

Rajesh Kumar Jyothi
Pankaj Kumar Parhi *Editors*

Clean Coal Technologies

Beneficiation, Utilization, Transport
Phenomena and Prospective

 Springer

Clean Coal Technologies

Rajesh Kumar Jyothi • Pankaj Kumar Parhi
Editors

Clean Coal Technologies

Beneficiation, Utilization, Transport
Phenomena and Prospective

 Springer

Editors

Rajesh Kumar Jyothi
Convergence Research Center for
Development of Mineral Resources (DMR)
Korea Institute of Geoscience and Mineral
Resources (KIGAM)
Daejeon, Republic of Korea

Pankaj Kumar Parhi
Department of Chemistry
Fakir Mohan University
Balasore, Odisha, India

ISBN 978-3-030-68501-0

ISBN 978-3-030-68502-7 (eBook)

<https://doi.org/10.1007/978-3-030-68502-7>

© The Editor(s) (if applicable) and The Author(s), under exclusive license to Springer Nature Switzerland AG 2021

This work is subject to copyright. All rights are solely and exclusively licensed by the Publisher, whether the whole or part of the material is concerned, specifically the rights of translation, reprinting, reuse of illustrations, recitation, broadcasting, reproduction on microfilms or in any other physical way, and transmission or information storage and retrieval, electronic adaptation, computer software, or by similar or dissimilar methodology now known or hereafter developed.

The use of general descriptive names, registered names, trademarks, service marks, etc. in this publication does not imply, even in the absence of a specific statement, that such names are exempt from the relevant protective laws and regulations and therefore free for general use.

The publisher, the authors, and the editors are safe to assume that the advice and information in this book are believed to be true and accurate at the date of publication. Neither the publisher nor the authors or the editors give a warranty, expressed or implied, with respect to the material contained herein or for any errors or omissions that may have been made. The publisher remains neutral with regard to jurisdictional claims in published maps and institutional affiliations.

This Springer imprint is published by the registered company Springer Nature Switzerland AG
The registered company address is: Gewerbestrasse 11, 6330 Cham, Switzerland

Preface

In global scenario, coal is one of the vital sources, strategically utilized for generation of energy. The coal source has received broader attention worldwide for its beneficiation owing to bear value adding physical and chemical constituents in it. In similar to coal, the fly ash source management is becoming an emerged area of research. Coal fly ash (CFA) is usually generated as a by-product after the combustion of coal, and the liberation of the fly ash from the various power plants and industries is abundant. Both coal and fly ash comprising REEs and other valuable metals/non-metals ascertain about their potential applicability by developing suitable technology for recovery metal values as well as their utilization as activated sorbent material for various environmental remediation processes. In addition, there is significance of numerous applications of both as source of raw material for making promising composite material(s). Ample amount of studies are being devoted on beneficiation-cum-management of coal, coal ash, and fly ash through various physical, chemical and biological processing approaches.

This book accomplishes various prospective applications of coal and fly ash, and extensive research studies are being taken up by researchers on physical/chemical beneficiation, slurry stabilization behaviour, rheology and prospective utilization of making various advanced building construction as well as value-adding material such as cement, brick, geo-polymer, zeolites, concrete, filtering composite material and activated sorbent material(s) including bio-char through numerous methodologies thereof. The entire prospective utilization, beneficiation and development of environmental friendly technology of coal have been categorically covered in several chapters as described herein.

Generation of fly ash, its rheology, transport behaviour and proposed mechanism on stabilization of fly ash slurry using additives have been detailed. Fly ash is considered as a waste material often dumped in various disposal sites directly leading to cause several environmental concerns. Therefore, it could be transported to the disposal site after proper pre-treatment; then the issues due to the contamination as well as cost of waste management could be minimized. Unlike coal water slurry, fly ash slurry is being made to do the pipeline transportation in which water acts as a medium, and with the help of a pump, fly ash particles are transported from power

stations to ash ponds. The role of additive is a critical one; presently, natural organic surfactants that are used as promising additive in the stabilization of fly ash slurry are comprehensively illustrated.

Beneficiation of coal accomplishes physical concentration method, e.g. agglomeration approach that appears to be versatile towards the treatment of ultra-fine coal particles. The critical parameter affecting the agglomeration has been extensively discussed and reported. The researchers have developed the technology on environmental remediation by utilizing several activated coal for removal of toxic heavy metals. Pre-treatment of the coals, activating agent(s) and operative factors such as temperature, heating rate, reagent dosage and holding time, influencing the nature of the activated coal product that resulted, is systematically summarized and presented. The other way of beneficiation of coal is through biological processes. The heterotrophs and acidophilic microbes are adopted under acidic environment to remove organic sulphur by converting it to sulphite form via 4S pathway. The sulphur found at the pyrite gets oxidized to produce sulphuric acid by microbes. The bioleaching approach with the adoption of iron-reducing bacteria could effectively dissolve the sulphur content from the coal phase, which substantially resulted as sulphuric acid. In addition to it, the content of rare and heavy metals in both coal and fly ash phases lured to the metallurgist to extract out by hydro-processing approach. Chemical and bioleaching of these metals are carried out by optimizing the operating leaching parameters. Thereby, the coal ash and fly ash phases are benefited after the removal of organic and inorganic components for their further utilization.

The typical bio-char was also synthesized and its physical and chemical behaviour was examined. The equilibrium sorption studies using the bio-char were investigated. After the activation studies of bio-char and its effective applications for substantial removal, the study of several metals and other ionic contaminants from wastewater has been overviewed and presented. Desulphurization of coal is essential by adopting suitable environmental friendly processes. The attempt on desulphurization study by adopting various biological approaches was reviewed and presented. The surface modification studies of bio-char have been investigated to ascertain on upgrading of the physicochemical characteristic properties. This would lead to improve on increase in chemical interactions accomplishing electrostatic attraction, surface complexation and ion exchange behaviour, as described.

The coal fly ash generated out of coal (utilized at thermal power plants) is usually dumped as such to the environment, but its economic importance for claiming various valuable metals, including rare earth metals as well as other components, ensures for its potential source in metallurgical prospective. Several processing approaches on recovery of these REEs and other metal as well as non-metal values out of the CFA followed by their safe disposal to the environments are extensively investigated as stated. Furthermore, the critical aspect of fly ash as economic source of metals, non-metals and the assessment in contest of its environmental impact has been illustrated. The CFA as potential sources of REEs and incorporation of carbon mineralization process for recovering REEs has been reviewed and reported.

The insight of understanding about the incorporation of nano-particles for improving the effectiveness of activated carbon for its application in wastewater purification study is reviewed as presented.

Balasore, Odisha, India
Daejeon, Republic of Korea

Pankaj Kumar Parhi
Rajesh Kumar Jyothi

Contents

1 Mineral Beneficiation and Processing of Coal	1
Tonmoy Kundu, Surya Kanta Das, Dinesh Kumar Biswal, and Shivakumar I. Angadi	
2 Natural Dispersant in Coal Water Slurry Stabilization	39
Debadutta Das, Prativa Kar, Bijnyan Ranjan Das, Ranjan Kumar Mohapatra, Subrata Narayan Das, Pankaj Kumar Parhi, and Umakanta Behera	
3 Application of Biotechnological Approach for Making Coal an Environmentally Friendly Fuel	59
Haragobinda Srichandan, Puneet Kumar Singh, Pankaj Kumar Parhi, and Snehasish Mishra	
4 Oil Agglomeration Towards Quality Enhancement of High-Ash Coals: The Indian Scenario	71
Saswati Chakladar, Ashok Kumar Mohanty, and Sanchita Chakravarty	
5 Preparation of Coal-Derived Activated Carbon and Its Application for Adsorption of Metals from Aqueous Solutions	83
Kurniawan and Sookyung Kim	
6 Characteristic and Equilibrium Adsorption Studies of Biochar	143
Vijetha Ponnamp, Subbaiah Tondepu, and Rajesh Kumar Jyothi	
7 Bio-Desulfurization of Coal Using Biotechnological Approach, Making Coal a Less Harmful Fuel	161
Hafiz Ahmad Ishfaq, Ayantika Banerjee, and Sanaullah Qamar	
8 Environmental Benign Biochar Technologies: Strategic Utilization for CO₂ Capture and Wastewater Treatment	181
Mohd Danish Khan and Ji Whan Ahn	

9	Role of Nanomaterials: Enhancing the Adsorption Efficiency of Activated Carbon in Wastewater Treatment	215
	Kiranmai Reddy Majji, Venkata Naga Suresh Reddy Kachireddy, Shashi Kumar Kuruva Nandyal, and Sreenivasa Rao Battula	
10	Adsorption of Metals Using Activated Carbon Derived from Coal . .	233
	Parag Girhe, Divya Barai, and Bharat Bhanvase	
11	Generation, Transportation and Utilization of Indian Coal Ash	267
	Ranjan Kumar Mohapatra, Pradeep Kumar Das, Dulal C. Kabiraz, Debadutta Das, Ajit Behera, and Md. Kudrat-E-Zahan	
12	Studies on Extraction of Heavy Metal (s) from Fly Ash through Hydroprocessing Approach	289
	Saroj Sekhar Behera, Surendra Hansdah, Debadutta Das, Pankaj Kumar Parhi, and Rajesh Kumar Jyothi	
13	Investigation on Extraction and Recovery of Rare Earth Elements from Coal Combustion Products	311
	Verónica Cristina Arellano Ruiz, Pankaj Kumar Parhi, Jin-Young Lee, and Rajesh Kumar Jyothi	
14	Recovery of Rare Earth and Some Other Potential Elements from Coal Fly Ash for Sustainable Future	339
	Harshit Mahandra, Brendan Hubert, and Ahmad Ghahreman	
15	Coal Fly Ash Utilisation and Environmental Impact	381
	Shanjida Sultana, Saifuddin Ahsan, Sakib Tanvir, Nawshad Haque, Firoz Alam, and Mohan Yellishetty	
16	Utilization of Circulating Fluidized Bed Combustion Fly Ash for Simultaneous Recovery of Rare Earth Elements and CO₂ Capture	403
	Quang Tuan Lai, Thriveni Thenepalli, and Ji Whan Ahn	
17	Developments in Characterization and Mineral Processing of Coal Fly Ash for Recovery of Rare Earth Elements	431
	Tumuluri Sreenivas, Md Serajuddin, Ramkaran Moudgil, and Kacham Anand Rao	
18	Coal Burn Ash: A Sustainable Future Resource for Critical Metals Production	473
	Manis Kumar Jha, Archana Kumari, Rekha Panda, Rukshana Parween, Sanchita Chakravarty, and Rajesh Kumar Jyothi	
19	Characterization and Utilization of Coal Ash for Synthesis of Building Materials	487
	Shaswat Kumar Das, Subhabrata Mishra, Debadutta Das, Syed Mohammed Mustakim, Cyriaque Rodrigue Kaze, and Pankaj Kumar Parhi	

20	Prospective Utilization of Coal Fly Ash for Making Advanced Materials	511
	Aritra Kumar Dan, Dipanjan Bhattacharjee, Saikat Ghosh, Saroj Sekhar Behera, Birendra Kumar Bindhani, Debadutta Das, and Pankaj Kumar Parhi	
21	Biochar Production for Green Environment	533
	Ayantika Banerjee	
22	Distribution of Rare Earth Elements in Coal and Coal Fly Ash	557
	Sanjay Agarwal, Vishal Kumar Dubey, Kyung Ho Park, and Jin-Young Lee	
23	Recent Development in Metal Extraction from Coal Fly Ash	575
	Hong Vu, Tomáš Frýdl, Tadeáš Bastl, Petr Dvořák, Eva Kristianová, and Tomáš Tomáško	
24	Application of Geochemical Modeling in Rare Earth Elements Leaching of Coal Combustion and Secondary Residues	605
	Joyce N. Odimba and Rafael M. Santos	
25	Ionic Liquids for the Recovery of Rare Earth Elements from Coal Combustion Products	617
	Isaac Kwabena Danso, Ana Belen Cueva-Sola, Zubair Masaud, Jin-Young Lee, and Rajesh Kumar Jyothi	
	Index	639

Contributors

Sanjay Agarwal Metal Extraction and Recycling Division, CSIR-National Metallurgical Laboratory, Jamshedpur, Jharkhand, India

Ji Whan Ahn Resources Recycling Department, University of Science and Technology (UST), Daejeon, Republic of Korea

Center for Carbon Mineralization, Mineral Resources Research Division, Korea Institute of Geosciences and Mineral Resources (KIGAM), Daejeon, Republic of Korea

Saifuddin Ahsan North West Power Generation Company Limited (NWPGL), Dhaka, Bangladesh

Firoz Alam School of Aerospace, Mechanical and Manufacturing Engineering, RMIT University, Melbourne, VIC, Australia

Kacham Anand Rao Mineral Processing Division, Bhabha Atomic Research Centre, AMD Complex, Begumpet, Hyderabad, Telangana, India

Shivakumar I. Angadi AcSIR—Academy of Scientific and Innovative Research, New Delhi, India

CSIR-Institute of Minerals and Materials Technology, Bhubaneswar, Odisha, India

Ayantika Banerjee Decontamination and Decommissioning Division, Korea Atomic Energy Research Institute (KAERI), Daejeon, Republic of Korea

Quantum Energy Chemical Engineering, University of Science and Technology (UST), Daejeon, Republic of Korea

Divya Barai Department of Chemical Engineering, Laxminarayan Institute of Technology, Rashtrasant Tukadoji Maharaj Nagpur University, Nagpur, MS, India

Tadeáš Bastl Department of Metals and Corrosion Engineering, University of Chemistry and Technology Prague, Prague 6 – Dejvice, Czech Republic

Sreenivasa Rao Battula Department of Chemistry, GITAM Institute of Science, GITAM (Deemed to be University), Vishakhapatnam, Andhra Pradesh, India

Ajit Behera Department of Metallurgical & Materials Engineering, National Institute of Technology (NIT), Rourkela, Odisha, India

Saroj Sekhar Behera CSIR-Institute of Minerals and Materials Technology (IMMT), Bhubaneswar, Odisha, India

Umakanta Behera Department of Mining Engineering, Government College of Engineering, Keonjhar, Odisha, India

Bharat Bhanvase Department of Chemical Engineering, Laxminarayan Institute of Technology, Rashtrasant Tukadoji Maharaj Nagpur University, Nagpur, MS, India

Dipanjan Bhattacharjee Materials Research Laboratory (MRL), School of Biotechnology & School of Chemical Technology, Kalinga Institute of Industrial Technology (KIIT) Deemed to be University, Bhubaneswar, Odisha, India

Birendra Kumar Bindhani Materials Research Laboratory (MRL), School of Biotechnology & School of Chemical Technology, Kalinga Institute of Industrial Technology (KIIT) Deemed to be University, Bhubaneswar, Odisha, India

Dinesh Kumar Biswal AcSIR—Academy of Scientific and Innovative Research, New Delhi, India

CSIR-Institute of Minerals and Materials Technology, Bhubaneswar, Odisha, India

Saswati Chakladar Analytical and Applied Chemistry Division, CSIR-National Metallurgical Laboratory (NML), Jamshedpur, Jharkhand, India

Sanchita Chakravarty Analytical and Applied Chemistry Division, CSIR-National Metallurgical Laboratory (NML), Jamshedpur, Jharkhand, India

Ana Belen Cueva-Sola Convergence Research Center for Development of Mineral Resources (DMR), Korea Institute of Geoscience and Mineral Resources (KIGAM), Daejeon, Republic of Korea

Resources Recycling, Korea University of Science and Technology (UST), Daejeon, Republic of Korea

Aritra Kumar Dan Materials Research Laboratory (MRL), School of Biotechnology & School of Chemical Technology, Kalinga Institute of Industrial Technology (KIIT) Deemed to be University, Bhubaneswar, Odisha, India

Isaac Kwabena Danso National Centre for Efficacy Evaluation of Respiratory Disease Products, Korea Institute of Toxicology, Jeongeup, Republic of Korea

Department of Human and Environmental Toxicology, Korea University of Science and Technology (UST), Daejeon, Republic of Korea

Bijnayan Ranjan Das Department of Chemistry, College of Engineering & Technology, Biju Patnaik University of Technology, Bhubaneswar, Odisha, India

Debadutta Das Department of Chemistry, Sukanti Degree College, Subarnapur, Odisha, India

Pradeep Kumar Das Department of Chemistry, N. C. (Autonomous) College, Jajpur, Odisha, India

Shaswat Kumar Das Green Tech Concrete and Research (GTCR), Industrial Estate, Mancheswar, Bhubaneswar, Odisha, India

Subrata Narayan Das Department of Mining Engineering, Government College of Engineering, Keonjhar, Odisha, India

Surya Kanta Das AcSIR—Academy of Scientific and Innovative Research, New Delhi, India

CSIR-Institute of Minerals and Materials Technology, Bhubaneswar, Odisha, India

Vishal Kumar Dubey Metal Extraction and Recycling Division, CSIR-National Metallurgical Laboratory, Jamshedpur, Jharkhand, India

Petr Dvořák Department of Metals and Corrosion Engineering, University of Chemistry and Technology Prague, Prague 6 – Dejvice, Czech Republic

Tomáš Frýdl Department of Metals and Corrosion Engineering, University of Chemistry and Technology Prague, Prague 6 – Dejvice, Czech Republic

Ahmad Ghahreman The Robert M. Buchan Department of Mining, Queen's University, Kingston, ON, Canada

Saikat Ghosh Materials Research Laboratory (MRL), School of Biotechnology & School of Chemical Technology, Kalinga Institute of Industrial Technology (KIIT) Deemed to be University, Bhubaneswar, Odisha, India

Parag Girhe Department of Chemical Engineering, Laxminarayan Institute of Technology, Rashtrasant Tukadoji Maharaj Nagpur University, Nagpur, MS, India

Surendra Hansdah Department of Chemistry, Fakir Mohan University, Balasore, Odisha, India

Nawshad Haque Commonwealth Scientific and Industrial Research Organisation (CSIRO), Melbourne, VIC, Australia

Brendan Hubert The Robert M. Buchan Department of Mining, Queen's University, Kingston, ON, Canada

Hafiz Ahmad Ishfaq Fuel Cell Research Center, Korea Institute of Energy Research (KIER), Daejeon, Republic of Korea

Department of Advanced Energy and System Engineering, University of Science and Technology (UST), Daejeon, Republic of Korea

Manis Kumar Jha Metal Extraction & Recycling Division, CSIR-National Metallurgical Laboratory, Jamshedpur, Jharkhand, India

Rajesh Kumar Jyothi Convergence Research Center for Development of Mineral Resources (DMR), Korea Institute of Geoscience and Mineral Resources (KIGAM), Daejeon, South Korea

Department of Resources Recycling, University of Science and Technology (UST), Daejeon, South Korea

Dulal C. Kabiraz Department of Chemistry, Faculty of Science, University of Rajshahi, Rajshahi, Bangladesh

Venkata Naga Suresh Reddy Kachireddy Department of Chemistry, GITAM Institute of Science, GITAM (Deemed to be University), Vishakhapatnam, Andhra Pradesh, India

Prativa Kar Gandhi Institute of Engineering and Technology University, Gunupur, Odisha, India

Cyriaque Rodrigue Kaze Laboratory of Applied Inorganic Chemistry, Faculty of Science, University of Yaoundé I, Yaoundé, Cameroon

Mohd Danish Khan Resources Recycling Department, University of Science and Technology (UST), Daejeon, Republic of Korea

Center for Carbon Mineralization, Mineral Resources Research Division, Korea Institute of Geosciences and Mineral Resources (KIGAM), Daejeon, Republic of Korea

Sookyung Kim Mineral Resources Research Division, Korea Institute of Geoscience and Mineral Resources (KIGAM), Daejeon, Republic of Korea

Resources Recycling, Korea University of Science and Technology, Daejeon, Republic of Korea

Eva Kristianová Department of Metals and Corrosion Engineering, University of Chemistry and Technology Prague, Prague 6 – Dejvice, Czech Republic

Md. Kudrat-E-Zahan Department of Chemistry, Faculty of Science, University of Rajshahi, Rajshahi, Bangladesh

Archana Kumari Metal Extraction & Recycling Division, CSIR-National Metallurgical Laboratory, Jamshedpur, Jharkhand, India

Tonmoy Kundu AcSIR—Academy of Scientific and Innovative Research, New Delhi, India

CSIR-Institute of Minerals and Materials Technology, Bhubaneswar, Odisha, India

Kurniawan Mineral Resources Research Division, Korea Institute of Geoscience and Mineral Resources (KIGAM), Daejeon, Republic of Korea

Resources Recycling, Korea University of Science and Technology, Daejeon, Republic of Korea

Shashi Kumar Kuruva Nandyal Department of Humanities & Sciences, Annamacharya Institute of Technology and Sciences, Kadapa, Andhra Pradesh, India

Quang Tuan Lai Department of Resources Recycling, University of Science & Technology, Daejeon, Republic of Korea

Tectonic and Geomorphology Department, Vietnam Institute of Geosciences and Mineral Resources (VIGMR), Hadong District, Hanoi, Vietnam

Center for Carbon Mineralization, Mineral Resources Research Division, Korea Institute of Geosciences and Mineral Resources (KIGAM), Daejeon, Republic of Korea

Jin-Young Lee Convergence Research Center for Development of Mineral Resources (DMR), Korea Institute of Geoscience & Mineral Resources (KIGAM), Daejeon, Republic of Korea

Department of Resources Recycling, University of Science and Technology (UST), Daejeon, Republic of Korea

Harshit Mahandra The Robert M. Buchan Department of Mining, Queen's University, Kingston, ON, Canada

Kiranmai Reddy Majji Department of Environmental Science, GITAM Institute of Science, GITAM (Deemed to be University), Vishakhapatnam, Andhra Pradesh, India

Zubair Masaud Fuel Cell Research Center, Korea Institute of Energy Research (KIER), Daejeon, Republic of Korea

Department of Advanced Energy and System Engineering, Korea University of Science and Technology (UST), Daejeon, Republic of Korea

Snehasish Mishra School of Biotechnology, Kalinga Institute of Industrial Technology (KIIT) (Deemed to be University), Bhubaneswar, Odisha, India

Subhabrata Mishra Grøn Tek Concrete and Research (GTCR), Bhubaneswar, Odisha, India

Environment and Sustainability Department, CSIR- Institute of Minerals and Materials Technology (IMMT), Bhubaneswar, Odisha, India

Ashok Kumar Mohanty Analytical and Applied Chemistry Division, CSIR-National Metallurgical Laboratory (NML), Jamshedpur, Jharkhand, India

Ranjan Kumar Mohapatra Department of Chemistry, Government College of Engineering, Keonjhar, Odisha, India

Ramkaran Moudgil Mineral Processing Division, Bhabha Atomic Research Centre, AMD Complex, Begumpet, Hyderabad, Telangana, India

Syed Mohammed Mustakim Environment and Sustainability Department, CSIR—Institute of Minerals and Materials Technology (IMMT), Bhubaneswar, Odisha, India

Nneka Joyce Odimba School Engineering, University of Guelph, Guelph, ON, Canada

Rekha Panda Metal Extraction & Recycling Division, CSIR-National Metallurgical Laboratory, Jamshedpur, Jharkhand, India

Pankaj Kumar Parhi Department of Chemistry, Fakir Mohan (F.M.) University, Vyasa Vihar, Nuapadhi, Balasore, Odisha, India

Kyung Ho Park Center for Carbon Mineralization, Mineral Resources Research Division, Korea Institute of Geosciences and Mineral Resources (KIGAM), Daejeon, Republic of Korea

Rukshana Parween Metal Extraction & Recycling Division, CSIR-National Metallurgical Laboratory, Jamshedpur, Jharkhand, India

Vijetha Ponnam Department of Chemical Engineering, VIGNAN's Foundation for Science, Technology & Research (VFSTR) (Deemed to be University), Vadlmudi, Guntur, Andhra Pradesh, India

Sanaulah Qamar Fuel Cell Research Center, Korea Institute of Energy Research (KIER), Daejeon, Republic of Korea

Department of Advanced Energy and System Engineering, University of Science and Technology (UST), Daejeon, Republic of Korea

Verónica Cristina Arellano Ruiz Convergence Research Center for Development of Mineral Resources (DMR), Korea Institute of Geoscience & Mineral Resources (KIGAM), Daejeon, Republic of Korea

Department of Resources Recycling, University of Science and Technology (UST), Daejeon, Republic of Korea

Rafael M. Santos School Engineering, University of Guelph, Guelph, ON, Canada

Md Serajuddin Mineral Processing Division, Bhabha Atomic Research Centre, AMD Complex, Begumpet, Hyderabad, Telangana, India

Puneet Kumar Singh School of Biotechnology, Kalinga Institute of Industrial Technology (KIIT) (Deemed to be University), Bhubaneswar, Odisha, India

Tumuluri Sreenivas Mineral Processing Division, Bhabha Atomic Research Centre, AMD Complex, Begumpet, Hyderabad, Telangana, India

Haragobinda Srichandan School of Biotechnology, Kalinga Institute of Industrial Technology (KIIT) (Deemed to be University), Bhubaneswar, Odisha, India

Shanjida Sultana Institute of Mining, Mineralogy and Metallurgy, Bangladesh Council of Scientific and Industrial Research (BCSIR), Joypurhat, Bangladesh

Sakib Tanvir North West Power Generation Company Limited (NWPGL), Dhaka, Bangladesh

Thriveni Thenepalli Department of Chemistry, Indian Institute of Technology—Tirupati, Tirupati, Andhra Pradesh, India

Tomáš Tomáško Department of Metals and Corrosion Engineering, University of Chemistry and Technology Prague, Prague 6 – Dejvice, Czech Republic

Subbaiah Tondepu Department of Chemical Engineering, VIGNAN's Foundation for Science, Technology & Research (VFSTR) (Deemed to be University), Vadlmudi, Guntur, Andhra Pradesh, India

Hong Vu Department of Metals and Corrosion Engineering, University of Chemistry and Technology Prague, Prague 6 – Dejvice, Czech Republic

Mohan Yellishetty Resources Engineering, Department of Civil of Engineering, Monash University, Clayton, VIC, Australia

About the Editors



Pankaj Kumar Parhi, Ph.D. is presently working as an associate professor at Fakir Mohan (F.M.) University, Vyasa, Balasore, Odisha, India. Prior to his present assignment, he has served as assistant professor at Kalinga Institute of Industrial Technology (KIIT) deemed to be University. Dr. Parhi has obtained Ph.D. degree in chemistry from CSIR-IMMT, Bhubaneswar, Odisha, India, in the year 2009 and moved to pursue Postdoctoral Researcher-ship at Korea Institute of Geosciences and Mineral Resources (KIGAM), South Korea, during 2009–2012. In the year 2019, he has further visited to KIGAM, South Korea, as research advisor. He has over 16 years of research

and development experiences in non-ferrous extractive metallurgy, waste recycling, secondary solid waste management and aqueous chemistry domain. He has received the prestigious distinct INSPIRE Faculty Award (2012–2019) from Department of Science and Technology (DST), Govt. of India. In the year 2014, he was also conferred with Young Scientist Award from Science and Engineering Research Board (SERB), DST, Govt. of India. In addition, he has received INSC award as a Mentor, Ministry of MSME, Govt. of India in the year 2019. During his exposure to research, he has filled 5 patents and published ~140 research articles as peer-reviewed international journal research articles, book chapters and conference proceedings. He has also written a book on technology development for environmental remediation (ISBN: 9786202061124). Currently, he is actively working as editorial board member in the journal *Current Environmental Management* and as guest editor at the journal *Micro and Nano System*, Bentham Science Publishers. His published articles receive more than 1756 citations with h-index-22 and i10-index-34 (Google scholar data). Dr. Parhi's name has been listed as top 2% researchers in standard citation metrics database done by Stanford University under chemical engineering subject domain in the year 2020.



Rajesh Kumar Jyothi is working as a principal researcher and professor at Korea Institute of Geoscience and Mineral Resources (KIGAM), Daejeon, South Korea. He received his PhD in chemistry (subject of research is hydrometallurgy) from Sri Venkateswara University, Tirupati 517 502, Andhra Pradesh, India, and at Indian Institute of Chemical Technology (IICT), CSIR, Hyderabad 500 007, Telangana, India. Professor Dr. R. K. Jyothi has nearly two decades of hands-on experience on hydrometallurgical process developments for refractory, rare and precious metals from primary and secondary resources. He received following awards and honours:

- Listed top 2% researchers in the standard citation metrics database done by Stanford University, USA authors Jeroen et al., under Mining, Metallurgy and Chemical Engineering research areas, year 2020,
- Received Excellent Research Paper Award from Journal of the Korean Institute of Resources Recycling, KIRR Society, Seoul, Korea, 2020.
- Received the *Award* as one of the team members for *Top 100 Excellence R & D Projects* from Ministry of Science & ICT, Govt. of Korea, 2017.
- Korean National News Channels MBC & YTN Science telecast about his career achievements in KIGAM, Korea, on June 14th and 15th, 2016.
- KIGAM monthly bulletin published article on his achievements under Creative People, 07-08/2016.
- Received the *Award* as one of the team members for *Industrial Technology Transfer* from KIGAM, year 2014.
- Received *Award of the Best Scientific and Technological Innovation* from WasteEng¹² Organizing Committee at Porto, Portugal, year 2012.
- *First foreigner* to get a permanent position at Korea Institute of Geoscience & Mineral Resources (KIGAM), Daejeon, Korea, year 2009.
- Junior Scientist Award received from NESAC (National Environmental Science Academy), Delhi, India, year 2009.
- *Post-doctoral fellowship* awarded by KIGAM, Daejeon, Korea, year 2007–09.
- *Senior Research Fellowship Award* received from CSIR, New Delhi, India, year 2004–06.
- *Best Research Scholar Award* received from Sri Venkateswara University, Tirupati, India, year 2003.
- Recognized as an *Outstanding Reviewer* by ELSEVIER Journals such as Hydrometallurgy, Minerals Engineering, Separation and Purification Technology, Journal of Cleaner Production, Waste Management, Journal of Industrial Engineering and Chemistry and Journal of Photochemistry and Photobiology, B: Biology.

He has published several research publications as articles, reviews, book chapters and conference presentations in peer-reviewed top tier research journals and presented/contributed his research in national and international symposiums (Scopus Author ID: 57216781429 & ORCID ID: <https://orcid.org/0000-0001-8106-795X>). He has written two books on liquid-liquid extraction (ISBN: 978-3-639-24889-0 & 978-3-639-24635-3) and edited two more books, one book on Mineral Processing: Methods, Applications and Technology (ISBN: 978-1-53612-892-5) and the other on Rare-Earth Metal Recovery for Green Technologies: Methods and Applications, Springer, a part of Springer Nature (ISBN: 978-3-030-38105-9). Several patents were filled in various countries such as South Korea, World, European and the USA.

Chapter 1

Mineral Beneficiation and Processing of Coal



Tonmoy Kundu, Surya Kanta Das, Dinesh Kumar Biswal,
and Shivakumar I. Angadi

1.1 Introduction

Coal is a sedimentary rock formed due to the decay and decomposition of organic plant vegetation over millions of years under the influence of heat and pressure. Coal constitutes the second major energy resource of the world and accounts for about one-fourth of its energy consumption. Coal is primarily used as a fuel for the generation of power and as a reductant in the form of coke to produce steel.

Worldwide proven reserves of coal have been estimated to be about 1085 billion tonnes, as shown in Table 1.1. The United States has the largest reserves of coal, followed by Russia, Australia, India, and China. The global production of coal is roughly about 8 billion tonnes. India is the second-largest producer of coal in the world after China.

India has a total coal reserve of about 319.02 billion tonnes, out of which 148.79 billion tonnes contribute to the proven reserves category (<https://coal.nic.in/content/coal-reserves>). The proven coking coal reserves reported as 19.08 billion tonnes (Table 1.2).

The gradual depletion of coking coal reserves in conjunction with increased demand for production of steel has increased burden on the foreign exchequer for importing metallurgical grade coal to meet the requirement of steel industry. Venugopal et al. (2016) reported that about 79% of the total coal requirement of our nation is fulfilled by imports. Literature reports that only one-fourth of the nation's coking coal production caters to metallurgical requirement, while the rest has not contributed in the production of iron and steel (Venugopal et al. 2016). China is the

T. Kundu · S. K. Das · D. K. Biswal · S. I. Angadi (✉)

AcSIR – Academy of Scientific and Innovative Research, New Delhi, India

CSIR-Institute of Minerals and Materials Technology, Bhubaneswar, Odisha, India

e-mail: shivakumar@immt.res.in

Table 1.1 Global reserves and production of coal (2018) (List of Countries by Coal Reserves 2018; List of Countries by Coal Production 2018), million tonnes (MT) (https://en.wikipedia.org/wiki/List_of_countries_by_coal_reserves, https://en.wikipedia.org/wiki/List_of_countries_by_coal_production)

Countries	Proven reserves			Coal production (MT)
	Anthracite and bituminous (MT)	Sub-bituminous and lignite (MT)	Total (MT)	
United States	2,20,167	30,052	2,50,219	702.3
Russia	69,634	90,730	1,60,364	411.2
Australia	70,927	76,508	1,47,435	481.3
India	1,41,602	7185	1,48,787	716.0
China	1,30,851	7968	1,38,819	3523.2
Indonesia	26,122	10,878	37,000	461.0
Germany	3	36,100	36,103	175.1
Ukraine	32,039	2336	34,375	34.2
Poland	20,542	5937	26,479	127.1
Kazakhstan	25,605	0	25,605	111.1
Turkey	551	10,975	11,526	99.8
South Africa	9893	0	9893	252.3
New Zealand	825	6750	7575	2.9
Serbia	402	7112	7514	40.0
Brazil	1547	5049	6596	7.0
Canada	4346	2236	6582	59.5
Colombia	4881	0	4881	89.4
Pakistan	207	2857	3064	4.0
Vietnam	3116	244	3360	38.1
Hungary	276	2633	2909	8.0
Greece	0	2876	2876	37.8
Czech Republic	110	2547	2657	44.9
Mongolia	1170	1350	2520	49.5
Bulgaria	192	2174	2366	34.5
Uzbekistan	1375	0	1375	3.9
Mexico	1160	51	1211	10.4
Spain	868	319	1187	1.7
Thailand	0	1063	1063	16.3
Venezuela	731	0	731	0.3
Europe	0	0	0	490.1
Japan	0	0	0	1.3
Romania	0	0	0	25.7
South Korea	0	0	0	1.7
United Kingdom	0	0	0	4.2
Zimbabwe	0	0	0	2.7
<i>Grand Total</i>	7,69,142	3,15,930	10,85,072	8068.5

Table 1.2 Coal reserves in India as on 01.04.2018 (Type and category-wise Coal Resources of India, Ministry of Coal 2018) in million tonnes (MT) (<https://coal.nic.in/content/coal-reserves>)

Type of Coal	Proved	Indicated	Inferred	Total
<i>(A) Coking</i>				
Prime coking	4649	664	0	5313
Medium coking	13,914	11,709	1879	27,502
Semi-coking	519	995	193	1708
Sub-total coking	19,082	13,368	2073	34,522
<i>(B) Non-coking</i>	129,112	125,697	28,102	282,910
<i>(C) Tertiary coal</i>	594	99	895	1588
<i>Grand total</i>	148,787	139,164	31,069	319,020

leading producer of coal followed by India, the USA, and Australia. The largest reserves of coal are also available with these countries. Anthracite constitutes only 1% of the total world reserves of coal, bituminous accounts for 52%, while the rest includes the low-rank coals rich in sub-bituminous and lignite variety (The Coal Resource-A Comprehensive Overview of coal, World Coal Institute, 2009) (<https://www.worldcoal.org>).

1.2 Coal Characterization

1.2.1 Classification of Coal

Coal constitutes a heterogeneous mixture of transformed organic vegetal matter and associated inorganic materials. It is rich in carbon and mineral matter. Coalification refers to the series of processes involved during the transformation of this organic vegetation into coal. The first step in transforming vegetation into coal is the formation of peat upon decay and decomposition of the dead plants through biological processes. The continued deposition of mineral sediments over the peat bed for an indefinite period under the influence of heat and pressure facilitated the transformation of peat into coal. Each step of the transformation process represents the degree of coalification or rank of coal, which indicates its maturity level. The higher the rank of coal, the higher is its maturity. Table 1.3 shows the ASTM classification of coal based on rank.

Peat represents the lowest rank in the coal formation stage and is the least matured of all the ranks. It generally varies from light brown to blackish in colour. It has the highest level of moisture content as it is the least compressed phase of coal formation. Gradual application of heat and pressure squeezes the inherent moisture and leaves a solid porous residue. Lignite is commonly termed as brown coal and has less moisture content than peat. It is chiefly used in thermal power plants for the generation of power. Sub-bituminous coal is black in colour and has higher moisture content than the bituminous coal. It is also primarily used for power generation.

Table 1.3 ASTM classification of coals (Maynard et al. 2007)

Rank/class	Fixed carbon, % (daf)	Volatile matter, % (daf)	Gross calorific value, MJ/kg	Reflectance, %
Peat	60	> 60	14.7	0.2
Lignite	71	44–69	<19.3	<0.4
Sub-bituminous	80	40–50	19.3–25.5	0.4–0.5
High volatile bituminous	86	29–50	25.5–32.6	0.5–1.1
Medium volatile bituminous	90	22–31	36	1.1–1.5
Low volatile bituminous	91	14–22	36.4	1.5–2.0
Semi-anthracite	92	8–14	36	2.0–2.5
Anthracite	95	2–8	35.2	>2.5

Bituminous coal has a higher rank than sub-bituminous coal and is extensively used for metallurgical coke making applications. This rank of coal can be further subdivided into three categories based on volatile matter content and the end-use. Anthracite constitutes the highest rank of coal, black and shiny in appearance. It has the highest fixed carbon content and is the hardest amongst all the ranks of coal due to its maximum exposure to heat and pressure.

Coal is also classified based on their ability to form coke, which is further used as a raw material in steel making. Based on utility, coals are classified into coking type and non-coking type. Further, coking coals are subdivided into four groups: prime coking coal, medium coking coal, semi-coking coal, and weakly coking coal. Prime coking coals when subjected to the carbonization process at high temperature produce coke of metallurgical standards. The distinguishing features of this category of coal include 22–30% volatile matter, swelling index higher than 3, and caking index varying from 20 to 22. Medium coking coals cannot be directly used to produce coke without prior treatment, such as beneficiation, or requires blending with a better quality of coal. This category of coal can be further classified into high (VM > 32%), medium (VM 20–32%), and low (VM 15–20%) volatile coals. The volatile matter content of semi-coking coal is still higher and lies in the range of 33–44%. The semi-coking coals and weakly coking coals are difficult to beneficiate and can be utilized further only upon suitable blending.

Coking coal can be further classified based on the ash content, while semi- and weak coking coals on the basis of ash and moisture content. Non-coking coals, on the other hand, are classified on the basis of calorific value. Table 1.4 represents the coal classification based on grades.

It can be observed from the table that Steel Grade-I constitutes the best quality of coking coal, having an ash content of less than 15%. The quality of non-coking coal, on the other hand, is determined by the gross calorific value of its different grades. G-1 represents the best category of non-coking coal suitable for thermal power plants to generate electricity having maximum heating value.

Table 1.4 Classification of coals based on grades (Coal Grades, Ministry of Coal, 2019) (<https://coal.nic.in/content/coal-grades>)

Coking coal		Non-coking coal	
Grade	Ash content (A), moisture content (M)	GCV (K Cal./kg)	Grade
Steel Grade-I	Not exceeding 15%	> 7000	G-1
Steel Grade-II	15% < A < 18%	6700 < GCV < 7000	G-2
Washery Grade-I	18% < A < 21%	6400 < GCV < 6700	G-3
Washery Grade-II	21% < A < 24%	6100 < GCV < 6400	G-4
Washery Grade-III	24% < A < 28%	5800 < GCV < 6100	G-5
Washery Grade-IV	28% < A < 35%	5500 < GCV < 5800	G-6
Washery Grade-V	35% < A < 42%	5200 < GCV < 5500	G-7
Washery Grade-VI	42% < A < 49%	4900 < GCV < 5200	G-8
Semi-Coking Grade-I	(A + M) not exceeding 19%	4600 < GCV < 4900	G-9
Semi-Coking Grade-II	19% < (A + M) < 24%	4300 < GCV < 4600	G-10
		3700 < GCV < 4000	G-12
		3400 < GCV < 3700	G-13
		3100 < GCV < 3400	G-14
		2800 < GCV < 3100	G-15
		2500 < GCV < 2800	G-16
		2200 < GCV < 2500	G-17

1.2.2 Petrographic Components of Coal

Literature reports the occurrence of four distinct varieties of coal lithotypes or rock types that do not require any magnification and are visible through the naked eye. These are namely vitrain, clarain, durain, and fusain. The coal samples which appear to be bright in colour consist of vitrain and clarain lithotypes, while the dull type consists of durain variety, and fusain represents the fossil charcoal type of coal. These lithotypes or the coal bands, when analysed under a microscope, reveal the presence of macerals, which are the petrological components of coal. The heterogeneous nature of the coal sample is attributed to the distinct features of these inherent macerals. Table 1.5 shows the physical properties of different coal lithotypes and the Stokes-Herleen System of classification of macerals.

1.2.3 Coal Washability Studies

Washability studies are primarily conducted to analyse the yield of clean coal that can be obtained at a desired specific gravity and ash content. This is achieved by subjecting the coal sample to sink-float analysis, wherein the coal particles are treated in a series of fluids of known density. The respective specific gravity fractions are subsequently dried, weighed, and analysed to determine the ash content.

Table 1.5 Physical properties of coal lithotypes and Stokes-Herleen System of classification (Stopes 1935)

Megascopic	Physical properties		Microscopic	
	Lithotypes	General appearance	Specific gravity	Group macerals
Vitrain	Uniform shiny black bands	~1.3	Vitrinite	Collinite and telinite
Clarain	Laminated: composed of shiny and dull bands	~1.3	Vitrinite dominant	Collinite and telinite
			Exinite and	Sporinite, cutinite, alginite, waxes and resins
			Inertinite less prominent	Fusinite, micrinite, sclerotinite and semifusinite
Durain	Dull, non-reflecting, poorly laminated	1.25–1.45	Inertinite dominant	Fusinite, micrinite, sclerotinite and semifusinite
			Vitrinite and	Collinite and telinite
			Exinite less prominent	Sporinite, cutinite, alginite, waxes and resins
Fusain	Charcoal-like fragments	Soft Fusain: 1.35–1.45 Hard Fusain: ≥ 1.6	Inertinite	Fusinite

The most common organic liquids used for sink-float analysis include carbon tetrachloride, benzene, methyl iodide, bromoform, and diiodomethane. The weight percentage and ash content of respective specific gravity fractions, as analysed, are tabulated to represent the sink-float data. The washability curves are constructed based on the consolidation of these raw data on a weighted average basis into cumulative float and cumulative sink fractions. Table 1.6 shows a typical sink-float data of a coal sample used to construct the washability curves.

It can be seen from the above table that the given coal sample was subjected to sink-float analysis at a specific gravity of 1.3–2.1 with an interval of 0.1. The weight percentage of each density fraction is recorded in column 2. The ash content analysed for the respective specific gravity fractions is recorded in column 3. Column 2 is cumulated from top to bottom to calculate the cumulative float weight percentage in column 4. Cumulative float ash (column 5) is calculated by cumulating the products of columns 2 and 3 on a weighted average basis from top to bottom. Similarly, the cumulative sink weight percentage (column 6) is calculated by cumulating column 2 from bottom to top. The products of columns 2 and 3 are likewise accrued from the bottom upwards to derive the cumulative sink ash values (column 7). Near Gravity Material (NGM) represents the weight percentage of float material at an interval of ± 0.1 specific gravity. The lower the content of near gravity material present in the feed material, the better is the separation efficiency that is expected to be

Table 1.6 Typical sink-float data of a coal sample

Specific gravity	Wt., %	Ash, %	Cumulative float		Cumulative Sink		NGM, %	Ordinate,Z
			Wt., %	Ash, %	Wt., %	Ash, %		
1	2	3	4	5	6	7	8	9
-1.3	0.5	11.2	0.5	11.2	100.0	53.4		0.25
+ 1.3-1.4	4.1	15.6	4.6	15.1	99.5	53.6	12.2	2.6
+ 1.4-1.5	8.1	23.0	12.7	20.1	95.4	55.2	24.9	8.7
+ 1.5-1.6	16.8	34.7	29.5	28.4	87.3	58.2	27.1	21.1
+ 1.6-1.7	10.3	43.6	39.8	32.4	70.5	63.8	19.7	34.7
+ 1.7-1.8	9.4	52.6	49.2	36.2	60.2	67.3	19.0	44.5
+ 1.8-1.9	9.6	56.9	58.8	39.6	50.8	70.0	22.2	54.0
+ 1.9-2.0	12.6	62.6	71.4	43.7	41.2	73.0	23.7	65.1
+ 2.0-2.1	11.1	72.6	82.5	47.6	28.6	77.6	28.6	77.0
+ 2.1	17.5	80.8	100.0	53.4	17.5	80.8		91.3
	100.0	53.4						

achieved. The characteristic ash content (column 9) signifies the maximum theoretical ash content in any one particle at a given range of specific gravity. It is calculated using the formula mentioned in Eq. 1.1 (Corriveau and Schapiro 1979).

$$Z = X + Y / 2 \tag{1.1}$$

where X represents the cumulative float weight percentage value at a lower specific gravity, and Y represents the instantaneous weight percentage of particles at a specific gravity immediately higher than that of X.

Washability curves essentially comprise five sets of curves: cumulative float ash curve, cumulative sink ash curve, yield gravity curve, NGM curve, and characteristic ash curve. Figure 1.1 shows the set of washability curves constructed from sink-float data of Table 1.6.

The cumulative float ash curve is plotted between cumulative float weight percentage (column 4) and cumulative float ash percentage (column 5). This curve predicts the maximum theoretical ash content of the clean coal that can be achieved at a specific yield of the washed coal. Similarly, the cumulative sink ash curve is plotted between cumulative sink weight and ash percentage (column 6 vs. 7). This curve forecasts the maximum theoretical reject ash value which can be attained at a specific yield of the reject coal. The yield gravity curve is constructed by plotting the data of cumulative float weight percentage (column 4) versus specific gravity (column 1) and represents the theoretical yield of washed coal that can be obtained at a desired specific gravity. The near gravity material curve is plotted between the cumulative weight percentage of material (column 8) that lies in an interval of ±0.1 specific gravity range against the respective specific gravity (column 1). The characteristic ash curve is constructed by plotting the ordinate (column 9) versus the

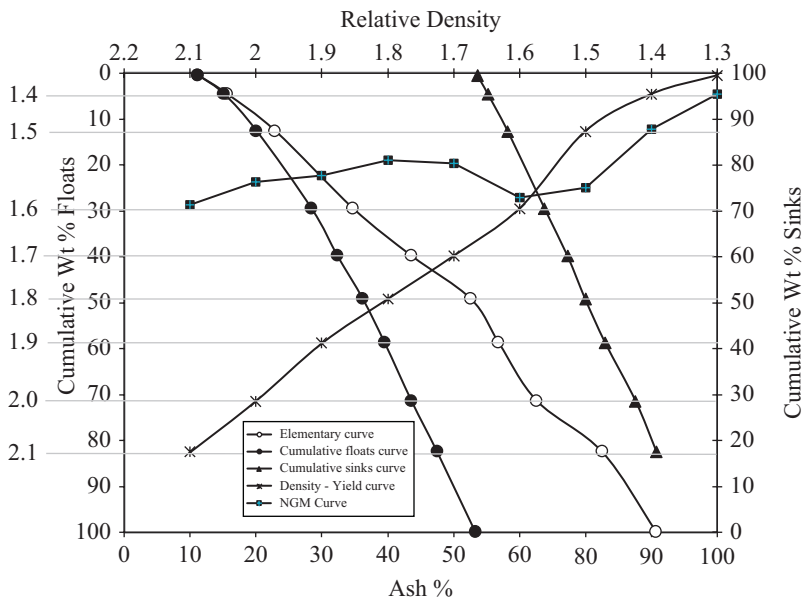


Fig. 1.1 Typical washability curves

cumulative float ash (column 5). This curve is a measure of the rate of change in the ash content at different specific gravities or yields.

1.3 Coal Preparation

The prime concern of a developing nation should be to utilize the available energy resources judiciously. Coal is one of the major sources of energy production. Hence, the activities revolving around coal utilization, such as mining, washing, and shipment, require a vigilant and systematic approach. One of the strategies that can be adopted is to explore the possibility of washing coal at its coarsest possible size, thereby eliminating the chances of over grinding. In turn, this reduces the operating cost of comminution circuit, handling and transportation costs, the difficulty encountered in dewatering of fine coal, and is also environment friendly.

Conventional gravity-based separators are generally employed to treat the coarse-sized coal fractions with a particle size in the range of $-80 + 15$ mm. Dense media cyclone is the most widely accepted technique to wash small size coal in the range of $-13 + 0.5$ mm. However, the problem lies with the treating of fine coal fraction having particle size finer than 0.5 mm. The mining techniques adopted in the present days further aggravate this problem, leading to generation of more fines. The continuous exploitation of the upper seam coals, followed by its increasing demand, urges it to wash difficult to wash coals meticulously. Oil agglomeration is

one such technique that is employed to wash fine-sized coal fraction. However, oil agglomeration suffers from the major drawback of increased diesel oil consumption, thereby adding to the process operating cost. In view of the above, froth flotation, water-only cyclone, and teeter-bed separators are the better options for treating fine coal.

The modern-day coal processing plants can be categorized into four different circuits, depending upon the size of the coal particles to be treated: (a) coarse coal processing circuit treating particles coarser than 10 mm, (b) small coal circuit for washing particles in the size range of 1-10 mm, (c) fine coal circuit for cleaning particles in size range of 0.15–1 mm, and (d) an ultra-fine coal processing circuit for treating particles finer than 0.15 mm (Luttrell and Honaker 2012; Angadi et al. 2015). Figure 1.2 shows the different range of equipment suitable to treat varying sized coal fractions of different circuits.

The series of equipment typically employed in various coal processing circuits can be broadly categorized into three groups depending on their ability to treat different particle size fractions: sizing devices, washing/cleaning devices, and dewatering devices (Luttrell and Honaker 2012). Sizing devices mainly include grizzly feeder, vibrating screen, sieve bend, classifying cyclone, etc. The various equipment used to wash coal includes drum separators, jigs, dense media cyclone, spiral concentrators, teeter-bed separators, water-only cyclone, shaking table, and flotation cell and columns. Solid-liquid separation in the coal processing circuits is achieved by employing different dewatering equipment such as high-frequency screens, centrifuges, thickeners, and filters. Different aspects of the listed equipment

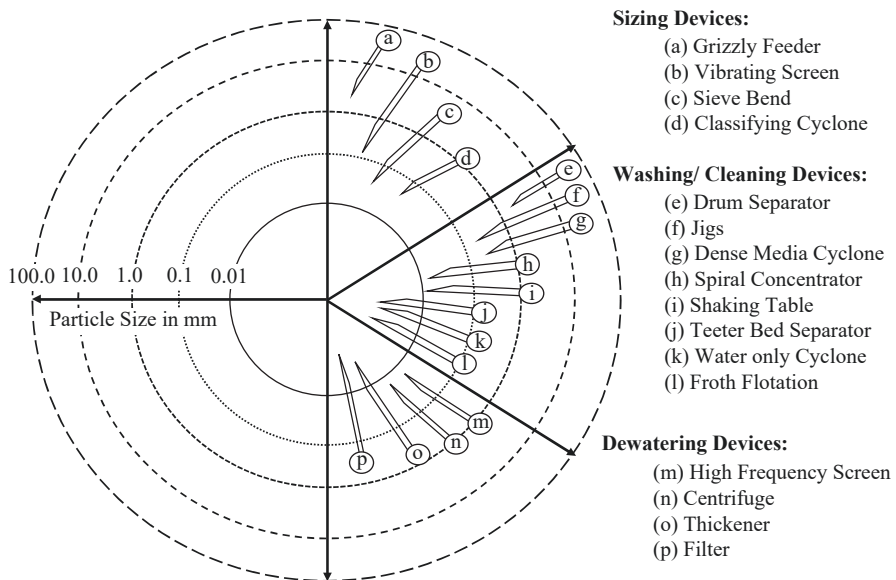


Fig. 1.2 Working size range of different coal processing equipment

typically utilized in the coal processing circuits are discussed in the subsequent section.

1.3.1 Sizing Devices

Sizing units are common in the processing of coals that are used throughout the circuit to perform different jobs. In the present-day coal preparation plants, sizing is done primarily for the following reasons:

- Removal of trash material or oversized boulders.
- Separation of coal particles based on the size required by the concentration unit.
- Retrieval of the heavy media used in the dense media coal cleaning circuit.
- Classification of ultra-fines in the fine coal cleaning circuit.
- Dewatering applications, etc.

Grizzly feeder is generally used to remove trash material from the feed of the comminution circuit to prevent any damage to the crushing surfaces. A vibrating screen is used to size or deslime the particles into coarse and fines fraction based on the requirement of different cleaning equipment of the washery circuit. The heavy media reporting along with the dense media cyclone overflow and underflow products in the coarse and small coal processing circuit is recovered using sieve bends and drain and rinse (D&R) screens. In the fines circuit, hydrocyclones are used to classify the ultra-fine coal particles. Whereas, high-frequency screens are utilized to dewater the coarse and fine coal products before discharging on to the conveyor belts.

1.3.1.1 Grizzly Feeder

The grizzly type fixed screens are chiefly utilized for primary screening applications in the coal preparation plants. ROM coal is pre-classified in a grizzly feeder to remove the undersize material, which otherwise may lead to choking problems, if directly fed to the primary crusher. The oversize material is recirculated to the primary crusher for desired size reduction.

Grizzly feeders are also employed to scalp the oversized material generally coarser than 50 mm in size (Luttrell and Honaker 2012). Figure 1.3 shows a typical grizzly feeder installed at the mine-site for heavy-duty applications to protect the downstream crushing equipment from the oversized feed material. The heavy-duty grizzly bars are constructed of cast manganese steel to withstand the impact and abrasive loads (Colman and Tyler 1980).

These screens essentially consist of evenly spaced parallel running grizzly bars or rails tapered towards the end. The grizzlies are generally mounted at a slope of 45–50 degrees to the horizontal for aiding the flow of feed material by gravity (Gupta and Yan 2006a). The static grizzlies are less efficient than the vibrating screens, especially due to the absence of any vibrating counterpart to assist in separating particles based on its size.

Fig. 1.3 Grizzly feeder
(Courtesy: FLSmidth India Limited)



1.3.1.2 Vibrating Screens

The separation efficiency of every processing equipment in the coal preparation plant is directly related to the feed particle size being treated. In general, a specific range of particle size is usually treated in any cleaning equipment to operate satisfactorily. However, coal in the form of lumps needs controlled size reduction and separation for further treatment in the washery circuit to reduce its ash content. Vibrating screens are operated in the coal preparation plants to regulate the crusher product particle size, deslime feed to heavy media separation circuits, and also dewater the clean coal and rejects.

A vibrating screen is a mechanical sizing device used to separate particles based on their size. The screens vibrate with a circular or elliptical motion generated due to the eccentric mounting of screen on the shaft (Lockwood et al. 2007). These screens are inclined to assist in the smooth flow of materials and impart a vibrating motion to the screening surface that further aid efficient separation of particles, as shown in Fig. 1.4.

Vibrating screens are applied to size coal particles having feed size varying from 300 mm to 45 μm (Hilden and David 2006). Generally, dry screening is preferred for coarser particles having size coarser than 5 mm, while wet screening is practiced for finer sized coal particles. The separation efficiency of vibrating screens is higher as compared to the static screens, such as grizzly feeders and sieve bends.

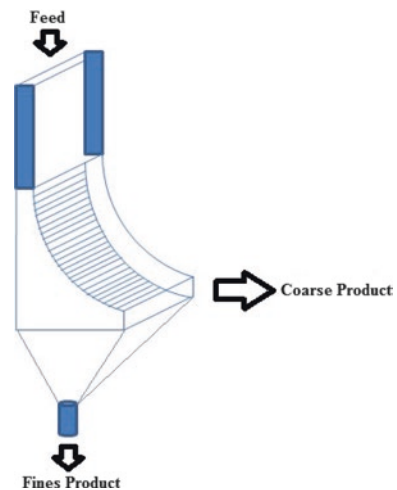
1.3.1.3 Sieve Bend

Sieve bends are used in coal preparation plants to confiscate the ultra-fine coal and drain the dense media cyclone products. These screens can handle a high throughput of coal slurry without blinding the apertures. The overflow product from the sieve bends mostly consists of water and a considerable amount of undersized



Fig. 1.4 Vibrating screen (Courtesy: FLSmidth India Limited)

Fig. 1.5 A sieve bend—
schematic representation



material. This undersize material is recovered upon further treatment in the drain and rinse screens. The application of sieve bends in the washery circuit has significantly reduced the vibrating screening area.

The sieve bends are stationary curved screens, composed of horizontal wedge bars or stainless steel wires curved to a quarter of a circle, as shown in Fig. 1.5. The slurry is tangentially fed at its top and flows downward in a perpendicular direction to that of the screening surface.

Separation of particles up to about 50 microns in size is attained every time a stream of particles comes across the screen surface, and a thin portion is peeled off to the underflow of the screen (Hilden and David 2006). They are essentially used

for dewatering applications in the DMC circuit, prior to feeding the products of dense media cyclones to the drain and rinse screens.

1.3.1.4 Classifying Cyclone

Cyclone or hydrocyclone is a centrifugal classifier that utilizes centrifugal force to classify coal particles, having size finer than 500 μm . The cyclones have the ability to obtain fine cuts even at a sharper separation. In coal preparation plants, a hydrocyclone is chiefly employed to classify undersize of the desliming screen, which is generally finer than 1000/500 μm . The underflow and overflow of classifying cyclones are further treated separately based on the required product coal quality.

The separation of particles based on size differences by using mechanized screening devices is economical for coarse particles (up to 50 microns in size). For finer separations, classifying cyclones are preferred because of their low capital and maintenance cost and higher separation efficiency. Figure 1.6 shows a bank of hydrocyclones installed in the processing plant for the classification application.

When the coal slurry is pumped and fed tangentially to the classifying cyclone, the particles swirling motion develops an outwardly directed centrifugal force and an inwardly directed counterbalancing drag force. The centrifugal force throws away the coarse particles having higher settling rates and discharges them through the apex. The finer particles are drawn into the vortex of the cyclone and are discharged through the vortex finder at the top. Classifying cyclones are extensively used in the coal processing circuit to stratify particles in size range of 0.1–0.15 mm (Luttrell and Honaker 2012).

1.3.2 Washing/Cleaning Devices

The coal quality and impurities present in the feed material play a significant role in deciding its end-uses. The thermal power plants utilize the heat value of coal for electricity generation, which is related to the composition of moisture, sulphur, and



Fig. 1.6 A bank of classifying hydrocyclones (Courtesy: FLSmidth India Limited)

ash values of the coal. On the other hand, steel plants evaluate coal quality based on its coking strength, sulphur, phosphorous, fixed carbon and ash contents, and the ability to form coke of requisite standards by suitable blending. The impurities present in the coal can be categorized into ash-forming and sulphur-containing type. Both of them can be further classified into the inherent and extraneous type of impurities. The inherent impurities are an integral component of the coal and cannot be separated by any physical or chemical means. However, the extraneous impurities, such as shale, sandstone, and clay, can be isolated from the clean coal by various available cleaning techniques. The choice of cleaning equipment is based on the liberation and washing characteristics of the coal. The feed particle size and the product ash requirement are the two basic features that govern particular cleaning equipment selection. Drum separators and jigs are essentially used in the coal washeries to treat coarse coal. Dense media cyclone is used for washing small-sized coal fraction. Spiral concentrator, shaking table, teeter-bed separator, water-only cyclone, and froth flotation are generally employed to wash the fine-sized coal fractions.

1.3.2.1 Drum Separators

Drum separators are gravity-based dense media separators, which consist of a cylindrical rotating drum. These separators essentially employ a heavy medium, such as magnetite, which creates a separation density up to 2.5 kg/l for separating clean coal from its associated shale impurities. Figure 1.7 shows a single-compartment drum separator.

As the coal slurry is fed to the drum separator, the heavier particles are constantly removed by lifters attached to the rotating drum. In comparison, the lighter particles discharge through an overflow weir, situated at an opposite end to the entry of feed particles (Napier-Munn 2006). These separators are efficient in treating a wide range of coal particles varying from 6 to 300 mm (Gupta and Yan 2006a, b). However, the separation efficiency decreases with an increase in fineness in the feed particle size. This is because settling of the fine particles is too slow under the influence of gravity to yield an efficient separation (Luttrell and Honaker 2012).

1.3.2.2 Jigs

Jigs comprise a class of conventional gravity separators, wherein particles stratify into layers of varying density gradient due to repeated upward and downward movement of the fluid medium. Jigs normally stratify coarse particles with a size in the range of 3–10 mm based on differences in their specific gravity (Holtham 2006). Unlike dense medium circuits, jigs do not require a media recovery circuit. They are cheaper to operate and preferred if the near gravity material is relatively less in the feed sample. Jigs have found wide applications in the beneficiation of coal, cassiterite, tungsten, gold, barite, and iron-bearing minerals. Figure 1.8 shows a water-pulsated jig.

Fig. 1.7 Wemco drum separator (Courtesy: FLSmidth India Limited)

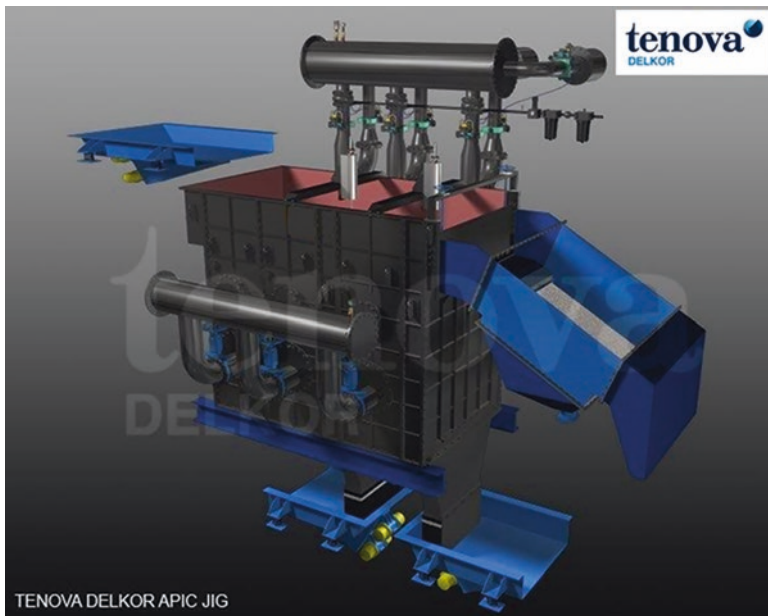


Fig. 1.8 Water-pulsated Jig (Courtesy: Tenova India Private Limited)

Particle stratification is achieved due to the pulsation and suction strokes that lift the bed of particles, dilates it, and eventually contracts it simultaneously and continuously. As the bed is lifted upwards during the pulsion stroke, the particles experience a difference in initial acceleration, which is predominantly dependent on the density of the solid particles and the fluid medium. As a result, the heavier coarse particles are completely separated from the lighter fine particles. The particles

thereafter attain terminal velocities, and hindered settling effect prevails, which leads to equal settling rates of the coarse light and fine heavy particles. The separation of such type of particles with similar settling rates is achieved during the suction stroke, wherein the bed contracts and allows only the fine heavy particles to trickle through the interstitial spaces between the coarse heavy particles and settle at the bottom.

Baum and Batac jigs are two types of air-pulsated jigs, which have found extensive applications in the coal industry. Stratification of particles in a Baum jig is caused due to the effect of pressurized air into the jig water system, which in turn causes alternate pulsation and suction of coal particles fed over the ragging bed. Baum jigs are high-capacity jigs, which can handle about 1000 t/hr. of coal particles (Holtham 2006). However, Baum jigs suffer a major drawback in generating an unequal stratification force along the entire width of the jig bed. This leads to a loss in separation efficiency of coal particles. This drawback has been successfully overcome in the design of Batac jigs, which has multiple air chambers situated all along the entire width of the jig bed so as to enable uniform air distribution for proper and efficient stratification of the bed of particles.

There is no dearth of literature on coal beneficiation using jigs, of which only a few are listed below. Research investigations conducted on jigging of a coal sample of size $-4.76 + 3$ mm using a laboratory Denver jig indicated a reduction in ash content of the clean coal to 16.55% from feed ash of 24.32% (Kumar and Venugopal 2017). It is reported that jigging studies conducted on a non-coking sample using a laboratory-scale Denver jig could achieve a clean coal product of 22.6% ash content and 64.15% combustible recovery at optimized conditions (Tripathy et al. 2016). Pilot-scale jigging studies conducted on a non-coking coal sample of Samleshwari mines using a Baum Jig washer revealed a reduction in ash content of the clean coal to 36% at a yield of 52% from a feed of 50% ash content (Gouricharan et al. 2009).

1.3.2.3 Dense Media Cyclone (DMC)

Dense media cyclone, a centrifugal type dense media separator, has been extensively adopted in coal washeries to wash coal particles of 0.5–12.5 mm size range (Luttrell and Honaker 2012). Provision for a high centrifugal force and low medium viscosity enables the centrifugal gravity separators to yield a finer separation than the gravitational separators. DMCs also utilize an external medium, such as magnetite, for washing coal, similar to the drum separators. Figure 1.9 shows a dense media cyclone.

The coal feed slurry is mixed with a desired ratio of magnetite by volume and pumped to the cyclone. The particles within the DMC are subjected to a swirling motion due to their tangential entry. Further, when the feed slurry encounters heavy medium within the centrifugal force field, denser particles, i.e. mostly shale particles, are thrown at the cyclone outer walls, finally collected as rejects at the spigot end. The lighter clean coal particles enter into the cyclone vortex and are discharged upwards through the vortex finder as the clean coal. However, magnetite also gets

Fig. 1.9 A dense media cyclone (Courtesy: FLSmidth India Limited)



distributed into the clean coal and reject products along with the particles, which has to be recovered. The media recovery circuit is the main drawback of DMC, which adds to the capital as well as the operating cost of the plant. The media recovery circuit consists of drain and rinse (D&R) screens and other associated auxiliary items such as tanks and pumps for both the cleans product and the rejects. The media recovered from the drain section of D&R screens is recirculated back to the DMC. However, the media recovered from the rinse section of the screens is diluted and can be reused only after treating and recovering it in a low-intensity magnetic separator.

Literature reports an extensive application of dense media cyclones to wash the coarse size coal fraction. Dense media separation studies conducted on a coal sample of West Bokaro coal washery indicated a decrease in ash content of the clean coal product to 17.5% from a feed of 36% with a yield of 33% while maintaining a media-to-coal ratio of 1:4 (Sripriya et al. 2007).

1.3.2.4 Spiral Concentrators

A spiral concentrator is another conventional gravity-based concentrator that separates valuable minerals from the gangue particles based on their specific gravity differences. The spiral concentrator was deployed commercially for the first time in the year 1943 by I.B. Humphreys Jr. to concentrate the chromite bearing sands in Oregon, USA (Holtham 2006). Spirals can efficiently treat and recover valuable particles in the size range of 3 mm to 75 μm . The operation of the spiral concentrator is simple and techno-economic, which makes them suitable for the treatment of a wide range of minerals, such as chromite, ilmenite, zircon, rutile, monazite, iron ore, and coal.

The spiral concentrators operate on the principle of flowing film concentration. As the feed slurry flows spirally downwards, valuable minerals are separated from the gangue particles due to their specific gravity differences. The separation is attained on account of the synergistic effects of interstitial trickling of particles through the flowing film, their differential settling rates and centrifugal force

(Holtham 2006). These effects result in forcing the lighter particles to travel along with water to the outer band, thereby retaining the heavier particles inwards. On the contrary, Mills (1978) reported hindered settling to be responsible for the separation of the particles along the troughs of the spiral concentrator. Bonsu (1983) identified reverse classification to be responsible for particle segregation within a spiral concentrator.

A spiral concentrator is extremely rugged and compact in construction, which is simple to operate and economical, and is the most versatile of all the available gravity-based separation units. Figure 1.10 shows a bank of spiral concentrators. The presence of these features facilitates a wide range of applications. Spirals are generally used for recovering gold from the hard rock ores, alluvial deposits, or the jig tailings. Spirals are also suitable, for instance, when the feed material consists of only a single sulphide phase having siliceous or other impurities, which requires its removal before flotation. Spirals are extensively used in the concentration of tin, tantalum, tungsten, and other associated heavy minerals from the hard rock ores, alluvial deposits, or the jig tailings. Spirals also find application in the beneficiation of beach sand minerals, such as ilmenite, rutile, leucoxene, zircon, and monazite. In view of the steel industry requirement to reduce the silica, phosphorous, Al_2O_3 , and K_2O levels in concentrates, spirals have been invariably used to enrich iron ores. Separation of chromite from silica-bearing minerals demands the application of spiral concentrators.

Coal beneficiation using spirals is an age-old technique and is still widely accepted, operated satisfactorily worldwide to reduce the ash content of the coal. A handful of research outcomes on the application of spiral concentrators for beneficiating coal have been listed in this section. Benusa and Klima (2008) reported that spirals reduced the ash content from 11.4% in the bituminous coal feed to 9.8% in the clean coal product, with a yield of 66.3%. The authors (Benusa and Klima 2009)



Fig. 1.10 A bank of spiral concentrators

also carried out similar research investigations on anthracite coal and reported ash reduction to 37.9% from 71% in the feed at a yield of 23.1%. Richards et al. (2007) reported that spirals could effectively reduce the ash content of a coking coal sample from a feed of 20% ash to 10% in the concentrate, with 80% yield. Similar observations were also reported for non-coking samples, wherein the ash content of the cleans product decreased from 35% to 20% at a yield of 60%.

1.3.2.5 Shaking Tables

The shaking table is a flowing film gravity concentrator that separates particles based on specific gravity differences. Shaking tables are used to stratify particles in size range of 0.3–9.5 mm (Gupta and Yan 2006b). These concentrators have found wide applications in the processing of coal, iron, tantalum, tin, tungsten, titanium, and, to a lesser extent, silver, gold, uranium, etc. Figure 1.11 shows a Denver Wilfley laboratory table supplied by M/s. Denver, USA.

The particles experience a longitudinal force, a slow forward stroke followed by a rapid return stroke exerted by the table deck. Furthermore, the flowing film of water applies a perpendicular force onto the particles. Under the influence of these two forces, particles move across the deck diagonally and in a parallel direction to the shaking table's vibration. The stratification of particles occurs behind the riffles, within the protected pockets. As a result, fine heavy grained particles travel farthest and report in the concentrate launder, while the coarse light particles are washed out by the flowing film of water and report into the tailing launder. Moderate elevation of the table deck along its vibration motion allows the heavier particles to advance easily compared to the lighter particles, thereby leading to a sharper cut between the concentrate and the tailing products.

Studies conducted on a coal sample using a shaking table could lessen the ash content from a feed of 38.1–18% in the concentrate (Cicek et al. 2008). Several researchers have reported similar applications of shaking table for washing coal fines (Zimmerman 1950; Tiernon 1980).



Fig. 1.11 Wilfley shaking table

1.3.2.6 Teeter-Bed Separators (TBS)

Teeter-bed separator, a type of hindered settling column, essentially consists of a vessel, which is open at the top, as shown in Fig. 1.12. These separators have found wide applications in the mineral processing industries (Hearn 2002; Littler 1986; Kumar et al. 2009) as classification units as well as gravity concentration units. Literature also reports TBS applications for the beneficiation of coal (Sarkar et al. 2008; Tripathy et al. 2013). Particles in the size range of 75 μm to a few millimetres are efficiently treated in these types of separators. Several published literature reveals the working principle of TBS (Doroodchi et al. 2004; Luttrell et al. 2006; Zimmels 1985).

Feed particles are allowed to fall through the column by gravity. In contrast, fluidized water is introduced upwards into the column in the opposite direction to that of feed for creating a teetered bed of suspended particles. The interstitial spaces situated within the bed of TBS generate high velocities of the upward moving stream of water, which prevents the settling of fine-light particles. As a result, coarse-heavy particles having higher settling rates than the upward stream of water can only settle through the teeter bed and are finally collected at the bottom discharge of the separator. The finer and lighter particles are carried to the top of the separator by the rising water stream and are finally discharged into a collecting



Fig. 1.12 Reflux classifiers (Courtesy: FLSmidth India Limited)

launder. Galvin et al. (1999) reported the application of dense media separation technique to evaluate the separation efficiency of teeter-bed separators.

Reflux Classifier: Reflux classifier is another gravity-based separation equipment that uses the synergistic effects of fluidized bed separation, autogenous dense medium separation, and lamella settling techniques to treat coal particles in size range of 0.25–2 mm (Galvin et al. 2002). There are two separation zones within a Reflux classifier. In the *fluidized bed zone*, separation of particles occurs in line with a similar working principle of the teeter-bed separators. The incoming coal particles are subjected to a rising stream of fluidization water, as a result of which the coal particles having velocity higher than the fluidization water will settle down, while the lighter particles report to the top. The accumulated coal particles in the fluidized bed zone result in the formation of a zone with a constant density, which is termed as a dense autogenous media. *Lamella zone* is an additional separation zone consisting of multiple parallel inclined plates, which allows the passage of only finer and lighter particles through the channels, while the denser and coarser particles are returned back to the fluidization zone. The recycling of coarser and denser particles develops a reflux action, which minimizes the possibility of misplacement. This leads to higher separation efficiency and better product quality, as compared to the teeter-bed separators. Kopparthi et al. (2019) reported that applying a Reflux classifier resulted in a reduction of ash content in the overflow product to 7.9–20% from a feed of 28% ash, at a yield varying from 31% to 64%.

1.3.2.7 Water-Only Cyclone (WOC)

Water-only cyclone (WOC) is used to treat coal particles in size range of 0.15–1 mm (Luttrell and Honaker 2012). Separation within a classifying hydrocyclone is predominantly due to the size effect. In water-only cyclones, the density of particles plays a predominant role in separation. The water-only cyclone is designed with a modification in the geometry of the existing classifying hydrocyclone.

Wider cone angle, an elongated cylindrical portion, and increased length of the vortex finder are the distinguishing features of a water-only cyclone, as shown in Fig. 1.13. The cone angle of a water-only cyclone may be as high as up to 120°, compared to 10–20° of the conventional classifying cyclones (Gupta and Yan 2006b). The wider cone angle creates a condition of hindered settling within the conical portion of the cyclone, and thereby increases the effect of particle density. Increased length of the vortex finder towards the apex implies a reduction in the distance between the vortex finder end and the conical walls of the cyclone. The extended cylindrical portion leads to increased particle retention time within the cyclone resulting in better separation efficiency.

WOCs are simple to function and are economical. They overcome the intrinsic drawbacks of dense media separators and froth flotation units as they do not require any consumables such as surfactants or artificial medium to separate particles. However, since the separation efficiency achieved is lower than the dense medium

Fig. 1.13 Bank of water-only cyclones



cyclones, these cyclones serve as suitable pre-cleaning devices for subsequent downstream operations based on the liberation characteristics of the feed material.

These cyclones are widely operated in coal processing circuits for its superior performance (Suresh et al. 1995, Hacifazlioglu 2012, Liu et al. 2013, Hore et al. 2012 and Majumder and Barnwal 2011). Sun et al. (2016) reported that the application of WOC for treating fine coal reduced the ash content in the overflow product to 23.49% from a feed of 28.64%. Similar studies conducted on a coal sample of the Cherat region in Pakistan indicated achieving a cyclone overflow product of less than 15% ash from a feed of 30% (Abbas and Muhammad 2016). Research investigations conducted by Kalyani et al. (2008) indicates a reduction in ash content of the fine coal to 20.98% from feed ash of 25.3% at a yield of 85.82%.

1.3.2.8 Froth Flotation

Froth flotation is an efficient technique for the treatment of fine and liberated particles. The conventional gravity separators are inefficient in treating the fines since a density difference between the valuables and the rejects is marginal. At present, it is a widely accepted and proven technique for the separation of coal particles finer than 150 microns (Luttrell and Honaker 2012). Also, it finds wide applications in the treatment of sulphide ores of copper, lead, zinc, platinum, nickel, and gold, oxide ores of iron, copper, and tin, and even non-metallic ores such as fluorites and phosphates (Luttrell and Honaker 2012). Froth flotation is a combination of physical and chemical separation processes that separates valuable minerals from its associated gangue impurities by utilizing differences in their surface wettabilities.

There are three major types of reagents that are widely used in the coal flotation process. The surface of the valuable mineral is rendered hydrophobic by the addition of *collectors*, which adsorbs on the coal surface and allows it to be recovered in

the froth product. Stability of the coal froth is rendered by the addition of *frothers*, which adsorbs on the air-water interface, reduces its surface tension, stabilizes the bubble, and allows its transportation and easy collection in the froth product. *Regulators* or *modifiers* are other groups of surfactants, which when added alter the surface properties of rejects or valuable minerals to the extent that only desired valuables are floated and collected in the froth product. Modifiers can be further subdivided into activators, depressants, and pH modifiers based on their applications in froth flotation. Activators are chemicals that aid in enhancing the adsorption possibility of the collector on the hydrophobic surfaces, whereas depressants are chemicals which influence the selectivity of flotation by getting adsorbed only on the hydrophilic surfaces and consequently depress them. On the other hand, the pH regulators modify the pulp alkalinity to create an environment for optimum performance of the other flotation reagents and the coal slurry.

Mechanical and pneumatic flotation cells are broadly used in the coal industry. As shown in Fig. 1.14, the mechanical flotation machine consists of a rotating impeller that keeps the slurry in suspension and allows uniform mixing of the air bubbles and flotation reagents with the coal slurry. The operating cost of these cells is generally higher due to the mechanical rotating arrangement embodied with the equipment. However, this drawback overcame after the invention of flotation column, which does not have moving parts. In the flotation column, feed slurry is fed into the column in a countercurrent direction to airflow. Air is dispersed from the bottom through a series of spargers to create aeration and facilitate particle suspension in the column. The froth and non-froth products are continuously collected in the respective launders situated at the top and bottom of the flotation column simultaneously. There are plenty of published literatures available elsewhere with regard to flotation of coal (Vanangamudi and Rao 1986, Rao et al. 1989, Angadi and Suresh 2005, Angadi et al. 2012, Ahmed and Jameson 1983, Aplan 1989, Arnold and Aplan 1989, Aston et al. 1983, Chander et al. 1994, Fuerstenau and Pradip 1982, Horsley and Smith 1951).

Fig. 1.14 A bank of flotation cells (Courtesy: Tenova India Private Limited)



1.3.3 Dewatering Devices

Coal industries are continuously striving to adopt innovative methods of coal cleaning. This results in the production of coals desired by the user industries. The moisture present in the washed coal product plays a major role in determining its value, which is responsible for reducing the heating value, increasing the transportation charges, adding on to the difficulty in handling and shipping, and lowering the yield and strength of metallurgical coke. Therefore, the product coal should be dewatered to the maximum possible extent before loading the conveyors for transportation. The most common difficulty encountered in dewatering of coal is the increase in surface area of the coal particles with a reduction in particle size. As a result, fine coals are more difficult to dewater compared to coarse coals. The dewatering equipment is responsible for removing only the free or surface moisture, which is present on the surface and between the particles. The inherent moisture, however, cannot be removed as such. There are several dewatering equipment in the coal washeries, deployed at different stages of processing on the basis of the feed particle size to be treated and the required product moisture to be achieved. High-frequency screens and centrifuges are used for dewatering the coarse fraction, while filters and thickeners are used for dewatering the fines fraction.

1.3.3.1 High-Frequency Screens

High-frequency screens constitute a special category of screens, which are essentially employed for dewatering of coal fine slurry. An electromagnetic vibrator is mounted on top of the screen and directly connected to it, as shown in Fig. 1.15, which imparts necessary vibrating motion to the screen.

Fig. 1.15 High-frequency dewatering screen
(Courtesy: *FLSmidth India Limited*)



Solid-liquid separation is attained by its characteristic features, such as high frequency (3600 rpm) and low amplitude (1.2–2.0 mm) of vibration. The vibration motion of high-frequency screens results in the particles' elliptical motion over the screen bed, thereby allowing only the oversized particles to be retained on the screen surface (Hilden and David 2006). The high-frequency vibrating screens are typically inclined to enhance the separation efficiency of the solid-liquid separation process. The inclination can be as high as 45 degrees. The apertures of the high-frequency screens are very fine and prone to blockage, which necessitates pre-treatment of the feed slurry.

1.3.3.2 Centrifuge

Centrifuges are used in coal processing circuits to dewater coarse and fine coal slurry. These can be broadly classified into three types, based on their ability to handle different sized coal fractions. Figure 1.16(a) shows a *horizontal vibrating basket* centrifuge used to dewater coarse coal fraction (+0.5 mm) generated in the DMC circuit. The clean coal and reject coal fractions of the DMC circuit are dewatered in this type of centrifuge to generate a product moisture content of 5–8%. Dewatering is accomplished by using centrifugal forces within the conical filtering basket in conjunction with the generated vibrating force. These centrifuges rotate at a low speed of 60–200 rpm, capable of generating centrifugal force of 44–62 g (Bickert 2007).

The second variety constitutes the *screen scroll basket centrifuges* (Fig. 1.16(b)) used to dewater products of spiral concentrators and teeter-bed separators, with a particle size of $-2 + 0.1$ mm. The presence of fine coal particles in the feed slurry demands a higher rotational speed (700 rpm) of the screen scroll and hence a higher centrifugal force (360 g) for its efficient dewatering. Product moisture from the screen scroll centrifuge is of the order of 12–18%. *Screen bowl centrifuges* (Fig. 1.16(c)) are used for dewatering ultra-fine coal slurry, having particles finer than 0.125 mm. The centrifugal force generated within the bowl is much higher than the other two types of centrifuges and can go up to 3000 g. Generally, flotation

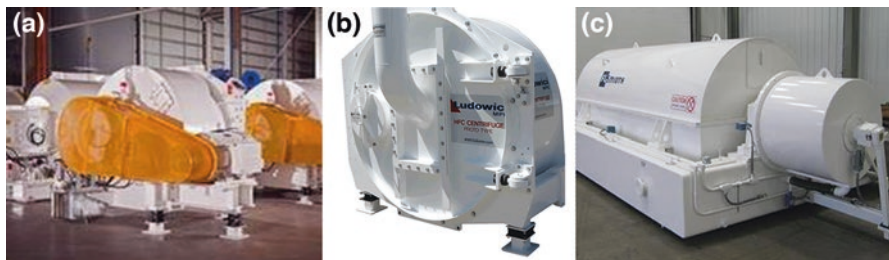


Fig. 1.16 Centrifuges: (a) horizontal vibrating basket centrifuge, (b) screen-scroll centrifuge, and (c) screen-bowl centrifuge (Courtesy: FLSmidth India Limited)

products of the fine coal circuit are treated in a screen bowl centrifuge to produce a dewatered product having moisture content in the range of 16–27% (Bickert 2007).

1.3.3.3 Thickener

Thickeners are circular tanks made of reinforced concrete or mild steel structures, as shown in Fig. 1.17. These are used to increase the solids concentration of the coal slurry by effective dewatering. Thickeners essentially employ flocculants to form flocs that aid in the settling process of the coal slurry.

The slurry is fed centrally through a feed well into the thickener. The clarified supernatant liquid continuously flows upwards and radially outwards, and finally overflows through a launder at the top of the thickener. This clarified water may be further reused as process water in the plant. On the other hand, the solids flow continuously downwards and inwards, settle at the bottom, and are withdrawn by rakes located radially across the thickener through an outlet at the centre of the thickener. The thickened underflow is usually discharged from the bottom of the thickener through a pumping arrangement.

1.3.3.4 Filter

Filtration units are also used for dewatering coal fines, especially when lower product moisture is desired. The filtration process involves the separation of solid particles from a liquid by subjecting the slurry into a pressurized/vacuum chamber, which is connected to the porous medium at the rear end. The liquid penetrates through the porous medium, while solid particles are retained. This is achieved either under the influence of a vacuum or an external pressure. The three major types of vacuum filters predominantly used in the coal processing applications are

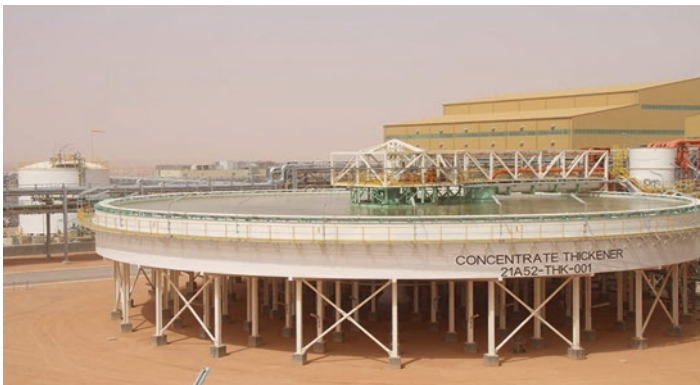


Fig. 1.17 Conventional thickener (Courtesy: Tenova India Private Limited)

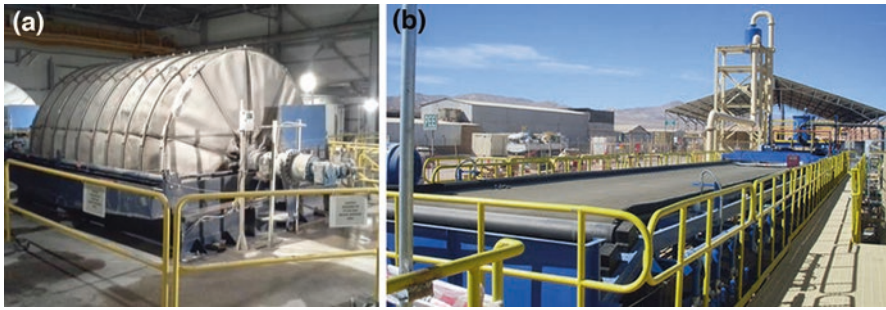


Fig. 1.18 Vacuum filters: (a) disc filter (Courtesy: FLSmidth India Limited), (b) horizontal belt filter (Courtesy: Tenova India Private Limited)



Fig. 1.19 Press filter (Courtesy: Tenova India Private Limited)

drum filter, disc filter, and horizontal belt filter (Bickert 2007). Figure 1.18 shows a schematic representation of different types of vacuum filters.

The vacuum drum filter comprises a large drum covered with a filter cloth around its circumference. A portion of the drum is immersed in the pool of slurry. During the drum rotation, the vacuum sucks liquid from the slurry forming a cake on the filter cloth surface. Solids accumulated in the form of cake are discharged at the end of the filtration cycle. Disc filters also operate on the same principle of dewatering solid particles under the application of a vacuum. However, disc filters provide a much larger filtration area as compared to the drum filters and hence can handle higher throughput capacity. Horizontal belt filters consist of a filter cloth located below a moving grooved belt, under which the vacuum is applied. The feed slurry is fed at one end of the belt filter, which gradually dries up and forms a cake as it reaches the other end of the belt. It has the ability to handle coarse particles of size up to 2 mm. Product moisture from the vacuum filters lies in the range of 20–25% for coal-based applications (Bickert et al. 2007).

The fine particles have a greater surface area and hence acquire higher moisture content. So, the dewatering of ultra-fine coal particles requires the application of pressurized force to lower the moisture content in the fine coal slurry. The

hyperbaric filter is one such filter similar to disc filter in appearance but utilizes pressurized compressed air (600 kPa) to dewater coal slurry (Bickert et al. 2007). Chamber filter press, commonly known as plate and frame filter press, consists of perforated plates along with alternate hollow frames mounted on a steel frame, as shown in Fig. 1.19.

Coal slurry is pumped into the frame under pressure and forms cake on the filter cloths fixed on both sides of the perforated plates. Press filters operate in a batch process, and cakes are discharged by opening the chamber plates. Membrane filters have an additional flexible membrane, usually made of rubber, to squeeze the cake by applying compressed air or injection of pressurized water behind the membrane.

The cake is discharged at the end of the filtration cycle after relieving the membrane pressure. These pressure filters produce a dewatered cake having product moisture content of 4–5% less compared to the vacuum filters (Bickert et al. 2007). Belt press filters also use pressure filtration techniques to dewater the thickened coal tailings. The flocculated slurry is fed under gravity through a series of rollers, wherein the shear forces generated by the rollers help in squeezing the cake and dewater it. Product moisture from belt press filters is in the range of 35–45%.

1.4 Plant Practices

The Indian origin coals have high ash content, and the impurities are dispersed throughout the coal seam. The near gravity material (NGM) content of such coals is high, generally greater than 30%. The liberation of valuable coal particles is achieved at a finer size. The presence of fines and ultra-fine particles poses difficulty in washing coals and consequently results in lower yield and less organic efficiency. Difficult to wash characteristics of coals eliminates the possibility of having a unified washery circuit in general for all Indian coals. Table 1.7 shows the various washing schemes adopted in the different coking coal washeries of India. Most of them utilize DMC as the washing equipment in small coal circuits to counter the effect of the presence of a relatively high NGM.

1.4.1 Typical Coking Coal Washery Circuit

The coal preparation plant plays a vital role in the techno-economics of steel production. The coal washery circuit is largely based on the qualities of raw material and the product needed. A typical coking coal washery circuit is outlined in Fig. 1.20.

The ROM coal lumps are reclaimed through a series of belt conveyors to feed the comminution circuit, wherein the coal lumps are reduced in particle size using rotary breaker and roll crushers. The crushed ore is stored in storage silos to ensure continuity in the plant operation throughout the year, even when the mining activity

Table 1.7 Existing Indian coking coal washeries with washing schemes (Venugopal et al. 2016)

Sl. no.	Name of washery	Washing technology			Year of commissioning	Design capacity (MTPY)
		Coarse coal	Small coal	Fine coal		
1	Jamadoba	–	–13 + 0.5 mm (Dense media cyclone)	–0.5 mm Flotation	1952	0.9
2	Kargali	–300 + 30 mm (Coarse Coal Jig)	–	–	1958	2.78
3	Durgapur	–80 + 20 mm (Dense media bath)	–20 + 1 mm (Small coal jig)	–1 + 0.25 mm (Spiral) –0.25 mm (Flotation)	1960	1.5
4	Bhojudih	–75 + 25 mm (Dense media bath)	–25 + 0.5 mm (Batac Jig)	–0.5 mm Flotation	1962	1.7
5	Dugda-II	–	–13 + 0.5 mm (Dense media cyclone)	– 0.5 mm Flotation	1968	1.8
6	Chasnalla	–80 + 20 mm (Dense media bath)	–20 + 0.5 mm (Small coal jig)	–0.5 + 0.15 mm (Spiral) –0.15 mm (Clean coal)	1968	1.5
7	Kathara	–80 + 13 mm (Drewboy bath)	–13 + 0.5 mm (Dense media cyclone)	–0.5 mm Flotation	1969	3
8	Swang	–80 + 20 mm (Deshaler Jig)	–20 + 0.5 mm (Dense media cyclone)	–0.5 mm Water-only cyclone	1970	0.75
9	Sudamdih	–	–37 + 0.5 mm (Dense media cyclone)	–0.5 mm Flotation	1981	1.6
10	West Bokaro-II	–	–13 + 0.5 mm (Dense media cyclone)	–0.5 mm Flotation	1982	1.8
11	Moonidih	–	–30 + 0.5 mm (Dense media cyclone)	–0.5 mm Water-only cyclone	1983	1.6
12	Nandan	–75 + 13 mm (Coarse coal jig)	–13 + 0.5 mm (Fine coal jig)	–0.5 mm Flotation	1984	1.2
13	Rajrappa	–80 + 16 mm (Batac jig)	–16 + 0.5 mm (Fine coal jig)	–0.5 mm Flotation	1988	3
14	Mohuda	–	–25 + 0.5 mm	–0.5 mm	1990	0.63

(continued)

Table 1.7 (continued)

Sl. no.	Name of washery	Washing technology			Year of commissioning	Design capacity (MTPY)
		Coarse coal	Small coal	Fine coal		
15	Bhelatand	–	(Dense media cyclone) –13 + 0.5 mm	Flotation –0.5 mm	1994	0.86
16	West Bokaro-III	–	(Dense media cyclone) –13 + 0.5 mm	Flotation –0.5 mm	1994	2.1
17	Kedla	–80 + 15 mm (Batac jig)	–15 + 0.5 mm (Fine coal jig)	–0.5 mm Flotation	1997	2.6
18	Madhuband	–	–13 + 0.5 mm (Batac jig)	–0.5 mm Flotation	1998	2.5

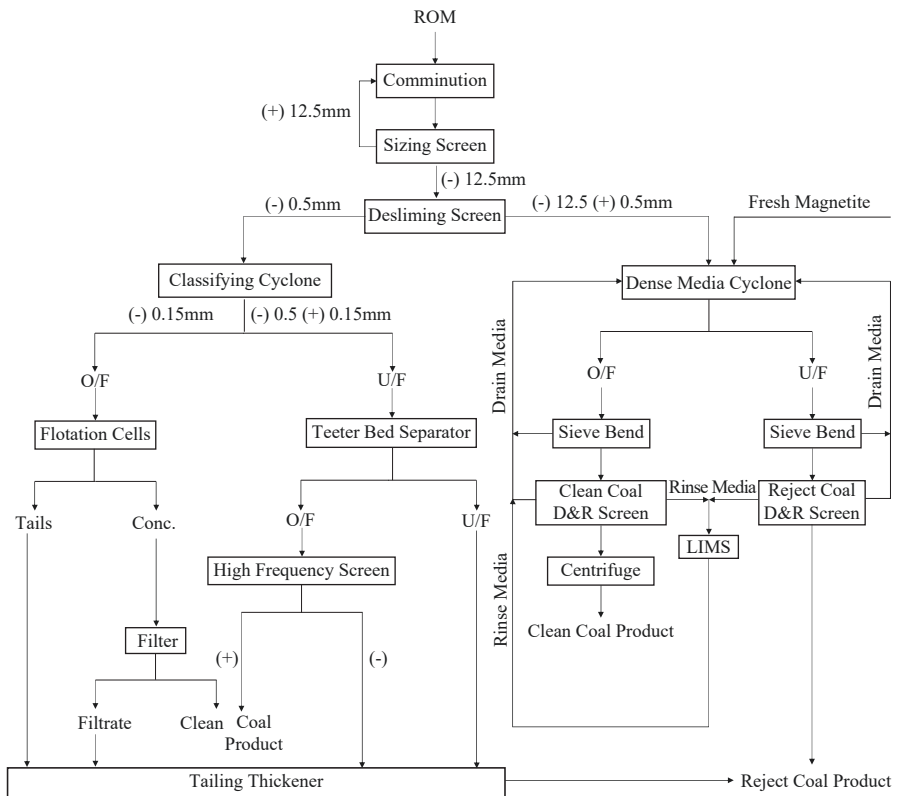


Fig. 1.20 Process flowsheet of a typical coking coal washery

is ceased. The crushed ore is then fed to the sizing screen to remove the particles coarser than 12.5 mm. The coarser particles are recycled back to the comminution circuit for further size reduction. The undersized particles are deslimed in a desliming screen at an aperture size of 0.5 mm to remove the ultra-fine particles from the heavy media circuit. The ultra-fine particles enhance the viscosity of the medium in dense media circuits, thereby affecting the separation efficiency.

The desliming screenoversize (i.e. $-12.5 + 0.5$ mm) is fed to the dense media cyclone. Fresh magnetite is added to the correct media tank along with water to prepare a medium of suitable specific gravity. The magnetite slurry is then pumped to the dense media cyclone to separate lighter coal particles from its associated heavy impurities effectively. The tangential entry of the particles develops a swirling motion, which leads to the generation of centrifugal force within the DMC. A counteracting inwardly directed drag force also develops to balance the outwardly directed centrifugal force. As a result, the heavier reject particles are thrown at the cyclone walls and are discharged through the apex, while the lighter coal particles report in the vortex finder. The cyclone overflow and underflow are treated in a sieve bend followed by D&R screens to drain the media and recirculating it back to the correct media tank for further feeding DMC. Spray water is added all along the length of D&R screens, which dilutes the media. This diluted media, which is recovered from the rinse section of D&R screens, is concentrated in a low-intensity magnetic separator (LIMS) to recover the correct media. The overflow of the D&R screen is fed to the centrifuge to dewater the clean coal product. The overflow of reject coal D&R screen is fed to the tailings thickener.

The undersize of the desliming screen (-0.5 mm) is treated in a classifying cyclone to cut it at a particle size of 0.15 mm. The cyclone underflow ($-0.5 + 0.15$ mm) is treated in a teeter-bed separator to separate the lighter coal particles reporting in the overflow and the shale impurity reporting in the underflow. The underflow of the teeter-bed separator is sent to the tailings thickener to dewater the coal reject, whereas the overflow is further treated in a high-frequency screen to dewater the clean coal of the fine coal processing circuit.

The cyclone overflow (-0.15 mm) is collected and pumped to flotation cells to float the clean coal. The froth product of the flotation cells is further processed in a filter to dewater the clean coal from the fines processing circuit.

1.4.2 Typical Non-coking Coal Washery Circuit

The thermal power plants receive coal from various mines that differ in calorific value, ash content, etc. Non-coking coal washing is practiced to provide consistent quality feed material to the thermal power plants. Figure 1.21 shows a typical non-coking coal washery circuit practiced in India.

Non-coking coal washery circuits are less complicated than the coking coal circuits. After suitable size reduction, the raw coal is fed to a desliming screen to separate the coarse and fines fraction. The coarser fraction is treated in a dense media

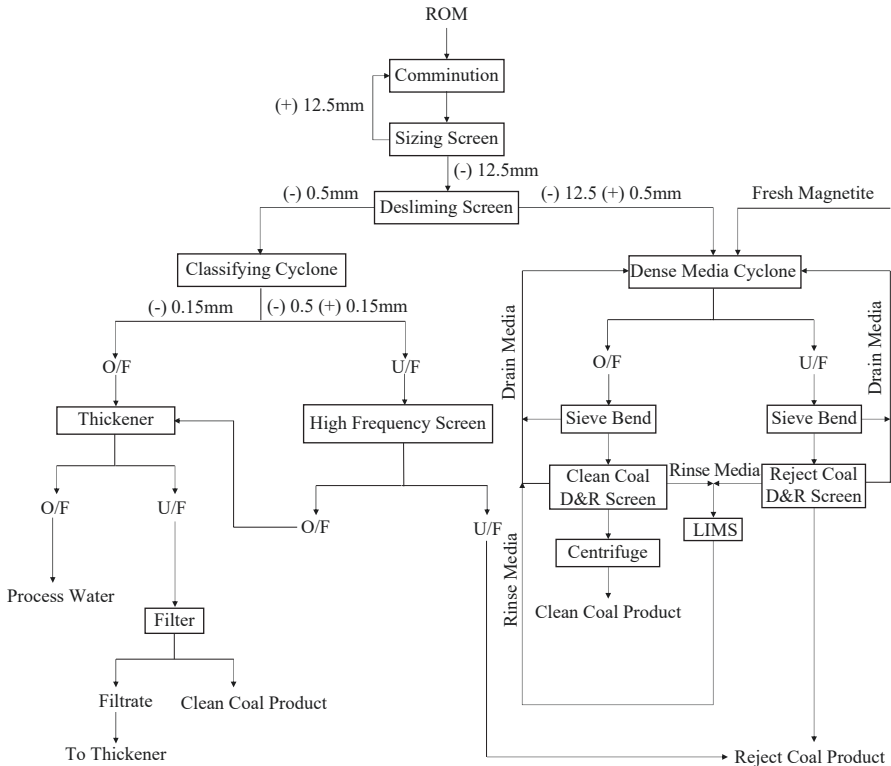


Fig. 1.21 Schematic diagram representing a typical non-coking coal washery circuit

cyclone to reduce its ash content at the coarsest possible particle size. Magnetite is generally used as the dense medium to aid the separation of particles based on specific gravity. The dense medium is recovered from the DMC circuit using sieve bends, D&R screens, and suitable pumping arrangements. The overflow product of DMC, having density lighter than the medium, is dewatered in a centrifuge and discharged as clean coal product on the conveyor belt. On the other hand, the underflow product, having a density higher than that of the separating medium, is discharged on the reject conveyor without the need for further dewatering.

Although the coarse coal processing circuits are similar in both cases, the fine coal processing circuits are different. The deslimed coal slurry is classified in a hydrocyclone to remove the coarser impurities. The overflow reports to a thickener, wherein the thickener underflow after being partially dewatered is processed further in a filter to achieve clean coal with a desired moisture content. The clarified water is recirculated back to the washery circuit and reused as process water. The underflow of hydrocyclone, on the other hand, is dewatered in a high-frequency screen, and the dewatered product is transferred to the reject coal conveyor for disposal.

1.4.3 Modular Plants

The modular concept has been successfully implemented for various mineral and coal processing plants in the recent past. Modularization of process plants has proved to be very promising in addressing various forthcoming requirements and logistic issues of the process industries. It allows greater flexibility and interchangeability of the available resources. The modular coal preparation plants offer significant advantages over the traditional conventional plants. It provides the opportunity to be operated even at remote sites, especially when access to the site and space availability become hindrances. The modular plants can cater to various mine sites due to its ease in shipment and transportation and facilitates easy installation. Some of the coal preparation applications where the modular concept has been employed include crushers, screens, hydrocyclones, spirals, jigs, and dense medium separators.

Figure 1.22 shows a modular plant consisting of screens, spiral concentrator, cyclone, thickener, etc. The plant is designed by M/s. CDE Asia Ltd. for treating coking coal fines. The feed coal sample is deslimed at 1 mm to remove the oversize material. The undersize of the desliming screen is pumped to a bank of spiral concentrators for further cleaning. The spiral concentrate is dewatered in a screen and discharged on to a product conveyor. The tailings of a spiral concentrator, and the overflow of hydrocyclone are fed to a tailings thickener. The overflow of the tailings thickener is recirculated back and caters to the process water requirement of the plant. About 90–95% of the process water is recovered and recycled back to the washery circuit.

Figure 1.23 shows a modular non-coking coal plant that consists of classifying cyclones and thickener designed by M/s. CDE Asia Ltd. The fines (<1 mm) of raw coal sample is fed to a desliming screen to separate the ultra-fine particles. The



Fig. 1.22 Modular spiral concentrator plant for treating coking coal fines



Fig. 1.23 Modular washing plant for treating non-coking coal fines

oversize product is discharged onto the product conveyor. The undersize of the desliming screen is pumped to a classifying cyclone for further cleaning. The cyclone underflow is subjected to a dewatering screen and discharged over a product conveyor. The tailings, hydrocyclone overflow, on the other hand, are fed to a tailings thickener. The overflow of the tailings thickener (clarified water) is recirculated back and caters to the process water requirement of the plant. The recovered process water from the tailings thickener overflow of about 90–95% is recycled back to the process plant.

1.5 Concluding Remarks

Coal is a valuable asset, which contributes to about 41% of the global electricity generation. Also, coal represents a vital part in manufacture of steel. However, a major part of the coals (about 70% in India) find application in generation of electricity. The raw coal quality available at the mine site is not suitable for end-use because of its high ash and low fixed carbon contents. This necessitates the cleaning or washing of raw coal for its further utilization in the power and steel industries. The beneficiation techniques adopted for washing thermal coals are much simpler and easier to operate than the metallurgical coals. Generally, froth flotation is not employed for treating the fine fraction of thermal coals, which evades the requirement of associated pumping and feeding arrangements. The techniques involved in coal preparation are environment-friendly and do not emit any toxic pollutants into the atmosphere. However, carbon dioxide gas emits during the electricity generation at the coal-fired thermal power stations. In recent times, the energy system across the world is facing a serious challenge to keep a balance between the increasing demand and supply of unpolluted and safe energy at a reasonable rate. Scientific inventions, such as the capture of emitted CO₂ gas, will allow us to cope up with the

growing demand for clean and harmless energy. In view of the above, judicious utilization of the coal reserves will lead to better economic development.

Acknowledgments The authors would like to thank M/s. FLSmidth India Limited, M/s. Tenova India Private Limited, and M/s. CDE Asia Limited for furnishing the figures of various equipment and modular plants included in this manuscript. The authors would like to thank the Director, CSIR-Institute of Minerals and Materials Technology, Bhubaneswar, India, for permitting to publish this chapter.

References

- Abbas, N., & Muhammad, K. (2016). Optimisation of operating and design parameters of Water-Only Cyclone using Cherat coal in Pakistan. *Journal of Nuclear Energy Science & Power Generation Technology*, 5, 2. <https://doi.org/10.4172/2325-9809.100049>.
- Ahmed, N., & Jameson, G. J. (1983). The effect of bubble size on the rate of flotation of fine particles. *International Journal of Mineral Processing*, 14, 195–215.
- Angadi, S. I., Jeon, H.-S., & Nikkam, S. (2012). Experimental analysis of solids and water flow to the coal flotation froths. *International Journal of Mineral Processing*, 110–111, 62–70.
- Angadi, S. I., Sreenivas, T., Jeon, H. S., Baek, S. H., & Mishra, B. K. (2015). A review of cassiterite beneficiation fundamentals and plant practices. *Minerals Engineering*, 70(2015), 178–200. <https://doi.org/10.1016/j.mineng.2014.09.009>.
- Angadi, S. I., & Suresh, N. (2005). A kinetic model for the prediction of water reporting to the froth products in batch flotation. *Transactions of the Institution of Mining and Metallurgy*, Sect. C, 114, 225–232.
- Aplan, F. F. (1989). Coal flotation—the promise and the problems. In S. Chander & R. R. Klimpel (Eds.), *Advances in Coal and Mineral Processing Using Flotation* (pp. 95–104). Littleton, CO: SME.
- Arnold, B. J., & Aplan, F. F. (1989). The hydrophobicity of coal macerals. *Fuel*, 68, 651–658.
- Aston, J. R., Drummond, C. J., Scales, F. J., & Healy, T. W. (1983). Frother chemistry in fine coal processing. In R. I. Whitmore (Ed.), *Proc. 2nd Aust. Coal Prep. Congress* (pp. 148–160). Brisbane: Westminster Press.
- Benusa, M. D., & Klima, M. S. (2008). An evaluation of a two-stage spiral processing ultrafine bituminous coal. *International Journal of Coal Preparation and Utilization*, 28(4), 237–260. <https://doi.org/10.1080/19392690802402978>.
- Benusa, M. D., & Klima, M. S. (2009). An evaluation of a two-stage spiral processing fine anthracite refuse. *International Journal of Coal Preparation and Utilization*, 29, 49–67. <https://doi.org/10.1080/19392690902784804>.
- Bickert, G. (2007). Solid–liquid separation technologies for coal, Chapter 13. In D. Osborne (Ed.), *The coal handbook: towards cleaner production (part II: Coal extraction and preparation)*. Woodhead Publishing Limited. <https://doi.org/10.1533/9780857097309.2.422>.
- Bickert, G., Joyce, J., Munro, M., Starr, D., & Firth, B. (2007). Dewatering of product coal, chapter 15. In G. J. Sanders (Ed.), *The principles of coal preparation* (4th ed., pp. 1–20) Australian Coal Preparation Society, ISBN: 978-0-9750337-4-6.
- Bonsu, A.K. (1983). Influence of pulp density and particle size on spiral concentration efficiency, *M.Phil.Thesis*, Camborne School of Mines.
- Chander, S., Polat, H., & Mohal, B. R. (1994). Flotation and wettability of a low-rank coal in the presence of surfactants. *Journal of Minerals Metallurgy*, 55–61.
- Cicek, T., Cocen, I., & Engin. and V. T., Cengizler, H. (2008). An efficient process for recovery of fine coal from tailings of coal washing plants. *Energy Sources, Part A: Recovery, Utilization, and Environmental Effects*, 30, 1716–1728. <https://doi.org/10.1080/15567030701443533>.

- Coal Grades, Ministry of Coal (2019). Retrieved September 30, 2020, <https://coal.nic.in/content/coal-grades>.
- Colman, K. G., & Tyler, W. S. (1980). Selection guidelines for size and type of vibrating screens in ore crushing plants, Chapter 15. In A. L. Mular & R. B. Bhappu (Eds.), *Mineral processing plant design* (2nd ed., pp. 341–361). Society of Mining Engineers of the American Institute of Mining, Metallurgical and Petroleum Engineers, Inc.
- Corriveau, M. P., & Schapiro, N. (1979). Projecting data from samples, Chapter 4. In J. W. Leonard (Ed.), *Coal preparation* (4th ed., pp. 4–3. – 1-55). New York: The American Institute of Mining, Metallurgical and Petroleum Engineers.
- Doroodchi, E., Fletcher, D. F., & Galvin, K. P. (2004). Influence of inclined plates on the expansion behaviour of particulate suspensions in a liquid fluidized bed. *Chemical Engineering Science*, 59, 3559–3567.
- Fuerstenau, D. W., & Pradip. (1982). Adsorption of frothers at coal/water interface. *Colloids and Surfaces*, 4, 229–243.
- Galvin, K. P., Doroodchi, E., Callen, A. M., Lambert, N., & Pratten, S. J. (2002). Pilot plant trial of the reflux classifier. *Minerals Engineering*, 15, 19–25. [https://doi.org/10.1016/S0892-6875\(01\)00193-5](https://doi.org/10.1016/S0892-6875(01)00193-5).
- Galvin, K. P., Pratten, S. J., & Nicol, S. K. (1999). Dense medium separation using a teetered bed separator. *Minerals Engineering*, 12(9), 1059–1081. [https://doi.org/10.1016/S0892-6875\(99\)00092-8](https://doi.org/10.1016/S0892-6875(99)00092-8).
- Gouricharan, T., Chattopadhyay, U. S., Singh, K. M. P., Kabiraj, S., & Haldar, D. D. (2009). Pilot-Scale Baum Jig Washing for beneficiation of a high-ash Indian noncoking coal. *International Journal of Coal Preparation and Utilization*. <https://doi.org/10.1080/19392690902936396>.
- Gupta, A., & Yan, D. S. (2006a). Screening, chapter 11. In *Mineral processing design and operation, An introduction* (pp. 293–353). Elsevier B. V. <https://doi.org/10.1016/B978-044451636-7/50012-7>.
- Gupta, A., & Yan, D. S. (2006b). Gravity separation, chapter 15. In *Mineral processing design and operation, An introduction*, 494–554. Elsevier B. V. <https://doi.org/10.1016/B978-044451636-7/50012-7>.
- Hacifazlioglu, H. (2012). Application of the modified water-only cyclone for cleaning fine coals in a Turkish washery, and comparison of its performance results with those of spiral and flotation. *Fuel Processing Technology*, 102, 11–17.
- Hearn, S. (2002). *Mineral processing plant design, practice and control proc.*, 1 (p. 929). USA: SME.
- Hilden, M. and David, D. (2006). Industrial screening, chapter 8, In B. A. Wills and T. Napier-Munn, *Mineral processing technology, An introduction to the practical aspects ore treatment and mineral recovery* (7th ed., pp. 186–202), Elsevier Science and Technology Books., ISBN: 0750644508.
- Holtham, P. (2006). Gravity concentration, chapter 10. In B. A. Wills & T. Napier-Munn (Eds.), *Mineral processing technology, An introduction to the practical aspects ore treatment and mineral recovery* (7th ed., pp. 225–245). Elsevier Science and Technology Books. ISBN: 0750644508.
- Hore, S., Das, S. K. R., Singh, R., & Bhattacharya, K. K. R. (2012). Efficiency study of a water only cyclone by experimental and data modelling techniques when cleaning Indian coal fines. *International Journal of Coal Preparation and Utilization*, 32(4), 193–209.
- Horsley, R. M., & Smith, H. G. (1951). Principles of coal flotation. *Fuel*, 30, 54.
- Kalyani, V. K., Gouricharan, T., Halder, D. D., Sinha, A., & Suresh, N. (2008). Coal-fine beneficiation studies of a bench-scale water-only cyclone using artificial neural network. *International Journal of Coal Preparation and Utilization*, 28(2), 94–114. <https://doi.org/10.1080/19392690802069918>.
- Kopparthi, P., Sachinraj, D., & Awasthi, A. (2019). Intermediate size fine coal beneficiation by reflux classifier using statistical approach. *Powder Technology*. <https://doi.org/10.1016/j.powtec.2019.11.078>.

- Kumar, C. R., Tripathy, S. K., & Rao, D. S. (2009). Characterisation and pre-concentration of chromite values from plant tailings using floatex density separator. *Journal of Minerals & Materials Characterization & Engineering*, 8, 367–378.
- Kumar, S., & Venugopal, R. (2017). Performance analysis of jig for coal cleaning using 3D response surface Methodology. *International Journal of Mining Science & Technology*, 27, 333–337. <https://doi.org/10.1016/j.ijmst.2017.01.002>.
- List of Countries by Coal Production (2018). Retrieved October 19, 2020, from https://en.wikipedia.org/wiki/List_of_countries_by_coal_production.
- List of Countries by Coal Reserves (2018). Retrieved October 19, 2020, https://en.wikipedia.org/wiki/List_of_countries_by_coal_reserves.
- Littler, A. (1986). Automatic hindered-settling classifier for hydraulic sizing and mineral beneficiation. *Mineral Processing and Extractive Metallurgy*, 95, 133–138.
- Liu, A., Gao, J., & Fan, M. (2013). Performance of an air-injected water-only cyclone for theseparation of fine coal. *International Journal of Coal Preparation and Utilization*, 33(5), 218–224.
- Lockwood, G., Lumsden, D., & Dauncey, N. T. (2007). Crushing and screening, chapter 8. In G. J. Sanders (Ed.), *The principles of coal preparation* (4th ed., pp. 149–192) Australian Coal Preparation Society, ISBN: 978-0-9750337-4-6.
- Luttrell, G. H., & Honaker, R. Q. (2012). Coal preparation. In R. A. Meyers (Ed.), *Encyclopedia of sustainability science and technology*. New York, NY: Springer. https://doi.org/10.1007/978-1-4419-0851-3_431.
- Luttrell, G. H., Westerfield, T. C., Kohmuench, J. N., Mankosa, M. J., Mikkola, K. A., & Oswald, G. (2006). Development of high-efficiency hydraulic separators. *Minerals and Metallurgical Processing*, 23, 33–39.
- Majumder, A. K., & Barnwal, J. P. (2011). Processing of coal fines in a water-only cyclone. *Fuel*, 90(2), 834–837.
- Maynard, B., Smith, C., & Preston, K. (2007). Coal in the ground, chapter 1. In G. J. Sanders (Ed.), *The principles of coal preparation* (4th ed., pp. 1–20) Australian Coal Preparation Society ISBN: 978-0-9750337-4-6.
- Mills, C. (1978). Process design, scale-up and plant design for gravity concentration. In A. L. Mular & R. B. Bhappu (Eds.), *Mineral processing plant design*. New York: AIMME.
- Napier-Munn, T. (2006). Dense medium separation (DMS), chapter 11. In B. A. Wills & T. Napier-Munn (Eds.), *Mineral processing technology, An introduction to the practical aspects ore treatment and mineral recovery* (7th ed., pp. 246–266) Elsevier Science and Technology Books, ISBN: 0750644508.
- Rao, T. C., Govindarajan, B., & Vanangamudi, M. (1989). A kinetic model for batch coal flotation. *Minerals Engineering*, 2(3), 403–414. [https://doi.org/10.1016/0892-6875\(89\)90009-5](https://doi.org/10.1016/0892-6875(89)90009-5).
- Richards, R. G., Hunter, J. L., & Holland-Bhatt, A. B. (2007). Spiral concentrators for fine coal treatment. *Coal Preparation*, 1(2), 207–229. <https://doi.org/10.1080/07349348508945549>.
- Sarkar, B., Das, A., & Mehrotra, S. P. (2008). Study of separation features in floatex density separator for cleaning fine coal. *International Journal of Mineral Processing*, 86, 40–49.
- Sripriya, R., Banerjee, P. K., Soni, B., & A. D. (2007). Dense-medium cyclone: Plant experience with high near-gravity material Indian coals. *Coal Preparation*, 27, 78–106. <https://doi.org/10.1080/07349340701249729>.
- Stopes, M. C. (1935). On the petrology of banded Bituminous coal. *Fuel*, 14(1), 4–13.
- Sun, M., Wei, L., & Cui, G. (2016). Studies of a water-only cyclone with a three-stage cone for fine coal beneficiation. *International Journal of Coal Preparation and Utilization*. <https://doi.org/10.1080/19392699.2016.1138943>.
- Suresh, N., Vanangamudi, M., & Rao, T. C. (1995). A performance model for water-only gravity separators treating coal. *Fuel*, 75(7), 851–854., 1996. [https://doi.org/10.1016/0016-2361\(96\)00020-8](https://doi.org/10.1016/0016-2361(96)00020-8).
- The Coal Resource-A Comprehensive Overview of coal, World Coal Institute (2009). Retrieved September 30, 2020, from <https://www.worldcoal.org>.

- Tiernon, C. H. (1980). Concentrating tables for fine coal cleaning. *Minerals Engineering*, 32, 1228–1230.
- Tripathy, A., Panda, L., Sahoo, A. K., Biswal, S. K., Dwari, R. K., & Sahu, A. K. (2016). Statistical optimization study of jigging process on beneficiation of fine size high ash Indian non-coking coal. *Advanced Powder Technology*. <https://doi.org/10.1016/j.apt.2016.04.006>.
- Tripathy, S. K., Mallick, M. K., Singh, V., & Rama Murthy, Y. (2013). Preliminary studies on teeter bed separator for separation of manganese fines. *Powder Technology*, 239, 284–289. <https://doi.org/10.1016/j.powtec.2013.02.015>.
- Type and category-wise Coal Resources of India, Ministry of Coal (2018). Retrieved September 30, 2020, from <https://coal.nic.in/content/coal-reserves>.
- Vanangamudi, M., & Rao, T. C. (1986). Modelling of batch coal flotation operation. *International Journal of Mineral Processing*, 16, 231–243. [https://doi.org/10.1016/0301-7516\(86\)90033-5](https://doi.org/10.1016/0301-7516(86)90033-5).
- Venugopal, R., Patel, J. P., & Bhar, C. (2016). Coal washing scenario in India and future prospects. *International Journal of Coal Science & Technology*, 3(2), 191–197. <https://doi.org/10.1007/s40789-016-0133-2>.
- Zimmels, Y. (1985). Theory of density separation of particulate system. *Powder Technology*, 43, 127–139.
- Zimmerman, R. E. (1950). The cleaning of fine sizes of bituminous coals by concentrating tables. *Minerals Engineering*, 187, 956–966.

Chapter 2

Natural Dispersant in Coal Water Slurry Stabilization



**Debadutta Das, Prativa Kar, Bijnyan Ranjan Das,
Ranjan Kumar Mohapatra, Subrata Narayan Das,
Pankaj Kumar Parhi, and Umakanta Behera**

2.1 Introduction

One of the parameters of the social improvement is economic development. Economic development depends on factors like man, material and machine. Machine requires both renewable and non-renewable energy. Renewable energy cannot match with the requirement. Therefore non-renewable energy is essential which is costly. All sources of non-renewable energy pertaining to coal are comparatively less costly than fuel oil or capital intensive, either thermal or atomic sources. Nevertheless, navigation of coal from mining head to generation site become a major location for cost effectiveness. Hence, the idea of transporting the coal from mining to the energy generation point through a pipeline in medium water has been considered suitable for cost cutting. Accordingly, attempts have been made

D. Das (✉)

Department of Chemistry, Sukanti Degree College, Subarnapur, Odisha, India

P. Kar

GIET University, Gunupur, Odisha, India

B. R. Das

Department of Chemistry, College of Engineering and Technology, Biju Patnaik University of Technology, Bhubaneswar, Odisha, India

R. K. Mohapatra

Department of Chemistry, Government College of Engineering, Keonjhar, Odisha, India

S. N. Das · U. Behera

Department of Mining Engineering, Government College of Engineering, Keonjhar, Odisha, India

P. K. Parhi

Department of Chemistry, Fakir Mohan University, Balasore, Odisha, India

to ferry the coal in the medium of water by using some chemical additives to facilitate concentration and viscosity and stability. Chemicals are not a gift of nature for which some more cost are involved. Therefore, introduction of bio-additive has been thought of for cost effectiveness of a product.

2.2 Brief History of Coal

A glimpse of the prehistoric era of the earth unfolds many untold stories of chronological development of coal. The earth was in dense forest in these periods. Due to natural calamities those swamp forest got buried under the earth. Layers of sand and soil deposited year after year causing increase in temperature of the buried vegetation resulting in carburization. The age of buried vegetation determined the quality of carbonization which in other words indicates the quality of coal that is concentrated carburization. Coal produces more than half of the total energy production in India.

2.3 Classification of Coal

High pressure and heat in the crest of earth created chemical, physical and biological changes in the buried vegetation which is called as coal. Time factor and metamorphism of the vegetation determines the quality of the coal. Besides, volatile matter and moisture are also factors to determine the nature of coal. The primary quality is peat whereas the highest quality is anthracite. In between there exist lignite, bituminous, and sub-bituminous. The utility of these qualities is as follows:

Peat: It is used as fuel and considered as forefather of coal.

Lignite: In the ladder the next step is lignite which has a calorific value of 4000–8300 BTU per pound and moisture content is of 25–35%. It is used for electricity generation.

Sub-bituminous coal: The next grade is sub-bituminous which contains heating value of 8300 to 13,000 BTU/pound. It has carbon content of 35–45% and is used in steam electric power generation.

Bituminous: Next grade is bituminous coal which contains heating value 11,000–15,500 BTU/pound. With the addition of heat and pressure lignite is converted to bituminous. Carbon content present in the bituminous coal is 45–86% and is used in the generation of electricity in steel industries and iron industry.

Steam coal: It is ranked in between bituminous and anthracites. It is used as fuel for steam locomotive. It is also used for domestic purpose.

Anthracites: It is the product of high temperature and pressure of the earth and categorized as high-rank coal. For its properties it is highly valued. Its glossy surface makes it look like metallic. It has heat capacity 15,000 BTU /pound. Its carbon content is around 86–97%.

Graphite: Though on the highest rank it is difficult to ignite. It is not used as fuel. Tip of pencils is made of graphite, and powder form of graphite is used as lubricants.

2.4 Background of Coal Water Slurry

Energy is an essential part of human civilization. Fuel oil was the main ingredient for energy generation till 1970. The quantum of fuel required had to be imported which tells upon the resources of states. Consequent on paucity of fuel oil due to dwindling oil reserve and extra requirement the cost of energy production is enhanced. As a result some alternative was thought of. Coal is the alternative (Li et al. 2017; Mochida et al. 1998; Belgiorno et al. 2003; Miura et al. 1991).

Coal in the process of power generation has to be pulverized and used. Use of pulverized coal for power generation had a number of disadvantages such as health hazard, loss in process, and less power generation. To avoid these difficulties coal has been used in the form of a slurry. The main ingredients in the slurry are coal and fuel oil. Fuel oil being a costly product, the cost of power generation was not favourable for development. An alternative to fuel oil was sought for. Attempts were made to form slurry of coal methanol and coal methanol water which proved to be uneconomical due to high cost of ethanol oil (Natoli et al. 1985). At these stages water is thought of as a substitute. Further investigation revealed that, with some additives, is the most suitable medium to form CWS to satisfy low viscosity, high concentration as well as stability without any adverse effect on the environment, without health hazard, with uninterrupted transportation, and without natural and man-made difficulties for power generation.

2.5 Viscosity Measurement of CWS

Efficiency of better fuel depends upon viscosity as per the van der Waals forces which shows coal conglomeration of particles (Das et al. 2020a, b, c, Meher et al. 2019). Flow behaviour of coal water slurry to the maximum 1000 mPas is essential for pipeline transport (Mishra and Kanungo 2000). Stability is also another factor responsible for concentration and storage.

Resistance to flow increases when coal is added to water as compared to water in the pipeline. Such resistance has to be reduced for smooth transportation. Pipeline flow behaviour is of either Newtonian and non-Newtonian. Newtonian flow behaviour requires application of nil force but non-Newtonian requires some force to facilitate flow.

While adding coal to the water, the viscosity of the slurry invariably increases compared to that of water alone. The coal particles make the coal-water solution thicker and hence they have an effect on the velocity distribution in a laminar flow

and, in turn, on viscosity. The suspension viscosity is the laminar flow parameter which directly relates velocity gradient to shear stress. Depending upon the variation of shear rate with shear stress fluids are described as Newtonian or non-Newtonian. If a plot is drawn between shear rate and shear stress, a straight line passing through the origin is obtained for a Newtonian fluids, as expressed in Eq. 2.1 (Fig. 2.1).

$$\eta = \frac{\tau}{\frac{du}{dy}} \quad (2.1)$$

where η is the coefficient of viscosity, τ is the shear stress, (du/dy) is shear rate.

The other categories of fluids which do not follow Eq. 2.1 are called non-Newtonian fluid. The non-Newtonian behaviour can be time independent or time dependent depending on whether the shear stress changes with time or not. Bingham plastic fluids are non-Newtonian fluids which are characterized by a flow curve as shown in which an intercept τ_0 on the shear stress axis with a straight line, where $\tau > \tau_0$, (obeying Eq. 2.2) is obtained

$$\tau - \tau_0 = \frac{\eta}{\frac{du}{dy}} \quad (2.2)$$

where τ = shear stress, τ_0 = yield stress, η is the coefficient of viscosity, (du/dy) is shear rate.

For such fluids the initial obstruction is due to the existence of a three-dimensional structure of sufficient rigidity at rest which can resist the applied stress, less than the yield stress (Y -intercept in shear stress axis). If stress applied becomes more than

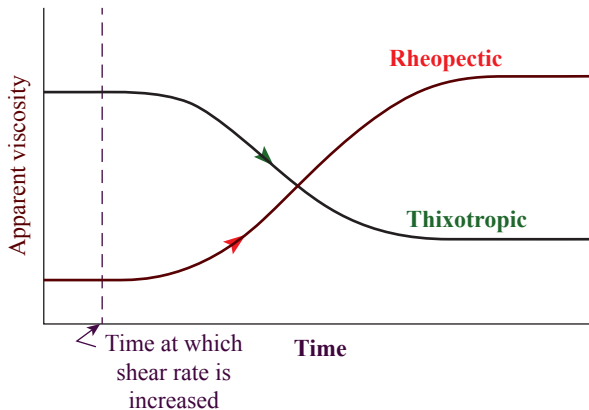


Fig. 2.1 Thixotropic and rheotropic fluid

the yield stress, then this structure disintegrates to form a dispersed system and the system behaves like a Newtonian fluid and flows under the shear stress ($\tau - \tau_0$). The structure reforms when applied shear stress falls below τ_0 . There are also some other kind of fluids which behave differently than Newtonian and Bingham Plastic fluids. The Power Law model as expressed in Eq. 2.3 is another pseudoplastic model obeyed by the fluids (Fig. 2.1).

$$\tau = \frac{K}{\left(\frac{du^n}{dy}\right)}, n < 1.0 \quad (2.3)$$

where n and K are constants for a particular fluid. The constant ' K ' is known as the 'consistency' of the fluid; if the value of K is higher, then viscosity of liquid becomes more.

For $n = 1$, that is for Newtonian behaviour, K corresponds to the Newtonian Viscosity. The constant ' n ' is the flow index parameter, the value of which measures the degree of departure from Newtonian character; the further ' n ' departs from unity, the more pronounced is the non-Newtonian behaviour. There are some fluids called dilatant fluids which can be described by the Power Law with a flow index $n > 1.0$. One more typical curve expressing the rheological behaviour of CWS is shown in Fig. 2.1 and is called Hershelly-Bulkely model which is similar to power law model having some yield stress. All these above category models are time-independent rheological models. The time-dependent models are obeyed by thixotropic and rheotropic fluid, depending on whether the shear stress decreases or increases with time at given conditions of shear rate and temperature (Fig. 2.1).

2.6 Isolation and Characterization of Natural Dispersant

2.6.1 Isolation of Natural Dispersant: (Chemical and Aqueous Extraction Process)

The *Sapindus laurifolia* fruits were collected from koraput district of southern Orissa, India. The pericarp was peeled out from the drupes and cut into pieces. The smaller pieces of pericarp were soaked with water about 12 h maintaining a solid-liquid ratio 1:3 by weight. Then the solid was squeezed off and again soaked in fresh water. The process was repeated four times and the extractant was collected in each time followed by concentration on heating. By adding ammonium sulphate precipitation takes place and the froth produced was collected and separated in n-butanol phase and recrystallized as thread shape mass. This was identified as saponin. When thin layer chromatogram is taken in the presence of the eluant hexane:chloroform a single spot was observed. The melting point of the compound saponin was 145 °C.

Extraction of saponin from *Sapindus mukorossi* was performed by taking 100 g of dry fruit followed by removing its pericarp and dissolving in 1000 ml of water to maintain solid liquid ratio as 1:10. Then the above mixture was agitated for 3 h by a magnetic stirrer followed by centrifugation.

2.6.2 Surface Activity of Natural Dispersant by Fluorimeter

The surface characteristics of *S. laurifolia* were investigated by taking the fluorescence spectra of isolated saponin in the presence of probe pyrene. From the spectra it is observed that pyrene has five peaks in which first peak (I_1) at 370 nm and third peak at (I_3) 380 depends upon polarity of medium (Fig. 2.2) (Kalyanasundaram and Thomas 1977). The CMC of saponin was measured by variation of surfactant concentration with polarity parameter (ratio of I_3 to I_1). The ratio of I_3 to I_1 increases with saponin concentration increases up to 1.5 (0.8% of saponin concentration). Appearance of a plateau in the curve is due to the formation of micelle (Sahoo et al. 2002; Chander et al. 1987) (Fig. 2.3). The micelles are formed gradually through dimers, trimers, tetramers, etc. This is because of stepwise association of saponin molecule and the formation of excimer at very low concentrations of saponin.

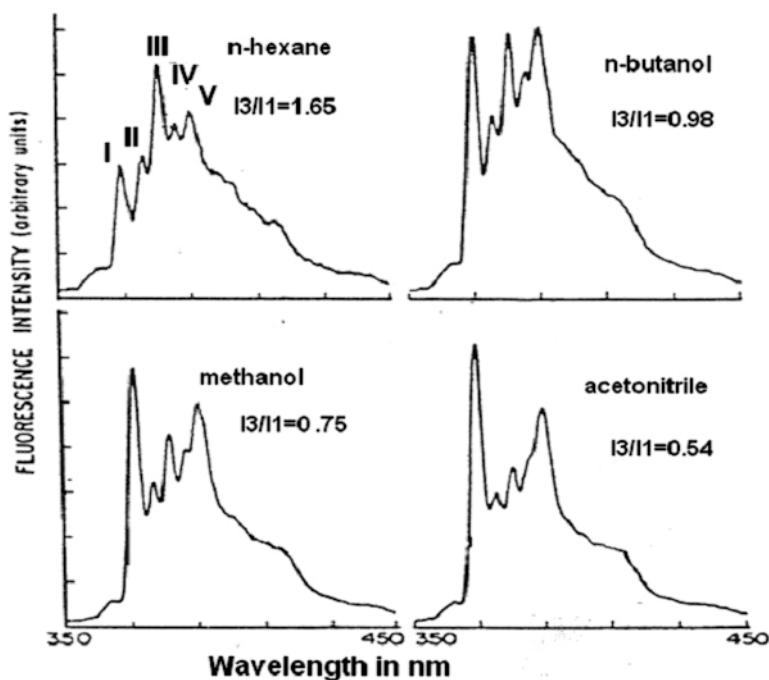


Fig. 2.2 Plot I_3 to I_1 of pyrene with solvent polarity

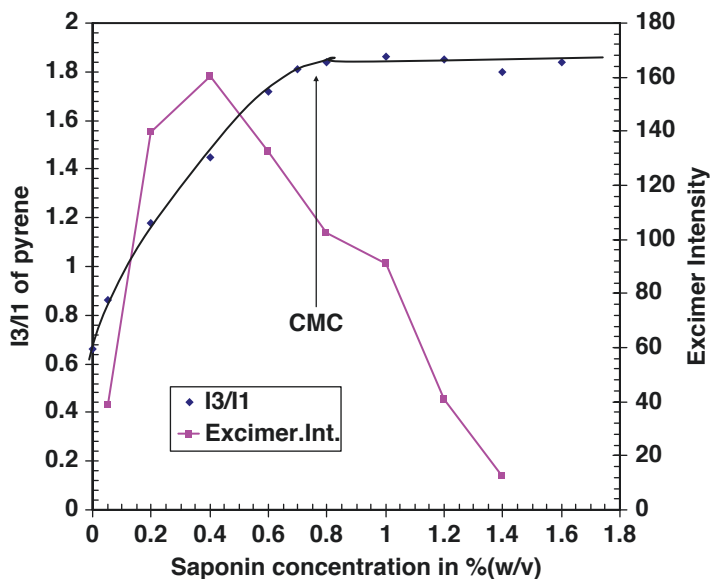


Fig. 2.3 I_3/I_1 ratio of pyrene vs. saponin concentration (Adapted with permission from Das et al. 2008 © ACS)

Initially the intensity of excimer increases, but after the formation of micelle, it decreases (Sahoo and Misra 2001; Singer 1983).

2.6.3 Surface Activity of Natural Dispersant by Surface Tension Measurement

ST-500MAN surface tensiometer was used to measure the surface tension of the diluted sample of natural surfactant containing various concentrations of saponin. Figures 2.4 and 2.5 represent the plot of surface tension aqueous saponin with concentration of saponin isolated by two different methods. Surface tension of pure water is 71 mN/m and level up to a minimum value at 39 mN/m at 0.007 g/cc for chemical extraction process. Similarly for saponin isolated by aqueous extraction process surface tension value saturates at 0.016 g/cc. Thus CMC of saponin was 0.007 g/cc and 0.016 (Figs. 2.4 and 2.5) by chemical and aqueous methods, respectively.

Fig. 2.4 Plot of concentration of saponin (aqueous) vs. surface tension value

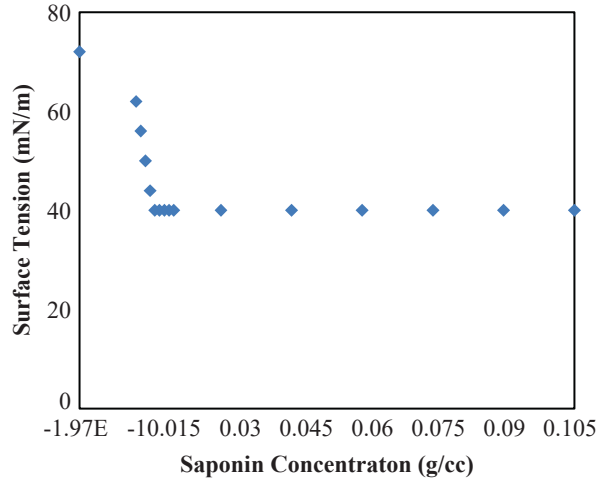
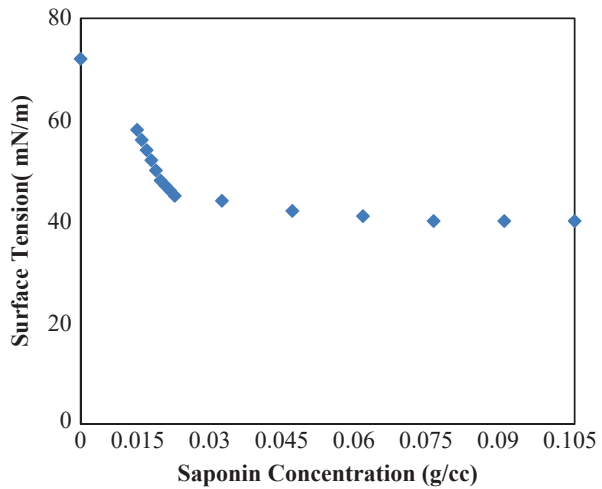


Fig. 2.5 Plot of concentration saponin (chemical) vs. surface tension value



2.7 Application of Natural Dispersant in Coal Water Slurry Stabilization

2.7.1 Effect of Coal Concentration on Apparent Viscosity of CWS

For economic slurry transportation in pipeline, concentration of solid particle should be maximum in an acceptable range of viscosity. This is because more is the concentration (volume fraction) of coal, lesser will be the transportation cost (Junguo et al. 2014).

The apparent viscosity of slurry increased with increase of coal load in the presence of the dispersant. The formation of CWS with maximum coal concentration and admissible viscosity depends upon the type of dispersants and the type of coals used for the preparation of CWS. Beyond these optimum concentrations of coal, the slurry becomes immeasurably optimum concentrations of coal; the slurry becomes immeasurably thick and rigid due to their strong inter-particle interactions. Formation of gel with increasing particle fraction in the slurry increases CWS viscosity (Tiwari et al. 2004).

Das et al. (2008) investigated the apparent viscosity of CWS for three types of coal having different ash contents, namely, coal-A, Coal-B and Coal-C. They measured the apparent viscosity of CWS in the presence of dispersant saponin concentration of 0.8% weight which is around critical micellar concentration (CMC). Saponins are isolated from plant *Sapindus laurifolia* and is utilized for preparation of CWS in the coal concentration ranging from 55% to 64%. Das et al. (2008) postulated particle-particle interaction is the main cause of increase in apparent viscosity. Beyond 64% coal concentration the slurry becomes thicker and disperse slowly. Figure 2.6 represents the plot between apparent viscosity with shear rate of coal concentration 64% and 60% of three types of coal A, B and C at optimized (0.8%) saponin concentration. Other authors (Tiwari et al. 2004) have also reported the similar behaviour of CWS. Das et al. (2008) established the relationship between ash content of coal with apparent viscosity. According to them, with increase in ash percentage of the coal, sample apparent viscosity increases. This may be due to strong interaction of water with hydrophilic ash. *Sapindus mukorossi* is another saponin-containing plant that can effectively stabilize coal water slurry as found by Routray et al. (2008). In their investigation, they measured the apparent viscosity of

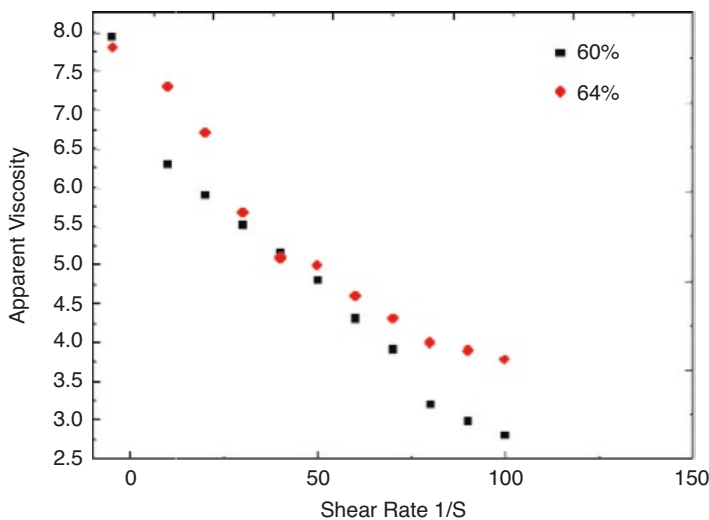


Fig. 2.6 Effect of apparent viscosity vs. shear rate of coal sample with coal concentration 60% and 64% in the presence of 0.8% of saponin

CWS in the studied range of coal concentration 55–65% at the CMC of the natural dispersant *Sapindus mukorossi*. The regular trend of increase in slurry viscosity with increase in coal concentration was observed because of increasing coal–coal association. Due to maximum hydrophobic nature of coal A (maximum C/O), water molecule has least tendency with coal particle A and remain adsorbed on the surface. This resulted in minimum viscosity for coal A among the three types of coal A, B and C.

2.7.2 Effect of Dispersant Concentration on Apparent Viscosity of CWS

The additive (surfactant) renders additional electrostatic or repulsive force (Karapte 2003) to reduce the van der Waals forces among the coal particles so that a well dispersion of coal in CWS can be maintained. Das et al. (2009) postulated when the natural dispersant saponin is adsorbed on the coal surface, a steric barrier is created because of the hydration of glucosides head groups oriented towards bulk water. This resulted in decrease in viscosity with increasing amount of dispersant saponin and this decreasing trend of viscosity continued as long as there is adsorbing tendency of saponin in CWS. Increasing the concentration of saponin beyond 0.8% of saponin that is above the CMC the apparent viscosity attains a minimum value which remains unchanged by adding saponin further (Das et al. 2008, 2009). After CMC, saponin shows its less affinity towards the coal surface due to formation of micelles. Since saponin forms monolayer only at coal water interface, maximum reduction of viscosity occurs at critical micellar concentration. Routray et al. (2008) isolated saponin from the plant *Sapindus mukorossi* by aqueous and chemical extraction process. They investigated that whatever may be the isolation process stabilizing action of saponin is same but aqueous extraction process is more economy than chemical extraction process. Out of the various types of interactions, such as hydrogen bonding (Rupprecht and Gu 1991), hydrophobic interaction (Misra et al. 2005), ion pairing (Snyder 1968), ion exchange (Snyder 1968), polarization of π electron (Giles et al. 1974), and dispersion forces (Kolbel and Kuhn 1959), which determine the interactions between the solid surface and substrate, the hydrophobic interactions are found to be more preferable for the saponin under consideration.

2.7.3 Change of Shear Stress with Shear Rate

Since the pipeline transport of the CWS demands a free-flowing tendency, the understanding on its flowing characteristics and the change of viscosity during flow is indispensable. Basing on the flowing characteristics, the fluids are classified into two categories. One is Newtonian fluid like water, alcohol, mineral oil, gasoline etc., and the other is non-Newtonian fluid. In Newtonian, viscosity does not depend upon change in shear or tensile stresses, while in non-Newtonian it depends (Shook

Fig. 2.7 Rheological behaviour of coal A in the presence of saponin and SDS

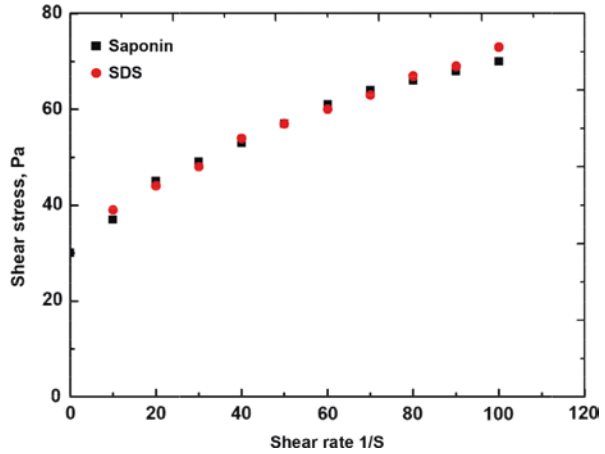
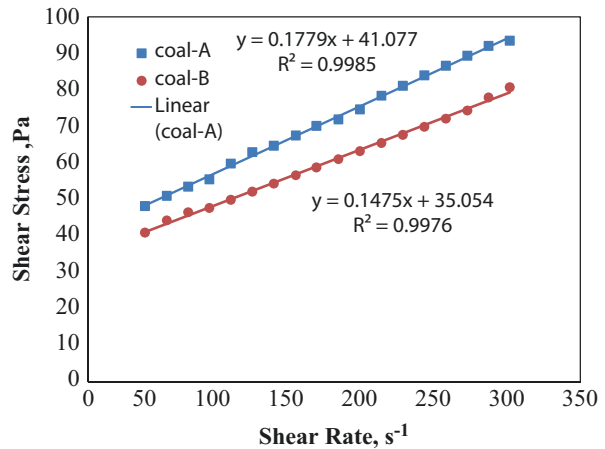


Fig. 2.8 Rheograms of CWS in the presence of 0.016 g/cc of saponin of *Sapindus*



et al. 1984). Thus the strain rate is not proportional to the rate of change of deformation in non-Newtonian fluid. Figure 2.7 represents the non-Newtonian nature of coal water slurry in terms of variation of shear rate with shear stress. Intercept of these linear plots gives the yield stress value of slurry and this value increases linearly with increase in percentage of coal load in the slurry. After this yield stress, the slurry exhibits Newtonian nature.

Das et al. (2008) compared the rheological behaviour of dispersant *Sapindus laurifolia* with a commercial dispersant SDS. Figures 2.7 shows the change of shear stress with shear rate at 64% concentration of coal and saponin 0.8%. They compared these data with a commercial dispersant sodium dodecyl sulphate (SDS) and found that saponin has similar stabilizing action with SDS.

Rheological behaviour of monomodal samples coal-A and coal-B of same particle size (<75 μm) was carried out in the presence of bio-additive (*Sapindus mukorossi*) is shown in Fig. 2.8. Saponin was isolated from this (*Sapindus mukorossi*) by two extraction methods. One is aqueous extraction method and the other is

chemical extraction method (Routray et al. 2008). Aqueous extraction method is more effective than chemical method because saponin present in aqueous method is more than chemical method.. So further rheological study for coal-A and coal-B has been carried out in the presence of saponin extracted from aqueous method.

mukorossi for particle size ($<75 \mu\text{m}$, $C_w = 55\%$).

2.7.4 Effect of Temperature

Viscosity of a slurry CWS is affected by slight variation of temperature. When temperature of any system increases, kinetic energy of particles increases, particles inside the system has more potential to move. Same theory can also be applied in the CWS system, and hence with rise in temperature of the CWS system, viscosity of coal slurry fuel decreases.

The variation of logarithm of apparent viscosity with reciprocal of temperature was studied by Mishra et al. (2002) for high ash only. The variation may be presented by Arrhenius expression.

$$\eta = A \exp^{E/RT}$$

Or

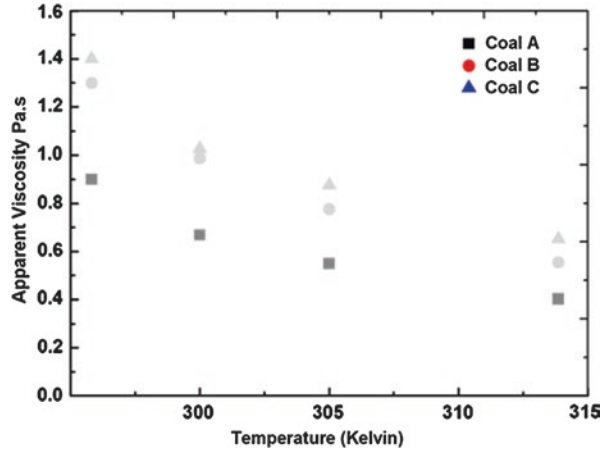
$$\ln \eta = E/RT + \ln A$$

where η and E are viscosity of the slurry and activation energy, respectively. According to Yamaguchi et al. (1979) variation of shear rate and solid concentration has no effect on apparent activation energy during fluid flow (Roh et al. 1995). It has been shown that K decreases considerably as the temperature is increased from 15 to 60 °C whereas η rises relatively little. In other words, a temperature rise has no significant effect on the non-Newtonian behaviour of CWS. The decrease in apparent viscosity is due to the decrease in the value of K and not that of decrease in η . Guzman Andrade equation can be used to study the effect of temperature on CWS viscosity in a certain range.

$$\eta = A_1 \exp(A_2 / T)$$

where A_1 and A_2 are constants and T is absolute temperature. The rate of reduction in viscosity is found to be slower at this temperature. In fact, it has been found by some investigators that after a certain value of temperature, a further increase in temperature has an adverse effect on CWS viscosity, viscosity increases and flowing behaviour decreases. The CWS tends to act non-Newtonian properties more strongly. This transition temperature appears to depend on different factors like nature of coal, the coal loading of CWS and the type and percentage of dispersing

Fig. 2.9 Temperature vs. apparent viscosity (coal concentration 64%, and saponin 0.8%)



agent or stabilizer, etc. (Roh et al. 1995). It also depends on combination of several factors (Fuerstenau et al. 1983; Hsiao and Dunning 1955) including thermal degradation of the chemical dispersant, increase in coal volume because of swelling, desorption of the molecular chains due to their solubility at high temperatures, entanglement of additive chains due to the increased entropy, etc.

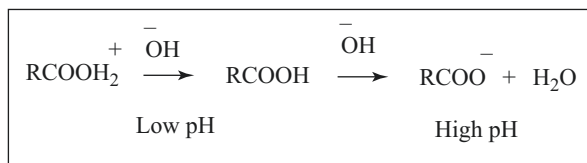
It has been studied by Das et al. (2008) that effect of temperature on apparent viscosity in the presence of natural dispersant *Sapindus laurifolia* is similar to any commercial dispersant. Exponentially decrease in viscosity with temperature was observed which is shown in Fig. 2.9. Decrease in inter-particle attraction among the particle with increase in kinetic energy of the coal particles is the main cause of reduction of viscosity of slurry. Similar type of experiments was carried out by Routray et al. (2008) in the presence of natural dispersant *Sapindus mukorossi*.

2.7.5 pH and Surface Charge of Coal

When coal is suspended in water it adsorbs either hydrogen or hydroxyl ion and thus coal surface acquires a surface charge which depends upon pH of the slurry. The increase of surface charge of coal prevents coal agglomeration and hence the stability of the slurry increases as suggested by DLVO theory (Verwey and Overbeek 1948).

Coal surface contains different type of polar groups such as like hydroxyl, carboxyl, and phenolic-hydroxyl (Whitehurst et al. 1980). These oxygen-containing functional groups play very important role for CWS preparation. Igarashi et al. (1984) investigated that hydroxyl and carboxyl group are main factors for determining the wettabilities of coal surfaces, and phenolic OH group is harmful to the coal slurry-forming ability. They also postulated that there exists an important relationship between oxygen-containing functional group and other structural parameters for coal and aqueous slurry. Zhu and Wang (1991) and Igarashi et al. (1984) have

Scheme 2.1 Dissociation of acidic functional group of coal at different pH



reported that air oxidation of coal increases the specific surface area, oxygen-containing functional group, wettabilities, equilibrium moisture content and slurry viscosity of coal.

At very low pH these functional groups are protonated rendering positive charge to coal. With increase of pH gradually the deprotonation takes place at two different steps (Scheme 2.1). The pH at which there is no residual charge on the coal surface is called isoelectric point. At this pH the probability of agglomeration of coal particle is very high and hence CWS becomes unstable. Usually the isoelectric point of coal lies within the range of 2–5 depending upon the rank of the coal depending on the extent of ash content. According to Kelebek et al. (1982) when CWS is allowed to keep certain time period, Fe^{2+} from pyrite undergoes oxidation to form Fe^{3+} . This causes the shifting of the isoelectric point.

Das et al. (2008) studied the relationship between zeta potential and pH of slurry. The zeta potential is known as electrophoretic mobility of the coal particles and is shown in Fig. 2.10 by changing the pH of the slurry and is represented in Fig. 2.10. Adsorption of saponin causes the shifting of isoelectric point and shear plane. Zeta potential value decreases because of the shifting of the shear plane by bulky surfactant molecule at the interface of coal and water. Depending upon the pH of the solution functional group of saponin molecule may be protonated or deprotonated producing surface charge on the coal particle. Figure 2.11 shows variation of apparent viscosity of different types of CWS of 60% coal concentration with pH. It is observed that surface hydroxylation produces large no of OH^- on the coal surface, which creates repulsion among coal particle causing reduction in viscosity of slurry.

It has been observed by Routray et al. (2008) that pH variation can significantly affect the apparent viscosity of slurry. They have carried out the experiment in the pH range from 1 to 10 in the presence of natural surfactant *Sapindus mukorossi*. From the results it has been observed that the apparent viscosity of slurry prepared from three different types of coal showed decreasing trend by increasing hydroxyl ion (increase in pH).

2.8 Mechanism of Stabilization

Saponin extracted from *Sapindus mukorossi* and *Sapindus laurifolia* are non-ionic surfactant (Das et al. 2020a, b, c). It consists of a polycyclic aglycone to which one or more sugar chain is attached. The sugar chain is hydrophilic in nature and is known as Glycone. part consists of more than one sugar unit. The polycyclic agly-

Fig. 2.10 Plot of zeta potential of coal with variation in pH (Adapted with Permission from Das et al. 2008 © ACS)

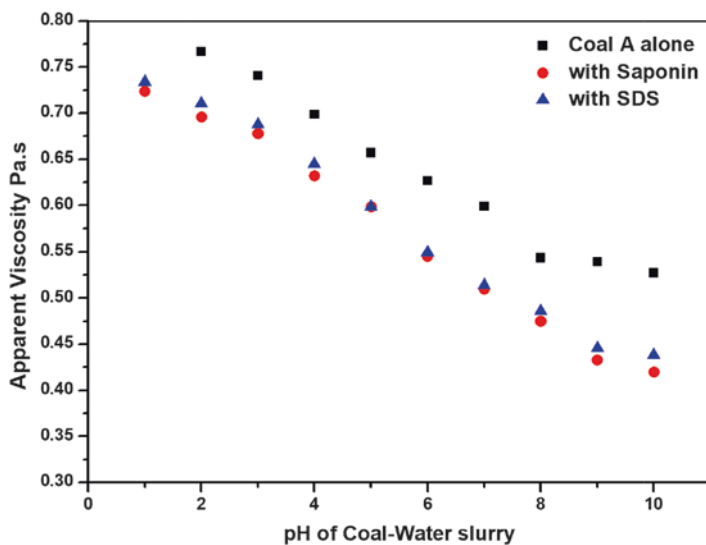
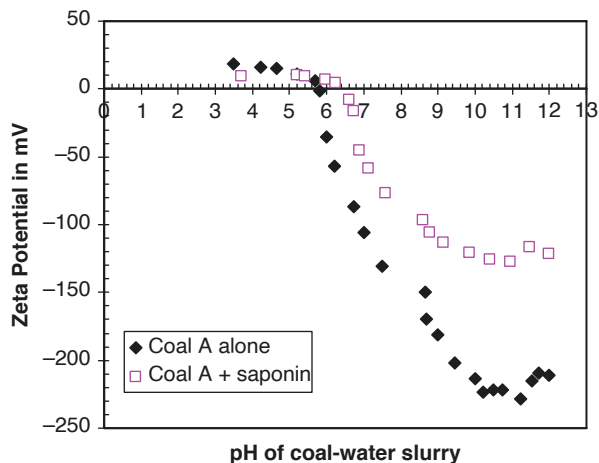


Fig. 2.11 Variation of pH with viscosity (coal concentration 60%, and saponin concentration 0.8%)

cone which is hydrophobic in nature may consist of a steroid or a triterpene ring. The saponin isolated from *Sapindus mukorossi* and *Sapindus laurifolia* is a triterpenoid saponin. The triterpenoid part is attached with saccharide residue through oxygen atom. The triterpene (hydrophobic) part of the saponin molecule adsorbs on the hydrophobic coal surface and sugar residue (hydrophilic) is projected towards aqueous phase (Das et al. 2008; Routray et al. 2008; Pattanaik et al. 2019; Routray et al. 2019; Das et al. 2019; Das et al. 2010a, b). Thus hydrated glycoside heads form a

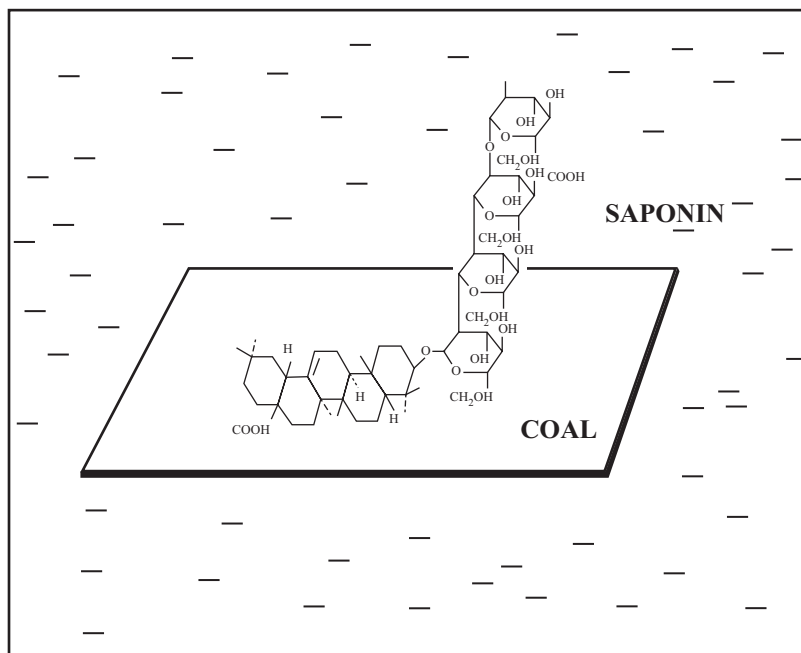


Fig. 2.12 Adsorption of saponin on coal particle (Adapted with permission from Das et al. 2008 © ACS)

coating on each coal particle. This creates a mechanical hindrance among the dispersed particles. Thus, this inhibits coal–coal association (Fig. 2.12).

2.9 Conclusions

Transportation of coal in aqueous form through pipeline to the power plant is the best mode of navigation. Because it is economical, devoid of environmental pollution. The coal conglomeration at high concentration however offers obstruction for the pipeline transportation and hence suitable additives are added to disperse the CWS. In order to get an effective fuel, the stability of the concentrated slurry should be considerably larger as well as its viscosity must be in acceptable value (<1000 mPa), which are usually achieved by adding dispersing agent (additive). High stability and lower in viscosity desire a good additive. The rheological parameter of CWS in the presence of saponin is fitted to Bingham plastic equation. Mobility of coal particle increases with temperature which is the cause of reduction in slurry viscosity. Increase in the pH of the slurry causes surface hydroxylation which decreases the viscosity. Dispersion of the CWS is mainly attributed to steric repulsions between coal particle. Advantage of CWS is that it can be stored with no

dust explosion, without danger of health hazard and very easily transported through pipeline. Hence, this technology has been put into commercial practice for transportation and combustion of coal, especially for power generation.

References

- Belgiorio, V., De Feo, C. D. R., & Napoli, R. M. A. (2003). Energy from gasification of solid wastes. *Waste Management*, 23(1), 1–15.
- Chander, P., Somasundaran, P., & Turro, N. J. (1987). Fluorescence probe studies on the structure of the adsorbed layer of dodecyl sulphate at the alumina-water interface. *Journal of Colloid and Interface Science*, 117, 31–46.
- Das, D., Dash, U., Nayak, A., & Misra, P. K. (2010a). Surface engineering of low rank Indian coals by starch-based additives for the formulation of concentrated coal-water slurry. *Energy & Fuels*, 24, 1260–1268.
- Das, D., Mohapatra, R. K., Belbsir, H., Routray, A., Parhi, P. K., & Hami, K. E. (2010b). Combined effect of natural dispersant and a stabilizer in formulation of high concentration coal water slurry: Experimental and rheological modeling. *Journal of Molecular Liquids*, 320, 114441.
- Das, D., Mohapatra, R. K., Parhi, P. K., Sarangi, A. K., Sahu, R., & Barik, S. R. (2020a). Sustainable & efficient route for the regeneration of carbonyl compounds from oximes using aqueous extract of *Sapindus laurifolia* under microwave radiation. *ACS Omega*, 5, 7716–7721.
- Das, D., Panigrahi, S., Misra, P. K., & Nayak, A. (2008). Effect of organized assemblies. Part 4: Formulation of highly concentrated coal-water slurry using a natural surfactant. *Energy & Fuel*, 22, 1865–1872.
- Das, D., Panigrahi, S., Misra, P. K., & Senapati, P. K. (2009). Effect of organized assemblies. Part 5: Study on the rheology & stabilization of a concentrated coal-water slurry using Saponin of the acacia *Concinna* plant. *Energy & Fuels*, 23, 3217–3226.
- Das, D., Pattanaik, S., Parhi, P. K., Mohapatra, R. K., Jyothi, R. K., Lee, J. Y., & Kim, H. I. (2019). Stabilization & rheological characteristics of fly ash-water slurry using a natural dispersant. *ACS Omega*, 4(25), 21604–21611.
- Das, D., Sarangi, A. K., Mohapatra, R. K., Parhi, P. K., Mahal, A., Sahu, R., & Zahan, K.-E. (2020b). Aqueous extract of *Shikakai*; a green solvent for deoxygenation reaction: Mechanistic approach from experimental to theoretical. *Journal of Molecular Liquids*, 309, 113133.
- Das, N., Biswal, S. K., & Mohapatra, R. K. (2020c). Recent advances on stabilization & rheological behavior of iron ore slurry for economic pipeline transportation. *Material Today: Proceeding*, doi:<https://doi.org/10.1016/j.matpr.2020.02.851>.
- Fuerstenau, D. W., Rosenbaum, J. M., & Laskowski, J. (1983). Effect of surface functional groups on the flotation of coal. *Colloids & Surfaces*, 8, 153–173.
- Giles, C. H., D'Silva, A. P., & Easton, I. A. (1974). A general treatment & classification of the solute adsorption isotherm. Part 2. Experimental interpretation. *Journal of Colloid & Interface Science*, 47, 766–778.
- Hsiao, L., & Dunning, H. (1955). A comparative study of non-ionic detergent adsorption by radio-tracer, spectrophotometric & surface tension methods. *Journal of Physical Chemistry*, 59, 362–366.
- Igarashi, T., Kiso, N., Hayasaki, Y., Yamamoto, M., Ogata, T., Fukuhara, K., & Yamajaki, S. (1984). Proc sixth Coal Slurry Combust Int. Symp, NTIS: Springfield.
- Junguo, L., Guanghua, Z., Ting, S., & Junfeng, Z. (2014). Synthesis, characterization & application of a dispersant based on rosin for coal-water slurry. *International Journal of Mining Science & Technology*, 24, 695–699.

- Kalyanasundaram, K., & Thomas, J. K. (1977). Environmental effects on vibronic B & intensities in pyrene monomer fluorescence & their application in studies of micellar systems. *Journal of the American Chemical Society*, 99, 2039–2044.
- Karatpe, N. (2003). Adsorption of a non-ionic dispersant on lignite particle surfaces. *Energy Conservation & Management*, 44, 1275.
- Kelebek, S., Salman, T., & Smith, G. W. (1982). An electrokinetic study of three coals. *The Canadian Journal of Metallurgy & Materials Science*, 21, 205–209.
- Kolbel, P. H., & Kuhn, I. P. (1959). Constitution und Eigenschaften grenzflächenaktiver Stoffe I. Messungen an p-n-Alkyl-Benzolsulfonate. *Angewandte Chemie*, 71, 211–215.
- Li, D., Liu, J., Wang, J., Bai, Q., Cheng, J., & Cen, K. (2017). Experimental studies on coal water slurries prepared from coal gasification wastewater. *Asia-Pacific Journal of Chemical Engineering*, 1–10.
- Meher, J., Das, D., Samal, A. K., & Misra, P. K. (2019). Role of maceral composition on the formulation of concentrated coal-water slurry using a natural surfactant. *Material Today Proceedings*, 9, 542–550.
- Mishra, S. K., & Kanungo, S. B. (2000). Factors affecting the preparation of highly concentrated coal water slurry (HCCWS). *Journal of Scientific & Industrial Research*, 59, 765–790.
- Mishra, S. K., Senapati, P. K., & Panda, D. (2002). Rheological behaviour of coal-water slurry. *Energy Sources*, 24, 159–167.
- Misra, P. K., Mishra, B. K., & Somasundaran, P. (2005). Organization of amphiphiles. Part 4. Characterization of the microstructure of the adsorbed layer of decylethoxylenenonyl phenol. *Colloids & Surfaces A*, 252, 169–174.
- Miura, K., Hayashi, J., & Hashimoto, K. (1991). Production of nuclear sieving carbon through carbonization of coal modified by organic additives. *Carbon*, 29(4–5), 653–660.
- Mochida, I., Sakanishi, K., Sazuki, N., Sakurai, M., Tsukui, Y., & Kaneko, T. (1998). Progresses of coal liquefaction catalyst in Japan. *Catalysis Surveys from Asia*, 2(1), 17–30.
- Natoli, J., Mahar, R. C., & Bobsein, B. R. (1985). Polycrylate thickeners for coal water slurries: Slurry formulation, stability & rheology. *International Chemical Engineering Symposium Series*, 95, 17–36.
- Pattanaik, S., Parhi, P. K., Das, D., & Samal, A. K. (2019). Acaciaconcinna: A natural dispersant for stabilization & transportation of fly ashwater. *Journal of the Taiwan Institute of Chemical Engineers*, 99, 193–200.
- Roh, S. N., Shin, D. H., Kim, D. C., & Kim, J. D. (1995). Effect of temperature on the flow properties of suspensions. *Fuel*, 74, 1220–1225.
- Routray, A., Das, D., Parhi, P. K., & Padhy, M. K. (2008). Characterization, stabilization, & study of mechanism of coal water slurry using SapindousMukorossi as an additive. *Energy Sources, Part A: Recovery, Utilization, & Environmental Effects*. <https://doi.org/10.1080/15567036.2018.1503755>.
- Routray, A., Senapati, P. K., Padhy, M. K., Das, D., & Mohapatra, R. K. (2019). Effect of mixture of a non-ionic & a cationic surfactant for preparation of stabilized high concentration coal water slurry. *International Journal of Coal Preparation & Utilisation*. <https://doi.org/10.1080/19392699.2019.1674843>.
- Rupprecht, H., & Gu, T. (1991). Structure of adsorption layers of ionic surfactants at the solid/liquid interface. *Colloid & Polymer Science*, 269, 506–522.
- Sahoo, L., & Misra, K. P. (2001). Characterization of the structure of polyoxyethylated alkyl phenols micelles at 300 K. *SU Journal of Science and Technology*, 13B, 18–22.
- Sahoo, L., Sarangi, J., & Misra, K. P. (2002). Organization of amphiphiles, part I: Evidence in favour of premicellar aggregates through fluorescence spectroscopy. *Bulletin Chemistry, Japan*, 75, 859–865.
- Shook, C. A., Gillies, R., Husb, W. H. W., & Small, M. (1984). Flow of coal slurry with a yield stress. *Journal of Pipeline*, 4, 289–297.
- Singer, L. A. (1983). In K. L. Mittal & E. J. Fendler (Eds.), *Solution behaviour of surfactants* (Vol. 1, p. 73). New York: Plenum.

- Snyder, L. R. (1968). Comparisons with adsorption on silica. *Journal of Physical Chemistry*, 72, 489–494.
- Tiwari, K. K., Basu, S. B., Bit, K. C., & Mishra, K. K. (2004). High concentration coal water slurry from Indian coal using newly developed additive. *Fuel Processing Technology*, 85(1), 31–42.
- Verwey, E. J. W., & Overbeek, J. T. G. (1948). *Theory of the stability of lyophobic colloids*. Amsterdam: Elsevier.
- Whitehurst, D. D., Mitchell, T. O., & Farcaiu, M. (1980). *Coal liquefaction*. New York, USA: Academic Press.
- Yamaguchi, K., Senna, M., & Kuno, H. (1979). Effect of temperature on the flow properties of suspensions. *Journal of Colloid & Interface Science*, 70, 584–591.
- Zhu, S. & Wang, Z. (1991). 16th International Conference on Coal & Slurry Technologies, *Clearwater*, FL, 435.

Chapter 3

Application of Biotechnological Approach for Making Coal an Environmentally Friendly Fuel



Haragobinda Srichandan, Puneet Kumar Singh, Pankaj Kumar Parhi, and Snehasish Mishra

3.1 Introduction

Coal is being considered as the prime source of energy since the ancient time. The coal reserve across the world is estimated to be 1.1 trillion tons (<https://www.world-coal.org/coal/where-coal-found>, Anon n.d.-c) among which the consumption rate is usually 8562 million tons per year (<https://www.worldometers.info/coal/>, Anon n.d.-a). As coal combustion is carried out, sulphur content of coal combines with oxygen and forms sulphur dioxide. This sulphur dioxide is emitted to the open environment and may lead to acid rain. Additionally, sulphur dioxide has other environmental consequences that are related to health of living organisms. So, legislation is being implemented throughout the world to reduce SO₂ emissions from coal. To fulfil the legislation, SO₂ emission is generally reduced by two operational mechanisms (Prayuenyong 2002): (1) the slurry containing alkaline agent, viz., limestone in water is applied over the flue gas. SO₂ reacts with limestone to get converted to gypsum and is discarded as wet sludge and the process is known as flue gas desulphurization. (2) In fluidized bed combustion (FBC), coal is grounded into small size particles followed by mixing with limestone. The resulting mixture is then injected with hot air into boiler. During coal combustion, limestone act as sponge material that captures sulphur. However, these processes are expensive to some extent and it is more vulnerable to reduce sulphur concentration in coal before the combustion. This can be done by several approaches, viz., physical, chemical and biological. The physical process of sulphur removal includes crushing, grinding and washing. About 90% of pyrite (sulphur mineral) is removed, by the process; however fine

H. Srichandan · P. K. Singh · S. Mishra (✉)

School of Biotechnology, Kalinga Institute of Industrial Technology (KIIT), Deemed to be University, Bhubaneswar, Odisha, India

P. K. Parhi

Department of Chemistry, Fakir Mohan University, Balasore, Odisha, India

particles of pyrite and organic sulphur may remain attached to coal (Klein 1998). The chemical method involves carbonization, air or wet oxidation, Mayers approach, chlorination treatment and removal with sodium hydroxide, etc. (Yaman et al. 1995). However, these methodologies are expensive, often generate hazardous waste and the structural integrity of coal may deteriorate.

Biological sulphur removal is an economical and environmentally friendly process due to a low-cost process (the substrates utilized by microbes are present within coal itself and no external source is needed), low downstream processing cost (mild acidic waste may be generated leading to low neutralization expenditure) and reduced waste generation. The sulphur in the coal is found in inorganic (mainly as pyrite) and organic (dibenzothiophene (DBT)) forms. Acidophilic microbes solubilize pyrite by utilizing iron and sulphur as their energy source and heterotrophs solubilize sulphur by degrading DBT.

3.2 Coal Structure and Availability in Nature

Coal is generally formed from the metamorphosis of plant residues left after anaerobic digestion. Coal is an insoluble, black, amorphous material and consists of two major phases, namely inorganic and organic (Akash 2013). Inorganic phases mainly include mineral substances such as sphalerite (ZnS), pyrite (FeS₂), arsenopyrite (FeAsS) and galena (PbS) (Prayuenyong 2002). There may be present the sulphate minerals, viz., barite (BaSO₄), anhydrite (CaSO₄) and gypsum (CaSO₄·2H₂O). The organic phase is made up of macerals, viz., vitrinite (derived from lignin and contain high volatile constituents), exinite (derived from algae, resin and spore, and volatile) and inertinite (highly condensed and charcoal-like material but can be soluble in certain solvent) (Akash 2013). The building blocks of bituminous are mainly of aromatic structures attached with numerous hydroxyl groups and in certain positions, thiol groups (an organic sulphur form), as well as amines, are attached (Akash 2013). The blocks of aromatic groups are linked with each other by methylene cross-link and oxygen-ether cross-link to form the meshwork of the coal structure. The structural integrity of hard coal (that often refers to anthracite) also represents aromatic structures in which inorganic form of sulphur, e.g. pyrite (FeS₂), is present in the dockyard of meshwork and organic sulphur in the form of thiophene ring and thiol group (Prayuenyong 2002).

3.3 Coal Stock and Production

Coal reserve around the world has been estimated to be 1.1 trillion tons (Fig. 3.1). The countries with the maximum reservoir of coal include the USA, Russia, China, Indonesia, Australia, India, Germany and South Africa (Ghosh et al. 2015; BP Statistical Review of World Energy 2013). Coal contributes to about 30% of total

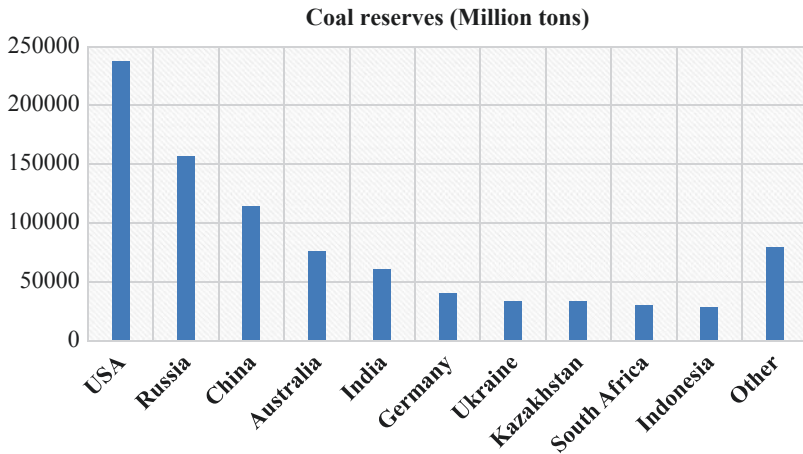


Fig. 3.1 Coal reserves countrywide (BP statistical review of world energy 2016)

energy and 42% of electricity around the globe (BP Statistical Review of World Energy 2013). The countries with major consumption of coal are China, the USA, India, Russia and Germany, and accounted for 77% of global coal consumption. Among the varieties, anthracite and bituminous are best-ranked coals with an estimated amount of 405 billion tons around the globe (BP Statistical Review of World Energy 2013). Although sub-bituminous and lignite are of lower ranks, their availability in nature is abundant (456 billion tons across the world). Generally, coal is of cooking and non-cooking types in which the former results in high heat value while the latter gives low heat value and high ash (www.coal.nic.in). India being one of the highest coal reservoirs in the globe contains mainly non-cooking type coal with low sulphur content. Out of total coal reserves of India, Jharkhand and Odisha are the highest coal repositories. India is considered as a rank holder of fifth position in the world as per coal reserve concerned. The 88% of Indian coal comes under the non-coking type while 0.5% are tertiary and the remaining are coking type.

Sulphur in coal is commonly found as inorganic (pyrite, elemental sulphur, inorganic sulphates and sulphides) and organic forms. The EIA (Energy Information Administration) has divided the coal into qualitative rating as per the sulphur content: high sulphur coal (≥ 1.68 pounds/million Btu), medium sulphur (0.61–1.67 pounds/million Btu) and low sulphur (≤ 0.60 pounds of sulphur per million Btu) (Ghosh et al. 2015).

3.4 Mechanism of Inorganic Sulphur Removal by Microbes

Pyritic sulphur removal by microbes mainly happens through two mechanisms: (1) direct and (2) indirect. The direct mechanism is often referred to as contact mechanism which needs the microbe to be in physical contact with pyrite while in the indirect mechanism, planktonic cells (free-living cells in solution) conduct the pyrite dissolution. Earlier it was speculated that during the contact mechanism microbes get attached to the mineral surface and solubilizes pyrite by enzymatic breakdown. However, later on, the reports have been made that instead of enzymatic dissolution of pyrite, attached microbe oxidize Fe^{2+} to Fe^{3+} (just like planktonic cells), which in turn oxidize pyrite and resulting in its solubilization (Rohwerder et al. 2003; Sandstrom 2009). The sulphur moiety that comes from pyrite dissolution can be further oxidized to sulphuric acid by microbes. Pyrite is an acid non-soluble mineral which cannot be solubilized by sulphuric acid that acts only to reduce the pH for the survival of microbes. The detailed process of pyrite removal by contact and non-contact mechanisms is discussed below.

3.4.1 Contact Mechanism

In contact mechanism approach, bacteria, e.g. *A. ferrooxidans*, is attached to pyritic mineral by its extracellular polymeric substances (EPS, Rohwerder et al. 2003). The space between ore surface and bacterial outer membrane is filled up by EPS layer of bacteria. The attachment happens at the edge, corner, defect and crack of the mineral (Jia et al. 2008). The EPS layer of bacteria contains the complex of Fe^{3+} -glucuronic acids which reacts with pyrite mineral. The Fe^{3+} accepts an electron from the pyrite and is reduced to Fe^{2+} (Tao and Dongwei 2014; Rohwerder et al. 2003). The Fe^{2+} at outer membrane is oxidized to Fe^{3+} by bacteria through electron transfer to oxygen via several intermediate locations (cytochrome (Cyc2), rusticyanin, periplasmic cytochrome (Cyc1) and cytochrome oxidase (Cox)) (Srichandan et al. 2019; Srichandan et al. 2020). Glucuronic acid further recruits Fe^{3+} to start another cycle, and after six sequential electron removal from pyrite by Fe^{3+} -glucuronic acids complex, the sulphur moiety and iron of pyrite are removed as thio-sulphate and Fe^{2+} , respectively. The thio-sulphate ($\text{S}_2\text{O}_3^{2-}$) is further oxidized by bacteria or Fe^{3+} via polythionates ($\text{S}_n\text{O}_6^{2-}$) to sulphuric acid. Several aggregates of elemental sulphur may be generated as by-product of reactions and oxidized by bacteria to sulphuric acid (Tao and Dongwei 2014; Rohwerder et al. 2003).

3.4.2 Non-contact Mechanism

The non-contact approach is carried out by planktonic bacterial cells. The Fe^{2+} and sulphur species present in the solution are oxidized by planktonic cells to Fe^{3+} and sulphuric acid, respectively. The generated Fe^{3+} and sulphuric acid become ready to conduct mineral solubilization; however pyrite being acid-insoluble is not susceptible to sulphuric acid attack whereas Fe^{3+} solubilize pyrite by oxidation-reduction reaction.

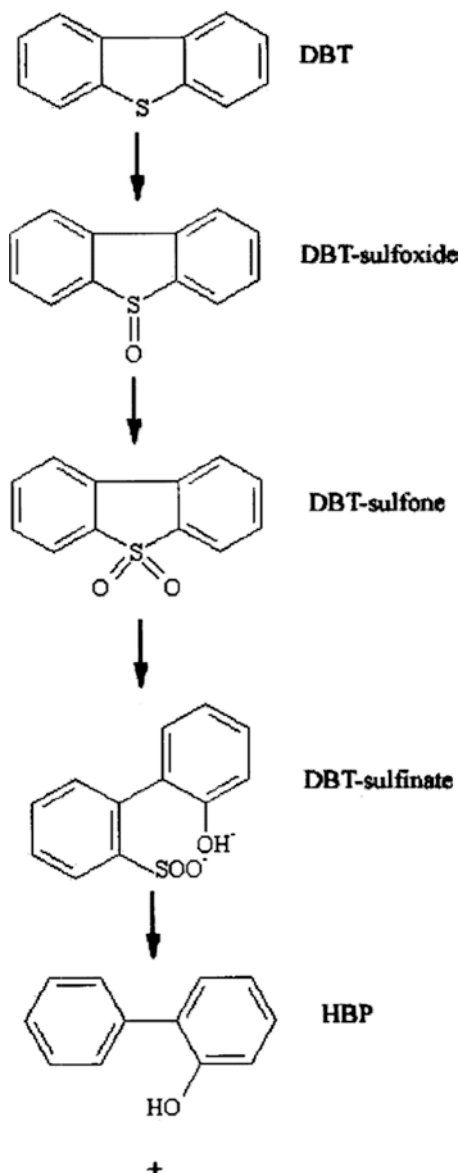
3.5 Microbes Take Part in Inorganic Sulphur Removal

Microbes that may take part in pyrite oxidation are chemolithotrophs (chemolithotrophs in the sense, they use inorganic material such as Fe^{2+} and sulphur species as their energy sources) which thrive at low pH condition of 2.0 or below. *A. ferrooxidans* being iron and sulphur oxidizer gain energy by oxidizing Fe^{2+} to Fe^{3+} and sulphur compounds, viz., S_8 , $\text{S}_2\text{O}_3^{2-}$, H_2S and polysulphide to sulphuric acid (Valdes et al., 2008). *A. ferrooxidans* grows optimally at a pH around 1.5–2.0. *Acidithiobacillus thiooxidans* (*A. thiooxidans*), a sulphur-oxidizer, survive at a pH up to 4.3 and gain energy by oxidizing sulphur compounds (Sivaji-Rao and Berger 1971). However, *A. thiooxidans* may not be able to solubilize pyrite, as it can only oxidize liberated sulphur species from pyrite oxidation that is performed by an iron oxidizer. *Leptospirillum ferriphilum* (*L. ferriphilum*) and *L. ferrooxidans* being Fe^{2+} oxidizer (Rohwerder et al. 2003) are capable of mineralizing pyrite. Moderate thermophilic bacteria grow at a higher temperature of 40–60 °C and are capable of oxidizing Fe^{2+} , thereby taking part in pyrite dissolution; one of such is *Sulfobacillus thermosulfidooxidans* (*S. thermosulfidooxidans*) capable of oxidizing both sulphur and iron (II) (Lizama and Suzuki 1989).

3.6 Microbes Involved in Organic Sulphur Removal and Mechanism

In coal, sulphur may be bound with organic carbon as dibenzothiophene (DBT) and removal of which using *R. erythropolis* has been reported (Prayuenyong 2002). The removal of sulphur from DBT is referred to as 4S pathway in which DBT is metabolized to HBP (hydroxybiphenyl) and sulphate via intermediate compounds such as DBT-sulfone and DBT-sulfinate (Fig. 3.2). Bacteria without cleaving C-C bond oxidizes sulphur atom which is finally removed as sulphite. The report has also been made in removal of sulphur from organically bound alkylated dibenzothiophenes such as 4,6-diethylbiphenyl using *R. erythropolis* (Lee et al. 1995). Likewise, sulphur removal from 3,4-benzo DBT, 2,8-dimethyl DBT and 4,6-dimethyl DBT using

Fig. 3.2 DBT
metabolization by *R.*
erythropolis for sulphur
removal as sulphite
(adopted from
Prayuenyong 2002)



R. erythropolis have also been stated (Lee et al. 1995). *Mycobacterium* sp. has also been revealed to be metabolizing 4,6-dimethyl DBT in removing sulphur (Nekodzuka et al. 1997). Sulphur that may have occurred in the form of benzothio-
phene (BT) can be metabolized by *Gordonia desulfuricans* (*G. desulfuricans*) via 4S pathway (Gilbert et al. 1998). Despite of structural similarity between BT and DBT, *G. desulfuricans* is not capable of metabolizing DBT and *R. erythropolis* is unable to metabolize BT (Prayuenyong 2002). The DBT can be undergone anaerobic

metabolism by certain microbes such as *Desulfovibrio desulfuricans* (*D. desulfuricans*) for removal of sulphur. The pathway is referred as Kodama pathway and includes important steps such as hydroxylation, ring cleavage and hydrolysis (McFarland et al. 1998).

3.7 Current Scenario of Sulphur Removal from Coal by Microbes

Sulphur removal from coal is dependent on experimental conditions; e.g. pyritic form of sulphur removed by microbes is influenced by coal particle size, pyritic quantity of coal, media composition, temperature, pH, aeration and bioreactor design, etc. Bio-depyritization is mainly available in the form of heap and slurry bio-desulphurization. The first one is less expensive due to simple arrangements and performed in open space while the second one is expensive due to needing fine grinding of coal, aeration arrangement system, closed bioreactor. However, the bio-desulphurization kinetic is faster with the second one. Hong et al. (2013) performed bio-desulphurization coal for pyritic sulphur removal using *A. ferrooxidans*. At the end of 16-day bioprocessing, 70% of pyritic sulphur and 51% total sulphur could be removed. In another study, first organic sulphur was removed using *R. erythropolis* at 30 °C and pH 7.0 followed by inorganic sulphur (pyritic sulphur) using *A. ferrooxidans* at acidic pH. At the end of two-step bio-desulphurization (30-days), 65% of total sulphur could be removed and the sulphur concentration of raw coal was reduced to 1.73% out of 4.98%. He et al. (2012) studied bio-desulphurization of coal using a thermophilic *Acidithiobacillus caldus* (*A. caldus*) and estimated 47% of pyrite removal and 19% of total sulphur. The sulphur removal resulted in corrosion on pyrite surface (He et al., 2012).

Biobleaching of pyrite from coal has also been investigated using mixed one culture composed of *A. ferrooxidans*, *L. ferrooxidans* and *A. thiooxidans*, in which the influence of three parameters such as nutrient medium type, pH and ferrous sulphate concentration was examined (Kiani et al. 2014). The maximum sulphur removal (50.3%) could be obtained at pH 1.0, ferrous sulphate concentration of 0.02 M and Noris medium. The total sulphur content of coal was reduced from 3.87% to 1.92%. A slurry biobleaching reactor study was conducted with coal for pyritic sulphur removal using *A. ferrooxidans* at a pulp density of 15% for a period of 96 h (Pandey et al. 2005). It was revealed on effective removal of pyritic kind sulphur which was resulted in the increment of caloric value of coal from 4400 to 6800 kcal/kg as reported in the above investigation. The maximum microbial growth (μ_{max}) and half saturation constant (K_s) obtained were 0.025/h and 0.220 g/L (as pyrite), respectively.

To date, only limited studies have been performed regarding the extraction of organic sulphur from coal. In a similar context, bio-desulphurization of organic sulphur was conducted using *R. erythropolis* strains PD1, R1, FMF and *Rhodococcus qingshengii* (*R. qingshengii*, Etemadifar et al. 2019). Among all the strains, PD1

was found to be more effective and could remove 46% of sulphur in its growing form as compared to 24% in resting (stationary) form. Bhanjadeo et al. (2018) studied the desulphurization of organic sulphur using four strains *R. rhodochrous*, *Arthrobacter sulfureus* (*A. sulfureus*), *Gordonia rubropertincta* (*G. rubropertincta*) and *R. erythropolis* at a DBT concentration of 0.5 mM. It was seen that almost quantitative (over 99%) desulphurization could be after 10-days of incubation. Further analysis of metabolites by HPLC revealed that DBT desulphurization might follow a variant of normal 4-S pathway; however the effective desulphurization as per the authors showed a path for implementation of process to petrochemicals and coal organic sulphur removal.

3.8 Drawbacks and Future Prospective

As discussed already, bio-desulphurization has some advantages (environmentally friendly and economical) over physical and chemical processes. However, there are several drawbacks in applying bioprocess for sulphur removal from coal. Bioprocess is a slow process and consumes significant time for effective removal of sulphur. Further, the microbes may suffer from adaption problems due to changes in the environment. The best solution to overcome the issue is to use microbe isolated from a similar environment or coal mines. Gomez et al. (1997) isolated microbes from Spanish coal and used for bio-desulphurization process. The 67% of total sulphur could be removed from coal. There are several other aspects which can be worked out for improvement in bio-desulphurization process: (1) recognizing the existing or new metabolism pathway of desulphurization by microbes and enhancement of metabolic pathway for improvement in efficiency, (2) development of improved microbes by genetic engineering process or recombinant DNA technology (RDT), (3) sequential use of distinctive processes and (4) use of modified or biphasic growth media.

To describe the impact of RDT, a recombinant strain of *Pseudomonas putida* (*P. putida*) was used for removal of organic sulphur from DBT (Galaan et al. 2001). The recombinant strain was prepared by transferring *dsz*-A, -C and -B genes from *P. putida* via plasmid construction and desulphurization was enhanced. Similarly, another *P. putida* strain containing *dsz*ABC gene from *P. putida* and *hpaC* from *E. coli* could increase desulphurization process by 140 under optimal condition (Martinez et al. 2015). The increment of desulphurization process was also influenced by the inclusion of acetic, citric and succinic acids (substrates) among which acetic acid led to the most positive impact on desulphurization process.

The sequential application of different processes may bring the positive impact on bio-desulphurization. Stevens et al. (1993) conducted desulphurization of coal using *A. ferrooxidans* and *L. ferrooxidans* integrated with physical method and removed 87% of pyritic sulphur. In a similar context, Aksoy et al. (2014) integrated gravity and floatation methods with bio-desulphurization to remove sulphur from coal. Gravity separation of concentrate followed by its bio-desulphurization results

in the reduction of total sulphur from 3.25% to 1.56%. Likewise, concentrates from flotation followed by its bio-desulphurization reduced total sulphur from 3.55% to 1.81%.

Application of modified or biphasic growth medium is also a prominent approach for improvement in bio-desulphurization; e.g. single-phasic medium may reduce bio-desulphurization efficiency attributed to the inability of microbes to overcome oil/water emulsions (hampers the mass transfer process) in the medium. In such a particular case, DBT conversion by *P. putida* encountered mass transfer limitation and overcome by adding additives and supplements. This led to the improvement in bio-desulphurization attributed to enhancement in the mass transfer process.

3.9 Conclusion

Coal being a primary energy source may lead to environmental pollution while undergoes the combustion process. The major pollution source is SO₂ which can be prevented by removal of sulphur from coal before the combustion process. Out of varieties of processes, the biological approach has been considered to be more economical and environmentally friendly. Inorganic sulphur which majorly presents as pyrite in coal can be removed by using acidophiles, e.g. *A. ferrooxidans* via the contact and non-contact mechanism while organic sulphur by heterotrophs, e.g. *R. thryopolis* through 4S pathway. Although significant studies have been performed and found to be successful in removal of sulphur, some additional prospectus may be considered for making the process more enlightened and feasible. Improvement in the metabolic pathways of sulphur removal, development of improved microbes by recombinant DNA technology, integration of different relevant processes along with bio-desulphurization, and use of modified or biphasic nutrient medium may be the suitable additional approaches for improvement in bio-desulphurization kinetic.

Acknowledgement The support and assistance provided by KIIT-BDTC, School of Biotechnology, KIIT (Deemed University) are highly acknowledged.

References

- Akash, B. A. (2013). Thermochemical liquefaction of coal. *International Journal of Thermal & Environmental Engineering*, 5, 51–60.
- Aksoy, D. O., Aytar, P., Toptaş, Y., Çabuk, A., Koca, S., & Koca, H. (2014). Physical and physicochemical cleaning of lignite and the effect of cleaning on biodesulfurization. *Fuel*, 132, 158–164.
- Anon. (n.d.-a) Coal left in the world, World Coal Statistic-Worldometer, <https://www.worldometers.info/coal/>
- Anon. (n.d.-c) Where is coal found? World Coal Association, <https://www.worldcoal.org/coal/where-coal-found>

- Bhanjadeso, M. M., Rath, K., Gupta, D., Pradhan, N., Biswal, S. K., Mishra, B. K., & Subudhi, U. (2018). Differential desulphurization of dibenzothiophene by newly identified MTCC strains: Influence of operon array. *PLoS One*, *13*, 0192536.
- BP Statistical Review of World Energy (2013). <http://www.bp.com/statisticalreview>.
- BP Statistical Review of World Energy 2016. <https://www.theglobaleducationproject.org/earth/energy-supply.php>
- Etemadifar, Z., Etemadzadeh, S. S., & Emtiazi, G. (2019). A novel approach for bioleaching of Sulphur, iron, and silica impurities from coal by growing and resting cells of *Rhodococcus* sp. *Geomicrobiology Journal*, *36*, 123–129.
- Galaan, S. B., Diaz, F. E., Ferrandez, B. A., Prieto, J. M. A., Garcia, L. J. L., Garcia-Ochoa, S. F., Garcia, C. E. (2001). Method for desulphurization of dibenzothiophene using a recombinant *Pseudomonas putida* strain as biocatalyst. Google Patents, WO/2001/070996.
- Ghosh, A., Sujata, A., & Pandey, B. D. (2015). Microbial bio-desulphurization of coal. In Abhilash, B. D. Pandey, & K. A. Natarajan (Eds.), *Microbiology for minerals, metals, materials and the environment*. Florida: CRC press.
- Gilbert, S. C., Morton, J., Buchanan, S., Oldfield, C., & McRoberts, A. (1998). Isolation of a unique benzothiophenedesulphurizing bacterium *Gordonasp.* Strain 213E (NCIMB 40816), and characterization of the desulphurization path-way. *Microbiology*, *144*, 2545–2553.
- Gomez, F., Amils, R., & Marin, I. (1997). Microbial ecology studies for the desulphurization of Spanish coals. *Fuel Process Technology*, *52*, 183–189.
- Hong, F. F., He, H., Liu, J. Y., Tao, X. X., Zheng, L., & Zhao, Y. D. (2013). Comparison analysis of coal bio-desulphurization and coal's pyrite bioleaching with *Acidithiobacillusferrooxidans*. *The Scientific World Journal*, *2013*, 184964.
- He, H., Hong, F. F., Tao, X. X., Li, L., Ma, C. Y., & Zhao, Y. D. (2012). Biondesulfurization of coal with *Acidithiobacillus caldus* and analysis of the interfacial interaction between cells and pyrite. *Fuel Processing Technology*, *101*, 73–77.
- Jia, Y., Tan, Q., Sun, H., Zhang, Y., Gao, H., & Ruan, R. (2008). Sulfide mineral dissolution microbes: community structure and function in industrial bioleaching heaps. *Green Energy and Environment*, *XX*, 1–92.
- Kiani, M. H., Ahmadi, A., & Zilouei, H. (2014). Biological removal of sulphur and ash from fine-grained high pyritic sulphur coals using a mixed culture of mesophilic microorganisms. *Fuel*, *131*, 89–95.
- Klein, J. (1998). Technological and economic aspects of coal bio-desulphurization. *Biodegradation*, *9*, 293–300.
- Lee, M. K., Senius, J. D., & Grossman, M. J. (1995). Sulphur-specific microbial desulphurization of sterically hindered analogs of dibenzothiophene. *Applied and Environmental Microbiology*, *61*, 4362–4366.
- Lizama, H. M., & Suzuki, I. (1989). Bacterial leaching of sulphide ore by *Thiobacillus ferrooxidans* and *Thiobacilluusthiooxidans*, part II, column leaching studies. *Hydrometallurgy*, *22*, 301–310.
- Martinez, I., Santos, V. E., Alcon, A., & Garcia-Ochoa, F. (2015). Enhancement of the bio-desulphurization capacity of *Pseudomonas putida* CECT5279 by co-substrate addition. *Process Biochemistry*, *50*, 119–124.
- McFarland, B. L., Boron, D. J., Deever, W., Meyer, J., Johnson, A. R., & Atlas, R. M. (1998). Biocatalytic Sulphur removal from fuels: Applicability for producing low Sulphur gasoline. *Critical Reviews in Microbiology*, *24*, 99–147.
- Nekodzuka, S., Kambe, T. N., Nomura, N., Lu, J., & Nakahara, T. (1997). Specific desulphurization of dibenzothiophene by *Mycobacterium* sp. strain G3. *Biocatalysis and Biotransformation*, *15*, 17–27.
- Pandey, R. A., Raman, V. K., Bodkhe, S. Y., Handa, B. K., & Bal, A. S. (2005). Microbial desulphurization of coal containing pyritic Sulphur in a continuously operated bench scale coal slurry reactor. *Fuel*, *84*, 81–87.

- Prayuenyong, P. (2002). Coal bio-desulphurization processes. *Journal of Science and Technology*, 24, 493–507.
- Rohwerder, T., Gehrke, T., Kinzler, K., & Sand, W. (2003). Bioleaching review part a. *Applied Microbiology and Biotechnology*, 63, 239–248.
- Sandstrom, A. (2009). *Compendium: Hydrometallurgy*. Sweden: Lulea Univeristy of Technology.
- Sivaji-Rao, G., & Berger, L. R. (1971). The requirement of low pH for growth of *Thiobacillusthiooxidans*. *Archives of Microbiology*, 79, 338–344.
- Srichandan, H., Mohapatra, R. K., Parhi, P. K., & Mishra, S. (2019). Bioleaching approach for extraction of metal values from secondary solid wastes: A critical review. *Hydrometallurgy*, 189, 105122.
- Srichandan, H., Mohapatra, R. K., Singh, P. K., Mishra, S., Parhi, P. K., & Naik, K. (2020). Column bioleaching applications, process development, mechanism, parametric effect and modelling: A review. *Journal of Industrial and Engineering Chemistry*, 90, 1–6.
- Stevens, C. J., Noah, K. S., & Andrews, G. F. (1993). Large laboratory scale demonstration of combined bacterial and physical coal depyritization. *Fuel*, 72(12), 1601–1606.
- Tao, H., & Dongwei, L. (2014). Presentation on mechanisms and applications of chalcopyrite and pyrite bioleaching in biohydrometallurgy—A presentation. *Biotechnology Reports (Amsterdam)*, 4, 107–119.
- Valdés, J., Pedroso, I., Quatrini, R., Dodson, R. J., Tettelin, H., Blake, R., ... & Holmes, D. S. (2008). Acidithiobacillus ferrooxidans metabolism: from genome sequence to industrial applications. *BMC genomics*, 9(1), 1–24.
- Yaman, S., Mericboyu, A. E., & Kucukbayrak, S. (1995). Chemical coal desulphurization research in Turkey. *Fuel Science and Technology International*, 13, 49–58.

Chapter 4

Oil Agglomeration Towards Quality Enhancement of High-Ash Coals: The Indian Scenario



Saswati Chakladar, Ashok Kumar Mohanty, and Sanchita Chakravarty

4.1 Introduction

Electricity generation worldwide largely depends on coal resources, particularly in India. Globally, coal fuelled power plants are responsible for 38% of electricity generation. India, being the third largest coal producer, has a vast energy infrastructure of coal, which comprises coal mining, extraction, transport and finally its utilization in power plants. However, Indian coals are of drift origin. This means the original plant materials, which were later transformed into coal, were transported by rivers and laid down as various mineral deposits. This results in contamination of plant materials with clay minerals, resulting in high ash content. This high ash content in Indian coal makes its utilization considerably challenging, be it for thermal power plants or metallurgical purposes. Over time, the quality of thermal coals in India has deteriorated as reflected in their ash content and calorific value. This is due to the depletion of improved quality coal reserves resulting in expansion of surface mining and mechanization. Although high-grade coals are typically the preferred option for commercial applications, in actuality it is the low-grade coals which are abundant and easily available. Hence, considerable effort is devoted to develop scientific technologies to beneficiate high-ash low-grade coals in a cost-effective manner.

Efficiency of beneficiation to ameliorate coal quality crucially depends on liberation of mineral matter, which is governed by the physical quality of coal as it varies with its particle size. In a typical coal beneficiation process, coal is subjected to a medium of defined specific gravity, containing both high-density and low-density liquids. Heavier material sinks (rejects or mineral matter) and lighter coal floats (clean coal). This specific gravity is defined by the 'washability' characteristics of

S. Chakladar · A. K. Mohanty · S. Chakravarty (✉)
Analytical and Applied Chemistry Division, CSIR-National Metallurgical Laboratory (NML),
Jamshedpur, Jharkhand, India
e-mail: sanchita@nmlindia.org

the coal seam which is not only specific for coal seam but also for the geographical area it belongs to. The existing methodologies are more directed towards cleaning of coarse coal. Fine coal beneficiation is more challenging and requires more attention in the present scenario owing to their increase in generation as a by-product for several physical processes.

4.2 Coarse Coal Cleaning

The presence of high near gravity material in Indian coals results in displacement of ash-bearing particles into clean coal stream rendering the coal difficult to clean. Coarse coal particles (particles with diameter greater than 1.0 mm) are traditionally treated by gravity separation technique. Coal washeries are typically preceded by one- or two-stage crushing to reduce the raw coal to a top size of 100, 75 or 50 mm. The smaller fractions of raw coal which are generated in the crushing process (–13, –10 or – 6.5 mm) which generally contains low ash (less than 30%) are left unwashed. The further utilization of a specific size for washing or direct consumption in power plants essentially depends upon their respective ash content and screening effectiveness. The coarser fractions are washed by conventional physical processes like jig, heavy medium bath or heavy medium cyclone to the extent that the combined ash of the washed coarse coal and the unwashed is within the permissible limit.

4.3 Fine Coal Cleaning

Fine coal processing is comparatively more challenging and expensive than coarse coal processing. Nevertheless, greater emphasis on fine coal recovery has resulted in the recovery of tailings from traditional coarse coal cleaning processes. There are several positive aspects to beneficiate coal fines. The coal fines which are lost in physical processing represent significant economic value. The removal of fine particles from effluent streams is gaining importance due to its potential in recyclability and increasingly stringent environmental regulations which are implemented now worldwide. With the increase in applications of fine coals, such as gasification, liquefaction, and fuel injection, the need to focus on its cleaning is of utmost importance. The two available techniques that can meet these criteria of simultaneous coal beneficiation coupled with coal fines recovery are froth floatation and oil agglomeration. However, although froth floatation technique works quite efficiently for high-rank coals and fines with larger particle size and low ash, it has its own limitations. The process of froth floatation results in low yield of beneficiated product with high moisture content when the particle size of coal fines is lower than 6 μm . Of

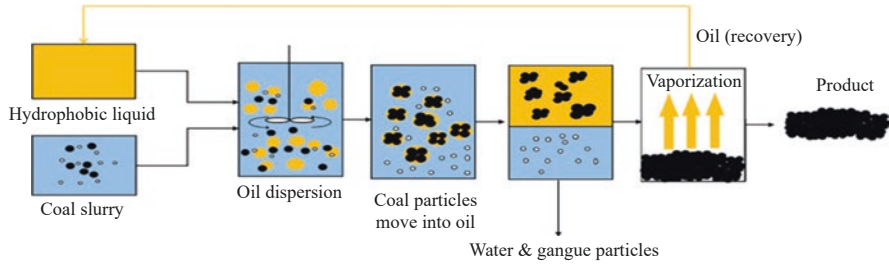


Fig. 4.1 The process of oil agglomeration in demineralization of coal

note, coals with altered surface properties due to oxidation are not amenable to beneficiation by flotation technique owing to increased surface hydrophilicity. Oil agglomeration, which is based on surface adsorption phenomenon, is an attractive alternative way to demineralize coal fines in sub-micron range (10 μm) with high mineral content. The process of oil agglomeration depends on selective wetting of coal particles by hydrocarbon oil under agitation conditions, leaving the uncoated mineral matter in the aqueous layer. The formed coal-oil agglomerates are subsequently sieved to obtain clean coal. The beneficiation process of oil agglomeration, however, is controlled by several crucial physical and chemical process parameters which monitor its efficiency. A pictorial representation of the process of oil agglomeration is shown in Fig. 4.1.

4.4 Key Factors Influencing Oil Agglomeration

4.4.1 Coal Rank

Based on experimental evidences, especially contact angle measurements, it has been found that the hydrophobicity of coal increases with its rank (Gutierrez-Rodriguez et al. 1984). The higher rank coals with high hydrophobicity agglomerate much more efficiently than lower rank coals with lower hydrophobicity (Hower et al. 1997; Carbini et al. 1992). Although oil agglomeration of bituminous coals has been considerably successful, on the contrary, low-rank coals posed numerous difficulties in getting agglomerated in an efficient manner. Several studies have been conducted in order to compare and analyse the agglomerates formed by graphite, coal and the mineral matter found in coal such as kaolin, iron pyrite and quartz (Drzymala et al. 1988; Venkatadri et al. 1988). The primary conclusion was that unlike the carbonaceous content like coal and graphite, which agglomerated with slight variations in nature of agglomerates, the mineral matter failed to agglomerate under similar conditions.

4.4.2 *Surface Chemistry of Coal Particles*

The surface chemistry of coal directly governs the hydrophobic properties of coal. Surface chemistry, in turn, is largely dictated by the maceral composition of coal and the extent of oxidation of its surface. Since oil agglomeration is a surface adsorption phenomenon, the compatibility between the bridging oil and the functional groups on the surface of coal fines is important in order to form agglomerate. Sub-bituminous and lignites contain large amounts of chemically bonded oxygen functional groups like phenolics and carboxylic acids on its surface, which makes them less oleophilic as compared to bituminous coals (Azik et al. 1994). The presence of oxygen-bearing functional groups (e.g. phenolics, carboxylics, ethers and esters) suppresses oil adsorption on coal surface, which is deleterious for agglomeration. Furthermore, it increases the negative charge on the coal particles resulting in electrostatic repulsion between them and the negatively charged oil droplets. Thus, in order to alter the surface hydrophobicity, surfactants as additives are often included as a pre-conditioning step towards improvement in agglomerate formation (Özer et al. 2017).

4.4.3 *Coal Particle Size*

The particle size of coal plays a significant role in the process of oil agglomeration. The selection of a suitable beneficiation process for coal is largely governed by the particle size of coal which is dealt with. The processing of fine coal is always more challenging and costly as compared to cleaning of coarse coal. The reduction in size of coal particles during grinding enhances the liberation of mineral matter and also improves the process of agglomeration (Garcia et al. 1995). Nevertheless, there is a fine line between sufficient grinding and doing it overly. Lin et al. and Chen et al. have shown that with increase in grinding time, the ash content of the agglomerates first decreased and then increased (Lin et al. 2012; Chen et al. 2013). The justification behind decrease in ash content of agglomerates is uncomplicated, indicating enhanced liberation of mineral. On the downside, prolonged grinding time leading to further reduction in particle size leads to increased mineral content in agglomerates owing to entrapment of fine particles of the mineral matter in the pores of agglomerates. It is important to note that the reduction in combustible recovery with reduction in coal particle size has been commonly observed by several researchers (Chary and Dastidar 2013; Sahinoglu and Uslu 2013). There are two possible explanations behind it, (a) enhancement in surface area owing to ultra-fine grinding results in insufficiency of bridging liquid to coat the entire coal particles and (b) difficulty in proper sieving of the small size agglomerates. The size of the agglomerates obtained is largely dependent on the coal feed size. However, there are limitations for individual feed sizes. Coarser coal particles, which are economically feasible, needing reduced grinding time, tend to form loose and voluminous

agglomerates (Ye and Miller 1988). On the other hand, fine coal particles which typically result in improved liberation of mineral matter tend to form larger agglomerates with higher moisture content (Fuerstenau et al. 1983). Hence, both technical and economical feasibility need to be contemplated in order to optimize the process parameters for coal oil agglomeration.

4.4.4 Bridging Liquid Nature and Concentration

The choice of bridging liquid in coal oil agglomeration is possibly the trickiest yet crucial parameter. Oil is typically used as bridging liquid for coal agglomeration; however, the most baffling issue is to choose the suitable oil type for a particular coal. Labuschagne used 41 different liquids possessing wide range of chemical properties, for example, paraffinic, olefinic and different cyclic hydrocarbons to investigate the effect of the chemical and structural properties of the bridging liquid obtained from various sources on the agglomeration process (Labuschagne 1986). However, drawing a single conclusion was complicated owing to the interdependency of other physical parameters which also affects coal agglomeration (Cebeci et al. 2002). Hitherto, petroleum fractions and edible vegetable oils like sunflower oil and soya bean oil have been widely used as agglomerants (Alonso et al. 1999; Aslan and Unal 2011; Chary and Dastidar 2013). Surprisingly, non-edible vegetable oils like Karanja oil, Jatropha oil and others have not been investigated to their best capacity.

The chemistry and physical properties of bridging liquid like viscosity, density and functional group distribution are of utmost importance to delineate the chemistry between coal surface and oil particles. Light oils were found suitable to agglomerate bituminous coals quite easily, whereas heavy oils are more effective for agglomeration of lower rank coals. The extent to which the oil molecules disperse during the agitation process is an important factor towards enhancing the probability of particle–oil-droplet collision. Under the high agitation conditions, light oils are expected to disperse to a greater extent as compared to heavy oils (Özer et al. 2017). Although light oils work efficiently for bituminous coals, it does not agglomerate lower rank coals quite well. The dissimilarity in the surface properties of bituminous coals and low-rank coals plays a vital role in selecting the suitable oil for their respective agglomeration. Typically, low-rank coals possess more hydrophilic functional groups on its surface such as hydroxyl, carboxylic acids and ethereal linkages. Hence, heavy oils with polar hydrophilic functionalities in their long-chain fatty acids are more suitable since they promote favourable chemical interactions with coal surface (Capes 1976). Hydrocarbons like pentane, hexane, xylene, benzene and cyclohexane have been thoroughly researched upon (Gray et al. 2001; Kim 1993). Cheaper oils like kerosene, diesel oil and fuel oil have been a common choice of agglomerant as well, more so due to their lower cost. Vegetable oils are commonly found to be efficient towards agglomeration of coal fines. The presence of the fatty acid group along with hydroxyl functionalities results in enhanced

emulsification in water, thus resulting in increased agglomerate recoveries with low ash content (Malik et al. 1999). Several studies have been conducted and are continuing to be explored where researchers are considering oil blend instead of a single oil to enhance the efficiency of agglomeration (Temel et al. 2009; Kaya and Ari 2019).

The concentration of bridging liquid used for agglomeration is extremely important to ascertain the cost effectiveness of the process. Furthermore, the concentration of bridging oil used dictates the size and nature of agglomerate being formed. There is a critical oil concentration, where the size and sphericity of micro-agglomerates formed is optimum for maximum ash rejection and sieving. Beyond that, the agglomerates tend to become dispersed and pasty in nature. The selection of type and concentration of bridging liquid is to be carefully done based on the coal type to be agglomerated.

4.4.5 Pulp Density

Pulp density or, in other words, the density of aqueous coal slurry affects the probability of collision and adhesion between the oil droplets and coal particles. Hence, it alters the efficiency of agglomeration to a large extent. There is an optimal pulp density for each coal, too high or too low, both are detrimental to the outcome of the process. Higher than optimal pulp density leads to insufficiency of oil droplets to coat the entire coal particles, thus leaving behind a large portion of untreated coal (Chen et al. 2013). On the other hand, if the pulp density is too low, the inter-particle distance between coal and oil particles is too high, resulting in inadequate coating of coal particles with oil (Rahmani 2001).

4.4.6 Pulp pH

The functional groups on the coal surface imparts it the characteristic hydrophilicity or hydrophobicity. These functional groups like carboxylic acids, hydroxyls and phenolics are expected to be responsible for development of negative charge on coal surface, which leads to repulsion between coal and oil particles. Typically, neutral pH works optimally for most coal types resulting in maximum recovery in the agglomeration process (Chary and Dastidar 2013; Temel et al. 2009). However, there are few reports when acidic pH worked better for some coals, while basic pH resulted in improved combustible yield as compared to neutral conditions. At lower pH, the hydrophilicity of the coal surface is enhanced which results in poor recovery of agglomerates. On the contrary, upon increasing the pH to basic conditions, the hydrophobicity of coal is reported to be enhanced which consequently improves the yield of combustible recovery from agglomeration process (Özer et al. 2017).

4.4.7 Ionic Strength

The role of electrolytes during the agglomeration process is primarily to destabilize the wetting films on coal surface. However, the presence of electrolytes works differently for hydrophobic coals and the hydrophilic ones. In case of hydrophobic coals, a positive electrolyte improves the compression of double layers of the negatively charged coal particles, which largely overcome the electrostatic repulsive forces between coal particles and oil droplets (Fan et al. 1992). On the other hand, for hydrophilic coals, the presence of electrolytes primarily affects the adsorption of cations onto the coal surface (Fan et al. 1987). The presence of inorganic electrolytes is believed to alter the surface chemistry of coal particles and mineral matter. There are several reports, wherein inclusion of NaCl during the agglomeration process for hydrophobic coals has been shown to improve the agglomeration recovery while decreased the induction time (Özer et al. 2017). Nevertheless, generalization of such an observation is rather difficult, since coals with less hydrophobicity tend to show an opposite effect of reduced agglomeration recovery upon inclusion of electrolytes.

4.4.8 Agitation Conditions

Agitation conditions are crucial parameters for the process of agglomeration wherein dispersion of oil particles and collision between dispersed oil and coal particles play a major role. The agitation intensity and duration affects the process significantly. High agitation conditions induce high shear and turbulence, induce improved and homogenous oil distribution and thereby increase the collision frequency. This leads to shorter induction time than exhibited at low mixing speeds. However, just like other process parameters, agitation intensity and duration also possess a critical point where both probability of collision and energy of collision of the oil-coated coal particles result in maximum agglomeration recovery. Nonetheless, optimization of agitation conditions is also specific for the type of coal used. Several contradictory observations are reported in literature. At low agitation speed (~2000 rpm), not only longer durations for agglomeration are required for optimum recovery, there are reports of higher ash content in the agglomerates formed (Bhattacharyya et al. 1977; Chen et al. 2013). Typically, higher agitation speed (~3000 rpm) results in optimum recovery of clean organic matter. On the downside, upon prolonged agitation duration at high intensity, the formed agglomerates tend to break resulting in loss of clean coal recovery. Therefore, the optimum agitation conditions need to be carefully deduced experimentally for each coal type.

4.5 Current Scenarios for Oil Agglomeration of High-Ash Indian Coals

The innate quality of Indian coal, along with the predominant practice of open cast mining, has resulted in very high quantity of mineral matter in low-grade coals. Typically, the low-grade coals in India have an average ash content of 35–50 percent and low Gross Calorific Value (1000–4000 kcal/kg), which poses considerable concern towards their utilization. The high ash content in coal leads to erosion in boilers, generation of excessive amounts of fly ash, poor emissivity and flame temperature. In addition to that, transportation of dirty coal across long distances is economically wasteful, as it carries large quantities of ash-forming minerals along with clean unnecessarily. In 2001, Ministry of Environment and Forest (MEF) has issued strict regulations mandate which requires raw coals to be cleaned to less than 34% ash if it requires to be transported for longer distances or if burned in environmentally sensitive areas such. Government policies in India are thus in favour of coal beneficiation and several mandates have been issued to power plants to improve upon the existing efficiency targets (Ministry of Environment 2015). Both thermal power plants and blast furnaces are required to use clean coal for their respective applications.

In India, the ash content in coal which is delivered to power plants currently averages about 40%. The coal is typically the low-grade non-coking variety which accounts for over 85% of the total reserve in our country. Despite the abundance of high-ash non-coking coal in India, very little work has been done towards beneficiation of such to ameliorate the efficiency of power plants. With the fast depletion of good quality coal, it is the need of hour to develop and implement efficient beneficiation techniques for these low-grade coals. The benefits of oil agglomeration as a suitable demineralization technique are well known in the scientific community. Nevertheless, the economic drawback associated with cost and availability of oil has halted its progress towards commercialization. Regardless of the chosen procedure, high-ash Indian coals are more challenging to beneficiate as compared to coals from the USA, China or Australia. Researchers have looked into optimization of demineralization of both non-coking and coking coals of Indian origin using oil agglomeration. The technical and economical benefit of beneficiation of Indian coals using oil agglomeration was documented initially by Mehrotra et al. (Mehrotra et al. 1980). One of the very first comprehensive studies to beneficiate coal fines was conducted by Rao and Vanangamudi (Rao and Vanangamudi 1984). They performed a detailed analysis of agglomeration of coking coal from Dugda-1 coal washery using varying dosages of furnace oil. Malik et al. optimized demineralization of five different Indian coals meant for both thermal and metallurgical sectors, using vegetable oils (Malik et al. 1999). They improved upon the ash rejection by including a pre-conditioning step using bacterial culture prior to oil agglomeration. Chary and Dastidar [Chary 2012, 2013] reported that Karanja oil enhanced the agglomeration of high-sulphur and low-ash Indian coal due to its high viscosity, when compared with rubber seed oil and jatropha oil. Baruah et al. explored the efficiency of

hydrocarbons such as xylene and hexane as agglomerants towards cleaning of high-sulphur Indian coals (Baruah et al. 2000). They concluded xylene to be relatively more efficient in both organic matter recovery (~92%) and ash rejection (~90%). Interestingly, sunflower oil could successfully agglomerate and demineralize heat-altered coal of Indian origin, commonly called Jhama coal, as reported by Chakladar et al. (Chakladar et al. 2020a, b). The ash content in the clean coal obtained was reduced by approximately 60%. Vegetable oils have been commonly implied as successful agglomerants for low-grade coals. Nevertheless, being edible in nature, the usage of such, for example, sunflower oil or soya bean oil is highly debatable, especially in a developing country like India. The quest for non-edible yet efficient bridging liquid as agglomerant is a continued effort among researchers. In this respect, turpentine oil, which is natural, abundant and non-edible in nature, was reported to be an efficient agglomerant of coking coals as recently published by Chakravarty and co-workers (Chakladar et al. 2020a, b). Apart from its efficiency, turpentine oil was found to be economical as well as easy to remove from the clean coal obtained. Most of the investigations which have been carried so far in Indian perspective for oil agglomeration have been batch process. Chary et al. reported agglomeration of high-ash thermal grade coal using Karanja oil as the bridging liquid under continuous mode of operation (Chary et al. 2015). Over the past four decades, the research on oil agglomeration in India primarily revolved around quality enhancement of coking coal or metallurgical coal aiming at reducing coal import for blast furnace applications. Despite the fact that more than 85% of our total reserve is indeed the high-ash non-coking variety mainly used in thermal power plants, negligible work has been conducted to demineralize such coals. Due to enhanced surface hydrophilicity, low-grade coals are less prone to agglomerate compared to high-grade coals; hence chemical modification of surface functionality is desirable. However, incorporation of surfactants would incur additional expense. Thus, keeping in mind the present economic and environmental circumstances in India, it is of paramount importance to divert our focus towards quality improvement of energy sector.

4.6 Economic Benefits of Coal Beneficiation in India

4.6.1 *Benefits to Plant Operations*

Power plants demonstrate much improved performance when the coal in use is of higher quality as opposed to when low-quality coals are used. By and large, there is an inverse relation of ash content in coal to the calorific value generated per unit weight of coal. When the ash content in coal is reduced, less quantity of coal needs to be burnt to produce equal amount of electricity. Usage of low-ash coals can significantly bring down the maintenance cost of boilers and can reduce damage to coal handling equipment such as conveyors, pulverisers and crushers. Coal

beneficiation improves overall power plant operations which directly affects the profitability of a coal plant over the long term.

4.6.2 Benefits to Transportation of High-Ash Coals

In India, the coal mines are typically located far from the power stations and hence extra transportation cost is incurred for coal to be hauled from distant mines. The coal with mineral matter puts an extra load on the railway system which carries it to power stations, apart from the environmental pollution it already comes with. Lower ash coal will also result in reduction in freight costs for transporting the same energy content considering the typical long haulage distances.

4.7 Future Prospects

The economic and environmental benefits of coal beneficiation at the national level often do not translate to financial savings directly at the plant level. However, owing to the fast depletion of the good coal, time has come when implementation of coal beneficiation techniques is crucial in order to save our environment. Oil agglomeration is versatile in its capability to beneficiate wide range of coals with varying chemistry, and thus holds tremendous prospects for future commercialization.

4.8 Concluding Remarks

Coal, being cheap and available, will continue to remain as one of the biggest energy sources for electricity generation in a developing nation like India. Unfortunately, Indian coals suffer from the biggest disadvantage of high ash content, which is associated with significant damaging impact on the environment. At the macro-economic level, coal demineralization leads to both economic efficiency and pollution control. On a positive note, beneficiation also adds value to Indian coals and improves their marketability. However, the realization of economic benefits of coal beneficiation is much needed. A government policy that is anchored to both economic and environmental considerations is likely to have greater impact than the one based only on the latter.

References

- Alonso, M. I., Valdes, A. F., Martinez-Tarazona, R. M., & Garcia, A. B. (1999). Coal recovery from fines cleaning wastes by agglomeration with vegetable oils: Effects of oil type and concentration. *Fuel*, *78*, 753–759.
- Aslan, N., & Unal, I. (2011). Multi-response optimization of oil agglomeration with multiple performance characteristics. *Fuel Processing Technology*, *92*, 1157–1163.
- Azik, M., Yurum, Y., & Gaines, A. F. (1994). Air oxidation of Turkish Beypazari lignite: 2. Effect of demineralization on structural characteristics in oxidation reactions at 150 °C. *Energy & Fuels*, *8*, 188–193.
- Baruah, M. K., Kotoky, P., Baruah, J., & Bora, G. C. (2000). Cleaning of Indian coals by agglomeration with xylene and hexane. *Separation and Purification Technology*, *20*(2), 235–241.
- Bhattacharyya, R., Moza, A., & Sarkar, G. (1977). Role of operating variables in oil-agglomeration of coal. In K. V. S. Sastry (Ed.), *Agglomeration* (Vol. 77, pp. 931–938). New York: American Institute of Mining, Metallurgical, and Petroleum Engineers.
- Capes, C. (1976). Erco award 1975: Basic research in particle technology and some novel applications. *The Canadian Journal of Chemical Engineering*, *54*, 3–12.
- Carbini, P., Ciccu, R., Ghiani, M., & Satta, F. (1992). Agglomeration of coals of different rank using mixtures of oils. *Coal Preparation*, *11*, 11–19.
- Cebeci, Y., Ulusoy, U., & Simsek, S. (2002). Investigation of the effect of agglomeration time, pH and various salts on the cleaning of Zonguldak bituminous coal by oil agglomeration. *Fuel*, *8*(9), 1131–1137.
- Chakladar, S., Banerjee, R., Mohanty, A., Chakravarty, S., & Patar, P. (2020a). Turpentine oil: A novel and natural bridging liquid for agglomeration of coal fines of high ash coals. *International Journal of Coal Preparation and Utilization*. <https://doi.org/10.1080/19392699.2020.1789976>.
- Chakladar, S., Chakravarty, S., Mohanty, A., Alex, T. C., & Kumar, S. (2020b). Quality improvement of heat altered coals: A preliminary feasibility study. *Environmental Technology and Innovation*. <https://doi.org/10.1016/j.eti.2020.100764>.
- Chary, G., & Dastidar, M. (2013). Comprehensive study of process parameters affecting oil agglomeration using vegetable oils. *Fuel*, *106*, 285–292.
- Chary, G. H. V. C., Gupta, A., & Dastidar, M. G. (2015). Oil agglomeration of coal fines in continuous mode of operation. *Particulate Science and Technology*, *33*(1), 17–22.
- Chen, B., Lin, S., Wu, S., Li, W., & Chen, W. (2013). Study on the cleaning of Peifeng coal with oil agglomeration. *Procedia Environmental Sciences*, *18*, 338–346.
- Dzrymala, J., Markuszewski, R., & Wheelock, T. D. (1988). Agglomeration with heptane of coal and other materials in aqueous suspensions. *Minerals Engineering*, *1*, 351–358.
- Fan, C., Markuszewski, R., & Wheelock, T. (1987). Coal and pyrite separation by oil agglomeration in salt solutions. *Fizykochemiczne Problemy Mineralurgii*, *19*, 17–26.
- Fan, C.-W., Markuszewski, R., & Wheelock, T. (1992). Effect of multivalent cations on oil agglomeration of coal and pyrite. *Coal Preparation*, *11*, 167–175.
- Fuerstenau, D., Rosenbaum, J. M., & Laskowski, J. (1983). Effect of surface functional groups on the flotation of coal. *Colloids and Surfaces*, *8*, 153–173.
- Garcia, A. B., Vega, J. G., & Martinez-Tarazona, M. R. (1995). Effects of oil concentration and particle size on the cleaning of Spanish high-rank coals by agglomeration with n-heptane. *Fuel*, *74*, 1692–1697.
- Gray, M., Champagne, K. J., Soong, Y., & Finseth, D. H. (2001). Parametric study of the column oil agglomeration of fly ash. *Fuel*, *80*, 867–871.
- Gutierrez-Rodriguez, J. A., Purcell, R. J., & Aplan, F. F. (1984). Estimating the hydrophobicity of coal. *Colloids and Surfaces*, *12*, 1–25.
- Hower, J. C., Kuehn, K. W., Parekh, B. K., & Andrews, W. M., Jr. (1997). Maceral and microliothotype response to oil agglomeration for selected eastern Kentucky high volatile A bituminous coals. *Fuel Processing Technology*, *50*, 185–198.

- Kaya, O., & Ari, M. (2019). Investigation of the factors affecting oil agglomeration using different reagent mixtures as a bridging liquid. *International Journal of Coal Preparation and Utilization*. <https://doi.org/10.1080/19392699.2019.1568999>.
- Kim, S. S. (1993). Development of a selective agglomeration process using light hydrocarbons for fine coal beneficiation. PhD diss., University of Pittsburgh.
- Labuschagne, B. (1986). Relationships between oil agglomeration and surface properties of coal: Effect of pH and oil composition. *Coal Preparation*, 3, 1–13.
- Lin, S., Chen, B., Chen, W., Li, W., & Wu, S. (2012). Study on clean coal technology with oil agglomeration in Fujian Province. *Procedia Engineering*, 45, 986–992.
- Malik, A., Singh, D., Sharma, S., Dastidar, M., & Roychoudhury, P. (1999). Oil agglomeration for recovery of coal fines: Effect of vegetable oil and bacterial pretreatment. *Coal Preparation*, 20, 247–268.
- Mehrotra, V., Sastry, K., & Morey, B. (1980). Oil agglomeration offers technical and economical advantages. *Mining Engineering*, 32, 1230–1234.
- Ministry of Environment (2015). Forest & climate change, India's intended nationally determined contribution: Working towards Climate Justice, page 10.
- Özer, M., Basha, O. M., & Morsi, B. (2017). Coal-agglomeration processes: A review. *International Journal of Coal Preparation and Utilization*, 37(3), 131–167.
- Rahmani, A. (2001). Effect of surfactant on spherical oil agglomeration of coal (research note). *International Journal of Engineering*, 14, 281–288.
- Rao, T. C., & Vanangamudi, M. (1984). Quantitative studies on the coal–oil agglomeration process. *Powder Technology*, 40, 195–205.
- Sahinoglu, E., & Uslu, T. (2013). Increasing coal quality by oil agglomeration after ultrasonic treatment. *Fuel Processing Technology*, 116, 332–338.
- Temel, A. H., Bozkurt, V., & Majumder, A. K. (2009). Selective oil agglomeration of lignite. *Energy & Fuels*, 23, 779–784.
- Venkatadri, R., Markuszewski, R., & Wheelock, T. D. (1988). Oil agglomeration of weakly hydrophobic coals and coal/pyrite mixtures. *Energy & Fuels*, 2, 145–150.
- Ye, Y., & Miller, J. D. (1988). Bubble/particle contact time in the analysis of coal flotation. *Coal Preparation*, 5, 147–166.

Chapter 5

Preparation of Coal-Derived Activated Carbon and Its Application for Adsorption of Metals from Aqueous Solutions



Kurniawan and Sookyung Kim

5.1 Introduction

Adsorption has been recognized as a powerful chemical engineering process which is widely employed in multiple fields, including for reduction of SO_x and NO_x from flue gases (Liemans et al. 2011; Silas et al. 2019; Wang et al. 2017), purification of hydrogen and helium gases (Augelletti et al. 2016; Jahromi et al. 2018; Saberimoghaddam and Nozari 2017; Shin et al. 2020), separation and purification of organic compounds/mixtures (Li et al. 2020; Ma et al. 2020), selective separation of leached gold and silver in cyanide solution (Oraby and Eksteen 2015; Parga et al. 2012; Yalcin and Arol 2002), control of water pollution/water treatment (Afroze and Sen 2018; Jiang et al. 2018; Uddin 2017; Xu et al. 2018), etc. Among these fields, adsorption of metals from such aqueous solutions during leaching and wastewater treatments contributes larger proportions to the total applications of adsorption process (Fig. 5.1), and becomes main parts of reasons to the more advanced understanding in adsorption process for the growing number of studies published dedicated to the adsorption of metallic ions from various aqueous solutions (Fig. 5.1).

Adsorption of metallic ions onto such adsorbents occurs through the surface interaction between the metallic ions and the surface of solid/liquid adsorbents, in which the metallic ions adhere to the surface of the adsorbents, and due to the unbalanced attraction forces, the metallic ions are accumulated and then adsorbed. This phenomenon is reversible; the adsorbed metals on the adsorbents can be released

Kurniawan · S. Kim (✉)

Resources Recycling, Korea University of Science and Technology,
Daejeon, Republic of Korea

Mineral Resources Research Division, Korea Institute of Geoscience and Mineral Resources
(KIGAM), Daejeon, Republic of Korea

e-mail: k.kurniawan@kigam.re.kr; skkim@kigam.re.kr

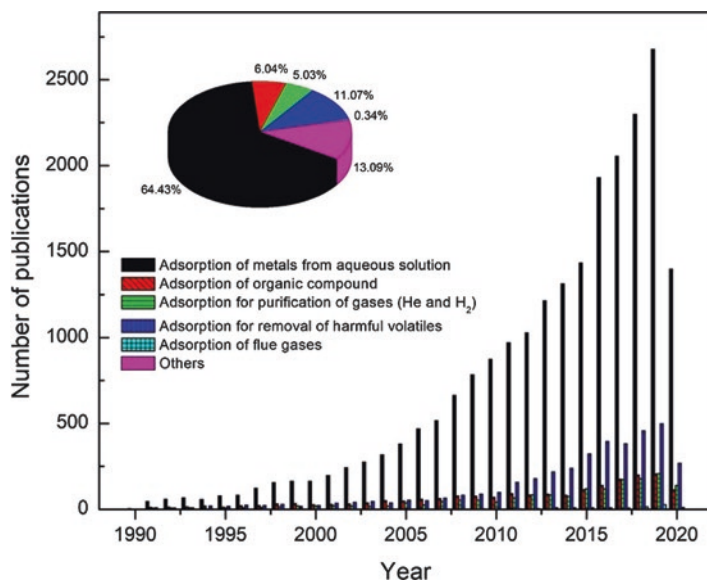


Fig. 5.1 Number of publications on the application of adsorption in various fields per year since 1990 to 30 June 2020. Data obtained from Web of Science with the key words: adsorption of metals from aqueous solution, adsorption of organic compound from aqueous solution, adsorption for purification of gases, adsorption for removal of harmful volatiles, and adsorption of flue gases. The inserted pie chart shows the corresponding percentages of each application

back/desorbed by performing chemical treatment of washing the loaded adsorbents with chemical reagents (Sukul et al. 2008; Wang et al. 2008). Desorption is the key factor of implementing adsorption system (Lee et al. 2020). The concept of adsorption-desorption has been realized for centuries, including the distinction between chemisorption and physisorption, but it remains one of the most studied processes in the recovery and separation/purification of metallic ions from aqueous solution and water treatment till present. This is in accordance with the growing understanding on the surface chemistry as the fundamental part of the adsorption-desorption process, and evidenced by a large number of studies/reviews gathered information on this field (Furmaniak et al. 2008; Largette and Pasquier 2016; Qiu et al. 2009; Wu et al. 2009).

Attention has also been paid to search for the most efficient adsorbents. The selection of adsorbents is crucial to achieve the successful adsorption practice. An efficient adsorbent is characterized by its maximum surface area with minimum volume (Cossu et al. 2018), along with other properties including its high recyclability and durability, chemical resistance and low production cost. Nowadays, a variety of adsorbents are available, including those from nature such as clays (bentonite, kaolinite, smectite) and zeolites, and those obtained after some physical and separation processes, viz. activated carbon (AC), silica gel, activated alumina, and polymers/resin. Zeolites have also been industrially manufactured by utilizing some

SiO₂-Al₂O₃ sources, such as bauxite and coal fly ash, and some natural clays have also been pretreated for enhancing their properties. These varied types of adsorbents pave the way for multiple applications of adsorption processes as mentioned earlier, and the major adsorbents used for adsorption of metallic ions from aqueous solutions are AC, polymers/resin, and zeolite (Table 5.1). AC, resin, and zeolite offer high efficiency to adsorb metals from broad types of solutions, but they can be distinguished and selected by their different physicochemical properties (Table 5.1). AC is often preferred for its advantages of larger surface area with well-developed pores, higher surface reactivity, high durability, and easiness of reusing the AC by simple heat treatment process. The understandings of metal adsorption with AC have also been well defined while those using resins and zeolites are often found to

Table 5.1 Physicochemical properties and applications of various types of adsorbents

Adsorbent	Properties	Application
Clay ^a	<ul style="list-style-type: none"> • Porous structure: Complex porous structure • Chemical composition: Si, Al, Fe, Ti, Ca, Na, K, Mg-oxides (depending on the types of clay) • Surface area: 60–300 m²/g 	<ul style="list-style-type: none"> • Adsorption of organic pollutant • Adsorption of dyes • Water remediation
Silica gel ^b	<ul style="list-style-type: none"> • Porous structure: Micropore, amorphous • Chemical composition: SiO₂ • Surface area: 500–650 m²/g 	<ul style="list-style-type: none"> • Dehumidification • Denitrogenation and desulfurization of flue gas
Activated alumina ^c	<ul style="list-style-type: none"> • Porous structure: Macroporous • Chemical composition: Al₂O₃ • Surface area: 150–500 m²/g 	<ul style="list-style-type: none"> • Dehumidification • Removal of halogens from water • Wastewater treatment
Activated carbon ^d	<ul style="list-style-type: none"> • Porous structure: Micro-, meso-, and macropores • Chemical composition: C, H, O, N • Surface area: 950–2000 m²/g 	<ul style="list-style-type: none"> • Gold and silver recovery from cyanidation • Wastewater treatment • Removal of SO_x and NO_x • Purification of helium and hydrogen gas
Fabricated zeolite ^e	<ul style="list-style-type: none"> • Porous structure: Micro-, meso-, and macropores • Chemical composition: Si-, Al-oxides • Surface area: 200–900 m²/g 	<ul style="list-style-type: none"> • Wastewater treatment • Catalysts • Removal of organic compounds • Removal of mercury from exhaust gases
Polymers/resin ^f	<ul style="list-style-type: none"> • Porous structure: micro-, meso-, and macropores • Chemical composition: Complex (mostly terpenes) • Surface area: 700–1000 m²/g 	<ul style="list-style-type: none"> • Water purification • Gold and silver recovery from cyanidation • Recovery of organic compounds

^aHan et al. (2019), Kausar et al. (2018), Rahman et al. (2013), Uddin (2017), Yadav et al. (2019)

^bLaredo et al. (2013), Menon and Komarneni (1998), Srivastava and Eames (1998)

^cBowen et al. (1967), Mohapatra et al. (2009), Srivastava and Eames (1998)

^dJiang et al. (2018), Lu and Xue (2019)

^eCid et al. (1983), Jiang et al. (2018), Srivastava and Eames (1998)

^fHu and Xu (2020)

be lacking for the varied types of polymers and zeolites which result in great differences in adsorption behavior (Ferreira et al. 2013; Mintova et al. 2006; Remy et al. 2013). Additionally, resin and zeolite could be degraded and hydrolyzed when they had contacted with highly acidic solutions to release carbonaceous acids, silicic acid, halloysite ($\text{Al}_2\text{Si}_2\text{O}_5(\text{OH})_4$) and gibbsite ($\text{Al}_2\text{O}_3 \cdot 3\text{H}_2\text{O}$) which thus reduce the adsorption capacity of the resin and zeolites (Antenucci et al. 1992; Cook et al. 1982; Li et al. 2016; Xue et al. 2018).

Researches on searching for the carbonaceous materials as the precursors of the AC are extensive, including the use of coal (Ahmadpour and Do 1997; Linares-Solano et al. 2000), nutshell (Kumar and Jena 2016; Li et al. 2017), rice husk (Kalderis et al. 2008; Teo et al. 2016), oil palm fronds (Salman and Hameed 2010, Salman et al. 2011), biomass (Schröder et al. 2007; Tay et al. 2009), bagasse (Kalderis et al. 2008), etc. Among them, coal is the most critical precursor, with advantages of higher carbon content, superior mechanical properties of the produced ACs, large supply and cheapness and readily primary pores (Ahmadpour and Do 1997; Linares-Solano et al. 2000). To date, hundreds of research articles, patents, and technical reports related to the preparation of coal-derived AC have been published, but reviews to collect and analyze the information based on the theoretical and technical aspects during the preparation of coal-derived AC are scarce (Durán-Valle et al. 2017; Silas et al. 2018). The present review is therefore intended to accumulate the information on the preparation methods of AC from coals. Examples of the application of the coal-derived AC for adsorbing metallic ions from such leaching and aqueous solutions are presented. Perspectives on the further opportunities and challenges of utilizing coals as the precursor of AC are given. Finally, the present review shows the evident utilization of coals in such green manner as an addition of the traditional utilization of coals as energy source to face the goal of clean coal technologies.

5.2 Physicochemical Properties of Activated Carbon

High adsorption capacity of AC is determined by its physicochemical properties, which include the crystalline structure, porous structure, and chemical composition as described below.

5.2.1 Crystalline Structure of Activated Carbon

Activated carbon (AC) has a 3-dimensional (3D) structure built by microcrystallite layers, where these layers are being less oriented with the interlayer spacing in the range 0.34–0.35 nm (Bansal and Goyal 2005). This disordered orientation, called as

turbostratic structure (Biscoe and Warren 1942), is resulted by the presence of $-\text{OH}$, $=\text{O}$, $-\text{O}-$, $-\text{N}-$, $-\text{S}-$ or $-\text{Si}-$ to form various functional groups which bounded on the surface of the carbon (Bansal and Goyal 2005) and defects (spot, line, and plans) generated during thermal preparation of the AC (Banhart et al. 2011).

Carbonaceous materials as the AC precursors can behave in two different graphitization classes during such thermal treatments (Franklin 1956). The first class is to obtain 3D graphitic carbon where the carbonization occurs continuously and homogeneously (Franklin 1956); the obtained product of graphitizing carbon composes of parallel multi-graphitic layers with well-organized orientation (Fig. 5.2a). The second class is to obtain non-graphitizing carbon with highly disordered orientation and well-developed pores (Fig. 5.2b). The AC is derived from this non-graphitizing carbon (Harris et al. 2008), where such thermal treatments at high temperature (1700–3000 °C) do not affect the microcrystallite orientation. In reality, parts of non-graphitizing carbon are graphitic layers (Franklin 1956); they tend to be more mutually orientated at temperatures 1700–3000 °C.

With the acceptance of models depicted in Fig. 5.2, the explanation on how the microcrystallite layers join each other, however, was still lacking in the study by Franklin. Jenkins et al. (1976) proposed that these joints are from twisted, bended, or intertwined cross-links, involving three microcrystallite layers which aligned each other in random orientations and creating the so-called strong confluence region. According to Mildner and Carpenter (1982), these cross-links are featured entirely with sp^2 carbons, and the more advanced development with respect to this idea was that sp^2 carbons featured cross-links have fullurene-like structure, comprising hexagonal and pentagonal rings (Harris et al. 2008; McDonald-Wharry et al. 2016).

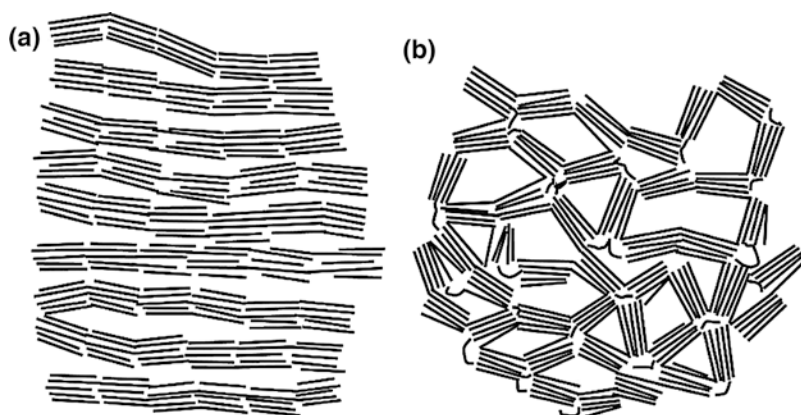


Fig. 5.2 Illustration of microcrystallite layers of (a) graphitizing carbon with well-organized orientation, (b) non-graphitizing carbon with well-developed pores (Adopted from Franklin (1951))

5.2.2 Pore Structure of Activated Carbon

The framework of non-graphitizing carbon/AC as shown in Fig. 5.2b shows the clear porous formed among the disordered microcrystallite layers. These pores have irregular shapes, such as slit-shaped capillaries (Chiang et al. 2001), V-shaped (Bayram and Ayranci 2010), ink-bottle shape (Dendooven et al. 2012), etc., and different sizes, which is determined by measuring the width or radius of the pores (Bansal and Goyal 2005). Basically, pores of AC are categorized into three size classes of micropores, mesopores, and macropores.

Micropores are characterized by their molecular dimensions with pore radii less than 2 nm. They typically have volume in the range 0.15–0.70 cm³/g (Bansal and Goyal 2005) with the surface area of 1300–2000 m²/g (Demiral and Demiral 2008). Their surface area becomes the major contributor of the total surface area of the ACs, and consequently they play specific role to control the sorption characteristics of the ACs. The adsorption occurring in the micropores is ruled by micropores-filling mechanism (Lorenc-Grabowska 2016; Mojoudi et al. 2019; Wang et al. 2020), where both physi- and chemisorption occur together (Alcañiz-Monge et al. 2002). This mechanism can be described as the following. The first step is physisorption phenomenon where the metal ions/adsorbates fill the micropores; in particular, the narrower pores are filled earlier (Alcañiz-Monge et al. 2002). Thereafter, the chemisorption occurs to the metal ions/sorbates which accumulated on the surface of the micropores. Accordingly, the adsorption energy becomes high (Bansal and Goyal 2005), and the adsorption is restricted to metal ions/sorbates with large radii due to being blocked to enter the micropores (Wang et al. 2020).

Mesopores are characteristically described as the following: pore radii, 2–50 nm; pore volume, 0.1–0.1 cm³/g; surface area, 10–200 m²/g (contribute to maximum 5% of total surface area of ACs) (Bansal and Goyal 2005). The adsorption occurring on the mesopores is characterized by physi- and chemisorption mechanism with lower adsorption energy and shorter equilibrium time than those of micropores (Hadi et al. 2015). These behaviors are attributed to the easier transportation of metallic ions/adsorbants towards the surface of the mesopores, and the further surface of the micropores.

Macropores have properties of >50 nm pore radii, 0.2–0.4 cm³/g pore volume, and ≤ 0.5 m²/g surface area (Bansal and Goyal 2005), and are less important for adsorption. Otherwise, they are more likely to act as conduits directing the metal ions/adsorbate towards the micro- and mesopores.

5.2.3 Chemical Composition of Activated Carbon

Typical AC contains C-atoms which bounded with O- and H-atoms as –C–OH, –C=O, –C–O–, –CO₃ and –CH (Fig. 5.3). The AC can also associate with other atoms of sulfur, nitrogen, halogens, and sometimes with cationic species of alkali, amines,

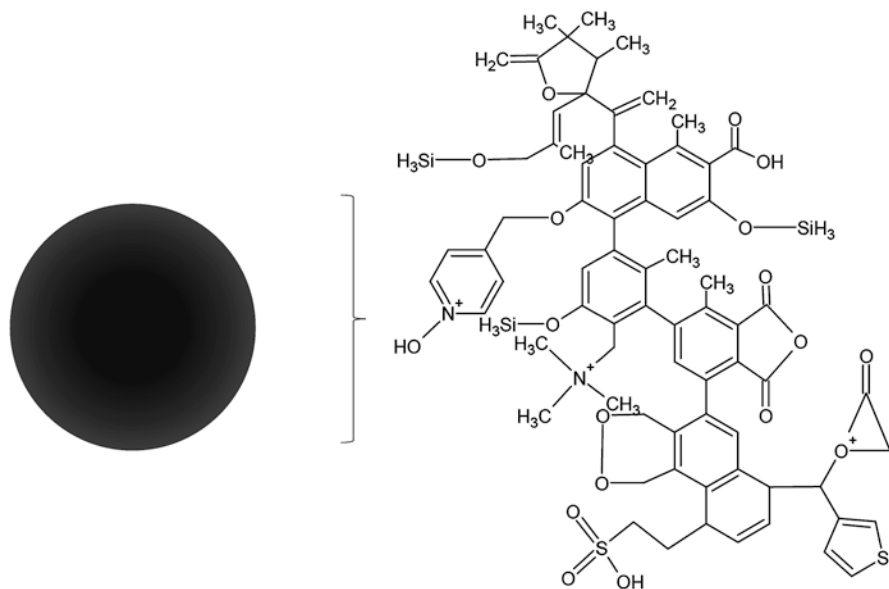


Fig. 5.3 Typical surface complex groups contained in the activated carbon

nitrobenzene, etc. on their surface (Fig. 5.3), which are derived from the carbon precursor or bonded/adsorbed during the AC preparation. These incorporated heteroatoms affect the characteristics and surface properties of the AC (Bansal and Goyal 2005). The very simple instance has been previously mentioned in Sect. 5.2.1, that the heteroatoms (oxygen, hydrogen, nitrogen, sulfur) bounded with C-atoms form the turbostratic structure of the ACs. The structural defects on the ACs for the self-doping heteroatoms have also been identified in numbers of studies (Chen et al. 2019; Hu et al. 2016). The incorporation of C-atoms with O-, S-, N-, and H-atoms forms the surface groups or surface complexes (Fig. 5.3) (Bansal and Goyal 2005), and determines the surface properties of the ACs, including wettability (Abbas et al. 2020; Liu et al. 2008), polarity (Furmaniak 2015; Rodriguez-Reinoso et al. 1992, 1997), acidity (Bagreev et al. 2001; Feng et al. 2005), chemical resistance (Szymański et al. 2002), thermal stability (Jaramillo et al. 2010), catalytic (Szymański et al. 2002), conductivity (Fan et al. 2013; Hulicova-Jurcakova et al. 2009; Xie et al. 2010), etc., which become parts of reason to the use of ACs as adsorbent.

5.3 Types and Properties of Coals as the Precursor for Activated Carbon

It is acknowledged that coal is categorized into four major types of lignite, bituminous, subbituminous, and anthracite. This categorization refers to the coal maturity, which is in strong meaning with the coalification process in nature (U.S. Geological Survey 2020) where the respective types have different physicochemical properties which affect the properties of obtained ACs when they are used as the precursors. For the sake of understanding the effect of coal types to the physicochemical properties of the AC, a brief discussion on the four types of coals is touched upon below.

Anthracite is placed in the highest rank, and characterized by its high carbon content (86%–98%) with low amount of volatile matter (2–12%) and moisture (3–6%) (Grammelis et al. 2016). The anthracite coal is hard and brittle, and has uniform wedge-shaped or narrow-neck pores (Gao et al. 2017; Liu et al. 2018a, 2018b) with average diameters of 1–50 nm (Guihong et al. 2010) and larger proportions of mesopores (38.5%) and micropores (38.5%) than macropores (23%) (Tan et al. 2020) due to the conversion of macropores to meso- and micropores during the coalification process (Guo and Guo 2018). Accordingly, the anthracite has the highest capacity for adsorption of CO₂ but the lowest capacities for water vapor and O₂ and N₂ gases (Liu et al. 2018a, b; Tan et al. 2020).

Bituminous is part of hard coals with carbon, volatile matter, and moisture contents ranging between 69–86%, 15–45%, and 2–15%, respectively (Grammelis et al. 2016). The bituminous coal has various pore shapes, such as cylindrical-, wedge-shaped, and narrow-neck pores (Liu et al. 2018a, b) with typical diameters ranging from 10 to 100 nm (Zhu et al. 2019) and proportions of 20% macro-, 40% meso-, and 40% micropores (Tan et al. 2020). The bituminous coal has higher water vapor and O₂ and N₂ gases adsorption capacities than the anthracite coal while it is expected that this coal has the lowest capacity for CO₂ gas (Liu et al. 2018a, 2018b; Tan et al. 2020).

Subbituminous is in the third rank in terms of carbon content with the approximated volatile matter and moisture contents of 25–45% and 15–30%, separately (Grammelis et al. 2016). The pores of subbituminous are predominant with mesopore range and have large variations of the shapes (silt-like/plate-like, cylindrical) (Cai et al. 2013; Nie et al. 2015).

Lignite is in the lowest place in the coal ranking system. This type of coal is characterized by its color ranging from brown to black, low carbon but high volatile matters and moisture contents (Grammelis et al. 2016). The lignite coal contains predominant macropores (Datta 2016) with largest adsorption capacities for water vapor and O₂ and N₂ gases (Liu et al. 2018a, b; Tan et al. 2020).

5.4 Preparation of Coal-Derived Activated Carbon

Figure 5.4 shows the common preparation method of coal-derived AC which can be grouped into physical and chemical-thermal preparation methods. The physical preparation is conducted through the stepwise thermal treatments of carbonization and activation. Both processes require different atmospheres; the former process is conducted at the inert atmosphere by injecting N_2 , argon, or other inert gas while the latter process is carried out at the oxidative environment while using steam (H_2O), CO_2 , O_2 , air, or their combination. In the chemical preparation, the coal is firstly impregnated with alkali (KOH, NaOH), chloride salts ($ZnCl_2$, $CaCl_2$, NaCl, KCl), phosphoric acid (H_3PO_4), or other salts ($KMnO_4$, $(NH_4)_2S_2O_8$, K_2CO_3); thereafter, the simultaneous carbonization and activation are performed simultaneously during the thermal treatment. In particular case where the minerals or ash content in the

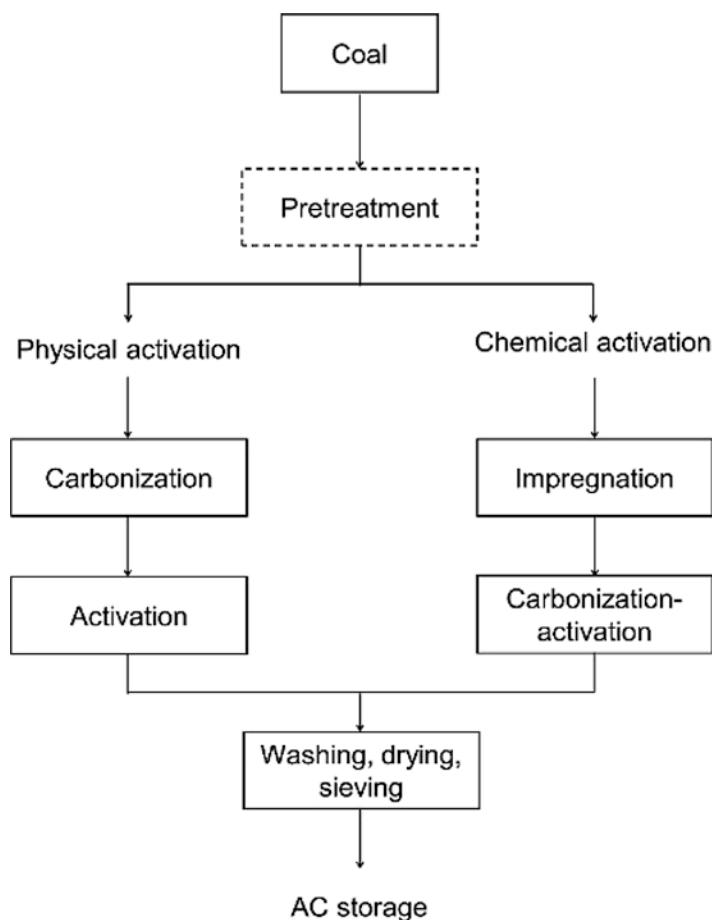


Fig. 5.4 Schematic of preparation of coal-derived activated carbon

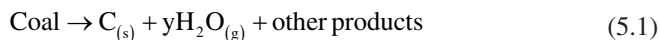
parent coals are considerably high, together with the nature thermoplastic properties of the coals, such pretreatment through oxidation or acid washing is required (Teng and Lin 1998; Teng et al. 1997; Wang et al. 2007). The pretreatment helps to form the primary pores which further assist the pore development during the thermal treatment (Wang et al. 2007).

5.4.1 Physical Preparation

Table 5.2 summarizes the carbonization and activation conditions employed during physical preparation of coal-derived AC. Both processes are further detailed as the following.

5.4.1.1 Carbonization

Carbonization, in strong meaning with pyrolysis, is aimed to decompose complex carbon groups and eliminate non-carbon compounds contained in the precursors; reaction that occurs during carbonization is simplified as Eq. (5.1). For the pyrolytic decomposition reactions, gases of H_2 , H_2O , CO_2 , CO , SO_2 , NO_x , CH_4 , C_2H_4 , etc., are released, and solid carbon-rich product of char is obtained. This char poses primary pores with the surface area range 110–120 m^2/g (Teng et al. 1997); these pores are conduits for the further pore development when undergoing the subsequent activation process.



Generally, carbonization is carried out in the temperature range 600–700 °C, heating rate 20–30 °C/min, and holding time of 1 h. As the carbonization significantly affects the properties of the final AC products, the operational parameters, viz. temperature, heating rate, gas flow rate, and holding time must be carefully maintained. Details on these parameters are addressed in Sect. 5.4.3.

5.4.1.2 Activation

After carbonization, the obtained char is subjected to the activation process. Here, activation refers to the thermal/gasification where O_2 -rich air, CO_2 , or H_2O steam is used as the activating agent. Reactions occurring during the activation process involve the selective oxidation of carbon to CO_2 (Eqs. 5.2–5.4) at temperature range 800–1000 °C for the typical reaction time of 1–2 h (while in several reports, longer reaction time is required (Table 5.2)), allowing to open the inaccessible pores, develop new pores, and widen the primary pores generated during carbonization

Table 5.2 Comprehensive studies on the physical preparation of coal-derived activated carbon

Precursor	Sample characteristics	Pre-oxidation/ pretreatment	Carbonization condition	Activation condition	Activated carbon characteristics	Highlight	Reference
Anthracite	<ul style="list-style-type: none"> Particle size (mm), <0.074 Chemical analysis (wt.%), VM = 7; ash, 2.5. 	–	1st step: N ₂ , 600 °C for 45 min Second step: N ₂ , 880 °C for 45 min	H ₂ O, 880 °C for 5 h	<ul style="list-style-type: none"> Surface area (m²/g), 817.6–1074 Pore volume (cm³/g), 0.43–0.58 with proportion of 90% micropores 	• Ni(NO ₃) ₂ was added to enhance the magnetic property of the AC • Ni catalyzed the carbonization and activation rate.	Zhang et al. (2011)
Bituminous	<ul style="list-style-type: none"> Particle size (mm), 0.4–1 Chemical composition (wt.%), C = 78.9; H = 5.4; O = 11.8; N = 3.3; S = 0.6. 	Preoxidation using air at 185 °C for 24 h	N ₂ , 900 °C with the flow rate of 30 °C/min	CO ₂ , 900 °C	<ul style="list-style-type: none"> Surface area (m²/g), 190–950 Pore diameter (nm), 2.0–2.2 	<ul style="list-style-type: none"> Development of surface area and pore diameter was a function of burning off level. 	Teng and Lin (1998)
Bituminous	<ul style="list-style-type: none"> Particle size (mm), 210–300 Chemical composition (wt.%), C = 78.9–83.2; H = 5.1–5.4; O = 7.4–11.8; N = 3.3–4.0; S = 0.6–0.8 	Preoxidation using O ₂ 200 °C for 6 h	CO ₂ , 800–950 °C with heating rate of 30 °C/min	CO ₂ , 950 °C	<ul style="list-style-type: none"> Surface area (m²/g), 496–704 Pore diameter (nm), 2.0–2.4 	<ul style="list-style-type: none"> The oxidation degree decreased with increasing the O/C ratio of the raw coals Preoxidation provided larger surface area 	Teng et al. (1997)
Bituminous	<ul style="list-style-type: none"> Particle size (mm), 0.85–1.4 Chemical composition (wt.%), C = 90.9; H = 1.2; O + S = 6.3; N = 1.6 	–	N ₂ , 900 °C for 1 h	CO ₂ , 900 °C for 1–15 h	<ul style="list-style-type: none"> Surface area (m²/g), > 1200 Pore diameter (nm), 0.35–0.4 	<ul style="list-style-type: none"> Atomic layers increased along with the increase of surface area 	Yoshizawa et al. (2000)

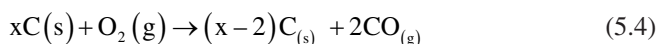
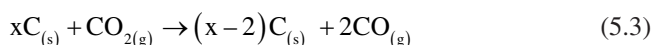
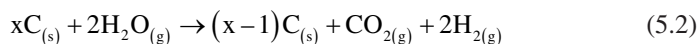
(continued)

Table 5.2 (continued)

Precursor	Sample characteristics	Pre-oxidation/ pretreatment	Carbonization condition	Activation condition	Activated carbon characteristics	Highlight	Reference
Bituminous	<ul style="list-style-type: none"> Particle size (μm), 75–1000 Chemical composition (wt.%), C = 80.2; H = 5.3; O = 9.5; N = 1.5; S = 3.5 	–	N ₂ , 600–900 °C with heating rate of 30 °C/min	H ₂ O, 650–750 °C	<ul style="list-style-type: none"> Surface area (m^2/g), 226.2 	<ul style="list-style-type: none"> Activation by steam increased the adsorption capacity of the AC 	Akash and O'Brien (1996)
Bituminous	NA	–	–	H ₂ O, 1000 °C for 6 h	<ul style="list-style-type: none"> Surface area (m^2/g), 857.1 Total pore volume (cm^3/g), 4.5×10^{-1}. 	–	El Qada et al. (2006)
Bituminous	<ul style="list-style-type: none"> Particle size (μm), 71–1000 Chemical composition (wt.%), C = 83.6; H = 5.1; O = 10; N = 1.1 	Preoxidation using air at 150–270 °C for 4–28 h	N ₂ , 700 °C for 1 h	H ₂ O, 800 °C for 6 h	NA	<ul style="list-style-type: none"> Carbonyl groups formed and α-CH₂ groups decreased during preoxidation. 	Wang et al. (2007)
Bituminous	<ul style="list-style-type: none"> Particle size (mm), <1.65 Chemical composition (wt.%), C = 77.1; H = 5.61; O = 16.3; N = 0.5; S = 0.5 	–	N ₂ , 800–950 °C for 2–5 min	H ₂ O, 880 °C for 4 h	<ul style="list-style-type: none"> Iodine adsorption capacity, 1000 mg/g 	<ul style="list-style-type: none"> Increasing carbonization temperature decreased the AC yield 	Kim et al. (1997)

Precursor	Sample characteristics	Pre-oxidation/pretreatment	Carbonization condition	Activation condition	Activated carbon characteristics	Highlight	Reference
Subbituminous	<ul style="list-style-type: none"> Particle size (μm), 325 Chemical composition (wt.%), C = 89.4–90.6; H = 3.9–6.9; O = 2.7–5.2; N = 0.8–1.2 	–	N ₂ , 630 °C for 0.5 h	1st step: CO ₂ , 600 °C for 20 min; Second step: H ₂ O, 900 °C for 2 h; Third step: H ₂ O, 950 °C for 2 h	<ul style="list-style-type: none"> Surface area (m^2/g), 1215–1223 Pore diameter (nm), 23.3–35.8 	<ul style="list-style-type: none"> FTIR analysis provided the information of carboxylic, phenolic, hydroxyl and carboxylic-OH groups 	Li et al. (2014)
Subbituminous	<ul style="list-style-type: none"> Particle size (μm), 210–300 Chemical composition (wt.%), C = 71; N = 1.1; H = 5.7; O = 22; S = 0.1 	–	N ₂ , 700–950 °C with heating rate of 30 °C/min	CO ₂ , 700–950 °C for 0.5 h	<ul style="list-style-type: none"> Surface area (m^2/g), 453–988 Pore diameter (nm), 1.92–24.1 	<ul style="list-style-type: none"> The maximum surface area and pore formation occurred at 750 °C, and decreased at the thereafter temperature Pore structure development could be controlled by activation temperature 	Teng and Lin (1998)
Lignite	<ul style="list-style-type: none"> Particle size (mm), < 0.2 Chemical composition (wt.%), C = 62.3–64.8; H = 5.4–5.7; O + S = 28.9–31.6; N = 0.6. 	–	Ar, 700 °C for 1 h	1st step: H ₂ O, 800–850 °C; Second step: Ammonia, 300–350 °C for 5 h	<ul style="list-style-type: none"> Surface area (m^2/g), 840–1000 Pore diameter (nm), 2.0–2.2 	<ul style="list-style-type: none"> Ammonoxidation aims to introduce nitrogen content to the AC, and takes place extensively during the first hour of the process Ammonoxidation increases the basicity of the surface of AC 	Pietrzak et al. (2007)

process; all these process increase the properties of AC (surface area, pore volume, pore size). Parameters of operational temperature, activating agent flow rate/dosage and reaction time affect in similar way to that of carbonization process on the AC yield (Teng et al. 1997; Yoshizawa et al. 2000) while selection of the activating agent appears to be the most important consideration. In terms of pore development process, H₂O steam is the most efficient to be employed as the activating agent (Akash and O'Brien 1996; Kim et al. 1997; Pietrzak et al. 2007; Wang et al. 2007). This is contributed to the smaller size of water molecule, leading to easier transportation of the molecule within the pores (Nor et al. 2013). And using the H₂O steam could result in faster kinetic reaction (two or three times) (Nor et al. 2013), making the process advantageous for the shorter reaction time.



5.4.2 Chemical Preparation

The chemical preparation refers to the process where activating agents (KOH, NaOH, ZnCl₂, CaCl₂, NaCl, KCl, H₃PO₄, KMnO₄, (NH₄)₂S₂O₈, K₂CO₃) are involved for preparing the AC; among them, ZnCl₂, H₃PO₄, NaOH, and KOH are the most common activating agents used. Impregnating the coal with these activating agents allows to lower the temperature required for the carbonization/activation. Basically, the chemical preparation is done at a temperature of 400–600 °C for ZnCl₂ and H₃PO₄ or 800–1000 °C for NaOH and KOH with the reaction time of 1–3 h. It is worth noting that the chemical reaction between the coal and activating agent is essential to determine the pore development process during carbonization-activation while operational parameters of thermal process play a role to extend the reactions (Molina-Sabio and Rodriguez-Reinoso, 2004). Therefore, it is worthwhile to pay greater attention to the effect of different activating agents used on the physico-chemical properties of the obtained ACs; this is addressed in Sect. 5.4.3.

The impregnation method is another consideration for the chemical preparation of AC. There are two types of impregnation methods, depending on the absence/presence of water during the process: physical and chemical impregnation. The physical impregnation, in strong correlation with physical mixing, is conducted by directly mixing the coal with the activating agent at room temperature; no water is added during the mixing. In the chemical impregnation, the coal is mixed in the solutions of activating agents; the mixing is performed at temperatures 50–60 °C, and followed by such drying process at temperature 110 °C prior the carbonization-activation process. The later impregnation method is advantageous over the first

method for the deeper penetration of activating agents into the surface of coal through their primary pores, and commonly applied in the works related to the chemical preparation of AC from various precursors.

Always, the obtained AC after the thermal process is washed to eliminate the remaining activating agents in the AC (Fig. 5.4) and allow to open the pores developed during the thermal process. The washing is basically carried out using acid or alkaline, depending on the type of activating agents used. In the final stage, the AC is washed with water to completely remove the remaining chemicals and control the pH of the AC. Table 5.3 presents comprehensive studies on the chemical preparation of coal-derived AC.

5.4.3 Effects of Carbonization-Activation Parameters on the Pore Development of Coal-Derived Activated Carbon

Pore properties (shape, volume, surface area) are the key drivers of implementing such adsorbents for the adsorption process. Here, discussions on the parameters affected the pore development during the coal-derived AC preparation, either through physical or chemical preparation, including pretreatment, coal/coal-based precursor types, activating agents (type, dosage) and thermal treatment variables are presented.

5.4.3.1 Effect of Pretreatment of the Coals

Pretreatment is an effort to enhance the physicochemical properties of the coal/coal-based precursors for the success of pore development process during the thermal process (Wang et al. 2017). The pretreatment is performed either through pre-oxidation involving oxygen-bearing gases or washing with mineral acid solutions.

- *Pre-oxidation*: Pre-oxidation is aimed to eliminate the thermoplastic properties of coals, which specifically appear in caking (bituminous, semianthracite–anthracite) coals. These particular properties are advantageous for coke-making but undesirable for the coal-derived AC production as they limit the pore development process. The process may occur naturally during coal stockpiling for the weathering (Aich et al. 2019; Maloney et al. 1982) or artificially by contacting the coal/coal-based precursors with oxygen-bearing gases at certain conditions (Pis et al. 1998; Ruiz et al. 2006; Teng et al. 1997; Worasuwanarak et al. 2002).

The natural weathering of coal, refer to the low-temperature oxidation, is a complex process (Worasuwanarak et al. 2002), involving oxidation of benzylic and aliphatic groups to carbonyl and carboxylic groups (Painter et al. 1980; Rhoads et al. 1983; Worasuwanarak et al. 2002), and even more complicated mechanisms

Table 5.3 Comprehensive studies on the chemical preparation of activated carbon

Precursor	Sample characteristics	Reagent	Activation method	Carbonization condition	Activated carbon characteristics	Highlight	Reference
Anthracite	<ul style="list-style-type: none"> Particle size (μm), 600–1000 Chemical composition (wt.%), ash = 11 	KOH	Impregnating the anthracite in KOH solution (1–5 g/10 ml) at the ratio of KOH/anthracite 1:1–5:1 for 2 h at 60 °C	N_2 , 800 °C for 2 h	<ul style="list-style-type: none"> Surface area (m^2/g), 2021–3290 Micropore distribution, 0.77–0.93 	<ul style="list-style-type: none"> Pore size greatly depended on the KOH amount and temperature The higher KOH amount reduced the micropore distribution while the increasing temperature resulted in the opposite direction 	Lozano-Castello et al. (2001)
Anthracite	<ul style="list-style-type: none"> Particle size (mm), < 0.6 Chemical composition (wt.%), C = 82.1–89.7; H = 3.1–3.2; O = 5.1–13.2; N = 1.1–1.2; S = 0.6–0.8 	NaOH	Impregnating the samples in NaOH solution with different NaOH/anthracite ratio (1:1–4:1) for 2 h at 60 °C	N_2 , 730 °C for 1 h	<ul style="list-style-type: none"> Surface area (m^2/g), 1045–2669 Pore volume (cm^3/g), 0.42–1.04 	<ul style="list-style-type: none"> Increasing the NaOH/coal ratio increased the adsorption capacity of the obtained AC Porosity development was higher when the coal had higher mineral content 	Lillo-Ródenas et al. (2001)
Anthracite	<ul style="list-style-type: none"> Particle size (μm) < 147 Chemical composition (wt.%), C = 61; H = 3.7; O = 27.5; N = 0.6; S = 1.5 	KOH	Mixing KOH/coal at a ratio of 1:3	Vacuum, heating at 693 W for 10 min	<ul style="list-style-type: none"> Surface area (m^2/g), 1770.5 Pore diameter (nm), 2.82 	<ul style="list-style-type: none"> The nature basicity of the AC was due to the KOH Carboxylic, lactonic and phenolic groups were detected on the surface of the AC 	Xiao et al. (2015)

Precursor	Sample characteristics	Reagent	Activation method	Carbonization condition	Activated carbon characteristics	Highlight	Reference
Anthracite	<ul style="list-style-type: none"> Particle size (μm), < 75 Chemical composition (wt.%), C = 86.8; VM = 5.8; ash = 5.7 	KOH	Mixing KOH/coal at ratio of 3:1, followed by drying at 400 °C for 1.5 h	N ₂ , 600–1000 °C for 2 h	<ul style="list-style-type: none"> Surface area (m^2/g), 2195–2398 Pore volume (cm^3/g), 0.99–1.5 	<ul style="list-style-type: none"> Preoxidation favored the pore development Using anthracite resulted in larger surface area than coals with lower ranks 	Zou and Han (2001)
Bituminous	<ul style="list-style-type: none"> Particle size (mm), 1.0–1.2 Chemical composition (wt.%), C = 77.7; H = 5.5; O = 10.4; N = 1.4; S = 5.3 	KOH	Mixing KOH/coal at a ratio of 3:1	N ₂ , 600–800 °C for 2 h	<ul style="list-style-type: none"> Surface area (m^2/g), 1906–1995 Pore diameter (nm), 2.82 	<ul style="list-style-type: none"> Pre-drying affected the carbonization behavior 	Jibril et al. (2007)
Bituminous	<ul style="list-style-type: none"> Chemical composition (wt.%), C = 83.2; H = 5.1; N = 3.7; O = 7.4; S = 0.6 	H ₃ PO ₄	Mixing the coal in H ₃ PO ₄ solutions with different concentrations (20%–80%) at 50–85 °C for 1–3 h	N ₂ , 400–600 °C for 1–3 h	<ul style="list-style-type: none"> Surface area (m^2/g), 510–551 Pore volume (cm^3/g), 0.28–0.3 	<ul style="list-style-type: none"> Time and temperature of carbonization affected the pore development Increasing the H₃PO₄ widened the pores 	Teng et al. (1998)
Lignite	<ul style="list-style-type: none"> Particle size (μm), 100–150 Chemical compositions (wt.%), C = 62.0–67.4; VM = 31.0–34.2; ash = 0.5–5.0 	KOH-ZnCl ₂ /NH ₄ Cl	Pretreating the samples in HCl, HF and NaOH solution. Thereafter, the coal was washed in KOH solution at 85 °C for 2 h, followed by mixing with ZnCl ₂ /NH ₄ Cl at activating agent/coal ratio of 3/1	N ₂ , 650–750 °C for 1 h	<ul style="list-style-type: none"> Surface area (m^2/g), 830.5–1200 Pore diameter (nm), 1.9–2.0 	<ul style="list-style-type: none"> Surface area increased with increasing the temperature Activation using ZnCl₂ resulted in AC with large surface area 	Kopac and Toprak (2007)

(continued)

Table 5.3 (continued)

Precursor	Sample characteristics	Reagent	Activation method	Carbonization condition	Activated carbon characteristics	Highlight	Reference
Lignite	<ul style="list-style-type: none"> • Particle size (mm), 0.09–0.125 • Chemical composition (wt.%), C = 51.4; S = 9.52; VM = 25.7 	ZnCl ₂ , CaCl ₂ , NaCl, KC	Mixing of coal with activating agent in HCl solution	N ₂ , 750 °C for 2 h	<ul style="list-style-type: none"> • Surface area (m²/g), 942 • Pore diameter (nm), 0.98 	<ul style="list-style-type: none"> • FTIR analysis showed the presence of carboxylic groups • ZnCl₂ was the most efficient activating agent 	Usmani et al. (1996)

(Larsen et al. 1986). The process occurs in slow kinetic reactions; therefore, its effects on the pore development are difficult to be directly observed (Pisupati and Scaroni 1993).

In order to increase the oxidation reaction rate and elucidate the effects of pre-oxidation on the pore development, artificial coal pre-oxidation with air (Parra et al. 1996; Pis et al. 1998; Ruiz et al. 2006; Serrano-Talavera et al. 1997; Teng and Lin 1998; Wang et al. 2007), O₂-rich gas (Teng et al. 1997), and mixed O₂-N₂ (Worasuwanarak et al. 2002) at an elevated temperature for a determined reaction time were reported. Non-oxidized and oxidized semianthracite coals (particle sizes, 1–3 and 0.125–0.425 mm; temperature, 270 °C; duration, 1–7 days; source, forced-air) were pyrolyzed under N₂ atmosphere at 850 °C with heating rate of 60 °C/min (Ruiz et al. 2006). The chars from oxidized coals have a wide micropore distribution with the surface area range 334–441 m²/g, increasing with the increase of oxidation duration and smaller particle size (Ruiz et al. 2006). In contrast, the obtained chars from fresh coal were present with macropores (surface area of 149 m²/g) and a lot of vacuoles on its surface which prevented the pore development. These were in well agreement with the results portrayed in studies by Pisupati and Scaroni (1993) (pre-oxidation conditions: coal type, bituminous; temperature, 200 °C; time, 2 and 72 h), Worasuwanarak et al. (2002) (coal type, bituminous; temperature, 250–330 °C; heating rate, 5 °C/min), Wang et al. (2007) (coal type, bituminous; temperature 150–270 °C; time, 4–28), Teng et al. (1997) (coal type, bituminous; temperature, 200 °C; time, 6 h), and others, to state that the pre-oxidation could improve the micropore distribution and surface area of resulted chars and ACs after carbonization-activation in the typical conditions (Sect. 5.4.1).

During the pre-oxidation process, only CO, CO₂, and H₂O gases were produced (Worasuwanarak et al. 2002). This implies that –OH and –CH groups contained in the cross-links of macromolecular parent coals were consumed (Larsen et al. 1986; Painter et al. 1980; Rhoads et al. 1983; Worasuwanarak et al. 2002), making the pore development process during carbonization-activation easier as the complex cross-links have been deconstructed. Inevitably, for the gas-solid chemical reactions of the oxygen and coal, particle size of the coal is an essential factor during the pre-oxidation. Accordingly, smaller particle size of coal could accelerate the oxidation reaction rate (Ruiz et al. 2006). The coal with particle size of 0.125–0.425 mm could reach a complete oxidation reaction within 1 day while the coal with larger particle size needed 5–7 days to obtain the similar conversion degree (Ruiz et al. 2006) because smaller particles had higher value of specific heat capacity ($C_p \frac{\partial T}{\partial t}$) (Li et al. (2014), as confirmed in studies (Akgün and Arisoy 1994; Gomez et al. 2014; Jiang et al. 2000; Teng and Hsieh 1998). However, the size of coal particles oxidized should be controlled at certain size to meet the requirement of final AC products. The typical activated carbon used for adsorption of metals from aqueous solution is granular activated carbon (GAC) with the effective size of 0.5–7 mm. Using fine coal particles is also disadvantageous to the lower AC yield and problems related to coal dust.

- **Acid washing.** Minerals/ashes (inorganic compounds) contained in the coals extremely affect the carbonization-activation behavior and physicochemical properties of the obtained AC. Studies show that the increase of minerals/ash content reduce the micropore distribution and surface area of the AC (Wang et al. 2019). Therefore, attempts to reduce the minerals/ash content in the parent coal/coal-based precursors have been being carried out by washing using strong mineral acids of HCl, HF, HNO₃, etc. Sometimes, multiple washing processes were performed to ensure the removal of the unnecessary constituents in the coals. A two subsequent acid leaching using HCl (HCl conc., 17 wt.%; temperature, 55–60 °C; time 30 min) and HF (HF conc., 48 wt.%; temperature, 55–60 °C; time 30 min) was applied to reduce the ash content from a bituminous coal (Linares-Solano et al. 2000). The parent and washed coals were carbonized (850 °C) under N₂ atmosphere and activated (850 °C) using CO₂ and H₂O steam; it is remarkable that the AC obtained from the washed coal yielded higher micropore distribution (surface area (m²/g), 1100) than the parent coal (surface area (m²/g), 800). The washing conditions are dependent on the characteristic of the coals used. Kopac and Toprak (2007) processed coals with ash content of 4.5–4.9 (wt.%) from local mining in Turkey in the subsequent HCl (15% at 60 °C for 1 h) and HF (25% at 60 °C for 2 h) washing processes; thereafter the ash content attained to be 0.4–0.5 (wt.%), and the surface area of the coals increased from 0.0008–1.2 to 0.95–1.2 m²/g. When the washed coals were chemically activated with mixed KOH and NH₄Cl at 750 °C under N₂ atmosphere, the surface area of the ACs attained to be 830.5 m²/g. Other studies, as the following: Ahmadpour and Do (1997) (coal samples: bituminous (ash (wt.%), 11.5); acid washing: 1.0 N HCl/H₂SO₄ at 1/1 for 2 days; activation: 25%–200% KOH/ZnCl₂ at temperatures 750–900 °C for 2 h), Musyoka et al. (2020) (samples: bituminous; acid washing: 20% HF for 2 h in the first stage, 10% HF in the second step, and 10% HCl in the third step for 12 h each steps at 55 °C; activation: KOH/treated CFA ratio of 4:1 at 800 °C for 1 h), Lv et al. (2020) (coal samples: bituminous (ash (wt. (%), 5.5); acid washing: 15% HCl at 80 °C for 6 h in the first step, and 40% HF at 70 °C for 6 h in the second step; activation: KOH/coal ratio of 1/1 at 750–950 °C for 30 min), Starck et al. (2006) (coal samples: lignite (mineral matter (wt.%), 6.2); acid washing: 5.0 N HCl in the first step, 22.0 N HF in the second step and 12.0 N HCl in the third step under heating; carbonization: 800 °C for 1 h; activation: H₂O at 700–800 °C for 70 min), proclaimed the similar results, that acid washing was effective to remove the inorganic compounds contained in the coal/coal-based precursors.

It is worth mentioning that the removal of inorganic compounds occurs through the dissolution/leaching reactions. The XRD analysis revealed that peaks of quartz, mullite, magnetite, and other inorganic phases in the parent coals disappeared after the acid washing (Liu et al. 2018a, b; Musyoka et al. 2020), in agreement with the SEM images which showed that there were a lot of open spaces on the surface of the washed coals (Musyoka et al. 2020), and the surface become dense and smooth (Liu et al. 2018a, b). To eliminate the side effects of remaining acid in the washed coals

on the thermal preparation, particularly when the chemical activation using alkali is chosen, the treated coals need to be washed thoroughly using water and dried prior performing the thermal processes. Other option related to the acid washing is to perform after carbonization-activation (Fig. 5.4), which can be suitable to the ACs after chemical preparation method (Wang et al. 2019).

5.4.3.2 Effect of Coal Types

As addressed in Sect. 5.3, each coal types has their specific physicochemical properties which extremely affect the carbonization-activation behavior and the properties of AC products. An instance has been addressed earlier related to the thermoplastic properties of the caking coals, and inorganic compounds in the parent coals (Sect. 5.4.3.1). Following the complex physicochemical properties of the coals, they are worth encouraging to be investigated.

There are many entities regarding the effect of coal types on the obtained chars. Coals with higher O/C ratio possess lower occurrence of caking effect to affect the efficacy of carbonization process. To confirm, three different coal samples with O/C atomic ratios of 0.11, 0.074, and 0.067 were carbonized under the following conditions: N₂, 800–950 °C, 30 °C/min (Teng et al. 1996); the obtained chars had surface areas of 10, 2 and < 1 m²/g, decreasing with the decrease of O/C ratios. A support by TGA analysis revealed that the coal with the highest O/C atom ratio had the lowest peak temperature (temperature where volatilizing reaches a maximum); the peak temperatures were 470, 479, and 505 °C for the respective coals, indicating that oxygen plays a role to determine the volatilization during carbonization. And during activation (CO₂, 900 °C), it was noticed that the reactions occurred stronger to the char from the coal with higher O/C atom ratio, the burn-off degree (64–70%) and micropore distribution (surface area range 432–1171 m²/g) increased with the increase of O/C atom ratios.

Studies found that low-rank coals note a higher weight loss than high-rank coals. Lignite and subbituminous coals were used to prepare the ACs through physical preparation (carbonization: Ar, 700 °C, 10 min, 25 °C/min; activation: H₂O steam, 700 °C, 30 min) (Gombojav et al. 2020); the AC yield as of 38.8% obtained from the lignite coal as compared to the subbituminous coal (56.1%), but the surface area of the first AC was higher than the latter AC (522 and 214 m²/g, respectively). A confirmation by FT-IR analysis portrayed that the phenolic compounds in the subbituminous were not decomposed, and the aromatization and condensation occurred, making the pores could not be developed efficiently. While using pre-oxidized samples of lignite, subbituminous and semi-anthracite coals as the AC precursors (6.0 M HNO₃ solution at 100 °C for 6 h) and chemical preparation KOH (5–30 wt.%) in water (0.5–3.0 cm³) at 700 °C at the heating rate of 5 °C/min and holding time of 1 h) (Alcaniz-Monge et al. 2010), the similar occurrence of the increase of weight loss as the decrease of coal rank was obtained. In line, the micropore distribution increased with the lower coal rank. Similar tendencies were reported in other studies under the conditions as the following: Illán-Gómez et al. (1996) (coal

samples: anthracite, high VM bituminous, low VM bituminous, subbituminous-lignite; activation: KOH, 500–700 °C, 5 °C/min, 1–2 h), Dalai et al. (1996) (coal samples: high VM bituminous, subbituminous, lignite; activation: H₂O steam, 700–850 °C for 0.5–4 h), Purevsuren et al. (2017) (coal samples: anthracite, bituminous, subbituminous, lignite; carbonization: N₂, 700 °C; activation: H₂O steam at 800 °C for 2 h), and others.

The conclusion above is attributed to the higher reactivity of low-rank coals towards the activating agents during the thermal processes. Additionally, this is in line with the fact that the cross-links in the low-rank coals, particularly aliphatic groups, are more readily evolved to form new pores and maintain the primary pores which are from the parent coals or opened during the pretreatment stage (Alcaniz-Monge et al. 2010; Illán-Gómez et al. 1996).

5.4.3.3 Effect of Activating Agents

– *Gaseous activating agents*: The performance comparison among the gaseous activating agents has been briefly touched upon in Sect. 5.4.1.2 with the H₂O steam being apparently the most efficient activating agent to develop the AC pores (Akash and O'Brien 1996; Kim et al. 1997; Pietrzak et al. 2007; Wang et al. 2007). The considerable reasons for this conclusion can be ascribed as the following. The reaction (5.3) during CO₂ activation majorly occurs on the surface of the chars to develop new pores (Zhou et al. 2019), and consequently the reactions are slower for the dense cross-links on the surface of the chars. In contrast, the reaction (5.2) happens inside of the char matrix as the H₂O is more prone to diffuse (Zhou et al. 2019), making the reaction occurs faster to enlarge the primary pores to mesopores while at the same time develop micropores. This is well-agreed with the SEM studies (Guizani et al. 2016; Zhou et al. 2019), that the AC produced after CO₂ activation has a sponge-like surface, while that after H₂O steam activation has an intact and smooth surface with only some alterations observed near periphery of the primary pores. The faster kinetic reaction during H₂O steam activation is also attributed to the more sensitivity of H₂O steam to the minerals in the coals. For instance, when calcium compounds are present in the chars/coals, they react with the H₂O steam to catalyze the formation of the mesopores or wide micropores (Zhou et al. 2019). Other elements of potassium, sodium, and magnesium give a similar impact on catalyzing the H₂O activation reactions, as reported by many (Feng et al. 2016; Miura et al. 1989; Yu et al. 2020). And also, the faster kinetic reaction using H₂O steam is due to the weak H–O bonding in water than the C=O bonding in CO₂ (Everson et al. 2006). H₂O is also well known to have high emissivity to enhance the heat transfer (Yi et al. 2014).

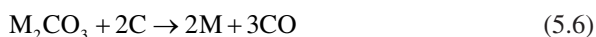
In short, the pore development using CO₂ occurs through the stepwise processes of pore opening and micropore development, while the pore development using

H₂O steam happens through the widening of the primary pores and micropore development. This description says that selecting H₂O steam as the activating agent must be preceded with an effective primary pore development process. Therefore, such pretreatments to the coal are strongly recommended (Yu et al. 2020), making the AC preparation downstream become more complex. And the obtained AC is often found to have lower micropore volume than those after CO₂ activation (Rodríguez-Reinoso et al. 1995), which may be overcome by operating the activation at high temperatures (Table 5.2).

With the pros and cons in the use of CO₂ or H₂O steam as the gaseous activating agent, attempts to combine both gases (Hecht et al. 2012; Jayaraman and Gokalp 2015) or conduct the stepwise CO₂-H₂O activation (Zhou et al. 2019) were reported. This idea relies on the explanation above; using CO₂ provides new pores to allow the H₂O to diffuse and react with the carbon. The reactions are faster, and the obtained ACs are superior with well-developed pores (Hecht et al. 2012; Jayaraman and Gokalp 2015; Zhou et al. 2019).

- *Chemical activating agent:* Given that NaOH, KOH, ZnCl₂, and H₃PO₄ are commonly used for activation purpose of coal-derived ACs (Table 5.3), the respective chemical reagents present different behaviors during the chemical preparation of coal-derived AC. The KOH is superior to produce AC with high micropore distribution, volume and surface area with the maximum temperature 700–800 °C. The AC with the surface area of 3100 m²/g was obtained from a lignin coal after chemically preparing using KOH at operational temperature of 700 °C (Fierro et al., 2008), in accordance with those reported in other studies (Table 5.3). While comparing to NaOH, KOH is more excellent. Using the same sample and experimental condition while replacing the KOH to NaOH, for instance, AC with lower surface area (2400 m²/g) was obtained (Fierro et al. 2008). Anthracite coal was also used to prepare ACs through chemical activation using KOH and NaOH; the obtained ACs had surface areas of 2750 and 2700 m²/g, respectively (Lillo-Ródenas et al. 2001). Reasons of this behavior can be ascribed as the following. It is worth noticing that the activations using KOH and NaOH occur through the similar behavior (Yahya et al. 2015), where the KOH/NaOH atom intercalate in the cross-links and play roles as donor electron to encourage the gasification reaction (Eq. 5.5), and the oxygen contained in the KOH/NaOH plays a role as an accelerator. However, KOH is more volatile and readily oxidized than NaOH (Fierro et al., 2008), making the reaction between the KOH and carbon atoms easier. This is in accordance with the thermodynamic point of view; that the Gibbs free energy of reaction with KOH starts to be a negative value at temperature 620 °C ($\Delta G_{893K} = -0.17$ kJ) while that involving NaOH is at temperature 960 °C ($\Delta G_{1233K} = -0.55$ kJ). By this fact, the charring occurs more readily than the activation reaction when the thermal treatment is conducted using NaOH (Fierro et al., 2008). Although the Na⁺ has smaller ionic radius (0.102 nm) than K⁺ (0.138 nm) which implies that the Na⁺ is easier to

diffuse into the char matrix and result in narrower micropores, the activity of the by-product Na_2CO_3 is much slower than K_2CO_3 (Hayashi et al. 2000). The K_2CO_3 by-product may help the char gasification through Eq. (5.6) to widen the primary pores and open new pores.



where M is the alkali, either K or Na.

Comparing to the alkali metal reagents, ZnCl_2 and H_3PO_4 are less favorable to be used in the coal-derived AC preparation. Instead, they are more suitable to be applied to the precursors which are less carbonized, such as lignocellulosic materials (Yahya et al. 2015). Using the ZnCl_2 and H_3PO_4 as the activating agent is characterized by the lower operational temperature; the maximum pore development could be reached at 500–600 °C (Hayashi et al. 2000) and the variation depends on the type of the coals, resulting in AC with similar surface as those of commercial AC. Even so, it is worth noticing that using ZnCl_2 can produce AC with higher surface area than H_3PO_4 . As confirmed by Usmani et al. (1996), when the activation was operated at 650 °C, coal/ ZnCl_2 ratio of 1/2 and 1 h duration, the obtained AC had surface area of 942 m^2/g , which was considerably higher than that reported by Teng et al. (1998) while using H_3PO_4 to perform the carbonization-activation at 500 °C for 3 h; the obtained AC had surface area of 551 m^2/g . This is due to the difference in mechanisms involved. Using ZnCl_2 as the activating agent involves water consumption/dehydrogenation to promote the modification of cross-links in the coals and increase the surface area; the process even starts at low temperature (< 200 °C) (Ahmadpour and Do 1997). Here, ZnCl_2 acted as a Lewis acid to increase the evolution reactions of molecular hydrogen in the cross-links and result active sites on the modified spots (Allothman et al. 2011). On the other hand, using H_3PO_4 could result in the pyrolytic decomposition and cross-link reformation (Teng et al. 1998; Wang et al. 2011), making the cross-link lost the hydrogen, oxygen, and sulfur atoms to accelerate the aromatization through phosphate ester groups and develop the micropores to mesopores.

A conclusion is thus derived that the effectiveness degree of the chemical activating agents to be used in the coal-derived ACs follows the order of $\text{KOH} > \text{NaOH} > \text{ZnCl}_2 > \text{H}_3\text{PO}_4$. Eventhough the process using KOH and NaOH undergoes at high temperatures, the process is apparently more environmentally friendly (Yahya et al. 2015). And the remaining KOH/NaOH can be easily washed out using acid while also helps to enhance the AC pore characteristics (Wang et al. 2019).

5.4.4 Effects of Thermal Treatment Parameters

Parameters of temperature, heating rate, gas flow rate/activating agent dosage, and holding time affect significantly on the AC pore development and properties. The significant order of these parameters is observed as the following: temperature > heating rate > reagent dosage > holding time.

- *Temperature*: Temperature is essential to determine the success of both physical and chemical preparation and affects the properties of the AC produced. In general, the higher operational temperature decreases the char/AC yield as more carbon is burned-off, while the lower temperature leads to the incomplete conversion of the carbon groups in the parent coals; moisture, volatiles, and tar remain in the obtained char/AC.

Bituminous coal was used to prepare ACs through physical preparation using steam under four different carbonization temperatures (600, 700, 800, and 900 °C) (Akash and O'Brien 1996). Predictably, the higher weight losses occurred at higher temperatures. Another highlight is that there were substantial drops in H- and O-atoms contained in the chars as the temperature increased; carbon content increased along with the increase of temperature; N- and S-atom contents were not affected by varying the temperatures. These behaviors imply that the charring occurs due to the steam formation (Yahya et al. 2015).

Other coal type, subbituminous coal, was used as the feed of carbonization in the presence of CO₂ gas (Teng et al. 1997, 1998). The increase of the burn-off percentages and the developments of pore properties (surface area, volume, size distribution, average diameter) with the increase of carbonization temperature were noted. However, when the burn-off percentages enhanced to above 50%, the surface area, pore volume, and micropore distribution decreased which was in contrast to the mesopore distribution and average diameter. When bituminous coal was used, the similar parabolic tendency was noted (Yoshizawa et al. 2000). The XRD analysis reflected that the carbonization occurred through the following mechanism. First, free carbon atoms are preferentially oxidized; removal of these free carbon atoms introduces micropore development in the cross-links. Second, the pore-developed cross-links are gasified to further develop the pores, including meso- and macropores.

Operational temperature during chemical preparation depends on the type of activating agent used (Sect. 5.4.3.3). Said the typical activating agents, namely ZnCl₂, H₃PO₄, K₂CO₃, Na₂CO₃, KOH, or NaOH is used, the carbonization behavior as the function of temperature (500–900 °C) is ascribed as follows. Using ZnCl₂ and H₃PO₄, the maximum pore volume (micropores + mesopores) was achieved at 600 °C (Hayashi et al. 2000); increasing the temperature decreased the total volumes. Using K₂CO₃, the maximum pore volume was achieved while operating the process at 800 °C; the decrease of total volume was noted when the temperature increased to 900 °C, but the mesopore proportion increased. The Na₂CO₃ did not work at temperatures <700 °C which correlated to the low activity of the salt, and the maximum pore achieved at 900 °C. Interestingly, the increase of pore volume

was driven by the increase of mesopore fraction. The total volume when using KOH increased as a function of temperature, but the ratio between micropores and mesopores decreased. The NaOH exhibited similar behavior to that of KOH, but increasing temperature from 800 to 900 °C could not enhance the total volume; instead, the micropore distribution decreased significantly.

Working with bituminous coal to prepare AC using 40% H₃PO₄ in a TGA under N₂ atmosphere at temperature range 30–800 °C (Teng et al. 1998), for an instance, the results were described as the following. Expectedly, the carbon yield decreased as the increase of temperature. Strong evolution occurred at temperature below 300 °C, representing the volatilization of water, CO₂, and hydrocarbons. At 400–600 °C, the tar evolution was suppressed by the H₃PO₄ to develop phosphate-based cross-links. Other works reported by Jibril et al. (2007) (KOH activation with temperature varied from 600 to 800 °C), Lozano-Castello et al. (2001) (KOH activation from 700 to 800 °C), Zou and Han (2001) (KOH activation from 510 to 910 °C), Lillo-Ródenas et al. (2001) (NaOH activation from 500 to 960 °C), Usmani et al. (1996) (ZnCl₂ activation from 650 to 850 °C), etc., clearly showed the thermal behaviors as described above. Conducting the carbonization-activation at the higher temperature contributes to enlarge the micropores to mesopores, resulting in the decreases of pore properties (Hayashi et al. 2000; Jibril et al. 2007; Lillo-Ródenas et al. 2001; Lozano-Castello et al., 2001; Usmani et al. 1996; Zou and Han 2001).

- *Heating rate*: Expectedly, increasing heating rate escalates the pore development process but decreases the AC yield. A bituminous coal was used to prepare AC while carbonization was performed under two different heating rates of 5 and 10 °C/min (Pallarés et al. 2018), and the obtained chars had the surface area and micropore volume as of 718 to 789 m²/g and 0.29 to 0.33 cm³/g, respectively. While using bituminous coal and varying the heating rates from 5 to 40 °C/min, Luo et al. (2001) reported the increase of surface area from 4.9 to 16.3 m²/g. Guldogan et al. (2000) specifically investigated the effect of heating rates on the carbonization kinetics of lignite samples. They varied the heating rate parameter (10–80 °C/min), and the results showed that the respective char yields and activation energies decreased from 68.9% to 66.5% and 45.6 to 28.9 kJ/mol as the increase of heating rates in the tested range. Wang et al. (2007) employed three heating rates of 4.4, 7.7, and 20 °C/min; Lozano-Castello et al. (2001) used two heating rates of 5 and 20 °C/min; Singh and Lal (2009) conducted carbonization while using heating rates of 2.5, 5, and 10 °C/min; these studies also found that the pore developments varied proportionally to the AC yield.

Clearly, the rapid heating rate is advantageous to encourage the carbonization reactions to occur larger than the slow heating rates; this is understandable for such reasons. During the thermal treatment, two competing phenomena of volatilization and char formation occur. When the higher heating rate is applied, the reaction time for tar volatilization is shorter. Shifting of the gaseous products as the more charring reactions is observed, from hydrogen and hydrocarbons to CO₂ (Seebauer et al. 1997). The more charring reactions, however, tend to reserve to the pore properties as more carbons inside the matrix are being graphitized (Harris et al. 2008).

Additionally, melting and sintering processes may occur on the surface of the AC (Pallarés et al. 2018), which is disadvantageous to the pore properties as the melting and sintering products may block the pores. It is thus suggested to operate the thermal treatment for preparation of coal-derived ACs at the heating rate range 20–40 °C (Tables 5.2 and 5.3). However, the heating rate appeared to be the secondary influencer upon the pore developments of the chars, behind the other parameters (Singla et al. 1983).

- *Reagent dosage:* Here, reagents refer to the inert gas (N₂, Ar, He), oxidizing gas (CO₂, H₂O), and chemical activating agents (KOH, NaOH, ZnCl₂, H₃PO₄) which are used during the physical and chemical preparation of ACs. Inert gases play a role to create oxygen-free atmosphere inside the carbonization reactor and sweep vapor phases generated during the process. Accordingly, increasing inert gas flow rate increases the gas yield but decreases the char yield for the sweeping effect of the inert gas to liberate the char from condensed volatiles which may seal the primary pores and hinder the pore development process. Using N₂ gas with flow rate range of 20 to 200 ml/min, the proportional increase of weight loss from 41.7% to 43.4% was noted during carbonization of bituminous sample at the conditions of 600 °C temperature, 0.5 °C/min heating rate, and 1 h duration (Song et al. 2008), well agreed with the results reported by Pallarés et al. (2018) while intensifying the gas dosage from 500 to 2500 ml/min, Choudhury et al. (2014) from 50 to 200 ml/min, Gercel (2002) from 25 to 100 ml/min, Lua (2019) from 5 to 40 ml/min, Liu et al. (2007) from 40 to 300 ml/min, etc. while using various type of inert gases under the typical carbonization conditions. The effect somehow was considerably less significant than those of temperature and heating rate. For an instance, the BET surface area of chars obtained after carbonizing the bituminous coal in the study reported by Pallarés et al. (2018) could only improve from 759 to 788 m²/g and the micropore volume from 0.32 to 0.33 cm³/g.

It is worth noting that there is negligible difference found among the chars obtained when the carbonization is operated in N₂, Ar, and He atmospheres, implying that the selection of inert gas to be used in the carbonization should consider the price of the respective inert gases rather than their efficiency. Still, using inert gas is cost driver. Therefore, some studies suggested to replace some fractions of the inert gases to the more economical oxidizing gases (CO₂, H₂O steam), but these attempts affect the quality of the chars (Teng et al. 1997). Vacuum technology has been seen as a sufficient alternative to replace the inert gas (Lua 2019; Xiao et al. 2015).

Expectedly, increasing the oxidizing gas flow rate during activation process results in similar behavior as depicted above. Using subbituminous and lignite coals as the precursors and CO₂ as the oxidizing gas, there was a small increase in the gasification rate when the CO₂ pressure increased from 0.1 to 1 atm, but it turned to be significant when the CO₂ pressure set at 21 atm (Tomaszewicz et al. 2017). Norman and Cha (1995) varied the CO₂ flow rate from 0.094 to 0.755 l/min to activate char using microwave with input power of 700 Watts, and obtained the consistent results of increasing the carbon gasification rate as the increase of CO₂ flow rate. Using steam (range dosage of steam (ml/min), 0.02–0.12) to activate chars at

the temperature of 900 °C for 3 h activation time, the burn-off percentage, AC yield, and ash content were also found to be extremely dependent on the variation of steam (Essuah and Buah 2019). Both burn-off percentage and ash content increased as the increase of steam dosage, but the AC yield decreased, in agreement with the results reported in other studies (El Qada et al. 2006; Grzyb et al. 2009; González et al. 1994; Izquierdo and Rubio 2008; Li et al. 2014; Manocha et al. 2010; Maroto-Valer et al. 1999; Pietrzak et al. 2007; Zhang et al. 2011). These behaviors can be simply explained by the more carbon to be gasified to open new pores through Eqs. 5.2 and 5.3. However, in the case of surface area of the pores, the increase of oxidizing gases dosage does not always have positive impact. For an instance, the BET measurement by referring to the iodine adsorption number in the study of Essuah and Buah (2019) noted that the iodine numbers increased when the steam dosage increased from 0.031 to 0.046 ml/min, but it then decreased in the thereafter increase of the steam dosage. These phenomena were confirmed in other studies (Grzyb et al. 2009; Manocha et al. 2010), which is explained by the widening of micropores to mesopores. Hence, the pore properties can be controlled by controlling the oxidizing gas dosage.

The curve trend of the pore properties is also observed in the chemical activation process. Here, the term used is the ratio of activating agent to the coal. The surface area of ACs from anthracite coal firstly increased from 726 to 3290 m²/g when the KOH/anthracite ratio increased ratio from 1/1 to 4/1 but then it decreased to 3183 m²/g at the KOH/anthracite ratio of 5/1 (Lozano-Castello et al., 2001); the activation was carried out at 700 °C for 1 h, as also observed while working with bituminous coal (Yan and Sorial 2011). The exact turning point can be varied, depending on other carbonization factors, such as coal types, activating agent used, temperature, duration, etc. (Lozano-Castello et al., 2001). Ahmadvour and Do (1997) when activating a bituminous sample at temperature 700 °C and duration 1 h noted that the decline of surface area of the obtained ACs occurred when KOH/bituminous ratio exceeded 2/1. A study reported by Teng et al. (1998) showed that increasing H₃PO₄/bituminous ratio (range 1/1–4/1) gradually increased the surface area, pore volume, and diameter; however, at the higher ratio, the surface area and pore volume decreased while the pore diameter kept increasing. A study using ZnCl₂ as the activating agent also exhibited a similar behavior (Usmani et al. 1996) that exceeding the ZnCl₂ ratio to 1/2 decreased the burning-off degree and the pore properties.

- *Holding time:* Increasing holding time means that more chances of carbon groups to be decomposed/gasified. Practically, 30 min to 1 h is required to obtain the maximum char product, and 1–3 h is required to ensure the complete char gasification process. Extending the holding time lowers the char/AC yield and pore properties which is due to the similar reason as discussed earlier. And shortening the holding time results in insufficient time for the reactions to proceed completely. The BET surface area of ACs after carbonization at KOH/bituminous ratio of 2/1 and temperature 650 °C increased from 1085 to 1476 m²/g when the carbonization duration was prolonged from 1 to 3 h (Yan and Sorial 2011); how-

ever, for the longer holding time of 5 h, the surface area reduced because more carbon in the micropore matrixes was gasified to widen as mesopores. Confirmation by Ganan et al. (2004) while comparing two holding times of 1 and 2 h to carbonize bituminous coal using KOH (300 °C), Lozano-Castello et al. (2001) when using at three different holding times of 0.5, 1, and 2 h to carbonize anthracite using KOH (KOH/coal ratio, 2/1; temperature (°C), 700), Sudaryanto et al. (2006) who varied the holding times from 1 to 3 h (KOH/precursor ratio, 1/1; temperature (°C), 650), Usmani et al. (1996) from 1 to 3 h (ZnCl₂/coal ratio, 1/2; temperature (°C), 650), and others stated similar tendencies. Determining the optimum holding time must also consider other factors, as depicted before. For an instance, operating the carbonization-activation at higher temperature can shorten the holding time to obtain the similar AC after carbonization-activation at lower temperature. Using caking-coals also requires shorter holding time to prevent the caking reactions. Despite its effect to the AC yield and properties, optimizing the holding time of carbonization-activation is important to reduce the consumption of energy for the heating.

5.4.5 Kinetic Aspect

Preparation of coal-derived AC involves the primary solid-gas reactions and secondary tar-gas reactions. The heterogeneous reactions occurred during the thermal preparation can be affected by three factors of (1) deconstruction and transformation of cross-links, (2) change of surface reaction of the coals, and (3) diffusion of gases/activating agent and reaction products (Kok and Pamir 2003).

It has been presented that such operational conditions of the thermal preparation determine the AC properties (Sect. 5.4.3). And the kinetic studies of the thermal preparation of AC from coals can be an important factor to optimize the process. Basically, the kinetic studies have been performed either using isothermal or non-isothermal methods in a thermogravimetric analysis (TGA) for the carbonization/pyrolysis and activation processes through different kinetic models.

5.4.5.1 Kinetic Models of Carbonization

The Arrhenius equation (Eq. 5.7) is the fundamental expression of such kinetic studies (Yahya et al. 2015).

$$k(T) = A \exp\left(-\frac{E}{RT}\right) \quad (5.7)$$

where $k(T)$ is reaction rate, T is temperature, E is the activation energy, A is exponential constant, and R is the universal gas constant.

Formally, such kinetic data can be calculated using Eq. (5.8):

$$\frac{d\alpha}{dt} = k(T)f(\alpha)^n \quad (5.8)$$

where $f(\alpha)$ is the conversion function indicating the reaction model and representing the controlling mechanism (Yahya et al. 2015) and n is the reaction order.

While the k value in Eq. (5.8) is from the Arrhenius equation (Eq. 5.7), and assuming that the reaction is first-order kinetic (Kök 2005), Eq. (5.8) can be written as the following:

$$\frac{d\alpha}{dt} = A \exp\left(-\frac{E}{RT}\right) f(\alpha) \quad (5.9)$$

$$\frac{d\alpha}{dt} \frac{1}{f(\alpha)} = A \exp\left(-\frac{E}{RT}\right) \quad (5.10)$$

Taking its logarithm form, Eq. (5.10) can be rewritten as:

$$\log\left[\left(\frac{d\alpha}{dt}\right) \frac{1}{f(\alpha)}\right] = \log A - \frac{E}{2.303RT} \quad (5.11)$$

And by plotting the $\log\left[\left(\frac{d\alpha}{dt}\right) \frac{1}{f(\alpha)}\right]$ as a function of T , a straight line (slope = $-\frac{E}{2.303R}$) is obtained.

When the carbonization is conducted under non-isothermal condition with a constant heating rate, say β ($\beta = \frac{dT}{dt}$ C/min), Eq. (5.8) can be transformed into:

$$\frac{d\alpha}{dT} = \frac{d\alpha}{dt} \frac{dt}{dT} \quad (5.12)$$

By substituting Eq. (5.9) into Eq. (5.12), the kinetic rate of non-isothermal can be written as follows:

$$\frac{d\alpha}{dT} = \frac{A}{\beta} \exp\left(-\frac{E}{RT}\right) f(\alpha) \quad (5.13)$$

The integrated form of Eq. (5.13), as expressed in Eq. (5.14), can be used to calculate the E by plotting the $\log\left[\frac{f(\alpha)}{T^2}\right]$ against $1/T$. Here, the assumption used the $E/2.303R$ is that is a constant, which is applicable for the high E_a and a moderate temperature (Ma et al. 1991).

$$\log\left[\frac{f(\alpha)}{T^2}\right] = \log\left[\frac{AR}{\beta(E+2RT)}\right] - \frac{E}{2.303RT} \quad (5.14)$$

Zou et al. (2017) and Ahmaruzzaman and Sharma (2005) have investigated the n -order carbonization reactions ($f(\alpha) = (1 - \alpha)^n$) of bituminous coals under non-isothermal conditions. Eq. (5.14) could further be presented as the following:

$$\ln \left[\frac{-\ln(1-\alpha)}{T^2} \right] = \ln \left(\frac{AE}{\beta R} \right) - \frac{E}{RT} \text{ for } n = 1 \tag{5.15}$$

$$\ln \left[\frac{1-(1-\alpha)^{1-n}}{T^2(1-n)} \right] = \ln \left(\frac{AE}{\beta R} \right) - \frac{E}{RT} \text{ for } n \neq 1 \tag{5.16}$$

Urbanovici et al. (1999) improved the accuracy of the general Eq. (5.14) by correcting the temperature integral approximation. The corrected equation was as follows:

$$\ln \left[\frac{f(\alpha)}{T^2} \right] - \ln [Q(x)] - \ln \left(\frac{AR}{\beta E} \right) + \frac{E}{RT} = 0 \tag{5.17}$$

where x is E/RT and $Q(x)$ is a third-degree rational approximation with an error $< 1.6 \times 10^{-3}\%$ when the $x \geq 10$, that written as the following:

$$Q(x) = \frac{(x^3 + 10x^2 + 18x)}{(x^3 + 12x^2 + 36x + 24)} \tag{5.18}$$

Slyusarskiy et al. (2017) approached the correction of the temperature integral approximation based on the following equation:

$$\log P(x) = -2.315 + 0.457x \tag{5.19}$$

And the E is defined using Eq. (5.20):

$$\ln \left[\frac{\beta}{H(x)} \right] = \ln \left(\frac{0.00484AE}{Rf(\alpha)} \right) - \frac{1.0516E}{RT} \tag{5.20}$$

where $H(x) = \frac{e^{-x}Q(x)/x^2}{0.0484e^{-1.05616x}}$ and $Q(x) = \frac{(x^4 + 18x^3 + 88x^2 + 96x)}{(x^4 + 20x^3 + 120x^2 + 240x + 120)}$.

The iteration of the above questions based on the procedures of the beginning $H(x)$ is 1 to calculate the E_1 , then by using Eq. (5.19) and the slope of Eq. (5.20), the new value of E_2 is obtained. The new values of $E_3, E_4, E_5, \dots, E_n$ are obtained by repeating the procedure, and the correction value is supposed to be less than 1%.

Nunn et al. (1985) suggested a simple kinetic model of pyrolytic decomposition of coal, as expressed in Eq. (5.21). This model works based on the ultimate yield of carbonization products (volatiles and gases) (Zabaniotou et al. 2000).

$$-\frac{dV_i}{dt} = K_i (V^\infty - V_i)^n \quad (5.21)$$

where K_i is Arrhenius kinetic constant ($K_i = k_{0i} e^{E_i/RT}$), V^∞ is the ultimate yield of volatiles and gases, V_i is the percentage of products in time t .

Using Gaussian distribution to the E_i of Eq. (5.21) (De Jong et al. 2007), the following expression can be obtained:

$$\frac{V^\infty - V}{V^\infty} = \frac{1}{\sigma\sqrt{2\pi}} \int_{-\infty}^{\infty} \exp \left[-A \int_0^t \exp \left(-\frac{E}{RT} \right) dt - \frac{(E - E_0)^2}{2\sigma^2} \right] dE \quad (5.22)$$

where σ is the width of the Gaussian distribution.

A parallel model by assuming that the coal carbonization occurs through the independent parallel reactions (Seo et al. 2011) and there is such T_{peak} to satisfy $\frac{d^2V_i}{dT^2} \Big|_{T=T_{\text{peak}}} = 0$ has also been used to describe the kinetics of coal carbonization (Eq. 5.23).

$$\ln \frac{\beta}{T_{\text{peak}}^2} = \ln \frac{A_i R}{E_i} - \frac{E_i}{RT_{\text{peak}}} \quad (5.23)$$

The kinetic parameters of each products can be obtained by plotting the $\ln \frac{\beta}{T_{\text{peak}}^2}$ against $1/T_{\text{peak}}$ and the intercept value of $\ln \frac{A_i R}{E_i}$. Further details of this model were presented by Seo et al. (2010).

5.4.5.2 Kinetic Models of Activation

Kinetic models for the activation/carbon gasification can be grouped into theoretical and semi-empirical models (Zhang et al. 2010). There are several well-known examples of theoretical kinetic models that have been widely used in studies (Yahya et al. 2015; Zhang et al. 2010), as the following.

- The VRM assumes that the gasification reactions occur homogeneously on all the active sites without any structural changes. The reaction is given as follows:

$$\frac{dx}{dt} = k_v (1 - x) \text{ or } -\ln(1 - x) = k_v t \quad (5.24)$$

- where k_v is the rate constant, and x is the conversion.
- The SCM considers that the shrinking core occurs progressively on the surface of nonporous grains. The simplified equation is written as the following (Eq. 5.25).

$$\frac{dx}{dt} = k_s (1-x)^{2/3} \text{ or } 3 \left[1 - (1-x)^{1/3} \right] = k_s t \quad (5.25)$$

- where k_s is the rate constant for the surface reaction.
- The RPM counts that all the pores develop and overlap as the function of gasification reactions. The reaction rate is defined as:

$$\frac{dx}{dt} = k_p (1-x) \sqrt{1-\psi \ln(1-x)} \text{ or } \left(\frac{2}{\psi} \right) \sqrt{1-\psi \ln(1-x)} = k_p t \quad (5.26)$$

- where k_p and ψ are the rate constant for the pore reaction and pore surface parameter (dimensionless) which are calculated using the pore length and porosity, respectively. It is worth noticing that the RPM is much more flexible than the VRM and SCM (Zhang et al. 2010). When the $\psi = 0$, the RPM turns to be the VRM, and at the $\psi = 1$, it approaches the SCM. Even so, the complexity of the chars affects the determination of the exact value of the ψ , and sometimes fitting treatment must be done (Kajitani et al. 2006). More importantly, the RPM can be used when the $x < 0.393$ (Zhang et al. 2010).
- The models above are sometimes found to be unsatisfactory to fit the experimental data. Efforts to develop semi-empirical models to reconcile the experimental data were reported. For an instance, Zhang et al. (2008) modified the conventional RPM by adding two dimensionless parameters of c constant and p power law constant, as indicated below:

$$\frac{dx}{dt} = k_p (1-x) \sqrt{1-\psi \ln(1-x)} \left(1 + (cx)^p \right) \quad (5.27)$$

Dutta et al. (1977) introduced the factor a into the rate equation (Eq. 5.29), which represented the relative availability of pore surface area at any stage of conversion as a function of the initial available pore surface area.

$$\frac{dx}{dt} = ak(1-x) \quad (5.28)$$

where $a = 1 \pm 100x^{\nu\beta}e^{-\beta x}$, and ν ($0 \leq \nu \leq 1$) and β are constants of a given char.

The rate of carbon gasification can also be expressed as Eq. (5.29), which was proposed by Johnson (1974). Here, the $(1-x)^{2/3}$ expresses the active surface area where the reactions undergo, and the $e^{-\alpha x^2}$ describes the relative influence of the effective surface area, which decreases as the increase of gasification. The value of α depends on the temperature and gas composition (Goyal et al. 1989).

$$\frac{dx}{dt} = k(1-x)^{2/3} e^{-\alpha x^2} \quad (5.29)$$

According to Adschiri et al. (1986), the rate of char gasification should consider the value of surface area, and the empirical equation can be described as the following:

$$\frac{dx}{dt} = S_{(x)}k(1-x) \quad (5.30)$$

And an empirical model by modifying the conventional VRM was reported (Wu et al. 2009). Here, it assumes that the k_v changes with the conversion (Eq. 5.31).

$$\frac{dx}{dt} = k_{(x)}(1-x) \text{ or } -\ln(1-x) = k_{(x)}t \quad (5.31)$$

5.5 Application of Activated Carbon for Adsorption of Metals in Aqueous Solutions

Figure 5.1 shows the fact that the adsorption system has been dominantly applied to deal with metallic ions in aqueous solutions, either to separate/recover metals from leach solutions or to treat wastewater, with the particular use of ACs as the adsorbents. Table 5.4 presents the application of coal-derived ACs to adsorb metals from various aqueous solutions.

5.5.1 Recovery of Gold and Silver from Cyanide Solution

The use of AC for the recovery of gold and silver in gold-silver processing plants has become the traditional example of the application of adsorption system to handle metal ions in aqueous solutions. A flowsheet illustrating the industrial application of adsorption with AC to recover gold and silver from cyanide leaching solution is depicted in Fig. 5.5.

Extensive works have been reported to understand the adsorption mechanism. The ionic pair mechanism of $[M^{n+}][Au(CN)_2^-/Ag(CN)_2^-]_n$ was proposed (Davidson 1974), where M refers to Ca, Mg, K, Na, etc. These cations have lower solubility than the gold- and silver-cyanide anions in the adsorption medium, and it was found out that the strength of the adsorptivity of the $Au(CN)_2^-$ and $Ag(CN)_2^-$ anions towards the ACs follow the sequence of $Ca^{2+} > Mg^{2+} > H^+ > Li^+ > Na^+ > K^+$ (Davidson 1974). These mechanisms have been well accepted by numerous gold and silver adsorption studies (Adams et al., 1987, Adams 1990, Adams 1992). McDougall et al. (1980) noted that there was subsequent reduction of the $Au(CN)_2^-$ and $Ag(CN)_2^-$ anions to $Au(CN)_x$ and $Ag(CN)_x$ after the ion-pairing, respectively. Cook et al. (1989), Tsuchida and Muir (1986), Van Deventer (1986), and others observed that the converted species were $Au(CN)$, $Ag(CN)$, and their metallic forms ($Au_{(s)}$).

Table 5.4 Applications of coal-derived AC for adsorption of metals in aqueous solutions

Type of coals	Preparation method	Type of solutions	Targeted metals	Adsorption conditions	Relevant issue	References
Anthracite	CO ₂ activation	Cyanide	Au (100 ppm), Ag (53.9 ppm), CN ⁻ (530 ppm)	–	<ul style="list-style-type: none"> – Adsorption of metals correlates with the total pore volume – Au was adsorbed in the form of Au(CN)₂⁻ while Ag as Ag(CN)₃²⁻; Ag(CN)₂⁻ was reduced for the excess CN⁻ in the solution – Hydrophobic surfaces of the ACs contributed to the adsorption of Au and Ag – Increasing the Ag concentration firstly increased and then decreased the AC sorption capacity of the AC – Sulfite affected the Ag recovery for the formation of stable Ag-thiosulfate complex and the increase of basicity 	Jia et al. (1998)
Anthracite	NA	Thiosulfate	Ag (19.5–117.5 mg/L)	–	<ul style="list-style-type: none"> – Adsorption efficiencies followed the order of Cu > Pb > Zn > Cd – Adsorption did not occur at the solutions with very low pH – Sorption competition among the metals – Optimum conditions were defined as the following: 70 °C, 3 h 	Kononova et al. (2007)
Anthracite	Air activation	Simulated leach solution	Zn, Cd, Cu, Pb (2.5 g/L for each)	pH 2.0–6.0	–	Petrov et al. (1992)
Anthracite	NA	Waste solution	Pt (57.6 mg/L)	pH 3.5, 25–80 °C, 1–5 h	–	Aktas and Morcalli (2011)
Bituminous	H ₂ O activation	Cyanide	Au (21 ppm), Cu (3800 ppm), CN ⁻ (3000 ppm)	–	<ul style="list-style-type: none"> – Adsorption of Au occurred through the monolayer formation – ACs from activation at 850 °C for 1.5 h showed better sorption properties 	Martínez-Mendoza et al. (2020)

(continued)

Table 5.4 (continued)

Type of coals	Preparation method	Type of solutions	Targeted metals	Adsorption conditions	Relevant issue	References
Bituminous	H ₂ O activation, followed by impregnating with sulfur donor extractants (tris(hydroxymethyl)aminomethane)	Chloride leach solution	Pt (110 mg/L), Pd (110 mg/L), Cu (47 mg/L), Ni (51 mg/L)	0.1 M HCl, 12–24 h	<ul style="list-style-type: none"> – Metal ionic appearances depended on the pH – Adsorption of the Pt and Pd occurred through the complexation with the thio- and amine-complexes contained in the ACs; the impregnated ACs did not react with cu and Ni 	Kasaini et al. (2005)
Bituminous	O ₂ + H ₂ O	Wastewater	Cr, Cd, Cu (30 mg/L for each)		<ul style="list-style-type: none"> – Initial metal concentration was found to be the most affected parameter; followed by pH, temperature and contact time – At pH 2.0, the metal adsorption order was Cu > Cr > Cd; at pH 4.0, the order was Cu > Cr > Cd 	de Lima et al. (2011)
Bituminous	NA	Simulated wastewater	Hg (1 µg/L)	–	<ul style="list-style-type: none"> – Pretreatment of the coal precursor by washing with acid affected the sorption capacity of the AC for the reintroduction of the carbon groups in the coal 	Pandey and Chaudhuri (1982)
Bituminous	ZnCl ₂ activation	Simulated wastewater	U (50–200 ppm)	pH 2–8, 30–70 °C, 5 mins to 8 h	<ul style="list-style-type: none"> – Best conditions were defined as the following: pH 5, U conc. 50 ppm, 4 h contact time, 30 °C; U recovery of 96% – pH affected the U-complexes; increasing the U concentration increased the interaction between the U and ACs; the adsorption occurred endothermally with the enthalpy (ΔH°) = 33.49 kJ/Mol 	Kütahyalı and Eral (2004)

Type of coals	Preparation method	Type of solutions	Targeted metals	Adsorption conditions	Relevant issue	References
Bituminous	H ₂ S and N ₂ activation	Simulated wastewater	Hg, Cd, Pb (3.8 × 10 ⁻² –7.3 mol/L for each)	pH 4.4–6.2	<ul style="list-style-type: none"> ACs after H₂S activation revealed higher adsorption capacity towards the targeted metals Metal adsorption efficiencies reduced significantly when the pH lowered to 2.0, particularly Cd and Pb 	Gomez-Serrano et al. (1998)
Bituminous	H ₂ O activation	Simulated wastewater	Cr (5–50 mg/L)	pH 2–14, 20 °C	<ul style="list-style-type: none"> Adsorption occurred through the reduction of Cr⁶⁺ to Cr³⁺, followed by adsorption of the reduced species onto the surface of the AC At pH > 7.0, anionic competition among the CrO₄²⁻, OH⁻ and Cl⁻ occurred 	Di Natale et al. (2007)
Bituminous	H ₂ O activation	Wastewater	Hg (500–5000 µg/L)	pH 1–4, 27–60 °C	<ul style="list-style-type: none"> Adsorption depended on the ionic species of the hg Cationic HgOH⁺ and Hg²⁺ could be adsorbed easier than HgCl⁺, and such competition with H₃O⁺ ions occurred At neutral pH, adsorption was more sensitive to the changes of adsorption conditions 	Di Natale et al. (2011)
Bituminous	NA	Simulated leach solution	Cu, Zn, Cd, Co, Pb (1000 mg/L for each)	pH 5, 22 °C, 1–360 min	<ul style="list-style-type: none"> Adsorption activity order of Pb > Cd > Cu > Zn > Co with complex sorption mechanisms (combination of physical and chemical adsorptions) Adsorbed metals could be eluted using mineral acids 	Kolodyńska et al. (2017)

(continued)

Table 5.4 (continued)

Type of coals	Preparation method	Type of solutions	Targeted metals	Adsorption conditions	Relevant issue	References
Lignite	NA	Wastewater	Hg, Cd (100 ppm for each)	pH 2.0–6.0, 1 h	<ul style="list-style-type: none"> Optimum recovery was achieved at pH 4.0 with the order of Hg > Cd The adsorbed metals could be eluted using EDTA 	Karabulut et al. (2001)
Lignite	H ₂ O activation	Wastewater	Cu (5–50 mg/L), Fe (5–100 mg/L), Cr (5–50 mg/L), Au (5–400 mg/L)	pH 1.5–5.0, 2 h	<ul style="list-style-type: none"> Adsorption efficiencies: Au > Fe > Cu >> Cr Strong acid (pH ~ 1.5) was the most suitable condition for the adsorption of Au 	Vassileva and Detcheva (2010)
Lignite	NaOH activation	Wastewater	Pb, Zn, Cu, Cd (1–500 mg/L for each)	pH 5.0, 6 h	<ul style="list-style-type: none"> Metal adsorption order of Pb >> Cu ≥ Cd > Zn Adsorption depends on the natural properties of the AC; the zero point charge of the adsorbent used was ~5.0 Adsorption competition among the metals ion and free H⁺ 	Havelcova et al. (2009)
Lignite	H ₂ O activation	Simulated leach solution	Zn, Cd, Cu, Pb (2.5 g/L for each)	pH 1.0–6.0	<ul style="list-style-type: none"> Metal adsorption order of Pb > Cu > Zn > Cd The adsorption was negligible at strong acid solution; the strong adsorption occurred at pH 3.0–4.0 	Budinova et al. (1994)
Lignite	NA	Simulated wastewater	Zn (5–50 mg/L)	pH 7.0, 30–80 °C, 10–60 min	<ul style="list-style-type: none"> Temperature and time affected positively the sorption efficiency, while initial metal concentration showed contrast effect 	Shrestha et al. (2013)

NA not available

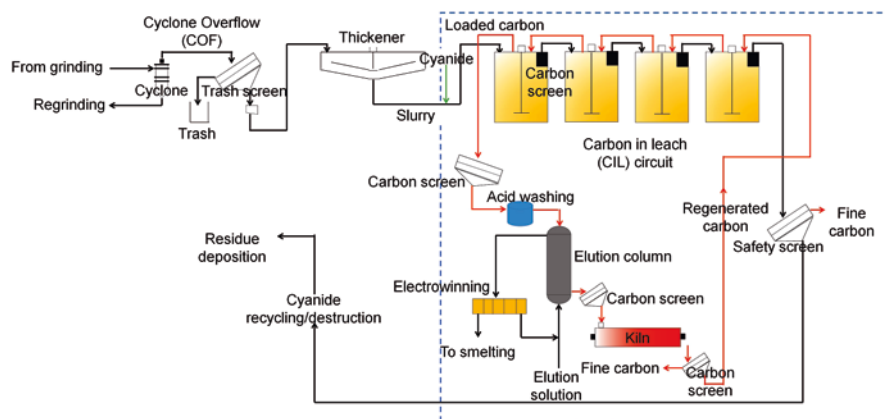


Fig. 5.5 Simplified flowsheet of carbon-in-leach (CIL) process for gold and silver recovery

and $\text{Ag}_{(0)}$). These findings were in opposition to those reported by other researches (Ibrado and Fuerstenau 1995; Klauber 1988, 1991), that the $\text{Au}(\text{CN})_2^-$ and $\text{Ag}(\text{CN})_2^-$ anions did not undergo any chemical species changes when they were adsorbed by the AC. The adsorbed species were oligomerized to tetramer $\text{Au}_4(\text{CN})_5^-$ and $\text{Ag}_4(\text{CN})_5^-$ when the loaded AC was washed with acid (Klauber 1988), in agreement with the results reported by Kongolo et al. (1990) for the escape of CN^- as HCN.

Researches also figured out that the surface functional groups of the AC played significant role in the gold and silver adsorption (Jia et al. 1998; Tsuchida and Muir 1986; Van der Merwe and Van Deventer 1988). O-atom in the functional groups enhanced the $\text{Au}(\text{CN})_2^-$ and $\text{Ag}(\text{CN})_2^-$ loading through the decomposition of the metal-cyanide complexes to obtain CO_3^{2-} , NH_3 , AuCN, and AgCN (Tsuchida and Muir 1986). Moreover, the O- and N-atoms provide the hydrophilicity of the AC surface to introduce the ion exchange mechanism during the metal adsorption (Jia et al. 1998). However, it is worthwhile that the graphitic plane contributes more to the adsorption of $\text{Au}(\text{CN})_2^-$ and $\text{Ag}(\text{CN})_2^-$ through π -donor mechanism (Ibrado and Fuerstenau 1995; Jia et al. 1998; Klauber 1988; Poinern et al. 2011).

The effects of AC pore structure and adsorption parameters, such as pH, cyanide concentration, dissolved oxygen, and temperature were also examined (Deveci et al. 2006; Jia et al. 1998). Expectedly, the ACs with more pore volume and surface area adsorb more $\text{Au}(\text{CN})_2^-$ and $\text{Ag}(\text{CN})_2^-$ anions (Ibrado and Fuerstenau 1995; Jia et al. 1998; Poinern et al. 2011). The low pH favors the adsorption process (Depci 2012; Petersen and Van Deventer 1991), but problems associated with the formation of harmful HCN must be taken into account. The excessed free CN^- is harmful for the $\text{Ag}(\text{CN})_2^-$ adsorption for the competitive sorption, but less affects to the $\text{Au}(\text{CN})_2^-$ anion (Jia et al. 1998). In the case of dissolved oxygen, this gas is consumed during the adsorption (Deveci et al. 2006; Ibrado and Fuerstenau 1995; Petersen and Van Deventer 1991), but its role is more likely to change the surface functional groups of the ACs, impart the hydrophilicity of the ACs, ensure the

ACs-solution contact, and promote the solution to diffuse into the internal pores. And increasing the operational temperature results in detrimental effect to the $\text{Au}(\text{CN})_2^-$ and $\text{Ag}(\text{CN})_2^-$ adsorption (Adams et al., 1987; Davidson 1974; McDougall et al. 1980); this implies to the reason of high temperature requirement for the elution process (Fig. 5.5).

5.5.2 Removal of Heavy Metals from Wastewater

The use of AC for removing heavy metals (Cd^{2+} , Pb^{2+} , Cr^{6+} , Cu^{2+} , Ni^{2+} , etc.) from wastewater has been the primary driver of applying adsorption process to the aqueous solution. To date, a large number of studies on the use of ACs for removing these metals from wastewater are still reported, along with a number of review articles which compile the information and discuss the factors that affect the application of AC in this field (Babel and Kurniawan 2003; Dias et al. 2007; Wong et al. 2018; Yahya et al. 2015), showing that the use of AC is economically and technically favorable for industries.

In similarity, adsorption of heavy metals from wastewater strongly depends on factors of the natural properties of metal ions (size, charge) and surface properties of the AC (functional groups, wettability, oxygen content, porosity, point of zero charge). Besides, operational parameters of AC dosage, temperature, solution pH, and initial metal concentrations are the other important considerations to optimize such process. It is worth notifying that such ion exchange mechanism contributes to the adsorption process (Aguayo-Villarreal et al. 2017), evidenced by the release of cations from the AC. And such sorption competition among the metals can also happen with the affinity order of $\text{Pb} > \text{Cu} > \text{Zn} > \text{Ni} > \text{Cd}$ (Aguayo-Villarreal et al. 2017; Loganathan et al. 2018).

5.5.3 Recovery/Separation of Leached Metals from Leaching Solutions

The use of AC to recover or separate metals from various types of leaching solutions was also reported. Kasaini et al. (2005) used commercial AC derived from bituminous coal to selectively separate platinum and palladium from chloride-based leach solutions containing base metals (Cu, Ni). They noted that the base metals could not be adsorbed at the solution pH of < 2 . And when the AC was functionalized with amine groups, the AC could even favorably adsorb Pt over Pd.

Pagnanelli et al. (2011) investigated selective recovery of molybdenum from acid leach solutions containing impurities of nickel and vanadium using AC. It showed that the nickel could be completely rejected from adsorbing onto the AC while vanadium was partially adsorbed. These results were explained by the

difference of ionic appearances between the molybdenum (as anion) and nickel (as cation), while the vanadium was present in the same form as molybdenum.

Navarro and Alguacil (2002) focused on the adsorption of arsenic and antimony from copper leach solutions. It was noted that the increase of AC to solution ratio and the decrease of temperature increased the metal uptakes, as expected. And the loaded arsenic and antimony onto the AC were noted as 2860 and 92 mg/g, respectively, after contacting the AC for 30 h into 160 g/L H₂SO₄ solutions containing 21.2 g/L As and 0.44 g/L Sb. Importantly, there was no copper and sulfuric acid loaded onto the ACs.

In particular case, the AC was modified with chemical treatments or functionalized with organic extractants. Recently, Kamran et al. (2019) chemically modified coal-derived AC by mixing with 6.0 M sodium nitrate (NaNO₃) solution at elevated temperature (80 °C) for 2 h stirring period. The modified AC showed a strong affinity towards Li⁺ ion when it was applied in alkaline solution (pH = 12) containing 30 mg/L Li⁺; the maximum adsorption percentage of 96% could be achieved. Often, AC was functionalized with tri-butyl phosphate (TBP) extractant to adsorb uranium from acid leach solutions (Gomaa et al. 2016; Saputra et al. 2019). The use of iron oxide to improve the adsorption rates of arsenic, mercury, lead, and copper was also reported (Kalaruban et al. 2019; Reed et al. 2000; Yang et al. 2009). The AC was also impregnated with anionic surfactants, viz. sodium dodecyl sulfate/SDS, sodium dodecyl benzene sulfonate/SDBS, dioctyl sulfosuccinate sodium/DSS (Ahn et al. 2009), ammonium pyrrolidinetithiocarbamate/APDC (Daorattanachai et al. 2005), metal salts/halides (Molina-Sabio et al. 1994; Tamon et al. 1996), MnO₂ (Kamran et al. 2019), etc. as efforts to improve the AC affinity towards specific metals in the various types of leach solutions while also showing the wide adaptability of AC to be subjected to physical and chemical treatments or applied in different environments.

5.6 Future Direction

With large numbers of studies related to the preparation of coal-derived AC, this field is still promising in the future through some directions as the following. Particular attention is being paid to the use of solid and liquid coal-derivatives generated during coal processing (either mining, crushing, grinding, transporting, combusting) as the AC precursors, including coal fly ash (CFA), coal bottom ash (CBA), coal dust, and coal tar pitch. Studies to use these materials as direct AC precursors or binder of AC precursors were reported (Arami-Niya et al. 2016; Choi et al. 2015; Gao et al. 2016; Grzyb et al. 2009; He et al. 2012; Izquierdo and Rubio 2008; Ma et al. 2010; Tian et al. 2018; Uddin et al., 2007; Wu et al. 2010; Zeng et al. 2013), showing their potential to be used as AC precursors. For an instance, Uddin et al. (2007) prepared AC from CFA while using heavy oil fly ash (HOFA) as the binder. The thermal treatment was performed at such conditions (temperature, 650 °C; holding time,

1 h), and the obtained AC had surface area of 500–800 m²/g, increasing with the decrease of CFA/HOFA ratio. Tian et al. (2018) emulsified coal-tar pitch from anthracite coal with starch, then carbonized the mixed material in two carbonization steps at 480 °C in the first step and 830 °C in the second step for 1 h each, followed by H₂O steam activation at 830 °C for 4 h, and the obtained AC had surface area in the range 790–838 m²/g with pore diameter < 2 nm. A mixture of coal dust and coal-tar pitch was chemically treated using KOH at 800 °C for 1 h under argon atmosphere to produce AC with surface area of 1044 m²/g (Arami-Niya et al. 2016). Wu et al. (2010) used CBA as the precursor, and reported the similar behaviors as those reported when using coal during the chemical preparation of AC using KOH; the surface area of the obtained AC was 1520 m²/g after treating the precursor at 780 °C for 1 h. He et al. (2012) mixed coal-tar pitch with MgO and thermally processed the mixture in the presence of KOH; Gao et al. (2016) produced the AC after mixing coal-tar pitch with H₃PO₄; Grzyb et al. (2009) used coal-tar pitch as the binder of polyacrylonitrile polymers, and prepared the AC by carbonization and H₂O steam activation; and many more studies related to the use of coal derivatives showed the capability of these materials to be considered as the AC precursors.

Understanding the natural properties of the respective coal derivatives is mandatory to determine the flow preparation process. Say CFA as the precursor, this material is characterized by its complex mineralogy, including unburnt carbon, SiO₂, Al₂O₃, Fe₂O₃, CaO, MgO, and others which can exceed 300 different minerals (Vassilev and Vassileva 2005). Typically, the CFA contains carbon in the range 2–5%, and even higher depending on the coal types fed to the coal-fired boiler (Styszko-Grochowiak et al. 2004). Knowing the fact that this material has low carbon content, together with the ultrafine particles of the CFA, utilizing the CFA as the AC precursor can be carried out by adding binder or performing such carbon enrichment (Uddin et al., 2007). The similar phenomena happen in the case of other coal derivatives, making the preparation process somewhat more complicated than the conventional use of coal as the precursor. Even so, these coal derivatives are worth encouraging to be considered as the AC precursors in the future investigation. Their huge production numbers are also another advantage, ensuring their readily supply when they are treated as the AC precursor. Utilizing these coal derivatives can be worth promising plan towards clean coal technology, reducing the amount of solid and liquid by-products generated during coal processing.

Chemical preparation, in strong correlation with catalytic carbonization, is also worth considering as the future direction of preparation of coal-derived AC. Although the existing process (as discussed in Sect. 5.4.2) has been well understood, along with its kinetic aspects and factors affected the optimization of such process, efforts on this field remain worthwhile particularly on seeking of new catalysts/activating agents which are powerful to develop pores of the AC while also bring benefits in the economical and environmental point of views. The uses of KOH and NaOH face problem on the high energy consumption while the uses of ZnCl₂ and H₃PO₄, despite

their lower efficiencies, must deal with environmental issues. The AC produced using $ZnCl_2$ is also not suitable for such particular applications in food and pharmacy (Yahya et al. 2015). Therefore, researches on the preparation of coal-derived AC are worth encouraging to search the other alternative of chemical agents/catalysts in near future. Additionally, knowing that different types of chemical agents/catalysts work on the activation process through different mechanisms (Sect. 5.4.2), investigation to understand such mechanisms while using new catalysts/activating agents is worth considering.

Another option worth encouraging is to impregnate the AC with chemical agents or organic extractants while aiming to obtain better sorption properties (selectivity, capacity, etc.). This route is predicted to be the future trend related to the application of AC. Researches related to the impregnation of coal-derived AC have been documented (Ahn et al. 2009; Daorattanachai et al. 2005; Gomaa et al. 2016; Kalaruban et al. 2019; Kamran et al. 2019; Saputra et al. 2019; Yang et al. 2009), but problems associated with the loss of impregnating agents to the aqueous solution, toxicity of the impregnating agents, and difficulties of the subsequent elution process were reported. Overcoming the aforesaid problems is strongly recommended in the future works related to the use of coal-derived AC. Making concerted efforts to recover the lost impregnating agents and search on the more environmentally friendly activating agents are worthwhile and unique to widen the application of coal-derived AC through the greener option.

5.7 Conclusion

Development of coal-derived activated carbon (AC) has been considered as one of the key factors towards the clean coal technology. The production of coal-derived AC has been studied for decades through the physical and chemical preparation processes, obtaining AC with excellent pore properties and adsorptivity towards metal ions in such aqueous solutions. Large numbers of coal resources, relatively inexpensive, high carbon content, and readily primary pores are advantages of using coals as the AC precursor in commercial scale. Successful applications of coal-derived AC to adsorb metal ions in aqueous solutions are reported in large number of studies. Although some limitations remain during both the preparation of coal-derived AC and its application to adsorb metal ions in aqueous solutions, researches can be subjected to search on the new and excellent activating agents and undergo modification of the surface properties of the AC. Utilization of coal-derived by-products generated during coal processing as the AC precursor is also expected to be the future of preparation of coal-derived AC while also contribute towards clean coal technology.

References

- Abbas, Q., Mirzaeian, M., Ogwu, A. A., Mazur, M., & Gibson, D. (2020). Effect of physical activation/surface functional groups on wettability and electrochemical performance of carbon/activated carbon aerogels based electrode materials for electrochemical capacitors. *International Journal of Hydrogen Energy*, 45(25), 13586–13595. <https://doi.org/10.1016/j.ijhydene.2018.04.099>.
- Adams, M. D. (1990). The mechanism of adsorption of aurocyanide onto activated carbon. I. Relation between the effects of oxygen and ionic strength. *Hydrometallurgy*, 25(2), 171–184. [https://doi.org/10.1016/0304-386X\(90\)90037-3](https://doi.org/10.1016/0304-386X(90)90037-3).
- Adams, M. D. (1992). The mechanisms of adsorption of $\text{Ag}(\text{CN})_2^-$ and Ag^+ on to activated carbon. *Hydrometallurgy*, 31(1–2), 121–138. [https://doi.org/10.1016/0304-386X\(92\)90112-D](https://doi.org/10.1016/0304-386X(92)90112-D).
- Adams, M. D., McDougall, G. J., & Hancock, R. D. (1987). Models for the adsorption of aurocyanide onto activated carbon. Part III: Comparison between the extraction of aurocyanide by activated carbon, polymeric adsorbents and 1-pentanol. *Hydrometallurgy*, 19(1), 95–115. [https://doi.org/10.1016/0304-386X\(87\)90044-2](https://doi.org/10.1016/0304-386X(87)90044-2).
- Adschiri, T., Shiraha, T., Kojima, T., & Furusawa, T. (1986). Prediction of CO_2 gasification rate of char in fluidized bed gasifier. *Fuel*, 65(12), 1688–1693. [https://doi.org/10.1016/0016-2361\(86\)90270-X](https://doi.org/10.1016/0016-2361(86)90270-X).
- Afroze, S., & Sen, T. K. (2018). A review on heavy metal ions and dye adsorption from water by agricultural solid waste adsorbents. *Water, Air, & Soil Pollution*, 229(7), 225. <https://doi.org/10.1007/s11270-018-3869-z>.
- Aguayo-Villarreal, I. A., Bonilla-Petriciolet, A., & Muñiz-Valencia, R. (2017). Preparation of activated carbons from pecan nutshell and their application in the antagonistic adsorption of heavy metal ions. *Journal of Molecular Liquids*, 230, 686–695. <https://doi.org/10.1016/j.molliq.2017.01.039>.
- Ahmadpour, A., & Do, D. D. (1997). The preparation of activated carbon from macadamia nutshell by chemical activation. *Carbon*, 35(12), 1723–1732.
- Ahmaruzzaman, M., & Sharma, D. K. (2005). Non-isothermal kinetic studies on co-processing of vacuum residue, plastics, coal and petrocrop. *Journal of Analytical and Applied Pyrolysis*, 73(2), 263–275. <https://doi.org/10.1016/j.jaap.2004.11.035>.
- Ahn, C. K., Park, D., Woo, S. H., & Park, J. M. (2009). Removal of cationic heavy metal from aqueous solution by activated carbon impregnated with anionic surfactants. *Journal of Hazardous Materials*, 164(2–3), 1130–1136. <https://doi.org/10.1016/j.jhazmat.2008.09.036>.
- Aich, S., Nandi, B. K., & Bhattacharya, S. (2019). Effect of weathering on physico-chemical properties and combustion behavior of an Indian thermal coal. *International Journal of Coal Science & Technology*, 6(1), 51–62. <https://doi.org/10.1007/s40789-018-0235-0>.
- Akash, B. A., & O'Brien, W. S. (1996). The production of activated carbon from a bituminous coal. *International Journal of Energy Research*, 20(10), 913–922. [https://doi.org/10.1002/\(SICI\)1099-114X\(199610\)20:10<913::AID-ER205>3.0.CO;2-7](https://doi.org/10.1002/(SICI)1099-114X(199610)20:10<913::AID-ER205>3.0.CO;2-7).
- Akgün, F., & Arisoy, A. (1994). Effect of particle size on the spontaneous heating of a coal stockpile. *Combustion and Flame*, 99(1), 137–146. [https://doi.org/10.1016/0010-2180\(94\)90085-X](https://doi.org/10.1016/0010-2180(94)90085-X).
- Aktas, S., & Morcali, M. H. (2011). Platinum recovery from dilute platinum solutions using activated carbon. *Transactions of Nonferrous Metals Society of China*, 21(11), 2554–2558. [https://doi.org/10.1016/S1003-6326\(11\)61091-1](https://doi.org/10.1016/S1003-6326(11)61091-1).
- Alcañiz-Monge, J., Linares-Solano, A., & Rand, B. (2002). Mechanism of adsorption of water in carbon micropores as revealed by a study of activated carbon fibers. *The Journal of Physical Chemistry B*, 106(12), 3209–3216. <https://doi.org/10.1021/jp014388b>.
- Alcañiz-Monge, J., Perez-Cadenas, M., & Lozano-Castelló, D. (2010). Effect of the pre-oxidation of coals in the preparation of chemically activated carbon pellets. *Energy & Fuels*, 24(6), 3385–3393. <https://doi.org/10.1021/ef901522k>.

- Alothman, Z., Habila, M., & Ali, R. (2011). Preparation of activated carbon using the copyrolysis of agricultural and municipal solid wastes at a low carbonization temperature. *Carbon*, 24, 67–72.
- Antenucci, D., Delaude, L., Fransolet, A. M., & Laszlo, P. (1992). Acidic degradation of zeolite catalysts in the course of aromatic chlorination using sulfuryl chloride. *Journal of Catalysis*, 135(1), 92–98. [https://doi.org/10.1016/0021-9517\(92\)90271-I](https://doi.org/10.1016/0021-9517(92)90271-I).
- Arami-Niya, A., Rufford, T. E., & Zhu, Z. (2016). Activated carbon monoliths with hierarchical pore structure from tar pitch and coal powder for the adsorption of CO₂, CH₄ and N₂. *Carbon*, 103, 115–124. <https://doi.org/10.1016/j.carbon.2016.02.098>.
- Augelletti, R., Frattari, S., & Murrura, M. A. (2016). Purification of hydrogen-methane mixtures using PSA technology. In *Enriched methane* (pp. 129–146). Cham: Springer. https://doi.org/10.1007/978-3-319-22192-2_8.
- Babel, S., & Kurniawan, T. A. (2003). Low-cost adsorbents for heavy metals uptake from contaminated water: A review. *Journal of Hazardous Materials*, 97(1–3), 219–243. [https://doi.org/10.1016/S0304-3894\(02\)00263-7](https://doi.org/10.1016/S0304-3894(02)00263-7).
- Bagreev, A., Adib, F., & Bandosz, T. J. (2001). pH of activated carbon surface as an indication of its suitability for H₂S removal from moist air streams. *Carbon*, 39(12), 1897–1905. [https://doi.org/10.1016/S0008-6223\(00\)00317-1](https://doi.org/10.1016/S0008-6223(00)00317-1).
- Banhart, F., Kotakoski, J., & Krashennnikov, A. V. (2011). Structural defects in graphene. *ACS Nano*, 5(1), 26–41. <https://doi.org/10.1021/nn102598m>.
- Bansal, R. C., & Goyal, M. (2005). *Activated carbon adsorption*. CRC press.
- Bayram, E., & Ayranci, E. (2010). Electrochemically enhanced removal of polycyclic aromatic basic dyes from dilute aqueous solutions by activated carbon cloth electrodes. *Environmental Science & Technology*, 44(16), 6331–6336. <https://doi.org/10.1021/es101177k>.
- Biscoe, J., & Warren, B. E. (1942). An X-ray study of carbon black. *Journal of Applied Physics*, 13(6), 364–371. <https://doi.org/10.1063/1.1714879>.
- Bowen, J. H., Bowrey, R., & Malin, A. S. (1967). A study of the surface area and structure of activated alumina by direct observation. *Journal of Catalysis*, 7(3), 209–216. [https://doi.org/10.1016/0021-9517\(67\)90098-X](https://doi.org/10.1016/0021-9517(67)90098-X).
- Budinova, T. K., Petrov, N. V., Minkova, V. N., & Gergova, K. M. (1994). Removal of metal ions from aqueous solution by activated carbons obtained from different raw materials. *Journal of Chemical Technology & Biotechnology*, 60(2), 177–182. <https://doi.org/10.1002/jctb.280600210>.
- Cai, Y., Liu, D., Pan, Z., Yao, Y., Li, J., & Qiu, Y. (2013). Pore structure and its impact on CH₄ adsorption capacity and flow capability of bituminous and subbituminous coals from Northeast China. *Fuel*, 103, 258–268. <https://doi.org/10.1016/j.fuel.2012.06.055>.
- Chen, D., Yang, L., Li, J., & Wu, Q. (2019). Effect of self-doped heteroatoms in biomass-derived activated carbon for supercapacitor applications. *ChemistrySelect*, 4(5), 1586–1595. <https://doi.org/10.1002/slct.201803413>.
- Chiang, Y. C., Chiang, P. C., & Huang, C. P. (2001). Effects of pore structure and temperature on VOC adsorption on activated carbon. *Carbon*, 39(4), 523–534. [https://doi.org/10.1016/S0008-6223\(00\)00161-5](https://doi.org/10.1016/S0008-6223(00)00161-5).
- Choi, P. R., Lee, E., Kwon, S. H., Jung, J. C., & Kim, M. S. (2015). Characterization and organic electric-double-layer-capacitor application of KOH activated coal-tar-pitch-based carbons: Effect of carbonization temperature. *Journal of Physics and Chemistry of Solids*, 87, 72–79. <https://doi.org/10.1016/j.jpccs.2015.08.007>.
- Choudhury, N. D., Chutia, R. S., Bhaskar, T., & Kataki, R. (2014). Pyrolysis of jute dust: Effect of reaction parameters and analysis of products. *Journal of Material Cycles and Waste Management*, 16(3), 449–459. <https://doi.org/10.1007/s10163-014-0268-4>.
- Cid, R., Arriagada, R., & Orellana, F. (1983). Zeolites surface area calculation from nitrogen adsorption data. *Journal of Catalysis*, 80(1), 228–230. [https://doi.org/10.1016/0021-9517\(83\)90247-6](https://doi.org/10.1016/0021-9517(83)90247-6).

- Cook, R., Crathorne, E. A., Monhemius, A. J., & Perry, D. L. (1989). An XPS study of the adsorption of gold (I) cyanide by carbons. *Hydrometallurgy*, 22(1–2), 171–182. [https://doi.org/10.1016/0304-386X\(89\)90048-0](https://doi.org/10.1016/0304-386X(89)90048-0).
- Cook, T. E., Cilley, W. A., Savitsky, A. C., & Wiers, B. H. (1982). Zeolite a hydrolysis and degradation. *Environmental Science & Technology*, 16(6), 344–350. <https://doi.org/10.1021/es00100a008>.
- Cossu, R., Ehrig, H., & Muntoni, A. (2018). Physical–chemical leachate treatment. In *Solid waste landfilling: Concepts, processes, technology* (pp. 575–632). Elsevier.
- Dalai, A. K., Chowdhury, A. I., Hall, E. S., Zaman, J., & Tollefson, E. L. (1996). Activation of Canadian coals in a fixed-bed reactor and an internally stirred horizontal kiln. *Fuel*, 75(3), 384–392. [https://doi.org/10.1016/0016-2361\(95\)00252-9](https://doi.org/10.1016/0016-2361(95)00252-9).
- Daorattanachai, P., Unob, F., & Imyim, A. (2005). Multi-element preconcentration of heavy metal ions from aqueous solution by APDC impregnated activated carbon. *Talanta*, 67(1), 59–64. <https://doi.org/10.1016/j.talanta.2005.02.006>.
- Datta, D. R. (2016). Coal, porosity. In G. Tiess, T. Majumder, & P. Cameron (Eds.), *Encyclopedia of mineral and energy policy*. Springer. https://doi.org/10.1007/978-3-642-40871-7_103-1.
- Davidson, R. J. (1974). The mechanism of gold adsorption on activated charcoal. *Journal of the Southern African Institute of Mining and Metallurgy*, 75(4), 67–76.
- De Jong, W., Di Nola, G., Venneker, B. C., Spliethoff, H., & Wójciewicz, M. A. (2007). TG-FTIR pyrolysis of coal and secondary biomass fuels: Determination of pyrolysis kinetic parameters for main species and NO_x precursors. *Fuel*, 86(15), 2367–2376. <https://doi.org/10.1016/j.fuel.2007.01.032>.
- De Lima, L. S., Araujo, M. D., Quinária, S. P., Migliorine, D. W., & Garcia, J. R. (2011). Adsorption modeling of Cr, cd and cu on activated carbon of different origins by using fractional factorial design. *Chemical Engineering Journal*, 166(3), 881–889. <https://doi.org/10.1016/j.cej.2010.11.062>.
- Demiral, H., & Demiral, İ. (2008). Surface properties of activated carbon prepared from wastes. *Surface and Interface Analysis*, 40(3–4), 612–615. <https://doi.org/10.1002/sia.2716>.
- Dendooven, J., Goris, B., Devloo-Casier, K., Levrau, E., Biermans, E., Baklanov, M. R., Ludwig, K. F., Voort, P. V., Bals, S., & Detavernier, C. (2012). Tuning the pore size of ink-bottle mesopores by atomic layer deposition. *Chemistry of Materials*, 24(11), 1992–1994. <https://doi.org/10.1021/cm203754a>.
- Depci, T. (2012). Comparison of activated carbon and iron impregnated activated carbon derived from Gölbasi lignite to remove cyanide from water. *Chemical Engineering Journal*, 181, 467–478. <https://doi.org/10.1016/j.cej.2011.12.003>.
- Deveci, H. A., Yazıcı, E. Y., Alp, I., & Uslu, T. U. (2006). Removal of cyanide from aqueous solutions by plain and metal-impregnated granular activated carbons. *International Journal of Mineral Processing*, 79(3), 198–208. <https://doi.org/10.1016/j.minpro.2006.03.002>.
- Di Natale, F., Erto, A., Lancia, A., & Musmarra, D. (2011). Mercury adsorption on granular activated carbon in aqueous solutions containing nitrates and chlorides. *Journal of Hazardous Materials*, 192(3), 1842–1850. <https://doi.org/10.1016/j.jhazmat.2011.07.021>.
- Di Natale, F., Lancia, A., Molino, A., & Musmarra, D. (2007). Removal of chromium ions from aqueous solutions by adsorption on activated carbon and char. *Journal of Hazardous Materials*, 145(3), 381–390. <https://doi.org/10.1016/j.jhazmat.2006.11.028>.
- Dias, J. M., Alvim-Ferraz, M. C., Almeida, M. F., Rivera-Utrilla, J., & Sánchez-Polo, M. (2007). Waste materials for activated carbon preparation and its use in aqueous-phase treatment: A review. *Journal of Environmental Management*, 85(4), 833–846. <https://doi.org/10.1016/j.jenvman.2007.07.031>.
- Durán-Valle, C. J., Botet-Jiménez, A. B., & Omenat-Morán, D. (2017). Hydrothermal carbonisation: An eco-friendly method for the production of carbon adsorbents. In *Adsorption processes for water treatment and purification* (pp. 77–108). Cham: Springer. https://doi.org/10.1007/978-3-319-58136-1_4.

- Dutta, S., Wen, C. Y., & Belt, R. J. (1977). Reactivity of coal and char. 1. In carbon dioxide atmosphere. *Industrial & Engineering Chemistry Process Design and Development*, 16(1), 20–30. <https://doi.org/10.1021/i260061a004>.
- El Qada, E. N., Allen, S. J., & Walker, G. M. (2006). Adsorption of methylene blue onto activated carbon produced from steam activated bituminous coal: A study of equilibrium adsorption isotherm. *Chemical Engineering Journal*, 124(1–3), 103–110. <https://doi.org/10.1016/j.cej.2006.08.015>.
- Essuah, E. Y., & Buah, W. K. (2019). Effects of steam dosage on the qualities of activated carbon developed from coconut shells in Ghana. *International Journal of Mining Science*, 5(4), 22–29. <https://doi.org/10.20431/2454-9460.0504002>.
- Everson, R. C., Neomagus, H. W., Kasaini, H., & Njapha, D. (2006). Reaction kinetics of pulverized coal-chars derived from inertinite-rich coal discards: Gasification with carbon dioxide and steam. *Fuel*, 85(7–8), 1076–1082. <https://doi.org/10.1016/j.fuel.2005.10.016>.
- Fan, L. Z., Qiao, S., Song, W., Wu, M., He, X., & Qu, X. (2013). Effects of the functional groups on the electrochemical properties of ordered porous carbon for supercapacitors. *Electrochimica Acta*, 105, 299–304. <https://doi.org/10.1016/j.electacta.2013.04.137>.
- Feng, D., Zhao, Y., Zhang, Y., Sun, S., Meng, S., Guo, Y., & Huang, Y. (2016). Effects of K and Ca on reforming of model tar compounds with pyrolysis biochars under H₂O or CO₂. *Chemical Engineering Journal*, 306, 422–432. <https://doi.org/10.1016/j.cej.2016.07.065>.
- Feng, W., Kwon, S., Borguet, E., & Vidic, R. (2005). Adsorption of hydrogen sulfide onto activated carbon fibers: Effect of pore structure and surface chemistry. *Environmental Science & Technology*, 39(24), 9744–9749. <https://doi.org/10.1021/es0507158>.
- Ferreira, A. F., Mittelmeijer-Hazeleger, M. C., van den Bergh, J., Aguado, S., Jansen, J. C., Rothenberg, G., Rodrigues, A. E., & Kapteijn, F. (2013). Adsorption of hexane isomers on MFI type zeolites at ambient temperature: Understanding the aluminium content effect. *Microporous and Mesoporous Materials*, 170, 26–35. <https://doi.org/10.1016/j.micromeso.2012.11.020>.
- Franklin, R. E. (1951). Crystallite growth in graphitizing and non-graphitizing carbons. *Proceedings of the Royal Society of London. Series A. Mathematical and Physical Sciences*, 209(1097), 196–218. <https://doi.org/10.1098/rspa.1951.0197>.
- Franklin, R. E. (1956). Homogeneous and heterogeneous graphitization of carbon. *Nature*, 177(4501), 239. <https://doi.org/10.1038/177239a0>.
- Furmaniak, S. (2015). Influence of activated carbon porosity and surface oxygen functionalities' presence on adsorption of acetonitrile as a simple polar volatile organic compound. *Environmental Technology*, 36(15), 1984–1999. <https://doi.org/10.1080/09593330.2015.1018843>.
- Furmaniak, S., Gauden, P. A., Terzyk, A. P., & Rychlicki, G. (2008). Water adsorption on carbons—Critical review of the most popular analytical approaches. *Advances in Colloid and Interface Science*, 137(2), 82–143. <https://doi.org/10.1016/j.cis.2007.08.001>.
- Fierro, V., Torné-Fernández, V., Montané, D., & Celzard, A. (2008). Adsorption of phenol onto activated carbons having different textural and surface properties. *Microporous and mesoporous materials*, 111(1–3), 276–284. <https://doi.org/10.1016/j.micromeso.2007.08.002>.
- Ganan, J., González-García, C. M., Gonzalez, J. F., Sabio, E., Macías-García, A., & Díaz-Díez, M. A. (2004). Preparation of activated carbons from bituminous coal pitches. *Applied Surface Science*, 238(1–4), 347–354. <https://doi.org/10.1016/j.apsusc.2004.05.222>.
- Gao, L., Dong, F. Q., Dai, Q. W., Zhong, G. Q., Halik, U., & Lee, D. J. (2016). Coal tar residues based activated carbon: Preparation and characterization. *Journal of the Taiwan Institute of Chemical Engineers*, 63, 166–169. <https://doi.org/10.1016/j.jtice.2016.02.029>.
- Gao, S., Ge, L., Rufford, T. E., & Zhu, Z. (2017). The preparation of activated carbon discs from tar pitch and coal powder for adsorption of CO₂, CH₄ and N₂. *Microporous and Mesoporous Materials*, 238, 19–26. <https://doi.org/10.1016/j.micromeso.2016.08.004>.
- Gercel, H. F. (2002). The effect of a sweeping gas flow rate on the fast pyrolysis of biomass. *Energy Sources*, 24(7), 633–642. <https://doi.org/10.1080/00908312.2002.11877438>.

- Gomaa, H., Gomaa, A., Farid, M., Cheira, M., Ahmed, T., & Seaf, S. E. (2016). Removal of uranium from acidic solution using activated carbon impregnated with tri butyl phosphate. *Biological and Chemical Research*, 313–340.
- Gombojav, U., Jambal, I., & Byambajav, E. (2020). Preparation of activated carbons from Mongolian lignite and sub-bituminous coal by a physical method. *Journal of Minerals and Materials Characterization and Engineering*, 8(03), 97. <https://doi.org/10.4236/jmmce.2020.83007>.
- Gomez, L. M., Colpas-Castillo, F., & Fernandez-Maestre, R. (2014). Cation exchange for mercury and cadmium of xanthated, sulfonated, activated and non-treated subbituminous coal, commercial activated carbon and commercial synthetic resin: Effect of pre-oxidation on xanthation of subbituminous coal. *International Journal of Coal Science & Technology*, 1(2), 235–240. <https://doi.org/10.1007/s40789-014-0033-2>.
- Gomez-Serrano, V., Macias-Garcia, A., Espinosa-Mansilla, A., & Valenzuela-Calahorro, C. (1998). Adsorption of mercury, cadmium and lead from aqueous solution on heat-treated and sulphurized activated carbon. *Water Research*, 32(1), 1–4. [https://doi.org/10.1016/S0043-1354\(97\)00203-0](https://doi.org/10.1016/S0043-1354(97)00203-0).
- González, M. T., Molina-Sabio, M., & Rodriguez-Reinoso, F. (1994). Steam activation of olive stone chars, development of porosity. *Carbon*, 32(8), 1407–1413. [https://doi.org/10.1016/0008-6223\(94\)90133-3](https://doi.org/10.1016/0008-6223(94)90133-3).
- Goyal, A., Zabransky, R. F., & Rehmat, A. (1989). Gasification kinetics of Western Kentucky bituminous coal char. *Industrial & Engineering Chemistry Research*, 28(12), 1767–1778. <https://doi.org/10.1021/ie00096a006>.
- Grammelis, P., Margaritis, N., & Karampinis, E. (2016). Solid fuel types for energy generation: Coal and fossil carbon-derivative solid fuels. In *Fuel flexible energy generation* (pp. 29–58). Woodhead Publishing. <https://doi.org/10.1016/B978-1-78242-378-2.00002-X>.
- Grzyb, B., Albiński, A., Broniek, E., Furdin, G., Maréché, J. F., & Bégin, D. (2009). SO₂ adsorptive properties of activated carbons prepared from polyacrylonitrile and its blends with coal-tar pitch. *Microporous and Mesoporous Materials*, 118(1–3), 163–168. <https://doi.org/10.1016/j.micromeso.2008.08.032>.
- Guihong, L. I., Zhang, H., Zhang, H., & Xiaozhong, S. O. (2010). Characteristics of fissures and pores of anthracite in Jincheng by SEM. *Mining Science and Technology (China)*, 20(5), 789–793. [https://doi.org/10.1016/S1674-5264\(09\)60282-9](https://doi.org/10.1016/S1674-5264(09)60282-9).
- Guizani, C., Jeguirim, M., Gadiou, R., Sanz, F. J., & Salvador, S. (2016). Biomass char gasification by H₂O, CO₂ and their mixture: Evolution of chemical, textural and structural properties of the chars. *Energy*, 112, 133–145. <https://doi.org/10.1016/j.energy.2016.06.065>.
- Guldogan, Y., Bozdemir TO, & Durusoy, T. (2000). Effect of heating rate on pyrolysis kinetics of Tuncbilek lignite. *Energy Sources*, 22(4), 305–312. <https://doi.org/10.1080/00908310050013901>.
- Guo, D., & Guo, X. (2018). The influence factors for gas adsorption with different ranks of coals. *Adsorption Science & Technology*, 36(3–4), 904–918. <https://doi.org/10.1177/0263617417730186>.
- Hadi, P., To MH, Hui, C. W., Lin, C. S., & McKay, G. (2015). Aqueous mercury adsorption by activated carbons. *Water Research*, 73, 37–55. <https://doi.org/10.1016/j.watres.2015.01.018>.
- Han, H., Rafiq, M. K., Zhou, T., Xu, R., Mašek, O., & Li, X. (2019). A critical review of clay-based composites with enhanced adsorption performance for metal and organic pollutants. *Journal of Hazardous Materials*, 369, 780–796. <https://doi.org/10.1016/j.jhazmat.2019.02.003>.
- Harris, P. J., Liu, Z., & Suenaga, K. (2008). Imaging the atomic structure of activated carbon. *Journal of Physics: Condensed Matter*, 20(36), 362201. <https://doi.org/10.1088/0953-8984/20/36/362201>.
- Havelcova, M., Mizera, J., Sýkorová, I., & Pekař, M. (2009). Sorption of metal ions on lignite and the derived humic substances. *Journal of Hazardous Materials*, 161(1), 559–564. <https://doi.org/10.1016/j.jhazmat.2008.03.136>.

- Hayashi, J. I., Kazehaya, A., Muroyama, K., & Watkinson, A. P. (2000). Preparation of activated carbon from lignin by chemical activation. *Carbon*, 38(13), 1873–1878. [https://doi.org/10.1016/S0008-6223\(00\)00027-0](https://doi.org/10.1016/S0008-6223(00)00027-0).
- He, X., Li, R., Qiu, J., Xie, K., Ling, P., Yu, M., Zhang, X., & Zheng, M. (2012). Synthesis of mesoporous carbons for supercapacitors from coal tar pitch by coupling microwave-assisted KOH activation with a MgO template. *Carbon*, 50(13), 4911–4921. <https://doi.org/10.1016/j.carbon.2012.06.020>.
- Hecht, E. S., Shaddix, C. R., Geier, M., Molina, A., & Haynes, B. S. (2012). Effect of CO₂ and steam gasification reactions on the oxy-combustion of pulverized coal char. *Combustion and Flame*, 159(11), 3437–3447. <https://doi.org/10.1016/j.combustflame.2012.06.009>.
- Hu, H., & Xu, K. (2020). Physicochemical technologies for HRP and risk control. In *High-risk pollutants in wastewater* (pp. 169–207). Elsevier. <https://doi.org/10.1016/B978-0-12-816448-8.00008-3>.
- Hu, L., Hou, J., Ma, Y., Li, H., & Zhai, T. (2016). Multi-heteroatom self-doped porous carbon derived from swim bladders for large capacitance supercapacitors. *Journal of Materials Chemistry A*, 4(39), 15006–15014. <https://doi.org/10.1039/C6TA06337C>.
- Hulicova-Jurcakova, D., Seredych, M., Lu, G. Q., & Bandosz, T. J. (2009). Combined effect of nitrogen- and oxygen-containing functional groups of microporous activated carbon on its electrochemical performance in supercapacitors. *Advanced Functional Materials*, 19(3), 438–447. <https://doi.org/10.1002/adfm.200801236>.
- Ibrado, A. S., & Fuerstenau, D. W. (1995). Infrared and X-ray photoelectron spectroscopy studies on the adsorption of gold cyanide on activated carbon. *Minerals Engineering*, 8(4–5), 441–458. [https://doi.org/10.1016/0892-6875\(95\)00009-F](https://doi.org/10.1016/0892-6875(95)00009-F).
- Illán-Gómez, M. J., García-García, A., Salinas-Martínez de Lecea, C., & Linares-Solano, A. (1996). Activated carbons from Spanish coals. 2. Chemical activation. *Energy & Fuels*, 10(5), 1108–1114. <https://doi.org/10.1021/ef950195+>.
- Izquierdo, M. T., & Rubio, B. (2008). Carbon-enriched coal fly ash as a precursor of activated carbons for SO₂ removal. *Journal of Hazardous Materials*, 155(1–2), 199–205. <https://doi.org/10.1016/j.jhazmat.2007.11.047>.
- Jahromi, P. E., Fatemi, S., Vatani, A., Ritter, J. A., & Ebner, A. D. (2018). Purification of helium from a cryogenic natural gas nitrogen rejection unit by pressure swing adsorption. *Separation and Purification Technology*, 193, 91–102. <https://doi.org/10.1016/j.seppur.2017.11.002>.
- Jaramillo, J., Álvarez, P. M., & Gómez-Serrano, V. (2010). Preparation and ozone-surface modification of activated carbon. Thermal stability of oxygen surface groups. *Applied Surface Science*, 256(17), 5232–5236. <https://doi.org/10.1016/j.apsusc.2009.12.109>.
- Jayaraman, K., & Gokalp, I. (2015). Effect of char generation method on steam, CO₂ and blended mixture gasification of high ash Turkish coals. *Fuel*, 153, 320–327. <https://doi.org/10.1016/j.fuel.2015.01.065>.
- Jenkins, G. M., Jenkins, A., & Kawamura, K. (1976). *Polymeric carbons: Carbon fibre, glass and char*. Cambridge University Press.
- Jia, Y. F., Steele, C. J., Hayward, I. P., & Thomas, K. M. (1998). Mechanism of adsorption of gold and silver species on activated carbons. *Carbon*, 36(9), 1299–1308. [https://doi.org/10.1016/S0008-6223\(98\)00091-8](https://doi.org/10.1016/S0008-6223(98)00091-8).
- Jiang, N., Shang, R., Heijman, S. G., & Rietveld, L. C. (2018). High-silica zeolites for adsorption of organic micro-pollutants in water treatment: A review. *Water Research*, 144, 145–161. <https://doi.org/10.1016/j.watres.2018.07.017>.
- Jiang, W., Nadeau, G., Zaghib, K., & Kinoshita, K. (2000). Thermal analysis of the oxidation of natural graphite—Effect of particle size. *Thermochimica Acta*, 351(1–2), 85–93. [https://doi.org/10.1016/S0040-6031\(00\)00416-0](https://doi.org/10.1016/S0040-6031(00)00416-0).
- Jibril, B. Y., Al-Maamari, R. S., Hegde, G., Al-Mandhary, N., & Houache, O. (2007). Effects of feedstock pre-drying on carbonization of KOH-mixed bituminous coal in preparation of activated carbon. *Journal of Analytical and Applied Pyrolysis*, 80(2), 277–282. <https://doi.org/10.1016/j.jaap.2007.03.003>.

- Johnson, J. L. (1974). Kinetics of bituminous coal char gasification with gases containing steam and hydrogen. In *Coal gasification* (pp. 145–178). ACS Publishing.
- Kajitani, S., Suzuki, N., Ashizawa, M., & Hara, S. (2006). CO₂ gasification rate analysis of coal char in entrained flow coal gasifier. *Fuel*, 85(2), 163–169. <https://doi.org/10.1016/j.fuel.2005.07.024>.
- Kalaruban, M., Loganathan, P., Nguyen, T. V., Nur, T., Johir, M. A., Nguyen, T. H., Trinh, M. V., & Vigneswaran, S. (2019). Iron-impregnated granular activated carbon for arsenic removal: Application to practical column filters. *Journal of Environmental Management*, 239, 235–243. <https://doi.org/10.1016/j.jenvman.2019.03.053>.
- Kalderis, D., Bethanis, S., Paraskeva, P., & Diamadopoulos, E. (2008). Production of activated carbon from bagasse and rice husk by a single-stage chemical activation method at low retention times. *Bioresource Technology*, 99(15), 6809–6816. <https://doi.org/10.1016/j.biortech.2008.01.041>.
- Kamran, U., Heo, Y. J., Lee, J. W., & Park, S. J. (2019). Chemically modified activated carbon decorated with MnO₂ nanocomposites for improving lithium adsorption and recovery from aqueous media. *Journal of Alloys and Compounds*, 794, 425–434. <https://doi.org/10.1016/j.jallcom.2019.04.211>.
- Karabulut, S., Karabakan, A., Denizli, A., & Yürüm, Y. (2001). Cadmium (II) and mercury (II) removal from aquatic solutions with low-rank Turkish coal. *Separation Science and Technology*, 36(16), 3657–3671. <https://doi.org/10.1081/SS-100108354>.
- Kasaini, H., Everson, R. C., & Bruinsma, O. S. (2005). Selective adsorption of platinum from mixed solutions containing base metals using chemically modified activated carbons. *Separation Science and Technology*, 40(1–3), 507–523. <https://doi.org/10.1081/SS-200042510>.
- Kausar, A., Iqbal, M., Javed, A., Aftab, K., Bhatti, H. N., & Nouren, S. (2018). Dyes adsorption using clay and modified clay: A review. *Journal of Molecular Liquids*, 256, 395–407. <https://doi.org/10.1016/j.molliq.2018.02.034>.
- Kim, S. C., Hong, I. K., & Park, K. A. (1997). Preparation and performance of the briquette type activated carbon based on bituminous coal. *Journal of Industrial and Engineering Chemistry*, 3(3), 218–222.
- Klauber, C. (1988). Acid induced oligomerization of aurocyanide adsorbed on carbon. *Surface Science*, 203(1–2), 118–128. [https://doi.org/10.1016/0039-6028\(88\)90198-7](https://doi.org/10.1016/0039-6028(88)90198-7).
- Klauber, C. (1991). X-ray photoelectron spectroscopic study of the adsorption mechanism of aurocyanide onto activated carbon. *Langmuir*, 7(10), 2153–2159. <https://doi.org/10.1021/la00058a030>.
- Kök, M. V. (2005). Temperature-controlled combustion and kinetics of different rank coal samples. *Journal of Thermal Analysis and Calorimetry*, 79(1), 175–180. <https://doi.org/10.1007/s10973-004-0581-6>.
- Kok, M. V., & Pamir, R. (2003). Pyrolysis kinetics of oil shales determined by DSC and TG/DTG. *Oil Shale*, 20(1), 57–68.
- Kołodźńska, D., Krukowska, J. A., & Thomas, P. (2017). Comparison of sorption and desorption studies of heavy metal ions from biochar and commercial active carbon. *Chemical Engineering Journal*, 307, 353–363. <https://doi.org/10.1016/j.cej.2016.08.088>.
- Kongolo, K., Bahr, A., Friedl, J., & Wagner, F. E. (1990). 197 au Mössbauer study of the gold species adsorbed on carbon from cyanide solutions. *Metallurgical Transactions B*, 21(2), 239–249.
- Kononova, O. N., Kholmogorov, A. G., Danilenko, N. V., Goryaeva, N. G., Shatnykh, K. A., & Kachin, S. V. (2007). Recovery of silver from thiosulfate and thiocyanate leach solutions by adsorption on anion exchange resins and activated carbon. *Hydrometallurgy*, 88(1–4), 189–195. <https://doi.org/10.1016/j.hydromet.2007.03.012>.
- Kopac, T., & Toprak, A. (2007). Preparation of activated carbons from Zonguldak region coals by physical and chemical activations for hydrogen sorption. *International Journal of Hydrogen Energy*, 32(18), 5005–5014. <https://doi.org/10.1016/j.ijhydene.2007.08.002>.

- Kumar, A., & Jena, H. M. (2016). Removal of methylene blue and phenol onto prepared activated carbon from fox nutshell by chemical activation in batch and fixed-bed column. *Journal of Cleaner Production*, 137, 1246–1259. <https://doi.org/10.1016/j.jclepro.2016.07.177>.
- Kütahyalı, C., & Eral, M. (2004). Selective adsorption of uranium from aqueous solutions using activated carbon prepared from charcoal by chemical activation. *Separation and Purification Technology*, 40(2), 109–114. <https://doi.org/10.1016/j.seppur.2004.01.011>.
- Laredo, G. C., Vega-Merino, P. M., Trejo-Zárraga, F., & Castillo, J. (2013). Denitrogenation of middle distillates using adsorbent materials towards ULSD production: A review. *Fuel Processing Technology*, 106, 21–32. <https://doi.org/10.1016/j.fuproc.2012.09.057>.
- Largitte, L., & Pasquier, R. (2016). A review of the kinetics adsorption models and their application to the adsorption of lead by an activated carbon. *Chemical Engineering Research and Design*, 109, 495–504. <https://doi.org/10.1016/j.cherd.2016.02.006>.
- Larsen, J. W., Lee, D., Schmidt, T., & Grint, A. (1986). Multiple mechanisms for the loss of coking properties caused by mild air oxidation. *Fuel*, 65(4), 595–596. [https://doi.org/10.1016/0016-2361\(86\)90056-6](https://doi.org/10.1016/0016-2361(86)90056-6).
- Lee, J. C., Kurniawan, H. H. J., Chung, K. W., & Kim, S. (2020). Separation of platinum, palladium and rhodium from aqueous solutions using ion exchange resin: A review. *Separation and Purification Technology*, 116896. <https://doi.org/10.1016/j.seppur.2020.116896>.
- Li, B., Chen, G., Zhang, H., & Sheng, C. (2014). Development of non-isothermal TGA–DSC for kinetics analysis of low temperature coal oxidation prior to ignition. *Fuel*, 118, 385–391. <https://doi.org/10.1016/j.fuel.2013.11.011>.
- Li, H., Yang, S., Riisager, A., Pandey, A., Sangwan, R. S., Saravanamurugan, S., & Luque, R. (2016). Zeolite and zeotype-catalysed transformations of biofuranic compounds. *Green Chemistry*, 18(21), 5701–5735. <https://doi.org/10.1039/C6GC02415G>.
- Li, X., Zhang, L., Yang, Z., Wang, P., Yan, Y., & Ran, J. (2020). Adsorption materials for volatile organic compounds (VOCs) and the key factors for VOCs adsorption process: A review. *Separation and Purification Technology*, 235, 116213. <https://doi.org/10.1016/j.seppur.2019.116213>.
- Li, Z., Liang, Q., Yang, C., Zhang, L., Li, B., & Li, D. (2017). Convenient preparation of nitrogen-doped activated carbon from macadamia nutshell and its application in supercapacitor. *Journal of Materials Science: Materials in Electronics*, 28(18), 13880–13887. <https://doi.org/10.1007/s10854-017-7236-4>.
- Liemans, I., Alban, B., Tranier, J. P., & Thomas, D. (2011). SO_x and NO_x absorption based removal into acidic conditions for the flue gas treatment in oxy-fuel combustion. *Energy Procedia*, 4, 2847–2854. <https://doi.org/10.1016/j.egypro.2011.02.190>.
- Lillo-Ródenas, M. A., Lozano-Castelló, D., Cazorla-Amorós, D., & Linares-Solano, A. (2001). Preparation of activated carbons from Spanish anthracite: II. Activation by NaOH. *Carbon*, 39(5), 751–759. [https://doi.org/10.1016/S0008-6223\(00\)00185-8](https://doi.org/10.1016/S0008-6223(00)00185-8).
- Linares-Solano, A., Martín-Gullón, I., de Lecea, C. S., & Serrano-Talavera, B. (2000). Activated carbons from bituminous coal: Effect of mineral matter content. *Fuel*, 79(6), 635–643. [https://doi.org/10.1016/S0016-2361\(99\)00184-2](https://doi.org/10.1016/S0016-2361(99)00184-2).
- Liu, C., Liang, X., Liu, X., Wang, Q., Teng, N., Zhan, L., Zhang, R., Qiao, W., & Ling, L. (2008). Wettability modification of pitch-based spherical activated carbon by air oxidation and its effects on phenol adsorption. *Applied Surface Science*, 254(9), 2659–2665. <https://doi.org/10.1016/j.apsusc.2007.10.026>.
- Liu, L., Yuan, Y., Kumar, S., Wang, Z., He, Y., Lv, Y., Liu, J., Gul-e-Rana, J., & Cen, K. (2018a). Catalytic effect of metal chlorides on coal pyrolysis and gasification part II. Effects of acid washing on coal characteristics. *Thermochimica Acta*, 666, 41–50. <https://doi.org/10.1016/j.tca.2018.06.001>.
- Liu, X., Yang, Y., Ji, W., Liu, H., Zhang, C., & Xu, B. (2007). Controllable growth of nanostructured carbon from coal tar pitch by chemical vapor deposition. *Materials Chemistry and Physics*, 104(2–3), 320–326. <https://doi.org/10.1016/j.matchemphys.2007.03.020>.

- Liu, Z., Zhang, Z., Choi, S. K., & Lu, Y. (2018b). Surface properties and pore structure of anthracite, bituminous coal and lignite. *Energies*, *11*(6), 1502. <https://doi.org/10.3390/en11061502>.
- Loganathan, P., Shim, W. G., Sounthararajah, D. P., Kalaruban, M., Nur, T., & Vigneswaran, S. (2018). Modelling equilibrium adsorption of single, binary, and ternary combinations of Cu, Pb, and Zn onto granular activated carbon. *Environmental Science and Pollution Research*, *25*(17), 16664–16675. <https://doi.org/10.1007/s11356-018-1793-9>.
- Lu, J. D., & Xue, J. (2019). Poisoning: Kinetics to therapeutics. In *Critical care nephrology* (pp. 600–629). Elsevier Publishing.
- Lua, A. C. (2019). A detailed study of pyrolysis conditions on the production of steam-activated carbon derived from oil-palm shell and its application in phenol adsorption. *Biomass Conversion and Biorefinery*, *11*, 1-1. <https://doi.org/10.1007/s13399-019-00447-9>.
- Luo, C., Watanabe, T., Nakamura, M., Uemiya, S., & Kojima, T. (2001). Gasification kinetics of coal chars carbonized under rapid and slow heating conditions at elevated temperatures. *Journal of Energy Resources Technology*, *123*(1), 21–26. <https://doi.org/10.1115/1.1345701>.
- Lorenc-Grabowska, E. (2016). Effect of micropore size distribution on phenol adsorption on steam activated carbons. *Adsorption*, *22*(4–6), 599–607. <https://doi.org/10.1007/s10450-015-9737-x>.
- Lozano-Castello, D., Lillo-Ródenas, M. A., Cazorla-Amorós, D., & Linares-Solano, A. (2001). Preparation of activated carbons from Spanish anthracite: I. Activation by KOH. *Carbon*, *39*(5), 741–749. [https://doi.org/10.1016/S0008-6223\(00\)00185-8](https://doi.org/10.1016/S0008-6223(00)00185-8).
- Lv, X., Zhang, T., Luo, Y., Zhang, Y., Wang, Y., & Zhang, G. (2020). Study on carbon nanotubes and activated carbon hybrids by pyrolysis of coal. *Journal of Analytical and Applied Pyrolysis*, *146*, 104717. <https://doi.org/10.1016/j.jaap.2019.104717>.
- Ma, J., Tan, J., Du, X., & Li, R. (2010). Effects of preparation parameters on the textural features of a granular zeolite/activated carbon composite material synthesized from elutriilite and pitch. *Microporous and Mesoporous Materials*, *132*(3), 458–463. <https://doi.org/10.1016/j.micromeso.2010.03.027>.
- Ma, L., He, M., Fu, P., Jiang, X., Lv, W., Huang, Y., Liu, Y., & Wang, H. (2020). Adsorption of volatile organic compounds on modified spherical activated carbon in a new cyclonic fluidized bed. *Separation and Purification Technology*, *235*, 116146. <https://doi.org/10.1016/j.seppur.2019.116146>.
- Ma, S., Hill, J. O., & Heng, S. (1991). A kinetic analysis of the pyrolysis of some Australian coals by non-isothermal thermogravimetry. *Journal of Thermal Analysis*, *37*(6), 1161–1177. <https://doi.org/10.1007/BF01913852>.
- Maloney, D. J., Jenkins, R. G., & Walker, P. L., Jr. (1982). Low-temperature air oxidation of caking coals. 2. Effect on swelling and softening properties. *Fuel*, *61*(2), 175–181. [https://doi.org/10.1016/0016-2361\(82\)90231-9](https://doi.org/10.1016/0016-2361(82)90231-9).
- Manocha, S. M., Patel, H., & Manocha, L. M. (2010). Effect of steam activation parameters on characteristics of pine based activated carbon. *Carbon Letters (Carbon Lett.)*, *11*(3), 201–205.
- Maroto-Valer, M. M., Taulbee, D. N., Schobert, H. H., Hower, J. C., Andersen, J.M. (1999). Use of unburned carbon in fly ash as precursor for the development of activated carbons. In International ash utilization symposium, paper 19 18.
- Martínez-Mendoza, K. L., Burgos, J. M., Marriaga-Cabrales, N., Machuca-Martínez, F., Barajas, M., & Romero, M. (2020). Production and characterization of activated carbon from coal for gold adsorption in cyanide solutions. *Ingeniería e Investigación*, *40*, 1. <https://doi.org/10.15446/ing.investig.v40n1.8012>.
- McDonald-Wharry, J. S., Manley-Harris, M., & Pickering, K. L. (2016). Reviewing, combining, and updating the models for the nanostructure of non-graphitizing carbons produced from oxygen-containing precursors. *Energy & Fuels*, *30*(10), 7811–7826. <https://doi.org/10.1021/acs.energyfuels.6b00917>.
- McDougall, G. J., Hancock, R. D., Nicol, M. J., Wellington, O. L., & Copperthwaite, R. G. (1980). The mechanism of the adsorption of gold cyanide on activated carbon. *Journal of the Southern African Institute of Mining and Metallurgy*, *80*(9), 344–356.
- Menon, V. C., & Komarneni, S. (1998). Porous adsorbents for vehicular natural gas storage: A review. *Journal of Porous Materials*, *5*(1), 43–58. <https://doi.org/10.1023/A:1009673830619>.

- Mildner, D. F., & Carpenter, J. M. (1982). On the short range atomic structure of non-crystalline carbon. *Journal of Non-Crystalline Solids*, 47(3), 391–402. [https://doi.org/10.1016/0022-3093\(82\)90215-0](https://doi.org/10.1016/0022-3093(82)90215-0).
- Mintova, S., Valtchev, V., Onfroy, T., Marichal, C., Knözinger, H., & Bein, T. (2006). Variation of the Si/Al ratio in nanosized zeolite Beta crystals. *Microporous and Mesoporous Materials*, 90(1–3), 237–245. <https://doi.org/10.1016/j.micromeso.2005.11.026>.
- Miura, K., Hashimoto, K., & Silveston, P. L. (1989). Factors affecting the reactivity of coal chars during gasification, and indices representing reactivity. *Fuel*, 68(11), 1461–1475. [https://doi.org/10.1016/0016-2361\(89\)90046-X](https://doi.org/10.1016/0016-2361(89)90046-X).
- Mohapatra, M., Anand, S., Mishra, B. K., Giles, D. E., & Singh, P. (2009). Review of fluoride removal from drinking water. *Journal of Environmental Management*, 91(1), 67–77. <https://doi.org/10.1016/j.jenvman.2009.08.015>.
- Mojoudi, N., Mirghaffari, N., Soleimani, M., Shariatmadari, H., Belver, C., & Bedia, J. (2019). Phenol adsorption on high microporous activated carbons prepared from oily sludge: Equilibrium, kinetic and thermodynamic studies. *Scientific Reports*, 9(1), 1–2. <https://doi.org/10.1038/s41598-019-55794-4>.
- Molina-Sabio, M., Perez, V., & Rodriguez-Reinoso, F. (1994). Impregnation of activated carbon with chromium and copper salts: Effect of porosity and metal content. *Carbon*, 32(7), 1259–1265. [https://doi.org/10.1016/0008-6223\(94\)90111-2](https://doi.org/10.1016/0008-6223(94)90111-2).
- Musyoka, N. M., Wdowin, M., Rambau, K. M., Franus, W., Panek, R., Madej, J., & Czarna-Juszkiewicz, D. (2020). Synthesis of activated carbon from high-carbon coal fly ash and its hydrogen storage application. *Renewable Energy*. <https://doi.org/10.1016/j.renene.2020.04.003>.
- Molina-Sabio, M., & Rodriguez-Reinoso, F. (2004). Role of chemical activation in the development of carbon porosity. *Colloids and Surfaces A: Physicochemical and Engineering Aspects*, 241(1–3), 15–25. <https://doi.org/10.1016/j.colsurfa.2004.04.007>.
- Navarro, P., & Alguacil, F. J. (2002). Adsorption of antimony and arsenic from a copper electrorefining solution onto activated carbon. *Hydrometallurgy*, 66(1–3), 101–105. [https://doi.org/10.1016/S0304-386X\(02\)00108-1](https://doi.org/10.1016/S0304-386X(02)00108-1).
- Nie, B., Liu, X., Yang, L., Meng, J., & Li, X. (2015). Pore structure characterization of different rank coals using gas adsorption and scanning electron microscopy. *Fuel*, 158, 908–917. <https://doi.org/10.1016/j.fuel.2015.06.050>.
- Nor, N. M., Lau, L. C., Lee, K. T., & Mohamed, A. R. (2013). Synthesis of activated carbon from lignocellulosic biomass and its applications in air pollution control—A review. *Journal of Environmental Chemical Engineering*, 1(4), 658–666. <https://doi.org/10.1016/j.jece.2013.09.017>.
- Norman, L. M., & Cha, C. Y. (1995). Production of activated carbon from coal chars using microwave energy. *Chemical Engineering Communications*, 140(1), 87–110. <https://doi.org/10.1080/00986449608936456>.
- Nunn, T. R., Howard, J. B., Longwell, J. P., & Peters, W. A. (1985). Studies of the rapid pyrolysis of sweet gum hardwood. In *Fundamentals of thermochemical biomass conversion* (pp. 293–314). Springer, Dordrecht. https://doi.org/10.1007/978-94-009-4932-4_16.
- Oraby, E. A., & Eksteen, J. J. (2015). The leaching of gold, silver and their alloys in alkaline glycine–peroxide solutions and their adsorption on carbon. *Hydrometallurgy*, 152, 199–203. <https://doi.org/10.1016/j.hydromet.2014.12.015>.
- Pagnanelli, F., Ferella, F., De Michelis, I., & Vegliò, F. (2011). Adsorption onto activated carbon for molybdenum recovery from leach liquors of exhausted hydrotreating catalysts. *Hydrometallurgy*, 110(1–4), 67–72. <https://doi.org/10.1016/j.hydromet.2011.08.008>.
- Painter, P. C., Snyder, R. W., Pearson, D. E., & Kwong, J. (1980). Fourier transform infrared study of the variation in the oxidation of a coking coal. *Fuel*, 59(5), 282–286. [https://doi.org/10.1016/0016-2361\(80\)90209-4](https://doi.org/10.1016/0016-2361(80)90209-4).
- Pallarés, J., González-Cencerrado, A., & Arauzo, I. (2018). Production and characterization of activated carbon from barley straw by physical activation with carbon dioxide and steam. *Biomass and Bioenergy*, 115, 64–73. <https://doi.org/10.1016/j.biombioe.2018.04.015>.

- Pandey, M. P., & Chaudhuri, M. (1982). Removal of inorganic mercury from water by bituminous coal. *Water Research*, 16(7), 1113–1118. [https://doi.org/10.1016/0043-1354\(82\)90127-0](https://doi.org/10.1016/0043-1354(82)90127-0).
- Parga, J. R., Rodríguez, M., Vázquez, V., Valenzuela, J. L., & Moreno, H. (2012). Recovery of silver and gold from cyanide solution by magnetic species formed in the electrocoagulation process. *Mineral Processing and Extractive Metallurgy Review*, 33(6), 363–373. <https://doi.org/10.1080/08827508.2011.601483>.
- Parra, J. B., Pis, J. J., De Sousa, J. C., Pajares, J. A., & Bansal, R. C. (1996). Effect of coal pre-oxidation on the development of microporosity in activated carbons. *Carbon*, 34(6), 783–787. [https://doi.org/10.1016/0008-6223\(96\)00030-9](https://doi.org/10.1016/0008-6223(96)00030-9).
- Petersen, F. W., & Van Deventer, J. S. (1991). The influence of pH, dissolved oxygen and organics on the adsorption of metal cyanides on activated carbon. *Chemical Engineering Science*, 46(12), 3053–3065. [https://doi.org/10.1016/0009-2509\(91\)85009-M](https://doi.org/10.1016/0009-2509(91)85009-M).
- Petrov, N., Budinova, T., & Khavesov, I. (1992). Adsorption of the ions of zinc, cadmium, copper, and lead on oxidized anthracite. *Carbon*, 30(2), 135–139. [https://doi.org/10.1016/0008-6223\(92\)90072-5](https://doi.org/10.1016/0008-6223(92)90072-5).
- Pietrzak, R., Wachowska, H., Nowicki, P., & Babel, K. (2007). Preparation of modified active carbon from brown coal by ammoxidation. *Fuel Processing Technology*, 88(4), 409–415. <https://doi.org/10.1016/j.fuproc.2006.11.001>.
- Pis, J., Parra, J., de la Puente, G., Rubiera, F., & Pajares, J. A. (1998). Development of macroporosity in activated carbons by effect of coal preoxidation and burn-off. *Fuel*, 77(6), 625–630. [https://doi.org/10.1016/S0016-2361\(97\)00156-7](https://doi.org/10.1016/S0016-2361(97)00156-7).
- Pisupati, S. V., & Scaroni, A. W. (1993). Effects of natural weathering and low-temperature oxidation on some aspects of the combustion behaviour of bituminous coals. *Fuel*, 72(6), 779–785. [https://doi.org/10.1016/0016-2361\(93\)90080-L](https://doi.org/10.1016/0016-2361(93)90080-L).
- Poinern, G. E., Senanayake, G., Shah, N., Thi-Le, X. N., Parkinson, G. M., & Fawcett, D. (2011). Adsorption of the aurocyanide, Au(CN)₂-complex on granular activated carbons derived from macadamia nut shells—a preliminary study. *Minerals Engineering*, 24(15), 1694–1702. <https://doi.org/10.1016/j.mineng.2011.09.011>.
- Purevsuren, B., Liou, Y. H., Davaajav, Y., Ariunaa, A., Batbileg, S., Avid, B., Jargalmaa, S., Huang, Y., & Lin, C. J. (2017). Investigation of adsorption of methylene blue from aqueous phase onto coal-based activated carbons. *Journal of the Chinese Institute of Engineers*, 40(4), 355–360. <https://doi.org/10.1080/02533839.2017.1308273>.
- Qiu, H., Lv, L., Pan, B. C., Zhang, Q. J., Zhang, W. M., & Zhang, Q. X. (2009). Critical review in adsorption kinetic models. *Journal of Zhejiang University-Science A*, 10(5), 716–724. <https://doi.org/10.1631/jzus.A0820524>.
- Rahman, A., Urabe, T., & Kishimoto, N. (2013). Color removal of reactive procion dyes by clay adsorbents. *Procedia Environmental Sciences*, 17, 270–278. <https://doi.org/10.1016/j.proenv.2013.02.038>.
- Reed, B. E., Vaughan, R., & Jiang, L. (2000). As (III), As (V), Hg, and Pb removal by Fe-oxide impregnated activated carbon. *Journal of Environmental Engineering*, 126(9), 869–873. [https://doi.org/10.1061/\(ASCE\)0733-9372\(2000\)126:9\(869\)](https://doi.org/10.1061/(ASCE)0733-9372(2000)126:9(869)).
- Remy, T., Peter, S. A., Van Tendeloo, L., Van der Perre, S., Lorgouilloux, Y., Kirschhock, C. E., Baron, G. V., & Denayer, J. F. (2013). Adsorption and separation of CO₂ on KFI zeolites: Effect of cation type and Si/Al ratio on equilibrium and kinetic properties. *Langmuir*, 29(16), 4998–5012. <https://doi.org/10.1021/la400352r>.
- Rhoads, C. A., Senftle, J. T., Coleman, M. M., Davis, A., & Painter, P. C. (1983). Further studies of coal oxidation. *Fuel*, 62(12), 1387–1392. [https://doi.org/10.1016/0016-2361\(83\)90104-7](https://doi.org/10.1016/0016-2361(83)90104-7).
- Rodríguez-Reinoso, F., Molina-Sabio, M., & González, M. T. (1995). The use of steam and CO₂ as activating agents in the preparation of activated carbons. *Carbon*, 33(1), 15–23. [https://doi.org/10.1016/0008-6223\(94\)00100-E](https://doi.org/10.1016/0008-6223(94)00100-E).
- Rodríguez-Reinoso, F., Molina-Sabio, M., & Gonzalez, M. T. (1997). Effect of oxygen surface groups on the immersion enthalpy of activated carbons in liquids of different polarity. *Langmuir*, 13(8), 2354–2358. <https://doi.org/10.1021/la961047u>.

- Rodriguez-Reinoso, F., Molina-Sabio, M., & Munecas, M. A. (1992). Effect of microporosity and oxygen surface groups of activated carbon in the adsorption of molecules of different polarity. *The Journal of Physical Chemistry*, *96*(6), 2707–2713. <https://doi.org/10.1021/j100185a056>.
- Ruiz, B., Parra, J. B., Pajares, J. A., & Pis, J. J. (2006). Effect of coal pre-oxidation on the optical texture and porosity of pyrolysis chars. *Journal of Analytical and Applied Pyrolysis*, *75*(1), 27–32. <https://doi.org/10.1016/j.jaap.2005.04.007>.
- Saberimoghaddam, A., & Nozari, A. (2017). An experimental and statistical model of a cyclic pressure swing adsorption column for hydrogen purification. *Korean Journal of Chemical Engineering*, *34*(3), 822–828. <https://doi.org/10.1007/s11814-016-0314-0>.
- Salman, J. M., & Hameed, B. H. (2010). Effect of preparation conditions of oil palm fronds activated carbon on adsorption of bentazon from aqueous solutions. *Journal of Hazardous Materials*, *175*(1–3), 133–137. <https://doi.org/10.1016/j.jhazmat.2009.09.139>.
- Salman, J. M., Njoku, V. O., & Hameed, B. H. (2011). Batch and fixed-bed adsorption of 2, 4-dichlorophenoxyacetic acid onto oil palm frond activated carbon. *Chemical Engineering Journal*, *174*(1), 33–40. <https://doi.org/10.1016/j.cej.2011.08.024>.
- Saputra, A., Swantomo, D., Ariyanto, T., & Sulistyio, H. (2019). Uranium removal from wastewater using mg (OH) 2-impregnated activated carbon. *Water, Air, & Soil Pollution*, *230*(9), 213. <https://doi.org/10.1007/s11270-019-4269-8>.
- Schröder, E., Thomauske, K., Weber, C., Hornung, A., & Tumiatti, V. (2007). Experiments on the generation of activated carbon from biomass. *Journal of Analytical and Applied Pyrolysis*, *79*(1–2), 106–111. <https://doi.org/10.1016/j.jaap.2006.10.015>.
- Seebauer, V., Petek, J., & Staudinger, G. (1997). Effects of particle size, heating rate and pressure on measurement of pyrolysis kinetics by thermogravimetric analysis. *Fuel*, *76*(13), 1277–1282. [https://doi.org/10.1016/S0016-2361\(97\)00106-3](https://doi.org/10.1016/S0016-2361(97)00106-3).
- Seo, D. K., Park, S. S., Hwang, J., & Yu, T. U. (2010). Study of the pyrolysis of biomass using thermo-gravimetric analysis (TGA) and concentration measurements of the evolved species. *Journal of Analytical and Applied Pyrolysis*, *89*(1), 66–73. <https://doi.org/10.1016/j.jaap.2010.05.008>.
- Seo, D. K., Park, S. S., Kim, Y. T., Hwang, J., & Yu, T. U. (2011). Study of coal pyrolysis by thermo-gravimetric analysis (TGA) and concentration measurements of the evolved species. *Journal of Analytical and Applied Pyrolysis*, *92*(1), 209–216. <https://doi.org/10.1016/j.jaap.2011.05.012>.
- Serrano-Talavera, B., Muñoz-Guillena, M. J., Linares-Solano, A., & Salinas-Martinez de Lecea, C. (1997). Activated carbons from Spanish coals. 3. Preoxidation effect on anthracite activation. *Energy & Fuels*, *11*(4), 785–791. <https://doi.org/10.1021/ef960105g>.
- Shin, C. W., Lee, E. H., Kim, S. K., Jin, H. G., Lee, D. W., Ahn, M. Y., Park, S. C., & Son, S. K. (2020). Design and experimental study of adsorption bed for the helium coolant purification system. *Fusion Engineering and Design*, *155*, 111687. <https://doi.org/10.1016/j.fusengdes.2020.111687>.
- Shrestha, S., Son, G., Lee, S. H., & Lee, T. G. (2013). Isotherm and thermodynamic studies of Zn (II) adsorption on lignite and coconut shell-based activated carbon fiber. *Chemosphere*, *92*(8), 1053–1061. <https://doi.org/10.1016/j.chemosphere.2013.02.068>.
- Silas, K., Ghani, W. A., Choong, T. S., & Rashid, U. (2018). Activated carbon monolith Co₃O₄ based catalyst: Synthesis, characterization and adsorption studies. *Environmental Technology & Innovation*, *12*, 273–285. <https://doi.org/10.1016/j.eti.2018.10.008>.
- Silas, K., Ghani, W. A., Choong, T. S., & Rashid, U. (2019). Carbonaceous materials modified catalysts for simultaneous SO₂/NO_x removal from flue gas: A review. *Catalysis Reviews*, *61*(1), 134–161. <https://doi.org/10.1080/01614940.2018.1482641>.
- Singh, A., & Lal, D. (2009). Influence of heating rate and temperature on carbon structure and porosity of activated carbon spheres from resole-type phenolic beads. *Carbon Letters (Carbon Lett.)*, *10*(3), 181–189.
- Singla, P. K., Miura, S., Hudgins, R. R., & Silveston, P. L. (1983). Pore development during carbonization of coals. *Fuel*, *62*(6), 645–648. [https://doi.org/10.1016/0016-2361\(83\)90302-2](https://doi.org/10.1016/0016-2361(83)90302-2).

- Slyusarskiy, K. V., Larionov, K. B., Osipov, V. I., Yankovsky, S. A., Gubin, V. E., & Gromov, A. A. (2017). Non-isothermal kinetic study of bituminous coal and lignite conversion in air and in argon/air mixtures. *Fuel*, *191*, 383–392. <https://doi.org/10.1016/j.fuel.2016.11.087>.
- Song, C., Wang, T., Qiu, J., Cao, Y., & Cai, T. (2008). Effects of carbonization conditions on the properties of coal-based microfiltration carbon membranes. *Journal of Porous Materials*, *15*(1), 1–6. <https://doi.org/10.1007/s10934-006-9044-8>.
- Srivastava, N. C., & Eames, I. W. (1998). A review of adsorbents and adsorbates in solid–vapour adsorption heat pump systems. *Applied Thermal Engineering*, *18*(9–10), 707–714. [https://doi.org/10.1016/S1359-4311\(97\)00106-3](https://doi.org/10.1016/S1359-4311(97)00106-3).
- Starck, J., Burg, P., Muller, S., Bimer, J., Furdin, G., Fioux, P., Vix Guterl, C., Begin, D., Faure, P., & Azambre, B. (2006). The influence of demineralisation and amoxidation on the adsorption properties of an activated carbon prepared from a Polish lignite. *Carbon*, *44*(12), 2549–2557. <https://doi.org/10.1016/j.carbon.2006.05.052>.
- Styszko-Grochowiak, K., Golaś, J., Jankowski, H., & Koziński, S. (2004). Characterization of the coal fly ash for the purpose of improvement of industrial on-line measurement of unburned carbon content. *Fuel*, *83*(13), 1847–1853. <https://doi.org/10.1016/j.fuel.2004.03.005>.
- Sudaryanto, Y., Hartono, S. B., Irawaty, W., Hindarso, H., & Ismadij, S. (2006). High surface area activated carbon prepared from cassava peel by chemical activation. *Bioresource Technology*, *97*(5), 734–739. <https://doi.org/10.1016/j.biortech.2005.04.029>.
- Sukul, P., Lamshöft, M., Zühlke, S., & Spiteller, M. (2008). Sorption and desorption of sulfadiazine in soil and soil-manure systems. *Chemosphere*, *73*(8), 1344–1350. <https://doi.org/10.1016/j.chemosphere.2008.06.066>.
- Szymański, G. S., Karpiński, Z., Biniak, S., & Świątkowski, A. (2002). The effect of the gradual thermal decomposition of surface oxygen species on the chemical and catalytic properties of oxidized activated carbon. *Carbon*, *40*(14), 2627–2639. [https://doi.org/10.1016/S0008-6223\(02\)00188-4](https://doi.org/10.1016/S0008-6223(02)00188-4).
- Tamon, H., Kitamura, K., & Okazaki, M. (1996). Adsorption of carbon monoxide on activated carbon impregnated with metal halide. *AIChE Journal*, *42*(2), 422–430. <https://doi.org/10.1002/aic.690420212>.
- Tan, B., Cheng, G., Zhu, X., & Yang, X. (2020). Experimental study on the physisorption characteristics of O₂ in coal powder are effected by coal nanopore structure. *Scientific Reports*, *10*(1), 1–1. <https://doi.org/10.1038/s41598-020-63988-4>.
- Tay, T., Ucar, S., & Karagöz, S. (2009). Preparation and characterization of activated carbon from waste biomass. *Journal of Hazardous Materials*, *165*(1–3), 481–485. <https://doi.org/10.1016/j.jhazmat.2008.10.011>.
- Teng, H., Ho, J. A., & Hsu, Y. F. (1997). Preparation of activated carbons from bituminous coals with CO₂ activation—Influence of coal oxidation. *Carbon*, *35*(2), 275–283. [https://doi.org/10.1016/S0008-6223\(96\)00137-6](https://doi.org/10.1016/S0008-6223(96)00137-6).
- Teng, H., Ho, J. A., Hsu, Y. F., & Hsieh, C. T. (1996). Preparation of activated carbons from bituminous coals with CO₂ activation. I. Effects of oxygen content in raw coals. *Industrial & Engineering Chemistry Research*, *35*(11), 4043–4049. <https://doi.org/10.1021/ie960170d>.
- Teng, H., & Hsieh, C. T. (1998). Influence of surface characteristics on liquid-phase adsorption of phenol by activated carbons prepared from bituminous coal. *Industrial & Engineering Chemistry Research*, *37*(9), 3618–3624. <https://doi.org/10.1021/ie970796j>.
- Teng, H., & Lin, H. C. (1998). Activated carbon production from low ash subbituminous coal with CO₂ activation. *AIChE Journal*, *44*(5), 1170–1177. <https://doi.org/10.1002/aic.690440514>.
- Teng, H., Yeh, T. S., & Hsu, L. Y. (1998). Preparation of activated carbon from bituminous coal with phosphoric acid activation. *Carbon*, *36*(9), 1387–1395. [https://doi.org/10.1016/S0008-6223\(98\)00127-4](https://doi.org/10.1016/S0008-6223(98)00127-4).
- Teo, E. Y., Muniandy, L., Ng, E. P., Adam, F., Mohamed, A. R., Jose, R., & Chong, K. F. (2016). High surface area activated carbon from rice husk as a high performance supercapacitor electrode. *Electrochimica Acta*, *192*, 110–119. <https://doi.org/10.1016/j.electacta.2016.01.140>.
- Tian, B., Li, P., Li, D., Qiao, Y., Xu, D., & Tian, Y. (2018). Preparation of micro-porous monolithic activated carbon from anthracite coal using coal tar pitch as binder. *Journal of Porous Materials*, *25*(4), 989–997. <https://doi.org/10.1007/s10934-017-0509-8>.

- Tomaszewicz, M., Tomaszewicz, G., & Sciazko, M. (2017). Experimental study on kinetics of coal char–CO₂ reaction by means of pressurized thermogravimetric analysis. *Journal of Thermal Analysis and Calorimetry*, *130*(3), 2315–2330. <https://doi.org/10.1007/s10973-017-6538-3>.
- Tsuchida, N., & Muir, D. M. (1986). Studies on role of oxygen in the adsorption of au (CN) 2– and ag (CN) 2– onto activated carbon. *Metallurgical Transactions B*, *17*(3), 529–533.
- U.S. Geological Survey (2020). Mineral commodity summaries 2020. U. S. Geological Survey, <https://doi.org/10.3133/mcs2020>.
- Uddin, M. K. (2017). A review on the adsorption of heavy metals by clay minerals, with special focus on the past decade. *Chemical Engineering Journal*, *308*, 438–462. <https://doi.org/10.1016/j.cej.2016.09.029>.
- Urbanovici, E., Popescu, C., & Segal, E. (1999). Improved iterative version of the coats-Redfern method to evaluate non-isothermal kinetic parameters. *Journal of Thermal Analysis and Calorimetry*, *58*(3), 683–700.
- Usmani, T. H., Ahmed, T. W., Ahmed, S. Z., & Yousufzai, A. H. (1996). Preparation and characterization of activated carbon from a low rank coal. *Carbon*, *34*(1), 77–82. [https://doi.org/10.1016/0008-6223\(95\)00137-9](https://doi.org/10.1016/0008-6223(95)00137-9).
- Uddin, M. A., Shinozaki, Y., Furusawa, N., Yamada, T., Yamaji, Y., & Sasaoka, E. (2007). Preparation of activated carbon from asphalt and heavy oil fly ash and coal fly ash by pyrolysis. *Journal of analytical and applied pyrolysis*, *78*(2), 337–342. <https://doi.org/10.1016/j.jaap.2006.09.004>.
- Van der Merwe, P. F., & Van Deventer, J. S. (1988). The influence of oxygen on the adsorption of metal cyanides on activated carbon. *Chemical Engineering Communications*, *65*(1), 121–138. <https://doi.org/10.1080/00986448808940248>.
- Van Deventer, J. (1986). Kinetic model for the reversible adsorption of gold cyanide on activated carbon. *Chemical Engineering Communications*, *44*(1–6), 257–274. <https://doi.org/10.1080/00986448608911359>.
- Vassilev, S. V., & Vassileva, C. G. (2005). Methods for characterization of composition of fly ashes from coal-fired power stations: A critical overview. *Energy & Fuels*, *19*(3), 1084–1098. <https://doi.org/10.1021/ef049694d>.
- Vassileva, P. S., & Detcheva, A. K. (2010). Adsorption of some transition metal ions [cu (II), Fe (III), Cr (III) and au (III)] onto lignite-based activated carbons modified by oxidation. *Adsorption Science & Technology*, *28*(3), 229–242.
- Wang, G., Zhang, Y., Wang, S., Wang, Y., Song, H., Lv, S., & Li, C. (2020). Adsorption performance and mechanism of antibiotics from aqueous solutions on porous boron nitride–carbon nanosheets. *Environmental Science: Water Research & Technology*. <https://doi.org/10.1039/D0EW00117A>.
- Wang, L., Guo, Y., Zou, B., Rong, C., Ma, X., Qu, Y., Li, Y., & Wang, Z. (2011). High surface area porous carbons prepared from hydrochars by phosphoric acid activation. *Bioresource Technology*, *102*(2), 1947–1950. <https://doi.org/10.1016/j.biortech.2010.08.100>.
- Wang, Q. B., Zhang, X. L., Xu, D. P., & Chen, Q. R. (2007). Effect of pre-oxidation on the properties of crushed bituminous coal and activated carbon prepared therefrom. *Journal of China University of Mining and Technology*, *17*(4), 494–497. [https://doi.org/10.1016/S1006-1266\(07\)60132-1](https://doi.org/10.1016/S1006-1266(07)60132-1).
- Wang, S., Ma, Q., & Zhu, Z. H. (2008). Characteristics of coal fly ash and adsorption application. *Fuel*, *87*(15–16), 3469–3473. <https://doi.org/10.1016/j.fuel.2008.05.022>.
- Wang, Y., Yang, H., Jin, L., Li, Y., Hu, H., Ding, H., & Bai, X. (2019). Effect of mineral in coal on preparation of activated carbon for methane decomposition to hydrogen. *Fuel*, *258*, 116138. <https://doi.org/10.1016/j.fuel.2019.116138>.
- Wang, Y., Zhao, L., Otto, A., Robinius, M., & Stolten, D. (2017). A review of post-combustion CO₂ capture technologies from coal-fired power plants. *Energy Procedia*, *114*, 650–665. <https://doi.org/10.1016/j.egypro.2017.03.1209>.

- Wong, S., Ngadi, N., Inuwa, I. M., & Hassan, O. (2018). Recent advances in applications of activated carbon from biowaste for wastewater treatment: A short review. *Journal of Cleaner Production*, 175, 361–375. <https://doi.org/10.1016/j.jclepro.2017.12.059>.
- Worasuwannarak, N., Nakagawa, H., & Miura, K. (2002). Effect of pre-oxidation at low temperature on the carbonization behavior of coal. *Fuel*, 81(11–12), 1477–1484. [https://doi.org/10.1016/S0016-2361\(02\)00083-2](https://doi.org/10.1016/S0016-2361(02)00083-2).
- Wu, F. C., Wu, P. H., Tseng, R. L., & Juang, R. S. (2010). Preparation of activated carbons from unburnt coal in bottom ash with KOH activation for liquid-phase adsorption. *Journal of Environmental Management*, 91(5), 1097–1102. <https://doi.org/10.1016/j.jenvman.2009.12.011>.
- Wu, Y., Wu, S., & Gao, J. (2009). A study on the applicability of kinetic models for Shenfu coal char gasification with CO₂ at elevated temperatures. *Energies*, 2(3), 545–555. <https://doi.org/10.3390/en20300545>.
- Xiao, X., Tian, F., Yan, Y., Wu, Z., Wu, Z., & Cravotto, G. (2015). Adsorption behavior of phenanthrene onto coal-based activated carbon prepared by microwave activation. *Korean Journal of Chemical Engineering*, 32(6), 1129–1136. <https://doi.org/10.1007/s11814-014-0317-7>.
- Xie, Y. B., Qiao, W. M., Zhang, W. Y., Sun, G. W., & Ling, L. C. (2010). Effect of the surface chemistry of activated carbon on its electrochemical properties in electric double layer capacitors. *New Carbon Materials*, 25(4), 248–254. [https://doi.org/10.1016/S1872-5805\(09\)60031-7](https://doi.org/10.1016/S1872-5805(09)60031-7).
- Xu, J., Cao, Z., Zhang, Y., Yuan, Z., Lou, Z., Xu, X., & Wang, X. (2018). A review of functionalized carbon nanotubes and graphene for heavy metal adsorption from water: Preparation, application, and mechanism. *Chemosphere*, 195, 351–364. <https://doi.org/10.1016/j.chemosphere.2017.12.061>.
- Xue, N., Vjunov, A., Schallmoser, S., Fulton, J. L., Sanchez-Sanchez, M., Hu, J. Z., Mei, D., & Lercher, J. A. (2018). Hydrolysis of zeolite framework aluminum and its impact on acid catalyzed alkane reactions. *Journal of Catalysis*, 365, 359–366. <https://doi.org/10.1016/j.jcat.2018.07.015>.
- Yadav, V. B., Gadi, R., & Kalra, S. (2019). Clay based nanocomposites for removal of heavy metals from water: A review. *Journal of Environmental Management*, 232, 803–817. <https://doi.org/10.1016/j.jenvman.2018.11.120>.
- Yahya, M. A., Al-Qodah, Z., & Ngah, C. Z. (2015). Agricultural bio-waste materials as potential sustainable precursors used for activated carbon production: A review. *Renewable and Sustainable Energy Reviews*, 46, 218–235. <https://doi.org/10.1016/j.rser.2015.02.051>.
- Yalcin, M., & Arol, A. I. (2002). Gold cyanide adsorption characteristics of activated carbon of non-coconut shell origin. *Hydrometallurgy*, 63(2), 201–206. [https://doi.org/10.1016/S0304-386X\(01\)00203-1](https://doi.org/10.1016/S0304-386X(01)00203-1).
- Yan, L., & Sorial, G. A. (2011). Chemical activation of bituminous coal for hampering oligomerization of organic contaminants. *Journal of Hazardous Materials*, 197, 311–319. <https://doi.org/10.1016/j.jhazmat.2011.09.093>.
- Yang, J. K., Park, H. J., Lee, H. D., & Lee, S. M. (2009). Removal of Cu(II) by activated carbon impregnated with iron(III). *Colloids and Surfaces A: Physicochemical and Engineering Aspects*, 337(1–3), 154–158. <https://doi.org/10.1016/j.colsurfa.2008.12.014>.
- Yi, B., Zhang, L., Huang, F., Mao, Z., & Zheng, C. (2014). Effect of H₂O on the combustion characteristics of pulverized coal in O₂/CO₂ atmosphere. *Applied Energy*, 132, 349–357. <https://doi.org/10.1016/j.apenergy.2014.07.031>.
- Yoshizawa, N., Maruyama, K., Yamada, Y., & Zielinska-Blajet, M. (2000). XRD evaluation of CO₂ activation process of coal-and coconut shell-based carbons. *Fuel*, 79(12), 1461–1466. [https://doi.org/10.1016/S0016-2361\(00\)00011-9](https://doi.org/10.1016/S0016-2361(00)00011-9).
- Yu, G., Yu, D., Liu, F., Han, J., Yu, X., Wu, J., & Xu, M. (2020). Different impacts of magnesium on the catalytic activity of exchangeable calcium in coal gasification with CO₂ and steam. *Fuel*, 266, 117050. <https://doi.org/10.1016/j.fuel.2020.117050>.

- Zabaniotou, A. A., Kalogiannis, G., Kappas, E., & Karabelas, A. J. (2000). Olive residues (cuttings and kernels) rapid pyrolysis product yields and kinetics. *Biomass and Bioenergy*, *18*(5), 411–420. [https://doi.org/10.1016/S0961-9534\(00\)00002-7](https://doi.org/10.1016/S0961-9534(00)00002-7).
- Zeng, C., Lin, Q., Fang, C., Xu, D., & Ma, Z. (2013). Preparation and characterization of high surface area activated carbons from co-pyrolysis product of coal-tar pitch and rosin. *Journal of Analytical and Applied Pyrolysis*, *104*, 372–377. <https://doi.org/10.1016/j.jaap.2013.06.010>.
- Zhang, J., Xie, Q., Liu, J., Yang, M., & Yao, X. (2011). Role of Ni (NO₃)₂ in the preparation of a magnetic coal-based activated carbon. *Mining Science and Technology (China)*, *21*(4), 599–603. <https://doi.org/10.1016/j.mstc.2011.01.003>.
- Zhang, Y., Ashizawa, M., Kajitani, S., & Miura, K. (2008). Proposal of a semi-empirical kinetic model to reconcile with gasification reactivity profiles of biomass chars. *Fuel*, *87*(4–5), 475–481. <https://doi.org/10.1016/j.fuel.2007.04.026>.
- Zhang, Y., Hara, S., Kajitani, S., & Ashizawa, M. (2010). Modeling of catalytic gasification kinetics of coal char and carbon. *Fuel*, *89*(1), 152–157. <https://doi.org/10.1016/j.fuel.2009.06.004>.
- Zhou, Y., Zhu, S., Yan, L., Li, F., & Bai, Y. (2019). Interaction between CO₂ and H₂O on char structure evolution during coal char gasification. *Applied Thermal Engineering*, *149*, 298–305. <https://doi.org/10.1016/j.applthermaleng.2018.12.037>.
- Zhu, J., He, F., Zhang, Y., Zhang, R., & Zhang, B. (2019). Fractal analysis in pore size distributions of different bituminous coals. *Scientific Reports*, *9*(1), 1–2. <https://doi.org/10.1038/s41598-019-54749-z>.
- Zou, C., Ma, C., Zhao, J., Shi, R., & Li, X. (2017). Characterization and non-isothermal kinetics of Shenmu bituminous coal devolatilization by TG-MS. *Journal of Analytical and Applied Pyrolysis*, *127*, 309–320. <https://doi.org/10.1016/j.jaap.2017.07.020>.
- Zou, Y., & Han, B. X. (2001). High-surface-area activated carbon from Chinese coal. *Energy & Fuels*, *15*(6), 1383–1386. <https://doi.org/10.1021/ef0002851>.

Chapter 6

Characteristic and Equilibrium Adsorption Studies of Biochar



Vijetha Ponnam, Subbaiah Tondepu, and Rajesh Kumar Jyothi

6.1 Introduction

In Guntur (Andhra Pradesh, India) district, chili production is more and so more amount of chili stalk waste was produced. To improve the production, more amount of carbofuran pesticide is used. Therefore the residue coming from the same fields is converted to biochar and can be used to remove carbofuran.

Previous findings on removal of carbofuran from adsorbent engaged in modifications in the adsorbents (Foo 2016). Few studies also reported biochar production without modification (Vijetha et al. 2019; Mayakaduwa et al. 2016). No such alterations are applied in the current research because the biochar preparation method could be user friendly to the farmers so that they can prepare and use it directly to adsorb pesticides and to improve soil health without any modifications. Thus, the production process of biochar is an environmentally friendly, low-cost, economical, and simplified technique.

Therefore, response to the elimination of carbofuran from water bodies was checked by the dried capsicum annum biochar (CABC). The tests were carried for distinct carbofuran concentrations, with varying CABC dosage, pH values, and adsorption time. Different isotherms and kinetic models were examined to clearly define the adsorption equilibrium and kinetics. These studies are discussed in detail in forthcoming sections.

V. Ponnam (✉) · S. Tondepu

Department of Chemical Engineering, VIGNAN's Foundation for Science, Technology & Research (VFSTR) (Deemed to be University), Guntur, Andhra Pradesh, India
e-mail: pv_chem@vignan.ac.in

R. K. Jyothi

Convergence Research Center for Development of Mineral Resources (DMR), Korea Institute of Geoscience and Mineral Resources (KIGAM), Daejeon, South Korea
e-mail: rkumarphd@kigam.re.kr

6.2 Preparation of CABC from CAW

Capsicum annum waste (CAW) has been obtained from the agricultural farms and was converted to biochar by the following methodology.

- The biomass was washed with distilled water.
- It was dried in sunlight for 3 days.
- Dried biomass is cut into pieces of approximately 1 cm.
- Cutted biomass was placed in oven at 105 °C for about 120 min.
- Dried biomass is milled and sieved to 80–120µm.
- Now the biomass is pyrolyzed into biochar by two methods.

Low-temperature Pyrolysis: Temperature of 300 °C for about 120 min.

High-Temperature Pyrolysis: Temperature of 700 °C for about 30 min.

CAW and CABC were analyzed for surface morphology, CHNS elements, specific surface area, and functional groups.

Elemental analysis is utilized to quantify the elements carbon, hydrogen, nitrogen, sulfur, and oxygen. In an oxygen-rich atmosphere, elemental analysis involves high-temperature combustion of the sample CHNS elemental analyzer.

By scanning the sample with an energy-rich electrical beam, the scanning electron microscope (SEM) creates images. During their interaction with the sample, electrons produce secondary electrons, spread electrons and X-rays. These signals are acquired by one or more sensors in order to create images that are shown on the computer. As the electron beam reaches the target material, relying on the increasing force and specimen composition it absorbs the sample up to a few microns depth.

In BET Analysis, the theory attempts to detail about adsorption of molecules on a solid and is the backbone for the assessment of the specific materials of the surface, such as the distributions of the pores. It offers a comprehensive surface area assessment of substances by means of nitrogen multilayer adsorption evaluated by a highly autonomous analyzer based on the pressure range. It represents surface area and porous area assessments to find the optimal surface area in m²/g, which provides significant data in various implementations in order to study the impact of the surface porosity and particle size.

FTIR is a powerful approach that is used to identify organic, polymer, and inorganic materials. Infrared light for scanning samples and for observing chemical properties are used by the FTIR analytical technique. FTIR transmits infrared radiation between 10,000 and 100 cm⁻¹, which receive and pass through such radiation. The radiation absorbed is converted into rotating or vibrational energy by the sample. The received image on the sensor generally shows a profile of the sample, from 4000 to 400 cm⁻¹. Every molecular or chemical arrangement creates another particular spectral picture and hence an FTIR study is a valuable method for material elucidation.

6.3 Adsorption Studies

Equilibrium tests have been carried out using the process of batch adsorption.

- In 250 mL volumetric flasks, carbofuran (98 percent purity) aliquots of 25–250 mg/L concentrations were made by mixing sufficient quantities of carbofuran in distilled water.
- Each flask was supplied with an adsorbent amount in the range 0.1–0.3 g and solutions were made to pH range of 2–12 and time of contact is varied between 0 and 210 min).
- These formulations were shook at 100 rpm in an orbital shaker.
- A filtering procedure was conducted using 0.45 μm whatman filter paper.
- The final carbofuran concentrations were measured.

Calibration curve was prepared using the following procedure:

- 5–250 ppm carbofuran standard solutions were made by adding distilled water.
- The absorbance was measured at a wavelength of 273 nm using UV-spectrophotometer.
- Calibration curve was drawn between absorbance and concentration of carbofuran solution.
- Concentrations of the unknown carbofuran solutions can be calculated using the calibration curve.
- % Removal and adsorption capacity can be calculated using the formulas

$$\%R = \frac{C_i - C_e}{C_i} * 100 \quad (6.1)$$

where %R = Percentage Removal.

C_i = Initial Concentration of adsorbate (mg/L).

C_e = Equilibrium concentration of adsorbate (mg/L)

$$q_e = \frac{(C_i - C_e)V}{m} \quad (6.2)$$

$$q_i = \frac{(C_i - C_i)V}{m} \quad (6.3)$$

where

q_e = mg of Carbofuran adsorbed / gm of adsorbent (mg/g)(equilibrium)

q_i = mg of Carbofuran adsorbed / gm of the adsorbent (mg/g)

V = Volume of the sample (L)

m = mass of the adsorbent (g)

6.4 Adsorption Isotherms Models

Isotherm tests were carried for solutions of carbofuran (25–250 mg / L) at pH 3.0, 0.3 g CABC dosage to obtain information about the adsorption mechanism.

Langmuir isotherm model

The Langmuir isotherm model is applicable under the following hypothesis:

- A consistent solid surface.
- Uniform surface energy adsorption.
- Lack of contact between adsorbed molecules.
- Single-layer adsorption (no adsorbate transmigration in the surface plane).

Langmuir isotherm is given by the following equation

$$qe = \frac{k_L q_m C_e}{1 + k_L C_e} \quad (6.4)$$

where q_e = mg of Carbofuran adsorbed per gram of the CABC at equilibrium (mg/g)

C_e = Equilibrium concentration of Carbofuran (mg/L)

q_m is the monolayer adsorption capacity of the CABC (mg/g) and

k_L is the Langmuir constant (L/g)

The equation in linear form is given as

$$\frac{1}{q_e} = \frac{1}{q_m} + \frac{1}{q_m K_L C_e} \quad (6.5)$$

where the Langmuir constants q_m and k_L are calculated from graph of $\frac{1}{q_e}$ vs. $\frac{1}{C_e}$

Another assessment on the grounds of the dimensionless parameter balance for the separation factor (R_L) may be carried out for the Langmuir equation which is given by

$$R_L = \frac{1}{(1 + K_L C_o)} \quad (6.6)$$

The isotherm type is explained by R_L values as shown below:

- $0 < R_L < 1$ (favorable)
- $R_L > 1$ (unfavorable)
- $R_L > 0$ (irreversible).

6.4.1 Freundlich Isotherm Model

In 1906, Freundlich formulated an isotherm called Freundlich isotherm on the basis that the adsorption is carried out on a heterogeneous area and adsorption is multi-layered, and with rise in concentration, the quantity of adsorbate adsorbed enhances continuously. The Freundlich isotherm is given by the following equation

$$q_e = k_f C_e^n \quad (6.7)$$

where k_f is a constant associated with the adsorbent adsorption capacity $(\text{mg/g})/(\text{mg/L})^n$ and n is an adsorption intensity-related analytical parameter.

n values vary with adsorbent heterogeneity and n value of 0.0–1.0 indicates favorable adsorption. The Freundlich isotherm in linearized form can be represented by

$$\log(q_e) = \log K_f + \frac{1}{n} \log C_e \quad (6.8)$$

The Freundlich constants K_f and n are evaluated from the plot of $\log q_e$ vs. $\log C_e$, respectively.

6.4.2 Temkin Isotherm Model

Temkin isotherm model considers the influence on the adsorption phase of indirect adsorbate / adsorbate connections; the adsorption heat of all the layer molecules is expected to decline linearly owing to surface coverage. The Temkin isotherm just applies to an average range of ion levels. The linear form of the equation is (Vijayaraghavan et al. 2006):

$$q_e = \frac{RT}{b_T} (\ln(A_T) + \ln(C_e)) \quad (6.9)$$

where b_T is Temkin constant and A_T is Temkin isotherm constant L/g

6.4.3 Dubinin-Radushkevich Isotherm Model

The isothermic model in Dubinin-Radushkevich is a scientific adsorption method that is typically used to describe the Gaussian energy distribution on heterogeneous surfaces. It is only appropriate for average values of adsorbate as it has unreasonable dynamical properties but does not anticipate the laws of Henry at reduced pressure. The method is a semi-empirical method, where a pore loading process opposes adsorption. It assumes that van der Waals has a multilayered character that applies to physical adsorption systems and is a basic method that objectively characterizes microporous adsorption of gasses and vapors.

The equation is given as

$$\ln(q_e) = \ln(q_s) - k_{ad} \varepsilon^2 \quad (6.10)$$

where q_s —Isotherm saturation capacity, (mg/g)

k_{ad} —DR isotherm constant, mol²/KJ²

ϵ —Isotherm constant.

6.5 Adsorption Kinetic Studies

The kinetic behavior of adsorption of carbofuran is interpreted using PFOM, PSOM-I, PSOM-II, EM, and IPDM .

PFOM: PFOM is described as the earliest adsorption fundamental analysis, for the kinetic processing of fluid and solid phase adsorption. Its equation is:

$$\ln(q_e - q_t) = \ln(q_e) - k_1 t \quad (6.11)$$

where q_e and q_t (mg/g) are equilibrium adsorption capacities and at time t (min), respectively. k_1 (min⁻¹) is the kinetic rate constant.

The first-order rate equation of Lagergren is named pseudo-first-order in order to classify kinetics dependency on adsorption efficiency and solution concentration. The adsorption of contaminants in water was commonly noted in several applications in recent times.

6.5.1 PSOM I and PSOM-II

In 1995, Ho adopted a concept of pseudo-second-order sorption rate resulting from the solid phase sorption capacity but not from the Sorbate concentration (Ho 2006).

PSOM I is given by

$$\frac{t}{q_t} = \frac{1}{k_2 q_e^2} + \frac{1}{q_e} t \quad (6.12)$$

PSOM II is given by

$$\frac{1}{q_t} = \frac{1}{k_2 q_e^2} \frac{1}{t} + \frac{1}{q_e} \quad (6.13)$$

where q_e and q_t (mg/g) are the equilibrium adsorption capacities and time t (min), respectively. k_2 (min⁻¹) is the rate constant.

6.6 Elovich Model (EM)

Elovich model is implemented for a deeper understanding of the chemisorption essence of adsorption. This model predicts the diffusion of a system's mass and surface, activation and deactivation energy. The model was used for gas systems at first but its validity has been significantly reduced to wastewater operations. The model predicts that the adsorption rate for solute is exponentially reduced with the increase of adsorbed solute.

$$q_t = \frac{1}{\beta} \ln(\alpha\beta) + \frac{1}{\beta} \ln(t) \quad (6.14)$$

α —Initial adsorption rate (mg/g min), β —desorption constant (g/mg).

IPDM: Model for intraparticle distribution to analyze the rate-limiting step all through adsorption was widely applied. Solute adsorption involves the mass transfer of adsorbates (film diffusion), the diffusion of surfaces, and the diffusion of pores. Film diffusion is an autonomous step, whereas concurrently surface and pores can occur. IPDM is studied by examining model,

$$q_t = K_{p1} t^{1/2} + C \quad (6.15)$$

where k_p —intraparticle diffusion rate constant (mg/g. min^{1/2}), C (mg/g)—constant.

6.7 Proximate and Ultimate Analysis

Proximate and ultimate analysis for CABC is assessed by regular procedure ASTM D 1762-84 for Raw stalk, CABC (300 °C), and CABC (700 °C) and is listed in Table 6.1. Current study shows that in CABC carbon content grew from 45.32% to 47.11% for a temperature rise from 300 to 700 °C. Oxygen and Hydrogen content decreases as pyrolysis proceeds due to release of volatile matter. The volatile components of CABC reduces slowly as the temperature increases, which shows that CABC formation depends on temperature (Buss et al. 2015).

As adsorption is a surface phenomenon, surface morphology, surface area, and pore volume play a major role and were studied using BET and SEM Analysis. For biochar formed at 300 °C the BET surface area and the pore volume were, respectively, 32.07 m²/g and 0.0635 cm³/g and for 700 °C it was 3.03 m²/g and 0.02 cm³/g. As the preparation temperature of char increases from 300 to 700°C, the value of the biochar surface area is declining due to splitting, shrinking, and fracturing on the biochar surface. The surface morphologies were examined at a magnification of 50µm using SEM and shown in Fig. 6.1. It was identified that in the case of CABC (300 °C) more pores are available compared to CABC (700 °C), and it was proved

Table 6.1 Elemental analysis

	Biomass	CABC (300 °C)	CABC (700 °C).
Ultimate analysis (wt. %)			
C	40.53	45.32	47.11
H	5.02	3.64	1.62
N	0.77	1.3	1.29
S	0.14	0.20	0.41
O	40.23	35.22	32.34
Proximate analysis (wt. %)			
Ash	0.82	15.32	12.12
Volatile matter	80.23	35.62	25.32
Fixed carbon	18.95	49.06	62.56
Moisture	3	–	–

by BET results. Thus, the low-temperature biochar, CABC (300 °C) is used throughout the work.

FTIR studies depict the difference in function (Fig. 6.2). The peak observed between 800 and 1000 cm^{-1} in raw biomass indicates the C-O stretching vibration of carboxyl groups, and a significant decrease in the transmittance from 87.04 to 82.86 reflects C-H bending. A peak at 1200 cm^{-1} confirmed the amount of nitro compounds with symmetric stretches. The peaks near 1500 cm^{-1} are affiliated to C=C aromatic ring (Ren et al. 2011).

A peak at 1100 cm^{-1} confirms the existence of aliphatic C-O-C and secondary alcohol, while the C-O stretch at 1000 cm^{-1} indicates hemicelluloses and cellulose in the chili stalk and CABC (300 °C). Broad peaks appeared for chili stalk decreased between 3500 and 3800 cm^{-1} in the case of CABC (300 °C), indicating cellulose and lignin desiccation. The strong absorption at 1000 in CABC-charged carbofuran indicated the existence of phenolic OH groups. The transformation of the phenolic OH peak in carbofuran-loaded CABC from 1000 to 1100 cm^{-1} affirms the high reactivity of carbofuran with CABC.

The value at about 1550 cm^{-1} shows stretching of C = N and C-N. The association of CABC phenolic groups with the amine and carbonyl groups of carbofuran molecules resulted in chemisorption (Mayakaduwa et al. 2016).

6.8 Effect of Initial Concentration and Contact Time

The impact on CABC carbofuran sorption was analyzed with varying time and concentrations (Fig. 6.3). Analysis was carried in 250 ml volumetric flasks at CABC dose of 0.3 g, with differing carbofuran concentrations from 25 to 250 mg/L. It was observed that, in the initial contact period of 30 min, carbofuran adsorption efficiency rises at a faster pace. The adsorption rate eventually rises gradually over time

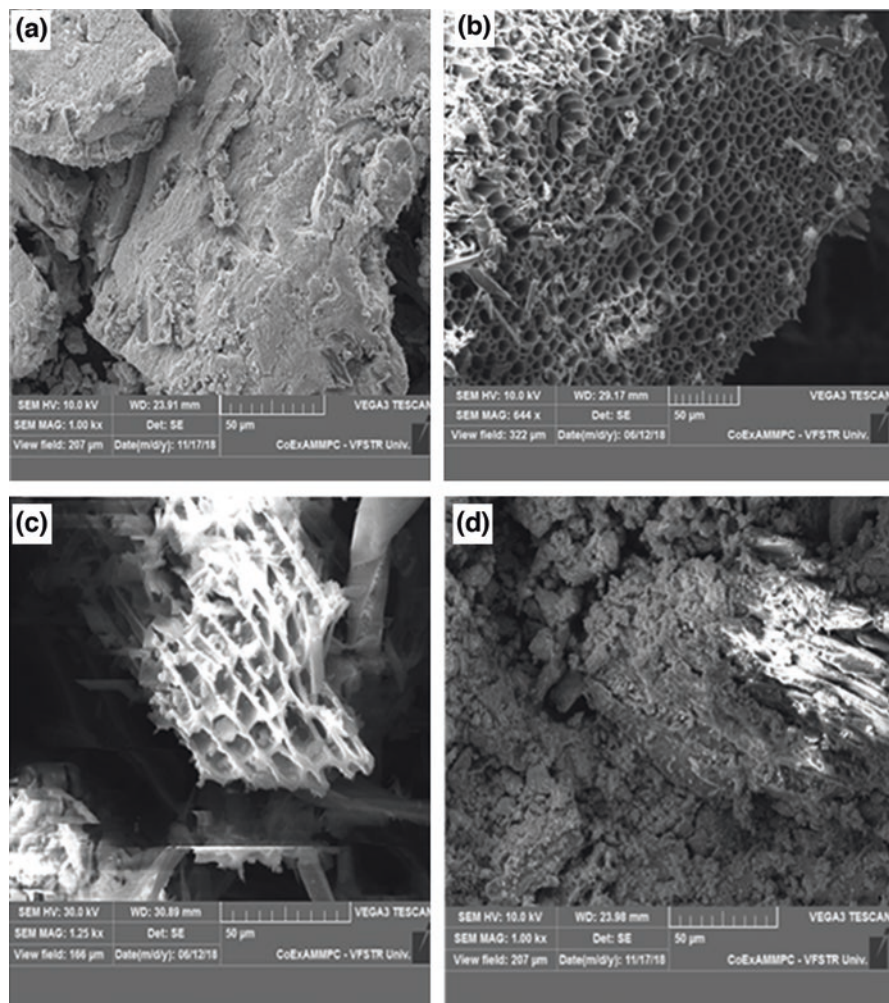


Fig. 6.1 SEM images of (a) Raw chili stalk, (b) CABC (300 °C), (c) CABC (700 °C), and (d) carbofuran-loaded biochar (Adapted, modified and reproduced from Vijetha et al. 2019)

and achieves equilibrium at 150 minutes. It indicates larger number of sites necessary for carbofuran sorption at the start of adsorption on the CABC surface. However, when the carbofuran concentration rises from 25 to 250 mg/L, the adsorption potential improved from 30 to 170 mg/g and the removal percentage decreased from 36% to 20.4% (Fig. 6.4) attributable to higher concentration difference and related patterns were found earlier (Hameed 2011).

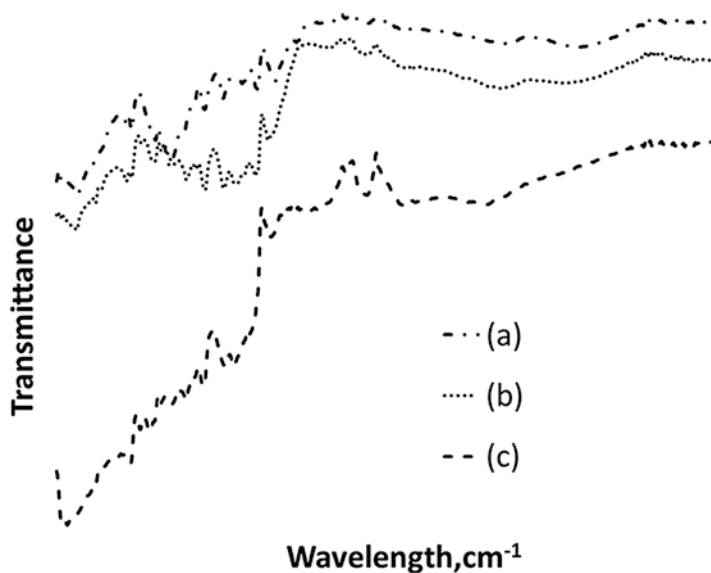


Fig. 6.2 FTIR spectrum of (a) raw chili stalk, (b) CABC (300 °C), and (c) carbofuran-loaded CABC. (Adapted, modified and reproduced from Vijetha et al. 2019)

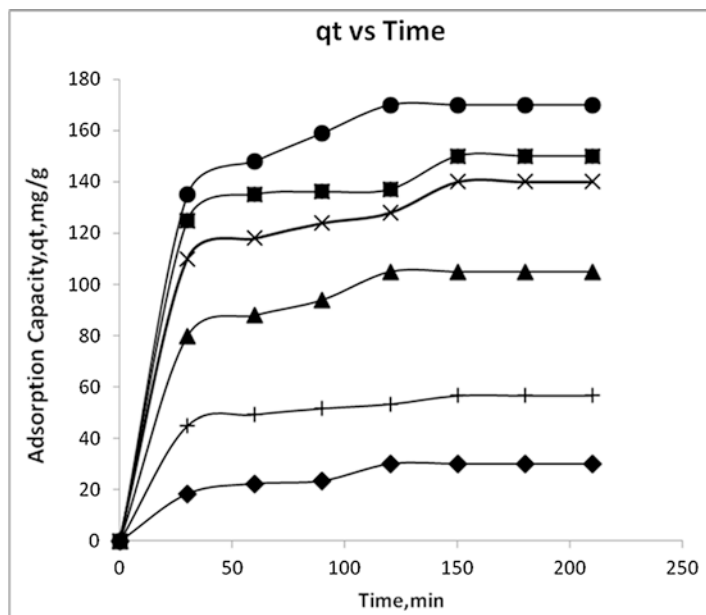


Fig. 6.3 Effect of contact time for different initial concentration (mg/L): (■), 25; (●), 50; (▲) 100; (▼), 150; 200 (◀) and 250 (▶) (Adapted, Modified and reproduced from Vijetha et al. 2019)

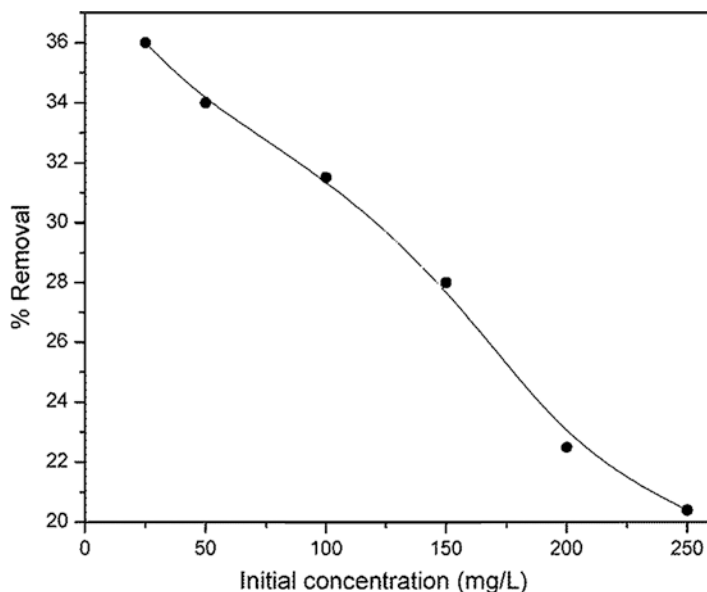


Fig. 6.4 Effect of initial concentration on % removal (Adapted, modified and reproduced from Vijetha et al. 2019)

6.9 Effect of pH

In pH range 2 to 12 (Fig. 6.5), the influence of pH on adsorption was studied. The absorption potential rises from 160 to 170 mg/g as the pH rises from 2 to 3 and a declining pattern in the pH level of 3–12 was found in comparison. In the experimental research done by Thilakarathnc 2014, the same value was observed. The basic medium contributes to anionic carbofuran molecules that show strong repulsion with negative CABC surface and resulted in unstable interaction (Batool et al. 2014).

6.10 Effect of Adsorbent Dosage

The impact of CABC dosage (grams of biochar per gram of carbofuran) on carbofuran adsorption was explored. The efficiency of adsorption rises as the sorbent dose rises to 1.2 g/g with the adsorption capacity of 170 mg/g indicating the excess amount of empty sites on CABC. As is apparent from Fig. 6.6, additional rise in sorbent dose decreases adsorption potential to 40 mg/g. It is because at higher CABC dose the CABC sorption potential required for carbofuran adsorbing was not completely used.

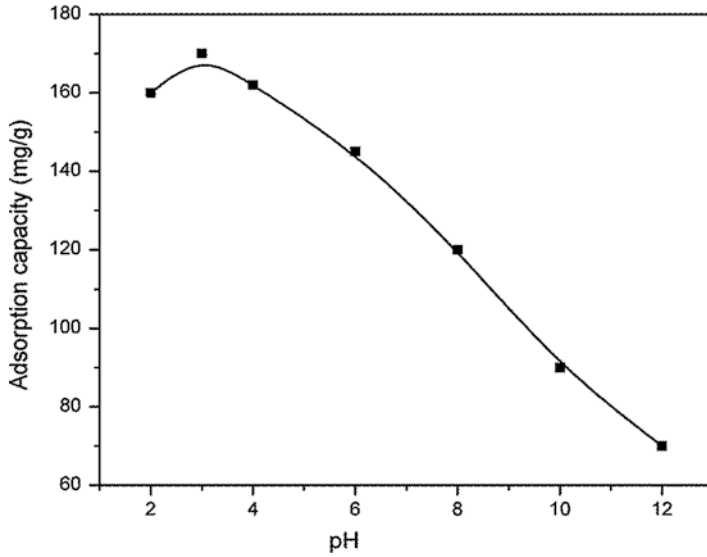


Fig. 6.5 Effect of solution pH

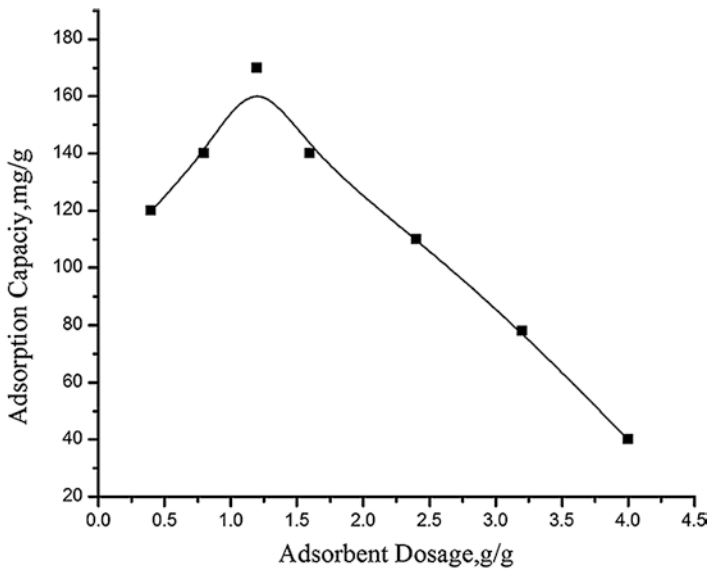


Fig. 6.6 Effect of adsorbent dosage

6.11 Adsorption Isotherms

The equilibrium data from Fig. 6.3 have been fitted to various isotherm models reported in Table 6.2.

Different models R^2 and ARE values suggest that the Langmuir model offers appropriate fitting to the adsorption results with higher R^2 (0.99) and lower average actual relative error (ARE)(0.08). This finding reveals that carbofuran monolayer adsorption occurs on homogeneous CABG surface. The maximum q_m obtained was 322.58 mg/g and the adsorption energy K_L Langmuir constant is 0.0064 L/g. The Langmuir adsorption isotherm fit was shown in Fig. 6.7(a).

The data also showed that carbofuran molecules were not interacted and transmitted in the surface plane (Foo 2016; Chang et al. 2014; Salman et al. 2011).

The separation factor R_L is also measured at various initial carbofuran concentrations, and the findings are seen in Fig. 6.7(b). Of all initial carbofuran concentrations, the value of R_L is between 0 and 1 which means that the sorption process is advantageous. Figure 6.7(b) represents the increasing trend with initial concentration up to CABG sites were saturated implying monolayer coverage.

Table 6.2 Isotherm models

Isotherm	Parameters	Values	Fitting parameters
Langmuir $\frac{1}{q_e} = \frac{1}{q_m} + \frac{1}{q_m K_L C_e}$ $R_L = \frac{1}{(1 + K_L C_o)}$ $\theta = \frac{K_L C_o}{(1 + K_L C_o)}$	q_m K_L	322.58 0.0064	R^2 0.99 ARE 0.08
Freundlich $\log(q_e) = \log K_F + \frac{1}{n} \log C_e$	K_F n	4.86 1.44	R^2 0.97 ARE 0.95
Temkin $q_e = \frac{RT}{b_T} (\ln(A_T) + \ln(C_e))$	b_T A_T	44.10 0.095	R^2 0.98 ARE 1.09
Dubinin–Radushkevich $\ln(q_e) = \ln(q_s) - k_{ad} \epsilon^2$ $\epsilon = RT \ln[1 + \frac{1}{C_e}]$	q_s k_{ad}	132.55 7×10^{-5}	R^2 0.85 ARE 2.33

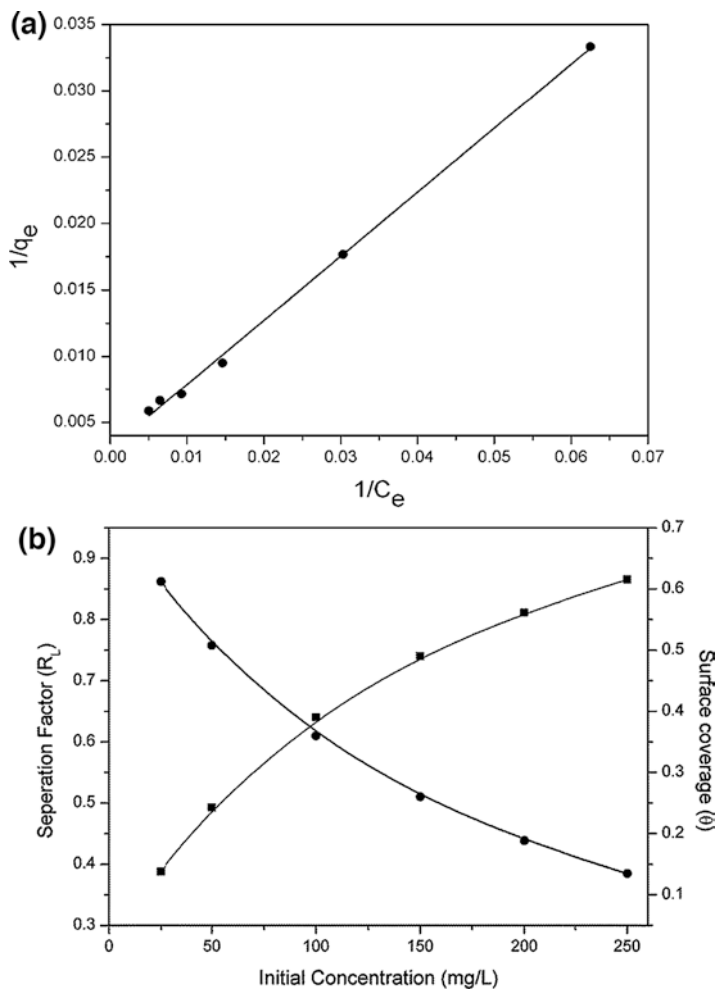


Fig. 6.7 (a) Langmuir isotherm model, (b) separation factor (●) and surface coverage (■) profile against initial carbofuran concentration for CABC

6.12 Adsorption Kinetics

Sorption kinetics of carbofuran was interpreted with PFOM, PSOM-I, PSOM-II, EM, and IPDM kinetic models. The models are listed in Table 6.3 and model fit of all kinetic models is shown in Fig. 6.8 for an initial concentration of 50 mg/L.

The kinetic data on carbofuran adsorption on the CABC was well depicted by PSO (Type-I) model, with a regression coefficient of 0.99. This depicts a chemical rate controlling mechanism in the sorption process. It also depicts that there are ample sites for sorption accessible on the surface with a low initial carbofuran concentration compared with the sorption capability of the CABC.

Table 6.3 Kinetic models

Model	Parameters	25 mg/L	50 mg/L	100 mg/L	150 mg/L	200 mg/L	250 mg/L
Pseudo-first-order model $\ln(q_e - q_t) = \ln(q_e) - k_1 t$	$k_1 \times 10^2$ q_e (mg/g) R^2	1.75 21.30 0.87	1.86 28.96 0.91	2.40 69.06 0.86	2.44 113.52 0.88	2.39 96.93 0.89	2.66 107.12 0.87
Pseudo-second-order (type -I) $\frac{t}{q_t} = \frac{1}{k_2 q_e} + \frac{1}{q_e} t$	$k_2 \times 10^3$ q_e R^2	1.82 32.36 0.98	2.42 58.13 0.99	0.91 109.89 0.99	0.67 144.92 0.99	0.92 153.84 0.99	0.71 175.43 0.99
Pseudo-second-order (type -II) $\frac{1}{q_t} = \frac{1}{k_2 q_e} + \frac{1}{k_1 q_e} + \frac{1}{k_2 q_e^2} t$	$k_2 \times 10^3$ q_e R^2	1.13 33.67 0.91	1.78 58.48 0.94	0.72 109.89 0.79	0.73 140.85 0.73	0.92 151.51 0.77	0.55 175.44 0.80
Elovich model $q_t = \frac{1}{\beta} \ln(\alpha\beta) + \frac{1}{\beta} \ln(t)$	α $\beta * 10^2$ R^2	3.29 14.86 0.90	234.38 15.60 0.98	77.75 6.49 0.87	244.94 5.72 0.86	2294.02 6.94 0.89	318.84 4.63 0.88
Intraparticle diffusion model $q_t = K_p t^{1/2} + C$	k_{p1} C R^2	1.42 11.33 0.88	1.36 38.39 0.95	3.29 61.44 0.86	3.84 86.36 0.90	3.14 106.44 0.92	4.59 109.42 0.87

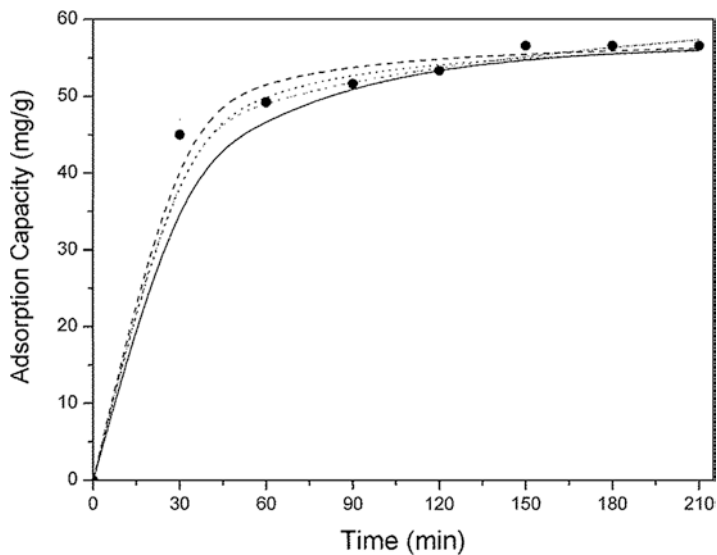


Fig. 6.8 Experimental data and modelled results based on PFOM (----), PSOM-I (-), PSOM-II (.....), and EM (-.-.-) models

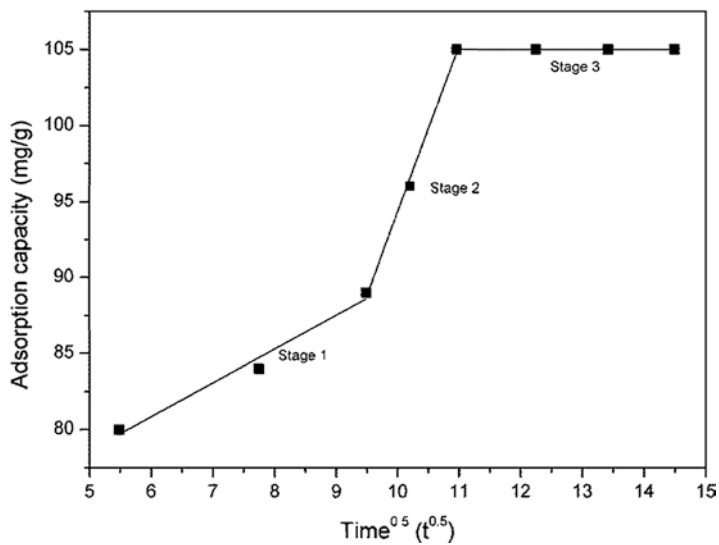


Fig. 6.9 Intraparticle diffusion model

In addition, IPDM was analyzed which illustrates the adsorption controlled by diffusion and the adsorption rate is calculated by the bio-sorbate's diffusion velocity to the adsorbent surface. Figure 6.9 shows the intraparticle diffusion model which shows three distinct zones indicating the large proportion of kinetic stages (Hafshejani et al. 2016).

In the overall adsorption process, the first stage shows the diffusion of carbofuran solution to the CABC surface, i.e., fluid transfer, the second stage shows the slower adsorption (film diffusion), and the third stage describes the equilibrium point owing to the reduction of CABC's active sites (Surface diffusion). In addition, the plot does not move through the origin revealing the possibility that the adsorption rate is regulated by the mechanism of diffusion.

6.13 Conclusions

In this chapter, CABC from CAW was prepared at 300 and 700 °C. These char samples were analyzed using SEM and BET Analysis. It was observed that CABC produced at 300 °C is having more surface area (32.07 m²/g) and pore volume (0.0635 cm³/g) compared to CABC at 700 °C surface area (3.03 m²/g) and pore volume (0.02 cm³/g) and hence CABC at 300 °C was used for adsorption studies. Langmuir adsorption isotherm was best matched with a q_m 322.58 mg/g and K_L 0.0064 L/g Here, the total adsorption rate follows a three-step process, carbofuran diffusion to CABC accompanied by gradual adsorption (film diffusion) and eventually a point of equilibrium (surface diffusion). The above findings are also useful in developing efficient and affordable low-temperature sorbent from agricultural fields to separate synthetic organic contaminant (Carbofuran) from CABC.

References

- Batool, S., Akib, S., Ahmad, M., Balkhair, K. S., & Ashraf, M. A. (2014). Study of modern nano enhanced techniques for removal of dyes and metals. *Journal of Nanomaterials*, 2014, 20. 864914.
- Buss, W., Masek, O., Margaret Graham, M., & Wüst, D. (2015). Inherent organic compounds in biochar -their content, composition and potential toxic effects. *Journal of Environmental Management*, 156, 150–157.
- Chang, K. L., Chen, C. C., Jun-HongLin, J. H., Hsiend, J. F., Wang, Y., Zhao, F., Shih, Y. H., Xinga, Z. J., & Chen, S. T. (2014). Rice straw-derived activated carbons for the removal of carbofuran from an aqueous solution. *New Carbon Materials*, 29, 47–54.
- Foo, K. Y. (2016). Value-added utilization of maize cobs waste as an environmental friendly solution for the innovative treatment of carbofuran. *Process Safety and Environment Protection*, 100, 295–304.
- Hafshejani, A. D., Hooshmand, A., Naseria, A. A., Mohammadi, A. S., Abbasi, F., & Bhatnagar, A. (2016). Removal of nitrate from aqueous solution by modified sugarcane bagasse biochar. *Ecological Engineering*, 95, 101–111.

- Hameed, B. H. (2011). Bentazon and carbofuran adsorption onto date seed activated carbon: Kinetics and equilibrium. *Chemical Engineering Journal*, 173, 361–368.
- Ho, Y. S. (2006). Second-order kinetic model for the sorption of cadmium onto tree fern: A comparison of linear and non-linear methods. *Water Research*, 40, 119–125.
- Mayakaduwa, S. S., Vithanage, M., Karunaratna, A., Mohan, D., & Ok, Y. S. (2016). Interface interactions between insecticide carbofuran and tea waste biochars produced at different pyrolysis temperatures. *Chemical Speciation & Bioavailability*, 28(1–4), 110–118.
- Ren, L., Zhang, J., Li, Y., & Zhang, C. (2011). Preparation and evaluation of cattail fiber-based activated carbon for 2,4-dichlorophenol and 2,4,6-trichlorophenol removal. *Chemical Engineering Journal*, 168, 553–561.
- Salman, J. M., Njoku, V. O., & Hameed, B. H. (2011). Bentazon and carbofuran adsorption onto date seed activated carbon: Kinetics and equilibrium. *Chemical Engineering Journal*, 173, 361–368.
- Thilakarathnc, H. M. A. G. (2014). Sorption properties of tea waste and rice husk biochar for carbofuran removal from aqueous media, University of Peradeniya Digital Library, 2014 (<http://dlib.pdn.ac.lk/handle/1/5908>).
- Vijayaraghavan, K., Padmesh, T. V. N., Palanivelu, K., & Velan, M. (2006). Biosorption of nickel(II) ions onto *Sargassum wightii*: Application of two-parameter and three-parameter isotherm models. *Journal of Hazardous Materials*, 133(1–3), 304–308.
- Vijetha, P., Tondepu, S., Aniya, V., Kumar, A., Bankupalli, S., & Mandapati, R. (2019). Torrefied and unmodified capsicum annuum biochar for the removal of synthetic hazardous pesticide (carbofuran) from watershed. *BRIAC*, 9(5), 4384–4393.

Chapter 7

Bio-Desulfurization of Coal Using Biotechnological Approach, Making Coal a Less Harmful Fuel



Hafiz Ahmad Ishfaq, Ayantika Banerjee, and Sanaullah Qamar

7.1 Introduction

Coal is known as the most abundant form of fossils fuel on earth. There is a persistent increase in the global demand of energy. To meet global energy demands commercialization and utilization of lower quality fossils fuels (Rajendran et al. 2020) is mandatory. Although coal is the most abundant, but most of the discovered coal is not of good quality. Clean coal is one of the most viable solutions to our energy requirement (Acharya et al. 2004). International Energy Agency sites to see the maximum increase in the amount of coal demand among all the primary energy resources. The demand has showed an increase of 38% in the decade of 2005 to 2015 will increase by a fold to 73% by 2030 as indicated in Fig. 7.1 (Patzek and Croft 2010).

There is a rampant need to develop clean coal technologies which can help us to attenuate the environmental aspect of coal as well as to improve the efficiency of the

Hafiz Ahmad Ishfaq, Ayantika Banerjee and Sanaullah Qamar contributed equally with all other contributors.

H. A. Ishfaq (✉) · S. Qamar
Fuel Cell Research Center, Korea Institute of Energy Research (KIER), Daejeon, South Korea

Department of Advanced Energy and System Engineering, University of Science and Technology (UST), Daejeon, South Korea
e-mail: sqamar.che5@scme.nust.edu.pk

A. Banerjee
Decontamination and Decommissioning Division, Korea Atomic Energy Research Institute (KAERI), Daejeon, South Korea

Quantum Energy Chemical Engineering, University of Science and Technology (UST), Daejeon, South Korea
e-mail: banerjee93@kaeri.re.kr

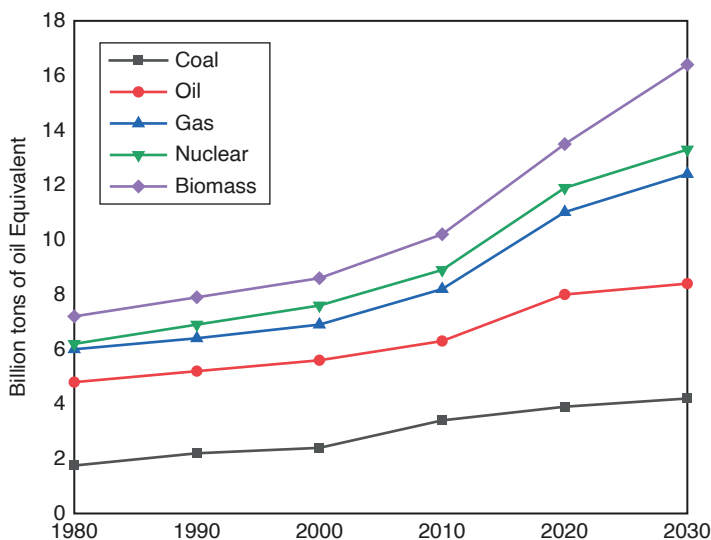


Fig. 7.1 International Energy Agency (IEA) data of World's primary energy Demand from 1980 to 2030 (Patzek and Croft 2010)

energy conversion process. Coal consists of inorganic and organic contents, mainly sulfur. Sulfur is contained in all forms of coal. Mostly it is found in three forms, namely inorganic sulfates, organic compounds, and in pyritic form. The removal of inorganic sulfur compounds can be easily done by physical techniques but organo-sulfur compounds need special chemical treatment. Coal contains organic compounds which are essential constituent of coal matrix, so this is really difficult to remove. Conventional methods already used coal can remove 50% of pyritic form of sulfur and 30% of total (Darmawan 2019). This sulfur cause huge problem to utilize coal as fuel. Removal of sulfur from coal is essential for coal utilization. Coal cleaning technology follows a lot of mechanism like physical, chemical, and biological methods of desulfurization.

7.1.1 Sulfur Contained in Coal: Need for Desulfurization

Burning coal not only results in increase of global warming but also releases airborne pollutants and toxins. Some of them contain toxic oxide gases like nitrogen oxide and sulfur oxide, particulate matter, and heavy metals like mercury and lead. Impurities present in coal when burnt along with coal release pollutant gases. Sulfur is naturally found in coal in small quantities of 1–3% (Çelik et al. 2019) and burning this sulfur-contained coal results in release of toxic gases which combine with water and that is one of the main cause of acid rain. Sulfur in coal mainly depends on the conditions for coal formation over the period of time. Coal formed under freshwater

environment comes up with a low content of sulfur as compared with coal formed under marine environments (Wynter et al. 2004). Removal of these impurities is mandatory and easier in the pre-burning stage instead of capturing and treatment of them from flue gas.

This chapter has described the process of desulfurization and also the mechanism of bio-desulfurization with biotechnological approaches.

7.2 Process for Desulfurization

To reduce the adverse environmental effects caused by coal combustion, different technologies have been developed. Desulfurization method is an important process of clean coal technology. This method can be classified into some categories according to the type of application:

- (a) Physical methods of desulfurization.
- (b) Chemical methods of desulfurization.
- (c) Biological methods of desulfurization.

Every desulfurization process comes up with difficulties and limitations. Only a limited form of inorganic sulfur can be removed from the physical coal cleaning technologies. This happens because of insufficient liberations (1998). Biological and chemical methods of desulfurization have the potential to remove the organic sulfur (Xuehui and Jinming 2009). Physical coal cleaning method can remove mainly large materials such as iron pyrites whereas chemical and biological methods remove fine materials. Physical cleaning method has been commercialized but biological or chemical methods are yet not fully commercialized.

7.2.1 Physical Methods of Desulfurization

Physical coal cleaning method is based on either specific gravity or surface properties and it can remove the sulfur only (Xuehui and Jinming 2009). Other physical characteristics of coal such as particle size, magnetic properties, and electrical conductivity help to develop the methods for physical removal of sulfur from coal. Physical desulfurization process has the ability to remove pyritic sulfur from coals without any kind of chemical modification or destructions (Ghosh et al. 2015). There are several process of physical methods of desulfurization such as flotation, gravimetric, magnetic, and power ultrasound process (Leonard et al. 1981). This can be done by simple processes of tabling, hydrocloning and jiggling, etc. (Harrison 1983). Impurities present in coal can be removed by simple technique like gravity separation. It depends on specific gravities of coal and its impurities. The lower values of the specific gravity of clean coal are 1.3 ~ 1.7, whereas mineral matter has the specific gravity of 2.5 ~ 5.0 (Fan 1984).

In *forth flotation*, being a hydrophobic compound coal binds itself with the bubbles of air and can be easily separated from the water. The impurities are soluble in aqueous suspension (Patterson et al. 1979). In *oil agglomeration*, instead of water we add a little quantity of oil to coal slurry. This results in coating of coal particles with oil and get agglomerated as larger clumps and that can be easily separated by screening the suspension (Leonard et al. 1981). *Magnetic separation* depends on the difference of magnetism of coal and water. *Electrical methods* make use of electrical charges as well as magnetic forces to separate the coal (Fan 1984). Difference of other properties such as dielectric effect and conductivity is also used by this separation method. A research group has developed a different technology called as *chemical comminution*, where the coal has been treated with a substance for instance anhydrous ammonia which can able to disrupt the natural bonds in coal to expose it as ash-forming minerals (Quackenbush et al. 1979). Lovás et al. (2011) has stated that pyrites can be removed as pyrites by absorbing microwave radiation and would be more effective if magnetite could be added while the coal would be processed with microwave and finally separated by magnetism.

Physical methods are good enough for desulfurization as all methods have been developed well, these methods are inexpensive, and there are no such difficulties. However, physical methods have the incapability to remove the impurities and organic sulfur.

7.2.2 Chemical Methods of Desulfurization

Pyrite found in coal always does react when it comes to the contact of air and that forms the poisonous sulfur oxides. The percentage of pyrites is generally high in coal, so the desulfurization is highly needed for protecting environment. One of the efficient methods of coal desulfurization is established on chemical and biological methods. In chemical methods there are several applications such as chemical desulfurization, leaching, extraction, flotation, and oxydesulfurization. The difficulty in removal of organic sulfur is this that it is fixed in the structure of coal. By using chemical methods it is possible to break the bonds and remove the organic sulfur partially (Li and Cho 2005). The sulfur in coal exists as organic or pyrite and organic sulfur stays in mercaptanes (RSH), disulfides (RS-S-R'), or sulfides (R-S-R') form (R' represents aliphatic group) (Meyers et al. 1979). Usually, burning of coal results in release of sulfur oxide gases such as SO₂ or SO₃, and both these gases get mixed to atmosphere and become main cause of "acid rain." Pyrite is predominant inorganic sulfur which has been randomly distributed in the form of crystal (Çelik et al. 2019). Chemical reagents like sodium hypochlorite, nitric acid, hydrofluoric acid, and sodium hydroxide are used for the extraction of sulfur (Steel and Patrick 2001; Abdollahy et al. 2006). Leaching is the most common method to extract the sulfur from coal. In this topic we are going to discuss about several chemical methods of desulfurization, and among those oxidative, reductive, caustic, and miscellaneous methods are mostly important (Chander et al. 2015).

7.2.3 *Oxidative Desulfurization (ODS)*

There are many ways to remove RS compounds from sulfur, for example, “adsorptive desulfurization,” “adsorptive desulfurization,” alkylation-based and “chlorinolysis-based desulfurization,” oxidative desulfurization(ODS), etc. (Abdollahy et al. 2006). After publishing the first report on ODS, several researches has been done on this topic and concluded this technique as a best technique for separation of organic sulfur compounds. ODS usually remove sulfur compounds through oxidation process in the presence of oxidative agent and that oxidant helps to form sulfones from sulfur and the sulfones can be removed as final end-product (Rajendran et al. 2020). Many oxidants like H₂O₂, molecular O₂, organic peracids, cyclo-hexanone hydroperoxide, ozone, nitrogen oxides, and air are published in many literatures (Ismagilov et al. 2011). The Chemical Construction Co. has showed the achievement on converting different forms of sulfur into aqueous form by process of oxidation process using air, at 150–200 °C under 220–1500 psi pressure (Chiang and Cobb 2000). There are some ODS catalysts which are reported as important, such as metal oxides, metal complexes, Titanosilicate (TS), and Polyoxometalates (Rajendran et al. 2020).

7.2.4 *Hydro-Desulfurization (HDS)*

Hydro-desulfurization is used mainly for removing high sulfur level. Gulf HDS process is known as best technique among all HDS techniques (Brunn et al. 1976). This technique is economically manageable as well as flexible. Typically, CoMoP/Al₂O₃-SiO₂ Hydro-desulfurization catalyst is well known for using it through wet-mixing kneading method (Brunn et al. 1976).

7.2.5 *Biological Method of Desulfurization*

Biological desulfurization known as microbial coal desulfurization process can be labeled as microbiological removal of sulfur at a certain temperature by Kilbane et al. (Kilbane 1989). Physical methods of desulfurization are not appropriate as it cannot remove pyritic sulfur, and chemical methods also demand not only high energy but also chemical consumption. So, the bio-desulfurization method has been developed through bioprocessing. Two pathways have been developed for bio-desulfurization. One, “direct mechanism,” which does emphasize on the independent action of ferric ions, and the other is, “indirect mechanism,” where the carbon ring structure or metal sulfides become oxidized to ferrous state (Ju 1992; Ghosh et al. 2015). According to Dastidar et al. (2000) study, it has been reported that microbial oxidation of compounds like pyrite is usually leading during the

exponential stag. While on the contrary, indirect process of electrochemical oxidation is probable to be observed at the stationary phase of growth.

Microbial exclusion of pyrites from coal had been tested and examined in several laboratories since past 30 years (Olson and Brinckman 1986). Bacteria and fungi have a great role in bio-desulfurization, as microorganisms have the ability to attack carbonaceous matter in coal (Ghosh et al. 2015). Several microorganisms like *Rhodococcus* sp. and *Pseudomonas* sp. have been reported with good ability of removing sulfur from coal (Kargi. and Robinson 1986). Meso-acidophilic bacteria named as *Acidithiobacillus ferrooxidans* is widely used in bio-desulfurization (Ghosh et al. 2015). Kargi and Robinson et al., (Kargi and Robinson 1985) reported that thermophilic bacteria, *Sulfolobus acidocaldarius*, has a good ability to eliminate 96% of organic sulfur and 50% of total sulfur from sample at 70 °C. Pinar et al. have showed that *A. ferrivorans*, a new member of *Acidithiobacillus* genus, has been able to remove 33% of total sulfur at pH 2.5 and 14 days of incubation time.

Various strains of *Thiobacillus ferrooxidans* are used widely as obligate autotrophs in coal desulfurization (Kargi. and Robinson 1986). These bacteria are gram-negative and mesophilic have been consumed for removal of pyritic sulfur under autotrophic conditions (Olsson et al. 1995). Although many *Thiobacillus*-type organisms are not good enough to remove organic sulfur from coal (Martínez et al. 1995) but “thermophilic” *Thiobacillus*-type organisms are used for pyritic sulfur removal from coal at 55 °C temperature (Brierley and Le Roux 1978). Cultures of *A. ferrooxidans*, *A. thiooxidans*, *Sulfolobus acidocaldarius* (Kargi and Robinson 1985), *Pseudomonas putida*, *Pseudomonas aeruginosa* (Rai and Reyniers 1988), *Acidianus brierleyi*, etc. have been used firstly for bio-desulfurization. Some researchers have reported that combined cultures of *T. ferrooxidans*, *T. thiooxidans*, *T. thiooxidans*, and *Leptospirillum ferrooxidans* show better efficiency for the removal of pyritic sulfur from coal (Malik et al. 2000). *Thiooxidans* and *ferrooxidans* can oxidize ferrous ion to ferric ion and also help to oxidize elemental sulfur to sulfate.

There are some researches which have concluded that fungi could be used for sulfur removal and as microorganisms. Van Hamme et al. reported that white rot fungi can metabolize dibenzyl sulfide. Later on, Aytar et al. have reported many studies on this topic and established the process of coal desulfurization by using *Alternaria* sp. Some studies reported that genetically modified *Acidithiobacillus* can have the ability of bioleaching (Koizumi 1994). As coal has a complex structure, so it is needed to identify the large-scale application which can serve a good aspects of bio-desulfurization. In this chapter, we will go through the advanced mechanisms and technologies regarding bio-desulfurization.

7.3 Bio-Desulfurization

Bio-desulfurization is a process that involves the oxidation process for converting organic sulfur or reduced form of sulfur in soluble compounds by the use of various microorganisms or enzymes that promotes the breakage of C-S bonds by various metabolic pathways. The concept of using various microorganisms for bio-desulfurization is important and has been discussed below.

7.3.1 Microorganisms Used for Bio-Desulfurization of Coal

Archaea bacteria were introduced in a phylogenetic tree that contains the varieties of sulfur-metabolizing archaea in the 1980s (Woese et al. 1990). This tree of archaea is typically divided into two main kingdoms named as Crenarchaeota and Euryarchaeota and illustrated in Fig. 7.2. Crenarchaeota kingdom contains variety of sulfur removing archaea and hence has thermophilic sulfur-reliant archaea used for microbial depyritization of coal. The Crenarchaeota is further divided into Sulfolobales and Thermoproteales which contain thermo-acidophilic sulfur-metabolizing archaea. *Sulfolobus*, *Acidianus*, and *Metallosphaera* (De Rosa et al. 1975; Huber et al. 1989; Kasmiarno and Chang 2020) are the sulfur-metabolizing bacteria which come under the category of Sulfolobales. The *Sulfolobus* and *Acidianus*, in their natural state, utilize sulfur as a source of energy. Some studies have reported that metallosphaera has been extensively used for coal desulfurization (Clark et al. 1993). Detz et al. (Barvinchak 1980) used thermophilic *Ferrobolus* and *Sulfolobus acidocaldarius* microorganisms to remove more than 90% organic sulfur from coal in 6 days of residence time. *S. acidocaldarius* has been reported to perform dual functions. It will not only degrade the organic sulfur compounds with an

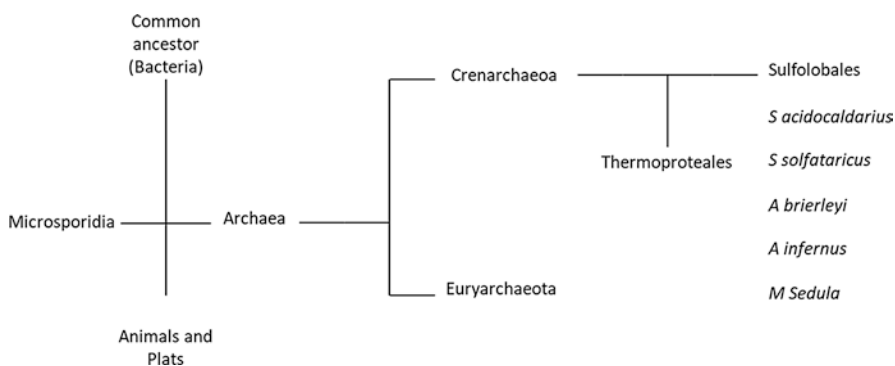


Fig. 7.2 The global phylogenetic tree showing the division of sulfur metabolizing archaea (adapted from Gutell and Woese 1990)

excellent behavior in removal of pyritic sulfur from coal but also effectively utilize the inorganic sulfur (De Rosa et al. 1975; Kargi 1987).

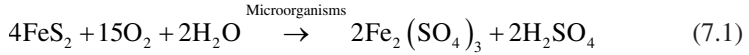
Thiobacterium, *Macromonas*, *Thiospira*, and *Beggiatoa* are some suitable bacteria which can effectively remove sulfur from coal (Acharya et al. 2004). The *Pseudomonas* is a well-known microorganism for its metabolic versatility that can efficiently remove organic sulfur from coal. This bacterium neither removed organic sulfur nor pyrite sulfur but could be used to remove thiophene sulfur from coal (Rossi 2014). *Bacillus*, *Xanthomonas*, and *Pseudomonas* have been used to degrade dibenzothiophene, and almost 20% organic sulfur has been removed in 15–20 days residence time (Kilbane 2017). Similarly, *Pseudomonas menacoas* and *Alcaligenes paradoxus* biovar are capable to confiscate around 22.2–32.0% organic sulfur from coal in the duration of 15 days (Wise and Kilbane 2018). These microorganisms for sulfur removal from coal have shown physiological and genetic differences and therefore could occur in an enormous variety of environments.

7.3.2 Mechanism of Pyrite Microbial Desulfurization

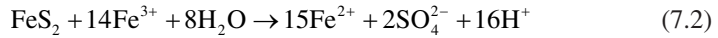
The oxidation process of coal conversion is possible by microorganisms after getting influenced by the polyfunctional coal structure and this process usually depends on two main factors: size or shape of coal and surface properties of microorganisms (Konishi et al. 1990). The morphology and distribution of pyrites are the crucial factors in the bio-desulfurization of coal. According to Silverman et al. (Silverman et al. 1961) in the direct contact mechanism, contact as physical in between bacteria and FeS_2 particles is required to oxidize the pyrite under aerobic conditions. In contrast, the regenerated Fe^{3+} ions by the bacterial oxidation of Fe^{2+} in pyrite can be further used for the oxidation of pyrite. Irrespective of an indirect and direct contact mechanism, the four vital steps which are involved in the microbial coal desulfurization are described as follows:

- Oxidative conversion of pyrite to ferrous (Fe^{2+}) ions catalyzed by *T ferrooxidans*.
- Oxidative conversion of Fe^{2+} to ferric (Fe^{3+}) ions catalyzed by *T ferrooxidans*.
- Chemically oxidative indirect conversion of pyrite into ferrous sulfate and hence to elemental sulfur by ferric sulfate.
- Sulfur to sulfuric acid conversion by the attack of microorganisms.

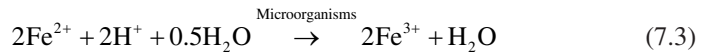
The conversion mechanisms are not yet completely elucidated because some studies support indirect mechanism (Keller and Murr 1982; Andrews and Maczuga 1984) whereas other researchers support the direct mechanism (Asai et al. 1992; Rohwerder and Sand 2007) for the coal desulfurization. A comprehensive description of the direct and indirect mechanism of pyrite microbial oxidation is suggested by Larsson et al. (Larsson et al. 1990). Direct mechanism of bio-desulfurization involves the direct oxidative conversion of pyrite by microorganism as:



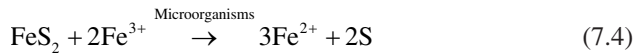
This process requires physical contact between microorganisms and the pyrite. Sulfuric acid usually produced by this reaction has a tendency to enhance the pH in the reaction container and therefore the control of pH value is necessary to remain these bacteria active. On the other hand, the indirect mechanism involves multiple paces. In the process of first step, chemical oxidation of pyrite by Fe^{3+} ions as:



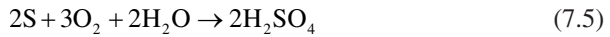
The microorganisms are then attacked on the Fe^{2+} ions and oxidized the produced Fe^{2+} to Fe^{3+} ions as:



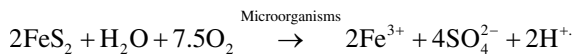
The elemental Fe is generated by the oxidation of ferrous iron in FeS_2 by ferric irons as:



The produced elemental sulfur in the above reaction is further converted to sulfuric acid through oxidation process, held by microorganisms and ferric iron, respectively, as:



However, the kinetics of reaction (7.5) is much faster than the reaction (7.6) and hence the oxidation of sulfur by microorganisms is energetically favorable (Fakoussa and Hofrichter 1999). The overall basic reaction for microbial pyrite oxidation can be summarized as:



7.3.3 Metabolic Pathways of Desulfurization of Coal

The most common compound called as Dibenzothiophene (DBT) is used like a model for organic sulfur compounds in coal. The degradation of DBT involves in various metabolic pathways to remove the sulfur from coal. These metabolic pathways are the chain of various chemical reactions that could occur in a typical microbial cell facilitated by enzymes. In bio-desulfurization process, microorganisms

obtain the energy required for its metabolism from the oxidative conversion of iron (Fe) in Pyrite (FeS_2) in the divalent state. The identification of these metabolic pathways is a complex task for the chemically bonded sulfur i.e., organic sulfur.

Kilbane et al. (Kilbane 1989) suggested a specific pathway contained sulfur represented as the “4S” pathway as shown in Fig. 7.3. The main thing in his represented pathway is the selective oxidation of a sulfur atom in DBT by microorganisms without the breakage of C-C bonds in coal and hence there is no change in the calorific value of coal (Kirimura et al. 2002; Bhanjadeo et al. 2018). This “4S” pathway involves the generation of four different molecules during sulfur metabolism, and for the oxidative conversion of organic sulfur, four genes are mainly responsible. These four genes included these following steps (Gupta et al. 2005): (1) The oxidation of DBT into sulfoxide and again it is oxidized to sulfone (dszC genes) by the action of DBT-monoxygenase, (2) DBT-sulfone is oxidized into 2-hydroxybiphenyl-2-sulfonic acid, the dszA gene, by DBT sulfone monoxygenase, (3) The 2-hydroxybiphenyl sulfinate undergoes desulfurization process that turn into HBP-sulfinate to 2-hydroxybiphenyl and sulfite (dszB genes), and (4) the generation of FMNH₂ required for first three oxidations. Gallagher et al. (Gallagher et al. 1993) proposed a similar “4S” metabolic pathway for *R. rhodochrous* (IGTS8) to remove sulfur from DBT. Similarly, the bacteria such as *Gordona* CYKS1 (Rhee et al. 1998), *Mycobacterium* sp. (Li et al. 2003), and *Paenibacillus* sp. (Konishi et al. 1997) are reported to desulfurize benzothiophene through the “4S” metabolic pathway.

Kodama et al. (Kodama et al. 1973) proposed another mechanism for bio-desulfurization of DBT as illustrated in Fig. 7.4. In their suggested pathway, the C-C bonding of DBT molecule is charged by microorganisms. The oxidative splitting of the C-C bond in their suggested metabolic pathway consists of three major steps: hydroxylation, ring split, and hydrolysis processes.

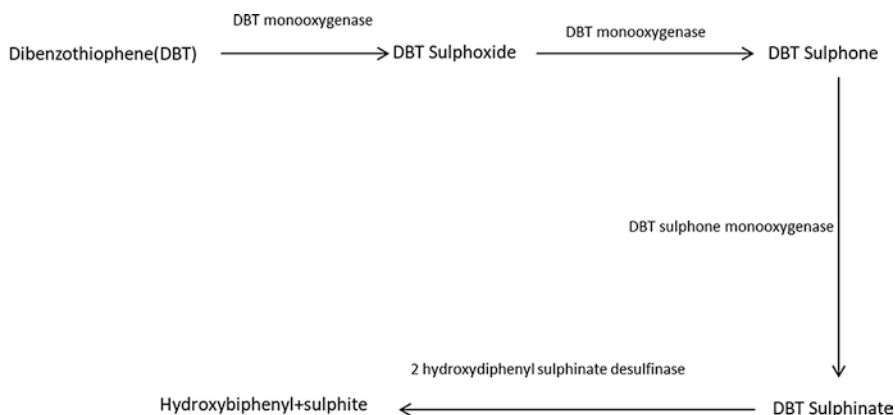


Fig. 7.3 The 4S metabolic pathway proposed by Kilbane for desulfurization of DBT (modified from Kilbane 1989)

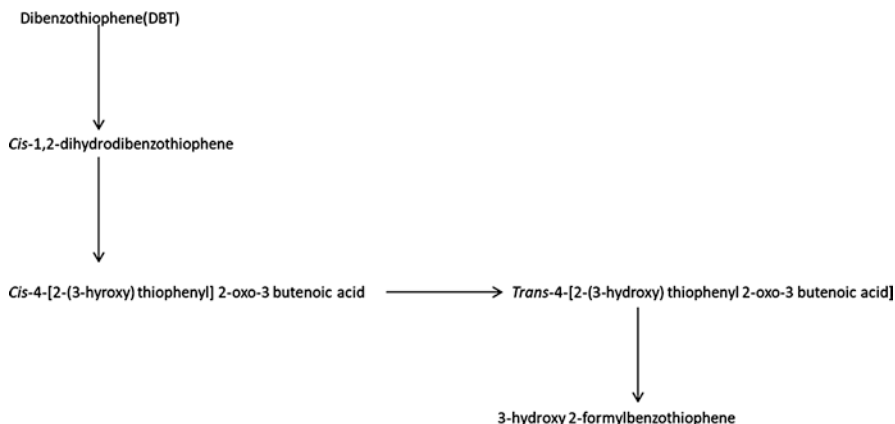


Fig. 7.4 The Kodama metabolic pathway for the DBT desulfurization (modified from Kodama et al. 1973)

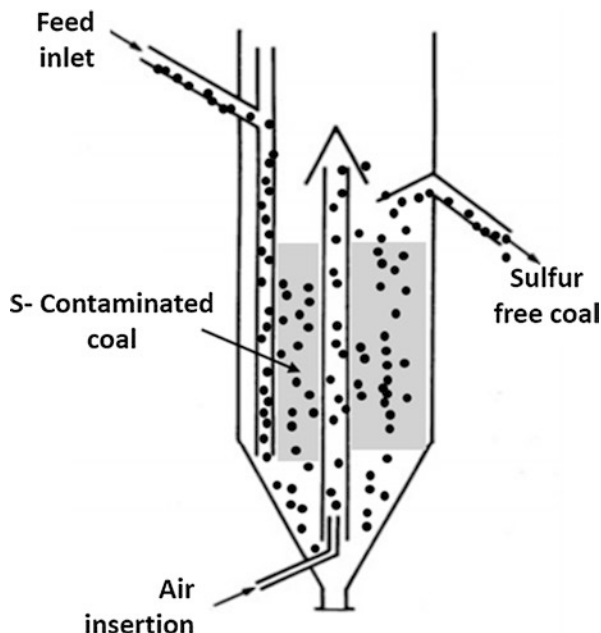
Several bacterias like *Beijerinckia* sp. (Laborde and Gibson 1977) and *Pseudomonas abikonesis* (Kodama et al. 1973) and fungus like *Pleurotus ostreatus* (Bezalel et al. 1996) and *Cunninghamella elegans* (Crawford and Gupta 1990) follow the Kodama's metabolic pathways for removing sulfur from DBT.

7.3.4 *Biotechnological Approaches towards Bio-Desulfurization of Coal*

Coal, the non-renewable fossil fuel, has been widely used as major resource of energy and industrial products but has harmful environmental impacts due to some contaminations, and sulfur is the main contaminant in coal which has been already discussed before. Except microbial desulfurization process some biotechnological approaches are there to desulfurize coal. There are bioreactors which has been designed to remove the impurities from coal. Here it has been discussed about some bioreactors and the technology behind that.

A bioreactor is a reactor in which a certain chemical process is carried out by using the various microorganisms such as bacteria or fungi. For the depyritization of coal biologically, various parameters access the overall performance of bioreactors. These parameters are the size of the tank, overall power requirements, the chemical compounds added to the bioreactor, the maintenance of bioreactor, and the purification of effluents. Two types of bioreactors in bio-desulfurization of coal are generally used, namely the Stirred Tank Reactor (STR) and Air Lift Reactor (ALR), also known as Pachuca tank. The ALR bioreactor is widely used in the bio-depyritization of coal and developed by a hydro metallurgist named Pachuca (Beyer et al. 1986), where this ALR reactor was used for the leaching of noble metals. The cylindrical tank of ALR bioreactor has narrowed bottom as shown in Fig. 7.5. The

Fig. 7.5 Working principle of Pachuca-type bioreactor with DMT model (adapted from Beyer et al. 1986)



pipe that is coaxial with tank has open ends on both sides. From the lower part of this pipe the air is inserted so that this pipe acts as an airlift. It works on the basis of density difference in pulp density within the pipe and outside of the pipe. The pulp density difference must be lower within the pipe than outside. This pressure difference causes the pulp to rise in the central pipe. In this way, the overflow pulp from the central pipe circulates the whole charge and the further desulfurization of coal proceeds continuously.

The performance of Pachuca-type bioreactors decrease abruptly when the concentration of solid rises beyond the value of 20% (Bailey and Hansford 1994). This limit of 20% of oxidizable solids concentration for the desulfurization of metal sulfides in ALRs is the main obstacle in these reactors as it increases both capital (including the cost of size of the reactor) and maintenance costs. Several authors claimed various reasons for this 20% limitation in ALRs in literatures (Bailey and Hansford 1994). The reasons they suggested are summarized as:

- The mechanical separation of microorganisms from the surface of coal due to the shear stresses acting in these bioreactors causes irretrievable destruction to microbial cells. In this way, the microorganisms lose their tendency to adhere to coal surfaces and the oxidization process is restarted.
- The proportion of solids that are able to oxidize has been shown as critical defining factor in the bio-desulfurization process as evidenced by Hansford and Bailey et al. (Bailey and Hansford 1993). The availability of less oxygen in these reactors due to the 20% limit, as indicated by the oxygen mass transfer coefficient (discussed in the next point) slows down the oxidation process.

- The oxygen mass transfer coefficient in Pachuca type bioreactors is defined by (Rossi 1999):

$$k_L \alpha = 2.29 \times 10^{-2} \left(\frac{P}{V} \right)^{0.66} \times \left[\frac{1}{p_o \ln \left(\frac{p_o + p_f g H}{p_o} \right)^{0.66}} \right]$$

where k_L is the overall liquid phase mass transfer coefficient (ms^{-1}), α is the interfacial area ($\text{m}^2 \text{m}^{-3}$), P is the produced power (kW), V is the volume of liquid that should be taken below the air-liquid boundary (m^3), p_o is the atmospheric pressure of air (Pa), p_f is the pressure of fluid (Pa) and H is the height of the pulp interface that must be taken above the bottom part of vessel (m). The reactor performance is enhanced by increasing the aeration that inevitably increased by the agitation and shear-stresses in suspension. But this in turn reduces the oxygen mass transfer coefficient's value that explains the reason behind the limitation of 20% solid concentrations (Rossi 1999). Interestingly, the experimental results for coal bio-desulfurization of pilot plant support these abovementioned remarks. These bench-scale tests in pilot plant were performed with these bioreactors successfully up to 40% coal at Deutsche Montan Technologie (DMT, Germany) and Delft University (Netherlands) (Huber et al. 1984; Beyer et al. 1986). To cope with the drawbacks associated with Pachuca type bioreactors, several modifications in design have been developed. These designs have various advantages of enhancing agitation to increase the oxygen transfer rate (OTR) with minimum shear stresses.

Aerated trough bioreactor: This bioreactor contains a large rectangular tank having a narrow bottom of V-shape which has an air sparger consisting of the perforated pipe as shown in Fig. 7.6 (Rossi 1999; Cooney 2019).

Low energy bioreactor: This design of bioreactor consists of a tank where the bio-desulfurization of coal is carried out. This tank has an agitator inside to reduce the shear stresses. This design has an aeration device which energetically aerated the pulp with the help of Venturi pipe, which is a type of pump used to recirculate the pulp in low energy bioreactor. The representation of this bioreactor is schematically shown in Fig. 7.7. This reactor maximizes the oxygen transfer rate without producing massive shear stresses in pulp. However, pulp inside the aerator is exposed to excessive turbulence and shear stresses caused by the agitator. These shear stresses are produced in the pulp through the impeller and pump which circulates the pulp periodically. Moreover, this reactor is mainly designed for low-grade ores resulting in around $6 \text{ g day}^{-1} \text{ dm}^{-3}$ iron leaching rates from FeS_2 . This performance is not remarkable compared to the value of $9.2 \text{ g day}^{-1} \text{ dm}^{-3}$ produced by stirred-type bioreactors of the pilot plant of Porto Torres (Rossi 1999; Cooney 2019). Hence, the aim is to promote a strong increasing rate in the population of microorganisms that can only be achieved by enhancing the value of the oxygen mass transfer coefficient. In these types of bioreactors, this much increase in the

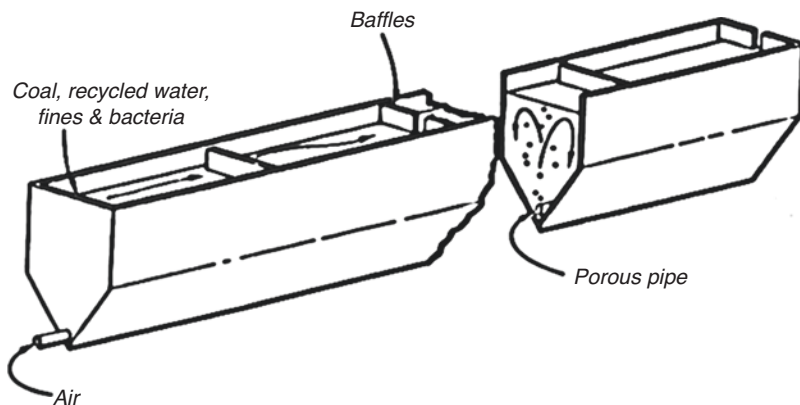
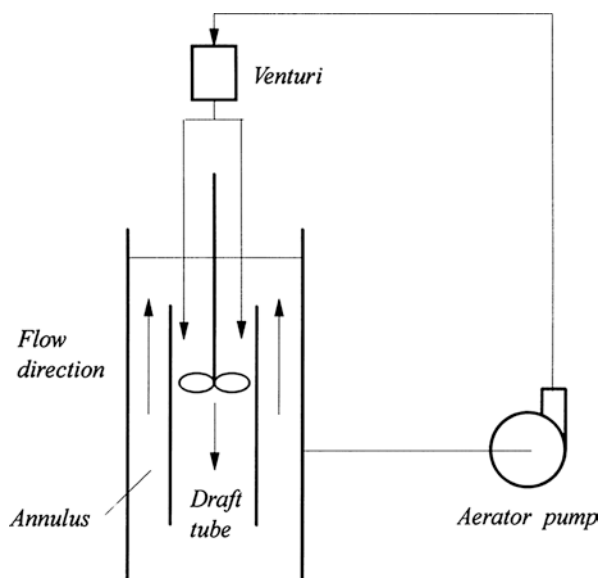


Fig. 7.6 The working principle of aerated trough bioreactor (permitted from Rossi 1999)

Fig. 7.7 The working principle of low energy bioreactor (permitted from Rossi 1999)



oxygen mass transfer coefficient has not been attained in pyrite solubilization of coal.

Revolving drum bioreactor (bio-rotor): The isometrical view of the bio-rotor is demonstrated in Fig. 7.8(b). This reactor consists of barrel having a cylindrical shape whose wall is lined with regular spaced-filters (L). These internally lined filters act as a tray where the suspension in the barrel is contained. Mixture of suspension, air, and CO_2 is passed via a pipe (T) which is fitted into the head (M) of the barrel, also called the *feed-head*. The rollers (R) cause the barrel to revolve so that the suspension in the filters is lifted in the upward direction. As the barrel revolves and achieves the highest position, the suspension is taken out from the barrel as a

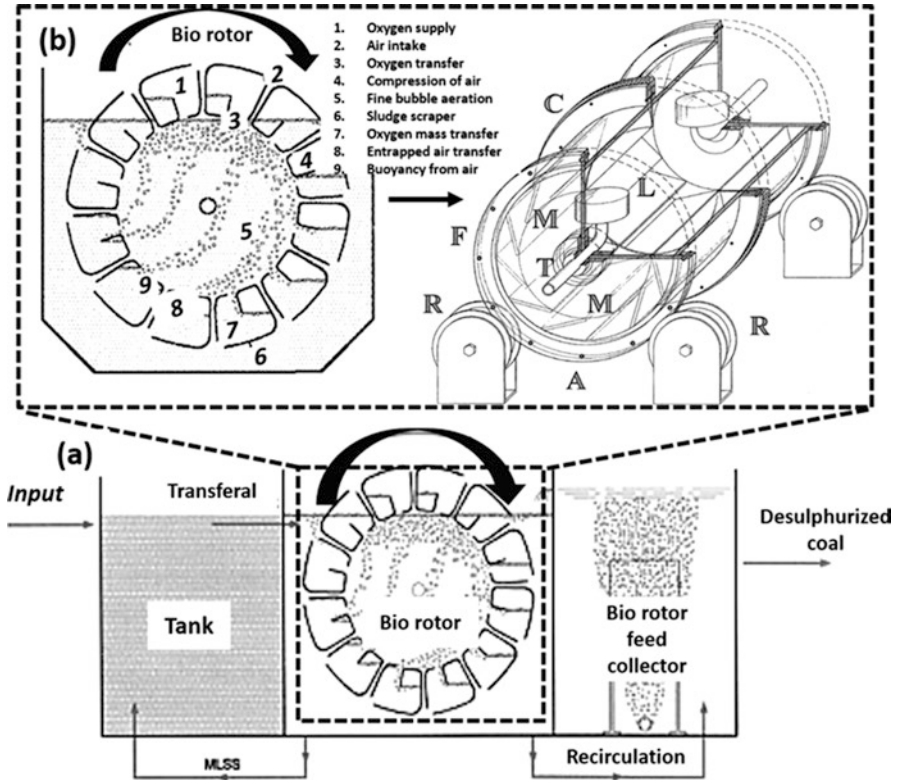


Fig. 7.8 (a) Schematic illustration of the bio-rotor process, (b) detailed description of the bio rotor’s components (modified and permitted from Rossi 1999)

thin contracting film. During the contraction of thin-film suspension, the mass transfer of oxygen usually occurs. The design of biorotor almost meets the requirements for an ideal bioreactor as:

- No “dead volumes” as mixing is complete due to the revolution of the barrel.
- No excessive shear stresses are acting on the suspension and these stresses are only limited to the comparative motion of plummeting film concerning the pulp in the barrel.
- The value of $k_L\alpha$ is in the range of one order of magnitude which is usually greater than that of STRs.

In bio-rotors, the OTR meets the value of $k_L\alpha$, i.e., oxygen is freely available to microorganisms to enhance growth kinetics of reactions. This remarkable feature of the bioreactor gives the yielded solubilization rates of pyrite (30% solids suspension) as high as about $600 \text{ g h}^{-1} \text{ m}^{-3}$ (Rossi 1999; Cooney 2019). Hence, bio-rotors utilize the potentials of microorganisms to increase the pyrite solubilization.

7.4 Conclusion

Coal is prior energy source for energy and as we already discussed that it is really challenging to remove sulfur from coal due to the presence of strong C-S bond in coal. There are lots of technologies which is under development to remove impurities as sulfur from coal. Physical methods of desulfurization are not able to remove organic sulfur, so it is needed to use chemical methods or biological methods to remove sulfur from coal. Selective microbes are able to desulfurize coal but the selection of microbial culture mainly depends on the type of sulfur present in the coal. Some researchers developed the theory of two-step bioleaching process in which both organic sulfur desulfurization bacteria and inorganic sulfur desulfurization bacteria are present (Pan et al. 2019). However the effects of leaching temperature, agitation time, etc. have a significant value on desulfurization. Bio-reactors do serve a good contribution towards desulfurization approaches but there are also some limitations related to the its overall bioreactor structure, type of operation, complicated designs, etc. Particle size has an another influence in the case of extraction process. If the particle size of coal would be smaller, the reactive area between coal and microorganisms would be greater and rate of transfer could be higher in that case. As we discussed before, Oxidative Desulfurization (ODS) process has been ongoing for the development since 30 years. Bio-depyritization is also a well-known process but has some limitations to its technicalities and economical profitability. Many concepts and mechanisms about the desulfurization of coal have been discussed in this chapter. Researches are still going on to find the optimized way-out for coal cleaning technology.

References

- Abdollahy, M., Moghaddam, A. Z., & Rami, K. (2006). Desulfurization of mezino coal using combination of "flotation" and "leaching with potassium hydroxide/methanol". *Fuel*, 85. <https://doi.org/10.1016/j.fuel.2005.10.011>.
- Acharya, C., Sukla, L. B., & Misra, V. N. (2004). Biodepyritisation of coal. *Journal of Chemical Technology and Biotechnology*, 79.
- Andrews, G. F., & Maczuga, J. (1984). Bacterial removal of pyrite from coal. *Fuel*, 63. [https://doi.org/10.1016/0016-2361\(84\)90003-6](https://doi.org/10.1016/0016-2361(84)90003-6).
- Asai, S., Konishi, Y., & Yoshida, K. (1992). Kinetic model for batch bacterial dissolution of pyrite particles by *Thiobacillus ferrooxidans*. *Chemical Engineering Science*, 47. [https://doi.org/10.1016/0009-2509\(92\)80207-S](https://doi.org/10.1016/0009-2509(92)80207-S).
- Bailey, A. D., & Hansford, G. S. (1993). Factors affecting bio-oxidation of sulfide minerals at high concentrations of solids: A review. *Biotechnology and Bioengineering*, 42. <https://doi.org/10.1002/bit.260421006>.
- Bailey, A. D., & Hansford, G. S. (1994). Oxygen mass transfer limitation of batch bio-oxidation at high solids concentration. *Minerals Engineering*, 7. [https://doi.org/10.1016/0892-6875\(94\)90071-X](https://doi.org/10.1016/0892-6875(94)90071-X).
- Barvinchak, G. (1980). Microbial desulfurization of coal, US Patent 4206288, United States.

- Beyer, M., Ebner, H. G., & Klein, J. (1986). Influence of pulp density and bioreactor design on microbial desulfurization of coal. *Applied Microbiology and Biotechnology*, 24. <https://doi.org/10.1007/BF00257061>.
- Bezalel, L., Hadar, Y., Fu, P. P., et al. (1996). Initial oxidation products in the metabolism of pyrene, anthracene, fluorene, and dibenzothiophene by the white rot fungus *Pleurotus ostreatus*. *Applied and Environmental Microbiology*, 62. <https://doi.org/10.1128/aem.62.7.2554-2559.1996>.
- Bhanjadeso, M. M., Rath, K., Gupta, D., et al. (2018). Differential desulfurization of dibenzothiophene by newly identified MTCC strains: Influence of operon array. *PLoS One*, 13. <https://doi.org/10.1371/journal.pone.0192536>.
- Brierley, C. L., & Le Roux, N. W. (1978). Bacterial leaching. *Critical Reviews in Microbiology*, 6. <https://doi.org/10.3109/10408417809090623>.
- Brunn, L. W., Montagna, A. A., Paraskos, J. A. (1976). Clean residual fuels from the Gulf HDS process. In: Preprints.
- Çelik, P. A., Aksoy, D., Koca, S., et al. (2019). The approach of biodesulfurization for clean coal technologies: A review. *International Journal of Environmental Science and Technology*, 16, 2115–2132. <https://doi.org/10.1007/s13762-019-02232-7>.
- Chander, A., Chen, X.-L., Naidu, D. G., et al. (2015). Subject index. *Minerals Engineering*, 10. <https://doi.org/10.1007/978-3-642-13757-0>.
- Chiang, S.-H., Cobb, J. T. (2000). Coal conversion processes, cleaning and desulfurization. In: Kirk-Othmer Encyclopedia of Chemical Technology.
- Clark, T. R., Baldi, F., & Olson, G. J. (1993). Coal depyritization by the thermophilic archaeon *Metallosphaera sedula*. *Applied and Environmental Microbiology*, 59. <https://doi.org/10.1128/aem.59.8.2375-2379.1993>.
- Cooney, C. L. (2019). Bioreactors: Design and operation. In: *Biotechnology and Biological Frontiers*.
- Crawford, D. L., & Gupta, R. K. (1990). Oxidation of dibenzothiophene by *Cunninghamella elegans*. *Current Microbiology*, 21. <https://doi.org/10.1007/BF02092161>.
- Darmawan, D. (2019). *Journal of Chemical Information and Modeling*, 53, 1689–1699. <https://doi.org/10.1017/CBO9781107415324.004>.
- Dastidar, M. G., Malik, A., & Roychoudhury, P. K. (2000). Biodesulfurization of Indian (Assam) coal using *Thiobacillus ferrooxidans* (ATCC 13984). *Energy Conversion Management*, 41. [https://doi.org/10.1016/S0196-8904\(99\)00085-0](https://doi.org/10.1016/S0196-8904(99)00085-0).
- De Rosa, M., Gambacorta, A., & Bu'lock, J. D. (1975). Extremely thermophilic acidophilic bacteria convergent with *Sulfolobus acidocaldarius*. *Journal of General Microbiology*, 86. <https://doi.org/10.1099/00221287-86-1-156>.
- Fakoussa, R. M., & Hofrichter, M. (1999). Biotechnology and microbiology of coal degradation. *Applied Microbiology and Biotechnology*, 52.
- Fan, C. (1984). Coal desulfurization and demineralization by chemical/physical treatments, IUM-I, Iowa State University.
- Gallagher, J. R., Olson, E. S., & Stanley, D. C. (1993). Microbial desulfurization of dibenzothiophene: A sulfur-specific pathway. *FEMS Microbiology Letters*, 107. <https://doi.org/10.1111/j.1574-6968.1993.tb05999.x>.
- Ghosh, A., Sujata, A., Pandey, B. D. (2015). Microbial biodesulfurization of coal. In: *Microbiology for Minerals, Metals, Materials and the Environment*.
- Gupta, N., Roychoudhury, P. K., & Deb, J. K. (2005). Biotechnology of desulfurization of diesel: Prospects and challenges. *Applied Microbiology and Biotechnology*, 66.
- Gutell, R. R., & Woese, C. R. (1990). Higher order structural elements in ribosomal RNAs: Pseudoknots and the use of noncanonical pairs. *Proceedings of the National Academy of Sciences of the United States of America*, 87. <https://doi.org/10.1073/pnas.87.2.663>.
- Harrison, J. S. (1983). Cleaning up coal: A study of coal cleaning and the use of cleaned coal. *Fuel*, 62. [https://doi.org/10.1016/0016-2361\(83\)90322-8](https://doi.org/10.1016/0016-2361(83)90322-8).
- Huber, G., Spinnler, C., Gambacorta, A., & Stetter, K. O. (1989). *Metallosphaera sedula* gen. et sp. nov. represents a new genus of aerobic, metal-mobilizing, Thermoacidophilic Archaeobacteria. *Systematic and Applied Microbiology*, 12. [https://doi.org/10.1016/S0723-2020\(89\)80038-4](https://doi.org/10.1016/S0723-2020(89)80038-4).

- Huber, T. F., Ras, C. and Kossen, N. W. F. (1984). "Design and scale-up of a reactor for the microbial desulphurization of coal: A kinetic model for bacterial growth and pyrite oxidation" in Third European Congress on Biotechnology, Munich, September 10–14, Verlag Chemie, Weinheim, Germany, pp. 151–159.
- Ismagilov, Z., Yashnik, S., Kerzhentsev, M., et al. (2011). Oxidative desulfurization of hydrocarbon fuels. *Catal Rev - Sci Eng*, 53. <https://doi.org/10.1080/01614940.2011.596426>.
- Ju, L. K. (1992). Microbial desulfurization of coal. *Fuel Science and Technology International*, 10, 1251–1290. <https://doi.org/10.1080/08843759208916050>.
- Kargi, F. (1987). Biological oxidation of thianthrene, thioxanthene and dibenzothiophene by the thermophilic organism *Sulfolobus acidocaldarius*. *Biotechnology Letters*, 9. <https://doi.org/10.1007/BF01027456>.
- Kargi, F., & Robinson, J. M. (1985). Biological removal of pyritic sulfur from coal by the thermophilic organism *Sulfolobus acidocaldarius*. *Biotechnology and Bioengineering*, 27. <https://doi.org/10.1002/bit.260270107>.
- Kargi, F., & Robinson, J. M. (1986). Removal of organic Sulphur from bituminous coal. Use of the thermophilic organism *Sulfolobus acidocaldarius*. *Fuel*, 65. [https://doi.org/10.1016/0016-2361\(86\)90302-9](https://doi.org/10.1016/0016-2361(86)90302-9).
- Kasmiarno, L. D., & Chang, J. S. (2020). Adsorption of gold from aqueous systems using microbial thermophilic proteins. *Journal of Engineering Technology Science*, 52. <https://doi.org/10.5614/j.eng.technol.sci.2020.52.1.9>.
- Keller, L., & Murr, L. E. (1982). Acid-bacterial and ferric sulfate leaching of pyrite single crystals. *Biotechnology and Bioengineering*, 24. <https://doi.org/10.1002/bit.260240108>.
- Kilbane, J. J. (1989). Desulfurization of coal: The microbial solution. *Trends in Biotechnology*, 7.
- Kilbane, J. J. (2017). Microbial removal of organic sulfur from coal: Current status and research needs. In: *Bioprocessing and Biotreatment of Coal*.
- Kirimura, K., Furuya, T., Sato, R., et al. (2002). Biotransformation of naphthothiophene and benzothiophene through selective cleavage of carbon-sulfur bonds by *Rhodococcus* sp. strain WU-K2R. *Applied and Environmental Microbiology*, 68. <https://doi.org/10.1128/AEM.68.8.3867-3872.2002>.
- Kodama, K., Umehara, K., Shimizu, K., et al. (1973). Identification of microbial products from dibenzothiophene and its proposed oxidation pathway. *Agricultural and Biological Chemistry*, 37. <https://doi.org/10.1080/00021369.1973.10860640>.
- Koizumi, J. (1994). Genetically engineered microorganisms exploitation for biocleaning of coal: A countermeasure to acid rain. *Fuel Energy Abstr* 36. [https://doi.org/10.1016/0140-6701\(95\)95322-1](https://doi.org/10.1016/0140-6701(95)95322-1).
- Konishi, J., Ishii, Y., Onaka, T., et al. (1997). Thermophilic carbon-sulfur-bond-targeted biodesulfurization. *Applied and Environmental Microbiology*, 63. <https://doi.org/10.1128/aem.63.8.3164-3169.1997>.
- Konishi, Y., Asai, S., & Katoh, H. (1990). Bacterial dissolution of pyrite by *Thiobacillus ferrooxidans*. *Bioprocess Engineering*, 5. <https://doi.org/10.1007/BF00376230>.
- Laborde, A. L., & Gibson, D. T. (1977). Metabolism of dibenzothiophene by a *Beijerinckia* species. *Applied and Environmental Microbiology*, 34. <https://doi.org/10.1128/aem.34.6.783-790.1977>.
- Larsson, L., Olsson, G., Holst, O., & Karlsson, H. T. (1990). Pyrite oxidation by thermophilic archaeobacteria. *Applied and Environmental Microbiology*, 56. <https://doi.org/10.1128/aem.56.3.697-701.1990>.
- Leonard, W. G., Greer, R. T., Markuszewski, R., & Wheelock, T. D. (1981). Coal desulfurization and Deashing by oil agglomeration. *Separation Science and Technology*, 16. <https://doi.org/10.1080/01496398108058317>.
- Li, F. L., Xu, P., Ma, C. Q., et al. (2003). Deep desulfurization of hydrodesulfurization-treated diesel oil by a facultative thermophilic bacterium *Mycobacterium* sp. X7B. *FEMS Microbiology Letters*, 223. [https://doi.org/10.1016/S0378-1097\(03\)00397-5](https://doi.org/10.1016/S0378-1097(03)00397-5).
- Li, W., & Cho, E. H. (2005). Coal desulfurization with sodium hypochlorite. *Energy and Fuels*, 19. <https://doi.org/10.1021/ef0400767>.

- Lovás M, Znamenáčková I, Zubrik A, et al. (2011). The application of microwave energy in mineral processing – a review. *Acta Montan. Slovaca* 16.
- Malik, A., Dastidar, M. G., & Roychoudhury, P. K. (2000). Biodesulphurization of coal: Rate enhancement by Sulphur-grown cells. *Biotechnology Letters*, 22. <https://doi.org/10.1023/A:1005603021710>.
- Martínez, O., Aller, A., Alonso, J., et al. (1995). Biodesulphurization of coals from the north of león (Spain). Optimization of process variables. *Coal Science Technology*, 24. [https://doi.org/10.1016/S0167-9449\(06\)80153-9](https://doi.org/10.1016/S0167-9449(06)80153-9).
- Meyers, R. A., Van Nice, L. J., & Santy, M. J. (1979). *Coal desulfurization* (p. 51). New York, NY: Combust.
- Olson, G. J., & Brinckman, F. E. (1986). Bioprocessing of coal. *Fuel*, 65.
- Olsson, G., Pott, B. M., Larsson, L., et al. (1995). Microbial desulfurization of coal and oxidation of pure pyrite by *Thiobacillus ferrooxidans* and *Acidianus brierleyi*. *Journal of Industrial Microbiology*, 14. <https://doi.org/10.1007/BF01569961>.
- Pan, J., Zhou, C., Tang, M., et al. (2019). Study on the modes of occurrence of rare earth elements in coal fly ash by statistics and a sequential chemical extraction procedure. *Fuel*, 237. <https://doi.org/10.1016/j.fuel.2018.09.139>.
- Patterson, E. C., Le, H. V., Ho, T. K., & Wheelock, T. D. (1979). Better separation by froth flotation and oil agglomeration. *Coal Process Technology*, 5.
- Patzek, T. W., & Croft, G. D. (2010). A global coal production forecast with multi-Hubbert cycle analysis. *Energy*, 35, 3109–3122. <https://doi.org/10.1016/j.energy.2010.02.009>.
- Quackenbush, V. C., Maddocks, R. R., & Higginson, G. W. (1979). Chemical communication: An improved route to clean coal. *Coal Min Process*, 16.
- Rai, C., Reyniers, J. P. (1988). Microbial desulfurization of coals by organisms of the genus *Pseudomonas*. *Biotechnol Prog* 4. <https://doi.org/10.1002/btpr.5420040406>.
- Rajendran, A., Cui, T. Y., Fan, H. X., et al. (2020). A comprehensive review on oxidative desulfurization catalysts targeting clean energy and environment. *Journal of Materials Chemistry A*, 8, 2246–2285. <https://doi.org/10.1039/c9ta12555h>.
- Rhee, S. K., Chang, J. H., Chang, Y. K., & Chang, H. N. (1998). Desulfurization of dibenzothiophene and diesel oils by a newly isolated Gordona strain, CYKS1. *Applied Environment Microbiology*, 64. <https://doi.org/10.1128/aem.64.6.2327-2331.1998>.
- Rohwerder, T., Sand, W. (2007). Mechanisms and biochemical fundamentals of bacterial metal sulfide oxidation. In: *Microbial Processing of Metal Sulfides*.
- Rossi, G. (1999). The design of bioreactors. *Process Metallurgy*, 9. [https://doi.org/10.1016/S1572-4409\(99\)80006-6](https://doi.org/10.1016/S1572-4409(99)80006-6).
- Rossi, G. (2014). The microbial desulfurization of coal. *Advances in Biochemical Engineering/Biotechnology*, 142. https://doi.org/10.1007/10_2013_178.
- Silverman, M. P., Rogoff, M. H., & Wender, I. (1961). Bacterial oxidation of pyritic materials in coal. *Applied Microbiology*, 9. <https://doi.org/10.1128/aem.9.6.491-496.1961>.
- Steel, K. M., & Patrick, J. W. (2001). The production of ultra clean coal by chemical demineralisation. *Fuel*, 80. [https://doi.org/10.1016/S0016-2361\(01\)00092-8](https://doi.org/10.1016/S0016-2361(01)00092-8).
- Wise, Kilbane, J. J. (2018). Microbial removal of organic sulfur from coal: Current status and research needs. In: *Bioprocessing and Biotreatment of Coal*.
- Woese, C. R., Kandler, O., & Wheelis, M. L. (1990). Towards a natural system of organisms: Proposal for the domains archaea, bacteria, and eucarya. *Proceedings of the National Academy of Sciences of the United States of America*, 87. <https://doi.org/10.1073/pnas.87.12.4576>.
- Wynter, C. I., May, L., Oliver, F. W., et al. (2004). Correlation of coal calorific value and Sulphur content with ⁵⁷Fe Mössbauer spectral absorption. *Hyperfine Interactions*, 153, 147–152. <https://doi.org/10.1023/B:HYPE.0000024719.48753.af>.
- Xuehui, M., Jinming, H. (2009). Coal, oil shale, natural bitumen, heavy oil and peat. In: *Coal, Oil Shale, Natural Bitumen, Heavy Oil and Peat*.

Chapter 8

Environmental Benign Biochar Technologies: Strategic Utilization for CO₂ Capture and Wastewater Treatment



Mohd Danish Khan and Ji Whan Ahn

8.1 Introduction

For a sustainable world, the implementation and execution of sustainable technologies are essential. Therefore, valorization of wastes originating from domestic, industrial, and agriculture can play a critical role in accomplishing sustainable goals (Khan et al. 2020). Agricultural, forest or any flora related organic wastes can be considered as biomass. For instance, the waste related to crop, forest, algae, organic municipal solid waste, sewage sludge, and manures can be included in biomass waste (Demirbas 2001). Globally, an estimated 12 billion tonnes of dried biomass waste are generated annually which highlights the presence of enormous amount of biomass waste (Pandey et al. 2015). Common applications of this waste biomass include animal feeding, as fuel, and production of biochar.

Biomass mainly contains hemicellulose, cellulose, and lignin in different proportions depending on the biomass type (Hao et al. 2014). The carbonaceous biochar can be obtained by applying thermal treatment on biomass waste in restricted or no oxygen. The yield of biochar greatly depends on the lignin concentration in respective biomass waste as lignin is the main source of carbon (Pandey et al. 2015). Major thermal treatments for the conversion of biomass into biochar include pyrolysis, microwave heating, hydrothermal carbonization, dry torrefaction, and gasification (Kambo and Dutta 2015; Liu et al. 2015). Each method differs in terms of temperature, oxygen content, duration, and therefore quality of produced biochar. The produced biochar offers two main advantages, i.e., the production process

M. D. Khan · J. W. Ahn (✉)

Resources Recycling Department, University of Science and Technology (UST),
Daejeon, Republic of Korea

Center for Carbon Mineralization, Mineral Resources Research Division, Korea Institute of
Geosciences and Mineral Resources (KIGAM), Daejeon, Republic of Korea
e-mail: ahnjw@kigam.re.kr

prevents the carbon dioxide emission by its conversion into stable form (carbon), restricting the greenhouse gas emission during biomass degradation (Creamer and Gao 2016). Secondly, biochar is an asset as adsorbent, providing environment friendly, low cost, and extraordinary performance in wastewater treatment (Inyang et al. 2015). The enhanced adsorption characteristics are the synergistic effect of large surface area and availability of ample functional groups. However, these physicochemical properties significantly depend on thermochemical decomposition technique, duration, production temperature, and feedstock pre/post treatments (Zhang et al. 2017a). These parameters are regulated depending on the type of feedstock and required applications. The pretreatment process includes physical (grinding, sieving, washing, drying), chemical (acid, alkali, or functional materials), and biological (treatment with bacteria) techniques (Son et al. 2018; Zhang et al. 2017a; Yao et al. 2015). Whereas the posttreatment includes physical (milling, carbon dioxide treatment, magnetization, etc.) and chemical (acid/alkali treatment) techniques (Cha et al. 2016; Tan et al. 2016; Dai et al. 2017). The biochar can be effectively used for the adsorption of heavy metals, anions, and organic pollutants in a wide range of concentration. Other applications include alternative of fuel particularly coal, catalyst/catalyst support, enhancing soil fertility, and adsorbent of air pollutant. Therefore, biochar can be considered as a potential solution for major global issues such as air/water pollution, climate change, and soil degradation (Creamer and Gao 2016).

Combustible natural resources, fuels, cement, and other chemical products are the major sources of environmental concern particularly global warming. Among all gases, CO₂ has been considered critical and required urgent mitigation as suggested by United Nations Framework Convention on Climate change and Intergovernmental Panel on Climate Change (IPCC). The major mitigation options provided by IPCC include renewable energy, nuclear power, CO₂ capture, sequestration, and mineralization. However, due to intensive cost involved, a renewable, efficient, and economic CO₂ sorptive materials are desired (Ello et al. 2013). Researchers globally are focussing on biochar performance against CO₂ sorption (Coromina et al. 2016; Deng et al. 2014). The carbon-rich biochar can probably last millennia and therefore can provide a strategic option for CO₂ sequestration. Numerous studies are evident of CO₂ sorption on biochar surface and therefore biochar amendment in soil can also be a promising option.

Continuous anthropogenic activities resulted in surface and underground water pollution causing severe environmental issues such as eutrophication, agitated pH, and metallic poisoning making water unfit for aquatic ecosystem (Khan et al. 2020; Wang et al. 2015c). Major point sources of water pollution include domestic, industrial, and agricultural sectors which leads to the introduction of heavy metals, organic, and anionic contaminants into surface waters. It has been estimated that on an annual basis, > 10 million tons of chemicals are discharged in water environments with the detection of almost >700 chemical compounds (Ali and Gupta 2006). Heavy metal ions such as Pb²⁺, As³⁺, As⁵⁺, Cd²⁺, and Cu²⁺ are toxic and responsible for severe health and environmental issues owing to their high solubility in aqueous medium (Dong et al. 2017; Wang et al. 2015c; Zhou et al. 2017).

Secondly, anions are required for aquatic life sustenance; however, beyond threshold limit they can cause severe damage to aquatic ecosystem and humans. Even a low concentration of anionic contaminants such as NO₃⁻, F⁻, PO₄³⁻, and ClO⁻ can illustrate adverse impacts, whereas contaminants such as CN⁻ and AsO₃³⁻/AsO₄³⁻ are toxic and hold the potential to trigger catastrophe (Bhatnagar et al. 2008; Hamadi et al. 2001; Wang et al. 2015c). Conventional removal techniques are generally expensive, possess high operation cost, generate secondary pollutant and toxic sludge, and often resulted in limited performance against lower, yet hazardous heavy metal and anionic contaminant concentrations in wastewater. Biochar derived from waste biomass can reduce the associated cost and environmental issues compared to conventional methods. While adsorption in aqueous medium, a highly porous biochar with excessive surface to mass/volume ratio and binding functional groups greatly enhance its performance (Wang et al. 2015d; Yao et al. 2014; Zhu et al. 2018). However, biochar has few drawbacks in terms of recycling, required cost intensive reagents, and sophisticated instruments.

In presented chapter, an overview of various biomass feedstocks, pre- and post-treatment methods, biochar production techniques, and performance against adsorption of metallic and anionic contaminants are presented. The adsorption mechanism of contaminants on biochar surface has been discussed. This critical chapter also focusses on the future research directions and perspectives of the biochar in the application of wastewater treatment.

8.2 Biomass Feedstocks

Among the three main component of biomass, lignocellulosic biomass (lignin and cellulose dominant) are preferred precursors for thermochemical conversion to biochar, with forestry and agricultural sectors being its primary sources (Collard and Blin 2014). The biomass feedstock accommodates various plant polymers, particularly hemicellulose, cellulose, and lignin. The highly complex characteristics of these plant macromolecules are responsible for the quality of biochar and other chemical products post thermochemical conversion (Channiwala and Parikh 2002; Parikh et al. 2005). In present study, the focus has been made on forestry (woody) and agricultural (herbaceous) biomass due to its wide availability and lignocellulosic content in biomass. The proximate and ultimate analysis of forestry and agricultural biomass feedstocks are depicted in Table 8.1.

The major point sources of waste woody biomass are forestry and pulp and paper industries. These biomass are dominant in lignin content which is a complex 3-D structure responsible for binding plant materials into compact fibers, transferring high strength to woody biomass structure (Hao et al. 2014). The thermochemical conversions not only provide biochar with enhanced physicochemical characteristics but also produce valuable bio-oil (depending on the type of thermochemical technique used) (Kambo and Dutta 2015; Liu et al. 2015). Another advantage of woody biomass is that it contains higher organic content which on thermal treatment

Table 8.1 The proximate and ultimate analysis of forestry and agricultural biomass feedstocks

Biomass	Proximate Analysis (Dry wt. %)			Ultimate Analysis (Dry wt. %)			References
	VM ^a	FC ^b	Ash	C	H	O	
<i>Forestry and hardwood biomass</i>							
Spruce wood	29.25	69.33	1.41	51.88	6.12	40.89	Demirbas (1997)
Beech wood	24.59	74.04	1.36	49.55	6.15	41.22	Demirbas (1997)
Bamboo wood	11.26	86.78	1.96	48.74	6.35	42.75	Channiwala and Parikh (2002)
Chaparral wood	18.57	75.20	6.22	46.94	5.11	40.09	Channiwala and Parikh (2002)
Wood chips	23.48	76.38	0.13	48.09	6.01	45.76	Parikh et al. (2005)
Neem wood	12.21	85.90	1.88	48.29	6.25	43.45	Channiwala and Parikh (2002)
Wood bark	31.78	66.57	1.64	53.08	6.09	40.63	Demirbas (1997)
Red wood	19.95	79.69	0.35	50.58	6.02	42.90	Parikh et al. (2005)
Ailanthus wood	24.77	73.52	1.71	49.53	6.17	40.98	Demirbas (1997)
Mulberry stick	22.72	75.05	2.22	44.19	6.63	46.27	Parikh et al. (2005)
Subabul wood	18.49	80.99	0.51	48.14	5.90	44.73	Channiwala and Parikh (2002)
<i>Agricultural biomass</i>							
Olive husk	26.04	70.24	3.71	49.94	6.24	42.22	Demirbas (1997)
Groundnut shell	21.57	72.66	5.76	48.61	5.61	39.51	Parikh et al. (2007)
Peanut hull	21.10	72.98	5.92	45.76	5.45	39.58	Parikh et al. (2007)
Rice husk	17.01	61.78	21.20	38.49	5.18	34.64	Channiwala and Parikh (2002)
Coconut shell	22.07	77.21	0.72	50.18	5.67	43.40	Channiwala and Parikh (2002)
Pistachio shell	16.90	81.97	1.12	48.83	5.89	43.40	Parikh et al. (2005)
Sal seed husk	27.99	62.61	9.40	48.10	6.51	35.95	Parikh et al. (2005)
Hazelnut shell	28.26	69.25	2.49	52.87	5.59	42.74	Demirbas (1997)
Walnut Shell	18.80	80.00	1.20	49.84	5.62	42.96	Channiwala and Parikh (2002)
Brazil nut shell	22.16	76.09	1.75	49.17	5.69	42.79	Parikh et al. (2007)

^aVolatile Matter^bFixed Carbon

like pyrolysis (as it valorize the organic content at ~500 °C) resulted in a development of complex pore network (Aller 2016). A recent study also reported that the resulting biochar pH is strongly dependent on pyrolysis temperature, i.e., higher the temperature, higher will be the biochar pH. It was suggested that the resulting pH rise is associated with the loss of acidic groups particularly alcohol and carboxyl functional groups along with enhancement of alkaline minerals (Zhang et al. 2017b).

8.3 Pretreatment Processes

Biomass feedstocks comprise varying physicochemical properties and thereby required appropriate pretreatment process prior to biochar production. Generally, pretreatment processes can be characterized into three major categories, i.e., physical, chemical, and biological pretreatment processes (Son et al. 2018; Zhang et al. 2017a; Yao et al. 2015).

The physical pretreatment methods broadly consist of crushing, washing, drying, and sieving of biomass feedstock. Generally, biomass feedstock with higher lignocellulosic content is dried at 105 °C until the weight reaches constancy followed by crushing into finer particles (Wang et al. 2016; Zhang et al. 2017a). In special cases particularly with plant feedstock possessing larger range of moisture content, step-wise drying is required. For instance, physical pretreatment of organic sludge includes initial dewatering with subsequent overnight drying in an oven, crushing, sieving, and finally storage in sealed containers (Agrafioti et al. 2013). Moreover, biomass feedstock based on their physicochemical properties sometimes required additional modifications. For instance, waste cardboards and newspapers are shredded, and feedstock is prepared after mixing with pulp (Randolph et al. 2017). The paper mill sludge generally has high content of minerals and therefore required acid-washing followed by rinsing with deionized water (Cho et al. 2017).

Chemical pretreatment methods include chemical reactions to modify and enhance the characteristics of biomass feedstock. The main reason behind chemical pretreatment is to induce functional agents and chemical precursors into biochar which may assist specific type of application. The treatment follows immersion of biomass feedstock into colloidal suspensions or specific chemical solutions, washing, and drying prior to biochar production (Tan et al. 2016). For instance, numerous biochar-based metal oxyhydroxide (i.e., MgO, Fe₃O₄, and AlOOH) rich nanocomposites can be synthesized through treatment of biomass with metal ion (MgCl₂, FeCl₃, and AlCl₃) solutions (Zhang et al. 2013; Son et al. 2018). Moreover, biomass can also be modified by induced engineered designed nanoparticles such as nanotubes, clay, and graphene which also resulted in production of nanocomposites (Inyang et al. 2015). To provide biomass/biochar with larger surface area and micro-pore volume, biomass often get treated with corrosive chemicals such as alkali, acids, and oxidants (Zhao et al. 2018).

Biological pretreatment is currently at emerging stage in the field of engineered biochar production, depending on biological processes such as bacterial treatment, biofuel processes, and anaerobic digestion. This treatment is relatively slow but has been proven to compel an efficient biologically activated biochar (Yao et al. 2015). It is evident from the literature that numerous biomass such as bagasse, sludge, and sugar beet were pretreated with anaerobic digestion prior to biochar production and resulted in improved physicochemical characteristics (Yao et al. 2011; Tang et al. 2019). It has been reported that anaerobic digestion enhances the adsorption performance and also improves surface area of resulted biochar (Yao et al. 2011). Other benefits of biological pretreatment include reduction in solid waste, economic

disposal, and eco-friendly bioenergy (Yao et al. 2015). Another example of biological pretreatment includes the conversion of biomass enriched with high content of heavy metals to biochar through bioaccumulation (Wang et al. 2017b). A recent study concluded that the conversion of heavy metal hyperaccumulating biomass into respective biochar through bioaccumulation can simultaneously provide two benefits, i.e., eco-friendly hyperaccumulator disposal and valorized biochar nanocomposites (Wang et al. 2017b).

8.4 Biochar Production Processes

Biochar production can be carried out through thermochemical processes such as pyrolysis, hydrothermal carbonization, dry torrefaction, and gasification. However, proper thermochemical process and appropriate operating conditions (i.e., pressure, temperature, moisture, reaction medium, residence time, and heating rate) are essential for obtaining a good quality biochar (Kambo and Dutta 2015; Liu et al. 2015). Table 8.2 provides the ranges of operating conditions and possible yields of biochar for different thermochemical processes.

Among aforementioned thermochemical processes, gasification and dry torrefaction processes are not appropriate for biochar production. A gasification process mainly includes a partial and rapid (10–20 s of residence time) combustion of biomass at relatively higher temperature range of 600–1200 °C. The main objective of gasification is to produce gaseous products from biomass feedstock such producer gas, syngas, H₂, and CO₂. Thus, gasification is not an ideal process to produce biochar; however biochar with very low yield (~ 10 wt.%) is produced (Brewer et al. 2009). The biomass contains inorganics and thus converted to oxide forms on high temperature combustion, also polycyclic aromatic hydrocarbons (PAHs) are produced as by-product from gasification process. Hence, metal oxides and PAHs in biochar are considered toxic and problematic for environmental remediation. Also, IBI firmly recommended a minimum accumulation of toxicants and air-pollutants in the produced biochar (IBI 2013).

Table 8.2 Ranges of operating conditions and possible yields of biochar for different thermochemical processes (Kambo and Dutta 2015; Liu et al. 2015)

Thermochemical process	Residence time	Heating rate (°C min ⁻¹)	Temperature (°C)	Pressure (Atm)	Yield (%)
Hydrothermal carbonization	10 min–12 h	5–15	180–260	12–25	40–70
Pyrolysis (flash)	<5 s	>800	400–1000	1	10–25
Pyrolysis (fast)	1–10 s	400–800	400–600	1	15–40
Pyrolysis (slow)	1–4 h	5–10	300–800	1	35–50
Gasification	10–60 s	50–100	600–1200	1	<10
Dry torrefaction	0.5–4 h	10–15	200–300	1	50–80

Dry torrefaction on the other hand is a thermochemical process that operates at moderate temperature (200–300 °C) and atmospheric pressure with a residence time ranges between 30 min and few hours (Bach and Tran 2015). Dry torrefaction generally increases the energy density by small portion (~10%) with the release of small fraction of volatile matter and considerable portion still resides in torrefied biochar. Therefore, this process is preferred as a pretreatment of biomass and mostly used in combustion related applications. Also, the physicochemical characteristics of torrefied biochar are in midst of biomass and biochar. Thus, technically torrefied biochar is not generally considered as biochar; however numerous literature argue over the physicochemical characteristics of biochar and torrefied biochar. Hence, the present work mainly focusses on pyrolysis and hydrothermal carbonization processes. Table 8.3 presents typical biochar yields and physicochemical characteristics of thermochemical processes.

8.4.1 Pyrolysis

Pyrolysis can be considered as a principal process for the production of biochar. This process mainly involves thermal decomposition of organic matter in biomass at exalted temperatures with constant heating rate and controlled inert medium such as constraint or no oxygen, nitrogen, and carbon dioxide. During pyrolysis, the volatile component of biomass decomposes and released in the form of gases leaving behind carbon dominating biochar as a residual solid. A fraction of volatile matter containing polar and higher molecular weight compounds liquefies (bio-oil) on cooling, whereas non-condensable gases with low molecular weight such as H₂ and CO₂ continue to be in gaseous phase.

On the basis of exalted temperature and heating rate, a pyrolysis process can be broadly categorized as slow, fast, and flash pyrolysis. Slow pyrolysis is usually carried out within a temperature range of 300–800 °C (>1 h) and a constant heating rate of 5–10 °C min⁻¹, providing comparatively higher yield of ~50% (Mohan et al. 2006). Fast pyrolysis is conducted within a temperature range of 400–600 °C (2–10 s) at a constant but rapid heating rate of 300–800 °C min⁻¹. Fast pyrolysis process generally provides high bio-oil yield and a small biochar yield of ~35% (Onay and Kockar 2003). Lastly, flash pyrolysis also dominates bio-oil yield, conducted at a higher temperatures ~1000–1200 °C (1–2 s) with a tremendous heating rate of ~1000 °C, providing very low biochar yield of ~15% (Onay and Kockar 2003).

In general, the pyrolysis products are strongly influenced by operating parameters, reactor conditions, and physicochemical characteristics of biomass feedstock. For instance, in slow pyrolysis with both low operating temperatures and heating rates, yield of solid product (biochar) dominates. In contrast, high operating temperatures, residence time, and heating rates have positive impact on high heating value and fixed carbon content of biochar. Volatile matters, such as C_xH_yO_z, C_xH_y, NH₃, CO₂, and CO, are released from biomass on pyrolysis at lower temperatures and the carbon content in biochar is gradually reduced (Becidan et al. 2007).

Table 8.3 Physicochemical characteristics of biochar synthesized from different thermochemical conversion processes

Biomass	Conversion Technique and operating conditions	SSA ^a (m ² g ⁻¹)	Yield (%)	Ash (%)	pH	Ultimate analysis			Reference
						C	H	N	
Chicken manure	Pyrolysis, 2 h (550 °C)	7.11	77	87.1	9.9	7.50	0.42	0.77	Zhao et al. (2020)
Rice straw	Pyrolysis, 2 h (550 °C)	4.14	33.5	43.0	10.3	45.69	2.11	1.18	Zhao et al. (2020)
Acacia	Pyrolysis, 2 h (~ 400 °C)	1.30	–	3.5	7.6	69.80	4.40	0.62	Arán et al. (2016)
Coconut fiber	Pyrolysis, 3 h (600 °C)	4.51	–	3.70	7.4	–	–	–	Wu et al. (2017a)
Almond shells	Pyrolysis (650 °C)	145	–	–	–	–	–	–	Kilic et al. (2013)
Sewage sludge	Pyrolysis, 2 h (550 °C)	8.17	78.9	68.9	7.6	19.00	1.69	2.91	Zhou et al. (2017)
Wheat straw	Pyrolysis, 5 h (600 °C)	26.2	–	41.0	9.8	51.00	2.41	1.00	Bogusz et al. (2017)
Rice husk	Pyrolysis, 1 h (650 °C)	21.8	34.0	36.1	–	60.28	0.11	0.40	Jian et al. (2018)
Citrus	Pyrolysis (300 °C)	~ 1.0	41.7	8.45	7.8	60.40	4.42	1.40	Wang et al. (2015a)
Anaerobic sludge	Pyrolysis, 2 h (600 °C)	163.0	52.8	–	–	28.10	1.29	9.71	Ni et al. (2019)
Rice husk	HTC, 1 h (260 °C)	3.5	28.0	2.7	–	73.4	5.0	2.8	Jian et al. (2018)
Rice husk	HTC, 20 min (300 °C)	358	80.6	60.0	–	–	–	–	Lju and Zhang (2011)
Sawdust	HTC, 12 h (190 °C)	7.88	–	–	–	60.88	6.01	0.96	Deng et al. (2019)
Banana peel	HTC, 2 h (230 °C)	31.7	15.7	0.55	–	71.40	6.31	0.61	Zhou et al. (2017)
Pinewood sawdust	HTC, 1 h (300 °C)	425	53.9	2.8	–	–	–	–	Lju and Zhang (2011)
Wood chips	Gasification, 1 h (1000 °C)	258	–	0.27	–	–	–	–	Runtti et al. (2014)

^aSpecific Surface Area

However, with higher temperature, the discharge of carbon-dominating compounds such as C_xH_yO_z and C_xH_y starts decreasing without affecting the random discharge of NH₃, CO₂, and CO, resulting in higher carbon content in the residual biochar. Also, higher the discharge of volatile matter, higher will be the pore volume and surface area in resulting biochar.

Apart from operating parameters discussed earlier, moisture content in biomass feedstock is also found to aid the biochar yield; however, it leads to energy intensive process. The lignocellulosic content of biomass also greatly modulates the biochar production. Numerous reports evident that biomass with higher lignin ratio such as pine wood begets or spruce wood resulted in biochar with both higher biochar yield and fixed carbon content (Antal and Grønli 2003). Another important parameter includes the proportion of inorganic compounds particularly containing alkaline earth metals in feedstock. It has been reported that these alkaline earth metals can play a catalytic role during thermochemical decomposition of biomass (Yaman 2004). Pretreatment of biomass feedstock with dilute acid or hot water has also been found to reduce the biochar yield and can be explained as hot water and dilute acid can considerably dissolve the alkaline earth metals from the biochar. Under hydrogen environment, pyrolysis of various biomass feedstocks such as woody, herbaceous, microalgae, and poultry litter showed a reduction in biochar yield and increment in polycyclic aromatic hydrocarbons PAHs with rise in temperature (Mcbeath et al. 2015). Biochar with higher carbon content such as derived from woody biomass possesses low ratio of PAHs and total organic carbon (TOC), whereas biochar derived from low carbon content biomass such as herbaceous biomass possesses high ratio of PAHs and TOC. Additionally, pH and surface area of the produced biochar are mainly influenced by pyrolysis temperature, while ash content, TOC, inorganic content, carbon content are predominantly affected by the group of biomass feedstock (Zhao et al. 2013). Experimental and modelling results in available literature are evident that with proper selection of biomass feedstock and pyrolysis operating conditions, the physicochemical characteristics of produced biochar can be altered suitable for specific applications.

Apart from biochar, pyrolytic products such as syngas (gas) and bio-oil (liquid) are other two important pyrolysis products, contributing to a distribution of almost 25–30% of overall pyrolysis products. All three products of pyrolysis are considered as renewable energies and can be used as fuel or fuel supplements. Therefore, the overall pyrolysis process can be considered as cost-effective and environmentally benign process (Zhang et al. 2010). A recent research examined the modelling and empirical relationship between biochar and bio-oil yield and economic trade-off. Through quadratic polynomial functions, optimum values of pyrolysis temperature for biochar/bio-oil price ratio under different economic conditions were estimated. The biochar or bio-oil yield and related characteristics are decidedly associated with type of biomass feedstock and pyrolysis operating conditions.

8.4.2 *Hydrothermal Carbonization (HTC)*

Hydrothermal carbonization (HTC) is an emerging thermochemical process where biochar is a dominating product. The chemistry involved in biochar formation and the reaction rates are still at infant stages due to limited research. Hydrothermal carbonization, hydrothermal gasification, and hydrothermal liquefaction are the three sub-classification of HTC process. Each process has different dominating final product and therefore used based on the required applications. The major advantages (other than high conversion efficiency) of HTC is that no pre-drying of biomass is required and operates at moderate temperatures (180–260 °C) with autogenous pressure controlled within a reactor for specific residence time (Hoekman et al. 2013).

The HTC process generally operates under subcritical condition where water properties and vapor pressure considerably vary with reaction temperature. The merit of water in subcritical state is that even at temperatures higher than 150 °C, water exist in liquid phase and resembles the characteristics of nonpolar solvent; for instance, at ~200 °C, it behave like methanol, whereas at ~300 °C, it behaves like acetone. With >374 °C, the dielectric constant of water decreases, thereby making the hydrogen bonds of water fragile which leads to higher ionization constant. This turns the water to act like an acid as the alienation of water increases and H₂O molecules start to break, forming H₃O⁺ and OH⁻ ions (Marcus 1999). Unlike normal water, the subcritical water encourages a competently higher H⁺ concentrate which can be considered extremely suitable for organic compound degradation through acid catalyzed reaction, though no acid was added, and therefore possessing a strong tendency to dissolve organic fraction of biomass in subcritical water. The polymeric portion of lignocellulosic biomass comprises low molecular weight compounds, and thereby during subcritical condition, the breakdown tendency of organic compounds particularly with COOH and OH bonds increases drastically and eventually dissolves in water. Additionally, there are reports emphasizing that the polychlorinated biphenyls and polychlorinated dibenzofurans, being a hazardous waste, can be destroyed under sub- and super-critical water (Weber et al. 2002).

HTC is the only thermochemical process suitable for wet biomass or biomass with high moisture content as water is a solvent used in this process. This leads to the elimination of biomass pre-drying step, thereby reducing the overall cost of the process as the pre-drying step is considered time consuming and energy intensive step. HTC process provides 3-phase products, i.e., biochar, bio-oil, and a mixture of gases dominated by CO₂. The distribution of these phases is dependent on operating conditions particularly temperature (Kambo and Dutta 2014). The biochar yield (wt.%) obtained from HTC process generally varies from 40% to 70%. The produced biochar is generally obtained in the form of slurry and thus required dewatering steps which include filtering, mechanical compressing, and drying prior its usage. The mechanical compressing reduces the moisture content to <50% because in the reactions involved in the dehydration and decarboxylation, a considerable fraction of oxygen is removed (Kambo and Dutta 2014). This significantly

suppresses the time and energy required for thermal/ solar drying for achieving further reduction in biochar moisture content making the process economical.

In the biochar producing process through thermochemical process, the rigid polymeric lignin content is reduced to low molecular weight chemical compounds. However, in HTC process, subcritical water initiates the hydrolysis of biomass which is the first step of biomass decomposition. The hydrolysis of biomass resulted in a rapid depolymerization forming water-soluble monomers and oligomers. Lignocellulosic biomass feedstocks generally contain various inorganics such as Na, Ca, Mg, P, S, and Fe which after thermochemical combustion process get converted to their respective oxide forms, i.e., Na₂O, CaO, MgO, P₂O₅, SO₃, and Fe₂O₃ and reside in ash (Tortosa Masia et al. 2007). These inorganic metal oxides are responsible for fouling, corrosion, clinker formation, and slagging. However, in the case of HTC process, acetic acid is formed as a by-product stream and due to acid solvation metals are leached out, thereby curtailing the distribution of ash in produced biochar (Liu and Balasubramanian 2014). Moreover, with chlorine-rich biomass feedstock, HTC process converts chlorine from organic to inorganic form and thus restrains the formation of corrosive and dioxins that are hazardous for the aquatic environment (Zhao et al. 2014).

The HTC process is a water intensive process and a continuous supply of massive amount of water for industrial HTC is a major challenge for a full-scale operation and also is economically nonviable. A recent study found that for the HTC conversion (at 260 °C) of miscanthus into 1 ton of biochar with ~50 wt. % yield, 12 tons of water is required. Therefore, for industrial HTC process, water recirculation and heat recovery is critical which will indirectly reduce both the amount and cost involved in wastewater treatment and lowers the expenditure for external heat (Stemann et al. 2013).

8.5 Posttreatment Processes

For the enhancement of physicochemical characteristics of produced biochar suited for diverse applications, required posttreatments are often carried out. Posttreatments generally modify the surface chemistry, pore volume, surface area, composited nanoparticles, and functional groups on produced biochar (Tan et al. 2016; Dai et al. 2017). Presented chapter briefly overviews the commonly applied posttreatments such as chemical, magnetization, and mechanical treatment.

Chemical or corrosive posttreatments of biochar generally include alkali, acid, and advanced oxidation for the alteration and modification in surface chemistry. The most commonly used chemicals are KOH, KMnO₄, NaOH, HNO₃, HCl, and H₂O₂ (Cha et al. 2016; Wang et al. 2017a). The main objectives of chemical treatment are to induce higher specific surface area, micropore volume, functional groups, and composites to improve the sorption capacity. Also, an integrated chemical treatment is also evident of providing superior physicochemical properties. For instance, an integrated NaOH(alkali)-HNO₃(acid) posttreatment on municipal sewage sludge

biochar resulted in induction of considerable oxygen-rich functional groups, generates porosity and thereby enhances the specific surface area of biochar, which significantly raises the adsorption capacity of tetracycline over 286 mg g^{-1} (Tang et al. 2018). KOH and KMnO_4 treatment on peanut-derived biochar increase the surface area and active sites and thereby significantly enhance the adsorption of Ni^{2+} in aqueous medium (An et al. 2019). An example of potential oxidant is H_2O_2 , a recent study provided evidence of generated oxygen and carboxyl groups on H_2O_2 -treated manure-based biochar surface, illustrating exceptional heavy metal adsorption capacity (Wang and Liu 2018).

Magnetization is a posttreatment process mainly employed to induce magnetic characteristics in treated biochar. The iron oxides such as CoFe_2O_4 , $\gamma\text{-Fe}_2\text{O}_3$, and Fe_2O_3 are generally used to load Fe content into biochar (Tan et al. 2016). An important advantage of magnetic modified biochar is that a magnetic separator can be used to isolate biochar from the aqueous solution (Son et al. 2018). A peanut hull-derived biochar has developed considerable adsorption rate for Cr^{6+} post treating with magnetic zero-valent iron (at 800°C), manifesting with higher surface area and loaded reductive iron (Liu et al. 2019a). The magnetic characteristics in biochar can also be introduced through Fe-based composites synthesized by direct coprecipitation of $\text{Fe}^{2+}/\text{Fe}^{3+}$ on the surface of the biochar. For instance, the switchgrass-derived Fe-based biochar composite prepared by treating with an aqueous solution of $\text{Fe}^{2+}/\text{Fe}^{3+}$ recorded the highest metribuzin adsorption capacity of 205 mg g^{-1} (Essandoh et al. 2017).

Mechanical posttreatment processes are often used to obtain a required particle size suitable for the adsorption-related applications. Mechanical posttreatment generally includes crushing or grinding followed by sieving. Ball milling is a most common mechanical posttreatment process owing to its simple operation and efficient performance. It utilizes the kinetic energy obtained from heavy metallic balls to crush/grind biochar, thereby breaking the chemical bonds and can reduce the particle size even up to nanoscales (Lyu et al. 2017). The physicochemical characteristics of biochar such as negative zeta potential, pore volume, surface area, and oxygen-rich functional groups greatly modify post ball milling (Wang et al. 2017a; Lyu et al. 2018). For instance, when compared with pristine bagasse biochar, ball milled biochar illustrates much higher adsorption capacities for both Ni^{2+} and aqueous methylene (Lyu et al. 2018). The superior performance can be the resultant effect of higher surface area due to induced cracks, uncover graphitic structure, and oxygen-rich functional groups. A recent study successfully developed nitrogen-doped biochar by simultaneous ball milling of ammonium hydroxide and pristine biochar. The nitrogen-doped biochar resulted in providing enhanced adsorption capacities against anionic reactive red and acidic carbon dioxide (Xu et al. 2019). Mechanical posttreatment therefore not only reduces the size of the particle but is also capable of elemental doping.

Although posttreatments feature numerous advantages, a wider range of research to extract maximum benefits still needs to be explored. For instance, recent research provides the possibilities for posttreatment of biochar by organic solvents. A biochar derived from municipal solid waste through methanol provides an esterification

between biochar and carbonyl groups, culminated with considerable enhancement in adsorption performance of tetracycline (Jing et al. 2014). Despite its significant performance, organic solvents are still not commercially used because of its volatile nature and high cost.

8.6 Biochar as an Adsorbent

8.6.1 CO₂ Capture

The conventional physical activation of thermochemically synthesized biochar not only exhibits improved structural properties but can also significantly adsorb CO₂. For instance, a study reported that biochar synthesized via pyrolysis of biomass (vine shoots) at 600 °C followed by physical activation in CO₂ medium for 3 h at 800 °C exhibited an improved surface area of 765 m² g⁻¹ where the surface area of unmodified biochar was 1.91 m² g⁻¹ (Manya et al. 2018). The more economic procedure can be the employment of single-step pyrolysis followed by physical activation as it will make the process less time consuming and hence consumes less energy. Another study performed an optimized work and reported the effect of activation time, temperature, and O₂:N₂ ratio on biochar synthesized from almond shells and olive stones under CO₂ environment (Gonzalez et al. 2013). It was observed that a cumulative CO₂ intake during both processes was 3.1 mmol g⁻¹. Chemical activation however shows greater tendency of CO₂ adsorption than physical activation. A study reported the synthesis of biochar derived from Africa palm shells via pyrolysis for 1 h at 600 °C in N₂ medium having a surface area of 365 m² g⁻¹. The synthesized biochar was then chemically activated by KOH with a ratio of 3:1 (dry biomass wt. %) heated for 1 h at 860 °C providing a surface area of 1250 m² g⁻¹. The improved surface area was the resultant effect of increased pore generation and nano- and micropore volume (Ello et al. 2013). In addition, the maximum CO₂ adsorption capacity increased from 1.9 mmol g⁻¹ (biochar) to 4.4 mmol⁻¹ (chemically activated biochar) at 25 °C and atmospheric pressure. Similar trend were observed with other biochar such as wheat flour, rice husk, vine shoots, camellia japonica, and pine nut shells with CO₂ adsorption capacities of 3.48, 3.71, 2.46, 5.0, and 5.0 mmol g⁻¹, respectively (Li et al. 2015; Hong et al. 2016; Coromina et al. 2016; Deng et al. 2014). This range of CO₂ adsorption falls in the range provide by other porous CO₂ adsorbent such as metal organic frameworks at ambient conditions (Oschatz and Antonietti 2018). Structural characteristics and CO₂ adsorption performance of thermochemically derived biochar is depicted in Table 8.4.

Considering the kinetic diameters of gaseous molecules post combustion (CH₄: 0.380, O₂: 0.346 nm, CO₂: 0.330 nm, N₂: 0.364 nm), selective CO₂ adsorption can be a serious challenge. Besides, elevated temperature is another factor which can reduce the CO₂ adsorption capacity due to high kinetic energy of gaseous molecules (Lahijani et al. 2018). Therefore, the interactions of CO₂ with biochar surface should

Table 8.4 Structural characteristics and CO₂ adsorption performance of thermochemically derived biochar

Biomass		Thermochemical conversion	Modification	Structural characteristics of biochar		Adsorption capacity (mmol g ⁻¹) at 25 °C			Reference
				SSA ^a (m ² g ⁻¹)	Pore volume (cm ³ g ⁻¹)	0.15 (bar)	1.0	20	
Mesquite wood	Hydrochar, 450 °C, 2 h	KOH exposure (5:1); heating (N ₂), 800 °C, 45 min	3162	1.63	–	6.5	–	Li et al. (2016)	
Jujun grass	Hydrochar, 250 °C, 2 h	KOH exposure (4:1); heating (N ₂), 700 °C, 1 h	3140	1.51	0.9	3.9	12.5	Coromina et al. (2016)	
Coconut shells	Pyrolysis (N ₂), 500 °C, 2 h	KOH exposure (3:1); heating (N ₂), 800 °C, 45 min	1169	0.45	1.43	4.21	–	Yang et al. (2017)	
Camellia Japonica	Hydrochar, 250 °C, 2 h	KOH exposure (2:1); heating (N ₂), 700 °C, 1 h	1350	0.56	1.43	5.1	14.0	Coromina et al. (2016)	
Pine nut shell	Pyrolysis, 500 °C, 1.5 h	KOH exposure (2:1); heating (N ₂), 700 °C, 1.5 h	1490	0.65	2.1	4.9	–	Deng et al. (2014)	
Jujun grass	Hydrochar, 250 °C, 2 h	KOH exposure (2:1); heating (N ₂), 700 °C, 1 h	1510	0.75	1.5	4.9	12.8	Coromina et al. (2016)	
Camellia japonica	Hydrochar, 250 °C, 2 h	KOH exposure (4:1); heating (N ₂), 800 °C, 1 h	3536	1.83	0.67	2.8	25.8	Coromina et al. (2016)	
<i>Adsorption capacity (mmol g⁻¹) at 0 °C</i>									
Vine shoots	Pyrolysis (N ₂), 600 °C, 1 h	KOH exposure (5:1); heating (N ₂), 700 °C, 1 h	1440	0.68	2.28	6.1	–	Manya et al. (2018)	
Arundo donax	Pyrolysis (single step)	KOH exposure (2:1); heating (N ₂), 600 °C, 2 h	1120	0.60	–	6.2	–	Singh et al. (2017)	
Vine shoots	Pyrolysis (N ₂), 600 °C, 1 h	KOH exposure (2:1); heating (N ₂), 600 °C, 1 h	1302	0.55	2.2	6.0	–	Manya et al. (2018)	
Pine nut shell	Pyrolysis, 500 °C, 1.5 h	KOH exposure (2:1); heating (N ₂), 700 °C, 1.5 h	1489	0.65	3.2	7.6	–	Deng et al. (2014)	

Vine shoots	Pyrolysis (N ₂), 600 °C, 1 h	Activation (CO ₂), 800 °C, 3 h	766	0.4	1.9	4.1	–	Manya et al. (2018)
				0 °C	25 °C	100 °C		
Almond shells	Pyrolysis (single step)	Activation (CO ₂), 750 °C, 4 h	860	0.35	–	2.6	0.9	Gonzalez et al. (2013)
Rice husk	Pyrolysis (N ₂), 520 °C, 20 min	KOH exposure (3:1); heating (N ₂), 780 °C, 1 h	2698	1.12	6.25	3.7	–	Li et al. (2015)
Africa palm shell	Pyrolysis (N ₂), 600 °C, 1 h	KOH exposure (3:1); heating (N ₂), 850 °C, 1 h	1249	0.6	6.1	4.3	–	Ello et al. (2013)
Wheat flour	Pyrolysis (N ₂), 900 °C, 2 h	KOH exposure (3:1); heating (N ₂), 700 °C, 1 h	1440	0.66	5.67	3.5	1.1	Hong et al. (2016)
Olive stones	Pyrolysis (single step)	Activation (CO ₂), 800 °C, 6 h	1211	0.50	–	3.0	0.8	Gonzalez et al. (2013)

^aSpecific surface area

be selective and strong enough to adsorb CO_2 molecules. As a nonpolar Lewis acid, CO_2 adsorption has been widely studied through surface functionalization which is found to improve alkalinity and hydrophobicity of biochar surface (Oschatz and Antonietti 2018; Rashidi and Yusup 2016; Choi et al. 2009). For the enhancement of CO_2 adsorption on biochar surface, surface functionalization generally includes heteroatom doping, metal and metal oxide impregnation, and N_2 -based thermal treatment. For instance, a study reported an amine functional group doping on black locust-derived biochar surface (Zhang et al. 2016). Biochar was synthesized via pyrolysis followed by KOH-based chemical activation providing large surface area and micropore volume. The activated biochar was then thermally treated under N_2 and NH_3 environment for the induction of amine functional groups on biochar surface. Compared to pristine biochar and activated biochar, the CO_2 adsorption capacity after amine functionalization increased 2.7 times (5.05 mmol g^{-1}) and 35% higher, respectively, at ambient condition (Zhang et al. 2016). The elevated temperature (50°C) resulted in reduction of CO_2 adsorption (3.37 mmol g^{-1}), still competitive with other activated biochar. However, surface functionalization without chemical activation showed ordinary CO_2 adsorption capacity. The biochar derived from rice husk and cotton stalk with amine surface functionalization (without chemical activation) did not show much improved CO_2 adsorption capacity (Zhang et al. 2014; Zhang et al. 2015). Other sources of nitrogen-based functional groups doping include urea, chitosan, melamine, and aminopropyl triethoxysilane (Singh et al. 2017; Bamdad et al. 2018). A recent study reported the CO_2 adsorption capacity of walnut-derived biochar which was KOH activated followed by amine functionalization via urea (Rouzitalab et al. 2018). Remarkable CO_2 adsorption capacity of 7.42 mmol g^{-1} was recorded with CO_2/N_2 selectivity of 12.7 at ambient condition (Rouzitalab et al. 2018).

Metal/metal oxide doping has also been found to enhance CO_2 adsorption capacity with considerable selectivity. The saw dust-derived biochar (activated by MgCl_2) doped with MgO showed remarkable CO_2 adsorption capacity of 5.45 mmol g^{-1} at 80°C and atmospheric pressure. Generally, CO_2 adsorption capacity decreases with increase in adsorption; however in this reported study the CO_2 adsorption capacities increased from 50°C to 80°C by 2.7 and 5.45 mmol g^{-1} , respectively, whereas decreased at 400°C with 1.3 mmol g^{-1} (Liu et al. 2013). Provided explanation suggested the strong hydrogen bond between OH and CO_2 and formation of MgCO_3 were responsible for stronger interaction at 80°C (Liu et al. 2013). Another study reported CO_2 adsorption on Persian wood-derived biochar doped with copper oxide (Nowrouzi et al. 2018). The CO_2 adsorption capacities of activated and metal oxide impregnated biochar were found to be 3.02 and 6.78 mmol g^{-1} , respectively, at 30°C and 1 bar. Similar CO_2 adsorption capacities were observed with Persian wood-derived biochar doped with other metal oxides such as MgO (5.98 mmol g^{-1}), Cu/Ni oxides (6.27 mmol g^{-1}), Al oxide (5.82 mmol g^{-1}), and Ni oxide (6.48 mmol g^{-1}).

8.6.2 Heavy Metals

Numerous biomass feedstocks derived biochar have been thoroughly investigated for the removal of heavy metal ions from natural and wastewater. Researchers have identified various factors such as solution pH, attached functional groups, specific surface area, synthesis dosage, and biochar modification that can influence the heavy metal selectivity and removal performance of biochar (Hong et al. 2019; Senthilkumar et al. 2020; Wang et al. 2013).

8.6.2.1 pH and Electric Charge

The electric charge and pH associated with biochar can be significant in deciding the adsorption capacity of particular heavy metal. These parameters mainly depend on the type of biomass and synthesis method (Hong et al. 2019). For instance, in the case of pyrolysis, as the temperature rises, biochar surface starts losing the attached acidic functional groups and results in rise of biochar pH, consequently enriching the alkaline characteristics (Kwak et al. 2019). The loss of acidic functional groups affecting the pH also indirectly regulates the adsorbent protonation, and thereby can modify biochar surface charge (Vijayaraghavan and Yun 2008). In general, low pH resembles presence of high concentration of H⁺ ions which can compete with cationic metal ions and therefore can reduce the adsorption capacity and vice versa (Vijayaraghavan and Yun 2008). It was observed that with biochar derived from corn stalk, the adsorption capacity of Pb(II) surged with increase in solution pH from 4 to 6. It was also concluded that the adsorption of Pb(II) ions were suppressed in acidic medium due to competition with H⁺ ions (Liu et al. 2019b). However, this is not the case with every metal ion as it was also found that the adsorption capacity of As(V) via biochar synthesized from *Ulva reticulata* increased by ~40% when the pH of the solution was raised from 2 to 4, and decreased thereafter. It was suggested that the form of arsenic within the pH range 4–6 is H₂AsO₄⁻ and HAsO₄²⁻, and the lack of high protonated active sites at higher pH weaken the electrostatic attraction (Senthilkumar et al. 2020).

8.6.2.2 Surface Functional Groups

Surface functional groups are considered as one of the most significant factor heavy metal ions removal because of their adsorption and chelate formation characteristics (Carrier et al. 2017). The organic functional groups present in lignocellulosic biomass particularly hardwood feedstocks can be transferred to biochar during thermochemical conversion, resulting in chelation with metal ions, electrostatic interaction, adsorption, and ion exchange (Xie et al. 2017). It was identified that the biochar chemical structure is enriched with functional groups such as carbonyl (-C=O), aliphatic carbon (-C-H), hydroxyl (-O-H), amine (-N-H), and numerous other aromatic

groups (Wang et al. 2013). The authors also investigated a temperature-dependent transformation of functional groups, i.e., when a pyrolysis temperature was raised from 500 to 700 °C, a considerable loss in amine and carbonyl groups were observed whereas aliphatic and hydroxyl groups were completely vanished (Wang et al. 2013). It has been noticed that the Cd^{2+} ions prefer to interact with deprotonated carboxyl groups on biochar surface, and being a weak Lewis acid, Cd^{2+} ions give preference to interactions with π electrons of carboxyl group (Harvey et al. 2011). Another study proposed that the metal ions such as Zn^{2+} , Cu^{2+} , and Ni^{2+} are removed due to carboxylate chelation, whereas Pb^{2+} , Mn^{2+} , and Ni^{2+} are removed by conversion to their oxide forms due to hydrolyses (Carrier et al. 2017).

8.6.2.3 Biochar Modification

Biochar modifications can further enhance the adsorption capacity by improving the physicochemical characteristics of biochar. Among all available biochar modification methods, metal or mineral impregnation, acid/base, and functional group modifications are most common (Rosales et al. 2017; Wan et al. 2018; Wang et al. 2015e; Liu et al. 2012).

Metal, metal oxide, and mineral impregnation are preferred to enhance the adsorption performance by improving pore porosity and functional groups development particularly enriched with oxygen. Electrostatic attraction, π —metal ions bonding, surface complexes, and ion exchange can be the possible interactions between biochar and metal cations (Rosales et al. 2017). A study reported a pyrolysis of a mixture of hickory chips, bagasse, and bamboo with clay for 1 h at 600 °C and found a surge of five times in adsorption potential when compared with only biochar (Yao et al. 2014). The impregnation of ferric chloride into biomass resulted in biochar with high surface area due to evaporation of ferric chloride during pyrolysis leaving behind highly porous structure (Yap et al. 2017). Another study revealed the generation of electrostatic adsorption sites, doubling the As adsorption capacity (429 mg kg^{-1}) post impregnation with iron oxide particles (Wang et al. 2015e). A nanocomposite fabricated from biochar and hydroxyapatite resulted in improved surface area (> 15 times) and doubling the Pb(II) adsorption capacity to 1000 mg g^{-1} against virgin biochar (Wang and Wang 2018). Impregnation of hydrated manganese oxide particles were carried out into biochar derived from peanut shells, sequestering Cd(II) and Pb(II) via manganese oxide induced -COO- and -CO- generated surface complexation (Wan et al. 2018). The improvement in terms of removal performance of Cd(II) and Pb(II) was found to be 4–6 times more than virgin biochar. Table 8.5 demonstrates various biochar modification techniques, adsorption characteristics, and the pattern involved in the removal of metal cations from wastewater.

The introduction of various functional groups on biochar surface has been proved to greatly enhance the adsorption performance. The functional groups can be incorporated through acid/base treatment by altering the porous structure and surface acidities. Chemicals such as HCl, H_3PO_4 , HNO_3 , H_2SO_4 , NaOH, and KOH are

Table 8.5 Modification, adsorption characteristics, and behaviors involved in the removal metal cations from wastewater

Type	Biomass	Modification and pyrolysis temperature	Target metal ions	Adsorption capacity (mg g ⁻¹)	Behaviors	Reference
Metallic nano-particles	Sugarcane leaf	MgO nanoflakes (550 °C)	Pb ²⁺	103	Nano sized carbon sponge enriched with -OH and Mg-OH groups	Li et al. (2018)
	Bamboo	H ₂ O ₂ + nZVI HNO ₃ + nZVI (600 °C)	As ⁵⁺ Ag ⁺	109.1 1218	Modifies surface free energy and atom structure, lowers nZVI's chemical reactivity	Wang et al. (2017a)
	Cornstalk	nZVI + HCl (500 °C)	Cr ⁶⁺	–	Modification resulted in improved efficiency of ~35%	Dong et al. (2017)
	Cottonwood	Fe ₂ O ₃ nanoparticles (600 °C)	As ⁵⁺	3147	Increases ferromagnetic property and surface area	Zhang and Gao (2013)
	Herbal residue	nZVI + sulfide	Cr ⁶⁺	130	Providing a precise core shell structure	Zhu et al. (2018)
Mineral loadings	Pinewood	MnCl ₂ ·4H ₂ O (600 °C)	As ⁵⁺	4.91	Adsorption enhanced by 72.3 times	Wang et al. (2015c)
	Oak bark	Fe ²⁺ / Fe ³⁺	Pb ²⁺	–	Provide porosity, O-containing group, and negative sites	Yao et al. (2014)
	Pinewood	Hematite (600 °C)	As ⁵⁺	0.43	Enhanced surface area and induce magnetic properties	Wang et al. 2015d
	Hickory chips	Fe impregnation (600 °C)	As ⁵⁺	2	Enhanced O-containing group through crystalline Fe(OH) ₂	Hu et al. (2015)
	Marine macroalgae	Magnetite	Cd ²⁺	55.86	Easy separation	Wang et al. (2019)

(continued)

Table 8.5 (continued)

Type	Biomass	Modification and pyrolysis temperature	Target metal ions	Adsorption capacity (mg g ⁻¹)	Behaviors	Reference
Surface oxidation/reduction	Rape straw	KMnO ₄ exposure (600 °C)	Cd ²⁺	80.9	Enhanced O-containing group and micropore creation	Li et al. (2017)
	Banana peels	20 wt. % H ₃ PO ₄ (230 °C)	Pb ²⁺	359	Enhances O/C ratio and surface area	Zhou et al. (2017)
	Municipal solid waste	KOH exposure (500 °C)	As ⁵⁺	31	Modifies functional group, texture, and surface area	Jin et al. (2014)
	Bamboo charcoal	10 wt. % HNO ₃	Hg ⁰	92.1	Enhances COOH and C=O groups	Tan et al. (2012)
	Broiler litter	Activated by steam	Cu ²⁺ , Cd ²⁺ , Ni ²⁺	–		

employed for desired modifications (El-Hendawy 2003; Liu et al. 2012). For example, it has been reported that a controlled exposure of HNO₃ to biochar resulted in the development of oxygen groups on biochar surface providing improved hydrated Pb²⁺ adsorption (El-Hendawy 2003). A recent study conducted an experiment on adsorption of tetracycline by H₂SO₄ and KOH-modified biochar (Liu et al. 2012). The results highlighted that KOH treatment provided better physicochemical characteristics to biochar such as porosity, carbon and oxygen-rich functional groups, and large surface area, in comparison to H₂SO₄-treated and unmodified biochar (Liu et al. 2012). In addition, hydrogen peroxide-exposed biochar synthesized from peanut hull showed oxygen enrichment in terms of carboxyl groups resulting in Pb(II) adsorption increment of 20 times compared to unmodified biochar (Yao et al. 2014).

8.6.3 Anions

The presence of anionic contaminants in water particularly derived from nitrogen, phosphorus, arsenic, and chromium even in trace amount can be catastrophic for all living organisms. For instance, nitrogen and phosphorus are among the vital nutrients for living organisms; however, exceeding threshold limits can cause eutrophication in surface waters such as lakes, rivers, and even oceans. Conventional processes for the removal of nitrogen and phosphorus include biological process as these processes are environmentally benign and cost effective. Although biological processes have advantages, they are generally slow particularly with high nitrogen

and phosphorus concentration in wastewater. Other common treatment methods include membrane filtration, electrochemical, adsorption, and ion exchange (Khan et al. 2020). Also, the most frequently observed heavy metals that exist in anionic form in wastewater are arsenic and chromium. Therefore, the removal processes and corresponding mechanisms for these heavy metal anions from wastewater differ from that of other heavy metal cations. Recently, the biomass-derived biochar and biochar composites have been widely studied and showed superior performances against adsorption of aforementioned anionic contaminants. Following subsections provide brief details of anionic adsorption performances through biochar. Table 8.6 summarizes the anionic adsorption characteristics of biochar.

8.6.3.1 Phosphorus

Phosphorus is mostly present in the form of phosphates (PO_4^{3-}) with high solubility in natural and wastewater. A recent study conducted on macroalgae revealed that the pyrolyzed biochar ($\sim 400\text{--}600\text{ }^\circ\text{C}$) showed considerable P removal performance with an adsorption capacity of $12.5\text{--}19.1\text{ mg g}^{-1}$, whereas raw macroalgae roots and derived biochar ($200\text{ }^\circ\text{C}$) showed no observable adsorption of phosphorus (Jung et al. 2016). The biochar derived from orange peel through pyrolysis within a temperature range of $250\text{--}400\text{ }^\circ\text{C}$ showed insignificant phosphorus adsorption. Same biochar when modified with Fe demonstrated much enhanced phosphorus adsorption capacity (Chen et al. 2011). Likewise, biochar when treated with AlCl_3 producing Al-based biochar nanocomposite exhibited improved phosphorus adsorption performance with an astonishing adsorption capacity $\sim 135\text{ mg g}^{-1}$, estimated through Langmuir modelling (Zhang and Gao 2013). In addition, a study reported an extraordinary phosphorus adsorption capacity of $\sim 887\text{ mg g}^{-1}$ when treated with Mg-Al-biochar nanocomposite synthesized through electro-assisted modification method with MgCl_2 as electrolyte and Al-electrode (Jung et al. 2015).

8.6.3.2 Nitrogen

Nitrogen is mostly present in the form of nitrates (NO_3^-) with high solubility in natural and wastewater. Numerous biomass feedstocks derived biochar have been used for the adsorption of nitrates from aqueous solution and real wastewater samples. For instance, a comparative study demonstrates that a biochar derived from waste bamboo provides better nitrate adsorption capacity ($\sim 1.25\text{ mg g}^{-1}$) than commercial activated carbon ($\sim 1.09\text{ mg g}^{-1}$), an enhanced performance by almost 15% (Mizuta et al. 2004). Similar comparative study was performed by Mishra and Patel (2009), reporting the nitrate adsorption capacities of biochar synthesized from mustard straw, wheat straw, and commercial activated carbon as 1.30, 1.10, and 1.22 mg g^{-1} , respectively. Here also the nitrate adsorption capacity of mustard straw is superior than commercial activated carbon (Mishra and Patel 2009). A study conducted on untreated biochar produced via fast pyrolysis showed a low nitrate

Table 8.6 Anionic adsorption characteristics of biochar

Biochar source/ modification	Target anion	Temperature (°C)	Initial concentration (mg L ⁻¹)	Adsorption performance	Reference
Bamboo powder	NO ₃ ⁻	900	10	1.25 mg g ⁻¹	Mizuta et al. (2004)
Cotton wood/ AlCl ₃ impregnation	PO ₄ ³⁻	600	1–1600	135 mg g ⁻¹	Zhang and Gao (2013)
Mustard straw	NO ₃ ⁻	300	25	–	Mishra and Patel (2009)
Peanut shell/ MgCl ₂ impregnation	NO ₃ ⁻	600	20	11.7%	Zhang et al. (2012)
Orange peel/ FeCl ₂ and FeCl ₃ modification	PO ₄ ³⁻	400, 700	2.4	11.0% (400 °C) 99.4% (700 °C)	Chen et al. (2011)
Oak sawdust/ LaCl ₃ impregnation	NO ₃ ⁻	600	20	1.96 mg g ⁻¹	Wang et al. (2015c)
Rice straw	Cr(VI)	300	50	100% (pH = 1) 98.4% (pH = 3) 34.7% (pH = 5)	Hsu et al. (2009)
Ramie residue	Cr(VI)	300, 600	20–800	82.23 mg g ⁻¹ (300 °C) 61.18 mg g ⁻¹ (600 °C)	Zhou et al. (2016)
Oak sawdust/LaCl ₃ impregnation	PO ₄ ³⁻	500	61.3	7.75 mg g ⁻¹	Wang et al. (2015c)
Coconut granular/ ZnCl ₂ treatment	NO ₃ ⁻	500	5–200	10.2 mg g ⁻¹	Bhatnagar et al. (2008)
Sugar beet tailings	Cr(VI)	300	50–800	123 mg g ⁻¹	Dong et al. (2011)
Waste tires/CO ₂ activation	Cr(VI)	900	60	29.93 mg g ⁻¹ (pH = 2)	Hamadi et al. (2001)
Pine wood/MnCl ₂ modification	As(V)	600	10	0.59 mg g ⁻¹	Wang et al. (2015b)
Chestnut shell/ magnetic gelation	As(V)	450	0.2–50	45.8 mg g ⁻¹	Zhou et al. (2016)
Corn straw/FeCl ₃ impregnation	As(V)	600	0.25–100	6.80 mg g ⁻¹	He et al. (2018)
Wheat straw/ bismuth impregnation	As(III)	500	5–200	16.21 mg g ⁻¹	Zhu et al. (2016)

(continued)

Table 8.6 (continued)

Biochar source/ modification	Target anion	Temperature (°C)	Initial concentration (mg L ⁻¹)	Adsorption performance	Reference
Perilla leaf	As(III)	700	0.05–7.0	11.01 mg g ⁻¹	Niazi et al. (2018b)
Rice straw/red mud treated	As(III)	600	1–50	0.52 mg g ⁻¹	Wu et al. (2017b)
Corn stover/FeCl ₂ and FeCl ₃ modification	Fluoride	500	1–100	4.11 mg g ⁻¹	Mohan et al. (2014)
Wood chips	Perchlorate	700	–	5.0 mg g ⁻¹	Fang et al. (2014)
Vermicompost	Red Congo	700	5–200	31.28 mg g ⁻¹	Yang et al. (2016)

adsorption capacity ~ 0.01 mg g⁻¹, and inversely proportional to pH of solution. Also, the adsorption capacity considerably decreased with co-existing ions such as sulfate and phosphate (Chintala et al. 2013). With untreated biochar, adsorbed nitrates were undetectable; however, post acid and hot water wash the nitrate adsorption capacity significantly enhanced with a value ~ 0.25 and ~ 0.048 mg g⁻¹, respectively (Gai et al. 2014). Literature are evident of biochar-based nanocomposites illustrating improved nitrate adsorption. For instance, a modified lanthanum-biochar nanocomposite was able to provide a nitrate adsorption capacity of ~ 100 mg g⁻¹ which is very high when compared with unmodified biochar ~ 8.94 mg g⁻¹ (Wang et al. 2015c).

8.6.3.3 Arsenic

The observable forms of arsenic anions in natural and wastewater are arsenite [As(III)] and arsenate [As(V)]. Numerous studies have reported positive adsorption performances by biochar against both forms of arsenic in wastewater. A biochar produced from raw pine cone showed As(III) adsorption efficiency of 66%, whereas same biochar when modified with Zn provided an adsorption efficiency of 88% (Vinh et al. 2015). Paper mill sludge recovered from wastewater treatment was used to produce biochar for the removal As(V) from aqueous solution. The biochar was indirectly doped with Fe, as FeSO₄ was used as coagulant during wastewater treatment, showed a As(V) adsorption capacity of 22.7 mg g⁻¹ and was easily recovered from wastewater due to developed magnetic properties (Yoon et al. 2017). Another study also reported an improved efficiency $\sim 89\%$, when As(V) was treated from wastewater with biochar synthesized from sewage sludge (Agrafioti et al. 2014). Fe-doped biochar produced from corn straw exhibited better A(V) adsorption capacity ~ 6.8 mg g⁻¹ whereas only 0.017 mg g⁻¹ was observed with unmodified corn straw biochar (He et al. 2018). A simultaneous removal of As(III) and As(V) from

water was examined by Niazi et al. (2018a, b), where biochar were synthesized from perilla leaf and Japanese oak wood. The measured adsorption capacities of As(III) and As(V) by perilla leaf-derived biochar were 11.0 and 7.2 mg g⁻¹, respectively, while with Japanese oak wood they were found to be 3.1 and 3.9 mg g⁻¹, respectively. It was observed that biochar produced from rice straw demonstrated a reasonable adsorption capacity for As(III) and As(V) as 0.45 and 0.55 mg g⁻¹, respectively. For the enhancement of metal oxide content, when the rice straw feedstock was mixed with red mud prior pyrolysis, the produced biochar showed improved performance with adsorption capacities for As(III) and As(V) as 0.52 and 5.92 mg g⁻¹, respectively (Wu et al. 2017b).

8.6.3.4 Chromium

The most common form of chromium anion present in wastewater is hexavalent dichromate [Cr(VI)]. Numerous studies explaining the adsorption of Cr(VI) on biochar have been reported. For instance, the adsorption capacity ~44.05 mg g⁻¹ was observed with a biochar produced from rubber wood sawdust at 30 °C. It was also identified that the adsorption capacity further enhances as the production temperature increases, i.e., biochar synthesized at 40 and 50 °C revealed an adsorption capacity of ~59.2 and 65.80 mg g⁻¹, respectively (Karthikeyan et al. 2005). The maximum adsorption capacities of Cr(VI) on biochar synthesized from sugar beet tailing and ramie residue were measured ~123 and ~82 mg g⁻¹, respectively (Dong et al. 2011; Zhou et al. 2016). A nanocomposite based on Zn-biochar with excess COO- functional group was produced from sugarcane bagasse, and the observed Cr(VI) maximum removal efficiency was almost twice to that of biochar without Zn impregnation (Gan et al. 2015). When compared the Cr(VI) removal performance with commercial activated carbon, biochar synthesized from coconut shell was found less effective; however, the one synthesized from waste tire had similar adsorption capacities, i.e., 44–53 mg g⁻¹ with biochar from waste tire and 48–58 mg g⁻¹ with commercialized activated carbon, respectively (Mohan et al. 2005). Another study reported successful catalytic reduction of Cr(VI) with biochar embedded with Ag nanoparticle, fixing the environmental issue of waste biomass contaminated with Ag (Liu et al. 2016).

8.6.3.5 Other Metallic Anions

Other than aforementioned anionic contaminants there are anions which can also adversely affect the aquatic ecosystem and humans when consumed beyond threshold limits. For instance, perchlorate (ClO₄⁻), fluoride (F⁻), anionic dye, etc.

Perchlorate (ClO₄⁻) is a rather new contaminant and therefore not much study has been conducted till date. It mainly disturbs the functioning of thyroid gland which regulates iodine controlling hormones in human body. A study conducted on biochar derived from wood via pyrolysis at 700 °C found a considerable

adsorption capacity of perchlorate of $\sim 10.5 \text{ mg g}^{-1}$. The suggested driving force for perchlorate adsorptions were hydrogen bonding and electrostatic attraction (Fang et al. 2014).

Anthropogenic activities are the major source of fluoride induction into natural waters and can be hazardous even in very low concentration ($> 1 \text{ mg l}^{-1}$). Biochar synthesized from pine wood via fast pyrolysis at $450 \text{ }^\circ\text{C}$ was found effective when treated at 2 pH and follows inverse relation with temperature (Mohan et al. 2011). Another study measured a fluoride removal efficiency of 83% when treated with biochar produced from *Cocos nucifera* shell with 10 mg l^{-1} of fluoride in aqueous solution; however this efficiency slightly reduced to 79% when a real water sample with 7 mg l^{-1} of fluoride was treated (Halder et al. 2016).

The rise in textile industries also boost the synthesis of various dyes that are posing severe environmental consequences. These dyes can be both cationic (methylene blue) and anionic (Congo red), where cationic dyes show good adsorption behavior on biochar, the anionic dyes show ordinary adsorption performance (Park et al. 2019). Congo red also consist of azo compounds making it even harder to adsorb. A rise in Congo red adsorption capacity of biochar with increasing synthesis temperature was reported, where biochar was produced via vermicompost and adsorption capacities were recorded in the range of $\sim 11.5\text{--}31.3 \text{ mg g}^{-1}$ (Yang et al. 2016). Fe₃O₄-assisted biochar produced from cellulose also exhibited superior Congo red removal performance with maximum adsorption capacity of $\sim 66 \text{ mg g}^{-1}$ (Zhu et al. 2011).

8.7 Summary and Future Perspectives

Biochar, a biomass derived thermochemically transformed product is a cost effective and potent adsorbent. It can be considered as renewable as biomass such as forestry residues, agricultural wastes, municipal wastes, sewage wastes, etc. are the sustainable source of biochar synthesis. The present chapter provides an overview of current biochar production techniques with focus on biomass pretreatment, thermochemical transformation, and posttreatment processes. It also provides a brief report summarizing the performance of biochar as an adsorbent in wastewater treatment particularly adsorption of heavy metal ions and cationic contaminants.

The denouement of this chapter can be construed as: (a) the characteristics of biochar are associated with biomass type, pre- and posttreatment techniques, and most importantly on the type of thermochemical conversion process. The biochar modifications in terms of induction of functional groups, gains much attention recently as the engineered biochar can divulge new possibilities in the field of wastewater treatment. (b) The modified biochar can be an efficient adsorbent of CO₂, heavy metal ion, and anionic contaminants with precise selectivity. The adsorption can be controlled by regulating mechanisms such as electrostatic attraction, ion exchange, chelation, complex formation, surface precipitation, and

hydrogen bonding. The engineered biochar shows a great potential as an alternative of commercial activated carbon; however, onsite applications need detailed investigation.

Although a lot of research has already been done on biochar production and application in wastewater, convergence of research gaps is still required. There is an utmost need to develop biochar modification processes with high efficacy at low cost. Pilot and semi-pilot plant level research is required to examine the proper functioning of engineered biochar. Regarding CO₂ capture, adsorption at high temperature still requires further research. Adsorption capacity of biochar is relatively better for heavy metal ions; however more research is required to further improve the adsorption efficacy of anionic contaminants. In addition, biochar itself contains PO₄³⁻ and NO₃⁻ developed through thermochemical conversion as phosphorus and nitrogen reside as nutrients in plants. The possibility of dissolution and influence of these anions on performance of wastewater treatment need to be explored.

Acknowledgement This work was supported by the National Strategic Project-Carbon Mineralization Flagship Center of the National Research Foundation of Korea (NRF) funded by the Ministry of Science and ICT (MSIT), the Ministry of Environment (ME), and the Ministry of trade, Industry and Energy (MOTIE) (2017M3D8A2084752).

References

- Agrafioti, E., Bouras, G., Kalderis, D., & Diamadopoulos, E. (2013). Biochar production by sewage sludge pyrolysis. *Journal of Analytical and Applied Pyrolysis*, 101, 72–78.
- Agrafioti, E., Kalderis, D., & Diamadopoulos, E. (2014). Arsenic and chromium removal from water using biochars derived from rice husk, organic solid wastes and sewage sludge. *Journal of Environmental Management*, 133, 309–314.
- Ali, I., & Gupta, V. K. (2006). Advances in water treatment by adsorption technology. *Nature Protocols*, 1(6), 2661–2667.
- Aller, M. F. (2016). Biochar properties: Transport, fate, and impact. *Critical Reviews in Environmental Science and Technology*, 46, 1183–1296.
- An, Q., Jiang, Y. Q., Nan, H. Y., Yu, Y., & Jiang, J. N. (2019). Unraveling sorption of nickel from aqueous solution by KMnO₄ and KOH-modified peanut shell biochar: Implicit mechanism. *Chemosphere*, 214, 846–854.
- Antal, M. J., & Grønli, M. (2003). The art, science, and technology of charcoal production. *Industrial and Engineering Chemistry Research*, 42, 1619–1640.
- Arán, D., Antelo, J., Fiol, S., & Macías, F. (2016). Influence of feedstock on the copper removal capacity of waste derived biochars. *Bioresource Technology*, 212, 199–206.
- Bach, Q. V., & Tran, K. Q. (2015). Dry and wet torrefaction of woody biomass—A comparative study on combustion kinetics. *Energy Procedia*, 75, 150–155.
- Bamdad, H., Hawboldt, K., & MacQuarrie, S. (2018). Nitrogen functionalized biochar as a renewable adsorbent for efficient CO₂ removal. *Energy & Fuels*, 32(11), 11742–11748.
- Becidan, M., Skreiberg, Ø., & Hustad, J. E. (2007). NO_x and N₂O precursors (NH₃ and HCN) in pyrolysis of biomass residues. *Energy & Fuels*, 21, 1173–1180.
- Bhatnagar, A., Ji, M., Choi, Y. H., Jung, W., Lee, S. H., Kim, S. J., Lee, G., Suk, H., Kim, H. S., Min, B., Kim, S. H., Jeon, B. H., & Kang, J. W. (2008). Removal of nitrate from water by adsorption onto zinc chloride treated activated carbon. *Separation Science and Technology*, 43(4), 886–907.

- Bogusz, A., Nowak, K., Stefaniuk, M., Dobrowolski, R., & Oleszczuk, P. (2017). Synthesis of biochar from residues after biogas production with respect to cadmium and nickel removal from wastewater. *Journal of Environmental Management*, 201, 268–276.
- Brewer, C. E., Schmidt-Rohr, K., Satrio, J. A., & Brown, R. C. (2009). Characterization of biochar from fast pyrolysis and gasification systems. *Environmental Progress & Sustainable Energy*, 28, 386–396.
- Carrier, A. J., Abdullahi, I., Hawboldt, K. A., Fiolek, B., & MacQuarrie, S. L. (2017). Probing surface functionality on amorphous carbons using X-ray photoelectron spectroscopy of bound metal ions. *Journal of Physical Chemistry C*, 121, 26300–26307.
- Cha, J. S., Park, S. H., Jung, S.-C., Ryu, C., Jeon, J.-K., Shin, M.-C., & Park, Y.-K. (2016). Production and utilization of biochar: A review. *Journal of Industrial and Engineering Chemistry*, 40, 1–15.
- Channiwala, S. A., & Parikh, P. P. (2002). A unified correlation for estimating HHV of solid, liquid and gaseous fuels. *Fuel*, 81, 1051–1063.
- Chen, B., Chen, Z., & Lv, S. (2011). A novel magnetic biochar efficiently sorbs organic pollutants and phosphate. *Bioresource Technology*, 102(2), 716–723.
- Chintala, R., Mollinedo, J., Schumacher, T. E., Malo, D. D., & Julson, J. L. (2013). Effect of biochar on chemical properties of acidic soil. *Archives of Agronomy and Soil Science*, 60, 393–404.
- Cho, D. W., Kwon, G., Yoon, K., Tsang, Y. F., Ok, Y. S., Kwon, E. E., & Song, H. (2017). Simultaneous production of syngas and magnetic biochar via pyrolysis of paper mill sludge using CO₂ as reaction medium. *Energy Conversion and Management*, 145, 1–9.
- Choi, S., Drese, J. H., & Jones, C. W. (2009). Adsorbent materials for carbon dioxide capture from large anthropogenic point sources. *ChemSusChem*, 2(9), 796–854.
- Collard, F. X., & Blin, J. (2014). A review on pyrolysis of biomass constituents: Mechanisms and composition of the products obtained from the conversion of cellulose, hemicelluloses and lignin. *Renewable and Sustainable Energy Reviews*, 38, 594–608.
- Coromina, H. M., Walsh, D. A., & Mokaya, R. (2016). Biomass-derived activated carbon with simultaneously enhanced CO₂ uptake for both pre and post combustion capture applications. *Journal of Materials Chemistry A*, 4(1), 280–289.
- Creamer, A. E., & Gao, B. (2016). Carbon-based adsorbents for postcombustion CO₂ capture: A critical review. *Environmental Science & Technology*, 50, 7276–7289.
- Dai, L., Fan, L., Liu, Y., Ruan, R., Wang, Y., Zhou, Y., Zhao, Y., & Yu, Z. (2017). Production of bio-oil and biochar from soapstock via microwave-assisted co-catalytic fast pyrolysis. *Bioresource Technology*, 225, 1–8.
- Demirbas, A. (1997). Calculation of higher heating values of biomass fuels. *Fuel*, 76, 431–434.
- Demirbas, A. (2001). Biomass resource facilities and biomass conversion processing for fuels and chemicals. *Energy Conversion and Management*, 42, 1357–1378.
- Deng, J., Li, X., Wei, X., Liu, Y., Liang, J., Tanga, N., Song, B., Chen, X., & Cheng, X. (2019). Sulfamic acid modified hydrochar derived from sawdust for removal of benzotriazole and Cu(II) from aqueous solution: Adsorption behavior and mechanism. *Bioresource Technology*, 290, 121765.
- Deng, S., Wei, H., Chen, T., Wang, B., Huang, J., & Yu, G. (2014). Superior CO₂ adsorption on pine nut shell-derived activated carbons and the effective micropores at different temperatures. *Chemical Engineering Journal*, 253, 46–54.
- Dong, H., Deng, J., Xie, Y., Zhang, C., Jiang, Z., Cheng, Y., Hou, K., & Zeng, G. (2017). Stabilization of nanoscale zero-valent iron (nZVI) with modified biochar for Cr(VI) removal from aqueous solution. *Journal of Hazardous Materials*, 332, 79–86.
- Dong, X. L., Ma, L. N. Q., & Li, Y. C. (2011). Characteristics and mechanisms of hexavalent chromium removal by biochar from sugar beet tailing. *Journal of Hazardous Materials*, 190(1–3), 909–915.
- El-Hendawy, A. N. A. (2003). Influence of HNO₃ oxidation on the structure and adsorptive properties of corn-cob-based activated carbon. *Carbon*, 41, 713–722.

- Ello, A. S., de Souza, L. K. C., Trokourey, A., & Jaroniec, M. (2013). Development of microporous carbons for CO₂ capture by KOH activation of African palm shells. *Journal of CO₂ Utilization*, 2, 35–38.
- Essandoh, M., Wolgemuth, D., Pittman, C. U., Mohan, D., & Mlsna, T. (2017). Adsorption of metribuzin from aqueous solution using magnetic and nonmagnetic sustainable low-cost biochar adsorbents. *Environmental Science and Pollution Research*, 24, 4577–4590.
- Fang, Q. L., Chen, B. L., Lin, Y. J., & Guan, Y. T. (2014). Aromatic and hydrophobic surfaces of wood-derived biochar enhance perchlorate adsorption via hydrogen bonding to oxygen-containing organic groups. *Environmental Science & Technology*, 48(1), 279–288.
- Gai, X., Wang, H., Liu, J., Zhai, L., Liu, S., Ren, T., & Liu, H. (2014). Effects of feedstock and pyrolysis temperature on biochar adsorption of ammonium and nitrate. *PLoS One*, 9, 1–19.
- Gan, C., Liu, Y., Tan, X., Wang, S., Zeng, G., Zheng, B., Li, T., Jiang, Z., & Liu, W. (2015). Effect of porous zinc-biochar nanocomposites on Cr(VI) adsorption from aqueous solution. *RSC Advances*, 5, 35107–35115.
- Gonzalez, A. S., Plaza, M. G., Rubiera, F., & Pevida, C. (2013). Sustainable biomass-based carbon adsorbents for post-combustion CO₂ capture. *Chemical Engineering Journal*, 230, 456–465.
- Halder, G., Khan, A. A., & Dhawane, S. (2016). Fluoride sorption onto a steam-activated biochar derived from Cocos nucifera shell. *Clean-Soil Air Water*, 44(2), 124–133.
- Hamadi, N. K., Chen, X. D., Farid, M., & Lu, M. G. Q. (2001). Adsorption kinetics for the removal of chromium (VI) from aqueous solution by adsorbents derived from used tyres and sawdust. *Chemical Engineering Journal*, 84, 95–105.
- Hao, W., Bjorkman, W., Lilliestrale, M., & Hedin, N. (2014). Activated carbons for water treatment prepared by phosphoric acid activation of hydrothermally treated beer waste. *Industrial and Engineering Chemistry Research*, 53, 15389–15397.
- Harvey, O. R., Herbert, B. E., Rhue, R. D., & Kuo, L. J. (2011). Metal interactions at the biochar-water interface: Energetics and structure-sorption relationships elucidated by flow adsorption microcalorimetry. *Environmental Science & Technology*, 45, 5550–5556.
- He, R. Z., Peng, Z. Y., Lyu, H. H., Huang, H., Nan, Q., & Tang, J. C. (2018). Synthesis and characterization of an iron-impregnated biochar for aqueous arsenic removal. *Science of the Total Environment*, 612, 1177–1186.
- Hoekman, S. K., Broch, A., Robbins, C., Zielinska, B., & Felix, L. (2013). Hydrothermal carbonization (HTC) of selected woody and herbaceous biomass feedstocks. *Biomass Conversion and Biorefinery*, 3, 113–126.
- Hong, M., Zhang, L., Tan, Z., & Huang, Q. (2019). Effect mechanism of biochar's zeta potential on farmland soil's cadmium immobilization. *Environmental Science and Pollution Research*, 26, 19738–19748.
- Hong, S. M., Jang, E., Dysart, A. D., Pol, V. G., & Lee, K. B. (2016). CO₂ capture in the sustainable wheat-derived activated microporous carbon compartments. *Scientific Reports*, 6, 34590.
- Hsu, N. H., Wang, S. L., Liao, Y. H., Huang, S. T., Tzou, Y. M., & Huang, Y. M. (2009). Removal of hexavalent chromium from acidic aqueous solutions using rice straw-derived carbon. *Journal of Hazardous Materials*, 171(1–3), 1066–1070.
- Hu, X., Ding, Z., Zimmerman, A. R., Wang, S., & Gao, B. (2015). Batch and column sorption of arsenic onto iron-impregnated biochar synthesized through hydrolysis. *Water Research*, 68, 206–216.
- IBI (2013). Pyrolysis and gasification of biosolids to produce biochar. IBI White Paper.
- Inyang, M., Gao, B., Zimmerman, A., Zhou, Y. M., & Cao, X. D. (2015). Sorption and cosorption of lead and sulfapyridine on carbon nanotube-modified biochars. *Environmental Science and Pollution Research*, 22, 1868–1876.
- Jian, X., Zhuang, X., Li, B., Xu, X., Wei, Z., Song, Y., & Jiang, E. (2018). Comparison of characterization and adsorption of biochars produced from hydrothermal carbonization and pyrolysis. *Environmental Technology and Innovation*, 10, 27–35.

- Jin, H., Capareda, S., Chang, Z., Gao, J., Xu, Y., & Zhang, J. (2014). Biochar pyrolytically produced from municipal solid wastes for aqueous as(V) removal: Adsorption property and its improvement with KOH activation. *Bioresource Technology*, 169(5), 622–629.
- Jing, X. R., Wang, Y. Y., Liu, W. J., Wang, Y. K., & Jiang, H. (2014). Enhanced adsorption performance of tetracycline in aqueous solutions by methanol-modified biochar. *Chemical Engineering Journal*, 248, 168–174.
- Jung, K. W., Jeong, T. U., Hwang, M. J., Kim, K., & Ahn, K. H. (2015). Phosphate adsorption ability of biochar/Mg₂Al assembled nanocomposites prepared by aluminum-electrode based electro-assisted modification method with MgCl₂ as electrolyte. *Bioresource Technology*, 198, 603–610.
- Jung, K. W., Kim, K., Jeong, T. U., & Ahn, K. H. (2016). Influence of pyrolysis temperature on characteristics and phosphate adsorption capability of biochar derived from waste-marine macroalgae (*Undaria pinnatifida* roots). *Bioresource Technology*, 200, 1024–1028.
- Kambo, H., Dutta, A. (2014). Hydrothermal carbonization (HTC): an innovative process for the conversion of low quality lignocellulosic biomass to hydrochar for replacing coal. In: Proceedings of the 9th Annual Green Energy Conference (IGEC-IX), Tianjin, China, 25–28.
- Kambo, H. S., & Dutta, A. (2015). A comparative review of biochar and hydrochar in terms of production, physico-chemical properties and applications. *Renewable and Sustainable Energy Reviews*, 45, 359–378.
- Karthikeyan, T., Rajgopal, S., & Miranda, L. R. (2005). Chromium(VI) adsorption from aqueous solution by Hevea Brasiliensis sawdust activated carbon. *Journal of Hazardous Materials*, 124(1–3), 192–199.
- Khan, M. D., Chottitissupawong, T., Vu, H. H. T., Ahn, J. W., & Kim, G. M. (2020). Removal of phosphorus from an aqueous solution by nanocalcium hydroxide derived from waste bivalve seashells: Mechanism and kinetics. *ACS Omega*, 5, 12290–12301.
- Kılıç, M., Mutlu, Ç. K. Ö. Ç., & Pütün, A. E. (2013). Adsorption of heavy metal ions from aqueous solutions by bio-char, a by-product of pyrolysis. *Applied Surface Science*, 283, 856–862.
- Kwak, J. H., Islam, M. S., Wang, S., Messele, S. A., Naeth, M. A., El-Din, M. G., & Chang, S. X. (2019). Biochar properties and lead(II) adsorption capacity depend on feedstock type, pyrolysis temperature, and steam activation. *Chemosphere*, 231, 393–404.
- Lahijani, P., Mohammadi, M., & Mohamed, A. R. (2018). Metal incorporated biochar as a potential adsorbent for high capacity CO₂ capture at ambient condition. *Journal of CO2 Utilization*, 26, 281–293.
- Li, B., Yang, L., Wang, C. Q., Zhang, Q. P., Liu, Q. C., Li, Y. D., & Xiao, R. (2017). Adsorption of Cd(II) from aqueous solutions by rape straw biochar derived from different modification processes. *Chemosphere*, 175, 332–340.
- Li, D., Ma, T., Zhang, R., Tian, Y., & Qiao, Y. (2015). Preparation of porous carbons with high low-pressure CO₂ uptake by KOH activation of rice husk char. *Fuel*, 139, 68–70.
- Li, R., Liang, W., Wang, J. J., Gaston, L. A., Huang, D., Huang, H., & Xiao, R. (2018). Facilitative capture of As(V), Pb(II) and methylene blue from aqueous solutions with MgO hybrid sponge-like carbonaceous composite derived from sugarcane leafy trash. *Journal of Environmental Management*, 212, 77–87.
- Li, Y., Ruan, G., Jalilov, A. S., Tarkunde, Y. R., Fei, H., & Tour, J. M. (2016). Biochar as a renewable source for high-performance CO₂ sorbent. *Carbon*, 107, 344–351.
- Liu, L., Huang, Y., Zhang, S., Gong, Y., Su, Y., Cao, J., & Hu, H. (2019b). Adsorption characteristics and mechanism of Pb(II) by agricultural waste-derived biochars produced from a pilot-scale pyrolysis system. *Waste Management*, 100, 287–295.
- Liu, P., Liu, W. J., Jiang, H., Chen, J. J., Li, W. W., & Yu, H. Q. (2012). Modification of bio-char derived from fast pyrolysis of biomass and its application in removal of tetracycline from aqueous solution. *Bioresource Technology*, 121, 235–240.
- Liu, W., Ling, L., Wang, Y., He, H., He, Y., Yu, H., & Jiang, H. (2016). One-pot high yield synthesis of Ag nanoparticle-embedded biochar hybrid materials from waste biomass for catalytic Cr(VI) reduction. *Environmental Science. Nano*, 3, 745–753.

- Liu, W. J., Jiang, H., Tian, K., Ding, Y. W., & Yu, H. Q. (2013). Mesoporous carbon stabilized MgO nanoparticles synthesized by pyrolysis of MgCl₂ preloaded waste biomass for highly efficient CO₂ capture. *Environmental Science & Technology*, 47(16), 9397–9403.
- Liu, W. J., Jiang, H., & Yu, H. Q. (2015). Development of biochar-based functional materials: Toward a sustainable platform carbon material. *Chemical Reviews*, 115, 12251–12285.
- Liu, Y., Sohi, S. P., Liu, S., Guan, J., Zhou, J., & Chen, J. (2019a). Adsorption and reductive degradation of Cr(VI) and TCE by a simply synthesized zero valent iron magnetic biochar. *Journal of Environmental Management*, 235, 276–281.
- Liu, Z., & Balasubramanian, R. (2014). Upgrading of waste biomass by hydrothermal carbonization (HTC) and low temperature pyrolysis (LTP): A comparative evaluation. *Applied Energy*, 114, 857–864.
- Liu, Z., & Zhang, F.-S. (2011). Removal of copper (II) and phenol from aqueous solution using porous carbons derived from hydrothermal chars. *Desalination*, 267, 101–106.
- Lyu, H. H., Gao, B., He, F., Ding, C., Tang, J. C., & Crittenden, J. C. (2017). Ball-milled carbon nanomaterials for energy and environmental applications. *ACS Sustainable Chemistry & Engineering*, 5, 9568–9585.
- Lyu, H. H., Gao, B., He, F., Zimmerman, A. R., Ding, C., Huang, H., & Tang, J. C. (2018). Effects of ball milling on the physicochemical and sorptive properties of biochar: Experimental observations and governing mechanisms. *Environmental Pollution*, 233, 54–63.
- Manya, J. J., Gonzalez, B., Azuara, M., & Arner, G. (2018). Ultra-microporous adsorbents prepared from vine shoots-derived biochar with high CO₂ uptake and CO₂/N₂ selectivity. *Chemical Engineering Journal*, 345, 631–639.
- Marcus, Y. (1999). On transport properties of hot liquid and supercritical water and their relationship to the hydrogen bonding. *Fluid Phase Equilibria*, 164(1), 131–142.
- Mcbeath, A. V., Wurster, C. M., & Bird, M. I. (2015). Influence of feedstock properties and pyrolysis conditions on biochar carbon stability as determined by hydrogen pyrolysis. *Biomass Bioenergy*, 73, 155–173.
- Mishra, P. C., & Patel, R. K. (2009). Use of agricultural waste for the removal of nitrate-nitrogen from aqueous medium. *Journal of Environmental Management*, 90(1), 519–522.
- Mizuta, K., Matsumoto, T., Hatate, Y., Nishihara, K., & Nakanishi, T. (2004). Removal of nitrate-nitrogen from drinking water using bamboo powder charcoal. *Bioresource Technology*, 95(3), 255–257.
- Mohan, D., Kumar, S., & Srivastava, A. (2014). Fluoride removal from ground water using magnetic and nonmagnetic corn Stover biochars. *Ecological Engineering*, 73, 798–808.
- Mohan, D., Pittman, C. U., & Steele, P. H. (2006). Pyrolysis of wood/biomass for bio-oil: A critical review. *Energy & Fuels*, 20, 848–889.
- Mohan, D., Sharma, R., Singh, V. K., Steele, P., & Pittman, J. C. U. (2011). Fluoride removal from water using bio-char, a green waste, low-cost adsorbent: Equilibrium uptake and sorption dynamics modelling. *Industrial and Engineering Chemistry Research*, 51(2), 900–914.
- Mohan, D. S., Singh, K. P., & Singh, V. K. (2005). Removal of hexavalent chromium from aqueous solution using low cost activated carbons derived from agricultural waste materials and activated carbon fabric cloth. *Industrial and Engineering Chemistry Research*, 44(4), 1027–1042.
- Ni, B. J., Huang, Q. S., Wang, C., Ni, T. Y., Sun, J., & Wei, W. (2019). Competitive adsorption of heavy metals in aqueous solution onto biochar derived from anaerobically digested sludge. *Chemosphere*, 219, 351–357.
- Niazi, N. K., Bibi, I., Shahid, M., Ok, Y. S., Burton, E. D., Wang, H., Shaheen, S. M., Rinklebe, J., & Luttge, A. (2018b). Arsenic removal by perilla leaf biochar in aqueous solutions and ground-water: An integrated spectroscopic and microscopic examination. *Environmental Pollution*, 232, 31–41.
- Niazi, N. K., Bibi, I., Shahid, M., Ok, Y. S., Shaheen, S. M., Rinklebe, J., Wang, H., Murtaza, B., Islam, E., Nawaz, M. F., & Luttge, A. (2018a). Arsenic removal by Japanese oak wood biochar in aqueous solutions and well water: Investigating arsenic fate using integrated spectroscopic and microscopic techniques. *Science of the Total Environment*, 621, 1642–1651.

- Nowrouzi, M., Younesi, H., & Bahramifar, N. (2018). Superior CO₂ capture performance on biomass-derived carbon/metal oxides nanocomposites from Persian ironwood by H₃PO₄ activation. *Fuel*, 223, 99–114.
- Onay, O., & Kockar, O. M. (2003). Slow, fast and flash pyrolysis of rapeseed. *Renewable Energy*, 28, 2417–2433.
- Oschatz, M., & Antonietti, M. (2018). A search for selectivity to enable CO₂ capture with porous adsorbents. *Energy & Environmental Science*, 11(1), 57–70.
- Pandey, A., Bhaskar, T., Stocker, M., & Sukumaran, R. K. (Eds.). (2015). *Recent advances in thermochemical conversion of biomass* (pp. 331–346). Amsterdam: Elsevier.
- Parikh, J., Channiwalla, S. A., & Ghosal, G. K. (2005). A correlation for calculating HHV from proximate analysis of solid fuels. *Fuel*, 84, 487–494.
- Parikh, J., Channiwalla, S. A., & Ghosal, G. K. (2007). A correlation for calculating elemental composition from proximate analysis of biomass materials. *Fuel*, 86, 1710–1719.
- Park, J. H., Wang, J. J., Meng, Y., Wei, Z., DeLaune, R. D., & Seo, D. C. (2019). Adsorption/desorption behavior of cationic and anionic dyes by biochars prepared at normal and high pyrolysis temperatures. *Colloids and Surfaces A: Physicochemical and Engineering Aspects*, 572, 274–282.
- Randolph, P., Bansode, R. R., Hassan, O. A., Rehrah, D., Ravella, R., Reddy, M. R., Watts, D. W., Novak, J. M., & Ahmedna, M. (2017). Effect of biochars produced from solid organic municipal waste on soil quality parameters. *Journal of Environmental Management*, 192, 271–280.
- Rashidi, N. A., & Yusup, S. (2016). An overview of activated carbons utilization for the post-combustion carbon dioxide capture. *Journal of CO₂ Utilization*, 13, 1–16.
- Rosales, E., Mejjide, J., Pazos, M., & Sanromán, M. A. (2017). Challenges and recent advances in biochar as low-cost biosorbent: From batch assays to continuous-flow systems. *Bioresource Technology*, 246, 176–192.
- Rouzitalab, Z., Maklavany, D. M., Rashidi, A., & Jafarnejad, S. (2018). Synthesis of N-doped nanoporous carbon from walnut shell for enhancing CO₂ adsorption capacity and separation. *Journal of Environmental Chemical Engineering*, 6(5), 6653–6663.
- Runtti, H., Tuomikoski, S., Kangas, T., Lassi, U., Kuokkanena, T., & Rämö, J. (2014). Chemically activated carbon residue from biomass gasification as a sorbent for iron(II), copper(II) and nickel(II) ions. *Journal of Water Process Engineering*, 4, 12–24.
- Senthilkumar, R., Reddy, P. D. M., Govindarajan, L., Saravanakumar, K., & Naveen, P. B. S. (2020). Synthesis of green marine algal-based biochar for remediation of arsenic(V) from contaminated waters in batch and column mode of operation. *International Journal of Phytoremediation*, 22, 279–286.
- Singh, G., Kim, I. Y., Lakhi, K. S., Srivastava, P., Naidu, R., & Vinu, A. (2017). Single step synthesis of activated bio-carbons with a high surface area and their excellent CO₂ adsorption capacity. *Carbon*, 116, 448–455.
- Son, E. B., Poo, K. M., Chang, J. S., & Chae, K. J. (2018). Heavy metal removal from aqueous solutions using engineered magnetic biochars derived from waste marine macro-algal biomass. *Science of the Total Environment*, 615, 161–168.
- Stemann, J., Erlach, B., & Ziegler, F. (2013). Hydrothermal carbonisation of empty palm oil fruit bunches: Laboratory trials, plant simulation, carbon avoidance, and economic feasibility. *Waste and Biomass Valorization*, 4, 441–454.
- Tan, X., Liu, Y., Gu, Y., Xu, Y., Zeng, G., Hu, X., Liu, S., Wang, X., Liu, S., & Li, J. (2016). Biochar based nano-composites for the decontamination of wastewater: A review. *Bioresource Technology*, 212, 318–333.
- Tan, Z., Sun, L., Xiang, J., Zeng, H., Liu, Z., Hu, S., & Qiu, J. (2012). Gas-phase elemental mercury removal by novel carbon-based sorbents. *Carbon*, 50(2), 362–371.
- Tang, L., Yu, J., Pang, Y., Zeng, G., Deng, Y., Wang, J., Ren, X., Ye, S., Peng, B., & Feng, H. (2018). Sustainable efficient adsorbent: Alkali-acid modified magnetic biochar derived from sewage sludge for aqueous organic contaminant removal. *Chemical Engineering Journal*, 336, 160–169.

- Tang, Y., Alam, M. S., Konhauser, K. O., Alessi, D. S., Xu, S., Tian, W., & Liu, Y. (2019). Influence of pyrolysis temperature on production of digested sludge biochar and its application for ammonium removal from municipal wastewater. *Journal of Cleaner Production*, 209, 927–936.
- Tortosa Masia, A. A., Buhre, B. J. P., Gupta, R. P., & Wall, T. F. (2007). Characterising ash of biomass and waste. *Fuel Processing Technology*, 88, 1071–1081.
- Vijayaraghavan, K., & Yun, Y. S. (2008). Bacterial biosorbents and biosorption. *Biotechnology Advances*, 26, 266–291.
- Vinh, V. N., Zafar, M., Behera, S. K., & Park, H. S. (2015). Arsenic(III) removal from aqueous solution by raw and zinc-loaded pine cone biochar: Equilibrium, kinetics, and thermodynamics studies. *International Journal of Environmental Science and Technology*, 12(4), 1283–1294.
- Wan, S., Wu, J., Zhou, S., Wang, R., Gao, B., & He, F. (2018). Enhanced lead and cadmium removal using biochar-supported hydrated manganese oxide (HMO) nanoparticles: Behavior and mechanism. *Science of the Total Environment*, 616–617, 1298–1306.
- Wang, B., Lehmann, J., Hanley, K., Hestrin, R., & Enders, A. (2016). Ammonium retention by oxidized biochars produced at different pyrolysis temperatures and residence times. *RSC Advances*, 6, 41907–41913.
- Wang, C., & Wang, H. (2018). Pb(II) sorption from aqueous solution by novel biochar loaded with nano-particles. *Chemosphere*, 192, 1–4.
- Wang, H., Gao, B., Wang, S., Fang, J., Xue, Y., & Yang, K. (2015e). Removal of Pb(II), Cu(II), and Cd(II) from aqueous solutions by biochar derived from KMnO₄ treated hickory wood. *Bioresource Technology*, 197, 356–362.
- Wang, L., Wang, Y., Ma, F., Tankpa, V., Bai, S., Guo, X., & Wang, X. (2019). Mechanisms and reutilization of modified biochar used for removal of heavy metals from wastewater: A review. *Science of the Total Environment*, 668, 1298–1309.
- Wang, S., Gao, B., Zimmerman, A. R., Li, Y., Ma, L., Harris, W. G., & Migliaccio, K. W. (2015a). Physicochemical and sorptive properties of biochars derived from woody and herbaceous biomass. *Chemosphere*, 134, 257–262.
- Wang, S., Gao, B., Zimmerman, A. R., Li, Y., Ma, L., Harris, W. G., & Migliaccio, K. W. (2015d). Removal of arsenic by magnetic biochar prepared from pinewood and natural hematite. *Bioresource Technology*, 175, 391–395.
- Wang, S., Zhou, Y., Gao, B., Wang, X., Yin, X., Feng, K., & Wang, J. (2017a). The sorptive and reductive capacities of biochar supported nanoscaled zero-valent iron (nZVI) in relation to its crystallite size. *Chemosphere*, 186, 495–500.
- Wang, S. S., Gao, B., Li, Y. C., Mosa, A., Zimmerman, A. R., Ma, L. Q., Harris, W. G., & Migliaccio, K. W. (2015b). Manganese oxide-modified biochars: Preparation, characterization, and sorption of arsenate and lead. *Bioresource Technology*, 181, 13–17.
- Wang, S. S., Gao, B., Li, Y. C., Ok, Y. S., Shen, C. F., & Xue, S. G. (2017b). Biochar provides a safe and value-added solution for hyperaccumulating plant disposal: A case study of *Phytolacca acinosa* Roxb. (Phytolaccaceae). *Chemosphere*, 178, 59–64.
- Wang, Y., Hu, Y., Zhao, X., Wang, S., & Xing, G. (2013). Comparisons of biochar properties from wood material and crop residues at different temperatures and residence times. *Energy and Fuels*, 27, 5890–5899.
- Wang, Y., & Liu, R. (2018). H₂O₂ treatment enhanced the heavy metals removal by manure biochar in aqueous solutions. *Science of the Total Environment*, 628–629, 1139–1148.
- Wang, Z., Guo, H., Shen, F., Yang, G., Zhang, Y., Zeng, Y., Wang, L., Xiao, H., & Deng, S. (2015c). Biochar produced from oak sawdust by lanthanum (La)-involved pyrolysis for adsorption of ammonium (NH₄⁺), nitrate (NO₃⁻), and phosphate (PO₄³⁻). *Chemosphere*, 119, 646–653.
- Weber, R., Yoshida, S., & Miwa, K. (2002). PCB destruction in subcritical and supercritical water evaluation of PCDF formation and initial steps of degradation mechanisms. *Environmental Science & Technology*, 36, 1839–1844.
- Wu, C., Huang, L., Xue, S. G., Huang, Y. Y., Hartley, W., Cui, M. Q., & Wong, M. H. (2017b). Arsenic sorption by red mud-modified biochar produced from rice straw. *Environmental Science and Pollution Research*, 24(22), 18168–18178.

- Wu, W., Li, J., Lan, T., Müller, K., Niazi, N. K., Chen, X., Xu, S., Zheng, L., Chu, Y., Li, J., Yuan, G., & Wang, H. (2017a). Unraveling sorption of lead in aqueous solutions by chemically modified biochar derived from coconut fiber: A microscopic and spectroscopic investigation. *Science of the Total Environment*, 576, 766–774.
- Xie, R., Jin, Y., Chen, Y., & Jiang, W. (2017). The importance of surface functional groups in the adsorption of copper onto walnut shell derived activated carbon. *Water Science and Technology*, 76, 3022–3034.
- Xu, X., Zheng, Y., Gao, B., & Cao, X. (2019). N-doped biochar synthesized by a facile ball-milling method for enhanced sorption of CO₂ and reactive red. *Chemical Engineering Journal*, 368, 564–572.
- Yaman, S. (2004). Pyrolysis of biomass to produce fuels and chemical feedstocks. *Energy Conversion and Management*, 45, 651–671.
- Yang, G., Wu, L., Xian, Q. M., Shen, F., Wu, J., & Zhang, Y. Z. (2016). Removal of Congo red and methylene blue from aqueous solutions by vermicompost-derived biochars. *PLoS One*, 11(5), e0154562.
- Yang, J., Yue, L., Hu, X., Wang, L., Zhao, Y., Lin, Y., Sun, Y., DaCosta, H., & Guo, L. (2017). Efficient CO₂ capture by porous carbons derived from coconut shell. *Energy & Fuels*, 31(4), 4287–4293.
- Yao, Y., Gao, B., Fang, J., Zhang, M., Chen, H., Zhou, Y., Creamer, A. E., Sun, Y., & Yang, L. (2014). Characterization and environmental applications of clay-biochar composites. *Chemical Engineering Journal*, 242, 136–143.
- Yao, Y., Gao, B., Inyang, M., Zimmerman, A. R., Cao, X., Pullammanappallil, P., & Yang, L. (2011). Biochar derived from anaerobically digested sugar beet tailings: Characterization and phosphate removal potential. *Bioresource Technology*, 102, 6273–6278.
- Yao, Y., Gao, B., Wu, F., Zhang, C., & Yang, L. (2015). Engineered biochar from biofuel residue: Characterization and its silver removal potential. *ACS Applied Materials and Interfaces*, 7, 10634–10640.
- Yap, M. W., Mubarak, N. M., Sahu, J. N., & Abdullah, E. C. (2017). Microwave induced synthesis of magnetic biochar from agricultural biomass for removal of lead and cadmium from wastewater. *Journal of Industrial and Engineering Chemistry*, 45, 287–295.
- Yoon, K., Cho, D. W., Tsang, D. C. W., Bolan, N., Rinklebe, J., & Song, H. (2017). Fabrication of engineered biochar from paper mill sludge and its application into removal of arsenic and cadmium in acidic water. *Bioresource Technology*, 246, 69–75.
- Zhang, C., Song, W., Ma, Q., Xie, L., Zhang, X., & Guo, H. (2016). Enhancement of CO₂ capture on biomass-based carbon from black locust by KOH activation and ammonia modification. *Energy & Fuels*, 30(5), 4181–4190.
- Zhang, H., Chen, C., Gray, E. M., & Boyd, S. E. (2017b). Effect of feedstock and pyrolysis temperature on properties of biochar governing end use efficacy. *Biomass Bioenergy*, 105, 136–146.
- Zhang, L., Xu, C., & Champagne, P. (2010). Overview of recent advances in thermo-chemical conversion of biomass. *Energy Conversion and Management*, 51, 969–982.
- Zhang, M., & Gao, B. (2013). Removal of arsenic, methylene blue, and phosphate by biochar/AlOOH nanocomposite. *Chemical Engineering Journal*, 226, 286–292.
- Zhang, M., Gao, B., Varnosfaderani, S., Hebard, A., Yao, Y., & Inyang, M. (2013). Preparation and characterization of a novel magnetic biochar for arsenic removal. *Bioresource Technology*, 130, 457–462.
- Zhang, M., Gao, B., Yao, Y., Xue, Y. W., & Inyang, M. (2012). Synthesis of porous MgO-biochar nanocomposites for removal of phosphate and nitrate from aqueous solutions. *Chemical Engineering Journal*, 210, 26–32.
- Zhang, X., Gao, B., Creamer, A. E., Cao, C., & Li, Y. (2017a). Adsorption of VOCs onto engineered carbon materials: A review. *Journal of Hazardous Materials*, 338, 102–123.
- Zhang, X., Zhang, S., Yang, H., Feng, Y., Chen, Y., Wang, X., & Chen, H. (2014). Nitrogen enriched biochar modified by high temperature CO₂-ammonia treatment: Characterization and adsorption of CO₂. *Chemical Engineering Journal*, 257, 20–27.

- Zhang, X., Zhang, S., Yang, H., Shao, J., Chen, Y., Feng, Y., Wang, X., & Chen, H. (2015). Effects of hydrofluoric acid pre-deashing of rice husk on physicochemical properties and CO₂ adsorption performance of nitrogen-enriched biochar. *Energy*, *91*, 903–910.
- Zhao, M., Dai, Y., Zhang, M., Feng, C., Qin, B., Zhang, W., Zhao, N., Li, Y., Ni, Z., Xu, Z., Tsang, D. C. W., & Qui, R. (2020). Mechanisms of Pb and/or Zn adsorption by different biochars: Biochar characteristics, stability, and binding energies. *Science of the Total Environment*, *717*, 136894.
- Zhao, P., Shen, Y., Ge, S., Chen, Z., & Yoshikawa, K. (2014). Clean solid biofuel production from high moisture content waste biomass employing hydrothermal treatment. *Applied Energy*, *131*, 345–367.
- Zhao, T., Yao, Y., Li, D., Wu, F., Zhang, C., & Gao, B. (2018). Facile low-temperature one-step synthesis of pomelo peel biochar under air atmosphere and its adsorption behaviors for ag(I) and Pb(II). *Science of the Total Environment*, *640–641*, 73–79.
- Zhao, X., Ouyang, W., Hao, F., Lin, C., Wang, F., Han, S., & Geng, X. (2013). Properties comparison of biochars from corn straw with different pretreatment and sorption behaviour of atrazine. *Bioresource Technology*, *147*, 338–344.
- Zhou, L., Liu, Y. G., Liu, S. B., Yin, Y. C., Zeng, G. M., Tan, X. F., Hu, X., Hu, X., Jiang, L., Ding, Y., Liu, S., & Huang, X. (2016). Investigation of the adsorption reduction mechanisms of hexavalent chromium by ramie biochars of different pyrolytic temperatures. *Bioresource Technology*, *218*, 351–359.
- Zhou, N., Chen, H., Xi, J., Yao, D., Zhou, Z., Tian, Y., & Lu, X. (2017). Biochars with excellent Pb (II) adsorption property produced from fresh and dehydrated Banana peels via hydrothermal carbonization. *Bioresource Technology*, *232*, 204–210.
- Zhu, H. Y., Fu, Y. Q., Jiang, R., Jiang, J. H., Xiao, L., Zeng, G. M., Zhao, S. L., & Wang, Y. (2011). Adsorption removal of Congo red onto magnetic cellulose/Fe₃O₄/activated carbon composite: Equilibrium, kinetic and thermodynamic studies. *Chemical Engineering Journal*, *173*(2), 494–502.
- Zhu, N., Yan, T., Qiao, J., & Cao, H. (2016). Adsorption of arsenic, phosphorus and chromium by bismuth impregnated biochar: Adsorption mechanism and depleted adsorbent utilization. *Chemosphere*, *164*, 32–40.
- Zhu, S., Huang, X., Wang, D., Wang, L., & Ma, F. (2018). Enhanced hexavalent chromium removal performance and stabilization by magnetic iron nanoparticles assisted biochar in aqueous solution: Mechanisms and application potential. *Chemosphere*, *207*, 50–59.

Chapter 9

Role of Nanomaterials: Enhancing the Adsorption Efficiency of Activated Carbon in Wastewater Treatment



Kiranmai Reddy Majji, Venkata Naga Suresh Reddy Kachireddy, Shashi Kumar Kuruva Nandyal, and Sreenivasa Rao Battula

9.1 Introduction

Water is a vital inorganic component for the endurance of life on this earth. An increase in population leads to the enhancement of agriculture and industries, which resulted in a decrease in water quality. Many treatment techniques were employed to retain water quality, such as screening, sedimentation, coagulation, flocculation, filtration, reverse osmosis, ion-exchange process, distillation, and adsorption. However, adsorption has drawn more attention because of its simple pattern and cost-effectiveness, and this technique has been widely used for industrial water treatment. The process of adsorption technique is a surface-based exothermic phenomenon. It is evident that specific molecules are adhering to a solid substance's surface by its nature of attraction when they come in contact with it. These molecules do not go more in-depth but remain on the surface of the substance. The collection or accumulation of molecules on the surface individually rather than in bulk is called adsorption (Sing et al. 1998). Forces present on the surface of adsorbent draw the pollutant (adsorbate) particles on its surface. Accumulation of pollutants rises as the surface area of the adsorbent increases. The other important factor in adsorption is enthalpy, which is negative always. When any substance is adsorbed,

K. R. Majji

Department of Environmental Science, GITAM Institute of Science, GITAM (Deemed to be University), Vishakhapatnam, Andhra Pradesh, India

V. N. S. R. Kachireddy (✉) · S. R. Battula

Department of Chemistry, GITAM Institute of Science, GITAM (Deemed to be University), Vishakhapatnam, Andhra Pradesh, India

e-mail: skachire@gitam.edu

S. K. Kuruva Nandyal

Department of Humanities & Sciences, Annamacharya Institute of Technology and Sciences, Kadapa, Andhra Pradesh, India

the molecules' freedom will be restricted, and a decrease in the entropy and enthalpy system was observed. Carbonaceous structure of activated carbon (AC), which is graphite-like, is ideal for adsorbing organic, inorganic, and aromatic functionality groups of substances (Cheng et al. 2005).

9.1.1 Importance of Activated Carbon

The most conventional adsorbent in water treatment is activated carbon. Internally it poses spongy structure with a diverse size of pores. Activated carbon occurs in different sizes such as macro (>50 nm), meso (2–50 nm), and micro (<2 nm) with branched internal structure. High surface area of activated carbon depends on porosity, resulting in many binding sites for adsorbate materials (Han et al. 2003; Pezoti et al. 2016; Sweetman et al. 2017). First, Raphael von Ostrejko got patent in 1900 and 1901 for developing commercial activated carbon. The pioneer substances used to prepare activated carbon are wood, lignite, bituminous coal, anthracite coal, peat shell, almond, olive stones and coconut shells, etc. containing 40–90% of carbon (Bansal et al. 1988). Pyrolytic decomposition of these pioneers leads to the formation of carbonaceous char. Chemical and physical treatment further enable the activity of this char (Ali et al. 2012). Intense temperature and steam is required to release carbon dioxide and air in physical treatment (Lizzio et al. 1990), whereas in chemical analysis H_2SO_4 , KOH, and $ZnCl_2$ were used as activators. The physical and chemical treatment depends on the heating rate, which significantly influences the pore shape of micro, prominent and mesopore, surface functional groups, and surface areas (Wigmans 1986; Bhatnagar et al. 2013). The important groups present on activated carbon are quinines, phenols, lactones, carbonyl, and carboxyl groups. Thermal treatment and post chemical-treatment lead to improved functional groups on the surface of activated carbon. The adsorption efficiency of activated carbon is increased by modifying the functional groups on the surface through suitable chemical and thermal treatment. In general, surface modification increases the activation process of carbon, and this can be performed by various applications such as acid-treatment, base-treatment, plasma-treatment, impregnation treatment, ozone-treatment, and surfactant-treatment (Lukens 2007; Bhatnagar et al. 2013; Ali et al. 2020).

9.1.2 Different Treatment Methods

Acid treatment improves the hydrophilic properties of activated carbon. Properties of cation exchange increase through replacing hydroxide groups, where a huge percentage of oxygen carriers appear on the surface of the carbon (Ahn et al. 2009; Ali et al. 2020). Commonly used acids in acid treatment are nitric acid and sulfuric acid; by replacing H^+ ions from the oxidized carbon surface, metal ion forms complexes

because of massive connection with negatively charged acid groups (Bhatnagar et al. 2013). Here pH shows an essential part in the expulsion of various metals. The metallic compounds adsorbance efficiency depends on the number of functional groups present on the activated carbon (Ahn et al. 2009). The use of nitric acid on activated carbon leads to oxidation, further changing ion-exchange behavior at different pH values.

Base treatment produces a positive charge on carbon, which adsorbs negative charged pollutants at high amounts (Faria et al. 2004; Shaarani and Hameed 2011). The active surface of activated carbon absorbs organic dye by electrostatic forces. The higher adsorption capacity was shown when carbon was modified with gaseous ammonia at 400 to 800 °C (Przepiorski 2006). Similarly, this modification also resulted in the easy removal of 2, 4 dichlorophenols from 232.56 to 285.71 mg/g (Shaarani and Hameed 2011).

The use of very fine chemicals or metals on the AC surface to remove the waste from water is called impregnation. Here metals like iron (Vaughan Jr. and Reed 2005), copper (Yeddou et al. 2011), silver (Miyanaga et al. 2002), and aluminum (Tchomgui-Kamga et al. 2010) were used to find the adsorption properties of activated carbon. When powder of metals or chemicals was added into activated carbon, the adsorption of pollutants increased ten times; this was confirmed by combining Fe^{+2} with AC to improve the adsorption of arsenate complexes from wastewater (Huang and Vane 1989). According to him, impregnated carbon has catalytic properties that promote synergism between activated carbon and impregnated material.

9.1.3 Efficient Removal of Inorganic Contaminants by Activated Charcoal

AC is readily available in different types such as PAC (packed AC), GAC (granular AC), and ACF (AC fiber) which are mostly used to remove organic pollutants such as dyes, inorganic metal ions, inorganic-pesticides, phenol-compounds, and many complex pollutants from wastewater. Encapsulated hulls of *Ceiba pentandra* are applied as AC to eliminate Hg^{2+} ions from wastewater (Rao et al. 2009). To their experience, they found more adsorption of 25.88 mg/L at pH 6.00. These studies are well pertinent with the Freundlich model and adsorption kinetics followed the pseudo-second-order model. Similarly, sulfuric acid-treated sago on activated carbon increased the elimination of Hg^{2+} ions at pH 5.00, which respect Langmuir equilibrium isotherm (Kadirvelu et al. 2004).

Many studies were carried out to eliminate arsenic contaminants from water using AC (Budinova et al. 2009; Kalderis et al. 2008). However, extracted AC from jute-stick and impregnated with iron was used for arsenic elimination (Asadullah et al. 2014). Here the iron oxide worked efficiently and changed the oxidation state of As (III) to As (V), which is adsorbed on its surface with 3.0 g/L, and the corresponding results are presented in Table 9.1. The AC loaded with iron oxide removes

Table 9.1 List of adsorbent materials used for the removal of pollutants from water

Pollutants	Adsorbent	Removing capacities	pH	References
Cd	Activated carbon (olive stone)	11.72 mg/g	–	Alslaibi et al. (2013) Wan et al. (2018)
	Hydrated manganese oxide nanoparticles coupled with biochar	53 mg/g		
Pb	AC (coconut buttons)	92.72 mg/g	–	Anirudhan and Sreekumari (2011) Wan et al. (2018)
	Hydrated manganese oxide nanoparticles coupled with biochar	94.5 mg/g		
	Ceria nanoparticles embedded in tamarind powder			
Cu	Activated carbon (coconut buttons)	73.60 mg/g	–	Anirudhan and Sreekumari (2011)
Hg(II)	Activated carbon (Ceiba pentandra hulls)	25.88 mg/g	6	Rao et al. (2009) Kadirvelu et al. (2004) Anirudhan and Sreekumari (2011) Pan et al. (2012)
	Activated carbon (sago industry waste)	55.6 mg/g	5	
	Activated carbon (coconut buttons)	78.84 mg/g		
	Mercapto-functionalized nanoscale Fe ₃ O ₄	522.9 mg/g		
As (V)	Iron-loaded activated carbon (jute stick)	3.0 µg/L	7	Asadullah et al. (2014) Yurum et al. (2014)
	Iron-loaded activated carbon (charcoal)	27.78 mg/g	7	
Diclofenac	Olive-waste cakes (activated carbon)	56.17 mg/g	–	Baccar et al. (2012)
Naproxen	Olive-waste cakes (activated carbon)	39.52 mg/g	–	Baccar et al. (2012)
Dyes	Copper oxide nanoparticles immobilized on activated carbon	172.42–212.79 mg/g	7.4–7.9	Ghaedi et al. (2019)
CV/MO	AgNPLs-AC	87.2 mg/g	7	Salam et al. (2017) Liu et al. (2019)
	Fe ₃ O ₄ -AC	150.35 mg/g		

99.90% of As (V) through a batch adsorption process within 5 minutes, and has a high adsorption rate of 27.78 mg/g at pH 7. It is also most suitable for Langmuir and pseudo-secondary kinetic models. Activated carbon is obtained from olivine by microwave treatment to remove Cd²⁺ ions in wastewater, which satisfies Langmuir and pseudo-second-order kinetics (Alslaibi et al. 2013). A list of adsorbents used for the expulsion of different metals is presented in Table 9.1. Coconut buttons are used to examine the adsorption process of heavy metals like Hg²⁺, Pb²⁺, and Cu²⁺. Good adsorption was shown for Pb²⁺ and Cu²⁺ at pH 6.0, whereas more adsorption of Hg²⁺ was monitored at pH 7.0 (Anirudhan and Sreekumari 2011) and these also satisfied Freundlich model and pseudo-second-order kinetics. Even Date Pit Activated Carbon (DPAC) was also used to extract Pb (II) from water. In the present work, phosphoric acid-embedded activated carbon was prepared and different parameters of DPAC such as structural, chemical, elemental, crystal, and surface nature were studied (Krishnamoorthy et al. 2019). The absorption capacity of DPAC towards Pb (II) was noted as 101.35 mg/g. The study also satisfied Langmuir and

pseudo-second order. The authors proved that DPAC can be reused four times before it loses its adsorption capacity and DPAC is also considered cost-effective. Similarly, high surface activated carbon from *Glycyrrhiza glabra* coupled with $ZnCl_2$ was prepared to remove Pb (II) and Ni (II) (Mohammadi et al. 2014). The adsorption of Pb (II) and Ni (II) was identified as 200 mg/g and 166.7 mg/g. Polyamidoxime modified magnetic activated carbon was used to adsorb the thallium and chromium (Adio et al. 2019).

9.1.4 Efficient Removal of Organic Contaminants by AC

Several research investigations were accomplished for the separation of industrial dyes from water. AC removed pollutants like trimethoprim, imidazole, and sulfonamides through the adsorption method (Mendez-Diaz et al. 2010). Similarly, 90% trimethoprim was removed using AC (Kim et al. 2010). Endocrine, a non-biodegradable compound, which cannot be removed by a conventional process, could be easily removed with the AC of natural products extractant (Baccar et al. 2012). In this observation, the adsorption processes also pursue the Langmuir model and pseudo-second-order adsorption kinetics. Lotus stalk-phosphorus activated carbon was used to remove oxyacids such as H_3PO_4 , $H_4P_2O_7$, HPO_3 , and H_3PO_3 . The sorption capacity was increased in the following manner $H_4P_2O_7 > H_3PO_4 > H_3PO_3 > HPO_3$, which respect both Langmuir and Freundlich models (Liu et al. 2012). These models describe specific binding sites that are restricted on the surface of the adsorbent, which forms a monolayer adsorbed molecules on its surface.

9.2 Nanomaterials as Adsorbents: Introduction

The emerging trend in water treatment is the use of nanomaterial-coated adsorbents for the successive expulsion of contaminants from wastewater. Nanomaterials, tiny in size of about 1–100 nm, are very active in removing pollutants from water. Nanotubes of carbon, titania nanotubes, ordered mesoporous carbon, grapheme, and carbon nanofibers are most popular nanomaterials which is efficiently used for wastewater treatment. The different structural properties, such as pore size, pore-volume, surface area, and porosity of their chemical composition and nanoparticles' thermal stability, depend on the synthesis and operating conditions. The nanoparticle synthesis methods are ion sputtering, sol-gel, mechanical milling, spray pyrolysis, impregnation, ion sputtering, chemical vapor deposition, etc. (Liu and Zhang 2007). The use of nanomaterials embedded with activated carbon in removing waste from water has gasped attention due to their small size. Nanoparticles were employed in many ways like metallic nanoparticles, magnetic nanoparticles, and metal oxide nanoparticles. Unique characteristics of these nanoparticles like small

size, high reactivity, large surface area with many pores, and high intermolecular force of attraction lead to more adsorption of pollutants from water than AC (Sadegh et al. 2017). The efficiency of nanoparticle embedded activated carbon is graphically presented in Fig. 9.1. Compared to bare activated carbon, nanoparticle encapsulated activated carbon shows high removal capacity since it can provide a large surface area, as shown in Fig. 9.1.

Many authors used the nanoparticles alone and nanoparticles embedded activated carbon to eliminate metals efficiently from water. As arsenic content in water can cause many diseases and sometimes leads to cancer, removing arsenic is crucial. Ethylenediamine-multiwall carbon nanotubes along with iron (III) were used for the expulsion of As (V) (Veličković et al. 2012). Similarly, the same kind of work presented in the literature (Tang et al. 2013) used magnesium ferrite nanoadsorbent to effectively remove As (V). Graphene is used as an adsorbent to purge certain dyes like methylene blue, methyl orange, phenols, and hydroquinones (Wang et al. 2016). Nanoadsorbents have shown remarkable success in removing hard biological pollutants (Nas et al. 2019). Cyanobacteria, which produce non-ribosomal peptides that are challenged to remove from water but by using carbon microtubules, can

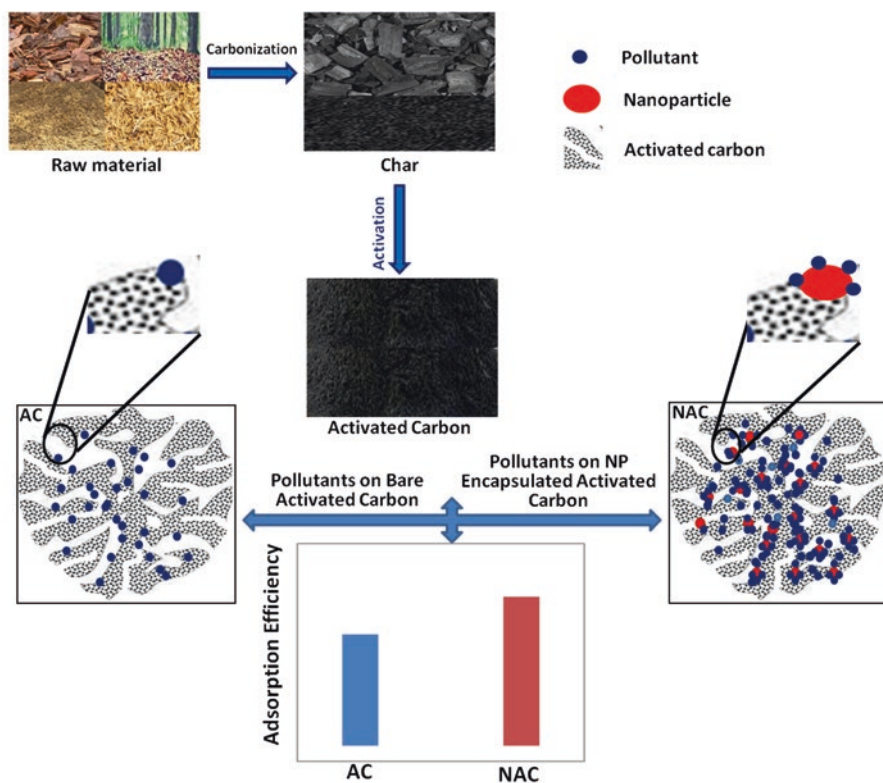


Fig. 9.1 Pictorial representation of adsorption efficiency of activated carbon and nanomaterial encapsulated activated carbon for removal of pollutants

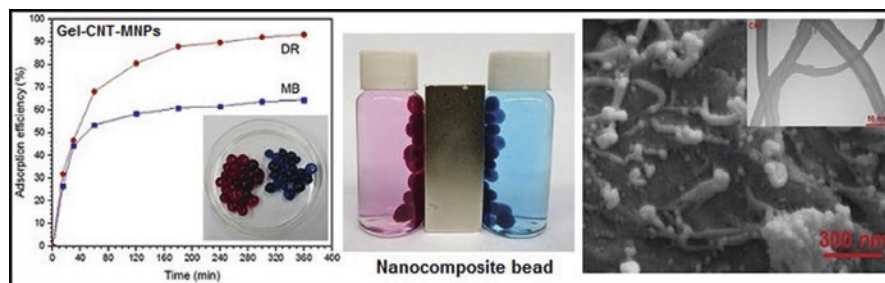


Fig. 9.2 Illustration of nanocomposite carbon bead for the adsorption of direct red 80 dye and methylene blue (Adapted and reproduced from reference Samandari et al. 2017 with the permission)

remove up to four times better and as much as 98% of contaminants (Yan et al. 2006). When nickel nanoparticles were covered in porous carbon or with carbon nanotube hybrids, the composites had a high surface area, large pore volume, and advanced graphitized wall, which worked excellently to remove many dyes such as malachite green, Congo red, rhodamine B, methylene blue, and methyl orange from water solution (Jin et al. 2018).

Similarly, gelatin-based -COOH modified multi-walled carbon nanotube (CNT) and embedded magnetic nanoparticles of iron oxide (MNPs) were used for the expulsion of direct red 80 dye (DR) and methylene blue dye (MB) (Samandari et al. 2017). Schematic description of nanocomposite bead usage in removal of dyes is presented in Fig. 9.2. By increasing the concentration of the solution, the adsorption of the dye on the magnetic nanocomposite beads can be enhanced, and the kinetic study follows the second-order model. The maximum adsorption identified was 96.1% DR and 76.3% MB.

A magnetic nanoporous carbon was prepared from carbon and iron salt to purge methylene blue (MB) from the aqueous solution. A significant change in the surface area of the material was observed through various surface characterization techniques. Greater adsorption of dye on adsorbent was noticed, and the used adsorbent was efficiently regenerated using ethanol. (Jiao et al. 2016).

9.2.1 Use of Nanomaterial Encapsulated Activated Carbon for the Removal of Inorganic Pollutants

The preparation of nanocomposite materials for the removal of waste from the water has drawn more attention in the current scientific era. A significant amount of Cd (II) was removed using $\text{EDTA@Fe}_3\text{O}_4$ loaded sawdust carbon as nanocomposites (Kataria and Garg 2018) as per the design shown in Fig. 9.3. Here in this work, first sawdust of poplar tree is converted into carbon, then coupled with EDTA and Fe_3O_4 to improve the adsorption capacity. The use of $\text{EDTA@Fe}_3\text{O}_4/\text{SC}$ showed better adsorption capacities when compare to $\text{Fe}_3\text{O}_4/\text{SC}$ at the same adsorbent dose. The

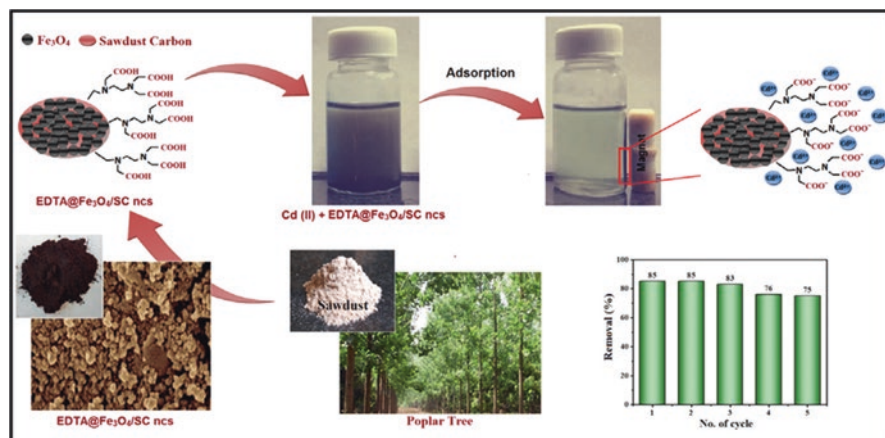


Fig. 9.3 EDTA@Fe₃O₄ loaded sawdust carbon as nanocomposite for the removal of cadmium (Adapted and reproduced from reference Kataria and Garg 2018 with the permission)

adsorption mechanism of C=O got disappeared indicating that EDTA used in this interacted with Cd (II). The chemical binding of Cd (II) involved in disappearance of carboxyl acid of C-O and O-H bonds. The study found that the Freundlich and Langmuir model were correctly fit for the removal of Cd (II) which also correlates with pseudo-second-order studies. According to their study, this work was considered eco-friendly, low cost for removing heavy metals using activated carbon.

Hydrated manganese oxide nanoparticles soaked in a peanut shell-evolved biochar were used to obtain an excellent nanocomposite to remove heavy metals (Wan et al. 2018). The comparative studies were carried out with biochar and hydrated manganese biochar to eliminate Pb (II) and Cd (II), which is presented in Fig. 9.4a. The results showed that hydrated manganese biochar showed 4–5 times higher ability in expelling Pb (II) and Cd (II) than biochar. The usage of activated charcoal coated titanate nanotubes (TNTs@PAC) was assessed to extract heavy metal, such as Pb (II). The faster adsorption of about 60 minutes was identified with a Langmuir extent of 318.5 mg/g through the mechanism depicted in Fig. 9.4b. Generally, natural organic matter (NOM) restricts the adsorption of metal ions over the TNT. When AC is coupled with TNT, NOM-Pb complexes, as well as free metal ions, are efficiently removed. Here, NOM-Pb is removed by charcoal, and TNT removes free metal ions. Moreover, the materials can be reused certain times by treating with EDTA (Ma et al. 2017).

Magnetic nanocomposites combined with activated carbon (NCAC) as sol-gel were used to remove Cr (VI) from wastewater. Magnetic properties of magnesium ferrite nanoparticles (MFNPs) were also tested and the corresponding mechanism is presented in Fig 9.4c. Different characterization methods were employed, such as FTIR, XRD, and SEM-EDX. The results showed that NCAC removed more amount of Cr (VI) when compared to MFNPs (Kaur et al. 2015). A mixture of pyrolyzed chestnut shell at 723 K with magnetic gelatin was used as biochar to remove As (V)

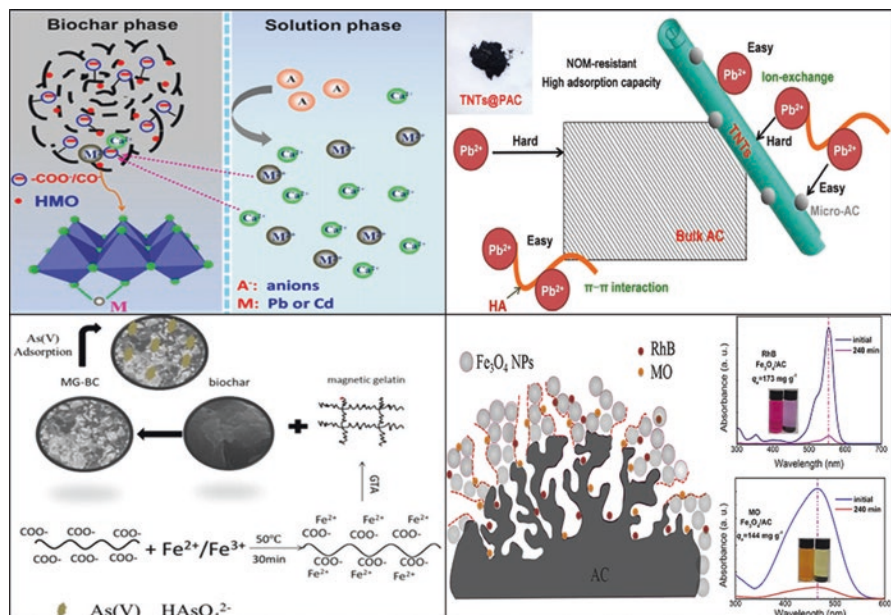


Fig. 9.4 (a) Removal of Pb (II) and Cd (II) with the help of hydrated manganese biochar (Adapted and reproduced from reference Wan et al. 2018 with the permission), (b) titanate nanotubes with PAC for the removal of lead (Adapted and reproduced from reference Ma et al. 2017 with the permission), (c) schematic illustration of chestnut shell with magnetic gelatin biochar for the removal of As(V). (Adapted and reproduced from reference Zhou et al. 2017 with the permission), (d) adsorption capacity of activated carbon immobilized with Fe₃O₄ nanoparticles (Adapted and reproduced from reference Liu et al. 2019 with the permission)

from industrial wastewater. The characterization was carried out with the help of VSM (vibrating sample magnetometer), FTIR, and XPS. The modified biochar has strong magnetic property, which removed As (V) from wastewater and showed an adsorption capacity as 45.8 mg/g correlated to unmodified biochar as 17.5 mg/g (Zhou et al. 2017).

Sewage sludge modified with nanostructured CaCO₃ (SSMNCB) was used as biochar to purge Cd (II) in aqueous solutions. The adsorption ability of adsorbent is well fitted to the Langmuir isotherm with the removal of Cd (II) with 36.5 mg/g (Zuo et al. 2017). It was also found that SSMNCB was very fast in removing Cd (II) compared to any other method. Nanopore and micropore activated carbon was prepared from *Limonia acidissima* shells (LASAC). Then it was modified chemically and thermally to enhance its adsorption extent. The scope of adsorption was identified as 3.2 mg/g for Cr (VI) and 2.7 mg/g for fluoride (Gaikwad and Balomajumder 2018). Expulsion of nitrate and phosphate from wastewater is carried out by handling nano-scale zero-valent iron functionalized with AC. Different composites of various mass were prepared and synthesized with ethanol medium, thermal treatment, acid treatment and both the treatments. The composite successfully increased

the efficiency of removal of nitrate by 50% and phosphate by 100%. This composite is also used to remove the hardness, humic acid, phosphorus, sulfate ions, etc. (Khalil et al. 2017).

9.2.2 Use of Nanomaterial Encapsulated Activated Carbon for the Removal of Organic Pollutants

Tannery dyes are one of the most pollution-causing substances released to water. These are very thick and take a very long time to undergo degradation. The efficiency of the removal of various dyes was increased by coupling the AC with copper oxide nanoparticles (Ghaedi et al. 2019). The equilibrium of these studies was followed Langmuir model and pseudo-second-order kinetics. The maximum adsorption capacity of copper oxide nanoparticles activated carbon for MG was 212.79 mg/g, RB 172.42 mg/g, and S was 149.25 mg/g. As well the study of the use of silver nanoparticles immobilized activated carbon for the expulsion of crystal violet dye worked effectively was also seen in the literature (Salam et al. 2017). The efficiency of AC-AgNPLs to remove crystal violet was more compared to AC. It also correctly fit in pseudo-second-order kinetics. Ferric oxide (Fe_3O_4) nanoparticle immobilized activated carbon has successfully used as an adsorbent for the removal of rhodamine B (rh B) and methyl orange (MO), and corresponding results were presented in Fig 9.4d. It shows the adsorption efficiency of $\text{Fe}_3\text{O}_4/\text{AC}$ for rh B and MO. The figure clearly describes the arrangement of Fe_3O_4 NPs on the surface of activated carbon which adsorbs rh B and MO with more percentage than activated carbon. Batch experiments were conducted which concluded that the adsorption capacity of rhB was 182.48 mg/g and MO was 150.35 mg/g, which also satisfies general order kinetic equation and Liu's isothermal model (Liu et al. 2019).

Phenols in the effluent can cause severe health hazards for both aquatic and human life. Magnetic cobalt nanoparticles functionalized on activated carbon (MCAC) used to remove phenols from waster (Mohammadi et al. 2020a, b). The removal efficiency has shown 107.5 mg/g, which also satisfies Langmuir, Freundlich models. One of the main components in the petroleum product is sulfur. Many conventional methods are employed for its removal, but it has several limitations. Adsorption through activated carbon shows a good result, but its efficiency has increased when this AC is coated with nanoparticles. Similarly, rubber tire activated carbon functionalized with copper nanoparticles efficiently removed the sulfur (Saleh 2018).

Activated carbon functionalized with copper sulfide nanorods (CuS-NRs-AC) were successfully prepared to remove malachite green and Pb^{2+} ions from wastewater. Various statistical designs were used to characterize CuS-NRs-AC through TEM, SEM-EDX, and XRD. Here in studies, MG and Pb^{2+} was removed with 3 and 25 mg/L, respectively (Sharif et al. 2018). The adsorption efficiency pursued Langmuir isotherm with pseudo-second-order kinetics in the removal of MG and

Pb^{2+} as 145.98 and 47.892 mg/g, accordingly. Similarly, the use of Ni-doped ferric oxy-hydroxide nanowires (Ni:FeO(OH)-NWs) embedded on activated carbon successfully removed Safranin-O (SO) and Indigo Carmine (IC) (Dastkhooon et al. 2017). The adsorption ability of SO was 37.85 mg/g and IC was 29.09 mg/g, which also satisfied Freundlich and pseudo-second order kinetic models.

A template of the metallic organic framework of nanostructured porous carbon material was handled to remove malachite green (MG) from the aqueous solution. The porosity, structure, magnetic, and morphology properties were analyzed using TEM, SEM, XRD, Raman spectroscopy, XPS, and VSM for surface area analysis. The adsorption of dyes was 499 mg/g at 30 °C and 863 mg/g at 60 °C. The pseudo-second order and Langmuir isotherm model were exceptionally suited to the adsorption system (Zang et al. 2015). A combination of polymer and biomass waste was functionalized with activated carbon used as adsorbent to purge ethyl acetate from water. The high adsorption capacity was noted with a range of 160–450 mg/g, which fitted into Langmuir model and Freundlich model. The removal of ethyl acetate depends on surface area provided by activated carbon (Stoycheva et al. 2016).

A nonzero valent combined with activated carbon (nZVI/GAC) was prepared (Hu et al. 2015) to remove nitrobenzene from the aqueous solution. Nonzero valent iron was uniformly distributed on the surface of granular activated carbon, removing 85% of nitrobenzene. An aggregation of strontium hexaferrite on to the surface of magnetic sewage sludge biochar was prepared to remove malachite green (MG) (Zang et al. 2016). It accurately fits with pseudo-second-order kinetic model. The reduced graphene oxide (rGO) coupled with activated charcoal was prepared to purge methylene blue (MB) dye (Riaz et al. 2020). Single use of reduced rGO, exposed to surface area, was hindering with electrolyte diffusion, so to eliminate this issue, activated charcoal was spaced on rGO sheets, which enhanced porosity, conductivity, and concentration of active sites to trap MB. This technique demonstrated the removal of 99% of methylene blue from water within 60 minutes of time period. Coconut shell activated carbon functionalized with active manganese oxide was used to remove azo dyes from water through hydrothermal method. The morphology of MnO_x @CSAC was changed through hydrothermal treatment led to in situ synthesis. MnO_x @CSAC removed 99% of azo dye at pH 3.0 and the same was confirmed by GC-MS analysis. It also removed other anionic dyes at 89.72–99.1% effectively (Xu et al. 2014). In another work, magnetic Co nanoparticles were introduced into the activated carbon (MAC/Co) by the co-precipitation method and removed cadmium (II) and methylene blue. The ability of adsorption for methylene blue and Cd (II) ion were observed as 192.3 and 123.5 mg/g, accordingly, within a short run time of 30 min (Mohammadi et al. 2020a, b). In contrast to the above works, recently, carbon-encapsulated MnFe_2O_4 nanoparticles (MFO) were used for the elimination of Cr (VI). The presence of carbon in MFO increases the elimination capacity of Cr (VI) to the maximum of 90.1% with the values 73.6 mg/g (Tuyen et al. 2020) represented in Table 9.2.

All studies' results revealed that nanoparticle encapsulated active carbon (NP/AC) were proved as an efficient adsorbent by providing more surface area through the accommodation of nanoparticles in its porous structure. The adsorption of

Table 9.2 Removal of pollutants using nanomaterials encapsulated activated carbon

Pollutant	Adsorbent	Removal efficiency	References
Cr (VI)	Carbon-encapsulated MnFe ₂ O ₄	73.6 mg/g	Tuyen et al. (2020)
Cd (II)	MAC/Co	123.5 mg/g	Mohammadi et al. (2020a, b)
Methylene blue		192.3 mg/g	
Methylene blue	rGO with activated charcoal	99%	Riaz et al. (2020)
rhB	Fe ₃ O ₄ NPs	182.48 mg/g	Liu et al. (2019)
Methyl Orange		150.35 mg/g	
Methylene blue	Pt-Co@GO	273.6 mg/g	Nas et al. (2019)
MG, CR, RB, MB and MO	Ni/PC-CNT	898,818, 395,312 and 271 mg/l	Jin et al. (2018)
Cd (II)	EDTA@ Fe ₃ O ₄ /SC	63 mg/g	Kataria and Garg (2018)
Cr (VI), fluoride	LASAC	3.2 mg/g, 2.7 mg/g	Gaikwad and Balomajumder (2018)
MG, Pb ²⁺	CuS-NRs-AC	145.98 mg/g, 47.892 mg/g	Sharif et al. (2018)
SO, IC	Ni:FeO(OH)-NWs	37.85 mg/g, 29.09 mg/g	Dastkhooon et al. (2017)
As (V)	Pyrolyzed chestnut magnetic gelatin	45.8 mg/g	Zhou et al. (2017)
Pb (II)	TNTs@PAC	318.5 mg/g	Ma et al. (2017)

pollutants over these NP/AC depends on types of interaction present between them, the amount of both active carbon and the size of nanoparticles besides the conventional parameters, i.e., and pH, temperature, and contact time. However, there is a demand to promote economical blended adsorbents on a large scale to treat wastewater generated by industries.

9.2.3 Challenges and Future Perspectives

Adsorption is one of the primary mechanisms for the elimination of pollutants from water. In this process, activated carbon plays a critical and widespread role as an efficient adsorbent. The efficiency of activated carbon is enriched by including the nanomaterials with different names and dimensions such as nanotubes, fullerene, mesoporous carbon, and graphene (Wang et al. 2013). Compared to other industries, stability is more important in environmental applications as metal-based nanomaterial leads to secondary contamination formation through leaching (Saputra et al. 2013). The great challenge focuses on manipulating nanomaterials with activated carbon, which might result in environmental pollution. Several authors reported that fullerenes were accumulated in rice seedlings and their vascular tissues (Lin et al. 2009). The presence of graphene in the soil reduced soil enzymes'

activity, resulting in microbes' antimicrobial properties (Chung et al. 2015). The emerging nano pollution needs to be monitored and addressed by developing environmentally friendly sustainable environment methods.

9.3 Conclusions

Past number of decades, one of the world's major global concerns is water pollution due to the expansion of agriculture, industries, and population growth. Many innovative attempts suggest that adsorption is one of the efficient methods in water treatment. Adopting activated carbon is an established method for eliminating pollutants, which to some extent works but not to the mark. When this activated carbon was encapsulated, impregnated, or fabricated with nanomaterials or nanoparticles, the efficiency rate has increased dramatically to remove organic and inorganic pollutants.

References

- Adio, S. O., Asif, M., Mohammed, A. R. I., Baig, N., Arfaj, A. A., & Saleh, T. A. (2019). Poly (amidoxime) modified magnetic activated carbon for chromium and thallium adsorption: Statistical analysis and regeneration. *Process Safety and Environmental Protection*, 121, 254–262. <https://doi.org/10.1016/j.psep.2018.10.008>.
- Ahn, C. K., Kim, Y. M., Woo, S. H., & Park, J. M. (2009). Removal of cadmium using acid-treated activated carbon in the presence of nonionic and/or anionic surfactants. *Hydrometallurgy*, 99, 209–213. <https://doi.org/10.1016/j.hydromet.2009.08.008>.
- Ali, I., Asim, M., & Khan, T. A. (2012). Low cost adsorbents for the removal of organic pollutants from wastewater. *Journal of Environmental Management*, 113, 170–183. <https://doi.org/10.1016/j.jenvman.2012.08.028>.
- Ali, M. E., Hoque, M. E., Hossain, S. K. S., & Biswas, M. C. (2020). Nanoadsorbents for wastewater treatment: Next generation biotechnological solution. *International journal of Environmental Science and Technology*, Review. <https://doi.org/10.1007/s13762-020-02755-4>.
- Alslaibi, T. M., Abustan, I., Ahmad, M. A., & Foul, A. A. (2013). Cadmium removal from aqueous solution using microwaved olive stone activated carbon. *Journal of Environmental Chemical Engineering*, 1, 589–599. <https://doi.org/10.1016/j.jece.2013.06.028>.
- Anirudhan, T. S., & Sreekumari, S. S. (2011). Adsorptive removal of heavy metal ions from industrial effluents using activated carbon derived from waste coconut buttons. *Journal Environmental Sciences*, 23, 1989–1998. [https://doi.org/10.1016/S1001-0742\(10\)60515-3](https://doi.org/10.1016/S1001-0742(10)60515-3).
- Asadullah, M., Jahan, I., Ahmed, M. B., Adawiyah, P., Malek, N. H., & Rahman, M. S. (2014). Preparation of microporous activated carbon and its modification for arsenic removal from water. *Journal of Industrial Engineering Chemistry*, 20, 887–896. <https://doi.org/10.1016/j.jiec.2013.06.019>.
- Baccar, R., Sarra, M., Bouzid, J., Feki, M., & Blaquez, P. (2012). Removal of pharmaceutical compounds by activated carbon prepared from agricultural by-product. *Chemical Engineering Journal*, 211, 310–317. <https://doi.org/10.1016/j.cej.2012.09.099>.
- Bansal, R. P., Donnet, J. P., & Stoeckli, F. (1988). *Active carbon*. New York: Marcel Dekker. <https://doi.org/10.1080/01932699008943255>.

- Bhatnagar, A., Hogland, W., Marques, M., & Sillanpaa, M. (2013). An overview of the modification methods of activated carbon for its water treatment applications. *Chemical Engineering Journal*, 219, 499–511. <https://doi.org/10.1016/j.cej.2012.12.038>.
- Budinova, T., Savova, D., Tsyntarski, B., Ania, C. O., Cabal, B., Parra, J. B., & Petrov, N. (2009). Biomass waste-derived activated carbon for the removal of arsenic and manganese ions from aqueous solutions. *Applied Surface Science*, 255, 4650–4657. <https://doi.org/10.1016/j.apusc.2008.12.013>.
- Cheng, W., Dastgheib, S. A., & Karanfil, T. (2005). Adsorption of dissolved natural organic matter by modified activated carbons. *Water Research*, 39, 2281–2290. <https://doi.org/10.1016/j.watres.2005.01.031>.
- Chung, H., Kim, M. J., Ko, K., Kim, J. H., Kwon, H., Hong, I., Park, N., Lee, S., & Kim, W. (2015). Effects of graphene oxides on soil enzyme activity and microbial biomass. *Science of the Total Environment*, 514, 307–313. <https://doi.org/10.1016/j.scitotenv.2015.01.077>.
- Dastkhooon, M., Ghaedi, M., Asfaram, A., Azghandi, M. H. A., & Purkait, M. K. (2017). Simultaneous removal of dyes onto nanowires adsorbent use of ultrasound assisted adsorption to clean waste water: Chemometrics for modeling and optimization, multicomponent adsorption and kinetic study. *Chemical Engineering Research and Design*, 124, 222–237. <https://doi.org/10.1016/j.cherd.2017.06.011>.
- Faria, P. C., Orfao, J. J., & Pereira, M. F. (2004). Adsorption of anionic and cationic dyes on activated carbons with different surface chemistries. *Water Research*, 38, 2043–2052. <https://doi.org/10.1016/j.watres.2004.01.034>.
- Gaikwad, M. S., & Balomajumder, C. (2018). Removal of Cr (VI) and fluoride by membrane capacitive deionization with nanoporous and microporous Limonia acidissima (wood apple) shell activated carbon electrode. *Separation and Purification Technology*, 195, 305–313. <https://doi.org/10.1016/j.seppur.2017.12.006>.
- Ghaedi, A. M., Karamipour, S., Vafaei, A., Baneshi, M. M., & Kiarostami, V. (2019). Optimization and modeling of simultaneous ultrasound-assisted adsorption of ternary dyes using copper oxide nanoparticles immobilized on activated carbon using response surface methodology and artificial neural network. *Ultrasonics-Sonochemistry*, 51, 264–280. <https://doi.org/10.1016/j.ultsonch.2018.10.007>.
- Han, S., Kim, S., Lim, H., Choi, W., Park, H., Yoon, J., & Hyson, T. (2003). New nanoporous carbon materials with high adsorption capacity and rapid adsorption kinetics for removing humic acids. *Microporous Mesoporous Materials*, 58, 131–135. [https://doi.org/10.1016/S1387-1811\(02\)00611-X](https://doi.org/10.1016/S1387-1811(02)00611-X).
- Hu, S., Yao, H., Wang, K., Lu, C., & Wu, Y. (2015). Intensify removal of nitrobenzene from aqueous solution using nano-zero valent iron/granular activated carbon composite as Fenton-like catalyst. *Water, Air & Soil Pollution*, 226(155), 1–13. <https://doi.org/10.1007/s11270-015-2421-7>.
- Huang, C. P., & Vane, L. M. (1989). Enhancing As⁵⁺ removal by a Fe²⁺-treated activated carbon. *Research Journal of Water Pollution Control Federation*, 61, 1596–1603. <https://www.jstor.org/stable/25043776>.
- Jiao, C., Wang, Y., Li, M., Wu, Q., Wang, C., & Wang, Z. (2016). Synthesis of magnetic nanoporous carbon from metal-organic framework for the fast removal of organic dye from aqueous solution. *Journal of Magnetism and Magnetic Materials*, 407, 24–30. <https://doi.org/10.1016/j.jmmm.2016.01.031>.
- Jin, L., Zhao, X., Qian, X., & Dong, M. (2018). Nickel nanoparticles encapsulated in porous carbon and carbon nanotube hybrids from bimetallic metal-organic-frameworks for highly efficient adsorption of dyes. *Journal of Colloid and Interface Science*, 509, 245–253. <https://doi.org/10.1016/j.jcis.2017.09.002>.
- Kadirvelu, K., Kavipriya, M., Karthika, C., Vennilamani, N., & Pattabhi, S. (2004). Mercury(II) adsorption by activated carbon made from sago waste. *Carbon*, 42, 745–752. <https://doi.org/10.1016/j.carbon.2003.12.089>.
- Kalderis, D., Koutoulakis, D., Paraskeva, P., Diamadopoulos, E., Otal, E., del Valle, J. O., & Fernández-Pereira, C. (2008). Adsorption of polluting substances on activated carbon prepared

- from rice husk and sugarcane bagasse. *Chemical Engineering Journal*, 144, 42–50. <https://doi.org/10.1016/j.cej.2008.01.007>.
- Kataria, N., & Garg, V. K. (2018). Green synthesis of Fe₃O₄ nanoparticles loaded sawdust carbon for cadmium (II) removal from water: Regeneration and mechanism. *Chemosphere*, 208, 818–828. <https://doi.org/10.1016/j.chemosphere.2018.06.022>.
- Kaur, M., Kaur, N., Jeet, K., & Kaur, P. (2015). MgFe₂O₄ nanoparticles loaded on activated charcoal for effective removal of Cr (VI)—A novel approach. *Ceramics International*, 41, 13739–13750. <https://doi.org/10.1016/j.ceramint.2015.08.040>.
- Khalil, A. M. E., Eljamal, O., Amen, T. W. M., Sugihara, Y., & Matsunga, N. (2017). Optimized nano-scale zero-valent iron supported on treated activated carbon for enhanced nitrate and phosphate removal from water. *Chemical Engineering Journal*, 309, 349–365. <https://doi.org/10.1016/j.cej.2016.10.080>.
- Kim, S. H., Shon, H. K., & Ngo, H. H. (2010). Adsorption characteristics of antibiotics trimethoprim on powdered and granular activated carbon. *Journal of Industrial Engineering Chemistry*, 16, 344–349. <http://hdl.handle.net/10453/13591>.
- Krishnamoorthy, R., Govindan, B., Banat, F., Sagadevan, V., Purushothaman, & Show, P. L. (2019). Date pits activated carbon for divalent lead ions removal. *Journal of Bioscience and Bioengineering*, 128, 88–97. <https://doi.org/10.1016/j.jbiosc.2018.12.011>.
- Lin, S., Reppert, J., Hu, Q., Hudson, J. S., Reid, M. L., Ratnikova, T. A., Rao, A. M., Luo, H., & Ke, P. C. (2009). Uptake, translocation and transmission of carbon nanomaterials in rice plants. *Small*, 5, 1128–1132. <https://doi.org/10.1002/smll.200801556>.
- Liu, H., Zhang, J., Bao, N., Cheng, C., Ren, L., & Zhang, C. L. (2012). Textural properties and surface chemistry of lotus stalk-derived activated carbons prepared using different phosphorus oxyacids: Adsorption of trimethoprim. *Journal of Hazardous Materials*, 235, 367–375. <https://doi.org/10.1016/j.jhazmat.2012.08.015>.
- Liu, P., & Zhang, L. X. (2007). Adsorption of dyes from aqueous solutions or suspensions with clay nano-adsorbents. *Separation and Purification Technology*, 58(1), 32–39. <https://doi.org/10.1016/j.seppur.2007.07.007>.
- Liu, X., Tian, J., Li, Y., Sun, N., Mi, S., Xie, Y., & Chen, Z. (2019). Enhanced dyes adsorption from waste water via Fe₃O₄ nanoparticles functionalized activated carbon. *Journal of Hazardous Materials*, 373, 397–407. <https://doi.org/10.1016/j.jhazmat.2019.03.103>.
- Lizzio, A. A., Jiang, H., & Radovic, L. R. (1990). On the kinetics of carbon (char) gasification—Reconciling models with experiments. *Carbon*, 28, 7–19. [https://doi.org/10.1016/0008-6223\(90\)90087-F](https://doi.org/10.1016/0008-6223(90)90087-F).
- Lukens, W. W. (2007). *Modified activated carbon perchlorate sorbents*. Berkeley: Lawrence Berkeley National Laboratory.
- Ma, J., Li, F., Qian, T., Liu, H., Liu, W., & Zhao, D. (2017). Natural organic matter resistant powder activated charcoal supported titanate nanotubes for adsorption of Pb (II). *Chemical Engineering Journal*, 315, 191–200. <https://doi.org/10.1016/j.cej.2017.01.029>.
- Mendez-Diaz, J. D., Prados-Joya, G., Rivera-Utrilla, J., Leyva-Ramos, R., Sanchez-Polo, M., Ferro-Garcia, M. A., & Medellin-Castillo, N. A. (2010). Kinetic study of the adsorption of nitroimidazole antibiotics on activated carbons in aqueous phase. *Journal of Colloid Interface Science*, 345, 481–490. <https://doi.org/10.1016/j.jcis.2010.01.089>.
- Miyanaga, S., Hiwara, A., & Yasuda, H. (2002). Preparation and high bacteriostatic action of the activated carbons possessing ultrafine silver particles. *Science and Technology of Advanced Materials*, 3, 103–109. [https://doi.org/10.1016/S1468-6996\(02\)00014-1](https://doi.org/10.1016/S1468-6996(02)00014-1).
- Mohammadi, S. Z., Darijani, Z., & Karimi, M. A. (2020b). Fast and efficient removal of phenol by magnetic activated carbon cobalt nanoparticles. *Journal of Alloys and Compounds*, 832, 154942. <https://doi.org/10.1016/j.jallcom.2020.154942>.
- Mohammadi, S. Z., Hamidani, H., & Moinadini, Z. (2014). High surface area-activated carbon from Glycyrrhiza glabra residue by ZnCl₂ activation for removal of Pb (II) and Ni (II) from water samples. *Journal of Industrial and Engineering Chemistry*, 20, 4112–4118. <https://doi.org/10.1016/j.jiec.2014.01.009>.

- Mohammadi, S. Z., Mofidinasab, N., Karimi, M. A., & Beheshti, A. (2020a). Removal of methylene blue and Cd(II) by magnetic activated carbon–cobalt nanoparticles and its application to wastewater purification. *International Journal of Environmental Science and Technology*, 63. <https://doi.org/10.1007/s13762-020-02767-0>.
- Nas, M. S., Calimli, M. H., Burhan, H., Yilmaz, M., Mustafav, S. D., & Sen, F. (2019). Synthesis, characterization, kinetics and adsorption properties of Pt-Co@ GO nano-adsorbent for methylene blue removal in the aquatic mediums using ultrasonic process systems. *Journal of Molecular Liquids*, 296, 112–100. <https://doi.org/10.1016/j.molliq.2019.112100>.
- Pan, S., Shen, H., Xu, Q., Luo, J., & Hu, M. (2012). Surface mercapto engineered magnetic Fe₃O₄ nanoadsorbent for the removal of mercury from aqueous solutions. *Journal of Colloid Interface Science*, 365, 204–212. <https://doi.org/10.1016/j.jcis.2011.09.002>.
- Pezoti, O., Cazetta, A. L., Bedin, K. C., Souza, L. S., Martins, A. C., Silva, T. L., Santos Junior, O. O., Visentainer, J. V., & Almeida, V. C. (2016). NaOH-activated carbon of high surface area produced from guava seeds as a high-efficiency adsorbent for amoxicillin removal: Kinetic, isotherm and thermodynamic studies. *Chemical Engineering Journal*, 288, 778–788. <https://doi.org/10.1016/j.cej.2015.12.042>.
- Przepiorski, J. (2006). Enhanced adsorption of phenol from water by ammonia-treated activated carbon. *Journal of Hazardous Materials*, 135, 453–456. <https://doi.org/10.1016/j.jhazmat.2005.12.004>.
- Rao, M. M., Reddy, D. H. K. K., Venkateswarlu, P., & Seshaiiah, K. (2009). Removal of mercury from aqueous solutions using activated carbon prepared from agricultural by-product/waste. *Journal of Environmental Management* 90(1):634–643. <https://doi.org/10.1016/j.jenvman.2007.12.019>.
- Riaz, R., Ali, M., Maiyalagan, T., Arbab, A. A., Anjum, A. S., Lee, S., Ko, M. J., & Jeong, S. H. (2020). Activated charcoal and reduced graphene sheets composite structure for highly electro-catalytically active counter electrode material and water treatment. *International Journal of Hydrogen Energy*, 45, 7751–7763. <https://doi.org/10.1016/j.ijhydene.2019.06.138>.
- Sadegh, H., Ali, G. A. M., Gupta, V. K., Makhlof, A. H., Goshekandi, R. S., Nadagouda, M. N., Sillanpaa, M., & Megiel, E. (2017). The role of nanomaterials as effective adsorbents and their applications in waste water treatment. *Journal of Nanostructure in Chemistry*, 7, 1–14. <https://doi.org/10.1007/s40097-017-0219-4>.
- Salam, A. H. A., Ewais, H. S., & Basaleh, A. S. (2017). Silver nanoparticles immobilized on the activated carbon as efficient adsorbent for removal of crystal violet dye from aqueous solutions. A kinetic study. *Journal of Molecular Liquids*, 248, 833–841. <https://doi.org/10.1016/j.molliq.2017.10.109>.
- Saleh, T. A. (2018). Simultaneous adsorptive desulfurization of diesel fuel over bimetallic nanoparticles loaded on activated carbon. *Journal of Cleaner Production*, 177, 2123–2132. <https://doi.org/10.1016/j.jclepro.2017.11.208>.
- Samandari, S. S., Samandari, S. S., Yekta, H. J., & Mohseni, M. (2017). Adsorption of anionic and cationic dyes from aqueous solution using gelatin-based magnetic nanocomposite beads comprising carboxylic action functionalized carbon nanotube. *Chemical Engineering Journal*, 308, 1133–1144. <https://doi.org/10.1016/j.cej.2016.10.017>.
- Saputra, E., Muhammad, S., Sun, H. Q., Ang, H. M., Tade, M. O., & Wang, S. B. (2013). Different crystallographic one-dimensional MnO₂ nanomaterials and their superior performance in catalytic phenol degradation. *Environment Science & Technology*, 47, 5882–5887. <https://doi.org/10.1021/es400878c>.
- Shaarani, F. W., & Hameed, B. H. (2011). Ammonia-modified activated carbon for the adsorption of 2,4-dichlorophenol. *Chemical Engineering Journal*, 169, 180–185. <https://doi.org/10.1016/j.cej.2011.03.002>.
- Sharif, P. E., Khafri, H. Z., Ghaedi, M., Asfaram, A., & Jannesar, R. (2018). Isotherms and kinetic study of ultrasound-assisted adsorption of malachite green and Pb²⁺ ions from aqueous samples by copper sulfide nanorods loaded on activated carbon: Experimental design optimization. *Ultrasonics-Sonochemistry*, 40, 373–382. <https://doi.org/10.1016/j.ultsonch.2017.07.030>.

- Sing, K. S. W., Rouquerol, J., & Rouquerol, F. (1998). *Adsorption by powders and porous solids*. San Diego, USA: Academic Press. <https://doi.org/10.1016/C2010-0-66232-8>.
- Stoycheva, I. G., Tsyntsarski, B. G., Petrova, B. N., Kumaneck, B., Budhinova, T. K., & Petrov, N. V. (2016). Adsorption of ethyl acetate from water by nanoporous carbon prepared from waste materials. *Water Air & Soil Pollution*, 227, 452. <https://doi.org/10.1007/s11270-016-3099-1>.
- Sweetman, M. J., May, S., Mebberson, N., Pendleton, P., Vasilev, K., Plush, S. E., & Hayball, J. D. (2017). Activated carbon, carbon nanotubes and graphene: Materials and composites for advanced water purification. *Journal of Carbon Research*, 18, 1–29. <https://doi.org/10.3390/c3020018>.
- Tang, W., Su, Y., Li, Q., Gao, S., & Shang, J. K. (2013). Superparamagnetic magnesium ferrite nano-adsorbent for effective arsenic (III, V) removal and easy magnetic separation. *Water Research*, 47, 3624–3634. <https://doi.org/10.1016/j.watres.2013.04.023>.
- Tchomgui-Kamga, E., Alonzo, V., Nansou-Njiki, C. P., Audebrand, N., Ngameni, E., & Darchen, A. (2010). Preparation and characterization of charcoals that contain dispersed aluminum oxide as adsorbents for removal of fluoride from drinking water. *Carbon*, 48, 333–343. <https://doi.org/10.1016/j.carbon.2009.09.034>.
- Tuyen, T. V., Chi, N. K., Tien, D. T., Nguyen, T., Quang, N. V., & Huong, P. T. L. (2020). Carbon-encapsulated MnFe₂O₄ nanoparticles: Effects of carbon on structure, magnetic properties and Cr(VI) removal efficiency. *Applied Physics A*, 126, 577. <https://doi.org/10.1007/s00339-020-03760-7>.
- Vaughan, R. L., Jr., & Reed, B. E. (2005). Modeling As (V) removal by an iron oxide impregnated activated carbon using the surface complexation approach. *Water Research*, 39, 1005–1014. <https://doi.org/10.1016/j.watres.2004.12.034>.
- Veličković, Z., Vuković, G. D., Marinković, A. D., Moldovan, M. S., Perić-Grujić, A. A., Uskoković, P. S., & Ristić, M. D. (2012). Adsorption of arsenate on iron (III) oxide coated ethylenediamine functionalized multiwall carbon nanotubes. *Chemical Engineering Journal*, 181–182, 174–181. <https://doi.org/10.1016/j.cej.2011.11.052>.
- Wan, S., Wu, J., Zhou, S., Wang, R., Gao, B., & He, F. (2018). Enhanced lead and cadmium removal using biochar-supported hydrated manganese oxide (HMO) nanoparticles: Behavior and mechanism. *Science of the Total Environment*, 616–617, 1298–1306. <https://doi.org/10.1016/j.scitotenv.2017.10.188>.
- Wang, S. B., Sun, H. Q., Ang, H. H., & Tade, M. O. (2013). Adsorptive remediation of environmental pollutants using novel graphene-based nanomaterials. *Chemical Engineering Journal*, 226, 336–347. <https://doi.org/10.1016/j.cej.2013.04.070>.
- Wang, Y., Mo, Z., Zhang, P., Zhang, C., Han, L., Guo, R., Gou, H., Wei, X., & Hu, R. (2016). Synthesis of flower-like TiO₂ microsphere/grapheme composite for removal of organic dye from water. *Materials & Design*, 5(99), 378–388. <https://doi.org/10.1016/j.matdes.2016.03.066>.
- Wigmans, T. (1986). Fundamentals and practical implications of activated carbon production by partial gasification of carbonaceous materials. In *Proceedings of the NATO advanced study institute on carbon and coal gasification*. Leiden: Martinus Nijhoff Publishers.
- Xu, L., Li, X., Ma, J., Wen, Y., & Liu, W. (2014). Nano-MnO_x on activated carbon prepared by hydrothermal process for fast and highly efficient degradation of azo dyes. *Applied Catalysis A: General*, 485, 91–98. <https://doi.org/10.1016/j.apcata.2014.07.041>.
- Yan, H., Gong, A., He, H., Zhou, J., Wei, Y., & Lv, L. (2006). Adsorption of microcystins by carbon nanotubes. *Chemosphere*, 62, 142–148. <https://doi.org/10.1016/j.chemosphere.2005.03.075>.
- Yeddou, A. R., Chergui, S., Chergui, A., Halet, F., Hamza, A., Nadjemi, B., Ould-Driss, A., & Belkouch, J. (2011). Removal of cyanide in aqueous solution by oxidation with hydrogen peroxide in presence of copper-impregnated activated carbon. *Minerals Engineering*, 24, 788–793. <https://doi.org/10.1016/j.mineng.2011.02.012>.
- Yurum, A., Kocabas-Atakli, Z. O., Sezen, M., Semiat, R., & Yurum, Y. (2014). Fast deposition of porous iron oxide on activated carbon by microwave heating and arsenic (V) removal from water. *Chemical Engineering Journal*, 242, 321–332. <https://doi.org/10.1016/j.mineng.2011.02.012>.

- Zang, C., Ye, F., Shen, S., Xiong, Y., Su, L., & Zhao, S. (2015). From metal-organic frameworks to magnetic nanostructured porous carbon composites: Towards highly efficient dye removal and degradation. *RSC Advances*, 5, 8228–8235. <https://doi.org/10.2166/wst.2016.386>.
- Zang, J., Liu, M., Yang, T., Yang, K., & Wang, H. (2016). A novel magnetic biochar from sewage sludge: Synthesis and its application for the removal of malachite green from wastewater. *Water Science Technology*, 74, 1971–1979. <https://doi.org/10.2166/wst.2016.386>.
- Zhou, Z., Liu, Y., Liu, S., Liu, H., Zeng, G., Tan, X., Yang, C., Ding, Y., Yan, Z., & Cai, X. (2017). Sorption performance and mechanisms of arsenic (V) removal by magnetic gelatin-modified biochar. *Chemical Engineering Journal*, 314, 223–231. <https://doi.org/10.1016/j.cej.2016.12.113>.
- Zuo, W., Chen, C., Cui, H., & Fu, M. (2017). Enhanced removal of Cd (II) from aqueous solution using CaCO₃ nanoparticle modified sewage sludge biochar. *RSC Advances*, 7, 16238–16243. <https://doi.org/10.1039/C7RA00324B>.

Chapter 10

Adsorption of Metals Using Activated Carbon Derived from Coal



Parag Girhe, Divya Barai, and Bharat Bhanvase

10.1 Introduction

Coal is a hard rock and an important solid fossil fuel. It is mostly made of carbon, but nitrogen, hydrogen, sulphur, and oxygen are also present in it (Blander et al. 1989). It is heterogeneous organic rock that includes mineral matter. It is a main source of energy for electricity production. Gasification and liquefaction of coal results into fuels (gases and liquids). However, utilization of coal as energy source may cause several health and environmental problems. Besides, it is also used as an energy source and it may be used as a valuable material in many pollution control process. This is because it is inexpensive material and easily found at many localities.

Outstanding adsorption properties of coal make it an attractive alternative for removing various inorganic and organic pollutants (Simate et al. 2016). Structure properties such as surface area, pore volume, and surface chemical composition influence physicochemical behaviour of coal making it applicable in many systems. Arpa et al. (Arpa et al. 2000) investigated low-rank coal for adsorption of different metals in wastewater received from mining plant and found promising results. Lakatos et al. (Lakatos et al. 2002) used wide range of coal to determine the characteristic of chromium removal with a purpose of reducing and removing chromium from effluent using coal.

The main sources of water pollution affecting our health and environment include industries like metal processing industries, chemical industry, mineral industry, waste management, and industries related to energy and fuel combustion. Indeed, industries tend to use great amounts of water and large-scale chemical inputs along with inefficient wastewater treatment methods resulting into large amounts of wastewater containing minerals and environmental pollutants. The metals present in

P. Girhe · D. Barai · B. Bhanvase (✉)

Department of Chemical Engineering, Laxminarayan Institute of Technology, Rashtasant Tukadoji Maharaj Nagpur University, Nagpur, MS, India

effluents are dangerous for the environment. In fact, they possess high toxicity and are prone to food accumulation, leading to various diseases, and are often carcinogenic in nature. For instance, lead (Pb) damages the liver, nervous system, and kidney, cadmium (Cd) causes respiratory diseases, and prolonged exposure to it can cause anaemia. Nickels leads to skin dermatitis, pulmonary fibrosis, and lung cancer, and zinc is important, but its excessive consumption leads to intestinal distress and diarrhoea. Even a small amount of metal such as chromium (Cr), arsenic (As), copper (Cu), mercury (Hg), lead (Pb), and cadmium (Cd) in drinking water and in effluent is very dangerous. In India, current permissible limit (ppm or mg/mL) for Cr, Cd, Cu, Ni, Zn, Pb, Hg, and As are 0.05, 0.01, 0.25, 0.20, 0.80, 0.006, 0.00003, and 0.050, respectively (Gopalakrishnan et al. 2015). Increase in the use of metals in industry accounts for increased amount of metals in natural water resources. Therefore, their removal from the wastewater streams should be carried out prior to their release in receiving waters. Technologies like precipitation, adsorption, membrane filtration, and ion-exchange are in use for removing metal impurities from water. However, adsorption is most effective and economical method for removing metals, dyes, and other pollutants from contaminated wastewater. Several adsorbents like silica, activated carbon, and graphene find application in water purification. Various toxic metals cannot be completely removed through chemical or simple physical treatments. Activated carbon (AC) is prepared from various raw materials such as agricultural, industrial, and natural sources. AC derived from coal is proved to be effective for removing various organic/inorganic pollutants. In fact, its high surface area and ability of the surface functional groups to form complexes with the pollutant metal ions makes it very useful for wastewater treatment. Table 10.1 depicts various properties of AC-derived from coal. The effectiveness of metal removal depends on a variety of factors such as concentration, ionic energy, initial pH, adsorbent modification, types of adsorbate, chemical nature of AC, its porosity, and surface area (Ansari and Sadegh 2007).

10.2 Need for Adsorption of Metals from Wastewater

Three major sources of wastewater originate from domestic, agricultural, and industrial activities. Significant volume of fresh water is utilized in these activities, which is later discharged as wastewater comprising of several impurities depending on the source. Industrialization has contributed much to water pollution. This is due to the emissions that contain large amount of toxic metal ions. Toxic metals mostly contained in wastewater from industries include chromium (Cr), lead (Pb), arsenic (As), cadmium (Cd), nickel (Ni), copper (Cu), iron (Fe), vanadium (V), manganese (Mn), mercury (Hg), molybdenum (Mo), cobalt (Co), etc., the amount and quantity of which is directly related to the processes performed in the industry. Metals in wastewater mainly originate from mining and metallurgy industries, chemical industries, tanneries, battery manufacturing industries, fossil fuel processing

Table 10.1 Analysis of AC derived from various types of coal

Coal type	Coal analysis				Activated carbon analysis						Reference			
	Proximate analysis (wt.%)		Ultimate Analysis (wt.%)		S _{BET} (m ² /g)	Pore Volume (cm ³ /g)	Pore Diameter (nm)	Ultimate Analysis (wt.%)						
	Ash	Moisture	Volatiles matter	Fixed carbon				Carbon	Hydrogen	Nitrogen		Sulphur		
Bituminous coal	5.54	3.26	30.89	60.31	73.73	4.43	1.44	0.24	1183	0.61	2.04	2.04	2.04	Lv et al. (2020)
Bituminous coal (New Zealand)	3.7	5.7	2.2	88.4	81.8	0.35	0.38	0.7	857.1	0.45	–	–	–	El Qada et al. (2006)
Bituminous coal	0.125	3.62	39.66	56.60	74.81	19.49	1.31	0.38	818.98	0.417	2.00	2.00	2.00	Liu et al. (2017)
Sub bituminous coal	3.68	11.79	32.70	56.64	73.50	6.55	0.91	0.51	933	0.70	2.99	2.99	2.99	Wang et al. (2018b)
Coal from Marit Kapit	–	–	–	63.6	71.52	1.14	4.45	–	1100.18	–	–	–	–	Jawad et al. (2018)
Discarded coal from Mpumalanga, South Africa	35.4	2.1	20	42.5	48.9	2.67	1.15	1.34	1826	1.25	2.77	2.77	2.77	Abdulsalam et al. (2019)
Coal from Xinjiang, China	2.92	5.54	29.13	62.41	78.15	3.75	0.83	0.42	2075	1.34	2.40	2.40	2.40	Gao et al. (2016)
Coal from Yulin, China	6.74	3.70	34.31	55.25	70.28	3.87	1.13	0.54	1212.5	0.69	2.26	2.26	2.26	Niu et al. (2018)
Coal from El-Maghara, Egypt	–	–	–	–	71.44	6.62	9.1	2.27	932	0.51	–	–	–	Elkady et al. (2020)
Coal gasification residue	9.56	–	14.88	75.56	–	–	–	0.56	1981	0.92	2.75	2.75	2.75	Wang et al. (2018c)
Coal liquefaction residue	10.16	0.37	43.87	45.6	83.46	6.79	1.14	1.74	1328	0.604	–	–	–	Wu et al. (2017b)

Table 10.2 Source and health effect of metal present in wastewater (Adapted and reproduced from reference Joseph et al. 2019 with the permission)

Metals	Human health effect	Common source	Oxidation state	Permissible limit, mg/L
Mercury	Kidney damage Nervous system damage	Fossil fuel combustion Electronic industry	+1, +2	0.01
Arsenic	Skin damage Circulatory system issue	Naturally occurring Electronic production	-3, +3, +5	0.02
Cadmium	Kidney damage Carcinogenic	Naturally occurring Various chemical industry	+2	0.06
Chromium	Allergic dermatitis Diarrhoea, nausea and vomiting	Naturally occurring Steel manufacturing	0, +2, +3, +6	0.05
Copper	Gastrointestinal issues Liver or kidney damage	Naturally occurring Household plumbing system	+1, +2	0.10
Lead	Kidney damage Reduce neural development	Lead-based product Household plumbing system	+1, +2	0.10

industries, etc. The various sources and health effects of metals are shown in Table 10.2. Metals released in environment cause significant water pollution leading to severe impact on human health. Therefore, their removal is very important.

Parameters associated with heavy metal removal are temperature, pH, existence of organic matter, and ionic strength. If left untreated, the metals can accumulate in various water sources, including ground water, rivers, and lakes. Metals are a serious threat to environment due to their persistence. They are indestructible and can accumulate in bodies of humans and animals through food grown on contaminated soil. Even if iron, zinc, copper, and chromium in the human body are vital, they can be toxic or even carcinogenic if present at concentrations higher than those required. Removal or degradation of these metals thus becomes a global priority as far as contamination of ground and surface water is concerned. Conventional remediation methods including ion exchange, precipitation, coagulation, ultrafiltration, nanofiltration, solvent extraction, etc. are not economically viable (Khulbe and Matsuura 2018). But, adsorption is the most economically beneficial, technically efficient, and environmentally friendly method (Mnasri-Ghnimi and Frini-Srasra 2019). Above all, adsorption offers opportunity for selection of adsorbent that has high performance for a specific pollutant. These include both commercial as well as bio-derived adsorbents (Renu et al. 2017).

10.2.1 Characteristics of Adsorbent Materials

Several materials are known as effective adsorbents for remediation of wastewater. These include commercially available-high surface area-carbon-based materials like commercial activated carbon, carbon nanotubes, graphene, alumina, various types of clays, etc. and bio-derived adsorbents like rice husk ash, sugarcane bagasse, coconut coir pith, egg shell, chitosan, etc. The main characteristic properties of an adsorbent for removal of any type of pollutant in wastewater treatment are surface area and particle size. Non-reactivity, non-toxicity, ease of regeneration, abundant availability, renewability, etc. are also other factors that must be considered. The process of synthesis of various adsorbents and the characteristics of the raw material of course largely affect all these properties.

Adsorption studies focus on intensification of the process variables to maximize its efficiency. AC produced from different raw materials including agriculture wastes, municipal solid waste, and industrial wastes has different characteristics depending upon the properties of raw material and the processing method. Activation process employed for preparation of AC also has major influence on its characteristics like porosity, morphology, and carbon content (Bergna et al. 2018). The pore structure is usually characterized by N_2 adsorption and desorption, thereby revealing macro- and mesopores, whereas CO_2 adsorption at 273 K is used for micropore structure analysis. Typically, macroporous or mesoporous carbon is responsible for removal of large molecules, whereas the micropores are responsible for removal of small molecules. Figure 10.1 shows different porosity development mechanisms.

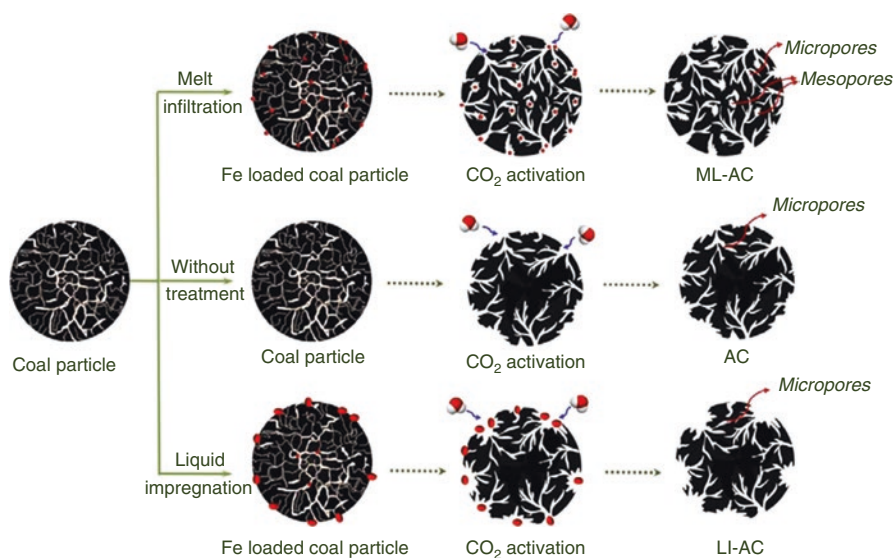


Fig. 10.1 Porosity development mechanism by various strategies (Adapted and reproduced from reference Wang et al. 2018a with the permission)

The ash content is another parameter for defining the characteristics of AC. Generally, the ash content of AC is less than 15%. The presence of carbon–oxygen groups in AC area is known by Boehm titration. The Raman spectrum measured from 1000 to 4000 cm^{-1} also provides with the molecular interactions, chemical structure, and crystallinity of an adsorbent. Furthermore, Fourier Transform Infrared spectroscopy (FTIR) gives information regarding the active groups present over the adsorbent, which are mainly responsible for efficient adsorption. Scanning Electron Microscopy (SEM) technique reveals the surface physical morphology. Also, during adsorption, there is a growing concern about the pH at which the net charge of total particle surface is equal to zero which is called as point of zero charge (PZC) that explains the mechanism of adsorption (Jawad et al. 2018). Another major concern bothering the adsorption process is separation of the adsorbent from the medium. In view of this, magnetic adsorbents are often used which can be easily separated and hence recovered through magnetic separation after treatment (Juang et al. 2018). Above all, liquid phase applications of adsorption further require the information regarding the micropore content which is achieved via measurement of iodine number of an adsorbent through adsorption of iodine from solution.

10.2.2 Mechanism of Adsorption

Adsorption is a mass transfer process, where a substance (adsorbate) is accumulated at the surface of another substance (adsorbent). For adsorption, the selection of an adsorbent having high capacity and selectivity, low cost, high adsorption rate, and rapid kinetics is vital. Further, for understanding mechanism of adsorption of the various organic and inorganic species onto the adsorbent, information about physical properties, chemical properties, and existing surface functional groups is required. However, the sorption mechanism varies from adsorbent to adsorbent as it is derived from different precursors. For solid-liquid adsorption (solid is the adsorbent and liquid is the adsorbate), there exists an equilibrium after certain degree of adsorption. The quantity of adsorbate that can be adsorbed depends on its temperature and concentration. Adsorption isotherm for such process is mathematically given by Eq. (10.1) (Malamis and Katsou 2013):

$$q_e = \frac{(C_o - C_e)V}{W} \quad (10.1)$$

where V is volume of the solution in L , q_e is adsorption capacity at equilibrium in mg/g , C_e is adsorbate concentration at equilibrium in mg/L , C_o is initial concentration of adsorbate in mg/L , and W is adsorbent mass used in g . Adsorption isotherms reveal the capacity of the sorbent, thereby providing details of surface properties and its ability to reach highest potential and are basically defined by Freundlich and Langmuir isotherm models. The Langmuir isotherm is applied to homogeneous sorption. It is a mechanistic model which assumes that all active sites upon the

adsorbent possess equal energies, adsorbed molecules do not interact with each other, localized adsorption, adsorption is a heterogeneous catalytic reaction (limiting reaction step is the surface reaction) (Arasteh et al. 2010). Thus, the metal ions-charged surface interaction can be given by Langmuir isotherm model defined by Eq. (10.2), linear form of which is defined by Eq. (10.3)

$$q_e = q_m \frac{K_L C_e}{1 + K_L C_e} \quad (10.2)$$

$$\frac{C_e}{q_e} = \frac{1}{q_m K_L} + \frac{C_e}{q_m} \quad (10.3)$$

where q_m is monolayer adsorption capacity in mg/g and K_L = the Langmuir constant in dm^3/g . Therefore, linear plot of C_e/q_e versus C_e validates Langmuir model.

Freundlich isotherm is another empirical model depicting relationship between equilibrium concentrations in liquid and solid phase. Adsorption on heterogeneous surface is depicted by Eq. (10.4), for which the linearized form is given by Eq. (10.5) (Malamis and Katsou 2013).

$$q_e = K_f C_e^{1/n_f} \quad (10.4)$$

$$\ln q_e = \ln K_f + \frac{\ln C_e}{n_f} \quad (10.5)$$

where K_f is model constant indicating relative adsorption capacity of adsorbent in $\text{mg/g}(\text{mg/L})^{-1/n_f}$ and $1/n_f$ represents intensity of adsorption. By plotting $\ln q_e$ vs. $\ln C_e$, the model parameters can be determined (Malamis and Katsou 2013). Pseudo-first- and -second-order mechanisms describe the initial adsorbent concentrations (Attari et al. 2017). For pseudo-first-order reaction, rate of solute adsorption from liquid phase is described by Eq. (10.6) (Boparai et al. 2011).

$$\ln(q_e - q_t) = \ln q_e - k_1 t \quad (10.6)$$

where k_1 is kinetic coefficient of pseudo-first-order reaction in min^{-1} and q_t is amount of sorbent adsorbed at time t in min. The plot of ' $\ln(q_e - q_t)$ ' versus ' t ' is linear if first-order kinetics are applicable. Comparison of the graphical q_e with that obtained from experiment determines validity of the first-order model (Sen Gupta and Bhattacharyya 2011).

Pseudo-second-order equation assumes chemical adsorption as the rate-limiting step. Eq. (10.7) depicts second-order kinetic model (Boparai et al. 2011).

$$\frac{t}{q_t} = \frac{1}{k_2 q_e^2} + \frac{t}{q_e} \quad (10.7)$$

where k_2 is second-order rate constant in (g/mg.min) and q_t is the temporal concentration. Plot of experimental values of (t/q_t) against t is linear if second-order kinetics are applicable (Boparai et al. 2011).

10.3 Synthesis of Activated Carbon from Coal

Charcoal is usually used as raw material for AC production. Also, coal has been a conventional raw material for AC and the AC thus produced is also known as activated coal. Coal offers an advantage as a raw material that may not be related to the AC having high surface area, but to the AC having lowest cost per unit area of pore surface area (Sun et al. 1997). Abundance of coal in earth's crust is the key reason of its use for various purposes specially in generating electricity. Thus, there are many probable waste products that are derived from these processes. Coal and the generated coal-based waste products are therefore suitable options for conversion into value-added products (Rashidi and Yusup 2016).

AC preparation conditions have significant impact on its adsorption capacity. Chemical and physical activation are the two most common techniques used to prepare AC as shown in Fig. 10.2. Sometimes combination of both can be used as per

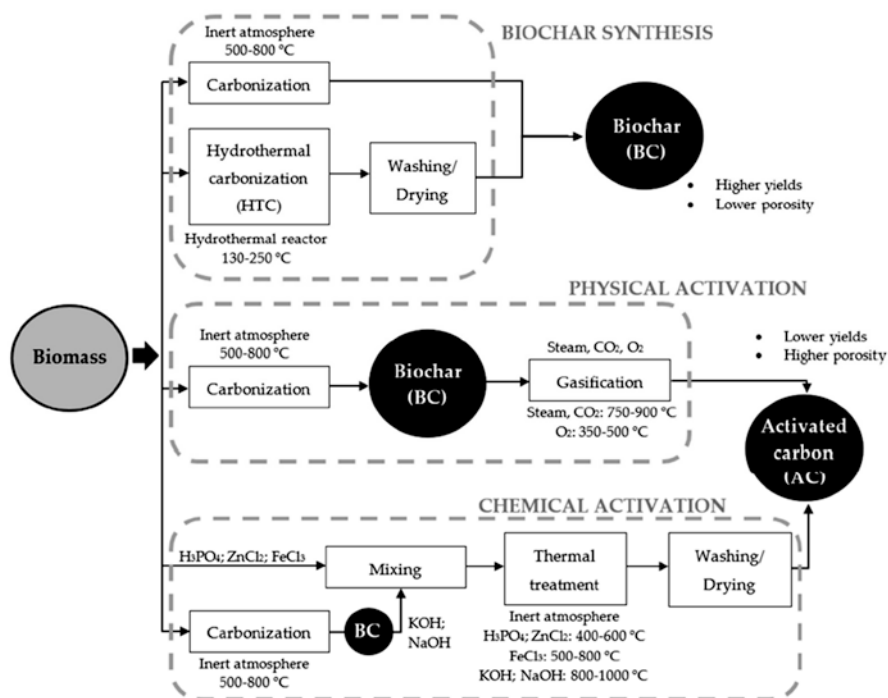
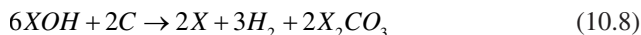


Fig. 10.2 Steps for synthesis of activated carbon (Adapted and reproduced from reference Bedia et al. 2018 with the permission)

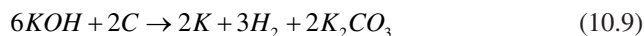
requirements. In physical activation, carbonization of raw material is carried out prior to high temperature activation in a CO_2 or steam atmosphere. In contrast, chemical activation involves carbonization of impregnated raw material. Impregnation agents are the chemicals such as ZnCl_2 , KOH , and H_3PO_4 . In general, chemical activation usually requires lower temperatures, less time, and yields AC with developed porosity compared to physical activation. Ahmadpour and Do (Ahmadpour and Do 1996) compared both the activation methods experimentally and summarized that chemical activation can provide desired pore size distribution. In contrast with this, some authors suggest that the physical activation process is better; it avoids usage of expensive chemicals and the need for wastewater treatment unlike chemical activation process, thereby resulting in economic and environmental benefits. The shapes of pores in AC are also found to be a function of the activation method used; physical activation yields cone-shaped pores, whereas chemical activation yields bottle-shaped pores (Kadlec et al. 1970).

10.3.1 Chemical Activation Method

Chemical activation is one-step process of preparing AC, even though it contains three stages; impregnation with chemicals (usually alkali- and alkaline earth metal-containing substances and other acids like ZnCl_2 , H_3PO_4 , NaOH , KOH , etc.), carbonization or thermal treatment (at temperatures depending on activating agent and in inert atmosphere), and washing (for removing remaining active agents and reaction by-products). The chemical reagents are conducive to dehydration, dehydrogenation, and they improve formation of cross-links, and solid skeletons, thereby resulting into formation of a rigid matrix. Also, they are used as oxidative inhibitors to reduce volatility and volume contraction upon carbonization and carbon loss of raw material at high temperatures. Eq. (10.8) represents chemical reaction which occurs during the chemical process using hydroxide, where $X = \text{K}, \text{Na}$.

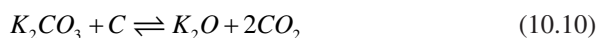


Among the chemical reagents, KOH is widely used. It mainly involves reactions between activating intermediate and carbon, thereby producing porosity, thus leading to high surface area, enhanced pore structure and distribution (Chunlan et al. 2005). Jibril et al. (Jibril et al. 2008) used KOH to produce AC having improved pore structure, higher surface area, and wider pore size distribution compared to that prepared using H_3PO_4 . Lillo-Ródenas et al. (Lillo-Ródenas et al. 2003) proposed that the reaction between carbon and KOH follows Eq. (10.9).



The activating agent to carbonaceous precursor ratio (impregnation ratio) has significant effect on AC texture characteristics. Wu et al. (Wu et al. 2010) reported

that increased amount of KOH enhances pore development and creates new pores due to reaction of more active sites with KOH. Niu et al. (Niu et al. 2018) showed that weight ratio of 3:1 of KOH:coal exhibited S_{BET} of 1212.50 m²/g and pore diameter 2.26 nm. Similarly, Abdulsalam et al. (Abdulsalam et al. 2019) found S_{BET} of 1826.41 m²/g and pore diameter of 2.77 nm for ratio of KOH to coal of 4:1. These two experimental studies clearly showed the positive effect of increasing impregnation ratio on AC porosity development. Abdulsalam et al. (Abdulsalam et al. 2019) experimented different weight ratio of activating agent and coal at different temperature. They concluded that a rise in temperature up to 800 °C and weight ratio of KOH:coal up to 4:1 increases surface area and pore volume significantly. Temperatures above 800 °C have resulted in lesser yield and poor pore size distribution. Decomposition of alkaline carbonate at above 800 °C leads to CO₂ evolution as one of the product of decomposition as shown in Eq. (10.10).



AC prepared using coal fly ash by chemical activation process at 800 °C with KOH in the ratio 1:4 (AC:KOH) exhibited specific surface area of 946.77 m²/g (Musyoka et al. 2020). Zou et al. (Zou and Han 2001) investigated the influence of particle size during chemical activation of coal using various activating agents (KOH, K₂CO₃, NaOH, and Na₂CO₃) in different proportions for adsorption of methylene blue. They observed that coal activated using KOH and NaOH had much higher adsorption capacity which was 380 mg/g and 126 mg/g, respectively, compared to K₂CO₃ and Na₂CO₃ for which 45 mg/g and 18 mg/g was recorded, respectively. Higher amount of KOH results in higher adsorption capacity and low yield of AC. Elkady et al. (Elkady et al. 2020) suggested low-cost and high-efficiency AC preparation by carbonizing the mixture of coal and NaOH solution at 550 °C for 90 min. This involved oxidation using nitric acid for producing active oxygen-containing groups and increasing hydrophilicity of carbon. Chemical activation process is therefore advantageous as a single-step process, requires low temperature, and yields large amount of product having high surface area and porosity.

10.3.2 Physical Activation Method

A physical activation method consist of two different thermal steps; firstly, carbonization (pyrolysis) of the precursor at temperatures nearly 700–900 °C under inert conditions to avoid combustion, and secondly, activation of the resultant product in the presence of CO₂ or steam as activating agents. During carbonization, heteroatoms and volatiles are removed, resulting in high carbon-containing char, but having low porosity development. Thus, rise in carbonization temperature results into increased carbon content. In the subsequent step, also known as gasification, characteristic porosity is generated in the product because of selective removal of reactive carbon atoms controlled gasification. Temperature of gasification usually

depends on gasification agent (typically steam, CO_2 , O_2) (Bedia et al. 2020). Conversion of carbonaceous raw material using steam and CO_2 can be explained by Eqs. (10.11) and (10.12), respectively (Linares-Solano et al. 2014).



Zhang et al. (Zhang et al. 2020) prepared AC by physical activation process under water vapour atmosphere by mixing coal with pyrite in different proportions at 900 °C using N_2 as carrier gas. Zhong et al. (Zhong et al. 2016) used physical activation method for preparing coal pitch-derived AC. The n-pentene was used to produce asphaltene from coal pitch by mixing with KOH in ratio of 1:4 and thereby carbonizing at low temperatures to get activation precursor (char) which was then activated by steam at 800 °C. Pyrolysis temperature has significant impact on specific surface area of AC derived from coal. AC prepared from carbonization of coal-blended sewage sludge by Li et al. (Li et al. 2018a) showed the impact of pyrolysis temperature on S_{BET} at specific temperature range for adsorption of various metals. The S_{BET} of synthesized material increased from 543 to 1052 m^2/g with temperature rise from 400 to 450 °C, reaching maximum of 1096 m^2/g at 500 °C for pyrolysis time of 30 min. Lv et al. (Lv et al. 2020) compared the AC and carbon nanotube in their experiment prepared by coal pyrolysis. The coal impregnated with KOH with equal quantity and heated up to final pyrolysis temperature of 900 °C for 90 min had maximum specific surface area of 1183 m^2/g . Further rise in pyrolysis temperature exhibited gradual decrease in specific surface area. The physical approach is therefore beneficial as it avoids usage of chemicals resulting into environmental and economic benefits.

10.3.3 Physicochemical Activation Method

The physical activation and chemical activation process have some drawbacks. In physical activation, high energy is required and the high burn off value during activation leads to relatively high cost. Similarly, in chemical activation, used chemical reagents are corrosive in nature and require additional washing process. Preparation of ideal AC is difficult only by adjusting the activation conditions; the improvement in physicochemical structure of coal in the pyrolysis process is the key factor. To make activated carbon surface interact specifically with the adsorbate, surface modifications have to be applied. This involves introduction of various oxygen, nitrogen, sulphur, phosphorus, or halogen containing groups to the AC surface. These modifications are carried out on carbon surface at specific conditions according to the process and the specifications of species that has to be adsorbed. Liu et al. (Liu et al. 2019) showed effect of pyrolysis condition on AC obtained from bituminous coal. They concluded that activation at 800 °C for 40 min is suitable for obtaining

disordered structure of carbon, plentiful initial pores, and active sites. Li et al. (Li et al. 2018b) compared AC with that activated using only ZnCl_2 and CO_2 (Fig. 10.3). The physiochemical activation process was achieved by heat treatment of mixture of ZnCl_2 and coal with CO_2 as reaction atmosphere. The demineralized coal was mixed with ZnCl_2 solution in mass ratio of 1:2 (coal- ZnCl_2), mixture of which was then gradually heated to 950°C in furnace. The AC prepared from physiochemical process had S_{BET} of $1823\text{ m}^2/\text{g}$ which was higher than $1529\text{ m}^2/\text{g}$ and $933\text{ m}^2/\text{g}$ achieved using chemical or physical activation, respectively.

Oxygen influences the application of the carbon. For instance, carbon-oxygen functional groups not only influence the surface behaviour, wettability, or electrical and catalytic properties of carbons, but also enables the possibility of tailoring the surface chemistry for the intended application via further functionalization (Bandosz and Ania 2006). With a high microporosity structure and BET surface area, AC showed significant mercury capture potential which was attributed to the intensified chemisorption due to presence of oxygen (Diamantopoulou et al. 2010). Sulphur-coated AC exhibited 40% increased efficiency in collecting elemental mercury in mixed gas situations compared to on-sulphur-coated AC (Uddin et al. 2009). For AC prepared by physical activation, Zhang et al. (Zhang et al. 2020) showed effect of addition of pyrite (FeS_2) on AC specific surface area and adsorption capacity. Addition of FeS_2 increased specific surface area up to certain concentration of FeS_2 (up to 2%), after which the specific surface area decreased due to decreases in gasification reaction and porosity blockage. The sulphur adsorption capacity exhibited by 2% FeS_2/AC was $65.2\text{ mg}/\text{g}$. It was 18.8% higher than that of commercial AC. This showed that FeS_2 influenced the physicochemical structure by enhancing

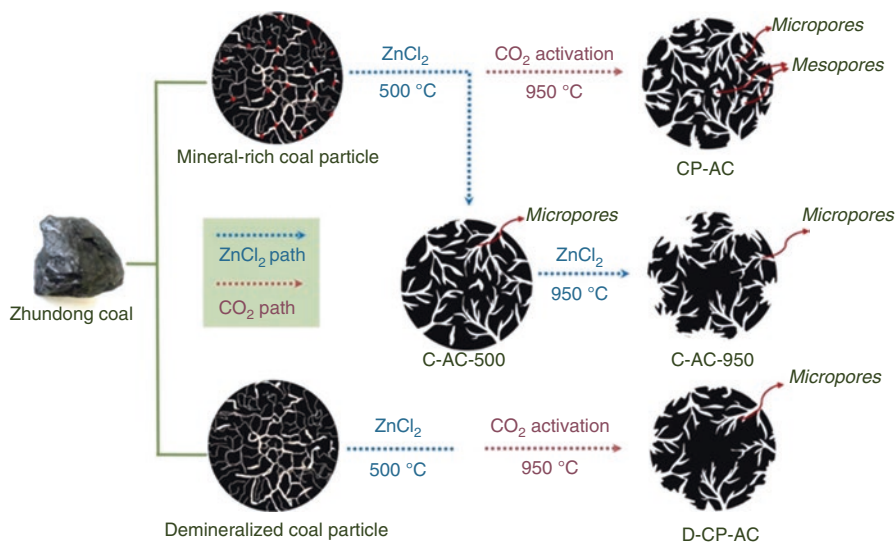


Fig. 10.3 Schematic illustration of preparation of AC (Adapted and reproduced from reference Li et al. 2018b with the permission)

the surface chemical properties and adsorption performance of AC. Fe_2O_3 is used as magnetic source in AC for improving adsorption capacity and increasing surface area. Gao et al. (Gao et al. 2016) used two-stage carbonization and activation process in the presence of Fe_2O_3 for preparation of AC having high S_{BET} of 2075 m^2/g and optimum porous structure. High S_{BET} was obtained at alkali:carbon ratio of 1 and Fe_2O_3 mass fraction of 12% at 1000 °C.

10.4 Adsorption of Metals Using Coal-Derived Activated Carbon

The understanding of the bonding of metals onto AC relates to its metal adsorption characteristics which may lead to development of better testing scheme to improve techniques for metals removal using AC. The AC prepared from coal shows promising results for adsorption of metals from wastewater.

10.4.1 Mercury Adsorption

Besides the natural occurrence of Hg, the main sources are mining, combustion of fossil fuels, and industrial processes mainly in chloro-alkali, plastics, metallurgy, and electronics industries. Hg is a toxic metal that can affect human health. Prolonged exposure to Hg at high concentrations can damage human brain, kidneys, and heart (Hsiao et al. 2011). As a result of the high mercury toxicity, the US Environmental Protection Agency (USEPA) classifies Hg emissions as 0.2 ppb. Many methods are used for removal of Hg like electrostatic precipitators (ESP), wet flue gas desulfurization, co-precipitation, coagulation, and reverse osmosis. Adsorption by coal-based AC is mature and its use is a promising approach for Hg capture from industrial flue gases and waste water as shown in Table 10.3. The physical characteristic of adsorbents, mass ratio of carbon and Hg, and AC composition are important factors that affect their adsorption capacities. AC with a rich pore structure exhibits excellent Hg adsorption (Min et al. 2017). However, adsorption is weakened by high temperatures (Huo et al. 2019). Hg removing efficiency increases with temperature up to some extent, after which it starts to decrease (Zhong et al. 2016). Similar effect is observed on S_{BET} at temperature between 700 and 800 °C.

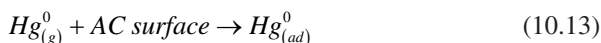
Attachment of sulphur group into the adsorbent surface enhances Hg adsorption potential. The amount of elemental Hg left in the coal appeared to be temperature dependent. Hsi et al. (Hsi et al. 1998) explained the importance of natural sulphur inherently present in coal in AC production for Hg^0 adsorption. Hg^0 adsorption increased up to some extent by sulphur coal-based AC. Similarly, Chen et al. (Chen et al. 2020) studied the coal liquefaction residue derived AC which was rich in

Table 10.3 Adsorption capacities of AC for mercury

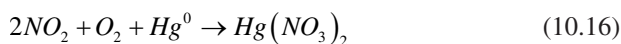
Source	Adsorption capacity	Adsorption, %	Temperature, °C	Optimum pH	Adsorption isotherm	Adsorption kinetics	Contact time	Reference
AC from coal	5.71 mmol/g	NA	35	4–5	Langmuir	NA	NA	Youssef et al. (1996)
AC from coal fly ash	NA	94	NA	NA	Freundlich	Pseudo-second order	120 min	Attari et al. (2017)
Thiol functional coal fly ash	361.61 mg/g	92	NA	8	Langmuir	Pseudo-second order	50 min	Dash et al. (2017)
Thiol modified magnetic AC	298.8 mg/g	NA	25	7	Langmuir	NA	NA	Chen et al. (2019)

NA not available

sulphur using KOH as activating agent at 800 °C. The efficiency of Hg removal was 97% at 60–120 °C. They observed that Hg removal efficiency decreased with increase in gas hourly space velocity. Sulphur-rich AC showed promising results in removing Hg. Addition of SO₂ enhanced the performance of sulphur-rich sorbent. Physical adsorption was important and active sulphur sites in sulphur-rich sorbent were widely available as HgS. Therefore, methods of removing Hg over rich sulphur sorbent may be approximately described as Eqs. (10.13) and (10.14). In this, physical and chemical adsorption occurs and influences Hg⁰ removal function of sulphur-rich sorbent (Chen et al. 2020).



Similarly, presence of NO has a positive impact on Hg⁰ removal efficiency in chemisorption. NO was easily oxidized to form active species (NO⁺, NO₂, NO₃⁻) which were used to remove Hg⁰. In this process, probable reactions to improve Hg⁰ capture can be defined as Eqs. (10.15) and (10.16).



Chemically treated AC has also been used to remove Hg. Among metal oxides, CeO₂ attached over the AC surface has high oxygen retention capacity and it promotes removal of Hg⁰ through the conversion of Ce⁴⁺/Ce³⁺ redox pairs (Tian et al. 2009; Fan et al. 2010). Zhao et al. (Wu et al. 2017a) experimentally compared Hg adsorption capacity of CeO₂/AC with different concentrations of Ce-Mn-based AC. They concluded that Ce-Mn-modified AC has better removal capacity than CeO₂/AC, especially, 3% Ce-Mn(0.7)/AC shows 90% Hg removal efficiency, although CeO₂/AC had higher S_{BET} and pore volume compared to Ce-Mn-based AC, when same Ce content was used. The impregnation of chemical agent on AC has high influence on its adsorption capacity. Sulphur-rich AC showed promising results for adsorption of Hg and the increase in temperature in some extent increased the adsorption performance of AC.

10.4.2 Cadmium Adsorption

Cd causes respiratory irritation, vomiting, and kidney dysfunction if ingested in human body. Also, long-term exposure of it can cause anaemia and yellow spots appearing in the tooth joint. It has a high concentration of sulfhydryl (-SH) protein groups competing with Zn(II) in biological systems. Cd ions are able to replace Zn(II) ions in metalloenzymes, thereby affecting the enzyme activity as well (IARC

2012). USEPA has limited Cd in drinking water to 0.002 mg/L, while the World Health Organization (WHO) has limited it to 0.003 mg/L (Rao et al. 2011).

Typical Cd removal methods include membrane separation, solvent extraction, ion exchange, and precipitation, but they are less effective at low concentrations. Adsorption is a promising technique for removal of Cd at low concentration as well. Karabulut et al. (Karabulut et al. 2001) used low-rank Turkish coal to remove Cd(II). The functional groups acted as sites for adsorption of metal by ion exchange mechanism. Low-rank coal had Cd(II) adsorption capacity of 1.42 mg/g at a pH 4. Vu et al. (Vu et al. 2020) synthesized mesopore molecular sieve from coal bottom ash. It had equilibrium adsorption capacity of 80.02 mg/g for Cd(II). Coal-based AC had higher adsorption capacities at optimum pH as shown in Table 10.4 as compared to raw coal. Erto et al. (Erto et al. 2013) prepared AC from bituminous coal by steam activation. The AC had high adsorption capacity even at low concentrations. The pH of solution also had significant impact on adsorption; increase in pH up to 7 increased adsorption of Cd. Youssef et al. (Youssef et al. 1996) used powdered AC for removal of Cd, Pd, and Hg from wastewater. Experiment was carried out at 0.15 mmol/g metal solution. Powdered AC was impregnated with ZnCl₂ at ratio of 1:2 followed by carbonation which showed high adsorption capacity of 4.25 mmol/g for Cd at pH of 6–7. Mesoporous AC prepared for removal of Cd(II) had maximum adsorption capacity of 27.3 mg/g at pH 7 (Asuquo et al. 2017). The grafting of mercaptopropyl group on the AC surface led to better adsorption of toxic metals from wastewater. Dash et al. (Dash et al. 2017) showed that thiol functionalized coal fly ash had a maximum efficiency of 72%. It was prepared from sewage sludge by coal blending for adsorption of Cu, Pb, Cd, and Ni from wastewater (Li et al. 2018a). Adsorption performance of thiol-functionalized AC for Cd(II) was 96.2 mg/g at pH 5. Magnetic properties of AC influenced the adsorption of Cd as studied by Vazquez et al. (González Vázquez et al. 2016). AC derived from bituminous coal had ferromagnetic properties which showed influence over adsorption of Cd. It removed 63% Cd from aqueous solution. Cd adsorption is mainly affected due to solution pH and the incorporated functional group. Adsorption capacity increased with pH of solution up to 7–8 after which it started to decrease.

10.4.3 Chromium Adsorption

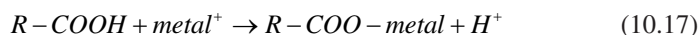
Many human activities are responsible for release of chromium (Cr) in the atmosphere which include mining, chemical industrial activities, battery manufacturing, production of plastics that use metals, etc. The oxidizing form of chromium, Cr(III) and Cr(VI), are most common forms of industrial pollutants, among which Cr(VI) form has high toxicity. Reduction of anionic species usually leads to formation of Cr(III), which is then precipitated as chromic hydroxide. But, this takes place at high concentrations of Cr and has many problems such as the production of waste, expense of disposal, and long-term environmental effects. Cr(VI) is more toxic than Cr(III) even at low concentrations (Ghasemi et al. 2020). Adsorption can remove Cr

Table 10.4 Adsorption capacities of AC for cadmium

Source	Adsorption capacity	Adsorption %	Temperature (°C)	Optimum pH	Adsorption Isotherm	Adsorption Kinetics	Contact time	Reference
Commercial AC	NA	84	NA	6	Langmuir	Pseudo-second order	5 hours	Wasewar et al. (2010)
AC from coal	4.25 mmol/g	NA	35	6–7	Langmuir	NA	NA	Youssef et al. (1996)
AC from sewage sludge with coal blended	96.2 mg/g	NA	NA	5	Langmuir	NA	NA	Li et al. (2018a)
Thiol functionalized AC	106.38 mg/g	72.14	NA	8	Langmuir	Pseudo-second order	80 min	Dash et al. (2017)
AC from coal fly ash	18.98 mg/g	66.5	NA	10	Langmuir	Pseudo-second order	NA	Papandreou et al. (2007)
Magnetic field effect on AC	NA	63	30	5	NA	NA	72 hours	González Vázquez et al. (2016)

NA not available

from wastewater efficiently even at low concentrations. Coal-based AC has properties which make it good adsorbent for Cr adsorption. Table 10.5 describes adsorption capacities of coal-derived AC. Functional groups present over AC significantly help in removing Cr ions. Carboxyl or hydroxyl groups participate in ion exchange according to Eqs. (17) and (18), where R is aromatic group (Gode and Pehlivan 2005).



Anwar et al. (Anwar et al. 2009) observed a rise in removal efficiency with pH and the best results are found at pH 8. At very low pH, functional groups over the coal are protonated resulting in less available active sites for adsorption, thereby decreasing the efficiency. Insoluble chromium hydroxide at pH > 8.5 began to precipitate, thereby complicating the true sorption studies. Therefore, pH of the solution must be high for best results, but not exceeding 8.5. Contradictorily, Arslan and Pehlivan (Arslan and Pehlivan 2007) suggested that adsorption efficiency of chromium increased in the lower range of pH. They found removal efficiency of 90% at pH 3. Various mechanisms like ion exchange, electrostatic forces, etc. should be considered when evaluating the effect of pH. Increase or decrease of Cr(VI) sorption at low or high pH depends on electrostatic attraction between chromium anionic species on active sites of the sorbent. In view of these assumptions, Cr(VI) removal occurs through physical adsorption (Arslan and Pehlivan 2007). At pH above 3.5, the sorption capacity decreases with increasing pH, which is attributed to the coordination bonds between metal ions and functional groups (Arslan and Pehlivan 2007). Golovina et al. (Golovina et al. 2018) experimented at low pH value and found removal efficiency of 79.9%. They performed experiments with black and brown coal and observed that brown coal has better removal capacity for Cr of 37.6 mg/g at pH 1.5–2. Cr is dependent on pH of solution and functionalized materials used for preparation of AC. At low pH, AC had high sorption capacity.

Table 10.5 Adsorption capacities of AC for chromium

Source	Adsorption capacity	Adsorption, %	Optimum pH	Adsorption isotherm	Contact time	Reference
AC from coal	37.7 mg/g	79.9	1.5–2	NA	NA	Golovina et al. (2018)
AC from coal	0.55 mmol/g	90	3	NA	80 min	Arslan and Pehlivan (2007)
AC from coal	2.6 mg/g	NA	8	Langmuir	40 min	Anwar et al. (2009)
AC coated with carbon nanotubes	9.0 mg/g	72	2	NA	60 min	Ali Atieh (2011)

NA not available

10.4.4 Lead Adsorption

Lead (Pb), another toxic metal, is used in production of lead acid batteries, cable sheathing, pigments, alloys, ammunition, and glazes (Deng et al. 2007). If inhaled or ingested, Pb causes serious illness and damage to central nervous system. Therefore, its removal from contaminated water and other sources is extremely necessary. AC having developed graphite structure has higher chances of effective adsorption of Pb(II) ions (Kuroki et al. 2019). At low pH, functional groups on AC surface are positively charged, thereby decreasing the number of adsorption active sites (Patnukao et al. 2008). As pH increases, many protonated groups, -COOH and -OH, get released and more active sites become available, which can promote interaction of Pb(II) with these functional groups, thereby improving its removal (Mouni et al. 2011; Yi et al. 2016). For Pb, maximum removal took place at around pH 6.0 which is mostly proposed by various researchers as shown in Table 10.6. Taraba and Vesela (Taraba and Veselá 2016) used coal-based AC for adsorption of Pb having adsorption capacity 0.2 mmol/g at pH 6. Dong et al. (Dong et al. 2016) utilized AC for removal of low concentration of metals and observed that it has adsorption efficiency of 62% at pH 6–8. Removal of Pb(II) was dependent on pH (Yi et al. 2016); pH for maximum Pb(II) adsorption capacity (162.33 mg/g) was in the range of 5.0–5.5. Mesopore molecular sieve synthesized from coal bottom ash was studied by Vu et al. (Vu et al. 2020). They found that coal bottom ash has maximum equilibrium adsorption capacity of 204.08 mg/g for Pb(II) at pH 5. Xu et al. (Xu and Chai 2018) used coal gasification slag-based material for preparation of AC with KOH activation at 750 °C for 80 min. High adsorption performance was achieved for Pb(II) removal at about 141 mg/g. Nano AC prepared by nitric acid oxidation had surface area of 932 m²/g with 62% Pb removal capacity (Elkady et al. 2020). Influence of pyrolysis temperature on specific surface area and functional group on AC adsorption capacity has been studied (Li et al. 2018a). The thiol functionalized AC modified from coal-blended sewage sludge exhibited adsorption performance of 238.1 mg/g at pH 5.

10.4.5 Arsenic Adsorption

Arsenic (As) ions present in natural water have become a global problem. It is a toxic chemical causing environment-related problems. Various technologies used for its removal, like precipitation, ion-exchange, and reverse osmosis, have some drawbacks. AC adsorption capacity for As is high at higher concentrations, whereas it has low selectivity and efficiency for As at low concentration due to competitive adsorption characteristics of other contaminants. In view of this, various elements like Fe, Cu, and Ag have been used for impregnation over AC to increase its performance as shown in Table 10.7. Surface impregnation is a key factor for promoting adsorption of metal species (Li et al. 2014). Rajakovic (Rajakovic 1992) found that

Table 10.6 Adsorption capacities of AC for lead

Source	Adsorption capacity	Adsorption, %	Temperature, °C	Optimum pH	Adsorption isotherm	Adsorption kinetics	Contact time	Reference
AC from coal	162.33 mg/g	92.96	25	5.0–5.5	Langmuir	Pseudo-second order	60 min	Yi et al. (2016)
AC from coal	6.38 mmol/g	NA	35	6	Langmuir	NA	NA	Youssef et al. (1996)
AC from coal	0.2 mmol/g	NA	60	6	Langmuir	Pseudo-second order	NA	Taraba and Veselá (2016)
Mesopore AC	20.3 mg/g	NA	25	7	Langmuir	Pseudo-first order	180 min	Asuquo et al. (2017)
Granular AC	13.33 mg/g	NA	NA		Langmuir	Pseudo-second order	5 min	Sulaymon et al. (2012)
AC from sewage sludge with coal blending	238.1 mg/g	NA	NA	5	Langmuir	NA	NA	Li et al. (2018a)
AC from coal gasification sludge	141 mg/g	NA	NA	NA	Freundlich	Pseudo-second order	NA	Xu and Chai (2018)

NA not available

Table 10.7 Adsorption capacities of AC for arsenic

Source	Oxidation state	Adsorption capacity	Optimum pH	Adsorption isotherm	Adsorption kinetics	Contact time	Reference
Coal-based AC	As(III)	1.491 mg/g	6	Langmuir	Pseudo-second order	60 min	Li et al. (2014)
	As(V)	1.760 mg/g					
Fe-incorporated AC	As(V)	1.43 mg/g	6	Freundlich	Pseudo-first order	NA	Kalaruban et al. (2019)
	As(III)	0.41 mmol/g	8	Langmuir	NA	NA	Rajakovic (1992)
AC impregnated with Cu ²⁺	As(V)	0.23 mmol/g					

NA not available

carbon pre-treated with Ag^+ or Cu^{2+} improved As(III) adsorption capacity but reduced As(V) adsorption capacity. Fe-incorporated AC had more adsorption capacity compared to AC without impregnation (Kalaruban et al. 2019). Increase in pH decreased zeta potential of AC, thereby decreasing its capacity to adsorb negatively charged As if electrostatic force governs the adsorption mechanism. Also, adsorption capacity of AC does not necessarily be a function of its surface area. Fe-incorporated AC had specific surface area of $876 \text{ m}^2/\text{g}$, and that of neat AC was $1124 \text{ m}^2/\text{g}$. However, Fe-incorporated AC exhibited higher adsorption capacity than neat AC (Kalaruban et al. 2019).

10.4.6 Copper Adsorption

Cu metal easily corrodes in water producing copper ions, Cu(II), which are more sensitive than copper metal because of their high toxicity (Yantasee et al. 2004). USEPA has limited Cu at 1.3 ppm in industrial wastewater. The adsorption of Cu-contaminated water depends on the pH as shown in Table 10.8. Removal of Cu(II) by adsorption increases with pH. The highest level of metal removal was 98.0–98.4% at pH range between 8 and 10 in case of Cu(II) (Sočo and Kalembkiewicz 2013). Papandreou et al. (Papandreou et al. 2007) prepared AC from coal fly ash which exhibited adsorption capacity of 20.92 mg/g for Cu of 20.92 mg/g at pH 10. Functional groups present in AC had significant effect on adsorption capacity. Thiol-functionalized AC prepared by coal blending (Li et al. 2018a) showed adsorption capacity of 87.7 mg/g for Cu. Amine-functionalized AC synthesized by Yantasee et al. (Yantasee et al. 2004) exhibited capacity between 40% and 90% of Cu(II) at pH 2–4, whereas neat AC could remove negligible quantity of Cu(II) at same pH. At low pH level, adsorption of Cu(II) from concentrated Cu-bearing waste is often effective (Yantasee et al. 2004). Fowle and Fein (Fowle and Fein 1999) showed that Cu started being adsorbed at pH of 3.5 and that a maximum adsorption of 70% was attained at pH of 6.5. After pH of 6.5, adsorption and precipitation were indistinguishable due to rise in highly carbonized materials.

10.5 Comparison of Adsorption of Metals Using Coal-Derived Activated Carbon with that Derived from Other Materials

Various processes are exploited to remove toxic metals from contaminated water. In particular, adsorption exhibits high efficiency, ease of operation, and economic benefits and therefore finds wide application in wastewater treatment. AC has been largely studied due to its ability to adsorb various substances including dyes, metals, and other organic materials. Many precursors are proposed to yield high surface area AC via various processes. These include agricultural-based materials,

Table 10.8 Adsorption capacities of AC for copper

Source	Adsorption capacity	Adsorption %	Mechanism	Optimum pH	Adsorption isotherm	Adsorption kinetics	Reference
Thiol functionalized AC	87.7 mg/g	NA	Chemisorption	5	Langmuir	NA	Li et al. (2018a)
AC from coal fly ash	20.92 mg/g	NA	NA	10	Langmuir	Pseudo-second order	Papandreou et al. (2007)
AC from coal fly ash	NA	98	Physisorption	8	Freundlich	NA	Sočo and Kalemkbkiewicz (2013)
Amine functionalized AC	0.86 mmol/g	NA	NA	2–4	Langmuir	NA	Yantasee et al. (2004)

NA not available

agro-waste materials, municipal solid-waste materials, industrial-waste materials, etc. Performance of AC depends on characteristics of raw material for AC preparation.

10.5.1 Performance Point of View

Different features of AC play their role in enhancing its metal adsorption performance. AC from different materials such as agricultural activities, industrial activities, and domestic activities are modified chemically using oxidizing agents to impart adsorption properties. This can be caused by enhancing surface and negative surface charge. Low-cost adsorbents have attracted much attention. Attari et al. (Attari et al. 2017) used coal fly ash for adsorption of Zn, Pb, and Cr(III). They observed that coal fly ash has adsorption capacity of 17.7 mg/g for Zn. It exhibited high adsorption capacity compared to natural clay and low-rank brown coal. Filho et al. (Filho et al. 1995) studied natural clay and Lafferty et al. (Lafferty and Hobday 1990) studied low-rank brown coal which, respectively, showed adsorption capacities of 0.92 and 14 mg/g for Zn(II). Malik et al. (Malik et al. 2007) compared groundnut shell AC with commercial powdered AC. Groundnut shell-based AC had higher surface area compared to commercial powdered AC. Both the AC samples were compared by varying adsorbent volume, contact time, and adsorbate concentrations. The groundnut shell-derived AC showed 94.5% dye removal in 30 minutes, whereas commercial AC removed 96% dye in 15 minutes. Orumwense (Orumwense 1996) used Kaolinitic clay as adsorbent in removing Pb from contaminated water, which showed maximum adsorption capacity of 7 mg/g. Blast furnace sludge as an adsorbent was tested by Lopez et al. (Lopez et al. 1995), which exhibited adsorption capacity of 64 mg/g, while coal-blended sewage sludge-based AC prepared by Li et al. (Li et al. 2018a) showed adsorption capacity of 238.1 mg/g of Pb. Removal of Rhodamine-B (RhB) using AC derived from rice husk was investigated by Ding et al. (Ding et al. 2014). AC prepared by KOH activation of rice husk (1:4 = rice husk:KOH by mass) at 400 °C (for 0.5 h) and later 800 °C (for 1 h) had S_{BET} of 2516 m²/g and exhibited adsorption capacity of 290 mg/g. Zhang et al. (Zhang et al. 2020) used coal-based AC incorporated with FeS for removal of RhB. The AC was prepared by mixing pyrite and coal in various proportions at 900 °C, and activated under water vapour by N₂ as carrier gas. The AC was incorporated with 1% FeS, and it exhibited 168 mg/g of RhB adsorption. Similarly, the adsorption of RhB using coal-based AC was observed by Li et al. (Li et al. 2018b). Pore size distribution and method for preparation of AC has significant impact on adsorption. The coal-based AC prepared from physiochemical activation process had adsorption capacity of 881.2 mg/g. Malkoc and Nuhoglu (Malkoc and Nuhoglu 2005) used tea waste-derived adsorbent for Ni(II) removal from wastewater. It showed maximum adsorption capacity of 18.4 mg/g. Li et al. (Li et al. 2018a) used coal-blended AC for adsorption of Ni(II) having adsorption capacity of 52.4 mg/g. From various experiments, it was concluded that the coal-based AC had high affinity for many

Table 10.9 Comparison of adsorbents

Adsorbent	Lead	Chromium (III)	Copper	Reference
Peanut Shell	39.9 mg/g	NA	NA	Taşar et al. (2014)
	NA	27.9 mg/g	25.4 mg/g	Witek-Krowiak et al. (2011)
Saw dust from poplar tree	21.1 mg/g	5.5 mg/g	6.6 mg/g	Li et al. (2007)
Coal Fly ash	45.3 mg/g	22.7 mg/g	NA	Attari et al. (2017)
	NA	NA	20.92 mg/g	Papandreou et al. (2007)
AC derived from coal	162.33 mg/g	NA	NA	Yi et al. (2016)
	NA	37.7 mg/g	NA	Golovina et al. (2018)
	NA	NA	87.7 mg/g	Li et al. (2018a)

NA not available

pollutants in contaminated water as shown in Table 10.9. Performance of AC was dependent on many factors like the raw material used for preparation of AC and activation method (physical activation or chemical activation method). In some cases, the functional groups of adsorbent had influence on adsorption capacity, while the affinity of adsorbate towards adsorbent has also been a major factor for adsorption of metal from wastewater. With the abundance of coal-based waste materials deriving from coal processing, there remains a certainty regarding the various adsorbent properties derived from them. Alternatively, agricultural-based materials pose a threat to adsorbent properties derived from them due to changes in their original properties, composition, and type which vary from region to region and time to time. Therefore, synthesis of adsorbents from materials that have constant properties becomes easier compared to those with variable properties. Different properties of the raw materials need different processing methods which not only complicate the synthesis process but also the adsorption performance.

10.5.2 Economic Point of View

Effectiveness and suitability of waste materials for AC preparation for removal of metal ions from wastewater has been studied widely. Due to local diversity in industrial and agricultural activities, different types of wastes are produced. The locally available materials used for preparation of AC reduce the cost for preparation of AC. Waste from agricultural, industrial, and domestic sources have shown its potential to remove metals from wastewater. Chemical modification has become a way to increase surface area of various materials, thereby enhancing its sorption performance. But, it requires additional cost due to chemicals. However, enhanced adsorption capacities can nullify it. In addition, after saturation of adsorbent from agricultural waste, its regeneration poses another cost-effective and environmental friendly advantage. In fact, regeneration can result into valuable metal in spent

adsorbent. However, characteristics of the renewed adsorbent and the significant losses during renewal can be of concern. Ioannidou and Zabaniotou (Ioannidou and Zabaniotou 2007) presented a review of different agricultural material-based AC and its production and properties. Sreenivas et al. (Sreenivas et al. 2014) studied biosorption using ash gourd peel. The peel powder had a particle size and specific surface area of 446 μm and 0.4854 m^2/g , respectively. Almost 91% Cr(VI) was adsorbed on it at pH of 1. Demirbas et al. (Demirbas 2002) studied hazelnut shell-derived AC for adsorption of Ni(II) which improved with rise in temperature. Similarly, Kobyas (Kobyas 2004) employed hazelnut shell-derived AC for Cr(VI) removal with an initial Cr(VI) concentration of 1000 mg/L. Approximately 170 mg/g adsorption capacity for Cr(VI)/g was exhibited.

Removal of Cd(II), Ni(II), and Cu(II) ions using AC derived from coir pith were examined (Kadirvelu et al. 2001). Maximum metal adsorption occurred at pH between 4 and 5. Feng et al. (Feng et al. 2004) observed that a pH between 3.5 and 8.5 and a pH between 5.2 and 8.5 was suitable for removal of Cu(II) and Pb(II). Among the industrial waste-based adsorbents, red mud (Zouboulis and Kydros 1993) exhibited an adsorption capacity of 160 mg/g for Ni(II) and that exhibited by blast-furnace slag (Dimitrova 1996) was 133.35 mg/g for Cu(II). Orange peel (Ajmal et al. 2000) exhibited adsorption capacity of 158 mg/g for Ni(II) and that exhibited by NaOH modified soybean hull and citric acid was 54.9 mg/g for Cu(II). Usage of coal bottom ash as adsorbent gave promising results, comparable to those given by adsorbents derived from other materials without causing environmental hazard. Reuse and regeneration of coal bottom ash may save the purchasing expense of fresh adsorbent (Rashidi and Yusup 2016). Vu et al. (Vu et al. 2020) studied coal bottom ash for adsorption of Cu, Pb, and Cd. The mesopore molecular sieve synthesized from coal bottom ash had maximum adsorption efficiencies of 41.66%, 43.98%, and 99.4%, for Cu, Cd, and Pb, respectively. Similarly, Li et al. (Li et al. 2018a) suggested low cost AC preparation from coal-blended sewage sludge for adsorption of metals. AC prepared from carbonation of coal-blended sewage sludge for adsorption of Cd(II), Cu(II), and Ni(II) exhibited adsorption capacities of 96.2, 87.7, and 52.4 mg/g for each metal, respectively, at pH 5.

Expense of adsorbents depends on its processing and availability. The cost efficacy of adsorbents for contaminants removal from wastewater is more if regenerated. Price can also be affected if more industries consider them for wastewater treatment. So far, no low cost adsorbent is made available for commercial use. Further research and development as well as in-depth study for scaling-up of production of adsorbents with outstanding removal performance and appropriate chemical regeneration is required. Coal processing gives rise to several waste materials which can be used as adsorbents to remove metal pollutants in wastewater. These substances are abundant and therefore large amount of value-added adsorbent materials can be produced.

10.6 Summary

Adsorption is a promising way to remove metals from wastewater. Coal-based AC is a sustainable solution for wastewater remediation as it has high adsorption performance, low cost, and abundant availability. Also, coal-based waste materials have potential to remove pollutants and at same time contribute to waste reduction, recovery, and reuse. In this study, coal-based AC was reviewed as adsorbent for the removal of Hg, Cd, Cr, As, Pb, and Cu from wastewater. Preparation method, surface properties, and structural and chemical modification of coal-based AC have significant impact on its characteristic. Adsorption performance is mainly affected due to pH of solution or temperature. pH of wastewater has significant impact on characteristics of present metal species. However, temperature has contradictory effect on adsorption, depending on metals; in some cases, metal adsorption capacity increases with temperature, whereas in some cases, it decreases with rise in temperature. Future prospective is related to enhancing the adsorption performance of coal-based AC and coal-based waste materials. The AC modification has led to the improvement in adsorption performance by appropriate chemical impregnation, surface chemistry, and composition modification of AC.

References

- Abdulsalam, J., Mulopo, J., Oboirien, B., Bada, S., & Falcon, R. (2019). Experimental evaluation of activated carbon derived from South Africa discard coal for natural gas storage. *International Journal of Coal Science and Technology*, 6, 459–477.
- Ahmadpour, A., & Do, D. D. (1996). The preparation of active carbons from coal by chemical and physical activation. *Carbon*, 34, 471–479.
- Ajmal, M., Rao, R. A. K., Ahmad, R., & Ahmad, J. (2000). Adsorption studies on *Citrus reticulata* (fruit peel of orange): Removal and recovery of Ni(II) from electroplating wastewater. *Journal of Hazardous Materials*, 79, 117–131.
- Ali Atieh, M. (2011). Removal of chromium (VI) from polluted water using carbon nanotubes supported with activated carbon. *Procedia Environmental Sciences*, 4, 281–293.
- Ansari, R., & Sadegh, M. (2007). Application of activated carbon for removal of arsenic ions from aqueous solutions. *E-Journal of Chemistry*, 4, 103–108.
- Anwar, J., Shafique, U., Salman, M., Waheed-uz-Zaman, Anwar, S., & Anzano, J. M. (2009). Removal of chromium (III) by using coal as adsorbent. *Journal of Hazardous Materials*, 171, 797–801.
- Arasteh, R., Masoumi, M., Rashidi, A. M., Moradi, L., Samimi, V., & Mostafavi, S. T. (2010). Adsorption of 2-nitrophenol by multi-wall carbon nanotubes from aqueous solutions. *Applied Surface Science*, 256, 4447–4455.
- Arpa, Ç., Başyılmaz, E., Bektaş, S., Genç, Ö., & Yürüm, Y. (2000). Cation exchange properties of low rank Turkish coals: Removal of Hg, Cd and Pb from waste water. *Fuel Processing Technology*, 68, 111–120.
- Arslan, G., & Pehlivan, E. (2007). Batch removal of chromium(VI) from aqueous solution by Turkish brown coals. *Bioresource Technology*, 98, 2836–2845.

- Asuquo, E., Martin, A., Nzerem, P., Siperstein, F., & Fan, X. (2017). Adsorption of Cd(II) and Pb(II) ions from aqueous solutions using mesoporous activated carbon adsorbent: Equilibrium, kinetics and characterisation studies. *Journal of Environmental Chemical Engineering*, *5*, 679–698.
- Attari, M., Bukhari, S. S., Kazemian, H., & Rohani, S. (2017). A low-cost adsorbent from coal fly ash for mercury removal from industrial wastewater. *Journal of Environmental Chemical Engineering*, *5*, 391–399.
- Bandosz, T. J., & Ania, C. O. (2006). Surface chemistry of activated carbons and its characterization. In T. J. Bandosz (Ed.), *Interface science and technology* (pp. 159–229). Elsevier.
- Bedia, J., Peñas-Garzón, M., Gómez-Avilés, A., Rodríguez, J., & Belver, C. (2018). A review on the synthesis and characterization of biomass-derived carbons for adsorption of emerging contaminants from water. *C*, *4*, 63.
- Bedia, J., Peñas-Garzón, M., Gómez-Avilés, A., Rodríguez, J. J., & Belver, C. (2020). Review on activated carbons by chemical activation with FeCl₃. *C Journal of Carbon Research*, *6*, 21.
- Bergna, D., Varila, T., Romar, H., & Lassi, U. (2018). Comparison of the properties of activated carbons produced in one-stage and two-stage processes. *C*, *4*, 41.
- Blander, M., Sinha, S., Pelton, A. D., Eriksson, G. (1989). Calculations of the Influence of Additives on Coal Combustion Deposits. *TMS Annual Meeting*, 340–346.
- Boparai, H. K., Joseph, M., & O'Carroll, D. M. (2011). Kinetics and thermodynamics of cadmium ion removal by adsorption onto nano zerovalent iron particles. *Journal of Hazardous Materials*, *186*, 458–465.
- Chen, H., Huo, Q., Wang, Y., Han, L., Lei, Z., Wang, J., Bao, W., & Chang, L. (2020). Upcycling coal liquefaction residue into sulfur-rich activated carbon for efficient Hg⁰ removal from coal-fired flue gas. *Fuel Processing Technology*, *206*.
- Chen, K., Zhang, Z., Xia, K., Zhou, X., Guo, Y., & Huang, T. (2019). Facile synthesis of thiol-functionalized magnetic activated carbon and application for the removal of mercury(II) from aqueous solution. *ACS Omega*, *4*, 8568–8579.
- Chunlan, L., Shaoping, X., Yixiong, G., Shuqin, L., & Changhou, L. (2005). Effect of pre-carbonization of petroleum cokes on chemical activation process with KOH. *Carbon*, *43*, 2295–2301.
- Dash, S., Chaudhuri, H., Gupta, R., Nair, U. G., & Sarkar, A. (2017). Fabrication and application of low-cost thiol functionalized coal fly ash for selective adsorption of heavy toxic metal ions from water. *Industrial and Engineering Chemistry Research*, *56*, 1461–1470.
- Demirbas, E. (2002). Removal of Ni(II) from aqueous solution by adsorption onto hazelnut shell activated carbon: Equilibrium studies. *Bioresource Technology*, *84*, 291–293.
- Deng, L., Su, Y., Su, H., Wang, X., & Zhu, X. (2007). Sorption and desorption of lead (II) from wastewater by green algae *Cladophora fascicularis*. *Journal of Hazardous Materials*, *143*, 220–225.
- Diamantopoulou, I., Skodras, G., & Sakellariopoulos, G. P. (2010). Sorption of mercury by activated carbon in the presence of flue gas components. *Fuel Processing Technology*, *91*, 158–163.
- Dimitrova, S. (1996). Metal sorption on blast furnace slag. *Water Research*, *30*, 228–232.
- Ding, L., Zou, B., Gao, W., Liu, Q., Wang, Z., Guo, Y., Wang, X., & Liu, Y. (2014). Adsorption of rhodamine-B from aqueous solution using treated rice husk-based activated carbon. *Colloids and Surfaces A: Physicochemical and Engineering Aspects*, *446*, 1–7.
- Dong, L., Liu, W., Jiang, R., & Wang, Z. (2016). Study on the adsorption mechanism of activated carbon removing low concentrations of heavy metals. *Desalination and Water Treatment*, *57*, 7812–7822.
- El Qada, E. N., Allen, S. J., & Walker, G. M. (2006). Adsorption of methylene blue onto activated carbon produced from steam activated bituminous coal: A study of equilibrium adsorption isotherm. *Chemical Engineering Journal*, *124*, 103–110.
- Elkady, M., Shokry, H., & Hamad, H. (2020). New activated carbon from mine coal for adsorption of dye in simulated water or multiple heavy metals in real wastewater. *Materials*, *13*, 2498.

- Erto, A., Giraldo, L., Lancia, A., & Moreno-Piraján, J. C. (2013). A comparison between a low-cost sorbent and an activated carbon for the adsorption of heavy metals from water. *Water, Air, and Soil Pollution*, 224.
- Fan, X., Li, C., Zeng, G., Gao, Z., Chen, L., Zhang, W., & Gao, H. (2010). Removal of gas-phase element mercury by activated carbon fiber impregnated with CeO₂. *Energy and Fuels*, 24, 4250–4254.
- Feng, D., Van Deventer, J. S. J., & Aldrich, C. (2004). Removal of pollutants from acid mine wastewater using metallurgical by-product slags. *Separation and Purification Technology*, 40, 61–67.
- Filho, N. L. D., Gushikem, Y., & Polito, W. L. (1995). 2-Mercaptobenzothiazole clay as matrix for sorption and preconcentration of some heavy metals from aqueous solution. *Analytica Chimica Acta*, 306, 167–172.
- Fowle, D. A., & Fein, J. B. (1999). Competitive adsorption of metal cations onto two gram positive bacteria: Testing the chemical equilibrium model. *Geochimica et Cosmochimica Acta*, 63, 3059–3067.
- Gao, S., Liu, L., Tang, Y., Jia, D., Zhao, Z., & Wang, Y. (2016). Coal based magnetic activated carbon as a high performance adsorbent for methylene blue. *Journal of Porous Materials*, 23, 877–884.
- Ghasemi, Z., Sourinejad, I., Kazemian, H., Hadavifar, M., Rohani, S., & Younesi, H. (2020). Kinetics and thermodynamic studies of Cr(VI) adsorption using environmental friendly multi-functional zeolites synthesized from coal fly ash under mild conditions. *Chemical Engineering Communications*, 207, 808–825.
- Gode, F., & Pehlivan, E. (2005). Adsorption of Cr(III) ions by Turkish brown coals. *Fuel Processing Technology*, 86, 875–884.
- Golovina, V. V., Eremina, A. O., Chesnokov, N. V., & Sobolev, A. A. (2018). Thermally activated Brown and Black coals as the sorbents of chromium(VI) from aqueous solutions. *Solid Fuel Chemistry*, 52, 240–246.
- González Vázquez, O. F., Del Rosario Moreno Virgen, M., Hernández Montoya, V., Tovar Gómez, R., Alcántara Flores, J. L., Pérez Cruz, M. A., & Montes Morán, M. A. (2016). Adsorption of heavy metals in the presence of a magnetic field on adsorbents with different magnetic properties. *Industrial and Engineering Chemistry Research*, 55, 9323–9331.
- Gopalakrishnan, A., Krishnan, R., Thangavel, S., Venugopal, G., & Kim, S. J. (2015). Removal of heavy metal ions from pharma-effluents using graphene-oxide nanosorbents and study of their adsorption kinetics. *Journal of Industrial and Engineering Chemistry*, 30, 14–19.
- Hsi, H. C., Chen, S., Rostam-Abadi, M., Rood, M. J., Richardson, C. F., Carey, T. R., & Chang, R. (1998). Preparation and evaluation of coal-derived activated carbons for removal of mercury vapor from simulated coal combustion flue gases. *Energy and Fuels*, 12, 1061–1070.
- Hsiao, H. W., Ullrich, S. M., & Tanton, T. W. (2011). Burdens of mercury in residents of Temirtau, Kazakhstan. I: Hair mercury concentrations and factors of elevated hair mercury levels. *Science of the Total Environment*, 409, 2272–2280.
- Huo, Q., Wang, Y., Chen, H., Han, L., Wang, J., Bao, W., Chang, L., & Xie, K. (2019). ZnS/AC sorbent derived from the high sulfur petroleum coke for mercury removal. *Fuel Processing Technology*, 191, 36–43.
- IARC. (2012). *Monographs on the evaluation of carcinogenic risks to humans: Radiation* (p. 274). World Health Organization.
- Ioannidou, O., & Zabaniotou, A. (2007). Agricultural residues as precursors for activated carbon production—a review. *Renewable and Sustainable Energy Reviews*, 11, 1966–2005.
- Jawad, A. H., Mehdi, Z. S., Ishak, M. A. M., & Ismail, K. (2018). Large surface area activated carbon from low-rank coal via microwave-assisted KOH activation for methylene blue adsorption. *Desalination and Water Treatment*, 110, 239–249.
- Jibril, B., Houache, O., Al-Maamari, R., & Al-Rashidi, B. (2008). Effects of H₃PO₄ and KOH in carbonization of lignocellulosic material. *Journal of Analytical and Applied Pyrolysis*, 83, 151–156.

- Joseph, L., Jun, B. M., Flora, J. R. V., Park, C. M., & Yoon, Y. (2019). Removal of heavy metals from water sources in the developing world using low-cost materials: A review. *Chemosphere*, 229, 142–159.
- Juang, R. S., Yei, Y. C., Liao, C. S., Lin, K. S., Lu, H. C., Wang, S. F., & Sun, A. C. (2018). Synthesis of magnetic Fe₃O₄/activated carbon nanocomposites with high surface area as recoverable adsorbents. *Journal of the Taiwan Institute of Chemical Engineers*, 90, 51–60.
- Kadirvelu, K., Thamaraiselvi, K., & Namasivayam, C. (2001). Removal of heavy metals from industrial wastewaters by adsorption onto activated carbon prepared from an agricultural solid waste. *Bioresource Technology*, 76, 63–65.
- Kadlec, O., Varhaníková, A., & Zukal, A. (1970). Structure of pores of active carbons prepared by water-vapour and zinc-dichloride activation. *Carbon*, 8, 321–331.
- Kalaruban, M., Loganathan, P., Nguyen, T. V., Nur, T., Hasan Johir, M. A., Nguyen, T. H., Trinh, M. V., & Vigneswaran, S. (2019). Iron-impregnated granular activated carbon for arsenic removal: Application to practical column filters. *Journal of Environmental Management*, 239, 235–243.
- Karabulut, S., Karabakan, A., Denizli, A., & Yürüm, Y. (2001). Cadmium (II) and mercury (II) removal from aquatic solutions with low-rank Turkish coal. *Separation Science and Technology*, 36, 3657–3671.
- Khulbe, K. C., & Matsuura, T. (2018). Removal of heavy metals and pollutants by membrane adsorption techniques. *Applied Water Science*, 8.
- Kobya, M. (2004). Removal of Cr(VI) from aqueous solutions by adsorption onto hazelnut shell activated carbon: Kinetic and equilibrium studies. *Bioresource Technology*, 91, 317–321.
- Kuroki, A., Hiroto, M., Urushihara, Y., Horikawa, T., Sotowa, K. I., & Alcántara Avila, J. R. (2019). Adsorption mechanism of metal ions on activated carbon. *Adsorption*, 25, 1251–1258.
- Lafferty, C., & Hobday, M. (1990). The use of low rank brown coal as an ion exchange material. 1. Basic parameters and the ion exchange mechanism. *Fuel*, 69, 78–83.
- Lakatos, J., Brown, S. D., & Snape, C. E. (2002). Coals as sorbents for the removal and reduction of hexavalent chromium from aqueous waste streams. *Fuel*, 81, 691–698.
- Li, J., Xing, X., Li, J., Shi, M., Lin, A., Xu, C., Zheng, J., & Li, R. (2018a). Preparation of thiol-functionalized activated carbon from sewage sludge with coal blending for heavy metal removal from contaminated water. *Environmental Pollution*, 234, 677–683.
- Li, L., Sun, F., Gao, J., Wang, L., Pi, X., & Zhao, G. (2018b). Broadening the pore size of coal-based activated carbon: Via a washing-free chem-physical activation method for high-capacity dye adsorption. *RSC Advances*, 8, 14488–14499.
- Li, Q., Zhai, J., Zhang, W., Wang, M., & Zhou, J. (2007). Kinetic studies of adsorption of Pb(II), Cr(III) and Cu(II) from aqueous solution by sawdust and modified peanut husk. *Journal of Hazardous Materials*, 141, 163–167.
- Li, W. G., Gong, X. J., Wang, K., Zhang, X. R., & Fan, W. B. (2014). Adsorption characteristics of arsenic from micro-polluted water by an innovative coal-based mesoporous activated carbon. *Bioresource Technology*, 165, 166–173.
- Lillo-Ródenas, M. A., Cazorla-Amorós, D., & Linares-Solano, A. (2003). Understanding chemical reactions between carbons and NaOH and KOH: An insight into the chemical activation mechanism. *Carbon*, 41, 267–275.
- Linares-Solano, A., Lillo-Ródenas, M. A., Marco-Lozar, J. P., Kunowsky, M., & Romero-Anaya, A. J. (2014). NaOH and KOH for preparing activated carbons used in energy and environmental applications. *Research and Applications for Energy, the Environment, and Economics*, 20, 59–92.
- Liu, D., Gao, J., Cao, Q., Wu, S., & Qin, Y. (2017). Improvement of activated carbon from Jixi bituminous coal by air preoxidation. *Energy and Fuels*, 31, 1406–1415.
- Liu, D. D., Jia, B. Y., Li, S., Dong, L. J., Gao, J. H., & Qin, Y. K. (2019). Effect of pyrolysis conditions on the improvement of the physicochemical structure of activated carbon obtained from Jixi bituminous coal. *Asia-Pacific Journal of Chemical Engineering*, 14, 1–12.

- Lopez, F. A., Perez, C., Sainz, E., & Alonso, M. (1995). Adsorption of Pb²⁺ on blast furnace sludge. *Journal of Chemical Technology & Biotechnology*, 62, 200–206.
- Lv, X., Zhang, T., Luo, Y., Zhang, Y., Wang, Y., & Zhang, G. (2020). Study on carbon nanotubes and activated carbon hybrids by pyrolysis of coal. *Journal of Analytical and Applied Pyrolysis*, 146, 104717.
- Malamis, S., & Katsou, E. (2013). A review on zinc and nickel adsorption on natural and modified zeolite, bentonite and vermiculite: Examination of process parameters, kinetics and isotherms. *Journal of Hazardous Materials*, 252–253, 428–461.
- Malik, R., Ramteke, D. S., & Wate, S. R. (2007). Adsorption of malachite green on groundnut shell waste based powdered activated carbon. *Waste Management*, 27, 1129–1138.
- Malkoc, E., & Nuhoglu, Y. (2005). Investigations of nickel(II) removal from aqueous solutions using tea factory waste. *Journal of Hazardous Materials*, 127, 120–128.
- Min, H., Ahmad, T., & Lee, S. S. (2017). Mercury adsorption characteristics as dependent upon the physical properties of activated carbon. *Energy and Fuels*, 31, 724–729.
- Mnasri-Ghnnimi, S., & Frini-Srasra, N. (2019). Removal of heavy metals from aqueous solutions by adsorption using single and mixed pillared clays. *Applied Clay Science*, 179.
- Mouni, L., Merabet, D., Bouzaza, A., & Belkhiri, L. (2011). Adsorption of Pb(II) from aqueous solutions using activated carbon developed from apricot stone. *Desalination*, 276, 148–153.
- Musyoka, N. M., Wdowin, M., Rambau, K. M., Franus, W., Panek, R., Madej, J., & Czarna-Juskiewicz, D. (2020). Synthesis of activated carbon from high-carbon coal fly ash and its hydrogen storage application. *Renewable Energy*, 155, 1264–1271.
- Niu, T., Zhou, J., Zhang, C., & Li, S. (2018). Fast removal of methylene blue from aqueous solution using coal-based activated carbon. *RSC Advances*, 8, 26978–26986.
- Orumwense, F. F. O. (1996). Removal of lead from water by adsorption on a kaolinitic clay. *Journal of Chemical Technology and Biotechnology*, 65, 363–369.
- Papandreou, A., Stournaras, C. J., & Panias, D. (2007). Copper and cadmium adsorption on pellets made from fired coal fly ash. *Journal of Hazardous Materials*, 148, 538–547.
- Patnukao, P., Kongsuwan, A., & Pavasant, P. (2008). Batch studies of adsorption of copper and lead on activated carbon from Eucalyptus camaldulensis Dehn. Bark. *Journal of Environmental Sciences*, 20, 1028–1034.
- Rajakovic, L. V. (1992). Sorption of arsenic onto activated carbon impregnated with metallic silver and copper. *Separation Science and Technology*, 27, 1423–1433.
- Rao, K., Mohapatra, M., Anand, S., & Venkateswarlu, P. (2011). Review on cadmium removal from aqueous solutions. *International Journal of Engineering, Science and Technology*, 2, 81–103.
- Rashidi, N. A., & Yusup, S. (2016). Overview on the potential of coal-based bottom ash as low-cost adsorbents. *ACS Sustainable Chemistry and Engineering*, 4, 1870–1884.
- Renu, Agarwal, M., & Singh, K. (2017). Heavy metal removal from wastewater using various adsorbents: A review. *Journal of Water Reuse and Desalination*, 7, 387–419.
- Sen Gupta, S., & Bhattacharyya, K. G. (2011). Kinetics of adsorption of metal ions on inorganic materials: A review. *Advances in Colloid and Interface Science*, 162, 39–58.
- Simate, G. S., Maledi, N., Ochieng, A., Ndlovu, S., Zhang, J., & Walubita, L. F. (2016). Coal-based adsorbents for water and wastewater treatment. *Journal of Environmental Chemical Engineering*, 4, 2291–2312.
- Sočo, E., & Kalemekiewicz, J. (2013). Adsorption of nickel(II) and copper(II) ions from aqueous solution by coal fly ash. *Journal of Environmental Chemical Engineering*, 1, 581–588.
- Sreenivas, K. M., Inarkar, M. B., Gokhale, S. V., & Lele, S. S. (2014). Re-utilization of ash gourd (*Benincasa hispida*) peel waste for chromium (VI) biosorption: Equilibrium and column studies. *Journal of Environmental Chemical Engineering*, 2, 455–462.
- Sulaymon, A. H., Mohammed, T. J., & Al-najar, J. (2012). Equilibrium and kinetics studies of adsorption of heavy metals onto activated carbon. *Canadian Journal on Chemical Engineering & Technology*, 3, 86–92.

- Sun, J., Hippo, E. J., Marsh, H., O'Brien, W. S., & Crelling, J. C. (1997). Activated carbon produced from an Illinois basin coal. *Carbon*, 35, 341–352.
- Taraba, B., & Veselá, P. (2016). Sorption of Lead(II) ions on natural coals and activated carbon: Mechanistic, kinetic, and thermodynamic aspects. *Energy and Fuels*, 30, 5846–5853.
- Taşar, Ş., Kaya, F., & Özer, A. (2014). Biosorption of lead(II) ions from aqueous solution by peanut shells: Equilibrium, thermodynamic and kinetic studies. *Journal of Environmental Chemical Engineering*, 2, 1018–1026.
- Tian, L., Li, C., Li, Q., Zeng, G., Gao, Z., Li, S., & Fan, X. (2009). Removal of elemental mercury by activated carbon impregnated with CeO₂. *Fuel*, 88, 1687–1691.
- Uddin, A., Ozaki, M., Sasaoka, E., & Wu, S. (2009). Temperature-programmed decomposition desorption of mercury species over activated Arbon sorbents for mercury removal from coal-derived fuel gas. *Energy and Fuels*, 23, 4710–4716.
- Vu, D. H., Bui, H. B., Bui, X. N., An-Nguyen, D., Le, Q. T., Do, N. H., & Nguyen, H. (2020). A novel approach in adsorption of heavy metal ions from aqueous solution using synthesized MCM-41 from coal bottom ash. *International Journal of Environmental Analytical Chemistry*, 100, 1226–1244.
- Wang, L., Sun, F., Gao, J., Pi, X., Pei, T., Qie, Z., Zhao, G., & Qin, Y. (2018a). A novel melt infiltration method promoting porosity development of low-rank coal derived activated carbon as supercapacitor electrode materials. *Journal of the Taiwan Institute of Chemical Engineers*, 91, 588–596.
- Wang, L., Sun, F., Gao, J., Pi, X., Qu, Z., & Zhao, G. (2018b). Adjusting the porosity of coal-based activated carbons based on a catalytic physical activation process for gas and liquid adsorption. *Energy and Fuels*, 32, 1255–1264.
- Wang, X. L., Shen, J., Niu, Y. X., Wang, Y. G., Liu, G., & Sheng, Q. T. (2018c). Removal of phenol by powdered activated carbon prepared from coal gasification tar residue. *Environmental Technology (United Kingdom)*, 39, 694–701.
- Wasewar, K. L., Kumar, P., Chand, S., Padmini, B. N., & Teng, T. T. (2010). Adsorption of cadmium ions from aqueous solution using granular activated carbon and activated clay. *Clean—Soil, Air, Water*, 38, 649–656.
- Witek-Krowiak, A., Szafran, R. G., & Modelski, S. (2011). Biosorption of heavy metals from aqueous solutions onto peanut shell as a low-cost biosorbent. *Desalination*, 265, 126–134.
- Wu, F. C., Wu, P. H., Tseng, R. L., & Juang, R. S. (2010). Preparation of activated carbons from unburnt coal in bottom ash with KOH activation for liquid-phase adsorption. *Journal of Environmental Management*, 91, 1097–1102.
- Wu, J., Zhao, Z., Huang, T., Sheng, P., Zhang, J., Tian, H., Zhao, X., Zhao, L., He, P., Ren, J., & Gao, K. (2017a). Removal of elemental mercury by Ce-Mn co-modified activated carbon catalyst. *Catalysis Communications*, 93, 62–66.
- Wu, M., Shi, L., & Mi, J. (2017b). Preparation and desulfurization kinetics of activated carbons from semi-coke of coal liquefaction residual. *Journal of Thermal Analysis and Calorimetry*, 129, 1593–1603.
- Xu, Y., & Chai, X. (2018). Characterization of coal gasification slag-based activated carbon and its potential application in lead removal. *Environmental Technology (United Kingdom)*, 39, 382–391.
- Yantasee, W., Lin, Y., Fryxell, G. E., Alford, K. L., Busche, B. J., & Johnson, C. D. (2004). Selective removal of copper(II) from aqueous solutions using fine-grained activated carbon functionalized with amine. *Industrial and Engineering Chemistry Research*, 43, 2759–2764.
- Yi, Z., Yao, J., Zhu, M., Chen, H., Wang, F., & Liu, X. (2016). Kinetics, equilibrium, and thermodynamics investigation on the adsorption of lead(II) by coal-based activated carbon. *Springerplus*, 5.
- Youssef, A. M., El-Wakil, A. M., El-Sharkawy, E. A., Farag, A. B., & Tollan, K. (1996). Adsorption of heavy metals on coal-based activated carbons. *Adsorption Science and Technology*, 13, 115–125.

- Zhang, H., Niu, J., Yin, X., Guo, Y., & Cheng, F. (2020). Role of inherent pyrite in coal on physico-chemical structure of activated carbon and adsorption capacity. *Fuel*, *262*, 116527.
- Zhong, L., Zhang, Y., Ji, Y., Norris, P., & Pan, W. P. (2016). Synthesis of activated carbon from coal pitch for mercury removal in coal-fired power plants. *Journal of Thermal Analysis and Calorimetry*, *123*, 851–860.
- Zou, Y., & Han, B. X. (2001). High-surface-area activated carbon from Chinese coal. *Energy and Fuels*, *15*, 1383–1386.
- Zouboulis, A. I., & Kydros, K. A. (1993). Use of red mud for toxic metals removal: The case of nickel. *Journal of Chemical Technology & Biotechnology*, *58*, 95–101.

Chapter 11

Generation, Transportation and Utilization of Indian Coal Ash



Ranjan Kumar Mohapatra, Pradeep Kumar Das, Dulal C. Kabiraz, Debadutta Das, Ajit Behera, and Md. Kudrat-E-Zahan

11.1 Introduction

The production of fly ash (FA) from several thermal power plants situated in various regions in India and also from all over the globe is really challenging to the environment. The most fly ash generating countries are India, China, the USA and Russia. This combustion product has numerous applications. However, it is considered as a waste material and is dumped in various disposal sites. Most of the thermal power stations prefer pipeline transportation to transport fly ash in the form of slurry to various disposal sites of power stations (called ash ponds). In pipeline transportation, water acts as a medium, and with the help of a pump, fly ash particles are transported from power stations to ash ponds. Fly ash slurry (FAS) has the same characteristics as a non-Newtonian fluid or Bingham fluid. The rheological properties of FAS had been discussed by FA concentration, particle size distribution, surfactant concentration, addition of BA (bottom ash) as additive, temperature and pH of the slurry (Pattanaik et al. 2019).

R. K. Mohapatra (✉)

Department of Chemistry, Government College of Engineering, Keonjhar, Odisha, India

P. K. Das

Department of Chemistry, N. C. (Autonomous) College, Jajpur, Odisha, India

D. C. Kabiraz · M. Kudrat-E-Zahan

Department of Chemistry, Faculty of Science, University of Rajshahi, Rajshahi, Bangladesh

D. Das

Department of Chemistry, Sukanti Degree College, Subarnapur, Odisha, India

A. Behera

Department of Metallurgical & Materials Engineering, National Institute of Technology (NIT), Rourkela, Odisha, India

Coal is a major source of fuel in today's India and China. We can find the use of coal in our every aspects of life from a very fundamental use as in cooking, other domestic purposes to largely in producing electricity. It has been the backbone of power generation everywhere in the world. China is the biggest coal consumer (global demand = 50%), whereas India is placed in second position. The global fly ash generation and utilization is shown in Fig. 11.1 (Gollakota et al. 2019). From the data, it is cleared that the top FA producers (India, China and the USA) have less utilization rate. This makes a huge challenge to the society and the environment. According to Bhatt et al. (2019), the common utilization of FA in India is shown in Fig. 11.2. It is a fine powder and has the tendency to travel far with the air. If not properly disposed, it may cause respiratory problems when inhaled. It will trigger asthma, silicosis and inflammation in lungs. According to some recent reports, these particulates are responsible for different respiratory diseases, heart diseases, stroke and cancer. Furthermore, the presence of toxic heavy metals (Cr, Pb, Hg, As, etc.) in such dusts may cause harmful effects on inhalation.

India is majorly depending on thermal power plants for generating electricity. Over the last few decades, there has been an increasing interest in innovating new techniques and technologies such as renewable and bioenergy worldwide due to severe environmental constraints on fossil fuels burning. Huge amount of particulate matters (such as dust, tiny parts of metals, soil, chemicals, and micro-plastics) are formed in air due to mainly burning fossil fuels, running of automobiles, etc.

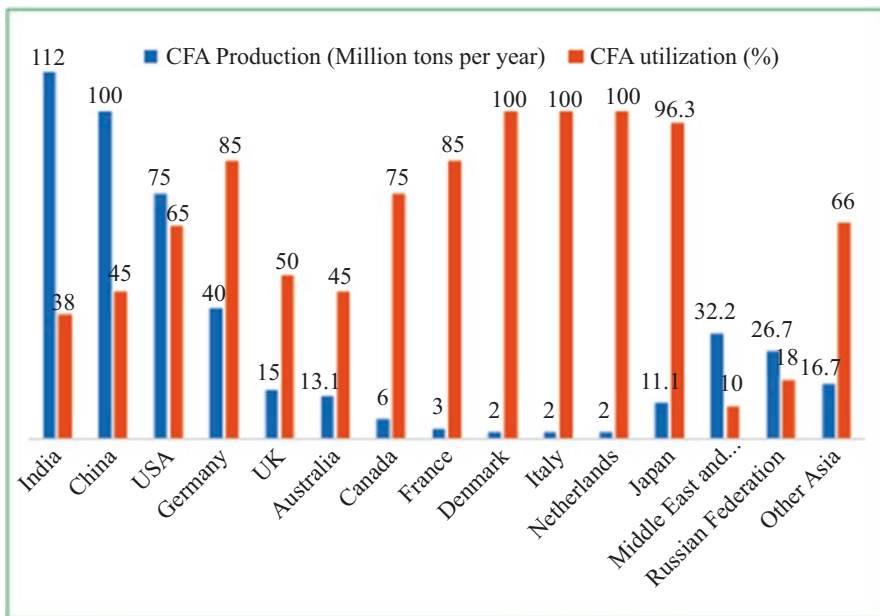


Fig. 11.1 The production and utilization of FA (Adapted with Permission from Gollakota et al. 2019 © Elsevier B. V.)

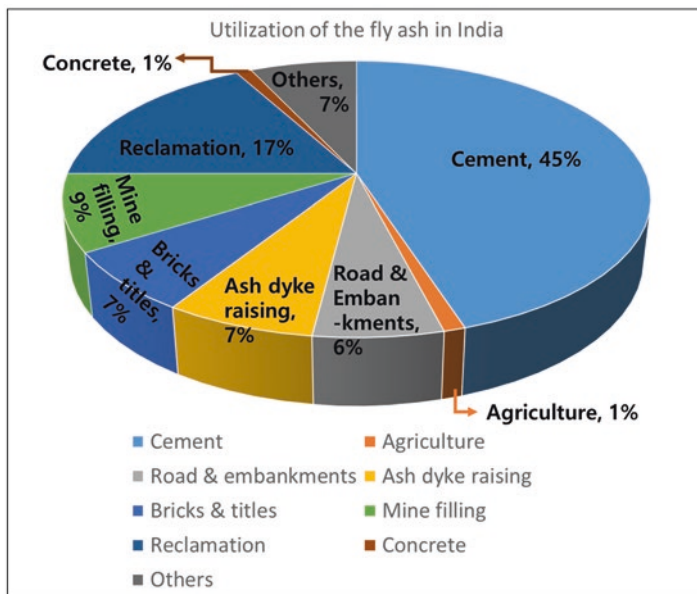


Fig. 11.2 Utilization of fly ash in India

Long-term exposure to fine particulate matter (SO₂, NO₂, etc.) may cause respiratory illness by reducing lung function. Moreover, these pollutants may cause relentless inflammatory response and ultimately raise the infection risk by targeting the airway. As per the study, poor air quality may allow people at higher risk and are vulnerable to serious illness and at times leading to death (Mohapatra et al. 2021).

Nowadays, the disposal of FA in the present situation has been a big challenge to the environment, as the need of electricity increases from time to time. This indicates the production of more and more amount of coal ash in near future. Hence, there is a constant need of handling such huge amount of fly ash. One conventional method is to dispose of both FA and bottom ash (BA) in the ash ponds around the thermal plant which requires vast tracts of land. The real challenge will start when one ash pond fills up; another has to be built at a great cost which leads to loss of or conversion of agricultural land. Moreover, numerous salts and metallic contents may leach down to the groundwater which contaminates it. Hence, the process is a sources of pollution for soil and water and also disrupts ecological cycles and set off environmental hazards. However, the best way to handle flue ash is to utilize it in many ways (Fig. 11.3) but not to dump in an open area. Presently, FA is used in manufacturing bricks and as an additive in cement industries. It is also used as a pozzolan in PCC applications. For the unique spherical shape of fly ash particles and size distribution, it acts as filler in hot mix asphalt applications. Moreover, the consistency and ample amount of FA show unique opportunities for its use in structural fills and other engineering works in many different locations (Ghazali and Kaushal 2015). In this chapter, we have described the generation of FA from

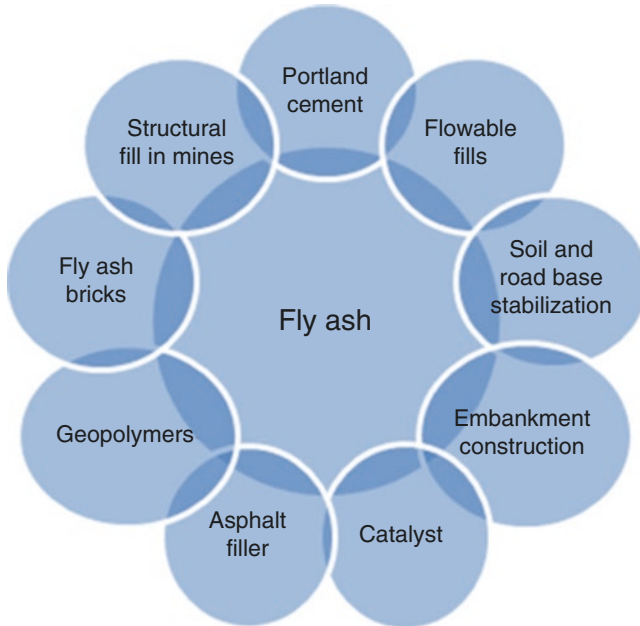


Fig. 11.3 The common uses of fly ash

different power plants, its stabilization for pipeline transportation and its utilization as fly ash bricks.

11.2 Generation of Fly Ash in India

The combustion of pulverized coal in power stations (in the boilers) produces energy along with different types of ash. During the combustion process, the volatile matter and fixed carbon burns in the boiler and the 'fine' ash fraction is moved upwards with flue gases and captured with the help of electrostatic precipitators before reaching the atmosphere (Fig. 11.4). It is mainly composed of extremely fine, glassy spheres and called FA which is a common by-product of thermal power plants. The residue part settles down at the bottom of the container and the cluster is called BA (Naik and Singh 1993). Moreover, burning of coal also produces boiler slag, flue-gas desulfurization residues, etc. The complete combustion of coal or biomass results inorganic residues due to the burning of organic and inorganic components present (Mishra and Gupta 2017; Karampinis et al. 2011; Chouhan et al. 2018; Das et al. 2020a, b). It is difficult to predict properly the properties of FA generated from combustion of coal which is mainly due to the interactions between the components of fuel mixtures. So, it is very essential to characterize the ashes fully produced from the burning of any fuel. The characteristics of particles of FA depend on

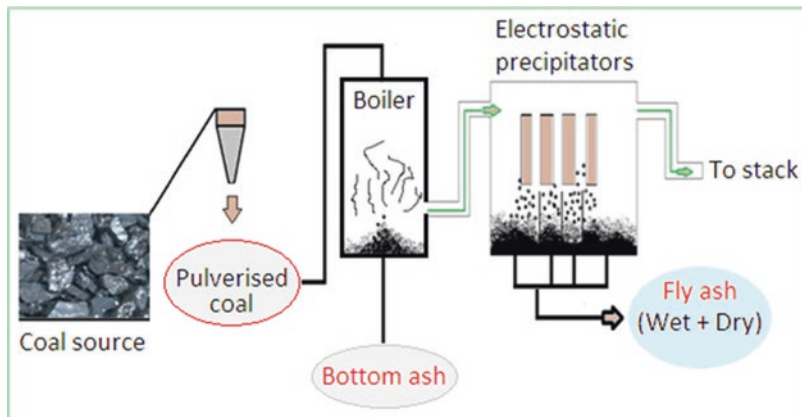
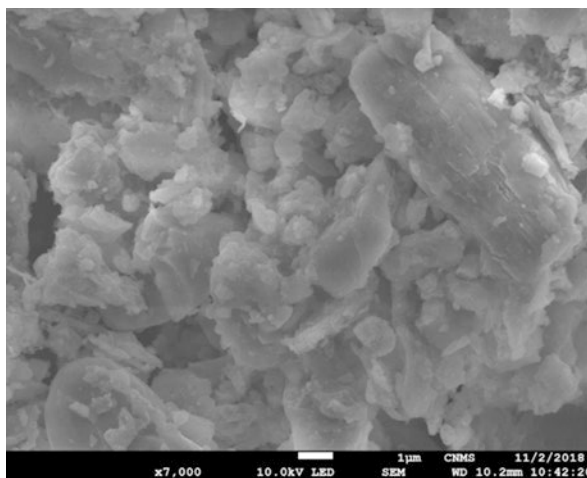


Fig. 11.4 Schematic representation for the generation of fly ash

Fig. 11.5 SEM photomicrograph of fly ash sample (Adapted with Permission from Pattanaik et al. 2019, © Elsevier B. V)



the quality of the fuel (coal) and efficiency of the boilers used in the production process. In India, low-grade coal is used having ash content 30-45%; however, imported foreign coals have low ash content (10-15%) (Sivalingam 2011). Thus, a huge quantity of ash is continuously generated at coal-based Indian thermal power plants. The ash production in various types of coals is as follows:

Peat >> Lignite >> sub-bituminous >> bituminous >> anthracite

There are usually three types of coal ash found near the thermal power plants (Fig. 11.5):

- *Dry fly ash:* This type of ash in coal burning is collected by using electrostatic precipitators, housing bags, or windscreen collectors.
- *Bottom ash:* This type is collected below the furnace (boiler) and characterized by better geotechnical properties.

- *Flue ash*: FA mixed with water in the form of slurry drawn into the ash ponds. In a pool of ash, the ashes are prepared and water as excessive. It is also termed as pond ash.

Pulverized coal during its burning in boiler produces fine-grained, glassy, powdery particles (size range from 2 to 10 μ m) which is moved with the flue gas and typically collected by using electrostatic precipitators, housing bags, or mechanical collection devices like cyclones. Generally, the electric producing industries use three major types of boiler furnaces (wet-bottom boilers, dry-bottom boilers, and cyclone furnaces). However, dry-bottom furnace is the most common sort of coal burning furnace. The pulverized coal on combustion produces 75% ash in a dry-bottom boiler, 50% ash in a wet-bottom or slag-tap furnace and 30–40% ash in a cyclone furnace. Around 70% energy requirement of India comes from thermal power plant and 90% of the thermal plants use lignite and bituminous coals of Indian origin for producing electricity. Thus, huge amount of coal ash is produced after combustion. The year wise approximate fly ash generation in India is listed in Table 11.1.

11.3 Types of Fly Ash

Normally, as per boiler operations, low-temperature fly ash (combustion temperature < 900 °C) and high-temperature fly ash (combustion temperature < 1000 °C) are

Table 11.1 Year wise approximate fly ash generation statistics

Year	Generation of electricity (TWh)	Coal requirement (million tonnes)	Generation of fly ash (million tonnes)
2018–19	1160	780	1002
2016–17	1135	745	194
2015–16	1098	710	186
2014–15	1083	670	179
2013–14	1050	637	172
2012–13	1012	608	167
2011–12	985	577	154
2010–11	932	546	145
2009–10	881	516	138
2008–09	833	488	130
2007–08	787	461	123
2006–07	744	436	116
2005–06	702	411	110
2004–05	662	388	103
2003–04	624	366	97
2002–03	589	345	92
2001–02	555	325	87
2000–01	522	306	82
1999–2000	491	288	77

generated. According to ASTM C618, FA is categorized into mainly two types as per their chemical properties (Ismail et al. 2007).

Type-C: this type of FA is formed from the combustion of sub-bituminous or lignite coals. Such FA contains CaO greater than 10% (as high as 30%) and has cementitious properties along with pozzolanic properties. Due to higher lime content, self-hardening characteristics are developed.

Type-F: this type of FA is generated from the combustion of bituminous or anthracite coals. This kind of FA is generated in larger quantities having low lime and contains greater combination of silica, iron and alumina (more than 70%). Such FA contains CaO less than 10% and has pozzolanic properties.

The major chemical compounds of FA are silica oxide (SiO), lime (CaO), aluminium oxide (Al_2O_3), and iron oxide (Fe_2O_3). These are also found in cement but the proportion is different. Fly ash has higher amount of reactive silicates. So, it is recommended to use FA with Portland cement (Fig. 11.6). Here, FA combines with free lime to produce same cementations compounds (calcium silicate hydrate) (Headwaters 2005).

11.4 Rheological Model

Rheology is the experimental characterization of rheological behaviour of a material. This is more applicable to non-Newtonian fluids having a complex microstructure like polymers, sludges, suspensions, etc. Bingham plastic fluid is a non-Newtonian fluid which finds a linear relation between shear rate and shear stress after an initial threshold (Das et al. 2008; Das et al. 2010; Das et al. 2019; Das et al. 2020a, b; Das et al. 2013). Shear stress also called yield stress is a significant parameter in pipeline transportation. The shear rate is applied to overcome yield stress in pipeline during pumping and the fluid is shown to flow linearly with increase in shear rate. Some examples of Bingham plastics fluids are mayonnaise, jam, toothpaste, etc. Thus, concentrated fly ash slurry being a non-Newtonian fluid starts to flow after an initial yield stress verge is reached. Hence, the fly ash slurry behaves as a Bingham plastic and follows the Bingham model.

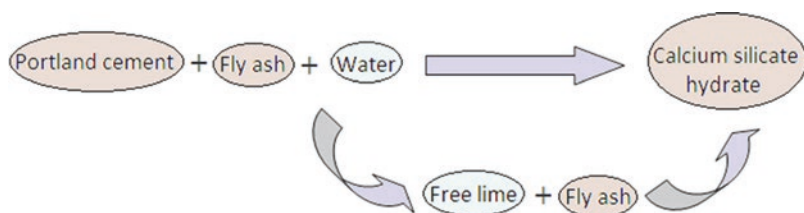


Fig. 11.6 Chemical reaction involving in Portland cement with fly ash

$$\text{i.e. } \tau = \tau_y + \frac{\partial v}{\partial y} \quad (11.1)$$

where τ_y = yield stress (N/m^2),
 η_p = plastic viscosity (Pas),
 $\frac{\partial v}{\partial y}$ = shear rate (s^{-1}),
 τ = shear stress.

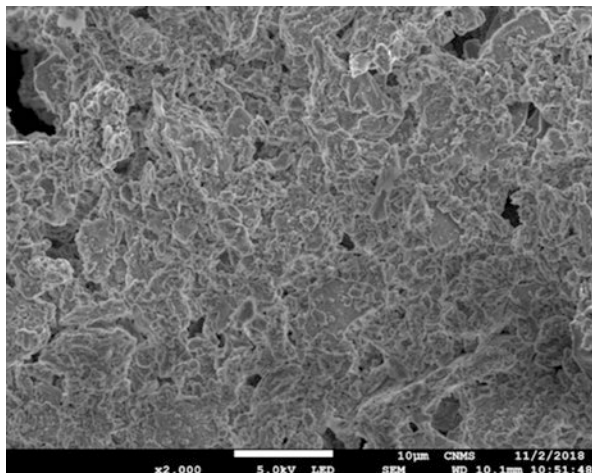
11.4.1 Stabilization of Fly Ash Slurry (FAS) by Using Surfactant

Surfactant is a surface active agent which reduces the surface tension and promotes the wetting of solid particles. This produces a well dispersion of solid particle in liquid by creating coating around each fly ash particle (Das et al. 2013). Naik et al. (2011) have investigated the mechanism of stabilization and rheological characteristics of FAS, a commercial dispersant CTAB in the studied range of shear rates ($25\text{--}1000$) s^{-1} and temperature ($20\text{--}40$) $^\circ\text{C}$. They have also studied the effect of sodium silicate as counter ion and concluded that wettability and suspension stability of FA is significantly improved.

Yang et al. (2018) have studied the flow behaviour and microstructure of alkali-treated FA pastes. The flow ability of FA paste was improved by using the dispersant sodium silicate. Chandel et al. (2009) investigated the combined effect of henko detergent and sodium carbonate on rheological characteristics and pressure drop of high concentrated FAS. They postulated that ash concentration up to 60% by weight can be easily transported through pipeline with minimum pressure drop. Moreover, Rhamsan gums, xanthan gum and carboxymethyl cellulose were used as stabilizing agent for pipeline transportation of dense FAS studied by Li et al. (2002). It was found that additives can effectively increase the slurry ability. Furthermore, Pani et al. (2015) have studied the non-Newtonian behaviour of 50-60% concentration fly ash slurry taking sodium silicate and ghadi detergent as dispersing agent. It was observed that the slurry exhibit non-Newtonian behaviour and fitted to Bingham plastic model with significant reduction in yield stress.

Singh and Lal (2012) have investigated the rheological property of 40% concentration of ash slurry by treating the FA particle with three different types of surface active agent, namely Cetylpyridinium chloride, SDS and Triton x-100. Stabilizing tendency of additive was evaluated on the basis of viscosity reduction and pH changes of bare slurry and treated slurry. Kolář et al. (1988) have studied flow behaviour fly ash slurry in an ash-slag hydro transport pipeline in the presence of a drag reducing polymer. They studied the different rheological parameters like pressure drop, velocities, fly ash concentration and concentration of polymers.

Fig. 11.7 SEM photomicrograph of air-drying FAS. (Adapted with Permission from Pattanaik et al. 2019 © Elsevier B. V)



In addition to synthetic and commercial drag reducing agent dispersant isolated from natural plant were found to stabilize FAS dispersion. Saponin isolated from the plant *Sapindus laurifolia* was used to prepare high concentrated FAS by Das et al. (2019). They investigated that the Wettability of FA particles was increased by addition of aqueous extract of *S. laurifolia* in comparison to slurry prepared by adding water only. This was confirmed by measuring the surface tension of both the slurry. SEM image of FA treated with saponin of *S. laurifolia* confirmed agglomeration of fly ash particle (Fig. 11.7). Similarly, another saponin-containing plant *Acacia concinna* may be utilized for stabilization of high concentrated fly ash slurry as reported by Pattanaik et al. (2019). They have investigated the effect of FA and saponin concentration, temperature and pH on apparent viscosity of FAS. Furthermore, Senapati et al. (2012) have used sodium silicate and selective bio-additive to study leaching and rheological characteristics of high-concentration FAS. Here, sodium silicate was used as a stabilizer.

11.4.2 Addition of Bottom Ash as Additive

Assefa and Kaushal (2015) have studied the role of bottom ash on the rheological characteristics of FAS taking FA (60–65%) and BA (10–40%). The slurry exhibited Bingham plastic behaviour. With increase in fly ash concentration result an increase in viscosity as well as shear stress. Chandel et al. (2010) have investigated the flow behaviour of high-concentration CAS by adding both FA and BA in the ratio of 4:1 proportion. Taking different concentrations of FA pressure drop was measured and velocity of flow was analysed. Singh et al. (2017a, b) studied the pipeline transportation of FAS containing multimodal particle size distribution with and without

addition of BA. It was concluded that addition of coarse fraction particle to finer ash particle improves the slurry rheology significantly.

Temperature has a significant effect on the rheology of mixture of bottom ash and fly ash mixture. Kumar et al. (2016) have studied the blending of both at various weight proportions in the ratio 8:2, 7:3 and 9:1. And rheological behaviour was enhanced by the addition of coarser particles. Rani and Jain (2017) have reported mixture of BA and FA during hydraulic transportation of FA in mine fill. Knezevic and Kolonja (2008) have studied the effect of FA concentration on flow behaviour and pressure drop in slurry transportation. It was found that there were noteworthy changes in flow behaviour by increasing FA concentration, particularly in the concentration range of 40–50%.

Iyer (2002) have reported the leaching of FA for transportation in the form of slurry. In his study ash (coarser) leaching chemistry of surface was evaluated for highlighting role of transfer of mass therefore postponing ash's elemental leaching, at times of disposal or additional value utilization. Distribution of particle on the basis of size after leaching was evaluated to be constant which demonstrated involvement of ash particle's surface exclusively during leaching. Particle gradation and size of the particle can affect the rheological characteristics of FAS in pipelines transportation was investigated by Kumar et al. (2003). They found that slurry containing a blend of both finer and coarser particle requires lesser amount of energy for pipeline transportation in comparison to slurry containing only fine particle.

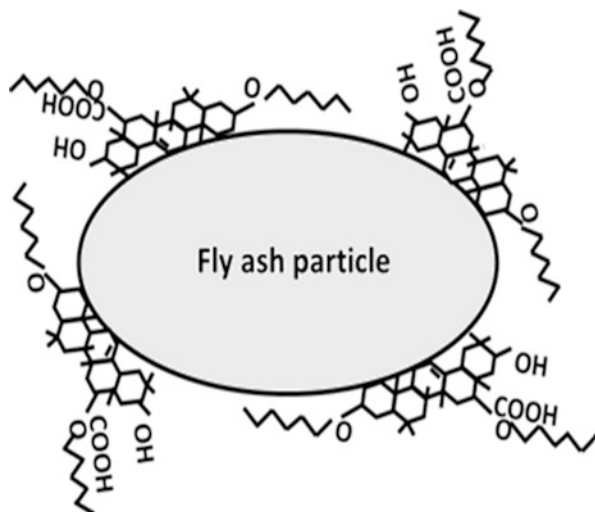
11.4.3 Mechanism of Stabilization

Major constituents of FA are Silica (SiO_2) and alumina (Al_2O_3) and their percentage are up to 54.6% and 32.8%, respectively. Any types of slurry stabilization mean to create a barrier among the solid particle in the slurry, so that particle-particle association is inhibited. This causes the steric wettability of FA particles (Pattanaik et al. 2019; Das et al. 2019). FAS stabilization mechanism can be explained by considering the Fig. 11.8. The non-polar part of the surfactant molecule which is hydrophobic in nature is attached on the silica particle by a specific interaction with hydrogen of silanol of FA, and the polar part which is bulky hydrophilic is attracted towards the water medium. This produces a coating around each particle and restricts agglomeration of FA particles.

11.5 Clay Brick (CB) to Fly Ash Brick (FAB)

The coal fly ash includes 188 mineral groups and 316 individual minerals, as per various FA samples on the basis of previous literatures. The main constituents of FA are metallic oxides (Fe_2O_3 , SiO_2 , Al_2O_3 , CaO , K_2O , MgO , etc.) and unburnt carbon compositions. Composition of the minor component will be varying based on type

Fig. 11.8 Interaction mechanism of fly ash and saponin from *Acacia concinna* plant (Adapted with Permission from Pattanaik et al. 2019 © Elsevier B. V)



of coal. Yao et al. (2015) have investigated on FA mineralogical properties and feasibility of their various application or disposal. Due to pozzolanic behaviour and high strength-to-weight, FA has much attention in many applications such as in construction industry, environmental protection, zeolite synthesis, depth separation, and reclamation, soil amelioration, ceramic industry, catalysis and chemical industries. In construction industries, fly ash gives a new direction towards green technology, globally. FA contains many cementitious compounds that have advantages as compared to the clay brick. The difference between the fly ash brick and clay brick has been given in Table 11.2. FAB is mainly utilized in constructing the buildings, road pavements and in furnace linings. Figure 11.9(a) shows the scanning electron microscopy of raw fly ash, which is used to produce the brick as shown in Fig. 11.9(b).

Naganathan et al. (2015) have investigated the compressive strength, modulus of rupture, ultrasonic pulse velocity, and water absorption behaviour in both the FA and BA bricks. He found out 7.13–17.36 MPa compressive strength in FAB which is much more than that of clay bricks and cement bricks. Ultrasonic pulse velocity and modulus of rupture is in the range of 2.2–2.96 km/s and 12.08–23.4 MPa, respectively, which is more than the conventional bricks. Cultrone and Sebastián (2009) have done analysis on petrophysical properties of fly ash brick that fired with 800 and 1000 °C temperatures. He found out that there is no increase in hydric properties when including fly ash in normal brick. Fly ash brick in exposure to salt crystallization cycles gives less damage as compared with the normal brick (Cultrone and Sebastián 2009). Kayali and Sharfuddin (2013) has been studied on the 100% fly ash brick (flash bricks) without addition of clay and shale. They found a 28% lighter brick than clay brick and has 40 MPa compressive strength. The class F fly ash in brick manufacturing with both fired and non-fired mode has also been investigated. Leiva et al. (2016) have studied the co-combustion FA in place of clay brick, in pollutant reduction. Due to the contribution of this type of brick in green

Table 11.2 Characteristics of FAB and normal bricks

Characteristics	Remarks
Colour	Colour depends on the absorption and emission factor which normally depends on composition of the brick. Appearance of FA is cement colour due to the presence of predominant ash. In case of general clay brick, the colour changes from brown (green structure) to red form (burnt final product)
Composition	Lime in both FAB and clay brick plays a major role in binding. A typical fly ash brick contains SiO ₂ (58.00 wt. %), Al ₂ O ₃ (29.30 wt. %), Fe ₂ O ₃ (5.60 wt. %), CaO (1.05 wt. %), TiO ₂ (1.70 wt. %), MgO (1.25 wt. %), P ₂ O ₅ (0.25 wt. %), K ₂ O (0.84 wt. %), Na ₂ O (0.61 wt. %), SO ₃ (0.41 wt. %), H ₂ O (0.20 wt. %). Whereas, clay brick contains 50-60 wt. % silica (sand), 20-30 wt. % alumina (clay), 2-5 wt% lime and ≤ 7 wt. % iron oxide
Texture	FA contains mostly globular oxide particles, silica and alumina found out in the cenosphere (hollow sphere, inert, and light weight) form. Clay bricks contain both the fine texture (due to the presence of silica) and multi-shape texture
Density	The fly ash bricks density is in the range of 1700-1850 kg/m ³ . Whereas the clay brick has nearly similar size particles and has the density in the range of 1600–1750 kg/m ³ . Due to the presence of more variety of cementitious particle, FAB has higher density. High density results in higher mechanical strength than that of the clay bricks
Mechanical strength	The compressive strength of clay brick is in the range of 30–35 kg/cm ² and fly ash brick in the range of 90–100 kg/cm ²
Porosity	The percentage of porosity in clay bricks is in the range of 15–35%, whereas in fly ash it is in the range of 30–65%
Water absorption capacity	Absorption capacity of the clay bricks is 15–25% and of fly ash bricks is 10–14%
Dimensional tolerance	Clay bricks are generally prepared manually whereas fly ash bricks are prepared by machine. So less dimensional tolerance has been observed. If clay bricks will be prepared by machine, then during plastering there is a variation observed in thickness
Thermal conductivity	Thermal conductivity of normal bricks is known to be 0.72 W/mK whereas for fly ash bricks it is 0.36 W/mK
Rupture strength	The rupture strength of the bricks is represented by their modulus of rupture. Experimental studies have shown that the modulus of rupture of clay bricks is 0.8 MPa (default value), which may vary from less than 1 MPa to greater than 2 MPa. FAB shows modulus of rupture of 10.3 MPa
Dry density	The maximum dry density of fly ash is 1.16 gm/cc whereas in clay brick it is 1.8–2.0 g/cc
Optimum moisture content (per cent)	Normal clay bricks have moisture content ranging between 0.1% and 0.2%. The optimum moisture content of fly ash is 18–38%
Permeability	Permeability is also known as hydraulic conductivity which describes the ease with which a fluid can move in between the pores of a material. For fly ash brick the permeability is 7×10^{-4} – 8×10^{-6} cm/s, which is higher than that of normal clay brick
Erosion resistance	Wear and tear resistance of fly ash is much more than that of clay brick

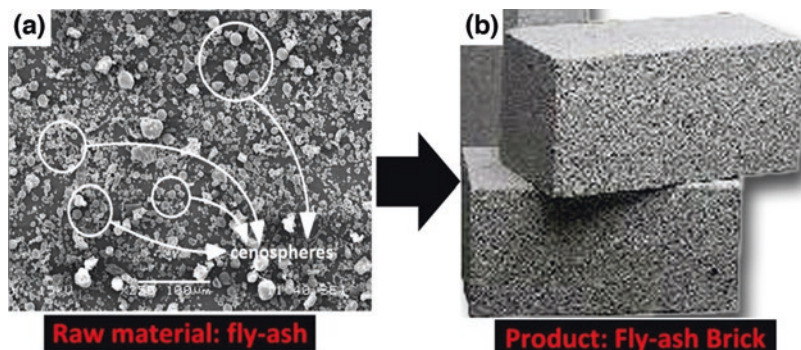


Fig. 11.9 (a) Micrograph of FA used for brick fabrication, (b) FAB

technology, FA got a huge attraction. The bricks having high ash content showed very high compressive strength at 1000 °C (firing temperature). The year wise approximate FA generation statistics is represented in Table 11.2.

Due to the presence of oxide stable particles, fly ash is a focus point in high-temperature structural material (Fuller et al. 2018). Singh and Badiger (2013) have studied the radiation blocking behaviour of FAB with respect to the percentage of FA that replaces the clay content in brick. By NaI(Tl) detector, coefficient of mass attenuation, absorption efficiency, half value layer, and effective electron density have been calculated at 661.6, 1173.2, and 1332.5 keV. They found that with higher percentage of FA in clay brick, which may be used as multi-layered exterior walls that able to protect the environment from low energy γ -rays (Singh and Badiger 2013; Mann et al. 2016). Li et al. (2015) have investigated the three types of bricks (recycled concrete bricks, CB, and FAB) to measure the coefficient of heat transfer. He found higher thermal insulation behaviour of fly ash brick (120 mm of sandwiched fly ash blocks) in comparison with other bricks. Shaikh and Aditya (2018) have doped the glass fibres (0.2–1.0%) in class F fly ash to enhance the strength of the brick. They found that, due to the presence of fibre the compressive strength increases up to 5.86 N/mm² and the water absorption capacity decreases to 12.32%. Addition of glass fibre only increases the cost of the brick. Tiwari and Choubey (2014) have examined the compressive strength of FAB with varying height-to-thickness ratio. They reported that the fracture that occurs at maximum stress mainly depends on the nature of bonding in particles. Singh (2018) has varied the sodium silicate binder in fly ash brick to increase the mechanical properties. He proved the increase of the mechanical strength due to action of binder in particle bonding. Mahudeswaran et al. (2014) have added Ironite as an admixture and reported the enhancement of FAB erosion strength. Safiuddin et al. (2016) have reported the compressive strength and water absorption capacity of FAB using artificial neural network in MATLAB. He reported that the predicted properties of FAB are close to that of experimental find out. Kishor et al. (2020a) have fabricated spark plasma sintered FAB, which results in a higher level of hardness, mechanical strength, erosion resistance, and corrosion resistance with higher density. Kishor et al. (2020b) have fabricated the fly ash-reinforced materials for high-temperature furnace lining

application. They have added separately the granite powder, black sand and Alite cement in FA to improve the bonding properties of the FA. Wang et al. (2015) have introduced the raw materials of FAB and its production process. They improved the brick manufacturing device by changing technical parameters.

11.5.1 Fabrication Techniques of FAB

The FAB properties are mainly influenced by the quality of raw materials (type of sand, fineness of binder, quality of stone dust), the composition of raw materials being used, environment (humidity, temperature, etc.), technique of mixing/curing and maximization of compressive strength (Singh et al. 2017a, b). The raw materials used to produce fly ash bricks are fly ash, stone dust or sand, lime, and gypsum (Liyanage et al. 2014). The manufacturing process involves the following steps:

- Mixing and grinding of raw materials.
- Pressing of the mixture in Moulding machine.
- Removal and stacking of the mix.
- Curing/Autoclaving.
- Cooling.
- Storing.

The properties like strength and colour of the FAB are controlled by composition of the raw materials while mixing them. Figure 11.10 shows scanning electron micrograph of various types of high-strength fly ash bricks that are granite-powder reinforced (Fig. 11.10a), alite-cement reinforced (Fig. 11.10b), and black-sand reinforced (Fig. 11.10c).

11.5.2 Mixing and Grinding of Raw Materials

The method of mixing and grinding depends upon the layout of the plant and the composition of raw materials used in the brick. To obtain high-strength calcium

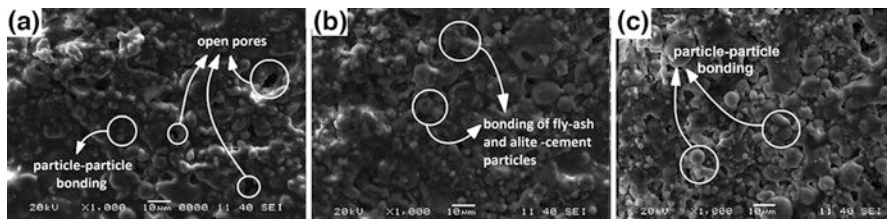


Fig. 11.10 Micrograph of (a) granite-powder reinforced fly ash brick, (b) alite-cement reinforced fly ash brick, and (c) black-sand reinforced fly ash brick. These bricks are made by powder metal-lurgy process

silicate materials the mixture of sand and lime should be mixed for a longer period. However, the fly ash can be mixed with the previous mixture for a shorter period. Shorter the periods for the mixing of fly ash with the mix so that only a portion of the mix receives grinding. For a good control over the operation, batch method is preferred over continuous process in the primary stage.

The raw materials and other necessary chemicals have been mixed using a U-shaped mixer/double mixer. Countercurrent mixer can also be used for this process, but is avoided because of its excessive cost. This mixing is carried out till the semi-dry mix is uniform throughout. Figure 11.11 is showing the phase formation in fly ash brick. Here the additives, granite powder, are varied, that is 5% (Fig. 11.11a), 10% (Fig. 11.11b), 15% (Fig. 11.11c), 20% (Fig. 11.11d), 25% (Fig. 11.11e), and 30% (Fig. 11.11f).

11.5.2.1 Pressing

The mix is instantly placed in a stripping mould which consists of an external vibrator. The compaction is done at 300 kg/cm² pressure on each brick. The compaction is to be carried out at high pressure, as the mixture is non-plastic in nature. After the compaction is done, a wooden plate is set up on the top and the mould is turned upside down. Now the mould is stripped by lifting. The press used in here should be very robust in nature to withstand high chemical strains, wear and tear.

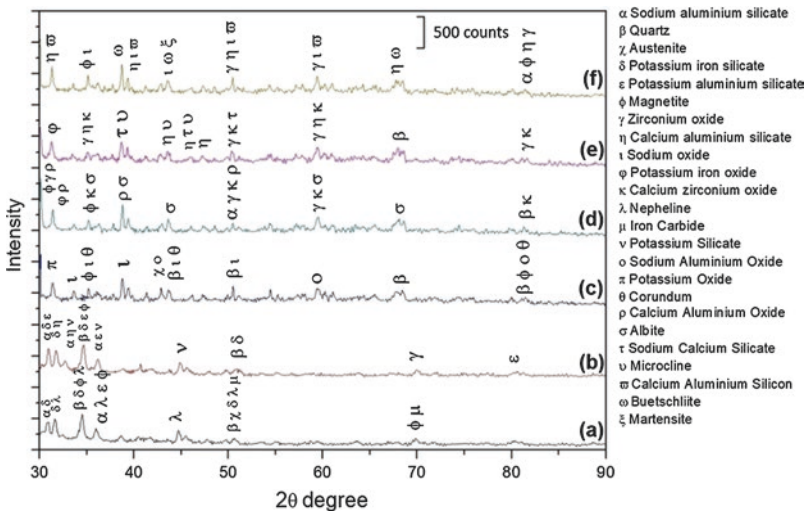


Fig. 11.11 Phase analysis of FAB with varying the additive (granite-powder) (a) 5%, (b) 10%, (c) 15%, (d) 20%, (e) 25%, and (f) 30%

11.5.2.2 Removal and Stacking

The bricks that are pressed can be removed manually or using an automatic press and brick stacking machine (working in conjunction with the pressing machine). These bricks are transported to the autoclave using trolley with capacity of 750–1000 bricks. The capacity of the autoclave is 20 trolleys.

11.5.2.3 Autoclaving

The trolleys are moved into the autoclave through the detachable end which is cylindrical in shape. The doors of the autoclave are closed tightly after the trolleys are placed inside. Steam is fed inside at normal pressure and curing is carried out for 6–8 h. The steam in the autoclave is released slowly through the release valve so that the bricks can be cooled down. Now the chamber is opened and trolleys were drawn out and cooled. These cooled bricks are then stored in yard. This makes immediate availability of the autoclave (Chen et al. 2018).

Cellular lightweight concrete (CLC) FAB is however having a slightly different procedure of manufacturing. FA and sand are the basic raw materials involved in making these bricks. Mixture of lime and cement is added as binders; lime and cement can also be added individually. The aeration of bricks is carried out by a foaming agent. ‘Neopor’ is a foaming agent that was developed and patented in German. Depending upon the productivity required and investment to be done, the procedure of manufacture varies. And, as per Indian requirements, very high-end sophisticated techniques are not required. The major equipment required for this process are a mixer, tunnel dryer, hydraulic press, and autoclaves which are available in industrial regions. The conditions required for the process are power, steam (10–12 kg/sq cm pressure) and water. The raw materials to be used depend upon the quality of bricks to be produced. The best quality CLC bricks are produced from dry FA and sand mixed proportionally. Calculated quantities of FA along with calcined gypsum are mixed in a dry state. After a uniform colour is obtained, cement is added to it. Whereas, foamer, lime and water are added at the last stage of the process to form thin slurry. Now the slurry is poured into the moulds and could get set for about 24 h. These set blocks are now de-moulded and autoclaved in steam for 8 h. The blocks are then water cured in the next step. The water curing period of these bricks is about 7 days. After this curing, these bricks are dispatched. Bulk density of these bricks varies between 0.4 and 1.8 gm/cm³ (Karolina and Sianipar 2018).

There were several studies made to manufacture FAB for different purposes by using different procedures. A study described the manufacture of insulating refractories bricks made of FA and clay. Five constituents were used in the manufacturing of these bricks. The composition was such that it had 20% of clay with respect to the FA utilized, where the composition of other ingredients was determined by performing several tests. Sodium silicate was one of the ingredients. The % of sodium silicate obtained was 15% with respect to fly ash. The other remaining components were hydrogen peroxide and water.

The first step of the manufacturing process was mixing the ingredients except for hydrogen peroxide, to obtain a homogenous mixture. After achieving desired degree of homogenization, hydrogen peroxide was added and was again mixed thoroughly. Moulds whose interior was made of plastic were used that were dismountable to ensure striking. The mixture remained in the box for 24 h. These samples were then removed and dried for 12 h at normal room temperature. Electric furnace with ceramic lining was used to fire the insulating bricks at a heating rate of 1 K/min. The temperatures used were 900°C, 1000°C, and 1100 °C with a dwell time of 60 min. And it was observed that the appropriate firing temperature was 1000 °C to obtain desired strength of the bricks (Pradhan and Bhargava 2008).

In a U.S. Patent, method of manufacturing of FAB has been described, using cellulose-based materials and binder in specific composition. As per this paper, the powder composition can include 71–82% of FA, and 18–29% of cellulose-based materials. The FA used was of class F and bottom ash. The process includes forming an aqueous emulsion comprising of about 1% of adhesive binder. Now all the components thoroughly mixed to form slurry like mixture. The slurry is then delivered to the mould. The slurry is then dried in the mould. During the drying of the slurry, it is compressed. After the article is prepared by pressing, it is cured in steam (Strabala and Colo 1996).

The manufacturing of FAB has been mentioned with the addition of admixture of ironite in its composition with certain ratio for strengthening of the bricks. Machinery used in the manufacturing process included a hydraulic pressure machine equipped with mixing barrel, brick mould, and pressure applying machine. Plank and plank lifter were used too. The manufacturing involved the following steps:

- All the components, i.e. FA, lime, sand/stone dust and gypsum, are mixed in a particular proportion. Gypsum and lime are added first to the mixture where they are grounded to make a dry mixture.
- The grinding is stopped while the mixing is being continued. Ash and sand are added next in a required quantity into the pan. To have uniform dry mixture, cement is added.
- Again, the mixture is grounded uniformly in dry condition until a uniform mixture is achieved.
- The next step is addition of water to the mixture in the pan mixture. For per kg of the mixture the water content ratio should not exceed 0.6%. The water content should be maintained in such a way that brick moulding can be carried out with ease.
- The next step is addition of ironite into the mixture for strengthening effect.
- The mixture is then filled into the moulds. The moulds are provided at the circular table which rotates in clockwise direction.
- The bricks are then pressed in the moulds and are pushed out automatically which are then collected in the planks provided.
- After the planks are filled up to their limit, they are taken out using a plank lifter and the bricks are sent to be air drying for around 2–3 days.
- The water curing is done as per the strength required.

Different samples with different ironite content were then examined to test the strengths of the samples. It was observed that the bricks manufactured by the process with the use of ironite were having good erosion resistance (Narmatha et al. 2014). Another work has been carried out in which FA used was obtained from circulating fluidized bed combustion of coal in power generation. The procedure used here was the common brick manufacturing technique. However, in addition to the steps followed in the brick manufacturing technique, sintering of the samples is also carried out.

Various clay and ash mixtures were prepared and mixed with water. The mixture should have enough water content so that the mixture has desirable amount of plasticity for easy working of the plastic mass. The optimum water content was evaluated by using a thermo-balance with IR radiation. The specimens were then extruded. These specimens are first dried in air for about 24 h and then in an oven at 105 °C for 48 h. The next step is sintering of these samples in a computer controlled furnace. Finally, these samples were furnace cooled and were taken out (Koukouzas et al. 2011).

Another technique for preparation of fly ash bricks was carried out by the process called spark plasma sintering (SPS). In this process, sintered compact is prepared under vacuum by providing high-density sintering in a short period. One of the advantages of this process is that, it prevents formation of pores due to entrapment of gases which usually occur in normal sintering. The sintering is performed by SPS apparatus. Following steps were carried out in this process:

- Initially FA was put in a graphite die having 100 mm diameter.
- These graphite punches are then applied a pressure of about 50 MPa.
- The temperature to be maintained during sintering was between 800 and 1100 °C with a pulse current.
- This sintered compact was cooled at room temperature for around 30 min.
- The process is carried out in vacuum of 10 Pa.
- All the conditions like temperature and pressure are controlled and monitored.

The density of the sintered sample was found to be 2.4×10^{-3} . Young's modulus and flexural strength of the sample was also calculated. It had a flexural strength of 25.6 MPa and Young's modulus of 23GPa (Hasezaki et al. 2007).

11.6 Summary

Coal is one of the major sources of fuel in today's world. We can find the use of coal in our every aspects of life from a very fundamental use as in cooking and domestic purposes to the use of coal in producing electricity. It has been the backbone of power generation everywhere in the world. Now-a-days, the disposal of FA in the present situation has been a big challenge to the environment, as the need of electricity increases from time to time. This indicates the production of more and more amount of coal ash in near future. Hence, there is a constant need of handling such

huge amount of fly ash. Year wise FA generation statistical data with their different applications has been given. The clear variation between the clay brick from the FAB has been given in this chapter. Fabrication steps of FAB have also been discussed.

References

- Assefa, K. M., & Kaushal, D. R. (2015). Experimental study on the rheological behaviour of coal ash slurries. *Journal of Hydrology and Hydromechanics*, 63(4), 303–310.
- Bhatt, A., Priyadarshini, S., Mohanakrishnan, A. A., Abri, A., Sattler, M., & Techapaphawit, S. (2019). Physical, chemical, and geotechnical properties of coal fly ash: A global review. *Case Studies in Construction Materials*, 11, e00263.
- Chandel, S., Seshadri, V., & Singh, S. N. (2009). Effect of additive on pressure drop and rheological characteristics of fly ash slurry at high concentration. *Particulate Science and Technology*, 27, 271–284.
- Chandel, S., Singh, S. N., & Seshadri, V. (2010). Transportation of high concentration coal ash slurries through pipelines. *International Archive of Applied Sciences and Technology*, 1(1), 1–9.
- Chen, T., Gao, X., & Ren, M. (2018). Effects of autoclave curing and fly ash on mechanical properties of ultra-high performance concrete. *Construction and Building Materials*, 158, 864–872.
- Chouhan, D., Upadhayay, V., & Ladhe, Y. (2018). A study of potential application for coal ash production as a raw material. *1(9)*, 438–446.
- Cultrone, G., & Sebastián, E. (2009). Fly ash addition in clayey materials to improve the quality of solid bricks. *Construction and Building Materials*, 23, 1178–1184.
- Das, D., Dash, U., Meher, J., & Misra, P. K. (2013). Improving stability of concentrated coal-water slurry using mixture of a natural and synthetic surfactants. *Fuel Processing Technology*, 113, 41–51.
- Das, D., Dash, U., Nayak, A., & Misra, P. K. (2010). Surface engineering of low rank Indian coals by starch-based additives for the formulation of concentrated coal–water slurry. *Energy & Fuels*, 24, 1260–1268.
- Das, D., Mohapatra, R. K., Belbsir, H., Routray, A., Parhi, P. K., & El-Hami, K. (2020a). Combined effect of natural dispersant and a stabilizer in formulation of high concentration coal water slurry: Experimental and rheological modeling. *Journal of Molecular Liquids*. <https://doi.org/10.1016/j.molliq.2020.114441>.
- Das, D., Panigrahi, S., Misra, P. K., & Nayak, A. (2008). Effect of organized assemblies. Part 4: Formulation of highly concentrated coal-water slurry using a natural surfactant. *Energy & Fuel*, 22, 1865–1872.
- Das, D., Pattanaik, S., Parhi, P. K., Mohapatra, R. K., Jyothi, R. K., Lee, J. Y., & Kim, H. I. (2019). Stabilization and rheological characteristics of fly ash–water slurry using a natural dispersant. *ACS Omega*. <https://doi.org/10.1021/acsomega.9b03477>.
- Das, S. N., Biswal, S. K., & Mohapatra, R. K., (2020b). Recent advances on stabilization and rheological behaviour of iron ore slurry for economic pipeline transportation, *Materials Today: Proceedings*, <https://doi.org/10.1016/j.matpr.2020.02.851>.
- Fuller, A., Maier, J., Karampinis, E., Kalivodova, J., Grammelis, P., Kakaras, E., & Scheffknecht, G. (2018). Fly ash formation and characteristics from (co-)combustion of an herbaceous biomass Andra Greek Lignite (low-rank coal) in a Pulverized Fuel pilot-scale test facility. *Energies*, 11, 1581. (1-38).
- Ghazali, M., & Kaushal, O. P. (2015). Characteristics of fly ash from thermal power plants and its management along with settling pond design. *International Journal of Engineering Research & Science*, 1(4), 24–32.

- Gollakota, A. R. K., Volli, V., & Shu, C.-M. (2019). Progressive utilisation prospects of coal fly ash: A review. *Science of the Total Environment*, 672, 951–989.
- Hasezaki, K., Nakashita, A., Kaneko, G., & Kakuda, H. (2007). Unburned carbon behavior in sintered coal fly-ash bulk material by spark plasma sintering. *Materials Transactions*, 48, 3062–3065.
- Headwaters, I. (2005). Proportioning fly ash concrete mixes. Retrieved from <http://www.flyash.com/>
- Ismail, K. N., Hussin, K., & Idris, M. S. (2007). Physical, chemical & mineralogical properties of fly ash, journal of nuclear and related technology. *Special Edition*, 4, 47–51.
- Iyer, R. (2002). The surface chemistry of leaching coal fly ash. *Journal of Hazardous Materials*, B93, 321–329.
- Karampinis, E., Nikolopoulos, N., Nikolopoulos, A., & Kakaras, E. (2011). Numerical investigation Greek lignite/cardoon co-firing in a tangentially fired furnace. *Applied Energy*, 97, 514–524.
- Karolina, R., & Sianipar, Y. G. C. (2018). The utilization of stone ash on cellular lightweight concrete. *IOP Conference Series: Materials Science and Engineering*, 309, 1–5.
- Kayali, O., & Sharfuddin, M. (2013). Assessment of high volume replacement fly ash concrete-concept of performance index. *Construction and Building Materials*, 39, 71–76.
- Kishor, M. S. V. R., Behera, A., Rajak, D. K., Menezes, P. L., & Catalin, P. I. (2020b). Manufacturing and mechanical characterization of Fly-ash-reinforced materials for furnace lining applications. *Journal of Material Engineering and Performance*. <https://doi.org/10.1007/s11665-020-05121-0>.
- Kishor, M. S. V. R., Sahoo, D. P., Sahoo, D. K., Behera, A., & Sarkar, S. (2020a). Nano-scale analysis on spark plasma sintered fly-ash bricks and their comparative study with SiN-Zr refractory bricks. *Micro and Nanosystems*, 12, 122–128.
- Knezevic, D., & Kolonja, B. (2008). The influence of ash concentration on change of flow and pressure in slurry transportation. *International Journal of Mining and Mineral Engineering*, I(1), 104–112.
- Kolář, V., Pollert, J., Sellin, R. H. J., & Vlasak, P. (1988). Experiments with a drag reducing polymer in an ash-slag hydro transport pipeline. *Journal of Hydraulic Research*, 26(2), 143–158.
- Koukouzas, Ketikidis, C., Itskos, G., Spiliotis, X., Karayannis, V., & Papapolymerou, G. (2011). Synthesis of CFB-Coal fly ash clay bricks and their characterisation, Nikolaos. *Waste Biomass Valor*, 2, 87–94.
- Kumar, K., Kumar, S., Gupta, M., & Garg, H. C., (2016). Effect of addition of bottom ash on the rheological properties of fly ash slurry at varying temperature, Material Science and Engineering, 149, IOP Conf. Series, Department of Mechanical Engineering, Guru Jambheshwar University of Science & Technology, Hisar, India.
- Kumar, U., Mishra, R., Singh, S. N., & Seshadri, V. (2003). Effect of particle gradation on flow characteristics of ash disposal pipelines. *Powder Technology*, 132, 39–51.
- Leiva, C., Arenas, C., Alonso-farinas, B., Vilches, L. F., Peceño, B., Rodriguez-galán, M., & Baena, F. (2016). Characteristics of fired bricks with co-combustion fly ashes. *Journal of Building Engineering*, 5, 114–118.
- Li, J., Cao, W., & Chen, G. (2015). The heat transfer coefficient of new construction—Brick masonry with fly ash blocks. *Energy*, 86, 240–246.
- Li, L., Usui, H., & Suzuki, H. (2002). Study of pipeline transportation of dense fly ash water slurry. *Coal Preparation*, 22, 65–80.
- Liyanage, M., Jayaranjan, D., Hullebusch, E. D. V., & Annachhatre, A. P. (2014). Reuse options for coal fired power plant bottomash and fly ash. *Reviews in Environmental Science and Biotechnology*, 13, 467–486.
- Mahudewaran, N., Mahudewaran, N., Aruna, R., & Saraswathi, M. (2014). Strengthening of Fly ash bricks by Ironite. *IOSR Journal of Mechanical and Civil Engineering*, 11, 21–26.
- Mann, H. S., Brar, G. S., Mann, K. S., & Mudahar, G. S. (2016). Experimental investigation of clay Fly ash bricks for gamma-ray shielding. *Nuclear Engineering and Technology*, 48, 1230–1236.

- Mishra, B., & Gupta, M. K. (2017). Use of fly ash plastic waste composite in bituminous concrete mixes of flexible pavement. *American Journal of Engineering Research*, 6(9), 253–262.
- Mohapatra, R. K., Das, P. K., Pintilie, L., & Dhama, K. (2021). Infection capability of SARS-CoV-2 on different surfaces. *Egyptian Journal of Basic and Applied Sciences*, <https://doi.org/10.1080/2314808X.2021.1907915>.
- Naganathan, S., Mohamed, A. Y. O., & Mustapha, K. N. (2015). Performance of bricks made using fly ash and bottom ash. *Construction and Building Materials*, 96, 576–580.
- Naik, H. K., Mishra, M. K., & Rao, K. U. M. (2011). Influence of chemical reagents on rheological properties of fly ash water slurry at varying temperature environment. *Coal Combustion and Gasification Products*, 3, 83–93.
- Naik, T. R., & Singh, S. S., (1993). Fly ash generation and utilization—an overview, Recent Trends in Fly Ash Utilization. Society of Forest & Environmental Managers (SOFEM). India, 1–25.
- Narmatha, M., Aruna, R., & Saraswathi, M. (2014). Strengthening of Fly ash bricks. *IOSR Journal of Mechanical and Civil Engineering*, 11, 21–26.
- Pani, G. K., Rath, P., Barik, R., & Senapati, P. K. (2015). The effect of selective additives on the rheological behaviour of power plant ash slurry. *Particulate Science and Technology*, 33, 418–422.
- Pattanaik, S., Parhi, P. K., Das, D., & Samal, A. K. (2019). Acacia concinna: A natural dispersant for stabilization and transportation of fly ash-water slurry. *Journal of Taiwan Institute of Chemical Engineers*, 99, 193–200.
- Pradhan, M., & Bhargava, P. (2008). Tailoring porosity and pore characteristics in oxide ceramic foams through controlled processing. *Transactions of the Indian Ceramic Society*, 67, 101–117.
- Rani, R., & Jain, M. K. (2017). Effect of bottom ash at different ratios of hydraulic transportation of fly ash during mine fill. *Powder Technology*, 315, 309–317.
- Safuiddin, M., Raman, S. N., Salam, M. A., & Jumaat, M. Z. (2016). Modeling of compressive strength for self-consolidating high-strength concrete incorporating palm oil fuel ash. *Materials*, 9, 1–13.
- Senapati, P. K., Mohapatra, R., Pani, G. K., & Mishra, B. K. (2012). Studies on rheological and leaching characteristics of heavy metals through selective additive in high concentration ash slurry. *Journal of Hazardous Materials*, 229-230, 390–397.
- Shaikh, F. U. A., & Aditya, P. (2018). Flexural behavior of hybrid PVA Fiber and AR-glass textile reinforced Geopolymer composites. *Fibers*, 6, 1–10.
- Singh, H., Brar, G., & Mudahar, G. (2017a). Evaluation of characteristics of fly ash-reinforced clay bricks as building material. *Journal of Building Physics*, 40, 530–543.
- Singh, K., & Lal, K. (2012). Effect of Cetylpyridinium chloride, Triton x-100 and sodium dodecyl Sulfate on rheology of fly ash slurry. *International Journal of Scientific and Research Publications*, 2(8), 1–5.
- Singh, M. K., Kumar, S., Ratha, D., & Kaur, H. (2017b). Design of slurry transportation pipeline for the flow of multi-particulate coal ash suspension. *International Journal of Hydrogen Energy*, 42, 19135–19138.
- Singh, N. B. (2018). Fly ash-based Geopolymer binder: A future construction material. *Minerals*, 8, 1–21.
- Singh, V. P., & Badiger, N. M. (2013). The gamma-ray and neutron shielding factors of fly-ash brick materials. *Journal of Radiological Protection*, 34, 89–101.
- Sivalingam, N., (2011). Project profile on fly ash bricks, Guindy, Chennai.
- Strabala, W. M., & Colo, A., (1996) Structural products manufactured from fly ash, United States Patent, Patent no.-5, 534, 058, July 9.
- Tiwari, V., & Choubey, U. B. (2014). Experimental study of fly-ash brick masonry under subjected to cyclic loading. *International Journal of Science Technology & Engineering*, 1, 1–7.
- Wang, L., Sun, H., Sun, Z., & Ma, E. (2015). New technology and application of brick making with coal fly ash. *Journal of Material Cycles and Waste Management*. <https://doi.org/10.1007/s10163-015-0368-9>.

- Yang, T., Zhu, H., Zhang, Z., Gao, X., Zhang, C., & Wu, Q. (2018). Effect of fly ash microsphere on the rheology and microstructure of alkali-activated fly ash/slag pastes. *Cement and Concrete Research*, *109*, 198–207.
- Yao, Z. T., Ji, X. S., Sarker, P. K., Tang, J. H., Ge, L. Q., Xia, M. S., & Xi, Y. Q. (2015). A comprehensive review on the applications of coal fly ash. *Earth-Science Reviews*, *141*, 105–121.

Chapter 12

Studies on Extraction of Heavy Metal (s) from Fly Ash through Hydroprocessing Approach



Saroj Sekhar Behera, Surendra Hansdah, Debadutta Das,
Pankaj Kumar Parhi, and Rajesh Kumar Jyothi

12.1 Introduction

Coal fly ash is generally a grey coloured powdered substance obtained from typically coal power plant. This typical solid waste is being generated from different industrial sectors that cause serious threat to environment because of its physico-chemical properties. At present scenario the management of fly ash (FA) is becoming a global challenge due to its enormous production. Annually, ~ 600 to 800 million tons of FA has been produced at the global scenario (Ahmaruzzaman 2010). At about 10% of this is contributed by the USA and Europe while that of India and China produces ~18% of the total production. Moreover, production rate is increasing day by day leading to raise a major issue for its disposal to environment. It is basically dumped for land filling purposes and thereby causes various environmental concerns (Yilmaz 2015; Wang et al. 2016; Kubonova et al. 2013). Furthermore, global utilization is somewhere in the range of 3–57%, with average of ~16% of the total ash content (Ahmaruzzaman 2010; Jones et al. 2012; Sarode et al. 2010; Neupane and Donahoe 2013). According to environmental information system (ENVIS) centre on fly ash production by India, it increases tremendously and may reach ~600 million tons per year by the year 2030. Accordingly, the utilization of

S. S. Behera

CSIR-Institute of Minerals and Materials Technology (IMMT), Bhubaneswar, Odisha, India

S. Hansdah · P. K. Parhi (✉)

Department of Chemistry, Fakir Mohan University, Balasore, Odisha, India

e-mail: parhipankaj@gmail.com

D. Das

Department of Chemistry, Sukanti Degree College, Subarnapur, Odisha, India

R. K. Jyothi

Convergence Research Center for Development of Mineral Resources (DMR), Korea Institute of Geoscience & Mineral Resources (KIGAM), Daejeon, South Korea

this fly ash with comparison to its production is very low and was seen in the Fig. 12.1. In India the main sources for production of FA generally are from different power plants (thermal) sectors and that is also being utilized in certain amount. Fly ash production and utilization scenario of different thermal plant is shown in Table 12.1. Mostly the fly ash which is being produced from different sources is used as it is for fabrication of concrete manufacture of bricks, blocks, tiles, etc. Due to bulk generation of fly ash from several industries it has been majorly used in low lying areas for reclamation, filling of underground, open mines, in agriculture as nutrient for plants. But over the period of time and due to direct contamination with soil level, it is again found as a major pollutant to the environment owing to the presence of trace toxic elements such as cadmium, lead, arsenic, antimony, mercury, chromium, nickel, zinc and selenium and which substantially contaminate the water bodies of the environment (Basu et al. 2009; Jones et al. 2012; Kubonova et al. 2013; Okada and Tomikawa 2012; Kai et al. 2011; Nagib and Inoue 2000; Cetina et al. 2012). In contrast, the key futuristic prospect of the FA is because of its economic importance due to the contentment of valuable metal mainly aluminium (Al), trace amount of heavy (Cu, Zn, Ni) as well as rare earth metals and high amount of silica (SiO₂) (Ahmaruzzaman 2010; Yilmaz 2015; Wang et al. 2016; Kubonova et al. 2013; Jones et al. 2012; Cheng-you et al. 2012; Xue et al. 2010; Tripathy et al. 2015). Accordingly, fly ash sources become a value additive material in extractive metallurgy area leading to exploit the metal value in particular of aluminium thereof. As of now, the research investigations in Indian scenario especially on recovery of metal values are limited, and therefore researchers have shown their interest to extract the metal values from it. In addition to Al other trace heavy/rare metals can also be extracted and later on the leached residue can either be applied for non-metallurgical application or can safely be disposed. In other aspect due to the attractive physico-chemical and geotechnical nature such as size of FA size, porosity,

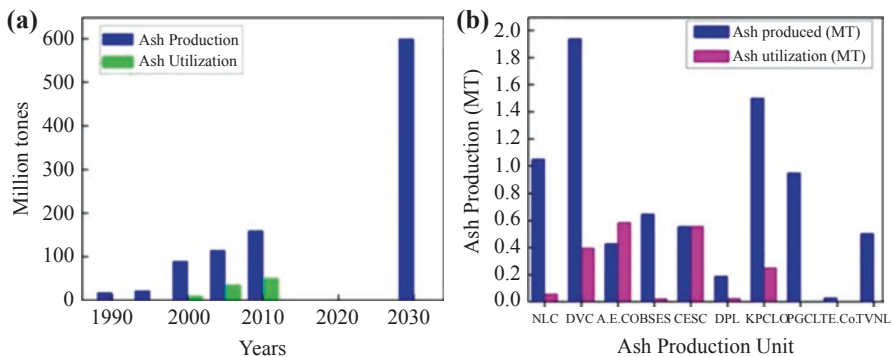


Fig. 12.1 (a) Scenario of global production and utilization of fly ash, (b) fly ash production and usage by several thermal power plant in Indian context

Table 12.1 Comparative study on leaching test methods used worldwide for extraction of metals from CFA

Reference	Location	Method	Metals
Kazonich et al. (1999)	Pittsburgh	Column	Na, Mg, K, Be, Ca, Ni, Cu, Cr, Pb, As, Sb
Georgakopoulos (2002)	Greece	SGLP leaching and column test	Na, Be, B, Si, Ca, Mg, Al, Ti, Ag, K, As, Fe
Vageesh and Siddaramappa (2002)	India	Column leaching test	Cr, Ni, Pb, Cd
Murarka (2003)	Abroad	–	Na, Al, K, Ca, Mn, Be, Fe, Cu, Zn, As, Sb, Pb,
Sushil and Batra (2006)	India	Digestion	Mn, Cu, Pb, Cr, Co, Ni, Zn
Tsiridis (2006)	Greece	TCLP 1311 and EN 12457–2	Ni, Cr, Zn, Mn, Ni, Pb
Ziemkiewicz and Knox (2006)	West Virginia	MWLP	Be, Cr, Mn, V, As, Ag, Cu, Hg, Mg, Se, and Tl
Takao (2007)	Japan	Column leaching	B, Na, Al, Si, Ca, Cr
Prasad (2008)	India	Cascade method	Cr, Zn, Fe, Mn, Co, Ni, Cu, Pb, Cd
Palumbo (2009)	Tennessee	Column leaching	Ve, Cr, Cu, Ag, Li, Al, Si, Ti, V, Fe, Co, Ni, Zn, Ba, Bi, Cs, Ga, Rb, Se, As, Pb, Cd
Arroyo et al. (2010)	Abroad	Batch leaching method	Mg, V, Ni, Zn, As, Sb
Sarode et al. (2010)	India	Batch and TLCP	Mn, Ni, Pb, Mg, Fe, Cu, Zn, Cd
Ward et al. (2010)	Australia	Batch test	Se, Mo, As
Vitkova et al. (2010)	Zambia	Static leaching test	Mg, S, Si, K, Ca, Co, Cu, Zn
Morar (2012)	US	CLT, WLT	As, Se, Cr, and Al
Pandeya et al. (2011)	India	Batch and column test	As
Sauer et al. (2012)	USA	CLT and WLT	Cr, Se, Ag, Cd
Shivpuri (2011)	India	TLCP	Zn, Ba, Fe, Mn
Barman (2012)	Abroad	CLT	Ca, K, Na
Lokeshappa and Dikshit (2012)	India	Pond	Cr, Se, Zn, As
Singh et al. (2012)	India	Batch test	Cr, Fe, Ni, Cu, Pb, Cd
Singh et al. (2015)	India	Batch test	Al, Si, Ti, Fe, Ca, V and K
Tiwari et al. (2015)	India	TLCP and toolumn	Mg, K, V, Co, Cu Be, Na, Al, Ca, Cr, Mn, Fe, Ni, Zn, Ag, Se, Tl, As, Sb, Hg
Gupta et al. (2017)	India	Batch test	Al, Fe, Mn, Zn, Mg, Si, Ti and K
Sen et al. (2016)	India	Batch test	AlI, Mg, Si, Fe, C, Na, Ca, and K

bulk density, water absorbing capacity and fly ash surface area, that is suitably applied as adsorbent for recovering/removing metals and or dyes from waste contaminated water. While adopting suitable processing approach for treating the raw fly ash by removing the trace hazardous metals, it can be used as one of the promising potential source for exploiting the targeted valuable metals. The abundance source and low cost of fly ash ensures on its effective utilization for the global need in context of the study on recovery of these above metals in an economical way (Sen et al. 2016, Dash et al. 2008, Mohapatra and Rao 2001, Tiwari et al. 2015, Nayak and Panda 2010, Narayani et al. 2017, Yao et al. 2014, Shemi et al. 2012, Agarwal and Rani 2017; Doucet et al. 2016). In consequences, the issues of the management of the fly ash in connection to environmental concern can be resolved. As per present statistics report all the fly ash being produced from various sources may contain significant amounts of silica (60–65%), alumina (25–30%), iron oxide (6–15%), calcium oxide and magnesium oxide which facilitate its application for the production of alum, precipitated silica and zeolites. However, the actual composition of fly ash may vary as per coal types that is used for burning and also the type of burner used (Ahmaruzzaman 2010; Yilmaz 2015; Wang et al. 2016; Kubonova et al. 2013; Jones et al. 2012; Cheng-you et al. 2012; Xue et al. 2010; Tripathy et al. 2015).

In consequence of time, the utilization of fly ash is ample for making artificial zeolite, cement and considered as suitable adsorbent also the significant source of heavy and traces metals. However, special attention is highly required since the generation of fly ash day by day is increasing which leads to cause the burden to the environment. Proper processing technology needs to be developed to overcome the above issue. The present investigation accomplishing the valuable metals recovery and trace metal impurities removal through integrated hydrometallurgical approaches urges the several advantages by lowering the production costs, reducing waste generation and preventing environmental pollution. In economical beneficiation aspect recovering of the valuable metals such as Al, Zn, Cu, and Ni would make value addition global market as the demand of these metals at present scenario is high due to their significant applications.

12.2 Physico-Chemical Properties of Coal Fly Ash

CFA is a grey powder material found in both solid as well as hollow spheres types with shining in nature. The main sources of fly ash are mainly from combustion of coal. This has been characterized by different techniques to understand the physical and chemical behaviours during their investigations. The major properties taken into considerations are (a) morphology of the particle, (b) mineralogical composition, (c) distribution analysis of particle size, and (d) specific surface area. Since CFA were produced from different resources, they may have wide variety of morphology. However, there is certain similarity between the different fly ash because they all are originated from coal. The morphology of the CFA was studied by different groups of researchers and they found mainly in spherical, oval as well as in

irregular forms of it (Sow et al. 2015; Brown et al. 2011; Zhao et al. 2010). The mineralogical composition of fly ash varies from one to another and mostly depends on geological factors. The geological factors are mainly related to the geographical area of deposition from where it was collected, its chemical composition and process adopted for its combustion. In all cases the mineralogical composition was different and was studied by different researchers with the help spectro-chemical techniques, i.e. XRD analysis. In maximum cases, the major phases of FA were quartz, kaolinite, illite, and sideraete. However, the less predominant phases include pyrite, calcite, hematite, rutile, corundum, thenardite, lime, and gahnite. Another important factor of fly ash is its surface area which plays the critical role of the fly ash in various fields. During the combustion of coal, the volatile compounds present in it was escaped out producing porosity on the surface of the by-product. So that the porosity developed on CFA particles surface increases the surface area and it does vary from one to other. The variability of the specific surface area was mainly based upon the chemical composition of the coal as well as technique followed during the combustion of that coal. As per the literature study as given in Table 12.2, it was seen that the specific surface area of different CFA was in the range of 0.16–6.10 m² g⁻¹. Another important parameter we observed in the FA was its particle size. The particle size of fly ash obtained from the combustion of different geographical resources coal has a major connection with its chemical composition. Therefore, the chemical composition plays a major role on not only the specific surface area but also size of FA particle as given in Table 12.3. Due to this structural behaviour like high specific surface area and small particle size there could be the enhancement of the other physic-chemical properties i.e. specific gravity, permeability, porosity, water holding capacity which makes them as a suitable candidate for the secondary beneficiation. It is widely used in the field of construction of roads, dams, structural fill, etc. Also it is widely used in the manufacturing of cement, building materials concrete, etc. Due to leachability nature of fly ash various toxic elements present in it was leached out to the environment and causes a serious environmental issue. Also the lacking of efficient industrial solid waste management, limited land for safety waste disposal as well as the uncontrolled dumping of fly ash cause serious threat to environment. Thus, it is urged to work on

Table 12.2 The specific surface area of some typical CFAs fly ash

Sl. No.	Reference	SSA of raw CFA/ m ² g ⁻¹	Sources of fly ash
1	Skvara et al. (2009)	0.21	Electric Thermal Power Plant, Czech Republic
2	Sakthivel et al. (2013)	2.00	Curtis H. Stanton Energy Centre, Florida
3	Nyale et al. (2013)	0.90	Power Station of Mpumalanga Province, South Africa
4	Cheng-you et al. (2012)	2.81	Thermal Power Station of Zhuzhou Huayin, China
5	Teng et al. (2019)	6.10	Shandong Zoucheng Power Plant of China

Table 12.3 Particle sizes distribution of some typical fly ash

Sl. No.	Reference	Particle size range (μm)	Sources of fly ash
1	Xu et al. (2018)	0–150	Shenhua Group Zhuneng Company Power Plant, China
2	Li et al. (2018)	50–230	Taigang Power Plant, China
3	Zhang et al. (2012)	0–25	Japan
4	Zhou et al. (2015)	0–200	Thermal Power Plant of Shenzhen Mawan, China
5	Sakthivel et al. (2013)	~ 20	Curtis H. Stanton energy Centre, USA
6	Tripathy et al. (2015)	0–150	National Aluminium Company, Bhubaneswar, India

development of technology on studying the leaching behaviour of metals in FA and its safe use.

12.3 Leaching Studies of Coal Fly Ash (CFA)

Mostly CFA is utilized for land filler purposes and once it comes in contact with water bodies after leaching out various elements with water that further causes serious environmental pollution. The water leaching is only possible because of the physico-chemical nature of CFA, i.e. the alkaline nature of particle, small size as well as very thin surface layer may bear a substantial amount of freely leachable elements, which is firmly deposited on the surface of CFA phase during cooling after combustion. Thus, it behaves as charged material by forming diffusion double layer during leaching which plays the major role of its leachability. To establish the actual mechanism of leaching, the elements found on the fly ash may be categorized into two different types based upon their concentration profile and particle size. The elements such as Co, Cr, Ni, Zn, Ln, Ga, Nd, Mn, Ba, Pb, Hg, V, As, Sb, Sn and S deposited at the surface of CFA are generally volatile up to a certain extent. However, the metals, namely Na, K, Rb, Cs, Mg, Ce and Nb show a lesser extent of volatilization during coal combustion and depend upon its particle size (Iyer 2002). On the other hand, some other elements (Si, Ca, Sm, Fe, Eu, Yb, Y, Tb, La, Ta and Zr.) deposited on CFA does not show any volatility behaviour during combustion. Moreover, the studies revealed that about 1–3% of total CFA was soluble in water (Keyser et al. 1978).

Number of leaching techniques were explained by various research groups for recovering metal values from FA through standard as well as enhanced leaching route in which leaching in deionized water, leaching under specific conditions as well as on natural conditions are kept fixed. Due to the presence of various elements such as metals (toxic as well as valuable heavy metals), non-metal and metalloids in coal fly ash (CFA) it acts as potential candidate of mineral sources. So the leach

ability of these resources was studied briefly. Generally the leaching of these elements from their resources is based upon three main purposes. The two main purposes include (a) separating out the toxic elements which causes serious threat to environment and (b) extracting the valuable elements for the fulfilment of the demand of the metal values.

12.3.1 The Removal of Toxic Elements

It was found that the fly ash causes a serious threat to environment by releasing their toxic element. Therefore, it is highly recommended that before its safe disposal a pretreatment process is applied to remove out the toxic element. However, in many places issues observed due to the adoption of standard of safe disposal and the policies made by local governing bodies and as a result of which the whole community is affected. Thus, the policy should strictly be maintained and newly developed technology should be adopted for its safety disposal. The objective should not be diverted at any circumstances regardless of technology and/or of policy. In certain cases it was found that even the fly ash contain very less concentration of pollutant (below the safety standard) and thereby causes serious threat because of the easy leachability properties of the fly ash. So it is highly warranted to remove out almost all the hazardous metal(s) found at FA phase. Generally, both mineral, organic acid and alkalis are well practised as a leaching agent for the extraction process.

12.3.1.1 Arsenic

Arsenic is a major pollutant and is generally found in the CFA (Finkelman 1995). When the extraction investigation was performed for the recovery of these metals from CFA, it becomes a difficult task for every researcher due to physico-chemical nature of CFA. When the combustion of coal was carried out at high temperature the arsenic present on them becomes arsenate and was accumulated over CFA surface. As it reacts with acid like sulphuric acid it produces $S-H_2AsO_4$ and gets accumulated onto CFA phase. This type of extraction behaviour was investigated and it demonstrated that the leaching of As from CFA showed to be pH dependant. At low pH (pH of 3–4) CFA was not extracted because at that pH it becomes arsenate form and gets accumulated on CFA surface. However, beyond pH > 9.0, maximum amount of As could be leached out. It was also noticed that the affinity of arsenate with different metal oxides showed to follow decreasing trend with increase in solution pH (Cornelis et al. 2008). As per statistics, it was seen that the major content (92–97%) of As in FA as As (V) and the major material that is found mostly in CFA phase are: iron oxide and calcium arsenate. So it is highly warranted to remove iron oxide and calcium arsenate from fly ash so that the As content in the fly ash may decline.

12.3.1.2 Chromium

Chromium was another hazardous element also contained in the CFA. It exists in variable oxidation states however; its hexavalent form is highly soluble in water. This hexavalent chromium can be transported and accumulated on the animal as well as humans body; it causes serious threat to environment by its carcinogenic nature (Huggins and Huffman 2004). On the other hand, Cr found in trivalent form was in trace amount and was of less concern to environment; its rate of leaching efficiency was very low. Therefore, it is essentially needed to be removed from the fly ash phase prior to its disposal into the environment. The leaching efficiency of Cr(III) from fly ash was studied by Dubikova 2006 in which 0.03% Cr was found in the fly ash phase after leaching. So due to the potential carcinogenic nature of hexavalent chromium, a number of investigations have been attempted to address contamination issues due to Cr present in FA. However, the leaching of Cr(VI) from fly ash was carried out on normal conditions, meanwhile for Cr(III) non-environmental conditions, i.e. high acid content, high temperature and pressure, was needed. Generally, major content of chromium was observed in fly ash produced after the incineration of bituminous coals.

12.3.1.3 Mercury

Mercury is also the major pollutant found in considerable level in fly ash. It comes into the environment in two different ways, either by atmospheric sedimentation or by auto-leaching process. Generally mercury is volatile in nature and directly enters into the atmosphere during combustion of coal. Initially it was present in their elemental form. During combustion it may react with sulphur and is converted to Hg sulphide. Also it may be chelated with other organic components forming organo-chelated Hg and is accumulated in the environment. As per data revealed by Wei et al. 2011, Hg is found in the environment in highest percentage in the surface of fly ash and then declined to atmospheric sedimentation and finally least amount was observed in the soils. When these elements come in contact with natural water bodies that get adsorbed by numerous inorganic and/or organic material in the aqueous phase. These Hg may further be converted to deadly poisonous material like methyl mercury during the microbial methylation process which was happening in water bodies due to the presence of numerous bacteria. The toxicity level of methyl mercury is approximately hundreds times higher than that of the elemental form of Hg. So it is highly needed that the poisonous metal like Hg must be separated from the fly ash to avoid secondary contamination. For the attainment of Hg-free fly ash and to avoid secondary problem, the pretreatment process is highly needed of the flue gas before discharging into the environment. This can be achieved by the adsorption of Hg from flue gas using fly ash and then the acid and/or alkali treatment of this adsorbed fly ash for Hg-free fly ash (Zhu et al. 2016; Li et al. 2016; Li et al. 2017; Bao et al. 2017; Tsiridis et al. 2012; Wang et al. 2020; Yang et al. 2018).

12.3.1.4 Cadmium and Lead

Some other elements like lead and cadmium were also found in trace amount in fly ash. Nevertheless, their toxicity level is much higher to that of the content of other toxic metals. Therefore, their removal from the fly ash phase is urged prior to the safe disposal. As of now there are limited works reported for removal of these two elements from CFA. One of the studies includes separation of Cd and Pb from CFA while treating it using both acid and alkalis. As per results of the work performed by Zhao et al. (2018) these two metals may have separated out in a wide range with supplement acid. The water or acid soluble form as well as ion exchangeable, reducible, oxidizable, and residual forms of metal leaching were observed. However, the techniques applied for the removal of toxic elements said above were not selective because leaching of other valuable elements were unavoidable. Up to the present stage of reported works, a significant level of outcome in context of obtaining selective leaching of high purity targeted elements from the Fly ash has not been attained and hence further study in this domain is essentially warranted.

12.3.2 Extraction of Valuable Metals

The leaching of valuable metals found in the CFA is highly needed to fulfil the public demand of the metal as well as the exploit of mines can be minimized in a certain way. Different group of researcher to extract the metal values from fly ash put extensive investigation forth. In several cases, it was observed that cations in water extract include Na and Ca, whereas the anions are reported as carbonates and hydroxides (Elseewi et al. 1980; Menon et al. 1980). However, the extraction behaviour for dissimilar fly ashes is markedly as different based on their compositions. Therefore, the extraction behaviour may depend upon CFA surface, chemical composition as well as the design process of flue gas treatment. Nevertheless, other factors like leaching reaction time, temperature lixiviant concentration, solid/liquid ratio and particle sizes play a key role as well during metal extraction phenomenon. Several perspectives on CFA leaching were studied by different researchers that are summarized and presented in Table 12.4 (Iyer 2002, Mohapatra and Rao 2001, Reijnders 2005, Prasad et al. 1996).

As per data given in Table 12.4, it was emphasized only on the valuable heavy metals including some rare earth because of their potential content, high value. The processing technology which is frequently applied for the extraction of metal from secondary solid waste through hydrometallurgical approach may need some activation techniques. However for leaching in certain cases activation techniques are highly essential for the enhancement of the leaching rate which may include addition of acid or alkali as well as calcinations and roasting that depends upon the nature of fly ash. For example, leaching of Al and Fe from CFA was studied by Yang et al. (2018) and in this investigation author chose pretreatment technique for obtaining maximum extraction efficiency. CFA was initially mixed with required

Table 12.4 Typical studies on extraction of metal values from fly ash

Sl. no.	Reference	Extraction method (s)	Extracted metals
1	Shivpuri (2011)	TLCP	Mn, Ba, Fe, Zn
2	Sarode et al. (2010)	Batch and TLCP	Ni, Fe, Mn, Cu, Zn, Mg, Pb, Cd
3	Cao et al. (2018)	Batch.	La, Ce, Nd
4	He et al. (2002)	Batch	Ga
5	Fan et al. (2012)	Batch	Ga
6	Lokeshappa and Dikshit (2012)	Pond	Cr, Zn, Se And As
7	Palumbo (2009)	Column	Li, Be, Al, Si, Ti, Ba, V, Fe, Cr, Co, Cu, Ni, Cs, Bi, As, Pb, Rb, Se, Cd
8	Sandeep et al. (2016)	TCLP	Fe, As
9	Takao (2007)	Column	B, Na, Al, Si, Ca, Cr
10	Georgakopoulos (2002)	SGLP leaching	Na, Al, S, Mg, K, Fe, Ti, B, Ba, Be, Bi, Br, Ag, As
11	Bhattacharyya et al. (2009)	SPLP	B, V, As, Cr, Mo, Se
12	Arroyo et al. (2010)	Batch	Ni, Zn, Mg, V, As, Sb
13	Tsiridis (2006)	TCLP 1311 and EN 12457-2	Zn, Cr, Mn, Ni, Cu and Pb
14	Akar et al. (2012)	TCLP and ASTM D-3987	Co, Cu, Ni, Zn, Pb and Cd
15	Vitkova et al. (2010)	Static leaching test	Mg, Si, S, K, Ca, Co, Cu, and Zn
16	Kazonich et al. (1999)	Column	Mg, Ca, Zn, As, Na, Be, Al, Ba, Cr, K, Fe, Ni, Mn, Cu, Pb, and Sb
17	Sauer et al. (2012)	WLT and CLT	Se, Ag, Cr, Cd
18	Jones et al. (2012)	TCLP and GJST	Na, Al, Ca, Mg, Fe, Mn, Ti, Ni, Cu, Zn, Cr, Cd, Pb
19	Vageesh and Siddaramappa (2002)	Leaching column test	Cr, Ni, Cd, Pb
20	Morar (2012)	WLT, CLT	Al, Cr, As, Se
21	Prasad (2008)	Cascade method	Mn, Fe, Cr, Zn, Cu, Ni, Co, Pb and Cd
22	Barman (2012)	CLT	Na, K and Ca
23	Sushil and Batra (2006)	Digestion	Mn, Co, Cr, Ni, Zn, Pb and Cu
24	Ward et al. (2010)	Batch test	Mo, As And Se

amount of Na_2CO_3 followed by calcined at $800\text{ }^\circ\text{C}$ for 2 h. Thereafter it was put under HCl leaching and subsequently more than 90% of Fe and Al has been leached. Similarly Liang et al. 2008 investigated on leaching behaviour of Al cum Fe from CFA while mixing it with sodium salt and then calcined. Further, the calcined fly ash was then treated with H_2SO_4 under microwave irradiation so that the leaching rate of Al and Fe could reach up to 59.2% and 49.2%, respectively. On the other hand, while leaching of REEs from CFA it was not essential on adoption of pretreatment techniques as most REEs bearing CFA get readily extracted during acid

leaching method. Cao et al. (2018) studied the leaching of REES such as La, Ce, Nd from CFA using HCl solution without any pretreatment approach and the leaching yield was reportedly of 71.9%, 61.9% and 66.0% for La, Nd and Ce, respectively. In many cases pretreatment approach was preferentially adopted by different group of researcher for the enhancement of metal leaching efficiency. To ascertain the extraction behaviour of metal from CFA, the usage of suitable lixiviant, adoption of technique(s) for the selective extraction of metals with high leaching yield and leaching through mono or multistage for sequential leaching of metals are systematically investigated and reported. Some of the typical valuable metal extraction studies have been investigated by researchers which have been discussed in following section.

12.3.2.1 Selenium

Selenium is one of the most critical elements observed to be present in coal CFA (He et al. 2019). The element Se is very prone to pH variation and make stable compound with calcium resulting in the compound form as CaSeO_3 and deposited at the CFA surface phase. At lower pH range, i.e. $\text{pH} \leq 2$, Se was found in the leachate in the form of H_2SeO_3 and was not adsorbed on to CFA phase (Pugh et al. 2008). However, with increase in pH Se was found as oxyselenide form, i.e. HSeO_3^- and SeO_3^{2-} , and was adsorbed with CF as illustrated by Otero-Rey et al. (2005). The Se was also found in their ionic form in the leach liquor with a wide range of variation. The Se metal found in the solution in the form of Se(VI) has a unique character and was not adsorbed onto the surface of the adsorbent. While in case of Se(IV) it was seen to be adsorbed by fly ash which was derived from bituminous coal at lower pH level as reported by Wang et al. (2017).

12.3.2.2 Manganese

Manganese is another valuable metal which was found as a vital one in the fly ash phase. It showed wide variation range of pH on its leachability. Maximum extraction efficiency was achieved only at highly acidic condition while with increase in its pH the extraction efficiency further followed decreasing order. It was also observed that Mn exist in the fly ash in different oxidation state ((II)/(III),(IV)); however, only divalent manganese form was showing better extraction efficiency as compared to others (Zhao et al. 2018). Warren and Dudas (1988) studied the leachability of Mn and in this investigation it was reported that Mn was found in two different phases, i.e. glassy phase and as symbiosis with ferromagnetic particles. Among these two phases Mn in glassy phase was quickly leached out in comparison to others.

12.3.2.3 Nickel

Nickel is another demandable element also found in fly ash with a considerable extent which can be extracted in an economical way for its reuse. It was noticed that the leachability of Ni from CFA was greatly influenced by pH and low pH showing better leaching efficiency than that of high pH (Kim et al. 2003). In this context a number of researches have been put forward by different group of researchers for the leachability property of Ni. Mostly the Ni present in fly ash was either of magnetic form or non-magnetic form. However, it was concluded that the non-magnetic form of Ni was extracted easily over the magnetic one.

12.3.2.4 Cobalt

Cobalt is another valuable metal also present in fly ash in a worthy quantity. However, its quantity is originated to be more in magnetic kind CFA in comparison to non-magnetic one. In the investigation on the cobalt extraction FA by Hansen et al. (1981) it was presumed that the presence of Co in the magnetic type FA mainly depends upon its ionic radii and overall a quantitative extraction of cobalt from CFA was achieved. Kukier et al. (2003) studied the degree of cobalt enrichment from CFA. This investigation has revealed that the enrichment of Co from magnetic fly ash was much lower than that of the magnetic one. Nevertheless, it was also noticed that the leaching of metallic cobalt from non-magnetic fraction was more over magnetic fraction.

12.3.2.5 Zinc

Another valuable metal like Zn is also present in different class of fly ash like class F and class C in which the concentration profile may vary while examining weathering of fly ash in water and this was observed by Catalano et al. 2012. In this study it was noticed about the structural changes of the the metal Zn present in class C type CFA (varies from 100% tetrahedral form to 65–75% tetrahedral and remaining 25–35% to octahedral) which is may be mainly depend upon weathering behaviour of CFA. Whereas in case of F class of fly ash, Zn was found in the form of spinel-like structure which may also further increase with increasing weathering. From the result of the investigation carried out by Rivera et al. (2017), it was noticed that Zn does exist CFA in three different forms i.e. (a) adsorbed form of Fe as (hydro)oxide (70–77%), (b) in a spinel-type structure equivalent to franklinite (ZnFe_2O_4 , 8–12%), and (c) as ZnO(14–20%). Overall, it was concluded that Zn was mainly found in the CFA in combined form with iron excepting its existence as the

ZnO form. Thus, leaching of Zn may also be resulted while leaching out the Fe (III) from CFA.

12.3.2.6 Copper

Another most abundant element like Cu was found in fly ash. Rivera et al. (2017) studied heavy metals leaching from FA and reported that Cu exists in fly ash in five different forms, including: (a) as Cu(II) in aluminosilicate glass (13–42%), (b) tenorite (17–29%, CuO), (c) as cuprite (20–27%, Cu₂O), (d) as chalcopyrite (0–14%), and (e) as Cu₂S (0–41%). The existence of chalcopyrite in CFA may be due to the content of incombustible form of copper sulphide. In an investigation on extraction of copper from CFA, as much as 42% of copper in FA in amorphous phase (aluminosilicate glass) has been extracted out to the environment in neutral and alkaline conditions. It was also noticed that the copper oxide, i.e. Cu₂O, and copper sulphide (Cu₂S) dissolution from CFA was pretty low at the studied experiment; however the amorphous form could be readily solubilized. Additionally, fly ash weathering by methanotrophic bacteria may also be helpful on the enhancement on dissolution of Cu from CFA.

12.3.3 *Proper Disposal of FA into the Environment*

The greater rate of the CFA generation from several industries including thermal power plant, refinery and several other sectors where coal is used as fuel is becoming a major issue in the environment. Most of the industries deliberately use this fly ash for landfill purposes. However, the fly ashes bearing both heavy and toxic metals are of key concern without suitable treatment prior to its conventional disposal into the environment. The environment is contaminated due to the fly ash bearing numerous toxic heavy metals including Cr, As, Hg, Pb and Cd. These metals are subsequently got into the aqueous water bodies and thereby cause water pollution. On the other hand, the losses due to the valuable metals like Cu, Zn, Co, Se and several other heavy as well as rare earth metals are incurred as well. Therefore, the extraction routed through leaching of above metals is one of the promising methodologies and inconsequence of which these metals could be freed out of fly ash phase. After extraction of all these metals, the treated fly ash phase becomes safe for its disposal into the environment. There have been ample amount of works are being devoted by many researcher and to understand the extensive investigations carried out in this domain, following section describes metal extraction research from the fly ash both in Indian and global context.

12.4 Current Research on Metal Extraction Status from Fly Ash

Though numbers of study have been reported on extraction and recovery of metal values from various fly ash, the sizeable quantity of Al found in it has attracted metallurgist to propose the suitable method on quantitative recovery of aluminium and relating to the extraction of aluminium from fly ash. In this connection a number of works have been reported and are summarized below. Following literatures include the reported works relating to extraction and separation of Al from different resources of fly ash.

Many research studies have been put forward by authors especially on fly ash utilization and process developed from various power plant based source as the valuable metal like aluminium concentration profile is present up to significant level. The approaches accomplish Pyro-, Hydro- and Bio-leaching methods for successful extraction of metal values from fly ash (Tiwari et al. (2015)). Yao et al. (2014) have studied on the recovery of Al from CFA (Thermal power plants by-product). In which comparative study and advantages as well as disadvantages of the various techniques used were extensively discussed. The recovery of Al from CFA by inorganic acid and gas phase extraction with acetyl acetone was investigated by Shemi et al. (2012). The application of gas phase extraction appears to be effective for the extraction of aluminium and its leaching efficiency was enhanced from 17.9% to 64% which is also 21% lesser than the acid leaching process. Moreover the advantages for applying gas phase are to mainly on targeting to shrink the time period and possibility on the recycling of the un-reacted acetyl acetone. In another study Lin et al. (2012) have extracted $\text{Al}(\text{OH})_3$ powder from thermal power plant fly ash by the application of dispersing agent and carbonization. Wu et al. (2014) investigated on extraction of aluminium from CFA produced from thermal power plant by sintering it with $(\text{NH}_4)_2\text{SO}_4$ to ammonium aluminium sulphate, where alumina can be extracted easily. The alumina recovery from CFA using mixture $\text{NaOH} + \text{Ca}(\text{OH})_2$ routed by hydrothermal process was investigated by Li et al. (2014) and from the results it was observed that aluminium extraction efficacy was increased with increasing temperature, calcium-silicon ratio and liquid-solid ratio and overall extraction resulted as 91.3%.

The extraction efficiency of aluminium from the CFA was studied in two steps: acid leaching process and with the application of acid leach-sinter-acid method. However, the extraction of aluminium was found to be 88.2% from CFA which is ~10% more compared to conventional lime-sinter method as reported by Shem et al. (2015). Fly ash produced from the thermal power plants' pulverized coal-fired boilers was treated to recover alumina and from which 92.02% aluminium was extracted by the application of mixed alkali solution, i.e. $\text{NaOH} + \text{Ca}(\text{OH})_2$ [Sun et al. 2016]. Calcination of the fly ash at 700 °C with supplement of mixture of NaOH and Na_2CO_3 showed the promising result on efficient (95%) extraction of alumina [Guo et al. 2013]. Aluminium extraction from South African ultrafine CFA by thermo-chemical treatment with ammonium sulphate was studied by Doucet

et al. (2016) where 95% of aluminium selectively extracted by thermo-chemical treatment at 600 °C.

Several studies have been reported by the researcher while recovering the metal values from various CFA. Since the nature of fly ash existence is different depending on the processes adopted in the industries, accordingly the elemental assay of fly ash varies. Following section discusses about the significance of fly ash and the approaches / processes for recovering metal values from numerous sources. The extraction of lead and zinc from municipals waste incineration based fly ash that bears 2.12% Fe, 10.7% Pb and 40.18% Zn. For this study, they apply both acid (hydrochloric-, acetic-, sulphuric-acid) leaching and alkali leaching (NaOH) for efficient extraction of Pb/Zn. In consequences of this study NaOH leaching followed by acid washing showed causative on substantial recovery of above metals. Toro et al. (2009) have recovered Pb, Cd, Cu, and Zn as well as the anion like chloride from MSWI and FA of combusted straw through wet extraction method using 1 M NaOH, 12 M NaOH and conc. H₂SO₄. They successfully extracted 75% of Cd, 40% of Pb, 14% of Cu and 90% of chloride ion at the condition of an L/S of 3, pH 3 and leaching time of 10 minute. Overall requirement of either of acid or alkali is quite high. The leaching study of toxic heavy metals, namely Cd, Pb and Cr, as well as the other components such as K, Na, Cl and Ca from municipal solid waste residues has been carried out by Quina et al. (2009). From the leaching it was apparent on the observations in context of the amphoteric behaviour of metals like Pb and Zn with low solubility of Pb at pH ~ 9.0. However in the study while the leaching Zn, it was reportedly minimized at the studied pH value of 10.00. Kubonova et al. (2013) comparatively studied on removal of copper, lead, zinc and cadmium from FA by the application of both thermal and hydrometallurgical approach. Though hydrometallurgical extraction approach was found to be more promising for removal of chromium and nickel by adopting the combination of both lixivants (alkali and acid), the combination of both pyro- and hydro-metallurgical extraction approach appears as suitable combination for fly ash treatment. Neupane and Donahoe (2013) leached Cr, As, Ni, Sb, Co, Se, V, Ti, and Zn in alkaline and acidic CFA by both batch and column leaching approach. It was noticed that the leaching rate of either of these metals consumes more time. Okada and Tomikawa (2012) investigated the extraction of Pb from the melting furnace fly ash (MFA). It was evident from the results that the leaching characteristics of Pb may be improved with increase in molar ratio of Cl either as Na or as K in incineration FA leading to the rapid rise in the Cl⁻ gas generation that on substantial promote on formation of water. The studies accomplishing on extraction of metal such as Cu, Pb and Cd from the fly ash derived from municipal solid waste (MSW) through thermal pretreatment and chlorination method as stated by Nayak et al. (2010). In this investigation initially sodium and calcium chloride was blended with CFA and subjected for pelletization and treated under rotary reactor at ~1000 °C. At about 90% of Cd as well as Pb along with 80% Zn and 60% Cu extraction was achieved while processing through above methodologies.

Kai and his co-workers (2011) developed the processing approach for extraction of metals MSW based FA and from the results ~98% Zn, 62% Cu, 82% Fe, 86% Pb,

96% Cd, 80% Al, extraction was attained while leaching with hydrochloric acid. Kubonova et al. (2013) investigated metal recovery from municipal solid waste fly ash with a comparison study based on thermal and hydrometallurgical treatment process. In case of thermal treatment to achieve more than 90% Pb and Cd extraction from fly ash it needs 800 °C-1000 °C where as in case of Cu it needs more than 1200 °C. In contrast through hydrometallurgical process >90% of Cu, Zn, Cr and Cd were removed through combination of both acidic (2 M H₂SO₄) and alkaline (3 M NaOH) mixture studied at 80 °C. Zhang et al. (2016) have leached Na, Ba, Ag, Cr, Cd, Cu, Al, Ca, K, Mn, Zn, As, Pb, Se including So₄⁻² MSW based Fly ash. From this investigation they found that leaching of Al and As showed amphoteric leaching prototype at highly acidic range (pH: 2.0) and alkaline ranges (i.e. ~pH 12.0) whereas Se and Ba leached out at higher pH, i.e. ~11.0. Also the remaining of the said elements was leached out at higher acidic condition (pH- 2). Kai et al. (2011) have investigated on the recovery of metals including Zn, Pb, Vd, Fe Cu and Al from municipal waste incineration (MWI) based FA. In this extraction process, they applied two steps. Initially fly ash freed the alkali/alkaline earth metals (Na, K, Ca) while washing with water and later on the washed content was treated with hydrochloric acid. In this way at about 82% of Fe, 86 98% of Zn, 96% of Cd, 62% of Cu, and 80% of Al was extracted and reported. Tiwari et al. (2015) proposed the sustainability of various leaching test methods from different sources of fly ash. In his review comparison data of leaching test used by worldwide has been covered as given in Table 12.1. However after efficient extraction of toxic and heavy metals fly ash was widely used in numerous fields. In the USA mostly the fly ash are used in the field of construction of road and architectural applications and it reaches at about 83% of total generated fly ash. The other minor applications include waste solidification, soil modification and mining application. Similar trend was also observed for another developed country, i.e. European union. About 98% of the total fly ash was being utilized in the making of road and architectural application. Generally more advanced techniques were being utilized in the USA and EU in comparison to other countries globally. Still these countries do not meet the standard goal. However the global rate of fly ash utilization in comparison to its generation does not meet the standard and also causes serious threat to environment. Arise of this inadequate situation is only due to its low demand for architectural application and road construction. Thus, it is highly essential to focus on the realistic research on the usage of fly ash.

12.5 Summary and Futuristic Prospective

Presently fly ash is one of the potential sources of secondary that appears as promising one for various futuristic applications. Fly ash was widely used in the field of preparing cement, constructing works (bricks, tiles, concrete, road, fly over, etc.), waste solidification and stabilization process. Nevertheless, the basic physico-chemical properties (mineralogical composition, high surface area, small particle

size high water adsorbs capacity) as well as its leachability make the fly ash as a potential candidate of pollutant and can have a negative impact on environment. So it is highly warranted to devote research on the fly ash treatment for reclamation of metal values for its safe disposal into the environment or use as precursor source for further applications. This chapter gives the brief information regarding the chemical composition of fly ash and its leach ability property of CFA. The harmful effect on environment was studied due to releases of the toxic metals associated with it. Not only the toxic metals but also some other heavy metals associated with this fly ash was studied. The importance, scarcity as well as the loss and finally the recovery of these heavy metals from fly ash were studied. Hence, pretreatment of FA is highly essential before its reuse. It gives an excellent methodology for recovering highly demanding metal, removing pollutant as well as toxic element that lead to almost in every aspect environmentally acceptable of pretreated fly ash in every sector. Hence, the proper utilization as well as the safe disposal of the fly ash can be achieved without harming the territory of the environment.

Acknowledgements All the co-authors are highly thankful and would like to acknowledge to their respective affiliated organization for providing the resources on framing this book chapter.

References

- Agarwal, S., & Rani, A. (2017). Adsorption of resorcinol from aqueous solution onto CTAB/NaOH/flyash composites: Equilibrium, kinetics and thermodynamics. *Journal of Environmental Chemical Engineering*, 5, 526–538.
- Ahmaruzzaman, M. (2010). A review on the utilization of fly ash. *Progress in Energy and Combustion Science*, 36, 327–363.
- Akar, G., Polat, M., Galecki, G., & Ipekoglu, L. (2012). Leaching behavior of selected trace elements in coal fly ash samples from Yenikoy coal-fired power plants. *Fuel Processing Technology*, 104, 50–56.
- Arroyo, F., Fernandez-Pereira, C., & Coca, P. (2010). Precipitation of germanium from coal fly ash leachates. *Coal Combustion and Gasification Products*, 2, 28–34.
- Bao, S. Y., Li, K., Ning, P., Peng, J. H., Jin, X., & Tang, L. H. (2017). Highly effective removal of mercury and lead ions from wastewater by mercaptoamine-functionalised silica-coated magnetic nano-adsorbents: Behaviours and mechanisms. *Applied Surface Science*, 393, 457–466.
- Barman, P. J. (2012). A study on leaching behavior of Na, Ca and K using column leach test. *World Academy of Science, Engineering and Technology*, 6, 679–683.
- Basu, M., Pande, M., Bhadoria, P. B. S., & Mahapatra, S. C. (2009). Potential fly-ash utilization in agriculture: A global review. *Progress in Natural Science*, 19, 1173–1186.
- Bhattacharyya, S., Donahoe, R. J., & Patel, D. (2009). Experimental study of chemical treatment of coal fly ash to reduce the mobility of priority trace elements. *Fuel*, 88, 1173–1184.
- Brown, P., Jones, T., & BéruBé, K. (2011). The internal microstructure and fibrous mineralogy of fly ash from coal-burning power stations. *Environmental Pollution*, 159, 3324–3333.
- Cao, S. S., Zhou, C. C., Pan, J. H., Liu, C., Tang, M. C., Ji, W. S., Hu, T. T., & Zhang, N. N. (2018). Study on influence factors of leaching of rare earth elements from coal fly ash. *Energy & Fuels*, 32, 8000–8005.
- Catalano, J. G., Huhmann, B. L., Luo, Y., Mitnick, E. H., Slavney, A., & Giammar, D. E. (2012). Metal release and speciation changes during wet aging of coal fly ashes. *Environmental Science & Technology*, 46, 11804–11812.

- Cetina, B., Aydileka, A. H., & Guney, Y. (2012). Leaching of trace metals from high carbon fly ash stabilized highway base layers. *Resources, Conservation and Recycling*, 58, 8–17.
- Cheng-you, W. U., Hong-fa, Y. U., & Hui-fang, Z. (2012). Extraction of aluminum by pressure acid-leaching method from coal fly ash. *Transactions of the Nonferrous Metals Society of China*, 22, 2282–2288.
- Cornelis, G., Johnson, C. A., Gerven, T. V., & Vandecasteele, C. (2008). Leaching mechanisms of oxyanionic metalloids and metal species in alkaline solid wastes: A review. *Applied Geochemistry*, 23, 955–976.
- Dash, B., Das, B. R., Tripathy, B. C., Bhattacharya, I. N., & Das, S. C. (2008). Acid dissolution of alumina from waste aluminium dross. *Hydrometallurgy*, 92, 48–53.
- Doucet, F. J., Mohamed, S., Neyt, N., Castleman, B. A., & Vander-Merwe, E. M. (2016). Thermochemical processing of a South African ultrafine coal fly ash using ammonium sulphate as extracting agent for aluminium extraction. *Hydrometallurgy*, 166, 174–184.
- Dubikova, M. (2006). *Modelling element mobility in water-fly ash interactions*. Australia: QCAT Technology Transfer Centre.
- Elsewi, A. A., Page, A. L., & Grimm, S. R. (1980). Chemical characterization of fly ash aqueous system. *Journal of Environmental Quality*, 9, 224.
- Fan, L. J., Liang, J., Shi, Y. Q., & Huang, Y. (2012). Experimental study of leaching gallium in fly ash with acid method (Chinese). *Coal Ash*, 2, 10–12.
- Finkelman, R. B. (1995). Modes of occurrence of environmentally-sensitive trace elements in coal. *Environmental Aspects of Trace Elements in Coal*, 2, 24–50.
- Georgakopoulos, A. (2002). Leachability of major and trace elements of fly ash from Ptolemais Power Station, Northern Greece. *Energy Sources*, 24, 103–113.
- Guo, Y., Li, Y., Cheng, F., Wang, M., & Wang, X. (2013). Role of additives in improved thermal activation of coal fly ash for alumina extraction. *Fuel Processing Technology*, 110, 114–121.
- Gupta, N., Gedam, V. V., Moghe, C., & Labhasetwar, P. (2017). Investigation of characteristics and leaching behavior of coal fly ash, coal fly ash bricks and clay bricks. *Environmental Technology & Innovation*, 7, 152–159.
- Hansen, L. D., Silberman, D., Fisher, G. L. (1981). Crystalline components of stack-collected, size-fractionated coal fly ash. *Environmental Science & Technology*, 15, 1057–1062.
- He, H. H., Pang, J. Y., Wu, G. L., & Lambers, H. (2019). The application potential of coal fly ash for selenium biofortification. *Advances in Agronomy*, 157, 1–54.
- He, J. Z., Hu, X. L., & Li, Y. Y. (2002). Leaching test conditions for gallium in fly ash (Chinese). *Fly Ash Compr Utilization*, 6, 11–12.
- Huggins, F. E., & Huffman, G. P. (2004). How do lithophile elements occur in organic association in bituminous coals? *International Journal of Coal Geology*, 58, 193–204.
- Iyer, R. (2002). The surface chemistry of leaching coal fly ash. *Journal of Hazardous Materials*, 93, 321–329.
- Jones, K. B., Ruppert, L. F., & Swanson, S. M. (2012). Leaching of elements from bottom ash, economizer fly ash, and fly ash from two coal-fired power plants. *International Journal of Coal Geology*, 94, 337–348.
- Kai, H., Inoue, K., Harada, H., Kawakita, H., & Ohto, K. (2011). Leaching behavior of heavy metals with hydrochloric acid from fly ash generated in municipal waste incineration plants. *Transactions of the Nonferrous Metals Society of China*, 21, 1422–1427.
- Kazonich, G., et al. (1999). The release of base metals during acidic leaching of fly ash. <http://www.flyash.info>.
- Keyser, T. R., Natusch, D. F. S., Evans, C. A., & Linton, R. W. (1978). Characterizing the surface of environmental particles. *Environmental Science & Technology*, 12, 768–773.
- Kim, A. G., Kazonich, G., & Dahlberg, M. (2003). Relative solubility of cations in class F fly ash. *Environmental Science & Technology*, 37, 4507–4511.
- Kubonova, L., Langova, S., Nowak, B., & Winter, F. (2013). Thermal and hydrometallurgical recovery methods of heavy metals from municipal solid waste fly ash. *Waste Management*, 33, 2322–2327.

- Kukier, U., Ishak, C. F., Sumner, M. E., Miller, W. P. (2003). Composition and element solubility of magnetic and non-magnetic fly ash fractions. *Environmental Pollution*, 123, 255–266.
- Li, G. B., Wang, Q., Han, X., & Yu, L. F. (2018). Research on ultrafine fly ash characteristics (Chinese). *Coal Ash*, 5, 14–15.
- Li, G. L., Wang, S. X., Wu, Q. R., Wang, F. Y., Ding, D., & Shen, B. X. (2017). Mechanism identification of temperature influence on mercury adsorption capacity of different halides modified bio-chars. *Chemical Engineering Journal*, 315, 251–261.
- Li, G. L., Wang, S. X., Wu, Q. R., Wang, F. Y., & Shen, B. X. (2016). Mercury sorption study of halides modified bio-chars derived from cotton straw. *Chemical Engineering Journal*, 302, 305–313.
- Li, H., Hui, J., Wang, C., Bao, W., & Sun, Z. (2014). Extraction of alumina from coal fly ash by mixed-alkaline hydrothermal method. *Hydrometallurgy*, 147–148, 183–187.
- Liang, J. K., Liu, X. R., Luo, L. G., Pan, T., & Hu, H. J. (2008). Research on strengthening leaching of the valuable elements in fly ash (Chinese). *Mining Metallurgical Engineering*, 28, 76–79.
- Lin, H., Wan, L., & Yang, Y. (2012). Aluminium hydroxide ultrafine powder extracted from Fly ash. *Advanced Materials Research*, 512–515, 1548–1553.
- Lokeshappa, B., & Dikshit, A. K. (2012). Behaviour of metals in coal fly ash ponds. *APCBEE Procedia*, 1, 34–39.
- Menon, M. P., Ghuman, G. S., James, J., Chandra, K., & Adriano, D. C. (1980). Physico-chemical characteristics of water extracts of different coal ashes and fly ash amended composts. *Water, Air, and Soil Pollution*, 50, 343–353.
- Mohapatra, R., & Rao, J. R. (2001). Review: Some aspects of characterisation, utilisation and environmental effects of fly ash. *Journal of Chemical Technology and Biotechnology*, 76, 9–26.
- Morar, D. L. (2012). Leaching of metals from fly ash-amended permeable reactive barriers. *Journal of Environmental Engineering*, 138, 815–825.
- Murarka, I. P. (2003). Leaching of selected constituents from ammoniated fly ash from a coal-fired power plant. In International ash utilization symposium. Paper – 81.
- Nagib, S., & Inoue, K. (2000). Recovery of lead and zinc from fly ash generated from municipal incineration plants by means of acid and/or alkaline leaching. *Hydrometallurgy*, 56, 269–292.
- Narayani, H., Augustine, R., Sumi, S., Jose, M., Nair, K. D., Samsuddin, M., Prakash, H., & Shukla, S. (2017). Removal of basic and industrial azo reactive dyes from aqueous solutions via Fenton-like reactions using catalytic non-magnetic Pd-flyash and magnetic Pd-Fe₃O₄-flyash composite particles. *Separation and Purification Technology*, 172, 338–349.
- Nayak, N., & Panda, C. R. (2010). Aluminium extraction and leaching characteristics of Talcher Thermal Power Station fly ash with sulphuric acid. *Fuel*, 89, 53–58.
- Neupane, G., & Donahoe, R. J. (2013). Leachability of elements in alkaline and acidic coal fly ash samples during batch and column leaching tests. *Fuel*, 104, 758–770.
- Nyale, S. M., Babajide, O. O., Birch, G. D., Böke, N., & Petrik, L. F. (2013). Synthesis and characterization of coal fly ash-based foamed geopolymer. *Procedia Environmental Sciences*, 18, 722–730.
- Okada, T., & Tomikawa, H. (2012). Leaching characteristics of lead from melting furnace fly ash generated by melting of incineration fly ash. *Journal of Environmental Management*, 110, 207–214.
- Otero-Rey, J. R., Mato-Fernández, M. J., Moreda-Piñeiro, J., Alonso-Rodríguez, E., Muniategui-Lorenzo, S., López-Mahía, P., & Prada-Rodríguez, D. (2005). Influence of several experimental parameters on as and se leaching from coal fly ash samples. *Analytica Chimica Acta*, 531, 299–305.
- Palumbo, A. V. (2009). Leaching of mixture of biochar and fly ash. <http://www.flyash.info>.
- Pandeya, V. C., Singha, J. S., Singha, R. P., Singh, N., & Yunus, M. (2011). Arsenic hazards in coal fly ash and its fate in Indian scenario. *Resources, Conservation and Recycling*, 55, 819–835.
- Prasad, B. (2008). Heavy metal leaching in Indian fly ash. *Journal of Environmental Science & Engineering*, 50, 127–132.

- Prasad, B., Banerjee, N. N., & Dhar, B. B. (1996). Environmental assessment of coal ash disposal: A review. *Journal of Scientific and Industrial Research India*, 55, 772–780.
- Pugh, J., Webb, T., Caughman, W., (2008). Chemical constituents in coal combustion product leachate: Thallium. Electric Power Research Institute.
- Quina, M. J., Bordado, J. C. M., & Quinta-Ferreira, R. M. (2009). The influence of pH on the leaching behaviour of inorganic components from municipal solid waste APC residues. *Waste Management*, 29, 2483–2493.
- Reijnders, L. (2005). Disposal, uses and treatments of combustion ashes: A review. *Resources, Conservation and Recycling*, 43, 313–336.
- Rivera, N., Hesterberg, D., Kaur, N., & Duckworth, O. W. (2017). Chemical speciation of potentially toxic trace metals in coal fly ash associated with the Kingston fly ash spill. *Energy & Fuels*, 31, 9652–9659.
- Sakthivel, T., Reid, D. L., Goldstein, I., Hench, L., & Seal, S. (2013). Hydrophobic high surface area zeolites derived from fly ash for oil spill remediation. *Environmental Science & Technology*, 47, 5843–5850.
- Sandeep, P., Sahu, S. K., Kothai, P., & Pandit, G. G. (2016). Leaching behavior of selected trace and toxic metals in coal fly ash samples collected from two thermal power plants, India. *Bulletin of Environment Contamination and Toxicology*, 97, 425–431.
- Sarode, D. B., Jadhav, R. N., Khatik, V. A., Ingle, S. T., & Attarde, S. B. (2010). Extraction and leaching of heavy metals from thermal power plant Fly ash and its admixtures. *Polish Journal of Environmental Studies*, 19, 1325–1330.
- Sauer, J. J., Benson, C. H., Aydilek, A. H., & Edil, T. B. (2012). Trace elements leaching from organic soils stabilized with high carbon fly ash. *Journal of Geotechnical and Geo Environmental Engineering*, 138, 968–980.
- Sen, S. K., Das, M. M., Bandyopadhyay, P., Dash, R. R., & Raut, S. (2016). Green process using hot spring bacterium to concentrate alumina in coal fly ash. *Ecological Engineering*, 88, 10–19.
- Shem, A., Ndlovu, S., Sibanda, V., & Dyk, L. D. (2015). Extraction of alumina from coal fly ash using an acid leach-sinter-acid leach technique. *Hydrometallurgy*, 157, 348–355.
- Shemi, A., Mpana, R. N., Ndlovu, S., Dyk, L. D., Sibanda, V., & Seepe, L. (2012). Alternative techniques for extracting alumina from coal fly ash. *Minerals Engineering*, 34, 30–37.
- Shivpuri, K. K. (2011). Metal leaching potential in coal fly ash. *American Journal of Environmental Engineering*, 1, 21–27.
- Singh, R., Singh, L., & Singh, S. V. (2015). Beneficiation of iron and aluminium oxides from fly ash at lab scale. *International Journal of Mineral Processing*, 145, 32–37.
- Singh, R. K., Gupta, N. C., & Guha, B. K. (2012). The leaching characteristics of trace elements in coal fly ash and an ash disposal system of thermal power plants. *Energy Sources Part A Recovery Utilization and Environmental Effects*, 34, 602–608.
- Skvara, F., Kopecky, L., Smilauer, V., & Bittnar, Z. (2009). Material and structural characterization of alkali activated low-calcium brown coal fly ash. *Journal of Hazardous Material*, 168, 711–720.
- Sow, M., Hot, J., Tribout, C., & Cyr, M. (2015). Characterization of spreader stoker coal fly ashes (SSCFA) for their use in cement-based applications. *Fuel*, 162, 224–233.
- Sun, Z., Li, H., Bao, W., & Wang, C. (2016). Mineral phase transition of desilicated high alumina fly ash with alumina extraction in mixed alkali solution. *International Journal of Mineral Processing*, 153, 109–117.
- Sushil, S., & Batra, V. S. (2006). Analysis of fly ash heavy metal content and disposal in three thermal power plants in India. *Fuel*, 85, 2676–2679.
- Takao, T (2007). Leaching test of coal fly ash for the landfill. <http://www.flyash.info>.
- Teng, F., Zhang, H. Y., & Qi, L. Q. (2019). Research on the adsorption performance of microwave combined with alkali modified fly ash for Cr (VI). *Conservation Utilization of Mineral Resource*, 39, 26–31.
- Tiwari, M. K., Bajpai, S., Dewangan, U. K., & Tamrakar, R. K. (2015). Suitability of leaching test methods for fly ash and slag: A review. *Journal of Radiation Research and Applied Sciences*, 8, 523–537.

- Toro, M. A., Calmano, W., & Ecke, H. (2009). Wet extraction of heavy metals and chloride from MSWI and straw combustion fly ashes. *Waste Management*, 29, 2494–2499.
- Tripathy, A. K., Sarangi, C. K., Tripathy, B. C., Sanjay, K., Bhattacharya, I. N., Mahapatra, B. K., Behera, P. K., & Satpathy, B. K. (2015). Aluminium recovery from NALCO fly ash by acid digestion in the presence of fluoride ion. *International Journal of Mineral Processing*, 138, 44–48.
- Tsiridis, V. (2006). Application of leaching tests for toxicity evaluation of coal fly ash. www.interscience.wiley.com.
- Tsiridis, V., Petala, M., Samaras, P., Kungolos, A., & Sakellariopoulos, G. P. (2012). Environmental hazard assessment of coal fly ash using leaching and ecotoxicity tests. *Ecotoxicology and Environmental Safety*, 84, 212–220.
- Vageesh, T. S., Siddaramappa, R. (2002). Leachate composition and soil quality assessment in coal fly ash amended soils, 17th WCSS, 14–21.
- Vitkova, M., Ettler, V., Hyks, J., & Astrup, T. (2010). Assessment of the leaching behaviour of fly ash from a cobalt smelter, zambia. In Proceedings Venice 2010, Third International Symposium on Energy from Biomass and Waste Venice, Italy (pp. 8–11). November 2010.
- Wang, H., Yu, W. S., Peng, X., Chen, Z. W., Wu, S. J., Yu, Q. Q., Yang, W., & Zhou, J. (2020). Highly efficient catalytic adsorbents designed by an “adaption” strategy for removal of elemental mercury. *Chemical Engineering Journal*, 388, 124220.
- Wang, L., Chen, Q., Jamro, I. A., Li, R. D., & Baloch, H. A. (2016). Accelerated co-precipitation of lead, zinc and copper by carbon dioxide bubbling in alkaline municipal solid waste incinerator (MSWI) fly ash wash water. *RSC Advances*, 6, 20173–20186.
- Wang, N. N., Chen, J. Q., Zhao, Q., & Xu, H. (2017). Study on preparation conditions of coal fly ash catalyst and catalytic mechanism in a heterogeneous Fenton-like process. *RSC Advances*, 7, 52524–52532.
- Ward, C. R., French, D., Stephenson, L., Riley, K., & Li, Z. (2010). Testing of interaction between coal ash leachates and rock minerals for mine backfill evaluation., 2, 16–27.
- Warren, C. J., & Dudas, M. J. (1988). Leaching behaviour of selected trace elements in chemically weathered alkaline fly ash. *Science of Total Environment*, 76, 229–246.
- Wei, Z., Wu, G. H., Su, R. X., Li, C. W., & Liang, P. Y. (2011). Mobility and contamination assessment of mercury in coal fly ash, atmospheric deposition, and soil collected from Tianjin, China. *Environmental Toxicology and Chemistry*, 30, 1997–2003.
- Wu, Y., Xu, P., Chen, J., Li, L., & Li, M. (2014). Effect of temperature on phase and alumina extraction efficiency of the product from sintering coal Fly ash with ammonium sulfate. *Chinese Journal of Chemical Engineering*, 22, 1363–1367.
- Xu, T., Lan, H. P., Yang, C., Li, N., Ji, Z. B., Zhang, J. N., & Zhang, R. H. (2018). Comparative research on physical and chemical properties of coal ash (Chinese). *Inorganic Chemistry Ind*, 50, 65–68.
- Xue, J., Wang, W., Wang, Q., Liu, S., Yang, J., & Wuid, T. (2010). Removal of heavy metals from municipal solid waste incineration (MSWI) fly ash by traditional and microwave acid extraction. *Journal of Chemical Technology and Biotechnology*, 85, 1268–1277.
- Yang, W., Hussain, A., Zhang, J., & Liu, Y. X. (2018). Removal of elemental mercury from flue gas using red mud impregnated by KBr and KI reagent. *Chemical Engineering Journal*, 341, 483–494.
- Yao, Z. T., Xia, M. S., Sarker, P. K., & Chen, T. (2014). A review of the alumina recovery from coal fly ash, with a focus in China. *Fuel*, 120, 74–85.
- Yilmaz, H. (2015). Characterization and comparison of leaching behaviours of fly ash samples from three different power plants in Turkey. *Fuel Processing Technology*, 137, 240–249.
- Zhang, B. P., Chen, Y. L., Wei, L., & Zu, Z. N. (2012). Study on the modification and adsorption capacity of coal fly ash. *Bulletin Chinese Ceramics Society*, 31, 675–678.
- Zhang, Y., Cetin, B., Likos, W. J., & Edil, T. B. (2016). Impacts of pH on leaching potential of elements from MSW incineration fly ash. *Fuel*, 184, 815–825.

- Zhao, S. L., Duan, Y. F., Lu, J. C., Gupta, R., Pudasainee, D., Liu, S., Liu, M., & Lu, J. H. (2018). Chemical speciation and leaching characteristics of hazardous trace elements in coal and fly ash from coal-fired power plants. *Fuel*, 232, 463–469.
- Zhao, Y. C., Zhang, J. Y., Tian, C., Li, H. L., Shao, X. Y., & Zheng, C. G. (2010). Mineralogy and chemical composition of high-calcium fly ashes and density fractions from a coal-fired power plant in China. *Energy & Fuels*, 24, 834–843.
- Zhou, Q., Duan, Y. F., Zhu, C., Zhang, J., She, M., Wei, H. Q., & Hong, Y. G. (2015). Adsorption equilibrium, kinetics and mechanism studies of mercury on coal-fired fly ash. *Korean Journal of Chemical Engineering*, 32, 1405–1413.
- Zhu, C., Duan, Y. F., Wu, C. Y., Zhou, Q., She, M., Yao, T., & Zhang, J. (2016). Mercury removal and synergistic capture of SO₂/NO by ammonium halides modified rice husk char. *Fuel*, 172, 160–169.
- Ziemkiewicz, P. F., & Knox, A. S. (2006). Prediction of coal ash leaching behavior in acid mine water: Comparison of laboratory and field studies. In K. S. Sajwan, I. Twardowska, T. Punshon, & A. K. Alva (Eds.), *Coal combustion byproducts and environmental issues*. New York, NY: Springer.

Chapter 13

Investigation on Extraction and Recovery of Rare Earth Elements from Coal Combustion Products



Verónica Cristina Arellano Ruiz, Pankaj Kumar Parhi, Jin-Young Lee, and Rajesh Kumar Jyothi

13.1 Introduction

The rare earth elements are a group of elements including the lanthanides series with atomic numbers ranging from 57 (lanthanum) to 71 (lutetium). The lanthanides do occur abundantly in nature, while promethium is extremely rare, appears in trace quantities in Earth's crust. Table 13.1 lists the physical and chemical properties of rare earth elements. The lanthanides are usually trivalent (3^+), with the exception of thulium ytterbium, samarium, thulium, ytterbium, and europium, which may exist as 2^+ ions form while cerium, praseodymium, and terbium do found as 4^+ ions form (Voncken 2015). REEs can be very easily the substitute for one making refinement to pure metal tough owing to their similarity (British Geological Survey 2011). Owing to the special unique properties, rare earth elements are extensively used in various diverse applications such as catalysts, magnets, phosphors, polishing powder, computer hard drives, electric motors, ceramics, liquid crystal displays (LCDs), etc. There is a sizable amount of REEs in the Earth's crust (Rudnick and Gao 2014). The crustal abundance of individual REEs varies extensively, from cerium, the richest, at the level of 0.28–43 ppm for thulium (Taylor and McLennan 1995).

In consequences of time, the market demand for rare earth elements has gradually increased, and consequently the production of REEs has been showing an upward trend. In the last few years, the majority of countries, which produce and export rare

V. C. Arellano Ruiz · J.-Y. Lee · R. K. Jyothi (✉)

Convergence Research Center for Development of Mineral Resources (DMR), Korea Institute of Geoscience & Mineral Resources (KIGAM), Daejeon, South Korea

Department of Resources Recycling, University of Science and Technology (UST), Daejeon, South Korea

e-mail: jinlee@kigam.re.kr; rkumarphd@kigam.re.kr

P. K. Parhi

Department of Chemistry, Fakir Mohan University (FMU), Balasore, Odisha, India

Table 13.1 Comparison of physical and chemical properties of rare earth elements (Gupta and Krishnamurthy 2005; McGill 2012; Peramaki 2006)

Element	Symbol	Atomic number	Atomic weight	Density (g cm ⁻³)	Melting point (°C)	Vicker's hardness	Physical appearance	Oxidation states	Specific heat capacity (J/mol K)
Lanthanum	La	57	138.9	6.146	918	37	Colorless	3	26.2
Cerium	Ce	58	140.1	8.16	798	24	Colorless	3 and 4	27.0
Praseodymium	Pr	59	140.9	6.773	931	37	Yellow-green	3 and 4	27.0
Neodymium	Nd	60	144.2	7.008	1021	35	Red-violet	3	27.5
Promethium ^a	Pm	61	145.0	7.264	1042	–	Pink	3	24.3
Samarium	Sm	62	150.3	7.52	1074	45	Yellow	2 and 3	29.6
Europium	Eu	63	151.9	5.244	822	17	Colorless	2 and 3	27.7
Gadolinium	Gd	64	157.2	7.901	1313	57	Colorless	3	37.1
Terbium	Tb	65	158.9	8.23	1356	46	Pale pink	3 and 4	28.9
Dysprosium	Dy	66	162.5	8.551	1412	42	Pale yellow-green	3	28.2
Holmium	Ho	67	164.9	8.795	1474	42	Yellow	3	27.2
Erbium	Er	68	167.2	9.066	1529	44	Pink	3	28.1
Thulium	Tm	69	168.9	9.321	1545	48	Pale green	2 and 3	27.0
Ytterbium	Yb	70	173.0	6.966	819	21	Colorless	2 and 3	26.7
Lutetium	Lu	71	174.9	9.841	1663	77	Colorless	3	26.9
Yttrium	Y	39	88.9	4.469	1522	38	–	3	25.5
Scandium	Sc	21	44.9	2.989	1541	85	–	3	26.5

^aPromethium: is a radioactive element

earth elements, have reduced their exports to the United States in order to safeguard their national industries. At present in global scenario, the largest world producer, consumer, and exporter of rare earth elements is China that controls more than 60% of the global REEs supply (Gambogi 2020). The Chinese Ministry of Commerce also imposes export duty on REEs for concentrates and oxides leaving the country. In general, the majority of rare earth elements have a 15% export tariff rate, while neodymium, yttrium, europium, dysprosium, terbium, and scandium have a 25% charge (British Geological Survey 2011). The rare earth elements (REEs) is being g increasingly incorporated in new technologies, and as a result of which, the industry market demand for the constituent REEs is significantly grown. Some analysts have established over the next 25 years, the lower and upper limits for REEs annual growth demand could be between 5% and 9% (Alonso et al. 2012). Consequently, looking for new alternative resources, it is imperative to satisfy the demand of REEs.

In concern with the REEs in coal ash/ fly ash, REEs are claimed to bear up to significant extent, though, their quantity is very small compared to primary sources. To ascertain about the REEs in coal phase it is important to know about the significance about the coal sources. Coal is majorly utilized in various scale of power plant sectors across the globe. Electricity is mostly generated by primary fossil fuels in the United States. Coal contributed with approximately 30% of the total electric power generated in 2017 (Jeffrey 2018). Coal combustion products (CCPs) are solid particles that are produced when coal is burned in coal-fired power plants in order to produce electricity (American Coal Ash Association 2020). These products are considered to be one of the largest types of industrial waste generated in the USA. According to the Coal Combustion Product Production & Use Survey, around 102 million tons of CCPs were generated in 2018. CCPs have been widely explored for their pro-environmental and pro-recovery uses. For example, FA and BA are reused in the construction industry. Based on this data, coal combustion products might be considered as a resource, rather than a waste.

In the United States, coal-fired power generation has been exponentially augmented in the last 10 years, the country has continued to generate vast quantities of fly ash, from which about a half is beneficially reused (American Coal Ash Association 2017). Fly ash is originated from the non-combustible constituents of coal, such as clay minerals and quartz. After combustion processes REEs are recollected and enriched in the fly ash (Seredin and Dai 2012). The principal application of fly ash (FA) is in the cement industry due to its chemical and physical properties that help on improving the compressive strength leading to which various mesoporous materials as well as zeolites are being synthesized out of it. In this way, fly ash is becoming an exciting area of research subject because of the contentment of REEs as alternative resources over the other primary and secondary ones. Therefore, numerous companies are inquiring methods to extract REEs from fly ash and investigating whether fly ash processing can become an economical and environmentally friendly alternative to recover REEs (Mayfield and Lewis 2013; Ketris and Yudovich 2009).

Several potential processes have been proposed to recover REEs from FA including physical separation, bioleaching, ion exchange, alkali-acid leaching, and

roasting approach. Fly ash (FA) is mainly composed of amorphous glass (aluminosilicate glass); thus pretreatment is necessary to dissolve amorphous glass to increase the REEs recovery efficiency. In view of which, this chapter provides a complete analysis of the technical viability of rare earth element extraction and recovery methods from coal fly ash. Moreover, the author presents an insight of the novel technologies in pyrometallurgy, hydrometallurgy, the chemical and physical principles, mechanisms, and their advantages as well as disadvantages.

13.2 Rare Earth Elements (REEs)

Rare earth elements are a particular group of 17 chemically analogous metallic elements. There are different categorizations of REEs, for instance, according to their atomic mass (light, medium, and heavy), market tendencies (critical, uncritical, and excessive), and geological orientation (Dai et al., 2018; Bünzli 2013). Rare earths are vital resources to several sectors of the world that is exponentially growing in the markets for usages including catalysts, magnets, ceramics, electronic devices, and others. Nevertheless, REEs constitute the base of critical technologies for clean energy, communication, and transport domain (Haque et al. 2014). Their chemical similarity justifies their combined use or reciprocal substitution in some uses, even though the end uses for REEs are diverse. Because of these factors, the criticality of some of the elements as compared to others could be determined (Reilly 2020).

13.2.1 Worldwide Rare Earth Resources

REEs geologically occur in a wide variety of igneous sedimentary and metamorphic rocks. Even though REEs are relatively common in the earth crust, they rarely can exist in economic concentrations. Resources are mostly found in four geologic environments (George et al. 2016). *Peralkaline igneous systems* are characteristically enriched in REEs, in some instances hosting high-grade deposits. Peralkaline igneous complexes are being explored due to their enriched content of heavy rare earth elements. Peralkaline igneous rock types in REE-bearing systems can differ substantially based upon their deposits. Hence, a notorious disadvantage is to generalize which peralkaline lithologies are steadily related to REEs deposits (Van Gosen et al. 2017).

Carbonatites intrusion occur in a diverse forms and its carbonate chemical compositions, encompassed from stocks, tabular bodies, dikes, irregular-shaped masses up to veins. However, the composition of carbonatites are different from other calcic, dolomitic, iron-carbonate, or siderite types (Van Gosen et al. 2017).

Ion-adsorption clay deposits are the primary world source of heavy rare earth elements in southern China. These deposits are generally formed in tropical regions

with moderate to high rainfall through different geological process (Van Gosen et al. 2017).

Monazite-xenotime-bearing placer deposits are two broad settings deposits, namely (a) coastal and nearshore deposits of sand and silt and (b) deposits of streams and rivers (fluvial deposits). In both deposits, heavy dense minerals (including monazite) are physically assorted and deposited together by water movement and gravity.

The resulting deposits of sediments which are conformed of sand and silt with narrow layers of heavy minerals are called “heavy-mineral sands.” Mountain Pass deposit in California is a project with high interest in the USA. Other significant projects are the Buena Norte mining in Brazil and in India in the State of Kerala (Van Gosen et al. 2017).

Figure 13.1 shows an example of the important rare earth element mining sites in the world in REEs production and significant projects. The most representative rare earth element sites for production are located in China, the USA, Burma, Australia, Russia, and India.

China has presently reported ~62.9% of global production (Van Gosen et al. 2017; Tse 2011); consequently, it is considered as the leading country in worldwide production of REEs. China imposed restrictions to the provision of REEs by the levy of quotas, licenses, and taxes in 2010 (Tse 2011; Hurst 2010). China’s new policies on REEs transformed the world rare-earth industry promoting increased stockpiling of REEs; incremented exploration and development of worldwide deposits and new efforts to conserve, recycle, and on finding alternative mine resources (Gong et al. 2018). According to the US Geological Survey, new mine production began in Australia in 2011 (2200 Mt) and in the United States in 2012 (7000 Mt), and additional exploration and development projects were in Thailand, Vietnam, Burma, Burundi, and others (Eggert et al. 2016). The average cost of rare-earth compounds and metals imported by the USA in 2015 was \$150 million while



Fig. 13.1 Examples of the important REEs mineral mine sites in the world (Barakos George et al. 2016)

in 2019 was \$170 million with an average increase of 4 million Mt. per year. The estimated distribution by application was catalysts around 75% including the use in the petroleum industry followed by metallurgical applications, polishing, and alloys ceramics-glass approximately 5% for each one and other application about 10% (Eggert et al. 2016).

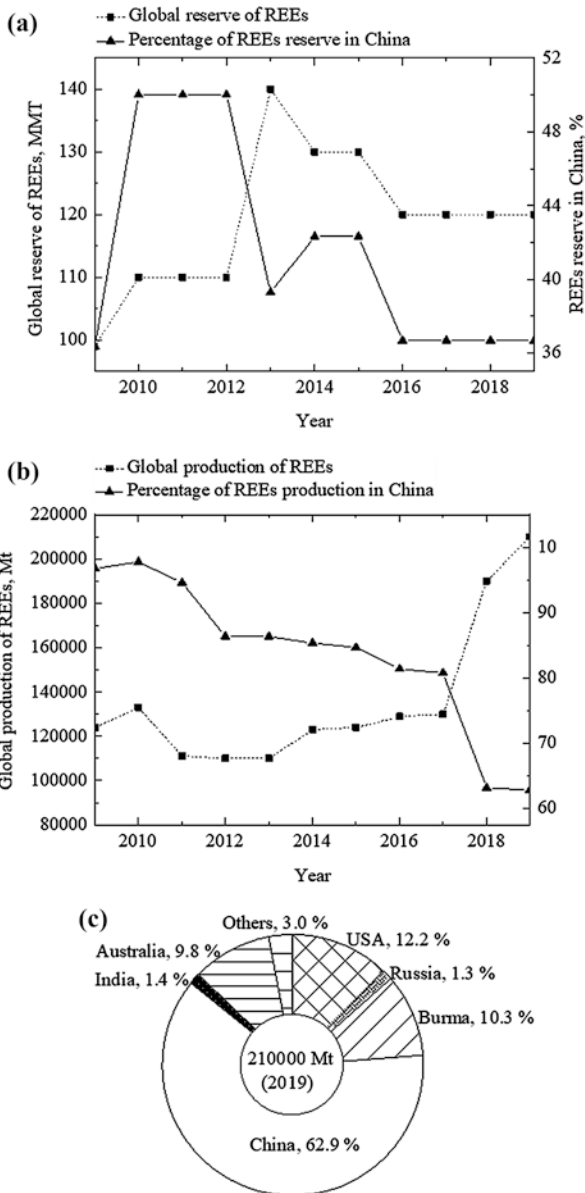
The top five focus companies for rare earth elements extraction in 2013 were: (1) Baota Steel Rare Earth (Group) Hi-Tech Co. Ltd., (2) China Rare Earth Holdings Ltd. (cre), (3) Solvay Group-Rhoda s.a., (4) Indian Rare Earths Ltd. (irel), and (5) Molycorp Inc. (Crull 2013). Therefore, Fig. 13.1 shows the mining processes and the upgrading processes for REEs mainly referring to the process used in these companies.

13.2.2 Rare Earths Global Reserve and Production

In 2010, a debate was proposed between the Chinese government and rare-earth producers in order to create policies on controlling the production and exports of REEs. The main objective was the preservation of the mineral resources and protection of the environment. Since 2010, Chinese rare earth elements have special tariffs and in this connection, Fig. 13.2(a) shows the global of REEs reserve and the percentage of REEs reserve in China. The total reserve of REEs has steadily increased owing to the increment of its worldwide market demand. While China maintains a commanding presence within the global rare earth reserve even though it has waned for in the last seven years. Figure 13.2(b) shows the production of REEs in China which was about approximately 95% until 2011. During the period of 2012–2017, China had provided over 80% of the world's rare earth elements as concentrates, intermediate products, and chemicals.

However, in 2019, China has slipped around 62.9% of the total production of REEs. Chinese rare earth reserves have equally fallen from 50% to 36.7% during 1995–2019 as can be seen from Fig. 13.2(a). Among the countries in the world, top five countries, e.g., China, Brazil, Vietnam, Russia, and India reserves major sources bearing rare earth elements (Reilly 2020). Figure 13.2(c) shows the global REEs production for different countries by 2019. China leads at the global rare earth elements production followed by Burma, the USA, Australia, and India. Nevertheless, it is well known that China rare-earth policies have a direct impact in the global production of rare earth elements. The policy changes have promoted the exploration and development of worldwide deposits such as Burundi, Vietnam, in 2016. Rare earths elements are found usually in negligible concentrations in the Earth's crust. The primary global use of REEs is the catalyst market estimated at about USD 33.9 billion in 2019 and is projected to raise by 4.4% per year from 2020 to 2027.

Fig. 13.2 (a) Global REEs production from 2009 to 2019 and the percentage of REEs production in China, (b) Global REEs reserve from 2009 to 2019 and percentage of REEs reserve in China, and (c) Global REEs production in several countries in 2019 (Gambogi 2010, 2011, 2012, 2013, 2014, 2015, 2016, 2017, 2018, 2019). *MMT* million metric ton, *Mt* metric ton



MMT = million metric ton, Mt = metric ton

The intensifying demand for catalysts from uses extend from chemical synthesis, polymers, petrochemicals, and others.

13.3 Hydrometallurgical Techniques Role on Metals Recovery

Hydrometallurgical processes have several advantages such as reasonably lowering of capital cost, reduced environmental impact, and high metal recovery rate with their suitability for small- and medium-scale applications (Tuncuk et al. 2012). A hydrometallurgical process of operation mainly follows the mechanical pretreatment, leaching of metals, purification, and recovery of metals. The refining using hydrometallurgy techniques to obtain ultra-high purity metals. The solution purification and concentration processes might encompass precipitation, distillation, adsorption, and solvent extraction processes.

13.4 Coal Combustion Products (CCPs)

The world electricity generation by coal source was 2472.3 TWh in 2019. According to the World Energy Balance, coal is the first electricity source for producing and consuming electricity around the world followed by natural gas, renewables, nuclear, and oil (International Energy Agency 2020; Jeffrey 2018). Coal combustion products (CCPs) are a result of burning of the coal used for generating electricity in coal-fired power plants. The U.S. Environmental Protection Agency coined the term “product” in order to promote recycling these and other industrial products (Environmental Protection Agency 2020; Union of Concerned Scientists 2020).

13.4.1 Coal Combustion Products Resources

Fly ashes are fine powdery particles retained by emission controls such as bag house, electrostatic precipitator, or scrubbers. The composition of fly ash is practically identical in its composition to volcanic ash with pozzolanic properties. Thereby, fly ash chemical composition is SiO_2 , Al_2O_3 , FeO_3 , and CaO . Fly ash has excellent cementation properties. In fact, over 50% of the American concrete produced uses fly ash in some percentage as a direct replacement for cement. Fly ash is used in Portland cement in the manufacture of concrete (American Coal Ash Association 2020; Kentucky Geological Survey 2020). In 2018, approximated 36 million tons of fly ash and around 50% were disposed in surface impoundments or

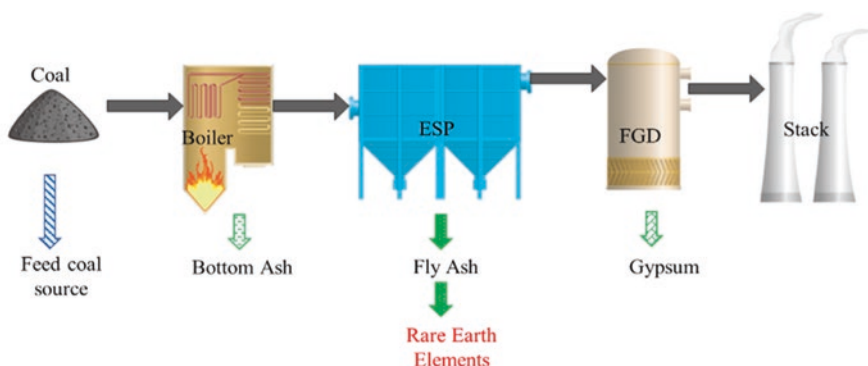
in landfills, but 40% to 45% is recycled as advantageous by-products (American Coal Ash Association 2018a, b).

Bottom Ashes are granular solid residues that are excessively large to be transported in the flue gases and that adhere on the furnace walls or fall down at the furnace bottom. The main disadvantage of bottom ash is that does not have any cementation properties. Bottom ash is usually used as an aggregate or filler material in construction (American Coal Ash Association 2020; Kentucky Geological Survey 2020). Approximately 15 million tons of bottom ash are produced each year in the United States, while only 1.5–2.25 million are recycled (American Coal Ash Association 2016). In winter, the production of FA and BA increases due to coal-fired power plants operating at full capacity.

Boiler Slag is collected at the base of slag tap and furnaces that is quenched with water; consequently, particles suffer fractures, crystallizes, and form pellets. The appearance is glassy and particle size fractions are in the range of 0.5 and 5.0 mm. Boiler slag is used as low silica blasting grit (American Coal Ash Association 2019; Kentucky Geological Survey 2020).

Flue Gas Desulfurization Gypsum is amply used to eliminate SO_2 from coal-fired flue gas and the wet limestone process by emissions control systems. These scrubbers are usually applied to eliminate sulfur, oxides and the wet limestone process from coal-fired power plant flue gas streams. FGD have different applications in construction as FGD gypsum (or “synthetic” gypsum) (American Coal Ash Association 2020; Kentucky Geological Survey 2020). There is a direct relationship between the amount of scrubbers installed in coal-fired power plants and the amount of FDG waste resulting in a growing in the production of FGD.

Other *coal combustion product* types are cenospheres, scrubber residues, and fluidized bed combustion ash. The schematic of the typical generation system of CCPs in coal-fired power plants is shown in Fig. 13.3.



ESP = electrostatic precipitators, FGD = flue gas desulfurization

Fig. 13.3 Schematic of typical generation system of coal combustion products (National Energy Technology Laboratory 2006). ESP electrostatic precipitators, FGD flue gas desulfurization

In many countries, regulations and projects have been created to decrease land-filling and research the opportunities to exploit the utilization of CPPs. These organizations assemble statistical data, and study the tendencies in the production and utilization of CPPs and their disposal practices. They are located in several countries accomplishing India under Fly Ash Utilization Program (FAUP), in the United Kingdom Quality Ash Association (UKQAA), in the USA as the American Coal Ash Association (ACAA), Ash Development Association of Australia (ADDA), and at the European Coal Combustion Products Association (ECOBA).

13.4.2 Physical and Engineering Properties of the Main CCPs

Table 13.2 summarizes the physical and engineering properties of some coal combustion products. FA is typically spherical with a diameter oscillating from 1 to 100 μm . FA is gray cohesive nature and has low permeability. BA and BS have sizes found in between 0.1 and 10.0 mm and are granular in form. FA possess a lower permeability than bottom ash, while boiler slag permeability is similar to sand. The dry densities of FA, BA, and BS fluctuate between 40 and 100 lb/ft^3 . Bottom ash and boiler slag have higher shear strength than FA. Depending on the type of system used (wet or dry), the FGD material physical characteristics vary. Wet FGD systems display diameters fluctuating from 0.001 to 0.05 mm. While dry FGD systems present 0.002–0.074 mm diameters. FGD material commonly has low porousness between 10–4 to 10–7 cm/s . FGD moisture content and the percentage of both fly ash and lime affect the unconfined compressive strength. The strength of wet FGD is enormously improved when FGD sludge is stabilized using a lime and fly ash mix (Ramme and Tharaniyil 2013).

As shown in Table 13.2, owing to the excellent cementation properties of coal combustion products, they are mainly used in the construction industry. Among these CCPs, fly ash is used mainly as the feedstock in cement manufacturing process. BA is often used as an aggregate and as a constituent in manufacturing

Table 13.2 Physical and engineering properties of some CCPs (American Coal Ash Association 2018a, b)

Physical properties	Fly ash	Bottom ash	FGD material	
			Wet	Dry
Particle size (mm)	0.001–0.1	0.1–10.0	0.001–0.05	0.002–0.074
Compressibility (%)	1.8	1.4	56–106	6–87
Dry density (lb/ft^3)	40–90	40–100	10–6–10-4	10–7–10-6
Permeability (cm/s)	10–6–10-4	10–3–10-1		
Shear strength cohesion (psi)	0.17	0		
Angle of internal friction (deg)	24–25	24–25		
Unconfined compressive strength (psi)			0–1600	41–2250

FGD material flue-gas desulfurization material

concrete blocks, synthetic gypsum in the manufacturing of wallboard, as well as waste stabilization, mine reclamation, and cement manufacturing (American Coal Ash Association 2018a, b).

13.4.3 Chemical Transformation

Generally, 95–99% of fly ash (FA) is composed of SiO_2 , Al_2O_3 , FeO_3 , and CaO . In addition, the components present in minor proportion are MgO , Na_2O , K_2O , SO_3 , P_2O_5 , and TiO_2 around 0.5–3.5% and unburnt coal (losses on ignition).

Fly ash and bottom ash are mainly amorphous glass (aluminosilicate glass) (Dai and Finkelman 2018; Hood et al. 2017; Wang et al. 2019) and the REEs present in these ashes are mainly associated with this amorphous glass. The chemical composition determines the melting behavior of the ash particles during combustion process. Figure 13.4 shows that during the process of combustion, there exist a transformation of minerals such as pyrite, aluminosilicates, and K-aluminosilicates. Figure 13.4 (a) and (b) illustrates the chemical composition of coal (wt. % minerals basis) and fly ash, respectively.

13.4.4 Coal Combustion Products Generation Global Wide

A vast share of worldwide electric power production and coal consumption has augmented enormously over the period and is expected to continue increasing as well. In America, one-third of electricity is being produced in the fired-coal power stations in which coal is used as the fuel. This process generates large volumes of coal combustion products (CCPs), notably fly ash and gypsum from emission control devices. According to the Statistical Review of World Energy, the total world-electricity generation was 27004.7 (TWh) and coal-fired generation accounted for 36% with 241 coal powered units across the United States in 2019 (Statistical

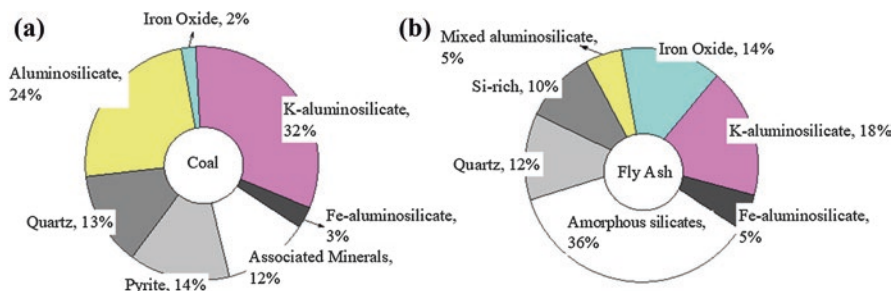


Fig. 13.4 Schematic of the chemical composition (wt. %) of (a) coal and (b) coal fly ash (FA) (L. D. Smoot 1993)

Review of World Energy 2020). In addition, in Asia coal is the principal fuel for electricity generation.

The present coal combustion products utilization is estimated to bear around 102 million tons and the percentage of utilization of CCPs was approximately 58.12% in the USA during 2018. The trend showed a progressive reduction in CCPs production in the USA probably due to the closing of coal-fired power stations owing to cheaper and cleaner natural gas and renewables options. In contrast, the trend of the demand market for CCPs showed a steady increase in the last five years (American Coal Ash Association 2020; US Environmental Protection Agency 2020). In fact, the American Coal Ash Association reported that coal usage is expected to grow by 3.4% over the next two decades due to the application of these products in different industries such as construction. In addition, fly ash has been one of the leading-CCPs products with around 47.6 million tons in 2018. According to American Coal Ash Association, fly ash production forecast to increase 2.6% by 2033. Due to improvement in technology in ash quality it is predicted an increase in the quantity of fly ash available for beneficial use. Moreover, this association categorized the key uses of fly ash as blended cement, feed for clicker, structural fills, and embankments due to the several advantages of fly ash such as good engineering mechanical properties (Li et al. 2017).

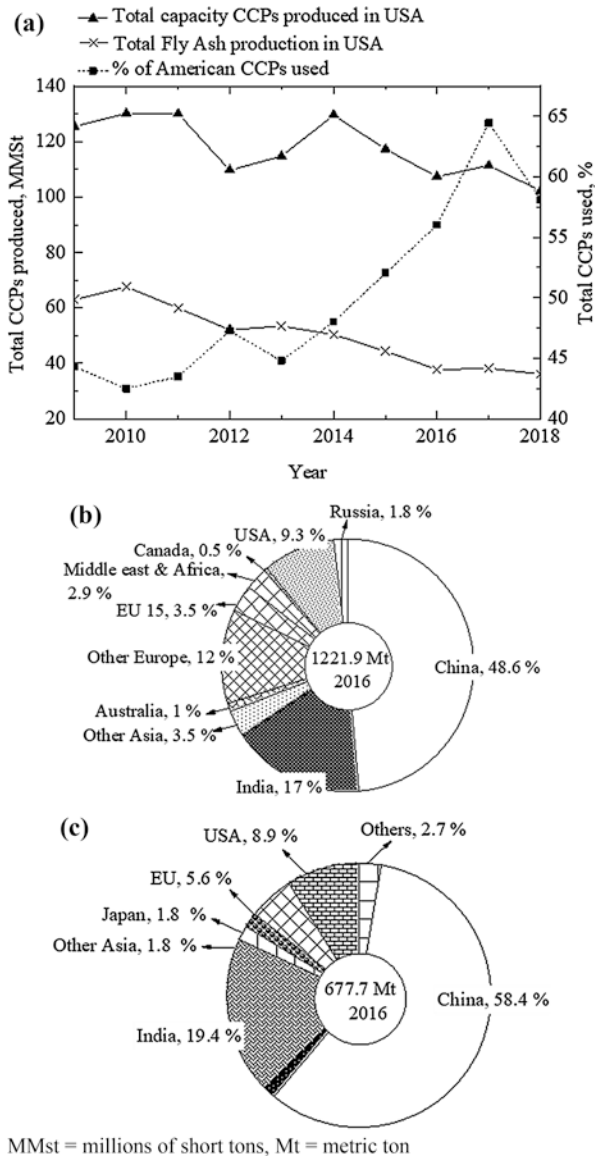
China is the largest coal combustion product producer in the world and accounts for 48.6% of the total CCPs production in 2016, followed by India (17%), European countries (12%), and the USA (9.3%) (Fig. 13.5). Due to the accelerated growth of China's economy, the demand of CCPs has rapidly increased too (Harris et al. 2019).

As shown in Fig. 13.5(c), China also led the global CCPs utilization in 2016 with a remarkable increase of 58.4% (equivalent to 395.7 Mt.). The principal uses of the Chinese fly ash are low value-added applications, such as construction, agriculture, and mineral extraction (Wang and Wu 2004; Cao et al. 2008; Lu et al. 2011). India is the second largest consumer of CCPs in the world; this can be attributed to the Indian government while achieving the distribution of electricity to every village in India by April 2018 (Philalay 2019).

13.5 Environmental Concerns Related to CCPs

Coal combustion products consist of silica, sand iron, aluminum, limestone, and oxidized clay. The chemical composition of coal combustion products and their mineralogy differed from coal-fired power plants primarily because of the type of coal and the combustion conditions adopted during the process of operation. Annually, an individual power plant might produce thousands of tons of CCPs. The CCPs disposal generally is on-site in places called landfills. However, the inadequate manage in the disposal of the CCPs has shown a potential risks of causing air pollution and water contamination (Sajwan et al. 2006).

Fig. 13.5 (a) Trend of capacity of CCPs production, percentage of the used CCPs, and total fly ash production in the USA (American Coal Ash Association 2010, 2011, 2012, 2013, 2014, 2015, 2016, 2017, 2018a, b), (b) Global CCPs production, and (c) Global CCPs utilization (Harris 2019). *MMst* millions of short tons, *Mt* metric ton



13.5.1 Air Emissions

The chemical composition of coal combustion products is similar to the volcanic ash. During this combustion process of ash, airborne toxins and pollutants are released to the atmosphere. The heavy metals have direct and negative impact on the human health and the primary pollutants in fly ash are sulfur dioxide, nitrogen oxides, particulates, and various other heavy metals.

Sulfur Oxide (SO₂) emissions from coal-fired power plants react with other elements in the atmosphere to form sulfate particles, a significant provider to the fine particle amalgam that circulates with the air. The sulfate particles are associated to significant number of serious human health problems such as cardiovascular or lung diseases. In addition, SO₂emissions also contribute to acid deposition or “acid rain.”

Mercury: The primary source of mercury to the air is fired-coal power plants, as well as other industrial sources. The mechanism consists in elemental mercury deposited slowly once emitted to the air and transported larger distance through the atmosphere.

Environmental Protection Agency (EPA) has been established to install pollution controls in plants to prevent the amount of emissions from coal-fired power plants. Both EPA and the Department of Energy (DOE) sponsor the cooperation along with several companies in the USA to induce financial support of the power plants. However, nowadays many of plants do not have these governmental sponsorship and consequently on lack of controls in the plants.

Table 13.3 displays emission limit levels for coal-fired power plant flue gases in Europe Union (EU). The regulations are to be implemented in large coal-fired power plants with a thermal capacity higher than 300 MWth. The regulation for plants built after 2003, the limit of SO₂ was 200 mg/m³ while after 2016 the limit reduced at 150 mg/m³.For nitrogen oxides permitted emission levels were the same. After 2016, dust emissions are to be lowered below 20 mg/m³ and for mercury there was a proposed emission limit level of 30 µg/m³.

While in India, the burning of coal is responsible for increasing PM_{2.5} levels. Thereby, the Indian government implemented the National Clean Air Program (NCAP), which consisted in a long-term program to reduce fine particulate matter (PM_{2.5}), and particulate matter (PM₁₀). The government has projected that the air pollution could be reduced in 20–30% by 2030. The World Bank states that around 7.7% of PM_{2.5} emissions were attributable to the coal combustion industry (Philalay 2019).

13.5.2 Water Contamination

According to the American Coal Ash Association, annually more than 100 Mt. of coal combustion products are generated in the USA. The inappropriate manage of

Table 13.3 European Union emission limits for large coal-fired power plants

Type of flue gas	Maximum limit (mg/m ³)
SO ₂ emissions for plants built after 2003	200
SO ₂ emission limits after 2016	150
NO ₂ emissions for plants built after 2003	200
NO ₂ limits after 2016	150
Dust emission limits after 2016	20
Proposed Hg emission limit	30

the coal combustion products lead to the release of waste which ends up in water bodies and after some years can contaminate waterways and drinking water supplies (Union of Concerned Scientists 2020).

In India, the inappropriate disposal of coal combustion products (FA, and BA) is considered a serious operational constraint and environmental risk. For instance, copper circulation in river sediments nearby a coal-fired power plant in India was attributed to coal combustion products disposal. In addition, the limited accessibility of data on the pollution of surface water and sediments do not allow a proper measure of the magnitude of the problem. Migration of toxic substances from waste disposal sites to adjacent ecosystems is a complex process. The ash particle surfaces bearing trace elements in it does leach out over time and then discharged in to contaminate the groundwater level. Toxicity can be measured in terms of increase in metal concentrations in surrounding ecosystems.

For example, in India the wet disposal methods are the most common practices for fly ash. This method consists of the discharge of fly ash in its slurry form upon mixing with water, which substantially settles down in a pond. After settlement, the formed supernatants are discharged into a receiving system usually natural water bodies like rivers. Even though there is no precedent of serious water contamination, in the USA the investigations of the effects of FA in lakes and streams have been conducted.

Some studies have proved that FA can be detrimental to aquatic life. Fly ash presence in sufficient quantities can be detected due to the increase in turbidity of the water, gill clogging, and increased alkalinity (Zhang 2014). Other negative impacts include acid rock drainage, the energy-water collisions, and the destruction of mountain streams and valleys. In order to prevent groundwater contamination produced by inappropriately handled CCPs there should be periodical monitoring of the drinking water wells close FA disposal sites to guarantee that the trace element concentrations stay below the regulatory levels.

United States Environmental Protection Agency diffused the Steam Electric Power generating Effluent Guidelines and Standards (40 CFR Part 423) in 1974, and revised the regulations from 1977 to 2020. The regulations considered the wastewater discharges from the coal-fired power plants operating as utilities. In 2020, US Environmental Protection Agency reviewed the specifications for two waste streams: (a) FGD wastewater and (b) BA transport water. In addition, the voluntary incentives program for FGD wastewater also subcategories were appended as well as new compliance dates were approved. (US Environmental Protection Agency 2020; Regulations.Gov 2020; Zhang 2016).

13.5.3 Climate Change Issues by Coal Ash Pollution

The climate change is the gravest long-term impact of the coal combustion products. According to the chemical composition, coal in majority consisted of carbon. Then after combustion process, coal reacts with oxygen to generate a heat-trapping gas (CO₂). In fact, the carbon dioxide increase above the normal limits produce the

warming of the earth. The coal combustion products typically are deposited in open pits. Therefore, overtime the groundwater sites end up with contamination by the leaching of toxic heavy metals from pits.

United States Environmental Protection Agency stated that coal combustion products did not need to be classified as a hazardous waste. In 2006, the US EPA standardized that mercury in coal combustion products were unlikely to be leached at a level of environmental concern. In 2010, EPA informed that CCPs were used as fill and contouring material in the Battlefield Golf Club construction in Chesapeake, and CCPs had no adverse impact on neither adjacent residential wells (groundwater) nor health effects. (US Environmental Protection Agency 2020).

Coal combustion products are considered an important secondary resource. In fact, coal combustion products (CCPs) are often more environmentally sustainable than raw alternatives. Products manufactured with coal combustion products perform better, cost less, and decrease environmental impacts. Actually, coal combustion products recycling result in avoiding one ton of greenhouse gas emissions when one ton of FA is used instead of traditional cement. In summary, the main advantages of fly ash in construction are the conservation of primary resources, reduction of greenhouses gas emissions, decrease of landfill disposal, and improvement in the durability and strength of materials (US Environmental Protection Agency 2020).

13.6 Rare Earths Recovery from Coal Ash

Coal combustion products are the potential sources for recovering REEs and that has shown an important alternative source of these metals. However, the REEs bound in aluminosilicate glasses are likely to be difficult to recover and requires aggressive approaches such as acid digestion, which may not be viable on a commercial scale (Franus et al. 2015). For instance, fly ash is among a range of coal-related products currently under consideration as potential REE sources. In some cases, such as in some low-rank coals, greater extractability of REEs may offset the fact that these coals have much lower overall REE contents than fly ash (Laudal et al. 2018). REEs in fly ash glasses, the most abundant constituent of fly ash, should be targeted using inventive approaches for extraction and concentration of REEs.

13.6.1 Roasting Treatment

The REEs are primarily found in *aluminosilicate glass*. Consequently, a simple acid leaching might not be effective to recover REEs. According to some authors, prior to the acid leaching, alkali-roasting treatments are carried out to enhance the REEs extraction efficiency. Taggart et al. proposed a roasting method using different additives with the coal ashes and roasting the mixture (Taggart et al. 2018). Some roasting additives that were evaluated are Na_2O_2 , NaOH , CaO , Na_2CO_3 , CaSO_4 , and $(\text{NH}_4)_2\text{SO}_4$. The FA

samples studied were from Illinois, Appalachian and Power River coal basins. The use of NaOH in the roasting process showed often increase in the REEs recovery (>90%). However, this study displayed that a high pH reduced the recovery rate of REEs.

As shown in Fig. 13.6, alkali roasting-water leaching-acid process is used to recover REEs and Ga, Nb, and Al. The feedstock for the alkali roasting in this process was from fly ash obtained from the Anwen Coal-fired Power Plant in Chongqing. The main processes consist of (a) alkali roasting using Na_2CO_3 under 1133 K for 30 min, (b) water leaching used to extract Ga and Al from roasting product, (c) acid leaching (HCl) used to recover REEs, and (d) ion adsorption resin to separate Ga and Al. As a result, REEs extraction was around 80% while Al and Ti reported a recovery of 68% and 76%, respectively (Liu et al. 2019).

13.6.2 Alkaline and Acid Leaching

Acid leaching is often used in the extraction of REEs from FA as the metal contents get readily leached out in the acidic media (Kashiwakura et al. 2013). Yet, the

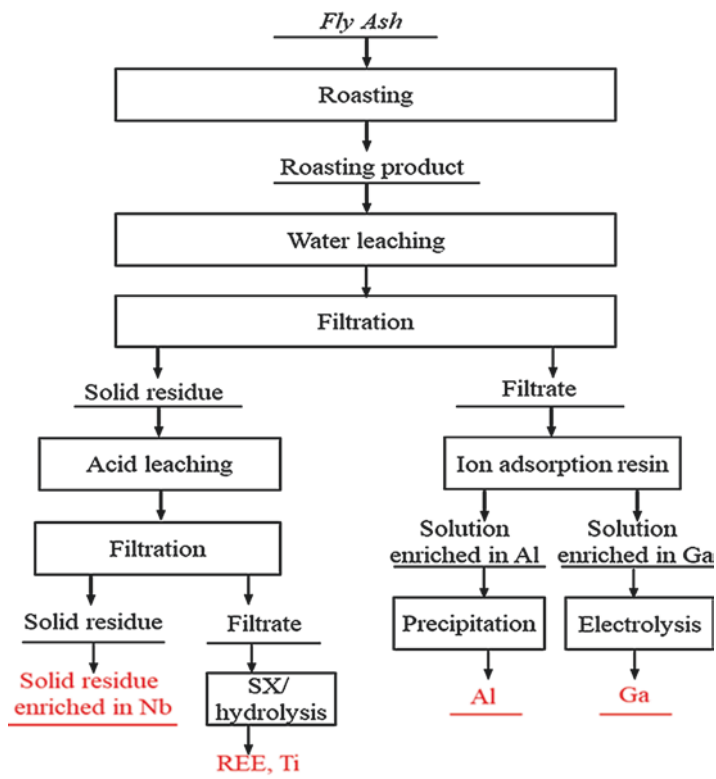


Fig. 13.6 Flowchart for recovering REEs, Ga, Nb, and Al from a fly ash using alkali roasting (Liu et al. 2015)

presence of impurities such as Al and Si might limit the effectiveness of the method (Hood et al. 2017; King et al. 2018). The REEs are primarily found in aluminosilicate glass. Therefore, a simple leaching with acid such as HCl and H_2SO_4 might not dissolve completely REEs. Hence, some alternative processes have been proposed.

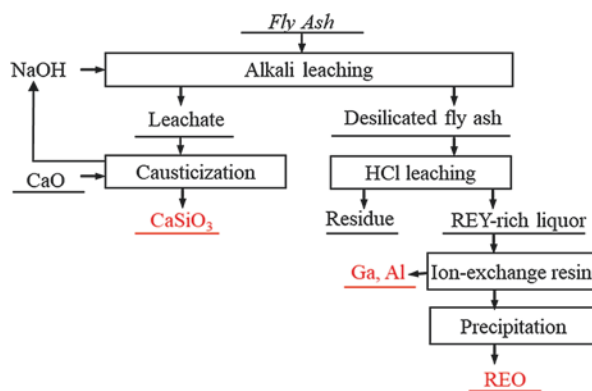
Wang et al. (2019) reported that around 70% REEs were presented in amorphous glass form, then successive acid and alkaline leaching was applied. REEs hydroxides precipitated by NaOH and silica became soluble (Wang et al. 2019). Figure 13.7 shows a flowchart of alkaline and acid leaching proposed by Wang et al. (2019).

King et al. (2018) applied a similar technology on three CCPs samples from Appalachians, Illinois, and Power River Basin (USA). The sample from Power River Basin was unique because of its high calcium content (King et al. 2018). After the extraction process, the recovery rate of REEs was reportedly excellent around 99%. On the other hand, CCPs samples from Illinois and Appalachia recovery rates of REEs were fewer than 40%. The improvement of recovery rate of REEs is imperative before the acid leaching. In addition, the variation of NaOH concentration had a direct relation with recovery rate of REEs and dissolution of glass. Li et al. 2017 performed hydrothermal treatment followed by leaching using 5 mol/L NaOH at experimental conditions S/L = 1:20, reaction temperature = 373 K, and reaction time 120 min. The hydrothermal treatment increases the REEs content in solid material from 366 to 806 ppm resulting in a low efficiency rate. However, none of the processes has produced high-grade final REEs compounds to be commercialized (Li et al. 2017).

13.6.3 Bioleaching

Bioleaching is based on the microbial dissolution of compounds. The advantages of bioleaching is that, the process is simple, low consume of chemicals/reagents with low energy costs associated, and finally overall waste generation out of the approach is less. In Russia, the incubation of acidophilic chemolithotrophic microbial

Fig. 13.7 Flowcharts of REEs extraction from fly ash using alkali and acid leaching (Wang et al. 2019)



community was used to recover 52%, 52.6%, and 59.5% of Se, Y, and La, respectively, from fly ash. Park and Liang suggested the bioleaching of trace elements and REEs from FA using three strains *Phanerochaete chrysosporium*, *Candida bombicola*, and *Cryptococcus curvatus* (Park and Liang 2019). The main advantage of these microorganisms is their tolerance to low pH values between three and four. The use of *Candida bombicola* showed the best leaching rates: 80.9% As, 79.5% Mo, 67.7% Yb, and 64.6% Er. Thus, bioleaching of coal ash could be seen as feasible using these strains and *Candida bombicola*.

13.6.4 Ionic Liquids

Rozelle et al. compared ammonium sulfate, an ionic liquid, and a eutectic solvent to evaluate their effectiveness in extracting REEs from CCPs (Rozelle et al. 2016). Extraction of REEs in each case produced high recovery rates of REEs to the solution (Painter et al. 2010). Deep eutectic liquid is a mixture of urea and chloride and has the advantage of reducing the solubility of silicon and aluminum oxides allowing the potentially selective recovery of REEs (Nockemann et al. 2006; Rozelle et al. 2016). Recovery rates of up to 89% REEs have been achieved using ammonium sulfate (Rozelle et al. 2016). However, the use of ionic liquids or eutectic solvents has not indicated an advantage on the recovery rate of REEs over ammonium sulfate. Huang et al. worked on the recovery of REEs from CCPs (China) using various ionic liquids. The REEs content from these CCPs was 1350 ppm (Huang et al. 2019). The ionic liquids used were: $[N_{1888}]Cl$, $[P_{6,6,6,6,14}]Cl$, $[P_{6,6,6,6,14}] [SOPAA]$, and $[P_{6,6,6,6,14}]$. 4 g of CCPs were mixed with different diluted acids (12 mol L⁻¹ HCl, 16 mol L⁻¹ HNO₃, and 23 mol L⁻¹ HF) and heated to 473 K for 9 h, cooled with air, and filtered. After filtration, the ionic liquid was added to the leachate. The recovery rate for REEs was 37.4%. Once the solution was purified, the REEs were precipitated using oxalic acid to obtain La, Ce, Y, Er, Tm, Yb, and Lu.

13.6.5 Physical Separation Processes

The physical separation target is to separate a high REE-containing fraction from a low REE-containing fraction. Therefore, physical separation process is commonly used as pretreatment owing to the elimination of unnecessary material present in the sample. Lanzerstorfer proposed a pre-processing of coal fly ash by classification for enrichment of rare earth elements. The author suggested that REEs enrich in the finest fractions by a factor of 1.05–1.65. HREEs were generally concentrated in fine fractions, while LREEs were concentrated in coarse ones (Lanzerstorfer 2018). The main advantage of the process is that since it is a dry process it is simple to be applied on an industrial scale. However, the degree of enrichment and supply

depends on the type of REEs. Suganal studied coal ash from the Pilimanan pilot plant. The REEs content in this material is 77.85 ppm. In this study, the authors attempted to increase the concentration of REEs by using the shaking table and the magnetic separator methods (Suganal 2018). The shaking table showed that REEs concentrations increased up to twice. However, the results for the magnetic separation technique were not significant. Lin et al. compared different physical separation methods such as separating by particle size, magnetic and density separation to evaluate their effectiveness on different CCPs samples (clean coal, coal ash, and clay-rich shale) (Lin et al. 2017). The results highlighted that the density separation method has the highest REEs enrichment rates. In addition, the other advantage is that separation processes can also be useful in the recovery of other elements (Al/Si, Fe, and Ca) during the REEs recovery process. Finally, Phuoc and Wang (2017) worked on a new method for separating and physically recovering REEs from coal ash using a laser beam.

To sum up, these processes helped to concentrate the REEs in a specific fraction, limiting the quantity of material to be treated. Furthermore, they could reduce the presence of iron oxides, which difficult the recovery process reducing the quantity of acid used during the recovery of REEs. Although the physical separation and the recovery techniques presented are promising, they are generally only one of the many steps in the recovery of REEs.

13.6.6 Other Methods

Periodic Products Chelok[®] technology was proposed by Laurino. This process consists of: (a) extraction and (b) polymerization and filtration. This technique is in development, the studies are focusing particle size, composition of the pregnant leach solution, contact time between the material and the extraction solution, etc. (Laurino 2016). The advantages of this process are high efficiency and cost effectiveness to remove and recover rare earth elements from CCPs. Another method in development is selective electro-deposition proposed by US Department of Environment (DOE).

Some researchers reported selective electrodeposition using ionic liquids (IL) which consists in dissolving fly ash directly into the ionic liquid solution, forming lanthanide complexes in situ, and use secondary complexing agents to selectively bind the different rare earth elements, making leaching process unnecessary. Selective electrodeposition at a controlled potential will recover and separate metals simultaneously (National Energy Technology Laboratory 2019).

The leach liquor obtained from the Central Appalachian Basin region in the USA was investigated using two different liquid membrane processes (liquid emulsion membranes, LEM, and supported liquid membranes, SLM) to compare their efficiency with the typical solvent extraction method for selective recovery of REEs from FA. SLM process was remarkably selective for HREEs while LEM and traditional conventional extraction processes were more selective for LREEs. The main disadvantage of both

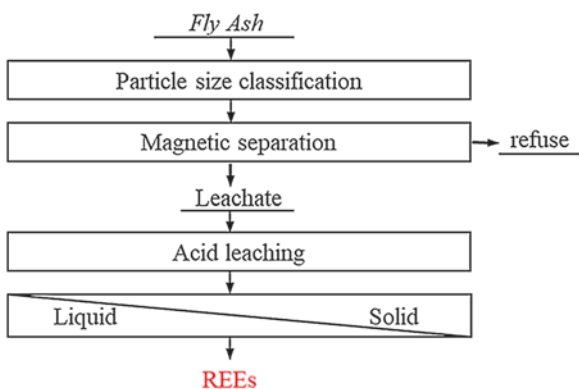
membranes is the low recovery rates. The recovery of REEs with LEM was incomplete due to diffuse mass transfer while the low recovery rates for SLM have to deal with the solvent chelator (Smith et al. 2019). Table 13.4 lists the advantages and disadvantages of the processes adopted (pyrometallurgy, alkaline and acid leaching, bioleaching, ion extraction, physical separation) to recover REEs from CCPs.

Various technologies might integrate or apply pretreatments to achieve optimum recovery at a minimal cost. To mitigate the disadvantages of traditional processes Pan J. et al. proposed an integrated physical separation and acid leaching of the rare earth elements and yttrium (REY) of fly ash (Pan et al. 2020). As shown in Fig. 13.8,

Table 13.4 Summary of the advantages and disadvantages of the methods to recover REEs from fly ash

Method	Advantages	Disadvantages
Roasting	<ul style="list-style-type: none"> • High recovery • Quick and simple process 	x High energy consumption
Alkaline and acid leaching	<ul style="list-style-type: none"> • REEs are transferred from solid into solution, that can be recovered • Relative simple process 	x Chemical product cost is high x Harsh leaching conditions x High alkali or acid consumption x % extraction depending on coal ash type
Bioleaching	<ul style="list-style-type: none"> • Simple process • Low chemical and energy costs • Reduced waste generated 	x High time consumption x Small scale application
Ion extraction	<ul style="list-style-type: none"> • Reduction in the solubility of silicon and aluminum oxide 	x Low recovery efficiency
Physical separation	<ul style="list-style-type: none"> • Concentration of REEs in a specific fraction • Elimination of unnecessary material and iron oxides • Low capital and operating cost • Application in industrial scale 	x Post treatments are necessary

Fig. 13.8 REEs extraction from fly ash using integrated physical separation and acid leaching (Pan et al. 2020)



the first step is the pre-concentration of REY to enrich the solution from 782 to 1025 mg/L by magnetic separation. After that process, acid leaching was applied.

The process was optimized to obtain the maximum efficiency using Taguchi three-level orthogonal design. The optimum leaching conditions are 400-rpm stirring rate, 3 mol/L acid concentration, S/L 1:10, leaching temperature 333 K, and 2 h. The leaching efficiency was approximately 80%. However, it could be increased using roasting prior to leaching and solvent extraction, membrane technology, and so on after leaching.

13.7 Concluding Remarks

In the recent decades, worldwide market demand for rare earth elements (REEs) has significantly increased owing to their utilization for diverse technological domain such as catalysts, metallurgical applications and alloys, ceramics and glass, and polishing. According to trend charts, the global reserves and production maintained a steady growth since past 10 years. However, the percentage of rare earth elements reserve and production of China keeps decreasing mainly due to policies adopted to control the exploitation of Chinese resources. Due to the unavoidable depletion of primary mineral resources as well as the strict policies established by the monopoly market of REEs in China, it is imperative to find suitable secondary sources for extraction of REEs. One of the potential sources for secondary REEs deposit includes CCPs, which so far are not classified as a hazardous waste but this could be an important source to develop a secondary recovery process of rare earth elements.

To generate energy, power plants use coal and other coal resources. The coal-fired power plants produce thousands of tons of CCPs per year. In the USA, the total capacity of CCPs produced in the USA has decreased mainly due to the closing of power plants owing to the development of new alternative fuels to produce energy. However, the percentage of utilization of CCPs is increasing due to the application in the construction industry as a cement additive. The CCPs require to be stored or disposed of in surface impoundments, landfills, mine, and quarry fills, from which surface impoundments are the most used to manage the coal combustion products in-site, whereas landfills are commonly used off-site.

Coal combustion products have been proving to be an interesting source of REEs and the techniques for recovering REEs depend on the type of CCPs composition, mineralogy, and combustion conditions. REEs are present in aluminosilicate matrix, which is difficult to dissolve. Hence, roasting process might be used as pretreatment to increase extraction efficiency of REEs. Based on the literature surveys, various methods to recover REEs from CCPs had been investigated such as alkaline or acid leaching, roasting, physical separation, bioleaching, ion extraction, and others. Physical separation shows promising in terms of process efficiency, yet posttreatments are necessary. According to some authors, alkali-acid leaching process has a proven efficiency between 70% and 90%. However, there is still no commercially feasible method established to recover REEs from CCPs.

Acknowledgments This work was supported by the National Research Council of Science & Technology (NST) grant by the Korea government (MSIT) (No.CRC-15-06-KIGAM).

References

- Alonso, E., et al. (2012). Evaluating rare earth element availability: A case with revolutionary demand from clean technologies. *Environmental Science & Technology*. <https://doi.org/10.1021/es203518d>.
- American Coal Ash Association (2010). CCP Survey Results, Michigan <https://www.aaa-usa.org/Portals/9/Files/PDFs/AAA-Brochure-Web.pdf>. Accessed 13 Jul 2020.
- American Coal Ash Association (2011). CCP Survey Results, Michigan <https://www.aaa-usa.org/Portals/9/Files/PDFs/AAA-Brochure-Web.pdf>. Accessed 13 Jul 2020
- American Coal Ash Association (2012). CCP Survey Results, Michigan <https://www.aaa-usa.org/Portals/9/Files/PDFs/AAA-Brochure-Web.pdf>. Accessed 13 Jul 2020
- American Coal Ash Association (2013). CCP Survey Results, Michigan <https://www.aaa-usa.org/Portals/9/Files/PDFs/AAA-Brochure-Web.pdf>. Accessed 13 Jul 2020
- American Coal Ash Association (2014). CCP Survey Results, Michigan <https://www.aaa-usa.org/Portals/9/Files/PDFs/AAA-Brochure-Web.pdf>. Accessed 13 Jul 2020
- American Coal Ash Association (2015). CCP Survey Results, Michigan <https://www.aaa-usa.org/Portals/9/Files/PDFs/AAA-Brochure-Web.pdf>. Accessed 13 Jul 2020
- American Coal Ash Association (2016). CCP Survey Results, Michigan <https://www.aaa-usa.org/Portals/9/Files/PDFs/AAA-Brochure-Web.pdf>. Accessed 13 Jul 2020
- American Coal Ash Association (2017). CCP Survey Results, Michigan <https://www.aaa-usa.org/Portals/9/Files/PDFs/AAA-Brochure-Web.pdf>. Accessed 13 Jul 2020
- American Coal Ash Association (2018a). CCP Survey Results, Michigan <https://www.aaa-usa.org/Portals/9/Files/PDFs/AAA-Brochure-Web.pdf>. Accessed 13 Jul 2020
- American Coal Ash Association (2018b). An American Recycling Success Story: Beneficial Use of Coal Combustion Products, Michigan <https://www.aaa-usa.org/Portals/9/Files/PDFs/AAA-Brochure-Web.pdf>. Accessed 13 Jul 2020
- American Coal Ash Association (2020). <https://www.aaa-usa.org/aboutaaa/joinaaa.aspx>. Accessed 15 Jul 2020.
- British Geological Survey (2011). Rare earth elements, <http://www.mineralsuk.com>. Nottingham, UK Accessed 26 Jul 2020.
- Bünzli, J.-C. G. (2013). Lanthanides. Kirk-Othmer Encyclopedia of Chemical Technology. doi:<https://doi.org/10.1002/0471238961.1201142019010215.a0>.
- Cao, D., Selic, E., & Herbell, J. (2008). Utilization of fly ash from coal-fired power plants in China. *Journal of Zhejiang University Science A*. <https://doi.org/10.1631/jzus.A072163>.
- Crull, A. W. (2013). Top ten companies in rare earth. BCC Research Market Research Reports. from <https://www.bccresearch.com/report/download/report/avm090a>
- Dai, S., & Finkelman, R. B. (2018). Coal as a promising source of critical elements: Progress and future prospects. *International Journal of Coal Geology*. <https://doi.org/10.1016/j.coal.2017.06.005>.
- Eggert, R., et al. (2016). Rare earths: Market disruption, innovation, and global supply chains. *Annual Review of Environment and Resources*. <https://doi.org/10.1146/annurev-environ-110615-085700>.
- Environmental Protection Agency (2020). Washington USA <https://www.epa.gov/> Accessed 15 Sep 2020.
- Franus, W., et al. (2015). Coal fly ash as a resource for rare earth element. *Environmental Science and Pollution Research*. <https://doi.org/10.1007/s11356-015-4111-9>.

- Gambogi, J. (2010). Mineral commodity summaries: Rare earths. U.S. Geological Survey, Washington, DC <https://www.usgs.gov/centers/nmic/rare-earths-statistics-and-information> Accessed 14 Jul 2020.
- Gambogi, J. (2011). Mineral commodity summaries: Rare earths. U.S. Geological Survey, Washington, DC <https://www.usgs.gov/centers/nmic/rare-earths-statistics-and-information> Accessed 14 Jul 2020.
- Gambogi, J. (2012). Mineral commodity summaries: Rare earths. U.S. Geological Survey, Washington, DC <https://www.usgs.gov/centers/nmic/rare-earths-statistics-and-information> Accessed 14 Jul 2020.
- Gambogi, J. (2013). Mineral commodity summaries: Rare earths. U.S. Geological Survey, Washington, DC <https://www.usgs.gov/centers/nmic/rare-earths-statistics-and-information> Accessed 14 Jul 2020.
- Gambogi, J. (2014). Mineral commodity summaries: Rare earths. U.S. Geological Survey, Washington, DC <https://www.usgs.gov/centers/nmic/rare-earths-statistics-and-information>. Accessed 14 Jul 2020.
- Gambogi, J. (2015). Mineral commodity summaries: Rare earths. U.S. Geological Survey, Washington, DC <https://www.usgs.gov/centers/nmic/rare-earths-statistics-and-information> Accessed 14 Jul 2020.
- Gambogi, J. (2016). Mineral commodity summaries: Rare earths. U.S. Geological Survey, Washington, DC <https://www.usgs.gov/centers/nmic/rare-earths-statistics-and-information> Accessed 14 Jul 2020.
- Gambogi, J. (2017). Mineral commodity summaries: Rare earths. U.S. Geological Survey, Washington, DC <https://www.usgs.gov/centers/nmic/rare-earths-statistics-and-information>. Accessed 14 Jul 2020.
- Gambogi, J. (2018). Mineral commodity summaries: Rare earths. U.S. Geological Survey, Washington, DC <https://www.usgs.gov/centers/nmic/rare-earths-statistics-and-information>. Accessed 14 Jul 2020.
- Gambogi, J. (2019). Mineral commodity summaries: Rare earths. U.S. Geological Survey, Washington, DC <https://www.usgs.gov/centers/nmic/rare-earths-statistics-and-information>. Accessed 14 Jul 2020.
- Gambogi, J. (2020). Mineral commodity summaries: Rare earths. U.S. Geological Survey, Washington, DC <https://pubs.usgs.gov/periodicals/mcs2020/mcs2020-rare-earths.pdf>. Accessed 14 Jul 2020.
- George, B. et al. (2016). An outlook on the rare earth elements mining industry. AusIMM Bulletin Available via file:///C:/Users/USER/Downloads/AnoutlookontherareearthelementsmineindustryAusIMMBulletin%20(4).pdf. Accessed 8 Aug 2020.
- Gong, X., et al. (2018). Chinese National Air Protection Policy Development: A Policy Network Theory Analysis. *International Journal of Environmental Research and Public Health*, 15(10), 2257. <https://doi.org/10.3390/ijerph15102257>.
- Gupta, K., & Krishnamurthy, N. (2005). *Extractive metallurgy of rare earths*. Washington: CRC Press.
- Haque, N. et al (2014). Rare earth elements: Overview of mining, mineralogy, uses, sustainability and environmental impact. Resources, doi:<https://doi.org/10.3390/resources3040614>.
- Harris, D., Heidrich, C. & Feuerborn, J. (2019). Coaltrans Conferences. from <https://www.coaltrans.com/insights/article/global-aspects-on-coal-combustion-products#:~:text=The%20largest%20coal%20combustion%20product,totaled%20nearly%201.2%20billion%20tonnes>. Accessed 15 Jul 2020.
- Hood, M. M. et al. (2017). Rare earth element distribution in fly ash derived from the Fire Clay coal, Kentucky. Coal Combust. Gasif. Products. doi:<https://doi.org/10.4177/CCGP-D-17-00002.1>.
- Huang, C., Wang, Y., Huang, B., Dong, Y., & Sun, X. (2019). The recovery of rare earth elements from coal combustion products by ionic liquids. *Minerals Engineering*, 130, 142–147.

- Hurst, C. (2010). China's rare earth elements industry: What can the west learn? Institute for the Analysis of Global Security. from <http://www.iags.org/rareearth0310hurst.pdf> Accessed 14 Aug 2020.
- International Energy Agency (2020). Electricity generated by resource <https://www.iea.org/reports/global-energy-review-2020>. Accessed 13 Aug 2020.
- Jeffrey, J. (2018). Annual Energy Outlook 2018 with projections to 2050. US Energy Information Administration, Washington. from <https://www.eia.gov/outlooks/aeo/pdf/AEO2018.pdf>. Accessed 15 Jul 2020.
- Kashiwakura, S., et al. (2013). Dissolution of rare earth elements from coal fly ash particles in a dilute H₂SO₄ solvent. *Open Journal of Physics and Chemistry*. <https://doi.org/10.4236/ojpc.2013.32009>.
- Kentucky Geological Survey (2020). <https://www.uky.edu/KGS/coal/coal-for-combustionbyproducts.php> Accessed 14 Sep 2020.
- Ketris, M., & Yudovich, Y. (2009). Estimations of clarkes for carbonaceous biolithes: World averages for trace element contents in black shales and coals. *International Journal of Coal Geology*. <https://doi.org/10.1016/j.coal.2009.01.002>.
- King, J. F., et al. (2018). Aqueous acid and alkaline extraction of rare earth elements from coal combustion ash. *International Journal of Coal Geology*. <https://doi.org/10.1016/j.coal.2018.05.009>.
- Lanzerstorfer, C. (2018). Preprocessing of coal combustion fly ash by classification for enrichment of rare earth elements. *Energy Reports*, 4, 660–663.
- Laudal, D. A., et al. (2018). Leaching behavior of rare earth elements in Fort Union lignite coals of North America. *International Journal of Coal Geology*. <https://doi.org/10.1016/j.coal.2018.03.010>.
- Laurino, J. P. (2016). The extraction and recovery of rare earth metals from coal combustion products. Periodic Products <http://www.periodicproducts.com/wp-content/uploads/2018/06/Rare-Earth-Metals-from-Coal-Ash-v2.2P.pdf> Florida USA Accessed 15 Sep 2020.
- Li, J., Zhuang, X., Querol, X., Font, O., & Moreno, N. (2017). A review on the applications of coal combustion products in China. *International Geology Review*. <https://doi.org/10.1080/00206814.2017.1309997>.
- Lin, R., et al. (2017). Enrichment of rare earth elements from coal and coal by-products by physical separations. *Fuel*. <https://doi.org/10.1016/j.fuel.2017.03.096>.
- Liu, P., Huang, R., & Tang, Y. (2019). Comprehensive understandings of rare earth element (REE) speciation in coal fly ashes and implication for REE extractability. *Environmental Science & Technology*. <https://doi.org/10.1021/acs.est.9b00005>.
- Lu, G., Xue, F., & Zhao, J. (2011). Some advice to the fly ash of China. *China Mining Magazine*, 20, 193–200. (in Chinese with English abstract).
- Lui, H., et al. (2015). Combined extraction of rare metals Ga-Nb-REE from the fly ash. *Journal of Engineering Science and Technology Reviews*. <https://doi.org/10.3981/j.issn.1000-7857.2015.11.006>.
- Mayfield, D. B. & Lewis, A. S. (2013). Environmental Review of Coal Ash as a Resource for Rare Earth and Strategic Elements. Paper presented at the World of Coal Ash, Lexington, Kentucky, 22–25 April 2013.
- McGill, I. (2012). *Rare earth elements in Ullmann's encyclopedia of industrial chemistry*. Weinheim: Wiley-VCH Verlag GmbH & KGaA.
- National Energy Technology Laboratory (2006). Clean Coal Technology. Washington USA. <https://www.netl.doe.gov/sites/default/files/netl-file/Topical24.pdf> Accessed 4 Nov 2020.
- National Energy Technology Laboratory (2019) 2019 Project Portfolio, Washington USA <https://www.netl.doe.gov/sites/default/files/2019-04/2019-REE-Project-Portfolio.pdf> Accessed 14 Sep 2020.
- Nockemann, P., et al. (2006). Task-specific ionic liquid for solubilizing metal oxides. *The Journal of Physical Chemistry B*. <https://doi.org/10.1021/jp0642995>.
- Painter, P., Pulati, N., Cetiner, R., Sobkowiak, M., Mitchell, G., & Mathews, J. (2010). Dissolution and dispersion of coal in ionic liquids. *Energy & Fuels*, 24(3), 1848–1853.

- Pan, J., et al. (2020). Recovery of rare earth elements from coal fly ash by integrated physical separation and acid leaching. *Chemosphere*. <https://doi.org/10.1016/j.chemosphere.2020.126112>.
- Park, S., & Liang, Y. (2019). Bioleaching of trace elements and rare earth elements from coal fly ash. *International Journal of Coal Science and Technology*. <https://doi.org/10.1007/s40789-019-0238-5>.
- Peramaki, S. (2006). Method development for determination and recovery of rare earth elements from industrial fly ash. Department of Chemistry, University of Jyväskylä, Finland. doi:<https://doi.org/10.1002/146518>.
- Philalay, M. (2019). Coal in India. Department of Industry, Innovation and Science. from <https://www.industry.gov.au/sites/default/files/2019-08/coal-in-india-2019-report.pdf>. Accessed 20 Jul 2020.
- Phuoc, T. X. & Wang, P. (2017). Laser separation of rare earth elements from coal ashes. World of Coal Ash (WOCA) Conference Lexington, KY.
- Ramme, B. W., & Tharaniyil, M. P. (2013). *Coal combustion products utilization handbook* (3rd ed.). Wisconsin.
- Regulations.Gov (2020). <https://www.regulations.gov/document?D=EPA-HQ-OW-2009-0819-7106>. Accessed 23 Jul 2020.
- Reilly, J. F. (2020). Mineral commodity summaries 2020. US Geological Survey. from <https://pubs.usgs.gov/periodicals/mcs2020/mcs2020.pdf>. Accessed 26 Jul 2020.
- Rozelle, et al. (2016). A study on removal of rare earth elements from U.S. Coal Byproducts by ion exchange. *Metallurgical and Materials Transactions E*. <https://doi.org/10.1007/s40553-015-0064-7>.
- Rudnick, R. L., & Gao, S. (2014). Composition of the continental crust. *Treatise on Geochemistry*. <https://doi.org/10.1016/b978-0-08-095975-7.00301-6>.
- Sajwan, K., et al. (2006). *Coal combustion byproducts and environmental issues* (pp. 14–17). New York: Springer.
- Seredin, V. V., & Dai, S. (2012). Coal deposits as potential alternative sources for lanthanides and yttrium. *International Journal of Coal Geology*. <https://doi.org/10.1016/j.coal.2011.11.00>.
- Smith, R. C., et al. (2019). Selective recovery of rare earth elements from coal fly ash leachates using liquid membrane processes. *Environmental Science & Technology*. <https://doi.org/10.1021/acs.est.9b00539>.
- Smoot, L. D. (1993). *Fundamentals for coal combustion: For coal and efficient use, coal science and technology*. Amsterdam, New York: Elsevier.
- Statistical Review of World Energy (2020). Statistical Review of World Energy 2020 London, UK. <https://www.bp.com/content/dam/bp/business-sites/en/global/corporate/pdfs/energy-economics/statistical-review/bp-stats-review-2020-full-report.pdf> Accessed 12 Sep 2020.
- Suganal, S. (2018). Rare earth elements enrichment of fixed-bed coal ash from a pilot plant gasification by physical methods. *Indonesian Mining Journal*, 21, 2.
- Taggart, R. K., et al. (2018). Effects of roasting additives and leaching parameters on the extraction of rare earth elements from coal fly ash. *International Journal of Coal Geology*. <https://doi.org/10.1016/j.coal.2018.06.021>.
- Taylor, S. R., & McLennan, S. M. (1995). The geochemical evolution of the continental crust. *Reviews of Geophysics*. <https://doi.org/10.1029/95rg00262>.
- Tse, P. (2011). China's Rare Earth Industry, U.S. Geological Survey. from <https://pubs.usgs.gov/of/2011/1042/of2011-1042.pdf> Accessed 14 Aug 2020.
- Tuncuk, A., Stazi, V., Akcil, A., Yazici, E. Y., & Deveci, H. (2012). Aqueous metal recovery techniques from e-scrap: Hydrometallurgy in recycling. *Minerals Engineering*, 25(1), 28–37. <https://doi.org/10.1016/j.mineng.2011.09.019>.
- Union of Concerned Scientists (2020). Coal Power Impacts. Cambridge. UK, <https://www.ucsusa.org/resources/coal-power-impacts>. Accessed 21 Jul 2020.
- Van Gosen et al. (2017) Critical Mineral Resources of the United States—Economic and Environmental Geology and Prospects for Future Supply. U S Geological Survey, Washington USA Available via <https://pubs.usgs.gov/pp/1802/o/pp1802o.pdf>. Accessed 15 Aug 2020

- Voncken, J. H. L. (2015). The rare earth elements an introduction. Springer Briefs in Earth Sciences. <https://doi.org/10.1007/978-3-319-26809-5>.
- Wang, F., & Wu, Z. (2004). *A handbook for fly ash utilization* (2nd ed.). Beijing: China Power Press. (in Chinese with English abstract).
- Wang, Z., Dwyer, G. S., Coleman, D. S., & Vengosh, A. (2019). Lead isotopes as a new tracer for detecting coal Fly ash in the environment. *Environmental Science & Technology Letters*. <https://doi.org/10.1021/acs.estlett.9b00512>.
- Zhang, X. (2014). Management of coal combustion wastes. International Energy Agency Clean Coal Center Available https://usea.org/sites/default/files/012014_Management%20of%20coal%20combustion%20wastes_ccc231.pdf?fbclid=IwAR39cevSRj-ZP5AuJW8a0ya8pn9DAIk7EWqlpsNAh6ZMuNQdfvvvUp_D7vI Accessed 7 Sep 2020.
- Zhang, X. (2016). Emission standards and control of PM_{2.5} from coal-fired power plant International Energy Agency Clean Coal Center. from <https://usea.org/sites/default/files/Emission%20standards%20and%20control%20of%20PM%202.5%20from%20coal%20fired%20power%20plant%20-ccc267.pdf> Accessed 7 Sep 2020.

Chapter 14

Recovery of Rare Earth and Some Other Potential Elements from Coal Fly Ash for Sustainable Future



Harshit Mahandra, Brendan Hubert, and Ahmad Ghahreman

14.1 Introduction

Coal is generated from dead plant matter under heat and pressure as rock hundreds of millions of years ago in nature. It is mainly composed of carbon (>50 wt%) with minor contribution of hydrogen, nitrogen, oxygen, and sulfur. In addition to this, coal is also found to contain a variety of elements and their compounds such as rare earth elements (REE), V, Ti, Al, Mg, Sr, Ba, Ca, Si, Ga, Ge, B, Se, Na, Fe, Se, Au, Pt, Ni, Co, and Cu in different proportions due to replenishment with time under different geological conditions (Abhilash and Akcil 2020). Global coal production has been increased by 3.3% in 2018 due to increase in steam and coking coal production (IEA 2019a). China is the leading coal producer since 1985 and retained the top position with the production of 3693 metric ton of coal in 2019 (IEA 2020). First time, in this century, the coal production is reduced by 0.9% than last year in India and amounted 769 metric ton in year 2019. The trend of fall in coal production in United States is continuing and reached 640 metric ton in 2019, the lowest level observed in the last four decades (IEA 2020). There is a marked difference in coal production between Organization for Economic Co-operation and Development (OECD) and non-OECD countries and the total production of coal from 1971 to 2018 in the world is represented in Fig. 14.1 (IEA 2019b).

Coal is primarily used for electricity and commercial heat generation and global consumption of coal for these purposes was 66.5% in 2017. The data of annual production (year 2017) of electricity, percent contribution of electricity via coal combustion, and quantity of fly ash generated in different countries have been shown in Table 14.1 (Abhilash and Akcil 2020).

H. Mahandra · B. Hubert · A. Ghahreman (✉)
The Robert M. Buchan Department of Mining, Queen's University,
Kingston, Ontario, Canada
e-mail: hm90@queensu.ca; ahmad.g@queensu.ca

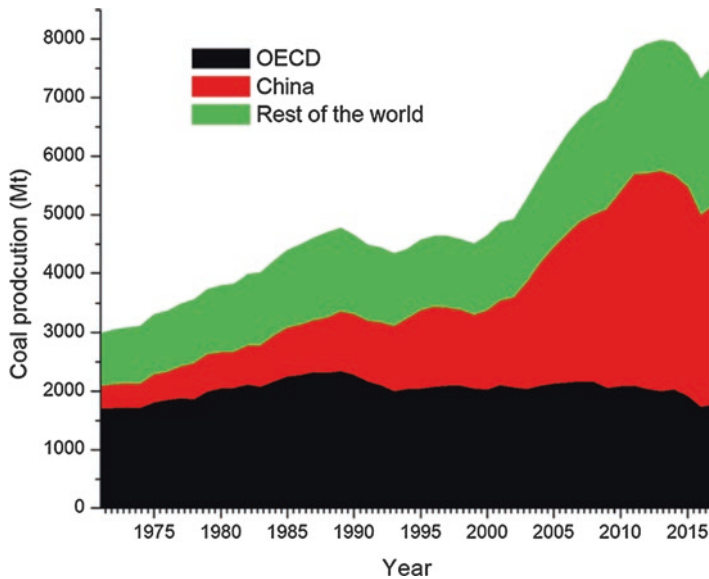


Fig. 14.1 World total coal production, 1971–2018

Table 14.1 Data for annual electricity and fly ash production of different countries in 2017

	United States	China	European Union	India	World
Electricity production (TWh/annum)	8182	6529	3886	1541	25,551
% contribution	26.0	66.5	20.6	76.0	27.0
Fly ash generated (MT/annum)	38	600	124	196	958

During the combustion of coal, fused particles of clays, shale, quartz, feldspar, etc. are carried along with flue gas and at low temperature form spherical particles called fly ash. The coal fly ash (CFA) produced as a by-product in thermal power plants contains about 5–20 wt.% of the feed coal and is generated as coarse bottom (70–85 wt.%) and fine fly ash (15–30 wt.%) (Akcil et al. 2015). On average, combustion of 1000 kg coal in a coal-fired power plant produces about 150 kg fly ash. The produced fly ash particles vary in size, shape, and composition. American society for testing and materials (ASTM) defined two different classes of fly ash, i.e., Class F and Class C on the basis of CaO content present in the fly ash. Class C fly ash contains 10–40% CaO and also called high lime fly ash. However, Class F generally possesses less than 10% CaO and designated as low lime fly ash (Dwivedi and Jain 2014; Sahoo et al. 2016). The dependency of world's thermal power plants on coal is responsible for an increase in CFA generation from 500 million tons in 2005 to 750 million tons in 2015, exponentially (Blissett and Rowson 2012; Gollakota et al. 2019). Around 25% of the globally produced CFA is utilized in different applications such as mining, cement, structure fills, and concrete products (Sahoo et al. 2016). The rest of the CFA is considered as waste and its disposal leads to soil, ground air, and water pollution. It has provided a chance to enhance

applications of CFA for geopolymers synthesis, silicon aerogels (thermal insulators), carbon nanotubes, and recovery of REE and other potential metals (Gollakota et al. 2019). The properties and chemical composition of CFA have been pointed out by various researchers which show the presence of REE along with some other valuable metals, e.g., Ga, Ge, Al, Se, and V in the CFA (Dai and Finkelman 2018; Kursun Unver and Terzi 2018; Meer and Nazir 2018; Gollakota et al. 2019). On the basis of research done for the REE and other elements recovery from CFA in the last decade, this work provides information about CFA recycling for the recovery of REE and other potential elements to find the knowledge gap for future research.

14.2 Rare Earth Elements

Rare earth elements are the seventeen chemical elements including 15 lanthanides from lanthanum (57La) to lutetium (71Lu) as well as scandium (21Sc) and yttrium (39Y). However, scandium and yttrium are not lanthanides but they have physical and chemical properties similar to those of lanthanides and found in combination with lanthanides, and therefore are called REE. REE are generally classified into light-REE (LREE) ranging from lanthanum (57La) to gadolinium (64 Gd) and heavy-REE (HREE) which include remaining lanthanides (Terbium to Lutetium). Yttrium is considered as HREE due to some similar properties, though Sc is in neither category. Sometimes, REE classification splits them into light (lanthanum to promethium), medium (samarium to gadolinium), and heavy REE (terbium to lutetium, scandium, and yttrium) (Ganguli and Cook 2018).

Rare earth elements find applications in various fields such as electronic, manufacturing, medical science, technology, and renewable energy that have a high consumption of REE (Ganguli and Cook 2018; Goodenough et al. 2018; Balaram 2019). These elements are also widely used in different products such as super magnets, autocatalytic converters, DVDs, phosphate binding agents, LED lighting, fluorescent materials, computer memory, glass additives, rechargeable batteries, solar panels, superconductors, mobile phones, and magnetic resonance imaging (MRI) agents due to their alloy strengthening, electrochemical, luminescent, and magnetic characteristics (Jyothi et al. 2020). Ganguli and Cook (2018) predicted the expected compounded annual growth between 2017 and 2021 for the global REE market to be 13.7%. The future supply of these elements may encounter shortages due to depletion of their primary resources and increasing global demand for green applications, e.g., hybrid cars, wind turbines, and electric car batteries (United State DOE 2017).

Coal fly ash has been identified as a secondary source for REE due to high or equal concentrations than those found in conventional REE ores. Recovery of REE from CFA is an exciting new area of research and some researchers believe the future of REE is in coal. However, increasing demand of HREE has been particularly challenging due to the absence of economically feasible HREE-enriched deposits outside of China. The 74 trace elements were detected in fly ash, and it is considered as an important source of HREE (Tang and Huang 2002). Zhang et al.

(2015b) have reported the REE concentration in coals of United States, China, Democratic People's Republic (DPR) of Korea, and Turkey. The concentration values of 101 ppm and 116 ppm were reported for the coals of China and Turkey whereas DPR Korea and US coals corresponds 72 ppm which is equal to the global average level. Nevertheless, there is uncertainty in this data due to different data reported by various authors, e.g., Seredin and Dai (2012) reported 138 ppm and 62 ppm concentration present in Chinese and US coals, respectively; however, the world coal average level was found to be 69 ppm. This difference in concentrations is due to several factors such as collection of samples, environmental, geological, and analytical methods used (Ketris and Yudovich 2009). It is estimated that around 50% of the REE minerals are found in coal deposits amounting to a total of 50 million metric ton. The well-known coalbeds for REE include Sydney Basin in Nova Scotia, Canada (72–483 ppm REE), Russian Far East coalfields (REE = 300–1000 ppm), and eastern United States with Fire Clay coal bed (REE = 500–4000 ppm) (Zhang et al. 2015b).

During the combustion process in the power plant, the REE are almost completely recovered into the fly ash, and thus the concentration of REE in the CFA is much higher in comparison to the coal. Assuming REE concentration in the coal to be 300 ppm, then the fly ash product would contain 2000 ppm REE (assuming coal to fly ash conversion ratio of 1000 to 150), which is equivalent to about 2500 to 3000 ppm REO. A concentration of 800–900 ppm of rare earth oxide (REO) in CFA is the cutoff for beneficial recovery of metals (Zhang et al. 2015a, b). Different methods have been used for the REE recovery from fly ash by various researchers in the past. The experimental details and outcome of studies performed by various researchers on REE beneficiation and extraction have been summarized in the following sections.

14.2.1 Recovery of REE Via REE Beneficiation Using Physical Separation Techniques

Physical separation methods are the simplest approach to enhance the recovery of REE from traditional acid leaching processes. These does not require any additional chemical reagents and serve to concentrate REE content in CFA samples based on physical traits to enhance recovery. A simple physical preconcentration method described by Lanzerstorfer (2018) exploited REE dependency on particle size fraction in CFA and classified ash particles by size prior to processing. In such a process, an air classifier would be installed within a coal plant's de-dusting system and separate ash particles by size into two or more size fractions which are either enriched or depleted in REE concentrations. It was found that particles in the finest size fraction ($<2.2 \mu\text{m}$) have 17% enrichment in total rare earth content. The distribution of LREE and HREE was also found to be dependent on particle size. The largest fraction of HREE was found in the finest particle fraction of $2.2 \mu\text{m}$ and the largest fraction of LREE was in the particle fraction of $19.4 \mu\text{m}$. Pan et al. (2020)

used physical separation techniques prior to acid leaching to enrich REE concentration in CFA samples (Fig. 14.2). Physical separation of CFA began with particle size separation to remove any particles larger than 38 μm . The remaining fine particles were then subjected to magnetic separation using a Davis tube with a current of 5 A to separate the CFA into magnetic and nonmagnetic fractions. Particles from the nonmagnetic fraction were collected for REE extraction. Using these physical separation methods, REE content in raw CFA was enriched from 782 to 1025 ppm. The enriched CFA was then subjected to acid leaching in 3 M HCl solution at conditions of 60 $^{\circ}\text{C}$, S/L = 10/1, stirring speed of 400 rpm, for 2 h. The leaching efficiency was increased from 43% to 78% using physical CFA preconcentration methods before leaching. The roasting of CFA, if economically feasible before leaching, was suggested to include for enhancing leaching efficiency.

14.2.2 Recovery of REE Using Direct Acid and Alkali Leaching

Acid leaching systems are among the most common systems used to recover REE from CFA. In these processes, acids or lixivants are brought into direct contact with CFA so that soluble constituents of the solid phase are dissolved. After the mixture

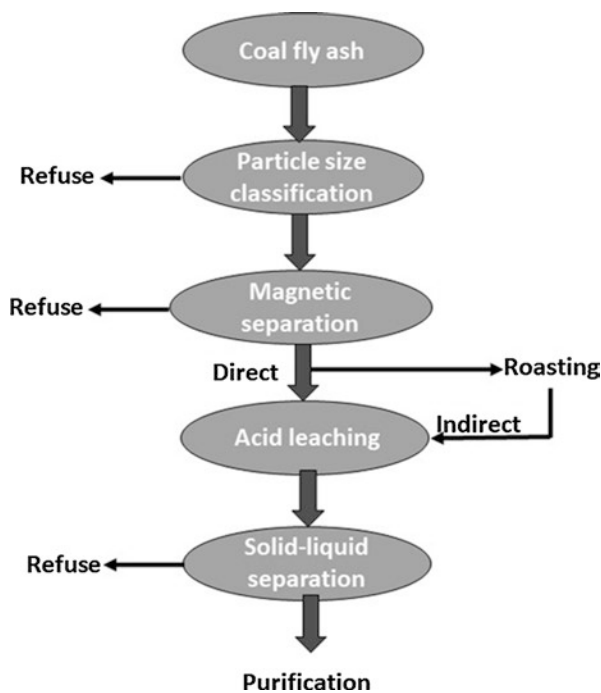


Fig. 14.2 Experimental flowsheet for proposed physical separation and acid leach system modified from (Pan et al. 2020)

is given adequate contact time, the acid solution loaded with dissolved metal is separated from the solid-liquid mixture. The recovered acid is then sent for further processing to recover the dissolved metals from solution. Despite its effectiveness, there are many factors which complicate this process and affect its feasibility in most industrial applications. REE present in CFA are distributed among a large span of different minerals, each requiring their own unique leaching conditions. The REE found in CFA can be classified into four different classes based on their modes of occurrence: (1) REE phosphates/hematite dissolved at pH < 1.5, (2) apatite dissolved at pH 2.0 to 3.5, (3) REE oxides/carbonates dissolved at pH 4.0 to 5.5, and (4) zircon and glass phase aluminosilicates nearly insoluble at any pH (Liu et al. 2019). This variation of REE bearing minerals coupled with the fact that the majority (>70%) of REE is typically trapped in insoluble glass phase aluminosilicates greatly reduces the effectiveness of single-step acid leaching systems. Additionally, acid leaching of the readily soluble noncrystalline REE bearing minerals results in significant levels of co-dissolution of other metal values, e.g., iron, magnesium, sodium, and phosphorous, further complicating later extraction processes.

A direct acid leaching system was developed by Cao et al. (2018) to leach REE from fly ash samples. Optimal leaching conditions of 3 M HCl, S/L = 1/10, 60 °C, 200 rpm stirring speed for 2 h leaching period resulted in REE leaching efficiencies of 71.9% for lanthanum, 66.0% for cerium, and 61.9% for neodymium. In this system, metal oxides present in the raw CFA samples are leached according to the reactions represented in Eqs. 14.1–14.3.



Rare earth oxides present in fly ash which are amenable to leaching follow a similar generalized leaching mechanism outlined in Eq. 14.4.



Rao et al. (2020) developed a similar direct acid leaching system using 1.5 M sulfuric acid. Owing to its classification as an economical extraction process, CFA samples in this process are subjected to only minor physical preconcentration prior to leaching using wet table shaking. Afterwards, CFA is leached using S/L = 1/5 at 25 °C for 5 h. This resulted in 90% and 50% solubilization of HREE and LREE, respectively, equivalent to a total REE recovery of about 60%. High recovery of HREE over LREE is achieved due to its presence with organic matter in raw coal. This causes HREE to be liberated during the combustion process after which they are adsorbed onto the surface of other solid minerals and behave as exchangeable type ions which make them easily leachable under acidic conditions. In comparison, LREE present in the CFA are more likely to be associated with the inorganic phases

of raw coal, most commonly zircon and monazite. These minerals entrap the LREE and prevent them from being leached without additional processing steps.

Leaching systems also utilized the combustion products derived from coal burning power plants which used fluidized bed combustion (FBC) technology. The lower temperatures used in fluidized bed combustion (700–900 °C) result in a lower tendency for glassy phases to form during the combustion and cooling process (Ohenoja et al. 2020). As a result, the combustion products produced from an FBC system are more amenable to acid leaching than those produced using pulverized coal (PC)-fired boilers. Tuan et al. (2019) achieved 62.1%, 55.5%, and 65.2% extraction of Y, Nd, and Dy, respectively, using coal ash from a circulating FBC system via acid leaching with 2 M HCl at 80 °C after 12 h leaching period. Similarly, Honaker et al. (2019) obtained REE recoveries of about 80% from pretreated FBC-derived coal combustion products with 1.2 M HCl acid leaching system using 1% pulp density at 75 °C for 5 h.

A comparative analysis on the effectiveness of various leaching acids for REE recovery from CFA samples has been conducted by Tuan et al. (2019) and Kumari et al. (2019). Both studies evaluated the performance of HCl, HNO₃, and H₂SO₄. Tuan et al. reported negligible performance differences between the three acids; however, Kumari et al. found that nitric acid could also function as an effective recovery agent. In order to avoid the production of nitrate effluent and owing to its ability to dissolve a greater range of REE, HCl was selected as the optimum extracting agent in both processes. Using a solution of 4 M HCl with S/L = 50 g/L at 90 °C, Kumari et al. achieved extractions of about 78%, 80%, 88%, and 35% of La, Ce, Nd, and Y, respectively, after a 2 h leaching period.

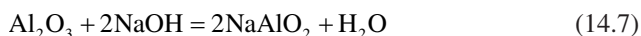
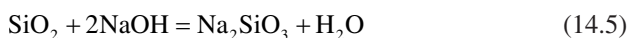
The acid and alkali leaching were employed for the extraction of REE from CFA samples (King et al. 2018). In the treatment of Appalachian Basin CFA, 6.25 M NaOH is used as an extractant instead of an acid. After mixing the ash and alkaline mixture together, the solid-liquid mixture was heated to 85 °C and left to react for 4 h. After allowing the mixture to react and cool, the system was leached using both deionized water and a mixture of 20% HCl to extract the REE from the digested ash. The recovery using deionized water was insignificant; however, samples leached with dilute acid after treatment with NaOH showed REE recoveries up to 85%. The recovery of REE with an alkaline treatment step was higher than those achieved using a standalone acid leaching system which recovered only about 60% of REE using the same ash samples, due to dissolution of glass phase aluminosilicates and liberation of REE in the NaOH treatment step.

A process described by Ma et al. (2019) sought to create a combined acid-alkali leaching system to extract valuable metals from coal combustion products. In this process, ash samples were treated 5-times alternating between solutions of HCl and NaOH. This system extracted 55% of all REE present; however, the indiscriminate behavior of the multiple leaching solutions used lead to significant co-dissolution of other major matrix elements such as Al and Si.

14.2.3 Recovery of REE Via Chemical Pre-Treatment of CFA

A hydrothermal alkali pre-treatment method for coal fly ash outlined by Lin et al. (2018) treated CFA samples with 5 M NaOH, S/L = 1/10 at 100 °C for 2 h. Using a 10-cycle NaOH treatment under these conditions, REE present in CFA samples were enriched from concentrations of 325 ppm to 877 ppm correlating to a 170% enrichment. Using a similar alkali pre-treatment step, Wang et al. (2019) treated CFA samples with 40% NaOH solution in a hydrothermal treatment process at S/L = 1/10 and 150 °C for 2 h. Pre-treatment of ash samples under these conditions correlated to a 41.1% removal efficiency of silica and an overall REE enrichment efficiency of 39.4%. Subsequent acid leaching of the resulting desilicated fly ash resulted in a leaching efficiency of 88.1%, much higher than the 32.4% efficiency obtained from samples of untreated fly ash under identical acid leaching conditions.

Coal fly ash treatment with chemical and thermal methods prior to acid leaching can destroy REE-bearing glassy aluminosilicate spheres. The destruction of these spheres serves to liberate the REE trapped within and improve acid leaching REE recoveries. The NaOH solutions used in these hydrothermal pre-treatment methods reacts with the major silicate and aluminosilicate matrix elements in CFA samples to liberate REE as shown in Eqs. 14.5–14.7 (Ding et al. 2017).



Taggart et al. (2018) tested the effectiveness of CFA roasting with an NaOH flux additive as a replacement for the established Na₂O₂ sintering method developed for geological sample analysis. Samples were roasted at 450 °C, well above NaOH flux melting point of 318 °C, for 30 min at a flux-CFA ratio of 1:1. Subsequent leaching of the treated samples using HNO₃ leaching system showed REE extraction greater than 70%. These recoveries were similar to the efficiencies achieved using the Na₂O₂ system suggesting the viability for NaOH to serve as a low-cost alternative pre-treatment additive.

Following the perceived benefits of alkali pre-treatment to REE recovery from fly ash, Tang et al. (2019) developed an alkali fusion CFA pre-treatment procedure for acid leaching systems. In this process a 1:1 ratio of Na₂CO₃ and CFA were added to corundum crucible and roasted at 860 °C for 30 min. Subsequent leaching of the roasted product resulted in 72.8% leaching efficiency and recoveries of REE in leachate solution were twice high than those obtained using a direct leaching method. Wen et al. (2020) used an alkali pre-treatment step before acid leaching process. CFA samples were added to 3 M NaOH aqueous solution with S/L = 1/8 at 80 °C for 3 h using 200 rpm stirring speed. Alkali treatment destroyed REE-bearing glassy aluminosilicate spheres which liberated the REE trapped within and greatly improved their availability for acid leaching. After alkali pre-treatment, CFA was

treated with 3 M HCl solution at 95 °C and 200 rpm for 90 min. Under these conditions, an average REE leaching efficiency of 95.5% (Nd 93.2%, Ce 89.9%, La virtually 100.0%) was achieved. However, additional economic considerations of the increased cost incurred from additional pre-treatment reagents must be considered when evaluating this process for its industrial feasibility.

14.2.4 Biological Methods for REE Recovery from CFA

Biological extraction methods have also been found suitable for REE and trace metals recovery from CFA. An indirect bioleaching method developed by Park and Liang (2019) found culture supernatant from the bacterial strain *C. bombicola* as an effective leaching agent for REE extraction from unprocessed CFA. Frozen stocks of the culture stored at -80 °C were revived and grown at 10% culture volume. Cultures were fermented for 3 days in darkness at 28 °C and shaking at 150 rpm before the culture was centrifuged for 15 min to separate into two distinct phases: a solid pellet containing all cell mass and any other particulates, and a liquid supernatant containing the organic acids secreted by *C. bombicola* used to leach the fly ash. The two phases were separated and the supernatant was used in leaching process at 28 °C with shaking at 50 rpm with 1% pulp density. The liquid-ash mixture was allowed to react for 6 h and the remaining undissolved solids were removed using a membrane filter. Using this indirect bioleaching method, high yield of HREE could be achieved with 64.6% and 67.7% of Er and Yb recovery, respectively. A highest mineral loss of 59.7% was achieved using *C. bombicola* broth in three fermentation days. The release of fatty organic acids decreases the pH of the system and can be responsible for leaching. The developed method required low energy input with low chemical cost and was found to be environmentally friendly. A flowsheet of the overall experimental design used in this work is presented in Fig. 14.3.

Despite the lower recoveries achieved using biological methods compared to their chemical leaching counterparts, biological leaching systems offer the advantages of being more environmentally friendly, requiring a much smaller energy input, and reduced chemical reagent costs. However, not all biological extraction systems function by leaching target metals indirectly. Direct bioleaching methods can also be used as a viable option to extract REE from fly ash. A process developed by Su et al. (2020b) combines a similar hydrothermal-alkali pre-treatment step used in other conventional REE leaching systems with a one-step biological leaching process. Hydrothermal-alkali pre-treatment of fly ash in this process was done by adding 4 M NaOH to raw CFA before placing the mixture at 150 °C and 0.476 MPa in a thermostatic incubator for 24 h. After treatment, the excess water was drained, and the pH of the fly ash was adjusted to 7.0. The treated ash was mixed with Waksman medium with 10% pulp density and the pH was adjusted to 3.5–4.0 using 0.1 M H₂SO₄. Next, a strain of *A. thiooxidans* which was specially cultivated to be able to withstand and grow steadily was added to the slurry media. The CFA slurry inoculated with the bacterium was then cultivated for 21 days at 30 °C and shaking

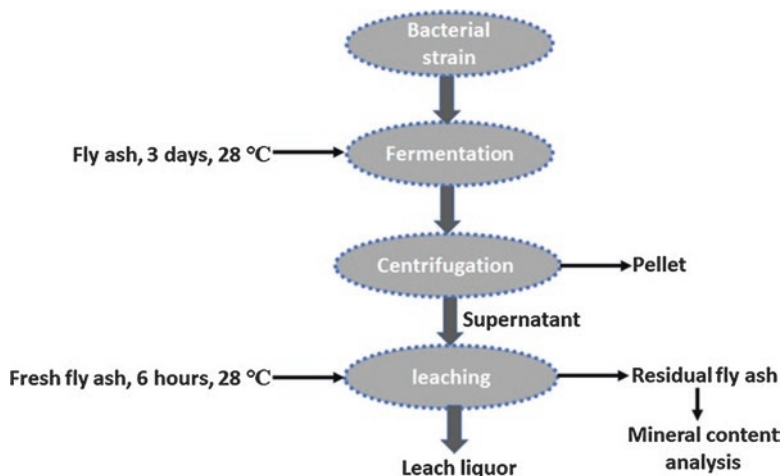


Fig. 14.3 Conceptual flowsheet of indirect bioleaching system modified from Park and Liang (2019)

at 165 rpm. Using this method, 67.0% of La and 97.6% of Ce present in the CFA were recovered. It is believed that using a direct bioleaching process compared to two-step indirect bioleaching methods actually enhances leaching efficiency. The main contributing phenomena to this effect could be the absorption of minerals to microorganism surfaces, the metabolism of microorganisms which change mineral surface properties and increase the ability for metals to participate in biochemical reactions, and by microbes adhering to mineral surfaces where they form a local environment for microbial energy exchange and biological oxidation processes.

14.2.5 *Methods for REE Separation from CFA Leachate Solutions*

Once REE are extracted from solid CFA into leachate solutions, further processing is required to selectively separate desired metals from other major soluble metal ions. Solvent extraction is generally used to separate rare earth metals from other undesired metal ions which co-dissolved during the acid leaching process. Such a process developed by Peiravi et al. (2017) and Smith et al. (2019) used Di-2-ethyl-hexylphosphoric acid (DEHPA) as an organic extractant in an organic carrier solvent of kerosene. Peiravi et al. reported solvent extraction as an extremely effective method for removing REE from aqueous leachate solutions with total REE recoveries of 98.8% using a 1:1 ratio of kerosene to DEHPA. However, this process suffers from the drawback of selectivity towards REE.

A novel process to extract REE from acidified leachate solutions with improved REE selectivity over other major soluble metal ions (Smith et al. 2019) used liquid

membrane separation process. Supported liquid (SEMs) and liquid emulsion membranes (LEMs) were used to recover REE from acidic leachate produced from CFA pre-treated by alkaline roasting. In the LEM process, a water in oil emulsion was first prepared by combining the oil phase comprised of 10% DEHPA, 2% Span 80 as surfactant, and 88% mineral oil with dropwise addition of 5 M HNO_3 under high stirring speed to a 1:1 ratio with the oil phase after which the coal ash leachate was immediately added. After a 1-h extraction time with mixing at 200 rpm, the solution was held static for 2 h to allow for the separation of the emulsion and aqueous phases. After decantation, the emulsion phase was separated into two phases and the acid containing dissolved REE was collected. In the SLM REE extraction process, a H-cell reactor comprised of two connect flanged glass jars was used. A 47 mm PVDF filter soaked in 10% DEHPA in kerosene was placed between the two glass chambers. Leach liquor and the strippant, i.e., 5 M HNO_3 , were added to the opposite chambers of the apparatus. A stirring speed of 700 rpm was used and the solutions were left for 24 h to attain equilibrium. After the extraction period the strippant phase with REE was recovered. A diagram of the reactor is shown in Fig. 14.4.

The LEM system was able to recover about 70% of total REE and achieved greater extraction efficiency of LREE over HREE. Conversely, extraction using the SLM system achieved high recoveries of 75% HREE but was only capable of recovering about 50% of LREE. The SLM extraction system also showed the greatest selectivity and recovered less than 10% of all undesired major metal constituents present in the leachate solution.

TEHDGA (*N,N,N',N'*-tetrakis-2-ethylhexyldiglycolamide), a commercial extractant used for REE separation from acidic nuclear waste solutions, has also been investigated for an application with CFA. This extraction method described by Mondal et al. (2019) uses a TEHDGA impregnated Amberlite XAD-7 resin to selectively extract REE from the matrix elements present in leached CFA solution. A packed column extraction procedure was used with the REE feed solution having a residence time of 40 min. Extraction proceeded until breakthrough of REE was observed in the effluent of the column after which a solution of 0.01 M nitric acid

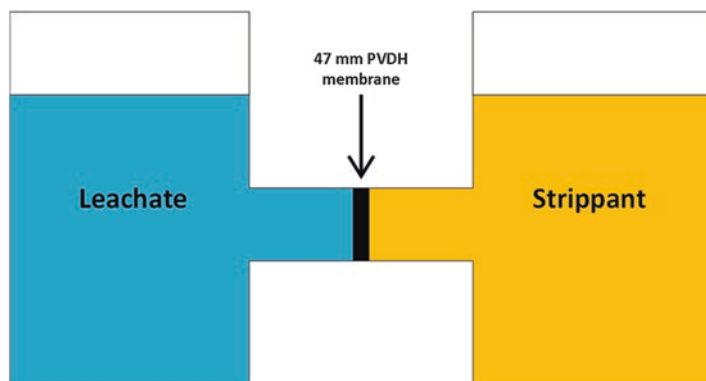


Fig. 14.4 Diagram of the H-cell reactor used in SLM extraction process

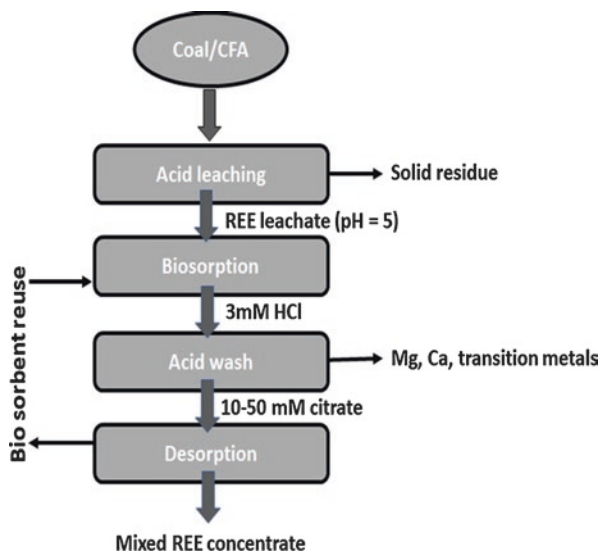
was flowed through the column for elution. Results from this procedure showed excellent selective recovery of REE from CFA with no reported co-extraction of major undesired elements such as silicon, aluminum, iron, magnesium, and calcium which were present in the feed with high stability of the resin allowing it to be recycled and reused.

A biosorption-based extraction process developed by Park et al. (2020) uses specially selected bacteria to selectively recover REE from leach liquor. In this process, a specific strain of *E. coli* which was engineered to display lanthanide binding tags on its cell surface and a native bacteria with a large REE adsorption capacity called *Arthrobacter nicotianae* were used as REE acceptors. Fly ash was leached in 1 M hydrochloric acid with $S/L = 1/10$ at 85 °C for 4 h and the leachate was centrifuged at 3000–5000 g for 15 min to remove undissolved particles. The pH of leach liquor was adjusted to 5. After culturing, bacteria cells were centrifuged and the supernatant was removed before the cells were resuspended in leachate to initiate biosorption. The cells were then centrifuged again for 5 min at 20,000 rpm and the supernatant decanted out. The cells were washed with 3.16 mM HCl to remove any unbound metals before they were centrifuged once more for 5 min. To desorb the bound REE, the cells were resuspended in equal volume of 10 mM and 50 mM citrate for *E. coli* and *A. nicotianae*, respectively. The selectivity of the microorganisms to biosorb desired REE over non-REE impurities can be enhanced via genetic engineering of cell surface functional groups. Using this process, 80% of total REE present in leachate solution were extracted with a separation factor greater than 30 for neodymium compared to all other non-REE metals. The high extraction efficiency and selectivity achieved with this process coupled with the ability to reuse cells for extraction independent of cell viability demonstrate the feasibility of this process for REE extraction from leach liquor (Fig. 14.5). The extracted concentrate has REE purity of 80% and 50% for coal and fly ash sample, respectively. Extraction and separation of REE from CFA using different methods are summarized in Table 14.2.

14.3 Aluminum

Aluminum is considered as the major element in the CFA after silicon. The abundance of Al in CFA is generally 11–30%. This results in the consideration of CFA as a possible replacement for bauxite in the production of Al_2O_3 (Fan et al. 2019). In spite of this fact, there is always risk associated with bauxite ores depletion. The processing of CFA for aluminum recovery can undoubtedly result in economic and environmental benefits along with the probable solution for bauxite depletion. Literature review revealed that CFA has been processed using different routes for the recovery of aluminum (Table 14.3). The acid leaching and alkali-sintering routes are not considered as feasible methods from all perspectives. However, bioleaching can be found as an effective method due to no consumption of acid or alkali with

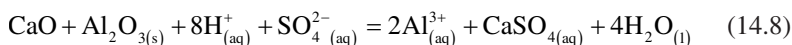
Fig. 14.5 Process flow diagram of biosorption REE extraction process modified from Park et al. (2020)



less amount of solid waste generated with the cost effectiveness recovery of aluminum.

14.3.1 Direct Acid and Alkali Leaching of Al from Fly Ash

Several techniques exist for the aluminum recovery from CFA. One of the most common techniques uses acid or alkali leaching to extract Al from CFA followed by a recovery process to separate the Al from the leachate solution. Shemi et al. (2014) showed the effectiveness of a direct acid leaching system to extract aluminum from the amorphous phase of fly ash and achieved 89.3% extraction efficiency for Al in 10.2 h using 6 M sulfuric acid as lixivant. Sangita et al. (2017) developed an acid leaching system for the recovery of Al using 18 M sulfuric acid with S/L = 1/2 at 200 °C from CFA. Despite the higher temperature and acid concentration, a similar amorphous phase aluminum extraction of 84.2% was achieved after 4 h of leaching. Aluminum was recovered as pure aluminum sulfate from leach liquor using pre-concentration and successive crystallization. Direct leaching of fly ash in such a system is obtained by $H_{(aq)}^+$ attack and the $H_{(aq)}^+$ ion of inorganic acid displaces the metal ion from the ash particle matrix (Eq. 14.8).



Building on past work conducted by Gajam and Raghavan (1985) which reported enhanced aluminum leaching rates of clays in the presence of fluoride ions, Tripathy et al. (2015) investigated the benefits of adding fluoride ions to CFA acid leaching

Table 14.2 Extraction and separation of REE from CFA using different methods

Element(s)	Method(s)	Experimental conditions	Percent recovery	References
REE	Acid leaching, solvent extraction	[HNO ₃] = 6 M, solids conc. = 30 g/L, 85 °C, 1 h	90.9% LREE, 94.2% HREE, 90.5% TREE*	Peiravi et al. (2017)
REE	Alkaline leaching, acid leaching	Alkali: [NaOH] = 6.25 M, 85 °C, 4 h Acid: 50% HCl/H ₂ O (v/v), 85 °C, 4 h	Alkali: 85% REE Acid: 40% REE	King et al. (2018)
REE	Alkali roasting, acid leaching	Roasting: Flux/ash ratio = 1:1, 350 °C, 0.5 h Leaching: [HNO ₃] = 1 M	>90% REE	Taggart et al. (2018)
REE (La, Ce, Nd)	Acid leaching	[HCl] = 3 M, 60 °C, S/L = 10, 200 rpm, 2 h	71.9% La, 66.0% Ce, 61.9% Nd	Cao et al. (2018)
REE	Dry air particle classification	Hosokawa Alpine Multi-Plex laboratory air classifier 100 MZR	TREE* enriched 17%	Lanzerstorfer (2018)
REE	Hydrothermal alkaline pre-treatment	[NaOH] = 5 M, solid/liquid = 1:20, 100 °C, 2 h	170% REE enrichment	Lin et al. (2018)
REE	Alkali fusion, acid leaching	Fusion: Mass ratio CFA/Na ₂ CO ₃ = 1:1, 860 °C, 0.5 h Leaching: [HCl] = 3 M, solid/liquid = 1/20, 400 rpm, 2 h	72.2% REE	Tang et al. (2019)
REE	Liquid emulsion membrane (LEM), supported liquid membrane (SLM)	LEM: [HNO ₃] = 5 M, 200 rpm, 1 h SLM: [HNO ₃] = 5 M, 700 rpm, 24 h	LEM: >70% TREE* SLM: 75% HREE, 50% LREE	Smith et al. (2019)
Sc, REE (Yb, Er)	Indirect bioleaching	Fermentation: <i>C. bombicola</i> , 28 °C, 150 rpm, 3d Leaching: 28 °C, 50 rpm, 6 h	63.0% Sc, 67.7% Yb, 64.6% Er	Park and Liang (2019)
REE	TEHDGA impregnated resin	Impregnation: 50 g Amberlite XAD-7, 50 g TEHDGA, 500 mL methanol, 1 h Extraction: 5 mL CFA solution, 0.1 g resin, 30 min	–	Mondal et al. (2019)
REE	Combined acid-alkali extraction	[NaOH] = 200 g/L, [HCl] = 230 g/L, solid/liquid = 1:5 (w/v), 90 °C	55% TREE*	Ma et al. (2019)

(continued)

Table 14.2 (continued)

Element(s)	Method(s)	Experimental conditions	Percent recovery	References
REE, Y	Alkali pre-treatment, acid leaching	Alkali: [NaOH] = 40%, solid/liquid = 1:10 (w/v), 150 °C, 2 h Acid: [HCl] = 8 M, solid/liquid = 1:30 (w/v), 60 °C, 2 h	88.15% TREE*	Wang et al. (2019)
REE	Acid leaching	[HCl] = 2 M, 80 °C, ρ_{pulp} = 100 g/L, 12 h	62.1% Y, 55.5% Nd, 65.2% Dy	Tuan et al. (2019)
REE	Acid leaching, solvent extraction, precipitation	Leaching: [HCl] = 4 M, 90 °C, ρ_{pulp} = 50 g/L, 2 h	78% Ce, 80% La, 88% Nd, and 35% Y	Kumari et al. (2019)
REE	Acid leaching	[HCl] = 1.2 M, solid concentration = 1%, 75 °C, 500 rpm	~80% REE	Honaker et al. (2019)
La, Ce, Nd	Alkali pre-treatment, acid leaching	Pre-treatment: [NaOH] = 3 M, 80 °C, L/S = 8:1, 3 h, 200 rpm Leaching: [HCl] = 3 M, 95 °C, 1.5 h, 200 rpm	~100% La, 90% Ce, 93% Nd	Wen et al. (2020)
REE, Y	Physical separation, acid leaching	[HCl] = 3 M, 60 °C, L/S = 10:1, 2 h, 400 rpm	~80%	Pan et al. (2020)
V, Sr, Y, La, Ce	Hydrothermal alkali treatment (HAKT), bioleaching	HAKT: [NaOH] = 4 M, 150 °C, 0.476 MPa, 24 h Bioleach: <i>A. thiooxidans</i> , pH = 3.5–4, 30 °C, 21d	90.8% V, 100% Sr, 79.3% Y, 70.0% La, 97.6% Ce	Su et al. (2020b)
REE	Acid leaching, biosorption	Leaching: [HCl] = 1 M, 85 °C, 4 h, ρ_{pulp} = 100 g/L Biosorption: <i>E. Coli</i> , <i>A. nicoitiana</i> , pH = 5	80% total REE	Park et al. (2020)
REE	Acid leaching	[H ₂ SO ₄] = 1.5 M, 25 °C, 5 h, 20% (w/w) solids	60% total REE (90% HREE, 50% LREE)	Rao et al. (2020)

*TREE total rare earth elements

systems. Using 25% pure sulfuric acid with a 10% pulp density at 90 °C, the recovery of alumina increased from 25% to ~92% after the addition of 1.5% hydrofluoric acid as a source for fluoride ions. Fluoride ions improve leaching by reacting with SiO₂ and destroying Si-Al bonds to form SiF₂ and release Al ions. Wei et al. (2018) used high temperatures in a sulfuric acid leaching system to improve aluminum recovery. Mullite, which is typically the dominant aluminum bearing crystalline mineral found in CFA, has been shown in past work by Harada et al. (1993) to decompose at temperatures above 230 °C. Based on this idea, Wei et al. (2018) reported a maximum aluminum leaching efficiency of 86% using sulfuric acid leaching system at 300 °C for 110 min leaching period.

Table 14.3 Extraction and separation of Al from CFA using different methods

Element	Method(s)	Experimental conditions	Percent recovery	Reference
Al	Sintering., alkali dissolution	Sintering: 1200 °C, 1 h Dissolution: [NaOH] = 60.78 g/L, 85 °C, 10 min	90% Al	Bai et al. (2010)
Al	Acid leaching, gas phase extraction	Leaching: [H ₂ SO ₄] = 6 M, solid/liquid = 1:4, 75 °C, 8.75 h Gas phase: Acetylacetone flowrate = 6 ml/min, 250 °C, 6 h	Leaching: 85% Al Gas phase: 64% Al	Shemi et al. (2012)
Al	Acid leaching	[H ₂ SO ₄] = 50%, 180 °C, 4 h	82.4% Al	Wu et al. (2012)
Al	Calcination, water leaching	Calcination: Al ₂ O ₃ /Na ₂ S ₂ O ₇ = 1:3 (PC); 1:5 (CFB), 420 °C, 2 h Leaching: Washed with distilled water	~93% Al	Guo et al. (2013a)
Al	Calcination, acid leaching	Calcination: NaOH/Na ₂ CO ₃ /CFA = 0.5:0.5:1, 700 °C, 2 h Leaching: [HCl] = 20%, solid/liquid = 1:3, 100 °C, 2 h	95% Al	Guo et al. (2013b)
Al	Acid leaching	[H ₂ SO ₄] = 6 M, solid/liquid = 1:4, 82 °C, 10.2 h	89.3% Al	Shemi et al. (2014)
Al	Calcination, acid leaching	Calcination: Na ₂ CO ₃ /CFA = 1:1, 850 °C, 2 h Leaching: [HCl] = 20 wt.%, solid/liquid = 1:4, 100 °C, 2 h	>90% Al	Guo et al. (2014)
Al	Mixed alkali hydrothermal method	[NaOH] = 40 wt%, 260 °C, solid/liquid = 1:12, reaction time = 45 min	91.3% Al	Li et al. (2014)
Al	Alkali leaching	[NaOH] = 45%, solid/liquid = 1:9, 280 °C, 1 h	92.31%	Yang et al. (2014)
Al	Sintering, acid leaching	Sintering: CFA/coal/CaCO ₃ = 5:4:1, 1150 °C, 3 h Leaching: [H ₂ SO ₄] = 6 M, solid/liquid = 1:4, 82 °C, 10.2 h, 150 rpm	88.2% Al	Shemi et al. (2015)
Al	Acid leaching	[H ₂ SO ₄] = 98%, solids concentration = 10%, 90 °C, 3 h	~92% Al	Tripathy et al. (2015)
Al	Two-step acid leaching	Leaching: [H ₂ SO ₄] = 10 M, 120 °C, solid/liquid = 1:2, 2 h Roasting: Na ₂ CO ₃ /SiO ₂ = 1:1 (molar), 860 °C, 2 h	99.83% Al	Zhu et al. (2015)
Al	Ammonium sulfate recovery	500 °C, CFA/(NH ₄) ₂ SO ₄ = 2:6 (w/w), 1 h	95% Al	Doucet et al. (2016)
Al	Acid leaching	[H ₂ SO ₄] = 18 M, 200 °C, 4 h, solid/liquid = 1:2	84.19% Al	Sangita et al. (2017)
Al, Li	Alkali pre-treatment, acid leaching	Alkali: 150 kg NaOH/1 m ³ CFA, solid/liquid = 1:3, 120 °C, 1 h Leaching: [HCl] = 6 M, 120 °C, solid/liquid = 1:20, 4 h	76.7% Al, 82.3% Li	Li et al. (2017)

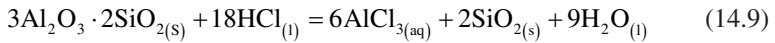
(continued)

Table 14.3 (continued)

Element	Method(s)	Experimental conditions	Percent recovery	Reference
Al	NaCO ₃ sintering, acid leaching	Sintering: 850 °C, Al/Na ₂ CO ₃ = 1:1 (molar), 2 h Leaching: [HCl] = 6.02 M, solid/liquid = 1:5, 2 h	~87% Al	Guo et al. (2017)
Al	Acid leaching	[H ₂ SO ₄] = 98 wt%, H ₂ SO ₄ /CFA = 1:2 (molar), 300 °C, 110 min	86% Al	Wei et al. (2018)
Al	Sintering pre-treatment, acid leaching	Sintering: CFA/CaCl ₂ = 1:1, 900 °C, 2 h Leaching: [H ₂ SO ₄] = 1 M, solid/liquid = 1:20	85% Al	Tanvar et al. (2018)
Al, Ce	Alkaline roasting, bioleaching	Roasting: Na ₂ CO ₃ /CFA = 1:0.22 (w/w), 850 °C, 2 h Bioleaching: Acidithiobacillus ferrooxidans, pyrite/CFA = 1.5:1, ρ _{pulp} = 20 g/L, pH = 1.75	91.2% Al, 63.4% Ce	Fan et al. (2019)
Al, Fe	Acid leaching	[HCl] = 20% (wt%), 95 °C, solid/liquid = 1:3.5, 5 h	42.75% Al, 35.10% Fe	Zhang et al. (2019)
Al	Acid leaching	[H ₂ SO ₄] = 15%, 90 °C, 2 h	91% Al	Tripathy et al. (2019)
Al	Alkaline roasting, acid leaching	Roasting: Na ₂ CO ₃ /Al = 1:2, 850 °C Leaching: [HCl] = 6.02 M, liquid/solid = 6 mL/g, 2 h	90.4% Al	Guo et al. (2019)
Al	Autoclave acid leaching	[HCl] = 345 g/L (30%), solid/liquid = 1:5, 190–200 °C, 3 h	90–95% Al	Valeev et al. (2019)
REE, Al	Combined acid-alkali extraction	[NaOH] = 200 g/L, [HCl] = 230 g/L, solid/liquid = 1:5 (w/v), 90 °C	55% TREE, 86% Al	Ma et al. (2019)
Al	Acid leaching, membrane electrolysis	Electrolysis: 2-membrane 3-chamber cell, 20 h	64.48% Al	Shi et al. (2020c)
Al	Acid leaching, electrolysis extraction	Electrolysis: 1 h, J = 600 A/m ²	83.25% Al	Shi et al. (2020b)
Al	Acid baking electrolysis	200 °C, 1.5 h, [H ₂ SO ₄] = 95–98 wt%	86% Al	Shi et al. (2020a)
Al, Li	NaCl roasting, acid leaching	Roasting: CFA/NaCl = 1:1, 800 °C Leaching: [HCl] = 6 M, 120 °C, 2 h	93% Al, 98% Li	Li et al. (2020)

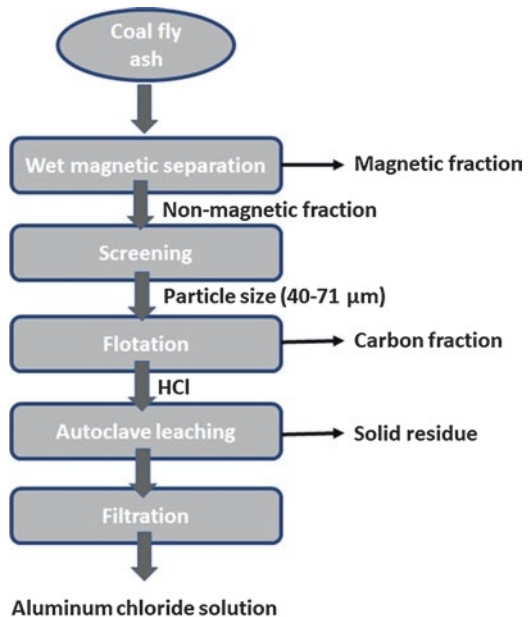
Acid leaching systems can also be enhanced by using physical beneficiation to concentrate Al content in CFA prior to leaching. Valeev et al. (2019) developed an enhanced HCl leaching system which used magnetic separation and carbon flotation steps to improve aluminum recovery. Physical separation of the fly ash resulted in the separation of both magnetic and carbon enriched waste streams and subsequent autoclave leaching of the resulting aluminum-enriched stream achieved ~95% aluminum extraction efficiency using 30% HCl at 200 °C for 3 h (Fig. 14.6). The

aluminum targeted by the autoclave leaching process occurred almost all in the mullite phase of the enriched ash and was dissolved following the mechanism outlined in Eq. 14.9.



Compared to CFA generated from traditional pulverized coal (PC) furnace, leaching systems which use CFA generated from circulating fluidized bed (CFB) boilers have been shown as a promising alternative feed material for aluminum recovery. Since a certain proportion of aluminum in CFA is present in the stable crystalline structure of mullite, the breaking of its crystalline structure to free trapped aluminum is a key focus of recovery processes using a PC derived CFA feed. In contrast, lower operating temperatures used in CFB boilers changes the mineral transformations which occur during combustion resulting in a much smaller proportion of crystal minerals with nearly all aluminum present in amorphous phases. When comparing the leaching activity of both PC and CFB coal ash, Guo et al. (2013a) found that amorphous structure bonds i.e., Si-O-Al bonds, were more active than those of crystal minerals leading to higher leaching activity. Yang et al. (2014) developed an alkali leaching system to investigate the benefits of using CFB-derived fly ash for aluminum recovery. Using 45% NaOH leaching solution with added calcium oxide using S/L = 1/9 at 280 °C, Yang et al. observed 92.3% aluminum recovery from CFB coal ash samples. Building on their work, Ma et al. (2019) developed a combined acid-alkali CFA treatment process which optimized the benefits offered by CFB coal ash. CFB ash samples were first leached in a solution of

Fig. 14.6 Combined flow sheet for physical separation and acid leach system (Valeev et al. 2019)



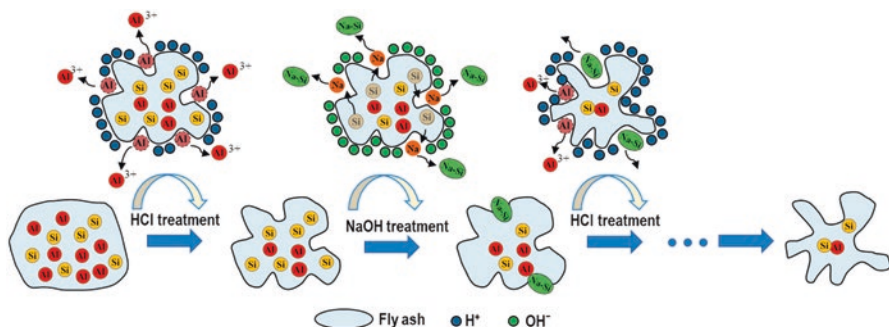


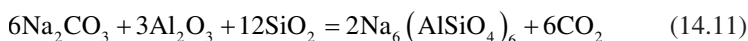
Fig. 14.7 Mechanism of the proposed combined acid-alkali CFB coal ash leaching (Ma et al. 2019)

230 g/L HCl to dissolve aluminum present on the particle surface. The CFB ash was then neutralized with deionized water before being treated with 5 M NaOH to dissolve SiO₂ which had accumulated on the ash particles and to break the Si-O-Al bonds in the residues. The newly exposed aluminum was then dissolved into solution by leaching once more with HCl. A further two more treatments were conducted to dissolve the maximum quantity of aluminum into the solution and an overall 86% Al extraction was achieved. The mechanism of dissolution of aluminum and silicon is shown in Fig. 14.7.

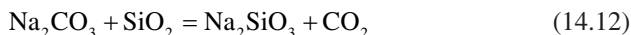
14.3.2 Recovery of Al Using CFA Pre-Treatment and Recovery Processes

Compared to traditional commercial aluminum process which uses bauxite, a mineral which possesses high aluminum content and low levels of impurities, fly ash contains comparatively low levels of alumina and high levels of silica (Fan et al. 2019). To address these shortcomings, many pre-treatment processes have been developed which improve aluminum recovery and lower operating costs. Thermal activation processes are commonly used pre-treatment processes in which fly ash is heated to high temperatures with other additives to improve aluminum leaching behavior. During heating, the fly ash and powdered additives react to decompose crystalline aluminosilicate structures such as mullite and quartz to form soluble aluminum compounds which can then be dissolved in subsequent leaching steps. A process developed by Guo et al. (2013b) used a combined NaOH and Na₂CO₃ additive in a thermal activation pre-treatment process to enhance aluminum recovery from HCl leaching system and a 95% recovery was reported from subsequent acid leaching with 20% HCl. A sole Na₂CO₃ calcination process at 900 °C was also studied by Guo et al. and showed strong CFA enhancement with 82% aluminum recovery. In this system, sodium carbonate reacts with aluminum and silicon-bearing minerals, i.e., mullite (3Al₂O₃•2SiO₂) and quartz (SiO₂) at temperatures around

800–900 °C to form minerals nepheline (NaAlSiO_4) and zeolite ($\text{Na}_6(\text{AlSiO}_4)_6$) which are amenable to acid leaching.



However, excess silicon in the system also reacts with sodium carbonate and forms sodium silicate following Eq. 14.12.



This undesired reaction contributes to a massive amount of reagent consumption with 0.8–1.2 tons of Na_2CO_3 required to activate one ton of fly ash greatly restricting the industrial viability of the process. In later work, the viability of using red mud (RM), a hazardous waste generated by the alumina industry, as an additive to reduce Na_2CO_3 consumption was investigated (Guo et al. 2014, 2017, 2019). In these processes, molar ratio of 1.3–1.8 for Si/Al was used to adjust it from around 0.6–0.8:1 to 1:1 in the CFA feed. An Si/Al molar ratio around 1:1 prevents excess silicon from reacting with Na_2CO_3 in the calcination process and greatly reduces reagent consumption. Incorporating RM into their feed stream, Guo et al. reduced Na_2CO_3 consumption in the calcination pre-treatment by 80%; however this solution also introduced impurities from RM which may make complicate Al separation from acid leachate. Fan et al. (2019) used a similar Na_2CO_3 calcination process to explore the effectiveness of CFA thermal activation in a bioleaching system. Fly ash was roasted at a temperature of 850 °C for 2 h using much smaller proportions of activating reagent at a 1:0.22 mass ratio of CFA to Na_2CO_3 . Subsequent bioleaching steps by meso-acidophilic *Acidithiobacillus ferrooxidans* resulted in 91.2% Al recovery after 12 days of incubation.

Shemi et al. (2015) investigated the feasibility of using a calcium carbonate sintering agent as part of a two-step acid leaching system. Fly ash was first leached in a pre-sinter leach step using sulfuric acid before the residues were mixed with CaCO_3 and sintered at 1150 °C for 180 min. Subsequent leaching of the treated ash in a post-sintering leaching step yielded aluminum recoveries of 88.2%. Ammonium sulfate was investigated by Doucet et al. (2016) as another alternative aluminum extraction agent. Ammonium sulfate offers the benefits of being a widely available, low-cost, and recyclable reagent which produces treated ash that can be leached using only water to recover aluminum. While unable to recover aluminum from crystalline phases, this process is capable of recovering up to 95% of amorphous phase aluminum. Tanvar et al. (2018) achieved aluminum extraction rates of 85% when leaching CFA which was pre-treated with calcium chloride at 900 °C for 2 h. Sodium chloride has also demonstrated the ability to promote the decomposition of mullite phases into soluble sodium salts when used as a thermal activating agent. Li et al. (2020) recorded aluminum extraction efficiencies of 93% using high alumina CFA roasted with NaCl at 800 °C. Other simpler pre-treatment processes performed

at more moderate temperatures focus on the desilication of raw fly ash by treatment with NaOH. Li et al. (2017) and Tripathy et al. (2019) presented the effectiveness of alkali desilication processes as a less energy-intensive alternative to sintering and calcination processes using temperatures around ~ 130 °C with reported aluminum recoveries of 76.7% and 91.0%, respectively. An added benefit of this process is its ability to generate useful silicon by-products while regenerating its alkali reagent.

14.3.3 Selective Recovery of Aluminum from CFA Pregnant Leach Solutions

Other extraction processes which function on different principals from acid leaching of raw or thermally treated coal fly ash have also been proposed for aluminum recovery. Aluminum can be extracted from other compounds in fly ash by gas phase extraction. Shemi et al. (2012) tested the feasibility of using acetylacetone to selectively extract aluminum(III) oxide from fly ash. The gas phase extraction using 6 mL/min gas flow rate at 250 °C for 6 h, 17.9% aluminum extraction was achieved representing 64% of the amorphous-phase aluminum present in the sample. Electrolysis has been studied as a much cleaner and more efficient extraction process which avoids the extensive use of hazardous chemicals. Shi et al. (2020a, b) developed electrolysis and baking-electrolysis process for Al_2O_3 recovery from leach liquor of CFA using sulfuric acid as a lixiviant. A novel two-membrane and three-chamber cell electrolysis aluminum recovery process developed by Shi et al. (2020c) was found efficient to extract aluminum as aluminum hydroxide from H_2SO_4 leached liquor. In this system, aluminum hydroxide and H_2 are liberated at cathodic and H_2SO_4 at the anodic chamber. Since H_2 can be used as a clean energy source and H_2SO_4 can be recycled back to be used in CFA acid leaching systems, no harmful by-products are directly generated by this process. Under optimized conditions, a $\text{Al}(\text{OH})_3$ yield of 64.5% was achieved after 20 h of operation with a synthetic sulfuric acid leachate.

14.4 Selenium

Trace amount of selenium is an essential nutrient for plant and animals. It is also used in fertilizers, manganese electrolysis, glass and alloy production, Li-Se batteries and solar cells. It is often produced as by-product during copper production as well as from metal sulfide ores refining. When present even at low concentrations, Se is assumed to be a toxic waste material. Selenium is also present in CFA and can be extracted from CFA enriched with Se. Wang et al. (2007) found that the maximum concentration of Se in CFA can be 200 ppm depending on the coal type and combustion method. Selenium is volatile in nature and accumulates in CFA via

volatilization-condensation process depending upon Coal source, CFA particle size, CFA composition, residence time, and combustion temperature.

Wang et al. (2009) explored bituminous and sub-bituminous CFAs to study leaching behavior of arsenic and selenium, two major toxic elements, in different type of CFAs. The maximum concentration of Se was 45.6 ppm in bituminous CFAs. In comparison to the sub-bituminous CFAs, selenium was significantly leached from bituminous CFAs with increase in S/L ratio and leaching time under alkaline pH (>12) conditions. The calcium precipitation resulted in minimizing leaching efficiency from sub-bituminous CFAs. Cantrell (2014) used deionized, rain, and ground water to study the leaching characteristics of fresh and weathered type sub-bituminous CFA for 2 and 6 h reaction time. The leached selenium concentrations were different in fresh and weathered type sub-bituminous CFA with different lixivants but were unaffected by extraction times. In all treatments, extractable selenium concentrations from fresh CFA were below 2.0 $\mu\text{g/L}$. However, water-extractable Se concentration from weathered CFA was 60.0 $\mu\text{g/L}$ with groundwater and rainwater which is nearly equal to the concentration obtained with deionized water, i.e., 57.6 $\mu\text{g/L}$. This is due to the formation of highly mobile and less toxic selenate (Se^{6+}) by the oxidation of selenite (Se^{4+}) during environmental weathering.

Schwartz et al. (2016) studied leaching of arsenic and selenium from CFA in sediment microcosms under aerobic and anaerobic conditions. Selenium was more dissolved (53 $\mu\text{g/L}$ at 24 h, pH = 7.1–7.4) under aerobic conditions due to oxidation of Se^{4+} to highly mobile selenate (Se^{6+}); however, there was rapid decrease in Se solubility under anaerobic conditions due to abundance of Se^{4+} species. He et al. (2019) reported potential application of CFA for Se biofortification. Selenium-rich CFA can be used to enhance plant growth and crop yields. It is a promising source of Se for soil amendment to fix selenium deficiency issues worldwide. He et al. (2020a) applied ultrasound-assisted sequential extraction (UASE) for the recovery of arsenic and selenium from CFA. The results showed quantitative and promising recoveries of As and Se. The conventional method was replaced with ultrasound with reaction times of 70 and 90 min for arsenic and selenium, respectively. The authors (He et al. 2020b) also investigated a fast screening of arsenic and selenium from CFA using microwave-assisted sequential extraction (MASE) methods. The recoveries of both elements were > 80% in all fractions and the operation time was significantly reduced from 24.5 h to 44 min. The technique was much improved and better than conventional sequential extraction CSE (Fig. 14.8).

14.5 Gallium and Germanium

Gallium has been widely used in semiconductor and biomedical applications, low melting alloys, electronic devices, and neutrino detection. Germanium found uses in fiber optics, infrared optics, polymerization catalysts, electronics and solar

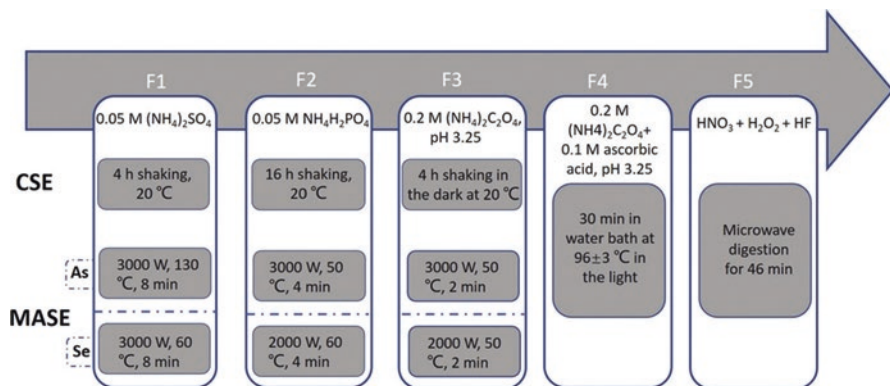
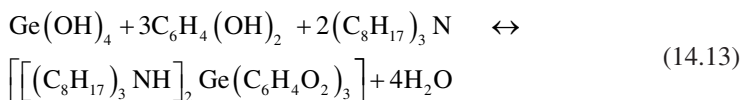


Fig. 14.8 Flow diagram of sequential extraction for CSE and MASE schemes (He et al. 2020b)

electric applications. Both metals are found in association with zinc and its mineral phases in the earth's crust. Coal is an abundant source of these metals and CFA is enriched with gallium and germanium due to condensation of both elements on CFA surface after coal combustion (Meawad et al. 2010). Qin et al. (2015a) reported Ga recovery from coal deposits and found that coal deposits are a promising source of Ga. Recovery of gallium and germanium from CFA has been reported by various researchers in the last decade.

Solvent extraction technique was used by Arroyo and Fernández-Pereira (2008) for Ge recovery from CFA obtained from integrated gasification with combined cycle (IGCC) process. Water was used as leaching agent and germanium was quantitatively leached at S/L = 1/5, 50 °C for 6 h. Germanium was extracted as Ge-catechol complex using trioctyl amine as an extractant at pH = 2–3 and A/O = 20/1.



The metal was stripped from organic phase using 1 M NaOH at A/O = 1/10 and the proposed scheme was claimed to be eco-friendly. Same authors (Torralvo and Fernández-Pereira 2011) have utilized ion exchange resin method with basic anionic resin (IRA-900) for Ge recovery from CFA leachate using water as leaching agent. Design of experiments was used to identify optimized conditions and 96.1% Ge retention was achieved using [Catechol]/[Ge] = 9 with [IRA-900]/[Ge] = 3. Germanium was eluted with 1 M HCl in 50% ethanol and reutilization of resin was confirmed with >99% efficiency. Arroyo et al. (2014) studied the variability of Ga and Ge in CFA generated from IGCC weekly (differences over 40–60 ppm), monthly (differences up to 72 and 94 ppm for Ga and Ge, respectively, over 2–3 months), and yearly (70 and 200 ppm for Ga and Ge, respectively). The group also focused on the extraction method for the metal's recovery from CFA. The Ga extraction was low in

comparison to Ge due to differences in their chemistry. The reduction in gallium extraction was due to decrease in reactivity of Al-Si fly ash matrix due to partial crystallization as an effect of aging. Germanium was quantitatively leached with 0.16 M oxalic acid at 50 °C, S/L = 5 in 1.5 h extraction period and considered as the most appropriate condition for high and regular Ge extraction. Arroyo et al. (2015) extended the developed process to pilot plant scale for Ge recovery and demonstration sized plant equipment was designed based on the results. The optimized conditions from previous studies were used with slight modifications. The pilot plant scale (5 kg fly ash/h) results were used to perform the mass balance of the demonstration plant (200 kg fly ash/h). The design, equipment options, process evaluation, and early investment calculation have been done for a demonstration plant. The tests were performed at pilot plant scale with the designed leaching reactor, filters including extraction-stripping equipment. It was derived that 200 kg fly ash/h resulted in the recovery of almost 61 g/h of GeO₂ and 1,800,000 euros were required to operate the demonstration plant. The same research group (Arroyo Torralvo et al. 2018) developed a low environmental impact process using ion exchange resin method with basic anionic resin (IRA-900) for Ge recovery from fly ash leachate using tartaric acid solution as leaching agent. The optimized leaching conditions (86% Ge leached) were S/L = 1/5, tartaric acid solution with pH = 1 for 3 h at 25 °C in an agitated vessel. Design of experiments was used to find out optimized conditions for ion exchange experiment and 90–98% Ge retention was achieved using 2–2.5 g/L IRA-900, 2–2.5 pH and 1.6–2.0 g/L tartaric acid. Germanium was eluted with 2, 3, and 4 M HCl resulting in >95% Ge recovery along with significant amount of Sb and V. Tannic acid was used for the precipitation of Ge from eluent and 99.3% of Ge was precipitated using 33.3 g tannic acid per g of germanium. Vanadium was also precipitated to some extent leaving other elements behind in the solution.

Kamran Haghghi et al. (2018) reported Ge recovery from synthetic leach solution of CFA using solvent extraction technique. Alamine 336 (tri-octyl/decyl amine), Aliquat 336 (N-methyl-N, N-diethyl chloride), and Cyanex 923 (phosphine oxide) have been explored as extractant and tartaric/oxalic acid as complexing agent to form extractable metal species. Germanium was selectively extracted from nickel, cadmium, cobalt, and zinc in each extraction system and extraction efficiency followed the order—Aliquat 336 > Alamine 336 > phosphine oxide. Germanium was stripped using 1 M HCl, 2 M HCl, and 0.1 M NaOH from the loaded Alamine 336, Aliquat 336, and phosphine oxide, respectively. Aliquat 336 was found to be promising extractant for the Ge recovery from CFA leached liquor. Zhao et al. (2020) reported Ga recovery from synthetic H₂SO₄ leach solution of CFA using P204 (bis(2-ethylhexyl) phosphonic acid), P507 (2-ethylhexyl phosphonic acid mono-2-ethylhexyl ester), and Cyanex 272 (Bis(2,4,4-trimethylpentyl) phosphonic acid) as extractants via solvent extraction technique. The pH effect was studied with all extraction systems and P507 along with Cyanex 272 was selected for further studies. Firstly, Ti and Fe were extracted using 1 M P507 at equilibrium pH ≤ 0.8 in 2-stage cross current extraction. Afterwards, Ga selectively extracted against Al using 0.5 M Cyanex 272 at equilibrium pH = 2.4–2.6. The overall process for the recovery of Ga is shown in Fig. 14.9. The ion exchange mechanism was proposed

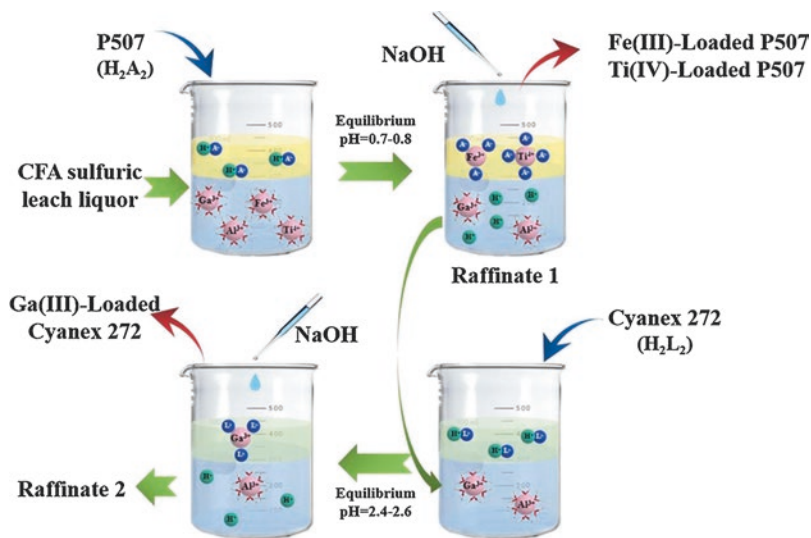


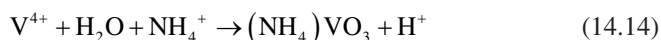
Fig. 14.9 Scheme for the recovery of Ga from synthetic leach solution of CFA (Zhao et al. 2020)

for Ga extraction and supported by slope analysis and spectroscopic methods. The selective stripping efficiency of 87.8% Ga was achieved with 0.5 M HCl as strippant and recyclability of Cyanex 272 was also confirmed.

14.6 Vanadium

Vanadium is frequently used as an alloying element in steel, as a catalyst in petrochemical industry, in aerospace, power generation, glass industry, and nuclear reactors. Although there are several reports for the recovery of vanadium from different matrices, CFA is considered as a promising source of vanadium due to vanadium enriched coal, e.g., >500 µg/g vanadium was found in the coal in southeastern China (Liu et al. 2017). The coal combustion leads to accumulation of V in CFA due to its low volatility and makes it a potential source of vanadium (Dai et al. 2010; Li et al. 2013; Tang et al. 2013). Most of the studies are focused on the recovery of V from spent catalyst, coal, coal stone, and vanadium bearing shale. Only a few studies have been reported for the recovery of V from fly ash. Wet leaching is one of the most commonly used method for vanadium recovery from CFA. Dan et al. (2013) reported enhancement in leaching efficiency of arsenic, selenium, molybdenum, and vanadium from trisodium hydrogen-di-carbonate dihydrate (trona) treated CFA. This happened due to the presence of more soluble fraction in trona ash as compared to control ash. Rastegar et al. (2015) adopted bioleaching process for vanadium, nickel, and copper recovery from oil-fired ash (OFA). Around 82%, 86%, and 87%, of vanadium, nickel, and copper were leached at 4% pulp density,

1 g/L Fe^{2+} and $\text{pH} = 1$ using *acidithiobacillus ferrooxidans* bacteria. Toxicity characteristic leaching procedure (TCLP) confirmed the detoxification of OFA after bio-leaching. Xiao et al. (2015) used hydrometallurgical extraction for the recovery of vanadium from bone coal and ash as vanadium pentoxide. Fluorosilicic acid (20%) was used as lixiviant for ash at 110 °C for 2 h using $\text{S/L} = 1/2.5$. Vanadium was precipitated as NH_4VO_3 from leach solution and calcinated to V_2O_5 as final product.



Rasoulnia and Mousavi (2016) employed *Aspergillus niger* and *Penicillium simplicissimum*, acid producing fungi for V and Ni recovery from CFA. The results confirmed quantitative recovery of V along with 50% Ni extraction with both type of fungi. The bioleaching showed improved recovery over chemical leaching for both the metals. Jung and Mishra (2018) recovered vanadium from OFA via carbon removal, roasting, and then leaching the resulting sample with water as a lixiviant. The vanadium content was enriched from 2.2% to 19% after carbon removal at 650 °C for 4 h. The resulted ash was roasted with Na_2CO_3 at 650 °C for 4 h to form water-soluble NaVO_3 . The resulting sample was leached using water as a lixiviant at 60 °C for 4 h, and 92% vanadium was leached under these conditions.

Abd El-Hamid and Abu Khoziem (2019) investigated possible optimized conditions for the recovery of metals from petroleum ash. Vanadium and nickel were found to be major elements in the ash. Around 98% of the metal values were leached under two different conditions using H_2SO_4 as lixiviant, MnO_2 as an oxidant and $\text{S/L} = 1/10$ at 80 °C for 6 h. Rahimi et al. (2020) recovered V as V_2O_5 from OFA using lemon juice containing citric, malic, and ascorbic organic acids as lixiviant via ultrasound-assisted leaching. Design expert 7 software and Response surface methodology (RSM), a statistical method were used to optimize conditions for V recovery and around 89% V was leached using 27.9% lemon juice, 10% H_2O_2 , 159 W ultrasound power and 0.01% S/L ratio for 2 h at 35 °C. Finally, V was precipitated as ammonium metavanadate from leach solution and calcinated to V_2O_5 at 550 °C for 4 h.

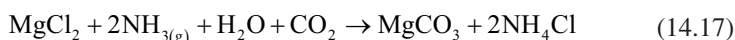
14.7 Lithium

Presently, lithium has been widely used in batteries, and other applications include in metallurgy, primary Al production, glass and ceramic production, lubricating greases, air purification, polymer, etc. Its demand is continuously increasing and therefore alternative sources for the production of Li must be identified. Coal is considered as a promising source for lithium and there is a huge gap in the research for lithium recovery from coal and CFA (Seredin et al. 2013; Qin et al. 2015b). Literature review reveals that many researchers have determined the content of Li in the coal and CFA samples. Ketris and Yudovich (2009) reported 12 ppm and 66 ppm

as the world average Li content in coal and CFA, respectively. The average high Li content (Guanbanwusu mine), i.e., 264 ppm and 1320 ppm was found for coal and CFA, respectively (Sun et al. 2012). These investigations lead to enforcement for the recovery of Li from CFA samples. Hu et al. (2018) investigated the distribution of Li in high alumina-CFA. The sequential separation of high alumina-CFA revealed the presence of 79–94% Li in glass phase, 5–16% in mullite-corundum-quartz (MCQ), and <5% in magnetic particles. The pre-desilication process followed by dissolution of glass phase was suggested for Li extraction. Li et al. (2017) reported Al and Li recovery from pre-desilicated CFA using acid pressure leaching. The pre-desilication was done with NaOH solution at 120 °C for 1 h. Thereafter, acid pressure leaching was performed using 6 M HCl, S/L = 1/20 at 120 °C for 4 h and resulted in 82.2% Li and 76.7% Al recovery. The work showed potential for future research for the recovery of Li from CFA.

14.8 Magnesium and Calcium

Magnesium/calcium is an alkaline earth metal and is found useful in mineral carbonation. The concentration of MgO and CaO in the CFA from different types of coal varies in between 1–10% and 1–40%, respectively (Sahoo et al. 2016). In mineral carbonation process, CO₂ is captured by MgO/CaO resulting in the form of magnesium carbonate. Weak or strong acidic/basic or ammonium reagents are employed as leaching medium for extraction. The ammonium medium is favorable one due to its selectivity towards magnesium.



The CFA having sufficient concentration of MgO/CaO can be considered as a potential source to recover high purity carbonates with the consumption of CO₂. The capturing power of CFA for CO₂ directly depends on the concentration of MgO/CaO. Brown CFA found in Victoria, Australia has high content of alkaline metal oxides and classified as highly alkaline CFA. Hosseini et al. (2013) leached magnesium and calcium from two different CFA samples (A and B) using 4 M ammonium chloride solution, S/L = 1/6 at 80 °C for 30 min. Sample B showed less recovery of magnesium due to the presence of chemically stable MgFe₂O₄. The metal carbonates were precipitated by bubbling 15 L/min CO₂ gas in to leach solution for 20 min with stirring at pH = 9–10 and more than 90% Mg/Ca carbonates were recovered from sample A. The authors (Hosseini et al. 2014) also studied capturing of carbon dioxide through indirect carbonation via multiple leaching-carbonation of brown CFA under similar experimental conditions. The regenerated ammonium chloride in carbonation step was further utilized for the extraction of Ca and Mg from CFA. The presence of metal oxides in CFA favored extraction and Ca was extracted much

faster than magnesium. The leaching kinetics of Mg resulted in pseudo-second-order reaction with an activation energy of 20.7 kJ/mol. Choo et al. (2016) investigated sodium sulfide, $\text{Na}_2\text{S}_2\text{O}_4$, and pyrite as reductant for the leaching of Fe and Mg from MgFe_2O_4 bearing brown CFA found in Victoria, Australia. The reductive leaching was performed with 2 M HCl as lixiviant, S/L = 1/6.67 at 200 °C, and using different reductants. Pyrite and $\text{Na}_2\text{S}_2\text{O}_4$ showed comparable leaching efficiencies for Fe^{2+} and Mg^{2+} and rise in temperature is favorable for pyrite. However, $\text{Na}_2\text{S}_2\text{O}_4$ due to its high dissolution showed effective leaching at 100 °C. There was no significant increase observed in leached iron concentration when pyrite was used as reductant due to its presence in solid leaching residue. Overall, the use of pyrite was recommended for the large-scale study.

14.9 Titanium and Molybdenum

Coal samples depending on their region of origin may have compositions which are enriched in certain trace elements such as titanium and molybdenum at levels high enough to be extracted at economically viable levels. Titanium due to its ability to withstand moderately high temperatures without deformation and strong corrosion resistance found applications in aerospace and automobile industries. The increasing demand for titanium coupled with increasingly scarce primary sources of the metal has resulted in more attention being given towards secondary sources for titanium recovery. Zhai et al. (2020) worked on early mine tailings derived from the Pangang Group's titanium mining operation in China, and demonstrated how waste from titanium mining operations could serve as an economically viable source for the metal with reported titanium concentrate recovery of 68.9%. Typically making up about ~1% of coal fly ash elemental material, coal samples and their combustion residues have also attracted the attention of researchers to exploit its potential as a secondary titanium resource. Coal combustion residue samples which are particularly enriched in Ti can be processed for Ti recovery using similar methods adopted for major CFA constituents. Kalemekiewicz and Chmielarz (2014) investigated different occurrence modes of titanium and titanium group elements from industrial fly ash. Speciation was determined by sequential chemical extraction to classify the ash samples into different modes of occurrences based on their relative leachability. The six classified fractions include soluble in water, exchangeable, soluble in acids, oxide, pseudo sulfide fraction, and residuals. After the fifth stage of the sequential chemical extraction procedure, the total solubility of the ash relative to the mass of the original sample only achieved 42.4%. This digested ash contained under 12% of the total titanium present in the ash sample with the remaining fraction trapped in undigested residuals. Similar to other valuable elements present in CFA, Ti tends to associate primarily with crystalline minerals which are not soluble in acidic leaching solutions. Hydrothermal alkali processes can be used to target titanium trapped

in crystalline minerals and CFA to improve its leachability. Su et al. (2020a) developed a process which used alkali treated CFA in a bioleach process for Ti extraction. CFA was mixed with 4 M NaOH and heated to 150 °C for 24 h to destroy Si-O-Si and Si-O-Al bonds on the mineral surface, thereby exposing the metals within. Subsequent bioleaching using a domesticated strain of *Aspergillus niger* showed a maximum Ti leaching rate increase of 89.2% in CFA with hydrothermal alkali treatment as compared to raw untreated ash samples. Since the acid leaching methods used to extract Ti result in the co-extraction of many other different metals and elements present in the CFA, selective recovery methods must be used to isolate and recover pure Ti from acid leachate solutions. Rushwaya and Ndlovu (2017) demonstrated that 99% of titanium could be recovered from an acidic aqueous leachate solution using a solvent extraction system. Using Primene JMT extractant, it was noted that the extraction of titanium was independent of hydrogen ion concentration and rather depended more heavily on the aqueous to organic solvent ratio (A/O) with better extractions recorded using higher organic ratios.

Molybdenum is another trace element which is typically extracted as a primary product or as a by-product in the copper production (Aydin et al. 2013). It is used in the production of corrosion and heat resistant stainless-steel alloys which accounts for 85% of all Mo consumption (IMO, 2020). In addition to its industrial applications, molybdenum is also a biological micronutrient essential to all living organisms where it functions as a co-factor in many different enzymatic reactions. By comparison, molybdenum distribution among chemical species CFA samples has been shown to follow a much more linear distribution when measured as a function of solubility. Aydin et al. (2013) conducted a sequential chemical separation analysis for molybdenum in coal ash separating occurrences into seven fractions: water soluble, exchangeable, carbonate, reducible, oxidizable, sulfide, and residuals. Results from this analysis showed the greatest fraction of molybdenum in this sample was present in the sulfide fraction with only about 26% of Mo left in undigested residuals. Long-term direct leaching of CFA samples under conditions meant to simulate those created by acid rain was performed by Lange et al. (2019) showed the higher mobility of Mo in CFA samples as compared to other leached elements. After 336 days of leaching under mildly acidic conditions, 70.7% of Mo had been leached from the sample; markedly higher than arsenic which was the second most leached element with 36.8% efficiency. A complete process for the extraction and recovery of Mo from CFA proposed by Ogata et al. (2011) involved first leaching ash samples under acidic conditions at pH 2. After adjusting the solution pH to 3 using sodium hydroxide, gibbsite, an amorphous aluminum oxide that had been calcined at 400 °C, was added to adsorb Mo in the leachate solution. Adsorption of Mo onto the gibbsite was shown to be associated with ion exchange and was capable of recovering 90% of Mo from fly ash leachate.

14.10 Radioactive Elements

Radioactive elements such as uranium have a large variety of industrial applications varying from energy production to medicine. Compared to other elements extracted from coal and coal by-products, the extraction of uranium from coal is not a novel concept. Coal is considered as a source of uranium for both the Soviet Union, Russia and the United States. The coal deposits, particularly rich in uranium, can be considered as a source of uranium for industrial extraction (Seredin 2012). The concentration of uranium in coal typically varies from 0.5 to 10.0 ppm; however, certain uranium-rich coals can have its concentrations upwards of hundreds or even thousands of ppm (Dai et al. 2015). The uranium removal from CFA has also paid attention on the grounds of environmental concerns which look to avoid the disposal of any coal ash contaminated with radioactive material into the environment. Though attention has steadily been drawn away from coal as a source for uranium after the discovery of other larger and richer deposits in other formations. In certain cases, enriched coal and coal combustion residues can still serve as an economically viable supplementary source for uranium (Table 14.4).

Maslov et al. (2010) utilized brown CFA of Mongolia as a resource for uranium recovery. Uranium was leached from the ash using an acid mixture of 8 M H_2SO_4 and 10% HF. A leaching period of 24 h resulted in leaching levels for uranium and radium of 99% and 97%, respectively. Afterwards, uranium could be selectively extracted from the leaching solution by an anion exchanger using Dowex 2 × 8 resin. Ash samples taken after leaching showed no natural radioactive elements demonstrating the efficiency of developed process for uranium extraction in order to remove hazardous radioactive elements from disposable CFA. A similar acid leach system approach for uranium extraction from coal ash samples was adopted by

Table 14.4 Extraction and separation of radioactive elements from CFA using different methods

Element(s)	Method (s)	Experimental conditions	Percent recovery	Reference
U, Ra	Acid leaching, anion exchange	Leaching: $[HNO_3] = 8$ M, $[HF] = 10\%$ in mixture, 24 h; Dowex 1X8 anion exchange resin, 2 M HCl eluent	Leaching-99% U, 97% Ra Anion exchange-90% U	Maslov et al. (2010)
U	Roasting, acid leaching	Roasting: 50% $CaCl_2$, 900 °C, 2 h Leaching: $[HNO_3] = 1$ M, 1 h	87.3% U	Lei et al. (2014)
U, Hf, Zr	Adsorption, precipitation	Dowex 1X8 anion exchange resin, 5 ml/min, pH = 1.5, H_2O_2 at pH = 1.5–3.5	78.73% U, 98.7% Zr, 20.5% Hf	Abd El-Hamid et al. (2015)
U	Acid leaching	$[H_2SO_4] = 0.3$ M, solid/liquid = 1:20 (g/L), 12 h, 60 °C	45.82% U	Yang et al. (2018)
Th, U	Precipitation	pH = 4.8 (selective precipitation)	100% Th, 47.9% U	Talan and Huang (2020)

Yang et al. (2018) on uranium-rich coal samples from the Yunnan Province of Southwest China. Around 45.8% uranium was leached using 0.3 M H_2SO_4 as lixiviant, $S/L = 1/20$, 60 °C, for 12 h reaction time. Like other metals and elements present in CFA, coal combustion at very high temperatures results in uranium encapsulation in $\text{SiO}_2\text{-Fe}_2\text{O}_3$ and $\text{SiO}_2\text{-Al}_2\text{O}_3$ lattice structures. This greatly reduces the fraction of active uranium in the CFA and large fractions of uranium left behind in the undigested ash residuals.

Lei et al. (2014) worked to enhance the performance of CFA for uranium leachability using a roast-leach extraction system. Samples of CFA were first mixed with powdered CaCl_2 , then heated to 900 °C for 2 h. Roasting of CFA with the CaCl_2 additive causes Ca to be incorporated into the mineral structural network and substituted for Si in Si-O-Si bonds. The relatively weaker strength of the newly formed Ca-O bond causes the silicate structure to weaken and become more susceptible to an acid attack. Subsequent leaching of roasted CFA under optimized conditions resulted in 87.3% uranium extraction as compared to the 25.5% removal achieved with direct leaching.

Investigations for the separation of uranium from CFA leach liquors have also been conducted. Abd El-Hamid et al. (2015) developed an adsorption process for uranium recovery from petroleum fly ash leach liquor using a Dowex 1X8 anion exchange resin in a packed column. Following elution, uranium was separated from other elements which were co-extracted and was precipitated from the U-rich eluant fractions. Uranium could either be precipitated using NaOH to form a precipitate containing uranium oxide at a purity of 68.5% or by adding hydrogen peroxide which formed precipitate of uranium peroxide at a purity of 94.7%. Talan and Huang (2020) discovered another process to remove dissolved uranium and thorium from acidified leach liquors. This study was concerned with the recovery of rare earth elements using coal and coal combustion products as a secondary resource with the removal of radioactive species as a contaminant rather than a product. A selective precipitation procedure was first employed which removed nearly 100% of Th and 47.9% of U at a pH of 4.8. Following the precipitation procedure, the leach solution was further processed using a two-stage solvent extraction system (50% tributyl phosphate, pH = 3.5, A/O = 1/3) which resulted in 79.6% rare earth recovery with 3.1% co-extraction of uranium.

14.11 Precious Metals

Gold, silver, platinum, and other precious noble metals have a vast number of applications across various industries. Gold has been used in jewelry from ancient to the present time. Other applications of gold and other precious metals include their use in electronics as a conductor and as industrial catalysts to reduce the levels of harmful emissions released into the atmosphere. Innovations in how we use these metals have been mirrored with innovation into new metal sources and methods for their extraction. Gold extraction from coal sources was first done in the United States

more than 100 years ago. As high-grade primary sources for precious metals are becoming increasingly scarce, attention has been drawn back towards coal and coal combustion residues as a potential secondary resource for these elements. Oleinikova et al. (2019) reported distribution of different elements including precious metals in brown coal samples of Amur river region. The average concentration for gold is found to be 3.0 and 4.4 parts per billion (ppb) in low-rank and hard coals, respectively (Dai et al. 2018). Despite these low averages for gold and other similarly low concentrations for other precious metals, certain coal deposits are particularly enriched in these metals. Correlations between coal compositions and Au have also been discovered with higher Au content shown to occur in coal with Si content between 6000 ppm and 8000 ppm and in coal particularly enriched in Ge (Chehreh Chelgani and Hower 2018; Dai et al. 2018). All precious metals have also shown a strong correlation with coal ash.

As coal is combusted in the high temperature zone of power plants (1200–1400 °C), gold is volatilized and is subsequently deposited on the glass spherules combustion products (Dai et al. 2018). These fine-grained particles of gold on the surface of combustion products were confirmed using scanning electron microscope technique. Seredin and Dai (2014) suggested that the metals could be further enriched using simpler concentrating methods. Based on the Ge-rich fly ash sample tested in this study, it was estimated that dozens of kilograms of Au could be extracted every year from the whole coal deposit using hydrometallurgical methods.

There are several methods which can be used to improve fractions of Au and other precious metals in coal combustion products. Sorokin and Ageev (2018) tested the effectiveness of physical separation methods to improve gold fractions in both furnace slag and CFA. The magnetic fraction of the furnace slag was first removed by magnetic separation and resulting nonmagnetic fraction was further separated into light and heavy particles. The heavy fraction of table concentrates showed a markedly higher gold concentration of 8.31 g/t as compared to the 0.05 and 0.88 g/t of the light fraction and magnetic fraction, respectively. Similar separation procedures on the fly ash sample showed comparable enrichment with gold content of 2.25 g/t in the concentrate compared to 0.93 g/t and 1.54 g/t in the light fraction and magnetic fraction, respectively. Chen et al. (2019) conducted a similar study which investigated the ability to use physical separation methods to enhance precious metal fractions in ash samples. Using gravity separation and flotation, platinum and palladium reached enrichment coefficients of 1.9 and 1.6, respectively, with corresponding recovery of 97% and 88%, respectively.

14.12 Economic Considerations

The huge consumption of primary REE sources lead to the scarcity of shortage in supply of REE. The recovery of REE from coal ash potentially converts the waste to value and supports the circular economy by linking coal mining, electric power, and REE industries. The CFA produced from the burning of coal has low

concentration of total REE but has high concentration of some expensive elements such as Sc and Nd. The economic feasibility of the developed process is generally evaluated using a modeling tool, Techno-economic analysis (TEA) (Das et al. 2018) before running at industrial scale. It is often used to make governmental decisions on different research projects in public sector. Cost and revenue are the two important parameters to analyze the economic feasibility of the process. The capital, labor, energy, reagents, and transport are the categories of cost. The revenue includes the selling price of the recovered REE and fly ash residue if good enough for other applications. Das et al. (2018) performed TEA for the supercritical extraction of REE from the samples of CFA. The value of recovered REE oxides per ton CFA is estimated to vary in between \$6–\$557 with a median of \$250. The scenario with high recovery of Sc from CFA with low cost input was found feasible with high revenue. Franus et al. (2015) analyzed twelve CFA samples for their elemental composition and sample number 6 obtained from bituminous coal combustion was found rich in individual and total REE content (543 ppm). Based on the data of sample number 6 and some reported data of elements in CFA samples, the maximum amount of elements in USD per metric ton of the fly ash has been calculated and summarized in Table 14.5. Noted that about 92% of the REE value in fly ash of this sample was with Sc, and total value of REE (excluding Sc) was below \$18, meaning the main target REE for extraction from fly ash should be Sc. Any element value >20 USD per metric ton of fly ash is considered as potentially possible for a beneficial recovery from fly ash. However, a value <20 USD is indication of non-economic feasible recovery of the element. In case of REE, most of the elements have value <20 USD except scandium. In spite of this, the total REE content, i.e., 543 ppm, is responsible for a significant value of 224.71 USD per metric ton of fly ash and can lead to economically feasible recovery compared to cost parameters.

14.13 Conclusion

This detailed review work provides a systematic description of advances in hydrometallurgical processes developed globally for the separation and recovery of REE and other potential elements such as aluminum, selenium, gallium, germanium, vanadium, lithium, calcium, magnesium, titanium, molybdenum, radioactive, and precious elements from CFA. The REE and other metal values will hold their importance in future due to their high demand in emerging fields. Improvement in the developed methods and discovery of a new path with safe environment and cost effectiveness are the potential way for the separation and recovery of metals from coal fly ash. The REE recovered from CFA may find applications in clean energy technologies such as electric vehicles, phosphors, and wind turbines. The recycling of CFA will help to reduce the environmental burden of hazardous waste and will improve the economy. The involvement of biohydrometallurgy in CFA recycling will result in fruitful results with several advantages such as minimization of waste production, no toxic gas emission, and clean extraction resulting in high REE and

Table 14.5 Price of elements and their concentrations in CFA sample with maximum element value in USD/metric ton CFA

REE	Price (USD/kg) (USGS 2020; Wikipedia 2020)	Concentration(ppm) (Franus et al. 2015)	Max. value (USD/metric ton CFA)	Other elements	Price (USD/kg) (USGS 2020; Wikipedia 2020)	Concentration (ppm) (Font et al. 2005; Franus et al. 2015)	Max. value (USD/metric ton CFA)
Scandium	4600	45.00	207	Aluminum	2.2	150,000	330.00
Yttrium	3	73.20	0.22	Selenium	44	4.2	0.18
Lanthanum	2	81.700	0.16	Gallium	570	186	106.02
Cerium	2	172.50	0.35	Germanium	1240	289	358.36
Praseodymium	65	20.51	1.33	Vanadium	26.22	500	13.11
Neodymium	50	81.30	4.07	Lithium	13	66	0.86
Samarium	2	17.00	0.03	Magnesium	5.22	2290	11.95
Europium	77	3.81	0.29	Calcium	2.21	2880	6.36
Gadolinium	37	14.65	0.54	Titanium	11.35	1380	15.66
Terbium	501	2.40	1.20	Molybdenum	26	18.4	0.48
Dysprosium	189	12.18	2.30	Uranium	101	10	1.01
Holmium	350	2.58	0.90	Gold	45,016	1.9	85.53
Erbium	180	7.41	1.33				
Thulium	3000	1.07	3.21				
Ytterbium	69	6.74	0.47				
Lutetium	1258	1.03	1.30				
Total REE value		543.08	224.71				

potential metals recovery. We believe the summarized information will be of keen interest for the people working in the area of REE/other potential metals extraction from CFA samples of different origin and will provide future research direction for utilizing CFA waste for wealth.

References

- Abd El-Hamid, A. A. M., & Abu Khoziem, H. A. (2019). Physical and chemical characterization of El Kriymat boiler ash to optimize the leachability of some valuable elements. *Journal of Environmental Chemical Engineering*, 7, 103362. <https://doi.org/10.1016/j.jece.2019.103362>.
- Abd El-Hamid, A. M., Zahran, M. A., Abou Elthana, S. M., et al. (2015). Recovery of uranium, hafnium and zirconium from petroleum ash leach liquor. *RSC Advances*, 5, 80245–80253. <https://doi.org/10.1039/c5ra11563a>.
- Abhilash, & Akcil, A. (2020). *Critical and rare earth elements: Recovery from secondary resources*. New York: CRC Press.
- Akcil, A., Vegliò, F., Ferella, F., et al. (2015). A review of metal recovery from spent petroleum catalysts and ash. *Waste Management*, 45, 420–433. <https://doi.org/10.1016/j.wasman.2015.07.007>.
- Arroyo, F., & Fernández-Pereira, C. (2008). Hydrometallurgical recovery of germanium from coal gasification fly ash. Solvent extraction method. *Industrial and Engineering Chemistry Research*, 47, 3186–3191. <https://doi.org/10.1021/ie7016948>.
- Arroyo, F., Fernández-Pereira, C., & Bermejo, P. (2015). Demonstration plant equipment design and scale-up from pilot plant of a leaching and solvent extraction process. *Minerals*, 5, 298–313. <https://doi.org/10.3390/min5020298>.
- Arroyo, F., Font, O., Chimenos, J. M., et al. (2014). IGCC fly ash valorisation. Optimisation of Ge and Ga recovery for an industrial application. *Fuel Processing Technology*, 124, 222–227. <https://doi.org/10.1016/j.fuproc.2014.03.004>.
- Arroyo Torralvo, F., Fernández-Pereira, C., García Villard, E., et al. (2018). Low environmental impact process for germanium recovery from an industrial residue. *Minerals Engineering*, 128, 106–114. <https://doi.org/10.1016/j.mineng.2018.07.022>.
- Aydin, F., Saydut, A., Gunduz, B., et al. (2013). Molybdenum speciation in coal bottom ash using a sequential extraction procedure and determination by FAAS. *Energy Sources, Part A Recover Utilization Environmental Effects*, 35, 2356–2363. <https://doi.org/10.1080/15567036.2010.535102>.
- Bai, G. H., Teng, W., Wang, X. G., et al. (2010). Alkali desilicated coal fly ash as substitute of bauxite in lime-soda sintering process for aluminum production. *Transactions of the Nonferrous Metals Society of China*, 20, 169–175. [https://doi.org/10.1016/S1003-6326\(10\)60034-9](https://doi.org/10.1016/S1003-6326(10)60034-9).
- Balaram, V. (2019). Rare earth elements: A review of applications, occurrence, exploration, analysis, recycling, and environmental impact. *Geoscience Frontiers*, 10, 1285–1303. <https://doi.org/10.1016/j.gsf.2018.12.005>.
- Blissett, R. S., & Rowson, N. A. (2012). A review of the multi-component utilisation of coal fly ash. *Fuel*, 97, 1–23. <https://doi.org/10.1016/j.fuel.2012.03.024>.
- Cantrell, M. A. (2014). *Leaching characteristics of selenium from coal fly ash*. University of Arkansas.
- Cao, S., Zhou, C., Pan, J., et al. (2018). Study on influence factors of leaching of rare earth elements from coal fly ash. *Energy and Fuels*, 32, 8000–8005. <https://doi.org/10.1021/acs.energyfuels.8b01316>.
- Chehreh Chelgani, S., & Hower, J. C. (2018). Relationships between noble metals as potential coal combustion products and conventional coal properties. *Fuel*, 226, 345–349. <https://doi.org/10.1016/j.fuel.2018.04.041>.

- Chen, T., Yan, B., Li, L., et al. (2019). Mineralogy characteristic study and exploration on the valuable metals enrichment of coal fly ash. *Advances in Polymer Technology*, 2019, 1–7. <https://doi.org/10.1155/2019/1839450>.
- Choo, T. K., Cashion, J., Selomulya, C., & Zhang, L. (2016). Reductive leaching of iron and magnesium out of Magnesioferrite from Victorian Brown coal fly ash. *Energy and Fuels*, 30, 1162–1170. <https://doi.org/10.1021/acs.energyfuels.5b01979>.
- Dai, S., & Finkelman, R. B. (2018). Coal as a promising source of critical elements—progress and future prospects. *International Journal of Coal Geology*, 186, 155–164.
- Dai, S., Yan, X., Ward, C. R., et al. (2018). Valuable elements in Chinese coals: A review. *International Geology Review*, 60, 590–620. <https://doi.org/10.1080/00206814.2016.1197802>.
- Dai, S., Yang, J., Ward, C. R., et al. (2015). Geochemical and mineralogical evidence for a coal-hosted uranium deposit in the Yili Basin, Xinjiang, northwestern China. *Ore Geology Reviews*, 70, 1–30. <https://doi.org/10.1016/j.oregeorev.2015.03.010>.
- Dai, S., Zhao, L., Peng, S., et al. (2010). Abundances and distribution of minerals and elements in high-alumina coal fly ash from the Jungar Power Plant, Inner Mongolia, China. *International Journal of Coal Geology*, 81, 320–332.
- Dan, Y., Zimmerman, C., Liu, K., et al. (2013). Increased leaching of As, Se, Mo, and v from high calcium coal ash containing trona reaction products. *Energy and Fuels*, 27, 1531–1537. <https://doi.org/10.1021/ef3020469>.
- Das, S., Gaustad, G., Sekar, A., & Williams, E. (2018). Techno-economic analysis of supercritical extraction of rare earth elements from coal ash. *Journal of Cleaner Production*, 189, 539–551. <https://doi.org/10.1016/j.jclepro.2018.03.252>.
- Ding, J., Ma, S., Shen, S., et al. (2017). Research and industrialization progress of recovering alumina from fly ash: A concise review. *Waste Management*, 60, 375–387. <https://doi.org/10.1016/j.wasman.2016.06.009>.
- Doucet, F. J., Mohamed, S., Neyt, N., et al. (2016). Thermochemical processing of a south African ultrafine coal fly ash using ammonium sulphate as extracting agent for aluminium extraction. *Hydrometallurgy*, 166, 174–184. <https://doi.org/10.1016/j.hydromet.2016.07.017>.
- Dwivedi, A., & Jain, M. (2014). Fly ash—Waste management and overview : A review. *Recent Research in Science and Technology*, 6, 30–35.
- Fan XL, Lv SQ, Xia JL, et al (2019) Extraction of Al and Ce from coal fly ash by biogenic Fe³⁺ and H₂SO₄. *Chemical Engineering Journal* 370:1407–1424. doi:<https://doi.org/10.1016/j.cej.2019.04.014>.
- Font, O., Querol, X., López-Soler, A., et al. (2005). Ge extraction from gasification fly ash. *Fuel*, 84, 1384–1392. <https://doi.org/10.1016/j.fuel.2004.06.041>.
- Franus, W., Wiatros-Motyka, M. M., & Wdowin, M. (2015). Coal fly ash as a resource for rare earth elements. *Environmental Science and Pollution Research*, 22, 9464–9474. <https://doi.org/10.1007/s11356-015-4111-9>.
- Gajam, S. Y., & Raghavan, S. (1985). A kinetic model for the hydrochloric acid leaching of kaolinite clay in the presence of fluoride ions. *Hydrometallurgy*, 15, 143–158. [https://doi.org/10.1016/0304-386X\(85\)90050-7](https://doi.org/10.1016/0304-386X(85)90050-7).
- Ganguli, R., & Cook, D. R. (2018). Rare earths: A review of the landscape. *MRS Energy Sustainability*, 5, 1–16. <https://doi.org/10.1557/mre.2018.7>.
- Gollakota, A. R. K., Volli, V., & Shu, C. M. (2019). Progressive utilisation prospects of coal fly ash: A review. *Science of the Total Environment*, 672, 951–989. <https://doi.org/10.1016/j.scitotenv.2019.03.337>.
- Goodenough, K. M., Wall, F., & Merriman, D. (2018). The rare earth elements: Demand, global resources, and challenges for resourcing future generations. *Natural Resources Research*, 27, 201–216. <https://doi.org/10.1007/s11053-017-9336-5>.
- Guo, C., Zou, J., Wei, C., & Jiang, Y. (2013a). Comparative study on extracting alumina from circulating fluidized-bed and pulverized-coal fly ashes through salt activation. *Energy and Fuels*, 27, 7868–7875. <https://doi.org/10.1021/ef401659e>.

- Guo, Y., Li, J., Yan, K., et al. (2019). A prospective process for alumina extraction via the co-treatment of coal fly ash and bauxite red mud: Investigation of the process. *Hydrometallurgy*, 186, 98–104. <https://doi.org/10.1016/j.hydromet.2019.04.011>.
- Guo, Y., Li, Y., Cheng, F., et al. (2013b). Role of additives in improved thermal activation of coal fly ash for alumina extraction. *Fuel Processing Technology*, 110, 114–121. <https://doi.org/10.1016/j.fuproc.2012.12.003>.
- Guo, Y., Zhao, Q., Yan, K., et al. (2014). Novel process for alumina extraction via the coupling treatment of coal gangue and bauxite red mud. *Industrial and Engineering Chemistry Research*, 53, 4518–4521. <https://doi.org/10.1021/ie500295t>.
- Guo, Y., Zhao, Z., Zhao, Q., & Cheng, F. (2017). Novel process of alumina extraction from coal fly ash by pre-desilicating—Na₂CO₃ activation—Acid leaching technique. *Hydrometallurgy*, 169, 418–425. <https://doi.org/10.1016/j.hydromet.2017.02.021>.
- Harada, Y., Kurata, N., & Furuno, G. (1993). Simultaneous determination of major constituents and impurities in high purity mullite using pressure acid decomposition. *Analytical Sciences*, 9, 99–103. <https://doi.org/10.2116/analsci.9.99>.
- He, H., Pang, J., Wu, G. L., & Lambers, H. (2019). The application potential of coal fly ash for selenium biofortification. *Advances in Agronomy*, 157, 1–54. <https://doi.org/10.1016/bs.agron.2019.05.002>.
- He, K. Q., Yuan, C. G., Shi, M. D., & Jiang, Y. H. (2020b). Accelerated screening of arsenic and selenium fractions and bioavailability in fly ash by microwave assistance. *Ecotoxicology and Environmental Safety*, 187, 109820. <https://doi.org/10.1016/j.ecoenv.2019.109820>.
- He, K. Q., Yuan, C. G., Shi, M. D., et al. (2020a). Fractions of arsenic and selenium in fly ash by ultrasound-assisted sequential extraction. *RSC Advances*, 10, 9226–9233. <https://doi.org/10.1039/c9ra08481a>.
- Honaker, R. Q., Zhang, W., & Werner, J. (2019). Acid leaching of rare earth elements from coal and coal ash: Implications for using fluidized bed combustion to assist in the recovery of critical materials. *Energy and Fuels*, 33, 5971–5980. <https://doi.org/10.1021/acs.energyfuels.9b00295>.
- Hosseini, T., Eng, Y. L., & Zhang, L. (2013). Using regenerative ammonium salt to extract and purify magnesium oxide from Victorian Brown coal fly ash. *World Coal Ash*, 1–14.
- Hosseini, T., Selomulya, C., Haque, N., & Zhang, L. (2014). Indirect carbonation of victorian brown coal fly ash for CO₂ sequestration: Multiple-cycle leaching-carbonation and magnesium leaching kinetic modeling. *Energy and Fuels*, 28, 6481–6493. <https://doi.org/10.1021/ef5014314>.
- Hu, P., Hou, X., Zhang, J., et al. (2018). Distribution and occurrence of lithium in high-alumina-coal fly ash. *International Journal of Coal Geology*, 189, 27–34. <https://doi.org/10.1016/j.coal.2018.02.011>.
- IEA. (2019a). *Coal 2019*. Paris: IEA. <https://www.iea.org/reports/coal-2019>.
- IEA. (2019b). *World total coal production, 1971–2018*. Paris: IEA. <https://www.iea.org/data-and-statistics/charts/world-total-coal-production-1971-2018>.
- IEA. (2020). *Coal information: Overview*. Paris: IEA. <https://www.iea.org/reports/coal-information-overview>.
- International Molybdenum Association (IMOA). (2020). <https://www.imoa.info/index.php>.
- Jung, M., & Mishra, B. (2018). Vanadium recovery from oil fly ash by carbon removal and roast-leach process. *JOM*, 70, 168–172. <https://doi.org/10.1007/s11837-017-2653-7>.
- Jyothi, R. K., Thenepalli, T., Ahn, J. W., et al. (2020). Review of rare earth elements recovery from secondary resources for clean energy technologies: Grand opportunities to create wealth from waste. *Journal of Cleaner Production*, 267, 122048. <https://doi.org/10.1016/j.jclepro.2020.122048>.
- Kalembkiewicz, J., & Chmielarz, U. (2014). Functional speciation and leachability of titanium group from industrial fly ash. *Fuel*, 123, 73–78. <https://doi.org/10.1016/j.fuel.2014.01.060>.
- Kamran Haghighi, H., Irannajad, M., Fortuny, A., & Sastre, A. M. (2018). Recovery of germanium from leach solutions of fly ash using solvent extraction with various extractants. *Hydrometallurgy*, 175, 164–169. <https://doi.org/10.1016/j.hydromet.2017.11.006>.

- Ketris, M. P., & Yudovich, Y. E. (2009). Estimations of Clarkes for carbonaceous biolithes: World averages for trace element contents in black shales and coals. *International Journal of Coal Geology*, 78, 135–148. <https://doi.org/10.1016/j.coal.2009.01.002>.
- King, J. F., Taggart, R. K., Smith, R. C., et al. (2018). Aqueous acid and alkaline extraction of rare earth elements from coal combustion ash. *International Journal of Coal Geology*, 195, 75–83. <https://doi.org/10.1016/j.coal.2018.05.009>.
- Kumari, A., Parween, R., Chakravarty, S., et al. (2019). Novel approach to recover rare earth metals (REMs) from Indian coal bottom ash. *Hydrometallurgy*, 187, 1–7. <https://doi.org/10.1016/j.hydromet.2019.04.024>.
- Kursun Unver, I., & Terzi, M. (2018). Distribution of trace elements in coal and coal fly ash and their recovery with mineral processing practices: A review. *Journal of Mining and Environment*, 9, 641–655. <https://doi.org/10.22044/jme.2018.6855.1518>.
- Lange, C. N., Flues, M., Hiromoto, G., et al. (2019). Long-term leaching of as, cd, Mo, Pb, and Zn from coal fly ash in column test. *Environmental Monitoring and Assessment*, 191, 1–12. <https://doi.org/10.1007/s10661-019-7798-0>.
- Lanzerstorfer, C. (2018). Pre-processing of coal combustion fly ash by classification for enrichment of rare earth elements. *Energy Reports*, 4, 660–663. <https://doi.org/10.1016/j.egy.2018.10.010>.
- Lei, X., Qi, G., Sun, Y., et al. (2014). Removal of uranium and gross radioactivity from coal bottom ash by CaCl₂ roasting followed by HNO₃ leaching. *Journal of Hazardous Materials*, 276, 346–352. <https://doi.org/10.1016/j.jhazmat.2014.05.052>.
- Li, H., Hui, J., Wang, C., et al. (2014). Extraction of alumina from coal fly ash by mixed-alkaline hydrothermal method. *Hydrometallurgy*, 147–148, 183–187. <https://doi.org/10.1016/j.hydromet.2014.05.012>.
- Li, H., Liu, G., Sun, R., et al. (2013). Relationships between trace element abundances and depositional environments of coals from the Zhangji coal mine, Anhui Province, China. *Energy Exploration & Exploitation*, 31, 89–107. <https://doi.org/10.1260/0144-5987.31.1.89>.
- Li, S., Bo, P., Kang, L., et al. (2020). Activation pretreatment and leaching process of high-alumina coal fly ash to extract lithium and aluminum. *Metals (Basel)*, 10, 1–14. <https://doi.org/10.3390/met10070893>.
- Li, S., Qin, S., Kang, L., et al. (2017). An efficient approach for lithium and aluminum recovery from coal fly ash by pre-desilication and intensified acid leaching processes. *Metals (Basel)*, 7, 272, 1–12. <https://doi.org/10.3390/met7070272>.
- Lin, R., Stuckman, M., Howard, B. H., et al. (2018). Application of sequential extraction and hydrothermal treatment for characterization and enrichment of rare earth elements from coal fly ash. *Fuel*, 232, 124–133. <https://doi.org/10.1016/j.fuel.2018.05.141>.
- Liu, P., Huang, R., & Tang, Y. (2019). Comprehensive understandings of rare earth element (REE) speciation in coal fly ashes and implication for REE extractability. *Environmental Science & Technology*, 53, 5369–5377. <https://doi.org/10.1021/acs.est.9b00005>.
- Liu, Y., Liu, G., Qu, Q., et al. (2017). Geochemistry of vanadium (V) in Chinese coals. *Environmental Geochemistry and Health*, 39, 967–986. <https://doi.org/10.1007/s10653-016-9877-2>.
- Ma, Z., Zhang, S., Zhang, H., & Cheng, F. (2019). Novel extraction of valuable metals from circulating fluidized bed-derived high-alumina fly ash by acid-alkali-based alternate method. *Journal of Cleaner Production*, 230, 302–313. <https://doi.org/10.1016/j.jclepro.2019.05.113>.
- Maslov, O. D., Tserenpil, S., Norov, N., et al. (2010). Uranium recovery from coal ash dumps of Mongolia. *Solid Fuel Chemistry*, 44, 433–438. <https://doi.org/10.3103/S0361521910060133>.
- Meawad, A. S., Bojinova, D. Y., & Pelovski, Y. G. (2010). An overview of metals recovery from thermal power plant solid wastes. *Waste Management*, 30, 2548–2559. <https://doi.org/10.1016/j.wasman.2010.07.010>.
- Meer, I., & Nazir, R. (2018). Removal techniques for heavy metals from fly ash. *Journal of Material Cycles Waste Management*, 20, 703–722. <https://doi.org/10.1007/s10163-017-0651-z>.
- Mondal, S., Ghar, A., Satpati, A. K., et al. (2019). Recovery of rare earth elements from coal fly ash using TEHDGA impregnated resin. *Hydrometallurgy*, 185, 93–101. <https://doi.org/10.1016/j.hydromet.2019.02.005>.

- Ogata, F., Tominaga, H., Yabutani, H., et al. (2011). Recovery of molybdenum from fly ash by gibbsite. *Toxicological and Environmental Chemistry*, 93, 635–642. <https://doi.org/10.1080/00272248.2011.558508>.
- Ohenoja, K., Pesonen, J., Yliniemi, J., & Illikainen, M. (2020). Utilization of fly ashes from fluidized bed combustion: A review. *Sustainability*, 12, 1–26. <https://doi.org/10.3390/su12072988>.
- Oleinikova, G. A., Vyalov, V. I., & Fadin, Y. Y. (2019). Distribution of trace elements in Brown coals from the Amur River region and in their submicron fractions. *Solid Fuel Chemistry*, 53, 175–183. <https://doi.org/10.3103/S0361521919030078>.
- Pan, J., Nie, T., Vaziri Hassas, B., et al. (2020). Recovery of rare earth elements from coal fly ash by integrated physical separation and acid leaching. *Chemosphere*, 248, 126112. <https://doi.org/10.1016/j.chemosphere.2020.126112>.
- Park, D., Middleton, A., Smith, R., et al. (2020). A biosorption-based approach for selective extraction of rare earth elements from coal byproducts. *Separation and Purification Technology*, 241, 116726. <https://doi.org/10.1016/j.seppur.2020.116726>.
- Park, S., & Liang, Y. (2019). Bioleaching of trace elements and rare earth elements from coal fly ash. *International Journal of Coal Science Technology*, 6, 74–83. <https://doi.org/10.1007/s40789-019-0238-5>.
- Peiravi, M., Ackah, L., Guru, R., et al. (2017). Chemical extraction of rare earth elements from coal ash. *Minerals and Metallurgical Processing*, 34, 170–177. <https://doi.org/10.19150/mmp.7856>.
- Qin, S., Sun, Y., Li, Y., et al. (2015a). Coal deposits as promising alternative sources for gallium. *Earth-Science Reviews*, 150, 95–101. <https://doi.org/10.1016/j.earscirev.2015.07.010>.
- Qin, S., Zhao, C., Li, Y., & Zhang, Y. (2015b). Review of coal as a promising source of lithium. *International Journal of Oil, Gas and Coal Technology*, 9. <https://doi.org/10.1504/IJOGCT.2015.067490>.
- Rahimi, G., Rastegar, S. O., Rahmani Chianeh, F., & Gu, T. (2020). Ultrasound-assisted leaching of vanadium from fly ash using lemon juice organic acids. *RSC Advances*, 10, 1685–1696. <https://doi.org/10.1039/c9ra09325g>.
- Rao, K. A., Serajuddin, M., RamaDevi, G., et al. (2020). On the characterization and leaching of rare earths from a coal fly ash of Indian origin. *Separation Science and Technology*, 1–17. <https://doi.org/10.1080/01496395.2020.1718705>.
- Rasoulnia, P., & Mousavi, S. M. (2016). V and Ni recovery from a vanadium-rich power plant residual ash using acid producing fungi: *Aspergillus Niger* and *Penicillium simplicissimum*. *RSC Advances*, 6, 9139–9151. <https://doi.org/10.1039/c5ra24870a>.
- Rastegar, S. O., Mousavi, S. M., Shojaosadati, S. A., & Sarraf Mamooory, R. (2015). Bioleaching of V, Ni, and Cu from residual produced in oil fired furnaces using *Acidithiobacillus ferrooxidans*. *Hydrometallurgy*, 157, 50–59. <https://doi.org/10.1016/j.hydromet.2015.07.006>.
- Rushwaya, M. J., & Ndlovu, S. (2017). Purification of coal fly ash leach liquor by solvent extraction: Identification of influential factors using Design of Experiments. *International Journal of Mineral Processing*, 164, 11–20. <https://doi.org/10.1016/j.minpro.2017.05.004>.
- Sahoo, P. K., Kim, K., Powell, M. A., & Equeenuddin, S. M. (2016). Recovery of metals and other beneficial products from coal fly ash: A sustainable approach for fly ash management. *International Journal of Coal Science and Technology*, 3, 267–283. <https://doi.org/10.1007/s40789-016-0141-2>.
- Sangita, S., Nayak, N., & Panda, C. R. (2017). Extraction of aluminium as aluminium sulphate from thermal power plant fly ashes. *Transactions of the Nonferrous Metals Society of China*, 27, 2082–2089. [https://doi.org/10.1016/S1003-6326\(17\)60231-0](https://doi.org/10.1016/S1003-6326(17)60231-0).
- Schwartz, G. E., Rivera, N., Lee, S.-W., et al. (2016). Leaching potential and redox transformations of arsenic and selenium in sediment microcosms with fly ash. *Applied Geochemistry*, 67, 177–185. <https://doi.org/10.1016/j.apgeochem.2016.02.013>.
- Seredin, V. V. (2012). From coal science to metal production and environmental protection: A new story of success. *International Journal of Coal Geology*, 90–91, 1–3. <https://doi.org/10.1016/j.coal.2011.11.006>.

- Seredin, V. V., & Dai, S. (2012). Coal deposits as potential alternative sources for lanthanides and yttrium. *International Journal of Coal Geology*, *94*, 67–93. <https://doi.org/10.1016/j.coal.2011.11.001>.
- Seredin, V. V., & Dai, S. (2014). The occurrence of gold in fly ash derived from high-Ge coal. *Mineralium Deposita*, *49*, 1–6. <https://doi.org/10.1007/s00126-013-0497-9>.
- Seredin, V. V., Dai, S., Sun, Y., & Chekryzhov, I. Y. (2013). Coal deposits as promising sources of rare metals for alternative power and energy-efficient technologies. *Applied Geochemistry*, *31*, 1–11.
- Shemi, A., Mpana, R. N., Ndlovu, S., et al. (2012). Alternative techniques for extracting alumina from coal fly ash. *Minerals Engineering*, *34*, 30–37. <https://doi.org/10.1016/j.mineng.2012.04.007>.
- Shemi, A., Ndlovu, S., Sibanda, V., & Van Dyk, L. D. (2014). Extraction of aluminium from coal fly ash: Identification and optimization of influential factors using statistical design of experiments. *International Journal of Mineral Processing*, *127*, 10–15. <https://doi.org/10.1016/j.minpro.2013.12.003>.
- Shemi, A., Ndlovu, S., Sibanda, V., & Van Dyk, L. D. (2015). Extraction of alumina from coal fly ash using an acid leach-sinter-acid leach technique. *Hydrometallurgy*, *157*, 348–355. <https://doi.org/10.1016/j.hydromet.2015.08.023>.
- Shi, Y., xi, J. K., & an, Z. T. (2020a). Cleaner extraction of alumina from coal fly ash: Baking-electrolysis method. *Fuel*, *273*, 117697. <https://doi.org/10.1016/j.fuel.2020.117697>.
- Shi, Y., xi, J. K., & an, Z. T. (2020b). A cleaner electrolysis process to recover alumina from synthetic sulfuric acid leachate of coal fly ash. *Hydrometallurgy*, *191*, 105196. <https://doi.org/10.1016/j.hydromet.2019.105196>.
- Shi, Y., xi, J. K., an, Z. T., & zhi, L. G. (2020c). Cleaner alumina production from coal fly ash: Membrane electrolysis designed for sulfuric acid leachate. *Journal of Cleaner Production*, *243*, 118470. <https://doi.org/10.1016/j.jclepro.2019.118470>.
- Smith, R. C., Taggart, R. K., Hower, J. C., et al. (2019). Selective recovery of rare earth elements from coal fly ash leachates using liquid membrane processes. *Environmental Science & Technology*, *53*, 4490–4499. <https://doi.org/10.1021/acs.est.9b00539>.
- Sorokin, A., Ageev, O. (2018). The technology of gold-containing concentrates recovery from the coal combustion products of the Yerkovetskoye brown coal deposit (the Amur Region, Russia). In: E3S Web of Conferences. pp 1–7.
- Su, H. F., Chen, H., & Lin, J. F. (2020a). A sequential integration approach using *Aspergillus Niger* to intensify coal fly ash as a rare metal pool. *Fuel*, *270*, 117460. <https://doi.org/10.1016/j.fuel.2020.117460>.
- Su, H. F., Tan, F., & Lin, J. F. (2020b). An integrated approach combines hydrothermal chemical and biological treatment to enhance recycle of rare metals from coal fly ash. *Chemical Engineering Journal*, *395*, 124640. <https://doi.org/10.1016/j.cej.2020.124640>.
- Sun, Y., Zhao, C., Li, Y., et al. (2012). Li distribution and mode of occurrences in Li-bearing coal seam # 6 from the Guanbanwusu Mine, Inner Mongolia, northern China. *Energy Exploration & Exploitation*, *30*, 109–130. <https://doi.org/10.1260/0144-5987.30.1.109>.
- Taggart, R. K., Hower, J. C., & Hsu-Kim, H. (2018). Effects of roasting additives and leaching parameters on the extraction of rare earth elements from coal fly ash. *International Journal of Coal Geology*, *196*, 106–114. <https://doi.org/10.1016/j.coal.2018.06.021>.
- Talan, D., & Huang, Q. (2020). Separation of thorium, uranium, and rare earths from a strip solution generated from coarse coal refuse. *Hydrometallurgy*, *197*, 105446. <https://doi.org/10.1016/j.hydromet.2020.105446>.
- Tang, M., Zhou, C., Pan, J., et al. (2019). Study on extraction of rare earth elements from coal fly ash through alkali fusion—Acid leaching. *Minerals Engineering*, *136*, 36–42. <https://doi.org/10.1016/j.mineng.2019.01.027>.
- Tang, Q., Liu, G., Zhou, C., & Sun, R. (2013). Distribution of trace elements in feed coal and combustion residues from two coal-fired power plants at Huainan, Anhui, China. *Fuel*, *107*, 315–322.

- Tang, X. Y., & Huang, W. (2002). Trace elements of coal and its significances on research. *Coal Geology China*, 14, 1–4.
- Tanvar, H., Chauhan, S., & Dhawan, N. (2018). Extraction of aluminum values from fly ash. *Material Today Proc*, 5, 17055–17063. <https://doi.org/10.1016/j.matpr.2018.04.112>.
- Torrvalvo, F. A., & Fernández-Pereira, C. (2011). Recovery of germanium from real fly ash leachates by ion-exchange extraction. *Minerals Engineering*, 24, 35–41. <https://doi.org/10.1016/j.mineng.2010.09.004>.
- Tripathy, A. K., Behera, B., Aishvarya, V., et al. (2019). Sodium fluoride assisted acid leaching of coal fly ash for the extraction of alumina. *Minerals Engineering*, 131, 140–145. <https://doi.org/10.1016/j.mineng.2018.10.019>.
- Tripathy, A. K., Sarangi, C. K., Tripathy, B. C., et al. (2015). Aluminium recovery from NALCO fly ash by acid digestion in the presence of fluoride ion. *International Journal of Mineral Processing*, 138, 44–48. <https://doi.org/10.1016/j.minpro.2015.03.010>.
- Tuan, L. Q., Thenepalli, T., Chilakala, R., et al. (2019). Leaching characteristics of low concentration rare earth elements in Korean (Samcheok) CFBC bottom ash samples. *Sustainability*, 11, 1–11. <https://doi.org/10.3390/su11092562>.
- United State DOE (2017). Report on Rare Earth Elements from Coal and Coal Byproducts. https://www.energy.gov/sites/prod/files/2018/01/f47/EXEC-2014-000442_for_Conrad_Regis_2.2.17.pdf.
- USGS (2020). Mineral commodity summaries 2020. U. S Geological Survey.
- Valeev, D., Kunilova, I., Alpatov, A., et al. (2019). Complex utilisation of Ekibastuz brown coal fly ash: Iron & carbon separation and aluminum extraction. *Journal of Cleaner Production*, 218, 192–201. <https://doi.org/10.1016/j.jclepro.2019.01.342>.
- Wang, T., Wang, J., Burken, J. G., et al. (2007). The leaching characteristics of selenium from coal fly ashes. *Journal of Environmental Quality*, 36, 1784–1792. <https://doi.org/10.2134/jeq2007.0143>.
- Wang, T., Wang, J., Tang, Y., et al. (2009). Leaching characteristics of arsenic and selenium from coal fly ash: Role of calcium. *Energy and Fuels*, 23, 2959–2966. <https://doi.org/10.1021/ef900044w>.
- Wang, Z., Dai, S., Zou, J., et al. (2019). Rare earth elements and yttrium in coal ash from the Luzhou power plant in Sichuan, Southwest China: Concentration, characterization and optimized extraction. *International Journal of Coal Geology*, 203, 1–14. <https://doi.org/10.1016/j.coal.2019.01.001>.
- Wei, C., Cheng, S., Zhu, F., et al. (2018). Digesting high-aluminum coal fly ash with concentrated sulfuric acid at high temperatures. *Hydrometallurgy*, 180, 41–48. <https://doi.org/10.1016/j.hydromet.2018.07.004>.
- Wen, Z., Zhou, C., Pan, J., et al. (2020). Recovery of rare-earth elements from coal fly ash via enhanced leaching. *International Journal of Coal Preparation and Utilization*, 1–15. <https://doi.org/10.1080/19392699.2020.1790537>.
- Wikipedia (2020). Prices of chemical elements. https://en.wikipedia.org/wiki/Prices_of_chemical_elements
- Wu, C. Y., Yu, H. F., & Zhang, H. F. (2012). Extraction of aluminum by pressure acid-leaching method from coal fly ash. *Transactions of the Nonferrous Metals Society of China*, 22, 2282–2288. [https://doi.org/10.1016/S1003-6326\(11\)61461-1](https://doi.org/10.1016/S1003-6326(11)61461-1).
- Xiao, W. D., Yang, X., & Zhang, P. (2015). Study of process mineralogy for hydrometallurgical extraction of vanadium and aluminum from bone coal. *Minerals and Metallurgical Processing*, 32, 155–160. <https://doi.org/10.1007/bf03402283>.
- Yang, Q. C., Ma, S. H., Zheng, S. L., & Zhang, R. (2014). Recovery of alumina from circulating fluidized bed combustion Al-rich fly ash using mild hydrochemical process. *Transactions of the Nonferrous Metals Society of China*, 24, 1187–1195. [https://doi.org/10.1016/S1003-6326\(14\)63178-2](https://doi.org/10.1016/S1003-6326(14)63178-2).

- Yang, Z., Li, Y., Ning, Y., et al. (2018). Effects of oxidant and particle size on uranium leaching from coal ash. *Journal of Radioanalytical and Nuclear Chemistry*, 317, 801–810. <https://doi.org/10.1007/s10967-018-5963-5>.
- Zhai, J., Wang, H., Chen, P., et al. (2020). Recycling of iron and titanium resources from early tailings: From fundamental work to industrial application. *Chemosphere*, 242, 125178.
- Zhang W, Groppo J, Honaker R (2015a) Ash Beneficiation for REE Recovery. In: 2015 World of Coal AshWorld of Coal Ash. pp 1–11.
- Zhang, W., Rezaee, M., Bhagavatula, A., et al. (2015b). A review of the occurrence and promising recovery methods of rare earth elements from coal and coal by-products. *International Journal of Coal Preparation and Utilization*, 35, 295–330. <https://doi.org/10.1080/19392699.2015.1033097>.
- Zhang, Y., Li, M., Liu, D., et al. (2019). Aluminum and iron leaching from power plant coal fly ash for preparation of polymeric aluminum ferric chloride. *Environment Technology (United Kingdom)*, 40, 1568–1575. <https://doi.org/10.1080/09593330.2018.1426639>.
- Zhao, Z., Cui, L., Guo, Y., et al. (2020). Recovery of gallium from sulfuric acid leach liquor of coal fly ash by stepwise separation using P507 and Cyanex 272. *Chemical Engineering Journal*, 381, 122699. <https://doi.org/10.1016/j.cej.2019.122699>.
- Zhu, P. W., Dai, H., Han, L., et al. (2015). Aluminum extraction from coal ash by a two-step acid leaching method. *Journal of Zhejiang University Science A*, 16, 161–169. <https://doi.org/10.1631/jzus.A1400195>.

Chapter 15

Coal Fly Ash Utilisation and Environmental Impact



Shanjida Sultana, Saifuddin Ahsan, Sakib Tanvir, Nawshad Haque, Firoz Alam, and Mohan Yellishetty

15.1 Introduction

The fine residue left after the coal burning contained within the flu gas exiting through chimney is called fly ash. Historically, fly ash was a waste product and contributed to environmental pollution. Coal-fired power plants are the largest generator of fly ash. Mined coal is transported to coal bunker or storage of a power plant from where it is sent to mill/pulveriser via conveyer belt. The milled coal or pulverised dust coal is blown to boiler from pulveriser by hot air. The combustion is instantaneous, and the coal burning raises the temperature inside the boiler up to 1300 °C. The carbon content in the coal dust is burnt in less than a second leaving all noncombustible materials/minerals as stream vapour rises through the boiler. As the stream rises and cools down, it solidifies into fly ash micro bits predominantly made up of mullite ($3\text{Al}_2\text{O}_3 \cdot 2\text{SiO}_2$), quartz (SiO_2), calcite or lime (CaO), and haematite (Fe_2O_3). It is also at this point that fly ash sets its characteristics. An electron

S. Sultana

Institute of Mining, Mineralogy and Metallurgy, Bangladesh Council of Scientific and Industrial Research (BCSIR), Joypurhat, Bangladesh

S. Ahsan · S. Tanvir

North West Power Generation Company Limited (NWPGL), Dhaka, Bangladesh

N. Haque (✉)

Commonwealth Scientific and Industrial Research Organisation (CSIRO), Melbourne, VIC, Australia

e-mail: nawshad.haque@csiro.au

F. Alam

School of Engineering (Aerospace, Mechanical and Manufacturing), RMIT University, Melbourne, VIC, Australia

M. Yellishetty

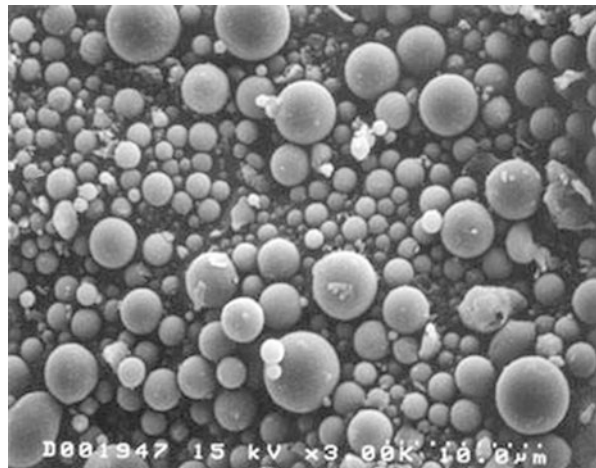
Department of Civil of Engineering, Monash University, Clayton, VIC, Australia

microscopic image of fly ash is shown in Fig. 15.1. The burning temperature, residue of burning time, and cooling rate influence the characteristics including the chemistry of fly ash. Generally, without treatment, the smoke coming out of a chimney stack is in fact the fly ash as shown in Fig. 15.2a. However, most fly ash is captured using Electro-Static Precipitators (ESP) or Fabric Filter Bag as shown in Fig. 15.2b. The captured fly ash conveys to ash silo from where ash carrying truck collects and removes the fly ash from the power plant. As shown in Fig. 15.3, if the fly ash is not removed from the silo, it is liquefied using water and pumped through pipe to nearest ash ponds for later collection or land fill. To reduce the environmental and occupational safety and health hazards, the process of receiving/removing fly ash, quality procedures, quality testing—all must be undertaken and managed by highly skilled and motivated personnel. To get best results, it is utmost important to employ competent and professional staff for dealing with the fly ash.

In addition to fly ash, the noncombustible coarser component (clinkers, slag, impurities, etc.) of coal (approximately 10% of the total waste) settles to the bottom of the power plant's boiler which is called bottom ash. It is mainly used as land fill material. A typical flow chart for bottom ash and fly ash collection in a coal-fired power plant is shown in Fig. 15.4.

Although coal is discouraged to be used for power generation for minimising environmental impact, coal is expected to remain principal low-cost energy source for power generation in the foreseeable medium-term future (Alam and Alam 2020a, b; Alam et al. 2019). Globally coal-fired power plants annually generate fly ash over 1 billion tonnes (Reid et al. 2020). China alone generates over 600 million tonnes (Mt) fly ash each year of which about 70% is processed into a range of industrial products (Baruya 2019). Despite considering fly ash a waste material, it is now regarded as an internationally traded commodity. The global fly ash market is expected to grow USD 4.5 billion in 2024 from USD 3.4 billion in 2018 with an annual growth rate of 6% due to the uses of fly ash in construction industry

Fig. 15.1 A 2000 times magnification of fly ash particles, adapted from (US Department of Transportation 2020)



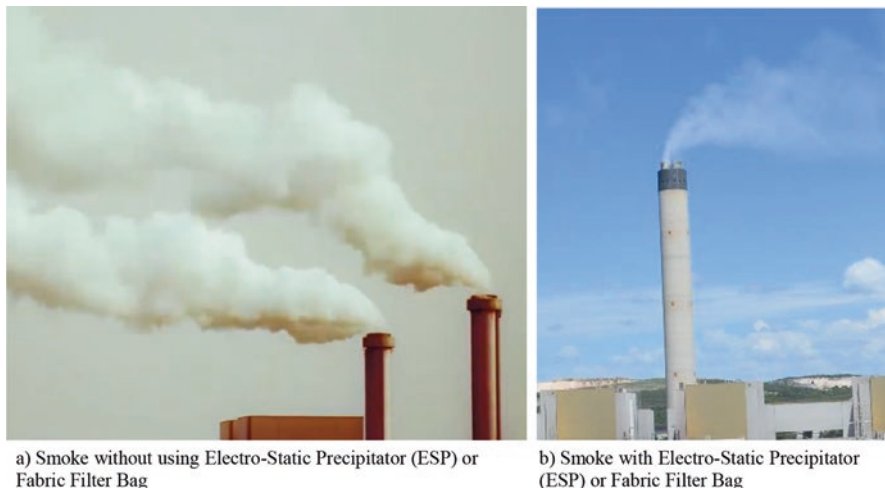


Fig. 15.2 Smoke without filtration (a) and with filtration (b) at coal-fired power plant



Fig. 15.3 Fly ash collection (a) and deposition (b)

especially in infrastructure and road paving (Market Research Report 2018). The global fly ash market is subgrouped into five regions: (1) North America (USA, Canada and Mexico), (2) Europe, (3) Asia Pacific including China, India, Australia, Japan, South Korea, Indonesia, Malaysia, (4) South America and (5) Middle East & Africa (South Africa, Gulf Cooperation Countries-Saudi Arabia, United Arab Emirates, Qatar, Bahrain, Kuwait, Oman, and all other Middle Eastern & African countries). The massive roads, bridges, infrastructures and building constructions in China, India, Indonesia, Malaysia, Thailand, Bangladesh, Vietnam, Pakistan, Australia, and other countries expand the Asia Pacific market for fly ash. The demand for fly ash in North American market is increasing due to construction sector. After Asia Pacific and North American fly ash markets, the European fly ash market considered world’s third largest.

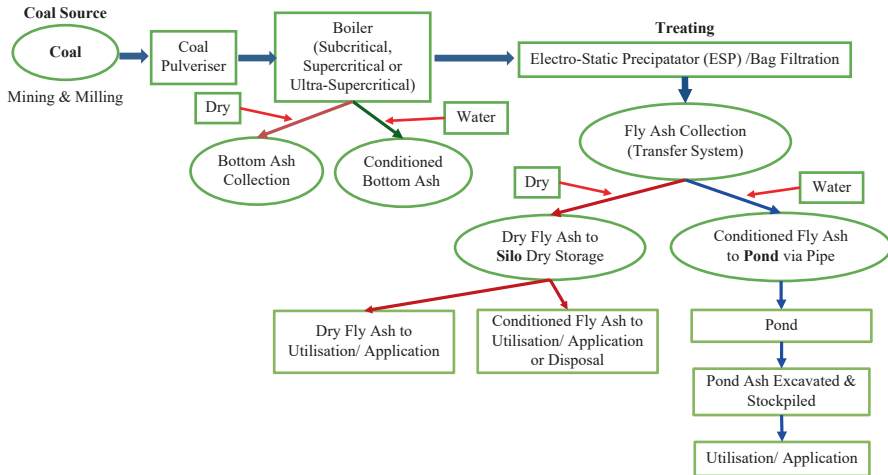


Fig. 15.4 Typical flow chart of a coal-fired power plant for ash collection, adapted from (US Department of Transportation 2020)

As per American Society for Testing and Materials (ASTM) C618 standard, three types of fly ash (e.g. Class N, Class F, and Class C) are widely used in cementitious materials. Class N fly ash is the raw/calcined natural pozzolans such as volcanic ashes or various minerals as they require calcination (i.e. clays and/or shales). Class F fly ash is produced by burning bituminous coal and anthracite coal. As it has pozzolanic properties and higher unburnt carbon, it requires more air entrainer. Class F fly ash has slow reaction during the initial hydration of the cement; however, it starts to react between 28 and 90 days of curing (Chelberg 2019; Hemalatha and Ramaswamy 2017). The lignite and subbituminous coal burning produced Class C fly ash. It has both cementitious and pozzolanic properties. These two properties enable Class C fly ash to possess higher compressive strength compared to Class F fly ash. Class C fly ash assists to have the early strength of concrete. As shown in Table 15.1, the percentage of CaO content distinguishes Class F from Class C as Class F must contain a minimum of 18% CaO (Hemalatha and Ramaswamy 2017). The properties of Class C and Class F are shown in Table 15.1.

Fly ash is used as a cementitious material as well as a partial cement replacement. It also serves as a fine aggregate in concrete (Khan et al. 2017; Xu and Shi 2018). According to American Coal Ash Association 2020, around 37% of 38 million tons of fly ash produced in the USA are used in concrete. The use of fly ash in construction as cementitious material and partial cement replacement material provides economic (it is considered waste product) benefit, environmental benefit as well as mechanical and structural advantages to the concrete mix (Chelberg 2019). Some mechanical and structural benefits are as follows:

- Fine particle size of fly ash raises concrete's density and lowers the permeability of concrete (Sumer 2012).

Table 15.1 Properties of Class C and Class F coal fly ash

Properties	Class C coal fly ash	Class F coal fly ash
Origin	Sourced from anthracite and bituminous coal	Produced from younger lignite and subbituminous coal
Lime content	Less than 20%, typically 10%	Contains more than 20%
Calcium content	Less than 12% in calcium hydroxide, calcium sulphate and glassy components	Typically, up to 40%
Alkali and sulphate content	Higher amounts	Lower amounts
Air entrainer	Requires an air entrainer	Does not require activator or air entrainer
Suitability for high sulphate condition	Used in high sulphate exposed conditions	Unsuitable for high sulphate conditions without additives
Uses	Used for high fly ash concrete mixtures. Specific uses include structural concrete, HP concretes and high sulphate exposure	Lower fly ash content in concrete. Primarily used for residential construction

Table 15.2 Typical oxide analyses of ash and Portland cement, adapted from (US Department of Transportation 2020)

Compound	Fly ash Class F (%)	Fly ash Class C (%)	Portland cement (%)
SiO ₂	55	40	23
Al ₂ O ₃	26	17	4
Fe ₂ O ₃ (haematite)	7	6	2
CaO (lime)	9	24	64
MgO	2	5	2
SO ₃ (sulphate)	1	3	2

SiO₂ and Al₂O₃ are together called mullite

- Fly ash decreases hydration heat of concrete thereby reducing thermal cracking (Bouzoubaâ and Lachemi 2001).
- Fly ash raises concrete's resistance to sulphate and acid attacks (Xu and Shi 2018).
- It considerably lowers the shrinkages of concrete (Gesoglu et al. 2009).
- The spherical shape of fly ash particle increases the fresh concrete's workability (Xu and Shi 2018).
- Class F fly ash increases the setting time (Nguyen et al. 2015).

Important variables are fly ash composition and properties are coal grade (e.g. fixed carbon, moisture, heating value and ash content), milling efficiency and combustor reaction conditions as shown in Table 15.1. Class F fly ash is generated from high-grade coal, and Class C is from low grade coal (i.e. lignite or brown coal). Class C ash is a 'high calcium' fly ash and is ideal for brick manufacture and structural concrete. Cenospheres and bottom ash make up 15% of the total ash with remainder of 85% fly ash from coal combustion. A comparative oxide analyses of fly ash Class C, Class F, and Portland cement are shown in Table 15.2. A recent large commercial application of fly ash was in the construction of the 55 km sea bridge

between Hong Kong and Macao which is one of the largest man-made structures in the world (Li et al. 2014).

15.2 Case Study: CFA Generation in Bangladesh

15.2.1 *Ash Production per Year from Coal-Fired Power Plants in Bangladesh*

The power generation of Bangladesh is greatly dependent on natural gas from indigenous sources over the years. However, with the depletion of most gas fields in the recent years, the government opted for liquefied natural gas (LNG) importation by setting up two floating LNG receiving and regasification terminals to make up deficits in gas supply. Furthermore, in order to diversify fuel mix in power generation and to reduce overall power generation cost, the government set a target to generate 35% electricity by using coal (either from domestic or international sources) under the power system master plan adopted in 2016. As a result, a good number of coal-fired power plants are under different stages of implementation in the public and private sectors. Currently, there are two existing coal-fired power plants in the country such as (1) Barapukuria Thermal Power Plant (2×125 MW + 1×275 MW) at Dinajpur under Bangladesh Power Development Board (BPDB) and (2) Payra 1320 MW (2×660 MW) Thermal Power Plant (Phase-1) at Patuakhali under the JV of North-West Power Generation Co. Ltd. (NWPGL), Bangladesh & CMC, China. Besides, another 21 power plants having an aggregated capacity of more than 22 GW have been initiated by public and private power generation companies including joint ventures. However, all of them may not be materialised for various reasons mostly due to lack of financing. Nevertheless, the following coal-fired power plants are at the construction phase and have either secured financing or at an advanced stage of financing and hence are most likely to be implemented by 2025.

- Moitree Super 1320 MW Thermal Power Plant at Bagerhat by JV of BPDB, Bangladesh and National Thermal Power Company Ltd. (NTPC), India.
- Payra 1320 MW Thermal Power Plant (Phase-2) at Patuakhali by JV of NWPGL, Bangladesh and CMC, China.
- Matarbari 1200 MW Coal-fired Power Plant, Cox's Bazar by CPGCBL, Bangladesh.
- Patuakhali 1320 MW Thermal Power Plant at Patuakhali by JV of RPCL, Bangladesh and Norinco, China.
- Barisal 307 MW Coal-fired Power Plant at Barguna by JV of Power China and ISO-Tech, China.

Under the above backdrop, the total installed capacity of coal-fired power plants would be more than 7.3 GW by 2025. During the operation of these power plants, a

significant amount of fly ash and bottom ash will be produced as a combustion by-product. However, the exact amount of ash production is dependent on four major factors:

Coal Quality: The coal consumption and ash production of a power plant are directly dependent on the calorific value of the coal to be used for combustion and percent of ash in the coal composition. Except for the Barapukira power plant, all coal-fired power plants of the country are designed based on imported coal. A common coal sourcing strategy observed among all power generation companies is to import a significant portion of coal from Indonesia due to its proximity to Bangladesh. However, the calorific value (CV) of Indonesian coal is generally lower (in the range of 16.7–20.6 MJ/kg or 4000–4300 kcal/kg, gross as-received basis) with high moisture content but low ash and sulphur content. Hence, Indonesian coal would require to be blended with higher CV coal of Australia, South Africa, or from other sources.

For this analysis, we are considering the calorific value of blended imported coal as 21 MJ/kg or 5050 kcal/kg (gross) or about 4700 kcal/kg (net) with ash content of 9.5% which is a typical average of Australian and Indonesian coal. On the other hand, for domestic coal available in the Barapukuria mine, the calorific value is 25 MJ/kg (6072 kcal/kg (gross) or 24.2 MJ/kg or about 5800 kcal/kg (net), using 4.18 MJ/1000 kcal conversion) with ash content of about 12.4%.

Efficiency of the power plant: Except for Barapukuria Power Plant which is using a subcritical boiler, other power plants are designed with supercritical or ultra-supercritical technology. For this analysis, we have considered 35% efficiency for the Barapukuria power plant at maximum continuous rating (MCR), and for other power plants, the average efficiency is considered as 42%.

Plant load factor: The plant factor is a function of relative power generation cost, grid demand, and reserve margin of the system. For a coal-fired power plant, the fuel cost for electricity generation is lower than imported LNG or liquid fuel-based power plants. Hence, coal plants get higher merit order dispatch to the grid. For this analysis, we have considered 75% annual plant factor for supercritical or ultra-supercritical power plants and 65% annual plant factor for subcritical power plants since currently there is a higher reserve margin in the electricity grid of Bangladesh.

Ash capturing equipment: Either electrostatic precipitators (ESP) or fabric filters are used in a modern coal-fired power plant to remove particulate matter from the fuel gas. ESP has a design efficiency of about 99.5%, whereas the efficiency of bag filters is even higher. Considering the ease of maintainability compared to fabric filters, all new coal plants of Bangladesh are using ESP. For this analysis, we have considered ash capturing rate of 99% for new plants and 97% for old plants in Barapukuria including ash handling losses.

Based on the above assumptions, the annual quantity of ash is calculated using the equation:

$$\text{Ash production per year (metric tonne)} = \frac{\text{Plant Capacity (kW)} \times \text{hours in a year (h)} \times \text{Plant Factor (\%)} \times \text{Plant Heat rate} \left(\frac{\text{kJ}}{\text{kWh}} \right) \times \text{Ash in coal (\%)} \times \text{Ash capture rate (\%)}}{\text{Calorific value of Coal (kJ/kg)} \times 1000 \left(\frac{\text{kg}}{\text{tonne}} \right)}$$

Using above equation, ash production is predicted in Year 2025 and is shown in Table 15.3.

Barapukuria thermal power plant (BTTP) was the only coal-based power plant in Bangladesh until 2019, and was established beside Barapukuria Coal Mine Co. Ltd. Barapukuria coal is mainly bituminous with an ash content of 10.2–14.0% with calorific value around 27.8 MJ/kg (or 12,000 Btu/lb) containing small amount of sulphur (0.63–0.71%). BTTP produces about 3000 tonnes of coal per day and burn to generate 250 MW electricity (Khan et al. 2013). The estimated CFA from BTTP is to be 120,000 tonnes per year. Thus, the ash production from the abovementioned seven power plants by 2025 would be about 2.0 million metric tonnes per annum, out of which about 90% would be fly ash and the rest are bottom ash. The ash production from coal-fired power plants will grow further beyond the year 2025 as some of the pipeline projects will be put into operation after 2025.

15.2.2 Ash Handling and Disposal Methods

The coal ash handling system of power plants generally vary in design. However, the typical design considerations of fly ash and bottom ash handling systems of a coal-fired power plant are described in the following:

Fly ash handling system of Power Plant: Each boiler of a power plant is generally equipped with one separate, routinely, and continuously operated fly ash handling system. The boiler unit contains a set of positive pressure concentrated phase pneumatic ash removal system for conveying fly ash collected in coal economiser and ESP hopper. Fly ash collected in the hoppers is transported sequentially to the fly ash silo (or slag bin) through the dense phase vessels by the compressed air. The system should be designed to segregate fine and coarse ash in separate silos.

In order to improve the fluidity of ash in the ash hopper and to ensure the smooth ash discharge, a set of fluidising devices is set up in each furnace in the ash removal system. Each set of fluidising device consists of hopper fluidising blowers, hopper air heaters, and fluidising slides. Multiple fly ash silos are generally provided for the temporary storage of ash until loaded to the disposal trucks of the buyers. Multiple outlets beneath the coarse and fine fly ash silos facilitate the loading of ash to the closed trucks and open trucks. Moreover, a separate ash slurry disposal system may be present to convey the coal ash to the ash pond.

Table 15.3 Ash production calculation (Year 2025 case)

Coal source	Capacity (MW)	Technology	Efficiency	Annual plant factor	Heat rate (kJ/kWh)	Ash % in coal	Ash capture rate	Coal CV (kJ/kg)	Ash quantity (metric tonne)
Imported coal	6787	SC/USC	42%	75%	8571.4	9.5%	99.0%	19,665	1,827,956
Domestic coal	525	Subcritical	35%	65%	10,285.7	12.4%	97%	24,267	152,400
	7312								1,980,356

Bottom ash handling system of Power Plant: Mechanical-type bottom ash handling system is generally used for removing the bottom ash from the furnace bottom which consists of conveying, storage, discharge of bottom ash. Firstly, the high-temperature bottom ash from the boiler furnace is discharged through the ash hopper to the steel conveyor. The bottom ash is then cooled by the cooling air. The cooling air can recover the heat of bottom ash to the boiler furnace. Then the bottom ash is conveyed to the bottom ash bin which serves as the temporary storage of bottom ash. Finally, the bottom ash is unloading to trucks of the buyers or conveyed to the ash pond.

Disposal from the site: The existing two coal-fired power plants of the country such as Barapukira and Payra Thermal Power Plants have entered into long-term selling agreements of coal ash to cement producers (coal ash buyers). In both cases, buyers are responsible for the collection, handling, and disposal of coal ash from the power plant sites. The buyers are also bound by the contract to dispose of the coal ash from the site in a timely manner. The violation of this condition may lead to penalty or liquidated damages.

15.2.3 Distribution of Value of Ash in Different Methods

The application of coal ash is contingent upon its compositions, quality, and strength. Ashes produced from Payra 1320 MW Thermal Power Plant using different quality of coal have been tested, and the ash compositions are shown in Table 15.4.

Coal ash has a wide range of applications in Portland cement production, in asphaltic concrete pavements, masonry products, ash bricks, cellular concrete, tiles, etc. It also has geotechnical applications such as soil stabilisation, embankments,

Table 15.4 Coal ash compositions from Payra 1320 MW Thermal Power Plant, Bangladesh

Ash component	Unit	Design coal (Indo 12)	High-quality coal (Aus 1)	Worst coal (Indo 6)
SiO ₂	%	40	61.3	43
Al ₂ O ₃	%	13.9	22.2	23.1
Fe ₂ O ₃	%	14.8	3.7	9
CaO	%	10.5	6.55	9.5
MgO	%	7.5	1.12	3.58
Na ₂ O	%	0.7	0.38	0.44
K ₂ O	%	1.7	0.71	1.48
TiO ₂	%	0.8	1.18	0.96
Mn ₃ O ₄	%	–	0.06	0.12
SO ₃	%	9.9	2.0	7.95
P ₂ O ₅	%	0.2	–	0.86
Others	%	–	0.8	0.01
Total	%	100	100	100

and mine reclamation. Coal ash also serves as filler in wood and plastic products, paints, and metal castings.

The most popular use of coal ash is in cement production. According to Bangladesh Cement Manufacturer Association (BCMA), total sales of cement in 2019 is 33.6 million metric tonnes out of which Portland Pozzolana Cement (PPC) was 23.5 million metric tonnes in which fly ash is used as an ingredient. Depending on the mixing pattern, cement manufacturers use 12–18% fly ash in PPC. However, the factories which have vertical roller mills can add 10% fly ash in cement along with other components such as clinker, gypsum, limestone, and slag. According to BCMA, fly ash demand in 2019 was about 3.0 million metric tonnes. The sector also experienced a growth of 13% in 2019.

Currently, cement manufacturers import fly ash mostly from India for which import cost breakdown is as follows:

- Freight on Board (FOB): USD 10.5–13 per metric tonne.
- Freight: USD 10–12 per metric tonnes (source country: India, destination: Dhaka, lighter vessels is used for transportation).
- Other costs (LC charge, Insurance, C&F agent fee, landing charge): About 4.0%.
- Custom Duties: 5.0% on sum of FOB, Freight, Insurance and landing charges.
- AIT & VAT are refundable for the manufacturers and hence are not included.
- Local transportation cost is not included.

Based on the above analysis of the current cement industry, the average import cost of fly ash is about USD 25 per metric tonne which gives a valuation of about USD 40–50 million per year for the estimated production of ash from the seven (07) coal-fired power plants listed above.

Alternatively, there is a potential market of fly ash in brick production since clay bricks are highly discouraged due to its adverse impact on the environment and loss of valuable topsoil. Besides, the fly ash brick has also technical advantages over clay bricks as listed in Table 15.5.

At present, there are no fly-ash bricks available in the Bangladesh market. Hence, for the valuation of fly ash bricks, a comprehensive market study is recommended.

Table 15.5 Properties comparison between clay bricks and fly ash brick

Properties	Red bricks/Clay bricks	Fly ash bricks	Remarks
Density	1600–1750 kg/m ³	1700–1850 kg/m ³	Higher load bearing
Compressive strength	2.94–3.43 MPa	8.83–9.81 MPa	Higher load bearing
Absorption	15–25%	10–14%	Less dampness
Dimensional stability	Very low tolerance	High tolerance	Saving in mortar up to 25%
Wastage during transit	Up to 10%	Less than 2%	Saving in cost up to 8%
Plastering	Thickness vary on both sides of wall	Even on both sides	Saving in plaster up to 15%.

In a study carried out in 2017 by the Department of Environment under the Ministry of Environment and Forest of Bangladesh, the brick industry of Bangladesh was estimated to be USD 2.53 billion per annum with an annual production of 23 billion bricks. The sector accounts for about 1% of the GDP of the country with an estimated annual growth of 2–3% over the next 10 years.

From the above discussion, it is evident that the market demand for coal ash is significantly higher than its domestic production. This gives the power generation companies privileges on selling of coal ash in a competitive market. This helps the power companies not only mitigate environmental and health effects in the process of ash disposal but also recover part of coal price by selling the waste coal ash. In Bangladesh, the potential coal ash use can be as ingredient for cement, admixture for concrete, material for road construction, as fertiliser and soil conditioner and for building artificial fish reef.

15.3 Coal Ash Uses in India

The fly ash and bottom ash use in India are transitioning to a modern ash and cement-based construction industry. The main applications include land reclamation, road surfacing, backfilling of exhausted mines and the creation of ash dykes at large scale. With the growing middle class and population in South Asia, brick manufacturing has grown exponentially over the years. In 2019 the Indian government ruled that all clay brick kiln manufacturers should switch to fly ash bricks if located within 300 km of a power plant. This is part of the initiative to reduce the emissions of CO₂ associated with the 100,000 kilns used by clay brick industry and to avoid the consumption of 400 Mt./y of fertile soil needed to supply raw clay materials for brick manufacturing. Traditional coal-fired brick kilns operate continuously except rainy season. This is a major source of pollutants including NO_x, SO_x and particulates in many parts of South Asia. In addition, incomplete combustion results in black smoke and CO emissions (Nath et al. 2018). In India, the industry produced 250 billion bricks per year without strictly adhering to environmental legislation. Restricted fly ash availability has forced brick manufacturers to operate at half capacity due to competition between the growing concrete industry and brick makers (Kapil 2019).

Flooding and river erosion are serious problems in India and downstream Bangladesh affecting millions of people. Initiatives to reclaim low lying land areas prone to flooding have used coal ash to avoid the depletion of valuable topsoil. This method has doubled in recent years accounting for 11 Mt. of ash in 2016–2017 which is over 6% of the total ash produced. Opencast mines also use similar quantity to fill mine passages preserving precious topsoil and sand extracted from the river system.

The direct application of coal ash in road building, embankment construction and ash dyke flood protection are significant activities, consuming over 6 Mt./y of fly ash. These projects are important infrastructure for flood mitigation during

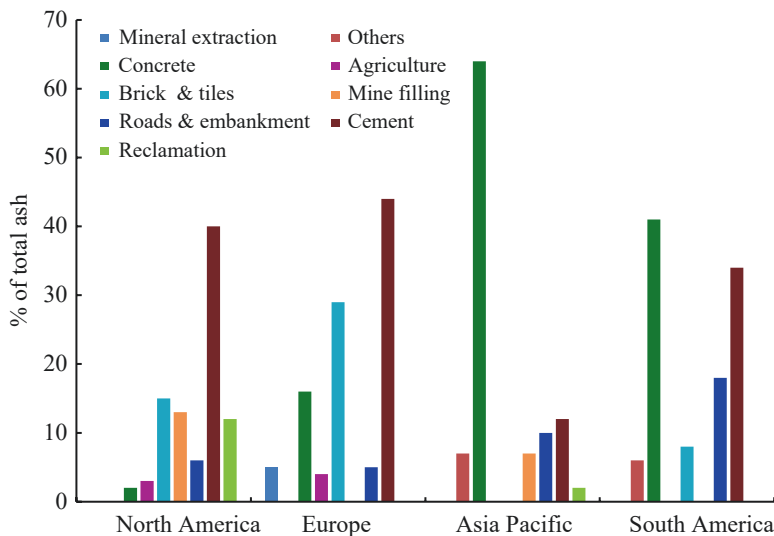


Fig. 15.5 Utilisation of fly ash in different regions in various industry sectors in the world, adapted from (Ma et al. 2017; Yadav and Fulekar 2018; American Coal Ash Association 2018)

annual monsoon season. An example of ash utilisation for several regions is shown in Fig. 15.5.

15.4 Potential Metal Value Contained in Coal Fly Ash

There are traces of metals available in coal ash as shown in Table 15.6. Some rare earth elements (REE) present in fly ash is shown in Table 15.7. Based on metal content, prices from London Metal Exchange and other sources for common and rare earth elements, the monetary values per tonne of coal fly ash is shown in Figs. 15.6–15.9.

About 70% value can be attributed to common metals of total US\$900/t CFA with remaining for rare earth elements. This is based on the content of the metal in CFA. However, if it is assumed 70% of this metal is recovered, potentially over US\$600 worth of metal value can be recovered from coal fly ash. The major common metals are Si, Al, K, Ti, Ca, and the main rare metals are Tm, Dy, Pr, Tb and Ce in terms of value.

In addition, cenosphere as an inert, lightweight and hollow sphere, comprised of mainly silica and alumina and filled with air/inert gas, can be utilised as fillers in cement to produce low-density concrete. It has also got a variety of applications including in foams, composites and in automotive industries after modification and treatment.

Table 15.6 Main elemental concentration of Fly ash (mg/kg), adapted from (EPRI 2009; Zhang 2014)

Main element	Concentration (mg/kg)	Main element	Concentration (mg/kg)
Aluminium	70,000–140,000	Cadmium	BDL–3.7
Calcium	7400–15,000	Chromium	27–300
Iron	34,000–130,000	Copper	62–220
Silicon	160,000–270,000	Lead	21–230
Magnesium	3900–23,000	Manganese	91–700
Potassium	6200–21,000	Mercury	0.01–0.51
Sodium	1700–17,000	Molybdenum	9–60
Sulphur	1900–34,000	Nickel	47–230
Titanium	4300–9000	Selenium	1.8–18
Antimony	BDL–16	Strontium	270–3100
Arsenic	22–260	Thallium	BDL–45
Barium	380–5100	Uranium	BDL–19
Beryllium	2.2–26	Vanadium	BDL–360
Boron	120–1000	Zinc	63–680 s

BDL below detection limit

Table 15.7 Concentration range of REE in CFA in different power plants, adapted from (Blissett et al. 2014; Franus et al. 2015; Mayfield and Lewis 2013)

REE	CFA from Polish and UK power plants, ppm	CFA from power plants in USA, Mexico and Europe, ppm
Cerium (Ce)	30.7–176.5	405–565
Lanthanum (La)	15.5–85.7	206–286
Yttrium (Y)	17.9–73.2	191–259
Neodymium (Nd)	12.7–81.3	183–256
Praseodymium (Pr)	3.3–20.51	49–68.4
Samarium (Sm)	2.8–17	–
Dysprosium (Dy)	2.61–12.18	32.1–50.3
Gadolinium (Gd)	2.85–14.65	–
Erbium (Er)	1.79–7.41	–
Terbium (Tb)	0.45–2.4	4.9–7.3
Europium (Eu)	0.56–3.81	3.9–5.9
Holmium (Ho)	0.59–2.58	–
Ytterbium (Yb)	1.8–6.74	–
Thulium (tm)	0.27–1.07	–
Scandium (Sc)	7–45	–
Lutetium (Lu)	0.3–1.03	–
Total REE	101.12–543.08	1213.6–1667.6

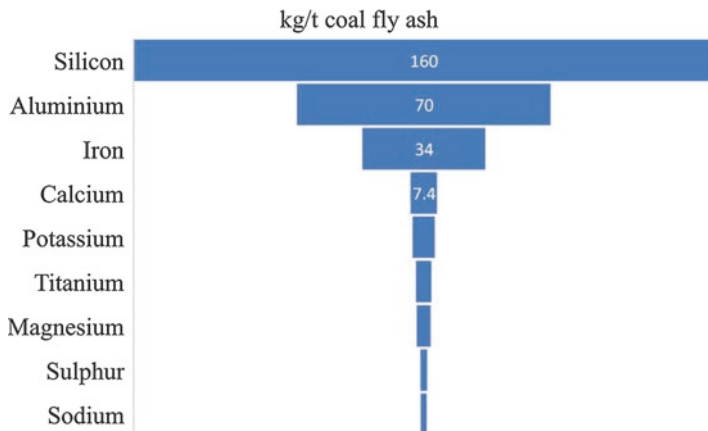


Fig. 15.6 Content of major metals (total of 290 kg metal content/t of coal ash)

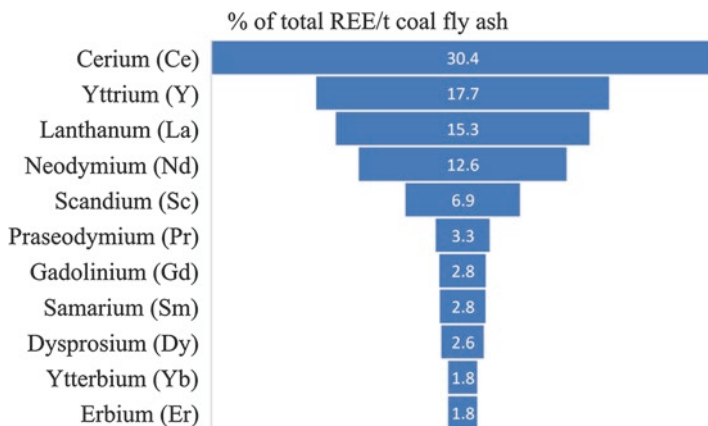


Fig. 15.7 Content of rare metals (total REE is over 100 ppm in coal ash)

15.5 Environmental Aspects of Coal Ash—CO₂ Emission Reduction Potential

15.5.1 Cement with Fly Ash

Cement industry uses approximately 190 million tonnes of clinker from domestic production in India during the year of 2014–15, with the balance from the imports. The total installed capacity of cement in India during the year 2014–15 was 390 million tonnes. Total cement production during the same year was 271 million tonnes. As per the government statistics cement industry grew at 5.6% in 2014–2015. Cement industry is likely to grow in coming years due to various initiative of

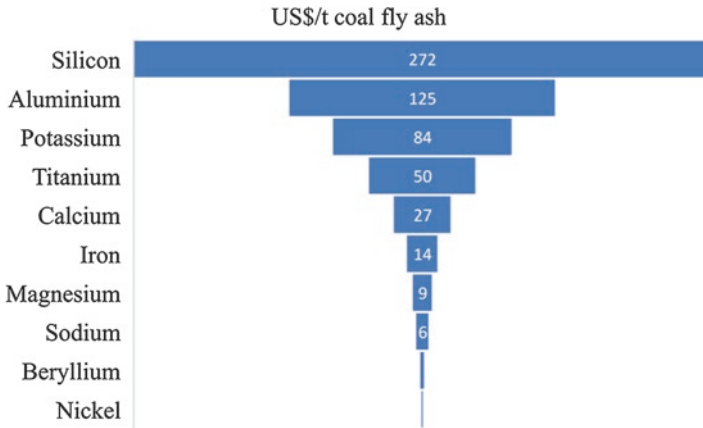


Fig. 15.8 Value of common metals in coal fly ash using indicative price in 2020

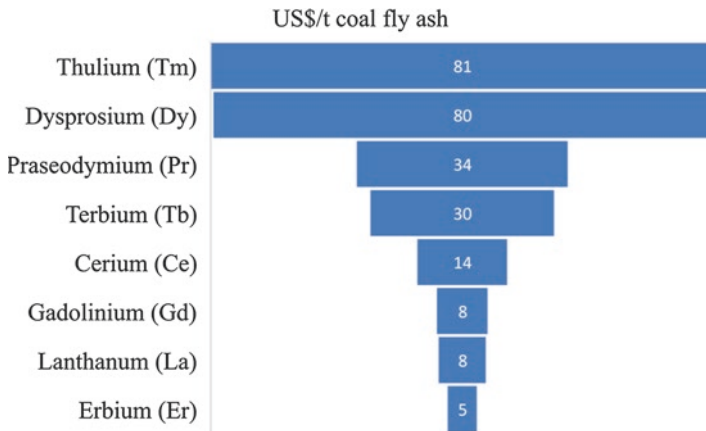


Fig. 15.9 Value of rare metals in coal fly ash using indicative price in 2020

Government of India like National highway project, 100 smart cities and housing for all.

Clinker production starts with reception of raw material at the factory gate and its internal transportation for pre-homogenisation and raw meal grinding where different raw materials are mixed to obtain the chemical composition required for cement. The homogenised raw meal is then fed to a pre-heater tower before sending to a pre-calciner and the rotary kiln. A preheater in the form of a series of vertical cyclones through which the raw meal is passed and comes in contact to swirling hot gases that is moving in the opposite direction. Pre-calcination occurs in a pre-calciner in which decomposition of limestone to lime happens. The reaction needs heat energy inputs at two points in the manufacturing process: (a) within the

'pre-calciner', a combustion chamber at the bottom of the pre-heater above the kiln, and (b) within the kiln itself. The pre-calcined meal then enters the kiln. The kiln's heat (~1450 °C) induces physical and chemical reactions partially melting the meal into 'clinker' which is an intermediate product in cement manufacturing that becomes the main substance in cement. It is a widely traded commodity.

The heated clinker from the kiln drops onto a grate cooler and cools down by incoming combustion air. It, therefore, minimises the energy loss in the system. Depending on the requirement, clinker can be stored in the silo to use for making different types of cement or transported to different locations. The life cycle-based CO₂-e emission of clinker from above process is 0.88 kg CO₂-e/kg clinker.

Indian cement plants are claimed to be relatively efficient in the world. Their thermal and electrical energy consumption is about 10% lower than the world. In India, various types of cements are manufactured like ordinary Portland cement, pozzolana Portland cement, Portland slag cement and white cement. Ordinary Portland cement is manufactured by mixing and grinding of clinker and gypsum in certain proportion. The strength of cement generally considered is between 43 MPa and 53 MPa.

The cement manufacturing process starts from clinker delivered and stored in silo. It includes clinker and additives blending and grinding in cement mill, internal transportation, cement product at a plant. The manufacturing of OPC starts with reception of clinker at the factory gate. The grinding of clinker and gypsum is undertaken in an appropriate proportion in a vertical roller mill or in a ball mill. The latest available technologies are vertical roller mill and energy-efficient fans. Indian cement industry has taken significant measures improving energy efficiency by installing better equipment, process optimisation, equipment retrofitting between 2014 and 2017. The life cycle-based CO₂ footprint of Indian cement is 0.9 kg CO₂-e/kg cement. The typical direct CO₂ emission with indirect CO₂ emission from various inputs is shown in Fig. 15.10. The life cycle-based water footprint is estimated to be 0.05 m₃ water/t of Portland cement. This can be reduced to 0.62 kg CO₂-e/kg cement if 30% CFA is replaced with clinker, or this provides a potential benefit of 30% in CO₂-e reduction per tonne of cement.

15.5.2 Fly Ash Brick

Fly ash bricks are produced by mixing fly ash with other raw materials under temperatures and pressures. Like clay bricks, the fly ash bricks are used in masonry building and construction.

In India, yearly production is about 7,727,951 tonnes. The processing starts with reception of raw material at manufacturing units. The manufacturing process to produce fly ash bricks is raw material provision, raw material mixing, pressing, curing, drying and dispatch, transport of raw materials to plant, and other required infrastructure. Material and energy requirement for administration was not included. Fly ash, lime, gypsum, and sand are manually feed into a pan mixer where water is

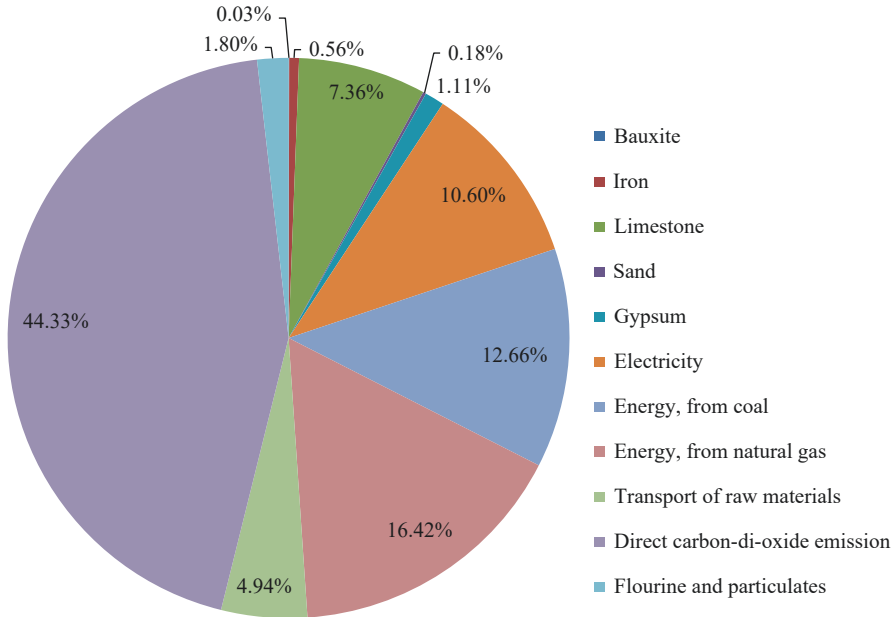


Fig. 15.10 Direct CO₂ (mainly from clinker production) and indirect CO₂ emission percent from various inputs for Portland cement

added to the required proportion for homogeneous mixing. After mixing, the mixture is to be transported on a belt conveyor through feed into an automatic brick making machine. The manufactured bricks are stored on wooden pallets and kept for 2 days. After 2 days, bricks are moved to an open area where bricks are water cured for 10–15 days. Thereafter, bricks are tested, sorted and stored for sale.

This fly ash brick carbon emission footprint can be compared with clay brick. The data for clay brick corresponds to a mix of different brick production technologies (i.e. different firing fuels) generally practised in Austria, Germany and Switzerland. The emission is compared with 1 kg of clay brick production using average inputs for 12 plants in Switzerland. This process includes first dry grinding and then wet process. The wet process comprises second grinding, mixing, plasticising, storage, forming, extruding moulding, cutting, drying, firing, loading, packing and storage. The waste heat is used again for drying, and no hard coal or coke is used. The wastewater and solid waste impact were not included. The life cycle-based carbon footprint for fly ash brick is 0.64 kg CO₂-e/kg brick. Over 90% of this is due to electricity use for the conveying system. The life cycle-based carbon footprint of a clay brick is 0.26 kg CO₂-e/kg brick. Of this about 5% is for clay making, 10% for electricity use and the remainder is for burning bricks. While carbon footprint is higher for CFA brick compared with clay brick; however, the saving of precious topsoil resources is important due to the use of a waste material compared with natural soil resource.

15.5.3 Fly Ash in Concrete

Fly ash can be used in ready-mix concrete production. The cost component for ready-mix concrete is raw materials, raw material mixing, transportation, energy, and plant use. In costing, the concrete transportation to site is not included. The amount of fly ash use in cement is regulated by national standards, and it varies from country to country. In Australia, it is regulated by Green Building Council of Australia. In Australia, the ready-mix concrete can have up to 30% fly ash with keeping cement's pozzolanic properties intact. The carbon footprint of concrete with 30% fly ash is 235 kg CO₂-e/m³ compared to 318 kg CO₂-e/m³ for standard concrete without any fly ash addition in Australian context. Therefore, adding 30% fly ash reduces a 26% CO₂ emission.

15.5.4 Radiation Impact of Fly Ash Product

Human activities such as nuclear fuel cycle (e.g. mining, processing, use or treatment of the nuclear fuel) and burning of fossil fuel including coal can release radionuclides. Airborne radionuclides can be inhaled by humans and animals. Furthermore, radionuclides can contaminate freshwater. The fresh water can be ingested by human, animals, plants and crops.

Radionuclides-induced damage is expressed per kBq activity level (1 kBq is equal to a decay of 1000 nuclei per second). The unit Becquerel (Bq) indicates the number of atom nuclei decay rate in each second. Becquerel (Bq) varies based on radiation types such as half-life of radionuclide and environmental fate of radionuclide. The indicative ionising radiation potential using life cycle assessment has been reported for various products (Fig. 15.11).

The radiation potential from ash and slag-based cement product is relatively higher compared with that from conventional cement. Cement manufacturing with 80% blast furnace slag is about four order of magnitude higher than that of the Portland cement. Cement made from fly ash can be an order or two magnitude higher than that of Portland cement depending on the percentage of ash used as ingredients. However, this is likely to be below the limit or threshold since many of these ashes or slag-based cement products got approval thorough regulatory systems for use in the construction.

15.6 Conclusions

Coal bottom ash and fly ash are not considered waste anymore. Their applications in various fields (construction, infrastructure, cement industry, mine rehabilitation, etc.) bring immense economic, environmental, and sustainable waste disposal

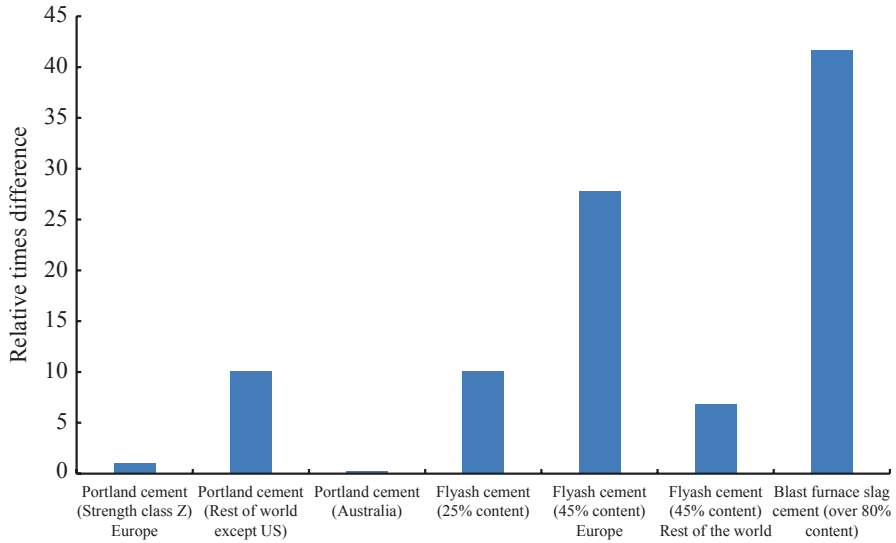


Fig. 15.11 Ionisation potential of Portland cement (assuming 1) compared with other ash and slag-based product

benefits. Fly ash contains some valuable rare earth materials harnessing of which will provide added economic value and supplementing industrial needs. The global market for fly ash is expanding rapidly. Therefore, a globally acceptable industrial standards needs to be devised for safe collection, transportation, and utilisation with minimal or no harm to humans, flora, fauna and water. Cost-effective and safe technology is also required to be developed for extracting valuable rare earth elements from the fly ash.

Acknowledgements The authors thank their respective employers for supporting them to write this chapter. The authors also thank Mr. Khondkar Saleque for minor input and personal discussion.

References

Alam, F., & Alam, Q. (2020b). Power generation and regional development in South Asia. In Q. Alam, A. Rahman, & S. R. U. Islam (Eds.), *The economic development of Bangladesh in the Asian century* (p. 240). Oxon: Routledge. ISBN 978-0-367-528768.

Alam, Q., & Alam, F. (2020a). Power generation and regional collaboration in South Asia. In M. A. Alam, Q. Alam, R. Khair, & M. R. Karim (Eds.), *Managing change for better public service delivery* (pp. 277–316). Oxon: Routledge. ISBN 978–0–367-47242-9.

Alam, Q., Alam, F., Chowdhury, H., Sarkar, R., & Paul, A. R. (2019). A review on the regional collaboration of power utilisation in South Asia. *Energy Procedia*, 160, 11–17.

American Coal Ash Association (2018). *Beneficial use of coal combustion products – an American success story*. Accessed on 5 September 2020 from: <https://www.aaa-usa.org/Portals/9/Files/PDFs/ACAA-Brochure-Web.pdf> Aurora, CO, USA American Coal Ash Association, p.8.

- American Coal Ash Association (2020). *Coal Combustion Product Production & Use Report 2017*. Accessed on 17 September 2020 from <https://www.acaa-usa.org/Portals/9/Files/PDFs/2017-Survey-Results.pdf>
- Baruya, P. (2019). *The economic and strategic value of coal*. CCC/296 (p. 115). London: IEA Clean Coal Centre.
- Blissett, R. S., Smalley, N., & Rowson, N. A. (2014). An investigation into six coal fly ashes from the United Kingdom and Poland to evaluate rare earth element content. *Fuel*, 119, 236–239.
- Bouzoubaâ, N., & Lachemi, M. (2001). Self-compacting concrete incorporating high volumes of class F Fly ash: Preliminary results. *Cement and Concrete Research*, 31(3), 413–420.
- Chelberg, M. (2019). *The effect of fly ash chemical composition on compressive strength of fly ash portland cement concrete*. M.S. Thesis, Ohio State University, USA, accessed on 16 September 2020 from https://etd.ohiolink.edu/etd.send_file?accession=osu1555611247091087&disposition=inline
- EPRI. (2009). *Coal ash: Characteristics, management and environmental issues. Technical update* (p. 12). Palo Alto, CA: Electric Power Research Institute.
- Franus, W., Wiatros-Motyka, M. M., & Wdowin, M. (2015). Coal fly ash as a resource for rare earth elements. *Environmental Science and Pollution Research*, 22(12), 9464–9474.
- Gesoğlu, M., Güneysi, E., & Özbay, E. (2009). Properties of self compacting concretes made with binary, ternary, and quaternary cementitious blends of Fly ash, blast furnace slag, and silica fume. *Construction and Building Materials*, 23(5), 1847–1854.
- Hemalatha, T., & Ramaswamy, A. (2017). A review on Fly ash characteristics—Towards promoting high volume utilization in developing sustainable concrete. *Journal of Cleaner Production*, 147, 546–559.
- Kapil, S. (2019). *Why are fly ash brick manufacturers in a tough spot?* Accessed on 10 September 2020 from <https://www.downtoearth.org.in/news/india/why-are-fly-ash-brick-manufacturers-in-a-tough-spot-63781> New Delhi, India, Down to Earth. p. 2.
- Khan, I., Castel, A., & Gilbert, R. I. (2017). Effects of Fly ash on early-age properties and cracking of concrete. *ACI Materials Journal*, 114(4), 673–681.
- Khan, M. A. A., Saha, M. S., Sultana, S., Ahmed, A. N., & Das, R. C. (2013). Coal Fly ash of Barapukuria thermal power plant, Bangladesh: Physico chemical properties assessment and utilization. *International Journal of Science and Engineering Research*, 4(11), 1456–1460.
- Li, J., Liu, K., Tu, L., & Jiao, Y. (2014). Crack control technology for concrete of super large section precast. *Applied Mechanics and Materials*, 578–579, 1240–1246.
- Ma, S. H., Xu, M. D., Qiqige, Wang, X. H., & Zhou, X. (2017). Challenges and developments in the utilization of fly ash in China. *International Journal of Environmental Science and Development*, 8(11), 781–785.
- Market Research Report (2018). *Fly ash market by type—Global Forecast to 2023*. Accessed on 22 September 2020 from <https://www.marketsandmarkets.com/requestsampleNew.asp?id=76345803>
- Mayfield, D., & Lewis, A. (2013). Coal ash: A resource for rare earth and strategic elements. *Ash at Work*, 1, 17–21.
- Nath, A. J., Lal, R., & Das, A. K. (2018). Fired bricks: CO₂ emission and food insecurity. *Global Challenges*, 2(4), 5.
- Nguyen, H. A., Chang, T. P., Shih, J. Y., Chen, C. T., & Nguyen, T. D. (2015). Influence of circulating fluidized bed combustion (CFBC) Fly ash on properties of modified high volume low calcium Fly ash (HVFA) cement paste. *Construction and Building Materials*, 91, 208–215.
- Reid, I., Carpenter, A.M., & Masili, A. (2020). *Beneficial uses of coal fly ash*. IEA Clean Coal Centre, Report number CCC/303. London, UK, ISBN 978–92–9029–626-3.
- Sumer, M. (2012). Compressive strength and sulphate resistance properties of concretes containing class F and class C Fly ashes. *Construction and Building Materials*, 34, 531–536.
- US Department of Transportation (2020). *Fly ash facts for highway engineers, Chapter 1—Fly ash—An engineering material*. Accessed on 20 September 2020 from, <https://www.fhwa.dot.gov/pavement/recycling/fach01.cfm>

- Xu, G., & Shi, X. (2018). Characteristics and applications of Fly ash as a sustainable construction material: A state-of-the-art review. *Resources, Conservation and Recycling*, 136, 95–109.
- Yadav, V. K., & Fulekar, M. H. (2018). The current scenario of thermal power plants and fly ash: Production and utilisation with a focus on India. *International Journal of Advanced Engineering and Research Development*, 5(4), 768–777.
- Zhang, X. (2014). *Management of coal combustion wastes*. CCC/231 (p. 68). London: IEA Clean Coal Centre.

Chapter 16

Utilization of Circulating Fluidized Bed Combustion Fly Ash for Simultaneous Recovery of Rare Earth Elements and CO₂ Capture



Quang Tuan Lai, Thriveni Thenepalli, and Ji Whan Ahn

16.1 Introduction

16.1.1 *The Rare Earths*

Rare earth elements (REE) represent a group of 15 elements of lanthanide series, atomic number from 59 (lanthanum) to 71 (lutetium), and scandium and yttrium (Table 16.1). Scandium and yttrium are placed into REE group due to their coexistence and chemically similar exhibition to the lanthanides. REE is relatively abundant in the Earth upper continental crust with the middling abundance of 0.3–64 ppm (Taylor and McLennan 1985). The elemental abundance of rare earth elements are compatible to the abundance of several popular elements such as cobalt, nickel, copper, tin, and tungsten at of 10, 20, 25, 55, and 2 mg/kg, respectively (Taylor and McLennan 1985). Particularly, the concentration of cerium (64 ppm) gives the position of 25th within the most 78 popular elements. However, the trivial name rare

Q. T. Lai

Department of Resources Recycling, University of Science & Technology,
Daejeon, Republic of Korea

Tectonic and Geomorphology Department, Vietnam Institute of Geosciences and Mineral
Resources (VIGMR), Hanoi, Vietnam

Center for Carbon Mineralization, Mineral Resources Research Division, Korea Institute of
Geosciences and Mineral Resources (KIGAM), Daejeon, Republic of Korea

T. Thenepalli

Department of Chemistry, Indian Institute of Technology—Tirupati,
Chittoor District, Andhra Pradesh, India

J. W. Ahn (✉)

Center for Carbon Mineralization, Mineral Resources Research Division, Korea Institute of
Geosciences and Mineral Resources (KIGAM), Yuseong-gu, Daejeon, Republic of Korea
e-mail: ahnjw@kigam.re.kr

Table 16.1 Overview of rare earth elements

Atomic number	Element	Symbol	Valence	Atomic mass	Electron configuration	Average abundance (ppm)	
						Continental crust ^a	Sedimentary rock ^b
21	Scandium	Sc	3	44.96	4s ² 3d ¹	11.0	9.6
39	Yttrium	Y	3	88.91	5s ² 4d ¹	22.0	29.0
57	Lanthanum	La	3	138.91	4f ⁰ 5d ¹	30.0	32.0
58	Cerium	Ce	3, 4	140.12	4f ¹ 5d ¹	64.0	52.0
59	Praseodymium	Pr	3, 4	140.91	4f ³ 5d ⁰	7.1	6.8
60	Neodymium	Nd	3, 4	144.24	4f ⁴ 5d ⁰	26.0	24.0
61	Promethium	Pm	3	145.00	4f ⁵ 5d ⁰	rare	rare
62	Samarium	Sm	2, 3	150.36	4f ⁶ 5d ⁰	4.5	5.5
63	Europium	Eu	2, 3	151.96	4f ⁷ 5d ⁰	0.9	0.9
64	Gadolinium	Gd	3	157.25	4f ⁷ 5d ¹	3.8	4.0
65	Terbium	Tb	3, 4	158.93	4f ⁹ 5d ⁰	0.6	0.7
66	Dysprosium	Dy	3, 4	162.50	4f ¹⁰ 5d ⁰	3.5	3.6
67	Holmium	Ho	3	164.93	4f ¹¹ 5d ⁰	0.8	0.9
68	Erbium	Er	3	167.26	4f ¹² 5d ⁰	2.3	1.7
69	Thulium	Tm	2, 3	168.93	4f ¹³ 5d ⁰	0.3	0.4
70	Ytterbium	Yb	2, 3	173.05	4f ¹⁴ 5d ⁰	2.2	2.0
71	Lutetium	Lu	3	174.97	4f ¹⁴ 5d ¹	0.3	0.4

^aTaylor and McLennan (1985)

^bGrigor'ev (2003)

earths arises by the International Union of Pure and Applied Chemistry (IUPAC) due to the scarcity of uniformly profitable deposits and the difficulty of individual separation.

REE has been playing integral role to emerging technologies, advanced energies, and defense industry depending on its unique electronic, electrical, optical, and magnetic properties (Hower et al. 1999). The excellent properties of rare earths could generate superior functionalities to the rare earths-bearing products serving industries and daily life (Fig. 16.1). As a result, rare earths is becoming indispensable and participates in multiple niche deployments such as magnetics, phosphors, metal alloys, catalysts, ceramics, glass and polishing, and defense (Awais 2016; Morrison and Tang 2012).

REE magnets have important functions in computer hard drives, microphone and speaker, automotive parts, anti-lock brake, electric vehicles, refrigeration, wind turbines, communication systems, MRI, etc. (Weedon 2019). REE efficiently promotes hydrogen storage and conversion in hybrid vehicles. REE magnets provide superior advantages such as superior magnetic moment and magnetic anisotropy to the products enhancing workability, reducing weight, increasing lifetime (Song et al. 2013). REE magnets effectively convert kinetic energy into electricity in wind turbines without external energy supply. REE magnets also efficiently convert batteries energy into mechanical power in electric vehicles (Tsamis and Coyne 2015).



Fig. 16.1 Niche deployments of rare earths for numerous beneficial uses

REE magnets could also help amplifying and enhancing resolution of signals in communication systems (Fernández Martínez et al. 1994).

REE phosphors are an important activator using in display screens, fluorescent lighting, medical imaging, laser, and optical fibers to produce desirable functions (Castor and Hedrick 2006). REE phosphors improve lighting efficiency, adjust the light's wavelength producing desired color, and reduce energy consumption of fluorescent lighting (Mueller-Mach and Mueller 2000). REE makes devices light up, transmits sound and images, and renders colors (Mikami et al. 2009). Gadolinium is used to increase the sensitivity and specificity as well as resolution and contrast of images in MRI machines. REE laser such as Ho:YAG laser has been widely applied for surgical purposes. Lasers emitted from Ho:YAG laser promote precise operation and minimum harm to surgical parts (e.g., joints, tissues, kidney, teeth) (Song et al. 2013).

REE are also using as additive strengthening functions of NiMH battery, fuel cell, steel, super alloys, and Al/Mg alloys to strengthen the workability of products. The occurrence of REE in the batteries reduces weight, enhances energy storage and conversion, makes it rechargeable and longevity (Lucas et al. 2015). Corrosion resistance and mechanical properties of magnesium alloys could be strengthened by adding neodymium (Yang and Li 2010). Lanthanum helps improving mechanical and electrical properties of copper alloys including corrosive and heat resistance, hardness and strength improvement, and conductivity modification (Ren et al. 2020).

The performance of many products of catalysts and ceramics domain is elevated by the partition of REE. REE-bearing catalysts have important role in petroleum refining, chemical processing, air pollution control, and catalytic converter. Capacitor, sensor, colorant, scintillator, and refractory are the important contribution of REE to ceramics, whereas the glass and polishing industry uses rare earths for polishing compounds, X-ray imaging, coating, producing UV-resistant and photo-optical glass (Song et al. 2013). Rare earth oxides (REO) are also prized as industrial polishing compounds for high-performance passive optics. The best example is cerium oxide (CeO_2), which is mixed with water in a polishing slurry that is used to polish lenses, wave plates and mirrors with unmatched speed and precision. Additionally, REE are irreplaceable position in national defense. The occurrence of REE secures the precise and controllable operation of devices and equipment in defense such as satellite communication, radar, missile guidance system, jet engine, night-vision goggle and submarine.

Rare earth elements only occupy a relatively small quantity in products and components, but achieve wonderful yields. The excellent performances of rare earths-bearing products derive by its atomic structure. All rare earths with minor exception have 4f electron configuration featured by low energy and indirectly combine with other elements in compounds (Gschneidner et al. 2019). Amounts of unpaired 4f electrons and diverse valences of REE are crucial governing the precious properties of products and components such as optical, magnetic, catalytic, electrical, metallurgical, and nuclear properties (Holleman et al. 2007).

16.1.2 Rare Earths Go Critical

The flexibility and specificity of REE is crucial toward a green-sustainable technological development, which is incomparable and unavailable substitution. However, the insecurity of rare earths supply triggers the growing constraint on the deployment and development of advanced and futuristic technologies. Starting from the late 1800s, the REE mining industry witnessed the distinguish changes. Initially, REE was primary mined from the placer monazite followed by the dominant role of the United States, lasted about 20 years from 1965 to 1984, in producing REE from the bastnasite ores in Mountain Pass area. Afterwards, rare earths industry underwent a transitional stage of major producer with the gradual replacement of China. This period ended by 1991. From 1991 onward, the increasing output of REE exploited in China, combined with the abandon of REE production in the USA, has made up China a monopoly position on the global REE market.

The accelerating uses of REE in the production of green and energy-efficient products toward sustainable technological development have put forward an

intensive demand for REE. The global demand of clean and energy-saving products in the sectors of rechargeable batteries, lighting products, catalytic converter, electric vehicles, and wind energy is growing steadily. The output of these sectors in 2016 were 580,125 Cps, 7720 million Cps, 95 million Cps, 35.75 million Cps (cars and bicycles), and 63,650 MW, respectively (Zhou et al. 2017). The respective output of these sectors are predicted to be 2.66 million Cps, 7216 million Cps, 117 million Cps, 66.53 million Cps (cars and bicycles), and 107,488 MW. Accordingly, the usage of REE in these products grows from 33.9 kt rare earth oxide in 2016 up to a predicted number of 51.9 kt REO in 2030 (Zhou et al. 2017). Meanwhile, Garside forecasts an rising demand of REO in the world, from 208.25 kt (2019) to 304.68 kt (2025) (Garside 2020a). Particularly, Alonso et al. anticipated the insistence of Nd and Dy between 2010 and 2035 could increase by about 700% and 2600% (Alonso et al. 2012).

The interaction of disruption potential versus the prerequisite of REE has made up critical REE. China dominates the world's REE mining and production. The ratio of REO mined and produced from China in 2019 occupied 62.85% and 90% globally (U.S. Geological Survey 2020). Accordingly, the 40% reduced of raw and manufactured REE export quota in 2010 of China provoked crisis of REE domain coupling with the surge of REE price (Fig. 16.2) (Garside 2020b; Report 2017; Schlinkert and van den Boogaart 2015; Statista 2015). While the substitutions or new deposits of REE are not available, the resilience on import has posed challenges to the rest of the world regarding deployment and development of emerging technologies. Afterwards, assorted REE elements have been specified as critical elements (European Commission (EC) 2020; National Environmental Research Council 2015; U.S. Department of Energy 2010).

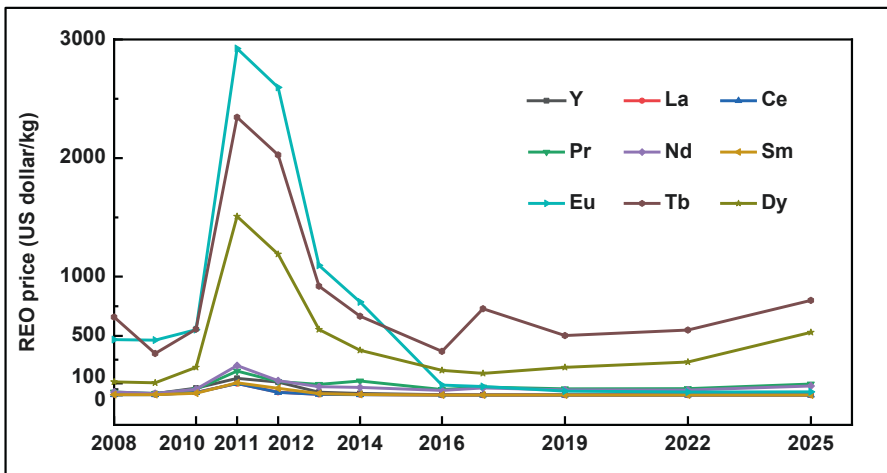


Fig. 16.2 Prices of REO from 2008 with the forecast to 2025

16.2 The Sources of Rare Earths

16.2.1 Conventional Sources for Rare Earths

The deposits of REE are observed in many nations. The estimated reserves of the global REO are at 120 million tons. The top six nations owning largest REO reserves are China, Brazil, Vietnam, Russia, India, and Australia with the corresponded reserves at of 44, 22, 22, 12, 6.9, and 3.3 million tons (U.S. Geological Survey 2020). This estimated reserve of global REE is believed to meet the global demand of REE (at level of the 2017 year) for the next 900 years. However, annual growth rate of REE demand was approximately 10%. Therefore, the global reserves of REO seem to be depleted beyond the middle of twenty-first century if the demand keeps growing, and there is no substitute or alternative sources for REE (Gschneidner et al. 2019). The statistics of the global REE mining and production in recent years are depicted in Fig. 16.3 (Gambogi 2017; U.S. Geological Survey 2020).

The known REE-bearing minerals are approximately 160 minerals. The idealized composition of REE minerals and their primary REE contents are shown in Table 16.2. However, just a few of them mined to produce products, for example, apatite, monazite, bastnasite, xenotime, loparite, and laterite clays (Golev et al. 2014). Monazite, bastnasite, and xenotime constitute 95% of commercial REO production of the world. In which, the output of REO produced from monazite, bastnasite, and xenotime was 55–60%, 70–75%, and 55–60%, respectively (Suli et al. 2017).

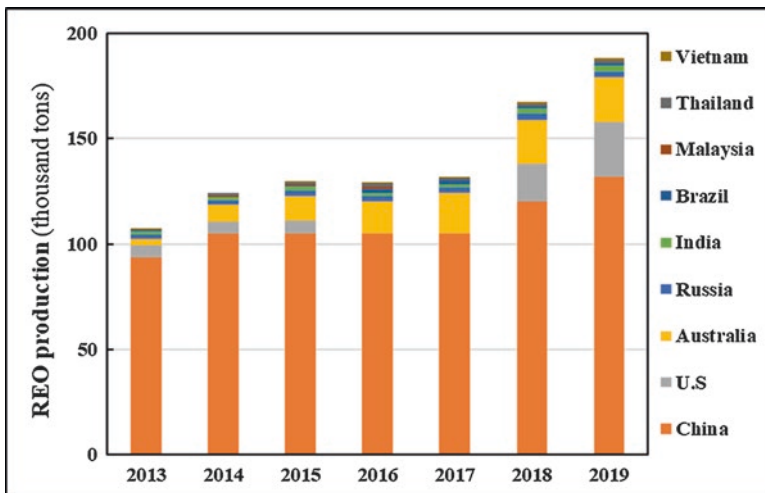


Fig. 16.3 Production of REO (thousand tons), by country

Table 16.2 Major REE-bearing minerals and its associated REE

Mineral	Composition	Primary rare earths
Allanite	$(R,Ca)_2(Al,Fe^{3+})_3(SiO_4)_3(OH)$	R-light REEs
Apatite	$(Ca,R)_5(PO_4)_3(F,Cl,OH)$	R-light REEs
Bastnasite	$R(CO_3)F$	R-light REEs
Laterite clays	SiO_2, Al_2O_3, Fe_2O_3	R-heavy REEs and yttrium
Loparite	$(R,Na,Sr,Ca)(Ti,Nb,Ta,Fe^{3+})O_3$	R-light REEs
Monazite	RPO_4	R-light REEs
Xenotime	RPO_4	R-heavy REEs and yttrium
Zircon	$(Zr,R)SiO_4$	R-all REEs

Table 16.3 Ore minerals and content of individual elements (in percentage of mass) of important REE deposits

Element	Bayan Obo, China (bastnasite)	Longnan, China (laterite)	Xunwu, China (laterite)	Mountain Pass, USA (bastnasite)	Mount Weld, Australia (monazite)	Kola Peninsula, Russia (loparite)	Lehat, Malaysia (xenotime)
Y	Trace	65	8	0.1	0.1	1.3	61
La	23	1.8	43.4	33.8	25.5	25	1.2
Ce	50	0.4	2.4	49.6	46.7	50.5	3.1
Pr	6.2	0.7	9	4.1	5.3	5	0.5
Nd	18.5	3	31.7	11.2	18.5	15	1.6
Sm	0.8	2.8	3.9	0.9	2.3	0.7	1.1
Eu	0.2	0.1	0.5	0.1	0.4	0.1	Trace
Gd	0.7	6.9	3	0.2	0.1	0.6	3.5
Tb	0.1	1.3	Trace	None	0.1	Trace	0.9
Dy	0.1	6.7	Trace	None	0.1	0.6	8.3
Ho	Trace	1.6	Trace	None	Trace	0.7	2
Er	Trace	4.9	Trace	None	Trace	0.8	6.4
Tm	Trace	0.7	Trace	None	None	0.1	1.1
Yb	Trace	2.5	0.3	None	None	0.2	6.8
Lu	Trace	0.4	0.1	Trace	None	0.2	1
Total	99.6	98.8	102.3	100	99.1	100.8	98.5

The origins of REE deposits currently profitably mined focus on four main types comprising: 1—ion-adsorption deposits; 2—placer deposits; 3—carbonatite magmas; and 4—alkaline magmas. The notable deposits of rare earths and the major corresponding rare earths minerals are shown in Table 16.3 (Gschneider et al. 2019). The origins of REE play key role in the processing routes. However, the overall process of REE production from ores typically include six distinguish phases. The whole process includes Ores exploration, exploitation, physical enrichment, chemical extraction, separation, and purification (Suli et al. 2017). Figure 16.4 visualizes the simplified ordered process for REE production from ores.



Fig. 16.4 Flow sheet of REE processing from ore minerals

16.2.2 *Alternative Sources for Rare Earths*

The intensive of REE supply has stimulated global hunt for finding new primary deposits and substitution and/or recovering REE from unconventional sources. While the production of REE from the ores is not practical due to enormously capital investment and associated negatively environmental threats, the newly economical deposits have not brought to the production. In addition, the substitutions are negligible and provide less effectiveness. Furthermore, numerous studies reported the abundance of rare earths at a considerable content in unconventional sources being tailing wastes, red mud, REE-containing end-use products, coal and coal combustion by-products, geothermal brine, etc. Therefore, numerous studies have been proceeded to evaluate the value of associated REE and to develop effective and economic routes recovering REE from those sources.

Processes to recover REE from mine tailing were also developed. A concentration of rare earths at 5000 ppm and 289.8 ppm were observed in the iron mining wastes and in the coalfield of East Kootenay, respectively (Kuppusamy et al. 2019; Peelman et al. 2016). Hydrometallurgical extraction processes were employed to extract REE at the level of 75–100% of heavy REE and < 40% of light REE from the iron mining wastes and of 85% REE from coal mine tailings.

The sum volume of REO consumed for producing high-tech components and products including permanent magnets, catalysts, alloys, glass, ceramics, and lighting devices were 121 kt and 159 kt in 2012 and 2016, respectively (Guyonnet et al. 2018). References estimated the potential amount of REO stocking in lamp phosphors, NiMH batteries, and permanent magnets at 375 kt by 2020. In which, 29.17 kt of REO are believed containing in old scrap in 2020. At the same time, the quantities of REO could be recycled, in the optimistic case, are approximately 10.68 kt. Thus, there are significant amounts of REE-containing end-of-life products, which are the futuristic unconventional sources for REE. Investigations reported the recovery of REE, mostly by hydrometallurgy processes, from permanent magnet, phosphor lamps, NiMH magnets, and fluorescent lamps were in the range of 90–100% with >99% purity (Bian et al. 2016; Dupont and Binnemans 2015; Meshram et al. 2016; Tunsu et al. 2015).

Additionally, byproducts of aluminum-making process called red mud constitute potential alternative sources for REE. Resources with scandium content between 20 and 50 ppm can be considered as an ore. However, the content of scandium contained in red mud from various sources such as Indian, Greek, Hungarian, and Australian was 50, 121, 54, and 54 ppm, which was equal or higher than the

profitable content of scandium in ore (Akcil et al. 2014; Borra et al. 2015; Ujaczki et al. 2015).

Coal combustion byproducts typically contain 200–500 ppm of REE with the global average at 445 ppm in coal fly ash (USDOE-NETL 2017). The notable concentration of 1385 ppm of REE in coal fly ash (CFA) was also reported (Mardon and Hower 2004). This makes coal ash (CA) in general and CFA in particular the most promising unconventional source for recycling REE (Taggart et al. 2016).

Recently, the development of science and technology as well as its applications has considered environmental protection. The unsecured supply of REE, fundamental for green energy, has imposed intensive barriers to the deployment and development of clean-advanced technologies. Recycling has been dragged great attention regarding reduction in the reliance of REE supply from conventional ores processing.

16.3 The Occurrence of Rare Earths in CFA

16.3.1 *The Abundance of Rare Earths in CFA*

The various origins of associated REE in coal basins were investigated. The enrichment mechanism of REE into coalfield based on genetic type was graphed by Bryan et al. (2015). Generally, four major pathways introduce REE into coal deposits, namely terrigenous type (Dai et al. 2012), tuffaceous type (Mardon and Hower 2004), infiltration type (Arbuzov and Ershov 2007), and exfiltration type (Seredin and Finkelman 2008). Terrigenous REE occurrence was driven by surface water leading to the transportation of REE-bearing minerals (e.g., apatite and zircon) into coal basins at the former formation stage. In the tuffaceous occurrence type, REE were introduced through settling of acid and alkaline pyroclastics down to coal accumulations simultaneously with explosive volcanic activity, for example, Songzao Coalfield (Dai et al. 2007) and Gunnedah Basin (Ward et al. 1999). Infiltrational and exfiltrational origin of REE-bearing coal incorporates with groundwater circulation. The descendant of groundwater brought REE components through the subsurface faults and cracks to coal bed in the epigenetic coal-formation stage making infiltration type. In contrast, the ascendant of REE-bearing groundwater through faults and cracks into coal bed in the epigenetic coal-formation stage making exfiltration type.

REE was brought from feed coal into coal combustion fly ash by the combustion process in power plants. Simultaneously, the combustion process multiplied REE content more than six folds from coal to CA (Erickson 2018; Joshi et al. 2013). Thus, various attempts proceeded to justify CFA as a source for rare earths. The understood concentration of REE from various CFA samples ranges from 200 to 550 ppm (Franus et al. 2015) with the average global basis at 445 ppm (Ketris and Yudovich 2009; USDOE-NETL 2017). REE content in several particular CFA was proved to be far exceed the world average (Fig. 16.5).

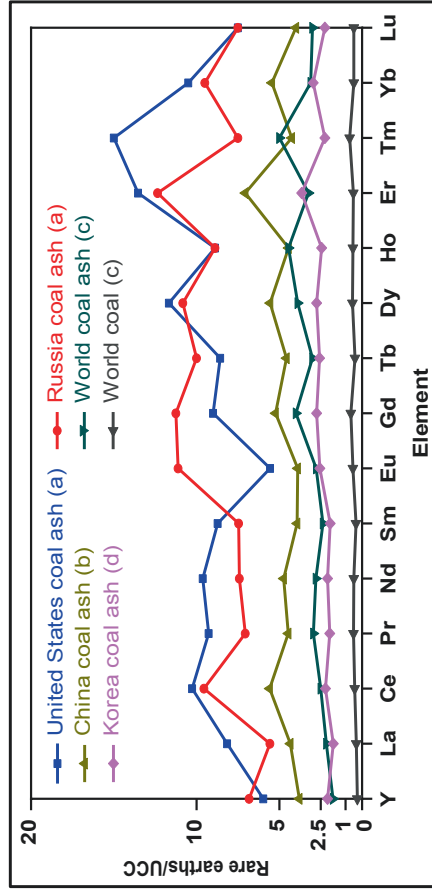


Fig. 16.5 Plots of REE standardized by median content of REE in the Upper Continental Crust (UCC) (Grigor'ev 2003). (a) Seredin and Dai (2012), (b) Pan et al. (2020), (c) Ketris and Yudovich (2009), (d) Tuan et al. (2019)

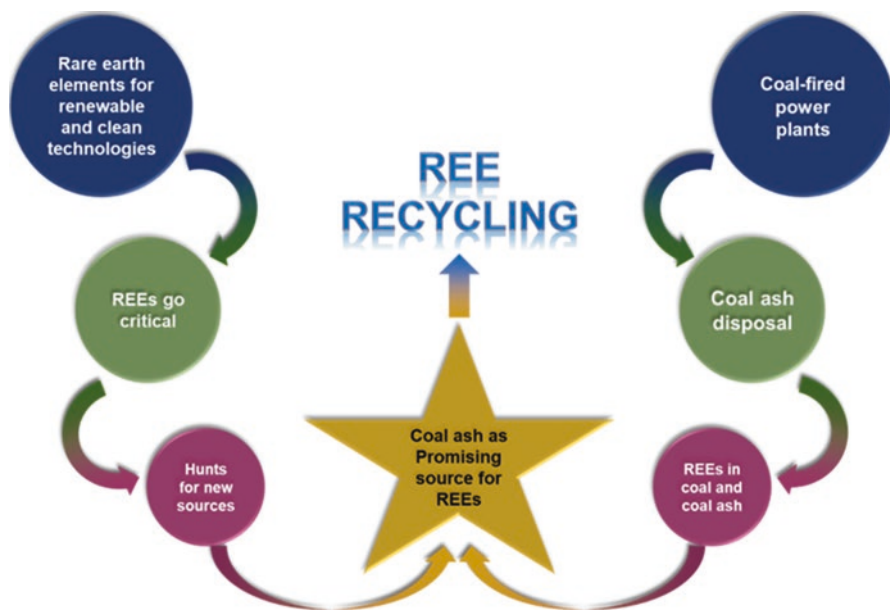


Fig. 16.6 CFA as a viable alternative source for REE

The extraordinary enrichment of REE in CFA has been reported in REE-rich samples from Russia, Mongolia, United States, and China. The range of total REE content from those sources among 721–8426 ppm (0.09–1.02%) with the average of 1000–2000 ppm (Seredin and Dai 2012). Nevertheless, a possible value of 7.1 million USD of REE was believed to be grasped in produced fly ash in Korea in 2013 (Park et al. 2015). In addition, the annual production of REO derived from the US CFA are 8.9 thousand tons, which are equivalent to an estimated value of 4.3 million USD (Taggart et al. 2016). Therefore, CFA is offering an alternative source for REE recycling (Fig. 16.6).

16.3.2 The Mode of Occurrence of REE in the CFA

CFA has been recognized as a viable secondary source expanding REE resources. Apparently, characterization of CFA with respect to REE occurrence is critical prior subsequent extraction routes. The work reported here reviews the properties of CFA and the mode of occurrence of REE. The characteristics of CFA particle regarding REE associations are governed by the quality of the feed-coal and the combustion technologies (Kutchko and Kim 2006). In general, there is not significant difference between FA in terms of size, shape, and geometry. However, the chemical compositions of FA are diversity due to the difference in coal sources and combustion process used (Bhatt et al. 2019).

CFA is separated from the flue gases coupling with a rapid cooling process. The size of particles is inconsistent between samples. Nevertheless, the dominant size of $<100\ \mu\text{m}$ of particles was reported. Pan et al. reported the mass of $<100\ \mu\text{m}$ particles of Faer and Panbei fly ashes (China) at 80–99% (Pan et al. 2019). The same results regarding the dominant of under $100\ \mu\text{m}$ particle size of FA with the cumulative distribution more than 95% were commonly established (Chindaprasirt et al. 2005; Lanzerstorfer 2018; Shearer 2014). Therefore, the FA samples are readily accessible.

The referred components of FA comprise organic compounds, feed-coal materials, and new-products (Franus et al. 2015; Goodarzi 2006; Kleinhans et al. 2018). Graphical illustration of FA particles based on the morphology and composition consisting of unburned carbon, unmolten particles, spherical molten, plerospheres, agglomeration and irregular-shaped particles is shown in Fig. 16.7. Of which, the mass of unburned carbon and unmolten particles (normally feldspars and quartz) is small in FA. The new products including spherical molten, plerospheres, agglomeration, and irregular-shaped particles are formed by the dissociation and fractionation of low melting ash/mineral particles in the fusion period or condensation and coagulation of volatilized matters in the post-combustion stage.

Chemical and mineralogical compositions of CFA are based on those in the feed coal and combustion conditions. For example, while the lignite is rich in Si, Al, Ca, Na, K, Cl, and S, the bituminous coal is just rich in Si, Al, Cl, K, Na, and S. This affects the mineral composition of feed coal, which results in the composition of corresponded CFA (Kleinhans et al. 2018). The major minerals of lignite are quartz, carbonate, and gypsum, whereas, quartz, kaolinite, illite, and pyrite are the major minerals found in bituminous coal. The composition of CFA after coal being burnt at high temperature is the consequence of decomposition, vaporization, coagulation, nucleation, and condensation processes (Kleinhans et al. 2018). However, the statistics of chemical compositions of CFA from 25 countries of Bhatt et al. showed that there are several typical elements in CFA such as SiO_2 , Al_2O_3 , Fe_2O_3 , CaO , and MgO (Bhatt et al. 2019). Accordingly, the CFA samples also contain some representative minerals including quartz, mullite, hematite/magnetite, anhydrite, and lime (Kleinhans et al. 2018; Mitchell and Gluskoter 1976).

The occurrence mode of REE in FA was investigated by sequential extraction procedure devised by researchers. Figure 16.8 illustrates the content of processes toward investigation of REE occurrence in fly ash proposed by Anand Rao et al. and Pan et al. (Rao et al. 2020; Pan et al. 2019). The mode of REE occurrence in FA was also characterized via a consecutive process comprising seven steps, which are reported by Lin et al. (2018). In addition, other processes, namely Tessier, BCR, toward speciation of particulate trace elements would be referred to characterize REE from fly ash (Pueyo et al. 2008; Tessier et al. 1979). The relatively similar processes to investigate REE occurrence were also shown in other researches (Lin et al. 2018; Park et al. 2020; Wang et al. 2019a, b).

CFA's compositions comprise crystalline and glassy phases. The mass of glassy compounds within CFA range from 60% to about 90%; the other 10–40% of CFA mass are occupied by the crystalline minerals (Chancey et al. 2010). Sequential chemical extraction (SCE) tests reported that REE is heterogeneously bound to

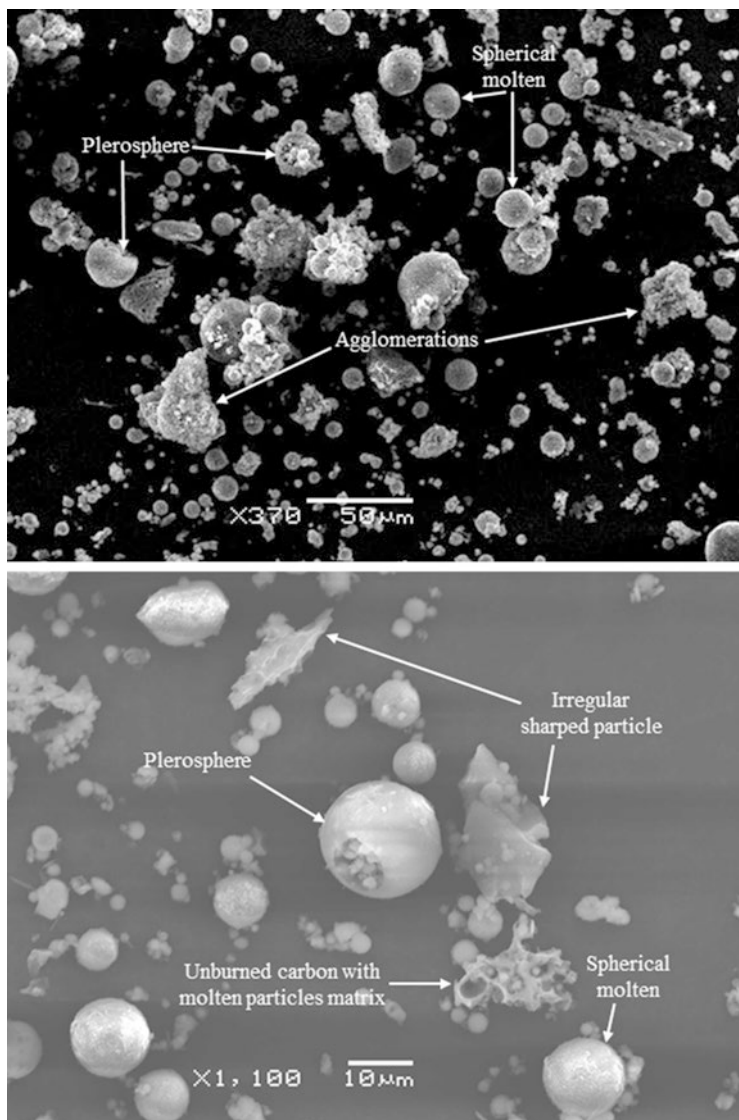


Fig. 16.7 Typical morphology of FA particles characterized by scanning electron microscope (SEM) analysis

several major bounding phases including ion-exchangeable, acid-soluble, metal oxides, organic, and silicate and aluminosilicate species. However, references reported that REE mainly participates in silicate and aluminosilicate species, especially the glassy phases (Stuckman et al. 2018; Pan et al. 2020; Kleinhans et al. 2018; Lin et al. 2018). Investigation of Lin et al. on characterization of Ohio power plant CFA found that 86.1% of REE was embedded within the aluminosilicate

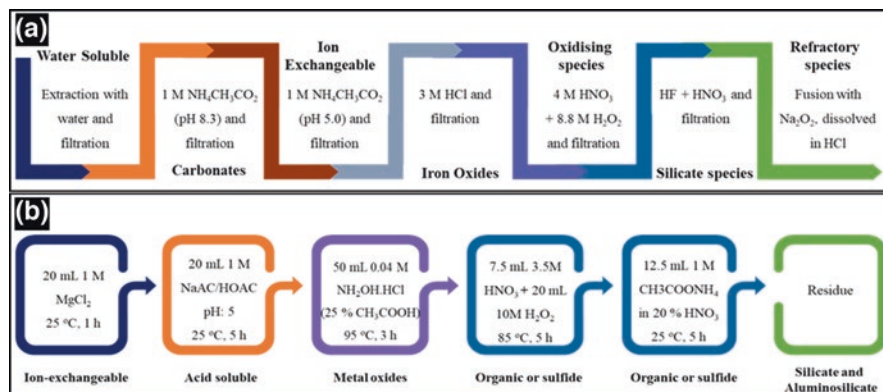


Fig. 16.8 Technique for speciation of mode of occurrence of REE in FA. Adapted from: (a) Anand Rao et al. (2020); (b) Pan et al. (2019)

species, which mostly comprise of glassy phase (Lin et al. 2018). A rate of 69% of REE combined to aluminosilicate phase of a CFA from China was also reported by Pan et al. (2020). Therefore, an effective route toward high REE extraction efficiency should overcome the issue of REE-glass phase bonding.

16.4 Rare Earths Recovery from Coal Fly Ash and CO₂ Capture

Hydrometallurgical and pyrometallurgical extraction processes constitute the effective routes of metal extraction from ores or recyclable sources. Metal extraction through pyrometallurgical process generally engages intensive energy and demands high-grade reserves. This method is conventionally adopted for proceeding mineral ores or concentrated available resources. Hydrometallurgical process is commonly proceeded prior recovery of value-added materials from low-grade unconventional or subeconomic resources, including recovery of REE from CFA. Proposed processes for REE recycling from CFA through hydrometallurgical techniques are inherently devised based on conventional ores processing techniques. The typical route of REE recycling from CFA is simply illustrated in Fig. 16.9.

Generally, extraction and recovery constitute two major operation stages of hydrometallurgical technique toward recycling of REE from CFA. Physical beneficiation processes are optionally deployed to upgrade REE content prior to processing in extraction stage. The extraction stage aims leaching of REE from solid to aqueous phase. Besides, the assistance of electromagnetic radiation and ultrasound waves possibly provides better REE extraction yields (Behera et al. 2019). Impurities are typically dissolved in the leaching process, which probably separated from the dissolved REE in the subsequent recovery process. The separation and purification

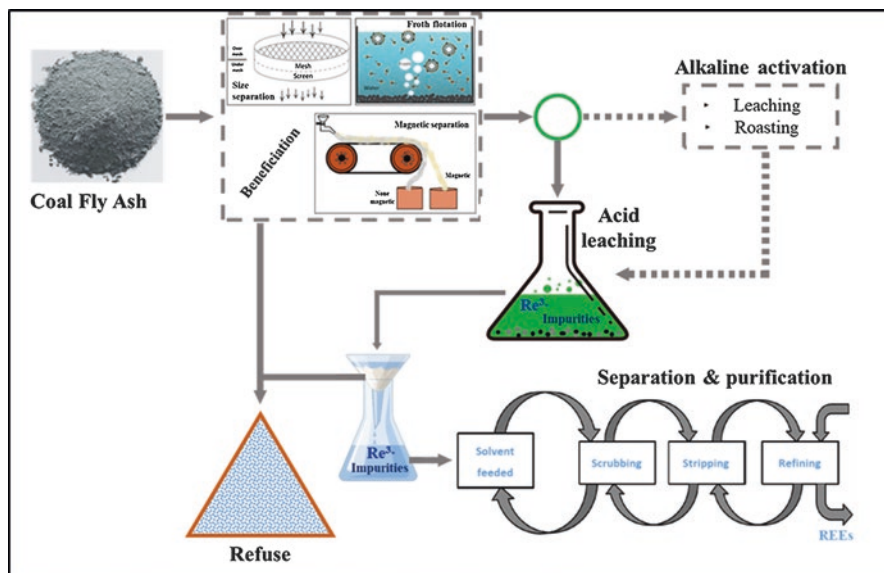


Fig. 16.9 Schematic diagram of the process to recover REE from CFA

methods include either adsorption, ion exchange, solvents extraction, or liquid membrane processes. However, solvents extraction is widely proceeded to recover REE from the leach liquor mixtures because of its selectivity and high efficiency.

16.4.1 Beneficiation of Rare Earths

The feed-coal has diverse compositions, which underwent a high-temperature combustion and rapid cooling. As a result, CFA particles are inconsistent and fractioned into divergent phases. Accordingly, beneficiation of REE rely on its distribution in CFA fractions. Based on the physical properties of CFA such as the gravity, particle size, magnetic strength, and hydrophobic property, the CFA is separated into fractions to level up the concentration of REE. Consequently, the obtained CFA beyond physical treatments has higher REE content and less fractions of unwanted impurities prior to chemical extraction processes.

The finer fractions of CFA typically concentrate more REE than the coarser fractions (Pan et al. 2019, 2020; Lin et al. 2017; Rosita et al. 2020). This means the concentration of REE increases when the particle size decreases. For example, total REE from Jungar power plant increased from 277 ppm to 648 ppm when the size of particles decreased from over 125 to minus 25 μm (Hower et al. 2016). Pan et al. observed the increase of REE content from 608 ppm at larger particle (150–100 μm) up to 896 ppm at smaller particle (–25 μm) (Pan et al. 2020). The similar phenomena was also observed in Panbei and Faer fly ash with the increase of total REE from

444 ppm and 495 ppm up to 499 ppm and 557 ppm as the particle size decreases from over 100 μm down to minus 25 μm (Pan et al. 2019). The contrast trend between particle size and REE content is explained by the bulk of small particle fractions and the strong affinity of REE to glassy phases, which have been proved occurring mostly at the finer fractions (Dai et al. 2014, 2010).

CFA particles are also separated into different fractions based on the magnetic properties. Investigation found that most of REE was preferentially partitioned within the nonmagnetic fraction of CFA. It means the magnetic susceptibility of CFA particles has the negative trend to the content of REE. Dai et al. found that the content of REE contained in the nonmagnetic fraction is higher than that contained in the magnetic one (261 ppm versus 202 ppm) (Dai et al. 2010). Blissett et al. recorded a concentration of 505 ppm of REO from the UK-1 CFA sample, which just have 270 ppm of REO contained in the magnetic fractions (Blissett et al. 2014). Lin et al. studied the distribution of REE corresponding to magnetic property of CFA from Ohio power plant (USA). The results showed that 80% in weight of CFA is nonmagnetic, which contained 360 ppm REE, accounting for 88% of total REE. Whereas, the magnetic fraction of CFA is 20% with the REE content at 196 ppm (Lin et al. 2018). An observation of Pan et al. on fly ash sample from China found that 60% of mass is nonmagnetic. Total REE of nonmagnetic fraction from this sample was reported at 63% with the concentration over 900 ppm (Pan et al. 2020).

Fractionation of REE is witnessed in density and hydrophobicity of CFA, which would be separated through froth floatation technique (Lin et al. 2017; Zhang et al. 2015b). REE is heterogeneously distributed in different fractions of CFA with respect to its density. Lin et al. reported that the more enriched density fraction of REE was at 2.71 ± 0.25 g/mL (Lin et al. 2017). Zhang et al. also reported a more enrichment of REE (521 ppm) in the -1.8 g/mL fraction rather than the over 1.8 g/mL fraction (376 ppm) (Zhang et al. 2015a). In addition, Pan et al. found that REE was more fractioned at the density of 2.4–2.6 g/mL, which is similar to quartz's density. The fraction of 2.4–2.6 g/mL of this sample accounted for 24% and 31% of ash yield and total REE recovery, respectively (Pan et al. 2020). However, the differences in mass recovery, REE concentration, and total REE of each fraction of density are insignificant. As a result, density separation targeting REE enrichment becomes less effective. Therefore, grinding is needed toward liberating REE from the glassy phase, which would increase the effectiveness of REE enrichment by density separation.

Deployment of beneficiation process could significantly elevate concentration of REE in CFA prior to subsequent chemical extraction as well as remove impurities, which could interfere with the efficiency of leaching process. An integrated process should be properly developed to effectively enrich and recover REE from CFA. There is no specific process for this matter. However, beneficiation processes commonly focus on some fundamental fractions including small particles, weak and nonmagnetic, and moderate density fraction (similar to quartz if needed). An emerged physical pretreatment process devised by Lin et al. toward REE enrichment including

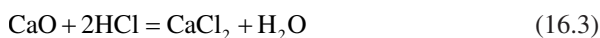
magnetic separation followed by size classification leveled up the concentration of REE from 325 ppm to 877 ppm with 49% total REE recovery (Lin et al. 2018).

16.4.2 Chemical Extraction of Rare Earths

Numerous recent studies proceeded to extract REE from various CFA sources through chemical leaching processes. Due to the relative differences of CFA sources, numerous leaching methods have been devised toward effective extraction of REE. Acidic leaching has been widely used to dissolve REE from CFA. However, in the chemical activation steps, alkaline activation could be either integrated prior to acidic leaching to produce higher extraction yields.

16.4.2.1 Acidic Leaching

Leaching is the utmost requisite step to dissolve REE from low-grade source like CFA. The requirement for high REE leaching efficiency has been satisfied by just acidic leaching. Reactions between acid-soluble fractions and REE of CFA with acid, taking HCl as an example, are described by Eqs. (16.1)–(16.4).



REE leaching from Illinois and Appalachian CFA using HCl was conducted by King et al. The leaching efficiency of 35–43% and 40–57% from Illinois and Appalachian CFA was documented as the condition of 12 mol/L HCl, 85 °C, and 4 h (King et al. 2018). Leaching of REE from Panbei fly ash using 3 mol/L HCl at 60 °C for 2 h provided 72%, 66%, and 62% leaching efficiency of lanthanum, cerium, and neodymium, respectively (Cao et al. 2018). Kashiwakura et al. also investigated the leaching behavior of lanthanum in Japan fly ash under the attack of H₂SO₄ solvent. The highest dissolution rate of lanthanum in H₂SO₄ at 80 °C for 2 h was about 44% (Kashiwakura et al. 2013).

Studies on REE leaching from circular fluidized bed combustion (CFBC) FA were also executed by Honaker et al., Tuan et al., and King et al. (Honaker et al. 2019; King et al. 2018; Tuan et al. 2019). Researchers witnessed a considerable leaching efficiency of REE from this fly ash type. Acid leaching using 2 mol/L HCl at 80 °C targeting REE dissolution from a Korean fly ash provided approximately 55%, 62%, and 65% for neodymium, yttrium, and dysprosium, respectively (Tuan et al. 2019). An experiment of REE leaching from calcined Illinois CFBC coal ash

using diluted HCl (1.2 mol/L) at 75 °C for 5 h was executed providing nearly 80% REE leached (Honaker et al. 2019). Particularly, a remarkable leaching yield of REE (80% to over 100%) from Powder River Basin fly ash at the condition of 12 mol/L HCl, 85 °C, and 4 h was reported (King et al. 2018). The higher leaching yield of REE from CFBC fly ash versus pulverized coal (PC) combustion FA could be explained by the lower combustion temperature (800–900 °C versus 1300–1450 °C) and desulfurization in the post-combustion step. The lower combustion temperature of CFBC boiler makes the coal materials less molten and less volatile resulting in the less of glassy components formation during rapid cooling stage. It means the REE partition within the acid-insoluble glassy phase in CFBC fly ash less than that in the pulverized CFA. Additionally, by adding limestone to remove sulfur in the desulfurization step promoted the higher partition of REE with more acid-soluble calcium compounds.

However, a relatively limited leaching efficiency was observed when solely applies acid leaching as the majority of REE are embedded in the glassy phase, which has low solubility in the acidic condition. Therefore, it makes recovery of REE from CFA by direct acidic leaching being inefficient. Recovered yield of REE from CFA by acidic leaching could be satisfied, but at the extensive conditions it requires high energy consumption and concentrated reagents.

16.4.2.2 Alkaline Activated-Acidic Leaching

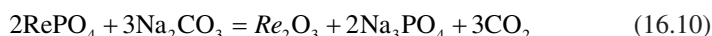
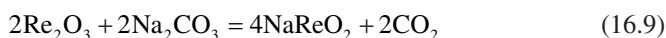
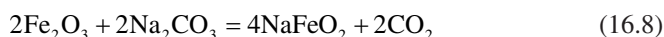
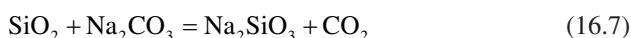
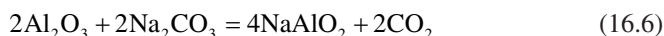
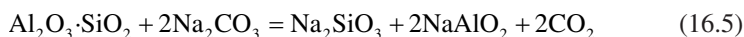
Alkaline Roasting-Acid Leaching

Roasting is a pretreatment method that uses elevated temperature and additives to modify sample's chemical and physical properties making the targeted materials to be more amenable in the downstream process. The temperature applied for roasting is lower than the fusion point of materials. The major portion of REE is partition in the compacted amorphous aluminosilicate matrix, which means the comprehensive breakage of the REE-aluminosilicate bond being important. Processes developed to extract Al and Si from CFA are a logically initial point because they intend decomposing aluminosilicate to access REE. The extraction yields of REE is reported to be intensified by roasting of CFA using alkaline reagents prior to acid leaching (Shoppert et al. 2017; Taggart et al. 2018; Tang et al. 2019).

Attempts on boosting REE leaching coupled with the assistance of alkaline roasting have proceeded. Alkaline roasting-acid leaching technique toward REE extraction from Appalachian and Illinois CFA was performed by Taggart et al. (2018). Formerly, the roasting condition was optimized by varying temperatures, roasting additives, and additive-ash ratio. Roasting with NaOH was found to provide the highest REE leaching effectiveness in comparison to Na₂CO₃, CaO, and CaSO₄. Downstream process was performed by leaching of roasted CFA in acidic condition followed by solid-liquid filtration and dilution for storage and inductively coupled plasma (ICP) analysis. The maximum leaching yield of REE from respective Appalachian and Illinois CFA was 93–97% and 90–150%, respectively, when

alkaline roasting-acid leaching was used: NaOH-fly ash was 6:1 at the temperature of 450 °C for 30 min followed by leaching with 20 mL of 2 mol/L HNO₃ within 1 week.

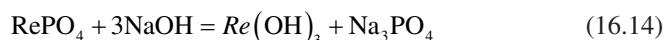
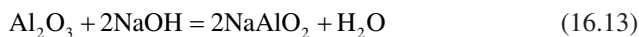
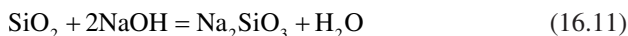
Extraction of REE from Guizhou CFA by alkaline fusion followed by acid leaching was promoted by Tang et al. (2019). The fusion stage used Na₂CO₃ as the additive with the additive:fly ash ratio being 1:1. This mixture was heated in the flux of 860 °C for 30 min and then was subjected to the leaching process using HCl 3 mol/L with the pulp density of 100 g/L (solid/liquid) for 2 h. The reactions occurred in the fusion process between CFA and Na₂CO₃ are outlined through Eqs. (16.5)–(16.10). This whole process enabled to leach approximately 72.8% of total REE occurred in the fly ash sample.

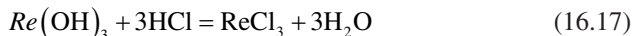
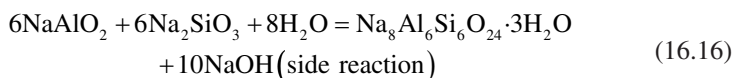
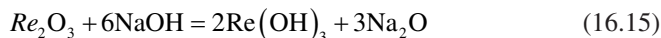


An integrated alkaline fusion-acid leaching was recognized as the comprehensive technique toward CFA processing (Shoppert et al. 2017). Alkaline fusion is the key opening the strong bond between REE and aluminosilicate phase by transforming silica into acid-soluble forms, which enhances REE accessible in the subsequent acid leaching process.

Alkaline Leaching-Acid Leaching

Alkali leaching of CFA prior to acid leaching exhibited high performance regarding REE leaching due to high desilication ability (Lin et al. 2018; Ma et al. 2019; King et al. 2018; Wang et al. 2019a, b). The purpose of leaching CFA using alkaline reagent is to dissolve aluminosilicate matrix toward liberation of the REE minerals prior to the subsequent acid leaching step. Mechanism of REE extraction from CFA through acid leaching-associated alkaline leaching was shown in Eqs. (16.11)–(16.17) (Ding et al. 2016).

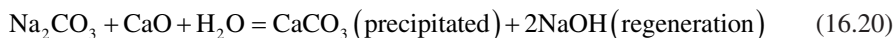
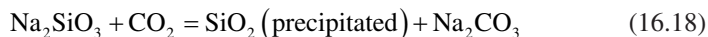




Leaching of CFA from Ohio power plant using NaOH 5 mol/L at elevated temperature for 2 h with a pulp density of 50 g/L providing desilication rate of 21.3% was performed by Lin et al. (2018). Accordingly, total REE was elevated to 803 ppm from a concentration of 366 ppm with a loss of 21%. A sequential extraction route was applied to extract REE from Luzhou CFA (China), which has over 90% REE associated with the glassy phase (70% weight of CFA) (Wang et al. 2019a, b). The experimental condition was alkaline leaching using NaOH 10 M at 150 °C for 2 h with a pulp density of 100 g/L (CFA/NaOH) followed by acid leaching using HCl 8 M at 60 °C for 2 h with a pulp density of 33.3 g/L (CFA/HCl). Accordingly, the results for desilication rate and REE leaching were 41.1% and 88.2%, respectively.

16.4.3 *CO₂ Capture and Chemical Regeneration via Integration of Carbon Mineralization*

Alkaline activation by either roasting or leaching methods followed by acid leaching are the fundamental steps to dissolve Si and Al for further recovery of them from CFA (Li et al. 2014; Zhang et al. 2016; Gong et al. 2019; Shoppert et al. 2017; Sedres 2016). Similarly, REE extraction from CFA couples with the dissolution of Si and Al, which could be recovered as extra valuable products. Si and Al ion presented in aqueous leaching solution (without the appearance of REE) could be easily recovered by carbonation process. The deployment of carbonation process by using CO₂ brings merits promoting REE recovery. Si and Al have been precipitated from aqueous alkali solution by solely injecting CO₂ gas (Chesley and Burnet 1987; Long et al. 2010; Yao et al. 2014). In addition to Si and Al recovery, coupling of carbonation process with the additional sources of calcium not only enables regeneration of alkaline reagents such as NaOH and Na₂O, which are costly and essential for REE recovery process, but also produces calcium carbonate, which has been used in many important applications. The reactions of Si and Al precipitation and NaOH regeneration during carbonation process are presented through Eqs. (16.18)–(16.20). Moreover, environmental benefits could be gained from carbonation process. While the high alkaline refused solution of chemical extraction process is neutralized, CO₂ and dissolved toxicities could be captured in precipitated carbonates (Chen et al. 2009). Therefore, the carbonation process should be integrated to promote green and economic recovery of REE from CFA.



16.4.4 Separation and Purification of Rare Earths

The leached REE in the leaching solution was subsequently separated from impurities and recovered through complexes of separation and purification steps. There exist several methods to separate and purify metal ion from the leach liquor such as ion exchange, solvent extraction (SX), liquid membrane, supercritical, electro-winning, and adsorption. However, SX is conventionally used to recover REE from rare earths ore processing process, which has been deployed in commercial scale based on the its capability of selective separation of REE (Pradip and Fuerstenau 2013; Suli et al. 2017; Thakur 2000; Peiravi et al. 2017).

SX is a technique that uses extractants such as Di-(2-ethylhexyl) phosphoric acid (DEHPA or D2EHPA), Cyanex 572, or Tributyl phosphate (TBP) to separate REE and unwanted impurities into immiscible organic and aqueous phase. The effectiveness of SX is governed by the natural behaviors of REE to the changes in solvent and aqueous phases. Therefore, the conditions of SX including extractant selection, pH, concentration of REE, and impurities in the leach liquor interact and contribute to the effectiveness of REE recovery (Xie et al. 2014).

16.5 Concluding Remarks

REE has been acclaimed for its vital positions to the deployment and development of clean-emerged technologies and national security. The intensive challenge of steady REE supply has made REE critical. However, increase in REE extraction from ores processing associates difficulties and negative effects. The significant concentration of REE in CFA has been dragged great attention with respect to REE recycling.

Numerous researches on the evaluation of REE value in CFA have been performed globally. Efforts on characterization properties of CFA have clarified the mode of occurrence of REE in CFA. The major content of REE in CFA is partition within the aluminosilicate compounds, particularly in the glassy phases. The recycling process prior to REE recovery from CFA should overcome the strong bonding of REE to the glassy phases.

There exist large amounts of studies to recover REE from CFA. Accordingly, numerous recycling routes were devised. Review on the established techniques for recycling of REE from CFA indicates three major processes, which are physical enrichment, chemical extraction, and REE separation and purification. The incorporation of carbon mineralization process into recycling process would promote associated economic and environmental benefits. However, there is not specific method that is universally acclaimed so far. Therefore, more attention and efforts should be paid for further development of recycling process toward green and effective recovery of REE from CFA.

Acknowledgments This research was supported by the National Strategic Project-Carbon Mineralization Flagship Center of the National Research Foundation of Korea (NRF) funded by the Ministry of Science and ICT (MSIT), the Ministry of Environment (ME), and the Ministry of Trade, Industry, and Energy (MOTIE) (2017M3D8A2084752).

References

- Akcil A., Akhmediyeva, N., Abdulvaliyev, R., & Abhilash, Meshram P. (2014). RedMud: a secondary resource for rare earth elements. In *International Bauxite, Alumina and Aluminium Symposium (IBAAS 2014)*.
- Alonso, E., Sherman, A. M., Wallington, T. J., Everson, M. P., Field, F. R., Roth, R., Kirchain, R. E. (2012). 2012-Evaluating rare earth element availability a case with revolutionary demand from clean technologies supporting information.pdf.
- Arbuzov, S. I., & Ershov, V. V. (2007) . *Geochemistry of rare elements in coals of Siberia*. Tomsk, Russia.
- Awais, M. (2016). What are rare earth elements, REEs? [WWW Document]. *Eur. Train. Netw. Des. Recycl. Rare-Earth Perm. Magn. Mot. Gener. Hybrid Full Electr. Veh.* Retrieved 22 October, 2020, from <https://etn-demeter.eu/what-are-rare-earth-elements-rees/>
- Behera, S. S., Panda, S. K., Mandal, D., & Parhi, P. K. (2019). Ultrasound and microwave assisted leaching of neodymium from waste magnet using organic solvent. *Hydrometallurgy*, 185, 61–70. <https://doi.org/10.1016/j.hydromet.2019.02.003>.
- Bhatt, A., Priyadarshini, S., Acharath Mohanakrishnan, A., Abri, A., Sattler, M., & Techapaphawit, S. (2019). Physical, chemical, and geotechnical properties of coal fly ash: A global review. *Case Studies in Construction Materials*, 11, e00263. <https://doi.org/10.1016/j.cscm.2019.e00263>.
- Bian, Y., Guo, S., Jiang, L., Liu, J., Tang, K., & Ding, W. (2016). Recovery of rare earth elements from NdFeB magnet by VIM-HMS method. *ACS Sustainable Chemistry and Engineering*, 4, 810–818. <https://doi.org/10.1021/acssuschemeng.5b00852>.
- Blissett, R. S., Smalley, N., & Rowson, N. A. (2014). An investigation into six coal fly ashes from the United Kingdom and Poland to evaluate rare earth element content. *Fuel*, 119, 236–239. <https://doi.org/10.1016/j.fuel.2013.11.053>.
- Borra, C. R., Pontikes, Y., Binnemans, K., & Van Gerven, T. (2015). Leaching of rare earths from bauxite residue (red mud). *Minerals Engineering*, 76, 20–27. <https://doi.org/10.1016/j.mineng.2015.01.005>.
- Bryan, R. C., Richers, D., Anderson, H. T., & Gray, T. (2015). *Assessment of rare earth elemental contents in select United States Coal Basins*. United States National Energy Technology Laboratory, Tetra Tech Inc., pp. 1–47.
- Cao, S., Zhou, C., Pan, J., Liu, C., Tang, M., Ji, W., Hu, T., & Zhang, N. (2018). Study on influence factors of leaching of rare earth elements from coal fly ash. *Energy and Fuels*, 32, 8000–8005. <https://doi.org/10.1021/acs.energyfuels.8b01316>.

- Castor, S. B., & Hedrick, J. B. (2006). Rare earth elements. In *Industrial minerals and rocks. Society for mining, metallurgy, and exploration* (pp. 769–792).
- Chancey, R. T., Stutzman, P., Juenger, M. C. G., & Fowler, D. W. (2010). Comprehensive phase characterization of crystalline and amorphous phases of a Class F fly ash. *Cement and Concrete Research*, *40*, 146–156. <https://doi.org/10.1016/j.cemconres.2009.08.029>.
- Chen, Q., Luo, Z., Hills, C., Xue, G., & Tyrer, M. (2009). Precipitation of heavy metals from wastewater using simulated flue gas: sequent additions of fly ash, lime and carbon dioxide. *Water Research*, *43*, 2605–2614. <https://doi.org/10.1016/j.watres.2009.03.007>.
- Chesley, J. A., & Burnet, G. (1987). Sulfate-resistant portland cement from Lime-Soda sinter process residue. *MRS Online Proceedings Library Archive*, *113*, 163. <https://doi.org/10.1557/PROC-113-163>.
- Chindapasirt, P., Jaturapitakkul, C., & Sinsiri, T. (2005). Effect of fly ash fineness on compressive strength and pore size of blended cement paste. *Cement and Concrete Composites*, *27*, 425–428. <https://doi.org/10.1016/j.cemconcomp.2004.07.003>.
- Dai, S., Jiang, Y., Ward, C. R., Gu, L., Seredin, V. V., Liu, H., Zhou, D., Wang, X., Sun, Y., Zou, J., & Ren, D. (2012). Mineralogical and geochemical compositions of the coal in the Guanbanwusu Mine, Inner Mongolia, China: Further evidence for the existence of an Al (Ga and REE) ore deposit in the Jungar Coalfield. *International Journal of Coal Geology*, *98*, 10–40. <https://doi.org/10.1016/j.coal.2012.03.003>.
- Dai, S., Zhao, L., Hower, J. C., Johnston, M. N., Song, W., Wang, P., & Zhang, S. (2014). Petrology, mineralogy, and chemistry of size-fractioned fly ash from the Jungar power plant, Inner Mongolia, China, with emphasis on the distribution of rare earth elements. *Energy and Fuels*, *28*, 1502–1514. <https://doi.org/10.1021/ef402184t>.
- Dai, S., Zhao, L., Peng, S., Chou, C. L., Wang, X., Zhang, Y., Li, D., & Sun, Y. (2010). Abundances and distribution of minerals and elements in high-alumina coal fly ash from the Jungar Power Plant, Inner Mongolia, China. *International Journal of Coal Geology*, *81*, 320–332. <https://doi.org/10.1016/j.coal.2009.03.005>.
- Dai, S. F., Zhou, Y. P., Ren, D. Y., Wang, X. B., Li, D., & Zhao, L. (2007). Geochemistry and mineralogy of the Late Permian coals from the Songzo Coalfield, Chongqing, southwestern China. *Science in China Series D: Earth Sciences*, *50*, 678–688. <https://doi.org/10.1007/s11430-007-0001-4>.
- Ding, J., Ma, S., Zheng, S., Zhang, Y., Xie, Z., Shen, S., & Liu, Z. (2016). Study of extracting alumina from high-alumina PC fly ash by a hydro-chemical process. *Hydrometallurgy*, *161*, 58–64. <https://doi.org/10.1016/j.hydromet.2016.01.025>.
- Dupont, D., & Binnemans, K. (2015). Rare-earth recycling using a functionalized ionic liquid for the selective dissolution and revalorization of $Y_2O_3:Eu^{3+}$ from lamp phosphor waste. *Green Chemistry*, *17*, 856–868. <https://doi.org/10.1039/c4gc02107j>.
- Erickson, B. E. (2018). From coal, a new source of rare earths: U.S. efforts to extract valuable elements from coal waste surge [WWW Document]. *Chemical & Engineering News*. Retrieved 11 October, 2020, from <https://cen.acs.org/materials/inorganic-chemistry/coal-new-source-rare-earth/96/i28>.
- European Commission (EC). (2020) *Critical raw materials resilience: Charting a path towards greater security and sustainability*.
- Fernández Martínez, V. M., Hornero del Castillo, E., & Pérez Muga, J. A. (1994). El poblado ibérico del Cerro de las Nieves (Pedro Muñoz). Excavaciones 1984–1991. In *Jornadas de Arqueología de Ciudad Real en la Universidad Autónoma* (pp. 111–130). de Madrid: Arqueología en Ciudad Real.
- Franus, W., Wiatros-Motyka, M. M., & Wdowin, M. (2015). Coal fly ash as a resource for rare earth elements. *Environmental Science and Pollution Research*, *22*, 9464–9474. <https://doi.org/10.1007/s11356-015-4111-9>.
- Gambro, J. (2017). *Minerals yearbook-rare earths*, U.S. Geological Survey.
- Garside, M. (2020a). Rare earth oxide demand worldwide from 2017 to 2025 [WWW Document]. *Statista*. Retrieved 22 Sept, 2020, from <https://www.statista.com/statistics/1114638/global-rare-earth-oxide-demand/>

- Garside, M. (2020b). Forecast rare earth oxide prices worldwide 2019–2025 [WWW Document]. *Statista*. Retrieved 24 Sept, 2020, from <https://www.statista.com/statistics/449838/forecast-average-rare-earth-oxide-prices-globally/>
- Golev, A., Scott, M., Erskine, P. D., Ali, S. H., & Ballantyne, G. R. (2014). Rare earths supply chains: Current status, constraints and opportunities. *Resources Policy*, *41*, 52–59. <https://doi.org/10.1016/j.resourpol.2014.03.004>.
- Gong, Y., Sun, J., Sun, S. Y., Lu, G., & Zhang, T. A. (2019). Enhanced desilication of high alumina fly ash by combining physical and chemical activation. *Metals (Basel)*, *9*(4), 411. <https://doi.org/10.3390/met9040411>.
- Goodarzi, F. (2006). Morphology and chemistry of fine particles emitted from a Canadian coal-fired power plant. *Fuel*, *85*, 273–280. <https://doi.org/10.1016/j.fuel.2005.07.004>.
- Grigor'ev, N. A. (2003). Average concentrations of chemical elements in rocks of the upper continental crust. *Geochemistry International*, *41*, 711–718.
- Gschneidner, Karl A., Pecharsky, J., Vitalij, K., Gregersen, E., Rafferty, J. P., & Young, G. (2019). Rare-earth element [WWW Document]. *Encyclopædia Britannica*. Retrieved 7 September, 2020, from <https://www.britannica.com/science/rare-earth-element/Minerals-and-ores>.
- Guyonnet, D., Lefebvre, G., Menad, N., 2018. Rare earth elements and high-tech products. In *Circular economy coalition for Europe* (pp. 1–11). <http://www.ccc4europe.eu>
- Holleman, A. F., Wiberg, E., & Wiberg, N. (2007). *Lehrbuch der Anorganischen Chemie (in German)* (102nd ed.). Walter de Gruyter.
- Honaker, R. Q., Zhang, W., & Werner, J. (2019). Acid leaching of rare earth elements from coal and coal ash: implications for using fluidized bed combustion to assist in the recovery of critical materials. *Energy and Fuels*, *33*, 5971–5980. <https://doi.org/10.1021/acs.energyfuels.9b00295>.
- Hower, J. C., Granite, E. J., Mayfield, D. B., Lewis, A. S., & Finkelman, R. B. (2016). Notes on contributions to the science of rare earth element enrichment in coal and coal combustion byproducts. *Minerals*, *6*(2), 32. <https://doi.org/10.3390/min6020032>.
- Hower, J. C., Ruppert, L. F., & Eble, C. F. (1999). Lanthanide, yttrium, and zirconium anomalies in the Fire Clay coal bed, Eastern Kentucky. *International Journal of Coal Geology*, *39*, 141–153. [https://doi.org/10.1016/S0166-5162\(98\)00043-3](https://doi.org/10.1016/S0166-5162(98)00043-3).
- Joshi, P. B., Preda, D. V., Skyler, D. A., Tsinberg, A., Green, B. D., & Marinelli, W. J. (2013). *Recovery of rare earth elements and compounds from coal ash*. US 8,968,688 B2.
- Kashiwakura, S., Kumagai, Y., Kubo, H., & Wagatsuma, K. (2013). Dissolution of rare earth elements from coal fly ash particles in a dilute H₂SO₄ solvent. *Open Journal of Physical Chemistry*, *03*, 69–75. <https://doi.org/10.4236/ojpc.2013.32009>.
- Ketris, M. P., & Yudovich, Y. E. (2009). Estimations of Clarkes for Carbonaceous biolithes: World averages for trace element contents in black shales and coals. *International Journal of Coal Geology*, *78*, 135–148. <https://doi.org/10.1016/j.coal.2009.01.002>.
- King, J. F., Taggart, R. K., Smith, R. C., Hower, J. C., & Hsu-Kim, H. (2018). Aqueous acid and alkaline extraction of rare earth elements from coal combustion ash. *International Journal of Coal Geology*, *195*, 75–83. <https://doi.org/10.1016/j.coal.2018.05.009>.
- Kleinhans, U., Wieland, C., Frandsen, F. J., & Spliethoff, H. (2018). Ash formation and deposition in coal and biomass fired combustion systems: Progress and challenges in the field of ash particle sticking and rebound behavior. *Progress in Energy and Combustion Science*, *68*, 65–168. <https://doi.org/10.1016/j.peccs.2018.02.001>.
- Kuppasamy, V. K., Kumar, A., & Holuszko, M. (2019). Simultaneous extraction of clean coal and rare earth elements from coal tailings using alkali-acid leaching process. *Journal of Energy Resources Technology Transactions of the ASME*, *141*, 1–7. <https://doi.org/10.1115/1.4043328>.
- Kutchko, B. G., & Kim, A. G. (2006). Fly ash characterization by SEM-EDS. *Fuel*, *85*, 2537–2544. <https://doi.org/10.1016/j.fuel.2006.05.016>.
- Lanzerstorfer, C. (2018). Fly ash from coal combustion: Dependence of the concentration of various elements on the particle size. *Fuel*, *228*, 263–271. <https://doi.org/10.1016/j.fuel.2018.04.136>.
- Li, H., Hui, J., Wang, C., Bao, W., & Sun, Z. (2014). Extraction of alumina from coal fly ash by mixed-alkaline hydrothermal method. *Hydrometallurgy*, *147–148*, 183–187. <https://doi.org/10.1016/j.hydromet.2014.05.012>.

- Lin, R., Howard, B. H., Roth, E. A., Bank, T. L., Granite, E. J., & Soong, Y. (2017). Enrichment of rare earth elements from coal and coal by-products by physical separations. *Fuel*, *200*, 506–520. <https://doi.org/10.1016/j.fuel.2017.03.096>.
- Lin, R., Stuckman, M., Howard, B. H., Bank, T. L., Roth, E. A., Macala, M. K., Lopano, C., Soong, Y., & Granite, E. J. (2018). Application of sequential extraction and hydrothermal treatment for characterization and enrichment of rare earth elements from coal fly ash. *Fuel*, *232*, 124–133. <https://doi.org/10.1016/j.fuel.2018.05.141>.
- Long, S. S., Zhang, G. F., Feng, Q. M., Ou, L. M., & Lu, Y. P. (2010). Desilicisation of alkaline leaching solution of roasted stone coal with carbonation method. *Transactions of Nonferrous Metals Society of China*, *20*, s132–s135. [https://doi.org/10.1016/S1003-6326\(10\)60027-1](https://doi.org/10.1016/S1003-6326(10)60027-1).
- Lucas, J., Lucas, P., Le Mercier, T., Rollat, A., & Davenport, W. (2015). Rare earths in rechargeable batteries. In *Rare earths* (pp. 167–180). Elsevier. <https://doi.org/10.1016/b978-0-444-62735-3.00010-3>.
- Ma, Z., Zhang, S., Zhang, H., & Cheng, F. (2019). Novel extraction of valuable metals from circulating fluidized bed-derived high-alumina fly ash by acid–alkali–based alternate method. *Journal of Cleaner Production*, *230*, 302–313. <https://doi.org/10.1016/j.jclepro.2019.05.113>.
- Mardon, S. M., & Hower, J. C. (2004). Impact of coal properties on coal combustion by-product quality: Examples from a Kentucky power plant. *International Journal of Coal Geology*, *59*, 153–169. <https://doi.org/10.1016/j.coal.2004.01.004>.
- Meshram, P., Pandey, B. D., & Mankhand, T. R. (2016). Process optimization and kinetics for leaching of rare earth metals from the spent Ni-metal hydride batteries. *Waste Management*, *51*, 196–203. <https://doi.org/10.1016/j.wasman.2015.12.018>.
- Mikami, M., Watanabe, H., Uheda, K., Shimooka, S., Shimomura, Y., Kurushima, T., & Kijima, N. (2009). New phosphors for white LEDs: Material design concepts. *IOP Conference Series: Materials Science and Engineering*, *1*, 012002. <https://doi.org/10.1088/1757-8981/1/1/012002>.
- Mitchell, R. S., & Gluskoter, H. J. (1976). Mineralogy of ash of some American coals: Variations with temperature and source. *Fuel*, *55*, 90–96. [https://doi.org/10.1016/0016-2361\(76\)90001-6](https://doi.org/10.1016/0016-2361(76)90001-6).
- Morrison, W., & Tang, R. (2012). *China's rare earth industry and export regime: Economic and trade implications for the United States*.
- Mueller-Mach, R., & Mueller, G. O. (2000). White-light-emitting diodes for illumination. In H. W. Yao, I. T. Ferguson, & E. F. Schubert (Eds.), *Light-emitting diodes: Research, manufacturing, and applications IV* (pp. 30–41). SPIE. <https://doi.org/10.1117/12.382840>.
- National Environmental Research Council. (2015). Risk list 2015: an update to the supply risk index for elements or element groups that are of economic value. *British Geological Survey*, *1*, 11. <https://doi.org/10.1017/CBO9781107415324.004>.
- Pan, J., Nie, T., Vaziri Hassas, B., Rezaee, M., Wen, Z., & Zhou, C. (2020). Recovery of rare earth elements from coal fly ash by integrated physical separation and acid leaching. *Chemosphere*, *248*, 126112. <https://doi.org/10.1016/j.chemosphere.2020.126112>.
- Pan, J., Zhou, C., Tang, M., Cao, S., Liu, C., Zhang, N., Wen, M., Luo, Y., Hu, T., & Ji, W. (2019). Study on the modes of occurrence of rare earth elements in coal fly ash by statistics and a sequential chemical extraction procedure. *Fuel*, *237*, 555–565. <https://doi.org/10.1016/j.fuel.2018.09.139>.
- Park, S., Kim, M., Lim, Y., Yu, J., Chen, S., Woo, S. W., Yoon, S., Bae, S., & Kim, H. S. (2020). Characterization of rare earth elements present in coal ash by sequential extraction. *Journal of Hazardous Materials*, *402*, 123760. <https://doi.org/10.1016/j.jhazmat.2020.123760>.
- Park, S.-U., Kim, J.-K., Seo, Y.-S., Hong, J.-S., Lee, H.-B., & Lee, H.-D. (2015). Evaluation of some rare metals and rare earth metals contained in coal ash of coal-fired power plants in Korea. *Journal of the Korean Institute of Resources Recycling*, *24*, 67–75. <https://doi.org/10.7844/kirr.2015.24.4.67>.
- Peelman, S., Sun, Z. H. I., Sietsma, J., & Yang, Y. (2016). Hydrometallurgical extraction of rare earth elements from low grade mine tailings. *Rare metal technology*, *2016*, 17–29.
- Peiravi, M., Ackah, L., Guru, R., Mohanty, M., Liu, J., Xu, B., Zhu, X., & Chen, L. (2017). Chemical extraction of rare earth elements from coal ash. *Minerals & Metallurgical Processing*, *34*, 170–177. <https://doi.org/10.19150/mmp.7856>.

- Pradip, P., & Fuerstenau, D. W. (2013). Design and development of novel flotation reagents for the beneficiation of Mountain Pass rare-earth ore. *Minerals & Metallurgical Processing*, 30, 1–9. <https://doi.org/10.1007/bf03402335>.
- Pueyo, M., Mateu, J., Rigol, A., Vidal, M., López-Sánchez, J. F., & Rauret, G. (2008). Use of the modified BCR three-step sequential extraction procedure for the study of trace element dynamics in contaminated soils. *Environmental Pollution*, 152, 330–341. <https://doi.org/10.1016/j.envpol.2007.06.020>.
- Rao, K. A., Serajuddin, M., RamaDevi, G., Thakurta, S. G., & Sreenivas, T. (2020). On the characterization and leaching of rare earths from a coal fly ash of Indian origin. *Separation Science and Technology*, 6395. <https://doi.org/10.1080/01496395.2020.1718705>.
- Ren, X. Y., Zhang, G. W., Hong, X., & Sun, F. E. (2020). Study on microstructure control and performance optimization of ZCuPb20Sn5 alloy by rare earth la. *Journal of Physics: Conference Series*, 1507, 042006. <https://doi.org/10.1088/1742-6596/1507/4/042006>.
- Report, C. (2017). Report: Medallion resources—REE prices are showing substantial price increases [WWW Document]. *Caesars Rep*. Retrieved 24 September, 2020, from <https://www.caesarsreport.com/reports/report-medallion-resources-ree-prices-showing-substantial-price-increases/>
- Rosita, W., Bendiyasa, I. M., Perdana, I., & Anggara, F. (2020). Sequential particle-size and magnetic separation for enrichment of rare-earth elements and yttrium in Indonesia coal fly ash. *Journal of Environmental Chemical Engineering*, 8, 103575. <https://doi.org/10.1016/j.jece.2019.103575>.
- Schlinkert, D., & van den Boogaart, K. G. (2015). The development of the market for rare earth elements: Insights from economic theory. *Resources Policy*, 46, 272–280. <https://doi.org/10.1016/j.resourpol.2015.10.010>.
- Sedres, G. (2016). *Recovery of SiO₂ and Al₂O₃ from coal fly ash* (Master Thesis).
- Seredin, V. V., & Dai, S. (2012). Coal deposits as potential alternative sources for lanthanides and yttrium. *International Journal of Coal Geology*, 94, 67–93. <https://doi.org/10.1016/j.coal.2011.11.001>.
- Seredin, V. V., & Finkelman, R. B. (2008). Metalliferous coals: A review of the main genetic and geochemical types. *International Journal of Coal Geology*, 76, 253–289. <https://doi.org/10.1016/j.coal.2008.07.016>.
- Shearer, C.R. (2014). *The productive reuse of coal, biomass, and co-fired fly ash* (pp. 1–242). Thesis.
- Shoppert, A. A., Loginova, I. V., Chaikin, L. I., & Rogozhnikov, D. A. (2017). Alkali fusion-leaching method for comprehensive processing of fly ash. *KnE Materials Science*, 2, 89. <https://doi.org/10.18502/kms.v2i2.952>.
- Song, X., Chang, M. H., & Pecht, M. (2013). Rare-earth elements in lighting and optical applications and their recycling. *JOM*, 65, 1276–1282. <https://doi.org/10.1007/s11837-013-0737-6>.
- Statista. (2015) *Prices of rare earth oxides worldwide from 2009 to 2013* [WWW Document]. Stat. Res. Dep. Retrieved 24 September, 2020, from <https://www.statista.com/statistics/449834/average-rare-earth-oxide-prices-globally/>
- Stuckman, M. Y., Lopano, C. L., & Granite, E. J. (2018). Distribution and speciation of rare earth elements in coal combustion by-products via synchrotron microscopy and spectroscopy. *International Journal of Coal Geology*, 195, 125–138. <https://doi.org/10.1016/j.coal.2018.06.001>.
- Suli, L. M., Ibrahim, W. H. W., Aziz, B. A., Deraman, M. R., & Ismail, N. A. (2017). A review of rare earth mineral processing technology. *Chemical Engineering Research Bulletin*, 19, 20. <https://doi.org/10.3329/ceb.v19i0.33773>.
- Taggart, R. K., Hower, J. C., Dwyer, G. S., & Hsu-Kim, H. (2016). Trends in the rare earth element content of U.S.-based coal combustion fly ashes. *Environmental Science & Technology*, 50, 5919–5926. <https://doi.org/10.1021/acs.est.6b00085>.
- Taggart, R. K., Hower, J. C., & Hsu-Kim, H. (2018). Effects of roasting additives and leaching parameters on the extraction of rare earth elements from coal fly ash. *International Journal of Coal Geology*, 196, 106–114. <https://doi.org/10.1016/j.coal.2018.06.021>.

- Tang, M., Zhou, C., Pan, J., Zhang, N., Liu, C., Cao, S., Hu, T., & Ji, W. (2019). Study on extraction of rare earth elements from coal fly ash through alkali fusion—Acid leaching. *Minerals Engineering*, *136*, 36–42. <https://doi.org/10.1016/j.mineng.2019.01.027>.
- Taylor, S. R., & McLennan, S. M. (1985). *The continental crust: Its composition and evolution : An examination of the geochemical record preserved in sedimentary rocks*. Oxford: Blackwell Scientific.
- Tessier, A., Campbell, P. G. C., & Bisson, M. (1979). Sequential extraction procedure for the speciation of particulate trace metals. *Analytical Chemistry*, *51*, 844–851. <https://doi.org/10.1021/ac50043a017>.
- Thakur, N. V. (2000). Separation of rare earths by solvent extraction. *Mineral Processing and Extractive Metallurgy Review*, *21*, 277–306. <https://doi.org/10.1080/08827500008914171>.
- Tsamis, A., & Coyne, M. (2015). *Recovery of rare earths from electronic wastes: An opportunity for high-tech SMEs*. https://doi.org/10.1007/978-94-017-5344-9_136.
- Tuan, L. Q., Thenepalli, T., Chilakala, R., Vu, H. H. T., Ahn, J. W., & Kim, J. (2019). Leaching characteristics of low concentration rare earth elements in Korean (Samcheok) CFBC bottom ash samples. *Sustain.*, *11*, 1–11. <https://doi.org/10.3390/su11092562>.
- Tunso, C., Petranikova, M., Gergorić, M., Ekberg, C., & Retegan, T. (2015). Reclaiming rare earth elements from end-of-life products: A review of the perspectives for urban mining using hydrometallurgical unit operations. *Hydrometallurgy*, *156*, 239–258. <https://doi.org/10.1016/j.hydromet.2015.06.007>.
- U.S. Department of Energy. (2010). *Critical materials strategy*.
- U.S. Geological Survey. (2020). *Mineral commodity summaries 2020*. U.S Department of the Interior, U.S Geological Survey. <https://doi.org/10.3133/mcs2020>.
- Ujaczki, É., Zimmermann, Y., Feigl, V., & Lenz, M. (2015). Recovery of rare earth elements from hungarian red mud with combined acid leaching and liquid–liquid extraction. In *Proceedings of the bauxite residue valorisation and best practices conference, Leuven, Belgium* (pp. 339–346).
- USDOE-NETL. (2017). *Report on rare earth elements from coal and coal byproducts*. <https://doi.org/10.1073/pnas.1115753108/>.
- Wang, X., Wang, X., Pan, Z., Yin, X., Chai, P., Pan, S., & Yang, Q. (2019a). Abundance and distribution pattern of rare earth elements and yttrium in vitrain band of high-rank coal from the Qinshui basin, northern China. *Fuel*, *248*, 93–103. <https://doi.org/10.1016/j.fuel.2019.03.054>.
- Wang, Z., Dai, S., Zou, J., French, D., & Graham, I. T. (2019b). Rare earth elements and yttrium in coal ash from the Luzhou power plant in Sichuan, Southwest China: Concentration, characterization and optimized extraction. *International Journal of Coal Geology*, *203*, 1–14. <https://doi.org/10.1016/j.coal.2019.01.001>.
- Ward, C. R., Spears, D. A., Booth, C. A., Staton, I., & Gurba, L. W. (1999). Mineral matter and trace elements in coals of the Gunnedah Basin, New South Wales, Australia. *International Journal of Coal Geology*, *40*, 281–308. [https://doi.org/10.1016/S0166-5162\(99\)00006-3](https://doi.org/10.1016/S0166-5162(99)00006-3).
- Weedon, A (2019). Rare earth mineral deal inked by US and Australia—What does that mean? [WWW Document]. *ABC News*. Retrieved 22 October, 2020, from <https://www.abc.net.au/news/2019-11-19/australian-critical-mineral-supply-to-be-guaranteed-by-us/11716726>
- Xie, F., Zhang, T. A., Dreisinger, D., & Doyle, F. (2014). A critical review on solvent extraction of rare earths from aqueous solutions. *Minerals Engineering*, *56*, 10–28. <https://doi.org/10.1016/j.mineng.2013.10.021>.
- Yang, Y., & Li, X. (2010). Influence of neodymium on high cycle fatigue behavior of die cast AZ91D magnesium alloy. *Journal of Rare Earths*, *28*, 456–460. [https://doi.org/10.1016/S1002-0721\(09\)60133-2](https://doi.org/10.1016/S1002-0721(09)60133-2).
- Yao, Z. T., Xia, M. S., Sarker, P. K., & Chen, T. (2014). A review of the alumina recovery from coal fly ash, with a focus in China. *Fuel*, *120*, 74–85. <https://doi.org/10.1016/j.fuel.2013.12.003>.
- Zhang, J. B., Li, S. P., Li, H. Q., & He, M. M. (2016). Acid activation for pre-desulfated high-alumina fly ash. *Fuel Processing Technology*, *151*, 64–71. <https://doi.org/10.1016/j.fuproc.2016.05.036>.

- Zhang, W., Groppo, J., & Honaker, R., 2015a. Ash beneficiation for REE recovery. 2015 World Coal Ash 11.
- Zhang, W., Rezaee, M., Bhagavatula, A., Li, Y., Groppo, J., & Honaker, R. (2015b). A review of the occurrence and promising recovery methods of rare earth elements from coal and coal by-products. *International Journal of Coal Preparation and Utilization*, 35, 295–330. <https://doi.org/10.1080/19392699.2015.1033097>.
- Zhou, B., Li, Z., & Chen, C. (2017). Global potential of rare earth resources and rare earth demand from clean technologies. *Minerals*. <https://doi.org/10.3390/min7110203>.

Chapter 17

Developments in Characterization and Mineral Processing of Coal Fly Ash for Recovery of Rare Earth Elements



Tumuluri Sreenivas, Md Serajuddin, Ramkaran Moudgil,
and Kacham Anand Rao

17.1 Introduction

Rare earths are a group of 17 elements comprising of 15 “Lanthanides”, namely ${}_{57}\text{La}^{138.9}$ to ${}_{71}\text{Lu}^{174.9}$ and two others— ${}_{21}\text{Sc}^{44.9}$ and ${}_{39}\text{Y}^{88.9}$. Sc and Y are grouped with the rare earth elements (REE) due to proximity of their physical and chemical properties with the lanthanides (Table 17.1). The crustal abundance of REEs is in the range of 130–240 $\mu\text{g/g}$. Evidently, they are not rare and in reality more abundant than Ag, Au and Pt group of metals (Zepf 2013). Amongst the REEs, elements like lanthanum, cerium, neodymium and yttrium are higher in abundance than the rest (Fig. 17.1) (Balaram 2019). However, these 17 elements donned the name of “Rare Earths” as it is uncommon to identify deposits of REE with tenor suitable enough for economical exploitation. The Japanese refer REEs as “the seeds of technology”, and in USA they are considered as “technology metals” (USDoE 2011; NRC 2008; Van Gosen et al. 2017). Many countries refer REEs as “critical metals” (CM) (USDoE 2011; EC 2014; Geoscience Australia 2013; Charalampides et al. 2015). A metal is referred to as “critical” if it is crucial (or high in demand) for green energy technologies (solar and wind energy, electric vehicles, etc.) and scarce by its geological occurrence (Hayes and McCullough 2018). At present there are no satisfactory replacements for some of the critical REEs like Dy, Nd, Tb, Eu and Y. Besides their use in green energy, the REEs are vital in many modern-day materials and

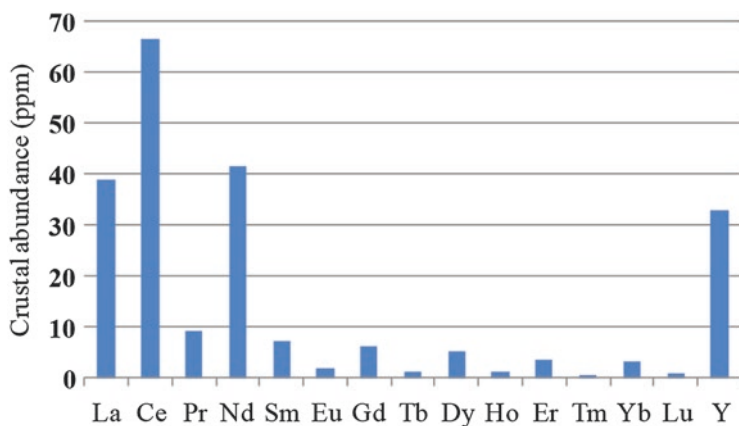
T. Sreenivas (✉) · M. Serajuddin · K. Anand Rao
Mineral Processing Division, Bhabha Atomic Research Centre, AMD Complex, Begumpet,
Hyderabad, Telangana, India
e-mail: tsreenivas@barc.gov.in

R. Moudgil
Mineral Processing Division, Bhabha Atomic Research Centre, AMD Complex, Begumpet,
Hyderabad, Telangana, India

Homi Bhabha National Institute, Mumbai, Maharashtra, India

Table 17.1 Important properties of rare earth elements

Elements	Symbol	Atomic number	Atomic weight	Density (g cm ⁻³)	Melting point (°C)	Vicker's hardness (10 kg load, kg/mm ²)
Scandium	Sc	21	44.95	2.989	1541	85
Yttrium	Y	39	88.90	4.469	1522	38
Lanthanum	La	57	138.90	6.146	918	37
Cerium	Ce	58	140.11	8.160	798	24
Praseodymium	Pr	59	140.90	6.773	931	37
Neodymium	Nd	60	144.24	7.008	1021	35
Promethium	Pm	61	145.00	7.264	1042	–
Samarium	Sm	62	150.36	7.520	1074	45
Europium	Eu	63	151.96	5.244	822	17
Gadolinium	Gd	64	157.25	7.901	1313	57
Terbium	Tb	65	158.92	8.230	1356	46
Dysprosium	Dy	66	162.50	8.551	1412	42
Holmium	Ho	67	164.93	8.795	1474	42
Erbium	Er	68	167.26	9.066	1529	44
Thulium	Tm	69	168.93	9.321	1545	48
Ytterbium	Yb	70	173.04	6.966	819	21
Lutetium	Lu	71	174.97	9.841	1663	77

**Fig. 17.1** Crustal abundance of REEs

technologies say in medical equipment, essential telecommunications, national security sectors and several types of electronic gadgets. They have played crucial role in miniaturization of various electronic devices.

The special properties of REEs are due to their atomic structure and the electronic configuration (EC), which is distinctive in the periodic table of elements. The ground-state EC of the lanthanides is generally of the type $(Xe)4f^n6s^2$. The element La with EC of $[(Xe)5d^16s^2]$ is outside this generalization yet shows +3 valence and

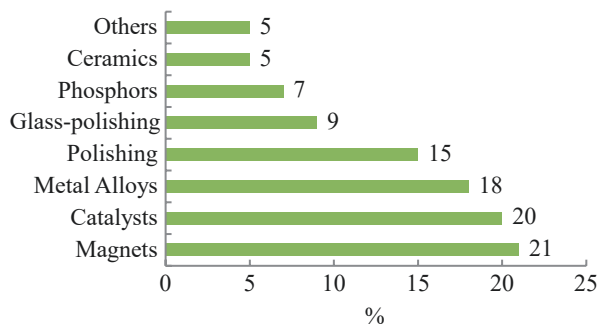
has similarities like other elements of the group. Among the lanthanides, three elements have exceptions to the pattern of EC, namely $(Xe)4f^n5d^06s^2$. They are Ce— $(Xe)4f^15d^1$, Gd— $(Xe)4f^75d^16s^2$ which is consistent with stabilized half-filled shell and Lu— $(Xe)4f^{14}5d^16s^2$. The common oxidation state of lanthanides is M^{3+} . However, Ce shows M^{4+} state also due to its tendency to lose the 4f and 5d electrons. Although the important chemical properties of REEs are very close to each other, critical physical properties like electrical, magnetic, spectroscopic and thermal are exclusive to a particular element. Such special properties are responsible for the desire of scientific and industry community for obtaining individual REEs of very high purity.

The consumption profile of REEs in various products/materials in recent times is shown in Fig. 17.2. Major share, about 20% each, was in magnets, catalyst and metal alloys. Closely following them was the polishing industry ~15% (NRCAN 2018). The compound annual growth rate (CAGR) of REEs for the block 2019–2025 was placed at 8.6% (Anon 2020) mainly due to their demand in technologies for climate control.

The sudden export restrictions imposed by China, which was the single dominant country for both REE reserves and production till 2010 (Krishnamurthy 2020), resulted in subsequent global efforts to bring in new supply chains such that the import dependency or uncertainties in the availability of REEs in general and critical REEs in particular can be waded off. The strategies that came into play as a consequence of 2010 supply disruptions are (a) exploration and mining for new REE primary resources/deposits and (b) exploitation of technospheric resources like urban electronic waste and/or end-of life products, bauxite residue (Evans 2016), phosphogypsum waste (Gijbels et al. 2017), fly ash of coal-fired thermal power plants (Seredin and Dai 2012), metallurgical slags, marine sediments, mine tailings, incinerator ash and waste water streams (Costis et al. 2019; Binnemans et al. 2015). Amongst the different alternative strategies conceived, the idea of using non-e-waste technospheric resources, gained importance for the simple fact that they are produced in large volumes and their utilization also serves the sustainability goals, which the entire world is embarking upon.

Though the use of coal as a fuel for energy generation has fallen in recent times due to the awareness on carbon footprint, it still reins supremacy in many countries.

Fig. 17.2 Consumption sectors of rare earth elements in 2018



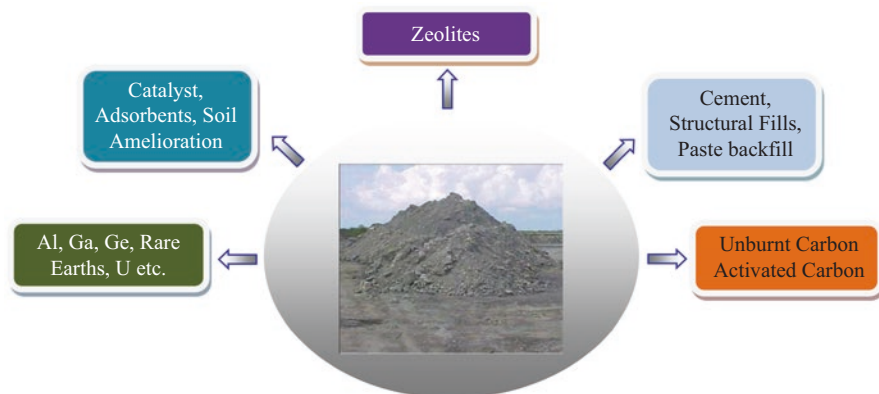


Fig. 17.3 Uses of coal fly ash

Coal-based energy corners about 38% share of the total energy output at the moment (BPSR 2019). Coal is forecasted to be the main raw material/fuel for energy generation even in the coming two decades.

Amongst the various effluents generated in coal-fired thermal power plants, the most important is the coal fly ash or CFA. Presently part of the CFA is used for making bulk products like cement supplement and geopolymers. These bulk uses form about 40% in USA and 65% in India. The rest of CFA is being put in landfills in many nations. It is to be realized that besides the pozzolanic character of CFA which is responsible for its bulk use, it also contains various value-added components like Al, Si, Fe and Ti metals whose demand is increasing in society with every passing day, and supplies from conventional resources is choking due to depletion in ore grades thus becoming uneconomical (Sahoo et al. 2016). Several other high-value metals like V, Ga, Ge, Se, Li, Mo, U, Pt, Au, Ag and rare earth elements (REEs) are also present in CFA in minor and trace quantities. Figure 17.3 illustrates multiple uses of CFA including those which are of potential nature. Valorization of CFA is an absolute necessity to achieve resource conservation and sustainability. This chapter gives a concise view on the potential of CFA as a source of REEs with special focus on presenting different studies that have been conducted and those which are in progress worldwide for the recovery of REEs.

17.2 Technospheric Resources of Rare Earths

Occurrence of over 200 different rare earth (RE) minerals was reported so far in different geological settings (Balaram 2019; Krishnamurthy 2020), and the most important RE minerals (Table 17.2) are bastnäesite and monazite. They assay (weight-wise) about 70% rare earth oxides (REO). Other REE minerals of economic significance are parisite-(Ce), synchysite-(Ce) and xenotime. While xenotime is a RE-phosphate mineral, the other two minerals are carbonates. The carbonate minerals are often found along with bastnaesite. Due to similarities in

Table 17.2 Economic minerals of rare earth elements

Mineral	Formula	Approximate REO %
Aeschnyite-(Ce)	(Ce,Ca,Fe,Th)(Ti,Nb) ₂ (O,OH) ₆	32
Allanite-(Ce)	(Ce,Ca,Y) ₂ (Al, Fe ³⁺) ₃ (SiO ₄) ₃ OH	38
Apatite	Ca ₅ (PO ₄) ₃ (F, Cl, OH)	19
Bastnasite-(Ce)	(Ce, La)(CO ₃)F	75
Fergusonite-(Ce)	(Ce, La, Nd)NbO ₄	53
Gadolinite-(Ce)	(Ce, La, Nd, Y) ₂ (Fe ²⁺ Be ₂ Si ₂ O ₁₀)	60
Kainosite-(Y)	Ca ₂ (Y, Ce) ₂ Si ₄ O ₁₂ CO ₃ ·H ₂ O	38
Loparite	(Ce, La, Na, Ca Sr)(Ti, Nb)O ₃	30
Monazite-(Ce)	(Ce, La, Nd, Th)PO ₄	65
Parasite-(Ce)	Ca(Ce, La) ₂ (CO ₃) ₃ F ₂	61
Xenotime	YPO ₄	61
Florencite-(Ce)	CeAl ₃ (PO ₄) ₂ (OH) ₆	32
Sychysite-(Ce)	Ca(Ce, La)(CO ₃) ₂ F	51
Samarskite-(Y)	(Y, Ce, U, Fe ³⁺) ₃ (Nb, Ta, Ti) ₅ O ₁₆	24

their ionic radii, the REEs are compatible in most minerals making their separation and concentration very challenging (Krishnamurthy and Gupta 2016; Jordens et al. 2013; Jha et al. 2016). Both monazite and bastnaesite (or other carbonate RE minerals) are richer in lighter rare earth elements (LREE: La to Sm), while xenotime has higher content of heavier rare earth element, namely yttrium (HREE: Eu to Lu and Y). Bastnaesite, monazite and xenotime account for the first-, second- and third largest % of RE deposits world over (Krishnamurthy and Gupta 2016).

The importance of technospheric resources of REEs in today's context is better understood if the pros and cons of exploitation of a primary deposit, and also the constraints in recycle of the e-waste type technospheric resources are objectively assessed. The exploration and mining of a new primary resource, either hard rock (carbonatites, alkaline igneous systems, etc.) or placers (riverine or beach), is expensive and has several associated socio-economic issues (Jaroni et al. 2019; Haque et al. 2014; Koltun and Tharumarajah 2014). Mining generates dust, creates noise pollution and consumes chemical explosives all of which are harmful for miners and other workers as well as to those living in the vicinities of mines. The surface footprint of the tailings dams, which stores the solid effluents, is also quite large. Some REE minerals like monazite contain significant radioactive elements (Th, U) causing radiation hazards. Weng et al. (2016) reports that the gross energy demand for mining of a conventional ore is about 2430 GJ per tonne of rare earth oxide (REO), and global warming potentials are approximately 230 tons CO₂-equivalent per ton of REO. Because of the chemically refractory nature of REE minerals, the energy demand and greenhouse gas emissions in REE production plants/mines is also high when compared to the other metal industries (Zaimes et al. 2015). The REE industry is capital-intensive and takes long gestation period, about a decade and half, for stabilizing the production process (USEPA 2012). The REO tenor in many of the new primary ore deposits located outside China after the 2010 export control affect is significantly low, less than about 2.5%, excepting the Steenkampskraal deposit in South Africa and the Gakara deposit in Burundi

(Guyonnet et al. 2018) which assayed 14.9% and 54.3% REO, respectively. Therefore viability, economical and environmental, of the lean tenor REO mines is a big question while deciding their candidatures for meeting the future demands of REOs (Wall et al. 2017) which is on upward trajectory consistently. It was reported that about 210,000 tons of REO was produced in 2019 itself (USGS 2020), and the production was chiefly from mines like Bayano Obo (China), Mountain Pass (USA) and Mt. Weld (Australia) deposits, all of which are higher in grade than those discovered outside China after 2010.

Recycling of e-waste or urban mining of e-waste for REEs is gaining attention as this approach/technology is ascribed with some advantages such as the following: (a) significantly lower environmental emissions when compared to emissions produced during mining and processing of a conventional primary deposits, (b) the issues linked to “RE-balance” are minimized and (c) e-waste is a viable resource for countries which are not in possession of exploitable or economical primary resources. The importance of recycling of e-waste for metal values for many countries is evident as 89% of the total 120 million tons of REO reserves identified so far occur in few countries, namely China, Brazil, Vietnam, Russia and India at present (USGS 2020). Unfortunately as on date only about 1% of the REEs are recycled from the e-waste due to several challenges. The issues are chiefly difficulty in selective separation of REEs from end-of-life materials which are multi-elemental in composition, low REE content and absence of economic incentives (Peelman et al. 2018; Ferron and Henry 2015; Massari and Ruberti 2013; Jowitt et al. 2018; Binnemans et al. 2013; ORNL 2015).

In comparison to the aforementioned primary and e-waste type technospheric REE resources, the other technospheric resources like bauxite residue, phosphogypsum, and coal fly ash (CFA) have distinct advantages with respect to the tenor (grade /assay) and quantities available, which include stock-piled material and also the additional volumes generated on annual basis. It is important to realize that the technospheric resources are well spread out across many geographical locations unlike the primary resources, thus giving scope for more diversified supply chain. In the case of bauxite residue, the feedstock was reported to be about 140 million tons on annual basis across the world, and the REE content in some residues was reported as high as 0.25% (Evans 2016; Vind et al. 2018). The phosphogypsum (PG) waste from phosphoric acid industry also contains interesting concentration of REE values. About 100–280 Mt./annum of (PG) waste was reported in this industry (Virolainen et al. 2019). In absolute terms, the contained REE values in PG produced from 30 different locations in European countries works out to 84,000 tons. Considering similar assay of REE (0.4%) in PG waste in rest of the world, the REE potential in this source could be 400,000–1,120,000 tons/annum. Similarly the coal fly ash (CFA) is another huge industrial waste generated at coal-fired thermal power stations which is now established to contain significant REE values (Seredin and Dai 2012; Seredin et al. 2013; Dai and Finkelman 2018; Blissett et al. 2014; Zhang et al. 2015a, 2020; Franus et al. 2015; Peiravi et al. 2017; NETL 2018; Hower et al. 2017; Taggart et al. 2016; USGS Fact Sheet 2019–3048; Pan et al. 2020; Anand Rao et al. 2020). About 958 million tons of CFA was reported to be generated world over in 2017 (Anand Rao and Sreenivas 2019) with countries like USA and India

contributing about 45 Mt. (Taggart et al. 2016) and 196 Mt. (CEA 2018), respectively, on annual basis. Reports point out that coal deposits carry nearly 50% of the REE reserve of traditional rare-earth-bearing mineral sources (Zhang et al. 2015a). Table 17.3 gives REE assay in CFAs of different locations across the world. The REE assay in CFA produced at different thermal power plants in various countries is in the range of 400–500 ppm. Recovering REEs from CFA has several benefits over recovering them from conventional rare earth ores (Zhang et al. 2020). The advantages include the following: (a) occurrence of relatively higher proportion of HREE and also critical REE in the total REE present, (b) reduced cost of production as REEs in CFA form a by-product of coal mining, (c) lower concentrations of harmful radio-nuclides (unlike monazite), (d) utilization of CFA contributes towards the goal of maximum utilization of mined material and (e) minimizes issues surrounding the landfills.

17.3 Rare Earths in Coal Fly Ash (CFA)

Coal fly ash (CFA) is a fine-particulate material originating from non-combustible components like quartz and clay present in coal. CFA is generated mainly from the coal-fired thermal power stations. Fly ash particles are captured from the flu gas exhaust of boilers using electrostatic precipitators or filter fabric bag houses. CFA forms 5–20% by weight of the total mass of coal used (Chen et al. 2019). According to ASTM 618 classification, CFA is of two different types, namely Class F and Class C (ASTM 2015). The demarcation is based on the chemical constituents occurring in the CFA. If the total weight of $\text{SiO}_2 + \text{Al}_2\text{O}_3 + \text{Fe}_2\text{O}_3$ is equal or higher than 70%, it is categorized as Class F CFA. The weight percent of these three oxides in Class C CFA is between 50 and 70. Partial chemical composition of CFA generated in some typical coal-fired (lignite and bituminous variety) thermal power plants in India is given in Table 17.4 (Anand Rao et al. 2020) along with average composition of samples from China (Wang et al. 2019). It is dominated by Si followed by Al. The other constituents in CFA include Ca, Fe, Mg and Ti. Several important metals like Cr, Ni, Zn, Sr and Ba are present in few hundred ppm concentration (Anand Rao et al. 2020; Wang et al. 2019). The morphology of particles in CFA is both crystalline and amorphous in nature with the former being more predominant (Fig. 17.4). The shapes of the particles are mostly as spherical and cenospherical form. According to Liu et al. (2019), the mineralogical composition of CFA of Class F type contained well-crystallized quartz, mullite, haematite and magnetite. Based on studies on different Class C type CFAs of USA, Liu et al. observed that those are of more complex mineralogy composed of quartz, anhydrite CaSO_4 , tricalcium aluminate ($\text{Ca}_3\text{Al}_2\text{O}_6$), lime (CaO) and periclase (MgO). Amorphous alumina-silicate glass was conspicuous in many CFA samples. Franus et al. (2015) investigated the mineralogy and morphology of the post-combusted coal ash from lignite and bituminous coals of Poland, and their data indicated similar mineralogical content but differed in the material morphology with the CFA from lignite coal being more amorphous.

Table 17.3 Rare earth elements (REE) and critical REEs content in typical CFA samples

Coal Basin	Total REEs (ppm)	Critical REEs* (%)	Reference	
Jungar, Inner Mongolia, China (Sample Code A)	192.1	28.8	USGS Fact Sheet 2019–3048 (https://doi.org/10.3133/fs20193048) Accessed on 8/9/2020	
Jungar, Inner Mongolia, China (Sample Code B)	229.7	28.7		
Jungar, Inner Mongolia, China (Sample Code C)	293.5	28.3		
Powder River basin +Appalachian basin mixed, US (Sample Code D)	313.8	39.2		
Powder River basin +Appalachian basin mixed, US (Sample Code E)	365.8	37.3		
Central Appalachian basin, US (Sample Code H)	524.5	39.5		
Eastern Interior (Illinois basin), US (Sample Code I)	366.5	39.4		
Powder River basin, US (Sample Code J)	345.2	34.5		
Central Appalachian basin, Fire Clay coal, US (Sample Code K)	1534.3	34.7		
Central Appalachian basin, Fire Clay coal, US (Sample Code L)	1667.6	36.5		
Central Appalachian basin, US (Sample Code M)	401.5	38.6		
Eastern Interior (Illinois basin, US) (Sample Code N)	312.1	36.2		
Central Appalachian basin, US (Sample Code O)	563.6	38.1		
Powder River basin, US (Sample Code P)	283.2	32.8		
Central Appalachian basin, Fire Clay coal, US (Sample Code Q)	626.6	36.7		
Central Appalachian basin, Fire Clay coal, US (Sample Code R)	723.4	35.1		
Central Appalachian basin, US (Sample Code S)	1175.2	38.4		
NLP II TPP, India	2207	44.4		Anand Rao et al (2020)
NLP I TPP, India	1222	41.7		
SN TPP, India	807	30.4		
R.G TPP, India	426	33.3		
Pavlovka-2, Seam I/a, Russian Far-East, Russia	4551	63.1	Seredin (2012)	
Pavlovka-2, Seam I/b, Russian Far-East, Russia	8426	63.2		
Lelchitsk, dh mine, Belorussia	5035	33.9		
Aduunchulvun, Mongolia	2263	48.6		
Nazar-Ailok, dh mine, Tadjikistan	950	60.7		
P1, CFA processing company RockTron Int. Ltd, Poland	358	35.6	Blisset et al (2014)	
P2, CFA processing company RockTron Int Ltd, Poland	308	35.6		
P3, CFA processing company RockTron Int. Ltd, Poland	359	36.1		
UK-1, CFA processing company RockTron Int. Ltd, UK	481	33.4		
UK-2, CFA processing company RockTron Int. Ltd, UK	294	35.1		
UK-3, CFA processing company RockTron Int. Ltd, UK	246	35.8		
Samcheonpo, South Korea	153	35.7	Thriveeni et al. (2015)	
Japan	119	35.4		
Coal (Bituminous) fired PP, Poland			Franus et al (2015)	
Sample – 1	373.09	34.6		
Sample – 2	373.05	35.4		
Sample- 3	394.59	35.6		
Sample- 4	340.15	35.6		
Sample – 5	380.00	34.6		
Sample – 6	543.08	36.2		
Sample – 7	413.71	35.7		
Sample – 8	307.65	35.5		
Sample – 9	264.8	36.3		
Coal (Lignite) fired PP, Poland				
Sample- 10	383.76	30.5		
Sample- 11	443.32	36.1		
Sample - 12	101.12	38.3		
Republika PP, Row 1, Bulgaria	227.8	34.7	Hower et al (2013)	
Republika PP, Row 2, Bulgaria	241.2	34.7		
Republika PP, Row 3, Bulgaria	240.4	34.9		
Bobov Dol PP, Row 1, Bulgaria	230.0	33.4		
Bobov Dol PP, Row 2, Bulgaria	230.1	33.2		
Bobov Dol PP, Row 3, Bulgaria	228.2	33.7		
Thermal PP, Turkey	208.8	36.1		
Thermal PP, Turkey	242.5	37.3		
Thermal PP, Turkey	212.4	35.0		
Thermal P Pt, Turkey	213.3	32.2		

*Critical REEs Y, Nd, Eu, Tb, Dy and Er. TPP—thermal power plant

Table 17.4 Chemical composition of typical CFA samples of Indian (Anand Rao et al. 2020) and Chinese origin (Wang et al. 2019)

Indian samples		Chinese samples (Avg. composition)					
Sample codes →	NLP/I	NLP/II	RG	SN	FHK	SLP	Chinese samples (Avg. composition)
<i>Percentage (%)</i>							
SiO ₂	47.4	44.1	57.8	52.5	60.8	36.8	48.0
TiO ₂	1.9	1.3	1.7	1.6	2.5	1.6	3.2
Al ₂ O ₃	30.3	22.6	26.4	23.2	28.5	10	27.8
Fe ₂ O ₃ (T)	3.3	8.6	4.7	3.4	6.3	9.7	12.0
MgO	3.4	3.7	1.3	0.9	1.3	1.7	0.8
MnO	0.01	0.01	0.1	0.1	0.1	0.1	0.07
CaO	8.6	14.3	3.8	3.5	2.1	30	3.6
Na ₂ O	0.4	0.8	0.1	0.1	0.5	0.6	0.6
K ₂ O	0.03	0.1	1.1	0.9	1.5	0.1	1.2
P ₂ O ₅	0.03	<0.01	0.2	0.1	<0.01	0.1	0.3
LOI	3	6	2	13	–	9.0	–
<i>Parts per million (ppm)</i>							
Cr	191	155	179	339	167	144	–
Ni	120	87	93	95	122	<5	–
Zn	301	809	114	55	202	55	–
Sr	470	636	615	109	441	314	–
Ba	402	1200	812	484	1358	–	–

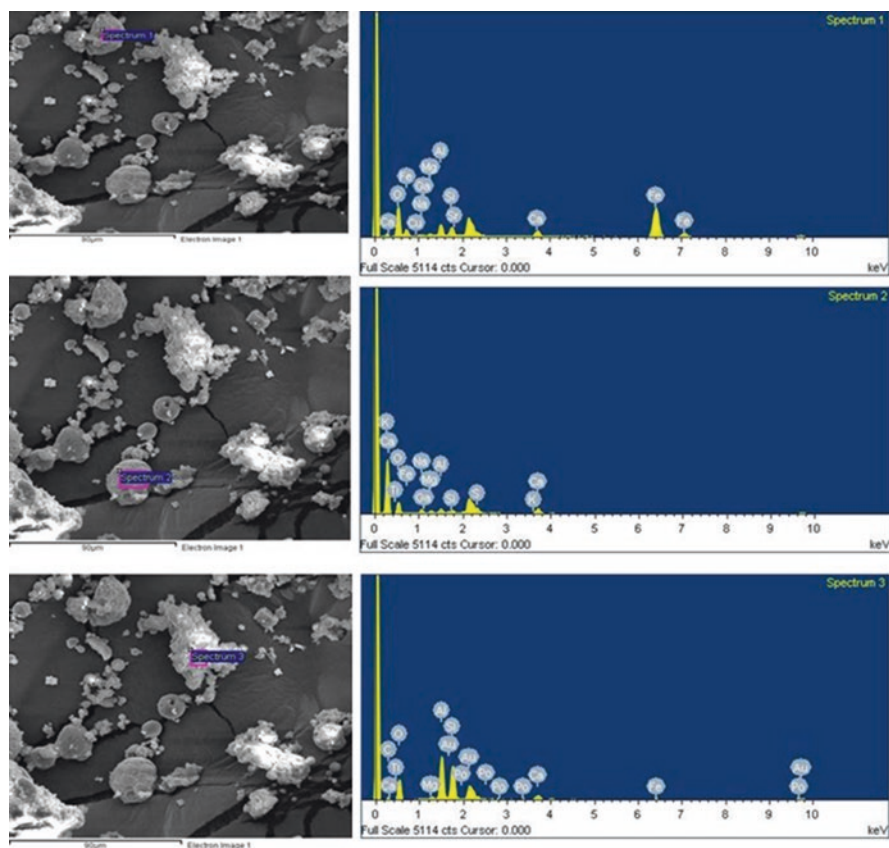


Fig. 17.4 Morphology (SEM image) of CFA in a lignite coal-fired thermal power plant

The geological aspects on deployment of REEs in coal and allied products were exhaustively reviewed in earlier literature by various authors (Seredin and Dai 2012; Dai et al. 2014; Hower et al. 2017; Hower et al. 2018; Zhang et al. 2020). The average REE content in lignite and bituminous coals was reported to be about 70 ppm. The REE assay in the resulting CFA is approximately 7–10 times their content in respective coals (Seredin and Dai 2012). Table 17.3 gives total REE content in different samples of CFA reported from various countries along with the percentage of critical REEs in it.

Seredin and Dai (2012) reported an average REE content of 400 ppm in CFA after analysing several samples collected across major coal fields worldwide. However, Taggart et al. (2016) reported slightly higher REE assay, about 500 ppm, in CFA of US coals (Taggart et al. 2016). Based on a recent mapping study on CFA from some coal-fired thermal power stations, Anand Rao and Sreenivas (2019) and Anand Rao et al. (2020) reported REE assay of 400–2100 ppm in India. Occurrence of CFA samples with few thousand ppm of REE was also sighted in different countries (Seredin and Dai 2012; Dai and Finkelman 2018; Hower et al. 1999; Blissett et al. 2014; Anand Rao et al. 2020). For instance, the Pavlovka coal deposit (Russian

Far East) analysed REE of about 1290 ppm. The CFA from this coal assayed 1% REE. Studies on the CFA produced from power stations using Kentucky Fire Clay Coal bed in USA showed REE content in the range of 0.12–0.167% (Mardon and Hower 2004; Hower et al. 1999). Anand Rao et al. (2020) and Anand Rao and Sreenivas (2019) reported REE assay of 0.12 and 0.22% in two different CFA samples collected from an Indian power plant using lignite coal. Some mines in China like the Changhe (K8), Sichuan and Tonghua mines, SW China too assayed 1400 and 1600 ppm of REE in the CFA of their coal. The CFA samples from Nazar-Ailok deposit, Tadjikistan, too contained 1000–2000 ppm of REE (Seredin and Dai 2012). Seredin and Dai (2012) have identified different genetic types of coal like Terrigenous, Tuffaceous, Infiltrational and Hydrothermal, for high REE accumulation (Table 17.5).

Seredin and Dai (2012) made a robust procedure for assessment of potential commercial value for REE recovery from CFAs. According to this method, which is driven by uses/market trends of REEs, the whole set of 17 elements were divided into 3 groups, namely critical (Nd, Eu, Tb, Dy, Y and Er), uncritical (La, Pr, Sm and Gd) and excessive (Ce, Ho, Tm, Yb and Lu). They defined two terms, namely C_{out} and $REE_{def,rel}$ as given in Eqs. (17.1) and (17.2), respectively, and used them for estimating the commercial potential.

$$x \text{ axis} = C_{out} = \frac{(\text{Nd} + \text{Eu} + \text{Tb} + \text{Dy} + \text{Er} + \text{Y}) / \text{total REE}}{(\text{Ce} + \text{Ho} + \text{Tm} + \text{Yb} + \text{Lu}) / \text{total REE}} \quad (17.1)$$

$$y \text{ axis} = REE_{def,rel} = 100 * \frac{\text{Nd} + \text{Eu} + \text{Tb} + \text{Dy} + \text{Y} + \text{Er}}{\text{total REE}} \quad (17.2)$$

Seredin and Dai (2012) made a plot with C_{out} as x -axis and $REE_{def,rel}$ as y -axis and divided the plot into three zones—Regions I, II and III as shown in Table 17.6. Any CFA resource falling in Regions II and III, that is with $C_{out} > 0.7$ and $REY_{def,rel} > 30\%$, was considered attractive for commercial exploitation.

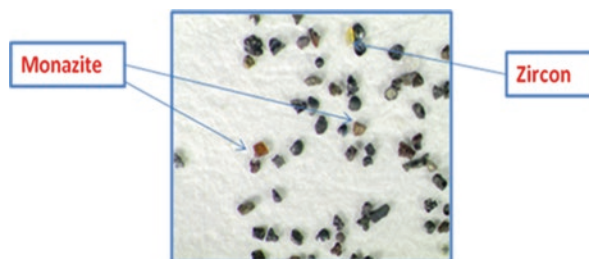
Because of the complexity involved in delineating the exact nature of occurrence of REEs in CFA, the researchers have used multiple techniques and different instruments with similar capabilities for analysing their department in different scales (Zhang et al. 2020; Liu et al. 2019). The instrumental techniques used for studying

Table 17.5 Main genetic types of coals with high rare earths content (after Seredin and Dai 2012)

Classification	REO assay in Ash%	Mines/deposits
Terrigenous	0.1–0.4	Jungar, China
Tuffaceous	0.1–0.5	Dean, USA
Infiltrational	0.1–1.2	Aduunchulun, Mongolia
Hydrothermal	0.1–1.5	Retikhovka, Russia

Table 17.6 Evaluation criteria for potential commercial exploitation of CFA for REE values (after Seredin and Dai 2012)

Region	C_{out}	$REY_{def-rel}$	Remarks
I	≤ 0.7	$\leq 26\%$	Unpromising
II	$0.7 \leq C_{out} \leq 1.9$	30–51%	Promising
III	> 2.0	$> 51\%$	Highly promising

Fig. 17.5 Occurrence of monazite and zircon grains in CFA of Indian origin

REE speciation at micro and molecular level included SEM/TEM coupled with EDX, μ XRF and μ XANES, EPMA LA-ICP-MS and synchrotron X-ray microscopy and synchrotron X-ray adsorption spectroscopy.

Burning of coal leads to enhancement of concentration/tenor of various metals in the resultant ash as they are non-combustible and REEs are no exception. Predominant presence of REEs was noticed in aluminosilicate glass and other minerals like haematite, ilmenite, lime and calcite either as inclusions or/and substitutions by several workers in various CFA samples (Montross et al. 2018; Stuckman et al. 2018; Anand Rao et al. 2020; Liu et al. 2019; Zhang et al. 2020; Taggart et al. 2018; Scott and Kolker 2019). The REEs in CFA are reported to be in the form of nanoscale crystalline minerals, overlapping ultra-fine minerals and as atomic dispersions within the glassy matrices. REE minerals like monazite, xenotime and rhabdophane, in discrete form have also been reported in CFA from coals of different origins in different countries (Liu et al. 2019; Anand Rao and Sreenivas 2019; Anand Rao et al. 2020; Zhang et al. 2020). Evidence on presence of discrete monazite, zircon and xenotime in CFA samples was noticed in samples collected from an Indian and Polish power plant as shown in Fig. 17.5. The size of the xenotime grains observed in Poland sample (Danuta Smolka-Danielowsjka 2010) ranged between 2 and 10 μ m. The morphology of the grains is in irregular and angular forms, quite often with characteristic pleochroic rim around the grain. Hood et al. (2017) and Liu et al. (2019) suggested that REE minerals like monazite and xenotime survive the combustion process but are reduced in size and become more widely distributed due to the thermal shock of the boiler. However, this argument was countered by Scott and Kolker (2019) in their recent study using ion microprobe technique (SHRIMP-RG). They advocated that dissemination of REEs in fly ash glasses and the similarity of distribution of REE in the glassy matrix to REE distribution in whole-sample imply that REEs in REE minerals are redistributed into glasses while the glasses are in the molten state during the combustion process. They further

noted that REE distributions for Al–Si aluminosilicate glasses are similar to, or slightly lower than, those of the bulk sample, confirming that REEs are partitioned into the glasses during coal combustion. Ca-, Fe- or Ca- and Fe-enriched aluminosilicate glasses are commonly REE-enriched relative to the more common Al–Si glasses. Scott and Kolker pointed out that as the proportion of Si to Al increases, the REE content decreases, which is consistent with the REE depletion observed in quartz. Another aspect commonly observed across different CFA samples is enrichment of REE values in relatively finer sizes. The presence of glassy material of CFA in finer size fractions is one of the chief reasons for REEs enrichment in such sizes over the coarser size fraction. The trend of enrichment of REEs in finer sizes is also due to the fact that the organic-bound REEs partially volatilize during combustion and subsequently deposit on the finer particles of fly ash. Besides such a phenomenon it was also inferred that the REEs associated with organic matter may form extremely small particles when the organic matter is combusted.

Figure 17.6 gives an example on enrichment ratio of REE as a function of size class in typical CFA samples of Indian origin which reiterates that nature and origin

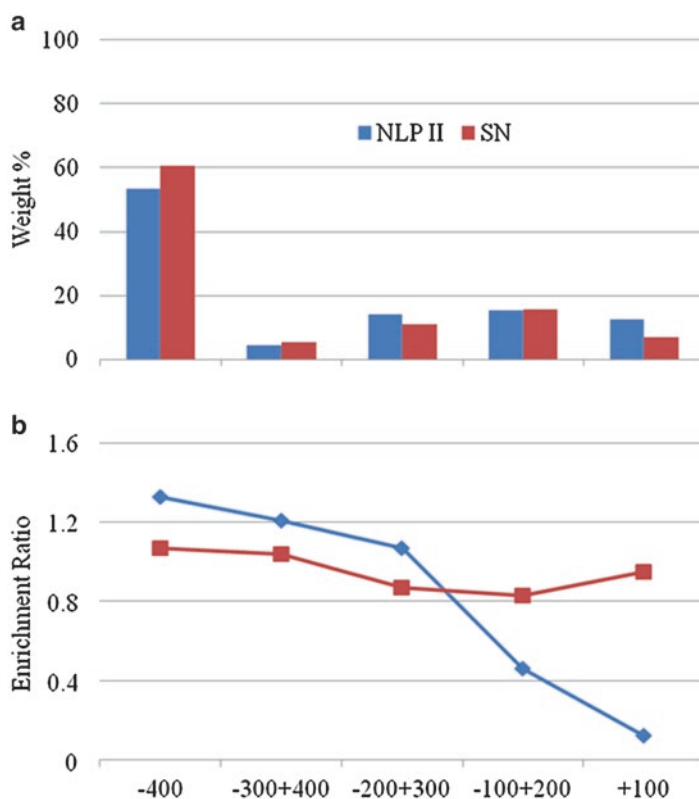


Fig. 17.6 (a) Particle size distribution and (b) enrichment ratio of REEs in two typical CFA samples of Indian origin

of coal and firing temperature in the power plant are very critical in the formation of resultant products and also on ER profile of REEs as a function of size. The enrichment ratio (ER = ratio of assay in a given stream/product to that present in the feed) of REEs in different size classes of CFAs showed that the -400# size fraction (<37 μ m) of the CFA from lignite coal has REEs enrichment of about 1.3 times over the feed value, and it decreased to <1 (lower than feed) in the sizes coarser than 300# size. Unlike this, the ER was practically invariant in the CFA sample originated from the bituminous coal.

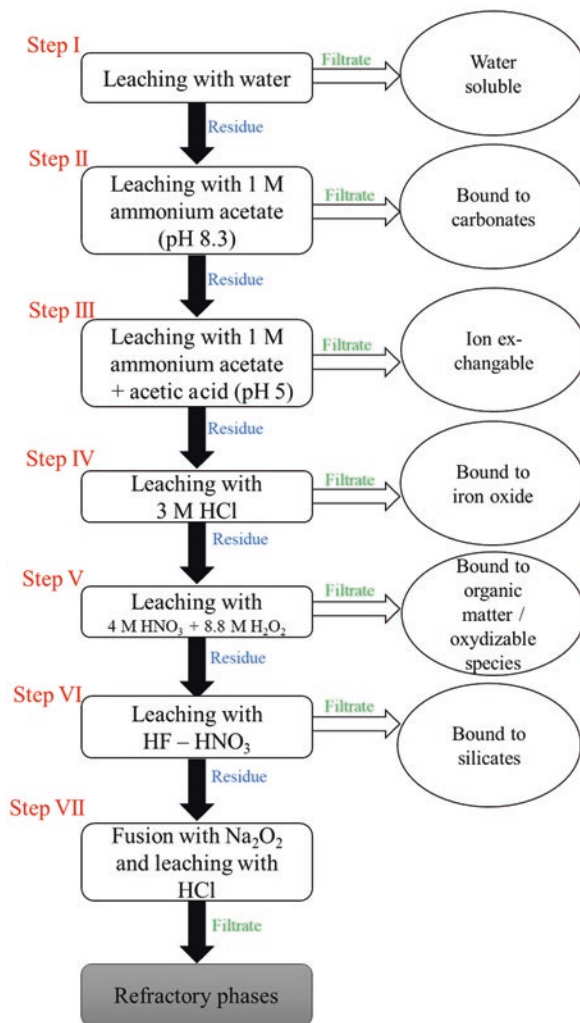
Sequential chemical extraction (SCE) is a widely used method for characterization of landfills in order to capture the department of the metals with various phases and understand their release into solution in a given chemical environment. The protocol or chemicals used in SCE schemes are tailor-made to suit the solid matrix under study. However, there also exists standard test procedures prescribed by the ASTM for SCE. SCE in CFA study helps in fractionation of the REEs into the following broad categories: (1) soluble in aqueous medium, (2) ion exchangeable and/or associated with acid soluble phases, (3) those in association with reducible material, (4) bound to oxidizable material and (5) in residuals or those associated with **silicates** (Dai et al. 2002). The protocol followed in SCE is to subject the residue or solid mass of ($i - 1$)th stage to chemical treatment defined in the i th stage. Figure 17.7 gives a detailed SCE protocol adopted for characterization of a REE-bearing CFA of Indian origin, and Fig. 17.8 gives a comparison of REE distribution in an SCE process for a typical CFA from India (Anand Rao et al. 2020) and another from south-west China (Pan et al. 2020). Both the samples showed contrasting behaviour with respect to their occurrence in the respective CFAs. The Chinese sample indicated maximum presence of REEs in glassy phase, while the Indian sample showed significant REE in ion-exchangeable form and in association with metal oxides. Liu et al. (2019) and Zhang et al. (2020) worked on finding out the difference in the department of REEs in Class F and C type CFAs using the SCE scheme. Their results revealed that REEs are associated, predominantly, with silicates and aluminosilicates in F type while they report with carbonates and oxides in the C type CFA.

Though some indication on the ease of extractability of REEs can be provided by SCE process, linking them to a particular mineral phase of CFA feedstock is misleading as the SCE process is not selective, the operating conditions are not designed for complete chemical attack of a desired or a particular phase always. At times the phases themselves may undergo alteration due to the chemical conditions adopted in the previous stages of SCE protocol and may result in inaccurate information.

17.4 Recovery of Rare Earths from CFA

The general strategy adopted for recovering REE values from a technospherical resource is to adopt a combination of physical beneficiation (including thermal pre-treatment) for pre-concentration of values which is then subjected to chemical/hydrometallurgical process for producing an intermediate-grade mixed

Fig. 17.7 Typical protocol of sequential chemical extraction (SCE) used for department of REE in an Indian CFA sample



RE-compound like RE-oxalate or RE-double sulphate or RE-chloride. Similar strategy has been adopted for recovery of REEs from CFAs by many Researchers, albeit with little or no success.

17.4.1 Physical Beneficiation

Pre-concentration of valuable minerals or/and metal-enriched particles present in a feedstock in a small mass prior to chemical processing is always an advantageous approach, both environmentally and economically. This is very essential in REEs recovery strategy from technospherical resources. The reasons for implementing

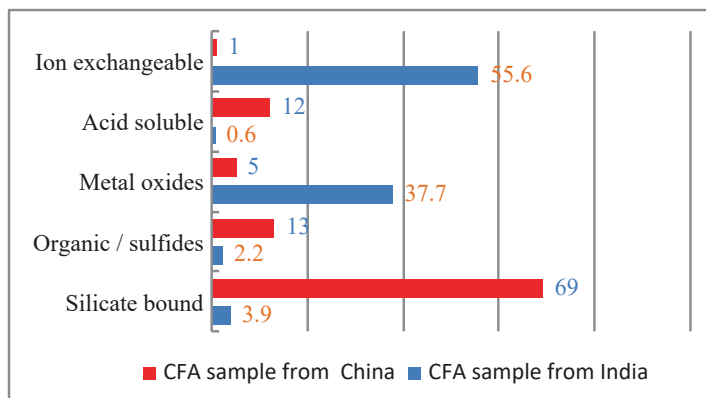


Fig. 17.8 Department of REEs in sequential chemical extraction of CFA from two different samples (Indian sample: after Anand Rao et al. 2020, Chinese sample: after Pan et al. 2020)

such a strategy are as follows: (a) REE minerals or compounds bearing them are chemically very refractory demanding drastic leaching conditions for dissolution and (b) the tenor of REEs in CFAs is generally lean. Additionally, pre-concentration by non-thermal physical beneficiation process will leave majority of the CFA feed-stock useful enough for bulk uses for which they are known at present (Fig. 17.3).

Pre-concentration is usually carried out by exploiting the differences in the physical/physico-chemical properties of various phases present in a resource. The properties used in the separation process include sorting, specific gravity, magnetic susceptibility, electrostatic and surface chemical differences. The success of the physical separation depends on the nature of occurrence of valuable mineral/metal values in the resource. The particle size distribution and shape too play very important role in physical beneficiation process. The particle size spectrum of CFA shows mix of both coarse ($300 \times 90 \mu\text{m}$) and finer size ($<90\mu\text{m}$) material. The coarser matter is composed of char, semi-cooked or coked carbon matters. The coarser matter arises due to low combustion efficiency in combustors and low-quality control in maintaining the particle size of the pulverized coal feed, besides other reasons. The fines are resulted due to alterations that various constituents of coal undergo during the combustion process as elaborated in previous discussions. Another important property that determines the efficiency of separation of desired values from barren in physical beneficiation process is the shape of particles. The particulate matter in CFA is irregular-shaped and contains vesicular, lacy, solid/hollow alumino-siliceous spheres. Capture of values present in sizes finer than about $25\mu\text{m}$ in the concentrate fraction during separation process is extremely difficult on conventional beneficiation equipment like gravity tables, wet high-intensity magnetic separators, electrostatic separators or by froth flotation using conventional reagents combine. In such cases equipment which enhances or amplifies the separating forces (or force multipliers) is made use of. The equipment and/or techniques in this category include the multi-gravity separator (centrifugal force: $10\text{--}13 \times \text{gravitational force (g)}$) or

Knelson separator (centrifugal force: 60–100 × *g*), high gradient magnetic separator (magnetic force 3–5 T) or froth flotation with mineral/metal specific collectors.

Physical beneficiation of REE values occurring in CFA was attempted in different countries using a variety of techniques. The techniques used included gravity, magnetic, froth flotation separation and also air classification. The CFA sample coded UK 1 containing 506 ppm of REE was processed according to flowsheet given in Fig. 17.9 by Blissett et al. (2014). The CFA was subjected to froth flotation initially to remove unburnt carbon in the float. The flotation sink was subsequently treated on a drum magnetic separator to separate magnetic and non-magnetic material. The REE values were distributed in both mags and non-mags, but the latter was relatively enriched in the REE values. The non-mags fraction was treated on a hydrocyclone classifier. In the classification stage, the REEs reported relatively more (enrichment ratio 1.26 times over feed REE assay) in the classifier overflow.

Zhang et al. (2015a) made an attempt to use froth flotation for selective flotation of REEs from CFA of Hazard 4 seam of UK analysing 640 ppm, using several collector molecules like oleic acid, sodium oleate, hydroxamic acid and Talon 9400. The results indicated evidence of marginal enrichment of REEs in the float fraction, but the recovery in this case also was very low. Anand Rao et al. (2020) processed unclassified CFA sample (Code NLP II) analysing 2100 ppm REE on a wet shaking gravity table fitted with slimes deck (Table 17.7), which is the deck configuration suitable for CFA samples of size spectrum as shown in Fig. 17.6. The CFA feed-stock has about 60% by weight in <37µm size (−400#). The metallurgical results indicated recovery of about 56% of REEs in Table Heavies fraction in about 40% weight indicating an overall enrichment ratio of 1.4 times over the feed REE assay. The LREEs were preferentially in Table Heavies, while the HREEs were reported in Table Lights (lower specific gravity). Microscopic observation of the separated fractions showed concentration of discrete REE minerals like monazite and zircon along with other heavy minerals in Table Heavies. The Table Lights are preferentially with very-fine-sized siliceous matter including glassy phases.

Lanzerstorfer (2018) explored the potential of Air Classifier (make: 100 MZR from Hosokawa Alpine) for separation of CFA sample of Poland into different size

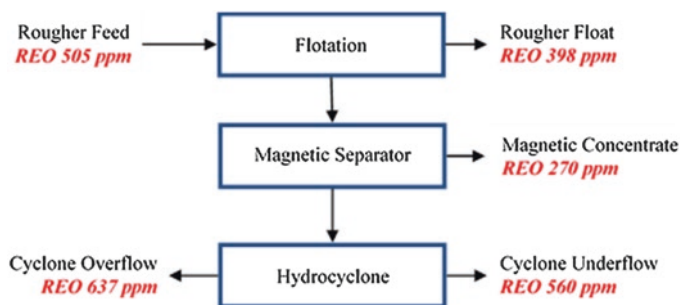



Fig. 17.9 Process flowsheet adopted for physical beneficiation of CFA (Code: UK1) from UK (after Blissett et al. 2014)

Table 17.7 Pre-concentration of REE values from a typical Indian CFA by gravity separation on slimes table (after Anand Rao et al. 2020)

Stream	Assay (ppm)	Wt%	Enrichment ratio of REE		
			Total	Lighter	Heavier
Table heavies		40	1.4	1.68	0.42
Table lights		60	0.73	0.55	1.45
Feed REE assay	2100				

Table 17.8 Physical beneficiation of REE values in CFA (Country: Poland) using Air Classifier (after Lanzerstorfer 2018)

Size Fraction →	Fines  Coarse				
Product ↓	Step I	Step II	Step III	Step IV	Step V
Enrichment Ratio of REEs					
LREE	1.11	0.61	0.89	1.23	0.77
HREE	1.34	0.78	1.01	0.99	0.65
Total REE	1.17	0.65	0.92	1.17	0.74

fractions which had different enrichment ratio of REEs. The procedure consists of separation of the finest size mass fraction in Step I, and the process is repeated subsequently by manipulating the separating force in steps such that at each step the size of the mass fraction collected increases progressively. The results of the experiment conducted are given in Table 17.8.

The finest size mass fraction (Step I) was relatively more enriched (ER) in REE values over the coarser size fractions collected in Steps II, III and thereon. The enrichment ratio of the LREE and HREE assays followed similar trend. Though the ER realized in the process was not very significant in the finer size mass fractions, Lanzerstorfer (2018) opines that very coarse material is definitely depleted in REE and can be stripped off for deriving some advantages. Zhang et al. (2015b) explored float-sink procedure for preferential separation of REE-enriched material in CFA samples. Their study indicated REE enrichment in the sink fraction when the heavy media liquid of specific gravity 1.8 was taken. In the studies conducted by Lin et al. (2017), the REE-rich mass was captured in the density range of 2.71–2.95 & 2.45–2.71.

Results of test work by other investigators too indicated suboptimal performance in pre-concentration of REE values during the physical beneficiation of CFA (Dai et al. 2014; Lin et al. 2017; Zhang et al. 2020; Costis et al. 2019) working on CFAs of different origin (either country and/or coal type). Presence of REEs in very fine size ranges, their encapsulations in refractory host matrices (composites) and deportment of REEs in multiple phases with varying physical properties in the fly ash are the chief reasons for the suboptimal performance noticed in many cases.

17.4.2 Leaching of REEs from CFA

The REE values in the CFA are leached by various methods such as the following: (i) direct leaching with mineral acids, (ii) alkali or/and thermal pre-treatment of feedstock followed by chemical leaching of pre-treated mass with mineral acids and (iii) bioleaching.

Mineral acids like HCl, H₂SO₄ and HNO₃ were used by researchers during direct leaching of REEs from CFAs. The leaching performance with different mineral acids was found to be varied with the nature of occurrence or department of REEs in the feedstock. For instance, the fly ash of Guizhou province of China gave REE leachability of about 70% with 3 M HCl in 2 h of reaction time at about 60 °C while it was only 32% even with 8 M HCl from CFA sample collected from Sichuan province of China (Cao et al. 2018; Wang et al. 2019). Addition of 4% HF to the Sichuan sample enhanced leachability to 90% at ambient temperature in 24 h of reaction time indicating the association of REEs with the refractory glassy matrix. Similarly, contrasting behaviour was also noticed with CFA samples of USA (King et al. 2018) with HCl. CFA from Powder River Basin gave 100% leaching of REEs with 12 M HCl at 85 °C itself as reported by King et al., and in the case of sample from Illinois Basin it was mere 35% under identical process conditions. Their studies have further shown that leachability was poor even with CFA of Appalachian Basin too with concentrated HCl. Interestingly, only 70% of REE values were leached even after using very strong concentration of 15 M HNO₃ with the Powder River Basin (USA) sample. King et al. (2018) observed correlation of Ca content/phases in CFA and the leachability of contained REE values. Sulphuric acid was studied as lixiviant for REEs from fly ash samples of Japan (Kashiwakura et al. 2013), India (Anand Rao et al. 2020) and Finland (Peramaki 2014). Kashiwakura et al. (2013) reported leachability of about 45% of the REE values from three different CFA samples of Japanese origin at 80 °C in dilute H₂SO₄ medium in 2 h. The leachability enhanced with further increase in temperature of reaction. Studies on a typical CFA sample (code: NLP II) from India by Anand Rao et al. (2020) with 1.5 M H₂SO₄ at ambient temperature gave about 90% leach recovery of HREEs and about 42% of LREEs. The Indian CFA sample gave better leaching results with equal concentration of H₂SO₄ (51%) over HCl (2%) and HNO₃ (29%). Furthermore, the filterability of leach slurry generated with H₂SO₄ as leachant was faster than the other two acids. The contrast in leachability of HREE and LREE during sulphuric acid treatment of CFA was investigated by Kashiwakura et al. (2013). The HREEs are generally associated with organic matter in coal and when the organic matter is burnt during the combustion process, the HREEs have tendency to adsorb on very-fine-size solid material (like CFA) which are surface-active and such HREEs are taken into solution by mineral acids and salts relatively easily. The mechanism of leaching expected here is by ion exchange process. It may be recalled that the results of sequential chemical extraction conducted on this Indian CFA sample (Fig. 17.8) show substantial presence of REEs in ion-exchangeable form. The suboptimal leachability of LREEs with the Indian sample can be explained on the basis of nature of their

occurrence. Some of the LREE values originate from refractory minerals like monazite and zircon (Fig. 17.5) which obviously require more aggressive leaching conditions than those used in the test work for maximizing the dissolution. The differential dissolution pattern between LREE and HREE observed by Anand Rao et al. (2020) with H_2SO_4 was also found in the work by Peiravi et al. (2017) in their studies on CFA from coal samples of different ranks, lignite to anthracite using nitric acid as lixiviant. Higher acid concentration, lower solids content during leaching and longer retention time were observed to result in higher recovery of LREEs. In the case of HREEs, higher concentration affected the HREE recovery instead, an intermediate molarity, 3 M, yielded better HREE dissolution, about 94%. Some workers like Vaisanen et al. (2013) used HNO_3 and H_2SO_4 combine for REE recovery and found success.

Many investigators (King et al. 2018; Taggart et al. 2018; Wang et al. 2019; Ma et al. 2019; Tang et al. 2019) observed that chemical and/or thermal pre-treatment of CFA prior to mineral acid leaching would result in better recoveries of REEs. The chemical pre-treatment uses highly concentrated alkalis (NaOH) or acids (HCl) and aggressive reaction conditions to facilitate unlocking of REE values from the glassy or silicate matrix. In the thermal treatment procedure, alkali roasting was followed, and in some cases roasting additives like Na_2O_2 , NaOH, CaO, Na_2CO_3 , CaSO_4 , and $(\text{NH}_4)_2\text{SO}_4$ were used (Taggart et al. 2018). The roasted mass was subjected to HCl leaching subsequently or in some cases plain water leaching was adopted for solubilising REE values. King et al. (2018) followed this dual treatment process (alkali + acid) for achieving higher leachability, about 85%, of REEs from Appalachian ashes of USA. The leachability in this method was significantly higher than using acid alone. Similar observations were noticed by Tang et al. (2019) on CFA samples of Panbei coal-fired power plant at Guizhou province of China. Alkali fusion with 1:1 mass ratio of CFA/ Na_2CO_3 , heating at 860 °C for 0.5 h followed by dissolution in 3 M HCl gave leaching efficiency of 0.6 while in direct HCl leaching it was only 0.22.

A comparison on success of these three mineral acids in leaching of REEs from different CFA feedstocks point out better score by HCl. The suboptimal performance with H_2SO_4 is attributed to formation of calcium gypsum during the leaching process. The freshly formed gypsum may sorb on the material surfaces, thus retarding transport of H^+ into the interiors of the particles (Borra et al. 2015). Cao et al. (2018) and King et al. (2018) conducted detailed studies on the role of reaction mechanism and effect of various operating and chemical parameters on the leaching of REEs from CFA. Cao et al. observed the mechanism of leaching is chemical reaction controlled; therefore temperature, lixiviant strength, solids content and contact time are highly influential, which was the observation of King et al. (2018) also Zhang et al. (2020) noted that the leaching efficiency varies with the temperature adopted in coal combustion process. REEs present in fly ash generated in a Fluidized Bed Combustion (FBC) chamber were more easily leached as against those originating from pulverized coal-fired (PCC) boilers mainly due to relatively lower temperature of combustion reactor in former case which results in lesser probability of formation of glassy phases with which REEs are generally associated.

Feasibility of bioleaching or bio-mining is relentlessly pursued world over due to their environmentally benign nature. Bioleaching of REEs from CFA was investigated by Russian Scientists (Muravyov et al. 2015) and others (Park and Liang 2019). Study by Muravyov et al. on ash samples containing relatively low amounts of REEs (in ppm), viz. Ce 80, La 46, Nd 39, Y 31, Pr 10, Sc 9.4, Sm 7.2, Gd 6.5, Dy 5.7, Er 3.6 and Eu 1.2, with acidophilic chemolithotrophic microbial communities in the presence of sulphur gave leachability of Sc, Y and La as 52.0, 52.6 and 59.5% after 10 days of bioleaching at 45 °C. The ratio of ash to elemental S, the substrate for sulphuric acid production by an acidophilic chemolithotrophic microbial community, is among the key parameters identified by authors for leaching of REEs. The results also indicated that low amounts of elemental S may result in insufficient concentrations of the leaching agent in the liquid phase, while its excess may result in lower economical efficiency of bioleaching. Park and Liang (2019) used three microbial strains, *Candida bombicola*, *Phanerochaete chrysosporium* and *Cryptococcus curvatus*, for testing leachability of REEs from CFA generated at S. Illinois University Carbondale power plant. All the microbial strains leached the metal values by releasing the organic acids, and they have been found to function effectively even at moderately higher acidities (pH 3–4). An important observation in this study was some of the REEs like Sc, Y, Dy, Er and Yb, majority of which are HREEs, are leached to an extent of about 60–65% while only about 25–30% of leachability was noticed for LREEs like La, Ce, Pr and Nd.

17.4.3 Separation and Purification of REEs from Leachates of CFA

The separation and purification of REEs from the leachates is conventionally performed at industrial scale using solvent extraction followed by precipitation (Krishnamurthy and Gupta 2016) and in some cases direct precipitation is also implemented. The properties utilized in the processes are (a) variation in the basicity of REEs as a consequence of decrease of their ionic radius across the period and (b) the variable oxidation states of some elements like Ce, Pr, Tb, Sm and Yb from the general oxidation state of +3 of REEs. Both the variations influence three important characteristics like solubility of the compounds, the hydrolysis behaviour of REE ions and the nature as well as type of REE complexes formed. In order to overcome some shortcomings in the above-cited processes, several other alternatives which are compatible with contemporary environmental regulations and also economical are explored in REE-laden leachate processing. An important thrust in some of the emerging techniques is to achieve selective separation of small concentrations of REE ions (<1 gpl) from leachates with the presence of high concentration of other dissolved solutes like Ca, Mg, Fe, Al, Mn, U, Th, SO_4^{2-} , NO_3^- , Cl^- , PO_4^{3-} to name a few. The alternatives processes/schemes include the following: ionic liquids (IL)-based separation, supported liquid phase extraction (SLE), solid phase

extraction (SPE), membrane-based separations, nano-filtration, solvent-impregnated resins (SIR), free-flow electrophoresis, supercritical fluid extraction and bio-sorption (GéoMégA 2016; KT 2015; Leenheer and Malcolm 1973; Royen and Fortkamp 2016; Silva et al. 2019a, b; Xie et al. 2014; Wang et al. 2017; Jha et al. 2016; Shibata et al. 2000; Smith et al. 2019; Mutlu et al. 2018; Li et al. 2018; Sinclair et al. 2017; Hu et al. 2018; Jin et al. 2017).

17.4.3.1 Solvent Extraction

In solvent extraction (SX) based purification processes, the REE cations are selectively extracted by organic (O) solvents initially. The commonly used solvents for REE-bearing leachates include di-(2-ethylhexyl) phosphoric acid (D2EHPA), 2-ethylhexylphosphonic acid mono-2-ethylhexyl ester (HEHEHP), neodecanoic acid (Versatic 10), tributyl phosphate (TBP), 2-ethylhexyl phosphonic acid mono-2-ethyl hexyl ester (PC 88 A) and tricaprylmethylammonium chloride (Aliquat 336) (Lucas et al. 2015; Thakur 2000; Xie et al. 2014; Mishra 2020; Jyothi et al. 2020). A stage of scrubbing follows after extraction to ensure elimination of extraneous ions or complexes which are co-extracted/entrained into the organic phase (O). The REEs in the organic phase are stripped back into aqueous phase using high concentration of a given acid reagent. The resultant aqueous solution after stripping is highly pure and yields precipitates of mixed REEs of good purity.

Published information on application of SX for purification of leachate from CFA is very limited. Peiravi et al. (2017), tested TBP, Cyanex 572 (mixture of organo phosphonic and phosphinic acids), D2EHPA for separation of REEs from leachate of a CFA sample of US origin assaying 51 ppm REE in HNO₃ medium. Amongst the solvents investigated, the performance of D2EHPA was found superior and exhibited good specificity for HREEs which was also reported by Peramaki (2014). Thriveni et al. (2015) applied PC 88A for selective separation of Y from a leachate of CFA sample produced at Samcheonpo power plant, S. Korea and also another of Japanese origin. PC 88A was observed to show better performance over other commercial solvents like Cyanex 272 and Cyanex 302. Joshi et al. (2013) developed a patented flowsheet for recovering REEs from CFA leachate in HNO₃ medium using TBP–kerosene mixture. Anand Rao and Sreenivas (2019) reported efficient extraction of REEs from a CFA sample leached in sulphuric acid medium using DEHPA–kerosene combine. Presence of impurities in the CFA leachate, particularly the dissolved silica, posed several problems during the SX process on Indian sample. The shelf life of the leachates was very short due to formation of gels. The process adopted for overcoming this involved prior removal of excess silica using gelatin. Though the HREEs were extracted with D2EHPA (12%) directly, quantitative loading of LREE necessitated partial saponification of

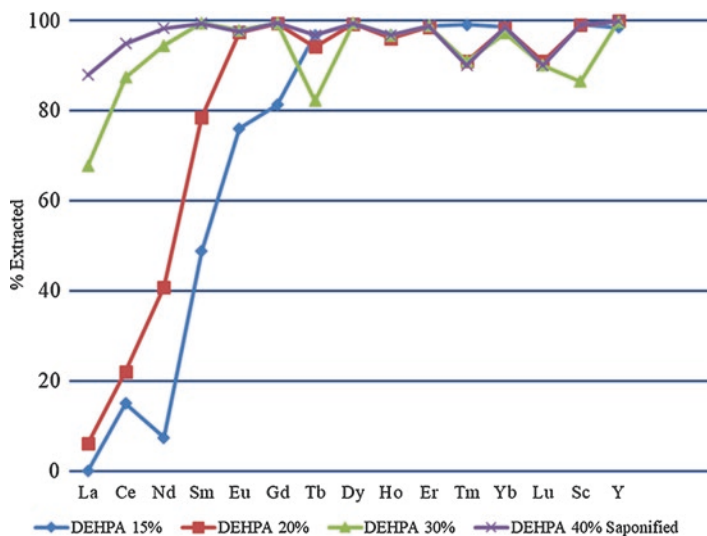


Fig. 17.10 Solvent extraction of REEs from leachate (sulphuric acid medium) of a typical CFA of Indian origin using DEHPA and role of saponification on extraction of LREEs

D2EHPA (40%) (Fig. 17.10). The schematic steps in the SX process developed by them are shown in Fig. 17.11. About 90% extraction of the total REE in the leachate could be accomplished in the loading sequence. Stripping with concentrated HCl gave 100% recovery in the form of two separate aqueous streams, a LREE-rich fraction and other enriched in HREEs. The two final purified strip liquors analysed 1.6 g/L HREE and 3 g/L LREE.

Though used quite extensively, SX is besieged with issues like (a) poor selectivity of solvents necessitating large number of stages, viz. 100–150 stages, especially for separating individual REE ions or complexes, (b) flammable and volatile nature of diluents generally used in contemporary processes, (c) highly acidic and voluminous quantities of raffinates, (d) stability, biodegradability and unfavourable economics of recycling of extractants is also a concern (Vahidi and Zhao 2017) and (e) toxic nature of various saponifiers (like ammonia salts) (Ding et al. 2020). Life cycle assessment studies on the technologies used on conventional ores containing REEs in the form of REE-fluorocarbonate minerals revealed that the purification stage of leachate accounts for about 30% of the total environmental impact and 70% of the ozone depletion impact (Vahidi and Zhao 2017; Lee and Wen 2017) Since the chemistry of SX process in separation and purification of REEs either from leachates of CFA or from conventional ores is broadly the same, the concerns highlighted in conventional ores are equally applicable in CFA processing also.

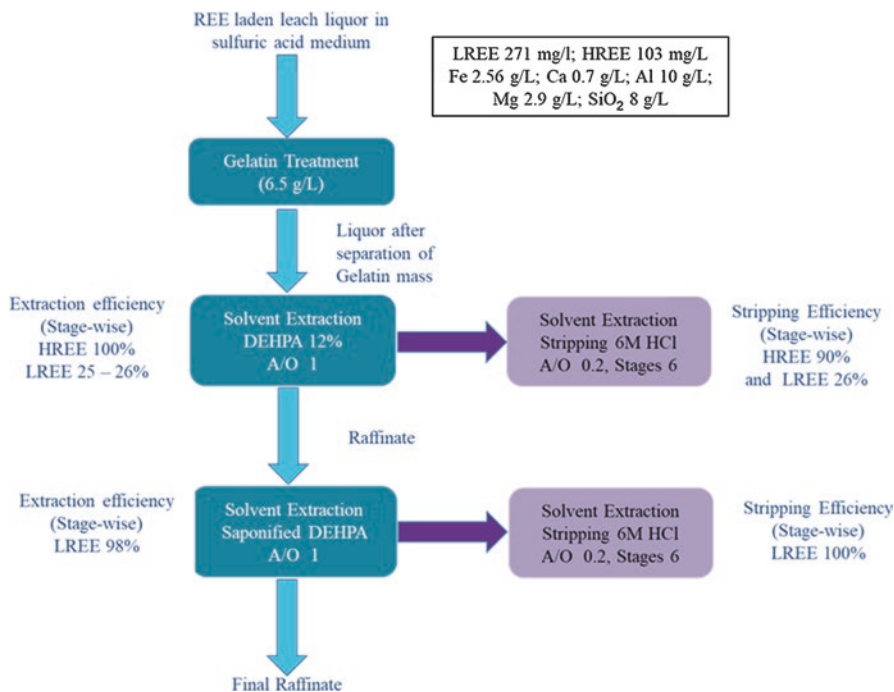


Fig. 17.11 Process flowsheet followed for separation of REEs from leachate of a typical CFA sample of Indian origin using DEHPA

17.4.3.2 Ionic Liquids

A recent development in the separation science and technology is the use of Ionic Liquids (ILs) and Deep Eutectic Solvents (DES) for resource leaching and also for leachate purification. They are bestowed with many positive attributes non-existent with conventional solvents. ILs has negligible vapour pressure at room temperature, lower fire load, higher thermal stability and a broader liquidus range. Rozelle et al. (2016) compared conventional precipitant— $(\text{NH}_4)_2\text{SO}_4$, an IL and a DES to evaluate relative effectiveness for extracting REEs from coal combustion products (CCP). Both IL and DES did not show any advantage over $(\text{NH}_4)_2\text{SO}_4$. Huang et al. (2019) worked on the recovery of REEs from CCPs of (China) assaying 0.0135% using various ILs, namely $[\text{N1888}]\text{Cl}$, $[\text{P6,6,6,6,14}]\text{Cl}$, $[\text{P6,6,6,6,14}][\text{SOPAA}]$ and $[\text{P6,6,6,6,14}]$ (Fig. 17.12). CCPs were mixed with different diluted acids and heated to 200 °C for 9 hours, cooled with air and filtered. The leachate was then put into contact with the ILs for recovery and purification. The recovery of REEs was 37.4%. Researchers at Skyhaven Systems, LLC (Jayne et al. 2019), claimed good measure of success in REE separation upon using conventional ILs and cheaper DES on a CFA of US origin. Efforts in replacing conventional leachants and solvents by less

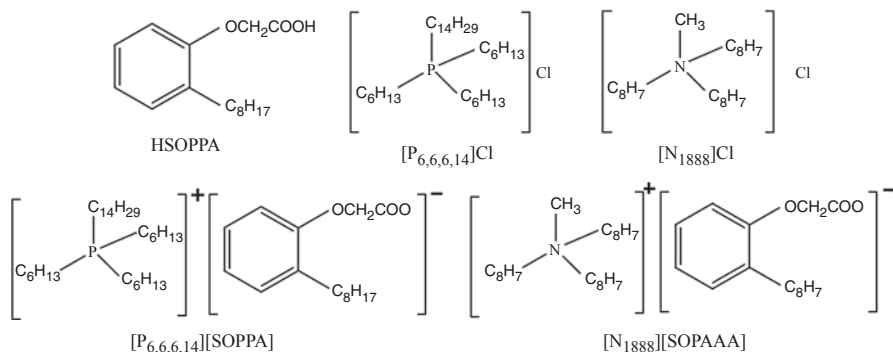


Fig. 17.12 Molecular structure of ionic liquids used in REE extraction from leachates of CFA of Chinese origin (after Huang et al. 2019)

harmful alternatives like ILs and DES, though in very nascent stage, is giving encouraging signs in the processing of secondary resources.

17.4.3.3 Membranes-Based Separation

Another group of techniques making inroads in the separation and purification of complex lean tenor leachates is the membrane-based technologies (MT) like emulsion liquid membrane (ELM), supported liquid membrane (SLM), and electrostatic quasi (pseudo) liquid membrane (EQLM). MTs are ascribed with superior operational efficiency and competitive economics (Bhave et al. 2018; Yaftian et al. 1998).

Smith et al. (2019) compared efficacy of conventional SX with ELM and SLM for capture of REEs very selectively from leachate of a typical CFA feedstock. D2EHPA in kerosene or mineral oil was the solvent in all the cases. The ELM technique where D2EHPA–oil emulsion was used gave performance akin to conventional SX process. In SLM technique, the hydrophobic matrix was grafted with D2EHPA, but the SLM process gave inferior kinetics in comparison to ELM process. Even with respect to selectivity, the ELM and SLM techniques gave different performances while SX and ELM were selective for LREEs while the SLM process showed higher affinity for HREEs.

Mutlu et al. (2018) investigated nano-filtration (NF) technique for separation of REEs from synthetic leachates similar in composition to that obtained with a typical CFA of Appalachian origin. Different commercially available membranes made of polyethersulphone, mixed cellulose ester, polycarbonate, and thin film composite were used in the studies. The feed solution was a synthetic leachate consisting of mixture of critical REE ions and impurities like Mg^{2+} , Ca^{2+} , Fe^{3+} , Al^{3+} , Si^{4+} and Na^+ , in nitric acid medium at pH 1. A pre-treatment step, by pH adjustment and microfiltration (MF), was incorporated to separate REEs from major impurity ions. Fairly good separation of REEs from major impurities in the leachate was achieved. However, Cantoni (2016) observed certain challenges in separation and purification

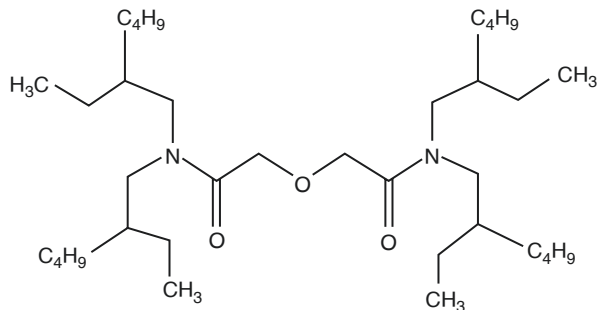
of real leachates obtained from a CFA by nano-filtration. The NF tests were conducted by this Group using four different commercially available membranes, namely NP010 (MicroDyn-Nadir), NP030 (MicroDyn-Nadir), DK (GE Osmonics) and Duracid (GE Osmonics). Synthetic leachates consisting of nitrate salts of REE, Na, Mg, Al, Ca and Fe gave encouraging separations, but when real leachates were tested the results demonstrated lower permeate flux and REEs rejection. The sub-optimal efficiency was attributed to high salt content in the real leachates, resulting in both membrane fouling, decreasing the permeate flux, Donnan potential reduction and increasing ions permeation, warranting more detailed studies.

17.4.3.4 Adsorption Methods

Various innovations in separation methods based on adsorption principle have taken place in recent times for selective capture of valuable metal ions including REEs from lean tenor leachates. Notable amongst such techniques are solid phase extraction (SPE), nano-adsorbents, solvent-impregnated resins (SIR), bio-sorption using microbes and other natural products (Shibata et al. 2000; Jelinek et al. 2007; Khaldun et al. 2008; Chun-fa et al. 2010; Helaly et al. 2012; Roosen and Binnemans 2014; Ponou et al. 2016; Jin et al. 2017; Shu et al. 2018; Hu et al. 2018; Li et al. 2018; Case et al. 2019; Jyothi et al. 2020). The advantages of using adsorption-based methods are multiple chiefly, simplicity, ease of handling, sludge-free operation and less expensive. The performance of adsorbents is enhanced by grafting ligands/functional groups on solid supports which are capable of delivering very high degree of affinity/selectivity for ions of interest in the leachate and also environmentally benign (Yang et al. 2013; Ansari et al. 2012; Ansari and Mohapatra 2017; Andreiadis et al. 2019; Yang et al. 2013; Gergoric et al. 2017; Mowafy and Mohamed 2017). Examples of such solvent molecules in diglycol amide family are as follows: *N,N,N',N'*-tetra-2-ethylhexyl diglycolamide (TEHDGA), *N,N,N',N'*-tetrabutyl diglycolamide (TBDGA), TODGA and DHD2DGA. Innovations in design and development of solid supports have also taken place such that the supports possess attributes like increased surface area, more active sites, endurance or recyclability to name a few. Some such adsorbents include carbon cloth supported nano-Mg(OH)₂ (Li et al. 2018), ordered mesoporous materials (Hu et al. 2018), natural polymers (Roosen and Binnemans 2014) and synthetic macromolecules like XAD-2, XAD-4, XAD-7, XAD-8, XAD-12 and XAD-16 (Shu et al. 2018).

The adsorption-based techniques were also explored on leachates of CFA by Mondal et al. (2019), Ponou et al. (2016) and Jin et al. (2017). Mondal et al. (2019) studied SIR technique for recovery of REEs from synthetic leach liquor having composition similar to a leachate generated from a typical REE-bearing CFA of a coal-fired Indian thermal power plant. Based on the complexation chemistry of diglycol amide functional group with various lanthanides and actinides, *N,N,N',N'*-tetra-2-ethylhexyl diglycolamide (TEHDGA) was impregnated on a commercially available poly acrylic polymer (XAD 7) backbone, and separation studies were performed (Fig. 17.13). The experimental results indicated that adsorption and elution

Fig. 17.13 Molecular structure of *N,N,N',N'*-tetra-2-ethylhexyl diglycolamide (TEHDGA)



behaviour of all the REEs depended on the charge density. REEs with higher charge density were sorbed more and gave higher loading capacity on the impregnated resin. Desorption of loaded REE was achieved by elution with 0.01 M nitric acid solution and good elution was also observed. The resin was recycled for 10 times and was found to retain its extraction and elution properties without much of degradation.

Ponou et al. (2016) reported biosorption-based method for separation and purification of REEs from leachates generated during CFA (DK-TOP) leaching (HCl medium). The leachate contained besides REEs other solutes like Li, Fe, Cu and Al. The leachate was processed on carbonized ginkgo leaves (GL450). Though good adsorption was noticed for typical lighter (La, Ce, Pr) and heavier REE (Y, Er) ions at pH 3, the desorption was satisfactory only for Er. The sorption was found to be columbic in nature and influenced significantly by reaction temperature and contact time. Biosorption was also explored by Jin et al. (2017) for separation of REEs from lean tenor feedstocks/leachates of CFA of Appalachian Basin, USA. The engineered bio-sorbents used are *Caulobacter crescentus* (*C. crescentus*) and *Escherichia coli* (*E. coli*). They showed good specificity for REE ions, and the investigators opined that the process is commercially also lucrative CFA feedstock of Appalachian Basin largely due to its high-value REE content.

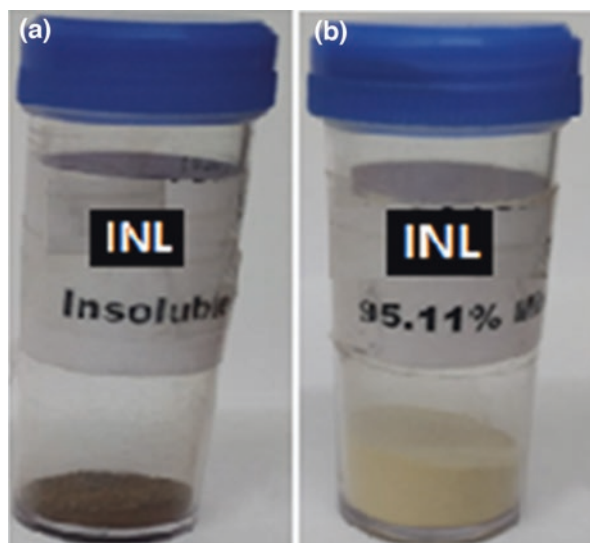
17.4.4 Precipitation of REEs from Leachates of CFA

The selective precipitation of REEs directly from the leachates or from purified liquors obtained after separation and purification stages like SX or any other alternative technique is dependent on the difference in solubility products of the complexes formed by REEs and other contaminants (Krishnamurthy and Gupta 2016). The chemical reagents used for REE precipitation are oxalic acid, ammonium/sodium hydroxide or ammonium/sodium bicarbonate/carbonate (Silva et al. 2019a; Silva et al. 2019b). The choice of a precipitant varies with the stage at which precipitation is introduced. For example when precipitation is carried out on impure leach liquors directly, the hydroxides or carbonate salts are used. If the feed liquor

for precipitation is the aqueous liquor after SX process, the REEs are precipitated using oxalic acid and the product is obviously of high purity. Though oxalates are formed with some dissolved impurity ions (Fe, Ti, Al, Zr) too, they exist in soluble form and only REE-oxalate product precipitates out in weakly acidic medium (pH 1–4) ensuring good quality/purity product (Chi and Xu 1999). Some plants using sulphuric acid as a leachant for REEs prefer using sodium sulphate as precipitant due to inexpensive nature of the reagent compared to others used for precipitation, the product being bulk REE-double sulphate. Pietrelli et al. (2002) opines that the double sulphate product is also of acceptable purity. Very recently, Han (2020) gave a detailed account on the role of different process parameters and solution chemistry on REE precipitation behaviour. They observe that nitrate systems are most favourable to precipitation followed by sulphate and chloride.

Literature on precipitation of REEs from leachates of CFA, either directly or after purification stage, is scanty. Wang et al. (2019) used oxalic acid as precipitant of REEs in leachate of CFA from the Luzhou power plant in Sichuan, SW China. Zhang and Honaker (2019) also preferred oxalic acid as precipitant for lean tenor RE leachates from coals of Kentucky region, USA. Serajuddin (2018) attempted multi-stage precipitation approach on a leachate obtained from a CFA sample of Indian origin. The leachate assayed 166 mg/L of REEs and had other impurities like Fe 680 mg/L, Ca 740 mg/L, Mg 2140 mg/L, Al 1.1%, dissolved SiO_2 1.56%. The pH of the leachate was 1.5. The strategy followed was bulk precipitation of dissolved solutes in the leachate directly with NaOH followed by re-dissolution of the bulk precipitate with HCl at pH 4. This step removed majority of the impurity solutes as solid residue thus produced (Fig. 17.14). The REEs in the filtrate were re-precipitated with NaOH and re-dissolved (pH 1.5) with same reagents, but the solids content in the second stage of re-dissolution with HCl was manipulated such that

Fig. 17.14 Recovery of rare earths from leachate of CFA sample of Indian origin by differential precipitation: (a) bulk precipitation of impurities and (b) rare earth oxalate of 95% purity



the leachate had relatively higher concentration of REEs. The REE values in leachate at this stage analysed 7 g/L which were then precipitated using oxalic acid. The purity of the final REE-oxalate product was 95%. Another study was also made in India on leachate which was purified using SX process utilizing both oxalic acid and sodium sulphate as precipitants. The REE content in the leachate was improved from about 300 mg/L to about 1.6 g/L in the SX step with D2EHPA. The other impurities in the purified liquor were Fe 19 g/L, Ca 0.27 g/L, Al 0.79 g/L, Mg 0.01 g/L and SiO₂ 0.02 g/L. This liquor gave good precipitation efficiency with oxalic acid, but with sodium sulphate the efficiency was suboptimal. Using 40% wt/vol. Na₂SO₄ and at 50 °C, the precipitation efficiency of REEs was only 68%. The results showed that the precipitation efficiency of LREE was almost complete, but the HREE was only 63%. The concentration of Na₂SO₄ could not be increased further as it bordered the solubility limits of sodium sulphate.

17.5 Flowsheet for Recovery of REE from CFA

The studies on the recovery of REEs from CFAs in different countries are still being evaluated on various counts—technical, economical and environmental, and the status of many of the flowsheet can be categorized as “suggested or conceptual” schemes only. However, in some instances the process schemes were tested at semi-continuous large-scale also. Amongst them, the patented process flowsheet called the ADP (Acid Digestion Process) by Battelle Group, Ohio (Fig. 17.15), has been studied in great detail on all aspects for its industrial adaptability (Peterson et al. 2017). The ADP flowsheet is a simple three-step scheme where the REE values are

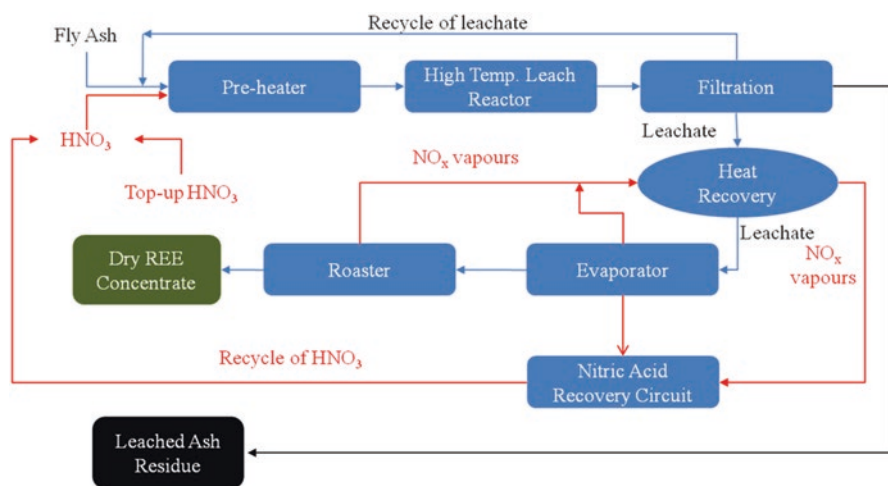


Fig. 17.15 Acid digestion process (ADP) flowsheet for recovery of REEs from CFA (modified after Peterson et al. 2017)

leached using HNO_3 followed by separation of the REE-laden leachate from the residual ash by vacuum filtration. The REE content in the liquor is enriched by partially bleeding the leachate and recycling the same to leach reactor. Further enrichment of REE in bled-out leachate is achieved in an evaporator. The REE nitrates from the evaporator are crystallized to REE-oxides and taken as solid product. The heart of the process is re-generation and recycles of nitric acid, conservation of heat and water by different ancillary processes. The design of the pilot-plant was made for ash throughput of 30,000 kg/h, and the Group finds it techno-economically attractive.

The authors of this article in India have developed and tested two alternative schemes for the recovery of REE from CFAs of Indian origin as shown in Fig. 17.16a–c. In both the alternatives, the lixiviant used was sulphuric acid and reaction temperature was 55–60 °C. Milder conditions during the leaching step were adopted deliberately to avoid unnecessary damage to the constituents of post-leached CFA which contribute for its bulk usages subsequently. Flowsheet A (Fig. 17.16a, b) uses solvent extraction (SX) with D2EHPA for purification and separation of REE values from a leachate generated using H_2SO_4 lixiviant on a CFA sample (REE ~2000 ppm) from a lignite coal-fired thermal power plant and recovers the REEs as REE-oxalate. The difficulties in stability of the leachate due to gel formation were overcome by gelatine strike of the leachate which lowers the dissolved silica content preventing formation of gels. Two separate oxalate products (Fig. 17.16b), namely LREE-rich (LREE: total REE = 0.98) and the other HREE-rich (HREE: total REE = 0.81), were obtained as final products (Table 17.9).

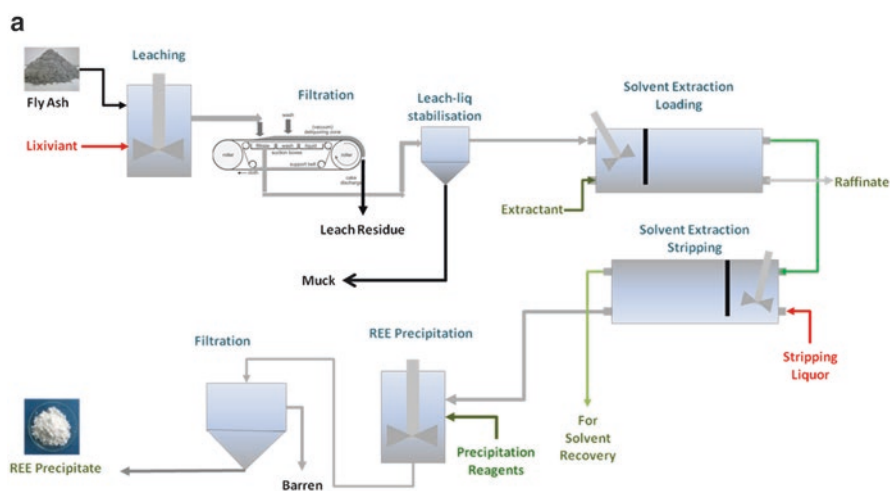


Fig. 17.16 (a) Process flowsheet for recovery of REE from CFA of Indian origin by sulphuric acid leaching—solvent extraction with D2EHPA—precipitation as REE-oxalate. (b) HREE- and LREE-rich products obtained from a CFA sample of Indian origin using sulphuric acid leaching—solvent extraction with D2EHPA—precipitation as REE-oxalate. (c) Process flowsheet for recovery of REEs from an Indian CFA sample by sulphuric acid leaching and differential precipitation route

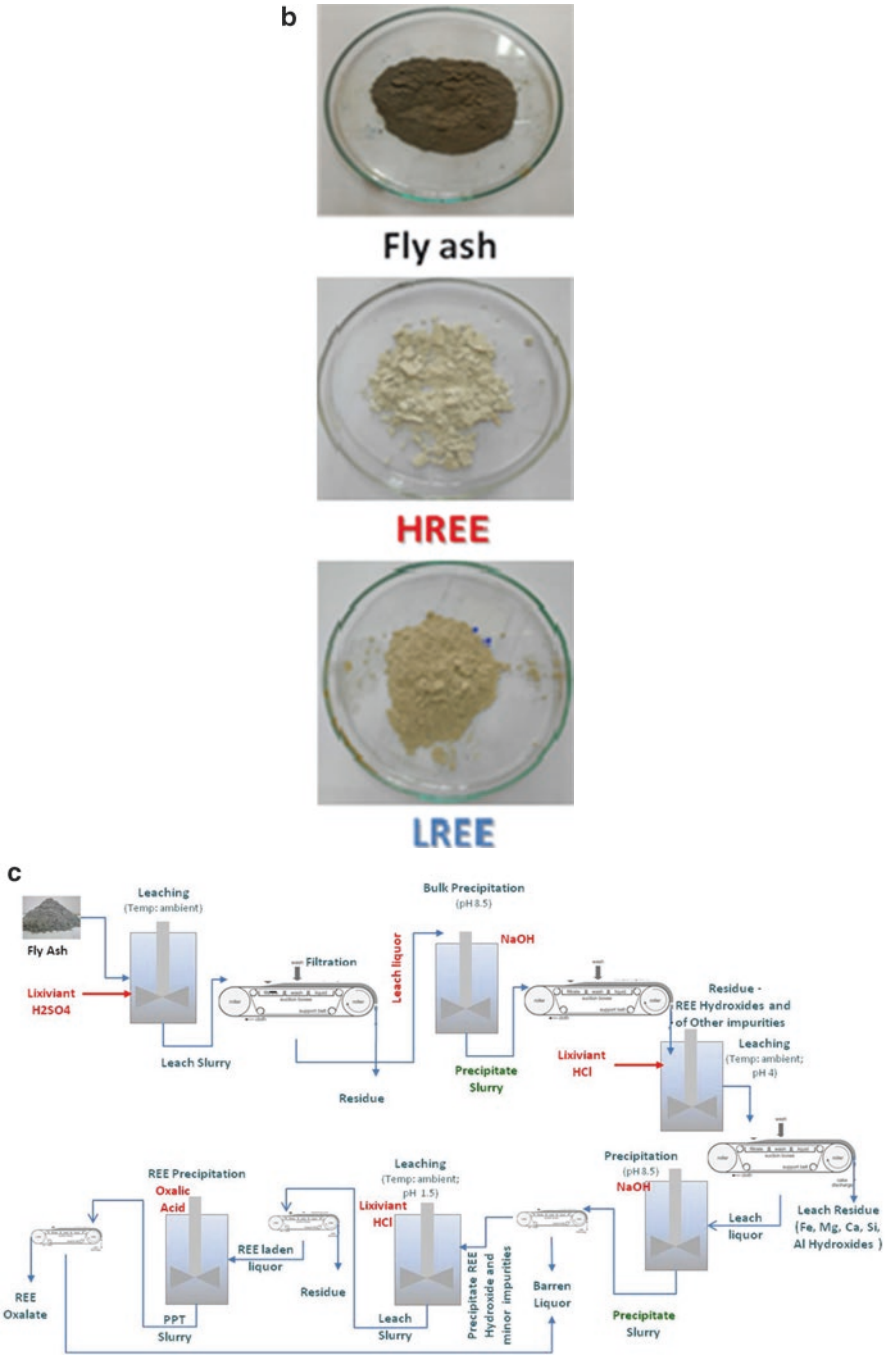


Fig. 17.16 (continued)

Table 17.9 Partial chemical composition of REE-oxalate product obtained from a typical Indian CFA sample using sulphuric acid leaching–solvent extraction (D2EHPA)–precipitation route

	REE	LREE	HREE	Fe	Ca	Al	Mg	SiO ₂
Stream	%							
Fly ash	0.21	0.14	0.06	50	4.2	6	7	13.4
HREE Conc.	16.3	3.3	13	0	0.6	0.1	0	0.5
LREE Conc.	8	7.9	0.05	0.2	8.7	0.1	0.03	0.1

Flowsheet B (Fig. 17.16c) too used CFA from lignite coal-fired thermal power plant as feedstock, but the REE content was only 1000 ppm. In this case the REE values from the sulphate leachate were recovered using differential precipitation with NaOH and multi-stage leaching of the precipitate with HCl. The final REE-oxalate product obtained in this scheme was 95% pure.

17.6 Pozzolanic Behaviour of Post-Leached CFA

Aluminium and siliceous matter form the major chemical constituents of CFA (Table 17.5). The pozzolans in CFA react with calcium hydroxide in the presence of moisture/water resulting in formation of cementitious material. This property/chemical reaction is responsible for bulk use of CFA in geopolymers, CFA bricks and supplementary cement presently. Major criticism encountered in the use of CFAs as a source of REEs is that the ash residue generated after leaching of CFAs with mineral acids loses its effectiveness as a pozzolan or its utility as supplementary pozzolanic material. This is because the processing conditions adopted prior to leaching as part of feed preparation or/and leaching latter are quite aggressive—either the temperature of roasting or/and type and concentration of acid/alkali reagents used to name a few. Such a treatment is essential for release of REEs from the glassy matrix essentially for maximizing the leach recovery of REEs. Some studies on overcoming this constraint is made by following alternative techniques for leaching of REEs like use of microbes, organic acids, ionic liquids and deep eutectic solvents (Wang et al. 2017). Some researchers (Anand Rao and Sreenivas 2019) adopted milder leaching conditions like moderate temperature with lower mineral acid concentration, such that the pozzolanic properties in the resulting leach residue are retained to certain extent, sacrificing even the leach recovery of REEs. Some of the apprehensions in using the mineral acids as leachants of REE from CFAs were addressed in a study made by Peterson et al. (2017). They investigated the variation in compressibility strength (CS) of different samples of leached CFA like ash from pulverized coal, from fluidized bed roaster and from coal liquefaction plant of USA, using HNO₃ as leachant. The results illustrated in Fig. 17.17 indicate that the CS of post-leached CFA is almost similar to that of unleached CFA.

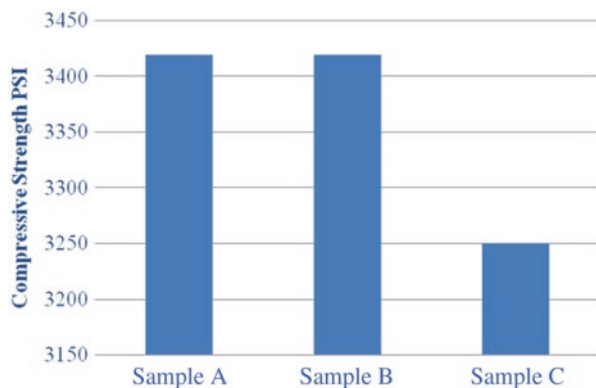


Fig. 17.17 Compressive strength of CFA sample leached with HNO_3 by ADP process and its comparison with unleached CFA (modified after Peterson et al. 2017). Sample A: Concrete with post-leached fly ash (Wt% of Cement: 77, Ash: 19, Sand: 4); Sample B: Concrete with untreated fly ash (Wt% of Cement: 77, Ash: 19, Sand: 4); Sample C: Concrete without addition of fly ash (Wt% of Cement: 77; Sand: 23%)

17.7 Conclusions

Coal fly ash (CFA) is a promising technospheric resource of rare earth elements. The availability of huge stock-piles of CFA and continuing use of coal as a fuel for energy generation across various nations show that it is a dependable and widespread resource for REEs. Exploiting the REE potential in CFAs also serves the sustainability objectives in natural resources utilization. Though the average REE content in CFA is about 0.05%, the nature of its occurrence is very complex. Characterization of CFAs of different origins of coal in various countries using very advanced instrumental techniques revealed their presence predominantly in fly ash glass. The department of REEs in multiple phases and in very finely disseminated state makes their pre-concentration by physical beneficiation prior to hydrometallurgical treatment almost improbable. However, thermal pre-treatment showed some encouraging response in exposing the REEs to the subsequent stage of chemical treatment. By and large recovery of REEs from many CFA feedstocks was studied by direct hydrometallurgical processing. Majority of the investigations at bench-scale reported reasonably good leach recovery. However, the process conditions adopted in bench-scale needs modifications and fine tuning when up-scaling campaigns are undertaken. The lean tenor of REE in the resultant leachates produced too posed several limitations in downstream processing, be it purification stage or at the REE precipitation stage, by conventional methods. The vast published literature on using CFAs as a resource of REEs clearly indicate that the shortcomings in existing processes are already identified and sustained research on developing newer techniques and tailor-made process schemes for different feedstocks of CFA, with maximum recovery of REEs and minimum environmental load (including that of water, energy and material inputs) is on-road. Needless to

underscore that any scheme for REE recovery from CFA should not degrade those properties of CFA, viz. the pozzolanic character, which contribute for their bulk uses, which is also equally important.

Acknowledgements The authors are thankful to Dr. Madangopal Krishnan, Director, Materials Group, BARC, for his interest in the work and encouragement. They are thankful to various Agencies in India who have generously provided the CFA samples for this research work. The support extended by their colleagues of Process Chemistry and Analysis Section is acknowledged with deep sense of gratitude.

References

- Anand Rao, K., Serajuddin Md., Rama Devi, G., Thakurta, S. G., & Sreenivas, T. (2020). On the characterization and leaching of rare earths from a coal fly ash of Indian origin. *Separation Science and Technology*. <https://doi.org/10.1080/01496395.2020.1718705>.
- Anand Rao, K., & Sreenivas, T. (2019). Recovery of rare earth elements from coal fly ash: a review. In A. A. Abhilash (Ed.), *Critical and rare earth elements: Recovery from secondary resources* (pp. 343–364). New York. ISBN-13: 978-0-367-08647-3: CRC Press (Taylor and Francis Group).
- Andreiadis, E., Miguirditchian, M., Pacary, V., & Hartmann, D. (2019). *Rare earth recovery and separation using diglycolamides*. ALTA 2019, Perth, Australia May 2019.
- Anon. (2020). *Global rare earths metal market*. Retrieved 17 September, 2020, from <https://www.zionmarketresearch.com/sample/rare-earth-metals-market>
- Ansari, S., & Mohapatra, P. K. (2017). A review on solid phase extraction of actinides and lanthanides with amide based extractants. *Journal of Chromatography A*, 1499, 1–20.
- Ansari, S. A., Pathak, P., Mohapatra, P. K., & Manchanda, V. K. (2012). Chemistry of diglycolamides: Promising extractants for actinide partitioning. *Chemical Reviews*, 112(3), 1751–1772. <https://doi.org/10.1021/cr200002f>.
- ASTM. (2015). *C618-15, Standard specification for coal fly ash and raw or calcined natural Pozzolan for use in concrete*. West Conshohocken, PA: ASTM International. www.astm.org.
- Balaran, V. (2019). Rare earth elements: A review of applications, occurrence, exploration, analysis, recycling, and environmental impact. *Geoscience Frontiers*, 10, 1285–1303. <https://doi.org/10.1016/j.gsf.2018.12.005>.
- Bhave A, Ramesh R, Daejin K, Peterson ES (2018). *Membrane assisted solvent extraction for rare earth element recovery*. United States. <https://www.osti.gov/servlets/purl/1438367>
- Binnemans, K., Jones, P. T., Blanpain, B., Gerven, T. V., & Pontikes, Y. (2015). Towards zero-waste valorisation of rare-earth-containing industrial process residues: A critical review. *Journal of Cleaner Production*, 99, 17–38.
- Binnemans, K., Jones, P. T., Blanpain, B., Gerven, T. V., Yang, Y., & Buchert, M. (2013). Recycling of rare earths: A critical review. *Journal of Cleaner Production*, 51, 1–22.
- Blissett, R. S., Smalley, N., & Rowson, N. A. (2014). An investigation into six coal fly ashes from the United Kingdom and Poland to evaluate rare earth element content. *Fuel*, 119, 236–239.
- Borra, C. R., Pontikes, Y., Binnemans, K., & Van, G. T. (2015). Leaching of rare earths from bauxite residue (red mud). *Minerals Engineering*, 76, 20–27.
- BPSR. (2019). *BP Statistical Review of World Energy 2019*, 68th ed. Retrieved 12 June, 2020, from Source: <https://www.bp.com/content/dam/bp/business-sites/en/global/corporate/pdfs/energy-economics/statistical-review/bp-stats-review-2019-full-report.pdf>
- Cantoni, B. (2016). *Recovery of rare earth elements from coal fly ash by nanofiltration*. MSc Thesis in Environmental and Land Planning Engineering, Politecnico di Milano, A.Y.

- Cao, S., Zhou, C., Pan, J., Liu, C., Tang, M., Ji, W., Hu, T., & Zhang, N. (2018). Study on influence factors of leaching of rare earth elements from coal fly ash. *Energy & Fuels*, 32(7), 8000–8005.
- Case, M., Fox, R., Baek, D., & Wai, C. (2019). Extraction of rare earths elements from chloride media with tetrabutyl diglycolamide in 1-octane modified carbon dioxide. *Metals*, 9(4), 429. <https://doi.org/10.3390/met9040429>.
- CEA. (2018). Retrieved 5 October, 2020, from http://www.cea.nic.in/reports/others/thermal/tcd/flyash_201718.pdf
- Charalampides, G., Vatalis, K. I., Apostoplos, B., & Ploutarch-Nikolas, B. (2015). Rare earth elements: Industrial applications and economic dependency of Europe. *Procedia Economics of Finance*, 24, 126–135.
- Chen, T., Yan, B., Li, L. L., Yan, Z. A., Wang, J., & Xiao, X. M. (2019). Mineralogy characteristic study and exploration on the valuable metals enrichment of coal fly ash. *Advances in Polymer Technology*, 1839450, 1–7. <https://doi.org/10.1155/2019/1839450>.
- Chi, R. A., & Xu, Z. (1999). A solution chemistry approach to the study of rare earth element precipitation by oxalic acid. *Metallurgical and Materials Transactions B: Process Metallurgy and Materials Processing Science*, 30(2), 189–195.
- Chun-fa, L., Yun-fen, J., Yong, L., Ping-guo, J., & Hua-ping, N. (2010). Adsorption-ex traction mechanism of heavy rare earth by Cyanex272-P507 impregnated resin. *Transactions of the Nonferrous Metals Society of China*, 20, 1511–1516.
- Costis, S., Mueller Kristin, K., Blais, J. F., Lavallée, A. R., Coudert, L., & Neculita, C. M. (2019). *Review of recent work on recovery of rare earths from secondary sources*. Final Report No. R1859; Natural Resources Canada, Ottawa, ISBN: 978–2–89146-926-5, July 2019.
- Dai, S., & Finkelman, R. B. (2018). Coal as a promising source of critical elements: Progress and future prospects. *International Journal of Coal Geology*, 186, 155–164.
- Dai, S., Zhao, L., Hower, J. C., Johnston, M. N., Song, W., Wang, P., & Zhang, S. (2014). Petrology, mineralogy, and chemistry of size-fractioned fly ash from the Jungar power plant, Inner Mongolia, China, with emphasis on the distribution of rare earth elements. *Energy and Fuels*, 28(2), 1502–1514.
- Dai, S. F., Ren, D. Y., & Li, S. S. (2002). Occurrence and sequential chemical extraction of rare earth elements in coals and seam roofs. *Journal of China University of Mining and Technology*, 31, 349–353.
- Ding, Y., Harvey, D., & Wang, N. H. L. (2020). Two-zone ligand-assisted displacement chromatography for producing high-purity praseodymium, neodymium, and dysprosium with high yield and high productivity from crude mixtures derived from waste magnets. *Green Chemistry*, 22(12). <https://doi.org/10.1039/d0gc00495b>.
- EC. (2014). European Commission 2014. Critical raw materials for the EU. Report of the ad hoc working group on defining critical raw materials European Commission, p 41.
- Evans, K. (2016). The history, challenges, and new developments in the management and use of bauxite residue. *Journal of Sustainable Metallurgy*, 2, 316–331.
- Ferron, C. J., & Henry, P. (2015). A review of the recycling of rare earth metals. *Canadian Metallurgical Quarterly*, 54(4), 388–394. <https://doi.org/10.1179/1879139515Y.0000000023>.
- Franus, W., Wiatros-Motyka, M. M., & Wdowin, M. (2015). Coal fly ash as a resource for rare earth elements. *Environmental Science and Pollution Research International*, 22(12), 9464–9474. <https://doi.org/10.1007/s11356-015-4111-9>.
- GéoMégA. (2016). *Resources Inc. Developing Rare Earths in Québec and Canada*, PDAC.
- Geoscience Australia. (2013). *Geoscience Australia review of critical metals*. Retrieved 8th September, 2020, from <https://www.ga.gov.au/about/projects/resources/critical-minerals>
- Gergoric, M., Ekberg, C., Foreman, M. R. S. J., Steenari, B. M., & Retegan, T. (2017). Characterization and leaching of neodymium magnet waste and solvent extraction of the rare-earth elements using TODGA. *Journal of Sustainable Metallurgy*, 3, 638–645.
- Gijbels, K., Pontikes, Y., Lacobescu, R. I., Schreurs, S., Schroyers, W., & Kuppens, T. (2017). Techno-economic and environmental analysis of alkali activated materials containing phosphogypsum and blast furnace slag. Sustainability assessments for the low-carbon

- economy, Interdisciplinary PhD expert course for young researchers, Hasselt, Belgium, 30/05–1/06/2017.
- Guyonnet, D., Lefebvre, G., & Menad, N. (2018). *Rare earth elements and high tech products*. Retrieved 16 September 2020, from https://www.cec4europe.eu/wp-content/uploads/2018/09/Chapter_3_3_Guyonnet_et_al_Rare_earth_elements_and_high_tech_products.pdf
- Han, K. N. (2020). Characteristics of precipitation of rare earth elements with various precipitants. *Minerals*, 10(2), 178. <https://doi.org/10.3390/min10020178>.
- Haque, N., Hughes, A., Lim, S., & Vernon, C. (2014). Rare earth elements: overview of mining, mineralogy, uses, sustainability and environmental impact. *Resources*, 3, 614–635. <https://doi.org/10.3390/resources30406140>.
- Hayes, S. M., & McCullough, E. A. (2018). Critical minerals: A review of elemental trends in comprehensive criticality studies. *Resources Policy*, 59, 192–199. <https://doi.org/10.1016/j.resourpol.2018.06.015>.
- Helaly, O. S., Abd El-Ghany, M., Moustafaa, I., Abuzaidn, H., & Ismail, M. (2012). Extraction of cerium(IV) using tributyl phosphate impregnated resin from nitric acid medium. *Transactions of the Nonferrous Metals Society of China*, 22, 206–214.
- Hood, M. M., Targgart, R. K., Smith, R. C., Hsu-Kim, H., Henke, K. R., Graham, U., Groppo, J. G., Unrine, J. M., & Hower, J. C. (2017). Rare earth element distribution in fly ash derived from the Fire Clay coal, Kentucky. *Coal Combust Gasificat Products*, 9, 22–33.
- Hower, J. C., Dai, S., Seredin, V. V., Zhao, L., Kostova, I. J., Silva, L. F. O., Mardon, S. M., & Gurdal, G. (2013). A note on the occurrence of yttrium and rare earth elements in coal combustion products. *Coal Combustion and Gasification Products*, 5, 39–47.
- Hower, J. C., Groppo, J. G., Henke, K. R., Graham, U. M., Hood, M. M., Joshi, P., & Preda, D. V. (2017). Pondered and land filled fly ash as a source of rare earth elements from a Kentucky power plant. *Coal Combustion and Gasification Products*, 9, 1–21. <https://doi.org/10.4177/CCGPD-17-00003.1>.
- Hower, J. C., Qian, D., Briot, N. J., Henke, K. R., Hood, M. M., Taggart, R. K., & Hsu-Kim, H. (2018). Rare earth element associations in the Kentucky State University stoker ash. *International Journal of Coal Geology*, 189, 75–82.
- Hower, J. C., Ruppert, L. F., & Eble, C. F. (1999). Lanthanide, yttrium, and zirconium anomalies in the Fire Clay coal bed, Eastern Kentucky. *International Journal of Coal Geology*, 39(1–3), 141–153.
- Hu, Y., Florek, J., Larivie're, D., Fontaine, F., & Kleitz, F. (2018). Recent advances in the separation of rare earth elements using mesoporous hybrid materials. *The Chemical Record*, 18, 1261–1276.
- Huang, C., Wang, Y., Huang, B., Dong, Y., & Sun, X. (2019). The recovery of rare earth elements from coal combustion products by ionic liquids. *Minerals Engineering*, 130, 142–147.
- Jaroni, M. S., Friedrich, B., & Letmathe, P. (2019). Economical feasibility of rare earth mining outside China. *Minerals*, 9, 576. <https://doi.org/10.3390/min9100576>.
- Jayne, K., Carr, D. R., Rowan, J., & Kimble, M. C. (2019). *Rare earth element extraction from coal fly ash*. United States. Retrieved 15 June 2020, from <https://www.osti.gov/biblio/1491487-rare-earth-element-extraction-from-coal-fly-ash>
- Jelinek, L., Wei, Y., Arai, T., & Kumagai, M. (2007). Selective Eu(III) electro-reduction and subsequent separation of Eu(II) from rare earths(III) via HDEHP impregnated resin. *Solvent Extraction and Ion Exchange*, 25(4), 503–513. <https://doi.org/10.1080/07366290701415911>.
- Jha, M. K., Kumari, A., Panda, R., Kumar, J. R., Yoo, K., & Lee, J. Y. (2016). Review on hydrometallurgical recovery of rare earth metals. *Hydrometallurgy*, 161, 77–101.
- Jin, H., Park, D. M., Gupta, M., Brewer, A. W., Ho, L., Singer, S. L., Bourcier, W. L., Woods, S., Reed, D. W., Lammers, L. N., Sutherland, J. W., & Yiao, Y. (2017). Techno-economic assessment for integrating biosorption into rare earth recovery process. *ACS Sustainable Chemistry & Engineering*, 5, 10148–10155.
- Jordens, A., Cheng, Y. P., & Waters, K. E. (2013). A review of the beneficiation of rare earth element bearing minerals. *Minerals Engineering*, 41, 97–114. <https://doi.org/10.1016/j.mineng.2012.10.017>.

- Joshi, P. B., Preda, D. V., Skyler, D. A., Tsinberg, A., Green, B. D., & Marinelli, W. J. (2013). *Recovery of rare earth elements and compounds from coal ash*. U.S. Patent 20130287653A1.
- Jowitt, S. M., Werner, T. T., Weng, Z., & Mudd, G. M. (2018). Recycling and secondary sources of the rare earth elements. In *28th Goldschmidt Conference, Boston, 12–17 August 2018*.
- Jyothi, R. K., Thenepalli, T., Ahn, J. W., Parhi, P. K., Chung, K. W., & Lee, J. Y. (2020). Review of rare earth elements recovery from secondary resources for clean energy technologies: Grand opportunities to create wealth from waste. *Journal of Cleaner Production*, 267, 122048.
- Kashiwakura, S., Kumagai, Y., Kubo, H., & Wagatsuma, K. (2013). Dissolution of rare earth elements from coal fly ash particles in a Dilute H₂SO₄ solvent. *Open Journal of Physical Chemistry*, 3, 69–75.
- Khalidun, I., Buchari, B., Amran, M.B., & Sulaeman, A. (2008). Separation of Sm(III) and Gd(III) using solvent-impregnated resin containing di-(2-ethylhexyl) phosphoric acid (D2EHPA) and tributylphosphate (TBP). In *Proceeding of The International Seminar on Chemistry 2008, 79–82, Jatinangor, 30–31 October 2008*.
- King, J. F., Taggart, R. K., Smith, R. C., Hower, J. C., & Hsu-Kim, H. (2018). Aqueous acid and alkaline extraction of rare earth elements from coal combustion ash. *International Journal of Coal Geology*, 195, 75–83.
- Koltun, P., & Tharumarajah, A. (2014). Life cycle impact of rare earth elements. *ISRN Metallurgy*, 2014, 1–10. <https://doi.org/10.1155/2014/907536>.
- Krishnamurthy, N., & Gupta, C. K. (2016). *Extractive metallurgy of rare earths (II Edition)*. CRC Press, Taylor & Francis Group. ISBN 9780367267575.
- Krishnamurthy, P. (2020). Rare metal (RM) and Rare earth element (REE) resources: World scenario with special reference to India. *Journal of the Geological Society of India*, 95, 465–474. <https://doi.org/10.1007/s12594-020-1463-7>.
- KT. (2015). K-Technologies Inc. Texas Rare Earth Resources Corp. Form 10-K, Annual Report Pursuant to Section 13 or 15(d) of the Securities Exchange Act of 1936, for the Fiscal Year Ended August 31, 2015.
- Lanzerstorfer, C. (2018). Pre-processing of coal combustion fly ash by classification for enrichment of rare earth elements. *Energy Reports*, 4, 660–663.
- Lee, J. C. K., & Wen, Z. (2017). Rare earths from mines to metals: Comparing environmental impacts from China's main production pathways. *Journal of Industrial Ecology*, 21(5), 1277–1290.
- Leenheer, J., & Malcolm, R. (1973). *Preparative free-flow electrophoresis as a method of fractionation of natural organic materials*, Geological Survey Water-Supply Paper 1817- D 1973.
- Li, Y., Tian, C., Liu, W., Xu, S., Xu, Y., Cui, R., & Lin, Z. (2018). Carbon cloth supported nano-Mg(OH)₂ for the enrichment and recovery of rare earth element Eu(III) from aqueous solution. *Frontiers in Chemistry*, 6, 118. <https://doi.org/10.3389/fchem.2018.00118>.
- Lin, R., Howard, B. H., Roth, E. A., Bank TL, Granite, E. J., & Soong, Y. (2017). Enrichment of rare earth elements from coal and coal by-products by physical separations. *Fuel*, 200, 506–520.
- Liu, P., Huang, R., & Tang, Y. (2019). Comprehensive Understandings of Rare Earth Element (REE) speciation in coal fly ashes and implication for REE extractability. *Environmental Science & Technology*, 53, 5369–5377.
- Lucas, J., Lucas, P., Mercier, T. L., Rollat, A., & Davenport, W. (2015). Rare earths science. *Technology, Production and Use*, Elsevier. <https://doi.org/10.1016/B978-0-444-62735-3.09992-7>.
- Ma, Z., Zhang, S., Zhang, H., & Cheng, F. (2019). Novel extraction of valuable metals from circulating fluidized bed derived high-alumina fly ash by acid-alkali-based alternate method. *Journal of Cleaner Production*, 230, 302–313. <https://doi.org/10.1016/j.jclepro.2019.05.113>.
- Mardon, S. M., & Hower, J. C. (2004). Impact of coal properties on coal combustion by-product quality: examples from a Kentucky power plant. *International Journal of Coal Geology*, 59(3–4), 153–169.
- Massari, S., & Ruberti, M. (2013). Rare earth elements as critical raw materials: Focus on International markets and future strategies. *Resources Policy*, 38, 36–43.

- Mishra, S. (2020). Comprehensive outlook for liquid-liquid extraction of rare earths (Chapter 7). In A. A. Abhilash (Ed.), *Critical and rare earth elements* (p. 165). NY: International Standard Book Number-13: 978-0-367-08647-3: CRC Press.
- Mondal, S., Ghar, A., Satpati, A. K., Sinharoy, P., Singh, D. K., Sharma, J. N., Sreenivas, T., & Kain, V. (2019). Recovery of rare earth elements from coal fly ash using TEHDGA impregnated resin. *Hydrometallurgy*, 185, 93–101.
- Montross, N., Verba, C., Chan, H. L., & Lopano, C. (2018). Advanced characterization of rare earth element minerals in coal utilization byproducts using multimodal image analysis. *International Journal of Coal Geology*. <https://doi.org/10.1016/j.coal.2018.06.018>.
- Mowafy, E. A., & Mohamed, D. (2017). Extraction of rare earth elements from nitrate solution using novel unsymmetrical diglycolamide. *Separation Science and Technology*, 52(6), 1006–1014.
- Muravyov, M. I., Bulaev, A. G., Melamud, V. S., & Kondrat'eva, T. F. (2015). Leaching of rare earth elements from coal ashes using acidophilic chemolithotrophic microbial communities. *Microbiology*, 84(2), 194–201.
- Mutlu, B. K., Cantoni, B., Turolla, A., Antonelli, M., Hsu-Kim, H., & Wiesner, M. R. (2018). Application of nanofiltration for rare earth elements recovery from coal fly ash leachate: Performance and cost evaluation. *Chemical Engineering Journal*, 349, 309–317.
- NETL. (2018). *Rare earth elements from coal and coal by-products*. National Energy Technology Laboratory. Retrieved 9 October 2018, from <https://www.netl.doe.gov/research/coal/rare-earth-elements>
- NRC. (2008). *National Research Council: Minerals, critical minerals, and the U.S. Economy* (p. 58). Washington, DC: National Academies Press.
- NRCAN. (2018). Retrieved 5 October, 2020, from <https://www.nrcan.gc.ca/our-natural-resources/minerals-mining/minerals-metals-facts/rare-earth-elements-facts/20522>
- ORNL. (2015). Oak Ridge National Laboratory, Critical Materials Institute. *Rare-earth recycling invention licensed to U.S. Rare Earths*. Retrieved 12 June 2020, from <https://www.ornl.gov/news/critical-materials-institute-rare-earth-recycling-inventionlicensed-us-rare-earths>
- Pan, J., Nie, T., Vaziri Hassas, B., Rezaee, M., Wen, Z., & Zhou, C. (2020). Recovery of rare earth elements from coal fly ash by integrated physical separation and acid leaching. *Chemosphere*, 248, 126112. <https://doi.org/10.1016/j.chemosphere.2020.126112>.
- Park, S., & Liang, W. (2019). Bioleaching of trace elements and rare earth elements from coal fly ash. *International Journal of Coal Science & Technology*, 6(1), 74–83.
- Peelman, S., Kooijman, D., Sietsma, J., & Yang, Y. (2018). Hydrometallurgical recovery of rare earth elements from mine tailings and WEEE. *Journal of Sustainable Metallurgy*, 4, 367–377.
- Peiravi, M., Ackah, L., Guru, R., Mohanty, M., Liu, J., Xu, B., Zhu, X., & Chen, L. (2017). Chemical extraction of rare earth elements from coal ash. *Mining, Metallurgy & Exploration*, 34, 170–177. <https://doi.org/10.19150/mmp.7856>.
- Peramaki, S. (2014). *Method development for determination and recovery of REE from industrial fly ash*. Research Report No. 178, Dept. of Chemistry, University of Jyväskylä, Finland. ISBN 978-951-39-6001-8.
- Peterson R, Heinrichs M, Giler J, Lanes A, & Taha, R. (2017). Recovery of REE from coal ash with recycling acid leach process. In *World Coal Ash (WOCA) Conference, KY, 9–11 May 2017*.
- Pietrelli, L., Bellomo, B., Fontana, D., & Montoreali, M. R. (2002). Rare earths recovery from NiMH spent batteries. *Hydrometallurgy*, 66, 135–139.
- Ponou, J., Dodbiba, G., Anh, J. W., & Fujita, T. (2016). Selective recovery of rare earth elements from aqueous solution obtained from coal power plant ash. *Journal of Environmental Chemical Engineering*, 4(4), 3761–3766.
- Roosen, J., & Binnemans, K. (2014). Adsorption and chromatographic separation of rare earths with EDTA-and DTPA-functionalized chitosan biopolymers. *Journal of Materials Chemistry A*, 2, 1530–1540.
- Royen, H., & Fortkamp, U. (2016). *Rare earth elements: purification, separation and recycling*. Stockholm, Sweden: IVL Swedish Environmental Research Institute. Report number C 211 ISBN 978-91-88319-12-8.

- Rozelle, P., Khadilkar, A. B., Pulati, N., Soundarajan, N., Klima, M. S., Mosser, M. M., Miller, C. E., & Pisupati, S. V. (2016). A Study on removal of rare earth elements from U.S. coal byproducts by ion exchange. *Metallurgical and Materials Transactions E*, 3(1), 6–17.
- Sahoo, P. K., Kim, K., Powell, M. A., & Equeenuddin, S. M. (2016). Recovery of metals and other beneficial products from coal fly ash: A sustainable approach for fly ash management. *International Journal of Coal Science & Technology*, 3(3), 267–283.
- Scott, C., & Kolker, A. (2019). *Rare earth elements in coal and coal fly ash: U.S. Geological Survey Fact Sheet No. 2019–3048*, Sept. 2019., 4p. <https://doi.org/10.3133/fs20193048>.
- Serajuddin Md (2018). Precipitation of rare earths from the leachate of a coal fly ash. In *International Seminar on Mineral Processing Technology 2018 (MPT 2018)*, Indian Institute of Mineral Engineers (IIME), IIT Dhanbad, Jharkhand, 10–12 October 2018.
- Seredin, V. V., & Dai, S. (2012). Coal deposits as potential alternative sources for lanthanides and yttrium. *International Journal of Coal Geology*, 94, 67–93. <https://doi.org/10.1016/j.coal.2011.11.001>.
- Seredin, V. V., Dai, S., Sun, Y., & Chekryzhov, I. Y. (2013). Coal deposits as promising sources of rare metals for alternative power and energy efficient technologies. *Applied Geochemistry*, 31, 1–11.
- Shibata, J., Matsumoto, S., & Yamamoto. (2000). A novel separation technology for a heavy rare earth residue using a solvent impregnated resin. *Solvent Extraction Research and Development Japan*, 7, 167–175.
- Shu, Q., Khayambashi, A., Wang, X., & Wei, Y. (2018). Studies on adsorption of rare earth elements from nitric acid solution with macroporous silica-based bis(2-ethylhexyl)phosphoric acid impregnated polymeric adsorbent. *Adsorption Science & Technology*, 36(3–4), 1049–1065. <https://doi.org/10.1177/0263617417748112>.
- Silva, R. G., Morais, C. A., & Oliveria, E. D. (2019a). Selective cerium removal by thermal treatment of mixed rare earth oxalates or carbonates obtained from non-purified rare earth sulphate liquor. *Minerals Engineering*, 139(105865), 1–15. <https://doi.org/10.1016/j.mineng.2019.105865>.
- Silva, R. G., Morais, C. A., Teixeira, L. V., & Oliveira, E. D. (2019b). Selective precipitation of high-quality rare earth oxalates or carbonates from a purified sulfuric liquor containing soluble impurities. *Mining, Metallurgy & Exploration*, 36, 967–977.
- Sinclair, L. K., Baek, D. L., Thompson, J., Tester, J. W., & Fox, R. V. (2017). Rare earth element extraction from pretreated bastnäsite in supercritical carbon dioxide. *Journal of Supercritical Fluids*, 124, 20–29.
- Smith, R. C., Taggart, R. K., Hower, J. C., Wiesner, M. R., & Hsu-Kim, H. (2019). Selective recovery of rare earth elements from coal fly ash leachates using liquid membrane processes. *Environmental Science & Technology*, 53(8), 4490–4499. <https://doi.org/10.1021/acs.est.9b00539>.
- Smolka-Danielowsjka, D. (2010). Rare earth elements in fly ashes created during the coal burning process in certain coal-fired power plants operating in Poland—Upper Silesian Industrial Region. *Journal of Environmental Radioactivity*, 101, 965–968.
- Stuckman, M. Y., Lopano, C. L., & Granite, E. J. (2018). Distribution and speciation of rare earth elements in coal combustion byproducts via synchrotron microscopy and spectroscopy. *International Journal of Coal Geology*, 195, 125–138.
- Taggart, R. K., Hower, J. C., Dwyer, G. S., & Hsu-Kim, H. (2016). Trends in the rare earth element content of U.S.-based coal combustion fly ashes. *Environmental Science and Technology*, 50(11), 5919–5926. <https://doi.org/10.1021/acs.est.6b00085>.
- Taggart, R. K., Hower, J. C., & Hsu-Kim, H. (2018). Effects of roasting additives and leaching parameters on the extraction of rare earth elements from coal fly ash. *International Journal of Coal Geology*, 196, 106–114. <https://doi.org/10.1016/j.coal.2018.06.021>.
- Tang, M., Zhou, C., Pan, J., Zhang, N., Liu, C., Cao, S., Hua, T., & Ji, W. (2019). Study on extraction of rare earth elements from coal fly ash through alkali fusion—Acid leaching. *Minerals Engineering*, 136, 36–42.

- Thakur, N. V. (2000). Separation of rare earths by solvent extraction. *Mineral Processing and Extractive Metallurgy Review*, 21(1–5), 277–306. <https://doi.org/10.1080/08827500008914171>.
- Thrivani, T., Jegal, Y., & Ahn, J. W. (2015). Characteristic studies of yttrium extracted from coal ash, South Korea. In *Recent advances on energy, environment, ecosystems, and development* (pp. 20–25). ISBN: 978:1–61804–291-0.
- USDoE. (2011). US Department of Energy, Critical materials strategy, Dec 2011.
- USEPA. (2012). United States Environmental Protection Agency, Rare earth elements: A review of production, processing, recycling and associated environmental issues.
- USGS. (2019). *USGS Fact Sheet 2019–3048, September 2019. Rare earth elements in coal and coal fly ash*. <https://doi.org/10.3133/fs20193048>.
- USGS. (2020). U.S. Geological Survey, Mineral Commodity summaries, January 2020. <https://pubs.usgs.gov/periodicals/mcs2020/mcs2020-rare-earths.pdf>
- Vahidi, E., & Zhao, F. (2017). Environmental life cycle assessment on the separation of rare earth oxides through solvent extraction. *Journal of Environmental Management*, 203(Pt 1), 255–263.
- Vaisanen A, Valkonen J, Peramaki S, Jyvaskyla FI, Soikkeli V (2013) Method for processing ash, particular fly ash. International Publication number WO 628 2013/079804A1.
- Van Gosen, B. S., Verplanck, P. L., Seal, R. R., Long, K. R., & Joseph, G. (2017). Rare earth elements. In K. J. Schulz, D. Y. JH Jr., R. R. Seal, & D. C. Bradley (Eds.), *Critical mineral resources of United States – Economic and environmental geology and prospects for future supply, USGS Professional Paper 1802* (pp. 1–31).
- Vind, J., Malfliet, A., Blanpain, B., Tsakiridis, P. E., Tkaczyk, A. H., Vassiliadou, V., & Panias, D. (2018). Rare earth element phases in bauxite residue. *Minerals*, 8(77), 1–32. <https://doi.org/10.3390/min8020077>.
- Virolainen, S., Repo, E., & Sainio, T. (2019). Recovering rare earth elements from phosphogypsum using a resin-in-leach process: Selection of resin, leaching agent, and eluent. *Hydrometallurgy*, 189(105125), 1–9.
- Wall, F., Rollat, A., & Pell, R. S. (2017). Responsible sourcing of critical metals. *Elements*, 13, 313–318.
- Wang, K., Adidharma, H., Radosz, M., Wan, P., Xu, X., Russell, C. K., Tian, H., Fan, M., & Yu, J. (2017). Recovery of rare earth elements with ionic liquids. *Green Chemistry*, 19, 4469–4493.
- Wang, Z., Dai, S., Zou, J., French, D., & Graham, I. T. (2019). Rare earth elements and yttrium in coal ash from the Luzhou power plant in Sichuan, Southwest China: Concentration, characterization and optimized extraction. *International Journal of Coal Geology*, 203, 1–14.
- Weng, Z., Haque, N., Mudd, G. M., & Jowitt, S. M. (2016). Assessing the energy requirements and global warming potential of the production of rare earth elements. *Journal of Cleaner Production*, 139, 1282–1297.
- Xie, F., Zhang, T. A., Dreisinger, D., & Doyle, F. (2014). A critical review on solvent extraction of rare earths from aqueous solutions. *Minerals Engineering*, 56, 10–28.
- Yaftian, M. R., Burgard, M., Dieleman, C. B., & Matt, D. (1998). Rare-earth metal-ion separation using a supported liquid membrane mediated by a narrow rim phosphorylated calixarene. *Journal of Membrane Science*, 144(1), 57–64.
- Yang, J. H., Cui, Y., Sun, G. X., Nie, Y., & Xia, G. M. (2013). Extraction of Sm(III) and Nd(III) with N,N,N',N'-tetrabutyl-3-oxy-diglycolamide from hydrochloric acid. *Journal of the Serbian Chemical Society*, 78(1), 93–100.
- Zaimes, G. G., Hubler, B. J., Wang, S., & Khanna, V. (2015). Environmental life cycle perspective on rare earth oxide production. *ACS Sustainable Chemistry & Engineering, American Chemical Society*, 3(2), 237–244.
- Zepf, V. (2013). Rare earth elements: What and where they are. In *Rare earth elements* (pp. 11–39). Berlin, Heidelberg., Springer Theses (Recognizing Outstanding Ph.D. Research): Springer. https://doi.org/10.1007/978-3-642-35458-8_2.
- Zhang, W., Groppo, J., & Honaker, R. (2015b). Ash beneficiation for REE recovery. In: *2015 World of Coal Ash (WOCA) Conference, Nashville, TN, USA, 5–7 May 2015*.

- Zhang, W., & Honaker, R. (2019). *Low cost selective precipitation circuit for recovery of rare earth elements from acid leachate of coal ash waste*. US Patent 2019/0136344 A1.
- Zhang, W., Noble, A., Yang, X., & Honaker, R. (2020). A comprehensive review of rare earth elements recovery from coal-related materials. *Minerals*, 10, 451.
- Zhang, W., Rezaee, M., Bhagavatula, A., Li, Y., Groppo, J., & Honaker, R. (2015a). A review of the occurrence and promising recovery methods of rare earth elements from coal and coal by-products. *International Journal of Coal Preparation and Utilization*, 35, 295–330.

Chapter 18

Coal Burn Ash: A Sustainable Future Resource for Critical Metals Production



Manis Kumar Jha, Archana Kumari, Rekha Panda, Rukshana Parween, Sanchita Chakravarty, and Rajesh Kumar Jyothi

18.1 Introduction

Natural resources are indispensable to this contemporary world and when they are susceptible to disturbed production, they are termed as critical materials. Country's monopoly in raw material supply or availability in politically conflicted zones are main reasons for their supply risk. Rare earth metals (REMs) is an example of Critical Raw Materials which are crucial strategic resources, more copious than precious metals, but their inimitable geochemical properties hold back to form economically feasible ore deposits (Binnemans et al. 2018). The unique, magnetic, luminescent, and electrochemical properties of REMs have made constant expansion in the field of technologies, defense as well as green energy sectors, thus augmented the requirement of REMs globally. Additionally, the exhausted situation of primary resources, lack of proper substitutes, and China's supremacy in universal REMs production have resulted in shortage of REMs globally (Tang et al. 2019; Kumari et al. 2018). The supply of REMs is mainly influenced by economic affairs and political situations due to their abnormal distribution in a few countries (Itoh et al. 2009). These factors have primarily boosted a level of concern for invariable availability of REMs and hence innovative REMs containing materials are being surveyed to guarantee satisfactory REMs requirement for upcoming use (Kumari et al. 2020; Blissett et al. 2014). As far as the REMs recuperation from their primary sources is concerned, they are reported to be complex in nature and adversely affect

M. K. Jha (✉) · A. Kumari · R. Panda · R. Parween · S. Chakravarty
Metal Extraction and Recycling Division, CSIR-National Metallurgical Laboratory,
Jamshedpur, Jharkhand, India
e-mail: mkjha@nmlindia.org

R. K. Jyothi
Convergence Research Center for Development of Mineral Resources (DMR), Korea Institute
of Geoscience and Mineral Resources (KIGAM), Daejeon, Republic of Korea

the environmental. Consequently, unconventional sources of REMs are gaining more attention, and some selected for REMs recovery include obsolete magnets, fluorescent lamps, waste catalyst, batteries, industrial process residue (red mud, steel plant slag, coal and coal ash, etc.), and municipal solid waste. Expansion of processes for REMs recuperation from alternative resources has become the thrust area owing to the fundamental part they contribute in a variety of sustainable technological applications. The low consumption of energy and cost highlights the quality of hydrometallurgical processes for the selective separation and recuperation of REMs from alternative sources (Rao et al. 2020; Kolker et al. 2017).

There are abundant alternative sources of REMs and among all options, coal combustion product, i.e., coal ash, is of immense importance because of the existence of significant quantity of REMs in it. Coal is a conventional, dependable, secure as well as a major resource for energy or a fuel intended for the generation of power in different sections of the world. Steel industries also utilize noteworthy quantity of coal during their manufacturing (Kumari et al. 2019a; Dai and Finkelman 2018). Accordingly, consumption of coal is incessantly rising that has increased the generation and disposal of enormous quantity of coal ash annually. However, maximum amount of coal ash are discharged as waste (Franus et al. 2015). These coal combustion products are reported to be earth's principal industrial waste, usually utilized (~25%) as an imperative constituent of reinforced concrete. Although some of the coal combustion products hold REMs, they are not processed consistently owing to their small REMs content and concerns related to the financial feasibility of extraction process. Worldwide, rare earth contents in natural coal are found to be 68.5 ppm and in its fly ash about 404 ppm. REMs concentration is reported to be larger (454 LREE $\mu\text{g/g}$) in fine particles (size $<25 \mu\text{m}$) of fly ash than the rough particles ($>25 \mu\text{m}$ fraction) which is found to be 156 $\mu\text{g/g}$ (Lin et al. 2017; Li et al. 2017).

REMs concentration in coal is investigated to be equivalent or more than that available naturally (Seredin and Finkelman 2008). In coal combustion product, concentration of REMs is investigated to fluctuate between 270 and 1480 ppm. This discrepancy in REMs concentration might be owing to inappropriate system of collecting samples, variation in coal geochemistry, or different analytical procedure being used. Thus, coal by-product can be an excellent preference for REMs recuperation as it contains light as well as heavy REMs (Kumari et al. 2019a). However, lack of appropriate processing in controlled manner results in the loss of these valuable metals. This reason has emphasized several researchers worldwide to distinguish novel processes to guarantee sufficient recovery of REMs to be utilized in different field. Concerning above facts, research work has been done which indicates the subsistence of significant quantity of REMs in the coal combustion products, i.e., coal ash. Sometimes, REMs concentration in certain coal samples is investigated to be superior than that exists in natural resources (Seredin and Finkelman 2008). Thus, presence of REMs in coal ashes was inveterate; however they are not regularly treated because of minor quantity of REMs in it. Research work for REMs recuperation from coal and its by-products focusing on its analytical, geological, beneficiation performances, and its chemical studies have been discussed in the following.

18.1.1 Analytical Studies of Coal and Coal Combustion Products

Major studies related to coal and coal combustion products are being carried out focusing on coal geochemistry and the behavior of elements/minerals present in coal combustion product (Kumari et al. 2020). Partial research work is investigated for the recuperation of REMs, but the existence of comparatively higher quantity of REMs in coal and its combustion products (coal ash) than its natural resources, gathered interest to examine the extraction scenario of REMs (Lin et al. 2017). It was observed that few laboratory-level research work were done to guarantee the possibility for recuperation of REMs. Analytical studies to notice the availability of REMs in naturally occurring resources were mainly carried out. The principal investigation of this analytical studies includes coal geochemistry, its distribution and mineralogy as well as variation in organic structure. Collection of coal fly ash samples was done in different regions of Europe showing significant REMs availability in coal ash of UK region and thus can be targeted to exploit on commercial scale (Blissett et al. 2014). Ion microprobe was used to verify REMs allocation as well as its division in various types of coal combustion products (Kolker et al. 2017). The quantity of REMs present in coal-ash sample of Powder River Basin was analyzed using Laser-induced breakdown spectroscopy (Phuoc et al. 2016). Researcher studied variety of coal seams of Talcher coalfield to observe the division of mineral species in them and alteration of their phases at different temperatures (Banerjee et al. 2016). REMs analysis of Appalachian coal was carried out quantitatively presenting the association of coal with organic matter (Lin et al. 2017). Lignite coal combustion product generated after power production was found to hold REMs, metalloids, and some strategic metals (Kermer et al. 2017).

18.1.2 Beneficiation of Coal and its by-Products to Get REMs Enriched Concentrate

REMs containing coal and its by-products are tremendously fine and are found to be interlocked with the host particles, thus require grinding to release the encapsulated REMs. This increases the operating cost of the process. As a result, physical beneficiation without size reduction produces only high-grade feedstock without any viable output. However, research work has been done to enrich the concentrate of REMs in a variety of coal and its combustion products; researchers performed decarbonization to clean coal followed by physical beneficiation studies. Gravity separation, magnetic separation, froth floatation, etc. techniques were used to enhance the concentration of REMs in coal and its refuse. It was observed that gravity separation enables enrichment up to a factor of 1.1. Separation based on size, density, and magnetic properties enriches the REMs containing coal concentrate by a ratio of 1.21, and these physical separations were reported to be unsatisfactory

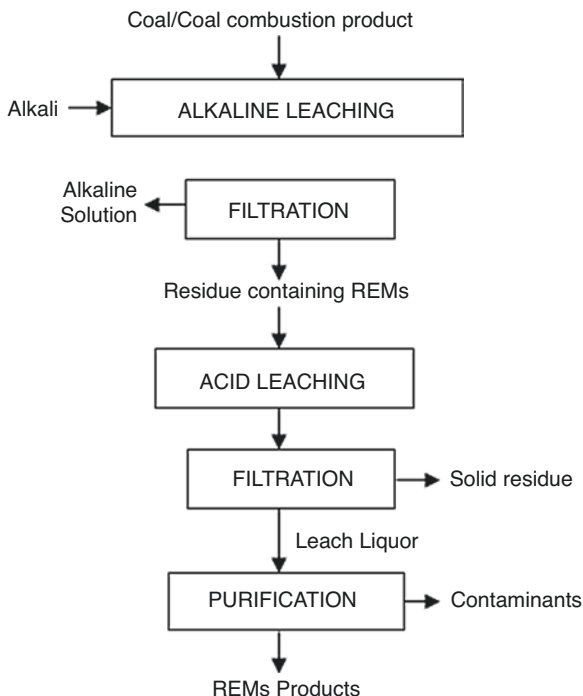
(Zhang et al. 2020). Surface hydrophobicity of particles were also used to separate the particles of REMs mainly available in decarbonized thickener underflows generated from coal-producing plants via froth flotation technique. Involvement of conventional flotation cells as well as column flotation using oleic acid as collector is reported, which require manifold treatment stages. Apart from this, hydrophobic–hydrophilic separation process was also reported where agglomeration of hydrophobic particles takes place using hydrocarbon oils, thus enhancing the recovery of micron-size particles along with dewatered product. Enrichment ratio was calculated to be 53:1. Although REMs separations are possible but are not economically feasible (Gupta et al. 2016).

18.1.3 Pretreatment of Coal and its Combustion Products to Improve REMs Leachability

Prior to REMs leaching from coal and its combustion products, researchers reported thermal and alkaline treatments to enhance the leaching efficiency of REMs. The pessimistic aspect of including alkali treatment is the cost of chemicals used as well as dissolution of alkalis used which contaminate the REMs and hinders the purification process. Necessity for investigation involving the increase of REMs leaching using diluted or weak alkalis is under process (Kuppusamy et al. 2019; Zhang et al. 2020).

Calcination or roasting is another scenario used to enhance REMs leaching efficiency during treatment of coal and its ashes. The organic matter of the coal material helped to maintain the temperature required during calcination and thus reduces the energy cost. Currently, studies were carried out showing that calcination followed by acid leaching is the best approach to recuperate REMs from coal and its by-products. However, feasibility test and some fundamental issues are essential to be resolved before validation. Figures 18.1 and 18.2 show the utilization of alkali pretreatment and thermal pretreatment both followed by acid leaching process to extort REMs from coal and its combustion products (Kuppusamy et al. 2019; Honaker et al. 2019). A flow sheet was proposed for treating coal fly ash of the Songzao coalfield to attain instantaneous extraction of REMs, Gallium (Ga) and Niobium (Nb). In this process, leaching of Ga and Al from the roasted product was carried out using water, whereas REMs remained in the solid residue, which was later recovered via acid leaching (Fig. 18.3) (Liu et al. 2015).

Fig. 18.1 Flow-sheet showing the use of alkali treatment before acid leaching. (Adapted from Kuppusamy et al. 2019)

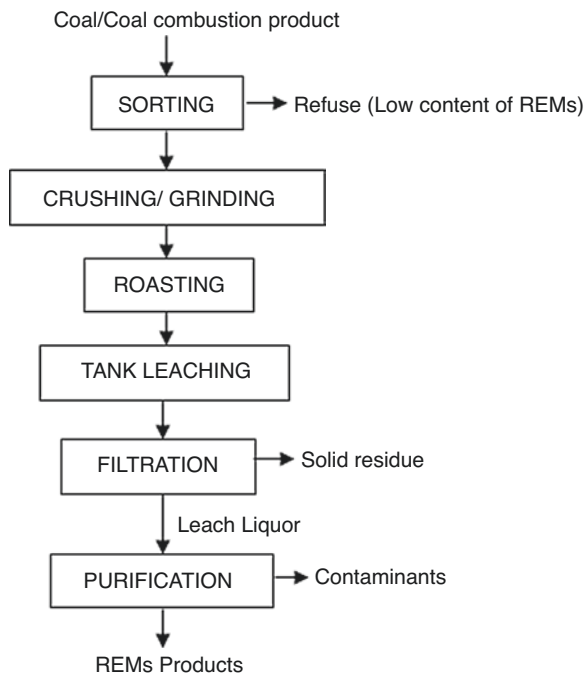


18.1.4 Acid Leaching of Coal and its Combustion Products to Extract REMs

Low concentration acid solutions show effective extraction of REMs from few coal sources. Using 0.5 M H_2SO_4 about 90% REMs recovery from lignite coal was observed due to complexation of REMs with organic acids in lignite coal, which get destroyed under acidic condition (Laudal et al. 2018). Using HNO_3 at 75 °C, 83% and 30% REMs were extracted from decarbonized Fire Clay middlings and decarbonized thickener underflow, respectively. It is reported that REMs extraction from middlings consumes lots of energy, thus it is not considered economically feasible (Huang et al. 2018). Apart from acid, salts are also reported to be used for REMs extraction from coal with unsatisfactory results and was concluded that salt leaching depends upon nature of the coal treated. Thus, alkaline and thermal treatment is essential prior to coal leaching to extract REMs using acid and salt leaching for high-grade coal. However, leaching performance of direct acid and salt in low-grade coal is quite satisfactory (Zhang et al. 2020).

Leaching of coal ash (fly ash or bottom ash) in acidic medium shows adequate recovery, and lots of work has been reported. Environmental Research and Educational Foundation developed a route to treat coal fly ash and recover REMs using a close loop leaching process was also investigated for REMs recuperation from coal ash (Taggart 2015; Peterson et al. 2017). Laboratory level experiments

Fig. 18.2 Process flow showing the use of thermal treatment before acid leaching. (Adapted from Honaker et al. 2019)



were performed to pretreat coal fly ash hydrothermally using NaOH and further subjected to acid (HCl) dissolution in order to view the leaching behavior of REMs present in coal fly ash. High temperature HNO_3 as well as H_2SO_4 leaching was also carried out, and in all three cases, more than 90% REMs get dissolved (Roth et al. 2017; Peiravi et al. 2017; Kashiwakura et al. 2013). Fly ash of the Powder River Basin was treated for REMs extraction and found that ~70% of total REMs present gets dissolved using 15 M HNO_3 at elevated temperature (Taggart et al. 2016). Investigation for complete extraction (~100%) of REMs from coal fly ash using 12 M HCl solution was done and observed that ~71% REMs gets extracted using much lower acid concentration of 1 M HCl (Zhang et al. 2020). Leaching efficiency of REMs from fluidized bed combustion bottom ash has also been studied and 2 M HCl at 80 °C was able to extract ~62% Y, 55% Nd and 65% Dy (Tuan et al. 2019). All mineral acids were used for REMs extraction from coal and its combustion products. HNO_3 and HCl show much better leaching efficiency compared to H_2SO_4 . But using HNO_3 is not recommend due to NO_x generation, and H_2SO_4 provide poor dissolution as huge quantity of calcium present in the coal sample which form complex with the sulfate resulting in loss of REMs. Thus, studies made till date prefer HCl for REMs leaching from coal and coal ashes.

Literature review allied to coal disclosed that insignificant contribution was made for REMs extraction/separation and recuperation. The intricate coal composition, presence of minor amount of REMs with heterogeneous distribution, and restrictions for REMs beneficiation procedure might be the reasons behind this

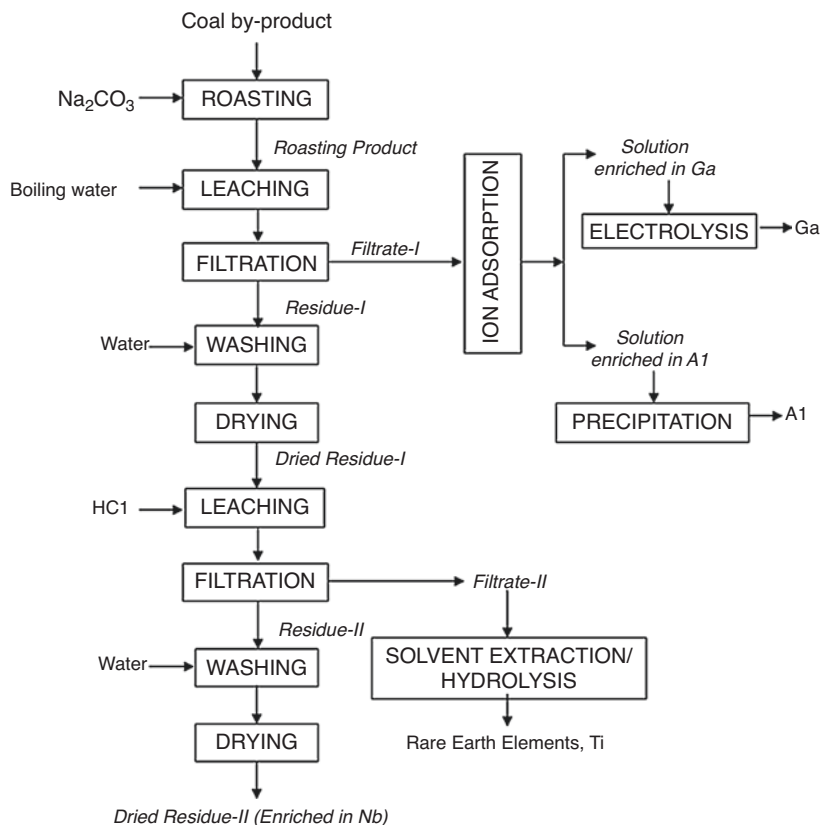


Fig. 18.3 Recovery of REMs from coal fly ash using alkali roasting. (Adapted from Liu et al. 2015)

negligence. Thus, deficiency of viable extraction of REMs from coal/coal ash still exist. As far as condition of REMs processing from coal combustion product in India is concerned, it must be noted that although more than 100 million tons of coal fly ash is generated in India, barely any consideration was made toward REMs inspection in coal ash (Kumari et al. 2019a). Hence, expansion of a viable route to recuperate REMs from coal/coal ash is accentuated. In view of this approach, studies were carried out primarily by CSIR-NML, India, to recover REMs from coal combustion product of Indian origin utilizing hydrometallurgical methods. Compared to other research work carried out earlier, present investigation reports systematic scientific research to separate and recuperate REMs from coal bottom ash of Indian origin.

18.2 Characterization and Distribution of REMs in Coal/Coal Ash

Investigation to calculate the quantity of REMs in coal and its combustion product is of utmost importance before processing in a feasible manner. Previously exhaustive literature review has been done by the author, and the amount of REMs found in different coal regions worldwide is presented in Table 18.1 (Kumari et al. 2019b).

The analysis of the Indian coal of eastern region revealed the presence of REMs. Based on its REMs contents, experiments were carried out to convert coal into its by-product. In order to prepare coal bottom ash obtained from thermal industry, the coal sample was initially crushed up to size in range 10–20 mm, in order to homogenize it and finally milled to decrease its particle size further. Lastly, the milled sample of coal of size 212 μ was burned at elevated temperature (450 °C) for 8 h to convert it into bottom ash. To calculate REMs content in the prepared coal bottom ash, the sample was chemically analyzed, and the result is presented in Table 18.2.

A total of 1036 g per ton of REMs is found in the sample prepared in CSIR-NML, Jamshedpur, which was further processed to extract REMs in a viable manner.

Table 18.1 Presence of REMs in coal ash in different parts of the world (Adapted from Kumari et al. 2019b)

Sl. no.	Origin of coal sample	Amount of REMs (ppm)
1.	ReckTron International Ltd.	2.43
2.	Electrical Power Company, Soma City, Fukushima Prefecture, Tohoku, Japan	2.8
3.	Sichuan Basin Deposit, China	4.0
4.	Coal Preparation Plant, Kentucky, USA	4.0
5.	Coal Power Plant, Ohio, USA	4.25
6.	Heshan Deposit, China	4.5
7.	Rakovka Deposit, Russia	5.0
8.	Fusui Deposit, China	5.0
9.	Coal Mine in NW of Spain	5.7 \pm 0.2
10.	Songzao Deposit, China	5.85
11.	Pavlovka Deposit, Russia	9.42
12.	Nazar-Ailok Deposit, Russia	10.16
13.	Yakhlinsk Deposit, Russia	15
14.	Rettikhovka Deposit, Russia	31

Table 18.2 Content of REMs in Indian coal bottom ash

REMs	La	Ce	Nd	Pr	Sm	Gd	Eu	Tb	Dy	Er	Lu	Ho	Yb	Y	Sc
g/ton	157	278	167	45	41	40	5.6	3.4	28	17	26	04	9.6	156	58

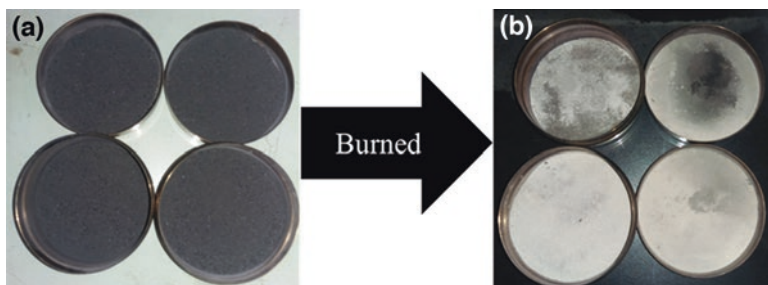


Fig. 18.4 (a) Indian coal, (b) coal bottom ash prepared

18.3 Extraction of REMs from Coal Bottom ash at CSIR-NML, Jamshedpur, India

Extraction of REMs from coal by-products was mainly reported using super-critical extraction and bioleaching methods but were not commercially viable. Thus, chemical leaching was opted for the study of REMs recovery from bottom ash. Coal bottom ash was prepared in the laboratory (Fig. 18.4) by burning coal at 450 °C for 8 h, and the same was used for the experimental purpose.

As far as drawback of chemical leaching is concerned, consumption of acid and its disposal is a major issue. To cope up with this, extraction of acid was also carried out to be re-used in an environmentally friendly manner. For poor and developing countries like India, use of acid to process tons of residue being generated is usually suggested. Thus, selection of cost-effective and feasible leachant as well as optimization of different process parameters is necessary for efficient leaching of REMs. Leaching of homogenized coal bottom ash was carried out in acidic medium in a three-mouthed glass reactor connected with a reflux condenser to avert loss of solution via evaporation. Coal bottom ash was further mixed with different leachants and heated using hot plate to get maximum dissolution of REMs. Stirring facility was provided which overlook the mass transfer effect on bottom ash leaching during the experiment, and sampling was done at different intervals of time. Once suitable leachant based on its efficiency toward leaching of metals was selected, different parameters like effect of temperature, leaching time, acid concentration, and solid-to-liquid ratio on REMs leaching performance were noticed. Initially, few sets of experiments were carried out to observe the performance of three mineral acids (nitric acid (HNO_3), hydrochloric acid (HCl) and sulfuric acid (H_2SO_4)) as well as a salt, ferric chloride (FeCl_3) in order to select best leachant for further sets of experiments.

It was observed that leaching coal bottom ash in diluted HCl for 2 h at 75 °C and solid-to-liquid ratio 100 g/L was observed to be appropriate for leaching most of the REMs present in coal ash sample. FeCl_3 was also found effective for heavy REMs, but HCl was preferred considering maximum REMs into the solution. The use of HNO_3 is not recommended owing to the generation of NO_x and effluent containing hazardous nitrate ions. Consequently, dilute HCl solution was used to carry out

further experiments. Major deviation in REMs dissolution was observed while using different leachant because of acid characteristics and existence of different other metals as impurity. To find out the definite need of leachant for maximum dissolution of REMs, studies were made varying concentration of selected leachant. Different sets of experiments were performed varying the amount of HCl used from 1 to 5 M. All sets of experiment were carried out for 120 min at temperature more than 70 °C maintaining solid-to-liquid ratio 100 g/L. Leaching efficiency of REMs was observed to be increased with HCl concentration from 1 to 4 M. This was because of the augmented flux of H⁺ ions across the boundaries of bottom ash particles. However, insignificant changes were noticed for REMs leaching on increasing the amount of acid further. Therefore, HCl concentration of 4 M was measured to be appropriate for maximum leaching of REMs from coal bottom ash. Various experimental sets were also arranged to observe the effect of leaching temperatures (ranging from 25 to 90 °C) maintaining HCl concentration 4 M and solid-to-liquid ratio 100 g/L for 120 min. Dissolution of REMs were found to increase with the increase in leaching temperature. Since aqueous medium was used for carrying out experiments, temperature beyond 90 °C is not suggested. Thus, 90 °C temperature was optimized for REMs dissolution. Similarly, effect of time was also studied and found that percentage dissolution of REMs increases up to 120 min. No remarkable changes in REMs dissolution were observed beyond 120 min. At last to limit the size of leaching reactor and find out the need of less leachant volume, the optimization of pulp density was carried out. 5, 10, and 15 g of coal bottom ash were put into 100 mL of 4 M HCl solution, maintaining a temperature of 90 °C and time of 120 min. Decrease in leaching percentage of REMs was observed with increase in solid-to-liquid ratio which might be owing to the insufficient availability of H⁺ for the reaction between the solid and liquid. Thus, 50 g/L solid-to-liquid ratio was selected for suitable leaching of REMs. Residues left after performing each experiment were dried and analyzed. Adequate material balance was observed with an utmost divergence of $\pm 2\%$ for all sets of experiment.

Leaching studies of coal bottom ash carried out revealed that most of the light REMs like La, Ce, and Nd were leached. After carrying out the leaching experiments, amount of acid present in the leach liquor gathered attention, which was essential to be reduced for selective precipitation of REMs. This was achieved using alkali. However, to diminish the use of alkali, liquid–liquid extraction procedure was performed to extort acid from the leached solution. It was observed that 70% TEHA diluted in kerosene was able to extract about 48% of HCl in 30 min of contact time and phase ratio 2:1 in single stage. Increase in the extraction stages can achieve total extraction of acid from the liquor. Afterward, hot deionized water was used to strip off acid efficiently from the loaded TEHA. The acid extracted from the liquor can be reutilized for dissolution of REMs, and the solution devoid of acid (containing rare earths and other metals) was subjected to precipitation method.

18.4 Final Product

After extracting acid from the liquor, it was further put to precipitation study. 35% pure ammonia solution ($\text{NH}_3(\text{aq})$) was used to upgrade REMs concentration in the solution for its easy recovery. Various sets of precipitation were carried out, and it was noticed that the precipitate of REMs was obtained at pH ~ 1.6 while other metal impurities were separated at different pHs. After attaining the required pH, the solution was allowed to settle for few hours and filtered. Distilled water was used to wash the obtained precipitate and was further dried out in oven maintaining 80 °C temperature for 120 min. The obtained salts of mixed REMs were found to attain extremely pure REMs content. Evolution of NH_4Cl fume during precipitation will be scrubbed, when experiments will be practiced in scale-up/pilot level. Liquor left after REMs precipitation was found to contain iron (Fe) in large amount. This Fe-containing liquor can be further treated to recover Fe as marketable product. The entire process developed at CSIR-NML is an optimization study for application-oriented research work.

Different solutions obtained during the entire research work were analyzed to calculate the amount of REMs present. Inductively Coupled Plasma-Optical Emission Spectrometer (ICP-OES)—Axial mode made by Thermo Fischer Scientific in USA (Model No. iCAP Duo 7600) was used to measure the REMs content. pH meter made by Metrohm, Switzerland (Model: 797 Basic titrino), was used to measure pH of the solution.

In view of environment, proper treatment or utilization of residues/effluent left after chemical processing is very crucial. After carrying out experiments of coal bottom ash to leach out REMs, the residues left was chemically analyzed. Minor amount of Fe with some other metals are present in it, which can be treated to recover valuable elements or used as a vital constituent of reinforced concrete. Finally, Toxicity Characterization Leaching Procedure test (TCLP) of the left-out residue will be done before its disposal. To the extent that effluent treatment of this developed process is concerned, acid content of liquor was reduced via extraction and the extracted acid could be reutilized. As far as the amount of ammonia in the liquor left after REMs precipitation is concerned, simple scrubbing procedure will be used to scrub off ammonia to be used again.

18.5 Conclusions

From the studies carried out to extract REMs from coal ash and after extensive literature search and experimental work carried out at CSIR-NML, India, the following conclusions have been made:

- Generation of coal ashes affects the environment due to its toxic contents, lack of proper disposal system, and its utilization.

- Coal ash has future potential to be adopted as a sustainable alternative resource for REMs extraction.
- Hydrometallurgical processing of coal ash to produce REMs will sustain as beneficial in view of economics and environment.

References

- Banerjee, A., Mishra, P. R., Mohanty, A., Chakravarty, K., Biswas, R. D., Sahu, R., & Chakravarty, S. (2016). Distribution of mineral species in different coal seams of Talcher coalfield and its transformation behavior at varying temperatures. *International Journal of Coal Science & Technology*, 3(2), 97–103.
- Binnemans, K., Jones, P. T., Muller, T., & Yurramendi, L. (2018). Rare earths and the balance problem: How to deal with changing markets? *Journal of Sustainable Metallurgy*, 4, 126–146.
- Blissett, R. S., Smalley, N., & Rowson, N. A. (2014). An investigation into six coal fly ashes from the United Kingdom and Poland to evaluate rare earth elements content. *Fuel*, 119, 236–239.
- Dai, S., & Finkelman, R. B. (2018). Coal as a promising source of critical elements: Progress and future prospects. *International Journal of Coal Geology*, 186(1), 155–164.
- Franus, W., Wiatros-Motyka, M. M., & Wdowin, M. (2015). Coal fly ash as a resource for rare earth elements. *Environmental Science & Pollution Research*, 22, 9464–9474.
- Gupta, N., Li, B., Luttrell, G., Yoon, R. H., Bratton, R., & Reyher, J. (2016). Hydrophobic-hydrophilic separation (HHS) process for the recovery and dewatering of ultrafine coal. In Proceedings of the 2016 SME Annual Conference and Expo, Phoenix, AZ, USA, 21–24 February 2016; pp. 706–709.
- Honaker, R. Q., Zhang, W., Werner, J., Noble, A., Luttrell, G. H., & Yoon, R. H. (2019). Enhancement of a process flowsheet for recovering and concentrating critical materials from bituminous coal sources. *Mining, Metallurgy & Exploration*, 37(1).
- Huang, Q., Noble, A., Herbst, J., & Honaker, R. (2018). Liberation and release of rare earth minerals from Middle Kittanning, Fire Clay, and West Kentucky No. 13 coal sources. *Powder Technology*, 332, 242–252.
- Itoh, M., Miura, K., & Machida, K. (2009). Novel rare earth recovery process on Nd-Fe-B magnet scrap by selective chlorination using NH_4Cl . *Journal of Alloy and Compound*, 477, 484–487.
- Kashiwakura, S., Kumagai, Y., Kubo, H., & Wagatsuma, K. (2013). Dissolution of rare earth elements from coal fly ash particles in a dilute H_2SO_4 solvent. *Open Journal of Physical Chemistry*, 3, 69–75.
- Kermer, R., Hedrich, S., Bellenberg, S., Brett, B., Schrader, D., Schonherr, P., Kopcke, M., Siewert, K., Gunther, N., Gehrke, T., Sand, W., Rauchle, K., Bertau, M., Heide, G., Weitkamper, L., Wotruba, H., Ludwig, H. M., Partusch, R., Schippers, A., Reichel, S., Glombitza, F., & Janneck, E. (2017). Light ash: Waste material or potential resource-investigation of metal recovery and utilization options. *Hydrometallurgy*, 168, 141–152.
- Kolker, A., Scott, C., Hower, J. C., Vazquez, J. A., Lopano, C. L., & Shifeng, D. (2017). Distribution of rare earth elements in coal combustion fly ash, determined by SHRIMP-RG ion microprobe. *International Journal of Coal Geology*, 184, 1–10.
- Kumari, A., Jha, M. K., Chakravarty, S., & Pathak, D. D. (2020). Indian coal ash: a potential alternative resource for rare earth metals (REMs). In: Rare Metal Technology 2020, The Minerals, Metals & Materials Society 2020, pp. 265–273.
- Kumari, A., Jha, M. K., & Pathak, D. D. (2018). Review on the processes for the recovery of rare earth metals (REMs) from secondary resources. In: Rare Metal Technology 2018, The Minerals, Metals & Materials Series, The Minerals, Metals & Materials Society 2018, pp. 53–65.

- Kumari, A., Jha, M. K., Pathak, D. D., Chakravarty, S., & Lee, J. C. (2019b). Processes developed for the separation of europium (Eu) from various resources. *Separation & Purification Reviews*, 48(2), 91–121.
- Kumari, A., Parween, R., Chakravarty, S., Parmar, K., Pathak, D. D., Lee, J. C., & Jha, M. K. (2019a). Novel approach to recover rare earth metals (REMs) from Indian coal bottom ash. *Hydrometallurgy*, 187, 1–7.
- Kuppusamy, V. K., Kumar, A., & Holuszko, M. (2019). Simultaneous extraction of clean coal and rare earth elements from coal tailings using alkali-acid leaching process. *Journal of Energy Resources Technology, Transactions of the ASME*, 141(7), 070708.
- Laudal, D. A., Benson, S. A., Addleman, R. S., & Palo, D. (2018). Leaching behavior of rare earth elements in Fort Union lignite coals of North America. *International Journal of Coal Geology*, 191, 112–124.
- Li, J., Zhuang, X., Querol, X., Font, O., & Moreno, N. (2017). A review on the applications of coal combustion products in China. *International Geology Review*, 60, 671–716.
- Lin, R., Howard, B. H., Roth, E. A., Bank, T. L., Granite, E. J., & Soong, Y. (2017). Enrichment of rare earth elements from coal and coal by-products by physical separation. *Fuel*, 200, 506–520.
- Liu, H., Tian, H., & Zou, J. (2015). Combined extraction of rare metals Ga-Nb-REE from fly ash. *Science & Technology Review*, 33, 39–43.
- Peiravi, M., Ackah, L., Guru, R., Mohanty, M., & Liu, J. (2017). Chemical extraction of rare earth elements from coal ash. *Minerals and Metallurgical Processing*, 34(4), 170–177.
- Peterson, R., Heinrichs, M., Glier, J., Lane, A., & Taha, R. (2017). Recovery of rare earth elements from coal ash with a recycling acid leach process. In Proceed. World of Coal Ash Conference, Lexington.
- Phuoc, T. X., Wang, P., & McIntyre, D. (2016). Detection of rare earth elements in powder river basin sub-bituminous coal ash using laser-induced breakdown spectroscopy (LIBS). *Fuel*, 163, 129–132.
- Rao, K. A., Serajuddin, M., RamaDevi, G., Thakurta, S. G., & Sreenivas, T. (2020). On the characterization and leaching of rare earths from a coal fly ash of Indian origin. *Separation Science and Technology*. <https://doi.org/10.1080/01496395.2020.1718705>.
- Roth, E., Macala, M., Lin, R., Bank, T., Thompson, R., Howard, B., Soong, Y., & Granite, E. (2017). Distributions and extraction of rare earth elements from coal and coal by-products, World of Coal Ash (WOCA) Conference, Lexington, KY.
- Seredin, V., & Finkelman, R. B. (2008). Metalliferous coals: A review of the main genetic and geochemical types. *International Journal of Coal Geology*, 76, 253–289.
- Taggart, R. (2015). Recovering rare earth metals from coal fly ash. In Proceed. World of Coal Ash Conference, Lexington.
- Taggart, R. K., Hower, J. C., Dwyer, G. S., & Hsu-Kim, H. (2016). Trends in the rare earth element content of U.S.-based coal combustion fly ashes. *Environmental Science & Technology*, 50, 5919–5926.
- Tang, M., Zhou, C., Pan, J., Liu, N. Z. C., Cao, S., Hu, T., & Ji, W. (2019). Study on extraction of rare earth elements from coal fly ash through alkali fusion—Acid leaching. *Minerals Engineering*, 136, 36–42.
- Tuan, L. Q., Thenepalli, T., Chilakala, R., Vu, H. H. T., Ahn, J. W., & Kim, J. (2019). Leaching characteristics of low concentration rare earth elements in Korean (Samcheok) CFBC bottom ash samples. *Sustainability*, 11, 2562.
- Zhang, W., Noble, A., Yang, X., & Honaker, R. (2020). A comprehensive review of rare earth elements recovery from coal-related materials. *Minerals*, 10(451), 1–28.

Chapter 19

Characterization and Utilization of Coal Ash for Synthesis of Building Materials



**Shaswat Kumar Das, Subhabrata Mishra, Debadutta Das,
Syed Mohammed Mustakim, Cyriaque Rodrigue Kaze,
and Pankaj Kumar Parhi**

19.1 Introduction

Coal is considered as one of the most significant sources of global energy at present, and it is being consumed widely all through the world for production of electricity. It was estimated that at present, as per the World Coal Association reports, the total share of the coal in global energy consumption is 38% (WCA 2019), a graphical representation of the global energy shares in reference with the sources is presented in Fig. 19.1. Regardless of the progress made on the renewable sources of energy in the energy sectors, the portion of coal will be 24% of the total number by 2035 (Bhatt et al. 2019).

It is reported that around 15–18.75 tons of coal is required to produce 1 megawatt of electricity, which also produces 4.3–11 tons of FA and BA (Jayaranjan et al. 2014; Asokan et al. 2005). As a result, a huge amount of coal ashes will be

S. K. Das (✉) · S. Mishra

Grøn Tek Concrete and Research (GTCR), Bhubaneswar, Odisha, India

CSIR – Institute of Minerals and Materials Technology (IMMT), Bhubaneswar, Odisha, India
e-mail: shsawatdas_sce@gcekjr.ac.in

D. Das

Department of Chemistry, Sukanti Degree College, Subarnapur, Odisha, India

S. M. Mustakim

CSIR – Institute of Minerals and Materials Technology (IMMT), Bhubaneswar, Odisha, India

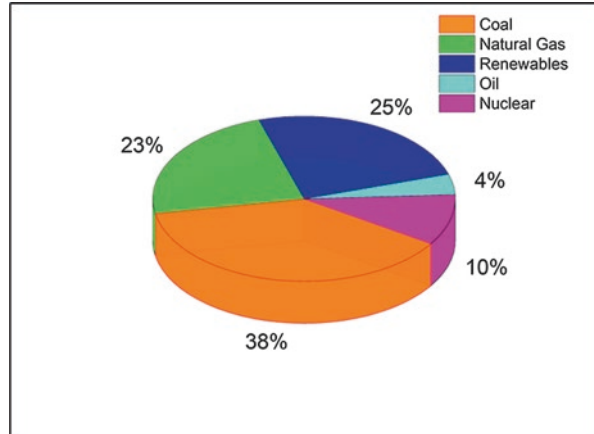
C. R. Kaze

Laboratory of Applied Inorganic Chemistry, Faculty of Science, University of Yaoundé I,
Yaoundé, Cameroon

P. K. Parhi

Department of Chemistry, Fakir Mohan (F.M.) University, Vyasa Vihar,
Balsore, Odisha, India

Fig. 19.1 Global energy share for the year 2019
(Data source: WCA 2019)



generated worldwide in these coming years that have the potential to contaminate both air and water (Pattanaik et al. 2019). On the contrary, construction sector is one of the major consumers of natural resources and hence it impacts the environment adversely. Therefore, several scientific investigations were made (Blissett and Rowson 2012; Queralt et al. 1997; Wang et al. 2016; Kim 2015; Jaturapitakkul and Cheerarot 2003), and also many technologies were commercialized using coal ashes as different components in building materials. Hence this chapter discusses the characteristics and utilization of coal ashes in building material synthesis. Extensive discussion has been provided on the usages of coal ash in cement composite, alkali-activated concrete, bricks/blocks, and asphalt concrete. The critical analysis has also been made on the challenges and opportunities of coal ashes in building material production to widen its practical applicability.

19.2 Coal Ash

During the combustion of coals in thermal power plants, a residual mass generates, the quantity of generation of this residue depends upon the ash content of the coal, and this residue is called coal ash (Das et al. 2019) or coal combustion residuals (CCRs). A schematic diagram has been provided in Fig. 19.2 detailing the generation of these coal ashes. The major classification of these ashes are fly ash (FA) and bottom ash (BA). This classification was done considering several parameters of the generated ash, for instance, the FA is the lighter one with very fine particles, whereas the BA is relatively heavier with large particles. The FA is extensively used in civil engineering applications, especially in cement concretes as a supplementary cementitious material (SCM) due to its good pozzolanic properties (Deschner et al. 2012). However, the BA does not possess required properties to be used as SCM in cement composites, hence most of the previous work has been conducted taking BA

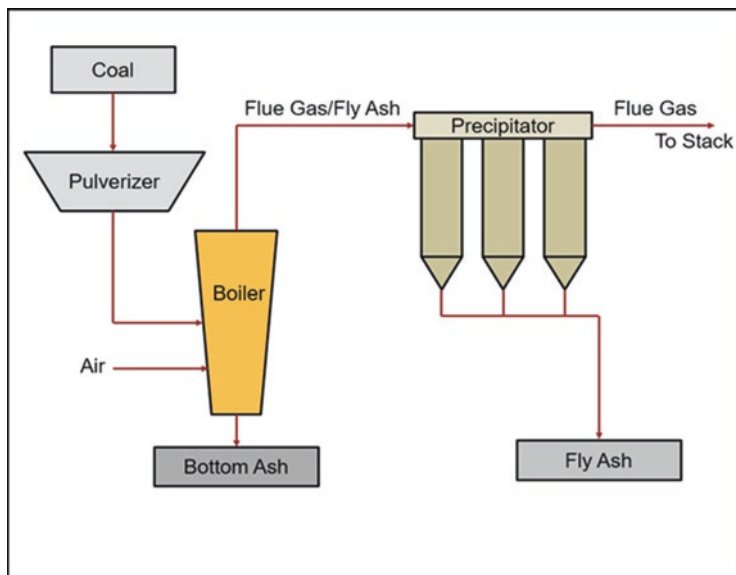


Fig. 19.2 Schematic flow chart of coal ash generation

as an alternative one to fine aggregates (Sand of river) in concrete (Singh and Siddique 2016; Andrade et al. 2009).

19.3 Physical and Chemical Properties

The physical properties of the coal ashes (both FA and BA) depend on many aspects; however, the major factors are coal grade, type and quantity of rock detritus existing inside the fissures of the coal seams, degree of pulverization before firing, the coal firing temperature, and so on. The primary distinctions in properties of both the FA and BA are discussed below taking several earlier conducted studies on the same in a more generalized approach.

19.3.1 Specific Gravity

The Specific gravity of the coal ashes depends on the chemical constituents of the ash, mostly on the iron and calcium content. In a study, it is mentioned that if the iron content of the ash is above 10%, then the value of the specific gravity will be directly proportional to the iron percentage; however if the lime content is more than 25%, the value of the specific gravity will be more irrespective to the iron

percentage (Singh and Siddique 2013). In general, the specific gravity of coal ashes lies close to 2.0; however, it can range from 1.6 to 3.1 depending upon several factors such as chemical composition (iron and calcium content), particle size, and porosity.

19.3.2 Particle Size Distribution

Particle size distribution of coal ashes plays a vital role in providing the initial rough approximations of its essential material properties such as permeability, reactivity, and specific surface area as well as its utility for different applications. For instance, a fine material with high reactivity is suitable for cement replacement, whereas a coarser material with less reactivity is more suitable for replacement of fine aggregates (natural river sand) in cement concrete. In general, the particles of FA are very fine and mostly fall under 400 μm , whereas the BA has coarser particles which could range from 1 to 2000 μm . Besides, the particle size distribution of both the ashes could vary from the abovementioned numbers depending upon several factors such as degree of pulverization of coal, firing temperature, and extent of combustion. A study conducted taking FA and BA from a thermal power plant situated at Ropar, Punjab, India (Kumar et al. 2014) where it was observed that the FA has very fine particle size gradation as compared to BA. It was found that 80% of the total FA particles are under 90 μm , whereas only 13.5% of the total BA particle fraction falls under 90 μm .

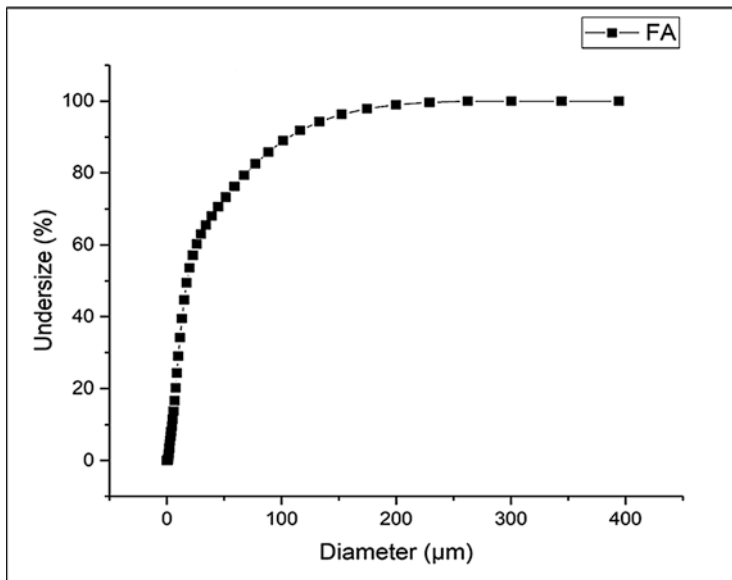


Fig. 19.3 Particle size distribution of FA from NTPC, Kaniha, Talcher, India

Figure 19.3 represents the detail distribution of particle size for FA obtained from a power plant of National Thermal Power Corporation (NTPC), Govt. of India, situated at Kaniha, Talcher, Odisha, India. The FA obtained from the NTPC had a median and mean particle size of 17.71 and 39.17 μm , respectively, whereas the d_{10} , d_{50} , and d_{90} of the same FA was 4.60, 17.71, and 106.68 μm , respectively. From the result, it can be concluded that the FA has very fine particles, whereas the BA has coarser grains in comparison.

19.3.2.1 Chemical Composition

Coal ashes are very complex to analyse, the heterogeneous composition with highly variable mineralogy provoke a major issues in concern with mineralogical characterization aspect and so as the usages of these ashes. For instance, it is found that at about 316 and 188 minerals/mineral groups was detected with coals and coal ashes, respectively (Vassilev and Vassileva 2007). However, major chemical constituents in both the FA and BA are silica (SiO_2) and alumina (Al_2O_3) with small amount of calcium content (CaO). Furthermore, as per the American Society for Testing and Materials (ASTM), the FA is classified into two-category classification based on its chemical composition (ASTM C311/C311M-18 2018), and this classification of FA is accepted worldwide. Whereas, there is no specific classification for the BA has been done, such inequality to the BA in terms of classification could be due to its limited applicability and comparatively less utility as compared to the FA. As per the ASTM classification, the FA containing 50–70% (wt.%) of $\text{SiO}_2 + \text{Al}_2\text{O}_3 + \text{Fe}_2\text{O}$ are Class C and the FA that contains more than 70% (wt.%) of the abovementioned constituents are categorized as Class F kind. Generally, the Class F type FA contains very less amount of CaO and has no self-cementitious properties, whereas the Class F type FA contains more than 10% CaO and possesses some self-cementing properties. The Class F type FA is more reactive and has higher pozzolanic characteristics, thus mostly used in cement plants as a replacement to the clinkers. The use of Class F FA is also widely seen in concrete batching plants as a suitable alternative of Portland cement (PC) during production of ready-mix concrete (RMC). The chemical composition of the coal ashes is dependent on the grade and composition of coals. For instance, the burning of lignite or sub-bituminous coals results in high calcium content coal ashes, while anthracite and bituminous coal typically result in ashes with less CaO content (Bhatt et al. 2019). The chemical assays of coal ashes reported by different authors are tabulated in Table 19.1, and it can be noticed that the major proportion of the chemical constituents are silica and alumina as discussed earlier.

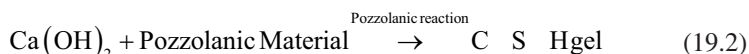
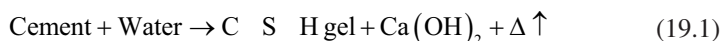
Table 19.1 Chemical assay of fly ash (FA) and bottom ash (BA)

Fly ash (FA)									
Authors	Composition								
	SiO ₂	Al ₂ O ₃	Fe ₂ O ₃	CaO	MgO	TiO ₂	Na ₂ O	K ₂ O	LOI
Sutcu et al. (2019)	50.97	27.20	4.11	10.56	1.82	1.54	0.30	0.99	0.51
Van Jaarsveld et al. (2002)	61.40	33.00	1.10	0.60	0.30	2.00	0.10	0.10	0.40
Das et al. (2020b)	60.34	30.83	3.34	0.80	0.05	1.87	0.08	1.26	NA
Palomo et al. (1999b)	53.20	26.00	7.95	3.57	0.97	1.38	0.29	2.59	2.22
Fernandez-Jimenez et al. (2007)	53.09	24.80	8.01	2.44	1.94	NA	0.73	3.78	3.59
Bottom ash (BA)									
Sutcu et al. (2019)	65.02	19.18	6.86	1.76	2.00	0.93	0.85	1.93	0.05
Jang et al. (2016)	44.20	31.50	8.90	2.00	2.60	NA	NA	NA	NA
Baite et al. (2016)	62.32	27.21	3.57	0.50	0.95	2.15	0.70	2.58	NA
Kim (2015)	45.74	25.33	6.86	0.99	1.25	3.03	0.70	3.71	12.6
Cherif et al. (1999)	56.00	26.70	5.80	0.80	0.60	1.30	0.20	2.60	4.6

NA Not available

19.3.2.2 Pozzolanic Characteristics

The pozzolanic property of any material is referred depending on the ability of material in order to react with lime and water by forming hydrated compounds similar to C-S-H gel (Thomas 2007). In general, when the pozzolanic materials are added to the cementitious composites, they react with the free lime (Ca(OH)₂) obtained from hydration of cement to produce a secondary form of calcium silicate hydrate (C-S-H) gel (see Eqs. 19.1 and 19.2). This reaction is called as pozzolanic reaction, and the materials which possess such properties are called pozzolanic materials. Interestingly, the pozzolanic materials does not have self-cementitious property; they only react in the presence of lime and water. The pozzolanic reactions are comparatively slower than the hydration of cement and hence the mechanical strength developments in pozzolan blended cements are quite slow and gradual. The pozzolanic reaction can be represented as follows:



Pozzolanic characteristics of the coal ashes are proportional to the aluminosilicate (Si and Al) material content, amount of reactive silica, and the ratio of Ca(OH)₂ to pozzolana. The pozzolanic reactivity of any material is being tested by the strength activity index method as referred by ASTM standard ASTM C 311 (ASTM C311/C311M-18 2018). The strength activity index test is generally conducted for ensuring whether the adopted FA results in a satisfactory standard of strength

development when blended in hydraulic cement of cement concrete. The BA shows very less pozzolanic activity due to large particle size and less reactivity. Hence the BA is mostly used as a replacement to sand in concrete and mortars. Moreover, some research works have been conducted to enhance the pozzolanic activity of the BA by applying mechanical activation method (pulverizing) (Cheriaf et al. 1999; Jaturapitakkul and Cheerarot 2003). The authors suggested that the pulverized BA can be used as a pozzolanic material in cementitious materials up to 20%; the increase in reactivity of the BA could be due to increase in specific surface area (SSA) imposed by mechanical grinding. The FA shows very good pozzolanic activity due to high reactivity, and it is being used widely in cement-based materials as an SCM.

19.3.3 Microstructural and Mineralogical Properties

The coal ashes are mostly composed of spherical particles both compact and hollow. The scanning electron microscope image of both FA and BA obtained from NTPC (Kaniha, Talcher, India) is provided in Figs. 19.4 and 19.5.

From the above figures, it can be observed that the microstructure of both the FA and BA is identical, and the same has been reported in several earlier studies (Cheriaf et al. 1999; Das et al. 2020b). It is also claimed in several occasions that the spherical shapes of these ashes help in achieving good workability performance of the blended concrete due to ball-bearing effect caused by these spherical-shaped grains (Mustakim et al. 2020). Though the FA and BA have similar microstructures in terms of morphology, but the FA founds to be significantly more reactive than BA due to its high amorphous mineralogy. A comparative microstructural investigation

Fig. 19.4 SEM micrograph of FA from NTPC, Kaniha, Talcher, India

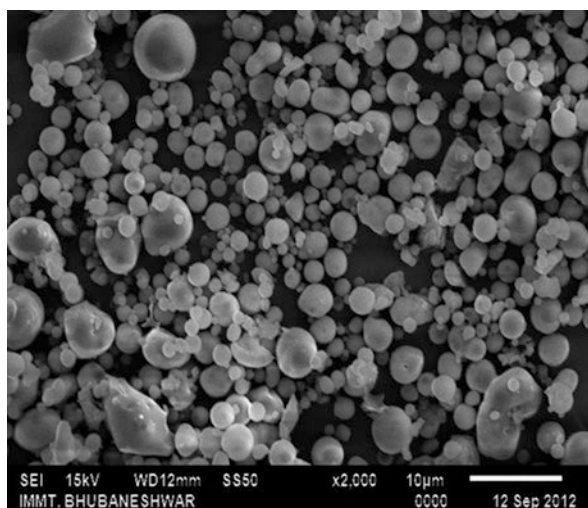


Fig. 19.5 SEM micrograph of BA from NTPC, Kaniha, Talcher, India

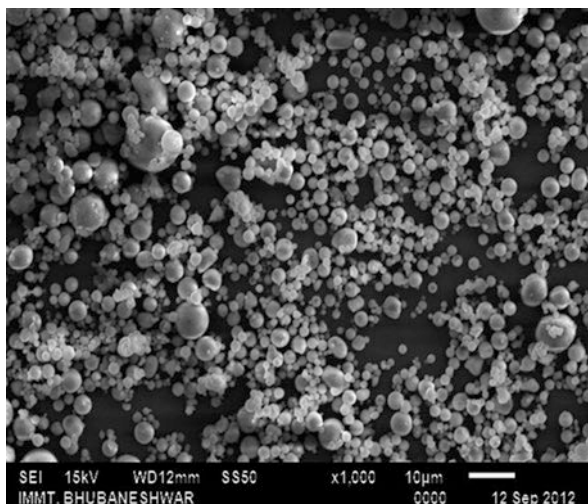
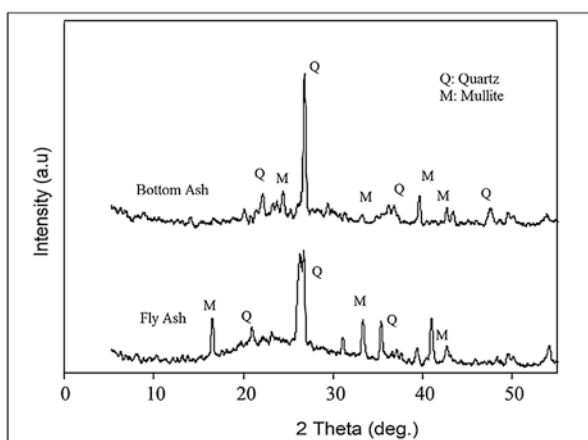


Fig. 19.6 Comparative X-ray diffractogram of FA and BA. (Adapted and reproduced from Chindaprasirt et al. 2009, with the permission)



conducted by Chindaprasirt et al. (2009) on FA and BA shows that the diffractogram (Fig. 19.6) of FA is comparatively more amorphous in nature, and thus possesses higher reactivity.

From the diffractogram it can be seen that in case of FA, there exist a broad hump in between 20 and 30° (2-theta position) revealing on the amorphous nature of the material. Whereas, in case of BA, the distinct peaks of quartz and mullite are found without any broad humps which specifies less reactivity. For more detailed investigation on the reactivity of FA, a detailed diffractogram of the FA obtained from NTPC (Kaniha, Talcher) is plotted in Fig. 19.7. The diffractogram of the FA shows same characteristics as obtained by Chindraprasirt et al.; however, in this case the amorphous hump located circa 15–25° (2-theta position).

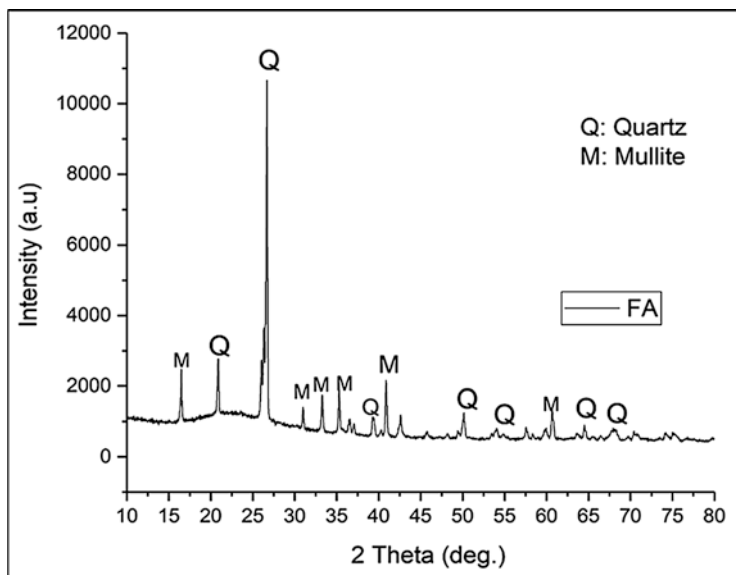
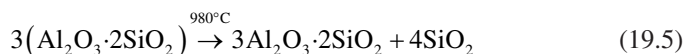
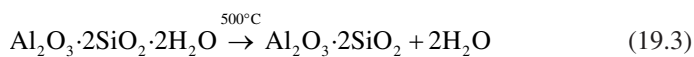


Fig. 19.7 X-ray diffractogram of FA from NTPC, Kaniha, Talcher, India

Analyzing the mineralogy, it is observed that the major components of coal ashes are quartz and mullite. Since quartz is naturally present in the coal and hence the occurrence of this phase in coal ashes is justified, but the presence of mullite does not found in coals. Therefore, it is assumed that the formation of mullite is caused by the thermal decomposition of naturally occurring kaolinite around 980 °C. The decomposition reactions for the kaolinite in FA is described by White and Case (White and Case 1990) and the same is represented as follows.



19.4 Utilization in Building Materials

19.4.1 Cement-Based Materials

Cement is one the most used material on the planet (Mishra et al. 2019), and its use is consistently raising due to the rapid urbanization and development of infrastructures. After looking close into the trend of production of cement, it can be seen that it is following a kind of geometric progression in an interval of each decade. By 1990, the global cement production was up to 1100 million tons, at present it is nearly 4370 million tons, and in 2030 the projection says it will be around 4830 million tons (Statista Research Department 2013). As the prime source of cement production is lime stone, huge amount of lime stone mining is done every year to meet the current demand. This mining activity is harshly damaging the ecosystem, and also the calcination of lime stone during cement production is causing severe environmental pollution by emitting CO₂ gas (Mishra et al. 2020). It is estimated that the carbon emission by the cement industries is around 7% of the total anthropogenic carbon discharge to the environment (Das et al. 2018). Meanwhile, both the FA and BA are considered solid waste that needs to be reused to minimize environmental pollution. These solid wastes can be reused in the cementitious materials as a replacement to cement or aggregates. These following sections summarized the utilization of FA and BA of cement and mortar as a supplement to cement/sand discussing their corresponding effect.

19.4.1.1 Fly Ash

Utilization of FA as an admixture in cement-based material has started and brought many possibilities to reuse it as a potential supplement of traditional construction of raw materials (viz. cement and sand). In 1995, Babu and Rao studied its efficiency in concrete to establish a relation between strength, water/cement ratio, age, and percentage of replacement (Ganesh Babu and Siva Nageswara Rao 1996). From their study, it was evidenced that with age the pozzolanic reaction of FA increases which increases the cementing efficiency. However, it depends on many physical and chemical characteristics like particle size, shape, and its distribution and chemical assay, glass or reactive content, respectively (Ganesh Babu and Siva Nageswara Rao 1996). In another study, Ravina (1997) used FA (Class F type) while replacing fine sand and then evaluated the properties of the fresh cement concrete. The FA mixed concrete achieved better workability as compared to the reference concrete. However, it consumed either the same or slightly higher water. It was further noticed that the FA mixed concrete required a higher setting time as compared to the reference concrete, which is caused owing to slow pozzolanic reaction. Later on, the ash handling division of NTPC Limited, India (NTPC Ash Utilization Division 2013), utilized FA as a mixer in cement for high-quality constructions, such as Delhi Metro Rail Corporation (DMRC) works and Bandra Worli Sea Link project. Different

proportions of FA were used to achieve the various grades of concrete, like M30, M35, or M60, as per the desired application. Also, they reported that the FA could be used as a supplement to the Portland cement (PC) in Ready Mixed Concrete (RMC) which can be utilized in housing and infrastructure projects. In a study, Cao et al. (Cao et al. 2008) investigated the Chinese FA, which was obtained from various powerplant of China, for further recovery of minerals like alumina (Al_2O_3) from it. The alumina value present in Chinese FA is more than 40% which is needed to recover. However, the study found that it has a lot of problems to recover alumina from the FA due to the complex technology that is available, hence for the time being it was limited in lab-scale study only. Furthermore, the study concluded that FA is a good option as a construction material to utilize in cement because of its good pozzolanic reactions.

Similarly, Nochaiya et al. used FA and silica fume (SF) as a replacement in PC and examined the workability, setting time, and compressive strength of the result concrete (Nochaiya et al. 2010). The obtained compressive strength of PC-FA-SF concrete was enhanced up to 145% as compared to PC-FA concrete. However, the workability of PC-FA-SF concrete remains similar to the control concrete mixture. Higher compressive strength of the PC-FA-SF concrete was achieved because of the pozzolanic reaction and filler effect of the SF and FA in the concrete mixtures. The use of FA along with SF in PC increases the strength of concrete which shows a better option to utilize both the by-products, i.e., FA and SF. The usage of FA as a replacement of PC in cement concrete is restricted to 40% by ASTM C 595 (ASTM International 2017) while it is limited to 35% by EN 197-1 (British Standard Institution 2011). However, these limits are increased to 50–75% for lab-scale testing to maximize the use of FA. In another study, Arezoumandi et al. experimentally examined strength of reinforcing steel in cement concrete where the cement was replaced by 50% FA. The prepared beams were tested and compared to the controlled beam prepared from normal cement concrete (CC) (Arezoumandi et al. 2013). The obtained results showed that the FA beams own comparable strength to that of normal CC beams. Arezoumandi and Volz extended their work to study the effect of the increased amount of FA on the beam strength (Arezoumandi and Volz 2013). The study shows that beam having 70% Class C FA has higher shear strength compared with the 50% FA and the normal CC beams. Furthermore, they found that increase in the amount of FA in concrete increases the bond strength of reinforcing steel concrete. It occurs due to the increase in mechanical properties like flexural strength, splitting tensile strength, and fracture energy. Also, the crack pattern and failure are similar for both FA and CC beams (Arezoumandi et al. 2015). Further, Hemalatha and Ramaswamy (Hemalatha and Ramaswamy 2017) performed a review analysis on the utilization of FA to make sustainable concrete based on the fly ash characteristics. It concluded that a higher replacement of cement by FA could be possible, i.e., up to 60% by the proper scientific method to maximize the utilization.

19.4.1.2 Bottom Ash

The BA particles are coarser in size which showed less reactivity than FA. However, the BA also can be utilized as a construction material like fly ash. Cheriaf et al. has examined the pozzolanic properties of BA (Cheriaf et al. 1999). The study evaluated its strength concerning the ages of the concrete mixture. The pozzolanic reactions are accelerated gradually after 28 days and become more significant after 90 days. The compressive strength test of prepared mortar was shown that BA can be used successfully in concrete. Besides, ball milling of BA for 6 h could improve their reactivity in alkaline media resulting in enhancement of the 28-day strength by 27%. In another study the milling effect of the BA in pozzolanic activity was examined by performing grinding up to 45 microns (Jaturapitakkul and Cheerarot 2003). Both before and after grind samples were taken, and their physical and chemical properties were investigated. The study unveils that due to grinding, particle size and porosity of BA decreases which resulted in a better pozzolanic reaction. With 20–30% replacement, the compressive strength of concrete could improve after 60 days. Oruji et al. (2017) took the BA from sub-bituminous coal and ground it to improve its fineness up to three times. Then the workability, setting time, and strength of the prepared mortar were investigated. The result shows that the workability and setting time increased by 21% and 14%, respectively, with regard to control. Similarly, the compressive strength improved by 120% at the age of 90 days. The pozzolanic reactivity of BA is improved which results in better strength and improved microstructure of cement mortar due to grinding of the coarse BA. Additionally, an experimental investigation was conducted by Pyo and Kim (Pyo and Kim 2017) to develop an ultra-high performance concrete (UHPC) by utilizing BA, FA, and two different types of slag powder. From the obtained results, it is evident that both BA and FA are promising to achieve significant workability and strength.

The use of BA as replacement of sand is extensively studied as compared to the studies where it is being used as an SCM. Several authors reported the excellent performance of the BA as replacement of sand in cement-based materials (Ramadoss and Sundararajan 2014; Baite et al. 2016; Torkittikul et al. 2017; Ngohpok et al. 2018). Ramadoss and Sundararajan examined the properties of masonry mortar by replacing fine aggregates by BA with a range of 20–50% (Ramadoss and Sundararajan 2014). The study reveals that at 20% BA incorporation, both compressive strength and modulus of rupture increase after 28 days by 1.7% and 2%, respectively. Therefore, BA can be used as fine aggregates replacing natural sand in cement concrete up to 20% replacement level. Due to average fineness and resemble particle size to natural sand, BA can be a good option for the replacement of sand in concrete manufacturing process. However, it demands more water than that of the normal cement mortar. The sorptivity and coefficient of absorption of the masonry mortar improve with inclusion of BA; this could be due to the filler effect of BA that reduces the pore spaces in masonry mortar. Moreover, Kim (2015) used ground BA powder as a coarse binder to prepare mortar with good compressive strength and workability. From experimental analysis results, it was noticed that more satisfying

workability of the BA-mortar mixture can be achieved over both the normal cement mortar mixture and FA-mortar mixture. Also, Baite et al. replaced sand at various volume fractions by fine aggregates of BA to obtain cementitious mortar (Baite et al. 2016). Incorporation of fine aggregates of BA in cementitious composite increases the porosity and hence water absorption rate. But, the utilization of BA reduces the specific weight due to low specific gravity as compared to the natural sand, and the thermal conductivity of the obtained composite is also reduced significantly. Thus, it promises a better option to utilize wastes, i.e., coal BA, with better performance in thermal insulation property of the building materials. It is also recommended that the BA-induced cementitious materials have better durability performance than the ordinary PC-based materials. A study was conducted by Jang et al., to perform an analysis to evaluate the deterioration in BA-mortar due to carbonation and chloride penetration (Jang et al. 2016). For a better comparison, ordinary mortar, FA-mortar, lightweight shell mortar, and slag cement mortar were included in the study. The results show that BA-mortar offered better resistance as compared to ordinary and lightweight mortar. However, FA-mortar and slag cement mortar have a better governing impact over BA-mortar while considering the chloride resistance, and the results are obvious comparing the pozzolanic reactivity of FA and slag with BA.

The thermal insulation property of the PC-based materials with BA was studied by Torkittikul et al. (2017). The study included BA as a substitute of sand at the various percentages (up to 100% replacement) and compared with the conventional mortar and concrete. The results of the conducted experiment show that the density decreases with an increase in BA% in the mortar and concrete mixture as compared to the controlled mixture; however, it does not influence the compressive strength significantly. The BA-mortar and concrete manifested enough thermal insulation properties; with an addition in BA%, the thermal conductivity reduces, which is in agreement with the earlier discussed study (Baite et al. 2016). The thermal conductivity of the BA-mortar and concrete with 100% replacement declined by 68.61% and 46.91% as compared to the control one. In another study, Ngohpok et al. have extended their study of BA in concrete (Ngohpok et al. 2018). They tested the thermal conductivity, mechanical properties, and sound absorption of pervious concrete by replacing the natural aggregates with the BA aggregates. The obtained results show that significant compressive strength can be achieved by replacing the limestone aggregates by BA aggregates. The BA-concrete achieves better thermal resistance as compared to that of natural limestone pervious concrete and hence encouraged to use.

19.4.2 Alkali-Activated Materials

The alkali activation is a chemical phenomenon that converts the glassy structures (partially/completely amorphous) of the coal ashes into a stable, compact, and strong composite with similar characteristics of cement-based materials (Palomo

et al. 1999b). The use of FA in alkali-activated materials (AAMs) is widely known and accepted, whereas the use of BA in AAMs is limited. The following subsections discuss different studies conducted on AAMs taking these coal ashes and their subsequent effect on the performance of the resulting AAM.

19.4.2.1 Fly Ash

The alkali activation of FA has been extensively investigated (Al-Majidi et al. 2016; Mustakim et al. 2020; Hardjito et al. 2004; Das et al. 2020b; Assaedi et al. 2020) and implemented widely in real-time application in countries like Australia and United States. In the year 1999, Palomo et al. (Palomo et al. 1999b) extensively studied the behavior of FA in alkali activation; their study established the FA as a viable material for the synthesis of AAMs. The FA was activated using a mixture of sodium hydroxide and sodium silicate solutions, and the highest mechanical strength of the final product was in a range of 60 MPa at 85 °C (5 h). Furthermore, a research group at the Curtin University, Perth, Australia, led by Prof. Rangan, made the first effort to develop FA-based alkali-activated concrete (geopolymer concrete); they published their experimental results in the materials journal of the American Concrete Institute (ACI Materials Journal) in the year 2004 (Hardjito et al. 2004). Prior to this research, all of the earlier conducted experiments were done only on alkali-activated FA paste or mortars (Van Jaarsveld et al. 2002; Palomo et al. 1999b), hence this research made an milestone in the development of the alkali-activated FA concrete for commercial applications. Though the developed alkali-activated FA concrete performed well in both strength and durability characteristics, due to certain other limitations such as elevated temperature curing and early setting issues, its implementation at large was restricted. Henceforth, several research works have been conducted to develop alkali-activated FA binder at atmospheric temperature that does not need elevated temperature curing to gain strength (Nath and Sarker 2012; Al-Majidi et al. 2016; Das et al. 2020b). Some authors recommended the incorporation of a high-calcium precursor material into the alkali-activated FA binder system (Rangan 2014; Deb et al. 2014); this will facilitate hydration and thus will generate heat of hydration; this heat of hydration will be beneficial for the geopolymerization process of FA. Therefore, in several occasions of ambient-cured FA geopolymer/AAM development, the blast furnace slag (BFS) is used as a supplementary binder to FA (Nath and Sarker 2014; Das et al. 2020a). Since BFS also contains good amount of aluminosilicate with considerable amount of CaO (30–50%), it helps in both geopolymerization and hydration processes. It is also advised that the BFS shall be pulverized before use, which is not cost-effective and at some places where BFS is not easily available, hence making FA-BFS blend AAM in those places is not economically viable. To take care of these issues with BFS, Das et al. (2020a, b) conducted a research experiment replacing FA with lime and silica fume (SF) in very small fractions (Das et al. 2020b). Their experimental results made another milestone on the FA-based alkali-activated concrete; at 2% SF and 7.5% lime the

FA-based composition exhibited a compressive strength greater than 60 MPa in 28 days of ambient curing.

Moreover, few research works have been conducted to use FA as a primary source material for the synthesis of one-part AAM (Hajimohammadi and van Deventer 2017; Abdollahnejad et al. 2015; Ouyang et al. 2020). One-part AAM denotes a class of binder that follows the same root of alkali activation/geopolymerization, but there is no need to add liquid alkaline activator separately, instead the activator is in the solid form mixed with the solid aluminosilicate materials (FA, BFS, etc.) and therefore the process of synthesis is same as hydraulic cement concrete, i.e., “just add water.” Considering the difficulty of supply chain and technological know-how of two-part AAM, one-part AAM emerged as a new sustainable alternative to both the cement-based and two-part alkali-activated concrete. Lv et al. conducted an experiment taking BFS and FA as a binder for one-part AAM (Lv et al. 2020). They have used a mixture of sodium carbonate, sodium hydroxide, and sodium silicate as alkaline activators. They claimed that their developed AAM showed great potential for practical applications since the resulted material claimed both high early and long-term strength; more than 25 MPa strength was developed within 3 days of casting and after 1 year the strength was nearly 73 MPa.

Moreover, the AAMs are more durable and less susceptible to chemical attacks. Several literatures have claimed that AAM shows excellent performance when immersed in aggressive solutions of different types such as seawater, deionized water, magnesium/sodium sulfate solution, and H_2SO_4 (Palomo et al. 1999a, b). For the better understanding of durability characteristics of any material, very profound observation is needed on its mineralogy and microstructure and essentially high mechanical strength of a material does not guarantees good durability property. Most of the durability issues of conventional cement-based materials are caused directly or indirectly by the calcium content of its binder. For instance, the sulfate attack caused by the reaction of C3A (tri-calcium aluminate) in the presence of free lime ($Ca(OH)_2$) with ingress sulfate ions from soil or water. This reaction generates ettringite and gypsum as reaction products that cause volumetric expansion leading to formation of cracks in the concrete. Another important case of durability reduction caused by lime is the reinforcement corrosion due to carbonation; in carbonation the free lime ($Ca(OH)_2$) reacts with the atmospheric CO_2 to form $CaCO_3$ precipitant. This process in cement concrete causes volumetric expansion with reduction in pH inside the matrix and hence the corrosion in reinforcements occurs. However, in case of the AAM, the reaction product that acts as the binder is an alkaline aluminosilicate gel with no free lime ($Ca(OH)_2$). Due to the unique mineralogy of AAM, it is extremely less susceptible to such chemical disintegration discussed above (Fernandez-Jimenez et al. 2007).

19.4.2.2 Bottom Ash

Though the BA does not have great reactivity like FA, still in several occasions it is being used as a precursor material for AAM. This less reactivity is generally caused by the large particle size coupled with the low specific surface area (SSA), therefore, it is suggested to pulverize the BA for enhanced reactivity before using in AAM (Osholana et al. 2020). In a study, conducted by Chindaprasirt et al. (Chindaprasirt et al. 2009), both FA- and BA-based AAM were synthesized using a mixture of NaOH and Na₂SiO₃ with three different concentrations of NaOH (5, 10, and 15 M). At a moderate level of alkali concentration (10 M), the BA-based composite exhibited a compressive strength of 18 MPa, whereas for FA the strength was 35 MPa. It is obvious that the FA will result comparatively better in mechanical properties than the BA, and the same has been reported in literature (Ul Haq et al. 2014). However, in a study it is reported that the elevated temperature curing can help achieve higher strength (Ul Haq et al. 2014); both FA and BA were taken as precursors for AAM separately, the FA-based composite resulted in 61.4 MPa, whereas the specimen made with BA shown a compressive strength of 55.2 MPa at 65 °C (48 h).

It is well known that the particle size and fineness of a material play a significant role in reactivity and the same has been reported in the case of BA in AAM. Chotetanorm et al. conducted an experiment taking different fineness of high-calcium BA (median particle sizes of 16, 25, and 32 μm) in AAM, and they have extensively investigated the mechanical properties and durability of the corresponding composites (Chotetanorm et al. 2013). Results revealed that relatively high strengths were achieved for the high-calcium BA-based geopolymer mortars. All of the specimens resulted in a compressive strength between 40.0 and 54.5 MPa. They further stated that the more fine is the BA, the better is its performance. The comparatively better performances of the fine BA were accredited to the high degree of reaction of the fine BA and the resulting less number of large pores inside the composite (0.05–100 μm) compared with those made from coarse BA. Furthermore, the BA can be used as an aggregate (fine) in AAM for the production of lightweight alkali-activated concrete (Wongsa et al. 2016) similar to the cement concrete as discussed earlier.

19.4.3 Brick and Paving Materials

19.4.3.1 Fly Ash

The ceramic industries have begun using fly ash (FA) by applying geopolymer technology for the production of ceramics materials like bricks, paver blocks, and tiles for building construction. Bricks contribute a major portion to the total consumption of building materials. Therefore, Queralt et al. used FA for making ceramic bricks (Queralt et al. 1997). The study revealed that FA could be a potential raw material

for the making of bricks, tiles, and paving stone. The particle size of FA is mostly below 75 micron which reduces the milling and grinding cost of the raw material, resulting in reduction in manufacturing cost. The strength of the FA bricks is more consistent or higher over the conventional bricks. However, due to changes in the mineralogical and chemical composition of FA from region to region, no general rules can be followed for standard manufacturing.

The use of FA in brick manufacturing is widely accepted and commercialized. In general, most of the brick manufacturer practices hydraulic cement as a supplementary binder with FA and thus the manufacturing cost of the bricks substantially increases. Hence, Reddy and Gaurav carried out the study to determine the strength of lime-FA brick by adding different additives to lower the cost of production (Reddy and Gourav 2011). From the study, it was observed that the lime-pozzolana reaction rate is slow at ambient temperature and requires a long curing duration to achieve comparable strength. The 28-day strength of lime-FA brick was 10 MPa with the addition of gypsum as an additive. Maximum compressive strength can be achieved by mixing only 2% gypsum; hence it is suggested to add some gypsum with the FA-lime-based bricks for the better results. Moreover, the compressive strength can be improved by curing the bricks in a steam chamber at 80 °C; this technic helps to control the relative humidity. In another study conducted by CSIR-IMMT, Bhubaneswar, the authors have mentioned a new technology called “mineral polymerization” by which the FA can be used for building brick production without using any cement (Dwari et al. 2020). However, this new technology needs special attention for its commercialization while considering techno-economic viability.

Experimental research was carried out by Wang et al. (2016) to innovate the possible technology for the utilization of coal FA. They produced FA brick with a replacement of 50–80%; strength grade and freezing–thawing resisting were evaluated. The study unveils that high-volume FA bricks can be used as building materials. Furthermore, Fernández-Pereira et al. used biomass gasification fly ash to prepare bricks (Fernández-Pereira et al. 2011). From that study, it was obtained that the prepared FA brick has similar properties like the commercially available bricks. It can be used commercially as low-density clay masonry units having excellent thermal insulating capacity. Similarly, Zhang et al. (2012) investigated on high sulfur content FA (more than 5% SO₃ by wt.) to prepare bricks, which was collected from circulating fluidized bed combustion (CFBC). Sulfur is a harmful substance while used in building material. In this study, CFBC-FA and slag were used to prepare brick, cured in the pressurized steam chamber (Autoclave), and then the strength was tested. The brick having 77% CFBC-FA, 20% CFBC slag, and 3% of cement attained the compressive strength of up to 14.3 MPa. Due to autoclave, the bricks are of good strength and can be used commercially.

Owing to the low specific gravity of FA while comparing with cement and sand, the lightweight building blocks can be well prepared using FA. In a study, Çiçek and Çinçin examined the performance of lightweight building blocks with FA (Çiçek and Çinçin 2015). The study investigated the mechanical performance of lightweight FA blocks to replace the conventional concrete blocks. It was found that the

FA blocks developed the significant strength and less weight. Also, their thermal resistance is excellent compared to conventional concrete blocks and superior to clay bricks. The utility of FA in pavements is also suggested and experimented. Mohammadinia et al. evaluated the effect of FA in crushed brick and reclaimed asphalt pavement (Mohammadinia et al. 2017). From the strength and durability test, it was found that the unconfined compressive strength and resilient modulus were maximum for 15% FA. The addition of FA to these mixtures increases the silica and alumina crystalline and increases the binding property that ensured the well cohesion between different particles within the whole system leading to the better mechanical performances. Also, the curing temperature plays a vital role in the strength of FA-mixture samples. Higher strength could be obtained at higher curing temperatures.

Consoli et al. (2020) used CFA and carbide lime (CL) as the enhancing agents in reclaimed asphalt pavement (RAP) and evaluated its durability and performance. The results showed that the compacted RAP-FA-CL mixtures well performed under wetting-drying than freezing-thawing conditions. The porosity/lime index also plays a key role in the mechanical strength and durability. The appropriate amount of porosity/lime index can be calculated as per the requirement by geotechnical engineers. However, more investigations are needed to use FA for pavement applications for optimum design mix and performance evaluation.

19.4.3.2 Bottom Ash

The use of BA in brick is generally not preferred since there is plenty amount of FA available for brick manufacturing. Hence, most of the generated BA goes directly into ash ponds thus creates sustainability issues. A study mentioned that the total percentage consumption of FA in construction industry is 47% of total generation, whereas, for BA the number is only 5.28% (Ashish et al. 2018). Considering the future trend in the construction industries, soon in the near future there will be a shortage of FA for making building bricks. Therefore, some studies have been conducted to use BA as a constituent material for manufacturing building bricks and paving materials (Mogili et al. 2020; Sutcu et al. 2019; Ashish et al. 2018; Aydin 2016; Santos et al. 2015; Naganathan et al. 2015; Colonna et al. 2012).

An experiment conducted by Ashish et al. used BA as a replacement to sand in FA-based cement bricks (Ashish et al. 2018). Their major aim was to reduce the use of natural river sand and to use BA in bricks; nevertheless, the developed FA-BA brick performed well in comparison with the reference one. Similarly, the use of BA as replacement to sand in paving blocks is reported (Santos et al. 2015). The results indicated that the BA taken for the manufacturing of paving blocks can be used up to 50% of the natural river sand without impacting its primary properties. Further, the use of BA for paving material application was extended by Aydin (2016). He suggested a BA-cement-lime-based composite that contains 70% of BA, 25% cement, and 5% lime for manufacturing of bricks, paving blocks and floor tiles. Due to the granular particle distribution of BA, it is also recommended that the BA can be used as an aggregate to the binder in pavement binder course. Colonna et al.

(2012) studied the characteristics of the flexible binder course with incorporation of BA in place of river sand. Their results revealed when a 15% of BA was added to the mix replacing a correspondent amount of sand, the mix performed perfectly as usual like the conventional mixture, there was no deteriorating effect on the mechanical properties of the bitumen mix in comparison to the control one. It means that BA could be used for various pavement applications, however, to promote the use of this waste material (BA) for practical applications; it is essential to issue new standards for the corresponding usages of BA.

19.5 Conclusion

The discussion made in this chapter narrated the possible utilization of coal ashes (both FA and BA) in several building material applications. With the critical analysis of the results obtained in several studies by various researchers, it can be concluded that the coal ashes have promising use in synthesis of both the building and road infrastructures. Furthermore, these are good sustainable alternative of naturally available construction materials like limestone, stone dust, and sand, and hence the utilization of coal ashes can help conserve the environment as well as the corresponding natural resources.

Acknowledgments Since this chapter has been written during the COVID 19 pandemic, the first author (S.K. Das) was at home during the manuscript preparation, he wants to thank his parents (Mr. Santosh K. Das and Mrs. Sasmita Das) for their continuous help and support in making the home a perfect place to write peacefully. All the authors are thankful to CSIR-Institute of Minerals and Materials Technology, Bhubaneswar, India, for the characterization study of coal ashes provided in the study. Mr. Jyotirmoy Mishra (Civil Engineering Department, VSSUT, Burla, India) and Mr. RS Krishna (CSIR-IMMT, Bhubaneswar, India) are also acknowledged for their valuable inputs in preparation of this work.

References

- Abdollahnejad, Z., Pacheco-Torgal, F., Aguiar, J. B., & Jesus, C. (2015). Durability performance of fly ash based one-part geopolymer mortars. *Key Engineering Materials*, 634, 113–120. <https://doi.org/10.4028/www.scientific.net/KEM.634.113>.
- Al-Majidi, M. H., Lampropoulos, A., Cundy, A., & Meikle, S. (2016). Development of geopolymer mortar under ambient temperature for in situ applications. *Construction and Building Materials*. <https://doi.org/10.1016/j.conbuildmat.2016.05.085>.
- Andrade, L. B., Rocha, J. C., & Cheriaf, M. (2009). Influence of coal bottom ash as fine aggregate on fresh properties of concrete. *Construction and Building Materials*. <https://doi.org/10.1016/j.conbuildmat.2008.05.003>.
- Arezoumandi, M., Looney, T. J., & Volz, J. S. (2015). Effect of fly ash replacement level on the bond strength of reinforcing steel in concrete beams. *Journal of Cleaner Production*. <https://doi.org/10.1016/j.jclepro.2014.10.078>.
- Arezoumandi, M., & Volz, J. S. (2013). Effect of fly ash replacement level on the shear strength of high-volume fly ash concrete beams. *Journal of Cleaner Production*. <https://doi.org/10.1016/j.jclepro.2013.06.043>.

- Arezoumandi, M., Wolfe, M. H., & Volz, J. S. (2013). A comparative study of the bond strength of reinforcing steel in high-volume fly ash concrete and conventional concrete. *Construction and Building Materials*. <https://doi.org/10.1016/j.conbuildmat.2012.11.105>.
- Ashish, D. K., Verma, S. K., Singh, J., & Sharma, N. (2018). Strength and durability characteristics of bricks made using coal bottom and coal fly ash. *Advances in Concrete Construction*. <https://doi.org/10.12989/acc.2018.6.4.407>.
- Asokan, P., Saxena, M., & Asolekar, S. R. (2005). Coal combustion residues—Environmental implications and recycling potentials. *Resources, Conservation and Recycling*. <https://doi.org/10.1016/j.resconrec.2004.06.003>.
- Assaedi, H., Alomayri, T., Kaze, C. R., Jindal, B. B., Subaer, S., Shaikh, F., & Alraddadi, S. (2020). Characterization and properties of geopolymer nanocomposites with different contents of Nano-CaCO₃. *Construction and Building Materials*. <https://doi.org/10.1016/j.conbuildmat.2020.119137>.
- ASTM C311/C311M-18. (2018). Standard test methods for sampling and testing fly ash or natural Pozzolans for use in Portland-cement concrete. *Annual Book of ASTM Standards*. https://doi.org/10.1520/C0311_C0311M-18.
- ASTM International. (2017). ASTM C595-17, standard specification for blended hydraulic cements. *ASTM International*. https://doi.org/10.1520/C0595_C0595M-17.
- Aydin, E. (2016). Novel coal bottom ash waste composites for sustainable construction. *Construction and Building Materials*. <https://doi.org/10.1016/j.conbuildmat.2016.07.142>.
- Baite, E., Messan, A., Hannawi, K., Tsobnang, F., & Prince, W. (2016). Physical and transfer properties of mortar containing coal bottom ash aggregates from Tefereyre (Niger). *Construction and Building Materials*. <https://doi.org/10.1016/j.conbuildmat.2016.08.117>.
- Bhatt, A., Priyadarshini, S., Mohanakrishnan, A. A., Abri, A., Sattler, M., & Techapaphawit, S. (2019). Physical, chemical, and geotechnical properties of coal Fly ash: A global review. *Case Studies in Construction Materials*. <https://doi.org/10.1016/j.cscm.2019.e00263>.
- Blissett, R. S., & Rowson, N. A. (2012). A review of the multi-component utilisation of coal fly ash. *Fuel*. <https://doi.org/10.1016/j.fuel.2012.03.024>.
- British Standard Institution. BS EN 197-1 Cement(2011). Composition, specifications and conformity criteria for common cements. *Bsi*. <https://doi.org/10.3989/mc.2012.07711>.
- Cao, D. Z., Selic, E., & Herbell, J. D. (2008). Utilization of fly ash from coal-fired power plants in China. *Journal of Zhejiang University: Science A*. <https://doi.org/10.1631/jzus.A072163>.
- Cherief, M., Rocha, J. C., & Péra, J. (1999). Pozzolanic properties of pulverized coal combustion bottom ash. *Cement and Concrete Research*. [https://doi.org/10.1016/S0008-8846\(99\)00098-8](https://doi.org/10.1016/S0008-8846(99)00098-8).
- Chindapasirt, P., Jaturapitakkul, C., Chalee, W., & Rattanasak, U. (2009). Comparative study on the characteristics of fly ash and bottom ash geopolymers. *Waste Management*, 29(2), 539–543. <https://doi.org/10.1016/j.wasman.2008.06.023>.
- Chotetanorm, C., Chindapasirt, P., Sata, V., Rukzon, S., & Sathonsaowaphak, A. (2013). High-calcium bottom ash Geopolymer: Sorptivity, pore size, and resistance to sodium sulfate attack. *Journal of Materials in Civil Engineering*. [https://doi.org/10.1061/\(ASCE\)MT.1943-5533.0000560](https://doi.org/10.1061/(ASCE)MT.1943-5533.0000560).
- Çiçek, T., & Çinçin, Y. (2015). Use of fly ash in production of light-weight building bricks. *Construction and Building Materials*. <https://doi.org/10.1016/j.conbuildmat.2015.07.029>.
- Colonna, P., Berloco, N., Ranieri, V., & Shuler, S. T. (2012). Application of bottom ash for pavement binder course. *Procedia - Social and Behavioral Sciences*. <https://doi.org/10.1016/j.sbspro.2012.09.945>.
- Consoli, N. C., Filho, H. C. S., Godoy, V. B., Rosembach, C. M. D. C., & Carraro, J. A. H. (2020). Durability of reclaimed asphalt pavement–coal fly ash–carbide lime blends under severe environmental conditions. *Road Materials and Pavement Design*. <https://doi.org/10.1080/14680629.2018.1506354>.
- Das, D., Pattanaik, S., Parhi, P. K., Mohapatra, R. K., Jyothi, R. K., Lee, J. Y., & In Kim, H. (2019). Stabilization and rheological behavior of fly ash-water slurry using a natural dispersant in pipeline transportation. *ACS Omega*. <https://doi.org/10.1021/acsomega.9b03477>.
- Das, S. K., Mishra, J., & Mustakim, S. M. (2018). Rice husk ash as a potential source material for geopolymer concrete: A review. *International Journal of Applied Engineering Research*, 13(7), 81–84.

- Das, S. K., Mishra, J., Singh, S. K., Mustakim, S. M., Patel, A., Das, S. K., & Behera, U. (2020a). Characterization and utilization of rice husk ash (RHA) in fly ash—Blast furnace slag based geopolymer concrete for sustainable future. *Materials Today: Proceedings*. <https://doi.org/10.1016/j.matpr.2020.02.870>.
- Das, S. K., Mustakim, S. M., Adesina, A., Mishra, J., Alomayri, T. S., Assaedi, H. S., & Kaze, C. R. (2020b). Fresh, strength and microstructure properties of geopolymer concrete incorporating lime and silica fume as replacement of fly ash. *Journal of Building Engineering*, 101780. <https://doi.org/10.1016/j.jobe.2020.101780>.
- Deb, P. S., Nath, P., & Sarker, P. K. (2014). The effects of ground granulated blast-furnace slag blending with fly ash and activator content on the workability and strength properties of geopolymer concrete cured at ambient temperature. *Materials and Design*. <https://doi.org/10.1016/j.matdes.2014.05.001>.
- Deschner, F., Winnefeld, F., Lothenbach, B., Seufert, S., Schwesig, P., Dittrich, S., Goetz-Neunhoeffer, F., & Neubauer, J. (2012). Hydration of Portland cement with high replacement by siliceous Fly ash. *Cement and Concrete Research*. <https://doi.org/10.1016/j.cemconres.2012.06.009>.
- Dwari, R. K., Sarangi, C. K., Mustakim, S. M., Dash, B., Tripathy, B. C., Ghosh, M. K., & Basu, S. (2020). R&D efforts of CSIR-IMMT toward solving some issues related to Aluminum production. *Journal of Sustainable Metallurgy*. <https://doi.org/10.1007/s40831-019-00250-w>.
- Fernandez-Jimenez, A., García-Lodeiro, I., & Palomo, A. (2007). Durability of alkali-activated fly ash cementitious materials. *Journal of Materials Science*. <https://doi.org/10.1007/s10853-006-0584-8>.
- Fernández-Pereira, C., De La Casa, J. A., Gómez-Barea, A., Arroyo, F., Leiva, C., and Luna, Y. (2011). Application of biomass gasification fly ash for brick manufacturing. *Fuel*. doi:<https://doi.org/10.1016/j.fuel.2010.07.057>
- Ganesh Babu, K., & Siva Nageswara Rao, G. (1996). Efficiency of fly ash in concrete with age. *Cement and Concrete Research*. [https://doi.org/10.1016/S0008-8846\(96\)85034-4](https://doi.org/10.1016/S0008-8846(96)85034-4).
- Hajimohammadi, A., & van Deventer, J. S. J. (2017). Characterisation of one-part geopolymer binders made from fly ash. *Waste and Biomass Valorization*, 8(1), 225–233. <https://doi.org/10.1007/s12649-016-9582-5>.
- Hardjito, D., Wallah, S. E., Sumajouw, D. M. J., & Vijaya Rangan, B. (2004). On the development of Fly ash-based Geopolymer concrete. *ACI Materials Journal*. <https://doi.org/10.14359/13485>.
- Hemalatha, T., & Ramaswamy, A. (2017). A review on fly ash characteristics—Towards promoting high volume utilization in developing sustainable concrete. *Journal of Cleaner Production*. <https://doi.org/10.1016/j.jclepro.2017.01.114>.
- Jang, J. G., Kim, H. J., Kim, H. K., & Lee, H. K. (2016). Resistance of coal bottom ash mortar against the coupled deterioration of carbonation and chloride penetration. *Materials and Design*. <https://doi.org/10.1016/j.matdes.2015.12.074>.
- Jaturapitakkul, C., & Cheerarat, R. (2003). Development of bottom ash as Pozzolanic material. *Journal of Materials in Civil Engineering*. [https://doi.org/10.1061/\(ASCE\)0899-1561\(2003\)15:1\(48\)](https://doi.org/10.1061/(ASCE)0899-1561(2003)15:1(48)).
- Jayaranjan, M. L. D., van Hullebusch, E. D., & Annachhatre, A. P. (2014). Reuse options for coal fired power plant bottom ash and Fly ash. *Reviews in Environmental Science and Biotechnology*. <https://doi.org/10.1007/s11157-014-9336-4>.
- Kim, H. K. (2015). Utilization of sieved and ground coal bottom ash powders as a coarse binder in high-strength mortar to improve workability. *Construction and Building Materials*. <https://doi.org/10.1016/j.conbuildmat.2015.05.017>.
- Kumar, S., Gandhi, B. K., & Mohapatra, S. K. (2014). Performance characteristics of centrifugal slurry pump with multi-sized particulate bottom and fly ash mixtures. *Particulate Science and Technology*. <https://doi.org/10.1080/02726351.2014.894163>.
- Lv, W., Sun, Z., & Su, Z. (2020). Study of seawater mixed one-part alkali activated GGBFS-Fly ash. *Cement and Concrete Composites*, 106(October 2019), 103484. <https://doi.org/10.1016/j.cemconcomp.2019.103484>.

- Mishra, J., Das, S. K., Krishna, R. S., & Nanda, B. (2020). Utilization of ferrochrome ash as a source material for production of Geopolymer concrete for a cleaner sustainable environment. *Indian Concrete Journal*, 94(7), 40–49.
- Mishra, J., Das, S. K., Singh, S. K., & Mustakim, S. M. (2019). Development of Geopolymer concrete for the protection of environment: A greener alternative to cement. *International Journal of Civil Engineering*, 6(3), 41–47. <https://doi.org/10.14445/23488352/ijce-v6i3p106>.
- Mogili, S., Mudavath, H., Gonavaram, K. K., & Paluri, Y. (2020). Strength and resilient behavior of lime modified pond ash as pavement layer. *Materials Today: Proceedings*. <https://doi.org/10.1016/j.matpr.2020.02.168>.
- Mohammadinia, A., Arulrajah, A., Horpibulsuk, S., & Chinkulkijniwat, A. (2017). Effect of fly ash on properties of crushed brick and reclaimed asphalt in pavement base/subbase applications. *Journal of Hazardous Materials*. <https://doi.org/10.1016/j.jhazmat.2016.09.039>.
- Mustakim, S. M., Das, S. K., Mishra, J., Aftab, A., Alomayri, T. S., Assaedi, H. S., & Kaze, C. R. (2020). Improvement in fresh, mechanical and microstructural properties of fly ash- blast furnace slag based geopolymer concrete by addition of nano and micro silica. *Silicon*. <https://doi.org/10.1007/s12633-020-00593-0>.
- Naganathan, S., Mohamed, A. Y. O., & Mustapha, K. N. (2015). Performance of bricks made using fly ash and bottom ash. *Construction and Building Materials*. <https://doi.org/10.1016/j.conbuildmat.2015.08.068>.
- Nath, P., and Sarker, P. K. (2012). Geopolymer Concrete for Ambient Curing Condition. *Australasian Structural Engineering Conference 2012: The Past, Present and Future of Structural Engineering*.
- Nath, P., & Sarker, P. K. (2014). Effect of GGBFS on setting, workability and early strength properties of FLY ash geopolymer concrete cured in ambient condition. *Construction and Building Materials*. <https://doi.org/10.1016/j.conbuildmat.2014.05.080>.
- Noghok, C., Sata, V., Satiennam, T., Klungboonkrong, P., & Chindaprasirt, P. (2018). Mechanical properties, thermal conductivity, and sound absorption of pervious concrete containing recycled concrete and bottom ash aggregates. *KSCE Journal of Civil Engineering*. <https://doi.org/10.1007/s12205-017-0144-6>.
- Nochaiya, T., Wongkeo, W., & Chaipanich, A. (2010). Utilization of Fly ash with silica fume and properties of Portland cement-fly ash-silica fume concrete. *Fuel*. <https://doi.org/10.1016/j.fuel.2009.10.003>.
- NTPC Ash Utilization Division (2013). *Fly ash for cement concrete*. Noida–201301: NTPC Limited. <https://www.ntpc.co.in/en/environment/ash-utilisation>
- Oruji, S., Brake, N. A., Nalluri, L., & Guduru, R. K. (2017). Strength activity and microstructure of blended ultra-fine coal bottom ash-cement mortar. *Construction and Building Materials*. <https://doi.org/10.1016/j.conbuildmat.2017.07.088>.
- Osholana, T. S., Dluđu, M. K., Oboirien, B., & Sadiku, R. (2020). Enhanced reactivity of Geopolymers produced from fluidized bed combustion bottom ash. *South African Journal of Chemical Engineering*. <https://doi.org/10.1016/j.sajce.2020.06.006>.
- Ouyang, S., Chen, W., Zhang, Z., Li, X., & Zhu, W. (2020). Experimental study of one-part geopolymer using different alkali sources. *Journal of Physics: Conference Series*, 1605, 012155. <https://doi.org/10.1088/1742-6596/1605/1/012155>.
- Palomo, A., Blanco-Varela, M. T., Granizo, M. L., Puertas, F., Vazquez, T., & Grutzeck, M. W. (1999a). Chemical stability of cementitious materials based on Metakaolin. *Cement and Concrete Research*. [https://doi.org/10.1016/S0008-8846\(99\)00074-5](https://doi.org/10.1016/S0008-8846(99)00074-5).
- Palomo, A., Grutzeck, M. W., & Blanco, M. T. (1999b). Alkali-activated Fly ashes: A cement for the future. *Cement and Concrete Research*. [https://doi.org/10.1016/S0008-8846\(98\)00243-9](https://doi.org/10.1016/S0008-8846(98)00243-9).
- Pattanaik, S., Parhi, P. K., Das, D., & Samal, A. K. (2019). Acacia Concinna: A natural dispersant for stabilization and transportation of Fly ash-water slurry. *Journal of the Taiwan Institute of Chemical Engineers*. <https://doi.org/10.1016/j.jtice.2019.03.020>.
- Pyo, S., & Kim, H. K. (2017). Fresh and hardened properties of ultra-high performance concrete incorporating coal bottom ash and slag powder. *Construction and Building Materials*. <https://doi.org/10.1016/j.conbuildmat.2016.10.109>.

- Queralt, I., Querol, X., López-Soler, A., & Plana, F. (1997). Use of coal fly ash for ceramics: A case study for a large Spanish Power Station. *Fuel*. [https://doi.org/10.1016/s0016-2361\(97\)00024-0](https://doi.org/10.1016/s0016-2361(97)00024-0).
- Ramadoss, P., & Sundararajan, T. (2014). Utilization of lignite-based bottom ash as partial replacement of fine aggregate in masonry mortar. *Arabian Journal for Science and Engineering*. <https://doi.org/10.1007/s13369-013-0703-1>.
- Ravina, D. (1997) Properties of fresh concrete incorporating a high volume of fly ash as partial fine sand replacement. *Mat. Struct.* 30, 473–479. <https://doi.org/10.1007/BF02524775>
- Rangan, B. V. (2014). Geopolymer concrete for environmental protection. *Indian Concrete Journal*, 88, 41.
- Reddy, B. V. V., & Gourav, K. (2011). Strength of lime-fly ash compacts using different curing techniques and gypsum additive. *Materials and Structures/Materiaux et Constructions*. <https://doi.org/10.1617/s11527-011-9738-5>.
- Santos, C. R., Tubino, R. M. C., & Schneider, I. A. H. (2015). Mineral processing and characterization of coal waste to be used as fine aggregates for concrete paving blocks. *Revista IBRACON de Estruturas e Materiais*. <https://doi.org/10.1590/s1983-41952015000100004>.
- Singh, M., & Siddique, R. (2013). Effect of coal bottom ash as partial replacement of sand on properties of concrete. *Resources, Conservation and Recycling*. <https://doi.org/10.1016/j.resconrec.2012.12.006>.
- Singh, M., & Siddique, R. (2016). Effect of coal bottom ash as partial replacement of sand on workability and strength properties of concrete. *Journal of Cleaner Production*. <https://doi.org/10.1016/j.jclepro.2015.08.001>.
- Statista Research Department (2013). Cement Production Worldwide 2030—Statistic. <https://www.statista.com/statistics/373845/global-cement-production-forecast/>
- Sutcu, M., Erdogmus, E., Gencel, O., Gholampour, A., Atan, E., & Ozbakkaloglu, T. (2019). Recycling of bottom ash and fly ash wastes in eco-friendly clay brick production. *Journal of Cleaner Production*. <https://doi.org/10.1016/j.jclepro.2019.06.017>.
- Thomas, M. D. A. (2007). *Optimizing the use of fly ash in concrete*. Portland Cement Association.
- Torkittikul, P., Nochaiya, T., Wongkeo, W., & Chaipanich, A. (2017). Utilization of coal bottom ash to improve thermal insulation of construction material. *Journal of Material Cycles and Waste Management*. <https://doi.org/10.1007/s10163-015-0419-2>.
- Ul Haq, Kunjalukkal Padmanabhan, E. S., & Licciulli, A. (2014). Synthesis and characteristics of fly ash and bottom ash based geopolymers—A comparative study. *Ceramics International*. <https://doi.org/10.1016/j.ceramint.2013.10.012>.
- Van Jaarsveld, J. G. S., Van Deventer, J. S. J., & Lukey, G. C. (2002). The effect of composition and temperature on the properties of fly ash- and kaolinite-based geopolymers. *Chemical Engineering Journal*. [https://doi.org/10.1016/S1385-8947\(02\)00025-6](https://doi.org/10.1016/S1385-8947(02)00025-6).
- Vassilev, S. V., & Vassileva, C. G. (2007). A new approach for the classification of coal fly ashes based on their origin, composition, properties, and behaviour. *Fuel*. <https://doi.org/10.1016/j.fuel.2006.11.020>.
- Wang, L., He, S., Sun, Z., & Ma, E. (2016). New technology and application of brick making with coal fly ash. *Journal of Material Cycles and Waste Management*. <https://doi.org/10.1007/s10163-015-0368-9>.
- WCA (2019). Coal & Electricity | World Coal Association. 2019. <https://www.worldcoal.org/coal/uses-coal/coal-electricity>
- White, S. C., & Case, E. D. (1990). Characterization of fly ash from coal-fired power plants. *Journal of Materials Science*. <https://doi.org/10.1007/BF00580153>.
- Wongsa, A., Zaetang, Y., Sata, V., & Chindapasirt, P. (2016). Properties of lightweight fly ash geopolymer concrete containing bottom ash as aggregates. *Construction and Building Materials*. <https://doi.org/10.1016/j.conbuildmat.2016.02.135>.
- Zhang, Z., Qian, J., You, C., & Changhua, H. (2012). Use of circulating fluidized bed combustion fly ash and slag in autoclaved brick. *Construction and Building Materials*. <https://doi.org/10.1016/j.conbuildmat.2012.03.006>.

Chapter 20

Prospective Utilization of Coal Fly Ash for Making Advanced Materials



Aritra Kumar Dan, Dipanjan Bhattacharjee, Saikat Ghosh,
Saroj Sekhar Behera, Birendra Kumar Bindhani, Debadutta Das,
and Pankaj Kumar Parhi

20.1 Introduction

Generally CFA is generated during the ablaze of coal for vitality creation. Its usage as a modern side effect has gotten a lot of consideration in recent decades as progressively manageable answers for squander issues have been looked for (Roviello et al. 2019). On average 90% of electricity is being produced by the combustion of brown coal (approximately 65 million tonnes per annum). In consequences of which, at about 1.13 million tonnes of FA by-products are being discharged for landfills purposes as it is without utilizing it further. FA generated from Brown coal (obtained out of sub-bituminous type coal) has different chemical properties compared with that generated from black CFA kind coal (Tennakoon et al. 2015). Due to the lack of a well-planned technique while dumping FA in Indian context, it poses a serious threat on making health hazards concern at the environmental prospective. The utilization and dumping of CFA with the above context is becoming a significant issue for those countries mainly depend on their power generation sectors from thermal plants source. Thus, attempts are being devoted on usages of FA as bulk material, soil stabilization purpose, and on further reclamation of land (Dutta et al. 2016). Multiple treatments have been developed over the last decades to resolve the FA-related issues. Over a period of time, the classical spectrum of FA treatments such as separation, solidification, stabilization, immobilization, and

A. K. Dan · D. Bhattacharjee · S. Ghosh · S. S. Behera · B. K. Bindhani
Materials Research Laboratory (MRL), School of Biotechnology & School of Chemical
Technology, Kalinga Institute of Industrial Technology (KIIT), Deemed to be University,
Bhubaneswar, Odisha, India

D. Das
Department of Chemistry, Sukanti Degree College, Subarnapur, Odisha, India

P. K. Parhi (✉)
Department of Chemistry, Fakir Mohan University, Balasore, Odisha, India

heating approaches has been extended to include microwave radiation, mechano-chemistry, electrochemistry, chemical fixation, thermal plasma, chemical reaction, and organic contaminants such as non-thermal hydrothermal method. Presently, researchers put the attention on FA making use of value adding materials like building block or upgrading it while blending with other secondary materials by investigating both the physical and chemical potential aspects of FA as it bears the chemical constituents like alumina-silicate to prepare various composite zeolites. Recovery of nutrients (P, N, S) from CFA biomass is important in the context of agriculture farming and that appears to be worth on investigating on the use of FA in a wider extent. The sophisticated reuse of FA offers more economic benefits and fosters in use of raw materials for future communities (Gianoncelli et al. 2013; Lokeshappa and Dikshit 2011; Ren et al. 2020). The audit at that point investigates the effect that a more than one stage adoption in this study showed appealing while analyzing the innovation fit for a progression of detachments to deliver empty microspheres, advanced carbon, attractive circles, fine debris item, and coarse debris item (Azhar et al. 2019). FA particles are fine, strong particulate buildup force out of the kettle with vent gases in the terminated coal force plants (Chen et al. 2020). There is a critical prospective for the expanded use of CFA both in its crude and its refined state. Thus by preparing the CFA, the degree of making new modern co-operative energies can be improved as illustrated by researchers (Asl et al. 2019). The effective applications for FA as a crude material like the making of zeolites, as dirt enhancement specialist of horticulture, blending of glass and earthenware production, meso-porous materials, amalgamation of geopolymers, as an adsorbent for gases and as source for extraction of metals (Ridtirud and Chindaprasirt 2019). Presently it very well may be utilized for making geopolymer which goes about as a concrete-like item (Moffatt et al. 2017). The innovation product like geopolymer gives a potential prospective for suitable utilization of FA with a minimal negative outcome. This survey sums up and looks at the logical advancement in terms of its properties, arrangement, and substantial utilization of FA-based geopolymer (De Rossia et al. 2020; Silva and Andrade 2017; Mármol et al. 2016). Some of the characteristics of FA put together with geopolymer are naturally reliant concerning the substance organization, concoction holding, and porosity. Mechanical properties and sturdiness may be improved by restoring conditions, calibrating the Si/Al proportions, salt arrangements, and incorporating slag, fiber, red mud, and rice husk ash (Zhuang et al. 2016; Tennakoon et al. 2014). Geopolymer is found to be an innovative binder that can be utilized with replacement over Portland Cement (Tennakoon et al. 2015; Hu et al. 2019); accordingly it has been substituted as alternatives to cement in concrete work for a longer period. By 2012 FA was exploited as a promising source with its bulk amount usages and as much as increased use up to 55.79% for making various commercial-level product (Shaikh and Supit 2015; Duan et al. 2016; Chen et al. 2019; Kim et al. 2020b). Apart from its environmental concerns, the proven technical amenities for utilization of FA with replacement of cement accomplish the creation of increasing workability, reduction of bleeding, reducing reinforcement corrosion at reinforced concrete, decreasing the rate of temperature that usually rises during hardening of concrete, reducing of drying shrinkage, and

that could lead to improvement in durability. Thus in the context of economical aspect of any of the resources, utilization of FA in place of cement is shown to be a very cost-effective technology with an outcome of promising waste management strategy instead of its direct disposal to the environment. In spite of the potential use of FA in concrete, overall consumption was achieved up to 25%, in a global prospective (Rivera et al. 2015). Nevertheless, the proper utilization of the industrial wastes including silica fume, FA, silica fume, and blast-furnace slag further ensures the benefaction prospective like concrete hydration, prevention of the issues due to diffusion of CO₂ and chlorides. The other aspects of FA usages in the concrete industry are to lower the use of cement and so on regulation of CO₂ emissions (Chousidis et al. 2015). It was assumed Portland Slag Cement (PSC) was affected by sulfate attack at the sulfate-rich environments. Hence to minimize this sulfate attack, the industrial by-products such as FA and slag are often mixed with PSC for improvement in its mechanical properties. But the impacts due to FA on concrete durability were not consistent since energy and time consumption seems very high (Nie et al. 2015; Fang and Zhang 2020). Various FA can be used as promising raw material sources for making geopolymer (Tennakoon et al. 2015; Zhang et al. 2014). The generation of FA-based geopolymer is worthwhile concerning oversolubility in base that is resulted at optimum conditions and mostly CO₂ emission is readily reduced than that of making of concrete using FA (Sharma and Akhai 2019; Natha et al. 2015). Thereby, the construction-based industrial sector showed their major interest in exploiting FA as a prime raw material, and more and more research studies are undertaken in this domain day-by-day. In cement supplement products, the use of pozzolans appears as a suitable alternative one. It is basically FA is being obtained as a by-product from electricity generation-based thermal plants. It is realized that the energy and cost component on production of Portland Slag Cement (PSC) is much higher, and approximately 1 tonnage of CO₂ emission is expected per ton on production of cement. Thus the substitution of FA could result on minimizing CO₂ emission and thereby, overall process becomes more economical as well as beneficial in a greater way (Pedrazaa et al. 2015; Velandia et al. 2016; Seto et al. 2017). On the other hand, another type product, namely Zeolites (hydrated alum inosilicate minerals), may be prepared from FA, kaolinite, etc. Usually kaolinite is subjected to calcination in the temperature ranges from 600 °C to 1000 °C, and as of now very limited works are reported. The synthesis approach includes hydrothermal processing route through pre-fusion treatment using alkali solution (Musyoka et al. 2015). However, some aspects are not properly obtained in the synthesis of zeolites by using kaolinite or FA. The most admissible perspective associated with the role of the synthesis is mainly depended on the function of time of crystallization, Si/Al at precursor phase, and temperature. The major use of pure form of kaolinite is mainly to make zeolite-An as a major one and minor phase as zeolite-X. However, the trace content of silicate minerals including quartz/illite phase is detected in kaolinite phase. In addition, it was proposed that the rate of crystallization of zeolite-A/ zeolite-X varies with time (Belviso et al. 2015).

Another useful utilization of FA could be the synthesis of artificial fertilizers by different methodologies. The versatile applicability prospective of CFA in making

various zeolite-based items is broadly demonstrated and shown almost in recent decades by applying distinctive unique techniques like basic direct transformation, basic combination, utilizing Si-concentrates, Al-rich fluid squanders, and for gasification using FA as a prime source. The cationic trade limit (CEC) and structure of typical zeolites (accomplishing zeolitic materials blended from the FA) provides greater prospective of the application of FA in various fields. Several research investigations in the context of the usages of above minerals have been accounted while addressing on natural and mechanical aspects at the earlier-mentioned modern exercises that include take-up of poisons from wastewaters, biological rebuilding, and soil revisions and organics squander fertilizing the soil. In similar, attention was paid at the synthesis of K-zeolites from FA and its impactful use which seems additionally intrigue and lead to the progress of the studies on concentrated amalgamation of phillipsite and chabazite for potential farming purposes. In recent development, the major interest for making has been investigated owing to the latent capacity application in farming as moderate discharge composts (Hermassi et al. 2020). Due to the various salient features, FA is broadly used in the manufacture of bricks, cement, and lighter construction aggregate, cellular concrete, concrete, and as soil stabilizer. At the same time, there is an increase in environmental concern in most countries on utilization of FA for various industrial practices, and it is being regulated by their respective governments through legislation. To illustrate in Indian scenario, clay brick industries will have to use a minimum of 25% FA in the brick-making system and if the industry of this domain found within 100 km of thermal plants (coal-based electricity generation) (Çiçek and Çinçin 2015).

Keeping in concerns over development of environmentally power sources that has led to exploration on application of hydrogen as an innovative and alternative energy carrier. Some research studies demonstrated about suitable adoption of materials-based storage as promising one for application of hydrogen storage prospective while making usages of mainly porous-based materials. This includes metal-organic frameworks (MOFs), zeolites, and activated carbons because of their excellent physical properties in order to capture hydrogen in it. One of the materials like carbons as template form which is typically a micro-/meso-porous material which is synthesized by combining carbon as a precursor with micro/meso-channels at the targeted inorganic template(s). As per reported works, the application of zeolites showed the potential one as it led to synthesis micro-/meso-porous carbon which has large pore volume, high surface area that ensures to be an excellent sorbent material on taking-up hydrogen. It is assessed that overall expenses for the synthesis of zeolite-X from FA cost approximately one-fifth of zeolite being manufactured commercially. Thus the usages of FA (derived zeolites) appear to be highly promising and impressive for manufacturing the zeolite-templated carbons while looking at its effectiveness and economical prospectives. The use of FA zeo-litization in synthesizing templated carbons further assures the scope on future larger use of CFA with greater beneficiation (Musyoka et al. 2015)

20.2 Environmental Pollution Due to Coal Waste

Thermal waste or CFA is the residue of coal after the complete coal combustion at 12,000–15,000 °C by the electricity generation power plants which have been creating serious environmental problems worldwide (Lieberman et al. 2015). India has the largest reservoir of coal among the other countries around the world. Several electricity generation plants use bituminous and sub-bituminous types of coal which produce a massive amount of CFA (Dwivedi and Jain 2014; Haleem et al. 2016; Alami and Akhtar 2011). Generally, bituminous and sub-bituminous types of coal contain more than 40% ash. At present, country like India generates about 180 Million ton of CFA waste and that is around 120 preexisting coal-based electricity power stations of India (Lokeshappa and Dikshit 2011; Tiwari et al. 2016). As the generation of FA is abundant and thereby, the required dumping area for their disposal is pretty high that may lead to cause the disposal issue as the toxicity concern is associated due to the water contamination occurs by leaching of substantial heavy metals into groundwater. It not only contaminates ground water but also directly affects the air quality leading to cause air pollution (Changa et al. 2009). In this way the disposal issue due to FA from resulted out of all CFAs causes serious issues at the environment. FA creations from an assortment of coal-burning units show a broad range of various kinds of elemental composition. For the most part, the components which are available in FA are underneath nuclear number 92 (Senapati 2011). At about 70 tons NO₂, 200 metric tons SO₂, and an ~500 tons FA are being generated on a daily basis by the 500 Megawatt thermal power plant. Therefore, one of the air pollutants such as particulate matter is regarded as a wellspring of air pollution which comprises from FA (Dwivedi and Jain 2014).

20.2.1 *Effects Due to Heavy Metals*

The toxic heavy metals including Ni, As, Cr, Pb, Cd, Sb, and several others are claimed to be in the FA phase. The fine particles of these toxic heavy metals which are present in CFA reach the pulmonary region of the lungs during the breathing process and accumulated there for a long period, which is generally a cumulative poison for our body (Zhipeng et al. 2015). Those submicron particles of the toxic heavy metals go further into the lungs which accumulated on the outside source of the alveolar wall after these particles could be moved to the circulatory system and mixed with blood plasma through the cell membrane. Those Silica residual particles (40–73%) cause silicosis, an interstitial lung disease (Dwivedi and Jain 2014; Senapati 2011). FA disposal can be done in both form (dry or wet) but in the dry state there is the possibility to be flown through the wind, so thermal industries dispose the FA in the wet state to minimize the FA flow due to wind. In the case of wet state, this coal waste also hampers the environment by transferring the heavy metal into the soil. The migration of heavy metals into soil from FA causes soil

pollution as well as groundwater pollution. Biologically these heavy metals are non-degradable and also do not get transformed into harmless products unlike other organic wastes. In a study conducted by the researchers in Japan, they have shown that CFA could fulfill the landfill disposal criteria up to a significant extent. In 1989, the waste management regulation assured that FA is non-hazardous if properly handled. So at present scenario, the thermal industries dumped the FA by setting up an ash pond (generally in slurry form) (Tiwari et al. 2016).

20.2.2 Effects Due to Toxic Trace Elements

The direct use of CFA in the construction of roadways has become a potential risk as it contains a significant amount of toxic elements such as As, Cd, Hg, Se, V, Pb, Ni, Ba, Cr, and Zn. In the present scenario, it is estimated that at 0.6 ha per MW thermal industries are needed to dispose FA with an overall amount of 82,200 Ha per annum (Dwivedi and Jain 2014; Tiwari et al. 2016). During dumping of FA in slurry form, it leaches out the soil when the toxic trace elements or metals particles are mixed up with the soil, so the leaching behavior of these toxic elements changed the soil properties, generally its fertility. Besides damaging the soil properties, these toxic trace elements also directly affect the groundwater and change its mineral levels, and substantially directly create concern health hazard. The pH-dependent tests are being used to understand or investigate the major toxic elements, so it can easily identify the environmental impacts (Komonweeraket et al. 2015). To address the environmental issues due to FA, some other processes that are being adopted by the thermal industries by which it can reduce the toxic amount in water. Generally, those thermal industries use high combustion temperature which could reduce Cd and Pb concentrations in FA by the volatile properties of metals (Gianoncelli et al. 2013).

20.2.3 Current Scenario of Manufacturing Products

CFA, being one of the wastes resulted out of high-temperature combustion process in coal industries, produce plenty of fine particles with high pozzolanic activity and concomitant heavy metals, which are proven to be hazardous to the environment. Hence many innovative technologies are coming up which dedicate them to produce different by-products made up of CFA. One of such processes which use hydrothermal approach has been adopted for the synthesis of tobermorite fibers, and to it slaked lime and CFA are blended (Cao et al. 2020). On the other hand, other study illustrates on sythesis of an environmentally friendly catalyst (used for methanolysis) using mixture of chicken eggshells and lignite-type carbon-based CFA (Pavlović et al. 2020). By the use of PET fibers with FA, properties of the structural performance of concrete (Kassa et al. 2019b) could be improved. It is also used in carbon

fixation, as a CO₂ storage medium, capture material, and as a catalyst for supporting CO₂ in numerous processes (Dindi et al. 2019). Furthermore, the porosity nature relies on its use as a suitable adsorbent of CFA, and overall the CFA shows the potential source in connection with the cost as well as environmental friendly aspect as it bears alumina-silicate which substantially helps in the removal of various water as well as air pollutants (Asl et al. 2019). The manufacture of sustainable and inexpensive material from high-calcium-bearing FA has been reported (Ngenkham et al. 2020).

20.2.3.1 Manufacturing Products Like Ceramic

CFA is comprised of various metals and non-metal oxides (Fe₂O₃, Al₂O₃, SiO₂, and CaO) which is regarded as a promising material for the production of various commercial products including various ceramics. The generation process mainly depended upon maintaining temperature of the feed CFA and the supplement co-reagents that is responsible for making the composite ceramic or glass. The filtering material (ceramic membranes) obtained out of CFA is effectively prepared on remediation study industrial effluent bearing dyes. CFA has been used as a suitable substitute by replacing kaolinite while assembling at the cordierite-type ceramic (Blissett and Rowson 2012). To safeguard the environmental concern, FA is investigated as the prime source for production of cordierite. These types of ceramics are generally utilized in making microelectronic-based segments which is used as a catalyst substrate during combustion of engine. Subsequently, an issue was sought after to assembling of the cordierite in an inexpensive way by dosing FA having the key components as alumina (Al₂O₃) and silica (SiO₂). Cordierite blend is done utilizing crude materials FA, dopants, and magnesia, for example, TiO₂, CeO₂, and ZrO₂ at various levels (5–20 wt.%). The hardness, fracture durability, and flexible strength were enhanced by the incorporation of the dopant into the cordierite matrix (Senthil et al. 2019; Kim et al. 2020a). FA was found as a promising natural waste material for making pure form of cordierite at the condition where low temperature supplement is needed, and the overall mechanical properties of the final product could considerably improve.

20.2.3.2 Manufacturing Products Like Concrete

The low content of FA does not provide adequate strength while in concrete phase as compared with pure concrete cement. From experimental studies, it was observed that the compressive strength usually improves at the concrete with a proportionate dose of FA and therefore it becomes essential to incorporate a requisite quantity of FA during concrete cement preparation process. Moreover, the improvement in such mechanical properties of concrete is warranted for longer run of its usages (Fanghui et al. 2015). The substitution of FA in place of cement in concrete further enhances the working ability and also reduces drying shrinkage, blending, reinforcement

corrosion of concrete by decreasing the temperature for hardening of concrete and thereby several beneficitation could be achieved (Rivera et al. 2015). The reason for attaining improved concrete performance due to the addition of FA or silica fume is owing to the production of C–S–H (Supit et al. 2014; Trisnaliani et al. 2019). In addition, high performance in terms of the strength on the structure of reinforced concrete is strongly influenced with penetration of chloride ion in it. Thus, FA is used in the process for reduction of permeability of concrete to protect the reinforced concrete (affected due to chloride ion effects encountered at the submarine and costal environments) (Chousidis et al. 2016). It was also noticed that the degree of fineness of FA particles could increase the performances in the context of offering better strength, quality and durability towards making concrete. Furthermore the consistency of concrete is again depended on the adequate content of silica to be incorporated as it is a bigger constituent for providing strength at the concrete phase.

20.2.3.3 Manufacturing Products Like Matrix

Metal matrix composite is manufactured to provide the best operating performance and wears resistance applications. During the operation of automobile components (crankshafts, brake, drums, cylinder liner piston), these metal matrices imparts resistance in over-the-counter source. For these purposes, aluminum matrix composite gives the best wear resistance during machine operations. The aluminum matrix composite (AMC) is produced by incorporating FA molecules in the range of 5–15% (weight ratio) with respect to the molten metal by casting stir route. As a result, the composite enhances the impact, hardness, and tensile cum compressive tensile strength, but the composite density follows a decreasing trend. By increasing the FA content, the dry sliding wear, as well as slurry erosive wear, got improved. The improvement in reduction of tensile strength and rise in compression strength during fabrication of AMC and FA molecules are observed at squeeze casting process, which are homogeneously dispersed since they are of porosity-free FA composite particle. Generally, a 20% FA molecule was thoroughly mixed with aluminum powder to form AMC in powder form. By the use of Pin on the disc machine, the composites are tested against the spheres of alumina. The high content of Si and Ca particles of FA showed improvement at the tribo-performance of aluminum matrix composite (AMC). At the same time the addition of FA dose as much as up to 15% leads to decrease in the wear resistance activity of overall composites. With the increase in FA percentage, the abrasive wear resistance of the composite increased, and ~5% of FA when mixed with MMC showed higher resistance to the rough wear over the other samples. During the squeeze casting process, a strong bond is created between FA particles and matrix material. All categories of the pore, size as well as the voids were removed with supplement load of squeeze pressure while carrying out squeeze casting process. This provides a compact bonding linkage among dispersed and continuous phase molecules resulting on increase in the composite strength of the product (Bharathi et al. 2017; Liu et al. 2019).

20.2.4 Types of Products

CFA is often obtained after combustion (burning coal) in electricity generation process. Over the past few decades, the utilization of FA as an industrial by-product for several applications has received remarkable attention in worldwide in the domain of industrial waste management. The diverse use of CFA as a valuable raw material ensures suitability of FA use in greater way and its potential economic importance. It can be used for soil improvement in agriculture, in the synthesis of ceramics and glass items of good economic value, formation of zeolites, generation of mesoporous, synthesis of geopolymers by the process of amalgamation, and acts as a good adsorbent for wastewater treatment processes and toxic gases, as catalysts and catalyst support, and for removal of trace as well as heavy metals that are detrimental to environment. By the upliftment of various new innovative technologies, a series of differentiation and different combinations are done to generate hollow microspheres, magnetic spheres, enriched carbon, coarse ash products, and fine ash products. Implementations of these CFA-based products are consistent and cost-effective. There is also a significant efficiency for the enhanced utilization of CFA in both its raw-cum-refined state. It is also a known fact now that by successfully preparing the CFA, the scope of initiating the innovative industrial synergies enhances and also turns to save the nature from the harmful effects of CFA (Blissett and Rowson 2012). The FA production and utilization from thermal power plant from the year 1997 to 2017 are shown in Table 20.1, Figs. 20.1 and 20.2.

20.2.4.1 Fabrication Microfiltration Membrane

The treatment process for the separation of oil from the oily wastewater has been done by several methods like gravity separation, skimming, de-emulsifications, dissolved air floatation, electro-coagulation process, and flocculation, but almost all of the methods do not achieve the efficient separation. Furthermore, they produce a large quantity of various secondary wastes. Ceramic membranes used for industrial applications are considered to be more prominent in the present scenario because it fulfills all of the features like mechanical, chemical, and thermal properties, long shelf life, better defouling aspect and suitable combinations of extraction efficiency (increase in the flux on resulting maximum separation efficiency during the treatment process). FA is incorporated in making of ceramic membrane which acts as a

Table 20.1 Production and utilization of fly ash (FA) in India

Description	2010–2011	2011–2012	2012–2013	2013–2014	2014–2015	2015–2016	2016–2017
FA production, %	131	145.4	163.5	172.8	184.1	176.7	169.2
FA utilization, %	55.8	58.5	61.4	57.4	55.7	60.9	63.3



Fig. 20.1 Thermal power plants distribution in India (MW/annum)

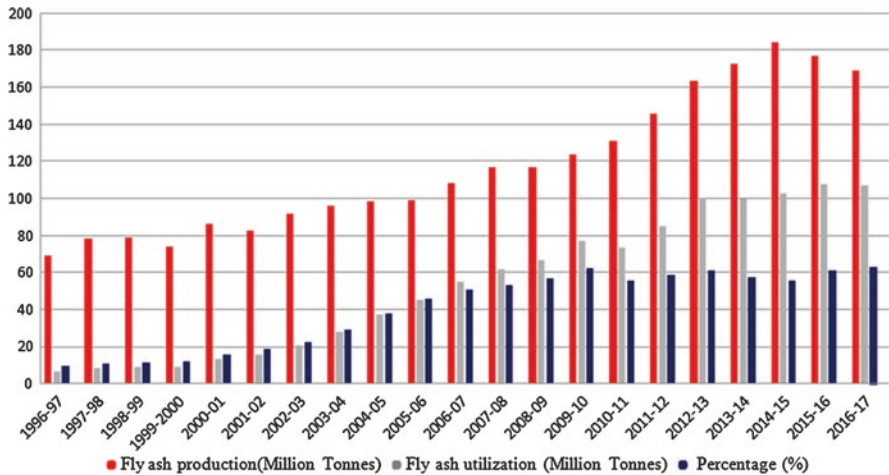


Fig. 20.2 FA production and utilization during 1996–1997 to 2016–2017 (Source-Report on FA Generation at Coal/Lignite based Thermal Power Station and its utilization, CEA, New Delhi)

major inorganic precursor for preparation of affordable and economical ceramic membranes through uni-axial dry compaction method and this it was reportedly successful for efficient oil–water emulsions separation. The average porosity was experimentally evaluated, i.e., 30 for M1, 39 for M2, and 43% for M3 types of three different membranes. Excellent chemical, thermal, and mechanical strength

properties of these membranes are shown when sintered at 1100 °C. The membrane porosity is being easily standardized by standardizing the concentration of CaCO₃ and FA. The prepared membrane with different concentrations of FA provides excellent mechanical strength (in the range of 1.68–9.25 MPa). The membrane permeability is estimated to be 5.384×10^{-6} , 6.508×10^{-6} , 9.53×10^{-6} m/s kPa, and the pore diameter is determined as 1.41, 1.36, and 1.53 μm at the above respective employed membrane sequences. The experimental research shows an excellent accomplishment in obtaining flux and the rejection of ceramic microfiltration membranes which are being prepared by the FA. On the other hand, it is also a cost-effective membrane manufacturing process (Suresh et al. 2016).

20.2.4.2 Geopolymer Synthesis

The particulate form of residue comes out of the coal-based power plant is commonly termed as CFA which is extensively used as a raw material for preparing the geopolymer product, and this kind of geopolymer appears to be an alternative replacement for the existing cement. This technology provides excellent usages of FA with minimum detrimental effects on nature (Zhuang et al. 2016). Some alkali-treated geopolymer copes up with the unfavorable results of concrete assembling. This type of geopolymer is generally made up of wood biomass and FA by the utilization of various curing strategies like control of water and temperature in the processes and control of the alkali (sodium hydroxide and silicate) activators. Cured geopolymers show diverse physical and chemical properties like adsorption of toxins and utilization as thick mortars (De Rossia et al. 2020; Kua et al. 2018). The high-calcium-based FA (HC) geopolymeric mortar incorporates natural zeolite (Z) and mullite, utilizes either Z or M or both together to enhance the fire resistivity of the geopolymeric composite. The strength quality is expended because of the formation of Yelimite and Wallastonite at very high temperatures, by the addition of Z and M (Bajpai et al. 2020; Wongsu et al. 2020). The process of geopolymerization follows the dissolution of alumina-silicate, alumina, and silica contained in the FA phase with the employed alkali solution. This further leads to the formation of combined speciation form of Al³⁺, Si⁴⁺ in the production of 3D amorphous type polymer (aluminum silicate). It was presumed that the polymerization prospective of geopolymer products out of Fa is mainly depending upon the physical properties along with the chemical assays in it. Furthermore, the role of curing conditions, alkali activators, and incorporation of fiber, slag, and red mud is shown to be critical in the above polymerization process (De Rossi et al. 2019).

20.2.4.3 Cements Production

Pozzolans type FA is found as a suitable alternative over the cement additives products. More than one ton CO₂ is being directly emitted into the environment out of one ton production of cement. Therefore, the adoption of FA (is being resulted from

thermal power plants) in cement manufacture industries appears to be worth, and as a result of which the CO₂ emission could be significantly minimized along with convincing low capital investment (Pedrazaa et al. 2015; Lee et al. 2016). The FA addition dose can be uplifting with increase in lime, and it mainly reacts with active lime resulting in enhancement of overall compressive strength during hydration process (Wu et al. 2014; Nguyen et al. 2015). The SiO₂ and Al₂O₃ of FA phase react with free lime and/or Ca(OH)₂ in order to increase the cement hydration process efficiency (Tudjonoa et al. 2014). FA is added to the cement composite to increase its performance to suit several conditions, such as to increase its ultimate strength. FA is composed of spherically shaped tiny particles which fits well with the available small voids and in consequences denser cement composites are formed. In this way, in installation process it needs lesser water content and thereby overall water consumptions could be reduced (Mohamad et al. 2019; Kassa et al. 2019a). FA is presently found as a complementary material with replacement of cement as much as 25–45%. **A noble approach including the adoption of FA** in aggregate form is practiced, and in that way the consumption of major dose of FA can be employed in the processes. Thus the usage of high-content FA leads to reduction in compressive strength and unit weight of product. The pozzolanic effect of FA causes a higher flexural strength. It may also result in the improved interracial transition zone with a greater value of FA usage ratio to that of the fine aggregate in place of sand during making of cement-based bricks (Fanghui et al. 2015; Bilir et al. 2015; Santamaria et al. 2016). The addition of FA in mortar mixtures showed resistance with a greater curing time and while adding ~23% of FA into the cement mixtures, which imparts several benefits. Overall, the manufacturing process becomes an inexpensive tool, and the issues due to the storing of huge quantity of FA in the power plants could be resolved. The overall utilization of FA for cement production from the year 2010 to 2019 is shown in Table 20.2.

20.2.4.4 Bricks Manufacturing

The synthetic pozzolanic character of FA is because of the constituents accomplishing amorphous silicate minerals. Usually pozzolanic ash does react with slaked lime and water to form the complex, i.e., CaO–Al₂O₃–SiO₂–H₂O (Çiçek and Çinçin 2015). The fired clay type bricks have been used on masonry constructed structures and at present scenario governmental authorities have put the regulation to use a greater quantity of FA and to conserve the natural resources, in brick-making processes. Apart from that, the use of fossil fuels for burning purpose in the production of clay bricks is being strictly avoided. Therefore, the adoption of FA bricks manufacture process provides the excellent salient features including air-cured and hydraulic-pressed nature which lead to have the solution of avoiding natural sources use as fuel in brick making and while conserving these natural source. In this way reduction of greenhouse emissions could be attained up to considerable extent (Sahu et al. 2019; Kirankumar et al. 2016). The key chemical constituents such as aluminum, silica oxide, and ferrites help providing strength to the bricks that are

Table 20.2 FA Utilization in India from 2014 to 2019

Mode of utilization	2014–2015		2015–2016		2016–2017		2017–2018		2018–2019	
	MT	%	MT	%	MT	%	MT	%	MT	%
Cement	43.33	42.36	43.38	40.32	40.59	37.9	50.29	25.6	25.03	26.85
Mine filling	13.3	13	10.3	9.57	11.78	11	12.51	6.66	4.8	5.15
Bricks and tiles	12	11.73	14.7	13.66	14.91	13.92	17.69	9.01	8.06	8.65
Reclamation of low-lying area	11	10.75	12.5	11.62	11.04	10.31	20.57	10.48	9.01	9.66
Ash dyke raising	9.8	9.58	10.6	9.85	11.89	11.1	13.55	6.9	8.52	9.15
Roads	3.4	3.32	5	4.65	6.19	5.78	6.67	3.4	2.51	2.1
Agriculture	1.9	1.86	2.2	2.04	1.92	1.79	0.573	0.29	0.071	0.77
Concrete	0.76	0.74	0.78	0.72	0.76	0.71	1.29	0.66	0.0966	1.04
Hydropower sector	0.01	0	0.04	0.03	0.02	0.02	0.007	0.004	0	0
Others	6.86	6.71	8.12	7.55	7.98	7.45	8.68	4.42	4.43	476
Total generation	102.33	55	107.62	60.8	107.1	63.28	131.83	67.42	62.53	539.37
Utilizes fly ash	81.68	44.39	69.38	39	62.16	36.72	64.57	32.87	29	31.28
Total	184		177		169.26		196.4		91.53	570.65

being prepared out of the manufacturing process. Moreover, the bricks' performance seems to be significantly improved due to the incorporation of sodium silicate in it. Furthermore, an increase in the volume of sodium silicate during brick-making process showed a reduction in the water consumption during making of bricks. The improvement in the compressive strength of the bricks is found to be mainly dependent upon the increase in the amount of sodium silicate incorporated in it, and in addition it again helps to improve corrosion resistivity to the CFA-based bricks. The possibility of insoluble metal silicates due to the reaction of the metals present in the FA phase with sodium silicate is encountered during the making of bricks (Moyo et al. 2019; Chen et al. 2020). Overall the conductivity due to heat of the CFA bricks determined to be $0.22 \text{ W m}^{-1} \text{ K}^{-1}$, thus assures much superior similarity index with the conventional aerated cellular concrete, and CFA brick seems promising over the fired clay bricks. In this way there are many practices of making CFA brick and thereby the disposal issues due to FA and so the environmental concern in this regard is seriously regulated. The incorporation of sodium silicate improves the execution of the bricks. The increase in the addition of FA dose results on the enhancement of apparent porosity as well as water absorption ability up to a significant level, and with a decrease in the bulk density and thermal conductivity (Ming et al. 2019).

20.2.4.5 Fertilizer Production

The chemical partition of phosphate by K-zeolites is extracted through hydrothermal transformation approach. The synthesis of Ca-bearing K-zeolites for further extracting the phosphate from the industrial effluent is investigated and reported by researchers. Generally those zeolites are by-product of CFA and are claimed to have enriched with the nutrient supplements (bears mainly good amount of P and K) and this prompts on potential use of CFA as slow-releasing fertilizer. The parameters like ratio of KOH-solution/FA, [KOH], time of activation time, and temperature were varied to investigate at two FA samples (FA-LB & FA-TE) and are reported. The resulted merlinoite and W containing zeolitic products from FA-LB and FA-TE were ascertained based on the analysis results after their sorption behavior toward the uptake of phosphate. The maximum phosphate loading capacity was of 250 mg P-PO₄/g for KP1-LB and 142 mg P-PO₄/g for the KP1-TE types of the zeolitic products. The phosphate sorption was consistent at the studied pH range (6–9) during the remediation study of waste effluents. It was reported that the above sorption process is based on diffusion-controlled mechanism in which phosphate ions are found in combined from with Ca. Thus this phosphate-enriched mineral in the CFA phase is used as an excellent sorbent material and that subsequently can be applied as a slow-release fertilizer (Hermassi et al. 2020). The overall utilization of FA in agriculture sector from the year 2010 to 2019 is shown in Fig. 20.3 and Table 20.2.

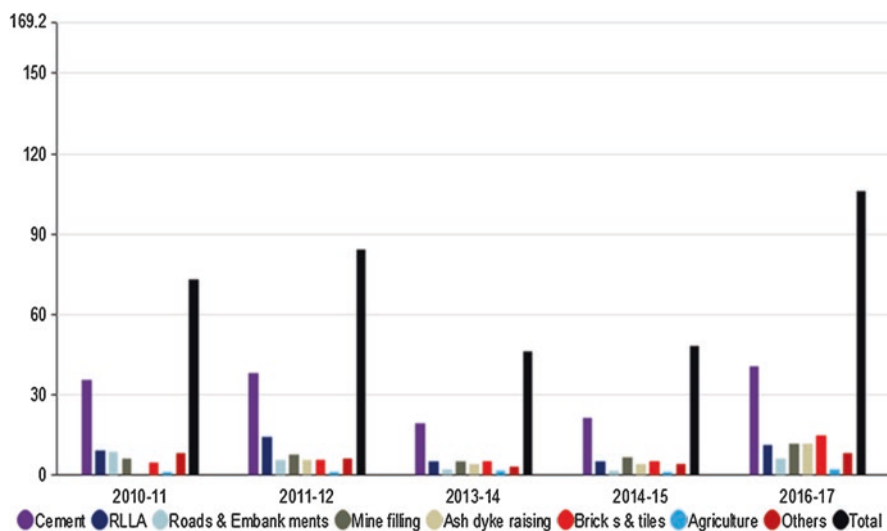


Fig. 20.3 Major modes of FA utilization from the year 2010–2011 to 2016–2017 (Source-Report on FA Generation at Coal/Lignite-based Thermal Power Station and its utilization in India, CEA, New Delhi)

20.2.4.6 Biodiesel Production

The synthesis of zeolitic material from FA is commonly termed as FA-ZM. In methanolysis process, CaO/-ZM catalyst shows more stability with comprehensively strong performances at optimum condition. Overall suitable condition; methanol/oil molar ratio of 6:1 at the set temperature of 60 °C was operated at the above reaction and where catalyst concentration has been kept constant, i.e., 6%. For the preparation of catalyst initially, zeolitic product was filtered and washed until the pH of the solution attained 9.0 by removing excess NaOH content. To obtain the pure form of the product after examining the catalytic activity, the resulted sample was subjected to drying (at 110 °C) and later on the chicken eggshells was properly washed with demineralized water to remove the entire impurities. The solid mass was finely ground to bring down the ZM into a fine powder form. By adding CaO powder with stick ZM stock, the overall content was periodically agitated at 700 rpm followed by hydration test which was examined for 6 h at 60 °C. Subsequently the hydrated product resulted was fed for further drying at 110 °C and calcined at 650 °C for the period of 4 h for obtaining CaO/ZM catalyst. The care was taken so as to avoid hygroscopic affinity of the respective catalyst; therefore, it was stored under desiccator. The generation of ME from the catalytic trans-esterification of oily feed stock was maximized to 97.8%. This process ensures the synthesis of an innovative catalytic product which is very cost-effective and is an active material made up of a very economical natural solid wastes like CFA and chicken eggshell. These processes comprise of methanolysis and that undergoes the trans-esterification process of sunflower oil for the production of the huge amount of Biodiesel (Pavlović et al. 2020).

20.2.4.7 Synthesis of Lathy Tobermorite Fibers

The newest value-added application of CFA is of synthesizing tobermorite fibers via the hydrothermal method. Due to its porous aggregation structures, tobermorite is a useful ingredient for making energy-saving building components. The porous aggregation structures look like calcium silicate board and aerated concrete block. In this way, the synthesis of tobermorite fibers from C would play a significant role in joining emission decrease in energy conservation. It is also noted that the porous aggregation structure can be destroyed with the addition of excessive high-concentration NaOH (above 40 g/L). The hydrothermal synthesis is a one-step method of tobermorite fibers synthesis by using a mixture of C and lime. Generally, tobermorite fibers are synthesized from a mixture of C and lime in aqueous solution at 170 °C for 12 h in 2000 L pilot-scale autoclave. Some researchers reported that the synthesis of tobermorite fibers from C is a “two-stage process.” In this process, alumina was first extracted from C by calcination followed by leaching, and the residue obtained in CFA after alumina extraction was further used to synthesize tobermorite fibers hydrothermally at 220 °C for 6 h. A huge amount of NaOH was used in the calcining-leaching or hydro-chemical processes for aluminum extraction from CFA which is difficult to control the suitable NaOH concentration for

tobermorite formation via the “two-stage process.” The synthesized tobermorite fibers show great properties as an adsorbent for the elimination of wastes from water. Furthermore, it shows the activity of thermally insulating material having possessed low thermal conductivity and apparent density (Ramanathan et al. 2020; Cao et al. 2020).

20.2.4.8 Fabrication of Composite Materials

In the automobile industry plastic products are widely used for various purposes in industries. It creates a harmful effect if it is not properly decomposed. Generally plastic materials takes too many years to get decomposed, and in addition it also causes air pollution while burnt in an open environment. Disposal of large quantities of plastic wastes creates a big problem for the environment due to its low biodegradability. So, at present there are significant research which are going to find the best possible ways for disposing of these wastes directly to the environment. The major components found from the municipality solid wastes (MSW) are of plastic which is a serious concern for the researchers to find an alternative possible way to use in making concrete like materials with good compact strength and light-weight feature of concrete. The most interesting way that was found by the researcher is the manufacturing of composite material by mixing of plastic powder and FA, which takes place in a vessel where the FA particles are uniformly dispersed in the melted plastic material. Then the resulting mixture is cooled to solidify the melted plastic powder material to form a hardened composite material. Plastic wastes can further be used by blending with the concrete mass without affecting its mechanical properties, but with a slight compromise in its strength. The combination of epoxy resin and the FA particles provided better the compressive strength of that composite and this may be due to the existence of strong interracial bond between FA particles and resin. SEM analysis suggests that the tiny ash particles are uniformly segregated (Gokulraj et al. 2019).

20.3 Conclusion

Fly ash obtained out of the thermal power plant sectors is becoming a vital source of raw material being exploited for making various advanced composite material. It is being widely utilized in the manufacturing of cement products, bricks, asbestos, wear resistance roads/embankments, and wall materials. The studies are administered for the improvement of crops, wastelands, and zeolites. The studies also show that these waste products have been discovered for wastewater treatment and purification as membrane filtration. It is being extensively utilized for manufacturing of wall materials and as a source for extracting out the metal values by various industries. It can even be utilized for massive production of biodiesel and fertilizer. FA bears the salient features accomplishing insensitiveness to change in moisture

content, nature of free draining, low relative density, simple compaction, and an excellent frictional property, and in consequences of which it can suitably be used on road making (as its zeolite form) in extensive way. The construction works and reclamation of low-lying areas can be accomplished by utilizing FA as a prime source. The key prospectives of fly ash utilization is of making value-added products which may substainly resolve the major environmental concerns that arise due to the issue of direct disposal. The futuristic prospective of FA utilization is challenging for the researchers, scientists, technologists, and engineers on development of eco-friendly technology with suitable disposition to the environment. As of now it has been realized that FA can be the promising source for building construction materials in an effective way. It has several advantages including the strength, economically feasibility, and environmentally acceptable relying which the various constructing products like bricks and concretes are being manufactured through various techniques. The guidelines for all electricity generation thermal stations regarding the disposal procedures or strategies should ensure the minimum opposite impact on the environment, and attempts should be consciously made to prevent the environmental damage by ensuring more effective disposal management of FA in the country like India, and the same prospective can be achievable across the other countries.

References

- Alami, J., & Akhtar, M. N. (2011). Fly ash utilisation in different sectors in Indian scenario. *International Journal of Emerging Trends in Engineering and Development*, 1(1), 1–14.
- Asl, S. M. H., Javadian, H., Khavarpour, M., Belviso, C., Taghavi, M., & Maghsudi, M. (2019). Porous adsorbents derived from coal fly ash as cost-effective and environmentally-friendly sources of aluminosilicate for sequestration of aqueous and gaseous pollutants: A review. *Journal of Cleaner Production*, 208, 1131–1147.
- Azhar, N. S. D. M., Zainal, F. F., & Abdullah, M. M. A. B. (2019). Effect of different ratio of geopolymer paste based fly ash-metakaolin on compressive strength and water absorption. *IOP Science, Materials Science and Engineering*, 701, 012010.
- Bajpai, R., Choudhary, K., Srivastava, A., Sangwan, K. S., & Singh, M. (2020). Environmental impact assessment of fly ash and silica fume based geopolymer concrete. *Journal of Cleaner Production*, 254, 120147.
- Belviso, C., Giannossa, L. C., Huertas, F. J., Lettino, A., Mangone, A., & Fiore, S. (2015). Synthesis of zeolites at low temperatures in fly ash-kaolinite mixtures. *Microporous and Mesoporous Materials*, 212, 35–47.
- Bharathi, V., Ramachandra, M., & Srinivas, S. (2017). Influence of fly ash content in aluminium matrix composite produced by stir-squeeze casting on the scratching abrasion resistance, hardness and density levels. *Materials Today: Proceedings*, 4, 7397–7405.
- Bilir, T., Gencel, O., & Topcu, I. B. (2015). Properties of mortars with fly ash as fine aggregate. *Construction and Building Materials*, 93, 782–789.
- Blissett, R. S., & Rowson, N. A. (2012). A review of the multi-component utilisation of coal fly ash. *Fuel*, 97, 1–23.
- Cao, P., Li, G., Luo, J., Rao, M., Jiang, H., Peng, Z., & Jiang, T. (2020). Alkali-reinforced hydrothermal synthesis of lathy tobermorite fibers using mixture of coal fly ash and lime. *Construction and Building Materials*, 238, 117655.

- Changa, C. Y., Wangb, C. F., Muib, D. T., & Chiangc, H. L. (2009). Application of methods (sequential extraction procedures and high-pressure digestion method) to fly ash particles to determine the element constituents: A case study for BCR 176. *Journal of Hazardous Materials*, 163, 578–587.
- Chen, F., Zhang, Y., Liu, J., Wang, X., Chu, P. K., Chu, B., & Zhang, N. (2020). Fly ash based lightweight wall materials incorporating expanded perlite/SiO₂ aerogel composite: Towards low thermal conductivity. *Construction and Building Materials*, 249, 118728.
- Chen, X., Wang, H., Najm, H., Venkateela, G., & Hencken, J. (2019). Evaluating engineering properties and environmental impact of pervious concrete with fly ash and slag. *Journal of Cleaner Production*, 237, 117714.
- Chousidis, N., Ioannou, I., Rakanta, E., Koutsodontis, C., & Batis, G. (2016). Effect of fly ash chemical composition on the reinforcement corrosion, thermal diffusion and strength of blended cement concretes. *Construction and Building Materials*, 126, 86–97.
- Chousidis, N., Rakanta, E., Ioannou, I., & Batis, G. (2015). Mechanical properties and durability performance of reinforced concrete containing fly ash. *Construction and Building Materials*, 101, 810–817.
- Çiçek, T., & Çiçin, Y. (2015). Use of fly ash in production of light-weight building bricks. *Construction and Building Materials*, 94, 521–527.
- De Rossi, A., Ribeiro, M. J., Labrincha, J. A., Novais, R. M., Hotza, D., & Moreira, R. F. P. M. (2019). Effect of the particle size range of construction and demolition waste on the fresh and hardened-state properties of fly ash-based geopolymer mortars with total replacement of sand. *Process Safety and Environmental Protection*, 129, 130–137.
- De Rossia, A., Simãoob, L., Ribeiroc, M. J., Hotza, D., & Moreira, R. D. F. P. M. (2020). Study of cure conditions effect on the properties of wood biomass fly ash geopolymers. *Journal of Materials Research and Technology*, 09, 7518–7528.
- Dindi, A., Quang, D. V., Vega, L. F., Nashef, E., & Abu-Zahra, M. R. M. (2019). Applications of fly ash for CO₂ capture, utilization, and storage. *Journal of CO₂ Utilization*, 29, 82–102.
- Duan, P., Yan, C., Zhou, W., & Ren, D. (2016). Fresh properties, compressive strength and microstructure of fly ash geopolymer paste blended with iron ore tailing under thermal cycle. *Construction and Building Materials*, 118, 76–88.
- Dutta, S., Nadaf, M. B., & Mandal, J. N. (2016). An overview on the use of waste plastic bottles and fly ash in civil engineering applications. *Procedia Environmental Sciences*, 35, 681–691.
- Dwivedi, A., & Jain, M. K. (2014). Fly ash – waste management and overview: A Review. *Recent Research in Science and Technology*, 6, 30–35.
- Fang, G., & Zhang, M. (2020). The evolution of interfacial transition zone in alkali-activated fly ash-slag concrete. *Cement and Concrete Research*, 129, 105963.
- Fannghui, H., Qiang, W., & Jingjing, F. (2015). The differences among the roles of ground fly ash in the paste, mortar and concrete. *Construction and Building Materials*, 93, 172–179.
- Gianoncelli, A., Zacco, A., Struis, R. P. W. J., Borgese, L., Depero, L. E., & Bontempi, E. (2013). Fly ash pollutants, treatment and recycling. In E. Lichtfouse, J. Schwarzbauer, & D. Robert (Eds.), *Pollutant diseases, remediation and recycling. Environmental chemistry for a sustainable world* (Vol. 04, pp. 103–213). Cham: Springer.
- Gokulraj, S., Shakthivel, T. K., Thirunavukarasu, S., & Myilnagaraja, B. (2019). brication of composite material using fly ash and plastic powder. *International Journal of Innovative Research in Advanced Engineering*, 06, 45–48.
- Haleem, A., Luthra, S., Mannan, B., Khurana, S., Kumar, S., & Ahmad, S. (2016). Critical ctors for the successful usage of fly ash in roads & bridges and embankments: Analyzing indian perspective. *Resources Policy*, 49, 334–348.
- Hermassi, M., Valderrama, C., Font, O., Moreno, N., Querol, X., Batis, N. H., & Cortina, J. L. (2020). Phosphate recovery from aqueous solution by K-zeolite synthesized from fly ash for subsequent valorisation as slow release fertilizer. *Science of the Total Environment*, 731, 139002.

- Hu, Y., Tang, Z., Li, W., Li, Y., & Tam, V. W. Y. (2019). Physical-mechanical properties of fly ash/GGBFS geopolymer composites with recycled aggregates. *Construction and Building Materials*, 226, 139–151.
- Kassa, R. B., Kanali, C., & Ambassah, N. (2019a). Engineering properties of polyethylene terephthalate fibre reinforced concrete with fly ash as a partial cement replacement. *IISTE Civil and Environmental Research*, 11, 25–34.
- Kassa, R. B., Kanali, C., & Ambassah, N. (2019b). Flexural performance evaluation of polyethylene terephthalate fibre reinforced concrete with fly ash as a partial cement replacement. *International Journal of Engineering Research and Technology*, 12, 1417–1422.
- Kim, M., Ko, H., Kwonb, T., Bae, H. C., Jang, C. H., Heo, B. U., & Parka, S. M. (2020a). Development of novel refractory ceramic continuous fibers of fly ash and comparison of mechanical properties with those of E-glass fibers using the Weibull distribution. *Ceramics International*, 46, 13255–13262.
- Kim, T., Ley, M. T., Kang, S., Davis, J. M., Kim, S., & Amrollahi, P. (2020b). Using particle composition of fly ash to predict concrete strength and electrical resistivity. *Cement and Concrete Composites*, 107, 103493.
- Kirankumar, G., Saboor, S., & Babu, T. P. A. (2016). Investigation of different window and wall materials for solar passive building design. *Procedia Technology*, 24, 523–530.
- Komonweeraket, K., Cetin, B., Benson, C. H., Aydilek, A. H., & Edil, T. B. (2015). Leaching characteristics of toxic constituents from coal fly ash mixed soils under the influence of pH. *Waste Management*, 38, 174–184.
- Kua, T. A., Imteaz, M. A., Arulrajah, A., & Horpibulsuk, S. (2018). Environmental and economic viability of Alkali Activated Material (AAM) comprising slag, fly ash and spent coffee ground. *International Journal of Sustainable Engineering*, 12, 223–232.
- Lee, H., Vimonsatit, V., & Chindaprasirt, P. (2016). Mechanical and micromechanical properties of alkali activated fly-ash cement based on nano-indentation. *Construction and Building Materials*, 107, 95–102.
- Lieberman, R. N., Green, U., Segev, G., Polat, M., Mastai, Y., & Cohen, H. (2015). Coal fly ash as a potential fixation reagent for radioactive wastes. *Fuel*, 153, 437–444.
- Liu, L., Peng, B., Yue, C., Guo, M., & Zhang, M. (2019). Low-cost, shape-stabilized fly ash composite phase change material synthesized by using a cile process for building energy efficiency. *Materials Chemistry and Physics*, 222, 87–95.
- Lokeshappa, B., & Dikshit, A. K. (2011). Disposal and management of coal fly ash. *IPCBBE*, 03, 11–14.
- Mármol, G., Savastano, H., Jr., Monzó, J. M., Borrachero, M. V., Soriano, L., & Payá, J. (2016). Portland cement, gypsum and fly ash binder systems characterization for lignocellulosic fiber-cement. *Construction and Building Materials*, 124, 208–218.
- Ming, L. Y., Sandu, A. V., Yong, H. C., Tajunnisa, Y., Azzahran, S. F., Bayuji, R., Abdullah, M. M. A. B., Vizureanu, P., Hussin, K., Jin, T. S., & Loong, F. K. (2019). Compressive strength and thermal conductivity of fly ash geopolymer concrete incorporated with lightweight aggregate, expanded clay aggregate and foaming agent. *Revista de Chimie*, 70, 4021–4028.
- Moftt, E. G., Thomas, M. D. A., & Him, A. (2017). Performance of high-volume fly ash concrete in marine environment. *Cement and Concrete Research*, 102, 127–135.
- Mohamad, M., Noor, M. M., & Key, T. P. (2019). Compressive strength of foamed cement composites with the addition of fly ash and polystyrene beads. *Advanced Journal of Technical and Vocational Education*, 03, 01–06.
- Moyo, V., Mguni, N. G., Hlabangana, N., & Danha, G. (2019). Use of coal fly ash to manufacture a corrosion resistant brick. *Procedia Manufacturing*, 35, 500–512.
- Musyoka, N. M., Ren, J., Langmi, H. W., North, B. C., & Mathe, M. (2015). A comparison of hydrogen storage capacity of commercial and fly ash-derived zeolite X together with their respective templated carbon derivatives. *International Journal of Hydrogen Energy*, 40, 12705–12712.

- Natha, P., Sarkera, P. K., & Rangan, V. B. (2015). Early age properties of low-calcium fly ash geopolymer concrete suitable for ambient curing. *Procedia Engineering*, *125*, 601–607.
- Ngernkham, T. P., Phiangphimai, C., Intarabut, D., Hanjitsuwan, S., Damrongwiriyunapap, N., Li, L. Y., & Chindaprasirt, P. (2020). Low cost and sustainable repair material made from alkali-activated high-calcium fly ash with calcium carbide residue. *Construction and Building Materials*, *247*, 118543.
- Nguyen, H. A., Chang, T. P., Shih, J. Y., Chen, C. T., & Nguyen, T. D. (2015). Influence of circulating fluidized bed combustion (CFBC) fly ash on properties of modified high volume low calcium fly ash (HV) cement paste. *Construction and Building Materials*, *91*, 208–215.
- Nie, Q., Zhou, C., Li, H., Shu, X., Gong, H., & Huang, B. (2015). Numerical simulation of fly ash concrete under sulfate attack. *Construction and Building Materials*, *84*, 261–268.
- Pavlović, S. M., Marinković, D. M., Kostić, M. D., Častvan, I. M. J., Mojović, L. V., Stanković, M. V., & Veljković, V. B. (2020). A CaO/zeolite-based catalyst obtained from waste chicken eggshell and coal fly ash for biodiesel production. *Fuel*, *267*, 117171.
- Pedrazaa, S. P., Pinedaa, Y., & Gutiérrez, O. (2015). Influence of the unburned residues in fly ash additives on the mechanical properties of cement mortars. *Procedia Materials Science*, *09*, 496–503.
- Ramanathan, S., Gopinath, S. C. B., Arshad, M. K. M., & Poopalan, P. (2020). Nanostructured aluminosilicate from fly ash: Potential approach in waste utilization for industrial and medical applications. *Journal of Cleaner Production*, *253*, 119923.
- Ren, X., Liu, S., Qu, R., Xiao, L., Hu, P., Song, H., Wu, W., Zheng, C., Wu, X., & Gao, X. (2020). Synthesis and characterization of single-phase submicron zeolite Y from coal fly ash and its potential application for acetone adsorption. *Microporous and Mesoporous Materials*, *295*, 109940.
- Ridtirud, C., & Chindaprasirt, P. (2019). Properties of light weight aerated geopolymer synthesis from high-calcium fly ash and aluminium powder. *International Journal of Geomate*, *16*, 67–75.
- Rivera, F., Martínez, P., Castro, J., & López, M. (2015). Massive volume fly-ash concrete: A more sustainable material with fly ash replacing cement and aggregates. *Cement and Concrete Composites*, *63*, 104–112.
- Roviello, G., Ricciotti, L., Molino, A. J., Menna, C., Ferone, C., Cio, R., & Tarallo, O. (2019). Hybrid geopolymers from fly ash and polysiloxanes. *Molecules*, *24*, 3510.
- Sahu, S., Sarkar, P., & Davis, R. (2019). Quantification of uncertainty in compressive strength of fly ash brick masonry. *Journal of Building Engineering*, *26*, 100843.
- Santamaría, A., Rojí, E., Skaf, M., Marcos, I., & González, J. J. (2016). The use of steelmaking slags and fly ash in structural mortars. *Construction and Building Materials*, *106*, 364–373.
- Senapati, M. R. (2011). Fly ash from thermal power plants waste management and overview. *Current Science*, *100*, 1791–1794.
- Senthil, K. M., Vanmathi, M., Senguttuvan, G., Mangalaraja, R. V., & Sakthivel, G. (2019). Fly ash constituent-silica and alumina role in the synthesis and characterization of cordierite based ceramics. *SILICON*, *11*, 2599–2611.
- Seto, K. E., Churchill, C. J., & Panesar, D. K. (2017). Influence of fly ash allocation approaches on the life cycle assessment of cement-based materials. *Journal of Cleaner Production*, *157*, 65–75.
- Shaikh, F. U. A., & Supit, S. W. M. (2015). Chloride induced corrosion durability of high volume fly ash concretes containing nano particles. *Construction and Building Materials*, *99*, 208–225.
- Sharma, V., & Akhai, S. (2019). Trends in utilization of coal fly ash in India: A review. *Journal of Engineering Design and Analysis*, *02*, 12–16.
- Silva, S. R. D., & Andrade, J. J. D. O. (2017). Investigation of mechanical properties and carbonation of concretes with construction and demolition waste and fly ash. *Construction and Building Materials*, *153*, 704–715.
- Supit, S. W. M., Shaikh, F. U. A., & Sarker, P. K. (2014). Effect of ultrafine fly ash on mechanical properties of high volume fly ash mortar. *Construction and Building Materials*, *51*, 278–286.

- Suresh, K., Pugazhenth, G., & Uppaluri, R. (2016). Fly ash based ceramic microfiltration membranes for oil-water emulsion treatment: Parametric optimization using response surcmethodology. *Journal of Water Process Engineering*, 13, 27–43.
- Tennakoon, C., Crentsil, K. S., Nicolas, R. S., & Sanjayan, J. G. (2015). Characteristics of Australian brown coal fly ash blended geopolymers. *Construction and Building Materials*, 101, 396–409.
- Tennakoon, C., Nazari, A., Sanjayan, J. G., & Crentsil, K. S. (2014). Distribution of oxides in fly ash controls strength evolution of geopolymers. *Construction and Building Materials*, 71, 72–82.
- Tiwari, M. K., Bajpai, S., & Dewangan, U. K. (2016). Fly ash utilization: A brief review in Indian context. *International Research Journal of Engineering and Technology (IRJET)*, 03, 949–956.
- Trisnaliani, L., Purnamasari, I., & Ahmadan, F. (2019). Performance of silica membranes from fly ash coal of PT semen baturaja in reducing metal content in mine acid water. *Indonesian Journal of Fundamental and Applied Chemistry*, 04, 9–14.
- Tudjonoa, S., Purwanto, X. X. X., & Apsari, K. T. (2014). Study the effect of adding nano fly ash and nano lime to compressive strength of mortar. *Procedia Engineering*, 95, 426–432.
- Velandia, D. F., Lynsdale, C. J., Provis, J. L., Ramirez, F., & Gomez, A. C. (2016). Evaluation of activated high volume fly ash systems using Na₂SO₄, lime and quicklime in mortars with high loss on ignition fly ashes. *Construction and Building Materials*, 128, 248–255.
- Wongsa, A., Wongkvanklom, A., Tanangteerapong, D., & Chindaprasirt, P. (2020). Comparative study of fire-resistant behaviors of high-calcium fly ash geopolymer mortar containing zeolite and mullite. *Journal of Sustainable Cement-Based Materials*, 9(5), 307–321.
- Wu, T., Chi, M., & Huang, R. (2014). Characteristics of CFBC fly ash and properties of cement-based composites with CFBC fly ash and coal-fired fly ash. *Construction and Building Materials*, 66, 172–180.
- Zhang, Z., Wang, H., Zhu, Y., Reid, A., Provis, J. L., & Bullen, F. (2014). Using fly ash to partially substitute metakaolin in geopolymer synthesis. *Applied Clay Science*, 88–89, 194–201.
- Zhipeng, T., Bingru, Z., Chengjun, H., Rongzhi, T., Huangpu, Z., & Fengting, L. (2015). The physiochemical properties and heavy metal pollution of fly ash from municipal solid waste incineration. *Process Safety and Environmental Protection*, 98, 333–341.
- Zhuang, X. Y., Chen, L., Komarneni, S., Zhou, C. H., Tong, D. S., Yang, H. M., Yu, W. H., & Wang, H. (2016). Fly ash-based geopolymer: Clean production, properties and applications. *Journal of Cleaner Production*, 125, 253–267.

Chapter 21

Biochar Production for Green Environment



Ayantika Banerjee

21.1 Introduction

Biochar is produced from several organic material feedstock such as agricultural waste, sewage sludge and municipal wastes under thermal combustion process. Biochar generally contains rich carbon and nutrients such as ammonia. Biochar has the property of rich carbon content, large surface area, porosity, high cation exchange capacity, etc. (Rizwan et al. 2016), generated by pyrolysis or carbonization process, is able to remove organic materials, immobilize heavy metals, improve the soil quality and enhance the soil quality with nutrients. Pyrolysis is a thermochemical conversion technology which works in the nonappearance of oxygen, with or without the presence of catalyst used as an important way to produce biochar from several wastes. A research group has developed a new method of conversion technique called 'Low Temperature Conversion (LTC)' followed the study of conversion of industrial, urban and agricultural wastes (Bernardino et al. 2017).

Biochar always applicable in multidisciplinary areas like science and engineering (Mohan et al. 2014). Some researchers reported that the biochar application could increase the efficiency of N-fertilizer and soil quality (Mohan et al. 2014). Several studies about biochar production and application showed that huge production of agro-forestry residuals, sewage sludge and human wastes offers an abundant source for biochar production and that is also a big solution of waste utilization. Some researchers observed that in insertion of C (Lehmann et al. 2008) sequestering and GHG gas emission reduction, biochar also can increase the efficiency of

A. Banerjee (✉)

Decontamination and Decommissioning Division, Korea Atomic Energy Research Institute (KAERI), Daejeon, South Korea

Quantum Energy Chemical Engineering, University of Science and Technology (UST), Daejeon, South Korea

e-mail: banerjee93@kaeri.re.kr

soil-water-holding capacity (Woolf et al. 2010), crop yields, soil fertility, etc. (Warnock et al. 2007).

The quality of the carbon balance depends on the efficiency of the waste residue pyrolysis facilities. The nutrient contents in biochar depends on so many factors such as pyrolysis/carbonization temperature, type of biomass and reactor configuration. In the time of 1990s, increasing amount of cultivation was the most important source to make living in Sudan for around 61% of the working inhabitants (Morgan 2013). Research in biochar use in soil comes forward recently, but the concept arrived from the ancient soils related study in the Basin of Amazon. 'Terra preta de Indio' or 'black soil of the Indians' has been designed by some people, thousands of years ago, at that time those people gathered charcoal and a variety of wastes, nutrient trash such as animal bones (Morgan 2013).

Pyrolysis of biomass is a complicated procedure where biomass goes through thermochemical conversion in an oxygen-limited conditions and as result various products are produced. Biochar can form in different states like solid, liquid and gas. Through this conversion technique biomass converts to not only biochar but also bio-oil, biogas, etc. Pyrolysis generally follows different steps, and elemental arrangements in biomass is an important role towards char production.

This chapter reviews the several processes of biochar production and the conditions behind all mechanisms along with biochar application in soil and beneficial effects of it.

21.2 Biochar: Definition and Properties

Biochar which is short form of 'bio-charcoal' is a carbon product created by heating raw materials such as animal compost, plant residues in a closed system in the absence of air and also in low temperature (<700 °C) (Lehmann et al. 2008). Biochar is a new technology which can resolve several ecological problems and energy deficiencies in economical way with great environmental advantages (Nguyen et al. 2010). Biochar is a new addition in a carbon-negative strategy for improving the soil quality and providing agricultural advantages, and the structure of carbon is the key reason behind this. Biochar consists of rich contents of total and organic carbon, high level of biodegradability and optimal concentration of micro and macroelements such as copper, zinc, potassium and sodium (Hernandez-Mena et al. 2014).

Biochar is naturally prepared from a range of biomasses that consists of many physical and chemical properties. Thermal conversion process mainly depends on the properties of biomasses. Biomasses feedstock such as bioenergy crops, forest residues and organic wastes are used for the production of Biochar. Different feedstocks have different ratios of elements and would transfer to biomass when it is produced from those feedstocks. The properties of Biochar are related to the characteristics of feedstock characterization and the method of preparation.

21.3 Preparation of Biochar

Biochar is created through several conversion processes such as pyrolysis, gasification and source of biochar preparation (Wu et al. 2019). Common wastes such as animal wastes, sludge and agricultural wastes are produced in a huge amount, all over the world. Various process of pyrolysis and their operational conditions have been illustrated in Fig. 21.1. Preparing biochar from all those biomasses can actually resolve the waste problem and meet the environmental sustainability. Carbonization usually decomposes parts of biomass but preserves the carbon contents and also the properties are altered, so the product became more carbonaceous.

21.3.1 Pyrolysis

The term ‘Pyrolysis’ came from ‘lysis’ = breaking down and ‘pyro’ = material by heat. So basically it defines the process where material is going through breakdown process by heating it. Pyrolysis generally happens under oxygen-free condition at the temperature of 300–900 °C (Cha et al. 2016). During this process, solid as biochar, liquid as bio-oil and gas as syngas consist of CO₂, hydrogen, NO₂, etc. produced (Wang and Wang 2019). Generally, the pyrolysis of forest or agricultural-derived biomass residues generates biofuel and that may be ploughed into soils in crop fields which enhance the soil fertility. Pyrolysis also divided according to the speed of the process. Slow pyrolysis usually processed when the feedstock placed into the reactor at the beginning of the pyrolysis process, whereas fast pyrolysis takes place where the feedstock adds to the reactor when the temperature reaches high (Wang and Wang 2019). Slow pyrolysis is usually defined as continuous process, but fast pyrolysis process can be described as ‘quick heat transfer’ process (Nartey and Zhao 2014). Fixed carbon content usually increases with the increase

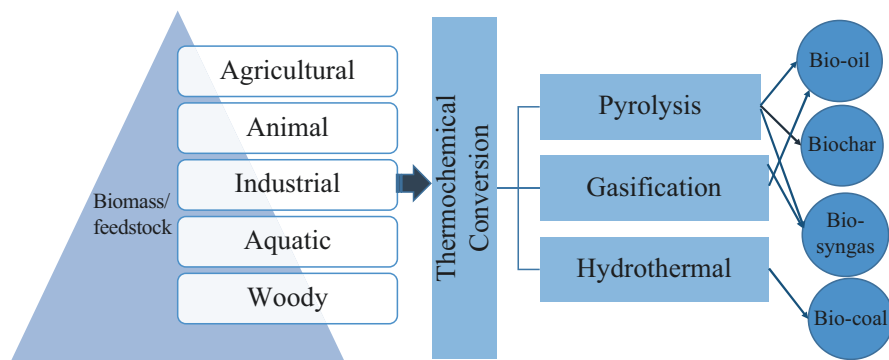


Fig. 21.1 Different procedure of biomass to generate biochar

of temperature, and peak temperature has an impact on surface area and core size of charcoal (Antal and Grønli 2003). Some studies reported that (Fig. 21.2) low surface area of charcoals can be pyrolyzed at a temperature of 500–550 °C (Khalil 1999). In the case of high moisture content, biomass pyrolysis is not suitable at all (Wang et al. 2018).

In the duration of fast pyrolysis, as temperature is high and for low residence time it enables the thermal cracking of biomass, which is the result of char formation (Mohan et al. 2006). To proceed the pyrolysis process, demand of energy is high and that is related to the production of charcoal by endothermic and exothermic reactions (Stenseng et al. 2001). The pressure for pyrolysis process also has an influence on the porosity of the produced charcoal. Some studies reported a little reduction in the total surface area by increasing pressure during the pyrolysis process.

21.3.1.1 Effects of Parameters on Pyrolysis Process

There are so many parameters such as temperature, pressure, surface area and functional group which have important effects on pyrolysis process.

Temperature and pressure: Temperature and pressure has a good impact on pyrolysis process. Pyrolysis process usually go through three stages (Lee et al. 2017) such as ‘pre-pyrolysis’, ‘main-pyrolysis’, ‘formation of by-products’. Heat rate change during the pyrolysis process affects the distribution of solid or liquid or gaseous products (Yadav and Jagadevan 2020). Lower heating rate is favourable for production of char in the second stage of pyrolysis, whereas at higher heating rate fragmentation of biomass takes place which is responsible for a higher yield of liquid and gaseous products (Yadav and Jagadevan 2020). The pyrolysis temperature is also related to the change in the physicochemical properties of biochar such

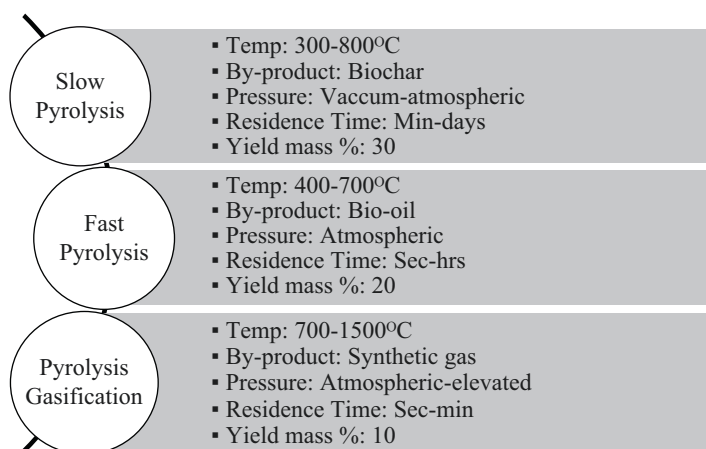


Fig. 21.2 Typical operational conditions of Pyrolysis processes for biochar production

as surface area, pH and functional group (Asadullah et al. 2007). In the first stage of pyrolysis (~200 °C), it is attributed to evaporate the moisture and volatiles, and in the second stage (200–500 °C) hemicelluloses and celluloses are decomposed and devolatilized at fast rate (Ding et al. 2016). Biochar produced at high temperature become hydrophobic in nature with a nice arrangement of C layers, whereas biochar produced at low temperature shows diversified orientation of organic compounds because of the aliphatic and cellulose-type structures (Park et al. 2010). To produce bio-oil, it is also found that heating rate change is required, as with increasing heating rate from 500 to 700 °C, 8% increment in bio-oil production has been shown (Park et al. 2010).

Pyrolysis process is also carried out under pressure, and the yield of biochar is generally enhanced while the pressure inside the reactor is higher than the atmospheric pressure (Park et al. 2010). Gaseous and liquid products are generally generated at fast pyrolysis by the production of volatile matter. The concentration of carbon is enhanced by increasing pressure that helps to enhance the density of energy of the produced biochar (Tag et al. 2016).

Size, shape and surface area: Particle size is an important factor for heat transfer during the pyrolysis of biomass. The relation between size of particle and the distance between the surface of the biomass and the core is proportional. Larger particle size could result for greater yield of solid biochar and longer size biomass particles conduct the reduction procedure in the yield of liquid products because of secondary reactions generation at higher temperature like 527 °C (Park et al. 2010). Besides size, the shape of particle is also involved in biochar production. Slab-shaped, cylindrical-shaped particle of biomass usually produces lesser yield of biochar, but spherical-shaped particle of biomass usually enhances towards high yield of biochar (Tag et al. 2016). The permeability of flow, thermal conductivity also depends upon the orientation of particle.

Specific surface area is one of the most important properties of biochar production and feedstock types. Feedstock like vine pruning or orange pomace has dead-ended pores and produce biochar with low surface area (Tag et al. 2016). Biochar produced from sugarcane has higher pore size and specific surface area. Pinecone biochars and peanut shell biochars have higher surface area than soybean cake biochar and corn stalk biochar (Tomczyk et al. 2020).

Residence time: The biochar yield is dependent on residence time. Longer residence time usually provides great ability for repolymerization of the constituents of feedstocks which enhances the yield of biochar, but the yield of biochar decreases when residence time is low (Yadav and Jagadevan 2020). Some kinds of biomass such as popular wood or yellow brown coal takes longer residence time and produces higher yield of biochar (Yeasmin et al. 1999). Some studies have stated some contradiction on this topic and according to their statement, residence time is not that much effective for biochar yield, while the composition and temperature have an important impact in biochar production (Tsai et al. 1997).

Composition of biomass: Different feedstocks have different kinds of element composition with various properties. Biochar composed from different biomass shows various elemental orientation. Feedstock is usually made up of cellulose,

hemi-cellulose and lignin which influence the nature of the produced biochar. Lignin-based biomass produces weak bonded biochar (Santos et al. 2013). Rate of lignin degradation usually depends on the amount of lignin present in the respective feedstock, and also the place of feedstock affects the biochar production. Straw-derived biochar is rich in potassium (961 mg/kg) with 9.5 pH, whereas wood-made biochar has shown a potassium content of 349 mg/kg with a pH of 8.0 (Vaughn et al. 2013). As higher volatile content can be removed easily through pyrolysis process than non-volatile contents, feedstock contained higher volatile compounds generates low yields of biochar (Wang and Wang 2019). At lower temperature degradation of cellulose leads to the formation of stable anhydrocellulose which can create higher biochar yield, but at higher temperature cellulose converts to volatile compounds (Brebti and Vasile 2010). Simultaneously, cellulose- and lignin-rich biomass can be converted to a mixture of liquid products easily. Moisture contents are also an important factor for pyrolysis. Researches stated that moisture content more than 30% is not good for pyrolysis but can produce bio-oil, whereas biomass with low content of moisture favours to produce biochar (Xiong et al. 2013).

Reactor configuration: To process the pyrolysis techniques, the reactor configuration is important to develop. There are several models of reactors which help to carry out the reaction inside it, such as cylindrical fixed-bed, packed bed, rotary kiln and fluidized bed reactor. Reactor has been made based on biomass movement. In fixed-bed reactor, biomass does not move, but in the moving-bed reactors biomass moves by enforcing mechanical force or force created by the flowrate of fluid (Yadav and Jagadevan 2020). Fixed-bed reactors are applicable for slow pyrolysis process and that is useful to produce charcoal. Fluidized bed reactor is a well-known technique which can be used commercially for fast pyrolysis process and that helps to produce a huge amount of bio-oil of 70–75% yields. This reactor uses a hydrodynamically stable bed with small size biomass particles and also used inert gas such as nitrogen (Verma et al. 2012). In the case of fixed-bed reactors the mode of heat transfers is solid-solid but in the case of fluidized bed reactors, heat transfers by the combined procedure of conduction and convection (Bridgwater et al. 1999). Ablative and cone reactors usually used for the production of huge amount of bio-oil, where fast pyrolysis is being involved and naturally thermal erosion of biomass comes into the contact of hot surface (Brassard et al. 2017). Huang et al. has been reported about microwave pyrolysis (Liu et al. 2014) which uses various lignocellulose feedstocks, and microwave generates heat to heat up the biomass particles and no external heat transfer is involved (Bridgwater 2012). The height of these reactors influences the percentage of yield products. Although biochar yield percentage does not depend on this factor, but if the height of bed from reactor increases more than 5–10 cm, it shows an increasing effect on the yield percentage of biochar (Zhang et al. 2009).

To produce large quantities of biochar, auger reactor is the best application which use intermediate pyrolysis technology (Washington State University 2011). Among all the reactor designs, auger reactor is the best in the view of technical design and the construction as well as operational technique is simple to handle (Washington State University 2011). In this reactor biomass is heated in oxygen-free condition

and because of rotational movement of the auger axis the volatile particles and gases leave the reactor, and biochar can be collected at the bottom (Brassard et al. 2017). To increase heat transformation, some of the auger reactor does use combination of small inert solid particulate heat carrier (Brassard et al. 2017). The residence time in this reactor is longer than fluidized bed reactors (Resende 2014). Vertical auger reactor is a way more suitable than other auger reactors to influence the pyrolysis operation. Several researches are going on to find the optimum condition or parameters of pyrolysis process according to auger reactor designs and techniques.

21.3.2 Gasification

Syngas and biochar are the main component produced from gasification process of biomass. To set the optimized condition for gasification according to the economy or efficiency, fixed-bed gasification model has been developed (Yao et al. 2018). Gasification is an important thermochemical process for biochar production by the conversion technique of biomass. Several models of gasification are being developed from the last few years. Hydrogen-rich gas can also be produced from biomass gasification by using gasifying agent as steam (Yao et al. 2016). Air, nitrogen, carbon dioxide, oxygen and various mixture of gases can also be used as agents for this process. This process is a partial oxidation which has been occurred at a high temperature of 800–900 °C (Yadav and Jagadevan 2020). The oxygen–carbon ratio can be used as an indicator which is useful to determine the efficiency of gasification process, and if the oxygen–carbon ratio is low in the process which increases the efficiency of gasification. Biochar yield via gasification process is usually lower than that produced during the pyrolysis. Feedstock from woods generally goes through gasification process because of the favourable elemental composition. Some researches stated various designs of gasifiers with different bed size and diameter.

21.3.3 Hydrothermal Carbonization

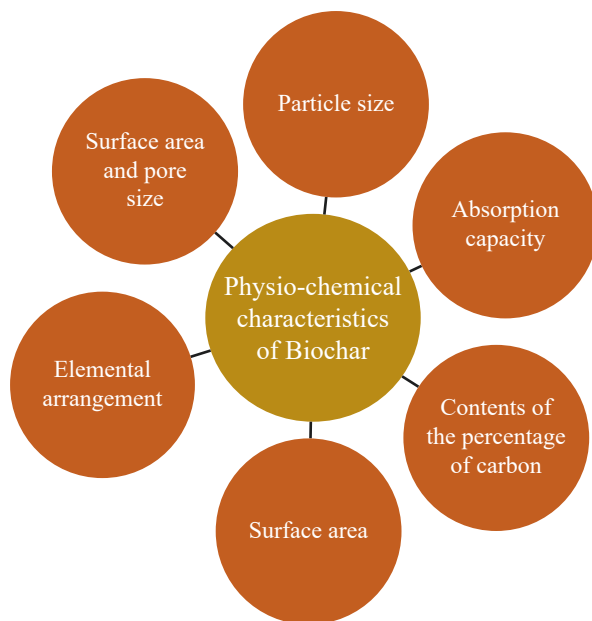
Hydrothermal carbonization is one of the most significant method after pyrolysis to convert biomass into biochar. This process has been coined by Bergius in the year of 1913 (Wang et al. 2018). For processing hydrothermal carbonization feedstock must be mixed with water in reactor. Temperature needed for this process is lower than gasification and pyrolysis, but the carbon content is high (Funke and Ziegler 2010). This process is attractive due to the ability of conversion of wet biomass to energy without predrying, and the product such as hydrochar or biochar is useful as it has the ability to produce precursors of activated carbon in the remediation of soil nutrition enrichment applications, wastewater pollution, etc. This application can be used for several wastes like municipal waste, sold wastes, sewages and municipal

solid wastes. This application is well known for its direct application in high moisture content biomass, but it is a bit difficult in terms of collection of by-products from it, and the costly equipment is required (Wang et al. 2018). Wet biomass can be proceeded by this technique but before that raw biomass need to be converted into lignite-like solid product and pre-drying is also not the necessity for this process (Knez et al. 2015). Temperature is needed relatively 180–250 °C, under autogenous pressure (Sharma et al. 2020). This process actually does not need any catalyst, but some report has stated ‘Fe’ as a catalyst which can increase the rate of hydrothermal carbonization (Sharma et al. 2020). HTC process gives the advantage to produce hydrochar by using water as a solvent. Hydrothermal carbonization upgrades fuel quality of waste biomass, by narrowing the differences among different biomasses, and it has the ability to homogenize the different feedstocks that can increase the potential of biomass utilization (Liu et al. 2013). The HTC process showed a new approach towards the biochar production since recent years.

21.4 Physiochemical Characteristics of Biochar

Physiochemical characteristics of biochar depend on the types of feedstock (Fig. 21.3). Biochar is rich in carbon which has high volatile contents and low ash. There is an important effect in between biochar type and the particle size (Fazeli Sangani et al. 2020). The performance of biochar in environmental sustainability

Fig. 21.3 Physiochemical characteristics of Biochar



depends on particle size distribution, elemental structural arrangements, surface area, porosity, etc. (Brewer et al. 2011).

As particle size has the strong influence in biochar, manipulating the particle size of source biomass prior to the conversion process is an important perspective for biochar design. Some researchers have reported that, if biochar particles are small, then pH equilibrium reaction in between soil and biochar mixtures and that increase the pH values (Chen et al. 2017). Some studies have stated that biochar produced from small particles feedstock had higher ash content which can enhance liming effects (Chen et al. 2017), and also larger particle feedstock generally produces biochar with higher sorption capacities and larger surface areas for nutrients (Xie et al. 2015). So many researches are going on to investigate the physiochemical characteristics of biochar production from anaerobically digested biomass like sugarcane bagasse, sugar beet tailings, or pig manure (Inyang et al. 2010), and aerobically digested biomass like swine manure (Meng et al. 2013).

21.5 Biochar and Its Environmental Impact

Biochar has huge impacts towards environmental sustainability because of its intrinsic properties (Fig. 21.4). It has a wide range of application in various fields like water, air and soil. Many field experiments have been carried out by researchers to profound the impact of biochar in agricultural field. Application of biochar increases the rate of bioremediation of organic compounds.

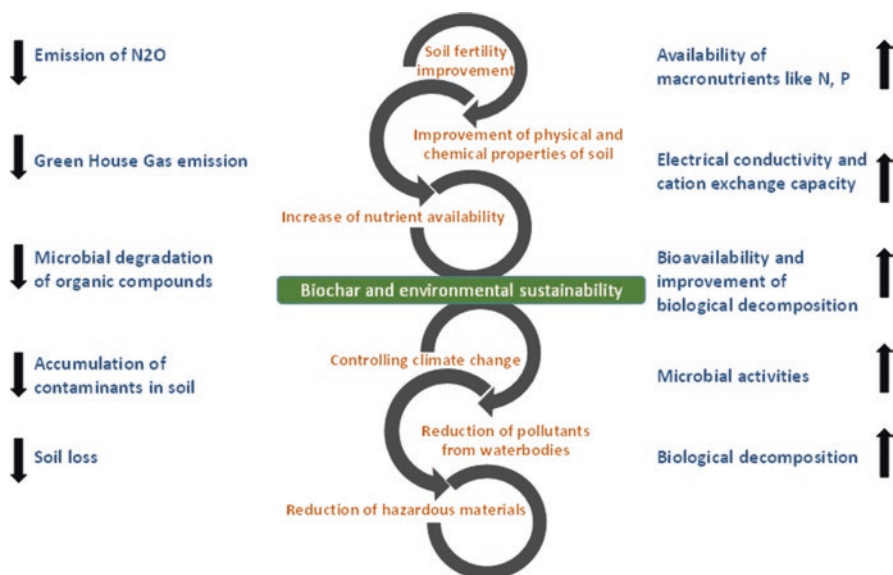


Fig. 21.4 Biochar and its contribution towards sustainability

21.6 Bioremediation and Amelioration of Soil

Bioremediation is a process where contaminated materials can be removed and that helps to clean the soil, water and other environments. Biochar application usually helps to remediate the soil from contaminations and organic materials. The bioremediation of soil by using biochar generally follows adsorption process (Ahmad et al. 2014).

Heavy metals removal from soil: Heavy metals or metalloids cannot be reduced or degraded from the environment, directly. Heavy metals also can be accumulated in the biota. Metal removing from soil has been followed by absorption and accumulation of heavy metal from soil and converting the heavy metals into lower toxic products (Sun et al. 2018). The ion exchanging mechanism can also remove heavy metals from soil. As the nature of biochar is alkaline and its surface contains negative charge, it can adsorb the toxic metals and also provides a favourable soil environment for some beneficial microorganisms. The immobilization mechanism follows by several techniques e.g., electrostatic attraction between cation as heavy metals and anion as minerals in biochar, cation exchange between minerals and metal ions, precipitation of heavy metals (Sun et al. 2018; Wu et al. 2019) with feedstock minerals, etc. (Table 21.1).

Some researches experienced that biochar made up of the manure of sheep and earthworms has an effect on immobilization of Pb in a contaminated soil (Boostani et al. 2019). The adsorption mechanism for reduction of Pb and Cd by using dairy manure biochar has been studied (Chen et al. 2019). Biochar from bamboo, rice straw and Chinese walnut shell can remove Cu from soil, and it has been examined that Cu uptake in roots was reduced by 15%, 35% and 26%, respectively (Wang et al. 2019). Biochar produced from sewage sludge, poultry litre, wheat straw and rice husk can remove Cd, Cu, Zn and Pb from soil. Some studies showed that concentration of Cu in wheat roots was reduced to 40.9% with high efficiency by the application of biochar (Jia et al. 2017). Biochar can reduce contaminants from soil, but different biochar has different ability to reduce the contaminants from the soil as a study has showed that bamboo biochar is much efficient in the case of reduction of Cu and Pb but not that much efficient in the case of Zn reduction (Yang et al. 2016). Poultry manure can remove Zn and Cr(VI) from the soil (Mandal et al. 2017). The reductive precipitation of Cr(VI) to Cr(III) in soil was magnified by the application of biochar (Choppala et al. 2012).

Table 21.1 Heavy metal immobilization with different mechanisms of remediation

Various methods of remediation	Polluted metal ions	References
Ion-exchange	Cd, Pb	Chen et al. (2019), Yang et al. (2016)
Precipitation, complexation and electrostatic interaction	Pb	Chander et al. (2015)
Sorption	Cr	Yang et al. (2016)

Mining affects large areas by destructing soil texture and reducing fertility which can cause harm to vegetation. Remediation and rehabilitation of these contaminated soil can be done through the application of biochar following phytostabilization technique (Sun et al. 2018). Many studies showed that biochar can enhance phytostabilization of metalloids including Cr, Cd, Cu, Ni, Zn and As (Uchimiya et al. 2012). By following different physical properties in the sense of pH and mobility, biochar with *Miscanthus* can be applied for the phytostabilization which reduce the As transfer to *Miscanthus* plants (Hartley et al. 2009). The pH, cation exchange capacity, nutrient retention or water-holding capacity of mine tailing are enhanced, and bioavailability of Zn, Pb, Cd decreases with the increase in the amount of biochar in soil (Fellet et al. 2014). Phytoextraction is also a mechanism related to biochar application and remediates the metalloid in soils. Several studies showed that the combination of biochar and phytoextraction such as *Brassica napus* L. is used with biochar to extract Cd from soil (Houben and Sonnet 2015).

Removal of organic compounds from soil: Biochar application can help to remove organic pollutants and decrease the activities of desorption and flow in the soil. Removal of organic compounds by biochar followed by different compositions of biomass or feedstock. Organic pollutants can be eliminated by electrostatic attraction or repulsion. Immobilized microorganisms' techniques with the application of biochar indicate the potential possibility for reducing soil pollutants. Biochar from bamboo can reduce organic pollutants like dibutyl phthalate and has 87–90% efficiency towards the removal (Qin et al. 2018). Phenanthrene, Imidacloprid, Tylosin and Chlorpyrifos can be removed by the biochar prepared from conifer, rice straw, wheat straw, hardwood, *Gossypium* spp. etc., simultaneously (Qin et al. 2018). Biochar prepared after pyrolysis thermal air oxidation can also increase the sorption of organic compounds, and also the degradation of organic pollutants by biochar deserves good focus on research as it can completely remove organic pollutants (Xiao et al. 2018). Biochar made up of fir wood chips, mixed wood shavings, rice husk or rice hull, corn straw and bamboo can remove 2,4-dichlorophenol (Gu et al. 2016), phenanthrene (Gu et al. 2016), pyrene and polychlorinated biphenyl (Bielská et al. 2018), dichlorodiphenyldichloroethylene (DDE) (Bielská et al. 2018), oxyfluorfen (Bielská et al. 2018), PAHs (Li et al. 2017), simultaneously.

Biochar application can increase the content of soil organic matter, available potassium, ammonium nitrogen, etc., in a significant way, but when the level of biochar increases in soil which inhibit the contents of nutrients in soil.

21.7 Improvement of Soil Fertility

According to many researches, biochar with an agronomic value by improving the composition, water retention etc. can enhance different soil qualities e.g. nutrient uptake (Major et al. 2010). Biochar depends on the composition of feedstock and the condition of pyrolysis process and the resulting biochar can contain good amount of fertilizing elements such as N, P and K. Several materials have been

reported for using as biomass in various parts of the world for enhancing the fertility of soil and plant nutrition. Freitas et al. observed that, available P in biochar made from different biomass is not proportional to the concentration of total P in biomass (Beheshti et al. 2017). Poultry litter biochar generally carried the mineral whitlockite, which can be utilized (Dari et al. 2016) as a slow-release P fertilizer. Biochar with compost mixtures is popular for improving soil fertility, mainly in the time of biochar mixed with feedstock before composting (Schulz and Glaser 2012). Biochar with composting can alter physicochemical properties of both materials.

21.8 Soil Treatment and Runoff

Biochar generally adsorbs organic and inorganic materials in soil and can reduce leaching to water courses. But some studies reported that due to biochar application nutrient leaching can be decreased (Sohi et al. 2010). High pyrolysis temperature, surface area, high pH, cation exchange capacity or anion exchange capacity, negative surface charge and hydrophobicity are advantageous properties for soil treatment, contamination remediation, amelioration. As pollutants like heavy metals could be immobilized on biochar, it can decrease probability of pollution because of leachate and run-off, which can be very much helpful from environmental perspective.

21.9 Soil Nutrient Dynamics by Using Biochar

Carbonaceous product as biochar generates from the pyrolysis process of feedstock in the total or partial absence of oxygen which increase the fertility of soil by affecting physical, chemical and biological trait (Song et al. 2018). Elemental arrangements in biochar depend on biomass type and other factors that have been discussed before. Nitrogen is important as the most limiting nutrient in soils, and an uninterrupted application of N in available form is important for various types of agricultural soils to nurture the crop production. In addition to organic forms of N such as hydrolysable-N and water-soluble N (Table 21.2), biochar can also contain inorganic N such as NO_3^- -N, N_2O -N, NH_4^+ -N (Liu et al. 2019). N content is not that high in biochar as during the pyrolysis of biomass some sort of N loss can be possible. The content of N in biochar decreases with an increase in pyrolytic temperature and also the conversion of the part of amino acids to pyridine-N and pyrolic-N is the reason behind N-loss in biochar (El-Naggar et al. 2019). N contents in chicken manure biochar were found at 2.79%, 2.45%, and 1.8% when the pyrolysis temperature was 250 °C, 350 °C, 550 °C (Xiao et al. 2018). All forms of nutrient N in biomass cannot be available in biochar, but the presence of metal elements in biomass can affect the conversion of N-contained compounds and in the amount and forms of N species (Xiao et al. 2018) in final biochar products.

Table 21.2 Availability of elements in biochar depends on various types of feedstock

Feedstock	Pyrolysis temperature (°C)	C/N ratio	N content		P content		K (%)	Ca (%)	Zn (mg/g)	Reference
			Total N	Available NH ₄ -N (g kg ⁻¹) (H ₂ O extract)	Total P	Available P (g kg ⁻¹) (H ₂ O extract)				
Chicken manure	250	12	2.79	0.06	1.91	5.08	4.16	1.98	—	Xiao et al. (2018)
Chicken manure	350	12	2.45	0.07	2.15	4.57	4.93	2.17	—	Xiao et al. (2018)
Chicken manure	550	13	1.81	—	2.96	2.93	5.93	3.03	—	Xiao et al. (2018)
Poultry litter	500–520	9	3.39	—	2.57	—	5.24	4.24	829.50	Brantley et al. (2016)
Poultry litter	400	5.85	—	2.57	—	3.88	2.83	—	—	Subedi et al. (2016)
Turkey litter	350	12	—	—	2.62	—	4.01	4.04	690	Cantrell et al. (2012)
Cow manure	300	58	—	—	0.19	—	0.26	—	—	Beheshti et al. (2017)
Bull manure	300	47	1.3	—	0.30	—	0.20	0.94	162	Enders et al. (2012)
Digested dairy manure	400	240	0.24	—	0.65	—	1.66	2.26	131	Enders et al. (2012)

The addition of Sydney bluegum wood biochar can increase Zn availability in soil at 1.5% rate, but if this biochar application is at 0.5%, it is unable to show any kind of significant change in Zn availability in soil (Namgay et al. 2010). Some research also showed that the biochar produced at 300 °C had a good impact for increasing P availability in soil (Naeem et al. 2017) than the biochar produced at 500 °C. Besides of this, soil microbes activity can affect the decomposition of soil organic matter and nutrient cycling (Song et al. 2018). Due to change in labile carbon and soil properties, the effect of biochar in soil can be varied. Biochar can increase or decrease microbial activity that can be measured by understanding the condition of soil type, pyrolysis temperature, etc. (Elzobair et al. 2016). Akbar et al. showed in result that with the application of corn biochar in calcareous soil, soil chemical traits, nutrient availability, and microbial availability can be changed. This study also suggested that increase of biochar at 2% application rate had the higher impact on P and K availability (Karimi et al. 2020). If we want to consider black soil, the minimum percent of P desorbed over lower P loads (19 mg/L) could rise from 35% to 40% with an increasing rate of biochar application, ranging between 1 and 11% (Oni et al. 2019). Hale et al. and Herath et al. showed that cacao shell biochar and corncob biochar desorbed 1483 mg/kg (Hale et al. 2012) and 175 mg/kg (Herath et al. 2015) of PO_4^{3-} , respectively. Different biochar types have different amount of nutrient content, so biochar can be utilized in several different ways in soils to obtain the nutrient supply effects.

21.10 Application of Biochar for Reducing the Greenhouse Gas Emission

Greenhouse gas emission is a huge problem and cause global warming which has a great contribution towards climate change. Carbon dioxide gas plays an important role for causing the global warming. Recent studies stated that the concentration of CO_2 in earth's atmosphere has been increased from 280 ppm to 410.6 ppm, from 1760 to 2019 (Rashidi and Yusup 2016). According to the IPCC (Intergovernmental Panel on Climate Change), the concentration of CO_2 could reach to 590 ppm, and the average temperature could rise by 1.9 °C by the end of twenty-first century (Li et al. 2014). The emission of carbon (IV) oxide emits from soil respiration which is 10 times higher than the emission form burning fossil fuel (Nguyen et al. 2010). Incubation and field studies both showed that biochar has the ability to reduce greenhouse gas emission (Lehmann and Joseph 2012; Shen et al. 2014). Biochar generally has an excellent stability which is able to decelerate the rate at which photosynthetically C is recovered. Biochar application helps to sequester C in the soil for a long period of time, and some studies said that could be more than 1000 years (Kuzyakov et al. 2014). Biochar and its capability to store C in soil can share the contribution to a reduction of 12% of current anthropogenic CO_2 emission (Woolf et al. 2010). Some studies observed that application of biochar in soil can

decrease CH₄ emissions due to the decrease of methanogens and methanotrophs in paddy soil (Feng et al. 2012). Rindin et al. reported that emissions of methane are almost zero while biochar has applied at a rate of 2% (w/w) to soil (Rondon et al. 2005). Sewage sludge biochar can decrease the N₂O emission significantly and help the paddy soil to absorb CH₄ (Khan et al. 2013). To reach the sustainability, biochar should be produced from those materials which could be decomposed, would not compete with food production, and the reactor should be specified which can prevent the production of GHG gases in the time of biochar production (Brassard et al. 2017). To avoid the generation of CO₂ and CO₂ in the duration of biomass decomposition, some studies reported a suppression of GHG emissions from agricultural soil while biochar has been used as an amendment (Wu et al. 2013). Some studies showed that biochar amendment can reduce total emission of CO₂ and CH₄ from rice fields (Zhang et al. 2010). A study showed the application of biochar made from swine manure (pyrolysis temperature 600–800 °C) or barely stover in two different soils (pyrolysis temperature 320 °C) and observed the emission of CO₂, CH₄, N₂O over a 36-d period (Yoo and Kang 2012). They showed that N-limited soil released less CO₂ and CH₄, and this reduction were likely offset by the increasing rate of N₂O emission. Kammann et al. (2012) experienced the effect of peanut hull biochar (pyrolysis temperature 500–800 °C) and hydrochar (pyrolysis temperature 200 °C), in the presence or absence of organic fertilizer, on soil greenhouse gas emission (Kammann et al. 2012). Kammann et al. and Yoo and Kang et al. reported from their study that if the pyrolysis temperature is high it reduces cumulative CO₂ release compared to the biochar which has lower pyrolysis temperature (Yoo and Kang 2012). There are some conditions on which effect of biochar on CO₂ emissions is dependent, such as soil type, pyrolysis temperature, incubation time and soil type. According to the report by Case et al. (2012), humidity of samples is necessary to know as CO₂ emission is both unaffected and increased by biochar addition (Case et al. 2012). Higher proportion of biochar with a C/N ratio greater than 100 resulted in an increase in CO₂ emission like 53%, but biochars with less C/N ratio comparatively resulted in a decrease in CO₂ emission (Brassard et al. 2017).

21.11 Application of Biochar in Waste Management

Several wastes from animal or agriculture can cause difficult environmental problems which can also harm the sustainability. So, the waste should be utilized well, and producing biochars through the pyrolysis process from those wastes can generate energy and also able to reduce the amount of wastes from ground. This mechanism can easily achieve the bio-economy. Some studies observed that pyrolysis provides a useful process of converting waste sludge to biochar which can improve the waste management issue and also reduce production values and as well as transport costs (Hossain et al. 2011). Biochar is a potential solution which can economically and immediately reduce the global impact of bio-waste and wastewater.

Wastewater treatment by biochar application: Biochar is the best application for treating the wastewater. China produces 25Mt of sewage sludge from wastewater treatment plants annually which is the reason of several environmental problems (Qambrani et al. 2017). The application of biochar for the reduction of heavy metal and organic matters from aqueous media is promising wastewater technology. Feedstock that contains cellulose, hemicellulos, lipids, etc. has a wide range of functional groups which can be physically activated through pyrolysis process or by CO₂ treatment which can improve the capability of biochar to adsorb contaminants. Biochar along with carbon-structured matrix which is coupled with its large surface area, high level of porosity and strong affinity towards non-polar substances such as dioxins and PAHs enables it to play an important role as a surface sorbent for reducing the contaminants in environment (Regmi et al. 2012). Biochar can be used as low-cost adsorbent widely for organic contaminants and heavy metal ions removal (Chen et al. 2011; Nguyen et al. 2007). Organic pollutants like microcystin-LR, norfloxacin, sulfamethoxazole, methylene blue, ibuprofen, salicylic acid and benzoic acid can be removed (80–99%) from water and waste water by applying biochar from chicken manure (Li et al. 2018), corn stalks, pinus radiation sawdust (Reguyal et al. 2017), mangosteen peel (Ruthiraan et al. 2017), cool planet LLC (Lin et al. 2017) and waste Douglas fir (Karunanayake et al. 2017), respectively, through pyrolysis temperature (600–800 °C). Biochar is an economical way to treat the wastewater, and this new mechanism opened several of research prospective towards future opportunity.

21.12 Limitation and Difficulties of Biochar Application

Some studies reported some limitations and disadvantages of the application of biochar. According to Mukherjee and Lal (2014), Biochar has negative aspects included leaching losses of carbon and nitrogen, mobility containment, various physical and chemical changes in soil biota (Mukherjee and Lal 2014). Some studies showed that biochar application in soil has some negative effects on the growth of fungi (Anyanwu et al. 2018). Biochar effects are more or less soil-specific, so the application of biochar not always plays a positive role for all types of soil (Zhu et al. 2015). Some study also reported the growth of weeds for biochar application. Safaei et al. (2018) observed that biochar application at comparatively higher rates of 15 t ha⁻¹ led an increase to 200% in weed growth during the culture of lentil and suggested to not to use biochar because it is not good for weed control (Safaei Khorram et al. 2018). Biochar affects soil NO_x emissions and NO_x increases tropospheric ozone concentration and that has serious effects on human health and ecosystem (Tisserant and Cherubini 2019). There are some issues with biochar application, but this application has high economical and beneficial perspective in so many aspects.

21.13 Conclusion

This chapter has reviewed about biochar preparation and overview of biochar application in agricultural fields. Conversion of organic wastes to biochar actually can help the environment to keep clean and sustainable. Pyrolysis is a thermochemical conversion process through which feedstock can be converted into biochar with the nutrient contents. Production of biochar depends on pyrolysis temperature, types of feedstocks, flow and heating rate, residence time, type of reactor configuration, etc. Biochar can be used as fertilizer for agriculture, and it can enhance the soil quality and help to improve the nutrients in soil. Biochar has a great capability to fix C in soil and reduce the GHG emission in environment. Also, as biochar has large surface area and porosity so it has the capacity to hold water in soil and the absorption of nutrients by decreasing soil loss which can actually increase the soil fertility.

The research of biochar in the aspect of climate change, organic pollutants removal and heavy metal immobilization has developed a lot in the past few years. Mitigation of GHG emissions is an important step to control the climate change and global warming. Thus, limiting the fertilizers and using biochar in the agricultural field can be useful to sequester C in the soil. This phenomenon of biochar can reduce the CO₂ from the atmosphere and particularly N₂O, a powerful GHG with a 298 times of potential of global warming that of CO₂ for a 100-year timescale. In this literature review, reactor configurations are also described. Pyrolysis auger reactor has been selected as a good technology for the conversion of feedstock, and it is simple to operate with less requirement of carrier gas and energy.

Small-scale impacts of biochar on soil nutrients and organic contaminants dynamics have been researched well, but long-term research should be focused on the biochar application. There are several limitations which need to overcome in the future research. Modification of biochar is an important part on this aspect of research. In the case of industrial application, the conditions of biochar preparation need to be improved further based on different soil properties and other factors, which can meet the environmental sustainability.

References

- Ahmad, M., Rajapaksha, A. U., Lim, J. E., Zhang, M., Bolan, N., Mohan, D., Vithanage, M., Lee, S. S., & Ok, Y. S. (2014). Biochar as a sorbent for contaminant management in soil and water: A review. *Chemosphere*, 99, 19–33. <https://doi.org/10.1016/j.chemosphere.2013.10.071>.
- Antal, M. J., & Grønli, M. (2003). The art, science, and technology of charcoal production. *Industrial and Engineering Chemistry Research*, 42(8), 1619–1640.
- Anyanwu, I. N., Alo, M. N., Onyekwere, A. M., Crosse, J. D., Nworie, O., & Chamba, E. B. (2018). Influence of biochar aged in acidic soil on ecosystem engineers and two tropical agricultural plants. *Ecotoxicology and Environmental Safety*. <https://doi.org/10.1016/j.ecoenv.2018.02.005>.
- Asadullah, M., Rahman, M. A., Ali, M. M., et al. (2007). Production of bio-oil from fixed bed pyrolysis of bagasse. *Fuel*, 86, 2514–2520. <https://doi.org/10.1016/j.fuel.2007.02.007>.

- Beheshti, M., Etesami, H., & Alikhani, H. A. (2017). Interaction study of biochar with phosphate-solubilizing bacterium on phosphorus availability in calcareous soil. *Archives of Agronomy and Soil Science*. <https://doi.org/10.1080/03650340.2017.1295138>.
- Bernardino, C. A. R., Mahler, C. F., Veloso, M. C. C., & Romeiro, G. A. (2017). Preparation of biochar from sugarcane by-product filter mud by slow pyrolysis and its use like adsorbent. *Waste and Biomass Valorization*, 8, 2511–2521. <https://doi.org/10.1007/s12649-016-9728-5>.
- Bielská, L., Škulcová, L., Neuwirthová, N., Cornelissen, G., & Hale, S. E. (2018). Sorption, bio-availability and ecotoxic effects of hydrophobic organic compounds in biochar amended soils. *Science of the Total Environment*. <https://doi.org/10.1016/j.scitotenv.2017.12.098>.
- Boostani, H. R., Najafi-Ghiri, M., Hardie, A. G., & Khalili, D. (2019). Comparison of Pb stabilization in a contaminated calcareous soil by application of vermicompost and sheep manure and their biochars produced at two temperatures. *Applied Geochemistry*. <https://doi.org/10.1016/j.apgeochem.2019.01.013>.
- Brantley, K. E., Savin, M. C., Brye, K. R., & Longer, D. E. (2016). Nutrient availability and corn growth in a poultry litter biochar-amended loam soil in a greenhouse experiment. *Soil Use and Management*. <https://doi.org/10.1111/sum.12296>.
- Brassard, P., Godbout, S., Raghavan, V., Palacios, J. H., Grenier, M., & Zegan, D. (2017). The production of engineered biochars in a vertical auger pyrolysis reactor for carbon sequestration. *Energies*. <https://doi.org/10.3390/en10030288>.
- Brebu, M., & Vasile, C. (2010). Thermal degradation of lignin: A review. *Cellulose Chemistry and Technology*, 44(9), 353–363.
- Brewer, C. E., Unger, R., Schmidt-Rohr, K., & Brown, R. C. (2011). Criteria to select biochars for field studies based on biochar chemical properties. *Bioenergy Research*, 4(4), 312–323. <https://doi.org/10.1007/s12155-011-9133-7>.
- Bridgwater, A. V. (2012). Review of fast pyrolysis of biomass and product upgrading. *Biomass and Bioenergy*, 38, 68–94. <https://doi.org/10.1016/j.biombioe.2011.01.048>.
- Bridgwater, A. V., Meier, D., & Radlein, D. (1999). An overview of fast pyrolysis of biomass. *Organic Geochemistry*. [https://doi.org/10.1016/S0146-6380\(99\)00120-5](https://doi.org/10.1016/S0146-6380(99)00120-5).
- Cantrell, K. B., Hunt, P. G., Uchimiya, M., Novak, J. M., & Ro, K. S. (2012). Impact of pyrolysis temperature and manure source on physicochemical characteristics of biochar. *Bioresource Technology*. <https://doi.org/10.1016/j.biortech.2011.11.084>.
- Case, S. D. C., McNamara, N. P., Reay, D. S., & Whitaker, J. (2012). The effect of biochar addition on N₂O and CO₂ emissions from a sandy loam soil—The role of soil aeration. *Soil Biology and Biochemistry*. <https://doi.org/10.1016/j.soilbio.2012.03.017>.
- Cha, J. S., Park, S. H., Jung, S. C., et al. (2016). Production and utilization of biochar: A review. *Journal of Industrial and Engineering Chemistry*, 40, 1–15.
- Chander, A., Chen, X.-L., Naidu, D. G., Gulati, S., Liu, Y., Munkacsi, A. B., Wilcox, L., Sturley, S. L., Gerelsaikhan, T., Chen, X.-L., Chander, A., Triggiani, M., Giannattasio, G., Calabrese, C., Loffredo, S., Granata, F., Fiorello, A., Santini, M., Gelb, M. H., et al. (2015). Subject index. *Minerals Engineering*, 10(2). <https://doi.org/10.1007/978-3-642-13757-0>.
- Chen, B., Chen, Z., & Lv, S. (2011). A novel magnetic biochar efficiently sorbs organic pollutants and phosphate. *Bioresource Technology*. <https://doi.org/10.1016/j.biortech.2010.08.067>.
- Chen, J., Li, S., Liang, C., Xu, Q., Li, Y., Qin, H., & Fuhrmann, J. J. (2017). Response of microbial community structure and function to short-term biochar amendment in an intensively managed bamboo (*Phyllostachys praecox*) plantation soil: Effect of particle size and addition rate. *Science of the Total Environment*. <https://doi.org/10.1016/j.scitotenv.2016.08.190>.
- Chen, Z. L., Zhang, J. Q., Huang, L., Yuan, Z. H., Li, Z. J., & Liu, M. C. (2019). Removal of Cd and Pb with biochar made from dairy manure at low temperature. *Journal of Integrative Agriculture*. [https://doi.org/10.1016/S2095-3119\(18\)61987-2](https://doi.org/10.1016/S2095-3119(18)61987-2).
- Choppala, G. K., Bolan, N. S., Megharaj, M., Chen, Z., & Naidu, R. (2012). The influence of biochar and black carbon on reduction and bioavailability of chromate in soils. *Journal of Environmental Quality*. <https://doi.org/10.2134/jeq2011.0145>.

- Dari, B., Nair, V. D., Harris, W. G., Nair, P. K. R., Sollenberger, L., & Mylavarapu, R. (2016). Relative influence of soil- vs. biochar properties on soil phosphorus retention. *Geoderma*. <https://doi.org/10.1016/j.geoderma.2016.06.018>.
- Ding, Y., Liu, Y., Liu, S., et al. (2016). Biochar to improve soil fertility. A review. *Agronomy for Sustainable Development*, 36(2), 1–18.
- El-Naggar, A., El-Naggar, A. H., Shaheen, S. M., Sarkar, B., Chang, S. X., Tsang, D. C. W., Rinklebe, J., & Ok, Y. S. (2019). Biochar composition-dependent impacts on soil nutrient release, carbon mineralization, and potential environmental risk: A review. *Journal of Environmental Management*. <https://doi.org/10.1016/j.jenvman.2019.02.044>.
- Elzobair, K. A., Stromberger, M. E., Ippolito, J. A., & Lentz, R. D. (2016). Contrasting effects of biochar versus manure on soil microbial communities and enzyme activities in an Aridisol. *Chemosphere*. <https://doi.org/10.1016/j.chemosphere.2015.06.044>.
- Enders, A., Hanley, K., Whitman, T., Joseph, S., & Lehmann, J. (2012). Characterization of biochars to evaluate recalcitrance and agronomic performance. *Bioresource Technology*. <https://doi.org/10.1016/j.biortech.2012.03.022>.
- Fazeli Sangani, M., Abrishamkesh, S., & Owens, G. (2020). Physicochemical characteristics of biochars can be beneficially manipulated using post-pyrolyzed particle size modification. *Bioresource Technology*. <https://doi.org/10.1016/j.biortech.2020.123157>.
- Fellet, G., Marmiroli, M., & Marchiol, L. (2014). Elements uptake by metal accumulator species grown on mine tailings amended with three types of biochar. *Science of the Total Environment*. <https://doi.org/10.1016/j.scitotenv.2013.08.072>.
- Feng, Y., Xu, Y., Yu, Y., Xie, Z., & Lin, X. (2012). Mechanisms of biochar decreasing methane emission from Chinese paddy soils. *Soil Biology and Biochemistry*. <https://doi.org/10.1016/j.soilbio.2011.11.016>.
- Funke, A., & Ziegler, F. (2010). Hydrothermal carbonization of biomass: A summary and discussion of chemical mechanisms for process engineering. *Biofuels, Bioproducts and Biorefining*. <https://doi.org/10.1002/bbb.198>.
- Gu, J., Zhou, W., Jiang, B., Wang, L., Ma, Y., Guo, H., Schulin, R., Ji, R., & Evangelou, M. W. H. (2016). Effects of biochar on the transformation and earthworm bioaccumulation of organic pollutants in soil. *Chemosphere*. <https://doi.org/10.1016/j.chemosphere.2015.11.106>.
- Hale, S. E., Lehmann, J., Rutherford, D., Zimmerman, A. R., Bachmann, R. T., Shitumbanuma, V., O'Toole, A., Sundqvist, K. L., Arp, H. P. H., & Cornelissen, G. (2012). Quantifying the total and bioavailable polycyclic aromatic hydrocarbons and dioxins in biochars. *Environmental Science and Technology*. <https://doi.org/10.1021/es203984k>.
- Hartley, W., Dickinson, N. M., Riby, P., & Lepp, N. W. (2009). Arsenic mobility in brownfield soils amended with green waste compost or biochar and planted with *Miscanthus*. *Environmental Pollution*. <https://doi.org/10.1016/j.envpol.2009.05.011>.
- Herath, H. M. S. K., Camps-Arbestain, M., Hedley, M. J., Kirschbaum, M. U. F., Wang, T., & van Hale, R. (2015). Experimental evidence for sequestering C with biochar by avoidance of CO₂ emissions from original feedstock and protection of native soil organic matter. *GCB Bioenergy*. <https://doi.org/10.1111/gcbb.12183>.
- Hernandez-Mena, L. E., Pecora, A. A. B., & Beraldo, A. L. (2014). Slow pyrolysis of bamboo biomass: Analysis of biochar properties. *Chemical Engineering Transactions*, 37. <https://doi.org/10.3303/CET1437020>.
- Hossain, M. K., Strezov Vladimir, V., Chan, K. Y., Ziolkowski, A., & Nelson, P. F. (2011). Influence of pyrolysis temperature on production and nutrient properties of wastewater sludge biochar. *Journal of Environmental Management*. <https://doi.org/10.1016/j.jenvman.2010.09.008>.
- Houben, D., & Sonnet, P. (2015). Impact of biochar and root-induced changes on metal dynamics in the rhizosphere of *Agrostis capillaris* and *Lupinus albus*. *Chemosphere*. <https://doi.org/10.1016/j.chemosphere.2014.12.036>.
- Inyang, M., Gao, B., Pullammanappallil, P., Ding, W., & Zimmerman, A. R. (2010). Biochar from anaerobically digested sugarcane bagasse. *Bioresource Technology*. <https://doi.org/10.1016/j.biortech.2010.06.088>.

- Jia, W., Wang, B., Wang, C., & Sun, H. (2017). Tourmaline and biochar for the remediation of acid soil polluted with heavy metals. *Journal of Environmental Chemical Engineering*. <https://doi.org/10.1016/j.jece.2017.04.015>.
- Kammann, C., Ratering, S., Eckhard, C., & Müller, C. (2012). Biochar and hydrochar effects on greenhouse gas (carbon dioxide, nitrous oxide, and methane) fluxes from soils. *Journal of Environmental Quality*. <https://doi.org/10.2134/jeq2011.0132>.
- Karimi, A., Moezzi, A., Chorom, M., & Enayatizamir, N. (2020). Application of biochar changed the status of nutrients and biological activity in a calcareous soil. *Journal of Soil Science and Plant Nutrition*. <https://doi.org/10.1007/s42729-019-00129-5>.
- Karunanayake, A. G., Todd, O. A., Crowley, M. L., Ricchetti, L. B., Pittman, C. U., Anderson, R., & Mlsna, T. E. (2017). Rapid removal of salicylic acid, 4-nitroaniline, benzoic acid and phthalic acid from wastewater using magnetized fast pyrolysis biochar from waste Douglas fir. *Chemical Engineering Journal*. <https://doi.org/10.1016/j.cej.2017.02.116>.
- Khalil, L. B. (1999). Porosity characteristics of chars derived from different lignocellulosic materials. *Adsorption Science and Technology*, 17. <https://doi.org/10.1177/026361749901700904>.
- Khan, S., Chao, C., Waqas, M., Arp, H. P. H., & Zhu, Y. G. (2013). Sewage sludge biochar influence upon rice (*Oryza sativa* L) yield, metal bioaccumulation and greenhouse gas emissions from acidic paddy soil. *Environmental Science and Technology*. <https://doi.org/10.1021/es400554x>.
- Knez, M. E., Hrnčič, M. K., Ravber, M., & Škerget, M. (2015). High pressure water reforming of biomass for energy and chemicals: A short review. *Journal of Supercritical Fluids*. <https://doi.org/10.1016/j.supflu.2014.06.008>.
- Kuzyakov, Y., Bogomolova, I., & Glaser, B. (2014). Biochar stability in soil: Decomposition during eight years and transformation as assessed by compound-specific ¹⁴C analysis. *Soil Biology and Biochemistry*. <https://doi.org/10.1016/j.soilbio.2013.12.021>.
- Lee, X. J., Lee, L. Y., Gan, S., et al. (2017). Biochar potential evaluation of palm oil wastes through slow pyrolysis: Thermochemical characterization and pyrolytic kinetic studies. *Bioresource Technology*, 236. <https://doi.org/10.1016/j.biortech.2017.03.105>.
- Lehmann, J., & Joseph, S. (2012). Biochar for environmental management: An introduction. In *Biochar for environmental management: Science and technology*. London: Routledge. <https://doi.org/10.4324/9781849770552>.
- Lehmann, J., Skjemstad, J., Sohi, S., et al. (2008). Australian climate-carbon cycle feedback reduced by soil black carbon. *Nature Geoscience*, 1. <https://doi.org/10.1038/ngeo358>.
- Li, H., Dong, X., da Silva, E. B., de Oliveira, L. M., Chen, Y., & Ma, L. Q. (2017). Mechanisms of metal sorption by biochars: Biochar characteristics and modifications. *Chemosphere*, 178, 466–478. <https://doi.org/10.1016/j.chemosphere.2017.03.072>.
- Li, J., Cao, L., Yuan, Y., Wang, R., Wen, Y., & Man, J. (2018). Comparative study for microcystin-LR sorption onto biochars produced from various plant- and animal-wastes at different pyrolysis temperatures: Influencing mechanisms of biochar properties. *Bioresource Technology*, 247, 794–803. <https://doi.org/10.1016/j.biortech.2017.09.120>.
- Li, K., An, X., Park, K. H., Khraisheh, M., & Tang, J. (2014). A critical review of CO₂ photoconversion: Catalysts and reactors. *Catalysis Today*, 224, 3–12. <https://doi.org/10.1016/j.cattod.2013.12.006>.
- Lin, L., Jiang, W., & Xu, P. (2017). Comparative study on pharmaceuticals adsorption in reclaimed water desalination concentrate using biochar: Impact of salts and organic matter. *Science of the Total Environment*. <https://doi.org/10.1016/j.scitotenv.2017.05.203>.
- Liu, C., Wang, H., Karim, A. M., Sun, J., & Wang, Y. (2014). Catalytic fast pyrolysis of lignocellulosic biomass. *Chemical Society Reviews*. <https://doi.org/10.1039/c3cs60414d>.
- Liu, L., Tan, Z., Gong, H., & Huang, Q. (2019). Migration and transformation mechanisms of nutrient elements (N, P, K) within biochar in straw-biochar-soil-plant systems: A review. *ACS Sustainable Chemistry and Engineering*. <https://doi.org/10.1021/acssuschemeng.8b04253>.
- Liu, Z., Quek, A., Kent Hoekman, S., & Balasubramanian, R. (2013). Production of solid biochar fuel from waste biomass by hydrothermal carbonization. *Fuel*. <https://doi.org/10.1016/j.fuel.2012.07.069>.

- Major, J., Rondon, M., Molina, D., Riha, S. J., & Lehmann, J. (2010). Maize yield and nutrition during 4 years after biochar application to a Colombian savanna oxisol. *Plant and Soil*. <https://doi.org/10.1007/s11104-010-0327-0>.
- Mandal, S., Sarkar, B., Bolan, N., Ok, Y. S., & Naidu, R. (2017). Enhancement of chromate reduction in soils by surface modified biochar. *Journal of Environmental Management*. <https://doi.org/10.1016/j.jenvman.2016.05.034>.
- Meng, J., Wang, L., Liu, X., Wu, J., Brookes, P. C., & Xu, J. (2013). Physicochemical properties of biochar produced from aerobically composted swine manure and its potential use as an environmental amendment. *Bioresource Technology*. <https://doi.org/10.1016/j.biortech.2013.05.086>.
- Mohan, D., Pittman, C. U., & Steele, P. H. (2006). Pyrolysis of wood/biomass for bio-oil: A critical review. *Energy and Fuels*, 20(3), 848–889.
- Mohan, D., Sarswat, A., Ok, Y. S., & Pittman, C. U. (2014). Organic and inorganic contaminants removal from water with biochar, a renewable, low cost and sustainable adsorbent: A critical review. *Bioresource Technology*, 160, 191–202. <https://doi.org/10.1016/j.biortech.2014.01.120>.
- Morgan, E. A. (2013). The biochar solution. Carbon farming and climate change. *Australian Planner*, 50(1), 79–80. <https://doi.org/10.1080/07293682.2012.670119>.
- Mukherjee, A., & Lal, R. (2014). The biochar dilemma. *Soil Research*. <https://doi.org/10.1071/SR13359>.
- Naem, M. A., Khalid, M., Aon, M., Abbas, G., Tahir, M., Amjad, M., Murtaza, B., Yang, A., & Akhtar, S. S. (2017). Effect of wheat and rice straw biochar produced at different temperatures on maize growth and nutrient dynamics of a calcareous soil. *Archives of Agronomy and Soil Science*. <https://doi.org/10.1080/03650340.2017.1325468>.
- Namgay, T., Singh, B., & Singh, B. P. (2010). Influence of biochar application to soil on the availability of As, Cd, Cu, Pb, and Zn to maize (*Zea mays* L.). *Australian Journal of Soil Research*. <https://doi.org/10.1071/SR10049>.
- Nartey, O. D., & Zhao, B. (2014). Biochar preparation, characterization, and adsorptive capacity and its effect on bioavailability of contaminants: An overview. *Advances in Materials Science and Engineering*, 2014.
- Nguyen, B. T., Lehmann, J., Hockaday, W. C., Joseph, S., & Masiello, C. A. (2010). Temperature sensitivity of black carbon decomposition and oxidation. *Environmental Science and Technology*. <https://doi.org/10.1021/es903016y>.
- Nguyen, T. H., Cho, H. H., Poster, D. L., & Ball, W. P. (2007). Evidence for a pore-filling mechanism in the adsorption of aromatic hydrocarbons to a natural wood char. *Environmental Science and Technology*. <https://doi.org/10.1021/es0617845>.
- Oni, B. A., Oziegbe, O., & Olawole, O. O. (2019). Significance of biochar application to the environment and economy. *Annals of Agricultural Sciences*. <https://doi.org/10.1016/j.aoads.2019.12.006>.
- Park, W. C., Atreya, A., & Baum, H. R. (2010). Experimental and theoretical investigation of heat and mass transfer processes during wood pyrolysis. *Combustion and Flame*. <https://doi.org/10.1016/j.combustflame.2009.10.006>.
- Qambrani, N. A., Rahman, M. M., Won, S., Shim, S., & Ra, C. (2017). Biochar properties and eco-friendly applications for climate change mitigation, waste management, and wastewater treatment: A review. *Renewable and Sustainable Energy Reviews*. <https://doi.org/10.1016/j.rser.2017.05.057>.
- Qin, P., Wang, H., Yang, X., He, L., Müller, K., Shaheen, S. M., Xu, S., Rinklebe, J., Tsang, D. C. W., Ok, Y. S., Bolan, N., Song, Z., Che, L., & Xu, X. (2018). Bamboo- and pig-derived biochars reduce leaching losses of dibutyl phthalate, cadmium, and lead from co-contaminated soils. *Chemosphere*. <https://doi.org/10.1016/j.chemosphere.2018.01.162>.
- Rashidi, N. A., & Yusup, S. (2016). An overview of activated carbons utilization for the post-combustion carbon dioxide capture. *Journal of CO₂ Utilization*. <https://doi.org/10.1016/j.jcou.2015.11.002>.
- Regmi, P., Garcia Moscoso, J. L., Kumar, S., Cao, X., Mao, J., & Schafran, G. (2012). Removal of copper and cadmium from aqueous solution using switchgrass biochar produced via

- hydrothermal carbonization process. *Journal of Environmental Management*. <https://doi.org/10.1016/j.jenvman.2012.04.047>.
- Reguyal, F., Sarmah, A. K., & Gao, W. (2017). Synthesis of magnetic biochar from pine sawdust via oxidative hydrolysis of FeCl₂ for the removal sulfamethoxazole from aqueous solution. *Journal of Hazardous Materials*. <https://doi.org/10.1016/j.jhazmat.2016.10.006>.
- Resende, F. L. P. (2014). Reactor configurations and design parameters for thermochemical conversion of biomass into fuels, energy, and chemicals. *Reactor and Process Design in Sustainable Energy Technology*. <https://doi.org/10.1016/B978-0-444-59566-9.00001-6>.
- Rizwan, M., Ali, S., Qayyum, M. F., et al. (2016). Mechanisms of biochar-mediated alleviation of toxicity of trace elements in plants: A critical review. *Environmental Science and Pollution Research*, 23, 2230–2248. <https://doi.org/10.1007/s11356-015-5697-7>.
- Rondon, M., Ramirez J. A., & Lehmann J. (2005). Greenhouse gas emissions decrease with charcoal additions to tropical soils | International biochar initiative. In *3rd USDA Symposium on Greenhouse Gases and Carbon Sequestration in Agriculture and Forestry*.
- Ruthiraan, M., Abdullah, E. C., Mubarak, N. M., & Noraini, M. N. (2017). A promising route of magnetic based materials for removal of cadmium and methylene blue from waste water. *Journal of Environmental Chemical Engineering*. <https://doi.org/10.1016/j.jece.2017.02.038>.
- Safaei Khorram, M., Fatemi, A., Khan, M. A., Kiefer, R., & Jafarnia, S. (2018). Potential risk of weed outbreak by increasing biochar's application rates in slow-growth legume, lentil (*Lens culinaris* Medik.). *Journal of the Science of Food and Agriculture*. <https://doi.org/10.1002/jsfa.8689>.
- Santos, R. B., Hart, P. W., Jameel, H., & Chang, H. M. (2013). Wood based lignin reactions important to the biorefinery and pulp and paper industries. *BioResources*. <https://doi.org/10.15376/biores.8.1.1456-1477>.
- Schulz, H., & Glaser, B. (2012). Effects of biochar compared to organic and inorganic fertilizers on soil quality and plant growth in a greenhouse experiment. *Journal of Plant Nutrition and Soil Science*. <https://doi.org/10.1002/jpln.201100143>.
- Sharma, R., Jasrotia, K., Singh, N., Ghosh, P., srivastava, S., Sharma, N. R., Singh, J., Kanwar, R., & Kumar, A. (2020). A comprehensive review on hydrothermal carbonization of biomass and its applications. *Chemistry Africa*. <https://doi.org/10.1007/s42250-019-00098-3>.
- Shen, J., Tang, H., Liu, J., Wang, C., Li, Y., Ge, T., Jones, D. L., & Wu, J. (2014). Contrasting effects of straw and straw-derived biochar amendments on greenhouse gas emissions within double rice cropping systems. *Agriculture, Ecosystems and Environment*. <https://doi.org/10.1016/j.agee.2014.03.002>.
- Sohi, S. P., Krull, E., Lopez-Capel, E., & Bol, R. (2010). A review of biochar and its use and function in soil. *Advances in Agronomy*. [https://doi.org/10.1016/S0065-2113\(10\)05002-9](https://doi.org/10.1016/S0065-2113(10)05002-9).
- Song, D., Tang, J., Xi, X., Zhang, S., Liang, G., Zhou, W., & Wang, X. (2018). Responses of soil nutrients and microbial activities to additions of maize straw biochar and chemical fertilization in a calcareous soil. *European Journal of Soil Biology*. <https://doi.org/10.1016/j.ejsobi.2017.11.003>.
- Stenseng, M., Jensen, A., & Dam-Johansen, K. (2001). Investigation of biomass pyrolysis by thermogravimetric analysis and differential scanning calorimetry. *Journal of Analytical and Applied Pyrolysis*, 58–59, 765–780. [https://doi.org/10.1016/S0165-2370\(00\)00200-X](https://doi.org/10.1016/S0165-2370(00)00200-X).
- Subedi, R., Taupe, N., Pelissetti, S., Petruzzelli, L., Bertora, C., Leahy, J. J., & Grignani, C. (2016). Greenhouse gas emissions and soil properties following amendment with manure-derived biochars: Influence of pyrolysis temperature and feedstock type. *Journal of Environmental Management*. <https://doi.org/10.1016/j.jenvman.2015.10.007>.
- Sun, W., Zhang, S., & Su, C. (2018). Impact of biochar on the bioremediation and phytoremediation of heavy metal(loid) s in soil. *Advances in Bioremediation and Phytoremediation*. <https://doi.org/10.5772/intechopen.70349>.
- Tag, A. T., Duman, G., Ucar, S., & Yanik, J. (2016). Effects of feedstock type and pyrolysis temperature on potential applications of biochar. *Journal of Analytical and Applied Pyrolysis*. <https://doi.org/10.1016/j.jaap.2016.05.006>.

- Tisserant, A., & Cherubini, F. (2019). Potentials, limitations, co-benefits, and trade-offs of biochar applications to soils for climate change mitigation. *Land*. <https://doi.org/10.3390/LAND8120179>.
- Tomczyk, A., Sokołowska, Z., & Boguta, P. (2020). Biochar physicochemical properties: Pyrolysis temperature and feedstock kind effects. *Reviews in Environmental Science and Biotechnology*. <https://doi.org/10.1007/s11157-020-09523-3>.
- Tsai, W. T., Chang, C. Y., & Lee, S. L. (1997). Preparation and characterization of activated carbons from corn cob. *Carbon*. [https://doi.org/10.1016/S0008-6223\(97\)84654-4](https://doi.org/10.1016/S0008-6223(97)84654-4).
- Uchimiya, M., Bannon, D. I., Wartelle, L. H., Lima, I. M., & Klasson, K. T. (2012). Lead retention by broiler litter biochars in small arms range soil: Impact of pyrolysis temperature. *Journal of Agricultural and Food Chemistry*. <https://doi.org/10.1021/jf300825n>.
- Vaughn, S. F., Kenar, J. A., Thompson, A. R., & Peterson, S. C. (2013). Comparison of biochars derived from wood pellets and pelletized wheat straw as replacements for peat in potting substrates. *Industrial Crops and Products*. <https://doi.org/10.1016/j.indcrop.2013.10.010>.
- Verma, M., Godbout, S., Brar, S. K., Solomatnikova, O., Lemay, S. P., & Larouche, J. P. (2012). Biofuels production from biomass by thermochemical conversion technologies. *International Journal of Chemical Engineering*. <https://doi.org/10.1155/2012/542426>.
- Wang, J., & Wang, S. (2019). Preparation, modification and environmental application of biochar: A review. *Journal of Cleaner Production*. <https://doi.org/10.1016/j.jclepro.2019.04.282>.
- Wang, T., Zhai, Y., Zhu, Y., Li, C., & Zeng, G. (2018). A review of the hydrothermal carbonization of biomass waste for hydrochar formation: Process conditions, fundamentals, and physicochemical properties. *Renewable and Sustainable Energy Reviews*. <https://doi.org/10.1016/j.rser.2018.03.071>.
- Wang, Y., Zhong, B., Shafi, M., Ma, J., Guo, J., Wu, J., Ye, Z., Liu, D., & Jin, H. (2019). Effects of biochar on growth, and heavy metals accumulation of moso bamboo (*Phyllostachy pubescens*), soil physical properties, and heavy metals solubility in soil. *Chemosphere*. <https://doi.org/10.1016/j.chemosphere.2018.11.159>.
- Warnock, D. D., Lehmann, J., Kuyper, T. W., & Rillig, M. C. (2007). Mycorrhizal responses to biochar in soil and concepts and mechanisms. *Plant Soil*, 300:9–20. <https://doi.org/10.1007/s11104-007-9391-5>
- Washington State University. (2011). Literature review of pyrolysis reactors. In *Methods for producing biochar and advanced biofuels in Washington State*.
- Woolf, D., Amonette, J. E., Street-Perrott, F. A., Lehmann, J., & Joseph, S. (2010). Sustainable biochar to mitigate global climate change. *Nature Communications*. <https://doi.org/10.1038/ncomms1053>.
- Wu, F., Jia, Z., Wang, S., Chang, S. X., & Startsev, A. (2013). Contrasting effects of wheat straw and its biochar on greenhouse gas emissions and enzyme activities in a Chernozemic soil. *Biology and Fertility of Soils*. <https://doi.org/10.1007/s00374-012-0745-7>.
- Wu, P., Ata-Ul-Karim, S. T., Singh, B. P., Wang, H., Wu, T., Liu, C., Fang, G., Zhou, D., Wang, Y., & Chen, W. (2019). A scientometric review of biochar research in the past 20 years (1998–2018). *Biochar*, 1(1), 23–43. <https://doi.org/10.1007/s42773-019-00002-9>.
- Xiao, R., Wang, J. J., Gaston, L. A., Zhou, B., Park, J. H., Li, R., Dodla, S. K., & Zhang, Z. (2018). Biochar produced from mineral salt-impregnated chicken manure: Fertility properties and potential for carbon sequestration. *Waste Management*. <https://doi.org/10.1016/j.wasman.2018.06.047>.
- Xie, T., Reddy, K. R., Wang, C., Yargicoglu, E., & Spokas, K. (2015). Characteristics and applications of biochar for environmental remediation: A review. *Critical Reviews in Environmental Science and Technology*. <https://doi.org/10.1080/10643389.2014.924180>.
- Xiong, S., Zhuo, J., Zhang, B., & Yao, Q. (2013). Effect of moisture content on the characterization of products from the pyrolysis of sewage sludge. *Journal of Analytical and Applied Pyrolysis*. <https://doi.org/10.1016/j.jaap.2013.05.003>.

- Yadav, K., & Jagadevan, S. (2020). Influence of process parameters on synthesis of biochar by pyrolysis of biomass: An alternative source of energy. In *Recent advances in pyrolysis*. <https://doi.org/10.5772/intechopen.88204>.
- Yang, X., Liu, J., McGrouther, K., Huang, H., Lu, K., Guo, X., He, L., Lin, X., Che, L., Ye, Z., & Wang, H. (2016). Effect of biochar on the extractability of heavy metals (Cd, Cu, Pb, and Zn) and enzyme activity in soil. *Environmental Science and Pollution Research*. <https://doi.org/10.1007/s11356-015-4233-0>.
- Yao, D., Hu, Q., Wang, D., Yang, H., Wu, C., Wang, X., & Chen, H. (2016). Hydrogen production from biomass gasification using biochar as a catalyst/support. *Bioresource Technology*. <https://doi.org/10.1016/j.biortech.2016.05.011>.
- Yao, Z., You, S., Ge, T., & Wang, C. H. (2018). Biomass gasification for syngas and biochar co-production: Energy application and economic evaluation. *Applied Energy*. <https://doi.org/10.1016/j.apenergy.2017.10.077>.
- Yeasmin, H., Mathews, J. F., & Ouyang, S. (1999). Rapid devolatilisation of Yallourn brown coal at high pressures and temperatures. *Fuel*. [https://doi.org/10.1016/S0016-2361\(98\)00119-7](https://doi.org/10.1016/S0016-2361(98)00119-7).
- Yoo, G., & Kang, H. (2012). Effects of biochar addition on greenhouse gas emissions and microbial responses in a short-term laboratory experiment. *Journal of Environmental Quality*. <https://doi.org/10.2134/jeq2011.0157>.
- Zhang, A., Cui, L., Pan, G., Li, L., Hussain, Q., Zhang, X., Zheng, J., & Crowley, D. (2010). Effect of biochar amendment on yield and methane and nitrous oxide emissions from a rice paddy from Tai Lake plain, China. *Agriculture, Ecosystems and Environment*. <https://doi.org/10.1016/j.agee.2010.09.003>.
- Zhang, H., Xiao, R., Huang, H., & Xiao, G. (2009). Comparison of non-catalytic and catalytic fast pyrolysis of corncob in a fluidized bed reactor. *Bioresource Technology*. <https://doi.org/10.1016/j.biortech.2008.08.031>.
- Zhu, Q., Peng, X., & Huang, T. (2015). Contrasted effects of biochar on maize growth and N use efficiency depending on soil conditions. *International Agrophysics*. <https://doi.org/10.1515/intag-2015-0023>.

Chapter 22

Distribution of Rare Earth Elements in Coal and Coal Fly Ash



Sanjay Agarwal, Vishal Kumar Dubey, Kyung Ho Park, and Jin-Young Lee

22.1 Introduction

Rare earth elements (REEs) are essential strategic elements which include 15 lanthanides with atomic numbers 57–71 [lanthanum (La), cerium (Ce), praseodymium (Pr), neodymium (Nd), promethium (Pm), samarium (Sm), europium (Eu), gadolinium (Gd), terbium (Tb), dysprosium (Dy), holmium (Ho), erbium (Er), thulium (Tm), ytterbium (Yb), and lutetium (Lu)] and two pseudo lanthanides with atomic numbers 21 and 39 [scandium (Sc) and yttrium (Y)]. Scandium and yttrium are treated as REEs because they have affinity toward lanthanides and exhibits similar chemical properties as that of REEs with different electric and magnetic properties (Tang et al. 2019; Zhang et al. 2015; Agarwal et al. 2017). Rare earth elements are present in appreciable amount in the earth crust however called rare because of their dispersed nature and are not found as concentrated mineral deposits, resulting in less economically viable ore deposit in the earth crust (Agarwal et al. 2020; Scott and Kolker 2019).

Except promethium, all REEs are more plentiful than precious metals like platinum, gold, and silver. On the basis of abundance of different elements in earth crust cerium comes in 25th position with 68 ppm, more abundant than copper (Van Gosen

S. Agarwal (✉) · V. K. Dubey
Metal Extraction and Recycling Division, CSIR-National Metallurgical Laboratory,
Jamshedpur, Jharkhand, India
e-mail: sanjay@nmlindia.org

K. H. Park
Center for Carbon Mineralization, Mineral Resources Research Division, Korea Institute of
Geosciences and Mineral Resources (KIGAM), Daejeon, Republic of Korea

J.-Y. Lee
Convergence Research Center for Development of Mineral Resources (DMR), Korea Institute
of Geoscience and Mineral Resources (KIGAM), Daejeon, Republic of Korea

et al. 2014). Average presence of REEs in the earth's crust is given in Table 22.1 (Van Gosen et al. 2014). Promethium [Pm, (atomic number 61)] is not included in this list because it is radioactive in nature. REEs are further classified into light (LREE—La, Ce, Pr, Nd, and Sm), medium (MREE—Eu, Gd, Th, Dy, and Y), and heavy (HREE—Ho, Er, Tm, Yb, and Lu). REEs are industrial vitamins because of their unique physicochemical properties, thus are widely used in today's industrial and technological applications (Van Gosen et al. 2014; Iftekhar et al. 2018). REEs are used extensively in next generation hybrid cars, power generation through wind turbines, high performance batteries, latest electronic gadgets, magnets, ceramic catalyst, super alloy steels, high-performance machine coolants, energy-efficient lighting equipments, military navigation systems, energy storing solar panels for the better performance of the new generation technologies (Zhang et al. 2020).

The major minerals of REEs are bastnasite, monazite, laterite, clays, and loparite. Others like apatite, gadolinite, euxenite and xenotime, allanite, fluorite, zircon, thorium minerals, uranium, iron tailings, and coal fly ash are also potential resources of rare earths. Global reserves of rare earths estimated on rare earth oxide basis to be about 130 million metric tons, where china has highest reserve followed by Brazil, Australia, and India (Van Gosen et al. 2014). China has greater grasp over REEs market which controls over more than 90% of worlds REEs supply. China has monopoly on production, supply chain, which led to a global concern for many countries like Japan, USA, India, and members of European union to tackle china's control on production and trading of REEs in global market. Therefore, there is inconsistency between higher demand and low production of REEs (Van Gosen et al. 2014). These problems lead to crisis in demand and supply chain, hence encouraged researchers and technological development teams across the world to

Table 22.1 List of REEs found in natural deposits. (Data source: Van Gosen et al. 2014)

Element	Symbol	Atomic number	Average abundance (in ppm)
Scandium	Sc	21	22
Yttrium	Y	39	33
Lanthanum	La	57	39
Cerium	Ce	58	66.5
Praseodymium	Pr	59	9.2
Neodymium	Nd	60	41.5
Samarium	Sm	62	7.05
Europium	Eu	63	2
Gadolinium	Gd	64	6.2
Terbium	Tb	65	1.2
Dysprosium	Dy	66	5.2
Holmium	Ho	67	1.3
Erbium	Er	68	3.5
Thulium	Tm	69	0.52
Ytterbium	Yb	70	3.2
Lutetium	Lu	71	0.8

recover REEs from secondary sources (Zhang et al. 2020; Franus et al. 2015). Among many secondary resources, coal fly ash is found to be a potential resource for the recovery of REEs. Coal fly ash is obtained as a by-product after combustion of coal in thermal power plant (Yao et al. 2015). On an average, the coal-based fly ash throughout the world contains around 400 mg/kg of REEs (Rao et al. 2020). As we know that energy is the basic requirement for the overall development of nations, it plays a very crucial role in their economic development. Developing countries are dependent on coal as natural resources for electricity production by thermal power plant which generate large amount of coal fly ash as a secondary product. (Rao et al. 2020; Yadav and Fulekar 2018) About 70–75% of India's and 40–45% of global energy requirement are fulfilled by coal-based thermal power plant which eventually produces a large amount of fly ash (Yadav and Fulekar 2018). India utilizes 60–70% and world utilizes about 45–50% of coal fly ash in different areas like cement industry, in roads and embankment construction, Mine filling, making bricks, and tiles (Haque 2013). The rest amount of fly ash remains unutilized and is a global concern to address. Abundance of REEs in coal fly across the world is about 5–10 times more than the concentration of REEs in coal. CFA is a very potential source of rare earth elements. This chapter reviews the detailed study of coal and coal fly ash, distribution of REEs in coal, coal-based fly ash, and different methods for the recovery of REEs from coal fly ash.

22.2 Coal

Coal is a combustible rock material containing mostly carbon along with hydrogen, sulfur, oxygen, and nitrogen as shown in Fig. 22.1. Coal is formed from the decay of dead plant matter, decayed organic matters which is buried under earth for

Fig. 22.1 A pictorial view of coal sample



millions of years under harsh geological conditions of heat and pressure. Coal formed from these matters are non-homogenous, and due to different geological conditions its structure becomes a heterogeneous one. Therefore, its structural determination is quite difficult. Coal structure is basically defined based on its size, i.e., primary structure having a size of 0.1–100 nm gives details about chemical subunits and bond nature between large molecules which are made up of condensed aromatic clusters linked by carbon bridge. Secondary structure having a size of 1 nm–10 μm reveals about local orientation of large molecules in the coal pore structures, and tertiary structures having size fraction of 1–100 μm gives idea about long-range arrangement of parallel structure in macerals and cluster of macerals with cross-links among themselves (Thomas 1986).

The heterogeneous nature of coal is due to the presence of macerals, distribution of inorganic matters. Macerals are organic compounds present in coals and are categorized into different groups such as vitrinite which is originated from humic gels wood bark or cortical tissues, exinite originated from fungal, spore's resins, secretions of plants, etc., inertinite originated from detrital matters, carbonized wood tissues, etc. Inorganic elements are incorporated in these organic matters. Almost all types of trace elements can be present in coal but in scarce amount. Some of the minerals which are found in coal are clay (kaolinite, illite, montmorillonite, chlorides), silica (quartz), sulfides (pyrites, pyrrhotite, sphalerite, marcasite, chalcopyrites, galena), carbonates (calcite, dolomite, siderite, aragonite, strontianite, witherite), and sulfates (gypsum, anhydrite, bassanite, barytes). When coal is heated, it is decomposed to coke with significant structural change. There are various types of chemical methods. There are various types of chemical methods used for the analysis of organic compounds in coal, namely dehydrogenation, oxidation, reduction, derivatization, and depolymerization (Thomas 1986).

7921 million tonnes of coal was produced in the year 2019. China, India, USA, Indonesia, and Australia are the top five coal-producing countries in the world. Around 85% of coal was consumed in the country where it was produced and rest 15% was traded in the international market. Table 22.2 gives the data of ten top coal producers of the world in 2019 (World Coal Production 2020; <https://www.worldcoal.org/coal/coal-mining>. Accessed on 23 November 2020). Our present-day life is unimaginable without electricity. Electricity is produced worldwide mainly by coal-based power plants. Thus coal plays a crucial role in the global electricity generation.

Table 22.2 Top 10 coal producer of world in 2019 (Data source: World Coal Production 2020; <https://www.worldcoal.org/coal/coal-mining>. Accessed on 23 November 2020)

Country	Qty. (million tons)	Country	Qty. (million tons)
China	3693	Russia	418
India	769	South Africa	254
USA	640	Germany	131
Indonesia	6161	Poland	112
Australia	503	Kazakhstan	104

22.2.1 *Distribution of REEs in Coal*

There are varied geological factors namely environment for deposition, physical, chemical and bio-geochemical factors which influences the enrichment and various modes of occurrence of REEs in coal (Equeenuddin et al. 2016). The accumulation mechanism and various modes of REEs occurrence in coal was studied by many geologists (Zhang et al. 2020). Coal enriched in REEs are formed under different geological conditions at various stages in Coal basins (Thomas 1986). Different genetic types are responsible for the occurrence of REEs in coal fly ash, namely source-rock-controlled types (Sediment source located near coal basin are important sources for incorporation of REEs in coal), Volcanic-ash-controlled type (Volcanic ash forms tonsteins which are incorporated into coal during different geological process. Alkaline tonsteins in coal were found to have a high content of REEs, whereas silicic tonsteins contained low REEs.), marine-environment-controlled type (coal deposits near marine environment are enriched in REEs not only because of sea water but also because of plankton which provided favorable environment for enrichment of REEs in coal), hydrothermal-fluid-controlled type (hydrothermal fluid in coal basin causes intrusion of igneous rocks into coal basin which enhances the concentration of REEs. It also affects the presence of organic matter), and groundwater-controlled type (ground water influences the occurrence of REEs in coal basin. REEs-enriched leachates were adsorbed by coal organic matter and intruded into the coal lying at the bottom level) (Dai et al. 2012). There are various REEs-bearing trace phases like monazite, allanite, zircon, xenotime, rhabdophane, and florencite which are discretely distributed in coal basins. Table 22.3 provides a comparison of different amounts of rare earth elements in coal samples of different countries throughout the world (Zhang et al. 2015; Mishra et al. 2019). In general, around 50–100 ppm of total REEs is found in coal samples across world.

Shifeng et al. studied coal enriched with boehmite mineral having higher portion of inertinite from Inner Mongolia, China. They collected coal sample from different region and categorized them based on boehmite to kaolinite ratio. These coal samples were completely characterized using different techniques like X-ray fluorescence spectroscopy (XRF), energy dispersive X-ray spectroscopy coupled with scanning electron microscope (EDS-SEM), induction coupled plasma (ICP), XRD, and chemical analysis. Elemental analysis revealed that there is higher concentration of Al_2O_3 in every sample, whereas in some coal samples CaO was present in appreciable quantity. Other element such as Th, Li, F, Se, Pb, Sc, Zn, Ga, Zr, Sr, U, In, REE, Hf, Ta, TiO_2 , W, and Nb were also present in them. In these coal samples they found that rare earth elements (La, Ce, Nd, Sm, Eu and Gd) are associated with Y, Sc, In, K_2O , Rb, Zr, HF, U, and P_2O_5 . On an average these coals contain about 172 $\mu\text{g/g}$ of REEs. Groundwater leaching during diagenesis causes the enrichment of REEs in coal. LREEs are leached preferably from parting and enriched into organic matter as compared to HRREs, which eventually increases the LREEs to HREEs ratio in coal stalls (Dai et al. 2012).

Table 22.3 The average content of REEs in coals throughout the world (in ppm) (Data source: Zhang et al. 2015; Mishra et al. 2019)

Elements	World coal	US coal	Chinese coal	DPR Korea coal	Indian coal
Sc	3.9	4.2	4	4.9	–
Y	8.4	8.5	9	7.2	4.9
La	11	12	18	14.5	8.50
Ce	23	21	35	27.2	7.1
Pr	3.5	2.4	3.8	2.9	6.8
Nd	12	9.5	15	11.1	18.6
Pm	–	–	–	–	–
Sm	2	1.7	3	2.3	2.2
Eu	0.47	0.4	0.65	0.5	0.1
Gd	2.7	1.8	3.4	1.4	1.2
Tb	0.32	0.3	0.52	0.3	0.4
Dy	2.1	1.9	3.1	2	2.2
Ho	0.54	0.35	0.73	0.4	–
Er	0.93	1	2.1	1.1	0.6
Tm	0.31	0.15	0.34	0.3	–
Yb	1	0.95	2.0	1	0.6
Lu	0.2	0.14	0.32	–	0.3

Eskenazy (1987) studied the columnar section of coal from pirin deposit of Bulgaria and observed that the bottom part of coal seam was enriched in REEs having high percentage of HREEs (Tb, Yb, Lu). Thin layers of coal in seam are comparatively enriched in REEs than thick layers. HREEs concentration is more compared to LREEs. There was enrichment of HREEs in composite shale and at the bottom of coal bed. Its concentration decreases as moved from bottom of coal bed to top. Similarly, concentration of LREEs decreases when moved from top to bottom of the bed. REEs have strong affinity toward aluminum silicate mineral matter and has positive correlation with ash amount. Presence of REEs in coal samples is due to suspended terrigenous matter which leached into river or ocean water and eventually incorporated into organic matter in coal (G.M. Eskenazy 1987).

Seredin (1996) studied rare earth elements distribution in coal from Russian far east deposits. Their findings revealed that coal seam contain REEs in the form of incorporated organic matter and clay particles. The REEs in coal is formed by two process, namely erosion and tectonic depression with weathering crust in basin and accumulation of REEs-enriched coal into garbens formed from volcanoes and tectonic disturbances (Seredin 1996).

Zheng et al. (2007) studied the distribution of REEs in permian coal deposits from Huaibei coalfield, China. Coal samples from partings and roof (top and bottom) were collected from Huaibei Coal field, which eventually provide idea about the source of rock with its mineral matter and sedimentary environment. Experimental data revealed that enrichment of REEs in coal is due to magmatic intrusion. Mineral matter present in coal mainly comprises of clay minerals and

carbonates. The main constituents of clay are lithophile elements like Si, Al, Fe, Ti, and Na with which REEs are positively correlated. Abundance of REEs in coal are higher than that of partings because of presence of mineral matter as well as REEs incorporated organic matters in coal (Zheng et al. 2007; Birk and White 1991).

Birk and White (1991) studied bituminous coal from Sydney Basin, Nova Scotia, and observed that the REEs are distributed in illite clay and zircon. REEs are found in macerals and are also present in resistate minerals such as monazite, xenotime, and florencite. These minerals are dispersed in bituminous coal which originate from suspended sedimentary deposits of rivers. HREEs are enriched in bituminous coal with low ash content which forms complexes with organic phase. Different REEs distribution patterns can be seen in individual seams which reflect depositional and diagenetic mineralogy. Sedimentation, water chemistry, ion exchange and chelation cause REEs partitioning between inorganic and organic phase in coal. Highly pyritized bands in seams gives low REEs in ash, whereas clay-rich bands have enrichment in LREEs concentration (Birk and White 1991).

Hower et al studied laterally persisted tonstein contained coal from central Appalachian basin, USA, and found that tonstein comprises of minerals like quartz, anatase, sanidine, euhedral zircon that provided exact evidence for volcanic origin of parting. REEs concentration in tonstein was found to be between 511 and 565 ppm. There was enrichment in REEs concentration in coal underlying at the bottom of tonstein. The enhancement in concentration is due to leaching of REEs contained volcanic components in tonstein. The leachate rich in REEs is incorporated as precipitate in mineral phase of the underlying coal (Hower et al. 1999).

Equeenuddin et al. (2016) studied the geochemical features and varied modes of occurrence of trace elements in coal from different areas of West Bokaro, India, and observed that coal was mainly constitute of quartz (SiO_2) and kaolinite ($\text{Al}_2\text{O}_3 \cdot 2\text{SiO}_2 \cdot 2\text{H}_2\text{O}$) as major phases, whereas analcime and illite as intermediate and pyrite, dolomite as minor phase. The coal comprises of metals, namely Mn, V, Cu, Cr, Zn, Ni, Co, As, and Cd. The concentration of manganese is maximum (7.6–483.4 mg/kg) followed by vanadium, copper, chromium, zinc, nickel, cobalt, arsenic, and cadmium. The enrichment of REEs in coal depends on geochemical and epigenetic processes in the course of their formation. Different metals and REEs are associated with organic and inorganic constituents, namely silicates, sulfides, oxides, carbonates, phosphates, and sulfate (Equeenuddin et al. 2016).

Mishra et al. (2019) studied the geochemistry of REEs in lower godwana and talcher coal of Indian origin and observed that coal mainly constitutes of clay mineral, quartz, and alumina. Clay and quartz mineral phases like kaolinite, illite, and montmorillonite are mainly present in all samples. There was an increase in REEs concentration from 29.6 to 179 ppm with an increase in the depth of coal, and on an average it contained about 91 ppm of REEs. Clay minerals in coal were found to be encapsulated with REEs-bearing phosphate minerals. REEs-based monazite mineral was found to be present in magnesium-aluminosilicate-based matrix as dispersed mineral. A positive correlation was observed for LREEs with phosphorus. Monazite was found in chlorite mineral present in coal which provide information

about formation of monazite due to hydrothermal alteration during coal formation (Mishra et al. 2019).

Different opinion was made about the usual content of REEs in coal throughout world. A typical coal reserve is spreaded widely throughout, and deposition of coal takes place in different coal formation periods under epigenetic evolution and coal formation environment. The abundance of REEs in coal can be categorized into different genetic types which helps to understand how REEs are incorporated into different coal deposits. According to Seredin (1996) and Zheng et al. (2007), usual content of REEs in coal throughout world is about 46 ppm. Seredin (1996) and Dai et al. (2012) reported that REEs abundance of coal worldwide is about 69 ppm. More than 80% of total rare earth elements reserve is with three countries (China, Australia, and United States of America) (Zhang et al. 2015). Thus coal becomes a respectable source for rare earth elements.

22.3 Coal Fly Ash

Coal fly ash (CFA) is a powdery substance mainly comprises of silica, alumina, iron oxide, and calcium oxide as shown in Fig. 22.2. It is formed as a result of pulverized coal combustion at boilers in thermal power plants as shown in Fig. 22.3 (Swaine 1995). These are formed mainly from organic and inorganic constituent of feed coal.

Coal fly ash mainly comprises of two phases, namely amorphous and crystalline. Bulk fly ash contains 60–90% amorphous phase, namely amorphous aluminum–silicon matrix, glass matrix, and amorphous silicon, and the rest in crystalline phase, namely quartz, mulite, hematite, magnetite, ferrite spinel's, traces of kennedyite, killalaite, and traces of calcium sulfate, anhydrite, melitite, merwinite periclase, tricalcium, aluminate, and lime. There are about 188 different types of minerals

Fig. 22.2 Pictorial view of coal fly ash



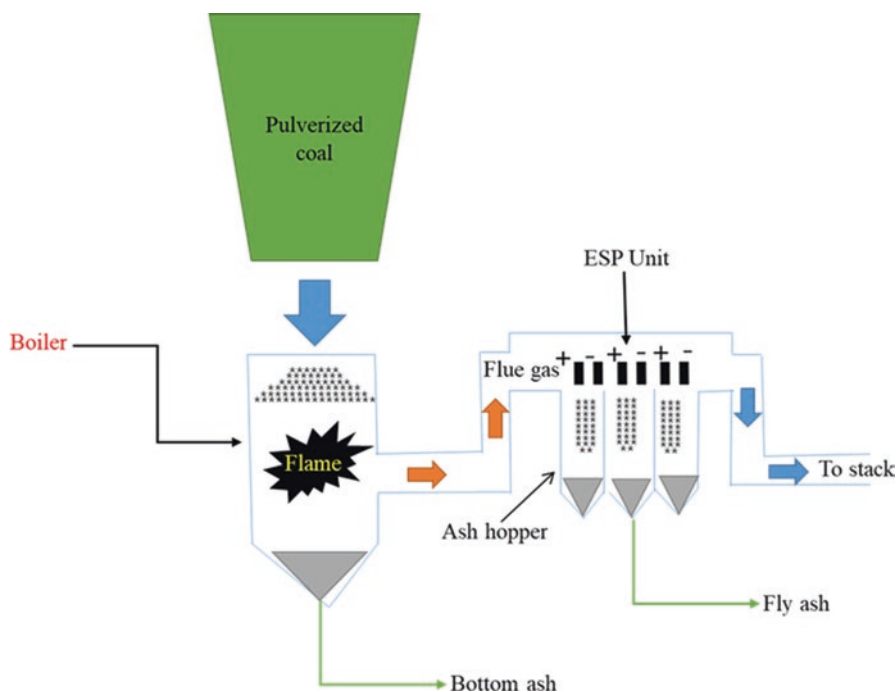


Fig. 22.3 Schematic diagram for generation of coal fly ash in thermal power plant (Re-drawn from reference Swaine 1995)

present in coal fly ash (Zhang et al. 2020; Rao et al. 2020; Yan et al. 2018; Medina et al. 2010). Because of light weight these coal fly ashes solidify while suspended in air from exhaust gases collected at electrostatic precipitators (Swaine 1995). The coal fly ash composition mainly depends on the chemistry of source coal, combustion process, and design of electrostatic precipitator (Franus et al. 2015). When pulverized coal is burnt, carbon, nitrogen, and sulfur present in organic matter oxidizes to CO_2 , NO_2 , SO_2 , and mineral matter present in coal is decomposed to residual solid that are bottom ash (contains approx. 20% of mineral matter) and fly ash (contains about 80% of mineral matter) (Swaine 1995).

Majority of fly ash is collected by electrostatic precipitators, fabric filters, fly ash arrestors, etc. According to American Society for Testing Materials (ASTM), CFA is categorized into two classes based on their physical and chemical characteristics and sum of (Fe_2O_3 , Al_2O_3 , CaO and SiO_2) content in coal fly ash. Class F fly ash is generated from high rank coal and Class C fly ash is generated from low rank coal. Class F fly ash has more than 70% of SiO_2 , Al_2O_3 , and Fe_2O_3 by mass and 20% of CaO , whereas Class C fly ash has more than 50% of SiO_2 , Al_2O_3 , and Fe_2O_3 and 30–40% of CaO (Chancey et al. 2010; Yousuf et al. 2020). Generally fly ash size ranges from 1 to 200 μm . Fly ash have different shapes like spherical called cenosphere, irregular shaped with rough and smooth surface (Mondal et al. 2019). Table 22.4 provides us a typical coal fly ash composition. The predominant elements

Table 22.4 Coal fly ash composition by coal type (wt.%) (Data source: Wikipedia Database 2020. Fly ash. https://en.wikipedia.org/wiki/Fly_ash. Accessed on 23 November 2020)

Type	Lignite	Sub-bituminous	Bituminous
SiO ₂	15–45	40–60	20–60
Al ₂ O ₃	20–25	20–30	5–35
Fe ₂ O ₃	4–15	4–10	10–40
CaO	15–60	5–30	1–12
LOI	0–5	0–3	0–15

in coal fly ash are Si, Al, Ca, and Fe and is a heterogeneous material (Singh and Subramanian 2018). Fly ash is utilized in a number of ways such as in cement making, brick blocks, as a construction and building material, as a filler material to replace sand in concrete production. Coal fly ash has mostly all the rare earth elements present in it, whereas many rare earth mineral mines have a few of them. Thus nowadays many countries/companies are exploring processes to recover REEs from coal fly ash in an economically and environmentally friendly way (Wikipedia Database 2020. Fly ash. https://en.wikipedia.org/wiki/Fly_ash. Accessed on 23 November 2020).

22.3.1 Distribution of REEs in Coal Fly Ash

It is important to explore and understand the REEs distribution in CFA so that effective recovery methods can be developed to extract REEs from them (Thomas 1986). Coal fly ash is a nonvolatile, noncombustible mineral matter of coal, hence major component of coal fly ash is mulite ($3\text{Al}_2\text{O}_3 \cdot 2\text{SiO}_2$), quartz (SiO_2), and iron oxide (hematite and magnetite). Thus 80% of coal fly ash composition consists of oxides of aluminum, silicon, and iron. REEs present in coal fly ash are embedded in the aluminosilicate glassy matrix structure. REEs bearing mineral phases such as monazite ($\text{Ce,La,Nd,Th}\text{PO}_4$), allanite ($\text{Ca,Ce,Y}_2(\text{Al,Fe}^{+3})_3(\text{SiO}_4)_3\text{OH}$), Zircon (ZrSiO_4), xenotime (YPO_4), rhabdophane ($(\text{La,Ce,Y}\text{PO}_4 \cdot \text{H}_2\text{O})$), Florencite $\text{CeAl}_3(\text{PO}_4)_2(\text{OH})_6$, Ce-Nd-bearing carbonates (Dai et al. 2012) are more commonly present in coal samples rather than in its coal fly ash. Coal-fired boilers working temperature is in the range of 1300 °C (Fluidized bed boilers) to 1700 °C (Pulverized coal-fired boilers). At these higher boiler working temperatures, coal having REEs bearing minerals gets melted, and their structure was broken leading to partitioning of REEs into the molten glass phases formed at these temperatures. This behavior is prevalent in natural igneous hydrothermal system where localized reduction/breakage of these phases occurs due to higher temperature-gradient thermal shocks present in the system. Thus to understand the REEs distribution in coal fly ash, the REE phases present in coal were reorganized at high temperature processing in the boilers to get incorporated into the aluminosilicate glassy matrix of coal fly ash. Swaine (1995) observed that with decrease in particle size of fly ash there was an increase in REEs

Table 22.5 REEs distribution in coal fly ash across the world (Data source: Rao et al. 2020; Franus et al. 2015; Rao et al. 2020; Tang et al. 2019; Lin et al. 2017, Franus et al. 2015; Mondal et al. 2019)

Elements (mg/kg)	China coal fly ash	USA coal fly ash	Poland coal fly ash	Indian coal fly ash
Sc	–	–	30	–
Y	57	–	48	–
La	82	319	60	62
Ce	184	662	123	137
Pr	21	79	14	20
Nd	85	300	53	46
Pm	–	–	–	–
Sm	16	62	11	6
Eu	3	7	2.4	4.3
Gd	14	62	9	4.4
Tb	2	10	1.5	1.2
Dy	12	63	8.3	4.9
Ho	2	12	1.8	0.9
Er	6	36	4.5	25.7
Tm	0.9	5	0.8	1.6
Yb	6	34	4.6	3.8
Lu	0.8	5	0.7	–

concentration (Yan et al. 2018). Calcium, iron-incorporated aluminosilicate in coal fly ash from their coal are comparatively REE-enriched due to the similarities in their ionic radii between divalent calcium and trivalent LREE and between divalent iron and trivalent HREEs (Wang et al. 2008).

Rao et al. (2020) observed that monazite mineral in fly ash was enriched in LREEs, whereas zircon in coal fly ash was enriched in HREEs (Franus et al. 2015; Rao et al. 2020). It was observed that maximum amount of REEs from the aluminosilicate glass-rich fraction of coal fly ash can be recovered. Table 22.5 gives the data of rare earth distributed across coal fly ash of different regions around the world (Tang et al. 2019; Lin et al. 2017; Franus et al. 2015; Mondal et al. 2019). The average REEs content present in all the coal fly ash is greater than 300 mg/kg. Major fraction being the rare earth elements (La, Ce, Nd, Pr, Sm, and Er).

22.3.2 Indian Fly Ash

India's power demand is mostly fulfilled from thermal power plant. About 70% of electricity generation depends on coal-based thermal power plant. They mostly use lignite coal as a raw material. These low-grade coals produce about 30–45% of fly ash and mainly composed of Al_2O_3 , CaO , TiO_2 , K_2O , SiO_2 , MgO , P_2O_5 , Fe_2O_3 , and SO_3 (Haque 2013; Van Gosen et al. 2014). More than 40% of fly ash comprises of

crystalline phase, namely quartz, mulite, hematite, magnetite, and rutile (Singh and Subramanian 2018). 217.04 million tons of fly ash was generated in India during 2018–2019 due to combustion of 667.43 million tons coal/lignite. Fly ash utilization during the same period was ~168.40 million tons which means ~77% of fly ash was effectively utilized in India (Yadav and Fulekar 2018).

Coal fly ash size ranges from 1 to 200 μm . SEM data revealed about different shapes of particles in fly ash (Dai et al. 2018). Indian data suggested that during the year 2018–2019, 75–78% of coal fly ash was utilized mainly in cement, mine filling, brick and tiles manufacturing, reclamation of low-lying area, ash dyke, road and flyover making, agricultural usage, concrete making, etc., and the remaining 22% was unutilized as shown in Fig. 22.4 (Chancey et al. 2010). More than 26% of fly ash was utilized in cement industry (Chancey et al. 2010). Class F type of fly ash contains less than 20% of CaO and has pozzolanic property due to which some of Portland cement content is replaced by these fly ashes (Van Gosen et al. 2014). Additionally alternate binders such as geopolymers (aluminosilicate) are prepared from fly ash which are used in structural applications (Singh and Subramanian 2018). Samples of coal fly ash from Bhusawal, Durgapur, Kaperkheda, Kota, and Panipat coal-fired power plant in India were studied for the REEs content in them

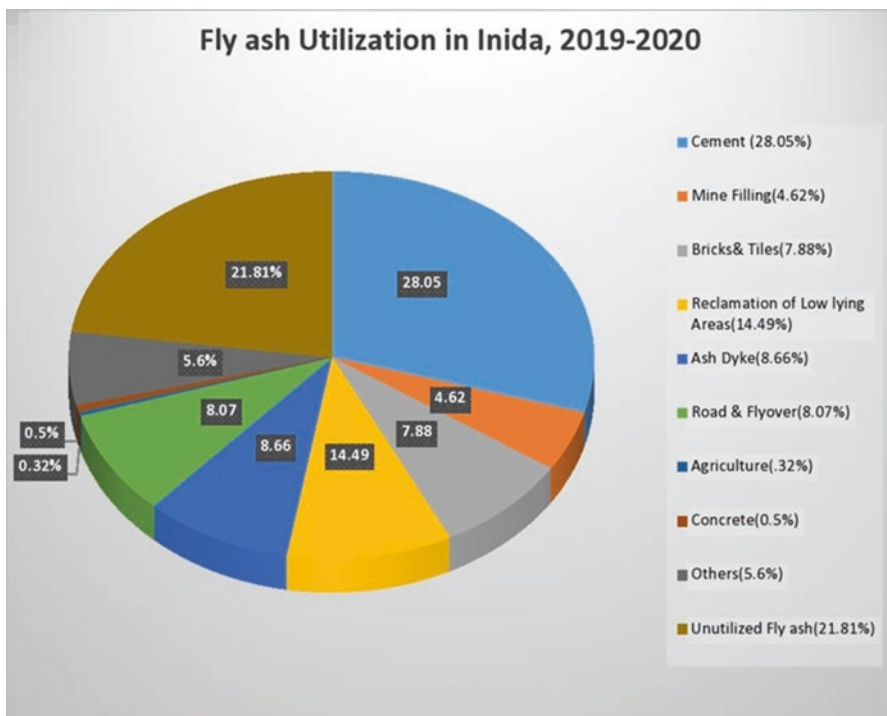


Fig. 22.4 Fly ash utilization in India (Data source: Dai et al. 2018; Chancey et al. 2010; Van Gosen et al. 2014; Singh and Subramanian 2018)

Table 22.6 REEs distribution in coal fly ash across India

REE/(mg/kg)	Bhusawal coal	Durgapur coal	Kaperkheda coal	Kota coal	Panipat coal
La	60	63	50	88.7	50.2
Ce	140	127	120	200	100
Pr	48	14.3	–	27	11.9
Nd	53	48	30	60	38.4
Sm	3.5	9.8	–	7.7	8.5
Eu	1.8	3.5	–	7.7	8.5
Gd	5.1	10.8	–	3.00	3.2
Tb	0.7	2.5	–	0.6	2.3
Dy	5.4	7.3	–	5.3	6.5
Ho	–	2.3	–	–	2.1
Er	–	4.6	120	–	4.0
Tm	–	1.6	–	–	1.5
Yb	4.3	4.2	2.0	5.0	3.7
Lu	1.8	1.6	–	2.0	1.5
Y	40	31.4	30	4.0	31
Sc	20.5	28.6	16	26	28
Total REEs	384.1	360.5	368	468.4	302.4

and are shown in Table 22.6 (Mondal et al. 2019). The average REEs were found to be 300–500 mg/kg (Mondal et al. 2019). This is a huge amount of fly ash which can be economically utilized to recover significant quantity of REEs from Indian fly ash.

22.4 Ways to Recover REEs from Coal Fly Ash

Based on physical and chemical characteristics of CFA, several studies were performed in order to concentrate REEs content in coal fly ash using different physical beneficiation techniques such as gravity, magnetic separation, and flotation techniques (Zhang et al. 2020; Lin et al. 2017). Lin et al. carried out physical separation feasibility studies to concentrate REEs from coal fly ash and observed that REEs were concentrated with finer size fractions in nonmagnetic fractions of coal fly ash using magnetic separation methods (Lin et al. 2017).

For the enhancement of REEs yield from CFA, direct chemical extraction of REEs was carried out using different acids by hydrothermal process (Zhang et al. 2020). Rao et al. (2020) studied the leaching recovery of REEs from Indian coal fly ash and observed that H_2SO_4 gave appreciable leaching recovery of 51% of total REEs as compared to 29% for HCl and 2% for HNO_3 . Leachability of HRREs was found to be high because they are mainly incorporated into organic phase, hence they are released freely from matrix during combustion, whereas LREEs leachability is less because they are incorporated in minerals like monazite and zircon (Rao et al. 2020). Tang et al. studied the extraction of REEs from fly ash through alkali

Table 22.7 Different REEs recovery process routes from coal fly ash (Data source: Rao et al. 2020, Tang et al. 2019, King et al. 2018 and Wang et al. 2020)

Sample	Pretreatment	Leaching condition	Recovery of total REEs	Reference
Coal fly ash, Neyveli lignite Corporation (NLC) India Ltd., Tamil Nadu, India	None	1 M H ₂ SO ₄ ; 60 °C, 20%(w/v), 6 h	51.60%	Rao et al. (2020)
		1 M HNO ₃ , 20%(w/v), 25 °C	29%	
		1 M HCl, 20%(w/v), 25 °C	2% ^s	
Coal fly ash, Panbei coal-fired power plant, Guizhou, China	Alkali fusion of coal fly ash with Na ₂ CO ₃ at 860 °C, (1:1) ratio of mixing of CFA and Na ₂ CO ₃ .	3 M HCl. Solid to liquid (1:2) g/ml, 2 h	72.78	Tang et al. (2019)
Fly ash from Illinois Basin, USA	None	12 M HCl, Liquid/solid ratio 100/1, 85 °C, 4 h	35–43%	King et al. (2018)
Fly ash/Bottom ash Sichuan, China	None	4% HF 50 g/L, 23–25 °C, 24 h	>90%	Wang et al. (2020)
Flay ash sample from Sichuan, China	40% NaOH, 10/1 (v/w), solid/liquid ratio, 150 °C, 2 h	8 M HCl Liquid/solid ratio 30/1 (v/w), 60 °C, 2 h	88.15%	
Coal Fly Ash from Powder River Basin, USA	None	15 M HNO ₃ , 10–50 g/l, 90 °C, 4 h	69.90%	Zhang et al. (2020)

fusion followed by acid leaching. They observed that alkali fusion prior to acid leaching gave higher recovery of 58.38% of REEs (Tang et al. 2019). The enhancement of REEs recovery is due to the fact that high temperature alkali fusion prior to acid leaching helps in breaking of REEs encapsulated Al-Si matrix (Yousuf et al. 2020). Moreover REEs enriched minerals like monazite and zircon are converted to ionic form which can easily be leached (Peiravi et al. 2017). A summary on relevant studies is provided in Table 22.7 (Rao et al. 2020; Tang et al. 2019; King et al. 2018; Wang et al. 2020). Highest recovery of total REEs from the coal fly ash was found to be ~90%.

22.5 Conclusion

Coal is a combustible rock mineral comprises of main elements like Al, Si, Ca, Mg, K, Cr, Mn, and P and minor elements like Mo, Cu, Pb, Zn, Cd, Sb, Au, Hg, Se, and As along with REEs. India has a rich resource of REEs in coal deposits. Pulverized

coal is consumed in thermal power plants to produce electricity, and it also generates a large amount of fly ash as a by-product. All the REEs present in coal gets into the coal fly ash. Even though coal fly ash is utilized in different sectors, namely cement, manufacturing, mine filling, brick making, road, and flyover making. More than 25% of the produced fly ash remains unutilized which eventually become environmental havoc. The coal fly ash is a very good secondary reserve for the production of REEs from it. Coal fly ash can be utilized in future for production of REEs with viable process without altering the chemical properties of ash. Economical recovery of REEs from fly ash will give a valuable aid to the coal fly ash industry.

References

- Agarwal, S., Kim, I. H., Park, K. H. and Lee, J. Y. (2017). Monazite mineral processing: Mineral processing. methods, application and technology, ed. Jyothi Rajesh Kumar, ISBN:978-1-53612-893-2 (eBook), 39-56. USA: Nova Science Publishers.
- Agarwal, S., Kim, I. H., Park, K. H., & Lee, J. Y. (2020). Thermodynamic aspects for rare earth metal production. In J. R. Kumar (Ed.), ISBN: 978-3-030-38106-6 (eBook) *Rare-earth metal recovery for green technologies, methods and applications* (pp. 39-56). Switzerland: Springer.
- Birk, D., & White, J. C. (1991). Rare earth elements in bituminous coals and underclays of the Sydney Basin, Nova Scotia: Element sites, distribution, mineralogy. *International Journal of Coal Geology*, 19(1-4), 219-251.
- Chancey, R. T., Stutzman, P., Juenger, M. C., & Fowler, D. W. (2010). Comprehensive phase characterization of crystalline and amorphous phases of a Class F fly ash. *Cement and Concrete Research*, 40(1), 146-156.
- Dai, S., Ren, D., Chou, C. L., Finkelman, R. B., Seredin, V. V., & Zhou, Y. (2012). Geochemistry of trace elements in Chinese coals: a review of abundances, genetic types, impacts on human health, and industrial utilization. *International Journal of Coal Geology*, 94, 3-21.
- Dai, S., Yan, X., Ward, C. R., Hower, J. C., Zhao, L., Wang, X., Zhao, L., Ren, D., & Finkelman, R. B. (2018). Valuable elements in Chinese coals: A review. *International Geology Review*, 60(5-6), 590-620.
- Equeenuddin, S. M., Tripathy, S., Sahoo, P. K., & Ranjan, A. (2016). Geochemical characteristics and mode of occurrence of trace elements in coal at West Bokaro coalfield. *International Journal of Coal Science & Technology*, 3(4), 399-406.
- Eskenazy, G. M. (1987). Rare earth elements in a sampled coal from the Pirin deposit, Bulgaria. *International Journal of Coal Geology*, 7(3), 301-314.
- Franus, W., Wiatros-Motyka, M. M., & Wdowin, M. (2015). Coal fly ash as a resource for rare earth elements. *Environmental Science and Pollution Research*, 22(12), 9464-9474.
- Haque, M. E. (2013). Indian fly-ash: production and consumption scenario. *International Journal of Waste Resources*, 3(1), 22-25.
- Hower, J. C., Ruppert, L. F., & Eble, C. F. (1999). Lanthanide, yttrium, and zirconium anomalies in the Fire Clay coal bed, Eastern Kentucky. *International Journal of Coal Geology*, 39(1-3), 141-153.
- Iftekhar, S., Ramasamy, D. L., Srivastava, V., Asif, M. B., & Sillanpää, M. (2018). Understanding the factors affecting the adsorption of Lanthanum using different adsorbents: a critical review. *Chemosphere*, 204, 413-430.
- King, J. F., Taggart, R. K., Smith, R. C., Hower, J. C., & Hsu-Kim, H. (2018). Aqueous acid and alkaline extraction of rare earth elements from coal combustion ash. *International Journal of Coal Geology*, 195, 75-83.

- Lin, R., Howard, B. H., Roth, E. A., Bank, T. L., Granite, E. J., & Soong, Y. (2017). Enrichment of rare earth elements from coal and coal by-products by physical separations. *Fuel*, *200*, 506–520.
- Medina, A., Gamero, P., Querol, X., Moreno, N., De León, B., Almanza, M., Vargas, G., Izquierdo, M., & Font, O. (2010). Fly ash from a Mexican mineral coal I: Mineralogical and chemical characterization. *Journal of Hazardous Materials*, *181*(1–3), 82–90.
- Mishra, V., Chakravarty, S., Finkelman, R. B., & Varma, A. K. (2019). Geochemistry of rare earth elements in lower Gondwana coals of the Talchir Coal Basin, India. *Journal of Geochemical Exploration*, *204*, 43–56.
- Mondal, S., Ghar, A., Satpati, A. K., Sinharoy, P., Singh, D. K., Sharma, J. N., Sreenivas, T., & Kain, V. (2019). Recovery of rare earth elements from coal fly ash using TEHDGA impregnated resin. *Hydrometallurgy*, *185*, 93–101.
- Peiravi, M., Ackah, L., Guru, R., Mohanty, M., Liu, J., Xu, B., Zhu, X., & Chen, L. (2017). Chemical extraction of rare earth elements from coal ash. *Minerals & Metallurgical Processing*, *34*(4), 170–177.
- Rao, K. A., Md, S., RamaDevi, G., G Thakurta, S., & Sreenivas, T. (2020). On the characterization and leaching of rare earths from a coal fly ash of Indian origin. *Separation Science and Technology*. <https://doi.org/10.1080/01496395.2020.1718705>.
- Scott, C. and Kolker, A. (2019). Rare earth elements in coal and coal fly ash, US Geological Survey: 2019–3048.
- Seredin, V. V. (1996). Rare earth element-bearing coals from the Russian Far East deposits. *International Journal of Coal Geology*, *30*(1–2), 101–129.
- Singh, G. B., & Subramanian, K. V. (2018). Characterization of Indian fly ashes using different experimental techniques. *Indian Concr. J*, *92*(3), 10–23.
- Swaine, D. J. (1995). The formation, composition and utilisation of flyash. In *Environmental aspects of trace elements in coal* (pp. 204–220). Dordrecht: Springer.
- Tang, M., Zhou, C., Pan, J., Zhang, N., Liu, C., Cao, S., Hu, T., & Ji, W. (2019). Study on extraction of rare earth elements from coal fly ash through alkali fusion–Acid leaching. *Minerals Engineering*, *136*, 36–42.
- Thomas, K. M. (1986). Coal structure. In *Carbon and coal gasification* (pp. 57–92). Dordrecht: Springer.
- Van Gosen, B.S., Verplanck, P.L., Long, K.R., Gambogi, J. and Seal II, R. R. (2014). The rare-earth elements: vital to modern technologies and lifestyles, US Geological Survey: 2014–3078.
- Wang, W., Qin, Y., Sang, S., Zhu, Y., Wang, C., & Weiss, D. J. (2008). Geochemistry of rare earth elements in a marine influenced coal and its organic solvent extracts from the Antaibao mining district, Shanxi, China. *International Journal of Coal Geology*, *76*(4), 309–317.
- Wang, X., Li, S., Zhao, L., Xu, C., & Gao, J. (2020). A DFT and TD-DFT study on electronic structures and UV-spectra properties of octaethyl-porphyrin with different central metals (Ni, V, Cu, Co). *Chinese Journal of Chemical Engineering*, *28*(2), 532–540.
- Wikipedia Database (2020). Fly ash. https://en.wikipedia.org/wiki/Fly_ash. Accessed on 23 November 2020.
- World coal production in (2020). <https://www.worldcoal.org/coal/coal-mining>. Accessed on 23 November 2020.
- Yadav, V. K., & Fulekar, M. H. (2018). The current scenario of thermal power plants and fly ash: production and utilization with a focus in India. *International Journal of Advance Engineering and Research. Development*, *5*(4), 768–777.
- Yan, K., Guo, Y., Ma, Z., Zhao, Z., & Cheng, F. (2018). Quantitative analysis of crystalline and amorphous phases in pulverized coal fly ash based on the Rietveld method. *Journal of Non-Crystalline Solids*, *483*, 37–42.
- Yao, Z. T., Ji, X. S., Sarker, P. K., Tang, J. H., Ge, L. Q., Xia, M. S., & Xi, Y. Q. (2015). A comprehensive review on the applications of coal fly ash. *Earth-Science Reviews*, *141*, 105–121.

- Yousuf, A., Manzoor, S. O., Youssouf, M., Malik, Z. A., & Khawaja, K. S. (2020). Fly Ash: Production and utilization in India—An overview. *Journal of Materials and Environmental Science*, *11*(6), 911–921.
- Zhang, W., Noble, A., Yang, X., & Honaker, R. (2020). A comprehensive review of rare earth elements recovery from coal-related materials. *Minerals*, *10*(5), 451.
- Zhang, W., Rezaee, M., Bhagavatula, A., Li, Y., Groppo, J., & Honaker, R. (2015). A review of the occurrence and promising recovery methods of rare earth elements from coal and coal by-products. *International Journal of Coal Preparation and Utilization*, *35*(6), 295–330.
- Zheng, L., Liu, G., Chou, C. L., Qi, C., & Zhang, Y. (2007). Geochemistry of rare earth elements in Permian coals from the Huaibei Coalfield, China. *Journal of Asian Earth Sciences*, *31*(2), 167–176.

Chapter 23

Recent Development in Metal Extraction from Coal Fly Ash



Hong Vu, Tomáš Frýdl, Tadeáš Bastl, Petr Dvořák, Eva Kristianová,
and Tomáš Tomáško

23.1 Introduction

With the major share of coal consumption going to the production of electricity, massive quantities of CFA are generated globally, but only part of them is utilized and the rest of unutilized CFA is stored in ash ponds or surface impoundments (Gollakota et al. 2019).

In 2018 the top coal consumers, China and India, produced 550 and 217 Mt. of CFA with the utilization rates at 75 and 77%, respectively (Yousuf et al. 2020; Luo et al. 2020). The CFA production in the USA stayed at 36 Mt. in 2018, but the rate of ash decreased by 10–55% since the previous year (ACAAssociation 2018). The production of CFA in the EU-15 in 2016 was 25.7 Mt., corresponding to the utilization rate of 94% (ECOBA 2016a). The updated global coal fly ash production and utilization is illustrated in Fig. 23.1.

Currently, CFA is utilized mainly in construction applications ranging from cement and concrete to road construction and filling materials, while small quantities of CFA are consumed in agriculture (Bhatt et al. 2019; Harris 2017; Gollakota et al. 2019). Many other potential options for reuse of CFA are being explored such as geopolymers, cenosphere, magnetite, aluminosilicate, carbon nanotubes, adsorbents for treatment of organic and inorganic pollutants or greenhouse emissions or raw materials for ceramics production (Bhatt et al. 2019; Tauanov et al. 2020; Gollakota et al. 2019). With the growing demands of metals for the low-carbon future and dismissing accessible metal-bearing resources, metal recovery from CFA has drawn great interests from academia, governments as well as from industry (Sahoo et al. 2016; Group 2017; Energy 2017; Harris 2017). The metallurgical

H. Vu (✉) · T. Frýdl · T. Bastl · P. Dvořák · E. Kristianová · T. Tomáško
Department of Metals and Corrosion Engineering, University of Chemistry and Technology
Prague, Praha 6 - Dejvice, Czech Republic
e-mail: Nguyen.Hong.Vu@vscht.cz

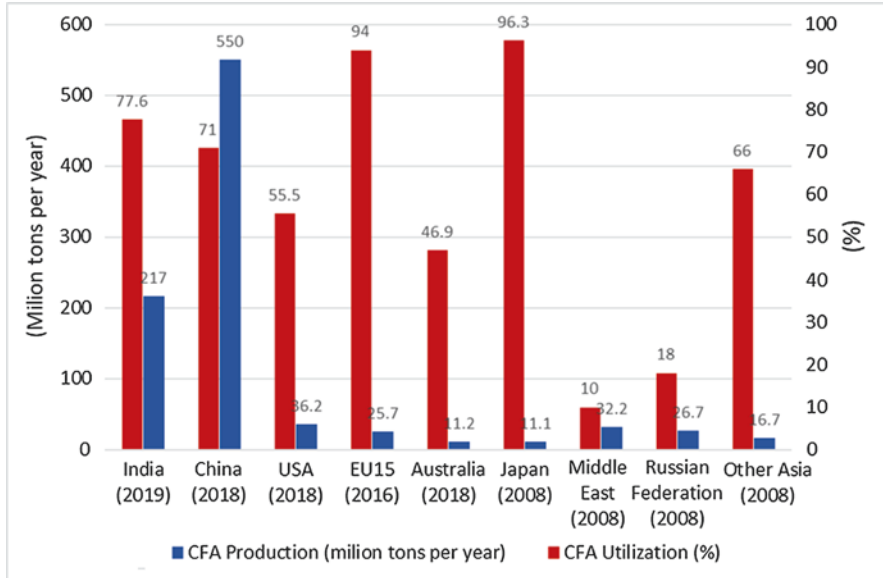


Fig. 23.1 Global coal fly ash production and utilization (Data source: Gollakota et al. 2019; ACAAssociation 2018; Luo et al. 2020; ECOBA 2016b; Yousuf et al. 2020; Ltd 2018)

treatment of CFA can reduce the environmental impacts of disposal and potential contamination of waste containing hazardous materials (Franus et al. 2015; Sahoo et al. 2016).

Coal fly ash is a very complex material with physical/chemical properties varying greatly according to the type of coal burnt and combustion techniques (Sahoo et al. 2016; Gollakota et al. 2019; Bhatt et al. 2019). The main components of all fly ashes are SiO_2 , Al_2O_3 , CaO , Fe_2O_3 , MgO , Na_2O and K_2O . The summary of coal fly ash composition from different countries and regions is presented in Table 23.1. Besides the main metals, CFA also contains trace metals at different concentrations as shown in Table 23.2 and rare earth metals as shown in Tables 23.3 and 23.4.

23.2 Metallurgical Methods for Processing Coal Fly Ash

23.2.1 Pyrometallurgical Methods

Pyrometallurgical methods in the processing of coal fly ash (CFA) can be divided into two big groups. The first one is direct extraction of selected metals which is accomplished via (carbo)chlorination. This method is capable of breaking up the structure of present minerals and thus enables the recovery of metals in the form of chlorides. The second approach is to transform insoluble compounds containing

Table 23.1 Content of oxides in CFA from different countries

Region	Country	Oxide content [wt.%]											Reference
		SiO ₂	TiO ₂	Al ₂ O ₃	Fe ₂ O ₃	MnO	MgO	CaO	Na ₂ O	K ₂ O	P ₂ O ₅		
Asia	China	35.7–57.7	0.2–3.2	18.8–55.0	1.3–19.4	0.1–0.4	0.2–6.6	1.1–9.6	0.1–1.3	0.3–2.1	0.3–1.5		Guo et al. (2019b), Pan et al. (2020), Guo et al. (2013), Shi et al. (2020b), Wu et al. (2019), Wang et al. (2019c), Guo et al. (2019a), Yan et al. (2012), Qi and Yuan (2011), Liu et al. (2004)
		50.2–65.1	0.8–2.7	14.0–32.4	1.0–4.7	0.8–1.4	0.1–2.1	0.6–2.6	0.1–1.2	0.1–4.7	0.1–0.6		Panda and Sangita (2020), Nayak and Panda (2010), Mishra and Das (2010), Dutta et al. (2009)
	Vietnam	37.4–57.0	0.6–0.8	17.4–25.0	4.2–5.6	0.04–0.1	1.1–1.4	0.8–6.6	0.1–0.2	5.0–6.7	0.1–0.2	Le et al. (2019)	
	Kazakhstan	35.3–68.9	0.9–1.8	18.2–29.5	4.0–7.6	N/D	0.8–3.9	2.0–8.4	N/D	N/D	N/D	Kaplan et al. (2020)	
	Borneo	50.9	1.0	28.7	9.0	N/D	2.2	3.3	0.8	0.9	N/D	Rosita et al. (2020)	
	South Sumatera	42.6	0.8	20.4	13.8	N/D	6.6	9.6	0.7	0.9	N/D	Rosita et al. (2020)	
	Israel	46.3	1.6	34.8	5.8	N/D	2.1	6.5	0.9	1.2	N/D	Shabtai and Mukmenev (1996)	
Africa	South Africa	49.3–67.0	1.1–2.0	14.3–34.0	2.5–5.8	0.02	0.8–2.4	2.8–9.5	0.1–0.4	0.7–0.7	0.2–1.0	Badenhorst et al. (2019), Doucet et al. (2016), Rushwaya and Ndlovu (2017), Matjie et al. (2005)	
Australia	Australia	48.8–66.0	1.3–3.7	17.0–27.8	1.1–13.9	N/D	0.3–2.0	2.9–5.3	0.2–1.3	1.1–2.9	0.2–3.9	Jankowski et al. (2006)	

(continued)

Table 23.1 (continued)

Region	Country	Oxide content [wt.%]										Reference
		SiO ₂	TiO ₂	Al ₂ O ₃	Fe ₂ O ₃	MnO	MgO	CaO	Na ₂ O	K ₂ O	P ₂ O ₅	
Europe	Czech Republic	30.0–54.0	1.2–3.4	15.1–29.5	5.4–8.2	N/D	0.3–1.3	2.9–31.2	0.2–0.6	0.9–2.7	0.1–0.3	KEJK (2010), Marko et al. (2019a)
	Bulgaria	30.1–57.4	0.7–1.0	16.6–25.4	5.9–21.2	0.04–0.23	1.1–2.9	1.5–24.8	0.5–1.9	0.8–4.0	0.1–0.4	Vassilev and Vassileva (2007)
	France	47.0–51.0	N/D	26.0–34.0	6.9–8.8	N/D	1.5–2.2	2.3–3.3	2.3–6.4	N/D	N/D	Biswas et al. (2003)
	Germany	20.0–80.0	0.1–1.0	1.0–19.0	1.0–22.0	N/D	0.5–11.0	2.0–52.0	0.1–2.0	N/D	N/D	Moreno et al. (2005)
	Italy	41.7–50.8	1.3–2.6	25.9–33.4	3.8–8.8	0.03–0.1	0.8–2.4	2.3–10.0	0.4–0.5	0.7–2.6	0.3–1.5	Moreno et al. (2005)
	Macedonia	40.5–48.6	0.5–0.6	23.2–25.9	N/D	0.2–0.4	2.6–4.0	6.9–13.2	1.2–1.5	1.9–2.6	0.3–0.4	Sijakova Ivanova et al. (2011)
	Russia	40.5–48.6	0.5–0.6	23.2–25.9	N/D	0.2–0.4	2.6–4.0	13.2	1.5	2.6	0.4	Bhatt et al. (2019)
	Slovakia	46.77	N/D	15.69	8.34	N/D	1.21	3.93	N/D	N/D	N/D	Škvarla et al. (2011)
	Spain	41.5–63.0	0.5–1.6	18.0–35.6	2.6–16.0	0.03–0.1	0.6–2.5	0.8–11.8	0.2–0.8	0.6–3.9	0.1–1.7	Font et al. (2007), Chimenos et al. (2013), Arroyo et al. (2009b), Moreno et al. (2005)
	USA	The United States	27.8–58.5	1.0–1.6	19.1–28.6	3.2–25.5	N/D	0.5–4.8	0.7–22.4	0.2–1.8	0.9–2.9	0.1–1.3

Table 23.2 Concentration of trace metals in CFA from different countries

No.	Country	Concentration of metals (ppm)							Reference
		Zn	Ga	Ge	As	Se	Rb	Sr	
1	China	275.2–280.4	48.9–66.8	12.5	26.0–132.6	22.8–26.5	9.9–21.6	910.5–2624.0	Pan et al. (2020), Wang et al. (2019c)
2	Macedonia	163.0–192.0	N/D	N/D	5.8–14.1	N/D	N/D	471.0–993.0	Sijakova Ivanova et al. (2011)
3	Vietnam	93.4–1799.2	N/D	N/D	N/D	N/D	167.8–267.2	52.9–135.3	Le et al. (2019)
4	Israel	110.0	N/D	N/D	26.0	N/D	N/D	N/D	Shabtai and Mukmenev (1996)
5	Poland	11.0–210.0	N/D	N/D	10.2–50.5	0.8–10.5	N/D	N/D	Franus et al. (2015)
6	Spain	6963.0–7230.0	155.0–324.0	194.0–432.0	898.0–955.0	18.6–19.0	310.0	112.0	Font et al. (2007), Arroyo et al. (2009b), Chimenos et al. (2013)
		Li	Be	V	Cr	Co	Ni	Cu	
7	China	162.2	4.3–12.5	391.5–520.6	207.3–272.3	51.2–51.5	97.2–116.4	206.6–248.9	Pan et al. (2020), Wang et al. (2019c)
8	Macedonia	N/D	N/D	N/D	93.0–114.0	22.0–26.0	58.0–68.0	61.2–80.0	Sijakova Ivanova et al. (2011)
9	Vietnam	N/D	N/D	N/D	98.5–514.5	N/D	43.9–156.1	35.0–85.3	Le et al. (2019)
10	Israel	N/D	N/D	260.0	225.0	N/D	N/D	96.0	Shabtai and Mukmenev (1996)
11	Poland	N/D	N/D	N/D	N/D	N/D	19.9–62.6	12.7–73.2	Franus et al. (2015)
12	Spain	271	14.8	3302.0–6256.0	85.0–155.0	31.0–62.4	2268.0–2296.0	242.0–392.0	Font et al. (2007), Arroyo et al. (2009b), Chimenos et al. (2013)

Table 23.3 Concentration of REE + Y and Sc in CFA from different locations

No.	Location	Concentration of elements (ppm)									Reference
		La	Ce	Pr	Nd	Sm	Eu	Gd	Tb	Dy	
1	China	134.4–138.7	266.4–290.3	29.8–30.3	113.6–114.7	21.6–22.0	3.5–4.1	20.9–23.0	3.2–3.4	20.0–20.5	Wang et al. (2019c), Pan et al. (2020)
2	Borneo	42.3	84.9	9.7	37.4	7.7	1.7	7.7	1.3	7.8	Rosita et al. (2020)
3	South Sumatera	34.5	70.0	8.1	32.8	7.1	1.5	6.9	1.2	7.2	Rosita et al. (2020)
4	India	50.0–88.7	100.0–200.0	11.9–48.0	38.4–60.0	3.5–9.8	1.8–3.5	3.1–10.8	0.6–2.5	5.3–7.3	Mondal et al. (2019)
5	Poland	15.5–81.7	30.7–172.5	3.3–20.5	12.7–81.3	2.8–17.0	0.6–3.8	2.9–15.7	0.5–2.4	2.6–12.2	Franus et al. (2015)
6	The United States	71.2	151.4	18.4	68.0	14.2	3.0	13.9	2.2	12.9	Pan et al. (2021)

Table 23.4 Concentration of REE + Y and Sc in CFA from different locations

No.	Location	Concentration of elements (ppm)								Reference
		Ho	Er	Tm	Yb	Lu	Y	Sc	REY	
1	China	4.0	12.0	1.7	10.9–11.1	1.6	105.2–109.9	25.9	779.5–782.1	Wang et al. (2019c), Pan et al. (2020)
2	Borneo	1.8	5.1	0.8	5.1	0.8	46.4	N/D	260.4	Rosita et al. (2020)
3	South Sumatera	1.5	4.4	0.7	4.5	0.7	44.5	N/D	225.7	Rosita et al. (2020)
4	India	2.1–2.3	4.0–4.6	1.5–1.6	2.0–5.0	1.5–2.0	30.0–40.0	16.0–28.6	302.4–468.4	Mondal et al. (2019)
5	Poland	0.6–2.6	1.8–7.4	0.3–1.1	1.8–6.7	0.3–1.0	17.9–73.2	7.0–45.0	101.1–543.1	Franus et al. (2015)
6	The United States	2.6	7.6	1.1	7.0	1.1	72.8	39.9	487.3	Pan et al. (2021)

metals of interest to compounds which can be dissolved in various leaching media. This is mainly achieved by the reaction of CFA with certain chemicals at high temperatures. Usually, these processes are named sintering, fusion or digestion.

Study by Burnet et al. (1977) describes high-temperature chlorination for Al and Fe recovery from the CFA. The experiments were carried out in the temperature range 700–1000 °C. The experimental setup included two beds of material in the furnace, on the first one CFA mixed with carbon and on the second one CFA without

any additives. Aluminium was recovered as AlCl_3 , together with FeCl_3 and SiCl_4 . Chlorination was used in the work (Kaplan et al. 2020), as well. Two ways of chlorination were used—sintering the fly ash with CaCl_2 and chlorination with Cl_2 gas in the presence of a small amount of coal as a source of carbon. Temperatures ranged between 950 and 1150 °C, and extraction efficiency of Al reached 98%. Carbochlorination was applied in the work by Wang et al. (2019b) for Mg and Ca extraction from CFA at temperatures 800–1000 °C. The work was focused rather on explaining the kinetics of the process; it did not explore the potential for the industrial application.

In the work by Fan et al. (2019), an activation of CFA by roasting with Na_2CO_3 at 850 °C was employed with the goal to transform insoluble Al compounds to an extractable form. Another method is sintering with CaCO_3 (at 1350 °C) or a mixture of CaCO_3 and Na_2CO_3 (at >1100 °C) (Gao et al. 2020). In all cases, fly ash with high Al content was used as the source material. The other option is sintering CFA with $(\text{NH}_4)_2\text{SO}_4$ (Gao et al. 2020; Doucet et al. 2016). Sintering temperatures ranged from 400 to 600 °C. For activation of fly ash sintering with CaCO_3 or CaO was used (Marko et al. 2019b). Sintering with NaOH appears in the work by Kumar et al. (2020). CFA was sintered at temperatures 250–900 °C. As an alternative option, sintering in a microwave furnace was investigated. In the study by Guo et al. (2019b), researchers carried out calcination with Na_2CO_3 and red mud at the same time at temperatures 600–900 °C. Alkali fusion with Na_2CO_3 at temperature higher than 857 °C was used in the work of Tang et al. (2019) to enable extraction of rare earth elements from CFA.

Besides abovementioned methods, there is also the possibility that CFA undergoes just reduction (Zhang and Xu 2016). The metal of interest (in this study Ge) was obtained by heating the mixture of fly ash and carbon under vacuum at temperatures 570–1030 °C. During the process, elemental Ge was formed, evaporated and subsequently condensed. In another work by Zhang and Xu (2017), distillation-chlorination stage for purification of the product obtained in the reduction stage was added. The temperatures used in the distillation-chlorination are quite low as the boiling temperature of GeCl_4 reaches 84 °C only.

Processing of CFA by calcining it with KHSO_4 can be included to the group of pyrometallurgical processes, even though the processing temperatures were not high (Guo et al. 2019a). The temperatures used in the study ranged only from 190 to 250 °C. Calcination process resulted in the formation of soluble $\text{K}_3\text{Al}(\text{SO}_4)_3$.

23.2.2 Hydrometallurgical Methods

23.2.2.1 Leaching

Hydrometallurgical methods for processing CFA include leaching and precipitation as well as solvent extraction, ion exchange and special types of electrolysis. For leaching, a whole range of leaching media is used—from acidic to alkaline. Solvent

extraction also uses various extractants, depending on the metal to be extracted. As mentioned above, hydrometallurgical techniques are often connected with pyrometallurgical “pretreatment” which changes the nature of material to make its components more soluble.

Leaching of CFA in H_2SO_4 solutions can be carried out directly, without any prior pyrometallurgical treatment (Nayak and Panda 2010). The results showed that the Al extraction efficiency was quite low at ambient temperature and low acid concentration. Changing l/s ratio and increasing acid concentration shifted extraction efficiencies to higher values; nevertheless, many other metals were dissolved along with Al, making the resulting leach liquor difficult to purify and obtain individual metals. In another work (Sangita and Panda 2020), the kinetics of Al dissolution from CFA was studied. In a study of Al and Fe leaching kinetics (Seidel and Zimmels 1998), self-inhibition effect of leaching was observed, the reason of which was the presence of Ca. It was suggested to remove it by pre-leaching of CFA in HCl. Using high-pressure HCl leaching (Valeev et al. 2020) makes the removal possible to reach very good extraction efficiency of Al and low co-extraction of other metals.

Leaching in alkaline media has brought various results. There are studies reporting relatively low extraction efficiencies of selected metals (Arroyo et al. 2014) as well as others showing quite high extraction efficiencies (Font et al. 2007). Sodium hydroxide leaching can also be used as a pretreatment of further leaching in acidic media (Wen et al. 2020). Acidic and alkaline leaching can be combined (Aphane et al. 2020). In acidic leaching step, mainly amorphous phase containing SiO_2 and Al_2O_3 is dissolved, and in alkaline step crystalline phase is decomposed.

Leaching may form the second step of combined pyrometallurgical–hydrometallurgical processes as mentioned above. In many cases, pyrometallurgical treatment is followed by leaching the product of sintering/digestion/fusion, etc., in water (Doucet et al. 2016; Gao et al. 2020; Shi et al. 2020a). However, depending on the pyrometallurgical pretreatment involved, subsequent leaching in H_2SO_4 (Marko et al. 2019b) or HCl (Guo et al. 2019b; Kumar et al. 2020) can be found.

Reported leaching media for processing CFA can include uncommon leaching reagents like NH_4HSO_4 (Wu et al. 2019). In this study high alumina extraction rates were achieved, but leaching must be carried out in autoclaves as leaching temperature exceeding 140 °C was required.

23.2.2.2 Bioleaching

Several studies have been published dealing with bioleaching for metal extraction from CFA. Using *Acidobacillus ferrooxidans* bacteria, Al and Ce can be extracted (Fan et al. 2019). A study on using another common type of bacteria—*Thiobacillus thiooxidans* (Seidel et al. 2001)—showed that the nature of CFA caused delay in starting the process of bioleaching; nevertheless, the overall good results were achieved. A method of bioleaching of CFA using thiobacillus was patented (Fass et al. 1993). An interesting contribution to the topic is the study on possibility of biomodification of coal fly ash using urease-producing bacteria (Zhang et al. 2021).

Even though it is not a method for direct metal recovery, some bioleaching was observed as well as microbially induced precipitation. Specific bacteria (*Rhodococcus* GIN-1) are capable of enriching Ti concentration in leachate (Shabtai and Mukmenev 1996). The process is based on biomagnetic separation. Bacteria, however, are not the only microorganisms used in CFA processing. Fungi *Aspergillus niger* was used in a combined leaching process (Su et al. 2020).

23.2.2.3 Solvent Extraction and Ion Exchange

Recovery of individual metals is accomplished usually by solvent extraction as liquors originating from leaching are mostly polymetallic. Nevertheless, precipitation and crystallization have been used, especially for Al_2O_3 recovery from acidic leach solutions (Seeley et al. 1981; Gabler and Stoll 1982). The low selectivity of sulphide precipitation can be shown on the example of Ge, where strong coprecipitation of As, Sb and Ni occurred (Arroyo et al. 2009a). Further refining steps were therefore necessary to obtain pure Ge. Certain improvement has brought using organic complexing agents, i.e. catechol and cetyltrimethylammonium bromide allowing Ge to be precipitated as an organic complex. For solvent extraction of metals from CFA, a whole range of extractants is used. As examples, JMT-Primene (Rushwaya and Ndlovu 2017) or Cyanex 923 (Gupta et al. 2007) can be mentioned. Application of stepwise extraction using two different extractants was also investigated (Zhao et al. 2020).

Ion exchange seems to be an efficient method for metal recovery from solutions originating from CFA leaching (Torralvo and Fernández-Pereira 2011). It is sufficiently selective; however, for potential industrial application it may be limited by higher costs.

It should also be mentioned about an example of uncommon method of metal recovery from CFA using two-membrane and three-chamber cell electrolysis (Shi et al. 2020b). Unfortunately, the study only used pure solution of $\text{Al}_2(\text{SO}_4)_3$, so no information on impurities behaviour was given.

23.3 Overview of Extraction of Selected Metals from Coal Fly Ash

23.3.1 Titanium

Titanium is found in the CFA in the amorphous phases of Si-Al-Ti-Fe, Al-Si-K-Fe-Ti or Al-Si-Ti, and partly also in the form of rutile (TiO_2), ilmenite (FeTiO_3) or perovskite (CaTiO_3). From the amorphous phases, Ti can be only extracted by chemical and thermochemical processes. Hydrometallurgical, biometallurgical or roasting processes are usually used for these purposes.

The most common hydrometallurgical process used for processing CFA is its leaching in H_2SO_4 (Matjie et al. 2005; Nayak and Panda 2010). During this process, Ti and other utility elements such as Al, Fe, As, Cd, Hg and Pb are also co-dissolved. The advantage of leaching in H_2SO_4 is prevention of SiO_2 dissolution as in alkaline leaching, which would otherwise be the main impurity in leaching liquor. The most significant challenge in this process is the co-extraction of accompanying impurities, mostly Ca, K, Na and Mg. Elements of interest can be extracted from the liquor by precipitation by pH adjustment with NaOH or $\text{NH}_3(\text{aq.})$ (Matjie et al. 2005; Shabtai and Mukmenev 1996), recrystallization or solvent extraction (Fontana et al. 2005; Sole 1999).

The degree of extraction of individual metals depends on the acid concentration, the leaching temperature, the process time and the solid to liquid ratio. It has been shown that a higher degree of Ti extraction can be achieved by increasing the concentration of H_2SO_4 , the leaching temperature and the liquid-to-solid ratio. By leaching in H_2SO_4 at the atmospheric pressure, maximum extraction rate of Ti of around 20% can be achieved. This efficacy was achieved under conditions of 18 mol/L H_2SO_4 , 200 °C and 4 h (Nayak and Panda 2010). Leaching is followed by filtering and purification of individual products. The sample processing flow charts are shown in Figs. 23.2 and 23.3. Since Ti in CFA is predominantly found in phases together with Si and Al oxides, the leaching extraction efficiency can be increased by roasting of CFA in the presence of CaCO_3 . Roasting with CaCO_3 at temperature of 1000–1200 °C is used to break down the original structures and create new Ca-rich phase. Titanium is activated by this process (Rushwaya and Ndlovu 2017; Nayak and Panda 2010).

Many extractants are known for selective separation of Ti by solvent extraction. The efficiency of this method is strongly dependent on the acidity of the aqueous phase and the extracting agent used. The most common extractant system used for Ti is di-2-ethylhexyl phosphoric acid (D2EHPA) dissolved in kerosene or benzene. Using this solvent, Ti can be extracted from sulphate, chloride and nitric acid media (Sole 1999; Biswas et al. 2003; Islam and Biswas 1981; Biswas and Begum 2000). Alongside D2EHPA, for the extraction of Ti from acidic solutions the following extractant systems are used: Primene-JMT (*tri*-alkyl-methylamine) dissolved in Shellsol D70 (Rushwaya and Ndlovu 2017), Cyanex 301 dissolved in Kerosene (Biswas and Karmakar 2014), Cyanex 302 dissolved in Kerosene (Karmakar and Biswas 2019), *tri*-*n*-octylphosphine oxide (TOPO) in cyclohexane (Sole 1999), 2-ethylhexyl phosphonic acid *mono*-2-ethylhexyl ester (EHEHPA) in kerosene (Fontana et al. 2005), *tri*-*n*-butyl phosphate (TBP) in kerosene (Seyfi and Abdi 2009), *trioctyl* tertiary amine (N235) in kerosene (Qin et al. 2019), Alamine 336 in *m*-xylene (Filiz and Sayar 2006) and Cyanex 923 in xylene (Saji John et al. 1999).

Biohydrometallurgical treatment of CFA by leaching in H_2SO_4 in the presence of *Rhodococcus* GIN-1 bacteria, followed by precipitation was explored. After bioleaching Ti is precipitated using a solution of $\text{NH}_3(\text{aq.})$, where the separation of individual metals is possible based on different pH values at which they precipitate in the form of sulphate-aqua-ammonium complexes. The Ti-bearing complex is precipitated at pH 2.05, the Al-bearing complex at pH 6.5, and the remaining

Fig. 23.2 Flow chart of two-step leaching of CFA in H_2SO_4 (Redrawn from Rushwaya and Ndlovu 2017)

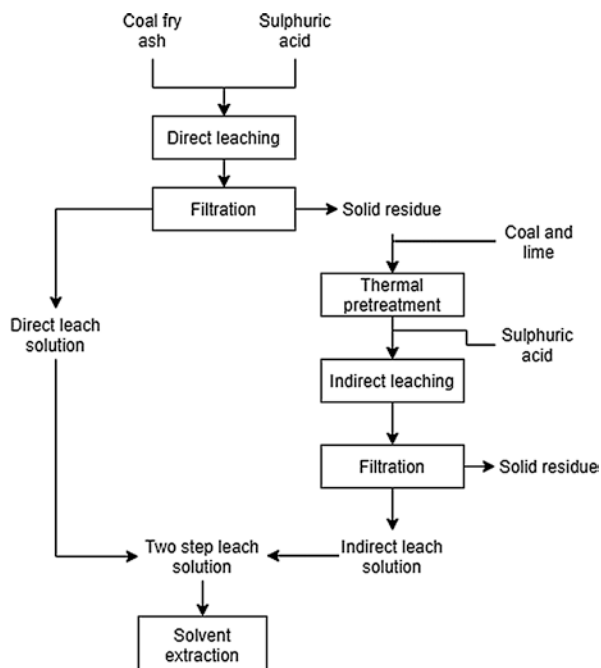
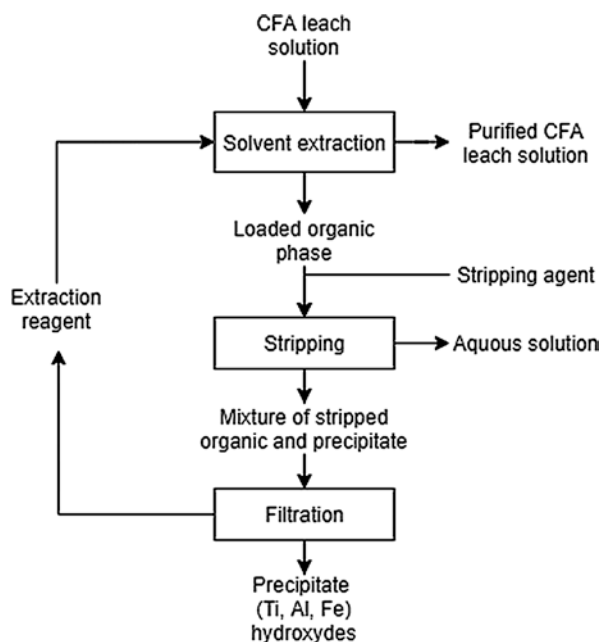


Fig. 23.3 Flow chart of solvent extraction of CFA leach solution (Redrawn from Rushwaya and Ndlovu 2017)

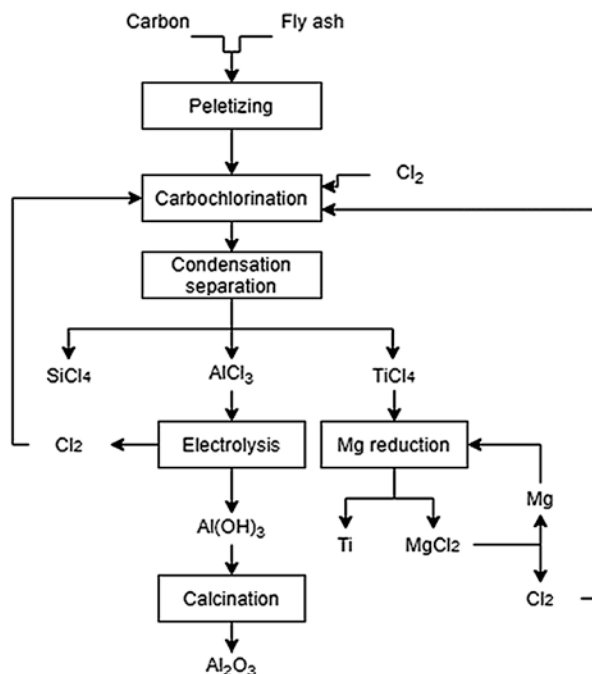


complexes of other metals at pH 8.5 and above. The method is considered entirely selective and economically advantageous. In the final step, the complexes are treated by short anneal for NH_3 removal. Efficiency of precipitation process of Ti higher than 80% was achieved using this method (Shabtai and Mukmenev 1996).

An alternative to hydrometallurgical processes is chlorination and carbochlorination of Ti-bearing CFA, which produces volatile TiCl_4 under reduction conditions in the presence of Cl_2 . A significant advantage of this process is in its effectiveness to extraction of Ti and valuable rare metals from CFA. Furthermore, it makes it easier to separate pure Ti product in the form of chloride, which is reduced by Mg to relatively pure metallic Ti. The process flow chart is shown in Fig. 23.4. As can be seen from the intended scheme, another advantage of this process is the possibility of separating individual carbochlorination reaction products, such as Al and Si chlorides. Aluminium and silicon chloride are separated from TiCl_4 by rectification, based on sufficiently different vapour pressures.

Studies show that the efficiency of TiO_2 chlorination depends on a large number of factors including the coal content of the pellets, the size of the pellets used, the reaction temperature and the flow rate of Cl_2 gas (Wang et al. 2019a; Yang and Hlavacek 1998). It was shown that higher chlorination efficiency can be achieved with temperatures above 1000 °C, smaller pellet sizes, higher Cl_2 flow rate and higher proportion of coal in the pellet (Wang et al. 2019a; Yang and Hlavacek 1998; Kaplan et al. 2020; Mehrotra et al. 1982).

Fig. 23.4 Process chart of the carbochlorination method (Redrawn from Wang et al. 2019a)



At the UCT Prague, a method linking Ti and Ga chlorination to cement roasting for the formation of cement clinker is being tested. In this method, CFA is roasted at an elevated temperature in the presence of CaCl_2 , CaCO_3 and coal. This method aims to maximize the recovery and evaluation of all components of CFA. The maximum degree of Ti conversion achieved by this method is around 40%.

Another known thermochemical process for extracting Ti from CFA is its roasting in the presence of $(\text{NH}_4)_2\text{SO}_4$ at around 600 °C and then leaching the sinter in water. The principle of the method is to convert the oxides of CFA into soluble sulphate-based compounds and/or double salts of ammonium metal sulphate-based compounds. The most represented minerals in the roast are millosevichite ($\text{Al}_2(\text{SO}_4)_3$) and godovikovite ($\text{NH}_4\text{Al}(\text{SO}_4)_2$). Along with Ti, Al, Ca, Fe and Mg are also co-dissolved in this process. The resulting Ti extraction efficiency is around 40% (Doucet et al. 2016).

23.3.2 Aluminium

Due to the large amount of Al_2O_3 contained in the CFA, this material is also considered a significant and inexpensive source of Al. The Al_2O_3 content is around 30–50% (Shi et al. 2020b). Aluminium is bound in CFA in various forms, such as oxides, hydroxides, aluminosilicates, zeolites, or refractory materials like mullite or andalusite. Methods for Al extraction from CFA are based on the form in which Al occurs in particular CFA. For example, for CFA with Al bound mainly in refractory materials, gravity and flotation treatment is suitable. When Al is primarily bounded in oxides, it is better to use hydrometallurgical extraction processes (Fečko et al. 2003).

As mentioned in the earlier in this chapter about Ti extraction and as shown in Figs. 23.1–23.4, many processes are used for extraction of Al as well as Ti. Therefore, direct leaching in H_2SO_4 followed by solvent extraction, precipitation, or membrane electrolysis is suitable for Al extraction (Shi et al. 2020b; Nayak and Panda 2010; Rushwaya and Ndlovu 2017; Panda and Sangita 2020; Seidel and Zimmels 1998). Increasing H_2SO_4 concentration, temperature and liquid-to-solid ratios has been shown to have a beneficial effect on Al extraction. The best results were achieved by leaching in 18 mol/L H_2SO_4 at 220 °C with a solid-to-liquid ratio of 1:3 and a leaching time of 4 h. Under these conditions, efficiency of 68–84% was achieved, depending on the CFA used (Seidel and Zimmels 1998; panda and Sangita 2020).

The pretreatment process by roasting CFA in the presence of Na_2CO_3 or NaOH was proven to increase the extraction efficiency of Al (Guo et al. 2019b). The method is based on the decomposition of mullite ($3\text{Al}_2\text{O}_3 \cdot 2\text{SiO}_2$), a chemically stable Al-containing fly ash constituent by soda or lye to form soluble compounds such as nepheline (NaAlSiO_4). Mullite phase was decomposed when roasted with NaOH at a temperature of 400 °C and up to 600 °C in the case of Na_2CO_3 . The best extraction efficiency of Al of 95% was achieved by roasting in the presence of mixture

Na_2CO_3 and NaOH at $700\text{ }^\circ\text{C}$, followed by leaching in 20 wt.% HCl at $100\text{ }^\circ\text{C}$ and for 2 h (Guo et al. 2013; Guo et al. 2019b).

Biohydrometallurgical treatment of CFA by leaching in H_2SO_4 in the presence of *Rhodococcus* GIN-1 followed by precipitation is another common process of extraction with Ti. Using this method 97% precipitation efficiency of Al from the leachate was achieved (Shabtai and Mukmenev 1996).

The principle of chlorination and carbochlorination method is applicable for Al extraction as in the case of Ti. The chlorination was carried out in the presence of Cl_2 and CaCl_2 . The highest efficiency, ranging from 84 to 96%, depending on the CFA used was achieved by chlorination with Cl_2 gas with the addition of 18 wt.% coal, at a temperature of $1100\text{ }^\circ\text{C}$. Similar efficacy was achieved by roasting with CaCl_2 with the ratio of CaCl_2 to CFA 1.3:1 at $1150\text{ }^\circ\text{C}$ (Kaplan et al. 2020; Wang et al. 2019a; Murtha and Burnet 1976).

The Al extraction was achieved by roasting in the presence of $(\text{NH}_4)_2\text{SO}_4$ and then leaching the sinter in water. All these methods go into more detail in the previous section. In the case of Al, extraction efficiency of up to 95% was achieved by this method (Doucet et al. 2016).

In addition to these procedures, other procedures are known for recovering Al and its compounds from CFAs. Study (Wu et al. 2019) showed that by leaching CFA with NH_4HSO_4 solution at $180\text{ }^\circ\text{C}$ for 240 min, more than 85% of Al can be extracted from CFA. High-pressure HCl leaching of CFA after separation of magnetic fraction was studied in paper (Valeev et al. 2020). More than 90% Al can be extracted by leaching CFA in HCl of concentration of 345 g/L at $210\text{ }^\circ\text{C}$ for 3 h. It was found that main control step in leaching is the surface reaction. The obtained AlCl_3 could be used as coagulant for waste water treatment (Valeev et al. 2020). Low temperature process by calcination with potassium bisulfate was used. This method is very similar to roasting in the presence of $(\text{NH}_4)_2\text{SO}_4$ with exception that the emerging soluble compound is not ammonium metal sulphate-based but potassium-metal sulphate-based ($\text{K}_3\text{Al}(\text{SO}_4)_3$). The extraction efficiency of Al_2O_3 from CFA reached up to 92.8% with the $\text{KHSO}_4/\text{Al}_2\text{O}_3$ molar ratio of 7:1 when calcination was carried out at $230\text{ }^\circ\text{C}$ for 3 h (Guo et al. 2019a).

23.3.3 Silicon

Silicon is together with Al major element in CFA, making it a promising material for zeolites synthesis. In this process, acid pretreatment is the necessary step to remove CaO and Fe_2O_3 from high-Ca and Fe-containing CFA as these elements compete with Al and Si for positions in zeolite structure. In the most common acid pretreatment CFA is treated in 3 mol/L HCl at $60\text{ }^\circ\text{C}$ for 1.5 h. The washed CFA is calcinated at $700\text{ }^\circ\text{C}$ to remove organic compounds. The next important step is alkali fusion as described by Lee et al. (2017), where quartz and mullite are transformed into water-soluble compounds necessary for zeolite synthesis. Another use of CFA

due to Si content is synthesis of silica aerogel or mesoporous membranes (Lee et al. 2017).

23.3.4 Germanium

For Ge extraction, CFA is mainly processed hydrometallurgically. This process comprises leaching the CFA in water, H_2SO_4 , HCl or NaOH solution (Survey 2013; Arroyo et al. 2009a; Zhang and Xu 2016; Arroyo et al. 2014). In the second step, Ge is obtained from the leach liquor, which contains a number of impurities. Known processes for extracting Ge from the leachate include the following:

- Separation by ion-exchange resins. These are mostly insoluble macromolecular resins that can bind the Ge–catechol complex. Known ion-exchange resins include IRA-900 and IRA-958 (Torralvo and Fernández-Pereira 2011).
- Ion flotation (Torralvo and Fernández-Pereira 2011; Arroyo et al. 2009a; Zhang and Xu 2016).
- Distillation of $GeCl_4$ from acid extracts (Marco-Lozar et al. 2007; Zhang and Xu 2016).
- Adsorption of the Ge-complex on active carbon. For this process, the key parameter is the selection of a suitable complex to ensure sufficient sorption capability and at the same time re-usability of active carbon, i.e. regeneration/desorption capability. For these purposes, the most commonly used is a catechol complex desorbed with HCl (Marco-Lozar et al. 2007).
- Solvent extraction of the Ge–catechol complex by means of *trioctylamine* dissolved in kerosene. The complex goes into the organic phase (Arroyo et al. 2009a; Zhang and Xu 2016).
- Precipitation with hydrolysed tannins. Tannins contain polyhydroxyl polyphenols, which have the ability to form chelates with Ge ions. Precipitate of the Ge–tanine complex is formed (Zhang and Xu 2016).
- Precipitation by H_2S to produce GeS_2 precipitate (Arroyo et al. 2009a).
- Precipitation of Ge–catechol complex (Ge–CAT) with cetyltrimethylammonium bromide (CTAB). Precipitation is based on a reaction of water-soluble GeCAT with CTA^+ by which insoluble CTA_2GeCAT_3 is formed (Arroyo et al. 2009a).

An alternative to the hydrometallurgical processing is the vacuum separation of Ge at an elevated temperature. The process is based on heating CFA together with coke to a temperature between 1200 and 1700 °C, at a pressure of 1–10 Pa. During the process, Ge compounds with predominantly GeO_2 are firstly reduced to metallic Ge, which is sublimated at higher temperatures. Up to 94% of the Ge from CFA is obtained by this technology, but the resulting desublimated Ge and its oxides are contaminated with $CaCO_3$, $CaSO_4$ and As compounds. Therefore, the resulting product of desublimation must be refined. Refining is performed by distilling $GeCl_4$ at 84 °C from a solution, which is produced by leaching the product of

desublimation in a solution of 8 mol/L HCl with addition of 30% H₂O₂, or possibly MnO₂ (Zhang and Xu 2016, 2017).

The second applicable thermochemical process for obtaining Ge from CFA is chlorination similar to the process obtaining Ti. The conversion to chloride is advantageous because GeO and GeS begin to sublime at around 700 °C, while the boiling point of GeCl₄ is only 84 °C (Survey 2013). Pure GeCl₄ is then hydrolysed with deionized water. The resulting Ge hydroxide is filtered and vacuum roasted to form GeO₂ (Butterman and Jorgenson 2005). The GeO₂ is reduced with H₂ at 760 °C to form Ge metal powder, which is then processed according to final needs. Germanium metal is most often refined by zone melting. The purity ranges from 4 N to 13 N. In addition to these methods, fractional crystallization of the unstable GeCl₄ is used to separate Ge from other metals. Flow chart of the manufacturing process is shown in Fig. 23.5 (Glavinović et al. 2017).

23.3.5 Gallium

Gallium is most commonly found in CFA in the form of Ga³⁺, which replaces Al³⁺ in the aluminosilicate mullite matrix (Arroyo et al. 2014). The processes for extracting this metal from CFA are derived from the processes by which Ga is currently obtained industrially. These are based on Ga extraction from leachate from Bayer's process and hydrometallurgical Zn production (Font et al. 2007).

The main procedures for the extraction of gallium from CFA include leaching in H₂SO₄ or NaOH. In both cases, Ga passes into solution, which is then processed. In the hydroxide process, the Ga content in the leachates is enriched by recirculation

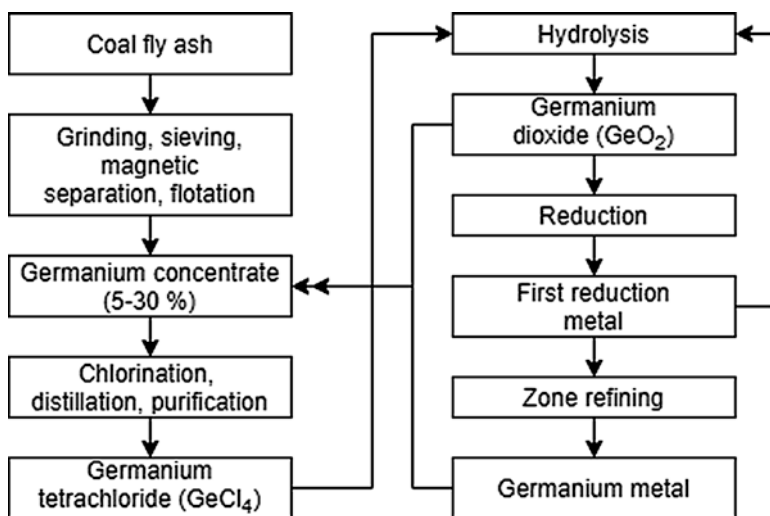


Fig. 23.5 Flow chart of Ge production from CFA (Butterman and Jorgenson 2005; Survey 2013; Glavinović et al. 2017)

of the alkaline extract solution, and Ga is subsequently precipitated from the enriched solution using CO_2 . Additionally, ion-exchange resins, direct electrolysis, or electrodeposition are used to extract Ga from this solution (Pan et al. 2018; Arroyo et al. 2014).

Ga is extracted by solvent extraction from the solution obtained by leaching in H_2SO_4 (Font et al. 2007). Known extractants for Ga include 2-ethylhexyl phosphonic acid *mono-2-ethylhexyl* ester (P507) dissolved in sulphonated kerosene (99%) (Zhao et al. 2020), *bis(2,4,4-trimethylpentyl)* phosphinic acid (Cyanex 272) in kerosene (Zhao et al. 2020) and Cyanex 923 in toluene (mixture of four *trialkyl*-phosphine oxides, namely dioctyl-hexyl-phosphine oxide (~42%), dihexyl-octylphosphine oxide (~32%), trihexyl-phosphine oxide (~8%) and trioctyl-phosphine oxide (~14%) (Gupta et al. 2007)).

Besides these traditional leaching media, the Ga extraction in H_2O_2 , HCl, $(\text{COOH})_2$ and catechol solution was also reported, but considerably higher extraction rate of Ga was not achieved in any of these leaching media.

23.3.6 Lithium

CFA from Inner Mongolia, Shanxi in China was found to contain up to 8–10 kg/t Li. According to the patents CN110643832A (Xingdong et al. 2020) and CN104477948A (En and Yinghong 2016), CFA is leached in an acidified aqueous solution with the addition of K_2CO_3 and Na_2CO_3 . When the leaching is finished, the mixture is filtrated, and the leaching liquor is concentrated, and CO_2 is added to obtain Li precipitate. The second process uses CFA, already free of Al and Fe, which reacts with CO_2 in an autoclave for 1–3 h to form Li_2CO_3 . Li was also extracted by biosorption together with Er (Ponou et al. 2016).

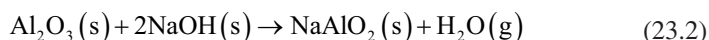
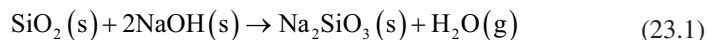
23.3.7 Rare Earth Metals with Yttrium and Scandium (REEs)

Rare earth metals are a group of 14 stable lanthanides, Y and Sc. REEs are strategic material, especially in high tech industries. The main uses are found in permanent magnets, automotive catalytic converters, superconductors, or green energy. China currently controls more than 86% of REEs production and in the last years steadily increases export taxes. Due to the constant development of new technologies, interest in REEs is also growing. It is, therefore, necessary to find new alternative sources of REEs. At the same time, global coal consumption and the associated amount of CFA are increasing. The CFA is an interesting potential source that contains on average 445 ppm/t of REEs (Jyothi et al. 2020; Kose Mutlu et al. 2018).

The form of occurrence of REEs in CFA depends on its origin. According to Pan et al. (2020), 69% of REEs and Y occur in the glassy aluminosilicate phase. The rest of REEs is found in organic (11.58%) and sulphide (13.56%) forms. Another study

(Wang et al. 2019c) shows that about 90% of REEs is found in glassy phase. The study (Rosita et al. 2020) shows that it is possible to enrich REEs by 23% by sequential sieving and magnetic separation. In the study by Pan et al. (2020) size classification followed by density fractionation and magnetic separation was used for enrichment. The content of REEs and Y in raw CFA can be enriched by 30%. The enriched product can be leached in HCl under optimal conditions: 3 mol/L HCl, $s/l = 1:10$, 60 °C, 2 h. Under these conditions, 78% extraction efficiency was obtained. In comparison to leaching raw CFA without enrichment by physical separation, the efficiency of leaching was 35% higher (Pan et al. 2020; Rosita et al. 2020).

Therefore, for processing CFA in order to obtain REEs, a pretreatment step is necessary. This can be accomplished by alkali fusion, by which the matrix of CFA containing quartz and aluminosilicates reacts with alkali carbonate or alkali hydroxide (Eqs. 23.1 and 23.2) at high temperature, and the matrix phases are converted into soluble compounds. It is a well-known method for processing materials with aluminosilicate structure (Lee et al. 2017). The most effective additive according to Pan et al. (2021) is NaOH or Na₂CO₃.



The products of roasting with these additives are Na₂SiO₃ and NaAlO₂, which dissolve readily in water. Leaching of roasting products in hot alkaline solution or water leads to their dissolution. REEs together with Fe, Ca and Mg remain in leach residue. The leaching in water results in porous CFA morphology, to which acid can easily penetrate during subsequent acid leaching. It was found (Pan et al. 2021) that recovery of more than 90% of REEs using Na₂CO₃ as a roasting additive requires a temperature of 850 °C while by using NaOH the recovery reached the maximum recovery of 70% at 235 °C, and it did not change when the temperature was increasing (Pan et al. 2021; Mondal et al. 2019; Lee et al. 2017).

A comparison between direct acid leaching of CFA and acid leaching after alkali fusion is described by Tang et al. (2019). It was found that the concentrations of all REEs in leachate are more than two times higher after alkali fusion. Moreover, the leaching after alkali fusion is significantly faster than direct leaching. The optimal conditions according to Tang et al. (2019) for maximum efficiency of leaching CFA are following: alkali fusion with Na₂CO₃ (mass ratio CFA:Na₂CO₃ = 1:1) at 860 °C for 30 min and leaching with 3 mol/L HCl at $s/l = 1:20$. Under these conditions, the total leaching efficiency of REEs is almost 73%. Another study (Roth et al. 2017) shows a comparison between NaOH digestion pretreatment and direct leaching. After direct leaching in 2 mol/L HCl, only 6% of REEs were extracted from CFA, but with NaOH pretreatment (leaching in 5 mol/L solution, $s/l = 1:10$, 93 °C) up to 90% of the REEs were extracted in subsequent HCl leaching (Tang et al. 2019; Roth et al. 2017). Study by Wang et al. (2019c) confirms that leaching of CFA in HCl only is not sufficient to extract majority of REEs. On the other hand, pre-leaching in NaOH with subsequent leaching in HCl results in more than 88% REEs extraction

from CFA. During the leaching in NaOH, SiO₂ is converted to soluble compound and REEs stay in insoluble residue. Alkaline pre-leaching leads to removal of more than 40% of SiO₂ and enrichment of REEs, increasing the extraction efficiency by HCl leaching (Wang et al. 2019c).

Study by Mondal et al. (2019) tried alkali fusion with a mixture of NaOH and NaNO₃ followed by leaching the insoluble residue in HNO₃ and selective extraction of REEs with TEHDGA (*N,N,N',N'-tetra(2-ethylhexyl)diglycolamide* (Ltd. 2019)) extractant impregnated on XAD-7 resin. The results showed selective separation of REEs from the extract, without extraction of Si, Al, Fe, Ca or Mg, and so a possible way of separating REEs from matrix elements from the extract. All REEs showed similar behaviour during elution with 0.01 mol/L HNO₃.

High efficiency of separation of Ga, Nd and Y from CFA can be achieved by the process described in patent WO2019022320A1 (Pyo et al. 2019). CFA first reacts with halogenic acid. Then, the non-halogenic acid is added to the filtrate and ultrasonic vibrations are applied. Using this procedure, it is possible to extract at least 90% of Ga and 98% of Nd and Y.

Leaching of CFA in strong acids, i.e. HNO₃, HCl, either direct or after alkaline fusion, leads to the formation of leachates, which have very low pH and contain besides REEs also many major elements like Si, Al, Fe and Na. The concentration of these major elements is 10²–10⁴ higher than the concentration of individual REEs. Kose Mutlu et al. (2018) studied micro- and nanofiltration to separate REEs from leach liquor to minimize high amounts of using chemical reagents. The use of microfiltration pretreatment followed by nanofiltration leads to concentrating the REEs in solution, while major elements are partially separated. Optimal conditions for separating REEs from major elements in leach liquors using nanofiltration are pH 3.5 and pressure 12 bar.

Possible extraction of REEs is also described in the patent CN108220630A (Kun et al. 2017). CFA is initially activated by H₂SO₄ and calcinated. The calcinated product is then leached in HCl or HNO₃ at 130–160 °C for 1–3 h. Iron and Al are then separated from REEs chlorides by chelating resin. The final step is elution of REEs from resin with demineralized water. It is necessary to add alkali (Na₂CO₃, NaOH or NH₃) to eluent to adjust pH to 5–7 in order to precipitate REE compounds and separate them from Ca and Mg.

As stated in patent US20130287653A1 (Green et al. 2013), REEs can be also extracted from CFA by solvent extraction. CFA is treated with a mineral acid to form an aqueous solution of REEs. The solution is mixed with the organic phase (tributylphosphate and kerosene), where the REEs salts are transferred to the organic phase followed by separation of the organic and aqueous phase. REEs are then re-extracted from the organic phase by suitable liquid to the pure aqueous phase.

Study by Ponou et al. (2016) described the biosorption/desorption of La, Ce and Er ions in an aqueous solution obtained from leaching CFAs on ginkgo leaves carbonized at 450 °C. Ashes were leached in HCl at various concentrations (0.25–10 mol/L). High concentrations of HCl of more than 3 mol/L were found to reduce leaching efficiency. The optimal concentration of HCl for leaching was found to be 2.5 mol/L. Furthermore, the best biosorption results were obtained at

pH 3 within 900 s. Er, Pr, Y, Ce and La were completely adsorbed. Desorption using 0.3 mol/L HCl resulted in obtaining more than 99% of Er together with other non-RE metals like Li, Fe and Ag. However, the desorption process was not effective for Ce, La and Cu.

The disadvantage of enriching and concentrating leach liquors is that it leads also to increasing content of Th and U. Th and U are always present together with REEs. Uranium occurs rather on the particle surface, while Th is associated mostly with the aluminosilicate matrix. Concentrating these elements during the purification of leach liquor could be hazardous, and these elements must be taken into account when processing CFA. By acid leaching 30–80% of U can be leached out. Because of high consumptions of chemicals during the acid leaching, patent CN108285981A (Zhongran et al. 2018) uses [Hbet] + [CF₃COO]-ionic liquid and *Aspergillus niger* bacteria. The U in the leaching solution is then recovered by ion-exchange process (Taggart et al. 2018; Zhongran et al. 2018).

Study by Couto et al. (2020) reported possible extraction of REEs from CFA by electrodialysis. CFA was leached in HNO₃ in vertical rotating mixer for 7 days. After leaching, 70–100% of light REEs and 17–88% of heavy REEs were extracted. With increasing pH of leaching solution, the efficiency decreased. The best results of leaching were achieved at pH 2.5. By electrodialysis process in two compartment cell more than 70% of REEs were removed from CFA.

Due to high content of REEs in Chinese Guizhou coal combustion at 1350 mg/kg, recovering REEs by different ionic-liquid extractants, e.g. [P6,6,6,14]Cl, [N1888]Cl, [P6,6,6,14][SOPAA] or [N1888][SOPAA] was studied (Huang et al. 2019). The recovery rate of REEs was more than 37%.

23.3.8 Trace Metals

Content of heavy metals in coal ranges from low to trace amounts. Taking into account that during the combustion of coal these elements are enriched up to 10 times and hundreds of millions of tons of CFA per year produced by power plants, the environmental impact of CFA increases rapidly. Particular contents of trace metals in different CFA are given in Table 23.2. For this reason, heavy metals in CFA are considered as environmental risk rather than possible source, but some studies have been carried out to address the challenges (Fernández-Turiel et al. 1994).

Copper occurs in CFA as a trace element in five different forms. Primarily 13–42% of Cu as Cu (II) in aluminosilicate glass and then in oxide and sulphide minerals like tenorite (19–29% of Cu, CuO), chalcopyrite (<15% of Cu, CuFeS₂), cuprite (20–27% of Cu, Cu₂O) and up to 41% of Cu as copper sulphide (Cu₂S). These values indicate that up to 42% of Cu is present in the amorphous phase in aluminosilicate glass. Copper from the amorphous phase can be leach out under neutral and alkaline conditions. Oxide and sulphide minerals of Cu can be leached in the presence of bacteria *Thiobacillus ferrooxidans* and *Thiobacillus thiooxidans*. For Cu-containing materials with a higher content of Fe and Ca, ammoniacal

leaching is used. The product of ammoniacal leaching is pure CuCO_3 solution, Fe and Ca stay in the leach residue (Wang et al. 2020; Jandová et al. 2018).

Zinc occurs in CFA in three forms. The majority of zinc of 70–77% is adsorbed to Fe (hydr)oxide, 14–20%, in ZnO and the rest in a spinel-like structure similar to franklinite (ZnFe_2O_4). According to Catalano et al. (2012), Zn compounds may vary depending on the CFA class. For the C class of CFA generated by burning of lignite or subbituminous coal, all Zn is in a tetrahedral structure in the raw CFA, after weathering the value drops to 65–75%, the rest of Zn is bound in octahedral structure. For the F class CFA generated by burning of anthracite of bituminous coal, Zn exists in raw CFA in spinel-like structure that is similar to franklinite and gahnite (ZnAl_2O_4) (Catalano et al. 2012; Office of Research 2016; Wang et al. 2020).

Arsenic is always present in coal along with pyrite. Almost all As in CFA is in the state (V), only 3–8% is in the state (III) (Wang et al. 2020). The environmental risk of Cr depends on its oxidation state. Chromium(VI) can easily dissolve as chromates and dichromates, known as carcinogenic substances, whereas Cr(III) is less soluble and less harmful to health and environment. Fortunately, Cr is present in most bituminous coal (CFA—Class F) in the (III) state. Chromium can be leached out at low pH and reducing conditions (Wang et al. 2020).

For environmental risk, heavy metals run-off during water leachability test is an important parameter. The highest mobility during water leachability test has Cd, which means Cd moves rapidly when the CFA is ponded or landfilled. Mobility of Co, Cu and Zn increases with the severity of extractions. Unlike these elements, the mobility of Ni and Pb is low (Fernández-Turiel et al. 1994).

By alkaline leaching with NaOH or NH_3 (aq.), only Pb and Zn are leached out. Other metals remain in the solid residue. When the alkaline leaching process is combined with subsequent leaching using acidic lixivants, Cu and Cd can be extracted. By leaching CFA in CH_3COOH , >97% of Zn and Pb can be extracted, while leaching in NaOH, only about 35% of Zn and 81% of Pb are leached out. An important method for the extraction of heavy metals from CFA is bioleaching. In this process, bacteria (*Thiobacillus*) are used. Using the *Thiobacillus thiooxidans* bacteria in aerobic acidic conditions (H_2SO_4), Co, Al and Ti can be extracted and then separated in a series of precipitation steps by controlling pH (Fass et al. 1994; Sahoo et al. 2016).

During Al_2O_3 refining, the Si contained in CFA is separated as CaSiO_3 , which looks promising as an adsorbent for heavy metals in aqueous solutions and water. According to Ma et al. (2018), CaSiO_3 powder is a great adsorbent for the removal of Cu, Ni, Zn and Co from solutions. With CaSiO_3 powder, up to hundreds of mg/g adsorption capacity can be reached. Calcium silica powder looks like a promising adsorbent for cleaning wastewaters containing heavy metals (Ma et al. 2018).

Another serious environment pollutant produced during the combustion of coal and other solid fuels is V_2O_5 . With toxicity comparable to As(V) (LD = 5–50 mg/kg), it is necessary to consider the removal of V_2O_5 from CFA. Acid leaching dissolves not only V but also other metals contained in CFA such as Al, Si, Cr, Ni and Zn. Therefore, it is preferable to use alkaline leaching to separate V. Study by Hakimi et al. (2020) tried alkaline leaching in NaOH (95 °C, 45 min) for separation

of V from CFA. During leaching, most V is dissolved into the solution in the form of NaVO_3 . Impurities like Al and Si are precipitated from the solution by adjusting pH to 8. Reaction with ammonium salts at pH 6 produces ammonium metavanadate, from which V_2O_5 is formed after calcination. With this method, it is possible to remove over 90% of V_2O_5 from CFA.

References

- ACAAssociation. (2018). *Coal ash recycling rate declines amid shifting production and use patterns*. Washington, D.C. <https://www.aaa-usa.org/Portals/9/Files/PDFs/Coal-Ash-Production-and-Use-2017.pdf>
- Aphane, M. E., Doucet, F. J., Kruger, R. A., Petrik, L., & van der Merwe, E. M. (2020). Preparation of sodium silicate solutions and silica nanoparticles from South African coal fly ash. *Waste and Biomass Valorization*, 11(8), 4403–4417. <https://doi.org/10.1007/s12649-019-00726-6>.
- Arroyo, F., Font, O., Chimenos, J., Pereira, C., Querol, X., & Llano, P. (2014). IGCC fly ash valorisation. Optimisation of Ge and Ga recovery for an industrial application. *Fuel Processing Technology*, 124, 222–227. <https://doi.org/10.1016/j.fuproc.2014.03.004>.
- Arroyo, F., Font, O., Fernández-Pereira, C., Querol, X., Juan, R., Ruiz, C., & Coca, P. (2009a). Germanium recovery from gasification fly ash: Evaluation of end-products obtained by precipitation methods. *Journal of Hazardous Materials*, 167(1), 582–588. <https://doi.org/10.1016/j.jhazmat.2009.01.021>.
- Arroyo, F., Pereira, C., Olivares, J., & Llano, P. (2009b). Hydrometallurgical recovery of germanium from coal gasification fly ash: Pilot plant scale evaluation. *Industrial & Engineering Chemistry Research*, 48, 3573–3579. <https://doi.org/10.1021/ie800730h>.
- Badenhorst, C. J., Wagner, N. J., Valentim, B. R., Santos, A. C., Guedes, A., Białecka, B., Calus, J., Popescu, L. G., Cruceru, M., Predeanu, G., & Viljoen, K. S. (2019). Char from coal ash as a possible precursor for synthetic graphite – Recent developments of the Charphite project. In: *Proceedings of the World of Coal Ash (WOCA)*, St. Louis, MO, USA (pp. 13–16).
- Bhatt, A., Priyadarshini, S., Acharath Mohanakrishnan, A., Abri, A., Sattler, M., & Techapaphawit, S. (2019). Physical, chemical, and geotechnical properties of coal fly ash: A global review. *Case Studies in Construction Materials*, 11, e00263. <https://doi.org/10.1016/j.cscm.2019.e00263>.
- Biswas, R. K., Banu, R. A., & Islam, M. N. (2003). Some physico-chemical properties of D2EHPA: Part 2. Distribution, dimerization and acid dissociation constants in n-hexane/1 M (Na⁺, H⁺) SO₄²⁻ system, interfacial adsorption and excess properties. *Hydrometallurgy*, 69, 157–168. [https://doi.org/10.1016/S0304-386X\(02\)00212-8](https://doi.org/10.1016/S0304-386X(02)00212-8).
- Biswas, R. K., & Begum, D. A. (2000). Kinetics of extraction and stripping of Ti(IV) in HCl–D2EHPA–kerosene system using the single drop technique. *Hydrometallurgy*, 55(1), 57–77. [https://doi.org/10.1016/S0304-386X\(99\)00074-2](https://doi.org/10.1016/S0304-386X(99)00074-2).
- Biswas, R. K., & Karmakar, A. K. (2014). Solvent Extraction of Ti(IV) from Acidic Sulphate Medium by Cyanex 301 Dissolved in Kerosene. *Separation Science and Technology*, 49(2), 278–289. <https://doi.org/10.1080/01496395.2013.837484>.
- Burnet, G., Murtha, M. J., & Wijatno, H. (1977). *Recovery of alumina from fly ash by high-temperature chlorination* (No. IS-M-142; CONF-7705131-1). Ames Lab., IA (USA).
- Butterman, W. C., & Jorgenson, J. D. (2005). Mineral commodity profiles: Germanium. *US Geological Survey Open-File Report*, 1218, 19. <https://doi.org/10.3133/ofr20041218>. (Online only edn.).
- Catalano, J. G., Huhmann, B. L., Luo, Y., Mitnick, E. H., Slavney, A., & Giammar, D. E. (2012). Metal release and speciation changes during wet aging of coal fly ashes. *Environmental Science & Technology*, 46(21), 11804–11812. <https://doi.org/10.1021/es302807b>.

- Chimenos, J. M., Fernández, A. I., del Valle-Zermeño, R., Font, O., Querol, X., & Coca, P. (2013). Arsenic and antimony removal by oxidative aqueous leaching of IGCC fly ash during germanium extraction. *Fuel*, 112, 450–458. <https://doi.org/10.1016/j.fuel.2013.05.059>.
- Couto, N., Ferreira, A. R., Lopes, V., Peters, S. C., Mateus, E. P., Ribeiro, A. B., & Pamukcu, S. (2020). Electrolytic recovery of rare earth elements from coal ashes. *Electrochimica Acta*, 359, 136934. <https://doi.org/10.1016/j.electacta.2020.136934>.
- Diaz, E. I., Allouche, E. N., & Eklund, S. (2010). Factors affecting the suitability of fly ash as source material for geopolymers. *Fuel*, 89(5), 992–996. <https://doi.org/10.1016/j.fuel.2009.09.012>.
- Doucet, F., Mohamed, S., Neyt, N., Castleman, B., & van der Merwe, E. (2016). Thermochemical processing of a South African ultrafine coal fly ash using ammonium sulphate as extracting agent for aluminium extraction. *Hydrometallurgy*, 166, 174–184. <https://doi.org/10.1016/j.hydromet.2016.07.017>.
- Dutta, B. K., Khanra, S., & Mallick, D. (2009). Leaching of elements from coal fly ash: Assessment of its potential for use in filling abandoned coal mines. *Fuel*, 88(7), 1314–1323. <https://doi.org/10.1016/j.fuel.2009.01.005>.
- ECOBA eV. (2016a). *EU statistics: Estimate on production*. e.V. ecoba. <http://www.ecoba.com/ecobaccpprod.html>.
- ECOBA eV. (2016b). *Production and utilisation of CCPs in 2016 in Europe (EU 15)*. UK Quality Ash Association. http://www.ukqaa.org.uk/wp-content/uploads/information/statistics/ECO-stat-2016_EU15_tab-1.pdf
- En, L. J., & Yinghong S. (2016). *Method for extracting lithium carbonate from coal ashes*. CN104477948A.
- Energy USDo (2017) *DOE Invests \$17.4 million in projects to advance recovery of rare earth elements from coal and coal byproducts*. U.S. Department of Energy. <https://www.energy.gov/articles/doe-invests-174-million-projects-advance-recovery-rare-earth-elements-coal-and-coal>
- Fan, X.-L., Lv, S.-Q., Xia, J.-L., Nie, Z.-Y., Zhang, D.-R., Pan, X., Liu, L.-Z., Wen, W., Zheng, L., & Zhao, Y.-D. (2019). Extraction of Al and Ce from coal fly ash by biogenic Fe³⁺ and H₂SO₄. *Chemical Engineering Journal*, 370, 1407–1424. <https://doi.org/10.1016/j.cej.2019.04.014>.
- Fass, R., Fleming, J. C., Geva, J., Shalita, Z. P., White, M. D. (1993). *Bioleaching method for the extraction of metals from coal fly ash using thiobacillus*. CA 2063687A1.
- Fass, R., et al. (1994). *Bioleaching method for the extraction of metals from coal fly ash using thiobacillus*. US5278069A.
- Fečko, P., Kušnierová, M., Lyčková, B., Čablík, V., & Farkašová, A. (2003). *Popílky*. Ostrava: VŠB—Technická univerzita Ostrava.
- Fernández-Turiel, J. L., de Carvalho, W., Cabañas, M., Querol, X., & López-Soler, A. (1994). Mobility of heavy metals from coal fly ash. *Environmental Geology*, 23(4), 264–270. <https://doi.org/10.1007/BF00766741>.
- Filiz, M., & Sayar, A. A. (2006). extraction of titanium(IV) from aqueous hydrochloric acid solutions into alamine 336-M-Xylene mixtures. *Chemical Engineering Communications*, 193(9), 1127–1141. <https://doi.org/10.1080/00986440500354457>.
- Font, O., Querol, X., Juan, R., Casado, R., Ruiz, C. R., López-Soler, Á., Coca, P., & Peña, F. G. (2007). Recovery of gallium and vanadium from gasification fly ash. *Journal of Hazardous Materials*, 139(3), 413–423. <https://doi.org/10.1016/j.jhazmat.2006.02.041>.
- Fontana, D., Kulkarni, P., & Pietrelli, L. (2005). Extraction of titanium (IV) from acidic media by 2-ethylhexyl phosphonic acid mono-2-ethylhexyl ester. *Hydrometallurgy*, 77(3), 219–225. <https://doi.org/10.1016/j.hydromet.2005.01.003>.
- Franus, W., Wiatros-Motyka, M. M., & Wdowin, M. (2015). Coal fly ash as a resource for rare earth elements. *Environmental Science and Pollution Research*, 22(12), 9464–9474. <https://doi.org/10.1007/s11356-015-4111-9>.
- Gabler, R. C., & Stoll, R. L. (1982). Extraction of leachable metals and recovery of alumina from utility coal ash. *Resources and Conservation*, 9, 131–142. [https://doi.org/10.1016/0166-3097\(82\)90068-2](https://doi.org/10.1016/0166-3097(82)90068-2).

- Gao, Y., Liang, K., Gou, Y., Sa, W., Shen, W., & Cheng, F. (2020). Aluminum extraction technologies from high aluminum fly ash. *Reviews in Chemical Engineering*. <https://doi.org/10.1515/revce-2019-0032>.
- Glavinović, M., Krause, M., Yang, L., McLeod, J. A., Liu, L., Baines, K. M., Friščić, T., & Lumb, J.-P. (2017). A chlorine-free protocol for processing germanium. *Science Advances*, 3(5), e1700149. <https://doi.org/10.1126/sciadv.1700149>.
- Gollakota, A. R. K., Volli, V., & Shu, C.-M. (2019). Progressive utilisation prospects of coal fly ash: A review. *Science of the Total Environment*, 672, 951–989. <https://doi.org/10.1016/j.scitotenv.2019.03.337>.
- Green DB, Joshi PB, Marinelli WJ, Preda DV, Skyler DA, Tsinberg A (2013) *Recovery of rare earth elements and compounds from coal ash*. US2013287653A1.
- Group WB. (2017). *The growing role of minerals and metals for a low carbon future*. Washington, DC: World Bank.
- Guo, C., Zou, J., Ma, S., Yang, J., & Wang, K. (2019a). Alumina extraction from coal fly ash via low-temperature potassium bisulfate calcination. *Minerals*, 9, 585. <https://doi.org/10.3390/min9100585>.
- Guo, Y., Li, J., Yan, K., Cao, L., & Cheng, F. (2019b). A prospective process for alumina extraction via the co-treatment of coal fly ash and bauxite red mud: Investigation of the process. *Hydrometallurgy*, 186, 98–104. <https://doi.org/10.1016/j.hydromet.2019.04.011>.
- Guo, Y., Li, Y., Cheng, F., Wang, M., & Wang, X. (2013). Role of additives in improved thermal activation of coal fly ash for alumina extraction. *Fuel Processing Technology*, 110, 114–121. <https://doi.org/10.1016/j.fuproc.2012.12.003>.
- Gupta, B., Mudhar, N., Begum, Z., & Singh, I. (2007). Extraction and recovery of Ga(III) from waste material using Cyanex 923. *Hydrometallurgy*, 87(1), 18–26. <https://doi.org/10.1016/j.hydromet.2007.01.001>.
- Hakimi, M., Kiani, P., Alikhani, M., Feizi, N., Bajestani, A. M., & Alimard, P. (2020). Reducing environmental pollution of fuel fly ash by extraction and removal vanadium pentoxide. *Solid Fuel Chemistry*, 54, 337–342.
- Harris, D. (2017). 21—Ash as an internationally traded commodity. In T. Robl, A. Oberlink, & R. Jones (Eds.), *Coal combustion products (CCP's)* (pp. 509–529). Woodhead Publishing. <https://doi.org/10.1016/B978-0-08-100945-1.00021-6>.
- Harris, D., & Heidrich, C., & Feuerborn, J. (2019). Global aspects on coal combustion products. In: *World of Coal Ash Conference, Conference Paper*.
- Hower, J. C., Robertson, J. D., Thomas, G. A., Wong, A. S., Schram, W. H., Graham, U. M., Rathbone, R. F., & Robl, T. L. (1996). Characterization of fly ash from Kentucky power plants. *Fuel*, 75(4), 403–411. [https://doi.org/10.1016/0016-2361\(95\)00278-2](https://doi.org/10.1016/0016-2361(95)00278-2).
- Huang, C., Wang, Y., Huang, B., Dong, Y., & Sun, X. (2019). The recovery of rare earth elements from coal combustion products by ionic liquids. *Minerals Engineering*, 130, 142–147. <https://doi.org/10.1016/j.mineng.2018.10.002>.
- IEA. (2020). *Coal-fired power*. IEA. <https://www.iea.org/reports/coal-fired-power>.
- IEA Agency. (2020). *IEA Energy Atlas*. International Energy Agency. <http://energyatlas.iea.org/#!/tellmap/2020991907/2>.
- Islam, M. F., & Biswas, R. K. (1981). The solvent extraction of Ti(IV), Fe(III) and Mn(II) from acidic sulphate-acetato medium with bis-(2-ethyl hexyl) phosphoric acid in benzene. *Journal of Inorganic and Nuclear Chemistry*, 43(8), 1929–1933. [https://doi.org/10.1016/0022-1902\(81\)80413-7](https://doi.org/10.1016/0022-1902(81)80413-7).
- Jandová, J., Vu, N. H., & Dvořák, P. (2018). Metody výroby neželezných kovů a zpracování odpadů. In *VŠCHT Praha* (pp. 201–202).
- Jankowski, J., Ward, C. R., French, D., & Groves, S. (2006). Mobility of trace elements from selected Australian fly ashes and its potential impact on aquatic ecosystems. *Fuel*, 85(2), 243–256. <https://doi.org/10.1016/j.fuel.2005.05.028>.
- Jyothi, R. K., Thenepalli, T., Ahn, J. W., Parhi, P. K., Chung, K. W., & Lee, J.-Y. (2020). Review of rare earth elements recovery from secondary resources for clean energy technologies: Grand

- opportunities to create wealth from waste. *Journal of Cleaner Production*, 267, 122048. <https://doi.org/10.1016/j.jclepro.2020.122048>.
- Kaplan, V., Dosmukhamedov, N., Zholdasbay, E., Daruesh, G., & Argyn, A. (2020). Alumina and silica produced by chlorination of power plant fly ash treatment. *JOM*, 72(10), 3348–3357. <https://doi.org/10.1007/s11837-020-04267-5>.
- Karmakar, A., & Biswas, R. K. (2019). A study on the kinetics of extraction of Ti(IV) from sulphate medium by Cyanex 302. *Separation and Purification Technology*, 221, 331–337. <https://doi.org/10.1016/j.seppur.2019.03.098>.
- Kejřík, P. (2010). *Rozpustnost elektrárenských popílků ve vysoce alkalickém prostředí*. Brno: Vysoké učení technické v Brně.
- Kim, B., & Prezzi, M. (2008). Evaluation of the mechanical properties of class-F fly ash. *Waste Management*, 28(3), 649–659. <https://doi.org/10.1016/j.wasman.2007.04.006>.
- Kose Mutlu, B., Cantoni, B., Turolla, A., Antonelli, M., Hsu-Kim, H., & Wiesner, M. R. (2018). Application of nanofiltration for Rare Earth Elements recovery from coal fly ash leachate: Performance and cost evaluation. *Chemical Engineering Journal*, 349, 309–317. <https://doi.org/10.1016/j.cej.2018.05.080>.
- Kumar, A., Agrawal, S., & Dhawan, N. (2020). Processing of coal fly ash for the extraction of alumina values. *Journal of Sustainable Metallurgy*, 6(2), 294–306. <https://doi.org/10.1007/s40831-020-00275-6>.
- Kun, C., Xiaoguang, C., Yin, D., Guimei, G., Jin, G., Zhaohua, G., Xinghui, H., Darui, L., Litaio, S., Hongbin, W., Yongwang, W., & Huijun, X. (2017). *Method for extracting rare earth from fly ash*. CN108220630A.
- Le, V. T., Ngo, T. T. C., Le, T. T. H., Nguyen, T. T., Hiroyuki, F. (2019). Properties of Fly Ashes from Thermal Power Stations in Relation to Use as Soil Amendments. *Sains Malaysiana* 48, 745–755. <https://doi.org/10.17576/jsm-2019-4804-06>.
- Lee, Y.-R., Soe, J. T., Zhang, S., Ahn, J.-W., Park, M. B., & Ahn, W.-S. (2017). Synthesis of nanoporous materials via recycling coal fly ash and other solid wastes: A mini review. *Chemical Engineering Journal*, 317, 821–843. <https://doi.org/10.1016/j.cej.2017.02.124>.
- Liu, G., Zhang, H., Gao, L., Zheng, L., & Peng, Z. (2004). Petrological and mineralogical characterizations and chemical composition of coal ashes from power plants in Yanzhou mining district, China. *Fuel Processing Technology*, 85(15), 1635–1646. <https://doi.org/10.1016/j.fuproc.2003.10.028>.
- Ltd. HGP (2018). *Annual production and utilisation survey report*. Ash Development Association of Australia, Kembla.
- Ltd. OCP. (2019). *N,N,N',N' Tetra (2 Ethylhexyl) Diglycolamide (TEHDGA)*. http://www.orion-chem.com/Tetra_2_Ethylhexyl_Diglycolamide_TEHDGA.html.
- Luo, Y., Wu, Y., Ma, S., Zheng, S., Zhang, Y., & Chu, P. K. (2020). Utilization of coal fly ash in China: A mini-review on challenges and future directions. *Environmental Science and Pollution Research*. <https://doi.org/10.1007/s11356-020-08864-4>.
- Ma, J., Qin, G., Zhang, Y., Sun, J., Wang, S., & Jiang, L. (2018). Heavy metal removal from aqueous solutions by calcium silicate powder from waste coal fly-ash. *Journal of Cleaner Production*, 182, 776–782. <https://doi.org/10.1016/j.jclepro.2018.02.115>.
- Marco-Lozar, J. P., Cazorla-Amorós, D., & Linares-Solano, A. (2007). A new strategy for germanium adsorption on activated carbon by complex formation. *Carbon*, 45(13), 2519–2528. <https://doi.org/10.1016/j.carbon.2007.08.020>.
- Marko, M., Opravil, T., Masilko, J., & Porizka, J. (2019a). Possibilities of fly ash activation in alumina recovery process. *IOP Conference Series: Materials Science and Engineering*, 583, 012003. <https://doi.org/10.1088/1757-899x/583/1/012003>.
- Marko, M., Opravil, T., Masilko, J., & Pořizka, J. (2019b). Possibilities of fly ash activation in alumina recovery process. *IOP Conference Series: Materials Science and Engineering*, 583, 012003. <https://doi.org/10.1088/1757-899X/583/1/012003>.

- Matjie, R. H., Bunt, J. R., & van Heerden, J. H. P. (2005). Extraction of alumina from coal fly ash generated from a selected low rank bituminous South African coal. *Minerals Engineering*, 18(3), 299–310. <https://doi.org/10.1016/j.mineng.2004.06.013>.
- Mehrotra, A. K., Behie, L. A., Bishnoi, P. R., & Svrcek, W. Y. (1982). High-temperature chlorination of coal ash in a fluidized bed. 2. Recovery of iron, silicon, and titanium. *Industrial & Engineering Chemistry Process Design and Development*, 21(1), 44–50. <https://doi.org/10.1021/i200016a009>.
- Mishra, D. P., & Das, S. K. (2010). A study of physico-chemical and mineralogical properties of Talcher coal fly ash for stowing in underground coal mines. *Materials Characterization*, 61(11), 1252–1259. <https://doi.org/10.1016/j.matchar.2010.08.008>.
- Mondal, S., Ghar, A., Satpati, A. K., Sinharoy, P., Singh, D. K., Sharma, J. N., Sreenivas, T., & Kain, V. (2019). Recovery of rare earth elements from coal fly ash using TEHDGA impregnated resin. *Hydrometallurgy*, 185, 93–101. <https://doi.org/10.1016/j.hydromet.2019.02.005>.
- Moreno, N., Querol, X., Andres, J., Stanton, K., Towler, M., Nugteren, H., Janssenjurkovicova, M., & Jones, R. (2005). Physico-chemical characteristics of European pulverized coal combustion fly ashes. *Fuel*, 84(11), 1351–1363. <https://doi.org/10.1016/j.fuel.2004.06.038>.
- Murtha, M., & Burnet, G. (1976). Recovery of alumina from coal fly ash by high temperature chlorination. *Proceedings of the Iowa Academy of Science*, 4, 125–129.
- Nayak, N., & Panda, C. R. (2010). Aluminium extraction and leaching characteristics of Talcher Thermal Power Station fly ash with sulphuric acid. *Fuel*, 89(1), 53–58. <https://doi.org/10.1016/j.fuel.2009.07.019>.
- Office of Research D, and Technology, Office of Safety, RDT. (2016). <https://www.fhwa.dot.gov/publications/research/infrastructure/structures/97148/cfa53.cfm>
- Pan, J., Hassas, B. V., Rezaee, M., Zhou, C., & Pisupati, S. V. (2021). Recovery of rare earth elements from coal fly ash through sequential chemical roasting, water leaching, and acid leaching processes. *Journal of Cleaner Production*, 284, 124725. <https://doi.org/10.1016/j.jclepro.2020.124725>.
- Pan, J., Nie, T., Vaziri Hassas, B., Rezaee, M., Wen, Z., & Zhou, C. (2020). Recovery of rare earth elements from coal fly ash by integrated physical separation and acid leaching. *Chemosphere*, 248, 126112. <https://doi.org/10.1016/j.chemosphere.2020.126112>.
- Pan, K., Li, Y., Zhang, J., & Zhao, Q. (2018). A facile and low-cost method to produce ultra-pure 99.99999% gallium. *Materials*, 11(11), 2308/2301–2308/2308. <https://doi.org/10.3390/ma11112308>.
- Panda, C. R., & Sangita, S. (2020). Kinetics of aluminium leaching from coal fly ash by sulphuric acid. *Indian Journal of Chemical Technology (IJCT)*, 27(4), 263–273.
- Ponou, J., Dodbiba, G., Anh, J.-W., & Fujita, T. (2016). Selective recovery of rare earth elements from aqueous solution obtained from coal power plant ash. *Journal of Environmental Chemical Engineering*, 4(4, Part A), 3761–3766. <https://doi.org/10.1016/j.jece.2016.08.019>.
- Pyo, H. J., Hyeok, J. J., Kwan, K. J., & Un, P. S. (2019). *Method for extracting rare metal elements from coal ash and apparatus for extracting rare metal elements*. WO2019022320A1,
- Qi, L., & Yuan, Y. (2011). Characteristics and the behavior in electrostatic precipitators of high-alumina coal fly ash from the Jungar power plant, Inner Mongolia, China. *Journal of Hazardous Materials*, 192(1), 222–225. <https://doi.org/10.1016/j.jhazmat.2011.05.012>.
- Qin, Z., Zhang, G., Luo, D., Li, C., Yue, H., & Liang, B. (2019). Separation of titanium from vanadium and iron in leach solutions of vanadium slag by solvent extraction with triocetyl tertiary amine (N235). *Hydrometallurgy*, 188, 216–221. <https://doi.org/10.1016/j.hydromet.2019.07.004>.
- Rosita, W., Bendiyasa, I. M., Perdana, I., & Anggara, F. (2020). Sequential particle-size and magnetic separation for enrichment of rare-earth elements and yttrium in Indonesia coal fly ash. *Journal of Environmental Chemical Engineering*, 8(1), 103575. <https://doi.org/10.1016/j.jece.2019.103575>.

- Roth, E., Macala, M., Lin, R., Bank, T., Thompson, R., Howard, B., Soong, Y., & Granite, E. (2017). Distribution and extraction of rare earth elements from coal and coal by-products. In *Paper Presented at the 2017 World of Coal Ash (WOCA), Lexington, KY*.
- Rushwaya, M. J., & Ndlovu, S. (2017). Purification of coal fly ash leach liquor by solvent extraction: Identification of influential factors using design of experiments. *International Journal of Mineral Processing*, 164, 11–20. <https://doi.org/10.1016/j.minpro.2017.05.004>.
- Sahoo, P. K., Kim, K., Powell, M. A., & Equeenuddin, S. M. (2016). Recovery of metals and other beneficial products from coal fly ash: A sustainable approach for fly ash management. *International Journal of Coal Science & Technology*, 3(3), 267–283. <https://doi.org/10.1007/s40789-016-0141-2>.
- Saji John, K., Saji, J., Reddy, M. L. P., Ramamohan, T. R., & Rao, T. P. (1999). Solvent extraction of titanium(IV) from acidic chloride solutions by Cyanex 923. *Hydrometallurgy*, 51(1), 9–18. [https://doi.org/10.1016/S0304-386X\(98\)00066-8](https://doi.org/10.1016/S0304-386X(98)00066-8).
- Sangita, S., & Panda, C. R. (2020). Kinetics of aluminium leaching from coal fly ash by sulphuric acid. *Indian Journal of Chemical Technology*, 27(4), 263–327.
- Seeley, F. G., McDowell, W. J., Felker, L. K., Kelmers, A. D., & Egan, B. Z. (1981). Determination of extraction equilibria for several metals in the development of a process designed to recover aluminum and other metals from coal combustion ash. *Hydrometallurgy*, 6(3), 277–290. [https://doi.org/10.1016/0304-386X\(81\)90045-1](https://doi.org/10.1016/0304-386X(81)90045-1).
- Seidel, A., & Zimmels, Y. (1998). Mechanism and kinetics of aluminum and iron leaching from coal fly ash by sulfuric acid. *Chemical Engineering Science*, 53(22), 3835–3852. [https://doi.org/10.1016/S0009-2509\(98\)00201-2](https://doi.org/10.1016/S0009-2509(98)00201-2).
- Seidel, A., Zimmels, Y., & Armon, R. (2001). Mechanism of bioleaching of coal fly ash by *Thiobacillus thiooxidans*. *Chemical Engineering Journal*, 83(2), 123–130. [https://doi.org/10.1016/S1385-8947\(00\)00256-4](https://doi.org/10.1016/S1385-8947(00)00256-4).
- Seyfi, S., & Abdi, M. (2009). Extraction of titanium (IV) from acidic media by tri-n-butyl phosphate in kerosene. *Minerals Engineering*, 22(2), 116–118. <https://doi.org/10.1016/j.mineng.2008.05.003>.
- Shabtai, Y., & Mukmenev, I. (1996). A combined chemical-biotechnological treatment of coal fly ash (CFA). *Journal of Biotechnology*, 51(3), 209–217. [https://doi.org/10.1016/S0168-1656\(96\)01598-2](https://doi.org/10.1016/S0168-1656(96)01598-2).
- Shi, Y., Jiang, K.-X., & Zhang, T.-A. (2020a). Cleaner extraction of alumina from coal fly ash: Baking-electrolysis method. *Fuel*, 273, 117697. <https://doi.org/10.1016/j.fuel.2020.117697>.
- Shi, Y., Jiang, K.-X., Zhang, T.-A., & Lv, G.-Z. (2020b). Cleaner alumina production from coal fly ash: Membrane electrolysis designed for sulfuric acid leachate. *Journal of Cleaner Production*, 243, 118470. <https://doi.org/10.1016/j.jclepro.2019.118470>.
- Sijkova Ivanova, T., Panov, Z., Blazev, K., & Zajkova, V. (2011). Investigation of fly ash heavy metals content and physico chemical properties from thermal power plant, Republic of Macedonia. *International Journal of Engineering Science and Technology (IJEST)*, 3, 8219–8225.
- Škvarla, J., Sisol, M., Botula, J., Kolesárová, M., & Krinická, I. (2011). The potential use of fly ash with a high content of unburned carbon in geopolymers. *Acta Geodynamica et Geomaterialia*, 2(162), 123–132.
- Sole, K. C. (1999). Recovery of titanium from the leach liquors of titaniferous magnetites by solvent extraction: Part I. Review of the literature and aqueous thermodynamics. *Hydrometallurgy*, 51(2), 239–253. [https://doi.org/10.1016/S0304-386X\(98\)00081-4](https://doi.org/10.1016/S0304-386X(98)00081-4).
- Su, H., Chen, H., & Lin, J. (2020). A sequential integration approach using *Aspergillus Niger* to intensify coal fly ash as a rare metal pool. *Fuel*, 270, 117460. <https://doi.org/10.1016/j.fuel.2020.117460>.
- Survey, B. G. (2013). *Critical metals handbook*. Nottingham, UK: Wiley. <https://doi.org/10.1002/9781118755341.ch9>.
- Taggart, R. K., Hower, J. C., & Hsu-Kim, H. (2018). Effects of roasting additives and leaching parameters on the extraction of rare earth elements from coal fly ash. *International Journal of Coal Geology*, 196, 106–114. <https://doi.org/10.1016/j.coal.2018.06.021>.

- Tang, M., Zhou, C., Pan, J., Zhang, N., Liu, C., Cao, S., Hu, T., & Ji, W. (2019). Study on extraction of rare earth elements from coal fly ash through alkali fusion—Acid leaching. *Minerals Engineering*, 136, 36–42. <https://doi.org/10.1016/j.mineng.2019.01.027>.
- Tauanov, Z., Azat, S., & Baibatyrova, A. (2020). A mini-review on coal fly ash properties, utilization and synthesis of zeolites. *International Journal of Coal Preparation and Utilization*, 1–23. <https://doi.org/10.1080/19392699.2020.1788545>.
- Torralvo, F. A., & Fernández-Pereira, C. (2011). Recovery of germanium from real fly ash leachates by ion-exchange extraction. *Minerals Engineering*, 24(1), 35–41. <https://doi.org/10.1016/j.mineng.2010.09.004>.
- Valeev, D., Kunilova, I., Shoppert, A., Salazar-Concha, C., & Kondratiev, A. (2020). High-pressure HCl leaching of coal ash to extract Al into a chloride solution with further use as a coagulant for water treatment. *Journal of Cleaner Production*, 276, 123206. <https://doi.org/10.1016/j.jclepro.2020.123206>.
- Vassilev, S. V., & Vassileva, C. G. (2007). A new approach for the classification of coal fly ashes based on their origin, composition, properties, and behaviour. *Fuel*, 86(10–11), 1490–1512. <https://doi.org/10.1016/j.fuel.2006.11.020>.
- Wang, L., Zhang, T.-A., Lv, G.-Z., Dou, Z.-H., Sun, W.-H., Zhang, W.-G., Niu, L.-P., & Zhang, Z.-M. (2019a). Titanium extraction from fly ash by carbochlorination. *JOM*, 71(12), 4624–4630. <https://doi.org/10.1007/s11837-019-03460-5>.
- Wang, L., Zhang, T.-A., Lv, G.-Z., Dou, Z.-H., Zhang, W.-G., Niu, L.-P., & Z-m, Z. (2019b). Kinetics of magnesium and calcium extraction from fly ash by carbochlorination. *JOM*, 71(8), 2798–2805. <https://doi.org/10.1007/s11837-019-03474-z>.
- Wang, N., Sun, X., Zhao, Q., Yang, Y., & Wang, P. (2020). Leachability and adverse effects of coal fly ash: A review. *Journal of Hazardous Materials*, 396, 122725. <https://doi.org/10.1016/j.jhazmat.2020.122725>.
- Wang, Z., Dai, S., Zou, J., French, D., & Graham, I. T. (2019c). Rare earth elements and yttrium in coal ash from the Luzhou power plant in Sichuan, Southwest China: Concentration, characterization and optimized extraction. *International Journal of Coal Geology*, 203, 1–14. <https://doi.org/10.1016/j.coal.2019.01.001>.
- Wen, Z., Zhou, C.-C., Pan, J., Cao, S., Hu, T., Ji, W., & Nie, T. (2020). Recovery of rare-earth elements from coal fly ash via enhanced leaching. *International Journal of Coal Preparation and Utilization*, 1–15. <https://doi.org/10.1080/19392699.2020.1790537>.
- Wu, Y., Yang, X., Li, L., Wang, Y., & Li, M. (2019). Kinetics of extracting alumina by leaching coal fly ash with ammonium hydrogen sulfate solution. *Chemical Papers*, 73(9), 2289–2295. <https://doi.org/10.1007/s11696-019-00779-w>.
- Xingdong, L., Jialong, L., Yanming, P., Shengqun, T., & Mengdie, W. (2020). *Method for extracting lithium from fly ash*. CN110643832A.
- Yan, L., Wang, Y., Ma, H., Han, Z., Zhang, Q., & Chen, Y. (2012). Feasibility of fly ash-based composite coagulant for coal washing wastewater treatment. *Journal of Hazardous Materials*, 203–204, 221–228. <https://doi.org/10.1016/j.jhazmat.2011.12.004>.
- Yang, F., & Hlavacek, V. (1998). Carbochlorination kinetics of titanium dioxide with carbon and carbon monoxide as reductant. *Metallurgical and Materials Transactions B*, 29(6), 1297–1307. <https://doi.org/10.1007/s11663-998-0053-7>.
- Yousuf, A., Manzoor, S. O., Youssouf, M., Malik, Z. A., & Khawaja, K. S. (2020). Fly ash: Production and utilization in india—an overview. *Journal of Materials and Environmental Science*, 11(6).
- Zhang, J., Wen, K., & Li, L. (2021). Bio-modification of coal fly ash using urease-producing bacteria. *Fuel*, 286, 119386. <https://doi.org/10.1016/j.fuel.2020.119386>.
- Zhang, L., & Xu, Z. (2016). An environmentally-friendly vacuum reduction metallurgical process to recover germanium from coal fly ash. *Journal of Hazardous Materials*, 312, 28–36. <https://doi.org/10.1016/j.jhazmat.2016.03.025>.

- Zhang, L., & Xu, Z. (2017). Application of vacuum reduction and chlorinated distillation to enrich and prepare pure germanium from coal fly ash. *Journal of Hazardous Materials*, 321, 18–27. <https://doi.org/10.1016/j.jhazmat.2016.08.070>.
- Zhao, Z., Cui, L., Guo, Y., Li, H., & Cheng, F. (2020). Recovery of gallium from sulfuric acid leach liquor of coal fly ash by stepwise separation using P507 and Cyanex 272. *Chemical Engineering Journal*, 381, 122699. <https://doi.org/10.1016/j.cej.2019.122699>.
- Zhongran, D., Dexin, D., Nan, H., Feng, L., Guangyue, L., & Hui, Z. (2018). *Method for extracting uranium from coal fly ash*. CN108285981A.
- Zierold, K. M., & Odoh, C. (2020). A review on fly ash from coal-fired power plants: Chemical composition, regulations, and health evidence. *Reviews on Environmental Health*, 35(4), 401–418. <https://doi.org/10.1515/reveh-2019-0039>.

Chapter 24

Application of Geochemical Modeling in Rare Earth Elements Leaching of Coal Combustion and Secondary Residues



Joyce N. Odimba and Rafael M. Santos

24.1 Introduction

Over 200 different minerals containing rare earth elements (REEs) naturally occur. While a large portion of these REEs are easily extracted, as they are speciated as carbonates or oxides, others are bonded to silicates and phosphates (Fig. 24.1), which are tough to infiltrate (Kumari et al. 2015; Rao et al. 2020). REEs are important to the world's economy as they are used in the production of rechargeable batteries, mobile phones, compact fluorescent light bulbs, catalytic converters, flat-screen display panels, hybrid vehicles, laptop computers, etc. (Edahbi et al. 2018).

REEs are commercially produced from bastnaesite, monazite, xenotime among other resources, however, due to depleting natural sources of these elements and their increasing industrial utilization; many studies have redirected their focus to the recovery of REEs from secondary/waste resources (Yang and Honaker 2020). These secondary resources include electronic waste recycling, coal ash (Fig. 24.2), mine waste streams, slags, wastewater, municipal solid waste incineration residues, and industrial wastes (Binnemans et al. 2013; Jha et al. 2016; Lin et al. 2017; Yang and Honaker 2020). Although the recovery of REEs from these secondary resources is usually low grade, it is still advantageous as it eliminates the cost of mining these elements from natural resources as well as other mining-associated costs.

The use of geochemical modeling has been employed in various leaching studies to predict and describe various leaching behaviors in different environmental fields such as solid waste, wastewater, and soil. As a popular tool, the geochemical equilibrium model is used to predict the phases and speciation of elements and the saturation index of minerals in solutions at equilibrium. The geochemical computer

J. N. Odimba · R. M. Santos (✉)
School Engineering, University of Guelph, Guelph, ON, Canada
e-mail: santosr@uoguelph.ca

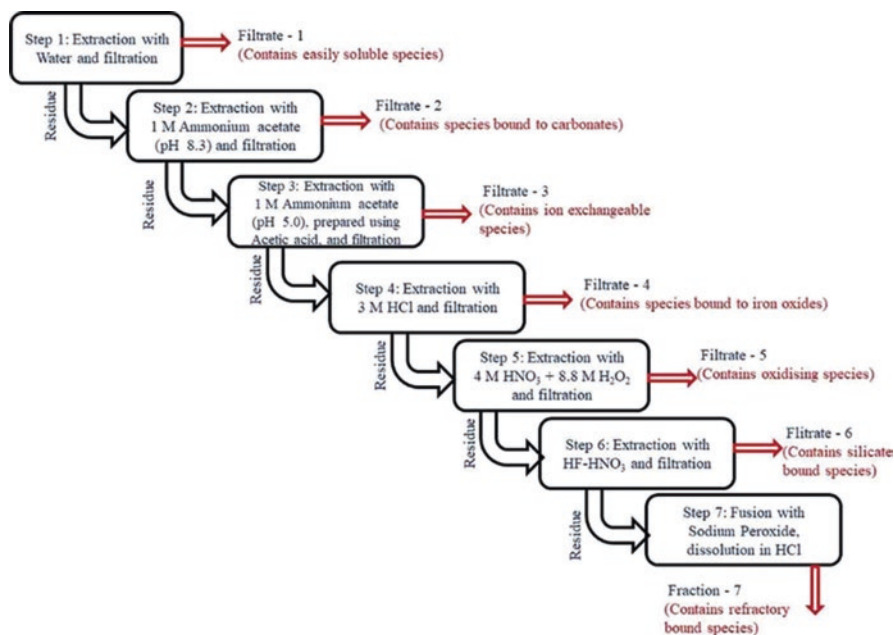


Fig. 24.1 Sequential chemical extraction scheme used by Rao et al. (2020) for spectating the REEs in coal fly ash (Rao et al. 2020); re-used with permission from Taylor & Francis (4962560438969)

software commonly used in environmental, geological, and other hydrometallurgical studies include Visual MINTEQ, PHREEQC, and Geochemist's Workbench. Thus, this review will focus on several REEs leaching studies that applied geochemical modeling in predicting and understanding various leaching behaviors such as dissolution-precipitation balance, acid-base balance, and saturation indices.

24.2 Motivation for Various REEs Leaching Studies

Although the leaching of REEs from secondary resources has been studied widely and even applied commercially, there are still quite some research gaps that different studies have been conducted to address some of these gaps.

Sea-floor deposits, including marine clays, ferromanganese nodules, and hydrogenic crusts, have been considered as alternative sources of REEs as they have significant REY (rare earth elements and yttrium) concentrations (Fujimoto et al. 2016; Menendez et al. 2017). Josso et al. (2018) reported that significant challenges of the economic exploitation of such sources include their comparative inaccessibility and the requirement for advanced mineral processing technologies. Their study noted a lack of knowledge on the processing of oceanic metalliferous sediments as an

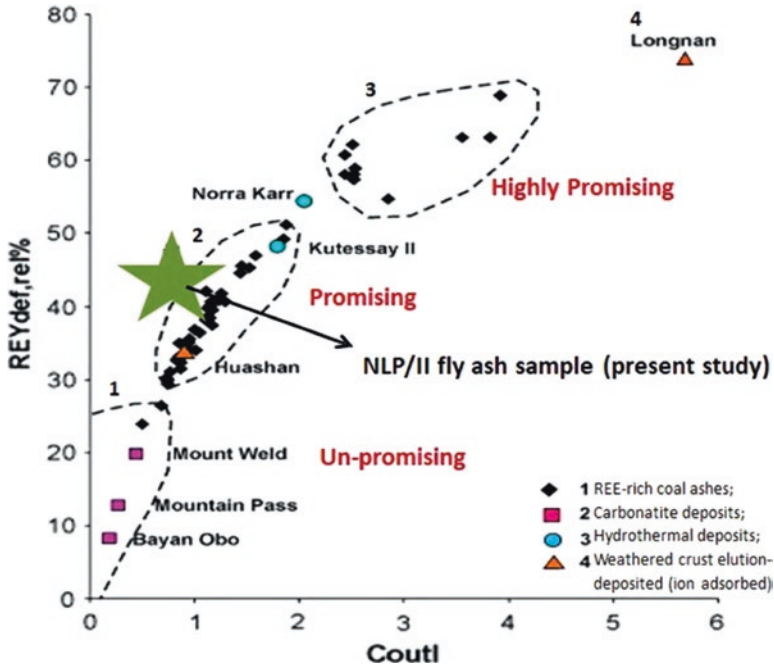


Fig. 24.2 Comparison between the REE content of coal ashes (diamond symbols), including the coal fly ash studied by Rao et al. (2020), to the REE content of typical ores (deposits) of REEs (Rao et al. 2020); re-used with permission from Taylor & Francis (4962560438969)

attractive source of REY. Hence, Josso et al. (2018) studied the extraction of REY from umbers (i.e., metalliferous sediments) as an alternative source of REY compared to magmatic deposits that are currently the preferred source of REEs to the global commercial market. Further, they utilized pH-dependent experiments and geochemical modeling in examining the efficiency of the selective recovery of REY present at relatively low concentrations (from other elemental components) present in the leaching liquor, using oxalate precipitation.

Acid mine drainages (AMD) produced from the processing operations of coal resources contain heavy metals and high concentrations of REEs, hence they are considered as secondary resources. However, Li and Wu (2017) noted that it is challenging to estimate and exploit the REE distribution patterns present in AMD. Thus, gaining comprehensive information about the geochemical characteristics of REEs in AMD through further research is essential, as relatively sparse amount of research has covered the geochemical behaviors and concentrations of REEs in AMD (Li and Wu 2017). To address this research gap, their study was aimed at determining the origin and distribution of REEs in AMD as well as identifying the factors responsible for the geochemical behaviors of REEs.

Moreover, Sharifi et al. (2013) reported that the water–rock interaction that governs the chemical make-up of acidic discharges from mining wastes can be

identified by the REE patterns. Thus, their concentration patterns aid in further understanding geochemical processes occurring over the course of AMD formation as these patterns can detect complex geochemical processes undergoing within natural systems. AMD and the stream waters that it impacts are rich in middle and heavy REEs as compared to solid samples which are rich in light REEs. These differences have been attributed to fractionation which can occur during weathering and solute transport (Gammons et al. 2003). Hence, in their research, Sharifi et al. (2013) studied the concentrations of REEs, their distribution pattern, and the inorganic speciation modeling of different mining-related and natural waters.

Furthermore, as a secondary source of REEs, the recovery of these elements can serve as a source of revenue and also lessen the cost of AMD treatments (Ayora et al. 2016; Moraes et al. 2020). Therefore, method of recovery is an important issue that has been investigated and still has a lot to be studied (Jha et al. 2016; Zhang and Honaker 2018). In the development of efficient, sustainable, and novel methods of REEs recovery from AMD, co-precipitation is at the top of the list. Thus, the study conducted by Moraes et al. (2020) focused on investigating the geochemistry of REEs in AMD and recovery of REEs via co-precipitation processes. The study also evaluated the chemistry and mineralogy of REE-rich precipitates resulting from AMD alkali treatment using different approaches including geochemical modeling.

The use of adsorbents has been considered as an effective method of extracting REEs from their sources. Komnitsas et al. (2017) have reported on the utilization of modified silica gel, sponge biomass, among other adsorbents, for the recovery of solubilized REEs; yet, very few studies have looked into the adoption of biochar for REEs adsorption. Biochar has been used for the adsorption of various organic and inorganic contaminants from both natural waters and wastewaters, but only a few studies report on the adsorption of REEs. Therefore, Komnitsas et al. (2017) investigated the efficiency of biochar-assisted adsorption of scandium and neodymium as well as the speciation of these REEs in the solution using geochemical modeling.

During the extraction of REEs from their ores or secondary resources, there are usually impurities present. Iron (Fe) has been observed as a common impurity in concentrates containing REEs, which must be removed in the early part of the mineral processing flowsheet before the REE separation step. Various methods have been used for the removal of Fe from the REE concentrates, and high temperature is usually an important factor in the removal process. Nascimento et al. (2019) state that there is a need for more comprehensive approaches that apply several methodologies that can enable accurate and reliable simulation of the behavior of complex hydrometallurgical processes. The major aim of the study was to obtain an aqueous solution with elevated REE concentrations, and conversely low concentration of Fe, which will be carried into subsequent separation and purification processes. Hence, in their study, thermodynamic modeling, statistical design, and multi-objective optimization were applied to elucidate the controlling process variables and their level of influence, in order to improve the extraction and recovery of REEs.

Further, the main challenge encountered in the extraction and separation of REEs from their concentrates, especially for satisfying the global commercial markets of REEs, is the need to improve the recovery of these elements during metallurgical

processing. To address this challenge, Yahya et al. (2019) noted that it is essential to consider the fundamental thermodynamics of such processes as it can constitute the ultimate guidance needed in selecting the reagents that should be used and their concentrations. This can be achieved by using the thermodynamic data graphed in the form of Pourbaix diagrams (i.e., Eh-pH diagrams), which will identify the conditions that favor the dissolution of specific REEs. Pourbaix diagrams show the relative stabilities of different chemical elements in solutions. However, Yahya et al. (2019) observed that no study had been conducted on the use of Pourbaix diagrams for investigating the acid leaching process for elevated temperatures.

In the separation of REEs from other fission products, rare earth oxalates precipitation is used extensively in hydrometallurgical processes. Rodriguez-Ruiz et al. (2018) reported that to gain a deeper conception and to optimize the control of supersaturation that leads to the precipitation of REEs, the thermodynamics of these processes must be fully understood. This can be accomplished by using various thermodynamic models that will calculate and analyze the activities of all chemical elements present in aqueous solution. Thus, their study was focused on performing thermodynamic modeling of systems consisting of oxalate-rare earth-nitric acid solutions, to investigate and gain comprehensive understanding of the reactive precipitation processes of neodymium and cerium.

24.2.1 Comment on the Papers' Similarities and Differences

The papers showed that temperature and pH are very important controlling factors for the extraction processes of REEs. They also focused their research on the exploitation of REEs from alternative sources rather than from natural resources. However, the first five papers reviewed were focused on determining the speciation of species in solution and the saturation index of the minerals in aqueous solution, while the last three papers in this review are focused on understanding the thermodynamics of the leaching process.

24.3 Methodologies

In their study, Josso et al. (2018) performed the modeling calculations using the PHREEQC software and thermodynamic data obtained from the Lawrence Livermore National Laboratory (LLNL) database. Stability constants for the different REE-oxalate complexes in solution were obtained from other sources (Chung et al. 1998; Schijf and Byrne 2001; Smith and Martell 2004).

Li and Wu (2017) used the Visual MINTEQ modeling software to determine the inorganic species of REEs present in AMD. The data used for the pH and concentrations were generated from the modeling program database. The speciation of the

elements in the solution was determined, and the saturation indices of the elements were calculated.

Likewise, Sharifi et al. (2013) used the Visual MINTEQ modeling software to obtain the equilibrium speciation of REEs in AMD. The thermodynamic data used for this modeling was generated from the MINTEQ program database and complemented with data from previous literature.

Moraes et al. (2020) analyzed the chemical modeling of the REEs in AMD using the PHREEQC modeling software. The database used for the modeling was the LLNL database and *Thermoddem_V1.10*. The saturation indexes were calculated based on data from the LLNL database, and the speciation of the REEs was calculated based on *Thermoddem_V1.10.dat*, with the exception of yttrium, which was modeled using the aforementioned LLNL database.

Komnitsas et al. (2017) used the PHREEQC modeling software and the LLNL database to define the speciation of both Nd and Sc in aqueous solutions. Additional solubility data was obtained from various sources to improve the reliability of the modeling results. The dominant oxidation species of the two REEs of interest were determined as well as the saturation indices of minerals at specific conditions were calculated.

To understand the thermodynamics of the REEs extraction process, Nascimento et al. (2019) used the HSC Chemistry software to calculate the Gibbs free energy of reactions. The data for the Gibbs free energy of formation was generated from the modeling software database, and the charts were plotted over the range of 100 °C–1000 °C to analyze the thermodynamics of acid roasting.

Further, Yahya et al. (2019) plotted the Pourbaix diagrams using the HSC Chemistry software, using different temperatures of 25 °C, 100 °C, 200 °C, and 300 °C. The coordinate of the stability boundaries was determined using the Gibbs energy of the various equilibria and used to create the Pourbaix diagram. The data used for the thermodynamics study was generated from the software database.

Rodriguez-Ruiz et al. (2018) used the Pitzer model realized in the PHREEQC modeling software to model both Ce and Nd systems. The Pitzer model was used because it allows the accurate estimation of ion activities over a broad range of pH values and ionic strengths. The calculations were activated via a COM interface with the software Matlab. The data used for the modeling was generated from the PHREEQC database and complemented with data previous literature and experimental data.

24.3.1 Comment on the Methodology Used in the Different Studies

The similarity between all the papers reviewed is that the data used for the modeling were all generated from the modeling software database. The data used in four of the studies were complemented with data from other sources. However, their

difference is the use of different modeling software. Two studies focused on thermodynamics modeling were conducted using the HSC Chemistry software, two other studies used the Visual MINTEQ modeling program while three of the studies used the PHREEQC software. From the papers reviewed, it was observed that the studies that used PHREEQC software for modeling usually complemented the data with the Lawrence Livermore National Laboratory (LLNL) database.

24.4 Results

Josso et al. (2018) utilized geochemical modeling in examining the efficiency of the selective extraction of low REY concentrations from other components/impurities present in leaching liquors, using an oxalate precipitation process. The modeling established that oxalate precipitates fractionate the REY in the decreasing order of middle REEs (MREEs) >> light REEs (LREEs) >> heavy REEs (HREEs), at equivalent molar REE concentrations in solution. Using the complexes predicted from the LLNL database and experimental conditions, oxalate-binding REE complexes dominated the REE complexation. Differences were observed between the REE speciation calculated using PHREEQC and experimental results. The model also showed that there was no precipitation of Er, Ho, Lu, Tb, Tm, and Yb. The fractionation of REEs obtained in the experiments were explained accurately by the modeling. The decrease in the recovery of REY was not as sharp in the experiments as they were predicted in the model. However, the model was able to show the leaching efficiency of REY using oxalate precipitation, it would be interesting to see the application of the modeling to describe the leaching kinetics.

The study conducted by Li and Wu (2017) was aimed at determining the origin and distribution of REEs in AMD as well as identifying the factors responsible for the geochemical behaviors of REEs. The modeling result showed that AMD samples are slightly more enriched with MREEs compared to LREEs and HREEs. This behavior was attributed to probable fractionation during acid leaching, weathering, and solute transport. The modeling calculation revealed that REE-sulfate complexes were the predominate species. The low pH and high concentrations of dissolved sulfate observed are necessary for forming stable REE-sulfate complexes, hence these conditions serve an important function in the presence of REEs in AMD. The mobility of REEs and the related geochemical behaviors were reportedly controlled by Fe-Al hydroxides/hydroxysulfate colloids and by accessory minerals. This may be because the stable REEs-sulfate complexes are adsorbed onto these Fe-Al hydroxides/hydroxysulfate and become co-precipitated together, leading to the removal of REEs from AMD. One uncertainty about the modeling is the fact that the data used were generated from the modeling software database and not experimental data, hence it is quite uncertain if the same result can be replicated in reality. However, the modeling result corresponds with the results observed by Josso et al. (2018) where it was observed that aqueous sources are more enriched with MREEs as a result of fractionation.

Sharifi et al. (2013) determined the concentrations and inorganic speciation of REEs, and the patterns of their distribution of various mining-related waters and natural waters. The result of the speciation modeling predicted that the predominant REE inorganic species dissolved in the solution were Ln^{3+} , $\text{Ln}(\text{SO}_4)^{2-}$, LnSO_4^+ , LnHCO_3^{2+} , $\text{Ln}(\text{CO}_3)^{2-}$ and LnCO_3^+ . Similar to the report given by Li and Wu (2017), the AMD studied was enriched with REE-sulfate and free metal species. It was also found that the AMD was enriched with MREEs, similar to the aforementioned studies. It would however be interesting to study the prediction of the leaching kinetics using the modeling software as this will serve as an opportunity for further research.

The study conducted by Moraes et al. (2020) focused on investigating the geochemistry of REEs in AMD and recovery of REEs via co-precipitation processes. The study also evaluated the chemistry and mineralogy of REE-rich precipitates resulting from AMD alkali treatment using different approaches including geochemical modeling. The modeling result revealed that REE complexed with sulfate except for praseodymium (Pr). The authors further noted that the absence of the Pr-sulfate complex may contribute to different behaviors of the element in the AMD system being studied, as REE-sulfate complexes have been noted to play an important role in the adsorption of REEs on precipitates in AMD. The result of the saturation index calculated showed that at low pH values, none of Al, Si, and Fe minerals were stable, as they presented negative SI indicating that they are expected to dissolve. However, goethite, hematite, and gibbsite precipitated from the aqueous system. Soluble REEs only started precipitating individually as REE hydroxides at slightly alkaline pH above 8.5. The different behaviors of the REE-sulfate complexes call for further research on decoding the exact mechanism of interaction between REE complexes and surfaces of precipitates in AMD systems.

Komnitsas et al. (2017) determined the efficiency of biochar-assisted adsorption of scandium and neodymium, and the chemical speciation of these REEs via geochemical modeling. The modeling results showed that under highly acidic conditions Nd was primarily present as positively charged species, Nd^{3+} and NdSO_4^+ . In comparison, under highly alkaline conditions (pH 11), this REE was predominantly present as negatively charged species, making up 66% of the speciation. On the other hand, Sc is only present as ScSO_4^+ under extremely high acidic conditions, usually pH values below 1.9. However, under acidic conditions above pH 1.9, Sc is predominantly present in its free ionic form. Under alkaline conditions, Sc is predominantly present as ScO_2H^0 and ScO_2^- . The saturation index (SI) calculation showed that $\text{Nd}(\text{OH})_3$ and $\text{Sc}(\text{OH})_3$ revealed positive SI values indicating possible precipitation at pH values over 6.7 and 4.8, respectively. However, the data used for this study were generated from the modeling software database, which was not compared to experimental data. In any case, the results of the geochemical modeling and speciation analysis can serve as a basis for the selection of the most efficient biochar and of the optimal experimental conditions needed to achieve greatest adsorption efficacy.

In their study, Nascimento et al. (2019) applied thermodynamic modeling, statistical design, and multi-objective optimization to identify the controlling process

variables and their level of influence adequate to improve the extraction of REEs. The result of the thermodynamic analysis revealed that at a roasting temperature of below 700 °C, iron sulfate formation was expected while at a temperature of above 780 °C, iron sulfate was expected to decompose. This means that the roasting temperature serves a crucial part in the control of Fe solubilization in the acid leaching process. Monazite was shown to be the main REE carrier phase, while goethite, hematite, and magnetite were found to be the main Fe-bearing phases. Hence, the study reported that the amount of acid used in the roasting should be just adequate to enable the Fe-sulfate to react with the monazite, while an excessive amount of acid would lead to undesirable iron leaching into the aqueous solution. This study sparked an interest as all of the results from the thermodynamic analysis were taken into consideration in the design of the laboratory experiment. This led to a high yield of REE and low Fe concentration. It will be interesting to see the result of applying the results of this thermodynamic analysis on the industrial production of REEs.

Pourbaix diagrams show the relative stabilities of different chemical elements in solutions, which is useful to determine possible REEs that may be present in the system. However, Yahya et al. (2019) observed that no study had been conducted on the use of Pourbaix diagrams for investigating the acid leaching process at elevated temperatures. Thus, the Pourbaix diagram was constructed for three main REEs in this study, namely La, Nd, and Ce. The constructed Pourbaix diagram for La-, Ce-, and Nd-PO₄-SO₄-H₂O revealed that temperatures of 200 °C–300 °C are suitable for the digestion process. Also, the Pourbaix diagram for La-, Ce-, and Nd-PO₄-SO₄-H₂O showed that acid concentration serves an important function in the control of REE concentrations. The result further showed that in the presence of sulfuric acid and phosphoric elements, the solubility of the REEs decreases in the order of Ce > La > Nd, as a function of increasing temperature and concentration. For further research, the Pourbaix diagram can be used to assess the stability areas in an aqueous system under alkaline leaching and identify the REEs present in such a system, as alkaline leaching has been reported to behave differently from acid leaching of REEs.

24.5 Conclusion

From the different studies reviewed in this paper, the role that geochemical modeling has to play in environmental studies, especially leaching studies, cannot be over-emphasized. As a predictive tool, the leaching behavior of rare earth elements predicted in most of the papers agrees with experimental results. In the papers discussed, only the precipitation/dissolution model and thermodynamic model were applied for analyzing the leaching behavior of REEs. However, further studies can be reviewed and conducted on the application of these geochemical models in understanding other leaching behaviors, such as the leaching kinetics. Further, these tools can also be tested in predicting the long-term stability of REEs in solid wastes,

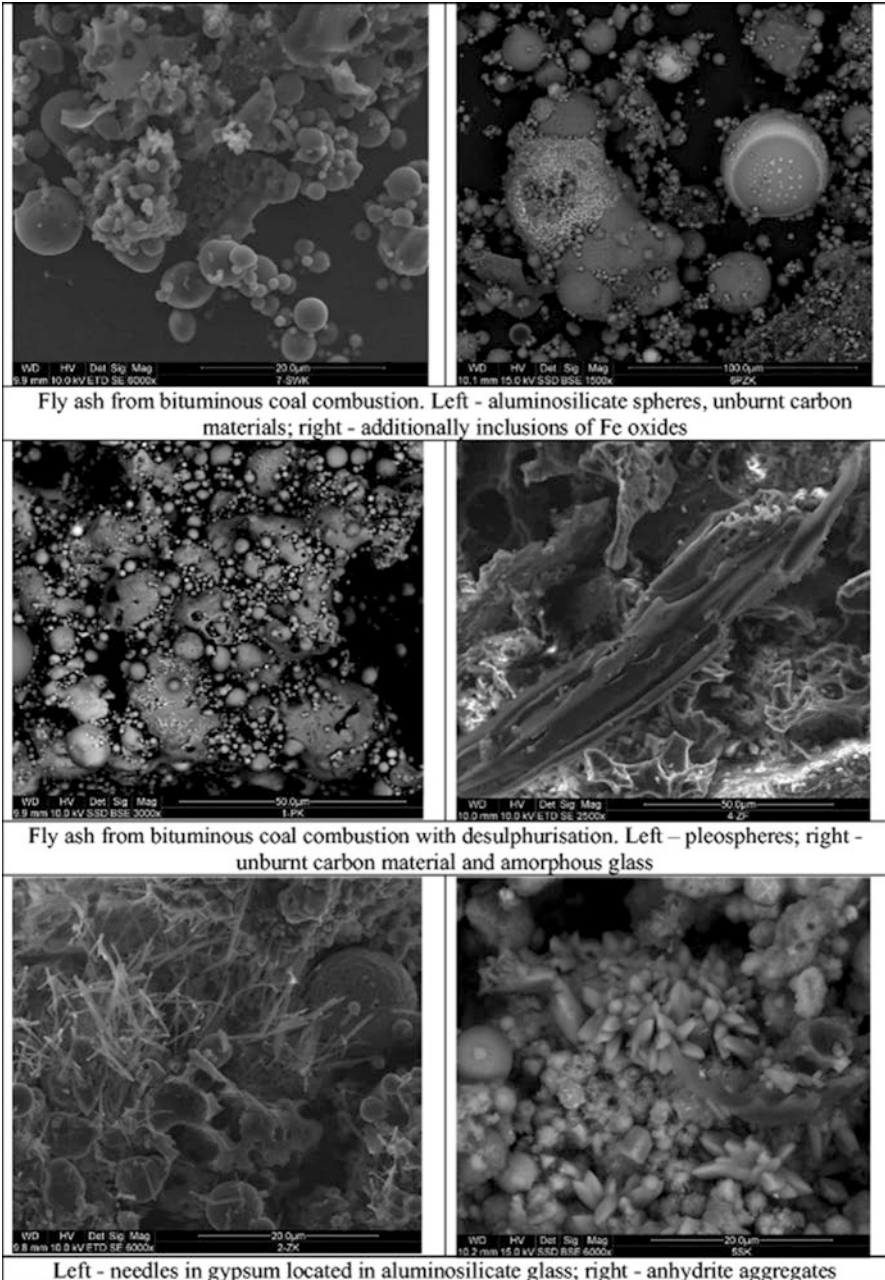


Fig. 24.3 SEM microphotographs of fly ashes from bituminous coal combustion (SEM photographs source: Franus et al. 2015); CC-BY

such as coal combustion residuals imaged in Fig. 24.3 (Franus et al. 2015; Razem, 2016; Hsu-Kim et al. 2018; Wang et al. 2019; Rao et al. 2020; Wen et al. 2020).

Acknowledgments Author Rafael M. Santos would like to acknowledge and say thanks to the financial assistance provided under a Discovery Grant from the Natural Sciences and Engineering Research Council of Canada (NSERC).

References

- Ayora, C., Macías, F., Torres, E., et al. (2016). Recovery of rare earth elements and yttrium from passive-remediation systems of acid mine drainage. *Environmental Science & Technology*, 50, 8255–8262.
- Binnemans, K., Jones, P. T., Blanpain, B., et al. (2013). Recycling of rare earths: A critical review. *Journal of Cleaner Production*, 51, 1–22.
- Chung, D. Y., Kim, E. H., Lee, E. H., et al. (1998). Solubility of rare earth oxalate in oxalic and nitric acid media. *Journal of Industrial and Engineering Chemistry*, 4, 277–284.
- Edabhi, M., Benzaazoua, M., Plante, B., et al. (2018). Mineralogical characterization using QEMSCAN® and leaching potential study of REE within silicate ores: A case study of the Matamec project, Québec, Canada. *Journal of Geochemical Exploration*, 185, 64–73.
- Franus, W., Wiatros-Motyka, M. M., & Wdowin, M. (2015). Coal fly ash as a resource for rare earth elements. *Environmental Science and Pollution Research*, 22(12), 9464–9474.
- Fujimoto, J., Tanaka, K., Watanabe, N., et al. (2016). Simultaneous recovery and separation of rare earth elements in ferromanganese nodules by using *Shewanella putrefaciens*. *Hydrometallurgy*, 166, 80–86.
- Gammons, C. H., Wood, S. A., Jonas, J. P., et al. (2003). Geochemistry of rare elements and uranium in the acidic Berkeley Pit Lake, Butte, Montana. *Chemical Geology*, 198, 269–288.
- Hsu-Kim, H., Smith, R., Taggart, R., et al. (2018). Recovery of rare earth elements from coal combustion residuals. 256th National Meeting and Exposition of the American-Chemical-Society (ACS) - Nanoscience, Nanotechnology and Beyond, Boston, MA. August, 2018, 19–23.
- Jha, M. K., Kumari, A., Panda, R., et al. (2016). Review on hydrometallurgical recovery of rare earth metals. *Hydrometallurgy*, 165, 2–26.
- Josso, P., Roberts, S., Teagle, D. A. H., et al. (2018). Extraction and separation of rare earth elements from hydrothermal metalliferous sediments. *Mining and Engineering*, 118, 106–121.
- Komnitsas, K., Zaharaki, D., Bartzas, G., et al. (2017). Adsorption of Scandium and Neodymium on Biochar Derived after Low-Temperature Pyrolysis of Sawdust. *Minerals*, 7, 200.
- Kumari, A., Panda, R., Jha, M. K., et al. (2015). Thermal treatment for the separation of phosphate and recovery of rare earth metals (REMs) from Korean monazite. *Journal of Industrial and Engineering Chemistry*, 21, 696–703.
- Li, X., & Wu, P. (2017). Geochemical characteristics of dissolved rare earth elements in acid mine drainage from abandoned high-As coal mining area, southwestern China. *Environmental Science and Pollution Research*, 24, 20540–20555.
- Lin, R., Bank TL, Roth, E. A., et al. (2017). Organic and inorganic associations of rare earth elements in central Appalachian coal. *International Journal of Coal Geology*, 179, 295–301.
- Menendez, A., James, R. H., Roberts, S., et al. (2017). Controls on the distribution of rare earth elements in deep-sea sediments in the North Atlantic Ocean. *Ore Geology Reviews*, 87, 100–113.
- Moraes, M. L. B., Murciego, A., Álvarez-ayuso, E., et al. (2020). The role of Al₁₃-polymers in the recovery of rare earth elements from acid mine drainage through pH neutralization. *Applied Geochemistry*, 113, 104466.
- Nascimento, M., Lemos, F., Guimarães, R., et al. (2019). Modeling of REE and Fe Extraction from a Concentrate from Araxá (Brazil). *Minerals*, 9, 451.

- Rao, K. A., Md, S., RamaDevi, G., et al. (2020). On the characterization and leaching of rare earths from a coal fly ash of Indian origin. *Separation Science and Technology*. <https://doi.org/10.1080/001496395.2020.1718705>.
- Razem, D. (2016). The extraction of rare earths from coal ash. *Kemija U Industriji Journal of Chemists and Chemical Engineers*, 65(3–4), 186.
- Rodríguez-Ruiz, I., Teychené, S., Vitry, Y., et al. (2018). Thermodynamic modeling of neodymium and cerium oxalates reactive precipitation in concentrated nitric acid media. *Chemical Engineering Science*, 183, 20–25.
- Schijf, J., & Byrne, R. H. (2001). Stability constant for mono- and dioxalato-complexes of Y and REE, potentially important species in groundwaters and surface waters. *Geochimica et Cosmochimica Acta*, 65, 1037–1046.
- Sharifi, R., Moore, F., & Keshavarzi, B. (2013). Geochemical behavior and speciation modeling of rare earth elements in acid drainages at Sarcheshmeh porphyry copper deposit, Kerman Province, Iran. *Chemie der Erde*, 73, 509–517.
- Smith, R. M., & Martell, A. E. (2004). *NIST critically selected stability constants of metal complexes database*. Version 8.0 for Windows. National Institute of Standards and Technology, Texas A&M University.
- Wang, Z., Dai, S. F., Zou, J. H., et al. (2019). Rare earth elements and yttrium in coal ash from the Luzhou power plant in Sichuan, Southwest China: Concentration, characterization and optimized extraction. *International Journal of Coal Geology*, 203, 1–14.
- Wen, Z. P., Zhou, C. C., Pan, J. H., et al. (2020). Recovery of rare-earth elements from coal fly ash via enhanced leaching. *International Journal of Coal Preparation and Utilization*. <https://doi.org/10.1080/19392699.2020.1790537>.
- Yahya, F. N., Suli, L. N. M., Ibrahim, W. H. W., et al. (2019). Thermodynamic Evaluation of the Aqueous Stability of Rare Earth Elements in Sulfuric Acid Leaching of Monazite through Pourbaix Diagram. *Mater Today: Proceed*, 19, 1647–1656.
- Yang, X., & Honaker, R. Q. (2020). Leaching Kinetics of Rare Earth Elements from Fire Clay Seam Coal. *Minerals*, 10, 491.
- Zhang, W., & Honaker, R. Q. (2018). Rare earth elements recovery using staged precipitation from leachate generated from coarse coal refuse. *International Journal of Coal Geology*, 195, 189–199.

Chapter 25

Ionic Liquids for the Recovery of Rare Earth Elements from Coal Combustion Products



Isaac Kwabena Danso, Ana Belen Cueva-Sola, Zubair Masaud, Jin-Young Lee, and Rajesh Kumar Jyothi

25.1 Rare Earth Metals

Modern technologies, which have contributed a significant improvement to human life including consumer electronics, energy, automobiles, and defense resources, largely rely on the use of rare earth elements. This critical commodity including the 15 lanthanides, yttrium, and scandium are relatively abundant in the earth's crust but limited minable concentrations. The largest of these reserves can be found in China; however, due to drastic extraction, these reserves have decreased significantly over the years, and China has suffered ecological destruction (Huang et al. 2019; Smith et al. 2019).

I. K. Danso

National Centre for Efficacy Evaluation of Respiratory Disease Products, Korea Institute of Toxicology, Jeongeup, Republic of Korea

Department of Human and Environmental Toxicology, Korea University of Science and Technology (UST), Daejeon, Republic of Korea

A. B. Cueva-Sola · J.-Y. Lee · R. K. Jyothi (✉)

Convergence Research Center for Development of Mineral Resources (DMR), Korea Institute of Geoscience and Mineral Resources (KIGAM), Daejeon, Republic of Korea

Resources Recycling, Korea University of Science and Technology (UST), Daejeon, Republic of Korea

e-mail: rkumarphd@kigam.re.kr

Z. Masaud

Fuel Cell Research Center, Korea Institute of Energy Research (KIER), Daejeon, Republic of Korea

Department of Advanced Energy and System Engineering, Korea University of Science and Technology (UST), Daejeon, Republic of Korea

25.1.1 Applications of REEs

Rare earth metals are utilized in a wide range of modern-day products such as liquid crystal display (LCD) and light-emitting diode (LED) electronic screens, battery alloys, hybrid automobiles, medical devices, and some military-grade weaponry and communication systems. Together with the quest for clean energy, REEs have a vital part to play, now and in the years to come, hence an upsurge in the demand for these elements (Zhou et al. 2017). Figure 25.1 shows the global distribution of REE end-use for the year 2019. It depicts that 75% of the global distribution of REE goes in the form of catalysts for use in major industries such as petroleum refineries, automotive industry, and water treatment plants. Some of the various applications in which they are used are shown in Table 25.1.

25.1.2 The Demand for REEs

REEs are abundant primarily in monazite and bastnaesite ore, and it is reported that China and the United States sit on the largest percentage of economic bastnaesite deposits. Although declining steadily in the last few years, China still commands a stronghold in the global production and reserves (Fig. 25.2) of rare earth metals shown in the bar graphs of Fig. 25.3a, b. Out of the 210,000 tons of REEs mined in the year 2019, China produced 132,000 tons, accounting for about 62.8% of global production (U.S. Geological Survey 2020). An estimated percentage of 20% of legal production is also alleged to be produced illegally (Liu 2016).

Fig. 25.1 Estimated global distribution of REE end-use, 2019 (Data source: U.S. Geological Survey 2020)

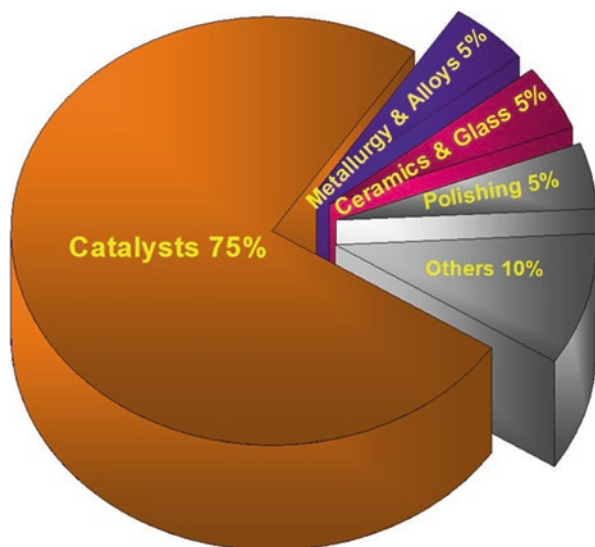
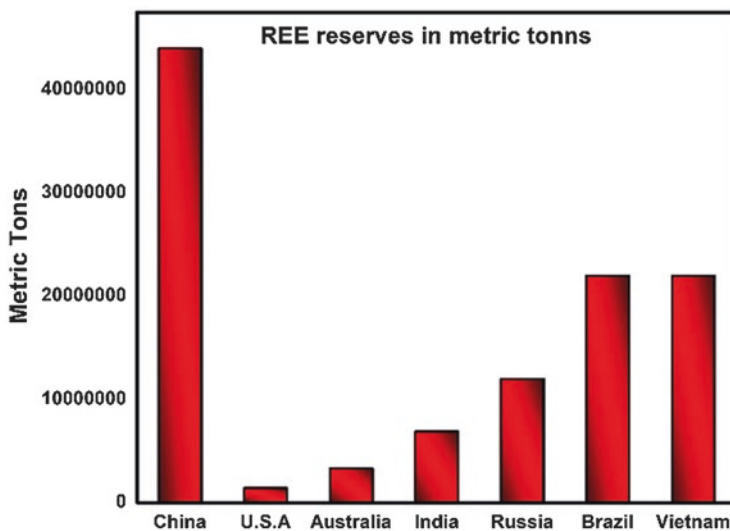


Table 25.1 The REE elements used in various sectors (Data source: Dutta et al. 2016)

Field	REE	Applications
Catalysts	La, Ce, Pr, and Nd	<ul style="list-style-type: none"> • Petroleum refinery • Automotive industry • Diesel additive • Water treatment
Polishing	Ce	<ul style="list-style-type: none"> • Polishing powders for cleaning glass, mirrors, and windshields.
Metallurgy and alloys	La, Ce, Pr, Nd, V, and Sm	<ul style="list-style-type: none"> • Batteries • Superalloys • Steel sector
Ceramic and glass	La, Ce, Pr, Nd, Gd, Er, Eu, and Ho	<ul style="list-style-type: none"> • Colorants • Fuel cells • Capacitors • Sensors • UV resistant glass • Thermal glass • Semi-conductors
Others		<ul style="list-style-type: none"> • Fertilizers • Medical tracers • Baseball bats • Lasers

**Fig. 25.2** REE reserves by country in metric tons (Data source: U.S. Geological Survey 2020)

The high global demand for REEs, accompanied by the monopoly of China, puts them in a high position in dictating the market for REEs, such that the recent export restrictions in 2010/2011 resulted in a global supply deficit (Mancheri et al. 2019). Before this era, China had minimal success in controlling the power and profits that

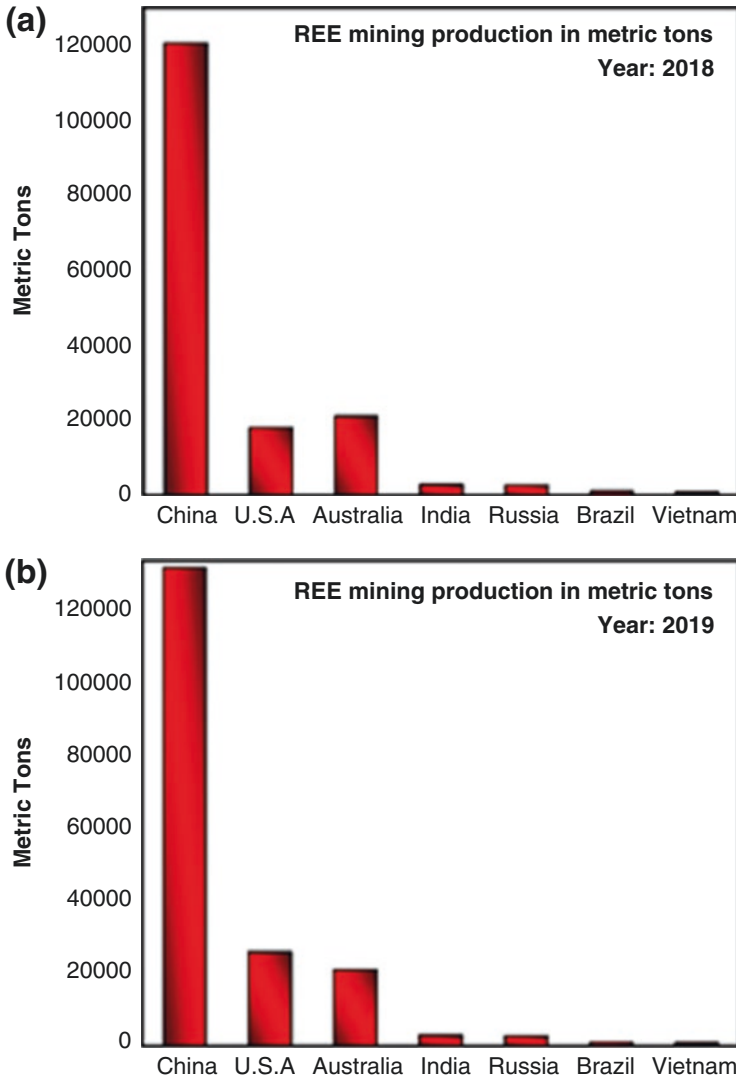


Fig. 25.3 REE mining production by country in (a) 2018 and (b) 2019 (Data source: U.S. Geological Survey 2020)

came with such a monopoly as large quantities of these rare earth products were exported, resulting in manipulative measures by importers to force down the prices (Hurst 2010; Cueva Sola et al. 2020).

Over the last few years, China has implemented certain policies to restrict the quota of REEs for export, and these policies have grown stringent over time. These policies were necessary as an attempt to conserve natural resources, to curb the environmental hazards that accompany the production of these REEs, and to

restructure the industry (Wübbeke 2013). However, the scarcity influenced the price and the market power in favor of China to a great extent (Mancheri et al. 2019). The global value of products that utilize REEs is estimated to be approximately 1.5–2 trillion dollars, representing almost 5% of the global Gross National Product. The economic impact from these restriction policies was therefore a big blow to the rest of the world. Consequently, as the availability of REEs is marred by this monopoly and restrictions, the global vision of transitioning into clean energy as well as the production of modern technology products is hampered (Tukker 2014).

There is an imminent risk of scarcity when the demand for REEs is perceived from an elemental point. Demand statistics have projected REEs usually in a collective way, and this approach fails to take into account that certain REEs are more critical in this era of clean energy technology than others. Dysprosium, terbium, yttrium, europium, and neodymium are projected to be the five vulnerable market elements (Dutta et al. 2016).

Because of limited supply, coupled with increasing demand and an attempt to break the issues of monopoly, the appraisal for alternative sources has come up with both private and public institutions. Researchers are already looking into the potential of coal fly ash, marine brines, and other waste residues, and coal-related materials have been discerned as a promising source (Zhang et al. 2020).

25.2 Coal Combustion Products (CCPs)

Recent scientific studies have been centered on the plausible uses of natural resources as knowledge of their detriments on biological and environmental systems widen, leading to a host of environmental protection reforms. The era of the industrial revolution thrived on the iron and a very important invention, the steam engine. As the utilization of these elements increased, it was accompanied by a symbiotic rise in the demand for coal (Wilde 2020).

Over the years, coal evolved into the world's most utilized energy source, especially in the generation of electricity (Munawer 2018). This generation of energy involves the combustion of coal in power plants, thereby producing what has generally been referred to as coal combustion products (CCPs), literally, coal combustion wastes or by-products (CCWs or CCBs, respectively). Collectively, residues of CCPs include fly ash, bottom ash, boiler slag, and flue gas desulfurization materials depending on the mineral composition of the coal and the combustion process utilized (Miller 2017).

China, currently holding the fourth largest coal reserves after the United States, Russia, and Australia, has been by far the largest producer as well as the largest consumer of coal worldwide. In the year 2019, China produced 1.8 billion metric tons representing 47.6% of the 3.9 billion tons of global coal production, and consumed 1.9 billion tons representing 51.7% of global coal consumption (Looney 2020). As a result, China produces the highest amount of CCPs. The first global statistical data on CCPs approximated a production of 780 million metric tons in

2010. In the said year, China produced 395 million metric tons, representing more than half of the global production. The United States was next in line with approximately 118 million metric tons (Heidrich et al. 2013). However, in 2017, this data was updated from 780 million metric tons to approximately 1.1 billion metric tons. In 2016, the global production of CCPs stood at approximately 1.2 billion metric tons with China ranking as the major producer and India, Europe, and the United States following in that order (Harris et al. 2019). As coal remains a dominant commodity in the energy industry, so shall the production of CCPs.

25.2.1 Adverse Effects of CCPs

Economically, coal was and still is a very beneficial commodity, yet its adverse effects on the environment are detrimental as coal combustion releases a series of gaseous components that pollute the atmosphere (Gasparotto and Da Boit Martinello 2020). Coal combustion emits CO_x , NO_x , and SO_x , gases with xenobiotic effects ranging from skin disorders to respiratory, blood, cardiovascular diseases, and some cancers. Carbon dioxide is vital to the livelihood of living organisms; however, an increased concentration in the atmosphere results in negative impacts on climate change. Carbon monoxide indirectly influences global warming by inhibiting the cleansing of other major greenhouse gases such as methane while also playing a vital role in lower atmosphere ozone formation (Munawer 2018). Acute exposure to increased atmospheric concentrations of carbon dioxide leads to adverse effects on health such as inflammations and low cognitive performance while chronic exposures may lead to oxidative stress, bone demineralization, and kidney calcification (Jacobson et al. 2019). Carbon monoxide poisoning, a condition that involves the binding of carbon monoxide to blood hemoglobin, is estimated to affect about 50,000 people a year in the United States. Recent studies have linked CO poisoning to profound cardiovascular effects and neurological trauma (Rose et al. 2017).

Oxides of sulfur from coal combustion affect ambient air and cause land and water pollution as well. Inhalation of SO_2 leads to cardiopulmonary impairments that could result in premature death. Atmospheric sulfur and nitrogen oxides could also form sulfuric acid and nitric acid, which affect the acidity of rainwater, leading to what is termed acid rains. These rains cause skin irritations and destroy statues and buildings. Acid rains are also known to have adverse effects on soil nutrients required for plant growth and in the process renders the soil and aquatic systems non-habitable for living organisms (Munawer 2018).

Coal combustion emissions of fly ash also play a major role in the environmental issue of particulate matter. Exposure to fine particulate matter ($\text{PM}_{2.5}$) could lead to cancer in the lungs and other severe cardiovascular injuries that could also result in early loss of life (Lin et al. 2019). Recent studies also showed that the synergistic impact of being co-exposed to SO_2 and $\text{PM}_{2.5}$ could lead to neurodegeneration (Ku et al. 2017).

25.2.2 *Components of Coal Combustion Products*

The coal combustion results in various types of products as waste materials (Zhang 2014) which are given as follows:

- *Fly Ash*: It can be found in the chimneys of the coal-fired power plants, which are typically fired at the range of 1100–1400 °C. They are basically ferroaluminosilicates with very fine particle size.
- *Boiler Slag*: The boiler slag is the viscous liquid-like substance formed as a result of the interaction of the molten slag with the water at a low temperature, respectively. This interaction causes the formation of a hard, black slag with a smooth and glassy appearance known as the boiler slag.
- *Bottom Ash*: These waste products of coal manufacturing are typically the particles that are too big to be carried by the flue gas and can be found on the furnace walls or the ash hoppers, which are located at the bottom of the furnace. The bottom ash is basically the agglomerated ash particles, which have a coarse particle size and can be found as a dry product on the walls or in the slurry form at the furnace bottom.
- *Others*: The other products of the coal combustion waste include fluidized bed combustion (FBC) ash, flue gas desulfurization (FGD) gypsum, spray dry absorption (SDA) FGD products, etc.

25.2.3 *Beneficial Use of CCPs*

Due to the dangers associated with the exposure of coal combustion products, their disposal in landfills has been an issue of environmental concern and has over the last few decades, seen advocacies and implementation of policies that support the agenda of recycling their use, coining the term “beneficial use.” By reusing CCPs, land and energy are saved, the cost of disposal is reduced, the environmental and biological exposure risk of harmful emissions is curbed, and the regulatory workload is reduced (Li et al. 2018). The quest for maximized power generation accompanied by the removal of uncontrolled air pollution emissions led to the development of the pulverized coal-fired power plant (Kitto 1996). This system increased the availability of CCPs, of which fly ash became the most abundant, propelling the need for its utilization (Chou 2012). The physical and chemical properties of fly ash make it a very important material in the construction industry. Fly ash has become a major component in making concrete products such as bridges, dams, roads, and buildings and has proven to be a potential alternative to ordinary portland cement in an attempt to reduce greenhouse gas emissions (Xu and Shi 2018). Other benefits of CCPs include the construction of concrete blocks and structural fills from bottom ash, the extensive use of synthetic gypsum from flue gas desulfurization, roofing granules and blasting grits from boiler slags, and the use of cenospheres as fillers in paints, plastics, and concrete (American Coal Ash Association 2017). In the United

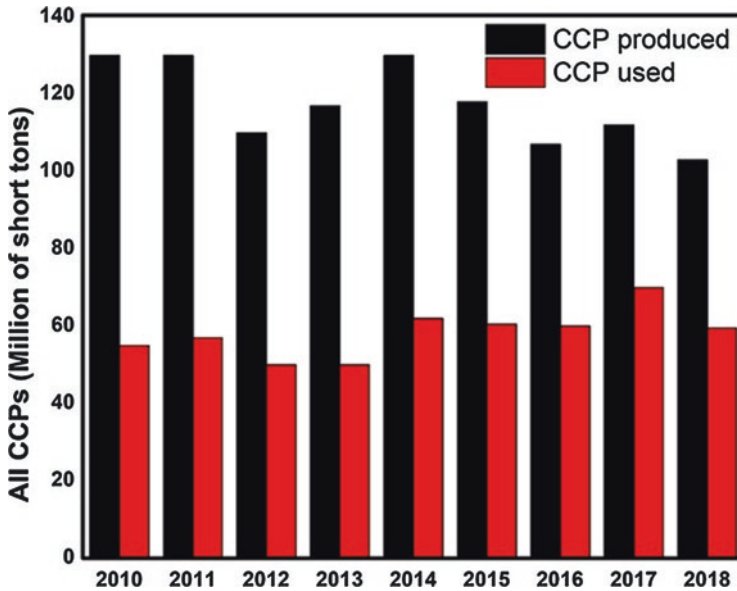


Fig. 25.4 CCPs produced and used in the USA over the year 2010–2018 (Data source: American Coal Ash Association 2019)

States, it was estimated by the Production and Use Survey conducted by the American Coal Ash Association that about 102.3 million tons of CCPs were produced in 2018, out of which, 59.4 million tons were put to beneficial use (Adams 2019). Moreover, the CCPs produced and used over this decade are shown in Fig. 25.4 (American Coal Ash Association 2019).

Among the applications of CCPs, the most exciting to this scope of the study is the knowledge that these ashes are enriched with a high level of rare earth metals, and there is a suggestion of possible extraction, although not easily exploitable (Taggart et al. 2016).

25.2.4 CCPs as Rare Earth Element Source

A few decades ago, the existence of REE-rich coal deposits was discovered, mostly in the Cenozoic weakly metamorphosed coal, in Far Eastern Russian basins. They came in beds ranging from a thickness of about 0.3–10.5 m and contained 0.2–0.3% REEs in concentrations of up to 1000 ppm. Not long after this discovery, similar samples were found to contain about 1% REE content, and subsequent discoveries were made in other parts of the world with contents as high as 4–11% (Seredin 1996; Seredin et al. 2009).

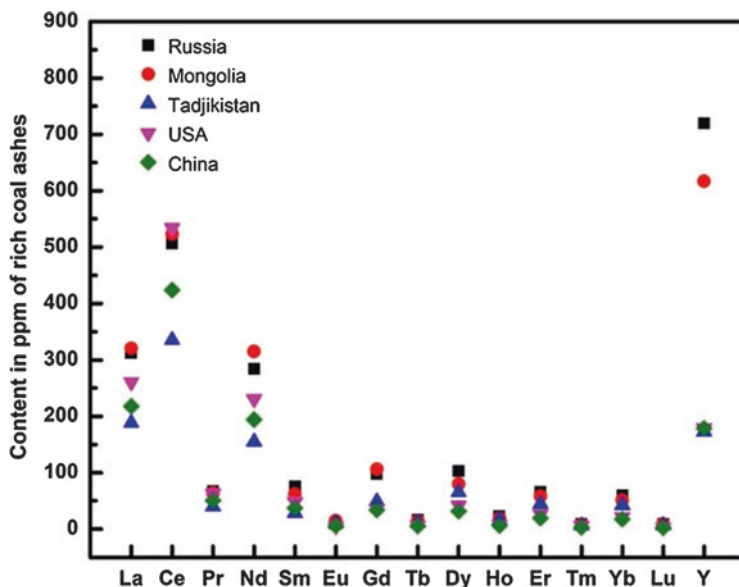


Fig. 25.5 Amount of rare earth element contents found in rich ashes across different countries (Data source: Seredin and Dai 2012; Taggart et al. 2016)

Recent studies have established new trends in the rare earth element content of coal combustion fly ashes from different locations. Results however suggested trends in accordance with geographical source. The statistical evaluations revealed that critical REE (Nd, Eu, Tb, Dy, Y, and Er) content of CCPs in the United States ranged from 28.5% to 41.0%. CCPs from Poland had a content of 35.6–36.1% REEs, the U.K. had 33.4–35.8% critical REE content CCPs. Chinese coal ash had 16.8–41.2%, Russia 31.5–63.2%, and Mongolia 48.6% (Taggart et al. 2016).

CCP samples from Jiangxi, Guizhou, and a power plant, all in China were assessed for their respective REE contents. The distribution of light REEs and heavy REEs revealed a similar trend in all three regions. The contents were dominated by Ce and La, while Y and Nd followed in that order. In Guizhou for instance, the overall content of REEs from CCP was 1350 mg/kg, out of which 487.25 mg/kg consisted of Ce (Huang et al. 2019).

The CCPs are an important source of rare earth elements. As discussed earlier, an immense amount of the CCPs is being produced daily across the various nations. These CCPs can be utilized as an effective source for the REE (Taggart et al. 2016). Moreover, in Fig. 25.5 the content of the various REE in the rich coal ashes found in various countries has been discussed. This graph is produced from the data given by Seredin et al. (Seredin and Dai 2012). It is evident from the analysis of the data at hand that REE such as Y, Ce, and La are present in a high quantity as compared to the other elements in the coal ashes regardless of the area. However, the coal ashes obtained in Russia are richer in REE as compared to any other country. The

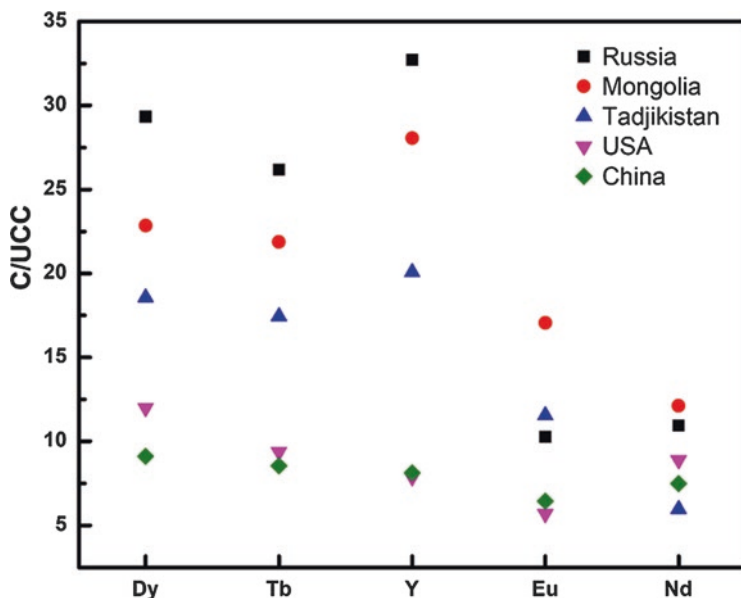


Fig. 25.6 C/UCC values calculated for critical REEs across various countries (Data source: Seredin and Dai 2012)

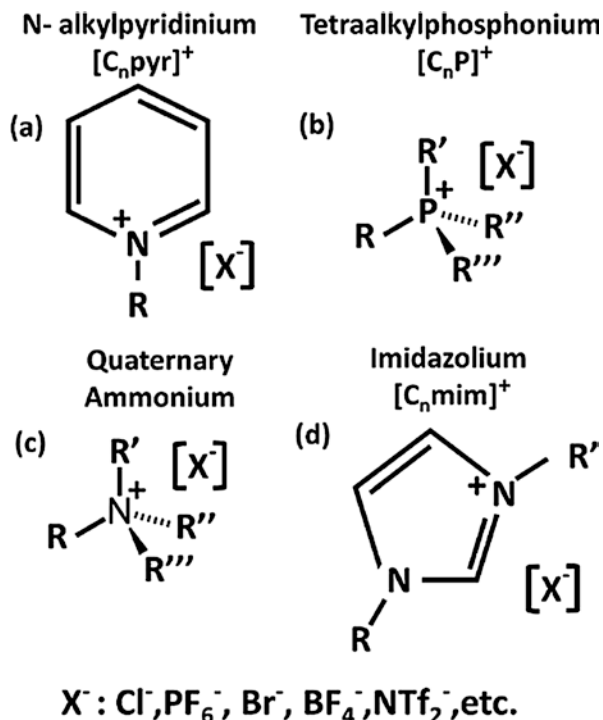
presence of critical REE elements such as Dy, Te, and Y is also notable in the data below.

However, to check whether an element is feasible for extraction for a certain source, the content it contains in the source (coal ash in this case) is compared with the content (in ppm) in the upper continental crust (UCC) (Rudnick and Gao 2003). This data is shown in Fig. 25.6, where the C/UCC values are calculated from the data provided by Seredin et al. (Seredin and Dai 2012). This data is plotted for the critical REEs. It can be seen that the U/UCC ratio in all the critical elements lies above five times, which shows the high concentration of the REE present in the coal ash. Considering USA as an example in Fig. 25.4, the country produced more than 100 million tons of CCP annually according to the latest data. From Fig. 25.6, it is also evident that the C/UCC values for critical elements including Dy, Tb, Y, Eu, and Nd are 12, 9, 8, 5.6, and 9 times respectively, which shows a higher concentration in the coal ash than in the upper continental crust. Thus, the extraction of REE from coal ash would be more feasible than mining from the UCC or primary ores.

25.3 Ionic Liquids and their Role in Metal Extraction

From a historical point of view, ionic liquids are not a new or a “green concept”; they have been studied since the nineteenth century by various chemists under the term “low-temperature molten salts.” Ionic liquids, as we know them currently, are salts having a melting point lower than the water boiling point; in addition, one of

Fig. 25.7 Main ILs used for metal extraction (IL structures are adapted from Renner 2001; Wilkes 2002; Davis 2004; Dietz 2006)



the most important characteristics of ionic liquids is their vast liquid range, which is the range between the freezing point and the boiling point of a liquid, that property gives ionic liquids the capacity to replace organic solvents due to their small to nearly not-volatility (Wilkes 2002). Ionic liquids are usually made of the combination of a large organic cation with a much smaller—usually inorganic—anion, giving them an almost infinite possibility of customization based on the purpose of their use, similarly to organic solvents they are able to dissolve a variety of organic compounds such as oils, plastics, inks, metals, among others while having an almost negligible vapor pressure, making them easily recyclable and reusable (Renner 2001).

Due to their vast uses and their recyclability, ionic liquids have found niche in among various applications including metal extraction, where most of the research done for the use of these compounds have been studied for a small group of molecules containing principally the cations shown in Fig. 25.7. Those cations, N-alkylpyridinium, tetraalkyl phosphonium, quaternary ammonium, and imidazolium, could be modified becoming a more bulky organic molecule changing the properties of the whole IL with a combination of a variety of anions (Davis 2004).

As mentioned above, the viscosity and melting point of the ionic liquid vary depending on the size of the cation, which usually contains alkyl substituents ranging from C2 to C8 in the different cations shown in Fig. 25.7. On the other hand, the anion usually forms a complex with the metal present in the aqueous phase controlling several important parameters such as reactivity, solubility, and speciation of the metal (Abbott et al. 2011).

Hydrometallurgy and specifically solvent extraction has been and will continue being the most used technology to recycle, recover, and separate rare earth metals. The main advantages the technique offer are the possibility to operate the system continuously, the simplicity of the equipment and process, the small amounts of extractant used and the possibility of its recycling and reusing, and the ability to treat large affluent in industrial scale. In addition, liquid–liquid extraction provides a great flexibility to tailor to different processes, metals, and systems having the advantage of working with a variety of organic compounds and in a wide pH range (Huddleston et al. 1998). However, the use of water immiscible extractants, most of which are volatile, toxic, flammable, etc. which should be disposed accordingly to the current strict regulations rising the cost of the whole production line and raising interest in the replacement of them for greener or less toxic options (Dietz 2006). Although ionic liquids offer a great variety of advantages over traditional extractants, it is not possible yet to ensure that they are a more environmental friendly alternative (Abbott et al. 2011).

25.3.1 Extraction of REEs by Ionic Liquids

The liquid–liquid extraction process consists basically in the contact of a large volume of aqueous affluent containing the REEs in a low concentration with an small volume of an immiscible organic phase creating a complex molecule with either the extractant or the ionic liquid—anions, cations, or both—which will transfer the metal ion into the organic phase. After the process the metal must be liberated again in an aqueous phase by the stripping process for further recovery (Habashi 1997, 2005). There are two main roles in which ionic liquids participate in the extraction process: the extraction of REEs using nonfunctional IL and the extraction of REEs using functional ionic liquids.

25.3.1.1 Nonfunctional Ionic Liquids for REE Recovery

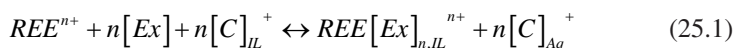
The first use that ionic liquids had in the extraction industry was in the substitution of noxious diluents such as benzene and toluene in the organic phase for the solvation of viscous liquids (Chauhan et al. 2018). When the term nonfunctional ionic liquid is used, the concept is based in that either the cation, anion, or both components of the IL do not show a coordinating (chelating) property with the rare earth counterparts present in the aqueous phase. There have been studies where both anion and cations do not contribute in the mass transfer of the metal into the organic phase; however, these tend to be scarce since REEs tend to stay in the aqueous phase due to the poor solubility of the metals in the IL (Wang et al. 2017). Thus, the use of nonfunctional ionic liquids alongside a proved extractant for the recovery of the rare earth elements has been vastly studied. In those systems, the ionic liquid cation or anion will be part of the extraction mechanism of the metal in either cation or anion

exchange mechanisms where either of the ions transfer into the aqueous phase allowing the formation of the complex between the extractant and the desired metal in the organic phase. However, the loss of any functional group in the ionic liquid into the aqueous phase is highly undesirable, hence it is necessary to choose the optimum extractant/nonfunctional IL to minimize the loss of ions during the extraction process.

Nakashima et al. showed that the use of Octyl(phenyl)-N,N-diisobutylcarbamoylmethylphosphine oxide (CMPO) as a extractant dissolved in 1-butyl-3-methyl-imidazolium hexafluorophosphate ([C4mim][PF6]) improved the selectivity of REEs and decreased greatly the concentration of CMPO necessary for the optimum extraction from 50 mmol/L to 3 mmol/L compared to the system CMPO dissolved in traditional solvents. Additionally, by using [C4mim][PF6], effective extraction can be achieved in deionized water without the necessity of the NO₃⁻ anions in the aqueous phase, improving the pH conditions of the system (Nakashima et al. 2003). The same group also studied the mechanism of the reaction and concluded that the effect of the anionic site of the IL can alter the extraction results of the process, so when using [C4mim][PF6] the extractability of the REEs was lower than when using [C4mim][Tf2N], this phenomena can be due to the effect of the anionic components on the hydrogen bonds existent in ionic liquids (Nakashima et al. 2005).

Another study showed that not only anions affected the extraction capacity of REEs. In the case of Nd³⁺ extraction with Cyanex 923 dissolved in small cations such as [C4mim][Tf2N] and [N1444][Tf2N] compared to ILs containing larger, more hydrophobic cations such as [C10mim][Tf2N], [P66614][Tf2N], or [N1888][Tf2N], the extraction efficiency decreased as the bulky hydrophobic cations tend to suppress the cation exchange mechanism necessary for the effective extraction (Rout and Binnemans 2014).

In general, several published works lead to the conclusion that the most common mechanism of REEs extraction with a neutral extractant dissolved in a nonfunctional ionic liquid is usually a cationic exchange in the form of the Eq. (25.1) below, where REE represents the rare earth metal, Ex the extractant, and C the cation side of the ionic liquid (Wang et al. 2017).

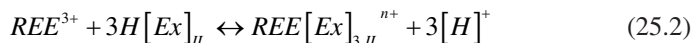


As observed in the mechanism, during the extraction process there is a loss of the cationic component of the IL to the aqueous phase, which limits the recycling and reuse of ionic liquids hindering their future applications for industrial processes.

On the other hand, anion exchange mechanisms tend to be scarcer due to the lack of published work about these topics; however, a conclusion cannot be drawn that this type of mechanism is less frequent in REE extraction with a traditional extractant dissolved in an IL. Jensen et al. presented the first study where 2-thenoyltrifluoroacetone (Htta) was used in the selective extraction of Nd³⁺ and Eu³⁺ dissolved in [C4mim][Tf2N]. The presence of the ionic liquid accelerated the formation of anionic complexes such as REE(tta)₄⁻ in contrast to previous report

where usually cationic species are formed in the extraction process. $\text{REE}(\text{tta})_4^-$ will become part of the IL forming the $[\text{REE}(\text{tta})_4]^- [\text{C4mim}]^+$ complex (Jensen et al. 2003). The main drawback of the process is that in order to recover the REE the ionic liquid will be destroyed, hindering the probabilities of the industrial application of the method as a cost-efficient, environmental friendly mechanism. Some solutions have been shown to reduce the affinity of the IL with the metal, specially using large anions in the ionic liquid, such as $[\text{NfO}]$ which shifts the mechanism from anion exchange to cation exchange, reducing the destruction of the ionic liquid. However, the extraction efficiency and selectivity of both systems was not compared making conclusions impossible to be drawn to which system is the best (Wang et al. 2017).

Neutral mechanisms for the extraction of REEs when the extractant is dissolved in a nonfunctional ionic liquid is the most desired mechanism with a promising opportunity of industrial applications. To guarantee the neutral mechanism, acidic extractants such as PC88A and DEPHA have been used to extract a wide variety of REE. The major drawback of the use of those extractants is their low solubility not only in low chain (more hydrophilic) ILs but also in the long chain ionic liquids; the lower solubility renders a smaller extraction efficiency compared to the traditional approach where the extractant is dissolved in an organic volatile solvent (Wang et al. 2017). The neutral mechanism of extraction with IL is the same as the one for traditional solvent extraction processes where REE represents the rare earth metal and Ex is the acidic extractant.



25.3.1.2 Functional Ionic Liquids for REE Recovery

One of the greatest features of ionic liquids is their diversity and the capacity to modify anions or cations for specific tasks. The ionic liquids synthesized with functional moieties are called either task-specific IL (Davis 2004) or functional ionic liquids. In the case of liquid–liquid extraction, ionic liquids are modified to act as both a solvent and an extractant; if both moieties have a specific role, then the IL is called a bifunctional IL, otherwise it would be a monofunctional IL.

As previously mentioned (Nakashima et al. 2005), CMPO is one of the best phosphorous-based extractants for REEs, thus there has been some studies where monofunctional ILs were synthesized using CMPO cations with $[\text{PF}_6^-]$ and $[\text{Tf}_2\text{N}^-]$ as anions to extract several rare earth compounds. When working with functionalized IL, the problem of getting the IL destroyed by losing the anions or cations to the aqueous phase is solved; however, ionic liquids tend to have a very high viscosity, which reduces the mass transfer between phases and inhibits the metal dissolution in the organic phase. Consequently, the distribution ratios for the extraction of rare earths in functionalized ILs was smaller than the results reported previously while using ILs as solvents for REEs extraction using CMPO. Using ILs as solvents

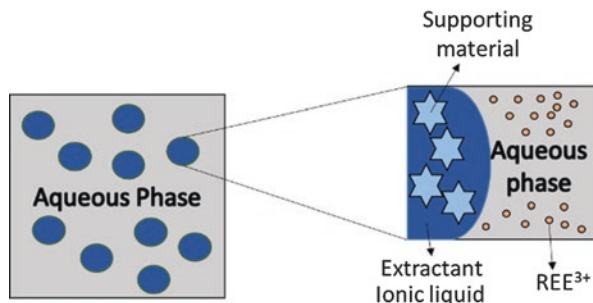
of task-specific ILs might be one solution to tackle the low mass transfer due to the high viscosity of the CMPO functional ILs (Mohapatra et al. 2013).

Another proven extractant for REEs is DEPHA, three different ionic liquids were prepared to understand the extraction mechanism of Nd^{3+} by these functional ILs (Rout et al. 2013). Compared with the extraction of Nd using DEPHA as extractant dissolved in nonfunctional ionic liquids, it was concluded that the extraction mechanism of $[\text{C}_6\text{mim}][\text{DEHP}]/[\text{N}_{1444}][\text{Tf}_2\text{N}]$ involves both the anion and cation of the functional ionic liquid, avoiding the disintegration of the molecule to the aqueous phase, and the distribution ratios are around 1000 at optimum conditions. In addition, it was observed that heavier REEs were effectively extracted while light rare earths such as lanthanum, cerium, and praseodymium were not (Rout et al. 2011). Based on those findings, DEPHA-based ionic liquids can be used for the separation of light and heavy rare earths and for the recovery of neodymium-rich secondary sources such as permanent Nd-Fe-B magnets.

The use of carboxyl groups as cations in the rare earth extraction by functional ILs was other broadly studied area. Betainium bis(trifluoromethyl-sulfonyl)imide, $[\text{Hbet}][\text{Tf}_2\text{N}]$ was synthesized to extract REEs among other metals, due to its interesting solubility behavior in water based on temperature (Mehdi et al. 2010). At the beginning of the extraction process, the temperature would be kept at 80°C forming only one phase where Fe can be extracted from previously roasted and grinded permanent magnet while REEs and Co stay in the aqueous phase when the temperature is reduced. Next, REEs and Co salts are precipitated using oxalic acid and then separated by selective leaching with ammonium hydroxide. The whole process yielded a 99.9% purity REEs oxalate which can be used to manufacture permanent magnets again (Dupont and Binnemans 2015).

Even though liquid–liquid extraction is the primary method for recovering rare earth metals in the industry, there are some drawbacks that need to be addressed and improved. Solid–liquid extraction using an extractant immobilized material offers solutions to problems such as low selectivity, impurities in the final recovered product, reduced contact area between the extractant, and the desired metal and low extraction efficiency. Ionic liquids can be impregnated in a matrix improving the surface contact area and reducing the losses of ionic liquid—extractant—with the aqueous phase during multiple I-I contacts alongside improving the quality of the final product. Figure 25.8 shows the concept of EIM for ionic liquids supported in a

Fig. 25.8 Schematic of the EIM system for REE recovery (Hidayah and Abidin 2017)



matrix that can be developed using different materials such as membranes, polymer, silica, and bio-materials and modified accordingly to improve the chemical and mechanical properties of the system for the recovery of rare earths; most of the researchers have used proven ILs such as Aliquat 336, [Cnmim][PF6], Cyphos IL-105, and [Cnmim][NTf2] in the EIM system to compare their capability against the traditional liquid–liquid extraction system (Hidayah and Abidin 2017).

25.3.2 Extraction of REEs from Coal Combustion Products by Ionic Liquids

Due to the high level of rare earths in the different coal-related materials such as coal refuse, mine drainage, combustion by-products, and coal fly ash around the world, it is only natural to think that ionic liquid technology could be applied for the recovery of those metals (Taggart et al. 2016) without the burden of mining and the depletion of primary metal sources from an attractive source such as coal combustion products. Huang et al. used [Methyltrioctylammonium][sec-octylphenoxy acetate] ([N1888] [SOPAA]) and [trihexyl(tetradecyl)phosphonium][sec-octylphenoxy acetate] ([P6,6,6,14][SOPAA]) to recover rare earth elements from three different sources in China from concentrates leached by acid treatments: HNO₃, HCl, and HF + HNO₃. They discovered that the amount of rare earths was the maximum in the Guizhou coal combustion product having 1350 ppm of rare earths from where 37.4% was recovered. The REEs found in the samples were La, Ce, Nd, Gd, Y, Er, Tm, Yb, and Lu (Huang et al. 2019). However, there is not many studies where ionic liquids are applied to the recovery of those elements, the great majority of studies are based in the leaching of rare earths from CCPs having a high acid consumption and being very dependent on the sample used for the leaching process (Zhang et al. 2020). Currently, searching for compelling ionic liquids and different technologies to recover and separate rare earth metals from rich secondary sources such as coal by-products must be of interest for different researchers.

25.3.3 Stripping of Rare Earths from IL Phase

Table 25.2 shows a variety of stripping methods used to obtain the REEs from the loaded organic containing the ionic liquid–REE complex. Wang et al. used 0.03 mol/L of HCl to strip lanthanum from [tricaprylmethylammonium]-[sec-octylphenoxy acetate] and [tricaprylmethylammonium]-[secononylphenoxy acetate] obtaining more than 95% recovery with a minimum loss of the ionic liquids used for the extraction (Wang et al. 2011). Additionally, Rout et al. scrubbed the ionic liquid loaded organic with NaOH to further strip 100% of neodymium

Table 25.2 Stripping mechanisms for REE from IL loaded organic (Huang et al. 2017)

Ionic liquid (IL)	Metal	Stripping agent	Stripping efficiency	Recycling method	Reference
[N ₁₈₈₈][CA12], [N ₁₈₈₈][CA100]	La(III)	0.5 mol/L H ₂ SO ₄	>95%	No extraction efficiency loss	Wang et al. (2011)
[A336][DGA]	Nd(III)	0.02 mol/L HCl/0.5 mol/L HNO ₃	100%	NaOH scrubbing and 96.5% efficiency for extraction	Rout and Binnemans (2014)
[N ₁₈₈₈][SOPAA]	REE(III)	Water	79.38%	–	Chen et al. (2016a)
[A336][P507], [A336][P204]	REE(III)	0.3 mol/L HNO ₃	>95%	Almost no extraction efficiency loss	Guo et al. (2014)
[P ₆₆₆₁₄][R ₂ POO]	Ni(II), REEs	2 mol/L HNO ₃	100%	NH ₃ scrubbing, negligible loss of extraction efficiency	Rout et al. (2014)
[P ₆₆₆₁₄][SOPAA]	Y(III), Lu(III)	0.008 mol/L HCl	100%	–	Dong et al. (2017)
[Hbet][Tf ₂ N]	REEs, Co(II)	1.5 mol/L H ₂ C ₂ O ₄	>99%	To prevent IL loss → Na ₂ SO ₄ scrubbing	Chen et al. (2016b)
[Hbet][Tf ₂ N]	Y(III), Eu(III)	1 mol/L HCl, 1.5 mol/L H ₂ C ₂ O ₄	100%	–	Dupont and Binnemans (2015)

using 0.5 mol/L of HNO₃ from trioctylmethylammonium dioctyl diglycolamate in four stripping stages (Rout and Binnemans 2014). Moreover, different rare earth elements were stripped using water in four stripping stages from [tricaprylmethylammonium]-[bis-sec-octylphenoxy acetate] having an efficiency of 79.38% (Chen et al. 2016a). Likewise, 0.008 mol/L of HCl was used as the stripping agent to separate Y and Lu using [trihexyl (tetradecyl) phosphonium]-[sec-octylphenoxy acetate] with a 100% recovery of the ionic liquid on one stripping stage.

Also, Dupont et al. successfully separated Y and Eu using [Hbet][Tf₂N] bifunctional ionic liquid recovering it by stripping with 1 mol/L of HCl and 1.5 mol/L of H₂C₂O₄ obtaining 100% of recycling of the IL (Dupont and Binnemans 2015). Finally, Wang et al. proposes a very innovative stripping method to recover bifunctional ionic liquids used in the extraction of rare earth elements by using supercritical CO₂, a process that also improves mass transfer accelerating the extraction process (Wang et al. 2017). The proposed system is shown in Fig. 25.9.

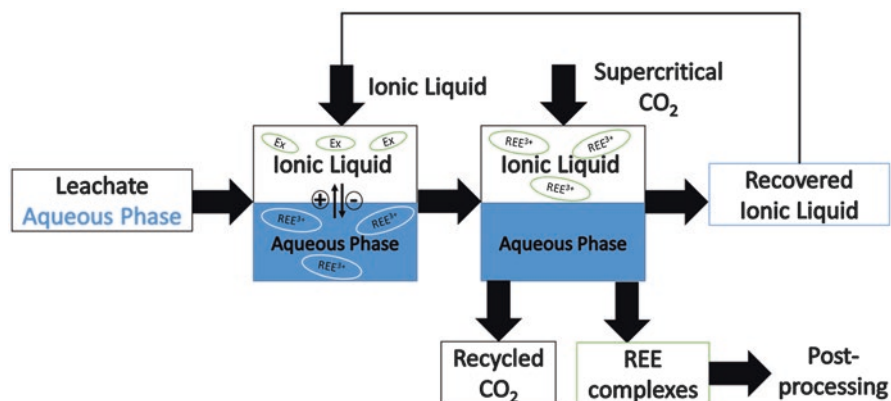


Fig. 25.9 Schematic of the extraction/stripping of REE using Sc-CO₂ to recycle and reuse bifunctional ionic liquids (Wang et al. 2017)

25.3.4 Challenges Surrounding Ionic Liquid Uses

There are some drawbacks surrounding the efficient and prolonged use of ionic liquids for rare earth metal recovery. The first issue that arises is the cost of ionic liquids themselves, according to Renner a pound of ionic liquids can cost up to 30,000 times the cost of a traditional solvent such as acetone or kerosene (Renner 2001). However, this problem can be improved while solving the second problem, the improvement of the recycling, and reuse of the ionic liquids, avoiding losses of the IL during the extraction process and leading to a cost-effective system in the long run. In addition, there is still a lot of research to be done in the development of greener processes to manufacture ionic liquids, which usually are synthesized using conventional solvents creating secondary waste (Dietz 2006). In addition, some ILs present a high viscosity, while some ILs could be slightly soluble in water, therefore the interaction and mechanism of these solvents with an aqueous phase and with the metals must be elucidated before scaling-up systems and use ionic liquids freely for liquid–liquid extraction (Abbott et al. 2011). The toxicity and environmental impact of ionic liquids and their derivatives have not yet been studied deeply, while the recyclability and reuse of the compounds for a long-term system are not yet proven in a medium-to-large scale. Several physicochemical and thermodynamics data for ILs and the mixture of them must be studied such as surface tension, solubility, viscosity, among others to understand and develop models to predict the behavior of new synthesized compounds (Dietz 2006).

25.4 Conclusion

The science of rare earth elements has become a very important topic in recent times due to their significant role in modern technological trends. China currently holds the largest production, consumption, as well as reserves of rare earth elements. As depletable natural resources, their supply is somewhat unassured to meet the projected rising future demands. The need to manage them properly while also curbing the environmental hazards that come with their mining led to the implementation of certain stringent measures by China. Although seen by many REE-dependent nations as manipulative tactics of monopoly, the significant global supply deficit that came with the restrictions raised concerns on the need to look to other plausible sources of REEs. Considering the conservation of the environment and the availability of the source materials, coal combustion products emerge as one of the most feasible options. Research has proven that coal ash is a REE-rich source and some available data by Seredin et al., projects that the extraction of REE from coal ash would be more feasible than mining from the UCC or primary ores, emphasizing Y, Ce, and La as present in a high quantities compared to other elements. Ionic liquids, considered “greener” options over traditional solvents and with a wide range of possibilities of tuneability, are one of the materials that are revolutionizing the solvent extraction field. As shown above, there has been different types of ionic liquids used for the recovery and separation of rare earth elements from secondary sources using nonfunctional, monofunctional, and bifunctional ionic liquids. However, the recovery of REEs from the by-products of coal combustion has not been vastly studied despite of it being a rich source of these technological crucial elements.

Acknowledgments This work was supported by the National Research Council of Science & Technology (NST) grant by the Korea government (MSIT) (No. CRC-15-06-KIGAM).

References

- Abbott, A. P., et al. (2011). Processing of metals and metal oxides using ionic liquids. *Green Chemistry*, 13(3), 471–481. <https://doi.org/10.1039/c0gc00716a>.
- Adams, T. H. (2019). Coal ash recycling rate declines amid shifting production and use patterns, 19 November, pp. 1–5. Available at: <https://www.prnewswire.com/news-releases/coal-ash-recycling-rate-declines-amid-shifting-production-and-use-patterns-300961238.html>
- American Coal Ash Association (2017). Beneficial use of coal combustion products, pp. 1–8.
- American Coal Ash Association (2019). *Coal combustion products production & use statistics, production & use reports*.
- Chauhan, G., et al. (2018). Novel technologies and conventional processes for recovery of metals from waste electrical and electronic equipment: Challenges & opportunities—A review. *Journal of Environmental Chemical Engineering*, 6(1), 1288–1304. <https://doi.org/10.1016/j.jece.2018.01.032>.
- Chen, J., et al. (2016a). Extraction behavior of bifunctional ionic liquid [N1888][SOPAA] and TBP for rare earth elements. *Journal of Rare Earths*, 34(12), 1252–1259. [https://doi.org/10.1016/S1002-0721\(16\)60161-8](https://doi.org/10.1016/S1002-0721(16)60161-8).

- Chen, L., et al. (2016b). Comprehensive appraisal and application of novel extraction system for heavy rare earth separation on the basis of coordination equilibrium effect. *Hydrometallurgy*, 165, 351–357. <https://doi.org/10.1016/j.hydromet.2015.12.007>.
- Chou, M.-I. M. (2012). Fly Ashfly ash. In R. A. Meyers (Ed.), *Encyclopedia of sustainability science and technology* (pp. 3820–3843). New York, NY: Springer New York. https://doi.org/10.1007/978-1-4419-0851-3_121.
- Cueva Sola, A. B., et al. (2020). Rare-earth metal recovery for green technologies, rare-earth metal recovery for green technologies. In R. K. Jyothi (Ed.). Cham: Springer International Publishing. <https://doi.org/10.1007/978-3-030-38106-6>.
- Davis, J. H. (2004). Task-specific ionic liquids., 33(9), 1072–1077. <https://doi.org/10.1246/cl.2004.1072>.
- Dietz, M. L. (2006). Ionic liquids as extraction solvents: Where do we stand? In *Separation science and technology* (pp. 2047–2063). Taylor & Francis Group. <https://doi.org/10.1080/01496390600743144>.
- Dong, Y., et al. (2017). A separation processing for industrial rare earth feed solution by phosphonium ionic liquid type saponification strategy. *Journal of Rare Earths*, 35(3), 290–299. [https://doi.org/10.1016/S1002-0721\(17\)60912-8](https://doi.org/10.1016/S1002-0721(17)60912-8).
- Dupont, D., & Binnemans, K. (2015). Recycling of rare earths from NdFeB magnets using a combined leaching/extraction system based on the acidity and thermomorphism of the ionic liquid [Hbet][Tf2N]. *Green Chemistry*, 17(4), 2150–2163. <https://doi.org/10.1039/c5gc00155b>.
- Dutta, T., et al. (2016). Global demand for rare earth resources and strategies for green mining. *Environmental Research*, 150, 182–190. <https://doi.org/10.1016/j.envres.2016.05.052>.
- Gasparotto, J., & Da Boit Martinello, K. (2020). Coal as an energy source and its impacts on human health. *Energy Geoscience*. <https://doi.org/10.1016/j.engeos.2020.07.003>.
- Guo, L., et al. (2014). Highly selective extraction and separation of rare earths(III) using bifunctional ionic liquid extractant. *ACS Sustainable Chemistry and Engineering*, 2(8), 1968–1975. <https://doi.org/10.1021/sc400541b>.
- Habashi, F. (1997). *Handbook of extractive metallurgy*. Wiley (Handbook of Extractive Metallurgy). from <https://books.google.co.kr/books?id=S6BlxwEACAAJ>.
- Habashi, F. (2005). A short history of hydrometallurgy. *Hydrometallurgy*, 79(1–2), 15–22. <https://doi.org/10.1016/j.hydromet.2004.01.008>.
- Harris, D., Heidrich, C. and Feuerborn, J. (2019). *Global Aspects on Coal Combustion products*. Available at: <https://www.coaltrans.com/insights/article/global-aspects-on-coal-combustion-products>
- Heidrich, C., Feuerborn, H. and Weir, A. (2013) ‘Coal Combustion Products : a Global Perspective’, in *2013 World of Coal Ash (WOCA) Conference*. Lexington. Available at: <http://www.flyash.info/2013/171-Heidrich-Plenary-2013.pdf>
- Hidayah, N. N., & Abidin, S. Z. (2017). The evolution of mineral processing in extraction of rare earth elements using solid-liquid extraction over liquid-liquid extraction: A review. *Minerals Engineering*, 112(March), 103–113. <https://doi.org/10.1016/j.mineng.2017.07.014>.
- Huang, C., et al. (2017). Efficient and sustainable regeneration of bifunctional ionic liquid for rare earth separation. *ACS Sustainable Chemistry and Engineering*, 5(4), 3471–3477. <https://doi.org/10.1021/acssuschemeng.7b00159>.
- Huang, C., et al. (2019). The recovery of rare earth elements from coal combustion products by ionic liquids. *Minerals Engineering*, 130(August 2018), 142–147. <https://doi.org/10.1016/j.mineng.2018.10.002>.
- Huddleston, J. G. et al. (1998). ‘Room temperature ionic liquids as novel media for “clean” liquid–liquid extraction’, *Chem. Commun.*, (16), pp. 1765–1766. <https://doi.org/10.1039/A803999B>.
- Hurst, C. (2010). ‘China ’ s Rare Earth Elements Industry’, *Institute for the Analysis of Global Security (IAGS)*, (March), p. 6.
- Jacobson, T. A., et al. (2019). Direct human health risks of increased atmospheric carbon dioxide. *Nature Sustainability*, 2(8), 691–701. <https://doi.org/10.1038/s41893-019-0323-1>.

- Jensen, M. P., et al. (2003). Mechanisms of metal ion transfer into room-temperature ionic liquids: The role of anion exchange. *Journal of the American Chemical Society*, 125(50), 15466–15473. <https://doi.org/10.1021/ja037577b>.
- Kitto, J. (1996). Developments in pulverized coal-fired boiler technology, *Missouri Valley Electric Association Engineering Conference*, (September), pp. 1–11.
- Ku, T., et al. (2017). Synergistic effects of particulate matter (PM_{2.5}) and sulfur dioxide (SO₂) on neurodegeneration via the microRNA-mediated regulation of tau phosphorylation. *Toxicology Research*, 6(1), 7–16. <https://doi.org/10.1039/c6tx00314a>.
- Li, J., et al. (2018). A review on the applications of coal combustion products in China. *International Geology Review*, 60(5–6), 671–716. <https://doi.org/10.1080/00206814.2017.1309997>.
- Lin, C. K., et al. (2019). A global perspective on coal-fired power plants and burden of lung cancer. *Environmental Health: A Global Access Science Source*, 18(1), 1–11. <https://doi.org/10.1186/s12940-019-0448-8>.
- Liu, H. (2016) RARE EARTHS : SHADES OF GREY—Can China Continue To Fuel Our Global Clean & Smart Future, pp. 1–63.
- Looney, B. (2020). ‘Statistical Review of World Energy’, Bp, 69, p. 66. Available at: <https://www.bp.com/content/dam/bp/business-sites/en/global/corporate/pdfs/energy-economics/statistical-review/bp-stats-review-2020-full-report.pdf>.
- Mancheri, N. A., et al. (2019). Effect of Chinese policies on rare earth supply chain resilience. *Resources, Conservation and Recycling*, 142, 101–112. <https://doi.org/10.1016/j.resconrec.2018.11.017>.
- Mehdi, H., et al. (2010). Hydrophobic ionic liquids with strongly coordinating anions. *Chemical Communications*, 46(2), 234–236. <https://doi.org/10.1039/b914977e>.
- Miller, B. G. (2017). The effect of coal usage on human health and the environment. *Clean Coal Engineering Technology*. <https://doi.org/10.1016/b978-0-12-811365-3.00003-x>.
- Mohapatra, P. K., et al. (2013). A novel CMPO-functionalized task specific ionic liquid: Synthesis, extraction and spectroscopic investigations of actinide and lanthanide complexes. *Dalton Transactions*, 42(13), 4343–4347. <https://doi.org/10.1039/c3dt32967d>.
- Munawer, M. E. (2018). Human health and environmental impacts of coal combustion and post-combustion wastes. *Journal of Sustainable Mining*, 17(2), 87–96. <https://doi.org/10.1016/j.jsm.2017.12.007>.
- Nakashima, K., et al. (2003). Ionic liquids as a novel solvent for lanthanide extraction. *Analytical Sciences*, 19(8), 1097–1098. <https://doi.org/10.2116/analsci.19.1097>.
- Nakashima, K., et al. (2005). Feasibility of ionic liquids as alternative separation media for industrial solvent extraction processes. *Industrial and Engineering Chemistry Research*, 44(12), 4368–4372. <https://doi.org/10.1021/ie049050t>.
- Renner, R. (2001). Ionic liquids: An industrial cleanup solution. *Environmental Science and Technology*. <https://doi.org/10.1021/es012505a>.
- Rose, J. J., et al. (2017). Carbon monoxide poisoning: Pathogenesis, management, and future directions of therapy. *American Journal of Respiratory and Critical Care Medicine*, 195(5), 596–606. <https://doi.org/10.1164/rccm.201606-1275CI>.
- Rout, A., & Binnemans, K. (2014). Solvent extraction of neodymium(III) by functionalized ionic liquid trioctylmethylammonium dioctyl diglycolamate in fluorine-free ionic liquid diluent. *Industrial and Engineering Chemistry Research*, 53(15), 6500–6508. <https://doi.org/10.1021/ie404340p>.
- Rout, A., et al. (2011). Room temperature ionic liquid diluent for the mutual separation of europium(III) from americium(III). *Separation and Purification Technology*, 81(2), 109–115. <https://doi.org/10.1016/j.seppur.2011.04.033>.
- Rout, A., et al. (2013). Liquid-liquid extraction of neodymium(III) by dialkylphosphate ionic liquids from acidic medium: The importance of the ionic liquid cation. *Physical Chemistry Chemical Physics*, 15(39), 16533–16541. <https://doi.org/10.1039/c3cp52218k>.

- Rout, A., Wellens, S. and Binnemans, K. (2014). Separation of rare earths and nickel by solvent extraction with two mutually immiscible ionic liquids. *RSC Advances*, 4(11), 5753–5758. <https://doi.org/10.1039/c3ra46261g>.
- Rudnick, R. L., & Gao, S. (2003). Composition of the continental crust. In *Treatise on geochemistry* (pp. 1–64). Elsevier. <https://doi.org/10.1016/B0-08-043751-6/03016-4>.
- Seredin, V. V. (1996). Rare earth element-bearing coals from the Russian Far East deposits. *International Journal of Coal Geology*, 30(1–2), 101–129. [https://doi.org/10.1016/0166-5162\(95\)00039-9](https://doi.org/10.1016/0166-5162(95)00039-9).
- Seredin, V. V., & Dai, S. (2012). Coal deposits as potential alternative sources for lanthanides and yttrium. *International Journal of Coal Geology*, 67–93. <https://doi.org/10.1016/j.coal.2011.11.001>.
- Seredin, V. V., et al. (2009). New data on the REY hydrothermal ores with extraordinarily high concentrations of rare earth elements. *Doklady Earth Sciences*, 425(2), 403–408. <https://doi.org/10.1134/s1028334x0903012x>.
- Smith, R. C., et al. (2019). Selective recovery of rare earth elements from coal fly ash leachates using liquid membrane processes. *Environmental Science and Technology*, 53(8), 4490–4499. <https://doi.org/10.1021/acs.est.9b00539>.
- Taggart, R. K., et al. (2016). Trends in the rare earth element content of U.S.-based coal combustion fly ashes. *Environmental Science and Technology*, 50(11), 5919–5926. <https://doi.org/10.1021/acs.est.6b00085>.
- Tukker, A. (2014). Rare earth elements supply restrictions: Market failures, not scarcity, hamper their current use in high-tech applications. *Environmental Science and Technology*. American Chemical Society, 9973–9974. <https://doi.org/10.1021/es503548f>.
- U.S. Geological Survey (2020). *Mineral commodity summaries 2020*, U.S Department OF The Interior, U.S Geological Survey.
- Wang, W., et al. (2011). Application of bifunctional ionic liquid extractants [A336][CA-12] and [A336][CA-100] to the lanthanum extraction and separation from rare earths in the chloride medium. *Industrial and Engineering Chemistry Research*, 50(12), 7534–7541. <https://doi.org/10.1021/ie2001633>.
- Wang, K., et al. (2017). Recovery of rare earth elements with ionic liquids. *Green Chemistry*, 19(19), 4469–4493. <https://doi.org/10.1039/C7GC02141K>.
- Wilde, R. (2020). *Coal Demand and the Industrial Revolution*, ThoughtCo. Available at: <https://www.thoughtco.com/coal-in-the-industrial-revolution-1221634> (Accessed: 30 November 2020).
- Wilkes, J. S. (2002). A short history of ionic liquids—From molten salts to neoteric solvents. *Green Chemistry*, 4(2), 73–80. <https://doi.org/10.1039/b110838g>.
- Wübbecke, J. (2013). Rare earth elements in China: Policies and narratives of reinventing an industry. *Resources Policy*, 38(3), 384–394. <https://doi.org/10.1016/j.resourpol.2013.05.005>.
- Xu, G. & Shi, X. (2018). Characteristics and applications of fly ash as a sustainable construction material: A state-of-the-art review. *Resources, Conservation and Recycling*, 136(August 2017), 95–109. <https://doi.org/10.1016/j.resconrec.2018.04.010>.
- Zhang, W., et al. (2020). A comprehensive review of rare earth elements recovery from coal-related materials. *Minerals*, 10(5), 451. <https://doi.org/10.3390/min10050451>.
- Zhang, X. (2014). *Management of coal combustion wastes*. Available at: <https://usea.org/publication/management-coal-combustion-wastes-ccc231>.
- Zhou, B., Li, Z., & Chen, C. (2017). Global potential of rare earth resources and rare earth demand from clean technologies. *Minerals*, 7(11). <https://doi.org/10.3390/min7110203>.

Index

A

- Accumulation mechanism, 561
- Acid-alkali leaching system, 345
- Acid dissolution process (ADP), 459
- Acid leaching, 327, 343, 355, 358, 582, 594, 613
- Acid mine drainages (AMD), 607
- Acid rains, 622
- Acidic leaching
 - CFBC, 419
 - efficiency, 419
 - glassy phase, 420
 - Illinois and Appalachian, 419
 - Panbei fly ash, 419
 - PC, 420
 - yields, 420
- Acidithiobacillus caldus*, 65
- Acidithiobacillus thiooxidans*, 63
- Acidobacillus ferrooxidans*, 582
- Acidophilic chemolithotrophic microbial community, 451
- Activated carbon (AC), 216
 - adsorption, 86, 218
 - advantage, 240
 - characteristics, 238
 - chemical activation, 241, 242
 - chemical composition, 88
 - coal-derived (*see* Coal-derived AC)
 - DPAC, 218
 - industrial dyes, 219
 - iron oxide, 217
 - microcrystallite layers, 87
 - micropores, 88
 - multi-graphitic layers, 87
 - non-graphitizing carbon, 87
 - organic pollutants, 217
 - physical activation, 241–243
 - physical and chemical treatment, 216
 - physicochemical activation, 243–245
 - precursors, 87
 - preparation conditions, 240
 - production, 240
 - properties, 234, 235
 - raw materials, 234
 - structure, 88, 216
 - surface complex groups, 89
 - synthesis, 240
 - 3D graphitic carbon, 87
 - thermal treatment, 216
- Activated carbons, 514
- Activated coal, 240
- Activating agent, 241
 - alkali metal reagents, 106
 - chemical activating agent, 105
 - CO₂-H₂O activation, 105
 - gaseous, 104
 - kinetic reaction, 104
 - KOH/NaOH atom, 105
 - micropore development, 105
 - micropore volume, 105
 - micropores, 106
- Additive, 41, 48, 54, 269, 274, 275
- Adsorbent materials, 218
- Adsorbents, 608
 - AC (*see* Activated carbon (AC))
 - adsorption capacity, 239
 - from agricultural waste, 257
 - Cr adsorption, 250
 - industrial waste-based, 258
 - low-cost, 256

- Adsorbents (*cont.*)
 - modification, 234
 - physical characteristics, 245
 - production, 258
 - silica, 234
 - synthesis, 257
 - waste-derived, 256
- Adsorption, 83, 215, 224–226
 - adsorbents, 85
 - adsorbents selection, 84
 - application, 84
 - mechanism, 238–240
 - metal, 85
 - metals from wastewater (*see* Wastewater)
 - organic compound, 84
 - performance, 259
 - properties, 233
 - properties and applications, 85
- Adsorption efficiency, 220
- Adsorption equilibrium, 143
- Adsorption isotherms models
 - carbofuran, 146, 155
 - Dubinin-Radushkevich isotherm model, 147
 - Freundlich isotherm, 146, 147
 - Langmuir isotherm model, 146, 155
 - Temkin isotherm model, 147
- Adsorption kinetics
 - carbofuran, 156
 - IPDM, 159
 - PFOM, 158
 - PSOM-I, 158
 - PSOM-II, 158
- Adsorption methods, 456
- Adsorption studies, 145
- Adsorption-based techniques, 456
- Adverse effects, CCP, 622
- Agitation conditions, 77
- Agricultural activities, 256
- Airborne radionuclides, 399
- Air lift reactor (ALR), 171
- Air-pulsated jigs, 16
- Alkali activation, 499
- Alkaline-activated acidic leaching
 - alkali leaching, 421, 422
 - roasting, 420–421
- Alkali-activated FA concrete, 500
- Alkali-activated materials (AAMs)
 - BA
 - mechanical properties, 502
 - particle size and fineness, 502
 - precursor material, 502
 - production, 502
 - SSA, 502
 - CaCO₃ precipitant, 501
 - durability characteristics, 501
 - FA
 - behavior, 500
 - BFS, 500
 - geopolymerization process, 500
 - one-part, 501
 - paste/mortars, 500
 - practical applications, 501
 - primary source material, 501
 - real-time application, 500
 - SF, 500
- Alkali concentration, 502
- Alkali leaching, 421, 422
- Alkaline fusion, 421
- Alkaline leaching, 595
- Alkaline reagents, 422
- Alkaline roasting-acid leaching
 - aluminosilicate, 420
 - fusion, 421
 - ICP analysis, 420
 - REE extraction, 420
 - temperature, 420
- Alumina, 237
- Aluminium, 587, 588
 - acid leaching system, 351–353
 - alkali desilication processes, 359
 - ammonium sulfate, 358
 - in CFA, 350
 - compounds, 357
 - extraction and separation, 354–355
 - fly ash, 351
 - leaching activity, 356
 - RM, 358
 - selective recovery
 - extraction processes, 359
 - sulfuric acid, 359
 - and silicon-bearing minerals, 357
 - sintering and calcination processes, 359
 - sodium salts, 358
 - traditional commercial aluminum process, 357
- Aluminosilicate, 421, 423, 501
- Aluminum matrix composite (AMC), 518
- Aluminum-making process, 410
- Ambient-cured FA geopolymer/AAM
 - development, 500
- Amelioration of soil, 542, 543
- American Coal Ash Association, 322
- American Concrete Institute (ACI), 500
- American society for testing and materials (ASTM), 340, 384, 491

- Amorphous aluminum–silicon matrix, 564
 Amorphous silicon, 564
 Anionic contaminants, 200
 Anthracite, 40, 90
 Anthropogenic activities, 205
 Application of biochar
 disadvantages, 548
 greenhouse gas emission, 546, 547
 limitations, 548
 waste management, 547, 548
 Aqueous extraction method, 50
 Arrhenius equation, 111, 112
 Arsenic (As), 234, 251, 253, 254, 295, 595
 Arsenic anions, 203
Arthrobacter nicotianae, 350
 Artificial fertilizers, 513
 Ash content, 4
 Ash-forming and sulphur-containing type, 14
 Ash utilization, building materials
 AAMs, 499–502
 applications, 505
 brick and paving materials, 502–505
 cement-based materials, 496–499
Aspergillus niger, 583
 ASTM classification, 3, 4, 491
 Atmospheric sulfur, 622
 Auger reactor, 538
 Autoclave leaching process, 356
- B**
- BA-based composite, 502
 BA-based geopolymer mortars, 502
 BA-cement-lime-based composite, 504
 Bacteria, 63
 BA-induced cementitious materials, 499
 BA-mortar mixture, 499
 Barapukira and Payra Thermal Power
 Plants, 390
 Barapukira power plant, 387
 Barapukuria thermal power plant (BTPP), 388
 Baum and Batac jigs, 16
 Belt press filters, 28
 Beneficiation, 4, 14, 16, 18, 20, 34
 Benzothiophene (BT), 64
 BET analysis, 144
 Bingham plastic equation, 54
 Bingham plastic fluids, 42, 43
 Bio-additive, 40, 49
 Biochar, 186, 189, 205
 amelioration of soil, 542, 543
 bioremediation, 542, 543
 carbon and nutrients, 533
 carbon balance, 534
 definition, 534
 elements, 545
 environmental impact, 541
 GHG gas emission reduction, 533
 LTC, 533
 multidisciplinary areas, 533
 N-fertilizer, 533
 organic material feedstock, 533
 physicochemical characteristics, 540, 541
 production, 533
 properties, 534
 soil, 534
 soil fertility, 544
 soil nutrient dynamics, 544, 546
 soil quality, 533
 soil treatment and runoff, 544
 sustainability, 541
 Biochar modifications, 198, 205
 Biochar nanocomposites, 186
 Biochar preparation
 biomass, 535
 conversion processes, 535
 gasification, 539
 hydrothermal carbonization, 539, 540
 pyrolysis (*see* Pyrolysis)
 Biochar production, 186
 dry torrefaction, 187
 HTC, 190
 magnetization, 192
 posttreatments, 191
 pyrolysis, 187
 Biochar technologies
 advantages, 181
 anionic adsorption, 202–203
 anions, 183
 biomass, 181, 183
 CO₂ adsorption, 193, 196
 CO₂ medium, 193
 combustible natural resources, 182
 contaminants, 183
 functional groups, 198
 KOH treatment, 200
 metal ions, 182
 metal/metal oxide doping, 196
 physicochemical characteristics, 188
 removal techniques, 183
 sustainable technologies, 181
 temperature, 193
 thermochemically, 194–195
 Biochar-assisted adsorption, 612
 Bio-charcoal, 534
 Bio-depyritization, 65, 176

- Bio-desulfurization, 165, 167
 - archaea bacteria, 167
 - conversion mechanisms, 168
 - Ferrobolus* and *Sulfolobus*, 167
 - microorganisms, 169
 - Pseudomonas* sp, 168
 - pyrites, 168
 - Bio-desulphurization
 - A. caldus*, 65
 - advantages, 66
 - application, 66
 - biphasic growth medium, 67
 - gravity and floatation methods, 66
 - gravity separation, 66
 - inorganic sulphur, 65
 - mass transfer process, 67
 - microbes, 66
 - organic sulphur, 65
 - pyritic sulphur removal, 65
 - Biodiesel production, 525, 526
 - Bio-economy, 547
 - Biohydrometallurgical treatment, CFA, 588
 - Bioleaching, 328, 451, 582, 583, 595
 - Biological extraction methods, 347
 - Biological pretreatment, 185
 - Biological sulphur removal, 60
 - Biomass, 183, 186
 - availability and lignocellulosic content, 183
 - biological pretreatment, 185
 - forestry and agricultural, 184
 - forestry and pulp, 183
 - pretreatment methods, 185
 - quality, 183
 - Bio-mining, 451
 - Bioprocess, 66
 - Bioreactor, 173, 174, 176
 - design, 173
 - Bioremediation, 542, 543
 - Biosorption, 350, 457
 - Biosorption-based extraction process, 350
 - Biosorption-based method, 457
 - Bituminous, 40, 90, 107, 108, 113
 - Blast furnace slag (BFS), 500
 - Boiler slag, 623
 - Bottom ash (BA), 275, 488, 623
 - temperature, 276
 - Brick and paving materials
 - BA
 - construction industries, 504
 - pavement applications, 505
 - pavement binder course, 504
 - replacement, 504
 - sustainability issues, 504
 - FA
 - building materials, 502
 - CFA, 504
 - CFBC, 503
 - experimental research, 503
 - geopolymer technology, 502
 - hydraulic cement, 503
 - lime-pozzolana reaction, 503
 - low-density clay masonry units, 503
 - maximum compressive strength, 503
 - mechanical performance, 503
 - mineral polymerization, 503
 - mineralogical and chemical composition, 503
 - particle size, 503
 - specific gravity, 503
 - strength and durability test, 504
 - Bricks, 514, 522, 523, 526, 527
 - Bridging oil, 76
 - Brown coal, 3
 - Buried vegetation, 40
- C**
- CABC carbofuran sorption, 150
 - Cadmium (Cd), 234, 247–249
 - Calcium silicate hydrate (C-S-H), 492
 - Capsicum annum biochar (CABC)
 - adsorbent dosage, 153, 154
 - adsorption rate, 150
 - carbofuran, 150, 156, 159
 - CAW, 144
 - contact time, 152
 - proximate and ultimate analysis, 149, 150
 - Capsicum annum waste (CAW), 144
 - Carbide lime (CL), 504
 - Carbochlorination, 581, 586, 588
 - Carbofuran
 - biochar, 143
 - CABC, 143, 150, 153, 159
 - isotherm tests, 146
 - kinetic behavior, adsorption, 148
 - kinetic data, 156
 - sorption kinetics, 156
 - Carbofuran-loaded biochar, 151
 - Carbon dioxide, 546, 622
 - Carbon gasification, 115
 - Carbon mineralization process, 424
 - Carbon monoxide, 622
 - Carbon nanotubes, 237
 - Carbonaceous materials, 86
 - Carbon-in-leach (CIL) process, 121

- Carbonization, 92, 107, 109, 242, 535
- Carbonization-activation, 101
 - coal particles, 101
- Carbonization reactions, 108
- Carcinogenic substances, 595
- CaSiO₃, 595
- Cation/anion exchange mechanisms, 629
- Cationic trade limit (CEC), 514
- Cellular lightweight concrete (CLC), 282
- Cement, 512, 513, 517, 521, 522
- Cement-based materials
 - BA
 - aggregates replacement, 498
 - alkaline media, 498
 - BA-mortar, 499
 - less reactivity, 498
 - mixture, 499
 - PC-based materials, 499
 - performance, 498
 - powder, 498
 - pozzolanic properties, 498
 - sub-bituminous coal, 498
 - thermal conductivity, 499
 - thermal resistance, 499
 - UHPC, 498
 - FA
 - admixture, 496
 - CC beams, 497
 - Chinese, 497
 - high-quality constructions, 496
 - lab-scale testing, 497
 - mixed concrete, 496
 - PC-FA-SF concrete, 497
 - pozzolanic reaction, 496
 - SF, 497
 - supplement, 497
 - production, 496
 - solid wastes, 496
 - urbanization and development, 496
- Cement concrete (CC), 497
- Cement industry, 395
- Cement manufacturing process, 397
- Cenospheres, 385
- Centrifuges, 25, 26
- Cerium oxide (CeO₂), 406
- CFA-based products, 519
- CFBC boiler, 420
- Chamber filter press, 28
- Char gasification, 116
- Charcoal, 240
- Cheaper oils, 75
- Chelok[®] technology, 330
- Chemical activation, 241, 242
- Chemical additives, 40
- Chemical analysis, 561
- Chemical assays, 491, 492
- Chemical composition, 321
- Chemical industry, 233
- Chemical method, 60
- Chemical preparation, 124
- Chemical pretreatment methods, 185
- Chili production, 143
- China, 558
- Chinese FA, 497
- Chlorination, 580, 588
- Chromium (Cr), 234, 248, 250, 296, 595
- Chromium anion, 204
- Circular fluidized bed combustion (CFBC), 419, 503
- Classifying cyclone, 13
- Clay and ash mixtures, 284
- Clays, 237
- Clean-emerged technologies and national security, 423
- Climate change, 325, 546, 549
- CO₂ capture
 - adsorption, 196
 - capacity, 196
 - chemical activation, 193
 - gaseous molecules, 193
 - performance, 193
 - structural characteristics, 194–195
- CO₂ emissions, 547
- Coal, 90, 161, 162, 176, 268, 339
 - activated carbon
 - synthesis, 241
 - adsorption properties, 233
 - anthracites, 40
 - aromatic structures, 60
 - bituminous, 40
 - building material synthesis, 488
 - burning, 162
 - chemical methods, 560
 - chronological development, 40
 - classification, 3–5
 - cooking and non-cooking types, 61
 - countries and consumption, 61
 - electricity production, 487
 - FBC, 59
 - and fuel oil, 41
 - global energy share, 487, 488
 - global reserves, 1, 2
 - gradual depletion, 1
 - graphite, 41
 - heterogeneous nature, 560
 - India, 61

- Coal (*cont.*)
- inorganic and organic contents, 162
 - inorganic elements, 560
 - inorganic phases, 60
 - legislation, 59
 - lignite, 40
 - limestone, 59
 - macerals, 560
 - magmatic intrusion, 562
 - non-homogenous, 560
 - non-renewable energy, 39
 - organic compounds, 162
 - organic phase, 60
 - peat, 40
 - petrographic components, 5, 6
 - plant practices (*see* Plant practices)
 - preparation (*see* Preparation)
 - production, 1, 2, 560
 - pulverized, 41
 - REEs, 559–564
 - reserves countrywide, 61
 - reserves in India, 1, 3
 - sample, 559
 - steam, 40
 - structure, 560
 - sub-bituminous, 40
 - sulphur content, 59
 - sulphur dioxide, 59
 - washability studies, 5–8
 - water pollution, 233
- Coal ash, 390
- availability, 392
 - carbon emission footprint, 398
 - in cement, 399
 - flooding and river erosion, 392
 - metals, 396
 - pre-calciner, 397
 - ready-mix concrete production, 399
 - in road building, 392
 - use in India, 392
 - utilisation, 393
- Coal ash compositions, 390
- Coal ash/coal combustion residuals (CCRs)
- chemical composition, 491
 - classification, 488
 - definition, 488
 - microstructural/mineralogical properties, 493–495
 - particle size distribution, 490, 491
 - physical and chemical properties, 489
 - pozzolanic property, 492, 493
 - specific gravity, 489
- Coal-based energy, 434
- Coal-based power plant, 521
- Coal beneficiation, 79–80
- Coal-blended AC, 256
- Coal bottom ash, 481
- Coal cleaning, 24
- Coal combustion emissions, fly ash, 622
- Coal combustion products (CCP), 313, 318, 326, 332, 454, 475
- adverse effects, 622
 - beneficial use, 623, 624
 - capacity, 323
 - chemical composition, 323
 - China, 621
 - coal combustion wastes/by-products, 621
 - components, 623
 - disposal, 325
 - emission limit levels, 324
 - energy source, 621
 - FGD, 319
 - fly ash, 318
 - furnace bottom, 319
 - global, 322
 - industrial revolution, 621
 - ionic liquids, 632
 - physical and engineering properties, 320
 - REEs, 332, 624–626
 - residues, 621
 - silica, 322
 - slag tap and furnaces, 319
 - SO₂ emissions, 324
 - toxic substances, 325
 - United States, 622
 - utilization, 320, 322, 332
 - volumes, 321
- Coal combustion residuals, 615
- Coal-derived AC, 86, 106
- adsorption, 83
 - agricultural, industrial, and domestic sources, 257
 - application, 116–120
 - arsenic (As), 251, 253, 254
 - cadmium (Cd), 247–249
 - chemical preparation
 - activating agents, 96
 - comprehensive studies, 98–100
 - impregnation, 96
 - temperature, 96
 - chromium (Cr), 248, 250
 - copper (Cu), 254, 255
 - economics, 257, 258
 - expense of adsorbents, 258
 - lead (Pb), 251, 252
 - mercury adsorption, 245–247

- performance, 256, 257
- physical preparation
 - activation, 92
 - carbonization, 92
 - operational temperature, 96
 - physical preparation, 93–95
- preparation, 91
- pretreatment, 92
- solid-gas reactions, 111
- Coal fly ash (CFA), 123, 242, 289, 294, 340, 434, 437
 - aluminium, 302
 - amorphous and crystalline, 564
 - arsenic, 295
 - ash ponds/surface impoundments, 575
 - beneficiation process deployment, 418
 - benefits, 437
 - categorization, 565
 - CFA, 447
 - chemical composition, 439
 - chromium, 296
 - coal consumers, 575
 - coal consumption, 575
 - cobalt, 300
 - components, 576
 - composition, 565, 566
 - construction applications, 575
 - CS, 463
 - Cu, 301
 - density and hydrophobicity, 418
 - diverse use, 519
 - economically and environmentally friendly, 566
 - in electricity generation process, 519
 - elements, 297
 - environmental pollution (*see* Environmental pollution, CFA)
 - factor, 293
 - fractions, 417
 - generation, 301, 565
 - H₂SO₄, 585
 - heavy metals, 297
 - Indian fly ash, 567–569
 - Indian origin, 442, 443
 - industrial waste, 436
 - leaching techniques, 294
 - lead and cadmium, 297
 - magnetic property, 418
 - manganese, 299
 - manufacturing products, 516, 517
 - ceramic, 517
 - concrete, 517–518
 - matrix, 518
 - mercury, 296
 - metal extraction (*see* Metal extraction, CFA)
 - metal values, 298, 303
 - metallurgical methods (*see* Metallurgical methods, CFA)
 - metallurgical treatment, 575–576
 - minerals, 564
 - modern side effect, 511
 - monazite/zircon grains, 442
 - morphology, 292, 440, 441
 - nickel, 300
 - nonmagnetic fraction, 418
 - organic and inorganic constituent, 564
 - oxide content, 577–578
 - particles, 417, 418
 - physical properties, 417
 - physical/chemical properties, 576
 - pollutant, 295
 - porosity, 293
 - powdery substance, 564
 - pretreatment process, 295
 - production, 576
 - production and utilization, FA in India, 519
 - rare earth metals, 580
 - recover REEs, 569, 570
 - REE, 418, 437, 566, 567
 - SCE, 444
 - selenium, 299
 - sizes distribution, 294
 - solvent extraction, 585
 - sources, 292
 - spectro-chemical techniques, 293
 - surface, 293, 294
 - thermal power plants distribution, 520
 - trace metals concentration, 579
 - typical, 293
 - USA, 575
 - uses, 434
 - utilization, 511, 576
 - valuable metals, 297
 - value-added application, 525
 - versatile applicability prospective, 513
 - water leaching, 294
 - Zn, 300
- Coal fly ash treatment, 346
- Coal formation environment, 564
- Coal fuelled power plants, 71
- Coal lithotypes, 5, 6
- Coal particle size, 74, 75
- Coal rank, 73
- Coal slurry, 28
- Coal types, 103

- Coal washeries, 72
 - Coal water slurry (CWS)
 - extraction, saponin, 44
 - flow behaviour, 41
 - Hershely-Bulkely model, 43
 - ingredients, 41
 - isolation, natural dispersant, 43
 - mechanism of stabilization, 52, 53
 - natural dispersant in stabilization
 - coal concentration, 46–48
 - dispersant concentration, 48
 - effect of temperature, 50, 51
 - pH and surface charge, 51–53
 - shear rate with shear stress, 48–50
 - pipeline flow behaviour, 41
 - surface activity, natural dispersant
 - by fluorimeter, 44, 45
 - by surface tension measurement, 45, 46
 - suspension viscosity, 42
 - thixotropic and rheotropic fluid, 42, 43
 - viscosity measurement, 41, 43
 - Coarse coal clean, 72
 - Coarse coal particles, 72, 74
 - Coking coal washery, 28, 30, 31
 - Coking coals, 4
 - Collectors, 22
 - Combustion process, 270
 - Commercial activated carbon, 237
 - Comminution circuit, 8
 - Compound annual growth rate (CAGR), 433
 - Compressibility strength (CS), 462, 463
 - Construction sector, 488
 - Contact mechanism approach, 62
 - Continuous anthropogenic activities, 182
 - Conventional methods, 162
 - Conventional remediation methods, 236
 - Copper (Cu), 234, 254, 255, 594
 - Corn biochar, 546
 - Corrosion resistance, 405
 - Critical analysis, 488, 505
 - Critical micellar concentration (CMC)
 - saponins, 44, 45, 47, 48
 - C-S-H gel, 492
 - Cured geopolymers, 521
 - Cyclone overflow, 31
 - Cyclone/hydrocyclone, 13
- D**
- Deep Eutectic Solvents (DES), 454
 - Dense media cyclone (DMC), 8, 16, 17
 - Denver jig, 16
 - Deslimed coal slurry, 32
 - Desliming screen, 31
 - Desorption, 84
 - Desulfovibrio desulfuricans*, 65
 - Desulfurization, 163, 176
 - biological, 165
 - bioreactor, 171
 - C-C bonding, 170
 - coal, 171
 - difficulties and limitations, 163
 - HDS, 165
 - hydrophobic compound, 164
 - microorganisms, 166
 - ODS, 165
 - organic sulfur, 164
 - physical coal cleaning method, 163
 - physical methods, 164
 - pyrites, 166
 - reagents, 164
 - sulfur metabolism, 170
 - Dewatering devices
 - centrifuges, 25, 26
 - filtration units, 26–28
 - heating value, 24
 - high-frequency screens, 24, 25
 - inherent moisture, 24
 - surface area, 24
 - thickeners, 26
 - Di-(2-ethylhexyl) phosphoric acid (DEHPA), 423, 584
 - Dibenzothiophene (DBT), 169
 - anaerobic metabolism, 65
 - 4S pathway, 63
 - Kodama pathway, 65
 - R. erythropolis*, 63, 64
 - Diffraction, 494
 - Diglycol amide functional group, 456
 - Direct acid leaching system, 344
 - Disc filter, 27
 - Distilled water, 483
 - Domestic activities, 256
 - Drain and rinse (D&R) screens, 10, 17, 31
 - Drum filter, 27
 - Drum separators, 14, 15
 - Dry torrefaction, 187
 - Dubinín-Radushkevich isotherm model, 147
- E**
- Economic benefits of coal beneficiation, India
 - plant operations, 79
 - transportation, high-ash coals, 80
 - Economic development, 39, 559
 - Either electrostatic precipitators (ESP), 387
 - Electric producing industries, 272
 - Electricity, 71, 621

- Electricity generation plants, 515
- Electricity production, 233, 559
- Electrodialysis, 594
- Electrolytes, 77
- Electromagnetic vibrator, 24
- Electronic configuration (EC), 432
- Electrostatic attraction, 198
- Electro-Static Precipitators (ESP), 382
- Electrostatic quasi (pseudo) liquid membrane (EQLM), 455
- Elemental analysis, 144, 150
- Elovich model (EM), 149
- Emulsion liquid membrane (ELM), 455
- Energy, 41, 559
- Energy consumption, 1
- Energy dispersive X-ray spectroscopy coupled with scanning electron microscope (EDS-SEM), 561
- Energy Information Administration (EIA), 61
- Environment pollutant, 595
- Environmental hazards, 635
- Environmental information system (ENVIS), 289
- Environmental pollution, CFA
 - air pollution, 515
 - bituminous and sub-bituminous types, 515
 - heavy metals, 515, 516
 - toxic trace elements, 516
- Environmental Protection Agency (EPA), 324
- Environmental sustainability, 541
- Equilibrium tests, 145
- Ethanol oil, 41
- European Union emission limits, 324
- Experimental flowsheet, 343
- Extracellular polymeric substances (EPS), 62
- Extraction behaviour, 297
- Extraneous impurities, 14
- F**
- FA-based alkali-activated concrete, 500
- FA-based geopolymer, 513
- FA graphical illustration, 414
- FA zeo-litization, 514
- FA-lime-based bricks, 503
- FA-mortar, 499
- Fast pyrolysis, 536
- Feed-coal, 417
- Feedstock, 540, 543
- Fertilizer, 549
- Fertilizer production, 524
- FGD wastewater, 325
- Filtration units, 26–28
- Fine coal beneficiation, 72
- Fine coal clean, 72, 73
- Fine coal particles, 75
- Fine particles, 27
- Fixed-bed gasification, 539
- Fixed-bed reactors, 538
- Flowing film concentration, 17
- Fluidized bed combustion (FBC), 59, 345, 450
- Fluidized bed reactor, 538
- Fluidized bed zone, 21
- Fluorosilicic acid, 364
- Fly ash (FA), 321, 381, 382, 384, 488, 623
 - annual quantity, 387
 - application, 390
 - ash slurry disposal system, 388
 - biodiesel production, 525
 - and bottom ash (BA), 269
 - brick fabrication, 279
 - bricks manufacturing, 522, 523
 - BTPP, 388
 - carbon content, 381
 - cement manufacturers, 391
 - chemical compounds, 273
 - clay bricks, 391
 - CO₂ emissions, 513
 - coal consumption, 387
 - coal economiser and ESP hopper, 388
 - coal, 382, 385
 - coal-fired power plants, 382, 386
 - combustion, 270
 - competitive market, 392
 - composition and properties, 385
 - concentration, 267
 - disposal, 269
 - effective applications, 512
 - electron microscopic image, 381–382
 - elemental concentration, 394
 - environmental and occupational safety, 382
 - ESP, 387
 - fabrication microfiltration membrane, 519, 521
 - fabrication, composite materials, 526
 - fertilizer production, 524
 - filtration, 383
 - fluidity, 388
 - gasification, 514
 - generation, 269, 271
 - geopolymer synthesis, 512, 521
 - handling system, 388
 - India, 268
 - inhalation, 268
 - magnification, 382
 - market, 383, 392

- Fly ash (FA) (*cont.*)
- mechanical and structural benefits, 384
 - noncombustible coarser component, 382
 - oxide analyses, 385
 - particles, 270
 - plant factor, 387
 - potential market, 391
 - power plant, 388
 - pozzolanic properties, 384
 - pozzolans type FA, 521, 522
 - production and utilization, 268
 - production calculation, 389
 - production, 267
 - soil pollution, 515–516
 - sophisticated reuse, 512
 - structural fills, 269
 - treatments, 511
 - type, 273
 - usages, 270, 391, 511, 514
 - utilization in India, 513, 514, 523
 - valuation, 391
- Fly ash brick (FAB), 397
- behaviour, 279
 - characteristics, 278
 - compressive strength, 277, 279
 - erosion, 279
 - manufacturing, 283
 - phase analysis, 281
 - properties, 280
 - raw materials, 280
 - strength and colour, 280
- Fly ash slurry (FAS)
- air-drying, 275
 - characteristics, 276
 - dispersion, 275
 - pipeline transportation, 274
 - stabilization, 276
 - viscosity, 275
- Fly ash utilization, 304
- Fly ashes (FA)
- bituminous coal combustion, 614
- Forth flotation, 164
- Fourier Transform Infrared spectroscopy (FTIR), 144, 150, 152, 238
- Free lime (Ca) (OH)₂, 501
- Freundlich and Langmuir isotherm models, 222, 238
- Freundlich isotherm, 146, 147, 239
- Freundlich model, 217
- Froth flotation, 9, 14, 21–23, 34, 72
- Frothers, 23
- Fuel oil, 41
- Functional ionic liquids, 630–632
- G**
- Gallium, 360
- fly ash leachate, 362
 - metal, 361
 - precipitation, 362
 - recovery, 363
- Gallium (Ga), 590, 591
- Gasification, 186, 233, 242, 539
- Gaussian distribution, 114
- Generalized leaching mechanism, 344
- Genetic types, 561
- Geochemical computer software, 605–606
- Geochemical equilibrium model, 605
- Geochemical modeling, REEs, 605–608, 611–613
- Geopolymerization, 500, 521
- Geopolymers, 512, 519, 521
- Germanium (Ge), 361, 362, 589, 590
- Glass matrix, 564
- Global warming, 546
- Gold, 369
- fine-grained particles, 370
 - and silver
 - ACs-solution contact, 122
 - mechanisms, 116
 - recovery, 116
 - structure and adsorption parameters, 121
 - surface functional groups, 121
- Gordonia desulfuricans*, 64
- Granular activated carbon (GAC), 101
- Graphene, 237
- Graphite, 41
- Gravity, 71
- Gravity-based dense media separators, 14
- Gravity concentrators, 19, 20
- Green energy technologies, 431
- Greenhouse gas (GHG) emission, 546, 547, 549
- Green-sustainable technological development, 406
- Grizzly feeder, 10, 11
- Groundnut shell-based AC, 256
- Groundwater-controlled type, 561
- Groundwater leaching, 561
- H**
- Heating rate, 108
- Heating value, 24
- Heavy metal immobilization, 542
- Heavy metals, 515, 516, 542, 595
- electric charge and pH, 197

- extraction, 291
 - impurities, 292
 - natural and wastewater, 197
 - surface functional groups, 197
 - Heavy oil fly ash (HOFA), 123
 - Heavy oils, 75
 - Heteroatoms, 242
 - Heterotrophs, 60, 67
 - High-ash Indian coals, 78, 79
 - High-frequency screens, 24, 25
 - High-volume FA bricks, 503
 - Holding time, 110
 - Horizontal belt filter, 27
 - Horizontal vibrating basket centrifuge, 25
 - HREEs, 561–563
 - HSC Chemistry software, 610
 - Hydrated manganese oxide nanoparticles, 222
 - Hydraulic cement, 503
 - Hydrocarbons, 75, 79
 - Hydrochar, 539
 - Hydro-desulfurization (HDS), 165
 - Hydrometallurgical extraction process,
 - 410, 416
 - Hydrometallurgical methods, 370
 - bioleaching, 582, 583
 - ion exchange, 583
 - leaching, 581, 582
 - solvent extraction, 583
 - Hydrometallurgical process, 318, 444, 463,
 - 474, 479
 - Hydrometallurgy, 628
 - Hydrothermal alkali pre-treatment
 - method, 346
 - Hydrothermal carbonization (HTC), 186, 187,
 - 190, 539, 540
 - biomass, 190
 - industrial, 191
 - moisture content, 190
 - organic compounds, 190
 - reaction temperature, 190
 - thermochemical process, 191
 - Hydrothermal-alkali pre-treatment, 347
 - Hydrothermal-fluid-controlled type, 561
 - Hyperbaric filter, 28
- I**
- Impregnation method, 96
 - Indian cement plants, 397
 - Indian coal bottom ash, 480
 - Indian coals
 - ash-bearing particles, 72
 - disadvantage, 80
 - drift origin, 71
 - high-grade coals, 71
 - thermal power plants, 71
 - Indian fly ash, 567–569
 - Indian origin coals, 28
 - Indirect bioleaching system, 348
 - Induction coupled plasma (ICP), 420, 561
 - Inductively Coupled Plasma-Optical Emission Spectrometer (ICP-OES), 483
 - Industrial activities, 256
 - Industrial revolution, 621
 - Industrial wastes, 513
 - Industrial water treatment, 215
 - Inorganic contaminants removal, 217, 218
 - Inorganic electrolytes, 77
 - Inorganic speciation modeling, 608
 - Inorganic sulphur removal, microbes
 - A. ferrooxidans*, 63
 - chemolithotrophs, 63
 - contact mechanism, 62
 - non-contact mechanism, 63
 - Integrated alkaline fusion-acid leaching, 421
 - Interaction mechanism, 277
 - International Energy Agency, 161
 - International Union of Pure and Applied Chemistry (IUPAC), 404
 - Intraparticle diffusion model, 158
 - Iodine adsorption number, 110
 - Ion exchange, 362, 583, 589
 - Ionic liquids (ILs), 329–331, 454, 455
 - Ionic liquids, metal extraction
 - advantages, 628
 - anion, 627
 - challenges, 634
 - characteristics, 627
 - green concept, 626
 - hydrometallurgy, 628
 - liquid–liquid extraction, 628
 - organic compounds, 627
 - organic solvents, 627
 - recyclability, 627
 - REEs (*see* REEs extraction, Ionic liquids)
 - solvent extraction, 628
 - viscosity and melting point, 627
 - water immiscible extractants, 628
 - Iron (Fe), 608
 - Isotherm models, 155
- J**
- Jigs, 14–16

K

Kaolinite, 256, 495, 513

Kinetic models

activation, 114

carbonization, 112

pyrolytic decomposition, 113

reaction model, 112

Kinetics

carbofuran, 148

model, 157

PFOM, 148

PSOM I, 148

PSOM II, 148

KOH/anthracite ratio, 110

K-zeolites, 524

L

Lamella zone, 21

Langmuir and pseudo-secondary kinetic models, 218

Langmuir isotherm, 146, 156, 238

Lanthanides, 433

Leaching, 164, 581, 582

Leaching systems, 345

Leaching, REEs, 606, 611, 613

Leaching–solvent extraction, 460

Lead (Pb), 234, 251, 252

Light oils, 75

Lignin-based biomass, 538

Lignite, 3, 40, 90

Lignocellulosic biomass feedstocks, 191

Limestone, 59

Liquefaction, 233

Liquefied natural gas (LNG) importation, 386

Liquid emulsion membranes (LEMs), 349

Liquid phase applications, 238

Liquid-ash mixture, 347

Liquid–liquid extraction, 628, 630, 631

Lithium, 364, 591

content, 365

pre-desilication, 365

Low Temperature Conversion (LTC), 533

Low-cost adsorbents, 256

Low-intensity magnetic separator (LIMS), 31

LREEs, 561–563

M

Macerals, 560

Macropores, 88, 101

Macroporous, 237

Magnesium

CFA, 365

solid leaching residue, 366

Magnesium/calcium, 365

Magnetic fraction, 370

Magnetic separation, 164

Magnetite, 32

Magnetization, 192

Manganese, 299

Manufacturing process, 283, 397

Marine-environment-controlled type, 561

Mechanical and pneumatic flotation cells, 23

Mechanical posttreatment, 192

Mechanical-type bottom ash handling system, 390

Medium coking coal, 4

Melting furnace fly ash (MFA), 303

Membrane electrolysis, 587

Membrane filters, 28

Membrane-based technologies (MT), 455

Mercury (Hg), 234, 296

Mercury adsorption, 245–247

electrostatic precipitators (ESP), 245

Mesopore fraction, 108

Mesopores, 88, 111

Mesoporous, 237

Metal extraction

aluminium, 587, 588

fly ash, 302

gallium, 590, 591

germanium, 589, 590

lithium, 591

REEs, 591–594

silicon, 588

titanium, 583, 584, 586, 587

trace metals, 594–596

Metal processing industries, 233

Metal removal

As, 251, 253, 254

Cd, 247–249

Cr, 248, 250

Cu, 254, 255

heavy, 236

Hg, 245–247

Pb, 251, 252

Metallic organic framework, 225

Metallurgical methods, CFA

hydrometallurgical methods, 581–583

pyrometallurgical methods, 576, 581

Metal-organic frameworks (MOFs), 514

Metals, 563

Methanolysis process, 525

Methylene blue (MB), 221

Microbes

inorganic sulphur removal

A. ferrooxidans, 63*A. thiooxidans*, 63

contact mechanism, 62

- non-contact mechanism, 63
 - organic sulphur removal, 63, 65
 - sulphur removal, coal, 65, 66
- Microbial coal desulfurization process, 165
- Microcrystallite layers, 87
- Microfiltration (MF), 455
- Micropore distribution, 101, 103
- Micropores, 88
- Microwave pyrolysis, 538
- Mine filling, 559
- Mineral industry, 233
- Mineral polymerization, 503
- Mineral processing, 20
- Mineralogy, 495
- Mining techniques, 8
- Ministry of Environment and Forest (MEF), 78
- Modern-day coal processing plants, 9
- Modular plants, 33, 34
- Molybdenum, 367
- Monazite, 563
- Mullite, 495
- Mullite-corundum-quartz (MCQ), 365
- Multiple washing processes, 102
- Multi-walled carbon nanotube (CNT), 221
- Municipal solid waste incineration
 - residues, 605
- Municipal solid waste (MSW), 303
- Municipal waste incineration (MWI), 304
- Municipality solid wastes (MSW), 526
- Mycobacterium* sp., 64

- N**
- N,N,N'N'-tetra-2-ethylhexyl diglycolamide (TEHDGA), 456, 457
- N₂O emission, 547
- Nanoadsorbents, 220
- Nanocomposite carbon, 221
- Nanocomposites combined with activated carbon (NCAC), 222
- Nano-filtration (NF), 455
- Nanomaterials, 219
 - acid treatment, 216
 - adsorption capacity, 221
 - charcoal, 222
 - nanocomposite, 221, 222
 - NCAC, 222
 - pollutants, 217, 226
 - TNT, 222
 - treatment, 215, 217
 - water treatment, 219
- Nanoparticles, 219
- Nanopore and micropore, 223
- NaOH regeneration, 422
- National Thermal Power Corporation (NTPC), 491
- Near gravity material (NGM), 28
- Newtonian flow behaviour, 41
- Nickel, 300
- Nitrogen, 201, 544
- Nitrogen oxides, 622
- Non-coking coal washery circuit, 31, 32
- Non-coking coals, 4
- Non-contact mechanism, 63
- Non-edible vegetable, 75
- Nonfunctional ionic liquids, 628–630
- Non-polar substances, 548
- Non-renewable energy, 39
- Nuclear fuel cycle, 399

- O**
- Octyl(phenyl)-N,N-diisobutylcarbamoylmethylphosphine oxide (CMPO), 629–631
- Ohio power plant (USA), 418
- Oil, 75
- Oil agglomeration, 164
 - agitation conditions, 77
 - beneficiation process, 73
 - bridging liquid and concentration, 75, 76
 - coal particle size, 74, 75
 - coal rank, 73
 - high-ash Indian coals, 78, 79
 - ionic strength, 77
 - process, 73
 - pulp density, 76
 - pulp pH, 76
 - surface adsorption, 73
 - surface chemistry, coal particles, 74
- Oil-fired ash (OFA), 363
- One-part AAM, 501
- Operational temperature, 107
- Optimal leaching conditions, 344
- Organic carbon, 63
- Organic contaminants removal, 219
- Organic material feedstock, 533
- Organic plant vegetation, 1
- Organic pollutants, 543, 548
- Organic sulphur removal, microbes, 63, 65
- Oxidation reaction rate, 101
- Oxidative desulfurization (ODS), 165, 176
- Oxidizing gas flow rate, 109
- Oxygen-carbon ratio, 539

P

- Pachuca tank, 171
 Pachuca-type bioreactors, 172
 Particulate matter (PM_{2.5}), 622
 PC-FA-SF concrete, 497
 Peat, 40
 Perchlorate (ClO₄⁻), 204
 Persian wood-derived biochar, 196
 pH, 153, 154
 pH-dependent tests, 516
 Phenols, 224
 Phosphogypsum (PG), 436
 Phosphorus, 201
 PHREEQC modeling software, 610
 Physical activation, 242, 243
 Physical cleaning method, 163
 Physical coal cleaning method, 163
 Physical desulfurization process, 163
 Physical quality of coal, 71
 Physical separation, 329, 342, 343
 Physicochemical activation, 243–245
 Phytoextraction, 543
 Phytostabilization technique, 543
 Plant practices
 coking coal washery, 28, 30, 31
 Indian origin coals, 28
 modular plants, 33, 34
 NGM, 28
 non-coking coal washery circuit, 31, 32
 washing schemes, 28–30
 Plastic wastes, 526
 Plate and frame filter press, 28
 Pollutants, 544
 Porosity development mechanisms, 237
 Portland cement (PC), 400, 491, 497
 Portland Pozzolana Cement (PPC), 391
 Portland Slag Cement (PSC), 513
 Posttreatment processes
 chemical/corrosive, 191
 KOH and KMnO₄ treatment, 192
 magnetization, 192
 mechanical, 192
 nitrogen-doped biochar, 192
 surface chemistry, 191
 Posttreatments feature, 192
 Pourbaix diagrams, 609, 610, 613
 Power plants, 79
 Pozzolanic activity, 493
 Pozzolanic ash, 522
 Pozzolanic materials, 492
 Pozzolanic reaction, 492
 Pozzolans, 462
 Precipitation, 369, 457–460, 462
 Preconcentration methods, 343
 Pre-oxidation, 97, 101
 Preparation
 communion circuit, 8
 conventional gravity-based separators, 8
 dewatering devices (*see* Dewatering devices)
 diesel oil consumption, 9
 energy resources, 8
 mining techniques, 8
 sizing devices (*see* Sizing devices)
 washing/cleaning devices (*see* Washing/cleaning devices)
 working size range, 9
 Press filter, 27
 Pretreatment, 97
 Prime coking coals, 4
 Promethium, 557, 558
 Proximate and ultimate analysis, 149
 Pseudo-first- and -second-order mechanisms, 239
 Pseudo-first-order reaction, 239
Pseudomonas putida, 66
 Pseudoplastic model, 43
 Pseudo-second-order equation, 239
 Pseudo-second-order kinetics, 224
 Pulp density, 76
 Pulp pH, 76
 Pulverized coal, 41, 272, 356, 420
 Pyrite (FeS₂), 60, 62
 Pyritic sulphur removal, microbes
 A. ferrooxidans, 63
 chemolithotrophs, 63
 contact mechanism, 62
 non-contact mechanism, 63
 Pyrolysis, 187
 auger reactor, 549
 biomass, 534
 biomass composition, 537, 538
 climate change, 549
 fast pyrolysis, 536
 fertilizer, 549
 forest/agricultural-derived biomass residues, 535
 heavy metal immobilization, 549
 operational conditions, 536
 organic pollutants removal, 549
 oxygen-free condition, 535
 particle shape, 537
 particle size, 537
 reactor configuration, 538
 residence time, 537
 slow pyrolysis, 535, 536

- small-scale impacts, 549
 - surface area, 537
 - temperature and pressure, 536, 537
 - thermochemical conversion technology, 533, 549
 - Pyrolysis temperature, 243
 - Pyrometallurgical extraction process, 416
 - Pyrometallurgical treatment, 582
- Q**
- Quick heat transfer' process, 535
- R**
- Radioactive elements, 368
 - Radionuclides-induced damage, 399
 - Raman spectrum, 238
 - RAP-FA-CL mixtures, 504
 - Rare earth elements (REE), 332, 393, 431, 580
 - abundance, 564
 - acid and alkali leaching, 345
 - acid leaching vs. CFA, 592
 - acid leaching, 594
 - adsorption, 608
 - advantages, 436
 - alkaline pre-leaching, 593
 - Al-Si glass, 443
 - AMD formation, 608
 - applications, 341, 619
 - calcination, 593
 - carbonate chemical compositions, 314
 - carbonates/oxides, 605
 - catalysts and ceramics, 406
 - categorizations, 314
 - CCPs, 313, 624–626
 - CFA, 344, 437, 440, 591–593
 - China, 591, 617, 635
 - Chinese and US coals, 342
 - classification, 558
 - coal ashes, 607
 - coal, 559–564
 - combustion process, 313, 342
 - commercial exploitation, 442
 - concentration, 559, 563
 - consumption sectors, 433
 - contentment, 313
 - co-precipitation processes, 612
 - critical elements, 407
 - crustal abundance, 432
 - demand, 618, 619, 621
 - dependency, 342
 - deposits, 314
 - description, 403
 - direct acid leaching system, 344
 - disruption potential, 407
 - electric and magnetic properties, 557
 - electrodialysis, 594
 - elemental abundance, 403
 - elements, 593
 - exploitation, 609
 - extraction of REY, 607
 - extraction, 316, 608
 - FA, 313
 - flexibility and specificity, 406
 - flowcharts, 328
 - fly ash, 450
 - fractionation, 611
 - genetic types, coals, 441
 - geochemical modeling, 605
 - geochemistry, 563
 - global distribution, 618
 - global reserves, 558
 - global, 316, 317
 - green and energy-efficient products, 406
 - H₂SO₄, 593
 - HCl leaching, 592, 593
 - hydroxides, 612
 - industrial utilization, 605
 - integral role, 404
 - ion-adsorption clay deposits, 314
 - lanthanides with atomic numbers, 557
 - leaching, 345, 449, 450, 606
 - leaching, roasting products, 592
 - LLNL database, 609
 - LREE and HREE, 342
 - magnets, 404
 - method of recovery, 608
 - microfiltration pretreatment, 593
 - mineral mine sites, 315
 - minerals, 435, 558
 - mining industry, 406
 - mining production, 620
 - mobility, 611
 - modern technologies, 617, 635
 - multiple niche deployments, 404, 405
 - NaOH/Na₂CO₃, 592
 - organic phase, 593
 - overview, 404
 - phosphors, 405
 - physical and chemical properties, 311, 312
 - physical beneficiation, 445–447
 - physicochemical properties, 558
 - precious metals, 557
 - pre-concentration, 448
 - production and exports, 316

- Rare earth elements (REE) (*cont.*)
- production, 311
 - properties, 432
 - provision, 315
 - quantity, 406
 - recovery from CFA, 459, 460
 - recovery, 341, 342, 444, 458, 605
 - acid leaching systems, 343
 - alkali pre-treatment, 346
 - biohydrometallurgy, 371
 - biological extraction methods, 347
 - biosorption, 351
 - concentrations, 372
 - consumption, 370
 - experimental design, 347
 - extraction and separation, 352–353
 - glass phase aluminosilicates, 344, 345
 - HCl and NaOH, 345
 - HREE, 344
 - LEM system, 349
 - NaOH flux melting point, 346
 - NaOH solutions, 346
 - physical preconcentration, 344
 - pre-treatment reagents, 347
 - separation, 371
 - SLM REE extraction process, 349
 - TEA, 371
 - TEHDGA, 349
 - USD, 371
 - REO, 407
 - reserve, 316, 619
 - SCE, 445, 446
 - sea-floor deposits, 606
 - secondary resources, 605
 - separation/purification, 451
 - solvent extraction, 593
 - speciation, 608, 610–612
 - strategic material, 591
 - strengthening functions, 405
 - supply disruptions, 433
 - SX, 452–454
 - technospheric resources, 434
 - thermodynamic models, 609, 611
 - uranium, 594
 - use, 314, 605
 - value metals, 434
 - via co-precipitation processes, 608
 - yttrium, 591, 592
- Rare earth metals (REM), 473
- acid leaching, 477, 478
 - alkali roasting, 479
 - alkali treatment, 477
 - availability, 473
 - by-products, coal, 475, 476
 - characterization, 480
 - coal, 474, 480
 - coal combustion products, 475
 - dissolution, 482
 - extraction process, 474
 - Indian coal bottom ash, 480–482
 - pretreatment, coal, 476
 - sources, 474
 - thermal treatment, 478
- Rare earth oxide (REO), 342, 406, 434
- Rare earths recovery
- beneficiation, 417–419
 - CFA, 416
 - coal combustion products, 326
 - extraction stage, 416
 - hydrometallurgical extraction
 - processes, 416
 - pyrometallurgical extraction processes, 416
 - recovering, 327
 - recycling, 416
 - roasting-water leaching-acid process, 327
 - solvents extraction, 417
 - subeconomic resources, 416
- Reactor configuration, 538
- Ready Mixed Concrete (RMC), 491, 497
- Reagents, 22
- Reagents dosage, 109
- Reclaimed asphalt pavement (RAP), 504
- Recombinant DNA technology (RDT), 66
- Recover REEs, 569, 570
- by-products of coal combustion, 635
 - EIM system, 631
 - functional ionic liquids, 630, 631
 - nonfunctional ionic liquids, 628–630
- Recovery rare earths, 569, 570
- Recycling, 411, 436
- Red mud (RM), 358
- Reduced graphene oxide (rGO), 225
- REE alternative sources
- CA, 411
 - CFA, 411
 - coal and coal combustion, 410
 - coal combustion by products, 411
 - deposits and substitution, 410
 - high-tech components, 410
 - hydrometallurgy processes, 410
 - iron mining wastes, 410
 - red mud, 410
 - REO stocking, 410
- REE chemical extraction
- acidic leaching, 419–420
 - alkaline-activated acidic leaching, 420–422

- CO₂ capture, 422
 - separation and purification, 423
 - REE concentration, 418
 - REE conventional sources
 - deposits, 409
 - minerals, 408
 - mining and production, 408
 - ore minerals, 409, 410
 - REO, 408
 - REE critical, 423
 - REE enrichment, 418
 - REE extraction efficiency, 416
 - REE laser, 405
 - REE occurrence mode, CFA
 - alternative source, 413
 - aluminosilicate species, 415–416
 - average global basis, 411
 - bituminous coal, 414
 - characterization, 413
 - chemical compositions, 414
 - chemical/mineralogical compositions, 414
 - coal basins, 411
 - countries, 413
 - crystalline/glassy phases, 414
 - flue gases coupling, 414
 - infiltrational and exfiltrational origin, 411
 - organic compounds, 414
 - power plants, 411
 - products, 414
 - SCE, 414
 - sequential extraction procedure, 414
 - surface water, 411
 - trace elements, 414
 - UCC, 412
 - REE recycling, 423, 424
 - REEs extraction, ionic liquids
 - CCPs, 632
 - liquid–liquid extraction process, 628
 - REE recovery
 - EIM system, 631
 - functional ionic liquids, 630–632
 - nonfunctional ionic liquids, 628–630
 - stripping methods, 632–634
 - REE-sulfate complexes, 611, 612
 - Reflux classifiers, 20, 21
 - Regulators/modifiers, 23
 - Reinforcement corrosion, 512
 - Remediation of wastewater, 237
 - Removing heavy metals
 - adsorption, 122
 - arsenic and antimony, 123
 - bituminous coal, 122
 - for industries, 122
 - molybdenum, 122
 - operational parameters, 122
 - vanadium, 122
 - Residence time, 537
 - Respective coal derivatives, 124
 - Rheological model
 - FAS, 274
 - surfactant, 274
 - Rheology, 273
 - Rhodamine-B (RhB), 256
 - Rhodococcus erythropolis*, 63–66
 - Rhodococcus GIN-1*, 583
 - Rhodococcus thryopolis*, 67
 - Roasting, 420
 - ROM coal lumps, 28
- ## S
- Saponin
 - CMC, 44, 45, 47, 48
 - on coal particle, 54
 - extraction from *Sapindus mukorossi*, 44
 - from *Sapindus mukorossi* and *Sapindus laurifolia*, 53
 - Scanning electron microscope (SEM), 144, 238
 - Screen bowl centrifuges, 25
 - Screen scroll basket centrifuges, 25
 - Screen-scroll centrifuge, 25
 - Sea-floor deposits, 606
 - Second-order kinetic model, 221, 239
 - Selenium, 299, 359
 - and arsenic, 360
 - calcium precipitation, 360
 - CFA, 360
 - concentration, 360
 - sequential extraction, 361
 - trace amount, 359
 - Semi-coking coals, 4
 - Semi-empirical models, 115
 - Sequential chemical extraction (SCE), 414, 444, 445
 - Sewage sludge biochar, 547
 - Shaking tables, 19
 - Sieve bends, 10–13
 - Silica fume (SF), 497, 500
 - Silicon, 588
 - Sizing devices
 - classifying cyclone, 13
 - coal preparation plants, 10
 - D&R screens, 10
 - grizzly feeder, 10, 11
 - sieve bends, 10–13
 - vibrating screens, 10–12
 - Slow pyrolysis, 535, 536

- Sodium dodecyl sulphate (SDS)
saponin, 49
- Sodium hydroxide leaching, 582
- Soil, 546
- Soil fertility, 544
- Solid-liquid adsorption, 238
- Solid-liquid extraction, 631
- Solid-liquid separation, 25
- Soil nutrient dynamics, 544, 546
- Soil nutrients, 622
- Soil quality, 534
- Solid phase extraction (SPE), 456
- Solvent extraction (SX), 361, 423, 452–454,
581–585, 589, 593, 628
- Solvent-impregnated resins (SIR), 456
- Sorption mechanism, 238
- Source-rock-controlled types, 561
- Spark plasma sintering (SPS), 284
- Speciation, 605, 610
- Specific surface area (SSA), 493, 502
- Spiral concentrators, 17–19
- Stability, 41, 54
- Stabilization
natural dispersant in CWS stabilization
coal concentration, 46–48
dispersant concentration, 48
effect of temperature, 50, 51
pH and surface charge, 51–53
shear rate with shear stress, 48–50
- Steam coal, 40
- Steel Grade-I constitutes, 4
- Steel industry, 1
- Steel making, 4
- Stokes-Herleen System, 5, 6
- Straw-derived biochar, 538
- Strength activity index test, 492
- Stripping mould, 281
- Subbituminous, 90
- Sub-bituminous coal, 3, 40
- Subsequent activation process, 92
- Sulfur, 503
- Sulphur dioxide, 59
- Sulphuric acid leaching, 460
- Supplementary cementitious material
(SCM), 488
- Supported liquid (SEMs), 349
- Supported liquid membrane (SLM), 455
- Surface area, 24
- Surface chemistry of coal, 74
- Surface functional groups, 197
- Sustainability, 541
- Sustainability goals, 433, 463
- T**
- Techno-economic analysis (TEA), 371
- Technology metals, 431
- Teeter-bed separator (TBS), 9, 20, 21, 31
- Temkin isotherm model, 147
- Temperature, 539, 540
- Thermal power plants, 78, 271, 559, 564, 565,
567, 571
- Thermal treatment, 216
- Thermal treatment parameters, 108
bituminous coal, 107
subbituminous coal, 107
temperature, 107
- Thermal waste, 515
- Thermochemical process, 590
- Thickeners, 26
- Thiobacillus thiooxidans*, 582, 595
- TiO₂ chlorination, 586
- Titanium
biohydrometallurgical treatment, CFA, 584
bioleaching, 584
carbochlorination method, 586
cement roasting, 587
CFA, 583, 584
chemical and thermochemical
processes, 583
chloride, 586
chlorination, 586
extraction, 584
H₂SO₄, 584
hydrometallurgical process, 584, 586
leaching, 584
solvent extraction, 584
thermochemical process, 587
- Titanium and molybdenum, 366
- Tobermorite fibers, 516, 525, 526
- Torrified biochar, 187
- Toxic metals, 234
- Toxicity Characterization Leaching Procedure
test (TCLP), 483
- Trace elements, 563
- Trace metals, 576, 579, 594–596
- Tributyl phosphate (TBP), 123, 423
- Turbostratic structure, 87
- Turpentine oil, 79
- U**
- Ultra-fine particles, 31
- Ultra-high performance concrete (UHPC), 498
- United States Environmental Protection
Agency, 326

- Upper Continental Crust (UCC), 412
Uranium, 368
U-rich eluant fractions, 369
US Environmental Protection Agency (USEPA), 245
- V**
Vacuum drum filter, 27
Vacuum filters, 26, 27
Vacuum technology, 109
Vanadium, 363
 and nickel, 364
 source, 363
Vegetable oils, 75, 79
Venturi pipe, 173
Vertical auger reactor, 539
Vibrating screens, 10–12
Visual MINTEQ modeling program, 609–611
Volatiles, 242
Volcanic-ash-controlled type, 561
- W**
Washability studies, 5–8
Washing/cleaning devices
 ash-forming and sulphur-containing type, 14
 coal quality, 13
 DMC, 16, 17
 drum separators, 14, 15
 extraneous impurities, 14
 Froth flotation, 22, 23
 jigs, 14–16
 shaking tables, 19
 spiral concentrators, 17–19
 TBS, 20, 21
 thermal power plants, 13
 WOC, 21, 22
Waste management, 233, 547, 548
Waste recycle, 436
Wastewater
 Cd, Pd, and Hg, 248
 characteristics, adsorbent materials, 237, 238
 conventional remediation methods, 236
 domestic, agricultural and industrial activities, 234
 heavy metal removal, 236
 industrial, 254
 iron, zinc, copper and chromium, 236
 mechanism of adsorption, 238–240
 metal ions, 257
 source and health effect, 236
 streams, 234
 toxic metals, 234
 treatment, 233, 234, 254
Wastewater treatment, 219, 548
Water leachability test, 595
Water-only cyclone (WOC), 9, 21, 22
Water-pulsated jig, 14, 15
Weak coking coals, 4
Wet biomass, 540
While semi-coking coal, 4
Wilfley shaking table, 19
World Coal Association reports, 487
- X**
Xenotime grains, 442
X-ray fluorescence spectroscopy (XRF), 561
XRD, 102, 107, 561
- Z**
Zeolites, 84, 513, 514, 588
Zeolitic material from FA (FA-ZM), 525
Zinc (Zn), 595